CURRENT TRENDS IN EXPLOITING MOLECULAR SIGNALING IN BACTERIA-HOST CROSSTALK

EDITED BY: Monica Cartelle Gestal, Carmen Mariana Chifiriuc, Alina Maria Holban and Karl Kuchler

PUBLISHED IN: Frontiers in Microbiology and Frontiers in Immunology

frontiers Research Topics



frontiers

Frontiers eBook Copyright Statement

The copyright in the text of individual articles in this eBook is the property of their respective authors or their respective institutions or funders. The copyright in graphics and images within each article may be subject to copyright of other parties. In both cases this is subject to a license granted to Frontiers.

The compilation of articles constituting this eBook is the property of Frontiers.

Each article within this eBook, and the eBook itself, are published under the most recent version of the Creative Commons CC-BY licence. The version current at the date of publication of this eBook is CC-BY 4.0. If the CC-BY licence is updated, the licence granted by Frontiers is automatically updated to the new version.

When exercising any right under the CC-BY licence, Frontiers must be attributed as the original publisher of the article or eBook, as applicable.

Authors have the responsibility of ensuring that any graphics or other materials which are the property of others may be included in the CC-BY licence, but this should be checked before relying on the CC-BY licence to reproduce those materials. Any copyright notices relating to those materials must be complied with.

Copyright and source acknowledgement notices may not be removed and must be displayed in any copy, derivative work or partial copy which includes the elements in question.

All copyright, and all rights therein, are protected by national and international copyright laws. The above represents a summary only. For further information please read Frontiers' Conditions for Website Use and Copyright Statement, and the applicable CC-BY licence.

ISSN 1664-8714
ISBN 978-2-88976-430-3
DOI 10.3389/978-2-88976-430-3

About Frontiers

Frontiers is more than just an open-access publisher of scholarly articles: it is a pioneering approach to the world of academia, radically improving the way scholarly research is managed. The grand vision of Frontiers is a world where all people have an equal opportunity to seek, share and generate knowledge. Frontiers provides immediate and permanent online open access to all its publications, but this alone is not enough to realize our grand goals.

Frontiers Journal Series

The Frontiers Journal Series is a multi-tier and interdisciplinary set of open-access, online journals, promising a paradigm shift from the current review, selection and dissemination processes in academic publishing. All Frontiers journals are driven by researchers for researchers; therefore, they constitute a service to the scholarly community. At the same time, the Frontiers Journal Series operates on a revolutionary invention, the tiered publishing system, initially addressing specific communities of scholars, and gradually climbing up to broader public understanding, thus serving the interests of the lay society, too.

Dedication to Quality

Each Frontiers article is a landmark of the highest quality, thanks to genuinely collaborative interactions between authors and review editors, who include some of the world's best academicians. Research must be certified by peers before entering a stream of knowledge that may eventually reach the public - and shape society; therefore, Frontiers only applies the most rigorous and unbiased reviews.
Frontiers revolutionizes research publishing by freely delivering the most outstanding research, evaluated with no bias from both the academic and social point of view. By applying the most advanced information technologies, Frontiers is catapulting scholarly publishing into a new generation.

What are Frontiers Research Topics?

Frontiers Research Topics are very popular trademarks of the Frontiers Journals Series: they are collections of at least ten articles, all centered on a particular subject. With their unique mix of varied contributions from Original Research to Review Articles, Frontiers Research Topics unify the most influential researchers, the latest key findings and historical advances in a hot research area! Find out more on how to host your own Frontiers Research Topic or contribute to one as an author by contacting the Frontiers Editorial Office: frontiersin.org/about/contact

CURRENT TRENDS IN EXPLOITING MOLECULAR SIGNALING IN BACTERIA-HOST CROSSTALK

Topic Editors:
Monica Cartelle Gestal, Louisiana State University Health Shreveport, United States
Carmen Mariana Chifiriuc, University of Bucharest, Romania
Alina Maria Holban, University of Bucharest, Romania
Karl Kuchler, Medical University of Vienna, Austria

Citation: Gestal, M. C., Chifiriuc, C. M., Holban, A. M., Kuchler, K., eds. (2022). Current Trends in Exploiting Molecular Signaling in Bacteria-Host Crosstalk. Lausanne: Frontiers Media SA. doi: 10.3389/978-2-88976-430-3

Table of Contents

06 ***Editorial: Current Trends in Exploiting Molecular Signaling in Bacteria-Host Crosstalk***
Carmen Mariana Chifiriuc, Monica Cartelle Gestal and Alina Maria Holban

09 ***An* Escherichia coli *Effector Protein EspF May Induce Host DNA Damage via Interaction With SMC1***
Muqing Fu, Song Liang, Jiali Wu, Ying Hua, Hanzong Chen, Zhikai Zhang, Jinyue Liu, Xiaoxia Li, Bao Zhang, Wei Zhao and Chengsong Wan

23 ***Bacteriostatic Potential of Melatonin: Therapeutic Standing and Mechanistic Insights***
Fang He, Xiaoyan Wu, Qingzhuo Zhang, Yikun Li, Yuyi Ye, Pan Li, Shuai Chen, Yuanyi Peng, Rüdiger Hardeland and Yaoyao Xia

38 **Lactobacillus casei Zhang *Counteracts Blood-Milk Barrier Disruption and Moderates the Inflammatory Response in* Escherichia coli*-Induced Mastitis***
Yuhui Zheng, Gang Liu, Wei Wang, Yajing Wang, Zhijun Cao, Hongjian Yang and Shengli Li

50 ***Protein Kinase R in Bacterial Infections: Friend or Foe?***
Robin Smyth and Jim Sun

72 ***Inhibitory Role of an* Aeromonas hydrophila *TIR Domain Effector in Antibacterial Immunity by Targeting TLR Signaling Complexes in Zebrafish***
Huai-ping Tang, Chen Huang, Chong-bin Hu, Hao Li, Tong Shao, Jian-fei Ji, Jun Bai, Dong-dong Fan, Ai-fu Lin, Li-xin Xiang and Jian-zhong Shao

89 ***Paeonol Attenuates Quorum-Sensing Regulated Virulence and Biofilm Formation in* Pseudomonas aeruginosa**
Dan Yang, Suqi Hao, Ling Zhao, Fei Shi, Gang Ye, Yuanfeng Zou, Xu Song, Lixia Li, Zhongqiong Yin, Xiaoli He, Shiling Feng, Helin Chen, Yu Zhang, Yuanze Gao, Yinglun Li and Huaqiao Tang

105 ***Dual Transcriptomic Analyses Unveil Host–Pathogen Interactions Between* Salmonella enterica *Serovar Enteritidis and Laying Ducks (*Anas platyrhynchos*)***
Yu Zhang, Lina Song, Lie Hou, Zhengfeng Cao, Wanwipa Vongsangnak, Guoqiang Zhu, Qi Xu and Guohong Chen

118 ***Respiratory Microbiota Profiles Associated With the Progression From Airway Inflammation to Remodeling in Mice With OVA-Induced Asthma***
Jun Zheng, Qian Wu, Ya Zou, Meifen Wang, Li He and Sheng Guo

132 ***Cytotoxic T-Cell Trafficking Chemokine Profiles Correlate With Defined Mucosal Microbial Communities in Colorectal Cancer***
Jiali Zhang, Ji Tao, Ruo-Nan Gao, Zhi-Yuan Wei, Yu-Shan He, Chun-Yan Ren, Qi-Chun Li, Yan-Shan Liu, Ke-Wei Wang, Gong Yang, Chengjia Qian and Jian-Huan Chen

147 **Lactobacillus rhamnosus *GR-1 Prevents* Escherichia coli*-Induced Apoptosis Through PINK1/Parkin-Mediated Mitophagy in Bovine Mastitis***
Yanan Li, Yaohong Zhu, Bingxin Chu, Ning Liu, Shiyan Chen and Jiufeng Wang

161 *Microbiota–Gut–Brain Axis and Epilepsy: A Review on Mechanisms and Potential Therapeutics*
Manqiu Ding, Yue Lang, Hang Shu, Jie Shao and Li Cui

177 *Uncovering the Oral Dysbiotic Microbiota as Masters of Neutrophil Responses in the Pathobiology of Periodontitis*
Zsombor Prucsi, Alicja Płonczyńska, Jan Potempa and Maja Sochalska

185 *Can Salivary Innate Immune Molecules Provide Clue on Taste Dysfunction in COVID-19?*
Aaron Ermel, Thankam Paul Thyvalikakath, Tatiana Foroud, Babar Khan and Mythily Srinivasan

191 *Oral Microbiota Analysis of Tissue Pairs and Saliva Samples From Patients With Oral Squamous Cell Carcinoma – A Pilot Study*
Ke Yang, Yuezhu Wang, Shizhou Zhang, Dongsheng Zhang, Lihua Hu, Tengda Zhao and Huajun Zheng

203 *Induction of Apoptotic Cell Death by Oral Streptococci in Human Periodontal Ligament Cells*
Ok-Jin Park, A Reum Kim, Yoon Ju So, Jintaek Im, Hyun Jung Ji, Ki Bum Ahn, Ho Seong Seo, Cheol-Heui Yun and Seung Hyun Han

214 *Glucocorticoids Elevate* Pseudomonas aeruginosa *Binding to Airway Epithelium by Upregulating Syndecan-1 Expression*
Dong Liu, Ying-Ying Zeng, Meng-Meng Shi and Jie-Ming Qu

224 Salmonella *Infantis Delays the Death of Infected Epithelial Cells to Aggravate Bacterial Load by Intermittent Phosphorylation of Akt With* SopB
Bing-Xin Chu, Ya-Nan Li, Ning- Liu, Lan-Xin Yuan, Shi-Yan Chen, Yao-Hong Zhu and Jiu-Feng Wang

238 *Long-Term Efficacy of Low-Intensity Single Donor Fecal Microbiota Transplantation in Ulcerative Colitis and Outcome-Specific Gut Bacteria*
Rongrong Ren, Xuefeng Gao, Yichao Shi, Jianfeng Li, Lihua Peng, Gang Sun, Zikai Wang, Bin Yan, Junli Zhi and Yunsheng Yang

250 *The Role of Flagellin B in* Vibrio anguillarum*-Induced Intestinal Immunity and Functional Domain Identification*
Quanxin Gao, Shaokui Yi, Yang Li, Jinping Luo, Qianqian Xing, Xia Yang, Ming Zhao, Minghua Min, Qian Wang, Yabing Wang, Lingbo Ma and Shiming Peng

268 *Fecal Microbiota Transplantation Controls Progression of Experimental Autoimmune Hepatitis in Mice by Modulating the TFR/TFH Immune Imbalance and Intestinal Microbiota Composition*
Ma Liang, Zhang Liwen, Song Jianguo, Dai Juan, Ding Fei, Zhang Yin, Wu Changping and Chen Jianping

279 Lacticaseibacillus casei *Strain T21 Attenuates* Clostridioides difficile *Infection in a Murine Model Through Reduction of Inflammation and Gut Dysbiosis With Decreased Toxin Lethality and Enhanced Mucin Production*
Wimonrat Panpetch, Pornpimol Phuengmaung, Thanya Cheibchalard, Naraporn Somboonna, Asada Leelahavanichkul and Somying Tumwasorn

294 *The Gut-Liver Axis in Health and Disease: The Role of Gut Microbiota-Derived Signals in Liver Injury and Regeneration*
Zhipeng Zheng and Baohong Wang

308 ***Critical Roles of Spätzle5 in Antimicrobial Peptide Production Against* Escherichia coli *in* Tenebrio molitor *Malpighian Tubules***
Maryam Ali Mohammadie Kojour, Tariku Tesfaye Edosa, Ho Am Jang, Maryam Keshavarz, Yong Hun Jo and Yeon Soo Han

326 ***Exploitation of the Host Ubiquitin System: Means by* Legionella pneumophila**
Jingjing Luo, Lidong Wang, Lei Song and Zhao-Qing Luo

338 ***Gut Microbiota and Acute Central Nervous System Injury: A New Target for Therapeutic Intervention***
Bin Yuan, Xiao-jie Lu and Qi Wu

356 ***Disturbance of Gut Bacteria and Metabolites are Associated With Disease Severity and Predict Outcome of NMDAR Encephalitis: A Prospective Case–Control Study***
Xue Gong, Yue Liu, Xu Liu, Aiqing Li, Kundian Guo, Dong Zhou and Zhen Hong

373 ***IL-17 Aggravates* Pseudomonas aeruginosa *Airway Infection in Acute Exacerbations of Chronic Obstructive Pulmonary Disease***
Fengming Ding, Lei Han, Qiang Fu, Xinxin Fan, Rong Tang, Chengjian Lv, Yishu Xue, Xue Tian and Min Zhang

388 ***The cGAS-STING Pathway in Bacterial Infection and Bacterial Immunity***
Nanxin Liu, Xiaoxiao Pang, Hua Zhang and Ping Ji

406 ***Accessory Gene Regulator (*agr*) Allelic Variants in Cognate* Staphylococcus aureus *Strain Display Similar Phenotypes***
Li Tan, Yuyang Huang, Weilong Shang, Yi Yang, Huagang Peng, Zhen Hu, Yuting Wang, Yifan Rao, Qiwen Hu, Xiancai Rao, Xiaomei Hu, Ming Li, Kaisen Chen and Shu Li

frontiers | Frontiers in Microbiology

EDITORIAL
published: 31 May 2022
doi: 10.3389/fmicb.2022.911558

Editorial: Current Trends in Exploiting Molecular Signaling in Bacteria-Host Crosstalk

Carmen Mariana Chifiriuc [1,2], Monica Cartelle Gestal [3] and Alina Maria Holban [1,2]*

[1] Department of Microbiology and Immunology, Faculty of Biology, University of Bucharest, Bucharest, Romania, [2] Earth, Environmental and Life Sciences Section, Research Institute of the University of Bucharest, Bucharest, Romania, [3] Louisiana State University Health Sciences Center-Shreveport, Shreveport, LA, United States

Keywords: bacterial infections, microbiota, crosstalk, biomarkers, anti-infective

Editorial on the Research Topic

Current Trends in Exploiting Molecular Signaling in Bacteria-Host Crosstalk

Despite antibiotics and immunization discovery, as well as tremendous progress made in medicine and environmental quality control, the global burden of infectious diseases still raises important new challenges for prevention, monitoring, diagnostic, and therapy. In case of bacterial infections, we are facing an unprecedented emergence and spread of antimicrobial resistance (AMR) globally, with medical and socio- economic disastrous consequences. Moreover, the coronavirus 2019 (COVID-19) pandemic has drastically changed the healthcare practices in terms of antibiotics and disinfectants use, eventually influencing, in a still unknown way, the dynamics of AMR. Many scientists are predicting that climate change will also influence the landscape of bacterial infections in many ways, such as the global warming will facilitate the more rapid growth and thus, the survival and spread of antibiotic-resistant bacteria and the exchange of resistance genes. This global context reiterates that multi-disciplinary and internationally concerted research is urgently needed to develop novel and efficient preventive and therapeutic strategies, for continuingly improving our preparedness and response to present and future threats from bacterial infections and AMR. Bacteria are able of intercellular communication and further, to sense and rapidly adapt to their environment through coordinated, multi-cellular responses. If their environment is the human body, pathogens' ability to sense, respond and manipulate host immune responses contributes greatly to their success to concur the host. The goal of this special issue was to present the current progress and perspectives regarding pathogen-host crosstalk, in the hope to provide a fruitful platform for feeding the pipeline for the future development of vaccines and anti-infective therapies.

By successfully fulfilling the declared goal of this Research Topic, the published papers present new, important and inspiring data concerning the effectors and mechanisms involved in the bacterial pathogens-host crosstalk during the infectious process as well as in the human microbiota dialogue with the human host organism. The presented results were obtained using state of the art methodology and infection models that could serve as inspiration for further research and offer new leads for the development of novel biomarkers and therapeutic strategies. Some valuable reviews on the above-mentioned subjects are adding to the original papers. According to their subject, the papers could be divided in three categories.

The first category presents novel effectors and pathogenic mechanisms involved in the interplay between different Gram-negative and Gram-positive bacteria and their animal or human host, during the infectious process and highlight their potential for the development of novel anti-infectious strategies. Liu et al. updated the major molecules involved in cyclic guanosine monophosphate (GMP)-adenosine monophosphate (AMP) (cGAMP) synthase (cGAS), along with

OPEN ACCESS

Edited and reviewed by:
Axel Cloeckaert, Institut National de recherche pour l'agriculture, l'alimentation et l'environnement (INRAE), France

****Correspondence:***
Carmen Mariana Chifiriuc
carmen.chifiriuc@gmail.com

Specialty section:
This article was submitted to Infectious Agents and Disease, a section of the journal Frontiers in Microbiology

Received: *02 April 2022*
Accepted: *05 April 2022*
Published: *31 May 2022*

Citation:
Chifiriuc CM, Cartelle Gestal M and Holban AM (2022) Editorial: Current Trends in Exploiting Molecular Signaling in Bacteria-Host Crosstalk. Front. Microbiol. 13:911558. doi: 10.3389/fmicb.2022.911558

the adaptor stimulator of interferon genes (STING) and the effects of the cGAS-STING pathway in various bacterial infections and bacterial immunity, which may pave the way for the development of new antibacterial drugs that specifically kill bacteria without harmful effects on the host. Luo et al. reviews the mechanisms by which *Legionella pneumophila* effectors interfere with host cells ubiquitination during the infectious process. Fu et al. focused on EspF, one of the virulence factors of Enterohemorrhagic *Escherichia coli* (EHEC) O157: H7, proving that it may mediate DNA damage, by regulating the subcellular localization and phosphorylation of SMC1. Using the *Tenebrio molitor* model, Kojour et al. unveil the role of the dimeric cytokine ligand Spätzle (Spz)5 in the innate defense against *E. coli* infection. Using a transcriptomic approach, Zhang et al. shed new insights in the mechanisms and effectors of *Salmonella enteritidis* infection in ducks, that could feed the pipeline for designing new therapeutic strategies. Chu et al. demonstrated that *Salmonella Infantis* inhibited the apoptosis of infected Caco-2 cells by intermittently phosphorylating Akt, allowing sufficient time for replication, thereby causing more severe inflammation. Liu et al. raises caution on using glucocorticoids in chronic lung disease, showing that they increase the expression of syndecan-1 (SDC1) and consequently, *Pseudomonas aeruginosa* binding to the airway epithelium. Ding et al. have shown that *P. aeruginosa* infection increases IL-17 production, augmenting inflammation in chronic obstructive pulmonary disease (COPD) patients and COPD mouse models and recommend IL-17A as a potential therapeutic strategy in controlling the outcomes of *P. aeruginosa* infection in COPD patients. Tang et al. reported for the first time a new mechanism by which *Aeromonas hydrophila* evades from host antibacterial defense by intervening CD80/86 signal, that could be targeted for the development of new therapeutic interventions. Gao et al. investigated the role of flagellin B from *Vibrio anguillarum*, an opportunistic pathogen of aquatic animals, on cell apoptosis, TLR5 expression, and production of IL-8 and TNF-α, in the perspective of future design of flagellin-based vaccines. Tan et al. offers the readers a fresh perspective regarding the correlation between the agr polymorphism and *S. aureus* pathogenic potential, while Smyth and Sun propose that Protein Kinase R (PKR), already well known as an important target in cancer, metabolic disorders, neurodegeneration, and antiviral defense, could be also be considered a promising lead for novel treatment strategies in bacterial infections. Park et al. have shown that most oral streptococci induce ROS production and subsequent apoptosis in human periodontal ligament cells, thus contributing to the progression of inflammatory conditions. Ermel et al. show that dysgeusia in COVID-19 is related to the salivary levels of innate immune response molecules such as the toll-like receptor-4, peptidoglycan recognition protein, and sACE2 and perturbation of oral biofilm.

The second batch of papers are moving the readers' focus to the human microbiota- host organisms crosstalk in health and disease. Ding et al. reviewed the role of microbiome and gut–brain axis in epilepsy, highlighting the possible pathogenic mechanisms and the novel therapies targeting the gut microbiota, Yuan et al. summarized the role of gut microbiota in acute central nervous system injuries, while Zheng and Wang offer the reader an update of molecular mechanisms by which gut microbiota-derived signals modulate liver injury and regeneration and the development of gut microbiota-based therapies. Zhang et al. have shown that the major cytotoxic T-cell trafficking chemokines (CTTCs) and chemokine-associated microbiota profiles are different in colorectal cancer (CRC) tumor vs. adjacent normal tissues, Yang et al. provide a detailed analysis of the oral microbiome in patients with oral squamous cell carcinoma and Prucsi et al. reviewed the involvement of oral microbiota in periodontal inflammation mediated by neutrophils. Using an *in vivo* mice model, Zheng et al.' study fills the knowledge gap regarding the dynamics and roles of respiratory microbiota in the different stages of asthma and their association with chronic asthma progression. By using a multi-omics approach, Gong et al. identified intestinal microbiota, fecal and serum metabolites and cytokines profiles which could predict for anti-N-methyl-D-aspartate receptor (NMDAR) encephalitis clinical severity and relapse. All these papers could inspire other researchers for developing novel microbiota-derived biomarkers used for risk prediction, early diagnosis and monitoring of cancer and other chronic diseases.

The third category of papers refer to novel antibacterial strategies based on natural compounds and on probiotics, updating or demonstrating their intimate mechanisms of actions. He et al. proposes that melatonin could be an effective approach against various pathogenic bacterial infections, acting by decreasing formation of reactive oxygen and nitrogen species, promoting detoxification and protecting mitochondrial damage, while Yang et al., demonstrate the anti-QS activities of the phenolic compound paeonol in a *Caenorhabditis elegans* infection model. Probiotics are used to alleviate the deleterious effects of inflammatory reactions, but the intimate mechanisms of action are still to be unveiled. Using *in vitro* and *in vivo* mastitis models, Zheng et al. have demonstrated that *Lactobacillus casei,* besides its direct competition with *E. coli,* could reduce the inflammation associated with *E. coli*-induced mastitis by consolidating the tight junctions and decreasing the expression of the inflammatory cytokines. In the same infection model, Li et al. have shown that *L. rhamnosus* GR-1 prevents *E. coli*-induced apoptosis induced PINK1/Parkin-mediated mitophagy that eliminated damaged mitochondria and reduced ROS production and NLRP3 inflammasome activation. The efficiency of *Lacticaseibacillus casei* T21 was demonstrated *in vitro,* on colonic epithelial cells and *in vivo,* on a murine *Clostridioides difficile* infection model, by assessing many reliable parameters. This could represent a model study for demonstrating the therapeutic efficiency of probiotic formulations and unveil their possible mechanisms of action (Panpetch et al.). Liang et al. show that fecal microbiota transplantation (FMT) controls progression of experimental autoimmune hepatitis in mice by modulating the follicular regulatory T cells and restoring the gut dysbiosis. Moving to huma studies, Ren et al. demonstrated the long-term efficacy and safety of single-donor, low-intensity FMT in treating ulcerative colitis (UC). The patients with UC sustained remission had a higher abundance of *Bifidobacterium breve*, while a higher level of *Bacteroides* spp. was observed in the relapse group.

We are very grateful to all authors and reviewers for their valuable contributions and hope that the readers will find our Research Topic selection interesting and inspiring for their future work.

AUTHOR CONTRIBUTIONS

All authors have contributed to the Editorial and approved the final paper.

FUNDING

This project was financed by the Ministry of Research, Innovation and Digitalization through Program 1—Development of the national R&D system, Subprogram 1.2—Institutional performance—Financing projects for excellence in RDI, project C1.2.PFE-CDI.2021-587, Contract no. 41 PFE/30.12.2021.

ACKNOWLEDGMENTS

We acknowledge the C1.2.PFE-CDI.2021-587 project.

Conflict of Interest: The authors declare that the research was conducted in the absence of any commercial or financial relationships that could be construed as a potential conflict of interest.

Publisher's Note: All claims expressed in this article are solely those of the authors and do not necessarily represent those of their affiliated organizations, or those of the publisher, the editors and the reviewers. Any product that may be evaluated in this article, or claim that may be made by its manufacturer, is not guaranteed or endorsed by the publisher.

Copyright © 2022 Chifiriuc, Cartelle Gestal and Holban. This is an open-access article distributed under the terms of the Creative Commons Attribution License (CC BY). The use, distribution or reproduction in other forums is permitted, provided the original author(s) and the copyright owner(s) are credited and that the original publication in this journal is cited, in accordance with accepted academic practice. No use, distribution or reproduction is permitted which does not comply with these terms.

frontiers in Microbiology

ORIGINAL RESEARCH
published: 26 May 2021
doi: 10.3389/fmicb.2021.682064

An *Escherichia coli* Effector Protein EspF May Induce Host DNA Damage via Interaction With SMC1

*Muqing Fu[1], Song Liang[1], Jiali Wu[1], Ying Hua[1], Hanzong Chen[1], Zhikai Zhang[1], Jinyue Liu[1], Xiaoxia Li[1], Bao Zhang[1], Wei Zhao[1] and Chengsong Wan[1,2]**

[1] Department of Microbiology, School of Public Health, Southern Medical University, Guangzhou, China, [2] Key Laboratory of Tropical Disease Research of Guangdong Province, Guangzhou, China

Enterohemorrhagic *Escherichia coli* (EHEC) O157: H7 is an important foodborne pathogen that causes human diarrhea, hemorrhagic colitis, and hemolytic uremic syndrome. EspF is one of the most important effector proteins injected by the Type III Secretion System. It can target mitochondria and nucleoli, stimulate host cells to produce ROS, and promote host cell apoptosis. However, the mechanism of the host-pathogen interaction leading to host oxidative stress and cell cytotoxic effects such as DNA damage remains to be elucidated. Here, we used Cell Counting Kit-8 (CCK-8) assays and 8-oxo-7,8-dihydro-2′-deoxyguanosine (8-OHdG) ELISA to study cell viability and DNA oxidative damage level after exposure to EspF. Western blot and immunofluorescence were also used to determine the level of the DNA damage target protein p-H2AX and cell morphology changes after EspF infection. Moreover, we verified the toxicity in intestinal epithelial cells mediated by EspF infection *in vivo*. In addition, we screened the host proteins that interact with EspF using CoIP-MS. We found that EspF may more depend on its C-terminus to interact with SMC1, and EspF could activate SMC1 phosphorylation and migrate it to the cytoplasm. In summary, this study revealed that EspF might mediate host cell DNA damage and found a new interaction between EspF and the DNA damage repair protein SMC1. Thus, EspF may mediate DNA damage by regulating the subcellular localization and phosphorylation of SMC1.

Keywords: EHEC (Enterohaemorrhagic *E. coli*), EspF, DNA damage, SMC1, protein interactions

OPEN ACCESS

Edited by:
Karl Kuchler,
Medical University of Vienna, Austria

Reviewed by:
Paul Dean,
Teesside University, United Kingdom
William T. Doerrler,
Louisiana State University, United States

***Correspondence:**
Chengsong Wan
gzwcs@smu.edu.cn

Specialty section:
This article was submitted to Infectious Diseases, a section of the journal Frontiers in Microbiology

Received: *17 March 2021*
Accepted: *30 April 2021*
Published: *26 May 2021*

Citation:
Fu M, Liang S, Wu J, Hua Y, Chen H, Zhang Z, Liu J, Li X, Zhang B, Zhao W and Wan C (2021) An Escherichia coli Effector Protein EspF May Induce Host DNA Damage via Interaction With SMC1. Front. Microbiol. 12:682064. doi: 10.3389/fmicb.2021.682064

INTRODUCTION

Enterohemorrhagic *Escherichia coli* (EHEC) O157:H7 is an important foodborne pathogen. It can cause bloody diarrhea, hemorrhagic colitis, and even life-threatening hemolytic uremic syndrome (Tarr et al., 2005). EHEC infection induces an increase in host reactive oxygen species levels and the activation of inflammatory signals, which both play an important role in mediating hemorrhagic colitis (Dahan et al., 2002; Pacheco and Sperandio, 2012). However, the mechanism of this host-pathogen interaction leading to host oxidative stress and DNA damage remains to be clarified.

EHEC O157: H7 adheres to the brush border of intestinal epithelial cells, and approximately 40 effector proteins are injected into host cells using the Type III Secretion System (Slater et al., 2018). EspF is one of the most important virulence factors for EHEC and enteropathogenic *E. coli* (EPEC) (Holmes et al., 2010). The N-terminus of EHEC-secreted effector protein EspF contains

a secretory signal (residues 1–21) that helps EspF secretion to host cells. Both a mitochondrial targeting signal (MTS, residues 1–24) and a nucleolar targeting domain (NTD, residues 21–74) enable EspF to target the mitochondria and nucleolus of host cells. Moreover, an essential role for leucine at position 16 was shown for mitochondrial targeting (Nagai et al., 2005), and mutation of this residue to glutamic acid (L16E) has been a pivotal tool for determining which of EspF's functions are dependent on mitochondrial targeting. The EspF C-terminus (residues 73–248) is composed of four highly homologous proline-rich repeats sequences, each of which contains an SNX9 protein binding site Src homology 3 (SH3) motif and a neuronal Wiskott-Aldrich syndrome protein (N-WASP) binding domain (Hua et al., 2018a).

Based on the structural characteristics of EHEC EspF, it can target mitochondria, destroy the mitochondrial membrane potential, induce the host to produce ROS (Wang et al., 2017), and mediate cell apoptosis (Zhao et al., 2013). In addition, EPEC EspF can also target the nucleolus to regulate ribosomal protein synthesis (Dean et al., 2010). As EPEC often leads to asymptomatic colonization, *E. coli* depletes host cell DNA mismatch repair (MMR) proteins in colonic cell lines and has been detected in colorectal cancer patients (Maddocks et al., 2009). EPEC EspF is critical for the depletion of MMR proteins, which can then lead to mutations in the *Apc* gene. The mechanism of EPEC modulation of the MMR protein is post-transcriptional and depends upon EspF mitochondrial targeting (Maddocks et al., 2013). In addition, EPEC EspF infection significantly increases spontaneous mutation frequency in host cells, which is a typical feature of colorectal tumors (De'Angelis et al., 2018).

In addition to the MMR pathway, Homologous Recombination (HR) and Non-Homologous End Joining are two important DNA double-strand break (DSB) repair pathways (Liu et al., 2017). Among them, HR repair requires a sister chromatid as a template to reduce errors in DNA and only functions in the S phase and G2 phase of the cell cycle (Stefanski et al., 2019). This repair pathway is mediated by serine/threonine kinase of ataxia telangiectasia-mutated (ATM). DSBs can activate ATM kinase and initiate downstream signaling pathways (Burma et al., 2001). SMC1 is an important target of ATM kinase (Yi et al., 2017). It can be phosphorylated by ATM and collaborates with the MRE11, Rad50, and NBS1 complex to regulate DNA replication fork formation and damage repair (Kitagawa and Kastan, 2005).

Although there is evidence that EspF can sequester host cell MMR proteins and cause host microsatellite instability (Maddocks et al., 2013), whether EHEC EspF causes DNA damage through other DNA damage repair proteins and the pathogenicity of EspF-host protein interaction is unclear. We, therefore, analyzed the ability of EspF to cause cell DNA damage and validated the DNA damage of intestinal epithelial cells in mice. Afterward, we demonstrated that EspF interacted with the DNA damage repair protein SMC1 by co-immunoprecipitation combined with mass spectrometry (CoIP-MS). Using CoIP and confocal microscopy, we further confirmed that EspF preferred to mediate the interaction with SMC1 through its C-terminus. EspF can also phosphorylate SMC1 and transfer it to the cytoplasm, affecting the cell's ability to repair DNA damage in the nucleus. Our research provides new insights into the pathogenesis of EHEC O157:H7 infection.

MATERIALS AND METHODS

Cell Lines and Strains

293T, Caco2 cells, and HT-29 cells were kindly gifted by Professor Bao Zhang, School of Public Health, Southern Medical University, Guangzhou. We cultured 293T and Caco2 cells overnight in DMEM (GIBCO, Waltham, MA, United States) containing 10% fetal bovine serum (FBS) and 1% penicillin and streptomycin at 5% CO_2 and 37°C. HT-29 cells were cultured overnight in RPMI-1640 (GIBCO) medium containing 10% FBS and 1% penicillin and streptomycin at 5% CO_2 and 37°C. The pEGFP-N1 plasmid, strain EHEC O157:H7 EDL933, Δ*espF*, and Δ*espF*/*pespF* were stored in our laboratory (Wang et al., 2017). DH5α-competent cells and LA high-fidelity enzyme were purchased from TaKaRa (Shiga, Japan). The restriction enzymes *Eco*RI and *Bam*HI were purchased from Thermo Fisher (Waltham, MA, United States). The primers used in this study were synthesized by Sangon Biotech (Shanghai, China). Gene sequencing was performed by IGE Biotechnology (Guangzhou, China).

Construction of pEGFP-EspF-3Flag, pEGFP-EspF-N-Flag, and pEGFP-EspF-C-Flag Plasmids

We amplified the *espF* gene, its N-terminus (1 − 219 bp), and C-terminus (220 − 747 bp) using the LA high-fidelity enzyme in the genome of EDL933. Each constructed plasmid was labeled with Flag. Primers *espF-F*: CCGGAATTCGCCACCATGCTTA ATGGAATTAGTAACGCTG and *espF-R*: CGCGGATCCCC GCTACCGCCGCTTCCCTTGTCCTTATCGTCGTCATCCTTG TAATCCTTATCGTCGTCATCCTTGTAATCCTTATCGTCGTC ATCCTTGTAATCCCCTTTCTTCGATTGCTCATA amplified the *espF* gene; primers *espF*/*N-F*: CCGGAATTCGCCACCATG CTTAATGGAATTAGACAC and *espF*/*N-R*: CGCGGATCCCC ACCAGAGCCACCCTTATCGTCGTCATCCTTGTAATCGGGA GTAAATGAAGTCACCTG amplified the *espF-N*; and primers *espF*/*C-F*: CCGGAATTCGCCACCATGTCTCGTCCGGCACCG CGCGCCCCCACC and *espF*/*C-R*: CGCGGATCCCCACCTC CCC amplified the *espF-C*. The PCR products were digested with *Eco*RI/*Bam*HI and T-linked to the pEGFP-N1 plasmid to generate pEGFP-EspF-3Flag, pEGFP-EspF-N-Flag, and pEGFP-EspF-C-Flag plasmids. Sequencing verified the integrity of the constructed plasmids.

We cultured 293T cells according to standard methods, and the cells were plated on 10 cm^2 culture dishes (NEST, Hong Kong, China). In accordance with the manufacturer's instructions, the

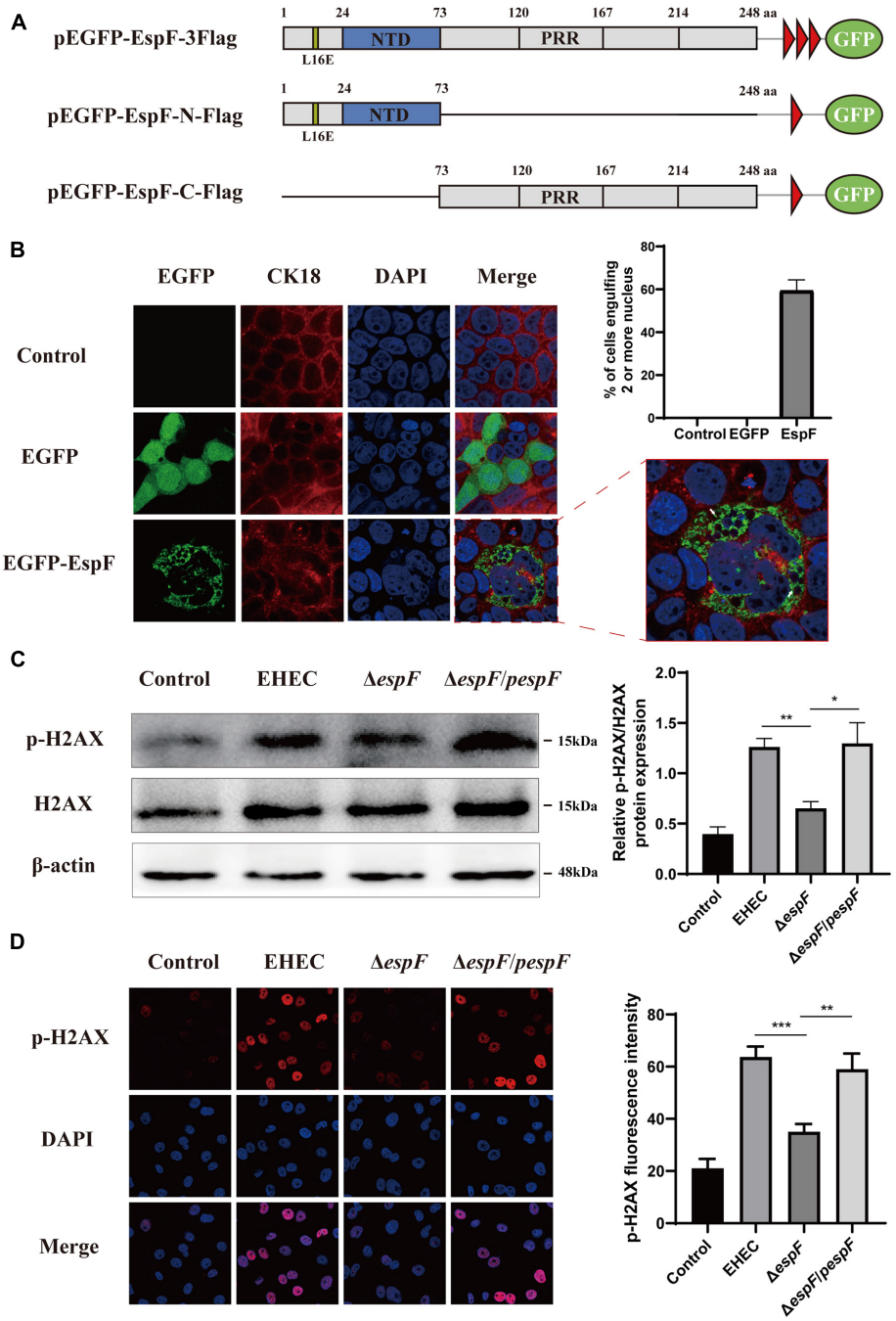


FIGURE 1 | EspF can increase H2AX phosphorylation and mediate cell multi-nucleation. **(A)** Diagram of pEGFP-EspF, pEGFP-EspF-N, and pEGFP-EspF-C plasmids used in this study. pEGFP-EspF, pEGFP-EspF-N, and pEGFP-EspF-C were tagged with Flag. aa: Amino acid. L16E: Mutation of Leucine at position 16 in mitochondrial targeting to Glutamic acid. NTD: Nucleolar Targeting Domain. PRR: Proline-rich repeats. **(B)** Immunofluorescent microscopy of CK18 protein. Caco2 cells transfected with plasmids for 48 h. The nucleus was labeled with DAPI in blue. CK18 was labeled with an anti-CK18 antibody in red. Green indicates fluorescence expressed by the fluorescent plasmid. Images were acquired on an FV1000 confocal laser scanning microscope using a 63 X oil objective. The white arrows represented cell internalization. The grayscale analysis of cells harboring four or more nuclei in cells transfection with EspF as indicated. **(C)** The levels and grayscale analysis of p-H2AX in Caco2 cells infected with strains as indicated. Relative protein levels were quantified using ImageJ software. Data are shown as the mean ± SD of three independent repeats. $^{*}P < 0.05$, $^{**}P < 0.01$, $^{***}P < 0.001$. **(D)** The fluorescence intensity and grayscale analysis of p-H2AX in Caco2 cells infected with strains for 6 h as indicated. Immunofluorescence was observed with an anti-p-H2AX antibody followed by a secondary antibody (red). Images were acquired on an FV1000 confocal laser scanning microscope using a 63 X oil objective.

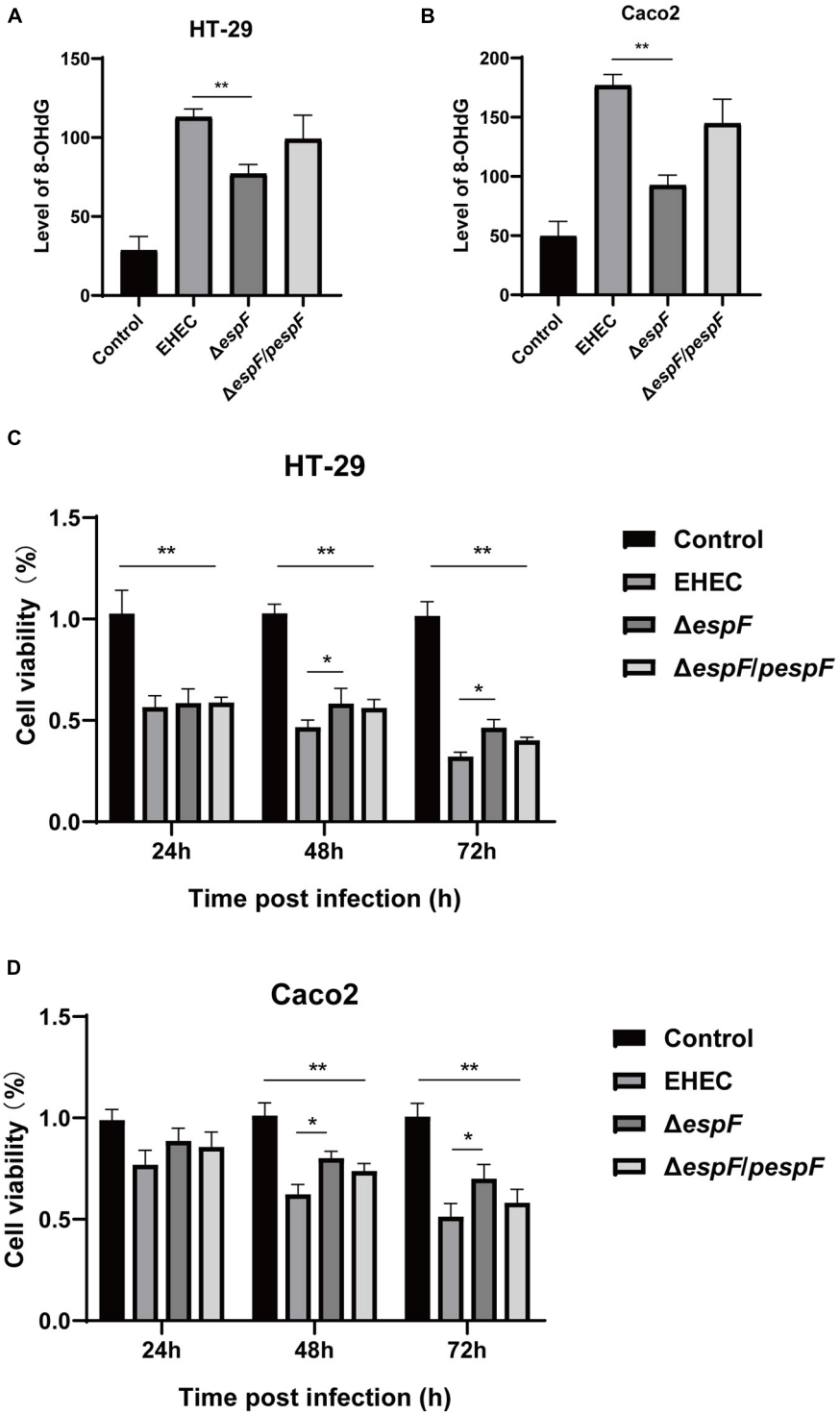


FIGURE 2 | EspF causes DNA oxidative damage and decreases cell viability. **(A)** The level of 8-OHdG in HT-29 cells after infection. HT-29 cells were infected with indicated strains, and DNA was extracted from cells for ELISA. Data are expressed as the mean ± SD from at least three independent experiments. $^{*}P < 0.05$, $^{**}P < 0.01$. **(B)** The level of 8-OHdG in Caco2 cells after infection. Caco2 cells were infected with indicated strains for 9 h, and DNA was extracted from cells for ELISA. Data are shown as the mean ± SD of at least three independent experiments. **(C)** Cell viability of HT-29 cells infected with indicated strains. HT-29 cells were infected with strains for 9 h, washed with PBS, and co-incubated in a medium containing gentamicin for 24 h, 48 h, and 72 h. Data are shown as the mean ± SD from at least three independent experiments. **(D)** Cell viability of Caco2 cells infected with strains. Caco2 cells were infected with strains for 9 h as indicated, washed with PBS, and then co-incubated in a medium containing gentamicin for 24 h, 48 h, and 72 h. Data are shown as the mean ± SD from at least three independent experiments.

cells were transfected with pEGFP-EspF-3Flag, pEGFP-EspF-N-Flag, and pEGFP-EspF-C-Flag plasmids using Lipofectamine 3000 (Thermo Fisher).

Immunofluorescence Assay

Caco2 cells were plated on a confocal dish (35 mm; NEST, Hong Kong) and transfected with pEGFP, pEGFP-EspF, pEGFP-EspF-N, or pEGFP-EspF-C vectors. After 48 h, the cells were gently washed with PBS three times and fixed in 4% paraformaldehyde for 15 min at room temperature, and then blocked with 0.1% Triton X-100 for 30 min. The fixed cells were stained with primary antibody overnight at 4°C (anti-p-H2AX/anti-CK18 [CST, Danvers, MA, United States]; anti-SMC1/anti-p-SMC1 [(Abcam, Cambridge, United Kingdom)], followed by incubation with a secondary antibody for 30 min. Then, the cells were stained with DAPI for 5 min. Cellular co-localization was observed with an FV1000 confocal microscope (Olympus, Tokyo, Japan).

Western Blot

The protein samples were loaded and separated by sodium dodecyl sulfate-polyacrylamide gel electrophoresis (SDS-PAGE). The electrophoresed proteins were transferred to polyvinylidene fluoride (PVDF) membranes (Merck Millipore, Darmstadt, Germany), then blocked with 5% bovine serum albumin (BSA, Gbcbio, China). Membranes were probed with anti-p-H2AX (CST, United States), anti-H2AX (CST, United States), anti-p-SMC1 (Abcam, United Kingdom), anti-SMC1 (CST, USA), or anti-βactin antibodies (Proteintech, China), followed by a goat anti-rabbit IgG secondary antibody (#SA00001-2, Proteintech, China) or goat anti-mouse IgG secondary antibody (#SA00001-1, Proteintech, China) for 1 h. The blots were visualized using an ECL chemiluminescence substrate kit (#WBKLS0100, Millipore, United States).

Bacterial Infection

The EHEC O157:H7 EDL933 strain was cultured in LB medium, Δ*espF* and Δ*espF*/*pespF* strains were cultured in LB medium containing kanamycin at 37°C for 12 h, and HT-29/Caco2 cells were seeded in 10-cm^2 culture dishes. When the cells reached 95% confluence, the cells were infected with bacteria at a multiplicity of infection (MOI) of 100:1 and incubated at 37°C and 5% CO_2. Then, the medium was aspirated, the cells were gently washed with PBS, and the proteins were collected for immunoblotting.

Determination of 8-OHdG

The strain EHEC O157:H7 EDL933 was cultured in LB medium, Δ*espF* and Δ*espF*/*pespF* strains were cultured in LB medium containing kanamycin at 37°C for 12 h, and HT-29/Caco2 cells were seeded in 10-cm^2 culture dishes. When cells reached 95% confluence, the cells were infected with bacteria at an MOI of 100:1 and incubated at 37°C and 5% CO_2. Celluar 8-oxo-7,8-dihydro-2′-deoxyguanosine (8-OHdG) was determined using a commercial competitive ELISA kit (CUSABIO, Wuhan, China). The concentrations were normalized to a standard sample and expressed in ng/mL.

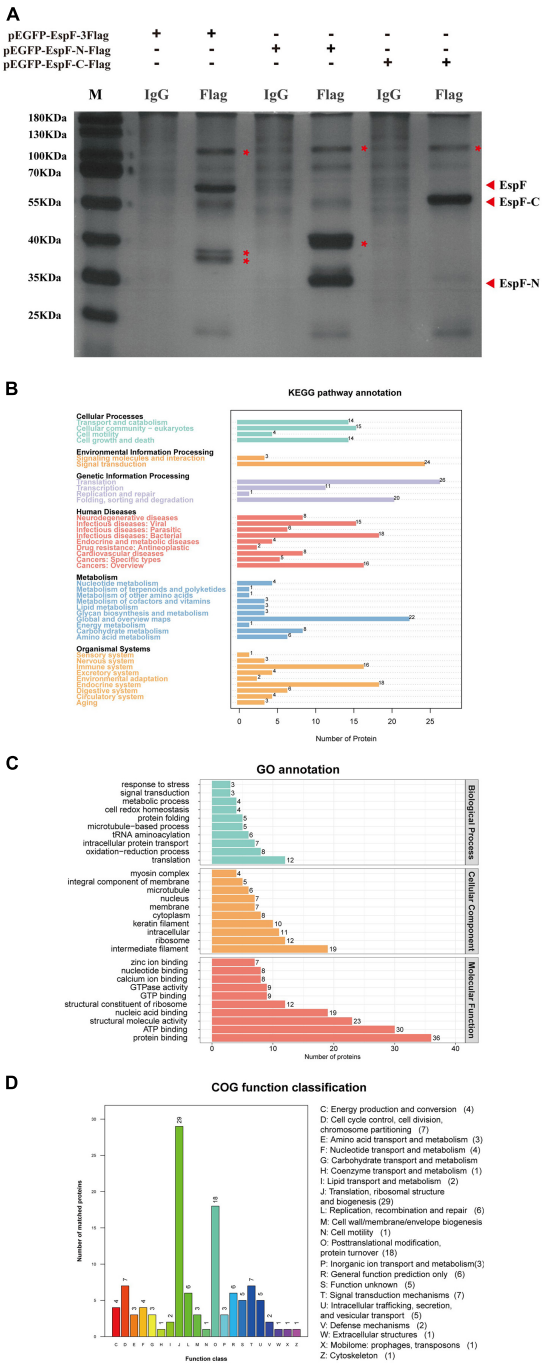


FIGURE 3 | Identification of host proteins that interact with EspF. **(A)** Additional bands from the pEGFP-EspF, pEGFP-EspF-N, and pEGFP-EspF-C groups. The plasmids were transfected into 293T cells. Cell lysates from pEGFP-EspF-transfected cells, pEGFP-EspF-N-transfected cells, or pEGFP-EspF-C-transfected cells were immunoprecipitated with anti-Flag/IgG protein monoclonal antibodies. Immunoprecipitated proteins were isolated by 10% SDS-PAGE and visualized by silver staining. The additional bands were shown with red asterisks (*). **(B)** KEGG analysis of the distribution of interacting protein pathways. **(C)** GO annotation of EspF-interacting proteins in terms of biological processes, cellular components, and molecular functions. **(D)** COG function classification of interacting protein pathways.

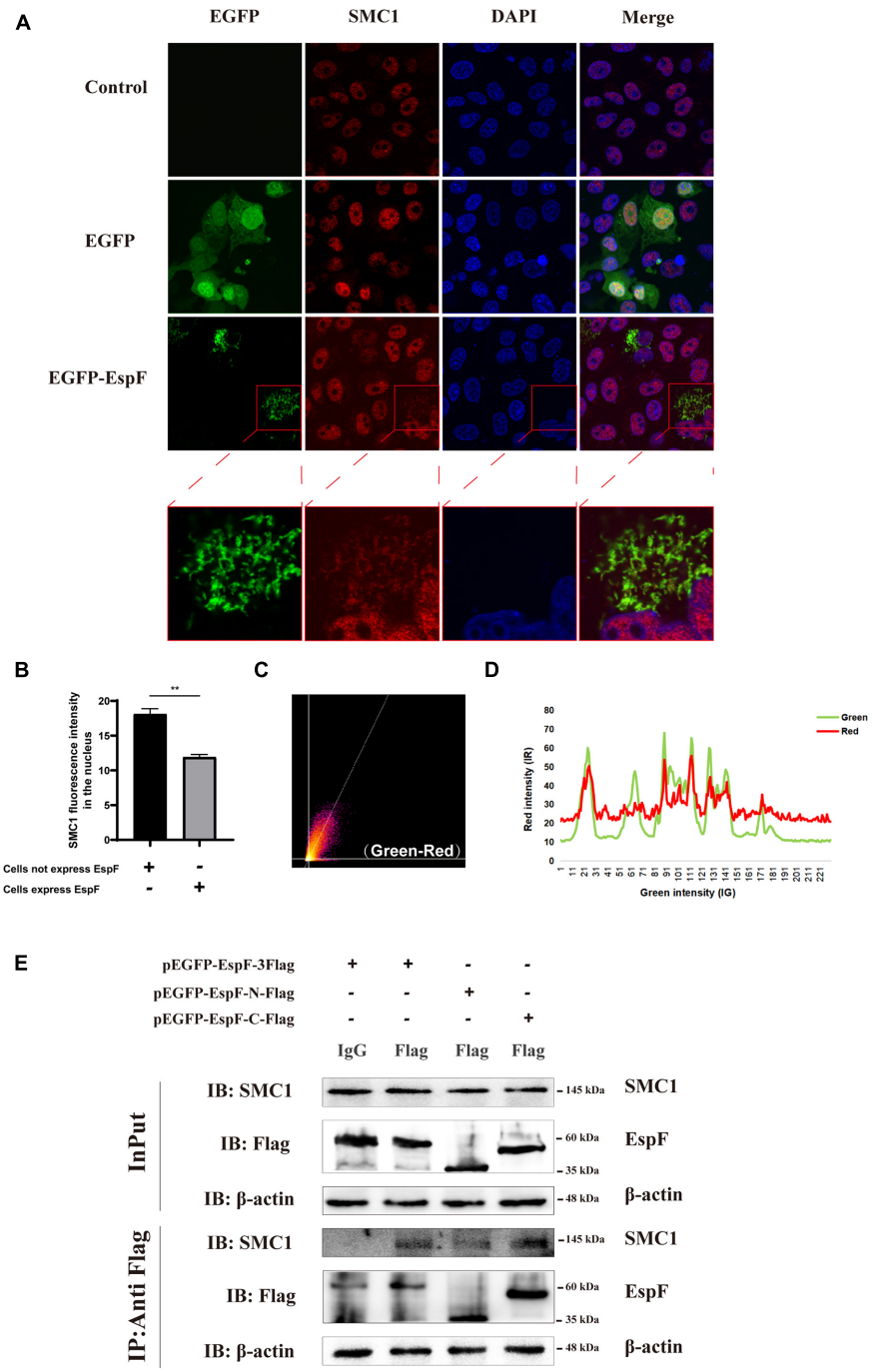


FIGURE 4 | EspF may interact with SMC1 via its C terminus. **(A)** EspF and SMC1 transiently co-localize in the cytoplasm. Caco2 cells were grown to 70% confluence in mock conditions and then transfected with pEGFP-N1 and pEGFP-EspF. After 48 h, cells were fixed, permeabilized, and immunostained with an anti-SMC1 antibody followed by a secondary antibody (red). Images were acquired on an FV1000 confocal laser scanning microscope using a 63X oil objective. The red boxes in panels A were enlarged in the bottom row. **(B)** EspF translocates SMC1 into the cytoplasm. Caco2 cells were transfected with pEGFP-EspF, then stained with an anti-SMC1 antibody. Grayscale analysis of fluorescence intensity of SMC1 in the nucleus as indicated. $^{**}P < 0.01$. **(C)** The scatter plot of co-localization between EspF and SMC1. the Pearson's correlation coefficient for the image above thresholds of EspF and SMC1 was 0.7034. **(D)** The plot profile of fluorescence intensity of red/green. **(E)** EspF may interact with SMC1 via its C terminus by CoIP. pEGFP-EspF-3Flag, pEGFP-EspF-N-Flag, or pEGFP-EspF-C-Flag were transfected into 293T cells for 48 h. Cell proteins were extracted and incubated with Flag/IgG agarose beads. Next, input and IP protein lysis were prepared for 10% SDS-PAGE gel. The indicated interacting proteins were immunoprecipitated with indicated antibodies (IB); normal mouse IgG was used as a negative control.

Measurement of Cell Viability

We used a Cell Counting Kit-8 (CCK-8) kit (Dojindo, Japan) to measure cell viability. A total of 1,000 cells in a volume of 100 μL per well were cultured in five replicate wells in a 96-well plate in a medium containing 10% FBS. HT-29/Caco2 cells were infected with strains as shown above. Then the cells were incubated in a medium containing gentamicin. The CCK-8 reagent (10 μL) was added to 90 μL DMEM to generate a working solution, of which 100 μL was added per well and incubated for 1.5 h. We performed this assay at 24 h, 48 h, and 72 h after infection.

Co-immunoprecipitation Assay

Following the instructions of the Pierce CoIP Kit (Thermo Fisher), we prepared 293T cells over-expressing pEGFP-EspF or pEGFP-EspF-N or pEGFP-EspF-C as mentioned above. We added 1 mg of cell lysates to 80 μl of the control agarose resin slurry to remove non-specifically bound proteins. Next, we placed 20 μl of AminoLink resin slurry into the spin column, added 15 μg of immunoglobulin G (IgG) antibody (ABclonal Technology, Woburn, MA, United States)/Flag antibody (Cell Signaling Technology, Danvers, MA, United States), and co-incubated the mixture for 1 h. The protein was added to the spin column and incubated at 4°C overnight. The resin was washed three times with IP lysis and then underwent 10% SDS-PAGE for immunoblotting. Anti-Flag (CST) and anti-SMC1 (CST) antibodies were added, and reactions were incubated overnight at 4°C. After three washes with TBST, the corresponding secondary antibody was added, the mixture was incubated at room temperature for 1 h, and the bands were visualized using an ECL chemical solution.

Silver Staining

After electrophoresis, SDS-PAGE gels were incubated in a fixing solution for 15 min in a shaker at room temperature. The gel was transferred to a sensitizer using gentle shaking. Then, we added the staining solution and left the mixture for 30 min on a shaker. After staining, the gel was washed with water three times (15 min each) and incubated in a developer solution until bands became visible. The gel was washed in water and then imaged. The different bands were cut out and sent to Huijun Biological Company (Guangzhou, China) for MS.

Survival Assay of Mice

A total of 30 adult female BALB/c mice (4–5 weeks old, 13.52 ± 0.59g) were randomly divided into three groups (EHEC, △*espF*, and Control group), with 10 mice in every group. The strains were cultured overnight in kanamycin at 37°C. The mice, respectively, received 0.2 mL of the bacterial suspension of different groups (approximately 5×10^{10} CFU/mL) by intragastric administration. After 12 h, the mice were infected again with the same amount of bacteria. The Control group received 0.2 mL LB broth. Prior to the gavage, the BALB/c mice were given sterile water containing streptomycin and were injected with mitomycin C (2.5 mg/kg) to enhance susceptibility to bacteria. The survival state of the mice was monitored every 12 h for 7 days. The survival rate and weight change of mice were calculated. After 7 days, the surviving mice were killed and their tissues were taken out. Subsequently, tissue immunohistochemical analysis was performed.

Statistical Analysis

All statistical analyses were performed using SPSS 20.0 (SPSS Inc., Chicago, IL, USA). The data are expressed as the mean ± SD. Comparisons between groups were made by one-way analysis of variance (ANOVA) followed by Dunnett's test for separate comparisons. $P < 0.05$ was considered statistically significant.

RESULTS

EspF Can Induce Extreme Multi-Nucleation and DNA Damage

The morphological changes of cells are often a manifestation of DNA damage. Mammalian-expression plasmids encoding full-length EspF, or the EspF-N and EspF-C terminus were fused to an N-terminus green fluorescent protein (GFP) with a flag tag (pEGFP-EspF-3Flag, pEGFP-EspF-N-Flag, and pEGFP-EspF-C-Flag) (**Figure 1A**). Caco2 cells were then transfected with these plasmids, and the medium was changed every two days to maintain cell viability. Cytokeratin 18 is a maker of the cell cytoskeleton. Cells expressing EGFP-EspF on day 2 post-transfection remained mono-nuclear. From day 2 to day 4 post-transfection, cells expressing EGFP-EspF exhibited a progressive increase in cell hypertrophy (maximal diameter) and multi-nucleation (defined as ≥ 15 nuclei). We then quantified the rate of the cell harboring four or more nuclei. Quantification results revealed that 59% ± 5.63% of EspF-expressing cells showed the phenomenon of cell multi-nucleation (**Figure 1B**), whereas non-transfected cells displayed near-zero levels of internalization. CK18 was rearranged in the cytoplasm and was accompanied by internalized nuclei. In addition, the CK18 protein co-localized with EspF in the cytoplasm. Meanwhile, in the EGFP and Control groups, cells still appeared to be mono-nuclear, and CK18 was distributed continuously along the cell membrane, with a complete structure and clear boundaries.

p-H2AX is a maker protein for DNA double-strand damage. To determine whether EspF could cause DNA damage, we next evaluated the level of p-H2AX in Caco2 cells by infecting them with different strains. Compared with the Δ*espF* group, the levels of p-H2AX in the EHEC and Δ*espF*/*pespF* groups were significantly increased (**Figure 1C**). Then, we infected Caco2 cells with different strains and observed the distribution of p-H2AX via immunofluorescence. As shown in **Figure 1D**, in non-infected Caco2 cells (Control), the p-H2AX fluorescence was lower. In the EHEC group, strong p-H2AX fluorescence was observable in the nucleus. By contrast, the Δ*espF* group had weakened punctate fluorescence in the nucleus. The p-H2AX fluorescence was recovered by complementation with *espF*. We then used ImageJ software version 1.8.0 to quantify the fluorescence intensity of p-H2AX in these images. The signal intensity of p-H2AX in the EHEC groups was almost two times higher than that in the Δ*espF* group. These results indicated that EspF may cause DNA damage

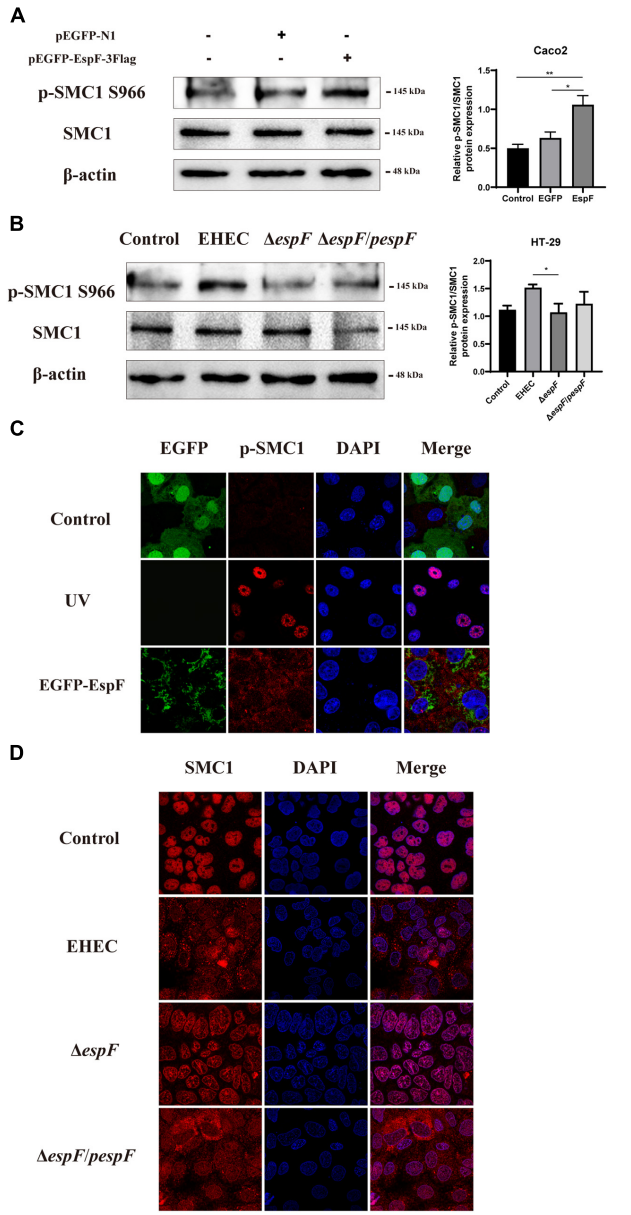


FIGURE 5 | EspF activates the phosphorylation of SMC1 and redistributes it to the cytoplasm. **(A)** EspF increases the phosphorylation of SMC1 in Caco2 cells. pEGFP-N1 and pEGFP-EspF were transfected into Caco2 cells for 48 h. The expression levels and grayscale analysis of p-SMC1/SMC1 were as indicated. Relative protein levels were quantified using ImageJ software. Data are shown as the mean ± SD from three independent repeats. $^{*}P < 0.05$, $^{**}P < 0.01$. **(B)** EspF increases the phosphorylation of SMC1 in HT-29 cells. HT-29 cells were infected with indicated strains. The expression levels and grayscale analysis of p-SMC1/SMC1 were as indicated. Relative protein levels were quantified using ImageJ software. Data are shown as the mean ± SD from three independent repeats. $^{*}P < 0.05$. **(C)** EspF alters the subcellular localization of p-SMC1. Immunofluorescence with anti-p-SMC1 antibody followed with a secondary antibody (red). Images were acquired on an FV1000 confocal laser scanning microscope using a 63X oil objective. **(D)** EspF alters the sub-cellular localization of SMC1. Immunofluorescence using an anti-SMC1 antibody followed by a secondary antibody (red). Images were acquired on an FV1000 confocal laser scanning microscope using a 63X oil objective.

and morphological changes such as cell multi-nucleation and internalization, along with the rearrangement of the cytoskeleton.

EspF Causes DNA Oxidative Damage and Decreases Cell Viability

The most common cell oxidative damage is the formation of mutagenic DNA adducts, including 8-OHdG (Kasai, 1997). We used an 8-OHdG ELISA kit to determine the level of DNA adducts after infection of HT-29 and Caco2 cells, which reflected the level of DNA oxidative damage. In HT-29 cells, the average DNA oxidative damage levels of Control, EHEC, Δ*espF*, and Δ*espF*/*pespF*-infected cells were 28.6, 113.1, 77.0, and 99.1 ng/mL, respectively (**Figure 2A**). Compared with the EHEC group, the DNA oxidative damage level in the Δ*espF* group was significantly reduced ($P < 0.01$). In Caco2 cells, the average DNA oxidative damage levels of Control, EHEC, Δ*espF*, and Δ*espF*/*pespF*-infected cells were 49.5, 176.8, 92.5, and 144.8 ng/mL, respectively (**Figure 2B**). The DNA oxidative damage level of the EHEC group was almost two times higher than that of the Δ*espF* group ($P < 0.05$). No differences were observed between the Δ*espF*/*pespF* and Δ*espF* groups, which may be caused by the instability of *espF* gene complementation.

CCK-8 assay can indirectly reflect the number of living cells. The effects of infection with different strains on cell viability were then measured with the CCK-8 assay. After HT-29 cells were infected with these strains, the cells were then treated with gentamicin (50 μg/ml) to remove adherent EHEC, followed by incubation for 24 h, 48 h, or 72 h. After infection with these strains, the cell viability was significantly lower than the Control group ($P < 0.01$). Compared with the EHEC group, the number of cells in Δ*espF* group increased by 2.0%, 11.6%, and 14.2% at 24 h, 48 h, and 72 h, respectively (**Figure 2C**), and the cell viability at 48 h and 72 h was statistically significant ($P < 0.05$). Similarly, in Caco2 cells, the cell viability of the EHEC group was 11.8%, 18.1%, and 19.5% lower than those of the Δ*espF* group at 24 h, 48 h, and 72 h ($P < 0.05$), respectively (**Figure 2D**). The Δ*espF*/*pespF* group was slightly lower than Δ*espF*, but the difference was not statistically significant.

Prediction and Analysis of Protein Interactions With EspF

After transfecting 293T cells with pEGFP-EspF-3Flag, pEGFP-EspF-N-Flag, and pEGFP-EspF-C-Flag plasmids for 48 h, we lysed cells and precipitated the proteins with Flag and IgG antibodies. These eluted proteins were resolved using 10% SDS-PAGE and visualized by silver staining. Protein expression of pEGFP-EspF-3Flag plasmid was at 60 kDa, that of pEGFP-EspF-N-Flag was at 35 kDa, and that of pEGFP-EspF-C-Flag was at 55 kDa, all of these band sizes were consistent with their anticipated sizes (**Figure 3A**). Three additional protein bands were specifically precipitated from pEGFP-EspF-transfected cells compared with the IgG group, two additional protein bands were specifically precipitated from pEGFP-EspF-N-transfected cells, and one additional protein band was observed from pEGFP-EspF-C-transfected cells. These additional protein bands in the Flag group and the same position as bands in the IgG group

were then cut off and digested by mass spectrometry. The pull-down proteins in the Flag group minus the pull-down proteins in the IgG group were considered to be the putative specific EspF-interacting proteins.

A total of 309 cellular proteins were shown to interact with EspF, while the EspF-N terminus alone interacted with 231 proteins, and 123 proteins interacted with the EspF-C terminus alone (**Supplementary Tables 1–3**). Kyoto Encyclopedia of Genes and Genomes (KEGG) pathway annotation of the host proteins interacting with EspF revealed that subclasses associated with metabolism, signal transduction, and the immune system were highly enriched (**Figure 3B**). Gene Ontology (GO) annotation analysis of interacting proteins revealed that subclasses associated with translation (23.1%) and redox process (15.4%) were enriched in Biological Processes (BPs). The most abundant subclasses in Cellular Components (CCs) included intermediate filaments (21.3%) and ribosomes (13.5%). Molecular Functions (MFs) mainly involved protein binding (22.4%) and ATP binding (18.6%) (**Figure 3C**). Clusters of Orthologous Groups (COG) analysis showed that the interacting proteins were mainly involved in translation, ribosomal structure, and post-translational modification (**Figure 3D**).

Among these proteins, Structural maintenance of chromosome protein 1A (SMC1) had a high interaction score with EspF. SMC1 is considered to be a chromosomal structural protein (Watrin and Peters, 2006). When cells are stimulated by DNA damage, SMC1 can be phosphorylated by ATM and plays a role in DNA damage repair in the ATM/NBS1 branch of the DSB repair pathway.

SMC1 Is a Novel EspF-Interacting Protein That May Interact via the EspF-C Terminus

Our MS results revealed that EspF could interact with SMC1. Confocal microscopy analysis and CoIP further validated this interaction between EspF and SMC1. We transfected pEGFP-EspF plasmids into Caco2 cells, and our IF results showed that SMC1 was mostly distributed in the nucleus in the Control group, but after transfection with EspF, SMC1 protein was partially transferred from the nucleus to the cytoplasm, and SMC1 and EspF co-localized in the cytoplasm (**Figure 4A**). We then quantified the fluorescence intensity of SMC1 protein in the nucleus, and the level of SMC1 in the cells expressing EspF was significantly lower than that in cells not expressing EspF, $P < 0.01$ (**Figure 4B**).

We next quantified the amount of co-localization between EspF and SMC1 in the cytoplasm. We used ImageJ to make a scatter plot of this co-localization (**Figure 4C**), and the Pearson's correlation coefficient (R^2) for the images above the thresholds for EspF and SMC1 was 0.7034. Moreover, the plot profile of co-localization showed that the red fluorescence intensity (SMC1) fluctuated with the green fluorescence intensity (EspF) (**Figure 4D**). These quantitative results clearly verified the interaction between EspF and SMC1.

We next used CoIP to confirm the interaction between EspF and SMC1 and the specific interaction domains required for this interaction. We transfected pEGFP-EspF-3Flag, pEGFP-EspF-N-Flag, and pEGFP-EspF-C-Flag into 293T cells and then obtained cell lysates. As shown in **Figure 4E**, we observed that the EspF and the EspF-C terminus co-precipitated with SMC1, whereas the N-terminus interacted very weakly with SMC1. Thus, SMC1 preferred to interact with the EspF-C terminus. The biological regulation of host SMC1 protein by EspF, however, still needs to be further studied.

EspF Can Activate SMC1 Phosphorylation and Change Its Subcellular Localization

To determine how EspF regulates the level of SMC1 in host cells, we measured SMC1 and its phosphorylation levels after transfecting pEGFP-EspF into Caco2 cells. After transfection with EspF, the level of SMC1 remained unchanged, but the phosphorylation of SMC1 was significantly higher compared with the EGFP group ($P < 0.05$) (**Figure 5A**). We confirmed this result by infecting HT-29 cells with the strains. The phosphorylation of SMC1 in cells infected with EHEC was higher than in those infected with Δ*espF* cells ($P < 0.05$) (**Figure 5B**).

We next observed the localization of phosphorylation of SMC1 in Caco2 cells by transfecting with pEGFP-EspF. As shown in **Figure 5C**, the level of p-SMC1 expression was low in the EGFP group. We used UV treatment as a positive control to induce DSBs. After exposure to 10 J/m^2 of UV, p-SMC1 was distributed in a punctate manner in the nucleus. While the level of p-SMC1 in the EspF group was significantly increased, p-SMC1 was typically transferred to the cytoplasm and co-localized with EspF protein. The above results verified that EspF could activate SMC1 phosphorylation and transfer it to the cytoplasm.

Then, we infected Caco2 cells with the strains. SMC1 was expressed in the nucleus in the Control and Δ*espF* groups, while in EHEC-infected cells, SMC1 was redistributed more from the nucleus to the cytoplasm. Also, the phenotype of SMC1 in cells infected with Δ*espF*/*pespF* was consistent with EHEC, suggesting that EspF prevented SMC1 from properly playing its DNA damage repair role in the nucleus (**Figure 5D**).

These findings suggested that EspF could change the subcellular localization of SMC1 protein from the nucleus to the cytoplasm, thereby preventing p-SMC1 from playing its role in the nucleus in DNA damage repair.

EspF Induces DNA Damage in Intestinal Epithelial Cells *in vivo*

To test our *in vitro* findings *in vivo*, we constructed an animal model of EHEC O157:H7 hemorrhagic enteritis based on our previous method (Wang et al., 2017). We improved this protocol by using streptomycin in sterile drinking water before gavage (**Figure 6A**), making EHEC O157:H7 the dominant intestinal bacteria strain and increasing the susceptibility of the BALB/c mice (Bohnhoff and Miller, 1962).

After the gavage of the strains, the mice showed sparse hair, poor mobility, and hind limb hemiplegia. The weight of mice decreased continually over the seven days. The weight of mice in the EHEC groups decreased faster, while the weight loss of the

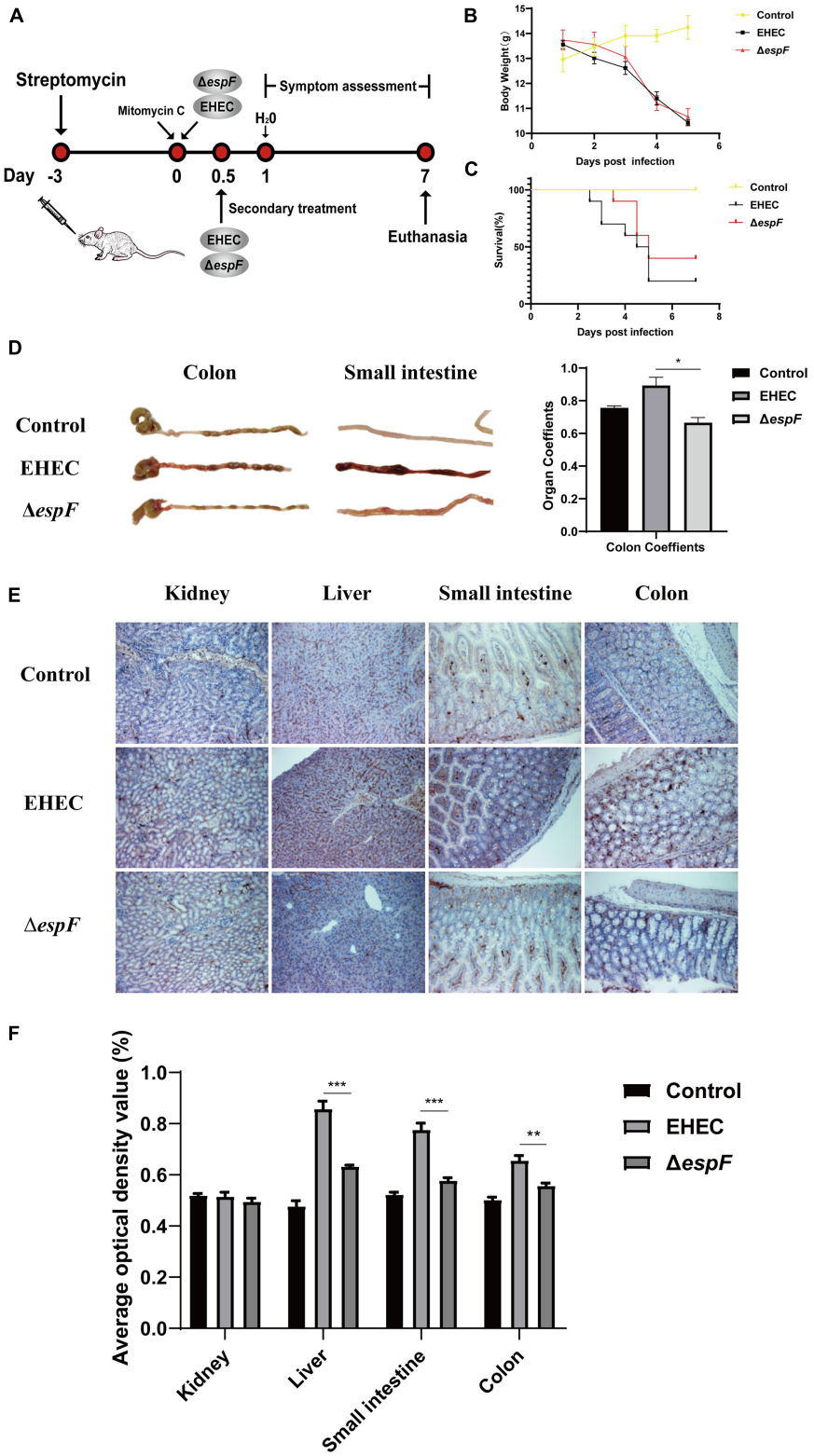


FIGURE 6 | Pathogenicity of EHEC O157:H7 mutant strains in BALB/c mice. **(A)** Construction of an animal model of EHEC O157:H7 hemorrhagic enteritis. **(B)** The bodyweight of the mice at 7 days post-infection. **(C)** Survival curves of BALB/c mice gavage with indicated strains. **(D)** The intestinal appearance and colon coefficient in mice. **(E)** Immunohistochemistry for p-H2AX in different tissues. **(F)** Grayscale analysis of p-H2AX in different tissues. The average optical density value was quantified using ImageJ software. Data are shown as the mean ± SD from three independent repeats. $^{*}P < 0.05$, $^{**}P < 0.01$, $^{***}P < 0.001$.

Δ*espF* group increased rapidly after the fourth day of infection (**Figure 6B**). Mice in the EHEC group had a rapid onset of disease, and the mice died on the 2.5 d of infection. The onset of the mice in the Δ*espF* group was, however, delayed. The mortality of the mice in the EHEC and Δ*espF* groups were 80 and 60%, respectively (**Figure 6C**).

After dissecting the mice, we found that the colon of the Control group was a normal yellow, and there was no redness or swelling in the small intestine or colon. In the EHEC group, the colon had edema and became bloody, the stool was black and granular, and small bowel lesions were more obvious, presenting as hemorrhagic colitis. The appearance of the colon in the Δ*espF* group was similar to that in the Control group, the colon lesions were mild, and the small bowel wall only had partial edema (**Figure 6D**). We weighed the colon of the mice and calculated the organ coefficient based on body weight (**Figure 6D**). The results showed that the colon coefficients of the EHEC group were significantly higher than those of the Δ*espF* group and Control group ($P < 0.05$), indicating that EspF could cause thickening of the colonic mucosa in mice and mediate severe edema and inflammation. These results demonstrated that EspF enhanced lethality and induced intestinal lesions in BALB/c mice.

We next examined the kidney, liver, small intestine, and colon tissue for p-H2AX levels using immunohistochemistry. The results showed that the normal lobule of the liver could be seen in the Control group, and only a few brown particles were seen in the nucleus. Compared with the Δ*espF* group, the phosphorylation of H2AX in the EHEC group was significantly increased. The intestinal tissue damage of mice was also more obvious (**Figure 6E**). We quantified the results of this immunohistochemistry by gray value analysis. Except for the kidney, the phosphorylation of H2AX in the EHEC group was significantly higher than that in the Δ*espF* group ($P < 0.05$) (**Figure 6F**), suggesting that EspF may mediate different degrees of DNA damage in various tissues.

DISCUSSION

It has been reported that EspF can lead to an increase in spontaneous mutations in host cells (Maddocks et al., 2013). However, the molecular mechanism of EspF-mediated DNA damage and microsatellite instability remains still unclear.

Cell morphological changes are also one of the manifestations of DNA damage, such as cell multi-nucleation and cell hypertrophy (Horn and Triantafyllopoulou, 2018). Some cells escape from cell cycle arrest and enter abnormal mitosis. This process is characterized by significant changes in cell morphology (Tyrer et al., 2014). Affected cells swell due to inappropriate cytokinesis, changing actin stress fibers, and form micro-nuclei and multi-nuclei. Studies have shown that EPEC EspF mediates cell multi-nucleation and this extreme phenotype depends on the C-terminus region of EspF (Dean and Kenny, 2013). Cell fusion relies on N-WASP, the protein that binds to the EspF-C terminus. In addition, EspF collaborates with CK18 and 14-3-3ζ (Viswanathan et al., 2004), resulting in the alteration of the intermediate-filament network. We hypothesized that EHEC EspF could also cause cell multi-nucleation. We transfected pEGFP-N1 and pEGFP-EspF into Caco2 cells, and cells expressing EspF showed multi-nucleation, accompanied by the rearrangement of the CK18 cytoskeleton, while the cells in Control and EGFP groups still maintained a single nucleus and had an intact cytoskeleton. These results indicated that EHEC EspF could induce host cell multi-nucleation and cytoskeletal rearrangement, and provided a basis for understanding EspF-mediated DNA damage.

One of the earliest events that occur after DNA damage is the phosphorylation of Ser139 on histone H2AX (p-H2AX), which is a known marker of DNA damage (Hong et al., 2016). In this study, we infected Caco2 cells with the strains. Compared with the Δ*espF* group, the phosphorylation of H2AX was higher in the EHEC and Δ*espF*/*pespF* groups. Immunofluorescence further confirmed that the EHEC and Δ*espF*/*pespF* groups had stronger red fluorescence signals. Therefore, we verified that EspF may induce host cell DNA damage.

EspF can increase the level of ROS in the host. It is worth noting that excessive ROS can lead to host DNA damage and form the mutagenic DNA adducts of 8-OHdG (Kasai, 1997; Kryston et al., 2011; Hua et al., 2013). The levels of 8-OHdG in the EHEC groups were significantly higher than those in the Δ*espF* group. Due to the instability of *espF* gene complementation, no statistically significant difference was observed between the Δ*espF*/*pespF* and Δ*espF* groups. Caco2 cells are more prone to DNA oxidative damage, which may be related to the characteristics of cell differentiation, such as intestinal cell differentiation and cell polarity (Gagnon et al., 2013).

During the infection of intestinal epithelial cells, the surface properties of EPEC/EHEC induce exogenous apoptotic pathways (Abul-Milh et al., 2001), whereas TIIISS effectors such as EspF and Map trigger intrinsic apoptotic pathways (Wong et al., 2011). EspF disrupts the mitochondrial membrane potential, leading to the release of cytochrome c and the cleavage of caspases 3 and 9, which eventually mediates cell apoptosis (Nougayrède and Donnenberg, 2004). Our research also confirmed that EspF reduced cell viability. Through CCK-8 assays, the cell viability of EHEC-infected cells was shown to be significantly lower than that of the Δ*espF* group at 48 h and 72 h after infection ($P < 0.05$). These results indicated that EspF could cause DNA oxidative damage, induce host cell apoptosis, and reduce cell viability. However, we noticed that compared with the Control group, the Δ*espF* strain still caused a significant decrease in cell viability. As we know, EHEC hemolysin employs outer membrane vesicles to target the mitochondria and cause endothelial and epithelial apoptosis (Bielaszewska et al., 2013). In addition, the EPEC effector Map imports into mitochondria, causing mitochondrial dysfunction and Ca^{2+} efflux into the host cytoplasm, resulting in the release of epidermal growth factors that stimulate the apoptosis signaling pathway (Ramachandran et al., 2020). Thus, activation of cell apoptosis may be a result of multiple factors.

We speculated that EspF may interact with specific host proteins to mediate DNA damage. Therefore, we used CoIP-MS

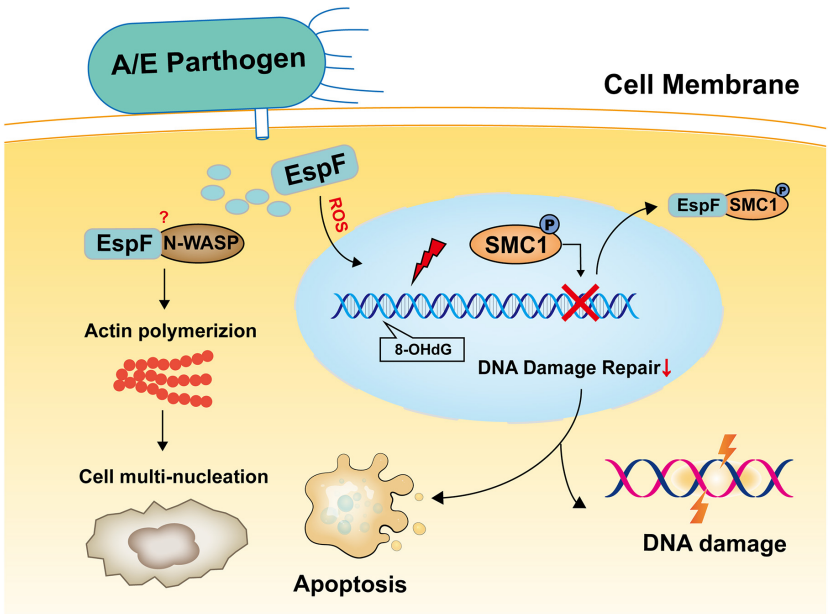


FIGURE 7 | Model of EspF may induce host DNA damage. EspF induces cell multi-nucleation, exacerbates DNA oxidative damage, inhibits cell viability, interacts with SMC1, transfers p-SMC1 into the cytoplasm, then may lead to DNA damage.

to identify the interactions between EspF and host proteins. Mass spectrometry identified the SNX9, SNX18, 14-3-3, and ANXA6 proteins which had previously been verified to interact with EspF, confirming the credibility of our mass spectrometry results. 309 host cell proteins interacting with EspF were revealed by CoIP-MS. Interacting proteins were mostly involved in metabolic pathways and ribosomal biological processes. We found that EspF interacted strongly with ribosomal RPL, RPS, and EIF family proteins. Previous proteomics studies have shown that the levels of many ribosomal proteins in intestinal cells decrease after EPEC infection (Hardwidge et al., 2004). In cells expressing EspF, pre-rRNA synthesis is blocked, and EspF-dependent EPEC infection reduces the expression level of the ribosomal protein RPL9 and changes the localization of RPS5 and U8 small nucleolar RNA (snoRNA) (Dean et al., 2010). Our results provided further support for the hypothesis that EspF might play its biological role by regulating ribosomal protein synthesis.

SMC1 had a higher score among our interacting proteins. It has also been shown to interact with EspF and be involved in multiple signal pathways via a bimolecular fluorescence complementation method (Hua et al., 2018b). It is shown that the SMC1 protein is specifically implicated in sister chromatid cohesion (Ball and Yokomori, 2008). The cohesin SMC1 is involved in ATM-dependent responses to DNA damage, and sister chromatid cohesive protein complexes play a key role in the HR-mediated repair of DSBs (Jessberger, 2009). DSBs can activate ATM kinase and initiate downstream signaling pathways. These downstream targets include the checkpoint kinase CHK1, CHK2, and SMC1, which regulate DNA replication forks and damage repair (Carrassa and Damia, 2017). We further verified the interaction between EspF and SMC1 by CoIP and immunofluorescence. Moreover, we demonstrated that the functional domain of interaction was most likely through the C-terminus of EspF. It is known that the binding of EspF to SNX9 and N-WASP proteins is based on the c-terminus SH3 and CRIB (Cdc42/rac interaction binding) motifs (Holmes et al., 2010). The EspF-C terminus, thus, may play a role as a scaffold, linking EspF with other proteins and exerting its biological functions.

We applied immunofluorescence and CoIP to further validate the interaction between EspF protein and SMC1 protein. Moreover, the interaction between SMC1 and the EspF-C terminus was stronger than that with the N terminus. In addition, the nuclear level of SMC1 in the cells expressing EspF was significantly lower than that in cells not expressing EspF, $P<0.01$, thus demonstrating the interaction between EspF and SMC1 can change the subcellular localization of SMC1.

We also examined the effect of sub-localization of SMC1 with strain infection. In HT29 cells, SMC1 concentrated in the nucleus in the Control and Δ*espF* groups, whereas EHEC and Δ*espF*/*pespF* infection lead SMC1 to migrate from the nucleus to the cytoplasm. Moreover, the phosphorylation of SMC1 was less expressed in EGFP groups, while it was punctated distributed in the nucleus in the UV treatment group. Transfection of EspF significantly activated the phosphorylation of SMC1 in the cytoplasm and co-localized with EspF. Therefore, we hypothesized that EspF might interact with SMC1 and transfer it to the cytoplasm, which decreased the SMC1 level in the nucleus, reducing the phosphorylation of SMC1 in the nucleus, and thus down-regulating the ability of DNA damage repair and inhibiting the HR pathway repair. However, the exact mechanism of EspF-SMC1 modulation of this deserves further study.

We also demonstrated that EspF may mediate DNA damage in intestinal epithelial cells *in vivo*. Mice have always been the

ideal animal model for studying EHEC infections (Wadolkowski et al., 1990; Mohawk and O'Brien, 2011). In this study, we added streptomycin to the drinking water to increase mice's susceptibility to pathogenic bacteria (Bohnhoff and Miller, 1962). Among these mice, the EHEC group had the highest mortality rate (80%), and the earliest disease onset. The appearance of the colon in the EHEC group showed hemorrhagic colitis such as edema and vacuoles, and the colon coefficient (0.912) was higher than the Δ*espF* group (0.663), $P < 0.05$. Immunohistochemistry for p-H2AX in different tissues showed that, except for the mice kidney, the phosphorylation of H2AX in EHEC groups was significantly increased than Δ*espF* group ($P < 0.05$). These results indicated that EspF can induce DNA damage in intestinal epithelial cells and mediate animal death.

This study did have some limitations. First, compared with EHEC, the expression of the complementation strains Δ*espF*/*pespF* was unstable. The *espF* gene was cloned into the pBAD33 plasmid to construct a complementary strain (Hua et al., 2015). Perhaps due to the pBAD expression system, the expression level of EspF was controlled by the regulation of L-arabinose, which caused the instability. Second, some of the host proteins that have been confirmed to interact with EspF were not identified in our MS results, such as N-WASP protein (Garber et al., 2018). This may be due to the size of N-WASP being about 55 kDa, it was not included in the bands we interrogated by MS. In addition, some weak interactions may not be detected. Further experiments to verify the interactions between EspF and host cell proteins would support these findings.

In summary, the results reported herein show that EspF induces cell multi-nucleation, exacerbates DNA oxidative damage, inhibits cell viability, and may lead to DNA damage and death in mice (**Figure 7**). In addition, the host proteins that interact with EspF are identified by CoIP-MS, and we verify that EspF interacts with a novel DNA damage repair protein SMC1. EspF can transfer p-SMC1 to the cytoplasm, making it unable to perform normal DNA damage repair in the nucleus and inhibiting the HR pathway. EspF, therefore, appears to cause DNA damage via interaction with the SMC1 protein, thus contributing to the pathogenicity of EHEC.

DATA AVAILABILITY STATEMENT

The raw data supporting the conclusions of this article will be made available by the authors, without undue reservation.

ETHICS STATEMENT

The animal study was reviewed and approved by Animal Experimental Committee of Southern Medical University.

AUTHOR CONTRIBUTIONS

MF, CW, and YH designed the research and wrote the manuscript. MF, SL, JW, and HC performed the research and conducted the data analysis. ZZ, JL, XL, BZ, and WZ supervised the project and edited the manuscript. All authors contributed to the article and approved the submitted version.

FUNDING

This work was supported by the Natural Science Foundation of Guangdong Province (No. 2018B030311063) and the Guangdong Basic and Applied Basic Research Foundation (Nos. 2019A1515111004 and 2021A1515011240).

SUPPLEMENTARY MATERIAL

The Supplementary Material for this article can be found online at: https://www.frontiersin.org/articles/10.3389/fmicb.2021.682064/full#supplementary-material

Supplementary Figure 1 | Supplementary data for **Figure 1**. Three independent Western blots to detect p-H2AX and H2AX protein in Caco2 cells.

Supplementary Figure 2 | Supplementary data for **Figure 4**. Three independent CoIP experiments to confirm the interaction between EspF, EspF-N, and the EspF-C terminus and SMC1 protein.

Supplementary Figure 3 | Supplementary data for **Figure 5**. Three independent Western blots to detect p-SMC1 and SMC1 protein in Caco2 cells and HT-29 cells.

Supplementary Figures 4–6 | Immunofluorescence figures of internalization phenomenon in Caco2 cells expressing EspF.

Supplementary Figure 7 | iTRAQ analysis of the differential proteins of EHEC and Δ*espF* strains infected with HT29 cells in the cell cycle pathway.

Supplementary Table 1 | The list of the proteins interacting with EspF protein.

Supplementary Table 2 | The list of the proteins interacting with EspF-N protein.

Supplementary Table 3 | The list of the proteins interacting with EspF-C protein.

REFERENCES

Abul-Milh, M., Wu, Y., Lau, B., Lingwood, C. A., and Barnett, F. D. (2001). Induction of epithelial cell death including apoptosis by enteropathogenic *Escherichia coli* expressing bundle-forming pili. *Infect. Immun.* 69, 7356–7364. doi: 10.1128/IAI.69.12.7356-7364.2001

Ball, A. J., and Yokomori, K. (2008). Damage-induced reactivation of cohesin in postreplicative DNA repair. *Bioessays* 30, 5–9. doi: 10.1002/bies.20691

Bielaszewska, M., Rüter, C., Kunsmann, L., Greune, L., Bauwens, A., Zhang, W., et al. (2013). Enterohemorrhagic *Escherichia coli* hemolysin employs outer membrane vesicles to target mitochondria and cause endothelial and epithelial apoptosis. *PLoS Pathog.* 9:e1003797. doi: 10.1371/journal.ppat.1003797

Bohnhoff, M., and Miller, C. P. (1962). Enhanced susceptibility to *Salmonella* infection in streptomycin-treated mice. *J. Infect. Dis.* 111, 117–127. doi: 10.1093/infdis/111.2.117

Burma, S., Chen, B. P., Murphy, M., Kurimasa, A., and Chen, D. J. (2001). ATM phosphorylates histone H2AX in response to DNA double-strand breaks. *J. Biol. Chem.* 276, 42462–42467. doi: 10.1074/jbc.C100466200

Carrassa, L., and Damia, G. (2017). DNA damage response inhibitors: mechanisms and potential applications in cancer therapy. *Cancer Treat. Rev.* 60, 139–151. doi: 10.1016/j.ctrv.2017.08.013

Dahan, S., Busuttil, V., Imbert, V., Peyron, J. F., Rampal, P., Czerucka, D., et al. (2002). Enterohemorrhagic *Escherichia coli* infection induces interleukin-8 production via activation of mitogen-activated protein kinases and the

transcription factors NF-kappaB and AP-1 in T84 cells. *Infect. Immun.* 70, 2304–2310. doi: 10.1128/iai.70.5.2304-2310.2002

Dean, P., and Kenny, B. (2013). A bacterial encoded protein induces extreme multinucleation and cell-cell internalization in intestinal cells. *Tissue Barr.* 1:e22639. doi: 10.4161/tisb.22639

Dean, P., Scott, J. A., Knox, A. A., Quitard, S., Watkins, N. J., Kenny, B., et al. (2010). The enteropathogenic *E. coli* effector EspF targets and disrupts the nucleolus by a process regulated by mitochondrial dysfunction. *PLoS Pathog.* 6:e1000961. doi: 10.1371/journal.ppat.1000961

De'Angelis, G. L., Bottarelli, L., Azzoni, C., De' Angelis, N., Leandro, G., Di Mario, F., et al. (2018). Microsatellite instability in colorectal cancer. *Acta Biomed.* 89, 97–101. doi: 10.23750/abm.v89i9-S.7960

Gagnon, M., Zihler, B. A., Chervet, N., Chassard, C., and Lacroix, C. (2013). Comparison of the Caco-2, HT-29 and the mucus-secreting HT29-MTX intestinal cell models to investigate *Salmonella* adhesion and invasion. *J. Microbiol. Methods* 94, 274–279. doi: 10.1016/j.mimet.2013.06.027

Garber, J. J., Mallick, E. M., Scanlon, K. M., Turner, J. R., Donnenberg, M. S., Leong, J. M., et al. (2018). Attaching-and-Effacing pathogens exploit junction regulatory activities of N-WASP and SNX9 to disrupt the intestinal barrier. *Cell Mol. Gastroenterol. Hepatol.* 5, 273–288. doi: 10.1016/j.jcmgh.2017.11.015

Hardwidge, P. R., Rodriguez-Escudero, I., Goode, D., Donohoe, S., Eng, J., Goodlett, D. R., et al. (2004). Proteomic analysis of the intestinal epithelial cell response to enteropathogenic *Escherichia coli*. *J. Biol. Chem.* 279, 20127–20136. doi: 10.1074/jbc.M401228200

Holmes, A., Mühlen, S., Roe, A. J., and Dean, P. (2010). The EspF effector, a bacterial pathogen's Swiss army knife. *Infect. Immun.* 78, 4445–4453. doi: 10.1128/IAI.00635-10

Hong, J., Chen, Z., Peng, D., Zaika, A., Revetta, F., Washington, M. K., et al. (2016). APE1-mediated DNA damage repair provides survival advantage for esophageal adenocarcinoma cells in response to acidic bile salts. *Oncotarget* 7, 16688–16702. doi: 10.18632/oncotarget.7696

Horn, V., and Triantafyllopoulou, A. (2018). DNA damage signaling and polyploid macrophages in chronic inflammation. *Curr. Opin. Immunol.* 50, 55–63. doi: 10.1016/j.coi.2017.11.002

Hua, K. F., Liao, P. C., Fang, Z., Yang, F. L., Yang, Y. L., Chen, Y.-L., et al. (2013). Generation of reactive oxygen species by polyenylpyrroles derivatives causes DNA damage leading to G2/M arrest and apoptosis in human oral squamous cell carcinoma cells. *PLoS One* 8:e67603. doi: 10.1371/journal.pone.0067603

Hua, Y., Ju, J., Wang, X., Zhang, B., Zhao, W., Zhang, Q., et al. (2018a). Screening for host proteins interacting with *Escherichia coli* O157:H7 EspF using bimolecular fluorescence complementation. *Future Microbiol.* 13, 37–58. doi: 10.2217/fmb-2017-0087

Hua, Y., Yan, K., and Wan, C. (2018b). Clever cooperation: interactions between EspF and host proteins. *Front. Microbiol.* 9:2831. doi: 10.3389/fmicb.2018.02831

Hua, Y., Sun, Q., Wang, X., Du, Y., Shao, N., Zhang, Q., et al. (2015). Construction of enterohemorrhagic *Escherichia coli* O157:H7 strains with espF gene deletion and complementation. *Nan Fang Yi Ke Da Xue Xue Bao* 35, 1546–1551.

Jessberger, R. (2009). Cohesin's dual role in the DNA damage response: repair and checkpoint activation. *EMBO J.* 28, 2491–2493. doi: 10.1038/emboj.2009.217

Kasai, H. (1997). Analysis of a form of oxidative DNA damage, 8-hydroxy-2'-deoxyguanosine, as a marker of cellular oxidative stress during carcinogenesis. *Mutat. Res.* 387, 147–163. doi: 10.1016/s1383-5742(97)00035-5

Kitagawa, R., and Kastan, M. B. (2005). The ATM-dependent DNA damage signaling pathway. *Cold Spring Harb. Symp. Quant. Biol.* 70, 99–109. doi: 10.1101/sqb.2005.70.002

Kryston, T. B., Georgiev, A. B., Pissis, P., and Georgakilas, A. G. (2011). Role of oxidative stress and DNA damage in human carcinogenesis. *Mutat. Res.* 711, 193–201. doi: 10.1016/j.mrfmmm.2010.12.016

Liu, C., Vyas, A., Kassab, M. A., Singh, A. K., and Yu, X. (2017). The role of poly ADP-ribosylation in the first wave of DNA damage response. *Nucleic Acids Res.* 45, 8129–8141. doi: 10.1093/nar/gkx565

Maddocks, O. D., Scanlon, K. M., and Donnenberg, M. S. (2013). An *Escherichia coli* effector protein promotes host mutation via depletion of DNA mismatch repair proteins. *mBio* 4:e0113-52. doi: 10.1128/mBio.00152-13

Maddocks, O. D., Short, A. J., Donnenberg, M. S., Bader, S., and Harrison, D. J. (2009). Attaching and effacing *Escherichia coli* downregulate DNA mismatch repair protein in vitro and are associated with colorectal adenocarcinomas in humans. *PLoS One* 4:e5517. doi: 10.1371/journal.pone.0005517

Mohawk, K. L., and O'Brien, A. D. (2011). Mouse models of *Escherichia coli* O157:H7 infection and shiga toxin injection. *J. Biomed. Biotechnol.* 2011:258185. doi: 10.1155/2011/258185

Nagai, T., Abe, A., and Sasakawa, C. (2005). Targeting of enteropathogenic Escherichia coli EspF to host mitochondria is essential for bacterial pathogenesis: critical role of the 16th leucine residue in EspF. *J. Biol. Chem.* 280, 2998–3011. doi: 10.1074/jbc.M411550200

Nougayrède, J. P., and Donnenberg, M. S. (2004). Enteropathogenic *Escherichia coli* EspF is targeted to mitochondria and is required to initiate the mitochondrial death pathway. *Cell Microbiol.* 6, 1097–1111. doi: 10.1111/j.1462-5822.2004.00421.x

Pacheco, A. R., and Sperandio, V. (2012). Shiga toxin in enterohemorrhagic *E.coli*: regulation and novel anti-virulence strategies. *Front. Cell Infect. Microbiol.* 2:81. doi: 10.3389/fcimb.2012.00081

Ramachandran, R. P., Spiegel, C., Keren, Y., Danieli, T., Melamed-Book, N., Pal, R. R., et al. (2020). Mitochondrial targeting of the enteropathogenic *Escherichia coli* map triggers calcium mobilization, ADAM10-MAP kinase signaling, and host cell apoptosis. *mBio* 11:e001397-20. doi: 10.1128/mBio.01397-20

Slater, S. L., Sågfors, A. M., Pollard, D. J., Ruano-Gallego, D., and Frankel, G. (2018). The Type III secretion system of pathogenic *Escherichia coli*. *Curr. Top. Microbiol. Immunol.* 416, 51–72. doi: 10.1007/82_2018_116

Stefanski, C. D., Keffler, K., McClintock, S., Milac, L., and Prosperi, J. R. (2019). APC loss affects DNA damage repair causing doxorubicin resistance in breast cancer cells. *Neoplasia* 21, 1143–1150. doi: 10.1016/j.neo.2019.09.002

Tarr, P. I., Gordon, C. A., and Chandler, W. L. (2005). Shiga-toxin-producing *Escherichia coli* and haemolytic uraemic syndrome. *Lancet* 365, 1073–1086. doi: 10.1016/S0140-6736(05)71144-2

Tyrer, P. C., Frizelle, F. A., and Keenan, J. I. (2014). *Escherichia coli*-derived outer membrane vesicles are genotoxic to human enterocyte-like cells. *Infect. Agent Cancer* 9:2. doi: 10.1186/1750-9378-9-2

Viswanathan, V. K., Lukic, S., Koutsouris, A., Miao, R., Muza, M. M., Hecht, G., et al. (2004). Cytokeratin 18 interacts with the enteropathogenic *Escherichia coli* secreted protein F (EspF) and is redistributed after infection. *Cell Microbiol.* 6, 987–997. doi: 10.1111/j.1462-5822.2004.00416.x

Wadolkowski, E. A., Burris, J. A., and O'Brien, A. D. (1990). Mouse model for colonization and disease caused by enterohemorrhagic *Escherichia coli* O157:H7. *Infect. Immun.* 58, 2438–2445. doi: 10.1128/IAI.58.8.2438-2445.1990

Wang, X., Du, Y., Hua, Y., Fu, M., Niu, C., Zhang, B., et al. (2017). The EspF N-Terminal of Enterohemorrhagic *Escherichia coli* O157:H7 EDL933w imparts stronger toxicity effects on HT-29 cells than the C-Terminal. *Front. Cell Infect. Microbiol.* 7:410. doi: 10.3389/fcimb.2017.00410

Watrin, E., and Peters, J. M. (2006). Cohesin and DNA damage repair. *Exp. Cell Res.* 312, 2687–2693. doi: 10.1016/j.yexcr.2006.06.024

Wong, A. R., Pearson, J. S., Bright, M. D., Munera, D., Robinson, K. S., Lee, S. F., et al. (2011). Enteropathogenic and enterohaemorrhagic *Escherichia coli*: even more subversive elements. *Mol. Microbiol.* 80, 1420–1438. doi: 10.1111/j.1365-2958.2011.07661.x

Yi, F., Wang, Z., Liu, J., Zhang, Y., Wang, Z., Xu, H., et al. (2017). Structural maintenance of chromosomes protein 1: role in genome stability and tumorigenesis. *Int. J. Biol. Sci.* 13, 1092–1099. doi: 10.7150/ijbs.21206

Zhao, S., Zhou, Y., Wang, C., Yang, Y., Wu, X., Wei, Y., et al. (2013). The N-terminal domain of EspF induces host cell apoptosis after infection with enterohaemorrhagic *Escherichia coli* O157:H7. *PLoS One* 8:e55164. doi: 10.1371/journal.pone.0055164

Conflict of Interest: The authors declare that the research was conducted in the absence of any commercial or financial relationships that could be construed as a potential conflict of interest.

Copyright © 2021 Fu, Liang, Wu, Hua, Chen, Zhang, Liu, Li, Zhang, Zhao and Wan. This is an open-access article distributed under the terms of the Creative Commons Attribution License (CC BY). The use, distribution or reproduction in other forums is permitted, provided the original author(s) and the copyright owner(s) are credited and that the original publication in this journal is cited, in accordance with accepted academic practice. No use, distribution or reproduction is permitted which does not comply with these terms.

frontiers in Immunology

REVIEW
published: 31 May 2021
doi: 10.3389/fimmu.2021.683879

Bacteriostatic Potential of Melatonin: Therapeutic Standing and Mechanistic Insights

Fang He[1,2†], Xiaoyan Wu[2†], Qingzhuo Zhang[2], Yikun Li[2], Yuyi Ye[2], Pan Li[1], Shuai Chen[3], Yuanyi Peng[1*], Rüdiger Hardeland[4] and Yaoyao Xia[2*]*

[1] College of Veterinary Medicine, Southwest University, Chongqing, China, [2] Guangdong Laboratory of Lingnan Modern Agriculture, Guangdong Provincial Key Laboratory of Animal Nutrition Control, Institute of Subtropical Animal Nutrition and Feed, College of Animal Science, South China Agricultural University, Guangzhou, China, [3] Institute of Subtropical Agriculture, Chinese Academy of Sciences, Changsha, China, [4] Johann Friedrich Blumenbach Institute of Zoology and Anthropology, University of Göttingen, Göttingen, Germany

OPEN ACCESS

Edited by:
Karl Kuchler,
Medical University of Vienna, Austria

Reviewed by:
Zhengkai Wei,
Foshan University, China
Shahzad Ali,
University of Veterinary and Animal Sciences, Pakistan

***Correspondence:**
Shuai Chen
chenshuai@mail.com
Yuanyi Peng
pyy2002@sina.com
Yaoyao Xia
yaoyaoxia2018@126.com

[†]These authors have contributed equally to this work

Specialty section:
This article was submitted to Microbial Immunology, a section of the journal Frontiers in Immunology

Received: 22 March 2021
Accepted: 13 May 2021
Published: 31 May 2021

Citation:
He F, Wu X, Zhang Q, Li Y, Ye Y, Li P, Chen S, Peng Y, Hardeland R and Xia Y (2021) Bacteriostatic Potential of Melatonin: Therapeutic Standing and Mechanistic Insights. Front. Immunol. 12:683879. doi: 10.3389/fimmu.2021.683879

Diseases caused by pathogenic bacteria in animals (e.g., bacterial pneumonia, meningitis and sepsis) and plants (e.g., bacterial wilt, angular spot and canker) lead to high prevalence and mortality, and decomposition of plant leaves, respectively. Melatonin, an endogenous molecule, is highly pleiotropic, and accumulating evidence supports the notion that melatonin's actions in bacterial infection deserve particular attention. Here, we summarize the antibacterial effects of melatonin *in vitro*, in animals as well as plants, and discuss the potential mechanisms. Melatonin exerts antibacterial activities not only on classic gram-negative and -positive bacteria, but also on members of other bacterial groups, such as *Mycobacterium tuberculosis*. Protective actions against bacterial infections can occur at different levels. Direct actions of melatonin may occur only at very high concentrations, which is at the borderline of practical applicability. However, various indirect functions comprise activation of hosts' defense mechanisms or, in sepsis, attenuation of bacterially induced inflammation. In plants, its antibacterial functions involve the mitogen-activated protein kinase (MAPK) pathway; in animals, protection by melatonin against bacterially induced damage is associated with inhibition or activation of various signaling pathways, including key regulators such as NF-κB, STAT-1, Nrf2, NLRP3 inflammasome, MAPK and TLR-2/4. Moreover, melatonin can reduce formation of reactive oxygen and nitrogen species (ROS, RNS), promote detoxification and protect mitochondrial damage. Altogether, we propose that melatonin could be an effective approach against various pathogenic bacterial infections.

Keywords: melatonin, bacteriostasis, MAPKs, NF-κB, ROS, inflammasome, sepsis

INTRODUCTION

Bacteria include both pathogenic and beneficial species and are universally present in all ecosystems as colonizers of hosts (1). Bacteria can be beneficial in multiple ways, for example, *Lactobacillus* and *Bifidobacterium* species are used for yoghurt production (2, 3), *Lactococcus* species and others in cheese production (4, 5), methane producing bacteria for methane production (6), *Corynebacteria*

for monosodium glutamate formation (7) and *Acetobacter* for vinegar generation (8). Bacteria, being a normal flora can also benefit hosts, such as, *Lactobacillus* species can inhibit inflammation by competing with pathogens or stimulating skin barrier recovery (9). Most, but not all bacteria present in the gut microbiome, which contains slightly more cells than a human body, can be also classified as being beneficial and relevant to health, as far as it possesses a favorable compostion (10). Pathogenic bacteria may cause mild, severe and even life-threatening diseases [e.g., septicemia (11), pneumonia (12) and meningitis (13)]. In terms of accessibility to treatments, the bacterial surface structures are of great importance. These are partially detectable by gram staining (14), according to which they are categorized as gram positive bacteria (GPB), gram negative bacteria (GNB), and others (15, 16). Examples of pathogenic GPB (PGPB) comprise *Staphylococcus aureus* (*S. aureus*) (17), *Streptococcus pneumoniae* (*S. pneumoniae*) (18) and *Bacillus anthracis* (*B. anthracis*) (19). Pathogenic GNB (PGNB) include *Escherichia coli* (*E. coli*) (20), *Helicobacter pylori* (*H. pylori*) (21), *Pseudomonas aeruginosa* (*P. aeruginosa*) (22), *Acinetobacter baumannii (A. baumannii)* (23), and *Klebsiella pneumoniae* (*K. pneumoniae*) (24). Another important pathogen, *Mycobacterium tuberculosis* (*M. tuberculosis*) (25) possesses a special waxy coating of its cell wall by mycolic acid, which largely prevents gram staining, although the cell wall structure resembles that of other GPBs and is, thus, devoid of an outer membrane (26). Also in genetic terms, *Mycobacterium* species are GPB-like, but the different surface has consequences to treatment.

Bacterial infections caused by pathogenic bacteria severely threaten public health worldwide (27, 28). Historically, the various antibiotics (e.g., penicillin, tetracycline and their derivatives as well as numerous other similarly acting compounds) usually represent the preferred armory for fighting bacterial infections (29). However, new problems (i.e., antibiotic resistance and residues) occur since the overuse and misuse of antibiotics (30–32); therefore, the development of new antibiotics that can effectively kill pathogenic bacteria and do not give rise to problematic metabolites is a matter of highest urgency. Given that very few compounds are currently under development or approval in the clinical setting, hence, repurposing compounds for novel application may become a productive alternate strategy for the combat against bacterial pathogens.

Melatonin, which shows a wide distribution within phylogenetically distant organisms from bacteria to humans (33), is synthesized from tryptophan and produced in pineal gland and in numerous other organs of vertebrates (e.g., gut, skin and bone marrow) (34–36). Melatonin is involved in many physiological processes, as summarized comprehensively (37, 38). In particular, this includes growth modulation and reproduction (39), immune regulation (40–43), anti-inflammation (44–47), antioxidative protection (48–51) and antioncogenic action (52, 53). Meanwhile, increasing evidence has accumulated for remarkable antibacterial actions of melatonin, including protection against damage by bacterial infections. For instance, melatonin has been reported to exert antibacterial effects in PGPB and PGNB *in vitro*, concerning *P. aeruginosa*, *A. baumannii* and *S. aureus* (54). Melatonin has also been shown to protect *Arabidopsis* and tobacco against *Pseudomonas syringae pv. tomato DC3000 (Pst DC3000)* (55), suggesting that melatonin reduces biotic stress by bacterial infection in plants. Also in mammals, several reports have demonstrated substantial effects of melatonin in protecting against or alleviating bacterial infections. In mice infected with *S. aureus* and *E. coli*, symptoms were strongly attenuated by melatonin (56). More impressive evidence has been obtained in septic mice treated with cecal ligation and puncture, in which the decisive effects of melatonin were related to inhibition of NO-mediated inflammation in connection with mitochondrial protection (57–59). Efficacy of melatonin was also multiply demonstrated in human sepsis, including that of neonates, which again underlines the excellent tolerability of this agent (60–62). Despite the emerging role of melatonin in fighting against bacterial infections, the protection mechanisms are only evident in the above-mentioned murine studies, plus additional anti-inflammatory effects that have been recently summarized (46, 63). Concerning protection against bacterial infections in plants, promising data have been obtained on the effects of stress-related genes and phytohormones, but still require further elucidation. Of note, with regard to these numerous highly valuable and beneficial organisms, which also represent an immunological quasi-self, one should melatonin not expect to generally act as an anti-bacterial agent. Moreover, various bacteria tested in this regard have been shown to synthesize themselves melatonin, sometimes in relevant quantities (64, 65). Among intestinal bacteria, the formation of melatonin was first described in *Escherichia coli* (66). Bacteria are even regarded as the evolutionary source of melatonin in eukaryotes, in connection with the uptake of α-proteobacteria and cyanobacteria as ancestors of mitochondria and plastids, respectively (67, 68). This has an important consequence for the consideration of melatonin as a bacteria-controlling agent. As many bacteria synthesize this compound or live, at least, in close community with melatonin-producing microbes, one cannot expect anti-bacterial effects at low doses of melatonin to which

Abbreviations: GPB, gram positive bacteria; GNB, gram negative bacteria; PGPB, pathogenic gram positive bacteria; PGNB, Pathogenic gram negative bacteria; *S. aureus*, *Staphylococcus aureus*; *S. pneumoniae*, *Streptococcus pneumoniae*; *B. anthracis*, *Bacillus anthracis*; *E. coli*, *Escherichia coli*; *H. pylori*, *Helicobacter pylori*; *P. aeruginosa*, *Pseudomonas aeruginosa*; *A. baumannii*, *Acinetobacter baumannii*; *K. pneumoniae*, *Klebsiella pneumoniae*; *M. tuberculosis*, *Mycobacterium tuberculosis*; *C. albicans*, *Candida albicans*; *B. subtilis*, *Bacillus subtilis*; *P. vulgaris*, *Proteus vulgaris*; MRSA, methicillin-resistant *S. aureus*; ALS, Amyotrophic lateral sclerosis; 5-MT, 5-methoxytryptamine; 6-MBOA, 6-methoxy-2-benzoxazolinone; ETEC, enterotoxigenic *Escherichia coli*; EHEC, enterohemorrhagic *E. coli*; EPEC, enteropathogenic *E. coli*; Xoo: *Xanthomonas oryzae pv. Oryzae*; AANAT, arylalkylamine-N-acetyltransferase; ASMT, N-acetylserotonin O-methyltransferase; PmCQ2, *Pasteurella multocida* serotype A strain CQ2; TB, tuberculosis; LA, Linoleic acid; LPO, peroxidation; CAT, catalase; CRP, C-reactive protein; SOD, superoxide dismutase; GSH, glutathione; NET, neutrophil extracellular trap; GM-CSF, granulocyte-monocyte colony-stimulating factor; OXI 1, oxidative signal-inducible.

these organisms are exposed anyway under physiological conditions. However, this does not hinder bacteriostatic actions at elevated concentrations and protection of hosts from damage by bacteria or by inflammatory responses induced by bacterial challenges.

In this review, we summarize the findings related to the antibacterial actions of melatonin *in vitro* and *in vivo*. Thereafter, we detailedly discuss the potential mechanisms whereby melatonin influences pathogenic bacteria as well as their deleterious effects on hosts. These concern: 1) *in vitro*: formation and detoxification of free radicals; regulation of bacterial replication by interference with the cell wall and exhaustion of intracellular substrates and micronutrients (e.g., iron); blockade of bacterial glucose and glutamate metabolism as related to bacterial cell division; 2) in plants: upregulation of genes related to phytohormone-dependent defense signaling as well as MAPK signaling; 3) in animals: involvement of multiple signaling pathways (e.g., NF-κB, STAT1 and Nrf2) related to anti-inflammatory and antioxidant control and mitochondrial protection. The review highlights the huge potential of melatonin in counteracting the growing threat of bacterial infections.

THE BASIC PHYSIOLOGY, PATHOPHYSIOLOGY AND CLINICAL SAFETY OF MELATONIN

Melatonin is a methoxyindole, mainly synthesized and secreted by the pineal gland at night under normal light and dark conditions, the main physiological functions of melatonin are related to hormonal properties (69). Melatonin transmits the information "darkness" and contributes to the synchronization of circadian oscillators (70), which is an important physiological sleep regulator in diurnal species including humans (71). In addition, melatonin is involved in numerous other physiological processes, such as regulation of blood pressure (72), glucose (73), and body temperature (74), suppression of oncogenesis (75), immune function (41), oxidative stress and inflammation (76). It is recognized that the "physiological" dose is the same as the peak plasma melatonin level at night, and the difference between the physiological and pharmacological effects of melatonin is not always clear, but is based on the consideration of the dosage rather than the duration of the hormone message (77). Indeed, the secretion of melatonin can be disturbed in the context of many pathophysiological conditions, which may increase the susceptibilities of the diseases (including infectious diseases) as well as increase the severity of symptoms or change the courses and outcomes of the diseases (78).

Of note, safety is important when melatonin is considered for clinical treatment. Clinically, 3mg, 6 mg and 10 mg melatonin showed satisfactory safety in patients (79–81). Moreover, there was no side effect of 1g/d melatonin for a month in humans (82). It has been shown that melatonin doses up to 800 mg/kg failed to cause any death in mice and it was impossible to obtain its LD50 (median lethal dose) in rats (83, 84). In study on Amyotrophic lateral sclerosis (ALS) patients, melatonin 300 mg/day was applied for 2 years and found to be safe (85). However, a trial of long-term controlled melatonin release for the treatment of sleep disorders in children with neurodevelopmental disabilities reported mild adverse effects, including seizures, cold/flu/infection, gastro-intestinal illness, agitation, anxiety and headache (86). In addition, the short- and intermediate-term administration of melatonin produced only minor adverse effects such as agitation, dizziness, headache, nausea and sleepiness in clinical studies on children; in clinical studies on adults, dizziness, paresthesias in the mouth, arms or legs, mild headaches, numbness and dyspnea aggravated; psychomotor impairment, sedation, disorientation, and amnesia in surgical patients; mild headache, increased sleepiness and skin rash in critically ill patients; daytime sleepiness in elderly (87, 88). Moreover, a recent systematic review showed that the most frequently reported melatonin adverse effects were daytime sleepiness (1.66%), dizziness (0.74%), headache (0.74%), other sleep-related adverse events (0.74%), and hypothermia (0.62%); but serious or clinical significance adverse events, including agitation, palpitations, nightmares, mood swings, fatigue, and skin irritation, were very few (89). Therefore, compared to other antibiotics, as a natural small molecule, melatonin is relatively safe with a low risk of side effects. However, the effect and safety of melatonin should be carefully monitored when melatonin is used clinically.

BACTERIOSTATIC ACTIONS OF MELATONIN *IN VITRO* AND THEIR UNDERLYING MECHANISMS

Historically, a great diversity of studies aimed to investigate whether melatonin does possess bacteriostatic actions. Initially, melatonin has only been shown to strongly reduce the lipid levels of the yeast *Candida albicans* (*C. albicans*) (90). Subsequently, one comparative study found that some pineal indoles that share a similar structure with melatonin possess antibacterial activities. For instance, 5-methoxytryptamine (5-MT), which is both a metabolite and precursor of melatonin (65), exhibits antibacterial actions against *S. aureus* and *Bacillus subtilis* (*B. subtilis*), and 6-methoxy-2-benzoxazolinone (6-MBOA) against *Proteus vulgaris* (*P. vulgaris*). However, no corresponding antibacterial effect was observed in the case of melatonin (91). Later, it has been reported that melatonin (31.25~125 mg/mL: 0.13-0.53 mM) is able to suppress the growth of PGPB (e.g., *S. aureus*) and PGNB (e.g., *P. aeruginosa* and *A. baumannii*) by reducing key intracellular substrates *in vitro* (54). Intriguingly, melatonin could also inhibit the growth of the atypical GPB *M. tuberculosis*, while the exact mechanism has not yet been identified (92). In this section, we present further evidence for antibacterial activities of melatonin against PGPBs and PGNBs *in vitro*, and we also discuss the potential mechanisms.

The antimicrobial resistance among GPBs (chiefly *S. aureus*, *Enterococcus faecium*, *Enterococcus faecalis* and *Streptococcus pneumoniae*) has become a serious threat to public health, spurring the development of new compounds against

infections (93, 94). In an early study, melatonin had been shown to moderately inhibit the growth of *S. aureus* (95). This was later also reported for the methicillin-resistant *S. aureus* (MRSA), but this required concentrations in the millimolar range (54). However, another investigation showed that the antibacterial action against *S. aureus* and/or MRSA of flouroquinolones was substantially diminished by melatonin *via* reduction of oxidative stress in the bacterial cells (96). Additional bacteria had been also tested in some studies (54, 95, 96), but melatonin's efficiency against other important PGPBs, such as *Enterococcus faecium*, *Enterococcus faecalis* and *Streptococcus pneumoniae* remains to be demonstrated.

PGNBs are also a major challenge in public health, such as *P. aeruginosa* (97) and *A. baumannii* (98). *P. aeruginosa* is one of the main opportunistic pathogenic bacteria in hospitals (99, 100), which often results in post-operative (101) or post-burn wound infections (102), bacteremia (103) and sepsis (104). Antimicrobial resistance also exists in *P. aeruginosa*, it has been discovered that melatonin has a direct suppressive role in carbapenem-resistant *P. aeruginosa* (54). CBR-4830 (a tricyclic indole analog which shows chemical similarity to melatonin), was supposed to suppress the growth of *P. aeruginosa* (105). *A. baumannii*, is a conditional pathogen (106), which often leads to pneumonia (107), meningitis (108) and bacteremia (109). It causes hospital infection frequently (110) and is often resistant to a variety of antimicrobial agents (111), bringing great difficulties to the clinical treatment. Fortunately, melatonin effectively inhibits the growth of *A. baumannii* (54), suggesting it may be suitable as adjunctive therapy in hospital infection. Similarly, we also found that melatonin could inhibit the growth of enterotoxigenic *Escherichia coli* (ETEC) and *Pasteurella multocida* serotype A strain CQ2 (PmCQ2) (unpublished data). Of note, melatonin was reported to moderately reduce surface hydrophobicity, a characteristic associated with the colonization of mammalian epithelia, inhibiting the adherence of *E.coli*; however, the reduction of surface hydrophobicity in *E. coli* remained at borderline and was only observed at high concentrations (0.2 mM) (112). In contrast, another study by the same group reported that melatonin instead increased cell surface hydrophobicity of *Neisseria meningitidis* (113). Thus, the influence of melatonin on surface hydrophobicity is obviously variable, which would require a convincing explanation, especially as the authors had tried to relate these effects to melatonin's antioxidant properties (112).

M. tuberculosis, an atypical PGPB whose cell wall is coated by mycolic acid (26), is the main pathogen of tuberculosis (TB) in humans (25, 114) and various mammals (115, 116). In addition to dormancy and persistence, drug resistance is a major obstacle in the treatment of TB (117). Therefore, it is urgent to seek for sensitive anti-TB drugs or methods to enhance the sensibility of existing antimicrobial agents. In the earlier literatures, the protective function of melatonin against *M. tuberculosis* was evaluated with isoniazid *in vitro*, experiments that did not reveal significant growth inhibitions by either isoniazid (0.005 to 0.01 μg/mL) or melatonin (0.26 nM to 2.6 nM) alone, but by a combination of isoniazid (0.005 μg/mL) and melatonin (0.01 mg/mL) (61, 92). Furthermore, the bacteriostatic capacity of melatonin was also reported for *M. tuberculosis* (3×10^7 CFU/mL, 3×10^5 CFU/mL, 3×10^3 CFU/mL) treated with different concentrations of melatonin (0.05, 0.1, 0.2 and 0.4 mg/mL) *in vitro* (118). However, the extent of inhibition was not quantified in that study. Collectively, melatonin can affect pathogenic bacteria in some cases directly (e.g., inhibition of growth and adherence), which has been summarized in **Table 1**. It is likely concluded that the effectiveness of melatonin on pathogenic bacteria is obvioulsy variable, and may depend largely on its working concentrations. Current studies have centered on melatonin's antibacterial activities on GNB, while the bacteriostatic capability of melatonin against other specific bacteria (especially antimicrobial resistant-GNB) is still poorly characterized.

As mentioned above, melatonin could exhibit bacteriostatic action against pathogenic bacteria; however, the potential mechanisms are not fully understood. Actually, there are two main hypotheses about bacteriostatic mechanisms of melatonin *in vitro*. It has been well documented that the growth of bacteria urgently requires metals, particularly free iron (121). Considering that melatonin has a high metal binding capacity, including iron, copper and zinc (122), thus, the addition of melatonin may reduce cytoplasmic availability of metal ions in bacteria to achieve the bacteriostatic effects (**Figure 1A**). Moreover, the membrane of bacteria is imbued with phospholipids (123, 124), and study has shown that melatonin can restrict the absorb of Linoleic acid (LA) used for facilitating cell proliferation (125). Therefore, melatonin may inhibit proliferation of bacteria by blocking the getting of bacterial growth factors (**Figure 1B**). These convincing findings indicate that melatonin inhibits the bacterial growth may through reducing intracellular substrates (54). Interestingly, a recent study declared that melatonin inhibits bacterial growth and proliferation by regulating the expression of genes associated with cell division (**Figure 1C**) and suppressing contents as well as activities of metabolism-related enzymes (**Figure 1D**) (119). These interesting results imply that melatonin could affect bacteria physiological condition by intrinsic molecular mechanisms; however, the experimental validation is still needed. Of note, our recent findings also demonstrated that melatonin exerts antibacterial activity against GNB (e.g., *Klebsiella*, *Pasteurella multocida* and *Pseudomonas aeruginosa*) through specifically inhibiting the activity of bacterial citrate synthase (**Figure 1E**), and the combination of colistin with melatonin enhances bacterial outer membrane permeability, oxidative damage and inhibits the effect of efflux pumps (**Figure 1F**) (126).

BACTERIOSTATIC ACTIONS OF MELATONIN *IN VIVO* AND THEIR UNDERLYING MECHANISMS

Melatonin not only has antibacterial effect *in vitro*, but also plays a significant role in the clinical prevention and treatment of

TABLE 1 | The antibacterial action of melatonin *in vitro* on different bacteria.

Bacteria	Dosage	Time	Effects	Ref.
Carbapenem-resistant *P. aeruginosa*	31.25 or 125 μg/mL (0.13 or 0.53 mM)	24 or 48 h	Inhibition of carbapenem-resistant *P. aeruginosa* growth	(54)
Carbapenem-resistant *A. baumannii*	31.25 or125 μg/mL (0.13 or 0.53 mM)	24 or 48h	Inhibition of crbapenem-resistant *A. baumannii* growth	(54)
Methicillin-resistant *S. aureus*	125 or 250 μg/mL (0.53 or 1.07 mM)	24 or 48h	Inhibition of methicillin-resistant *S. aureus* growth	(54)
S. aureus ATCC 29123	125 or 250 μg/mL (0.53 or 1.07 mM)	24 or 48h	Inhibition of *S. aureus* (ATCC 29123) growth	(54)
P. aeruginosa ATCC 27853	125 or 250 μg/mL (0.53 or 1.07 mM)	24 or 48h	Inhibition of *P.aeruginosa* (ATCC 27853) growth	(54)
M. tuberculosis H37Rv	26.0 nM 0.01 to 10 mM	unknown	Inhibition of *M. tuberculosis* H37Rv growth The antibacterial efficacy of melatonin with isoniazid increased at least a threefold	(92)
M. tuberculosis bovis BCG	0.13 to 10 mM	unknown	Inhibitin of *M. bovis* BCG growth	(92)
Multidrug-resistant M. tuberculosis (TBRI 40 and TBRI 204)	0.01 to 10 mM	unknown	Inhibition of multidrug-resistant *M. tuberculosis* (TBRI 40 and TBRI 204) growth	(92)
Xanthomonas oryzae pv. Oryzae (Xoo)	200 μg/mL	12, 21 or 24 h	Inhibition of Xoo proliferation, motility and biofilm formation Alteration of Xoo cells length Downregulation of mRNA expression of genes involved in cell division, carbohydrate metabolism and amino acid metabolism	(119)
Xanthomonas oryzae pv. Oryzicola Xoc)	200 μg/mL	24 h	Inhibition of Xoc growth, the motility and biofilm formation Reduction of mRNA expression of genes related to toxin and cell division	(120)

P. aeruginosa, Pseudomonas aeruginosa; A. baumannii, Acinetobacter baumannii; S. aureus, Staphylococcus aureus; M. tuberculosis, Mycobacterium tuberculosis; B. anthracis, Bacillus anthracis.

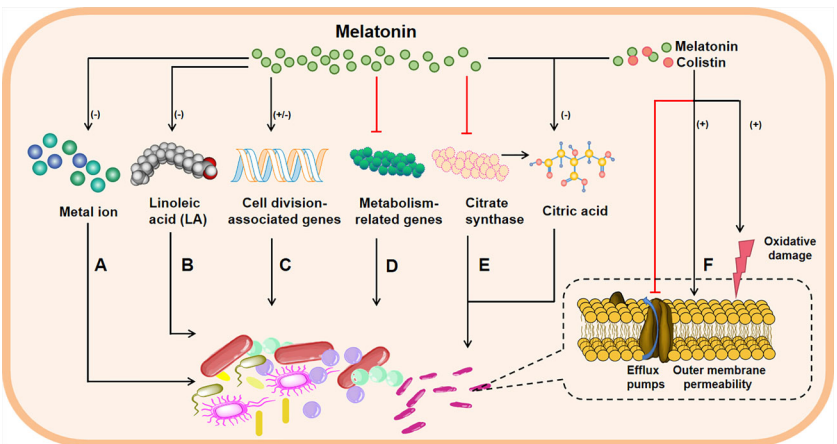


FIGURE 1 | The possible bacteriostatic mechanisms of melatonin *in vitro*. Melatonin inhibits the growth of bacteria through these avenues: reducing cytoplasmic availability of metal ion **(A)**; interfering cell wall formation, for example, melatonin restricts the absorb of Linoleic acid (LA), which makes up the cell wall, thus limiting cell proliferation **(B)**; melatonin can also regulate the expressions of genes associated with cell division **(C)** or suppress the content and activity of metabolism-related enzymes **(D)** to inhibit bacterial growth and proliferation; melatonin resists against Gram-negative bacteria through inhibiting bacterial citrate synthase and reducing the synthesis of citric acid **(E)**, besides, when melatonin is combination with colistin, bacterial outer membrane permeability and oxidative damage are enhanced, and the effect of efflux pumps is inhibited **(F)**, leading to increased bacteria damage. Note: minus in parentheses represents decrease; plus in parentheses represents increase; and the red line represents inhibition; the black arrow indicates activation.

bacterial infections *in vivo* (61). The inhibitory effects of melatonin *in vivo* includes both on PGPB [e.g., *S. aureus* (56) and *S. pneumoniae* (127)] and PGNB [e.g., *E.coli* (128), *H. Pylori* (129) and *K. pneumonia* (130)]. For example, in many GNB-infected animal models (e.g., sepsis), melatonin has a favorable effect in improving survival rates, ameliorating tissue damage and reducing levels of pro-inflammation mediators (e.g., TNF-α and IFN-γ), and increasing levels of anti-inflammation mediators (e.g., IL-10) (131, 132). Notably, various signaling have been described to shape bacterial infection *in vivo* by melatonin, including NF-κB, Nrf2, NLRP3 and ROS pathways. In this section, firstly, we present the evidence from studies that have used melatonin to resist bacterial infections *in vivo*. Subsequently, we illustrate the possible mechanisms.

S. aureus always causes many serious infections in human (133, 134). Virtually, melatonin not only inhibits the growth of *S. aureus in vitro*, but also has significant defensive effects against *S. aureus*-induced infection *in vivo*. For example, melatonin reduces lipid peroxidation (LPO), catalase (CAT), neutrophil recruitment, and TNF-α, IFN-γ, IL-6, iNOS, COX-2 and C-reactive protein (CRP), while increases superoxide dismutase (SOD) and glutathione (GSH) in animals infected by *S. aureus* (5×10^6 CFU/mL) (56). The pathogenicity of *S. pneumoniae* is second only to *S. aureus* in pyogenic cocci (135), which triggers major lobe pneumonia (136), meningitis (137), bronchitis (138). Fortunately, it has found that melatonin has a certain inhibitory effect on the infection of *S. pneumonia* (95). These aforementioned findings indicate that melatonin can target GPB to alleviate infections *in vivo*. However, it has been shown that melatonin therapy fails to reduce neuronal injury in *S. pneumoniae*-infected rabbit model, the possible reason may due to the 12 h delay in the administration of melatonin after the infection (139).

Historically, *E. coli* has been regarded as an integral part of the normal intestinal flora (140), and was considered to be non-pathogenic bacteria (141). Nevertheless, as the research moves along, some special serotypes of *E. coli* [e.g., ETEC (142), enterohemorrhagic *E. coli* (EHEC) (143) and enteropathogenic *E. coli* (EPEC) (144)] are shown to be pathogenic to humans and animals (especially infants and young animals) (145), causing severe diarrhea (146) and sepsis (147). Some studies have found that melatonin has a bacteriostatic effect in the animals infected by *E. coli*, for instance, melatonin reduces LPO, CAT, neutrophil recruitment, and TNF-α, IFN-γ, IL-6, iNOS, COX-2 and CRP, while increases SOD and GSH in animals infected by *E. coli* (2.5×10^7 CFU/mL) (56, 148). *H. Pylori* is the only microbial species known to survive in the human stomach (149) to induce gastritis (150), gastrointestinal hemorrhage (151) and gastric lymphoma (152). It has been revealed that *H. Pylori* infection inhibits gastric mucosal melatonin synthesizing enzymes [e.g., arylalkylamine-N-acetyltransferase (AANAT) and N-acetylserotonin O-methyltransferase (ASMT)] expression (153). Interestingly, melatonin facilitates *H. pylori* eradication in patients with gastroduodenal ulcer by omeprazole treatment (154–156), indicating melatonin can be used as an adjuvant clinical drug against *H. Pylori* infection. Furthermore, *K. pneumonia* is also a member of PGNB, isolated from the sputum of patients with pneumonia (157), mainly leads to pneumonia (158), septicemia (159) or bacteremia (160), meningitis (161) and peritonitis (162). An experimental study showed that the supply of 100 mg/kg of melatonin can reduce pro-inflammatory cytokines, inhibit microglial activation, and counteract neurocognitive damage in *K. pneumoniae*-infected rats (130). Likewise, we also found that melatonin can inhibit macrophage-mediated excessive inflammatory responses in *Pasteurella multocida* (PmCQ2)-infected mice (unpublished data). Of note, like GPB *S. pneumoniae*, the effect of melatonin on inactivated *Pasteurella multocida* (P52 strain) vaccine-mediated immune responses is time-dependent evidenced by exogenous melatonin administration at 4 h post vaccination augments immune responses in rats in comparison to 16 h post vaccination (163, 164).

Notably, melatonin has been demonstrated to increase survival rates and improve organ function in several sepsis models (165, 166). The oxidative imbalance is one of the characteristics of sepsis (167), and mitochondria play key roles in regulating sepsis-related redox dysregulation (168). Mechanistically, melatonin can alleviate sepsis symptoms by preventing mitochondria dysfunction *via* ROS/RNS scavenging (169) and many other pathways (e.g., intra-mitochondrial SIRT3 and MAPK/ERK pathway) (170–176). Inflammation is essential for the host to resist infection by pathogenic bacteria, however, excessive inflammation is another characteristic of the initial stage of sepsis, leading to organ dysfunction and eventually death (177, 178).

Melatonin as a signal molecule of stress can be induced by the pathogenic (but not the beneficial) bacteria invasion and the increased melatonin level in hosts can improve the protective effects or tolerance to the bacteria (179). In addition to inhibiting pathogenic bacteria, melatonin has a beneficial effect on intestinal flora (180, 181). For example, melatonin reprogramming of gut microbiota improves lipid dysmetabolism to prevent obesity in mice (182–185). Moreover, melatonin contributes to reshape gut microbiota to alleviate neuroinflammation and metabolic disorder in DSS-induced depression rats (186). Furthermore, melatonin ameliorates ochratoxin A-induced liver inflammation, oxidative stress and mitophagy involving in intestinal microbiota in mice (187). Altogether, as summarize in **Table 2**, melatonin may function as a novel compound to resist pathogenic bacterial infections *in vivo*. However, the defensive effects of melatonin against pathogenic bacteria are likely dose- and/or time-dependent.

Notably, the mechanisms whereby melatonin exerts bacteriostatic action *in vivo* are tightly associated with the immune responses, for example, during polymicrobial infection, melatonin treatment could promote the development of the neutrophil extracellular trap (NET), whereas inhibits the phagocytic activities of neutrophils (188). Indeed, mounting evidences suggest that melatonin always exerts its physiological effects *via* its receptors (e.g., MT1 and MT2). It has been discovered that melatonin is able to improve the survival rate of polymicrobial sepsis of mice through MT1 and MT2 receptor (**Figure 2A**) (189). Melatonin also alleviates acute lung injury induced by LPS *via* inhibiting the activation of NLRP3 inflammasome (**Figure 2B**) (190). Melatonin could dose-dependently reduce pro-inflammatory cytokine TNF-α, IL-6 and IL-8, increase anti-inflammatory cytokine IL-10 and improve survival, which are associated with p38MAPK and NF-κB signaling pathway (173, 191–195) (**Figure 2C**). Moreover, melatonin could block LPS (which is from *P. intermedia*)-induced activation of NF-κB signaling (**Figure 2D**) and STAT1 pathway (**Figure 2E**), thereby inhibiting the production of inflammatory mediators (e.g., NO and IL-6) (196, 197). Likewise, it has found that melatonin can reduce pro-inflammatory mediators [e.g., IL-1β, IL-6, NO and granulocyte-monocyte colony-stimulating factor (GM-CSF)], while increase anti-inflammatory cytokine (e.g., IL-10) by

TABLE 2 | The antibacterial action of melatonin *in vivo* infected with different bacteria.

Bacteria	Dosage	Time	Effects	Ref.
S. aureus	10 mg/kg	At 17:00, 17:30, 18:00	Reducing expression of LPO, CAT, iNOS, COX-2 and production of TNF-α, IFN-γ, IL-6, CRP, increasing the production SOD and GSH	(56)
S. pneumoniae	2 mg/mL	40 h	Suppressing bacterial growth at a high concentration	(95)
E. coli	10 mg/kg or 1nM	At 17:00, 17:30 and 18:00 or 70 s	Reducing expression of LPO, CAT, iNOS, COX-2 and production of TNF-α, IFN-γ, IL-6, CRP, increasing the production SOD and GSH	(56, 148)
H. Pylori	5 mg or 3 mg	21 days	Increasing efficacy of *H. pylori* elimination, Accelerating duodenal ulcer recovery	(154–156)
K. pneumonia	100 mg/kg	24 h	Counteracting neurocognitive damage inhibiting microglial activation, and reducing pro-inflammatory cytokine levels	(130)
Pasteurella multocida (P52)	100mg/kg	4 h	Exogenous melatonin at 4 h post vaccination augments immune responses in rats.	(163)
Pasteurella multocida (PmCQ2)	30 mg/kg, 60 mg/kg, 120mg/kg	12 h, 16 h, 24 h, 32 h	Inhibiting macrophage-mediated excessive inflammatory responses	Unpublished

S. aureus, Staphylococcus aureus; S. pneumonia, Streptococcus pneumonia; E. coli, Escherichia coli; H. Pylori, Helicobacter Pylori; K. pneumonia, Klebsiella pneumonia; LPO, lipid peroxidation; CAT, catalase; iNOS, inducible nitric oxide synthase, CRP, C-reactive protein; SOD, superoxide dismutase; GSH, glutathione.

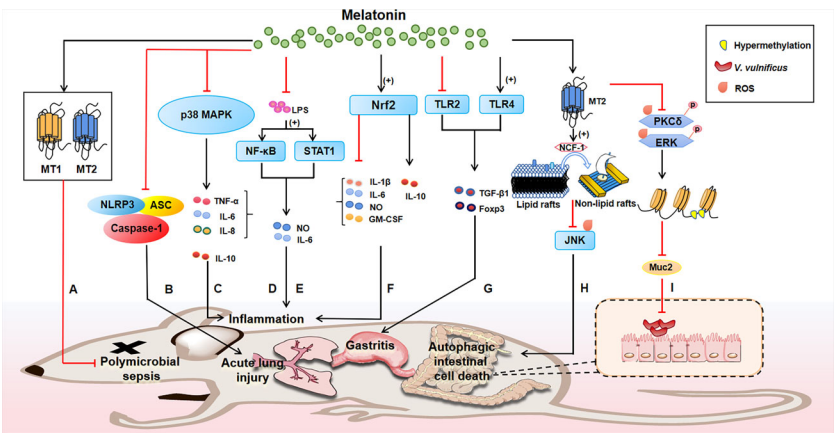


FIGURE 2 | The bacteriostatic mechanisms of melatonin in animals. Melatonin receptors (e.g., MT1 and MT2) play a great role in mediating the functions of melatonin. Melatonin reduces polymicrobial sepsis through MT1 and MT2, thus improving the survival rate of mice **(A)**; notably, the mechanisms whereby melatonin exerts bacteriostatic action *in vivo* are tightly associated with the immune responses, for instance, melatonin inhibits NLRP3 inflammasome to alleviate acute lung injury **(B)**; melatonin reduces pro-inflammatory cytokines, increases anti-inflammatory cytokines and improves survival through p38MAPK signaling pathway **(C)**; melatonin blocks LPS-induced activation of NF-κB **(D)** and STAT1 **(E)**, thus inhibiting the production of inflammatory factors to modulate inflammation. Likewise, suppression of inflammation also occurs when melatonin activates Nrf2, evidenced by reduced pro-inflammatory mediators (e.g., IL-1β, IL-6, NO and GM-CSF) and increased anti-inflammatory cytokine (e.g., IL-10) **(F)**; melatonin treatment can target TLR to alleviate *H. pylori*-induced gastritis by promoting TLR4 and inhibiting TLR2 to regulate TGF-β1 and Foxp3 expression **(G)**; of note, melatonin could be a therapeutic alternative agent to fight bacterial infections due to its antioxidant function. For example, melatonin signaling *via* MT2 promotes NCF-1 recruitment from lipid rafts to non-lipid rafts to block the ROS-mediated JNK pathway, preventing autophagic intestinal cell death **(H)**; moreover, MT2 signaling inhibits the ROS-mediated phosphorylation of PKCδ and ERK to reduce region-specific hypermethylation in the Muc2 promoter, combating *V. vulnificus* infection **(I)**. Note: plus in parentheses represents increase; and the red line represents inhibition; the black arrow indicates activation.

activating Nrf2 pathway (**Figure 2F**) (198). Actually, melatonin treatment can also alleviate *H. pylori*-induced gastritis through regulating TGF-β1 and Foxp3 expression *via* the suppression of TLR2 and activation of TLR4 (**Figure 2G**) (129), although the molecular target of melatonin in the TLR signaling warrants further investigation.

Moreover, it should be noted that melatonin could be a therapeutic alternative agent to fight bacterial infections due to its antioxidant function. Intriguingly, melatonin inhibits apoptotic cell dealth in colonic epithelial cells induced by *Vibrio vulnificus* VvhA *via* MT2 (199). Mechanistically, melatonin signaling *via* MT2 stimulates NCF-1 recruitment

into non-lipid rafts from lipid rafts to block the ROS-mediated JNK pathway, preventing rVvhA-induced apoptosis and autophagic intestinal cell death (**Figure 2H**). Similarly, melatonin treatment maintains the expression level of Muc2 in the intestine of *V. vulnificus*-infected mouse. Mechanistically, melatonin inhibits the ROS-mediated phosphorylation of PKCδ and ERK responsible for region-specific hypermethylation in the Muc2 promoter *via* MT2 receptor, restoring the level of Muc2 production in intestinal epithelial cells to resist *V. vulnificus* infection (**Figure 2I**) (200).

Collectively, melatonin could exert its bacteriostatic action *in vivo* by various potential mechanisms, including NF-κB, STAT1, Nrf2, TLR2/4, and ROS signaling (**Figure 2**). These aforementioned findings may provide promising strategies for controlling many diseases of public health importance. It should not be neglected that melatonin has a significant antibacterial effect *in vitro*; thus, whether the powerful effect of melatonin *in vivo* is also directly inhibiting bacterial growth remains further exploration.

BACTERIOSTATIC ACTIONS OF MELATONIN IN PLANTS AND THEIR UNDERLYING MECHANISMS

In addition to the significant bacteriostatic functions of melatonin *in vitro* and in animals, melatonin also exerts similar function against pathogenic bacterial infections in plants (201, 202). It has found that melatonin treatment inhibits the growth, motility and capsule formation of the bacterium *Xanthomonas oryzae pv. oryzae* (Xoo) (119), which leads to bacterial blight in rice (203, 204). Melatonin increases the resistance to *Verticillium dahlia* in cotton by regulating lignin and gossypol biosynthesis (205), although the molecular mechanisms are still not available. Authentically, it has been demonstrated that Serotonin N-acetyltransferase (SNAT)-deficient *Arabidopsis* shows lower melatonin levels and exhibits susceptibility to pathogen infection (206). Conformably, melatonin can trigger defense responses against *Pst* DC3000 infection in *Arabidopsis* and/or tobacco (55, 207, 208). Mechanistically, melatonin-induced rise of NO that favors in the expression of salicylic acid (SA)-related genes (e.g., *AtEDS1*, *AtPAD4*, *AtPR1*, *AtPR2* and *AtPR5*), conferring improved disease resistance against *Pst* DC3000 infection in *Arabidopsis* (**Figure 3**); however, the beneficial effects of melatonin could be jeopardized by using a NO scavenger (cPTIO) and/or lost in NO-deficient mutants of *Arabidopsis* (209). Furthermore, it has been discovered that melatonin can active MPK3 and MPK6 signaling (members of MAPKs), which are independent of G-protein and Ca^{2+} signaling, and the inhibition of MPK3 and/or MPK6 induces reduced expression of defense and pathogen resistance-related genes (e.g. *PR1*, *PR2*, and *PR5*) (55). Indeed, melatonin activates MPK3 and MPK6 *via* four MKKs (i.e., MKK4/5/7/9) (210), and MAPKKK 3 and OXI 1 (oxidative signal-inducible 1) kinases are responsible for triggering

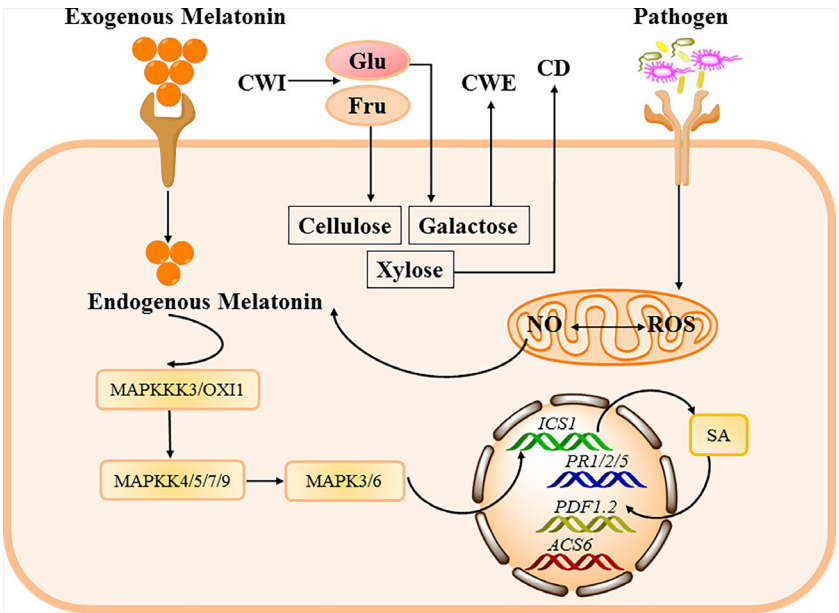


FIGURE 3 | The bacteriostatic mechanisms of melatonin in plants. Antibacterial mechanisms against plant pathogenic bacteria are characterized by up-regulation of defense genes such as *plant defensin1.2* (*PDF1.2*), *plant resistance 1/2/5* (*PR1/2/5*), and *1-aminocyclopropane-1-carboxylate synthase 6* (*ACS6*) through several signal transduction pathways, including augmentation of NO levels in plants, which collaborates with melatonin in up-regulating SA. Moreover, melatonin can stimulate mitogen-activated protein kinases (MAPKs) cascades, which in turn up-regulate SA biosynthesis gene *isochorismate synthase 1* (*ICS1*). Additionally, high cell wall invertase (CWI) activity within melatonin-treated *Arabidopsis* leads to improved cell wall strengthening and callose-depositing factors (cellulose, xylose, and galactose).

melatonin-induced defense signaling pathways (211). Therefore, melatonin could mediate pathogen resistance in *Arabidopsis* and tobacco by activating MAPKs signaling *via* MKK4/5/7/9-MPK3/6 cascades through the activation of MAPKKK 3 and OXI 1 (**Figure 3**). In conclusion, melatonin plays a critical bacteriostatic role in *Pst* DC3000-infected *Arabidopsis* by MAPKs pathway. Moreover, melatonin could improve cell wall strengthening and callose-depositing factors (cellulose, xylose, and galactose) by increasing cell wall invertase (CWI) activity in *Arabidopsis* infected with *Pst. DC3000* (**Figure 3**) (207). However, whether melatonin could function as a signaling molecule in modulating defense responses of other plants infected by various pathogenic bacteria are still poorly defined.

CONCLUDING REMARKS

Melatonin has multifarious functions, like circadian rhythm regulation (212, 213); anti-inflammatory/anti-tumor effects (214, 215); and, with particular relevance to this article, anti-bacterial function. Here, we summarize melatonin can directly influence bacteria *in vitro* (e.g., inhibition of growth) by reducing intracellular substrates. Considering that intestinal bacteria, *Enterobacter aerogenes*, responds to the melatonin by an increase in swarming activity, which is expressed rhythmically (216); thus, it is meaningful to further investigate the potential effects of melatonin in synchronizing bacterial rhythms *in vitro*. Notably, melatonin resists pathogenic bacterial infections *in vivo* by various pathways, such as NF-κB, TLR2/4, and ROS. Other pathways seem to get involved as well, but further experimental validation is needed. Furthermore, intestinal microbiota play a crucial role in the progress of different diseases, including bacterial infections *in vivo* (183, 217); therefore, it is necessary to further investigate the intestinal microbiota-mediated defensive roles of melatonin in attenuating bacterial infections *in vivo*. Melatonin serves as a signaling molecule to resist bacterial infections in *Arabidopsis* mainly through MAPK pathway, whether other specific pathways connecting to the bacteriostatic actions of melatonin in other plants or even other specific bacteria also remain an open question.

In addition to its significant antibacterial effect, it is thought that melatonin plays crucial roles in the fighting viral infections (61). Melatonin was found to effective against Ebola hemorrhagic shock syndrome by inhibiting Rho/ROCK signaling (218). Melatonin was also shown to protect mice infected with the Venezuelan equine encephalitis virus (VEEV) by reducing viral loads, brain apoptosis and oxidative stress (219, 220). Additionally, melatonin also was reported to exert protective and therapeutic effects against hemorrhagic disease virus (221), respiratory syncytial virus (RSV) (222), aleutian disease virus (223) and influenza virus (224). Recently, melatonin was proposed to be a potential candidate drug as an adjuvant treatment for patients with COVID-19 based on its antioxidant, anti-inflammatory and immunomodulatory properties (81, 225–227).

Overall, this review highlights melatonin as a novel and feasible preventive and therapy to tackle the increasing threat by bacterial infections. Based on the various physiological/pharmacological functions of melatonin and its significant anti-pathogenic effects, melatonin can be possibly used as clinical agent against pathogens and even viruses in the future.

AUTHOR CONTRIBUTIONS

FH, XW, and YX designed and wrote the review article. PL, SC, RH, and YX revised the review article. FH, XW, QZ, YL, YY, PL, SC, and YP helped with designing figures and finding relevant literatures. YX approved the final manuscript. All authors contributed to the article and approved the submitted version.

FUNDING

This work was supported by Ministry of China Agriculture & Rural Affairs and Finance: the National Modern Agricultural Industry Technology System (Beef/Yak Cattle, CARS-37), and Chongqing Science & Technology Commission (cstc2017jcyjAX0288).

ACKNOWLEDGMENTS

Our profound admiration and respect go to researchers in this field and in our laboratories, for their dedication and hard work. We apologize to scientists whose work is in this field if their papers are not cited owing to space limitations.

REFERENCES

1. Trdá L, Boutrot F, Claverie J, Brulé D, Dorey S, Poinssot B. Perception of Pathogenic or Beneficial Bacteria and Their Evasion of Host Immunity: Pattern Recognition Receptors in the Frontline. *Front Plant Sci* (2015) 6:219. doi: 10.3389/fpls.2015.00219
2. Jawad KI, Razavi SH. Characterization of Lactobacillus Plantarum as a Potential Probiotic In Vitro and Use of a Dairy Product (Yogurt) as Food Carrier. *Appl Food Biotechnol* (2017) 4:11–8. doi: 10.22037/afb.v4i1.13738
3. Kok CR, Hutkins R. Yogurt and Other Fermented Foods as Sources of Health-Promoting Bacteria. *Nutr Rev* (2018) 76:4–15. doi: 10.1093/nutrit/nuy056
4. Broadbent JR, Barnes M, Brennand C, Strickland M, Houck K, Johnson ME, et al. Contribution of Lactococcus Lactis Cell Envelope Proteinase Specificity to Peptide Accumulation and Bitterness in Reduced-Fat Cheddar Cheese. *Appl Environ Microbiol* (2002) 68:1778–85. doi: 10.1128/aem.68.4.1778-1785.2002
5. Abdelfatah EN, Mahboub HHH. Studies on the Effect of Lactococcus Garvieae of Dairy Origin on Both Cheese and Nile Tilapia (O. Niloticus). *Int J Vet Sci Med* (2018) 6:201–7. doi: 10.1016/j.ijvsm.2018.11.002
6. Mustapha NA, Hu A, Yu CP, Sharuddin SS, Ramli N, Shirai Y, et al. Seeking Key Microorganisms for Enhancing Methane Production in Anaerobic Digestion of Waste Sewage Sludge. *Appl Microbiol Biotechnol* (2018) 102:5323–34. doi: 10.1007/s00253-018-9003-8
7. Bampidis V, Azimonti G, Bastos ML, Christensen H, Dusemund B, Kos Durjava M, et al. Safety and Efficacy of Monosodium L-Glutamate Monohydrate Produced by Corynebacterium Glutamicum KCCM 80188 as a Feed Additive for All Animal Species. *Efsa J* (2020) 18:e06085. doi: 10.2903/j.efsa.2020.6085

8. Baek JH, Kim KH, Moon JY, Yeo SH, Jeon CO. Acetobacter Oryzoeni Sp. Nov., Isolated From Korean Rice Wine Vinegar. *Int J Syst Evol Microbiol* (2020) 70:2026–33. doi: 10.1099/ijsem.0.004008
9. Gueniche A, Benyacoub J, Philippe D, Bastien P, Kusy N, Breton L, et al. Lactobacillus Paracasei CNCM I-2116 (ST11) Inhibits Substance P-Induced Skin Inflammation and Accelerates Skin Barrier Function Recovery In Vitro. *Eur J Dermatol* (2010) 20:731–7. doi: 10.1684/ejd.2010.1108
10. Barko PC, McMichael MA, Swanson KS, Williams DA. The Gastrointestinal Microbiome: A Review. *J Vet Intern Med* (2018) 32:9–25. doi: 10.1111/jvim.14875
11. Huang M, Cai S, Su J. The Pathogenesis of Sepsis and Potential Therapeutic Targets. *Int J Mol Sci* (2019) 20:5376. doi: 10.3390/ijms20215376
12. Marangu D, Zar HJ. Childhood Pneumonia in Low-and-Middle-Income Countries: An Update. *Paediatr Respir Rev* (2019) 32:3–9. doi: 10.1016/j.prrv.2019.06.001
13. Koelman DLH, Brouwer MC, van de Beek D. Targeting the Complement System in Bacterial Meningitis. *Brain* (2019) 142:3325–37. doi: 10.1093/brain/awz222
14. Tripathi N, Sapra A. Gram Staining. In: *Statpearls*. Treasure Island (FL: StatPearls Publishing (2021). Copyright © 2021, StatPearls Publishing LLC.
15. Wang W, Wang Y, Lin L, Song Y, Yang CJ. A Tridecaptin-Based Fluorescent Probe for Differential Staining of Gram-Negative Bacteria. *Anal Bioanal Chem* (2019) 411:4017–23. doi: 10.1007/s00216-018-1465-0
16. Becerra SC, Roy DC, Sanchez CJ, Christy RJ, Burmeister DM. An Optimized Staining Technique for the Detection of Gram Positive and Gram Negative Bacteria Within Tissue. *BMC Res Notes* (2016) 9:216. doi: 10.1186/s13104-016-1902-0
17. Jenul C, Horswill AR. Regulation of Staphylococcus Aureus Virulence. *Microbiol Spectr* (2019) 7:1–21. doi: 10.1128/microbiolspec.GPP3-0031-2018
18. Kadioglu A, Weiser JN, Paton JC, Andrew PW. The Role of Streptococcus Pneumoniae Virulence Factors in Host Respiratory Colonization and Disease. *Nat Rev Microbiol* (2008) 6:288–301. doi: 10.1038/nrmicro1871
19. Norris MH, Kirpich A, Bluhm AP, Zincke D, Hadfield T, Ponciano JM. Convergent Evolution of Diverse Bacillus Anthracis Outbreak Strains Toward Altered Surface Oligosaccharides That Modulate Anthrax Pathogenesis. *PLoS Biol* (2020) 18:e3001052. doi: 10.1371/journal.pbio.3001052
20. Rueter C, Bielaszewska M. Secretion and Delivery of Intestinal Pathogenic Escherichia Coli Virulence Factors Via Outer Membrane Vesicles. *Front Cell Infect Microbiol* (2020) 10:91. doi: 10.3389/fcimb.2020.00091
21. Ji J, Yang H. Using Probiotics as Supplementation for Helicobacter Pylori Antibiotic Therapy. *Int J Mol Sci* (2020) 21:1136. doi: 10.3390/ijms21031136
22. Azam MW, Khan AU. Updates on the Pathogenicity Status of Pseudomonas Aeruginosa. *Drug Discov Today* (2019) 24:350–9. doi: 10.1016/j.drudis.2018.07.003
23. Harding CM, Hennon SW, Feldman MF. Uncovering the Mechanisms of Acinetobacter Baumannii Virulence. *Nat Rev Microbiol* (2018) 16:91–102. doi: 10.1038/nrmicro.2017.148
24. Martin RM, Bachman MA. Colonization, Infection, and the Accessory Genome of Klebsiella Pneumoniae. *Front Cell Infect Microbiol* (2018) 8:4. doi: 10.3389/fcimb.2018.00004
25. Le Chevalier F, Cascioferro A, Majlessi L, Herrmann JL, Brosch R. Mycobacterium Tuberculosis Evolutionary Pathogenesis and its Putative Impact on Drug Development. *Future Microbiol* (2014) 9:969–85. doi: 10.2217/fmb.14.70
26. Fu LM, Fu-Liu CS. Is Mycobacterium Tuberculosis a Closer Relative to Gram-Positive or Gram-Negative Bacterial Pathogens? *Tuberculosis (Edinb)* (2002) 82:85–90. doi: 10.1054/tube.2002.0328
27. Jones KE, Patel NG, Levy MA, Storeygard A, Balk D, Gittleman JL, et al. Global Trends in Emerging Infectious Diseases. *Nature* (2008) 451:990–3. doi: 10.1038/nature06536
28. Morens DM, Folkers GK, Fauci AS. The Challenge of Emerging and Re-Emerging Infectious Diseases. *Nature* (2004) 430:242–9. doi: 10.1038/nature02759
29. Lewis K. Platforms for Antibiotic Discovery. *Nat Rev Drug Discov* (2013) 12:371–87. doi: 10.1038/nrd3975
30. Neu HC. The Crisis in Antibiotic Resistance. *Science* (1992) 257:1064–73. doi: 10.1126/science.257.5073.1064
31. Martínez JL. Antibiotics and Antibiotic Resistance Genes in Natural Environments. *Science* (2008) 321:365–7. doi: 10.1126/science.1159483
32. Bush K, Courvalin P, Dantas G, Davies J, Eisenstein B, Huovinen P, et al. Tackling Antibiotic Resistance. *Nat Rev Microbiol* (2011) 9:894–6. doi: 10.1038/nrmicro2693
33. Cipolla-Neto J, Amaral FGD. Melatonin as a Hormone: New Physiological and Clinical Insights. *Endocr Rev* (2018) 39:990–1028. doi: 10.1210/er.2018-00084
34. Rusanova I, Martínez-Ruiz L, lorido J, Rodríguez-Santana C, Guerra-Librero A, Acuña-Castroviejo D, et al. Protective Effects of Melatonin on the Skin: Future Perspectives. *Int J Mol Sci* (2019) 20:4948. doi: 10.3390/ijms20194948
35. Tordjman S, Chokron S, Delorme R, Charrier A, Bellissant E, Jaafari N, et al. Melatonin: Pharmacology, Functions and Therapeutic Benefits. *Curr Neuropharmacol* (2017) 15:434–43. doi: 10.2174/1570159x14666161228122115
36. Wang B, Wen H, Smith W, Hao D, He B, Kong L. Regulation Effects of Melatonin on Bone Marrow Mesenchymal Stem Cell Differentiation. *J Cell Physiol* (2019) 234:1008–15. doi: 10.1002/jcp.27090
37. Hardeland R, Cardinali DP, Srinivasan V, Spence DW, Brown GM, Pandi-Perumal SR. Melatonin–a Pleiotropic, Orchestrating Regulator Molecule. *Prog Neurobiol* (2011) 93:350–84. doi: 10.1016/j.pneurobio.2010.12.004
38. Pandi-Perumal SR, Srinivasan V, Maestroni GJ, Cardinali DP, Poeggeler B, Hardeland R. Melatonin: Nature's Most Versatile Biological Signal? *FEBS J* (2006) 273:2813–38. doi: 10.1111/j.1742-4658.2006.05322.x
39. Reiter RJ. The Pineal and its Hormones in the Control of Reproduction in Mammals. *Endocr Rev* (1980) 1:109–31. doi: 10.1210/edrv-1-2-109
40. Plaimee P, Khamphio M, Weerapreeyakul N, Barusrux S, Johns NP. Immunomodulatory Effect of Melatonin in SK-LU-1 Human Lung Adenocarcinoma Cells Co-Cultured With Peripheral Blood Mononuclear Cells. *Cell Prolif* (2014) 47:406–15. doi: 10.1111/cpr.12119
41. Xia Y, Chen S, Zeng S, Zhao Y, Zhu C, Deng B, et al. Melatonin in Macrophage Biology: Current Understanding and Future Perspectives. *J Pineal Res* (2019) 66:e12547. doi: 10.1111/jpi.12547
42. Ren W, Liu G, Chen S, Yin J, Wang J, Tan B, et al. Melatonin Signaling in T Cells: Functions and Applications. *J Pineal Res* (2017) 62:e12394. doi: 10.1111/jpi.12394
43. Tan D-X, Hardeland R. Potential Utility of Melatonin in Deadly Infectious Diseases Related to the Overreaction of Innate Immune Response and Destructive Inflammation: Focus on COVID-19. *Melatonin Res* (2020) 3:120–43. doi: 10.32794/mr11250052
44. Mauriz JL, Collado PS, Veneroso C, Reiter RJ, González-Gallego J. A Review of the Molecular Aspects of Melatonin's Anti-Inflammatory Actions: Recent Insights and New Perspectives. *J Pineal Res* (2013) 54:1–14. doi: 10.1111/j.1600-079X.2012.01014.x
45. Álvarez-Sánchez N, Cruz-Chamorro I, Díaz-Sánchez M, Sarmiento-Soto H, Medrano-Campillo P, Martínez-López A, et al. Melatonin Reduces Inflammatory Response in Peripheral T Helper Lymphocytes From Relapsing-Remitting Multiple Sclerosis Patients. *J Pineal Res* (2017) 63:e12394. doi: 10.1111/jpi.12442
46. Hardeland R. Aging, Melatonin, and the Pro- and Anti-Inflammatory Networks. *Int J Mol Sci* (2019) 20:1223. doi: 10.3390/ijms20051223
47. Yawoot N, Govitrapong P, Tocharus C. Ischemic Stroke, Obesity, and the Anti-Inflammatory Role of Melatonin. *Biofactors* (2021) 47:41–58. doi: 10.1002/biof.1690
48. Reiter RJ, Tan DX, Burkhardt S. Reactive Oxygen and Nitrogen Species and Cellular and Organismal Decline: Amelioration With Melatonin. *Mech Ageing Dev* (2002) 123:1007–19. doi: 10.1016/s0047-6374(01)00384-0
49. Reiter RJ, Tan DX, Mayo JC, Sainz RM, Leon J, Czarnocki Z. Melatonin as an Antioxidant: Biochemical Mechanisms and Pathophysiological Implications in Humans. *Acta Biochim Pol* (2003) 50:1129–46. doi: 10.18388/abp.2003_3637
50. Hardeland R. Antioxidative Protection by Melatonin: Multiplicity of Mechanisms From Radical Detoxification to Radical Avoidance. *Endocrine* (2005) 27:119–30. doi: 10.1385/endo:27:2:119
51. Tian X, Wang F, Zhang L, Ji P, Wang J, Lv D, et al. Melatonin Promotes the In Vitro Development of Microinjected Pronuclear Mouse Embryos Via Its Anti-Oxidative and Anti-Apoptotic Effects. *Int J Mol Sci* (2017) 18:988. doi: 10.3390/ijms18050988

52. Hill SM, Frasch T, Xiang S, Yuan L, Duplessis T, Mao L. Molecular Mechanisms of Melatonin Anticancer Effects. *Integr Cancer Ther* (2009) 8:337–46. doi: 10.1177/1534735409353332
53. Samanta S. Melatonin: An Endogenous Miraculous Indolamine, Fights Against Cancer Progression. *J Cancer Res Clin Oncol* (2020) 146:1893–922. doi: 10.1007/s00432-020-03292-w
54. Tekbas OF, Ogur R, Korkmaz A, Kilic A, Reiter RJ. Melatonin as an Antibiotic: New Insights Into the Actions of This Ubiquitous Molecule. *J Pineal Res* (2008) 44:222–6. doi: 10.1111/j.1600-079X.2007.00516.x
55. Lee HY, Byeon Y, Back K. Melatonin as a Signal Molecule Triggering Defense Responses Against Pathogen Attack in Arabidopsis and Tobacco. *J Pineal Res* (2014) 57:262–8. doi: 10.1111/jpi.12165
56. Bishayi B, Adhikary R, Nandi A, Sultana S. Beneficial Effects of Exogenous Melatonin in Acute Staphylococcus Aureus and Escherichia Coli Infection-Induced Inflammation and Associated Behavioral Response in Mice After Exposure to Short Photoperiod. *Inflammation* (2016) 39:2072–93. doi: 10.1007/s10753-016-0445-9
57. López LC, Escames G, Tapias V, Utrilla P, León J, Acuña-Castroviejo D. Identification of an Inducible Nitric Oxide Synthase in Diaphragm Mitochondria From Septic Mice: its Relation With Mitochondrial Dysfunction and Prevention by Melatonin. *Int J Biochem Cell Biol* (2006) 38:267–78. doi: 10.1016/j.biocel.2005.09.008
58. Escames G, Acuña-Castroviejo D, López LC, Tan DX, Maldonado MD, Sánchez-Hidalgo M, et al. Pharmacological Utility of Melatonin in the Treatment of Septic Shock: Experimental and Clinical Evidence. *J Pharm Pharmacol* (2006) 58:1153–65. doi: 10.1211/jpp.58.9.0001
59. Ortiz F, García JA, Acuña-Castroviejo D, Doerrier C, López A, Venegas C, et al. The Beneficial Effects of Melatonin Against Heart Mitochondrial Impairment During Sepsis: Inhibition of iNOS and Preservation of Nnos. *J Pineal Res* (2014) 56:71–81. doi: 10.1111/jpi.12099
60. Henderson R, Kim S, Lee E. Use of Melatonin as Adjunctive Therapy in Neonatal Sepsis: A Systematic Review and Meta-Analysis. *Complement Ther Med* (2018) 39:131–6. doi: 10.1016/j.ctim.2018.06.002
61. Srinivasan V, Mohamed M, Kato H. Melatonin in Bacterial and Viral Infections With Focus on Sepsis: A Review. *Recent Pat Endocr Metab Immune Drug Discov* (2012) 6:30–9. doi: 10.2174/187221412799015317
62. Galley HF, Lowes DA, Allen L, Cameron G, Aucott LS, Webster NR. Melatonin as a Potential Therapy for Sepsis: A Phase I Dose Escalation Study and an Ex Vivo Whole Blood Model Under Conditions of Sepsis. *J Pineal Res* (2014) 56:427–38. doi: 10.1111/jpi.12134
63. Hardeland R. Melatonin and Inflammation-Story of a Double-Edged Blade. *J Pineal Res* (2018) 65:e12525. doi: 10.1111/jpi.12525
64. Tan DX, Zheng X, Kong J, Manchester LC, Hardeland R, Kim SJ, et al. Fundamental Issues Related to the Origin of Melatonin and Melatonin Isomers During Evolution: Relation to Their Biological Functions. *Int J Mol Sci* (2014) 15:15858–90. doi: 10.3390/ijms150915858
65. Tan DX, Hardeland R, Back K, Manchester LC, Alatorre-Jimenez MA, Reiter RJ. On the Significance of an Alternate Pathway of Melatonin Synthesis Via 5-Methoxytryptamine: Comparisons Across Species. *J Pineal Res* (2016) 61:27–40. doi: 10.1111/jpi.12336
66. Luo H, Schneider K, Christensen U, Lei Y, Herrgard M, Palsson B. Microbial Synthesis of Human-Hormone Melatonin at Gram Scales. *ACS Synth Biol* (2020) 9:1240–5. doi: 10.1021/acssynbio.0c00065
67. Tan DX, Manchester LC, Liu X, Rosales-Corral SA, Acuna-Castroviejo D, Reiter RJ. Mitochondria and Chloroplasts as the Original Sites of Melatonin Synthesis: A Hypothesis Related to Melatonin's Primary Function and Evolution in Eukaryotes. *J Pineal Res* (2013) 54:127–38. doi: 10.1111/jpi.12026
68. Hardeland R. Melatonin in the Evolution of Plants and Other Phototrophs. *Melatonin Res* (2019) 2:10–36. doi: 10.32794/mr11250029
69. Claustrat B, Brun J, Chazot G. The Basic Physiology and Pathophysiology of Melatonin. *Sleep Med Rev* (2005) 9:11–24. doi: 10.1016/j.smrv.2004.08.001
70. Hardeland R, Madrid JA, Tan DX, Reiter RJ. Melatonin, the Circadian Multioscillator System and Health: The Need for Detailed Analyses of Peripheral Melatonin Signaling. *J Pineal Res* (2012) 52:139–66. doi: 10.1111/j.1600-079X.2011.00934.x
71. Zisapel N. New Perspectives on the Role of Melatonin in Human Sleep, Circadian Rhythms and Their Regulation. *Br J Pharmacol* (2018) 175:3190–9. doi: 10.1111/bph.14116
72. Scheer FA, Van Montfrans GA, van Someren EJ, Mairuhu G, Buijs RM. Daily Nighttime Melatonin Reduces Blood Pressure in Male Patients With Essential Hypertension. *Hypertension* (2004) 43:192–7. doi: 10.1161/01.HYP.0000113293.15186.3b
73. Rodríguez C, Puente-Moncada N. Regulation of Cancer Cell Glucose Metabolism is Determinant for Cancer Cell Fate After Melatonin Administration. *J Cell Physiol* (2021) 236:27–40. doi: 10.1002/jcp.29886
74. Dollins AB, Zhdanova IV, Wurtman RJ, Lynch HJ, Deng MH. Effect of Inducing Nocturnal Serum Melatonin Concentrations in Daytime on Sleep, Mood, Body Temperature, and Performance. *Proc Natl Acad Sci U S A* (1994) 91:1824–8. doi: 10.1073/pnas.91.5.1824
75. Reiter RJ, Rosales-Corral SA, Tan DX, Acuna-Castroviejo D, Qin L, Yang SF, et al. Melatonin, a Full Service Anti-Cancer Agent: Inhibition of Initiation, Progression and Metastasis. *Int J Mol Sci* (2017) 18:843. doi: 10.3390/ijms18040843
76. Chitimus DM, Popescu MR, Voiculescu SE, Panaitescu AM, Pavel B, Zagrean L, et al. Melatonin's Impact on Antioxidative and Anti-Inflammatory Reprogramming in Homeostasis and Disease. *Biomolecules* (2020) 10:1211. doi: 10.3390/biom10091211
77. Ma Q, Reiter RJ, Chen Y. Role of Melatonin in Controlling Angiogenesis Under Physiological and Pathological Conditions. *Angiogenesis* (2020) 23:91–104. doi: 10.1007/s10456-019-09689-7
78. Claustrat B, Leston J. Melatonin: Physiological Effects in Humans. *Neurochirurgie* (2015) 61:77–84. doi: 10.1016/j.neuchi.2015.03.002
79. Mistraletti G, Umbrello M, Sabbatini G, Miori S, Taverna M, Cerri B, et al. Melatonin Reduces the Need for Sedation in ICU Patients: A Randomized Controlled Trial. *Minerva Anestesiol* (2015) 81:1298–310.
80. Mistraletti G, Sabbatini G, Taverna M, Figini MA, Umbrello M, Magni P, et al. Pharmacokinetics of Orally Administered Melatonin in Critically Ill Patients. *J Pineal Res* (2010) 48:142–7. doi: 10.1111/j.1600-079X.2009.00737.x
81. Zhang R, Wang X, Ni L, Di X, Ma B, Niu S, et al. Covid-19: Melatonin as a Potential Adjuvant Treatment. *Life Sci* (2020) 250:117583. doi: 10.1016/j.lfs.2020.117583
82. Nordlund JJ, Lerner AB. The Effects of Oral Melatonin on Skin Color and on the Release of Pituitary Hormones. *J Clin Endocrinol Metab* (1977) 45:768–74. doi: 10.1210/jcem-45-4-768
83. Barchas J, DaCosta F, Spector S. Acute Pharmacology of Melatonin. *Nature* (1967) 214:919–20. doi: 10.1038/214919a0
84. Sugden D. Psychopharmacological Effects of Melatonin in Mouse and Rat. *J Pharmacol Exp Ther* (1983) 227:587–91. doi: 10.1016/0160-5402(83)90069-4
85. Weishaupt JH, Bartels C, Pölking E, Dietrich J, Rohde G, Poeggeler B, et al. Reduced Oxidative Damage in ALS by High-Dose Enteral Melatonin Treatment. *J Pineal Res* (2006) 41:313–23. doi: 10.1111/j.1600-079X.2006.00377.x
86. Wasdell MB, Jan JE, Bomben MM, Freeman RD, Rietveld WJ, Tai J, et al. A Randomized, Placebo-Controlled Trial of Controlled Release Melatonin Treatment of Delayed Sleep Phase Syndrome and Impaired Sleep Maintenance in Children With Neurodevelopmental Disabilities. *J Pineal Res* (2008) 44:57–64. doi: 10.1111/j.1600-079X.2007.00528.x
87. Andersen LP, Gögenur I, Rosenberg J, Reiter RJ. The Safety of Melatonin in Humans. *Clin Drug Investig* (2016) 36:169–75. doi: 10.1007/s40261-015-0368-5
88. Ferlazzo N, Andolina G, Cannata A, Costanzo MG, Rizzo V, Currò M. Is Melatonin the Cornucopia of the 21st Century? *Antioxidants (Basel)* (2020) 9:1088. doi: 10.3390/antiox9111088
89. Besag FMC, Vasey MJ, Lao KSJ, Wong ICK. Adverse Events Associated With Melatonin for the Treatment of Primary or Secondary Sleep Disorders: A Systematic Review. *CNS Drugs* (2019) 33:1167–86. doi: 10.1007/s40263-019-00680-w
90. Ozturk AI, Yilmaz O, Kirbag S, Arslan M. Antimicrobial and Biological Effects of Ipemphos and Amphos on Bacterial and Yeast Strains. *Cell Biochem Funct* (2000) 18:117–26. doi: 10.1002/(sici)1099-0844(200006)18:2<117::aid-cbf863>3.0.co;2-1
91. Wang HX, Liu F, Ng TB. Examination of Pineal Indoles and 6-methoxy-2-benzoxazolinone for Antioxidant and Antimicrobial Effects. *Comp Biochem Physiol C Toxicol Pharmacol* (2001) 130:379–88. doi: 10.1016/S1532-0456(01)00264-2

92. Wiid I, Hoalvan HE, Hon D, Lombard C, Van HP. Potentiation of Isoniazid Activity Against Mycobacterium Tuberculosis by Melatonin. *Antimicrob Agents Chemother* (1999) 43:975–7. doi: 10.1128/AAC.43.4.975
93. Abbas M, Paul M, Huttner A. New and Improved? A Review of Novel Antibiotics for Gram-Positive Bacteria. *Clin Microbiol Infect* (2017) 23:697–703. doi: 10.1016/j.cmi.2017.06.010
94. Woodford N, Livermore DM. Infections Caused by Gram-Positive Bacteria: A Review of the Global Challenge. *J Infect* (2009) 59 Suppl 1:S4–16. doi: 10.1016/s0163-4453(09)60003-7
95. Atroshi F, Rizzo A, Westermarck T, Ali-vehmas T. Effects of Tamoxifen, Melatonin, Coenzyme Q10, and L-carnitine Supplementation on Bacterial Growth in the Presence of Mycotoxins. *Pharmacol Res* (1998) 38:289–95. doi: 10.1006/phrs.1998.0363
96. Masadeh MM, Alzoubi KH, Al-Azzam SI, Khabour OF, Al-Buhairan AM. Ciprofloxacin-Induced Antibacterial Activity Is Atteneuated by Pretreatment With Antioxidant Agents. *Pathogens* (2016) 5:28. doi: 10.3390/pathogens5010028
97. Thi MTT, Wibowo D, Rehm BHA. Pseudomonas Aeruginosa Biofilms. *Int J Mol Sci* (2020) 21:8671. doi: 10.3390/ijms21228671
98. Chen W. Host Innate Immune Responses to Acinetobacter Baumannii Infection. *Front Cell Infect Microbiol* (2020) 10:486. doi: 10.3389/fcimb.2020.00486
99. de Bentzmann S, Plésiat P. The Pseudomonas Aeruginosa Opportunistic Pathogen and Human Infections. *Environ Microbiol* (2011) 13:1655–65. doi: 10.1111/j.1462-2920.2011.02469.x
100. Redfern J, Enright MC. Further Understanding of Pseudomonas Aeruginosa's Ability to Horizontally Acquire Virulence: Possible Intervention Strategies. *Expert Rev Anti Infect Ther* (2020) 18:539–49. doi: 10.1080/14787210.2020.1751610
101. Augustin P, Tran-Dinh A, Valin N, Desmard M, Crevecoeur MA, Muller-Serieys C, et al. Pseudomonas Aeruginosa Post-Operative Peritonitis: Clinical Features, Risk Factors, and Prognosis. *Surg Infect (Larchmt)* (2013) 14:297–303. doi: 10.1089/sur.2012.084
102. Brandenburg KS, Weaver AJJr., Qian L, You T, Chen P, Karna SLR, et al. Development of Pseudomonas Aeruginosa Biofilms in Partial-Thickness Burn Wounds Using a Sprague-Dawley Rat Model. *J Burn Care Res* (2019) 40:44–57. doi: 10.1093/jbcr/iry043
103. Yoshida S, Suzuki K, Suzuki A, Okada H, Niwa T, Kobayashi R, et al. Risk Factors for the Failure of Treatment of Pseudomonas Aeruginosa Bacteremia in Critically Ill Patients. *Pharmazie* (2017) 72:428–32. doi: 10.1691/ph.2017.7453
104. Britt NS, Ritchie DJ, Kollef MH, Burnham CA, Durkin MJ, Hampton NB, et al. Importance of Site of Infection and Antibiotic Selection in the Treatment of Carbapenem-Resistant Pseudomonas Aeruginosa Sepsis. *Antimicrob Agents Chemother* (2018) 62:e02400–17. doi: 10.1128/aac.02400-17
105. Robertson GT, Doyle TB, Du Q, Duncan L, Mdluli KE, Lynch AS. A Novel Indole Compound That Inhibits Pseudomonas Aeruginosa Growth by Targeting MreB is a Substrate for Mexab-Oprm. *J Bacteriol* (2007) 189:6870–81. doi: 10.1128/jb.00805-07
106. Wareth G, Neubauer H, Sprague LD. Acinetobacter Baumannii - a Neglected Pathogen in Veterinary and Environmental Health in Germany. *Vet Res Commun* (2019) 43:1–6. doi: 10.1007/s11259-018-9742-0
107. Amaya-Villar R, Garnacho-Montero J. How Should We Treat Acinetobacter Pneumonia? *Curr Opin Crit Care* (2019) 25:465–72. doi: 10.1097/mcc.0000000000000649
108. Xiao J, Zhang C, Ye S. Acinetobacter Baumannii Meningitis in Children: A Case Series and Literature Review. *Infection* (2019) 47:643–9. doi: 10.1007/s15010-018-1234-1
109. Chusri S, Chongsuvivatwong V, Silpapojakul K, Singkhamanan K, Hortiwakul T, Charernmak B, et al. Clinical Characteristics and Outcomes of Community and Hospital-Acquired Acinetobacter Baumannii Bacteremia. *J Microbiol Immunol Infect* (2019) 52:796–806. doi: 10.1016/j.jmii.2019.03.004
110. Shi J, Sun T, Cui Y, Wang C, Wang F, Zhou Y, et al. Multidrug Resistant and Extensively Drug Resistant Acinetobacter Baumannii Hospital Infection Associated With High Mortality: A Retrospective Study in the Pediatric Intensive Care Unit. *BMC Infect Dis* (2020) 20:597. doi: 10.1186/s12879-020-05321-y
111. Fernández-García L, Fernandez-Cuenca F, Blasco L, López-Rojas R, Ambroa A, Lopez M, et al. Relationship Between Tolerance and Persistence Mechanisms in Acinetobacter Baumannii Strains With AbkAB Toxin-Antitoxin System. *Antimicrob Agents Chemother* (2018) 62:e00250–00218. doi: 10.1128/aac.00250-18
112. Uberos J, Augustin C, Liébana J, Molina A, Muñoz-Hoyos A. Comparative Study of the Influence of Melatonin and Vitamin E on the Surface Characteristics of Escherichia Coli. *Lett Appl Microbiol* (2001) 32:303–6. doi: 10.1046/j.1472-765x.2001.00908.x
113. Uberos J, Molina A, Liébana J, Augustin MC, Muñoz A. The Influence of Different Concentrations of Melatonin on the Cell Surface Hydrophobic Characteristics of Neisseria Meningitidis. *Lett Appl Microbiol* (2000) 31:294–8. doi: 10.1046/j.1472-765x.2000.00813.x
114. Gagneux S. Ecology and Evolution of Mycobacterium Tuberculosis. *Nat Rev Microbiol* (2018) 16:202–13. doi: 10.1038/nrmicro.2018.8
115. Pavlik A, Yayo I, Parmova W, Melicharek I, Hanzlikova I, Svejcova M, et al. Mycobacterium Tuberculosis in Animal and Human Population in Six Central European Countries During 1990-1999. *Vet Med* (2003) 48:8–89. doi: 10.17221/5754-VETMED
116. Chen Y, Chao Y, Deng Q, Liu T, Xiang J, Chen J, et al. Potential Challenges to the Stop Tb Plan for Humans in China; Cattle Maintain M. Bovis, and M. Tuberculosis. *Tuberculosis (Edinb)* (2009) 89:95–100. doi: 10.1016/j.tube.2008.07.003
117. Sarathy JP, Via LE, Weiner D, Blanc L, Boshoff H, Eugenin EA, et al. Extreme Drug Tolerance of Mycobacterium Tuberculosis in Caseum. *Antimicrob Agents Chemother* (2018) 62:e02266–02217. doi: 10.1128/aac.02266-17
118. Jasim TM, Alabbassi MG, Almuqdadi SF, Kamel H, Kamel J. Anti-Bacterial Properties of Melatonin Against Mycobacterium Tuberculosis In Vitro. *Iraqi J Pharm Sci* (2010) 19:59–63.
119. Chen X, Sun C, Laborda P, Zhao Y, Palmer I, Fu ZQ, et al. Melatonin Treatment Inhibits the Growth of Xanthomonas Oryzae Pv. Oryzae. *Front Microbiol* (2018) 9:2280. doi: 10.3389/fmicb.2018.02280
120. Chen X, Sun C, Laborda P, He Y, Zhao Y, Li Z, et al. Melatonin Treatments Reduce the Pathogenicity and Inhibit the Growth of Xanthomonas Oryzae Pv. Oryzicola. *Plant Pathol* (2019) 68:288–96. doi: 10.1111/ppa.12954
121. Ward CG, Bullen JJ, Rogers HJ. Iron and Infection: New Developments and Their Implications. *J Trauma* (1996) 41:356–64. doi: 10.1097/00005373-199608000-00030
122. Gulcin I, Buyukokuroglu ME, Kufrevioglu OI. Metal Chelating and Hydrogen Peroxide Scavenging Effects of Melatonin. *J Pineal Res* (2003) 34:278–81. doi: 10.1034/j.1600-079X.2003.00042.x
123. Rothfield L, Horecker BL. The Role of Cell-Wall Lipid in the Biosynthesis of Bacterial Lipopolysaccharide. *Proc Natl Acad Sci U S A* (1964) 52:939–46. doi: 10.1073/pnas.52.4.939
124. Hebeler BH, Chatterjee AN, Young FE. Regulation of the Bacterial Cell Wall: Effect of Antibiotics on Lipid Biosynthesis. *Antimicrob Agents Chemother* (1973) 4:346–53. doi: 10.1128/AAC.4.3.346
125. Dauchy RT, Dauchy EM, Davidson LK, Krause JA, Lynch DT, Tirrell PC, et al. Inhibition of Fatty Acid Transport and Proliferative Activity in Tissue-Isolated Human Squamous Cell Cancer Xenografts Perfused in Situ With Melatonin or Eicosapentaenoic or Conjugated Linoleic Acids. *Comp Med* (2007) 57:377–82. doi: 10.1023/A:1010330504668
126. Liu Y, Jia Y, Yang K, Tong Z, Shi J, Li R, et al. Melatonin Overcomes MCR-Mediated Colistin Resistance in Gram-negative Pathogens. *Theranostics* (2020) 10:10697–711. doi: 10.7150/thno.45951
127. Gerber J, Lotz M, Ebert S, Kiel S, Huether G, Kuhnt U, et al. Melatonin is Neuroprotective in Experimental Streptococcus Pneumoniae Meningitis. *J Infect Dis* (2005) 191:783–90. doi: 10.1086/427816
128. Sener G, Tuğtepe H, Velioğlu-Oğünç A, Cetinel S, Gedik N, Yeğen BC. Melatonin Prevents Neutrophil-Mediated Oxidative Injury in Escherichia Coli-Induced Pyelonephritis in Rats. *J Pineal Res* (2006) 41:220–7. doi: 10.1111/j.1600-079X.2006.00357.x
129. Luo J, Song J, Zhang H, Zhang F, Liu H, Li L, et al. Melatonin Mediated Foxp3-Downregulation Decreases Cytokines Production Via the TLR2 and TLR4 Pathways in H. Pylori Infected Mice. *Int Immunopharmacol* (2018) 64:116–22. doi: 10.1016/j.intimp.2018.08.034
130. Wu UI, Mai FD, Sheu JN, Chen LY, Liu YT, Huang HC, et al. Melatonin Inhibits Microglial Activation, Reduces Pro-Inflammatory Cytokine Levels,

and Rescues Hippocampal Neurons of Adult Rats With Acute Klebsiella Pneumoniae Meningitis. *J Pineal Res* (2011) 50:159–70. doi: 10.1111/j.1600-079X.2010.00825.x
131. Carrillo-Vico A, Lardone PJ, Naji L, Fernandez-Santos JM, Martin-Lacave I, Guerrero JM, et al. Beneficial Pleiotropic Actions of Melatonin in an Experimental Model of Septic Shock in Mice: Regulation of Pro-/Anti-Inflammatory Cytokine Network, Protection Against Oxidative Damage and Anti-Apoptotic Effects. *J Pineal Res* (2005) 39:400–8. doi: 10.1111/j.1600-079X.2005.00265.x
132. Maestroni GJ. Melatonin as a Therapeutic Agent in Experimental Endotoxic Shock. *J Pineal Res* (1996) 20:84–9. doi: 10.1111/j.1600-079X.1996.tb00244.x
133. de Jong NWM, van Kessel KPM, van Strijp JAG. Immune Evasion by Staphylococcus Aureus. *Microbiol Spectr* (2019) 7:GPP3-0061-201. doi: 10.1128/microbiolspec.GPP3-0061-2019
134. Smith TC, Wardyn SE. Human Infections With Staphylococcus Aureus CC398. *Curr Environ Health Rep* (2015) 2:41–51. doi: 10.1007/s40572-014-0034-8
135. Reddinger RM, Luke-Marshall NR, Sauberan SL, Hakansson AP. Streptococcus Pneumoniae Modulates Staphylococcus Aureus Biofilm Dispersion and the Transition From Colonization to Invasive Disease. *mBio* (2018) 9:e02089–02017. doi: 10.1128/mBio.02089-17
136. Zhao W, Pan F, Wang B, Wang C, Sun Y, Zhang T, et al. Epidemiology Characteristics of Streptococcus Pneumoniae From Children With Pneumonia in Shanghai: A Retrospective Study. *Front Cell Infect Microbiol* (2019) 9:258. doi: 10.3389/fcimb.2019.00258
137. Yau B, Hunt NH, Mitchell AJ, Too LK. Blood–Brain Barrier Pathology and CNS Outcomes in Streptococcus Pneumoniae Meningitis. *Int J Mol Sci* (2018) 19:3555. doi: 10.3390/ijms19113555
138. Priftis KN, Litt D, Manglani S, Anthracopoulos MB, Thickett K, Tzanakaki G, et al. Bacterial Bronchitis Caused by Streptococcus Pneumoniae and Nontypable Haemophilus Influenzae in Children: The Impact of Vaccination. *Chest* (2013) 143:152–7. doi: 10.1378/chest.12-0623
139. Spreer A, Gerber J, Baake D, Hanssen M, Huether G, Nau R. Antiinflammatory But No Neuroprotective Effects of Melatonin Under Clinical Treatment Conditions in Rabbit Models of Bacterial Meningitis. *J Neurosci Res* (2006) 84:1575–9. doi: 10.1002/jnr.21055
140. Mueller M, Tainter CR. Escherichia Coli. In: *Statpearls*. Treasure Island (FL: StatPearls Publishing (2020). Copyright © 2020, StatPearls Publishing LLC.
141. Köhler CD, Dobrindt U. What Defines Extraintestinal Pathogenic Escherichia Coli? *Int J Med Microbiol* (2011) 301:642–7. doi: 10.1016/j.ijmm.2011.09.006
142. Madhavan TP, Sakellaris H. Colonization Factors of Enterotoxigenic Escherichia Coli. *Adv Appl Microbiol* (2015) 90:155–97. doi: 10.1016/bs.aambs.2014.09.003
143. Bohnlein C, Kabisch J, Meske D, Franz CM, Pichner R. Fitness of Enterohemorrhagic Escherichia Coli (EHEC)/Enteroaggregative E. Coli O104: H4 in Comparison to That of EHEC O157: Survival Studies in Food and In Vitro. *Appl Environ Microbiol* (2016) 82:6326–34. doi: 10.1128/aem.01796-16
144. Hu J, Torres AG. Enteropathogenic Escherichia Coli: Foe or Innocent Bystander? *Clin Microbiol Infect* (2015) 21:729–34. doi: 10.1016/j.cmi.2015.01.015
145. Vijay D, Dhaka P, Vergis J, Negi M, Mohan V, Kumar M, et al. Characterization and Biofilm Forming Ability of Diarrhoeagenic Enteroaggregative Escherichia Coli Isolates Recovered From Human Infants and Young Animals. *Comp Immunol Microbiol Infect Dis* (2015) 38:21–31. doi: 10.1016/j.cimid.2014.11.004
146. Ramya Raghavan P, Purushothaman SA, Ramanathan T, Roy S. Diarrhegenic Escherichia Coli Replaces Shigella Spp. As the Predominant Bacteria Causing Childhood Diarrhea in Andaman and Nicobar Islands, India. *Am J Trop Med Hyg* (2018) 98:814–5. doi: 10.4269/ajtmh.17-0327
147. Khwaja J. Bilateral Adrenal Hemorrhage in the Background of Escherichia Coli Sepsis: A Case Report. *J Med Case Rep* (2017) 11:72. doi: 10.1186/s13256-017-1236-0
148. Paulose JK, Wright JM, Patel AG, Cassone VM. Human Gut Bacteria Are Sensitive to Melatonin and Express Endogenous Circadian Rhythmicity. *PloS One* (2016) 11:e0146643. doi: 10.1371/journal.pone.0146643
149. Dunne C, Dolan B, Clyne M. Factors That Mediate Colonization of the Human Stomach by Helicobacter Pylori. *World J Gastroenterol* (2014) 20:5610–24. doi: 10.3748/wjg.v20.i19.5610
150. Yang L, Zhang J, Xu J, Wei X, Yang J, Liu Y, et al. Helicobacter Pylori Infection Aggravates Dysbiosis of Gut Microbiome in Children With Gastritis. *Front Cell Infect Microbiol* (2019) 9:375. doi: 10.3389/fcimb.2019.00375
151. Lanas A, Dumonceau JM, Hunt RH, Fujishiro M, Scheiman JM, Gralnek IM, et al. Non-Variceal Upper Gastrointestinal Bleeding. *Nat Rev Dis Primers* (2018) 4:18020. doi: 10.1038/nrdp.2018.20
152. Kim SS, Ruiz VE, Carroll JD, Moss SF. Helicobacter Pylori in the Pathogenesis of Gastric Cancer and Gastric Lymphoma. *Cancer Lett* (2011) 305:228–38. doi: 10.1016/j.canlet.2010.07.014
153. Chojnacki C, Poplawski T, Blasiak J, Chojnacki J, Reiter RJ, Klupinska G. Expression of Melatonin Synthesizing Enzymes in Helicobacter Pylori Infected Gastric Mucosa. *BioMed Res Int* (2013) 2013:845032. doi: 10.1155/2013/845032
154. Malinovskaia NK, Rapoport SI, Zhernakova NI, Rybnikova SN, Postnikova LI, Parkhomenko IE. [Antihelicobacter Effects of Melatonin]. *Klin Med (Mosk)* (2007) 85:40–3.
155. Celinski K, Konturek PC, Konturek SJ, Slomka M, Cichoz-Lach H, Brzozowski T, et al. Effects of Melatonin and Tryptophan on Healing of Gastric and Duodenal Ulcers With Helicobacter Pylori Infection in Humans. *J Physiol Pharmacol* (2011) 62:521–6.
156. Osadchuk MA, Sibriaev AA, Kireeva NV, Kvetnoi IM. [The Influence of Melatonin Included in the Combined Treatment of Antichelicobaterial Therapy on Immunohistochemical Characteristics of Gastric Epitheliocytes From Patients With Duodenal Ulcer]. *Klin Med (Mosk)* (2012) 90:48–52.
157. Ikeda M, Mizoguchi M, Oshida Y, Tatsuno K, Saito R, Okazaki M, et al. Clinical and Microbiological Characteristics and Occurrence of Klebsiella Pneumoniae Infection in Japan. *Int J Gen Med* (2018) 11:293–9. doi: 10.2147/ijgm.s166940
158. Bueno MG, Iovine RO, Torres LN, Catao-Dias JL, Pissinatti A, Kierulff MC, et al. Pneumonia and Bacteremia in a Golden-Headed Lion Tamarin (Leontopithecus Chrysomelas) Caused by Klebsiella Pneumoniae Subsp. Pneumoniae During a Translocation Program of Free-Ranging Animals in Brazil. *J Vet Diagn Invest* (2015) 27:387–91. doi: 10.1177/1040638715584792
159. Bidewell CA, Williamson SM, Rogers J, Tang Y, Ellis RJ, Petrovska L, et al. Emergence of Klebsiella Pneumoniae Subspecies Pneumoniae as a Cause of Septicaemia in Pigs in England. *PLoS One* (2018) 13:e0191958. doi: 10.1371/journal.pone.0191958
160. Namikawa H, Yamada K, Sakiyama A, Imoto W, Yamairi K, Shibata W, et al. Clinical Characteristics of Bacteremia Caused by Hypermucoviscous Klebsiella Pneumoniae at a Tertiary Hospital. *Diagn Microbiol Infect Dis* (2019) 95:84–8. doi: 10.1016/j.diagmicrobio.2019.04.008
161. Carrie C, Walewski V, Levy C, Alexandre C, Baleine J, Charreton C, et al. Klebsiella Pneumoniae and Klebsiella Oxytoca Meningitis in Infants. Epidemiological and Clinical Features. *Arch Pediatr* (2019) 26:12–5. doi: 10.1016/j.arcped.2018.09.013
162. Dhruve MJ, Bargman JM. Klebsiella Pneumoniae Renal Abscess and Peritonitis in a Peritoneal Dialysis Patient: A Novel Route of Infection. *Perit Dial Int* (2017) 37:654–6. doi: 10.3747/pdi.2017.00094
163. Korde JP, Srivastava RS, Mishra SC, Sharma AK. Time Dependent Immunomodulatory Response of Exogenous Melatonin to Killed Pasteurella Multocida (P52 Strain) Vaccine in Albino Rats. *Indian J Physiol Pharmacol* (2005) 49:227–35.
164. Esquifino AI, Pandi-Perumal SR, Cardinali DP. Circadian Organization of the Immune Response: A Role for Melatonin. *Clin Appl Immunol Rev* (2004) 4:423–33. doi: 10.1016/j.cair.2004.08.002
165. Colunga Biancatelli RML, Berrill M, Mohammed YH, Marik PE. Melatonin for the Treatment of Sepsis: The Scientific Rationale. *J Thorac Dis* (2020) 12: S54–s65. doi: 10.21037/jtd.2019.12.85
166. Zhen G, Liang W, Jia H, Zheng X. Melatonin Relieves Sepsis-Induced Myocardial Injury Via Regulating JAK2/STAT3 Signaling Pathway. *Minerva Med* (2020). doi: 10.23736/s0026-4806.20.06626-4
167. Petronilho F, Giustina AD, Nascimento DZ, Zarbato GF, Vieira AA, Florentino D, et al. Obesity Exacerbates Sepsis-Induced Oxidative Damage in Organs. *Inflammation* (2016) 39:2062–71. doi: 10.1007/s10753-016-0444-x
168. Mantzarlis K, Tsolaki V. Role of Oxidative Stress and Mitochondrial Dysfunction in Sepsis and Potential Therapies. *Oxid Med Cell Longev* (2017) 2017:5985209. doi: 10.1155/2017/5985209
169. Tan DX, Manchester LC, Terron MP, Flores LJ, Reiter RJ. One Molecule, Many Derivatives: A Never-Ending Interaction of Melatonin With Reactive

Oxygen and Nitrogen Species? *J Pineal Res* (2007) 42:28–42. doi: 10.1111/j.1600-079X.2006.00407.x
170. Chen Y, Qing W, Sun M, Lv L, Guo D, Jiang Y. Melatonin Protects Hepatocytes Against Bile Acid-Induced Mitochondrial Oxidative Stress Via the AMPK-SIRT3-SOD2 Pathway. *Free Radic Res* (2015) 49:1275–84. doi: 10.3109/10715762.2015.1067806
171. Pi H, Xu S, Reiter RJ, Guo P, Zhang L, Li Y, et al. Sirt3-SOD2-mROS-dependent Autophagy in Cadmium-Induced Hepatotoxicity and Salvage by Melatonin. *Autophagy* (2015) 11:1037–51. doi: 10.1080/15548627.2015.1052208
172. Zhai M, Li B, Duan W, Jing L, Zhang B, Zhang M, Jing L, Zhang B, Zhang M, et al. Melatonin Ameliorates Myocardial Ischemia Reperfusion Injury Through SIRT3-Dependent Regulation of Oxidative Stress and Apoptosis. (2017) 63:e12419. doi: 10.1111/jpi.12419
173. Zhang J, Wang L, Xie W, Hu S, Zhou H, Zhu P. Melatonin Attenuates ER Stress and Mitochondrial Damage in Septic Cardiomyopathy: A New Mechanism Involving BAP31 Upregulation and MAPK-ERK Pathway. *J Cell Physiol* (2020) 235:2847–56. doi: 10.1002/jcp.29190
174. Kirkebøen KA, Strand OA. The Role of Nitric Oxide in Sepsis–an Overview. *Acta Anaesthesiol Scand* (1999) 43:275–88. doi: 10.1034/j.1399-6576.1999.430307.x
175. Escames G, León J, Macías M, Khaldy H, Acuña-Castroviejo D. Melatonin Counteracts Lipopolysaccharide-Induced Expression and Activity of Mitochondrial Nitric Oxide Synthase in Rats. *FASEB J* (2003) 17:932–4. doi: 10.1096/fj.02-0692fje
176. Crespo E, Macías M, Pozo D, Escames G, Martín M, Vives F, et al. Melatonin Inhibits Expression of the Inducible NO Synthase II in Liver and Lung and Prevents Endotoxemia in Lipopolysaccharide-Induced Multiple Organ Dysfunction Syndrome in Rats. *FASEB J* (1999) 13:1537–46. doi: 10.1096/fasebj.13.12.1537
177. Srinivasan V, Pandi-Perumal SR, Spence DW, Kato H, Cardinali DP. Melatonin in Septic Shock: Some Recent Concepts. *J Crit Care* (2010) 25:656.e651–656. doi: 10.1016/j.jcrc.2010.03.006
178. Zhou L, Zhao D, An H, Zhang H, Jiang C, Yang B. Melatonin Prevents Lung Injury Induced by Hepatic Ischemia-Reperfusion Through Anti-Inflammatory and Anti-Apoptosis Effects. *Int Immunopharmacol* (2015) 29:462–7. doi: 10.1016/j.intimp.2015.10.012
179. Tan DX, Hardeland R. Targeting Host Defense System and Rescuing Compromised Mitochondria to Increase Tolerance Against Pathogens by Melatonin may Impact Outcome of Deadly Virus Infection Pertinent to COVID-19. *Molecules* (2020) 25:4410. doi: 10.3390/molecules25194410
180. Yasmin F, Sutradhar S, Das P, Mukherjee S. Gut Melatonin: A Potent Candidate in the Diversified Journey of Melatonin Research. *Gen Comp Endocrinol* (2020) 303:113693. doi: 10.1016/j.ygcen.2020.113693
181. Ma N, Zhang J, Reiter RJ, Ma X. Melatonin Mediates Mucosal Immune Cells, Microbial Metabolism, and Rhythm Crosstalk: A Therapeutic Target to Reduce Intestinal Inflammation. *Med Res Rev* (2020) 40:606–32. doi: 10.1002/med.21628
182. Xu P, Wang J, Hong F, Wang S, Jin X, Xue T, et al. Melatonin Prevents Obesity Through Modulation of Gut Microbiota in Mice. *J Pineal Res* (2017) 62:e12399. doi: 10.1111/jpi.12399
183. Yin J, Li Y, Han H, Chen S, Gao J, Liu G, et al. Melatonin Reprogramming of Gut Microbiota Improves Lipid Dysmetabolism in High-Fat Diet-Fed Mice. *J Pineal Res* (2018) 65:e12524. doi: 10.1111/jpi.12524
184. Yin J, Li Y, Han H, Ma J, Liu G, Wu X, et al. Administration of Exogenous Melatonin Improves the Diurnal Rhythms of the Gut Microbiota in Mice Fed a High-Fat Diet. *mSystems* (2020) 5:e00002–20. doi: 10.1128/mSystems.00002-20
185. Hong F, Pan S, Xu P, Xue T, Wang J, Guo Y, et al. Melatonin Orchestrates Lipid Homeostasis Through the Hepatointestinal Circadian Clock and Microbiota During Constant Light Exposure. *Cells* (2020) 9:489. doi: 10.3390/cells9020489
186. Lv WJ, Liu C. Melatonin Alleviates Neuroinflammation and Metabolic Disorder in DSS-Induced Depression Rats. *Oxid Med Cell Longev* (2020) 2020:1241894. doi: 10.1155/2020/1241894
187. Zhang H, Yan A, Liu X, Ma Y, Zhao F, Wang M, et al. Melatonin Ameliorates Ochratoxin A Induced Liver Inflammation, Oxidative Stress and Mitophagy in Mice Involving in Intestinal Microbiota and Restoring the Intestinal Barrier Function. *J Hazard Mater* (2020) 407:124489. doi: 10.1016/j.jhazmat.2020.124489
188. Xu L, Zhang W, Kwak M, Zhang L, Lee PCW, Jin JO. Protective Effect of Melatonin Against Polymicrobial Sepsis Is Mediated by the Anti-Bacterial Effect of Neutrophils. *Front Immunol* (2019) 10:1371. doi: 10.3389/fimmu.2019.01371
189. Fink T, Glas M, Wolf A, Kleber A, Reus E, Wolff M, et al. Melatonin Receptors Mediate Improvements of Survival in a Model of Polymicrobial Sepsis. *Crit Care Med* (2014) 42:e22–31. doi: 10.1097/CCM.0b013e3182a63e2b
190. Zhang Y, Li X, Grailer JJ, Wang N, Wang M, Yao J, et al. Melatonin Alleviates Acute Lung Injury Through Inhibiting the NLRP3 Inflammasome. *J Pineal Res* (2016) 60:405–14. doi: 10.1111/jpi.12322
191. Lowes DA, Almawash AM, Webster NR, Reid VL, Galley HF. Melatonin and Structurally Similar Compounds Have Differing Effects on Inflammation and Mitochondrial Function in Endothelial Cells Under Conditions Mimicking Sepsis. *Br J Anaesth* (2011) 107:193–201. doi: 10.1093/bja/aer149
192. Shang Y, Xu SP, Wu Y, Jiang YX, Wu ZY, Yuan SY, et al. Melatonin Reduces Acute Lung Injury in Endotoxemic Rats. *Chin Med J (Engl)* (2009) 122:1388–93. doi: 10.3760/cma.j.issn.0366-6999.2009.12.006
193. Titheradge MA. Nitric Oxide in Septic Shock. *Biochim Biophys Acta* (1999) 1411:437–55. doi: 10.1016/s0005-2728(99)00031-6
194. Acuña-Castroviejo D, Escames G, López LC, Hitos AB, León J. Melatonin and Nitric Oxide: Two Required Antagonists for Mitochondrial Homeostasis. *Endocrine* (2005) 27:159–68. doi: 10.1385/endo:27:2:159
195. Deng SL, Zhang BL, Reiter RJ, Liu YX. Melatonin Ameliorates Inflammation and Oxidative Stress by Suppressing the P38mapk Signaling Pathway in LPS-Induced Sheep Orchitis. *Antioxidants (Basel)* (2020) 9:1277. doi: 10.3390/antiox9121277
196. Choi EY, Jin JY, Lee JY, Choi JI, Choi IS, Kim SJ. Melatonin Inhibits Prevotella Intermedia Lipopolysaccharide-Induced Production of Nitric Oxide and Interleukin-6 in Murine Macrophages by Suppressing NF-kappaB and STAT1 Activity. *J Pineal Res* (2011) 50:197–206. doi: 10.1111/j.1600-079X.2010.00829.x
197. Tamura EK, Cecon E, Monteiro AW, Silva CL, Markus RP. Melatonin Inhibits LPS-Induced NO Production in Rat Endothelial Cells. *J Pineal Res* (2009) 46:268–74. doi: 10.1111/j.1600-079X.2008.00657.x
198. Yu GM, Kubota H, Okita M, Maeda T. The Anti-Inflammatory and Antioxidant Effects of Melatonin on LPS-Stimulated Bovine Mammary Epithelial Cells. *PLoS One* (2017) 12:e0178525. doi: 10.1371/journal.pone.0178525
199. Lee SJ, Lee HJ, Jung YH, Kim JS, Choi SH, Han HJ. Melatonin Inhibits Apoptotic Cell Death Induced by Vibrio Vulnificus VvhA Via Melatonin Receptor 2 Coupling With NCF-1. *Cell Death Dis* (2018) 9:48. doi: 10.1038/s41419-017-0083-7
200. Lee YM, Park JP, Jung YH, Lee HJ, Kim JS, Choi GE, et al. Melatonin Restores Muc2 Depletion Induced by V. vulnificus VvpM via melatonin receptor 2 coupling with Gαq. *J Biomed Sci* (2020) 27:21. doi: 10.1186/s12929-019-0606-x
201. Debnath B, Islam W, Li M, Sun Y, Lu X, Mitra S, et al. Melatonin Mediates Enhancement of Stress Tolerance in Plants. *Int J Mol Sci* (2019) 20:1040. doi: 10.3390/ijms20051040
202. Yin L, Wang P, Li M, Ke X, Li C, Liang D, et al. Exogenous Melatonin Improves Malus Resistance to Marssonina Apple Blotch. *J Pineal Res* (2013) 54:426–34. doi: 10.1111/jpi.12038
203. Mansfield J, Genin S, Magori S, Citovsky V, Sriariyanum M, Ronald P, et al. Top 10 Plant Pathogenic Bacteria in Molecular Plant Pathology. *Mol Plant Pathol* (2012) 13:614–29. doi: 10.1111/j.1364-3703.2012.00804.x
204. Mahmood T, Jan A, Kakishima M, Komatsu S. Proteomic Analysis of Bacterial-Blight Defense-Responsive Proteins in Rice Leaf Blades. *Proteomics* (2006) 6:6053–65. doi: 10.1002/pmic.200600470
205. Li C, He Q, Zhang F, Yu J, Li C, Zhao T, et al. Melatonin Enhances Cotton Immunity to Verticillium Wilt Via Manipulating Lignin and Gossypol Biosynthesis. *Plant J* (2019) 100:784–800. doi: 10.1111/tpj.14477
206. Lee HY, Byeon Y, Tan DX, Reiter RJ, Back K. Arabidopsis Serotonin N-acetyltransferase Knockout Mutant Plants Exhibit Decreased Melatonin and Salicylic Acid Levels Resulting in Susceptibility to an Avirulent Pathogen. *J Pineal Res* (2015) 58:291–9. doi: 10.1111/jpi.12214
207. Zhao H, Xu L, Su T, Jiang Y, Hu L, Ma F. Melatonin Regulates Carbohydrate Metabolism and Defenses Against Pseudomonas Syringae Pv. Tomato

DC3000 Infection in Arabidopsis Thaliana. *J Pineal Res* (2015) 59:109–19. doi: 10.1111/jpi.12245
208. Qian Y, Tan DX, Reiter RJ, Shi H. Comparative Metabolomic Analysis Highlights the Involvement of Sugars and Glycerol in Melatonin-Mediated Innate Immunity Against Bacterial Pathogen in Arabidopsis. *Sci Rep* (2015) 5:15815. doi: 10.1038/srep15815
209. Shi H, Chen Y, Tan DX, Reiter RJ, Chan Z, He C. Melatonin Induces Nitric Oxide and the Potential Mechanisms Relate to Innate Immunity Against Bacterial Pathogen Infection in Arabidopsis. *J Pineal Res* (2015) 59:102–8. doi: 10.1111/jpi.12244
210. Lee HY, Back K. Mitogen-Activated Protein Kinase Pathways are Required for Melatonin-Mediated Defense Responses in Plants. *J Pineal Res* (2016) 60:327–35. doi: 10.1111/jpi.12314
211. Lee HY, Back K. Melatonin is Required for H2 O2 - and NO-Mediated Defense Signaling Through MAPKKK3 and OXI1 in Arabidopsis Thaliana. *J Pineal Res* (2017) 62:e12379. doi: 10.1111/jpi.12379
212. Wurtman RJ, Lieberman HR. Melatonin Secretion as a Mediator of Circadian Variations in Sleep and Sleepiness. *J Pineal Res* (1985) 2:301–3. doi: 10.1111/j.1600-079X.1985.tb00647.x
213. Li Y, Ma J, Yao K, Su W, Tan B, Wu X, et al. Circadian Rhythms and Obesity: Timekeeping Governs Lipid Metabolism. *J Pineal Res* (2020) 69:e12682. doi: 10.1111/jpi.12682
214. Fathizadeh H, Mirzaei H, Asemi Z. Melatonin: An Anti-Tumor Agent for Osteosarcoma. *Cancer Cell Int* (2019) 19:319. doi: 10.1186/s12935-019-1044-2
215. Nabavi SM, Nabavi SF, Sureda A, Xiao J, Dehpour AR, Shirooie S, et al. Anti-Inflammatory Effects of Melatonin: A Mechanistic Review. *Crit Rev Food Sci Nutr* (2019) 59:S4–s16. doi: 10.1080/10408398.2018.1487927
216. Paulose JK, Cassone VM. The Melatonin-Sensitive Circadian Clock of the Enteric Bacterium Enterobacter Aerogenes. *Gut Microbes* (2016) 7:424–7. doi: 10.1080/19490976.2016.1208892
217. Ren W, Wang P, Yan J, Liu G, Zeng B, Hussain T, et al. Melatonin Alleviates Weanling Stress in Mice: Involvement of Intestinal Microbiota. *J Pineal Res* (2018) 64:e12448. doi: 10.1111/jpi.12448
218. Junaid A, Tang H, van Reeuwijk A, Abouleila Y, Wuelfroth P, van Duinen V, et al. Ebola Hemorrhagic Shock Syndrome-on-a-Chip. *iScience* (2020) 23:100765. doi: 10.1016/j.isci.2019.100765
219. Bonilla E, Valero-Fuenmayor N, Pons H, Chacín-Bonilla L. Melatonin Protects Mice Infected With Venezuelan Equine Encephalomyelitis Virus. *Cell Mol Life Sci* (1997) 53:430–4. doi: 10.1007/s000180050051
220. Montiel M, Bonilla E, Valero N, Mosquera J, Espina LM, Quiroz Y, et al. Melatonin Decreases Brain Apoptosis, Oxidative Stress, and CD200 Expression and Increased Survival Rate in Mice Infected by Venezuelan Equine Encephalitis Virus. *Antivir Chem Chemother* (2015) 24:99–108. doi: 10.1177/2040206616660851
221. Crespo I, San-Miguel B, Sánchez DI, González-Fernández B, Álvarez M, González-Gallego J, et al. Melatonin Inhibits the Sphingosine Kinase 1/sphingosine-1-phosphate Signaling Pathway in Rabbits With Fulminant Hepatitis of Viral Origin. *J Pineal Res* (2016) 61:168–76. doi: 10.1111/jpi.12335
222. Huang SH, Cao XJ, Liu W, Shi XY, Wei W. Inhibitory Effect of Melatonin on Lung Oxidative Stress Induced by Respiratory Syncytial Virus Infection in Mice. *J Pineal Res* (2010) 48:109–16. doi: 10.1111/j.1600-079X.2009.00733.x
223. Ellis LC. Melatonin Reduces Mortality From Aleutian Disease in Mink (Mustela Vison). *J Pineal Res* (1996) 21:214–7. doi: 10.1111/j.1600-079x.1996.tb00288.x
224. Huang SH, Liao CL, Chen SJ, Shi LG, Lin GJ. Melatonin Possesses an Anti-Influenza Potential Through its Immune Modulatory Effect. *J Funct Foods* (2019) 58:189–98. doi: 10.1016/j.jff.2019.04.062
225. Shneider A, Kudriavtsev A. Can Melatonin Reduce the Severity of COVID-19 Pandemic? *Int Rev Immunol* (2020) 39:153–62. doi: 10.1080/08830185.2020.1756284
226. Zhou Y, Hou Y, Shen J, Huang Y, Martin W. Network-Based Drug Repurposing for Novel Coronavirus 2019-Ncov/SARS-Cov-2. *Cell Discov* (2020) 6:14. doi: 10.1038/s41421-020-0153-3
227. Bahrampour Juybari K, Pourhanifeh MH, Hosseinzadeh A, Hemati K, Mehrzadi S. Melatonin Potentials Against Viral Infections Including COVID-19: Current Evidence and New Findings. *Virus Res* (2020) 287:198108. doi: 10.1016/j.virusres.2020.198108

Conflict of Interest: The authors declare that the research was conducted in the absence of any commercial or financial relationships that could be construed as a potential conflict of interest.

Copyright © 2021 He, Wu, Zhang, Li, Ye, Li, Chen, Peng, Hardeland and Xia. This is an open-access article distributed under the terms of the Creative Commons Attribution License (CC BY). The use, distribution or reproduction in other forums is permitted, provided the original author(s) and the copyright owner(s) are credited and that the original publication in this journal is cited, in accordance with accepted academic practice. No use, distribution or reproduction is permitted which does not comply with these terms.

frontiers in Microbiology

ORIGINAL RESEARCH
published: 24 June 2021
doi: 10.3389/fmicb.2021.675492

Lactobacillus casei Zhang Counteracts Blood-Milk Barrier Disruption and Moderates the Inflammatory Response in *Escherichia coli*-Induced Mastitis

*Yuhui Zheng, Gang Liu, Wei Wang, Yajing Wang, Zhijun Cao, Hongjian Yang and Shengli Li**

State Key Laboratory of Animal Nutrition, College of Animal Science and Technology, China Agricultural University, Beijing, China

OPEN ACCESS

Edited by:
Monica Cartelle Gestal, Louisiana State University Health Shreveport, United States

Reviewed by:
Yunhe Fu, Jilin University, China
Anna Arís, Institute of Agrifood Research and Technology (IRTA), Spain
Carina Shianya Alvarez Villagomez, Universidad Juárez Autónoma de Tabasco, Mexico

***Correspondence:**
Shengli Li
lisheng0677@163.com

Specialty section:
This article was submitted to Microbial Immunology, a section of the journal Frontiers in Microbiology

Received: *03 March 2021*
Accepted: *07 May 2021*
Published: *24 June 2021*

Citation:
Zheng Y, Liu G, Wang W, Wang Y, Cao Z, Yang H and Li S (2021) Lactobacillus casei Zhang Counteracts Blood-Milk Barrier Disruption and Moderates the Inflammatory Response in Escherichia coli-Induced Mastitis. Front. Microbiol. 12:675492. doi: 10.3389/fmicb.2021.675492

Escherichia coli is a common mastitis-causing pathogen that can disrupt the blood-milk barrier of mammals. Although *Lactobacillus casei* Zhang (LCZ) can alleviate mice mastitis, whether it has a prophylactic effect on *E. coli*-induced mastitis through intramammary infusion, as well as its underlying mechanism, remains unclear. In this study, *E. coli*-induced injury models of bovine mammary epithelial cells (BMECs) and mice in lactation were used to fill this research gap. *In vitro* tests of BMECs revealed that LCZ significantly inhibited the *E. coli* adhesion ($p < 0.01$); reduced the cell desmosome damage; increased the expression of the tight junction proteins claudin-1, claudin-4, occludin, and zonula occludens-1 (ZO-1; $p < 0.01$); and decreased the expression of the inflammatory cytokines tumor necrosis factor (TNF)-α, interleukin (IL)-1β, and IL-6 ($p < 0.01$), thereby increasing trans-epithelial electric resistance ($p < 0.01$) and attenuating the lactate dehydrogenase release induced by *E. coli* ($p < 0.01$). *In vivo* tests indicated that LCZ significantly reduced the injury and histological score of mice mammary tissues in *E. coli*-induced mastitis ($p < 0.01$) by significantly promoting the expression of the tight junction proteins claudin-3, occludin, and ZO-1 ($p < 0.01$), which ameliorated blood-milk barrier disruption, and decreasing the expression of the inflammatory cytokines (TNF-α, IL-1β, and IL-6) in mice mammary tissue ($p < 0.01$). Our study suggested that LCZ counteracted the disrupted blood-milk barrier and moderated the inflammatory response in *E. coli*-induced injury models, indicating that LCZ can ameliorate the injury of mammary tissue in mastitis.

Keywords: ***Lactobacillus casei* Zhang, bovine mammary epithelial cells, blood-milk barrier, mastitis, inflammatory response**

INTRODUCTION

Bovine mastitis is a common disease that results in enormous economic losses for dairy farms worldwide (Sathiyabarathi et al., 2016; Angelopoulou et al., 2018). *Escherichia coli* (*E. coli*) is one of the most common mastitis-causing pathogens and often causes acute mastitis with a severe inflammatory response that disturbs the blood-milk barrier. The abuse of antimicrobials

in food animals has attracted public attention, and concerns relating to antimicrobial residues and anti-microbial resistance in bacteria have increased because of the increased use of antimicrobials (Lhermie et al., 2016; Muziasari et al., 2016). There is thus an urgent need to find new potential non-antimicrobials to prevent mastitis.

Lactobacillus is an important probiotic that contributes to the immunity and health of animals. Their probiotic properties play an important role in regulating gut microbiota (Igor et al., 2019), relieving intestinal diseases (Sanders et al., 2019), and enhancing body immunity (Garcia-Castilla et al., 2019) in addition to other functions (da Costa et al., 2016; Li et al., 2017). *Lactobacillus* is known to protect hosts against intramammary infection in both humans and cows by oral or intramammary administration (Jiménez et al., 2008; Arroyo et al., 2010; Fernández et al., 2016), but the mechanism of this protective effect remains unclear. Intramammary infusion of drugs is the most common and effective way for treating bovine mastitis in practice, and intramammary infusion of some *Lactobacillus* strains can effectively alleviate clinical symptoms of bovine mastitis (Ignacio et al., 2015; Pellegrino et al., 2017; Kitching et al., 2019). The clinical symptoms of mastitis in mice can be effectively alleviated through oral administration of *Lactobacillus casei* Zhang (LCZ; Ma et al., 2018). However, whether intramammary infusion of LCZ has a prophylactic effect on mastitis, as well as its underlying mechanism, remains unclear. Here, we studied the prophylactic effect of LCZ on *E. coli*-induced injury models and its mechanism using bovine mammary epithelial cells (BMECs) and mice in lactation.

MATERIALS AND METHODS

Bacterial Strains

Lactobacillus casei Zhang (provided by Inner Mongolia Agricultural University, Key Laboratory of Dairy Biotechnology and Engineering, Inner Mongolia, China) was grown in de Man, Rogosa, and Sharpe (MRS) broth (Solarbio, Beijing, China) at 37°C under microaerophilic conditions. The isolate of *E. coli* ATCC 25922 (provided by China General Microbiological Culture Collection Center, Beijing, China) was incubated in tryptone soya broth (Solarbio, Beijing, China) at 37°C. In all treatments, *E. coli* and LCZ were plated on tryptone soya agar (TSA, Solarbio, Beijing, China) and MRS agar (Solarbio, Beijing, China), respectively, to count colony-forming unit (CFU).

Cell Culture

Bovine mammary epithelial cells (provided by Yangzhou University, College of Animal Science and Technology Feed Engineering Technology Research Center, Yangzhou, China) were cultivated in Dulbecco's modified eagle medium (DMEM)-F12 medium (ThermoFisher, Waltham, MA, United States) containing 10% fetal bovine serum (FBS; ThermoFisher), 1% penicillin and streptomycin (Beyotime, Shanghai, China), 15 ng/ml epidermal growth factor (PeproTech, Cranbury, NJ, United States), 1% non-essential amino acids (ThermoFisher), and 1% insulin-transferrin-selenium (ITS, ThermoFisher) at 37°C in 5% CO_2 and 95% relative humidity. Briefly, BMECs (5×10^5) were seeded onto six-well cell culture plates in the aforementioned medium for 48 h and were then cultured in DMEM-F12 medium with 5% FBS, 1% penicillin and streptomycin, and 1% ITS for 72 h to ensure that a polarized and differentiated state was achieved. Before treatments, the medium was changed into DMEM-F12 alone, and both *E. coli* and LCZ were diluted by DMEM-F12. Cells were randomly treated under four conditions, and the dose of two bacteria was decided according to pretest: (1) Control group (DMEM alone); (2) 1×10^3 CFU *E. coli* treatment for 5 h (*E. coli* group); (3) 1×10^5 CFU LCZ pretreatment for 3 h, followed by 1×10^3 CFU *E. coli* treatment for 5 h (LCZ + *E. coli* group); and (4) 1×10^5 CFU LCZ treatment for 3 h (LCZ group). 5 h after LCZ treatment, cells were washed with phosphate buffer saline (PBS, ThermoFisher) and then incubated with *E. coli*. All cell experiments were repeated three times, and each experiment was performed in triplicate.

Cell Death Assay

Cell death was measured using the lactate dehydrogenase (LDH) method through a CytoTox 96 cytotoxicity assay (Solarbio, Beijing, China) based on the manufacturer's manual. In detail, the cell culture supernatant was used to detect the amount of LDH release.

Adhesion Assay

The BMECs were washed with PBS for three times, and 1 ml triton-X-100 (0.5% v/v, Solarbio, Beijing, China) was added to each well after incubation with LCZ or *E. coli*. The cells were scraped off, and the lysate was transferred to a centrifugal tube after 10 min of stabilization at room temperature. *E. coli* and LCZ were plated on TSA and MRS agar, respectively, to count CFU.

Trans-Epithelial Electric Resistance

Bovine mammary epithelial cells were seeded on transwell inserts (membrane area: 0.33 cm^2, pore size: 0.4 μm, Corning, NY, United States), cultivated for 120 h as described previously, and measured TEER daily. When cells reached a polarized and differentiated state which means that TEER reached 400 Ω cm^2, different treatments were applied. TEER was measured for three times per well using a Millicell Electrical Resistance System-2 (Millipore, MA, United States) and expressed as Ω cm^2 after subtracting the filter resistance value. The results of TEER were defined as the TEER change (TEER of monolayer cells after treatments – TEER of monolayer cells before treatments).

Animals

CD-1 mice (8–10 days in lactation; 50 ± 5 g; obtained from SPF Biotechnology Co., Ltd., Beijing, China) were reared at

25°C and fed with enough food and water. Twenty mice were randomly allocated to the four treatments, and the dose of two bacteria was decided according to pretest: (1) Control group (PBS alone); (2) 1×10^3 CFU *E. coli* treatment for 12 h (*E. coli* group); (3) 1×10^5 CFU LCZ pre-infusion for 24 h, followed by 1×10^3 CFU *E. coli* treatment for 12 h (LCZ + *E. coli* group); and (4) 1×10^5 CFU LCZ treatment for 24 h (LCZ group). Five mice were used as replicates in each group. Mice were anesthetized with Zoletil 50 (Virbac, Barneveld, France), and all treatments were conducted through intramammary infusion *via* the teat canal of the fourth teat. *E. coli* was injected 24 h after LCZ pretreatment. After treatments, the mice were killed to collect mammary tissues. All animal feeding and experimental protocols in this study were approved by the animal ethics committee of the National Institutes of Health Guide for the Care and Use of Laboratory Animals (GB14925-2010, China).

Histopathology

The general condition of each mammary tissue of the mice was assessed by clinical scoring. The clinical score ranked from 1 to 5, with higher scores corresponding to greater degrees of tissue damage. Specifically, 1 indicated no damage, 2 indicated slight redness, 3 indicated redness and slight bleeding, 4 indicated redness and bleeding, and 5 indicated redness and obvious bleeding.

The mammary tissues were fixed in 4% cell tissue fixative (Solarbio) immediately after the mice were killed. To evaluate histological changes, hematoxylin-eosin was used to stain tissue samples, and a microscope was used to observe the tissues. The semi-quantitative scoring was performed using a histological score based on the following criteria. The histological score ranged from 1 to 5, and higher scores corresponded to greater degrees of tissue damage. Specifically, 1 indicated the absence of histological features (i.e., necrosis, neutrophils, and lymphocytes), 2 indicated minimal histological features (i.e., individual neutrophils), 3 indicated mild histological features (i.e., a small amount of neutrophils), 4 indicated moderate histological characteristics (i.e., many neutrophils and slight damage to glandular structure), and 5 indicated severe histological characteristics (i.e., a large number of neutrophils and severe damage to glandular structure). Both clinical scoring and histological scoring were made by experienced veterinary pathologists who were blinded to the treatments.

Immunofluorescence

Two mammary tissue blocks (0.3 cm^3) were immediately sampled after the mice were killed and then stored in liquid nitrogen for tissue immunofluorescence to localized tight junction proteins. Briefly, cryosections of mammary tissues were fixed with 4% paraformaldehyde and then were incubated with 5% bovine serum albumin (BSA; ThermoFisher) at 25°C. After incubation using primary antibodies (zonula occludins-1 (ZO-1), claudin-3, and occludin, 1:2,000 dilution, Abcam, Cambridge, United Kingdom) at 4°C for 12 h, tissues were washed with PBS, and secondary antibodies (1:1,000 dilution, CoWin Biosciences, Beijing, China) were added and incubated at 25°C for 1 h. Blanks were treated in the same way except that the tissues were not incubated with primary antibodies. After washing with PBS and staining with 4′,6-diamidino-2-phenylindole (DAPI), a fluorescence microscope was used to obtain images.

Transmission Electron Microscope Analysis

Two mammary gland tissue blocks (10 mm^3) collected from each mouse were immediately stored in centrifuge tubes and filled with electron microscope fixative (Servicebio, Wuhan, China) for transmission electron microscopy (TEM; Gang et al., 2019). Cell samples were harvested and fixed with electron microscope fixative for TEM. Both tissue and cell samples were dehydrated with ethanol at 25°C for 15 min per step. Cells were then placed into epoxy resin acetone mixtures (Solarbio) for 2 h and then into pure resin (Solarbio) overnight at 37°C. Next, an ultramicrotome (Leica EM, Wetzlar, Germany) was used to cut ultra-thin sections, which were stained by uranyl acetate and lead citrate (1%, Solarbio) and detected using TEM (Hitachi H-7650, Tokyo, Japan).

Western Blot Analysis

Both BMECs and mammary tissues were collected after treatment, and protein content was determined using a BCA assay kit (Beyotime). Each sample was separated by 12% sodium dodecyl sulfate-polyacrylamide gels, transferred onto polyvinylidene fluoride membranes (Bio-Rad, CA, Hercules, United States), and blocked by 5% BSA for 12 h at 4°C. The membranes were cultured with primary antibodies (zonula occludins-1 (ZO-1), claudin-1, claudin-4, and occludin for BMECs, 1:500 dilution, Bioss Antibodies, Beijing, China; ZO-1, claudin-3, and occludin for mice mammary tissue, 1:2,000 dilution, Abcam, Cambridge, United Kingdom) at 25°C for 3 h. After washing with Tris-buffered saline with tween (NobleRyder, Beijing, China), the membranes were incubated with secondary antibodies (1:1,000 dilution, CoWin Biosciences) at 25°C for 1 h. Protein bands were visualized by a Beyo Enhanced Chemiluminescence reagent kit (Solarbio). MultiImager (Bio-Rad Gel Doc XR) and ImageJ software (National Institutes of Health, Bethesda, MD, United States) were used to detect protein expression.

Enzyme-Linked Immunosorbent Assay

Tumor necrosis factor (TNF)-α, IL-6, and IL-1β expression in both BMECs and mammary tissues of mice were detected using bovine (DG Biotech, Beijing, China) and mouse ELISA kits (ThermoFisher), respectively. In detail, the cell medium was moved to a sterile centrifuge tube and centrifuged at 4°C for 10 min at 1000 × g for further test. Each tissue sample was added with 2 ml of RIPA tissue lysate (Solarbio), the cracked samples were centrifuged at 10,000–14,000 g for 4 min, and the supernatant was removed for further test.

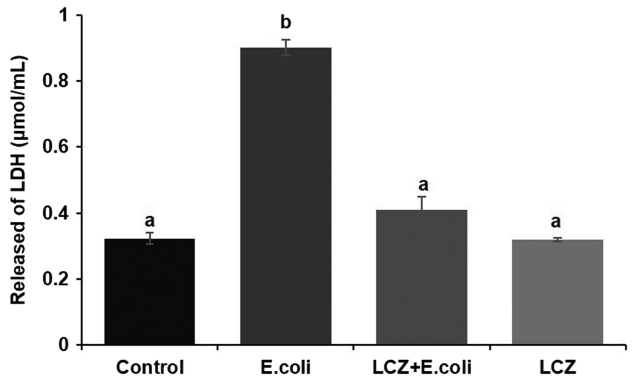


FIGURE 1 | Effect of *Lactobacillus casei* Zhang (LCZ) on changes in cell viability (n = 9). Cell viability was determined by the LDH method. Means with different superscripts differ significantly ($p < 0.01$).

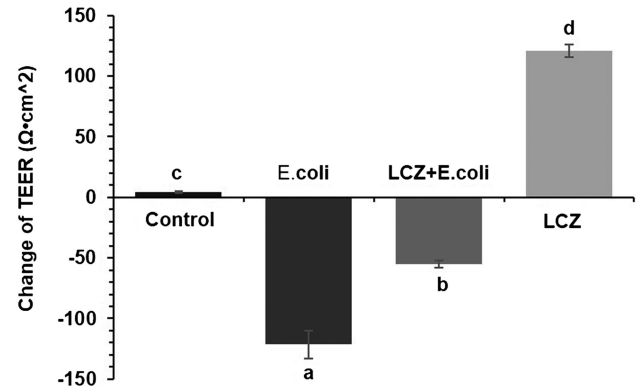


FIGURE 2 | Effect of LCZ on changes in TEER (n = 9). TEER was obtained using a Millicell Electrical Resistance System-2. TEER change = TEER of monolayer cells after treatment – TEER of monolayer cells before treatment. Means with different superscripts differ significantly ($p < 0.01$).

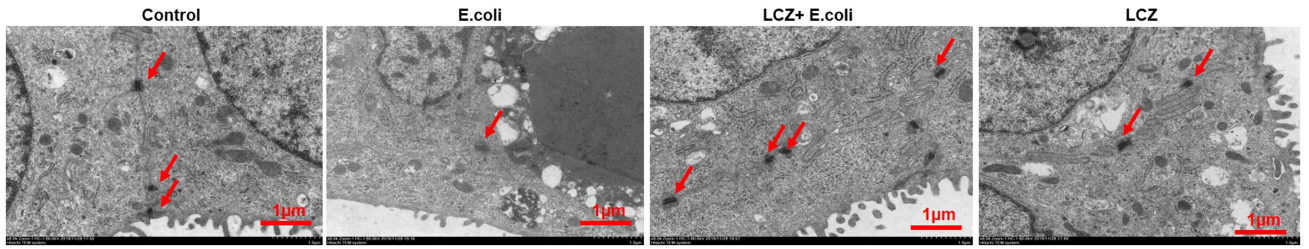


FIGURE 3 | Effect of LCZ on changes in blood-milk barrier structure (n = 9). Desmosome structure was detected using transmission electron microscopy (TEM). Scale bars: 1 μm. Means with different superscripts differ significantly ($p < 0.01$).

Statistical Analysis

All data were analyzed in SAS 9.2 (SAS Institute Inc., NYC, United States) and expressed as mean ± standard error of the mean (SEM). Graphs were produced with Origin 8.0 (Origin Lab, Northampton, MA, United States). Variance was analyzed using one-way ANOVA in SAS 9.2, followed by multiple comparisons using the Tukey method. The threshold for statistical significance was $p < 0.01$.

RESULTS

In vitro Pre-incubation With LCZ Reduces *E. coli*-Induced Damage of BMECs

Escherichia coli caused a significantly higher LDH release compared with the other groups ($p < 0.01$); there were no significant differences between the Control, LCZ + *E. coli*, and LCZ groups (**Figure 1**). TEER change in BMECs treated with *E. coli* was negative and significantly different from the other groups ($p < 0.01$). Specifically, although TEER change was significantly higher in the LCZ + *E. coli* group than in the Control group ($p < 0.01$), it was significantly less negative compared with the *E. coli* group ($p < 0.01$; **Figure 2**). The desmosome structure in the *E. coli* group was severely damaged and blurred as illustrated by TEM, whereas LCZ pretreatment noticeably alleviated desmosome structure damage. Moreover, the desmosome structure in the LCZ group was clearly visible, and no clear difference was detected compared with the Control group (**Figure 3**).

LCZ pretreatment significantly inhibited the *E. coli* adhesion rate to monolayer BMECs ($p < 0.01$), and the adhesion ability of LCZ to monolayer BMECs was significantly lower compared with *E. coli* ($p < 0.01$; **Figure 4**). The expression of claudin-1, claudin-4, occludin, and ZO-1 in BMECs was significantly decreased in the *E. coli* group compared with the other groups ($p = 0.02$; **Figure 5**), and LCZ pretreatment significantly increased the expression of these four proteins ($p = 0.02$). Moreover, ZO-1 expression in the LCZ group was significantly increased ($p = 0.02$); there were no significant differences in the expression of the other three proteins between the LCZ group and the Control group. The effect of LCZ on the expression of inflammatory cytokines in BMECs is shown in **Figure 6**. The expression of TNF-α, IL-6, and IL-β was significantly higher in the *E. coli* group than in the other groups ($p < 0.01$); LCZ pretreatment inhibited the expression of these cytokines ($p < 0.01$).

In vivo Pre-infusion With LCZ Reduces *E. coli*-Induced Injury in Mice Mammary Tissue

No redness or swelling was detected in the mammary tissues in the Control, LCZ + *E. coli*, and LCZ groups, and there was no significant difference in the injury score among these groups (**Figure 7**). However, visible redness and bleeding were observed in the *E. coli* group, and LCZ pretreatment significantly reduced the injury score ($p < 0.01$). No visible pathological damage was observed in the mammary acinar structure of the mice in the Control and LCZ groups; by contrast, *E. coli* caused remarkable pathological injury and led to the presence of a large number of neutrophils in the alveolar lumen (**Figure 8**). LCZ pretreatment significantly alleviated mammary acinar structure damage and the number of neutrophils compared with the *E. coli* group; furthermore, a significant decrease in the histological score was observed ($p < 0.01$). The tight junction structure in the *E. coli* group was severely damaged and blurred under TEM (**Figure 9**) but was visibly alleviated in the LCZ + *E. coli* group. The tight junction structure in the LCZ group was apparent, and there were no obvious differences between the LCZ group and the Control group.

The tight junction proteins claudin-3, occludin, and ZO-1 in mice mammary tissue were clearly localized on the interstitial side, as well as in the intercellular regions of the neighboring alveolar epithelial cells before *E. coli* infusion (Control group); nevertheless, the localization of these three proteins was disturbed by *E. coli*. In addition, LCZ pretreatment greatly promoted the positive reactions of these proteins in the alveolar lumen compared with the *E. coli* group. These three proteins were all localized on the interstitial side, and no differences were noted between the LCZ and Control groups (**Figures 10–12**). Tight junction protein expression in mice mammary tissues was significantly decreased in the *E. coli* group relative to the other groups ($p < 0.01$; **Figure 13**). LCZ pretreatment significantly increased the expression of these proteins compared with the *E. coli* group ($p < 0.01$), and no significant differences were noted between the LCZ and Control groups. The effect of LCZ on inflammatory cytokine expression in mice mammary tissue is shown in **Figure 14**. TNF-α, IL-6, and IL-1β expressions were significantly increased by *E. coli* ($p < 0.01$), whereas LCZ pretreatment significantly decreased the expression of these cytokines ($p < 0.01$). IL-1β expression was significantly higher in the LCZ group than in the Control group ($p < 0.01$), and no significant differences were detected in IL-6 and TNF-α expressions.

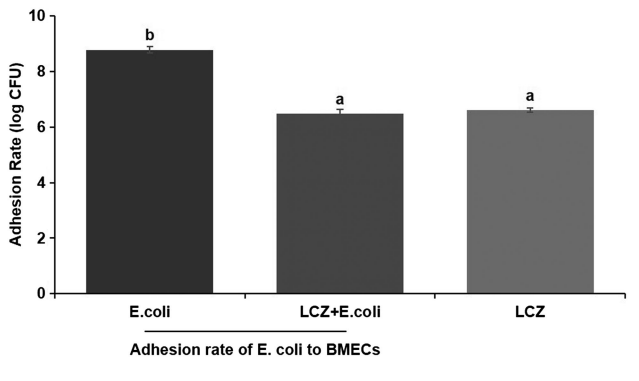


FIGURE 4 | Effect of LCZ on the adhesion rate of *E. coli* to bovine mammary epithelial cells (BMECs; $n = 9$). Means with different superscripts differ significantly ($p < 0.01$).

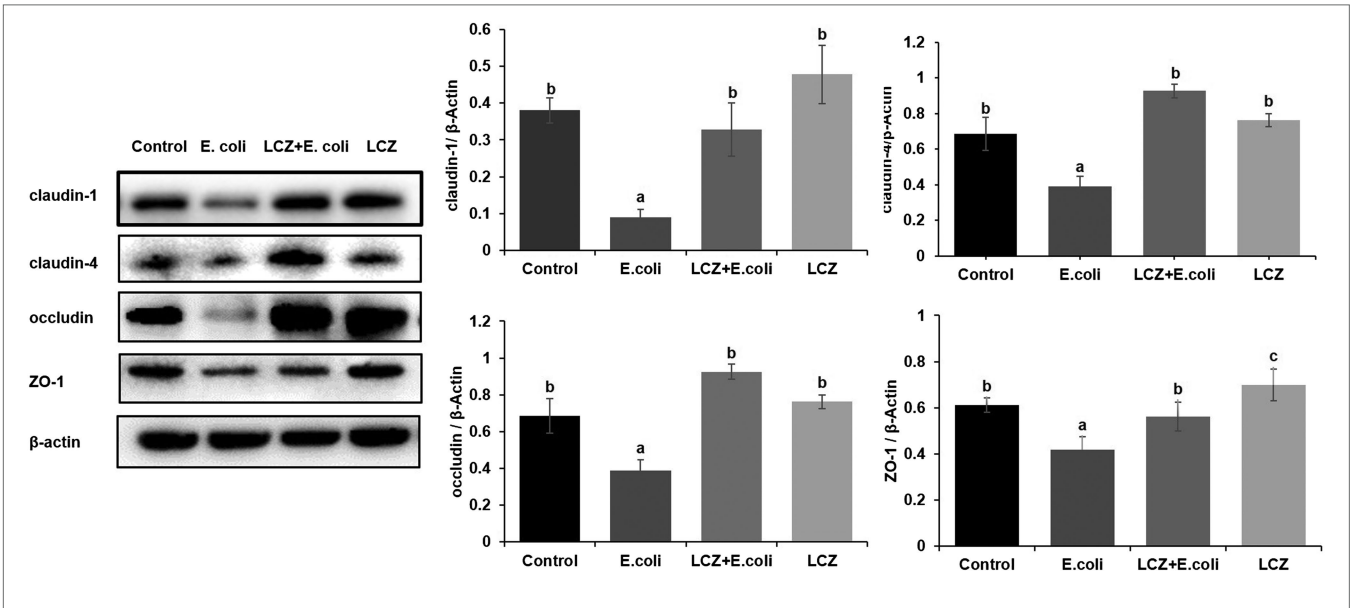


FIGURE 5 | Effect of LCZ on the tight junction protein expression of BMECs ($n = 9$). Quantification of proteins was normalized to β-actin. Means with different superscripts differ significantly ($p < 0.01$).

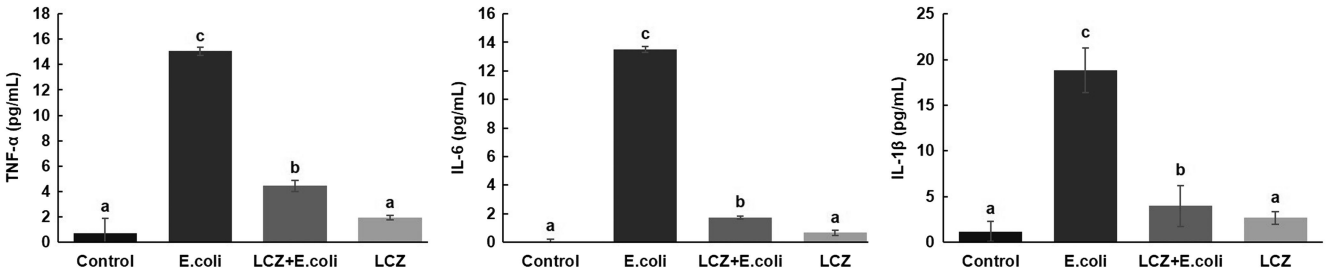


FIGURE 6 | Effect of LCZ on the inflammatory cytokine transcription of BMECs (n = 9). TNF-α, IL-1β, and IL-6 transcriptions were measured by ELISA. Means with different superscripts differ significantly ($p < 0.01$).

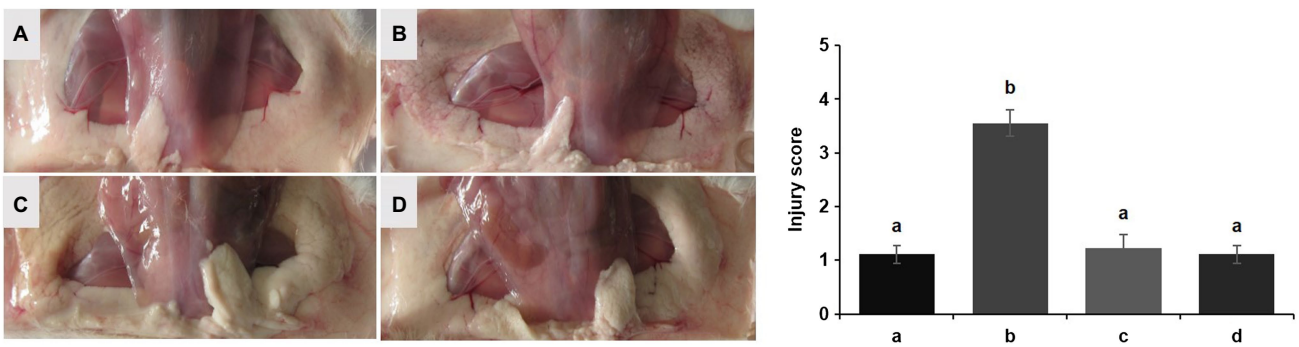


FIGURE 7 | Effect of LCZ on the histopathological impairment of mice mammary tissue. Injury score of mice mammary tissue from the Control **(A)**, *E. coli* **(B)**, LCZ + *E. coli* **(C)**, and LCZ **(D)** groups. The injury score ranged from 1 to 5, where 1 indicates no damage, 2 indicates slight redness, 3 indicates redness and slight bleeding, 4 indicates redness and bleeding, and 5 indicates redness and obvious bleeding. Data shown are means ± standard error of the mean (SEM) (n = 10). Means with different superscripts differ significantly ($p < 0.01$).

DISCUSSION

Lactobacillus casei Zhang has a promising prophylactic effect against several inflammatory diseases (Wang et al., 2013, 2016; Zhang et al., 2017), and recent research has shown that LCZ can have a prophylactic effect against mastitis in mice when administered orally (Ma et al., 2018). Here, both *in vitro* and *in vivo* tests were conducted to characterize the prophylactic effect of LCZ on *E. coli*-stimulated BMECs and mice mammary injury; its potential mechanism was also studied. In dairy farming, the treatment of mastitis is mainly carried out through milk duct infusion; therefore, in this study, intramammary infusion instead of oral infusion was chosen during *in vivo* test. This study revealed that LCZ pretreatment could dramatically counteract BMEC injury induced by *E. coli*, a finding that is consistent with previous studies (Chen et al., 2017; Dinić et al., 2017; Wang et al., 2018a). The prophylactic effect of LCZ on *E. coli*-induced mastitis in mice by intramammary infusion was also explored in this study. The result showed that pre-infusion of LCZ could reduce the number of neutrophils and relieve damage to mammary tissue, which was also consistent with the results of *in vitro* test, which shows that LCZ pretreatment decreases the release of LDH of BMECs. Recent studies have shown that intramammary infusion of *Lactococcus* does not cause inflammatory reactions; after intramammary infusion of *Lactococcus*, immune proteins acute phase proteins haptoglobin and milk amyloid A were significantly expressed in the mammary glands of healthy Holstein cows (Pyorala, 2003; Eckersall et al., 2006; Crispie et al., 2008), and no major bovine mastitis pathogen was detected (Pellegrino et al., 2017). Therefore, findings of this study indicate that LCZ can prevent bovine mastitis, which might be related to its ability to promote the production of lactic acid, antibacterial peptides, and other beneficial substances (Lebeer et al., 2018).

Several studies have indicated that pro-inflammatory cytokines play an important regulatory role in the disorder of tight junctions induced by inflammation (Schulzke et al., 2009; Zhang et al., 2018). The integrity of the blood-milk barrier could protect mammary epithelial cells from infection by pathogens and thus prevent an inflammatory reaction. TNF-α and IL-1β disrupt tight junctions, and IL-6 is associated with host defense against inflammatory disease (Rochfort et al., 2014; Cheng et al., 2018). In this study, the expression of TNF-α, IL-6, and IL-1β caused by *E. coli* decrease significantly when pretreated with LCZ, which is consistent with the results of Wu et al. (2016) showing that *Lactobacillus* pretreatment effectively reduce the upregulation of TNF-α, IL-1β, and IL-8 mRNA expressions induced by *E. coli*. This may because that LCZ pretreatment may promote an early alert state of the immune system which could improve the

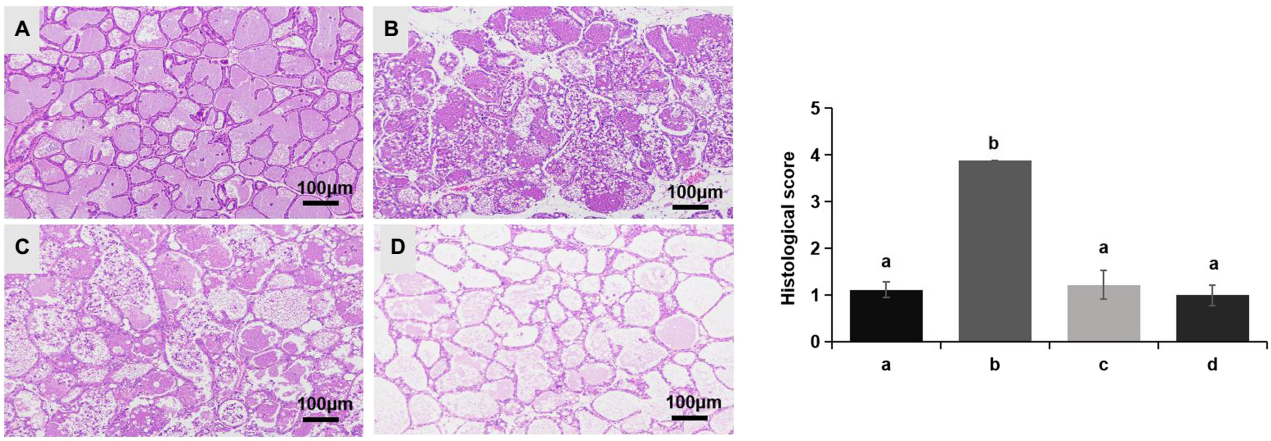


FIGURE 8 | Effect of LCZ on the histopathological impairment of mice mammary tissue. Histological score of hematoxylin-eosin-stained pathological sections from the Control **(A)**, *E. coli* **(B)**, LCZ + *E. coli* **(C)**, and LCZ **(D)** groups. Hematoxylin-eosin staining of formalin-fixed mammary gland. Scale bars: 100 μm. The histological score ranged from 1 to 5, where 1 indicates the absence of histological features (e.g., necrosis, neutrophils, and lymphocytes), 2 indicates minimal histological features (i.e., individual neutrophils), 3 indicates mild histological features (i.e., a small amount of neutrophils), 4 indicates moderate histological characteristics (i.e., many neutrophils and slight damage to glandular structure), and 5 indicates severe histological characteristics (i.e., a large number of neutrophils and severe damage to glandular structure). Data shown are means ± SEM (n = 10). Means with different superscripts differ significantly ($p < 0.01$).

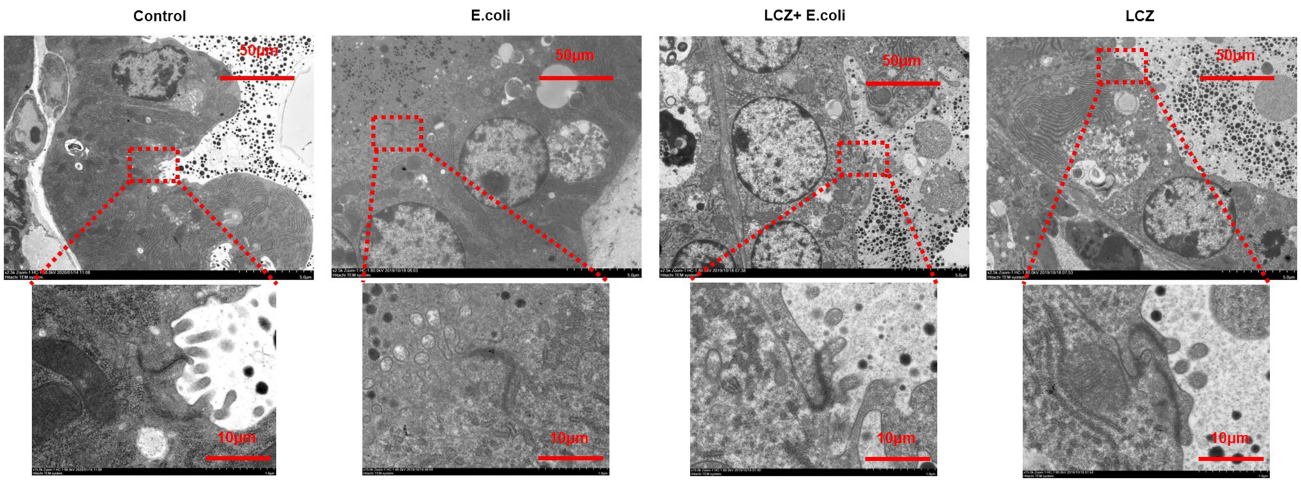


FIGURE 9 | Effect of LCZ on the tight junction structure of mice mammary tissue. The structure of the tight junction was observed by TEM.

alertness of the host defensive system, thus stopping a subsequent strong infection rapidly (Kingma et al., 2011). Furthermore, the previous studies have shown that the inflammatory response can decrease acinar tight junction protein expression (Hartwig et al., 2003; Oguro et al., 2011) and affect barrier function. *In vitro* test showed that LCZ could significantly inhibit inflammatory cytokine expression by inhibiting *E. coli* infection; we thus also measured inflammatory cytokine expression in mice mammary tissue and got the same result. Therefore, this study indicates that the prophylactic effect of LCZ may be achieved by increase the alert state increasing a little bit the levels of immune regulators, which allows to decrease the expression of inflammatory cytokines in both BMECs and mice mammary tissue caused by *E. coli*. Besides, in exploring the underlying mechanism of the prophylactic effect of LCZ against *E. coli*-treated cells and blood-milk barrier damage, this study found that LCZ pretreatment could significantly reduce the adhesion rate of *E. coli* to BMECs. These results are consistent with recent studies showing that *Lactobacillus* could significantly inhibit the adhesion of *E. coli* to Caco-2 (Behbahani et al., 2019) and HT-29 cells (Dhanani and Bagchi, 2013). Therefore, the prophylactic effect of LCZ on BMECs could be mediated by the inhibition of *E. coli* adhesion, so that the expression of cytokines was decreased lower, which lead to *E. coli* infection decrease.

Mammary epithelial cells form the blood-milk barrier through special connecting structures, such as tight junctions.

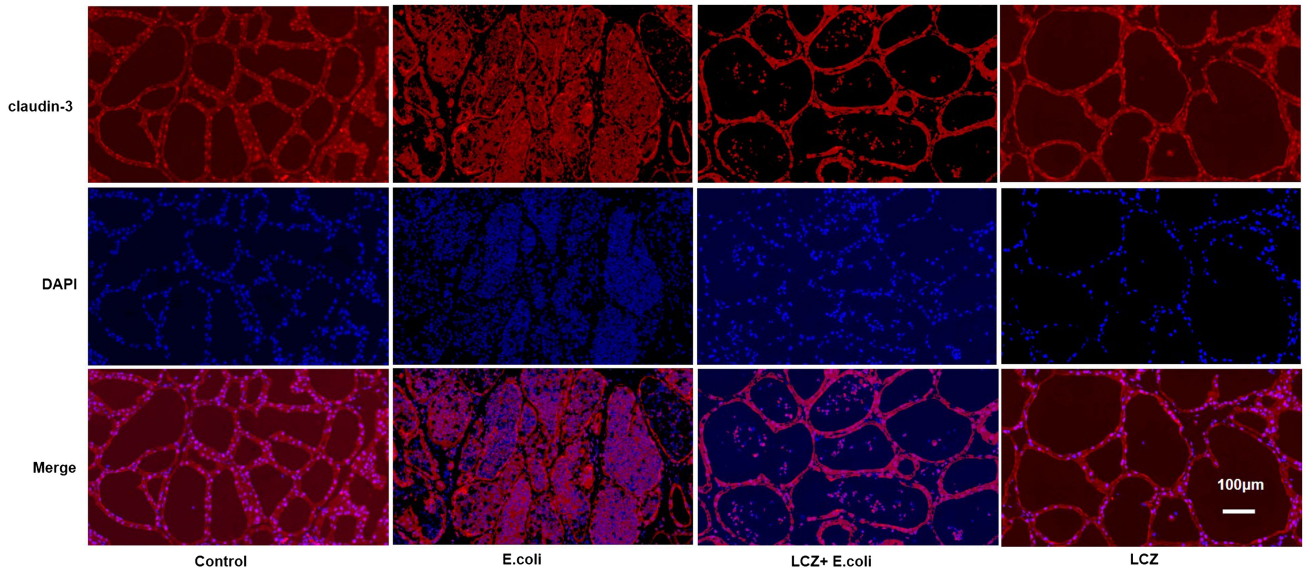


FIGURE 10 | Effect of LCZ on the location of claudin-3 in mice mammary tissue. Blue shows nuclei (DAPI), and red shows claudin-3. Scale bars: 100 μm.

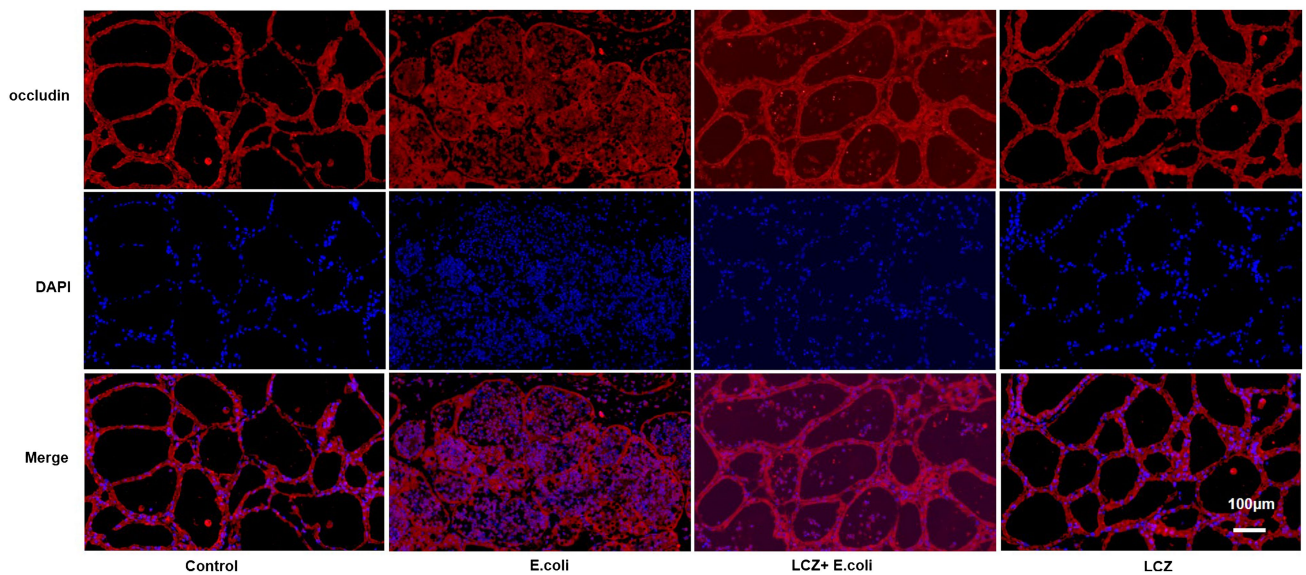


FIGURE 11 | Effect of LCZ on the location of occludin. Blue shows nuclei (DAPI), and red shows occludin. Scale bars: 100 μm.

Several mammary pathogenic bacteria, including *E. coli*, cause mastitis. The blood-milk barrier is leaky in bovine mastitis, which permits molecules to cross the barrier and occur in milk (Nguyen and Neville, 1998; Lehmann et al., 2013). Specifically, *E. coli* can damage tight junction structure, thereby increasing the permeability of the epithelial barrier and causing pathogens in the acinus to enter mammary tissue (Bruewer et al., 2006; Shen and Turner, 2006). TEER reflects the integrity of the monolayer cells, the ion conductance of the pathway adjacent to monolayer epithelial cells, and the pore size of tight junctions (Flavia et al., 2006). This study showed that LCZ pretreatment could significantly mitigate the reduction in TEER caused by *E. coli*. This result corroborated the findings of several previous studies showing that *Lactobacillus* could significantly promote the TEER of Caco-2 and NCM460 cells (Horibe et al., 1997; Liu et al., 2010; Qiu et al., 2017). Accordingly, this study proposes that LCZ enhances the densification of monolayer BMECs. The same conclusion was obtained based on TEM observations of the desmosome structure between cells. Furthermore, tight junction proteins

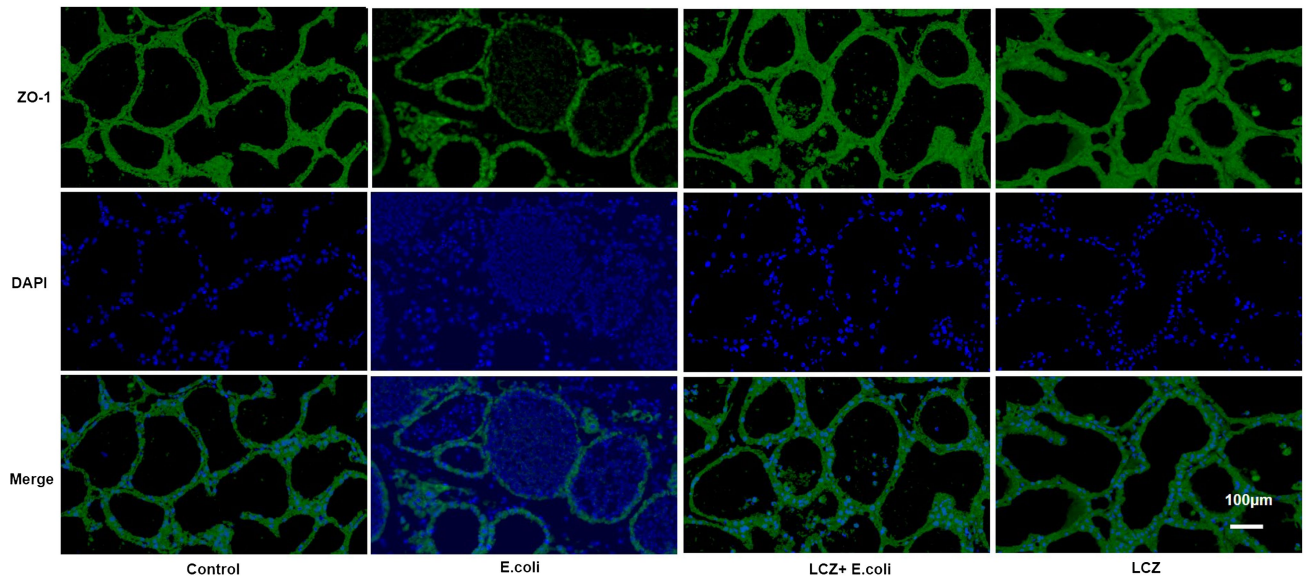


FIGURE 12 | Effect of LCZ on the location of ZO-1 in mice mammary tissue. Blue shows nuclei (DAPI), and green shows ZO-1. Scale bars: 100 μm.

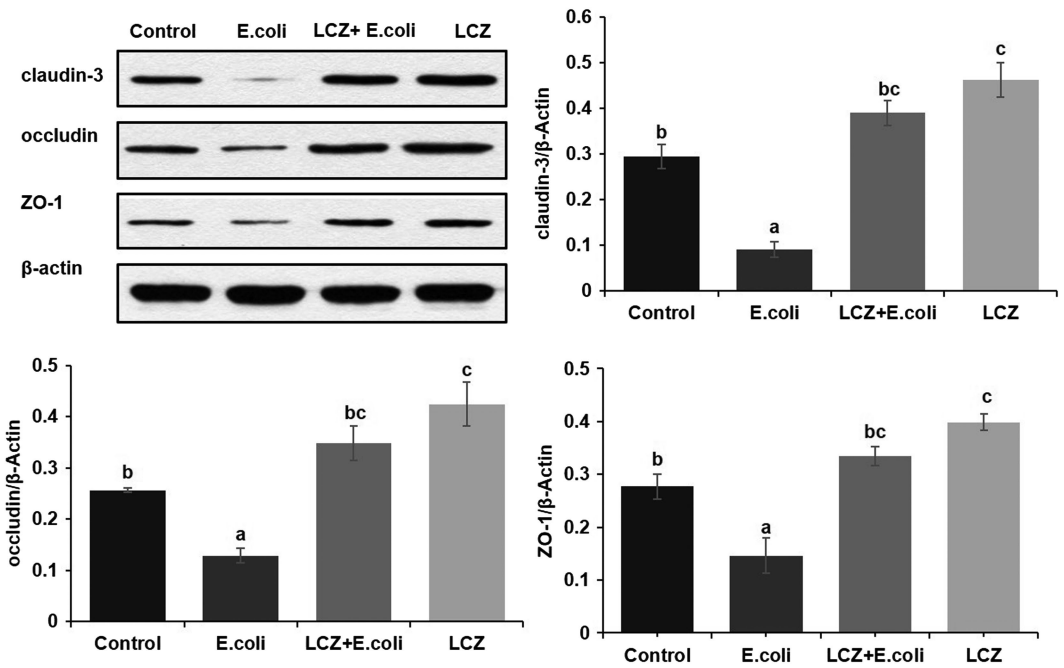


FIGURE 13 | Effect of LCZ on the expression of claudin-3, occludin, and ZO-1 in mice mammary tissue. Quantification of proteins was normalized to β-actin. Data shown are means ± SEM (n = 10). Means with different superscripts differ significantly ($p < 0.01$).

are known to maintain the structural integrity of tight junctions, which is necessary for the normal function of the blood-milk barrier (Shen et al., 2006; Guo et al., 2019). This study indicates that LCZ pretreatment could significantly increase tight junction protein expression in BMECs, which is consistent with the TEER results. These results are also consistent with those of Karczewski et al. (2010) and Wang et al. (2018b) showing that *Lactobacillus plantarum* could effectively promote occludin and ZO-1 expression in human intestinal cells as well as claudin-1 in IPEC-J2 cells. Moreover, Johnson et al. (2008) found that *Lactobacillus rhamnosus* could effectively promote claudin-1 and ZO-1 expression in T84 epithelial cells. The results of the Western blot, immunofluorescence, and the TEM *in vivo* test also showed that pre-infusion of LCZ could enhance

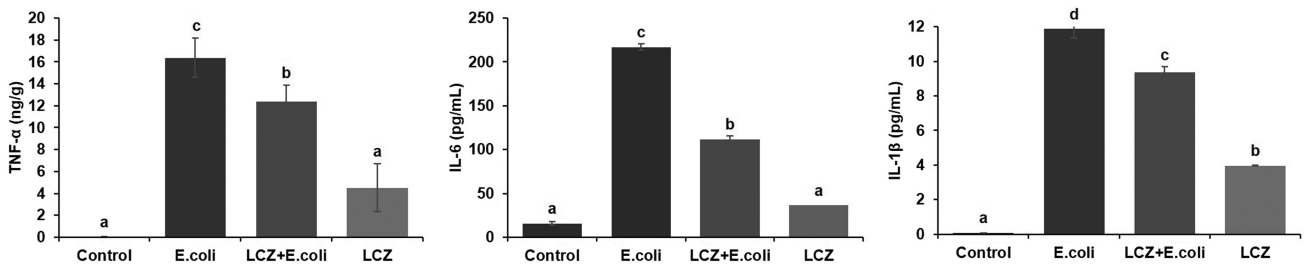


FIGURE 14 | Effect of LCZ on the inflammatory cytokine transcription of mice mammary tissue (n = 10). Levels of TNF-α, IL-1β, and IL-6 were measured by ELISA. Means with different superscripts differ significantly ($p < 0.01$).

the tight junction structure and upregulate tight junction protein expression in the mammary alveolar lumen in mice. This result is consistent with our *in vitro* test as well as previous studies, including Mennigen et al. (2009), Karczewski et al. (2010), and Patel et al. (2012), indicating that *Lactobacillus* can significantly promote the tightness of the intestinal epithelial barrier in both mice and humans by increasing tight junction protein expression. Consequently, this study found that LCZ could promote the integrity of the epithelial barrier *via* increasing tight junction protein expression in both BMECs and mice mammary tissues, and lead to lower expression of inflammatory cytokines, thereby alleviating damage to mammary tissue.

CONCLUSION

This study shows that LCZ has prophylactic effect on *E. coli*-induced injury of mammary gland. It could counteract the blood-milk barrier disruption and decrease the inflammatory response, which mechanism included the promotion of tight junction protein expression and the inhibition of *E. coli* infection in both BMECs and mice mammary tissue. This study provides a new perspective on the protective effect of LCZ as well as an effective prophylactic agent for preserving blood-milk barrier function during *E. coli*-induced mastitis.

DATA AVAILABILITY STATEMENT

The original contributions presented in the study are included in the article/supplementary material, and further inquiries can be directed to the corresponding author.

ETHICS STATEMENT

The animal study was reviewed and approved by the National Institutes of Health Guide for the Care and Use of Laboratory Animals (GB14925-2010, China).

AUTHOR CONTRIBUTIONS

YZ, GL, and SL conceived and designed the experiments. YZ performed the experiments, analyzed the data, and wrote the manuscript. GL, WW, and SL reviewed and edited the manuscript. GL, WW, YW, ZC, HY, and SL provided guidance for the experiments. All authors contributed to the article and approved the submitted version.

FUNDING

This work was supported by the National Natural Science Foundation of China (31772628).

ACKNOWLEDGMENTS

We thank the Key Laboratory of Dairy Biotechnology and Engineering, Inner Mongolia Agricultural University for providing Strain *Lactobacillus casei* Zhang, and the College of Animal Science and Technology Feed Engineering Technology Research Center, Yangzhou University for providing BMECs.

REFERENCES

Angelopoulou, A., Field, D., Ryan, C. A., Stanton, C., Hill, C., and Ross, R. P. (2018). The microbiology and treatment of human mastitis. *Med. Microbiol. Immunol.* 207, 1–12. doi: 10.1007/s00430-017-0532-z

Arroyo, R., Martín, V. M. A., Jiménez, E. F. L., and Rodríguez, J. M. (2010). Treatment of infectious mastitis during lactation: antibiotics versus oral administration of lactobacilli isolated from breast milk. *Clin. Infect. Dis.* 50, 1551–1558. doi: 10.1086/652763

Behbahani, B. A., Noshad, M., and Falah, F. (2019). Inhibition of *Escherichia coli* adhesion to human intestinal Caco-2 cells by probiotic candidate *Lactobacillus plantarum* strain L15. *Microb. Pathog.* 136, 103677–103684. doi: 10.1016/j.micpath.2019.103677

Bruewer, M., Samarin, S., and Nusrat, A. (2006). Inflammatory bowel disease and the apical junctional complex. *Ann. N. Y. Acad. Sci.* 1072, 242–252. doi: 10.1196/annals.1326.017

Chen, Z.-Y., Hsieh, Y.-M., Huang, C.-C., and Tsai, C.-C. (2017). Inhibitory effects of probiotic *Lactobacillus* on the growth of human colonic carcinoma cell line HT-29. *Molecules* 22:107. doi: 10.3390/molecules22010107

Cheng, Y., Desse, S., Martinez, A., Worthen, R. J., Jope, R. S., and Beurel, E. (2018). TNFα disrupts blood brain barrier integrity to maintain prolonged depressive-like behavior in mice. *Brain Behav. Immun.* 69, 556–567. doi: 10.1016/j.bbi.2018.02.003

Crispie, F., Alonso-Gómez, M., O'Loughlin, C., Klostermann, K., Flynn, J., Arkins, S., et al. (2008). Intramammary infusion of a live culture for treatment of bovine mastitis: effect of live lactococci on the mammary immune response. *J. Dairy Res.* 75, 374–384. doi: 10.1017/S0022029908003385

da Costa, W. K. A., Brandão, L. R., Martino, M. E., Garcia, E. F., Alves, A. F., de Souza, E. L., et al. (2016). Qualification of tropical fruit-derived *Lactobacillus plantarum* strains as potential probiotics acting on blood glucose and total cholesterol levels in Wistar rats. *Food Res. Int.* 8, 109–117. doi: 10.1016/j.foodres.2018.08.035

Dhanani, A. S., and Bagchi, T. (2013). *Lactobacillus plantarum* CS24.2 prevents *Escherichia coli* adhesion to HT-29 cells and also down-regulates enteropathogen-induced tumor necrosis factor-alpha and interleukin-8 expression. *Microbiol. Immunol.* 57, 309–315. doi: 10.1111/1348-0421.12038

Dinić, M., Lukić, J., Djokić, J., Milenković, M., Strahinić, I., Golić, G., et al. (2017). *Lactobacillus fermentum* postbiotic-induced autophagy as potential approach for treatment of acetaminophen hepatotoxicity. *Front. Microbiol.* 8:594. doi: 10.3389/fmicb.2017.00594

Eckersall, P. D., Young, F. J., Nolan, A. M., Knight, C. H., McComb, C., Waterston, M. M., et al. (2006). Acute phase proteins in bovine milk in an experimental model of *Staphylococcus aureus* subclinical mastitis. *J. Dairy Sci.* 89, 1488–1501. doi: 10.3168/jds.S0022-0302(06)72216-0

Fernández, L., Cárdenas, N., Arroyo, R., Manzano, S., Jiménez, E., Martín, V., et al. (2016). Prevention of infectious mastitis by oral administration of *Lactobacillus salivarius* PS2 during late pregnancy. *Clin. Infect. Dis.* 62, 568–573. doi: 10.1093/cid/civ974

Flavia, Z., Anne-Françoise, B., Giovanna, B., Jean, C., Arianna, C., Rosa, C., et al. (2006). An inter-laboratory study to evaluate the effects of medium composition on the differentiation and barrier function of Caco-2 cell lines. *Altern. Lab. Anim* 33, 603–618. doi: 10.1177/026119290503300618

Gang, L., Yin, J., Han, B., Barkema, H. W., Shahid, M., De Buck, J., et al. (2019). Adherent/invasive capacities of bovine-associated *Aerococcus viridans* contribute to pathogenesis of acute mastitis in a murine model. *Vet. Microbiol.* 230, 202–211. doi: 10.1016/j.vetmic.2019.02.016

Garcia-Castilla, V., Komatsu, R., Clua, P., Indo, Y., Takagi, M., Salva, S., et al. (2019). Evaluation of the immunomodulatory activities of the probiotic strain *Lactobacillus fermentum* UCO-979C. *Front. Immunol.* 10:1376. doi: 10.3389/fimmu.2019.01376

Guo, W., Liu, B., Hu, G., Kan, X., Li, Y., Gong, Q., et al. (2019). Vanillin protects the blood-milk barrier and inhibits the inflammatory response in LPS-induced mastitis in mice. *Toxicol. Appl. Pharmacol.* 365, 9–18. doi: 10.1016/j.taap.2018.12.022

Hartwig, W., Karen, W. B., Jörg, K., Gesa, R. E., Stefan, L., Stefan, H., et al. (2003). Localization of claudin-3 in tight junctions of the blood-brain barrier is selectively lost during experimental autoimmune encephalomyelitis and human glioblastoma multiforme. *Acta Neuropathol.* 105, 586–592. doi: 10.1007/s00401-003-0688-z

Horibe, Y., Hosoya, K., Kim, K.-J., Ogiso, T., and Lee, V. H. L. (1997). Polar solute transport across the pigmented rabbit conjunctiva: size dependence and the influence of 8-bromo cyclic adenosine monophosphate. *Pharm. Res.* 14, 1246–1251. doi: 10.1023/A:1012123411343

Ignacio, F., Pellegrino, M., Giraudo, J., Nader-Macias, M. E., and Cristina, B. (2015). Evaluation of beneficial lactic acid bacteria strains as a potential probiotic for the prevention of bovine mastitis. *Front. Immunol.* 6, 231–239. doi: 10.3389/conf.fimmu.2015.05.00231

Igor, S., Sharon, M. D., Zdislava, S., Vera, N. B., Eva, V., Vera, J., et al. (2019). Colonization of germ-free piglets with commensal *Lactobacillus amylovorus*, *Lactobacillus mucosae* and probiotic *E. coli* Nissle 1917 and their interference with *Salmonella typhimurium*. *Microorganisms* 7, 273–291. doi: 10.3390/microorganisms7080273

Jiménez, E., Fernández, L., Maldonado, A., Martín, R., Olivares, M., et al. (2008). Oral administration of *Lactobacillus* strains isolated from breast milk as an alternative for the treatment of infectious mastitis during lactation. *Appl. Environ. Microbiol.* 74, 4650–4655. doi: 10.1128/AEM.02599-07

Johnson, H. K. C., Donato, K. A., Shen, T. G., Gordanpour, M., and Sherman, P. M. (2008). *Lactobacillus rhamnosus* strain GG prevents enterohemorrhagic *Escherichia coli* O157: H7-induced changes in epithelial barrier function. *Infect. Immun.* 76, 1340–1348. doi: 10.1128/IAI.00778-07

Kingma, S. D., Li, N., Sun, F., Valladares, R. B., Neu, J., and Lorca, G. L. (2011). *Lactobacillus johnsonii* N6.2 stimulates the innate immune response through toll-like receptor 9 in Caco-2 cells and increases intestinal crypt Paneth cell number in biobreeding diabetes-prone rats. *J. Nutr.* 141, 102–1028. doi: 10.3945/jn.110.135517

Karczewski, J., Troost, F. J., Konings, I., Dekker, J., and Wells, J. M. (2010). Regulation of human epithelial tight junction proteins by *Lactobacillus plantarum* in vivo and protective effects on the epithelial barrier. *Am. J. Physiol. Gastrointest. Liver Physiol.* 298, G851–G859. doi: 10.1152/ajpgi.00327.2009

Kitching, M., Mathur, H., Flynn, J., Byrne, N., Dillon, P., Sayers, R., et al. (2019). A live bio-therapeutic for mastitis, containing *Lactococcus lactis* DPC3147 with comparable efficacy to antibiotic treatment. *Front. Microbiol.* 10:2220. doi: 10.3389/fmicb.2019.02220

Lhermie, G., Grohn, Y. T., and Raboisson, D. (2016). Addressing antimicrobial resistance: an overview of priority actions to prevent suboptimal antimicrobial use in food-animal production. *Front. Microbiol.* 7:2114. doi: 10.3389/fmicb.2016.02114

Lebeer, S., Peter, A. M., Marco, M. L., Van Pijkeren, J.-P., Motherway, M. O., Hill, C., et al. (2018). Identification of probiotic effector molecules: present state and future perspectives. *Curr. Opin. Biotechnol.* 49, 217–223. doi: 10.1016/j.copbio.2017.10.007

Lehmann, M., Wellnitz, O., and Bruckmaier, R. M. (2013). Concomitant lipopolysaccharide-induced transfer of blood-derived components including immunoglobulins into milk. *J. Dairy Sci.* 96, 889–896. doi: 10.3168/jds.2012-5410

Li, X.-X., Wang, H., Du, X.-X., Yu, W.-N., Jiang, J.-W., et al. (2017). Lactobacilli inhibit cervical cancer cell migration in vitro and reduce tumor burden in vivo through upregulation of E-cadherin. *Oncol. Rep.* 38, 1561–1568. doi: 10.3892/or.2017.5791

Liu, Z.-H., Shen, T.-Y., Zhang, P., Ma, Y.-L., Moyer, M. P., and Qin, H.-L. (2010). Protective effects of *Lactobacillus plantarum* against epithelial barrier dysfunction of human colon cell line NCM460. *World J. Gastroenterol.* 16, 5759–5766. doi: 10.3748/wjg.v16.i45.5759

Ma, C., Sun, Z., Zeng, B., Huang, S., Zhao, J., Zhang, Y., et al. (2018). Cow-to-mouse fecal transplantations suggest intestinal microbiome as one cause of mastitis. *Microbiome* 6, 200–217. doi: 10.1186/s40168-018-0578-1

Mennigen, R., Nolte, K., Rijcken, E., Utech, M., Loeffler, B., Senninger, N., et al. (2009). Probiotic mixture VSL#3 protects the epithelial barrier by maintaining tight junction protein expression and preventing apoptosis in a murine model of colitis. *Am. J. Physiol. Gastrointest. Liver Physiol.* 296, 1140–1149. doi: 10.1152/ajpgi.90534.2008

Muziasari, W. I., Pitkänen, L. K., Sørum, H., Stedtfeld, R. D., Tiedje, J. M., and Marko, V. (2016). The resistome of farmed fish feces contributes to the enrichment of antibiotic resistance genes in sediments below Baltic Sea fish farms. *Front. Microbiol.* 7:2137. doi: 10.3389/fmicb.2016.02137

Nguyen, D. A., and Neville, M. C. (1998). Tight junction regulation in the mammary gland. *J. Mammary Gland Biol. Neoplasia* 3, 233–246. doi: 10.1023/A:1018707309361

Oguro, M., Koike, M., Ueno, T., Asaoka, D., Mori, H., Nagahara, A., et al. (2011). Dissociation and dispersion of claudin-3 from the tight junction could be one of the most sensitive indicators of reflux esophagitis in a rat model of the disease. *J. Gastroenterol.* 46, 629–638. doi: 10.1007/s00535-011-0390-1

Patel, R. M., Myers, L. S., Kurundkar, A. R., Maheshwari, A., Nusrat, A., and Lin, P. W. (2012). Probiotic bacteria induce maturation of intestinal claudin 3 expression and barrier function. *Am. J. Pathol.* 180, 626–635. doi: 10.1016/j.ajpath.2011.10.025

Pellegrino, M., Berardo, N., Giraudo, J., Nader-Macías, M. E. F., and Bogni, C. (2017). Bovine mastitis prevention: humoral and cellular response of dairy cows inoculated with lactic acid bacteria at the dry-off period. *Benefic. Microbes* 8, 589–596. doi: 10.3920/BM2016.0194

Pyorala, S. (2003). Indicators of inflammation in the diagnosis of mastitis. *Vet. Res.* 34, 565–578. doi: 10.1051/vetres:2003026

Qiu, Y.-Q., Jiang, Z.-Y., Hu, S.-L., Wang, L., Ma, X., and Yang, X.-Y. (2017). *Lactobacillus plantarum* enhanced IL-22 production in natural killer (NK) cells that protect the integrity of intestinal epithelial cell barrier damaged by enterotoxigenic *Escherichia coli*. *Int. J. Mol. Sci.* 18, 2409–2414. doi: 10.3390/ijms18112409

Rochfort, K. D., Collins, L. E., Murphy, R. P., Cummins, P. M., and Koval, M. (2014). Downregulation of blood-brain barrier phenotype by proinflammatory cytokines involves NADPH oxidase-dependent ROS generation: consequences for interendothelial adherens and tight junctions. *PLoS One* 9:e101815. doi: 10.1371/journal.pone.0101815

Sanders, M. E., Merenstein, D. J., Reid, G., Gibson, G. R., and Rastall, R. A. (2019). Probiotics and prebiotics in intestinal health and disease: from biology to the clinic. *Nat. Rev. Gastroenterol. Hepatol.* 16, 1–13. doi: 10.1038/s41575-019-0173-3

Sathiyabarathi, M., Jeyakumar, S., Manimaran, A., Jayaprakash, G., Heartwin, A., Pushpadass, M., et al. (2016). Infrared thermography: a potential noninvasive tool to monitor udder health status in dairy cows. *Vet. World* 9, 1075–1081. doi: 10.14202/vetworld.2016.1075-1081

Schulzke, J. D., Ploeger, S., Amasheh, M., Fromm, A., Zeissig, S., Troeger, H., et al. (2009). Epithelial tight junctions in intestinal inflammation. *Ann. N. Y. Acad. Sci.* 1165, 294–300. doi: 10.1111/j.1749-6632.2009.04062.x

Shen, L., and Turner, J. R. (2006). Role of epithelial cells in initiation and propagation of intestinal inflammation. Eliminating the static: tight junction dynamics exposed. *Am. J. Physiol. Gastrointest. Liver Physiol.* 290, G577–G582. doi: 10.1152/ajpgi.00439.2005

Shen, L., Black, E. D., Witkowski, E. D., Lencer, W. I., Guerriero, V., Schneeberger, E. E., et al. (2006). Myosin light chain phosphorylation regulates barrier function by remodeling tight junction structure. *J. Cell Sci.* 119, 2095–2106. doi: 10.1242/jcs.02915

Wang, B., Li, J., Wang, S., Hao, Y., Zhao, X., and Chen, J. (2018a). *Lactobacillus plantarum* ameliorates tumour necrosis factor-induced bacterial translocation in Caco-2 cells by regulation of TLR4 expression. *J. Med. Microbiol.* 67, 982–991. doi: 10.1099/jmm.0.000762

Wang, J., Ji, H., Wang, S., Liu, H., Zhang, W., Zhan, D., et al. (2018b). Probiotic *Lactobacillus plantarum* promotes intestinal barrier function by strengthening the epithelium and modulating gut microbiota. *Front. Microbiol.* 9:1953. doi: 10.3389/fmicb.2018.01953

Wang, Y., Li, Y., Xie, J., Zhang, Y., Wang, J., Sun, X., et al. (2013). Protective effects of probiotic *Lactobacillus casei* Zhang against endotoxin-and d-galactosamine-induced liver injury in rats via anti-oxidative and anti-inflammatory capacities. *Int. Immunopharmacol.* 15, 30–37. doi: 10.1016/j.intimp.2012.10.026

Wang, Y., Xie, J., Li, Y., Dong, S., Liu, H., Chen, J., et al. (2016). Probiotic *Lactobacillus casei* Zhang reduces pro-inflammatory cytokine production and hepatic inflammation in a rat model of acute liver failure. *Eur. J. Nutr.* 55, 821–831. doi: 10.1007/s00394-015-0904-3

Wu, Q., Liu, M.-C., Yang, J., Wang, J.-F., and Zhu, Y.-H. (2016). *Lactobacillus rhamnosus* GR-1 ameliorates *Escherichia coli*-induced inflammation and cell damage via attenuation of ASC-independent NLRP3 inflammasome activation. *Appl. Environ. Microbiol.* 82, 1173–1182. doi: 10.1128/AEM.03044-15

Zhang, M., Wu, Y., Xie, L., Teng, C.-H., Wu, F.-F., Xu, K.-B., et al. (2018). Isoliquiritigenin protects against blood brain barrier damage and inhibits the secretion of pro-inflammatory cytokines in mice after traumatic brain injury. *Int. Immunopharmacol.* 65, 64–75. doi: 10.1016/j.intimp.2018.09.046

Zhang, Y., Ma, C., Zhao, J., Xu, H., Hou, Q., and Zhang, H. (2017). *Lactobacillus casei* Zhang and vitamin K2 prevent intestinal tumorigenesis in mice via adiponectin-elevated different signaling pathways. *Oncotarget* 8, 24719–24727. doi: 10.18632/oncotarget.15791

Conflict of Interest: The authors declare that the research was conducted in the absence of any commercial or financial relationships that could be construed as a potential conflict of interest.

Copyright © 2021 Zheng, Liu, Wang, Wang, Cao, Yang and Li. This is an open-access article distributed under the terms of the Creative Commons Attribution License (CC BY). The use, distribution or reproduction in other forums is permitted, provided the original author(s) and the copyright owner(s) are credited and that the original publication in this journal is cited, in accordance with accepted academic practice. No use, distribution or reproduction is permitted which does not comply with these terms.

frontiers in Immunology

REVIEW
published: 08 July 2021
doi: 10.3389/fimmu.2021.702142

Protein Kinase R in Bacterial Infections: Friend or Foe?

Robin Smyth[1] *and Jim Sun*[1,2]*

[1] Department of Biochemistry, Microbiology and Immunology, University of Ottawa, Ottawa, ON, Canada, [2] Centre for Infection, Immunity and Inflammation, University of Ottawa, Ottawa, ON, Canada

The global antimicrobial resistance crisis poses a significant threat to humankind in the coming decades. Challenges associated with the development of novel antibiotics underscore the urgent need to develop alternative treatment strategies to combat bacterial infections. Host-directed therapy is a promising new therapeutic strategy that aims to boost the host immune response to bacteria rather than target the pathogen itself, thereby circumventing the development of antibiotic resistance. However, host-directed therapy depends on the identification of druggable host targets or proteins with key functions in antibacterial defense. Protein Kinase R (PKR) is a well-characterized human kinase with established roles in cancer, metabolic disorders, neurodegeneration, and antiviral defense. However, its role in antibacterial defense has been surprisingly underappreciated. Although the canonical role of PKR is to inhibit protein translation during viral infection, this kinase senses and responds to multiple types of cellular stress by regulating cell-signaling pathways involved in inflammation, cell death, and autophagy – mechanisms that are all critical for a protective host response against bacterial pathogens. Indeed, there is accumulating evidence to demonstrate that PKR contributes significantly to the immune response to a variety of bacterial pathogens. Importantly, there are existing pharmacological modulators of PKR that are well-tolerated in animals, indicating that PKR is a feasible target for host-directed therapy. In this review, we provide an overview of immune cell functions regulated by PKR and summarize the current knowledge on the role and functions of PKR in bacterial infections. We also review the non-canonical activators of PKR and speculate on the potential mechanisms that trigger activation of PKR during bacterial infection. Finally, we provide an overview of existing pharmacological modulators of PKR that could be explored as novel treatment strategies for bacterial infections.

Keywords: Protein Kinase R, bacterial infection, macrophage signaling, antibacterial defense, EIF2AK2, cell death, autophagy, inflammation

OPEN ACCESS

Edited by:
Monica Cartelle Gestal, Louisiana State University Health Shreveport, United States

Reviewed by:
Som G. Nanjappa, University of Illinois at Urbana-Champaign, United States
Yuan Liu, Yangzhou University, China
Alan S. Cross, University of Maryland, Baltimore, United States

***Correspondence:**
Jim Sun
jim.sun@uottawa.ca

Specialty section:
This article was submitted to Microbial Immunology, a section of the journal Frontiers in Immunology

Received: *29 April 2021*
Accepted: *28 June 2021*
Published: *08 July 2021*

Citation:
Smyth R and Sun J (2021) Protein Kinase R in Bacterial Infections: Friend or Foe? Front. Immunol. 12:702142. doi: 10.3389/fimmu.2021.702142

INTRODUCTION

Interferon-induced, double-stranded RNA-activated protein kinase, also known as protein kinase R (PKR), is a ubiquitously and constitutively expressed serine-threonine kinase that is specifically found in vertebrate cells (1). PKR is encoded in humans by the *EIF2AK2* gene located on chromosome 2 and is 551 amino acids in length (2, 3). This kinase senses and responds to

multiple types of cellular stress by regulating cell-signaling pathways involved in inflammation, cell death, and autophagy. As such, dysregulation of PKR expression or activation has been linked to multiple human diseases, including neurodegeneration, cancer, metabolic disorders, and viral infections [reviewed in-depth previously: (4–6)]. In particular, the most well-characterized function of PKR is to sense viral double-stranded RNA (dsRNA) for its canonical role in antiviral defense (7).

The best characterized transcriptional inducers of PKR are type I interferons (IFN). Type I IFN are produced in response to pathogen-associated molecular patterns (PAMPs) and signal through the IFNα/IFNβ receptor (IFNAR) to induce transcription of numerous genes that assist in antiviral defense [reviewed in-depth previously (8)]. These genes are referred to as interferon-stimulated genes (ISGs) and include *EIF2AK2*. Indeed, the PKR promoter contains an interferon-stimulated response element (ISRE), thus prompting transcription of the *EIF2AK2* gene in response to type I IFN signaling (9). The PKR promoter also contains a kinase conserved sequence upstream of the ISRE, which possesses binding sites for the transcription factors Sp1 and Sp3 (9, 10). Sp1 and Sp3 cooperatively activate basal PKR expression in the absence of IFN stimulation (10). The canonical activator of PKR is viral dsRNA (7); however, PKR can also be activated in response to a variety of stress signals, including serum starvation and endoplasmic reticulum (ER) stress (11). This activation of PKR in the absence of viral dsRNA is mediated by PKR protein activator (PACT). PACT is phosphorylated under cellular stress and physically interacts with PKR to trigger its activation (11). The more well-characterized roles of PKR include regulation of protein translation and apoptosis in response to viral infection, controlling cell proliferation and differentiation, and supressing tumour growth [reviewed in-depth previously: (4, 12)].

Structurally, PKR has a C-terminal kinase domain and an N-terminal dsRNA binding domain (dsRBD). The dsRBD consists of two dsRNA binding motifs (dsRBM1 and dsRBM2), both of which are required for the high-affinity interaction with viral dsRNA (13). Recognition and binding of dsRNA by the dsRBMs triggers homodimerization of PKR and its subsequent autophosphorylation (14, 15). PKR is autophosphorylated at multiple serine and threonine residues, including Thr446 and Thr451, which are consistently phosphorylated during PKR activation (14, 16). Once activated, PKR phosphorylates serine 51 (Ser51) on the alpha subunit of eukaryotic initiation factor-2 (EIF2α). PKR belongs to a family of four EIF2α kinases, all of which share the same substrate. The other three EIF2α kinases are heme-regulated inhibitor, PKR-like endoplasmic reticulum kinase (PERK), and general control non-depressible 2 (GCN2), which are activated by heme depletion (17), ER stress (18), and amino acid starvation (19), respectively.

Phosphorylation of EIF2α by PKR or any of the other three EIF2α kinases results in inhibition of protein translation. Mammalian EIF2 is critical for initiating polypeptide chain synthesis since it promotes the delivery of initiator methionyl transfer RNA (Met-tRNAi) to the 40S ribosome. EIF2α binds Met-tRNAi in a GTP-dependent manner, forming a ternary complex that interacts with the 40S subunit. Following Met-tRNAi delivery, EIF5 promotes GTP hydrolysis of EIF2-GTP, triggering the release of EIF2-GDP from the 48S initiation complex. EIF2-GDP must be regenerated to EIF2-GTP by the GTP exchange factor EIF2B, since EIF2-GDP is inactive. When Ser51 on EIF2α is phosphorylated, the affinity of EIF2 for EIF2B is increased up to 100-fold (20). Consequently, phosphorylated EIF2α competes with EIF2-GDP for binding of EIF2B. This competitive inhibition prevents the regeneration of active EIF2-GTP and as such, initiation of translation is substantially reduced (21). Functionally, this mechanism prevents the translation of both cellular and viral messenger RNA (mRNA), thereby inhibiting viral replication.

Although the canonical role of PKR is to inhibit protein translation during viral infection [reviewed in-depth previously: (12, 22–24)], PKR is in fact a versatile kinase that controls signal transduction pathways to mediate transcription and cellular processes. Given that PKR regulates critical immune cell functions in inflammation, cell death, and autophagy – processes that are critical for host immunity against bacterial infections – it is logical to expect that the role of PKR extends beyond that of antiviral defense. Surprisingly, the role of PKR in antibacterial defense is understudied and underappreciated relative to its role in antiviral defense. However, there is accumulating evidence demonstrating that PKR contributes significantly to the immune response to a variety of bacterial infections. This review provides an overview of immune cell functions regulated by PKR and includes an exhaustive summary of the current knowledge on the role and function of PKR in pathogenic bacterial infections. Specifically, we organized the sections by grouping bacteria under Gram-positive, Gram-negative, or mycobacteria, and included every report that we could find which linked PKR to pathogenic bacteria that cause human disease. We also review the non-canonical activators of PKR and speculate on the potential mechanisms that trigger PKR activation during bacterial infection. Finally, we provide an overview of existing pharmacological modulators of PKR that could be explored for treatment of bacterial infections.

PKR IN IMMUNE CELL FUNCTION

Inflammation

PKR regulates inflammation by activating multiple downstream effectors. One mechanism utilized by PKR to regulate inflammation is by activating mitogen-activated protein kinases (MAPK) such as p38 and c-Jun N-terminal kinase (JNK) (25–27) **(Figure 1)**. p38 and JNK trigger activating transcription factor-2 (ATF2) and c-Jun to induce the expression of proinflammatory cytokines such as interleukin (IL)-1β and tumour necrosis factor-alpha (TNFα) (28, 29) **(Figure 1)**. JNK is activated by MAPK kinase (MKK)4 or MKK7, whereas p38 is activated by MKK3 or MKK6. Depletion of PKR by stable knockdown impaired the phosphorylation of JNK and p38 in response to dsRNA or a mutant strain of vaccinia virus (25). Another group observed that PKR expression was required for full activation of JNK and p38 in

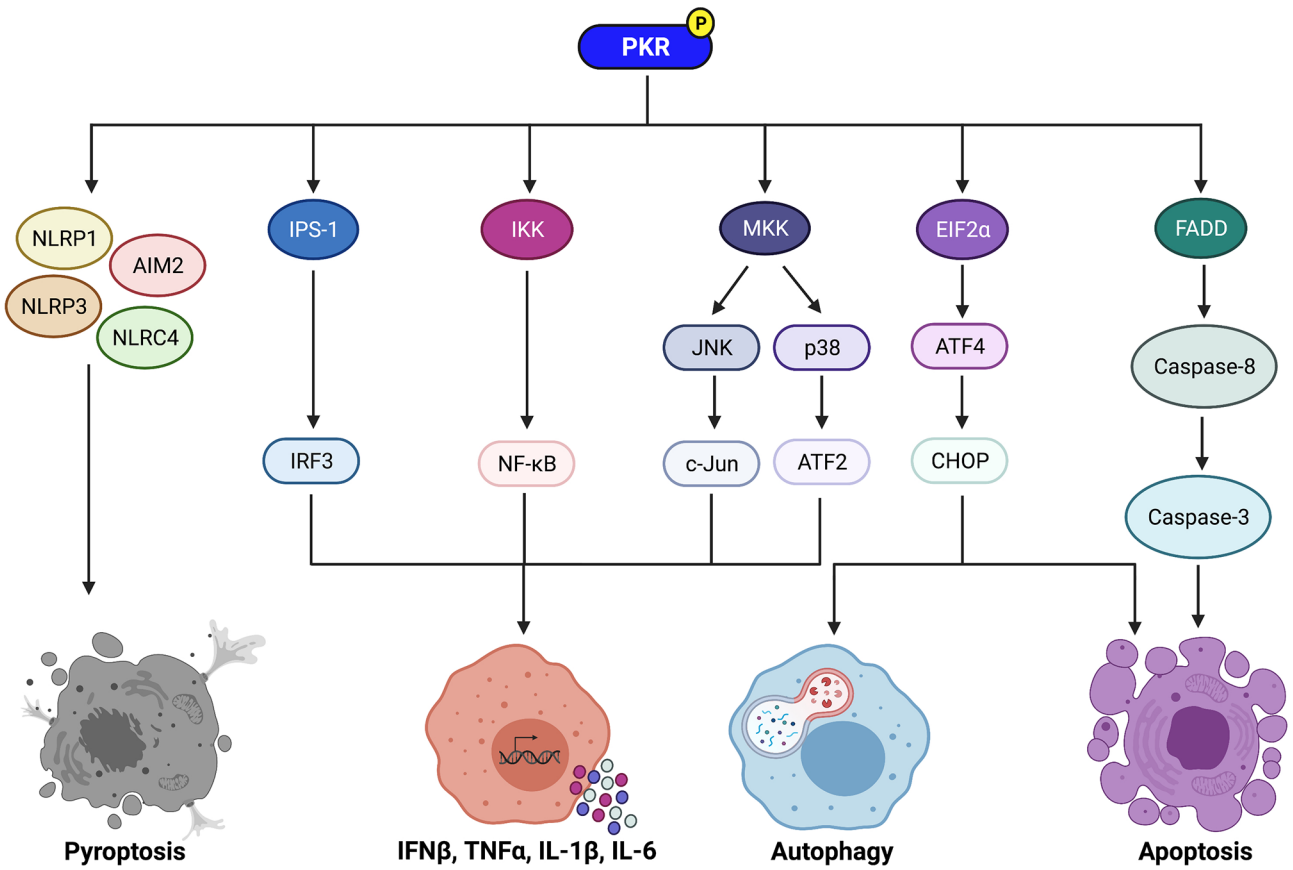


FIGURE 1 | Signaling pathways regulated by PKR to control immune cell functions. PKR regulates downstream effectors such as IPS-1, IKK, and MKK to activate IRF3, NF-κB, and the MAP kinases JNK and p38, respectively. IRF3 induces transcription of IFNβ, whereas NF-κB induces transcription of pro-inflammatory cytokines such as TNFα, IL-1β, and IL-6. Active JNK and p38 trigger c-Jun and ATF2 activation, respectively, which also induce transcription of pro-inflammatory cytokines. PKR also plays a role in induction of pyroptosis via activation of the NLRP1, AIM2, NLRP3, and NLRC4 inflammasomes. Phosphorylation of EIF2α by PKR leads to increased translation of ATF4, which then increases expression of CHOP. ATF4 and CHOP trigger activation of autophagy by inducing transcription of essential autophagy genes. In addition, CHOP promotes apoptosis during periods of prolonged cellular stress. PKR can also induce apoptosis independently of EIF2α phosphorylation via activation of the FADD/caspase-8/caspase-3 pathway. Created with BioRender.com.

response to polyinosinic:polycytidylic acid [poly(I:C)], lipopolysaccharide (LPS), IL-1β, and TNFα (26). In that same study, deletion of PKR in mouse embryonic fibroblasts (MEFs) was observed to inhibit MKK4 and MKK3/6 phosphorylation in response to the same stimuli. Interestingly, PKR deletion did not impact p38 or JNK activation in response to stressors that impact cellular components on a global scale, such as ultraviolet radiation, osmotic shock, and heat shock. The PKR-dependent stress stimuli were limited to pro-inflammatory ligands that bind distinct receptors, i.e. PKR as a receptor for dsRNA, CD14 and toll-like receptor (TLR)-4 for LPS, and the respective cytokine receptors for IL-1β and TNFα. Thus, it is suggested that PKR mediates activation of p38 and JNK in response to "receptor-mediated" pro-inflammatory stress stimuli, but not in response to "globally acting" stressors (26). Results from a different study support the observation that PKR activates p38 by acting upstream of MKK6 (27).

PKR can also regulate inflammation through its effects on NF-κB (**Figure 1**). PKR indirectly activates NF-κB by activating IκB kinase (IKK) (30). Active IKK targets IκB, a negative regulator of NF-κB, for proteasomal degradation, thereby triggering its dissociation from NF-κB. NF-κB is then free to translocate to the nucleus, where it induces transcription of genes encoding pro-inflammatory cytokines such as IL-1, IL-6, and TNFα (30, 31) (**Figure 1**). PKR triggers NF-κB activation in response to poly(I:C) and viral infection (30, 32, 33). While PKR physically associates with IKK (31), it remains unclear whether PKR is a structural or catalytic component in the activation of IKK (4, 12). Furthermore, although there are numerous reports of PKR activating NF-κB, there exists some contradictory evidence. Indeed, two independent studies have reported that PKR deficiency results in normal or only slightly decreased NF-κB activity in response to TNFα (34, 35). These findings suggest that PKR may play an important role in activating NF-κB in

response to certain stimuli (e.g. dsRNA), but not others (e.g. TNFα treatment).

A third pathway by which PKR mediates inflammation is inducing type I IFN (**Figure 1**). The canonical function of type I IFN is antiviral defense as they can directly limit intracellular viral replication and induce antiviral responses from T cells, natural killer cells, and B cells [reviewed in-depth previously: (36)]. However, there is increasing evidence to show that type I IFN also play a role in regulating inflammation, since they can alter the production of both pro- and anti-inflammatory mediators. For example, IFNβ treatment has been observed to increase MCP-1 and IP-10 production *via* STAT1 activation, which are crucial chemoattractants that recruit immune cells to the site of infection (37). On the other hand, IFNβ treatment also increases the production of the anti-inflammatory cytokine IL-10 and inhibits the secretion of pro-inflammatory cytokines such as IL-6 and TNFα *via* STAT3 activation in LPS-stimulated cells (37). In addition, type I IFN have been shown to regulate inflammation by controlling inflammasome activation (38). Interestingly, IFNβ was shown to enhance AIM2-dependent IL-1β secretion in response to *Francisella tularenis* or *Listeria monocytogenes* infection (39, 40) and mediates caspase-11-dependent pyroptosis during *Escherichia coli* and *Salmonella* Typhimurium infection (41, 42). These findings provide evidence that type I IFN regulate inflammation in the context of bacterial infections.

PKR activates IFNβ promoter stimulator-1 (IPS-1) signaling, which induces interferon regulatory factor 3 (IRF3) and subsequent transcription of IFNβ (43) (**Figure 1**). Numerous studies have found that PKR deficiency impairs IFNβ production upon stimulation with poly(I:C) or viral infection (44). Curiously, Schultz and colleagues observed that IFNβ transcription was highly induced in PKR-deficient cells following encephalomyocarditis virus (EMCV) infection, but little or no IFNβ protein was produced (45). This suggested that PKR impacts the post-transcriptional regulation of IFNβ production. Indeed, further investigation revealed that IFNβ transcripts produced in EMCV-infected PKR-deficient cells completely lack a poly(A)tail (45). This indicates that PKR is required for the integrity of IFNβ mRNA and its translation into functional protein. As such, PKR has reported roles in increasing both transcription and translation of IFNβ. Since type I IFN modulates inflammation, the ability of PKR to induce type I IFN is another mechanism that allows the kinase to regulate the inflammatory response.

Collectively, PKR plays a central role in regulating inflammation through numerous downstream effectors, including MAPK p38 and JNK, NF-κB, and type I IFN (**Figure 1**). Although acute inflammation assists with microbial clearance, chronic inflammation can result in tissue damage and deleterious effects to the host. In addition, many of the signaling pathways that regulate inflammation also have key roles in the control of cell death, a major cellular response that has consequences for bacterial infections. Inflammation must therefore be tightly regulated to achieve an optimal outcome for the host during bacterial infection.

Cell Death

As mentioned in the previous section, inflammation and cell death share common signaling pathways and are tightly intertwined. It is thus unsurprising that PKR has reported roles in regulating cell death pathways such as apoptosis and pyroptosis. PKR was first shown to induce apoptosis in 1994, when expression of the kinase in HeLa cells triggered rapid apoptosis, an effect that was not observed in cells expressing a mutant form of PKR (46). Later studies using MEFs from PKR knockout mice or NIH3T3 cells expressing a catalytically inactive PKR mutant reinforced the finding that PKR plays a pro-apoptotic role during cellular stress (47, 48). The ability to induce apoptosis of virus-infected cells is now a well-known function of PKR (4, 49). Indeed, PKR regulates apoptosis in response to numerous viruses, including poxviruses, influenza, and EMCV (50–52). Importantly, PKR can induce apoptosis in the absence of viral infection, such as in response to LPS, TNFα, serum starvation, or ER stress (47, 48, 53, 54), suggesting a role for this kinase in non-viral contexts. PKR-dependent apoptosis in the absence of viral infection is reported to rely on PACT, which triggers PKR activation in response to numerous stressors such as serum withdrawal and ER stress (11, 55).

PKR regulates apoptosis through EIF2α-dependent mechanisms (32, 47) (**Figure 1**). Phosphorylation of EIF2α results in repression of global protein translation but preferential translation of activating transcription factor-4 (*ATF4*) mRNA (56). ATF4 increases expression of C/EBP homologous protein (CHOP), a transcription factor that promotes apoptosis during periods of prolonged cellular stress. CHOP induces apoptosis by increasing expression of the pro-apoptotic protein Bim and decreasing expression of the anti-apoptotic protein Bcl-2 (57, 58). PKR can also induce apoptosis independently of EIF2α phosphorylation. One such mechanism is through activation of the FADD/caspase-8/caspase-3 pathway (59–61) (**Figure 1**). In addition, NF-κB, ATF-3, and p53 are downstream effectors of PKR that are speculated to contribute to PKR-mediated apoptosis (4, 12), although the exact mechanisms remain unclear.

In addition to apoptosis, PKR is reported to regulate inflammasome activation and pyroptosis (**Figure 1**). Lu and colleagues observed that activation of PKR was triggered by multiple inflammasome activators, and deletion of PKR inhibited high mobility group protein B1 (HMGB1) release, IL-1β secretion, and caspase-1 activation in response to inflammasome-inducing stimuli (62). Importantly, deletion of PKR also prevented cell death of macrophages treated with inflammasome activators. In the same study, PKR was shown to physically associate with NLRP1, NLRP3, NLRC4, and AIM2 inflammasomes. A non-phosphorylatable PKR mutant failed to bind NLRP3 and was unable to activate the inflammasome, indicating that phosphorylated PKR physically interacts with inflammasomes to induce their activation (62).

However, the role of PKR in pyroptosis remains controversial, as a study by Yim et al. reported that PKR represses inflammasome activation (63). Nigericin-treated peritoneal macrophages from PKR knockout or kinase-dead PKR mice resulted in elevated

levels of IL-1β and IL-18, and enhanced caspase-1 activity. Ablation of PKR expression or kinase activity also promoted the expression or assembly of inflammasome components such as NLRP3 and pro-IL-1β. Since EIF2α phosphorylation impairs protein translation, the authors speculated that PKR represses translation of inflammasome constituents by its kinase activity on EIF2α. Indeed, pre-treatment of peritoneal macrophages with the small molecule ISRIB, which counteracts the effect of EIF2α phosphorylation, increased the expression of pro-IL-1β. Yim and colleagues attribute the discrepancy between their findings and those from Lu et al. to a difference in the mouse models used (63). Notably, Lu et al. used mice from a mixed 129Sv/BALB/c background, which have attenuated inflammasome activity due to diminished caspase-11 expression (64). To complicate matters further, He et al. showed that PKR is dispensable for inflammasome activity (65). However, the *in vitro* differentiation of mouse macrophages from this study is considered to be the source of the discrepancy compared to findings from the Yim et al. study, where primary macrophages were used without further manipulation *in vitro* (63). Altogether, these conflicting reports show that the animal and cellular model is a key determinant in whether PKR mediates inflammasome activation and pyroptotic cell death.

Nevertheless, the role of PKR in cell death has major implications for bacterial infections because the mode of cell death in bacteria-infected cells influences the outcome of infection. For example, apoptotic cell death is generally considered as a pro-host response during *Mycobacterium tuberculosis* infection, since it enhances cross-priming of T cells and limits inflammation (66). In contrast, pyroptotic cell death is considered as an anti-host response during *M. tuberculosis* infection, since it results in bacterial dissemination and host tissue damage (67, 68). As such, the ability of PKR to regulate cell death pathways such as apoptosis and pyroptosis is pertinent for host immunity against bacterial pathogens.

Autophagy

PKR has been shown to induce autophagy, which may be a mechanism to balance its role in activating cell death and inflammation. Autophagy is a homeostatic process that generates nutrients by degrading cytoplasmic constituents, and this pathway is speculated to be protective against cell death (69). Although the canonical targets of autophagic degradation are organelles and proteins, it is now known that the autophagy pathway can selectively target pathogens for degradation in a process termed xenophagy (70, 71). Indeed, the autophagy pathway has been shown to degrade intracellular bacteria, viruses, and parasites (70–73). In the context of bacterial infections, selective autophagy allows for progressive elimination of bacteria (73), decreased bacterial burden (71), and improved control of inflammation (74). As such, autophagy is a critical pathway in antibacterial defense.

There is increasing evidence for PKR's role in autophagy. An initial study by Tallóczy and colleagues found that EIF2α phosphorylation by the yeast EIF2α kinase GCN2 was essential for starvation-induced autophagy of yeast cells (75). Expression of PKR in GCN2-disrupted yeast rescued autophagy in these cells, indicating a role for PKR in induction of autophagy. A follow-up study by the same group showed that PKR can induce autophagy during viral infection (76). Infection of PKR knockout MEFs with a Herpes Simplex Virus-1 (HSV-1) mutant lacking the PKR-inhibiting virulence factor ICP34.5 significantly inhibited colocalization of virions with autophagosomes and resulted in increased viral titres compared to wild-type cells (76). More recently, Ogolla and colleagues reported that PKR induces autophagy in RAW264.7 macrophages during infection with the parasite *Toxoplasma gondii* (77). Indeed, PKR expression was required for LC3 accumulation around the parasite and lysosomal fusion with vacuole-containing *T. gondii* in macrophages, which are crucial events during selective autophagy. The autophagy-inducing role of PKR during *T. gondii* appears to be critical for controlling infection, as PKR knockout mice exhibited higher parasite loads compared to wild-type mice (77).

The mechanism of PKR-dependent induction of autophagy is likely through phosphorylation of EIF2α **(Figure 1)**. Indeed, Tallóczy and colleagues observed that MEFs expressing a non-phosphorylatable EIF2α mutant displayed diminished xenophagic degradation of HSV-1 proteins to the same extent as PKR knockout MEFs, and the viral titres were equivalent between the two cell-lines (76). This indicates that PKR-induced autophagic degradation of HSV-1 is mediated through phosphorylation of EIF2α. Phosphorylation of EIF2α increases the expression of transcription factors ATF4 and CHOP, which then induce transcription of essential autophagy genes such as *Map1lc3b*, *Atg12*, *Atg3*, *Atg7*, and *Becn1* (78). It is also possible that PKR induces autophagy through its downstream effects on MAPK p38 and JNK. Although the specific mechanisms by which p38 and JNK activate autophagy during bacterial infection have not yet been elucidated, these MAPK are reported to induce autophagy during starvation through indirect effects on Beclin-1, a crucial protein in the autophagy pathway. Specifically, p38 activates MK2 and MK3, which results in the phosphorylation of Beclin-1 (79). In contrast, JNK phosphorylates a negative regulator of Beclin-1, Bcl-2 (80), to trigger its dissociation from Beclin-1 (81). Given the critical role of autophagy against intracellular bacterial pathogens, the ability of PKR to trigger autophagy is likely a key cellular response to certain bacterial pathogens.

PKR IN GRAM-POSITIVE BACTERIAL INFECTIONS

Staphylococcus aureus

Staphylococcus aureus is a Gram-positive, facultative intracellular bacterium that is commonly found in the upper respiratory tract and skin flora of humans. Although *S. aureus* is typically a commensal bacterium, it can become an opportunistic pathogen and cause a range of illnesses with varying severity, including cellulitis, osteomyelitis, pneumonia, and meningitis. *S. aureus* was initially characterized as an extracellular bacterium. However, it is now understood that *S. aureus* is phagocytosed by neutrophils and

macrophages, where it manipulates the phagosome maturation pathway to avoid lysosomal degradation (82, 83). *S. aureus* secretes a pore-forming toxin known as α-toxin, which assists *S. aureus* in escaping from macrophage phagosomes (82) and leads to activation of the autophagy pathway (84). PKR was first suspected to play a role during *S. aureus* infection when Kloft and colleagues observed that autophagy is activated in α-toxin-treated HaCaT cells and that phosphorylation of EIF2α was required for the accumulation of autophagosomes (85). Further examination revealed that both PKR and GCN2 are phosphorylated in response to α-toxin, whereas PERK is not. These findings suggest that PKR- and/or GCN2-mediated phosphorylation of EIF2α activates autophagy during *S. aureus* infection (85). However, further investigation is required to determine which of these EIF2α kinases is responsible for this effect. Interestingly, PKR might also play a proapoptotic role during *S. aureus* infection, although the current evidence is limited. Treatment of cardiac cells with RNA extracted from *S. aureus* was shown to trigger PKR activation and induce apoptosis, whereas cells treated with a PKR inhibitor were resistant to apoptosis (86) (**Table 1**). *S. aureus* RNA induced cleavage of capase-8, caspase-3, and caspase-9, an effect that was prevented following treatment with a PKR inhibitor (86). As such, PKR may activate caspase-8- and caspase-9-mediated apoptosis during

TABLE 1 | Role of PKR in different bacterial infections.

Bacterium	Experimental model	Method of PKR modulation	Live bacterium	Effect of PKR modulation[a]	Bacterial burden[a]	Citation
S. aureus	Human cardiac myocytes	Pharmacological inhibition	No (RNA)	Decreased apoptosis	N.D	(86)
B. anthracis	Mouse BMDMs	Genetic deletion	Yes	Decreased apoptosis	N.D	(87)
	Mouse peritoneal macrophages	Genetic deletion	No (toxin)	Decreased pyroptosis Decreased inflammasome activation	N.D	(62)
	J774 macrophages	siRNA knockdown	No (toxin)	Decreased pyroptosis Decreased inflammasome activation	N.D	(88)
L. monocytogenes	Mouse BMDCs and BMDMs	Pharmacological inhibition	Yes	Reduced expression of CHOP	N.D	(89)
***S.* Typhimurium**	Mouse BMDMs	Genetic deletion	Yes	Decreased apoptosis	N.D	(87)
	Mouse peritoneal macrophages	Genetic deletion	Yes	Decreased pyroptosis Decreased inflammasome activation	N.D	(62)
E. coli	C57BL/6J mice	Genetic deletion	Yes	Decreased inflammasome activation	Decreased (spleen, peritoneal cavity)	(62)
	Mouse peritoneal macrophages		Yes	Decreased pyroptosis Decreased inflammasome activation	N.D	
	Mouse BMDCs		No (RNA)	Decreased inflammasome activation		
	C57BL/6J mice	Genetic deletion	Yes	N.D	Unaffected (lungs, liver, blood, spleen)	(90)
	Mouse peritoneal macrophages			Decreased IFNα and IFNβ	N.D	
	C57BL/6J mice	Genetic deletion	Yes	Decreased IL-1β mRNA in the liver	Unaffected (blood)	(91)
	Human cardiac myocytes	Pharmacological inhibition	No (RNA)	Decreased apoptosis	N.D	(86)
Y. pseudotuberculosis	Mouse BMDMs	Genetic deletion	Yes	Decreased apoptosis	N.D	(87)
C. trachomatis	MEFs	Genetic deletion	Yes	Increased bacterial invasion	N.D	(92)
	Human mDCs	Pharmacological inhibition	Yes	Decreased IFNβ	N.D	(93)
	Mouse BMDMs	Genetic deletion		Decreased IFNβ mRNA		
L. pneumophilia	U937 macrophages	shRNA knockdown	Yes	Decreased IL-6	Unaffected	(94)
***M. bovis* BCG**	Human primary monocytes	Pharmacological inhibition	Yes	Decreased IL-6, TNFα, IL-10	N.D	(95)
M. tuberculosis	C57BL/6J mice	Genetic deletion	Yes	No effect	Unaffected (spleen, lungs)	(96)
	THP-1 monocytes	Genetic deletion Pharmacological activation	Yes	N.D	Increased Decreased	(97)
	THP-1 macrophages	Genetic deletion Genetic overexpression	Yes	Decreased selective autophagy Increased selective autophagy	Increased Decreased	(98)

[a]*Based on "Method of PKR modulation" column. N.D, not determined.*

S. aureus infection. Although the findings from the aforementioned studies suggest a role for PKR in the antibacterial response to *S. aureus*, neither of these studies examined the overall effect of PKR expression on the control of bacterial replication. Furthermore, these studies did not use live *S. aureus* infection, but instead examined the effect of bacterial RNA or α-toxin. As such, future investigation is required to determine whether PKR plays a role during infection with the live bacterium.

Bacillus anthracis

Bacillus anthracis is a Gram-positive, extracellular bacterium that is the causative agent of anthrax. *B. anthracis* secretes a major virulence factor known as lethal toxin, which enters host cells and cleaves MAPK kinases to impair MAPK signaling pathways (99). In doing so, lethal toxin disrupts crucial processes such as proliferation, survival, and inflammation in host cells. Anthrax lethal toxin has been shown to trigger phosphorylation of PKR in murine peritoneal macrophages (62), which suggests that PKR would be activated by *B. anthracis* infection. The role of PKR during *B. anthracis* infection remains unclear; however, there is evidence to suggest that PKR regulates cell death during infection with this bacterium. Indeed, Hsu and colleagues observed that deletion of PKR in bone marrow-derived macrophages (BMDMs) infected with live *B. anthracis* had markedly reduced apoptosis levels compared to wild-type macrophages (87) **(Table 1)**. Further examination into the mechanism revealed that PKR is required for TLR4-dependent apoptosis of *B. anthracis*-infected macrophages (87). Hett and colleagues provided further evidence that PKR regulates TLR4-dependent apoptosis in response to *B. anthracis*, since pharmacological inhibition of PKR protected LPS-sensitized macrophages from apoptosis in response to lethal toxin (88). Interestingly, Lu and colleagues observed that PKR was required for inflammasome activation in lethal toxin-treated mouse peritoneal macrophages, as indicated by impaired caspase-1 activation, IL-1β cleavage, and HMGB1 release in PKR-deficient cells (62) **(Table 1)**. Furthermore, PKR deficiency protected macrophages from lethal toxin-induced cytotoxicity. Consistent with the findings from Lu et al., Hett and colleagues reported that PKR is required for pyroptosis in response to lethal toxin challenge (88). Indeed, PKR knockdown protected J774 macrophages from cell death following treatment with lethal toxin, and was accompanied by reduced caspase-1 activity and IL-18 secretion **(Table 1)**. Interestingly, lethal toxin was not observed to induce PKR phosphorylation, and treatment with pharmacological inhibitors of PKR did not protect macrophages from lethal toxin-induced cell death. These findings indicate that the catalytic activity of PKR is not required for PKR-dependent pyroptosis in response to lethal toxin. As such, the authors speculate that PKR mediates activation of pyroptosis through physical interactions with inflammasomes (88). Since PKR regulates inflammasome activation in response to anthrax lethal toxin, it is possible that PKR would have the same activity in response to infection with live *B. anthracis*. However, findings from studies focusing on one virulence factor *in vitro* at the expense of studying whole organism infections with the live bacterium must be interpreted with caution. For example, Kang and colleagues reported that *B. anthracis* spores and lethal toxin induce IL-1β *via* functionally distinct pathways, demonstrating that different components of the same bacterium can mediate different signaling pathways (100). In fact, spore-induced IL-1β was observed to limit *B. anthracis i*nfection, whereas lethal toxin-induced IL-1β enabled *B. anthracis* to escape host defenses (100). Furthermore, although PKR expression was reported by Hsu et al. to be required for TLR4-dependent macrophage apoptosis in response to live *B. anthracis* infection, Moayeri and colleagues reported later that same year that lethal toxin-mediated lethality in mice was independent of TLR4 function (101). Altogether, these studies emphasize the need for *in vivo* studies with the live bacterium, since experiments focusing on single components/ virulence factors of a bacterium *in vitro* can produce different results. In addition, the overall effect of PKR expression on bacterial burden during live *B. anthracis* infection has not been investigated.

Listeria monocytogenes

Listeria monocytogenes is a Gram-positive, facultative intracellular bacterium that causes listeriosis, which can manifest as sepsis, meningitis, pneumonia, urinary tract infections, and gastroenteritis (102). This bacterium has been shown to induce phosphorylation of EIF2α in the murine macrophage cell-line RAW264.7, which indicates that PKR or another EIF2α kinase is activated during *Listeria* infection (103). Expression of a non-phosphorylatable mutant of EIF2α in MEFs resulted in increased bacterial invasion, suggesting an important role for EIF2α kinases in the antibacterial response to *Listeria* (103). Indeed, our group observed that *L. monocytogenes* infection triggers increased levels of total and phosphorylated PKR protein in the human macrophage cell-line THP-1 (98). Since *L. monocytogenes* is established to invade the cytosol and initiate a type I IFN response, and type I IFN signaling induces PKR transcription, Valderrama and colleagues examined the effect of *L. monocytogenes* infection on *EIF2AK2 (PKR)* mRNA levels (89). As expected, *L. monocytogenes* infection resulted in increased PKR transcription levels in murine bone marrow-derived dendritic cells (BMDCs) and BMDMs. Interestingly, an LLO knockout strain of *L. monocytogenes*, which lacks the LLO virulence factor required for phagosome escape, was able to induce transcription of PKR, although not to the same extent as wild-type *L. monocytogenes* (89). This indicates that cytosolic localization of *L. monocytogenes* is not required to induce transcription of PKR. Further investigation revealed that murine myeloid cells treated with a PKR inhibitor have reduced expression of CHOP following *L. monocytogenes* infection (89) **(Table 1)**. CHOP expression is increased following EIF2α phosphorylation and induces a number of effects such as proinflammatory cytokine secretion and inflammasome activation (104–107). As such, the authors speculate that PKR-dependent activation of CHOP triggers an inflammatory response to *L. monocytogenes* infection. However, this inflammatory role of PKR during *Listeria* infection may be

harmful to the host, since CHOP knockout mice had decreased splenic cell death, decreased bacterial proliferation, and better survival compared to wild-type mice (89). Nevertheless, the direct effects of PKR modulation on *L. monocytogenes* survival and host outcome have yet to be studied.

PKR IN GRAM-NEGATIVE BACTERIAL INFECTIONS

Salmonella enterica

Salmonella enterica serovar Typhimurium is a Gram-negative, facultative intracellular bacterium that causes gastroenteritis in humans. *Salmonella* Typhimurium can infect both humans and animals, and infection is commonly acquired by consuming contaminated food products. *S.* Typhimurium infection has been observed to increase mRNA levels of *EIF2AK2* in MEFs (108), and we and others have reported that *S.* Typhimurium increases total and phosphorylated PKR protein levels in macrophages (87, 98). These findings suggest that PKR plays a role in the antibacterial response to *Salmonella*. Indeed, PKR has been shown to regulate host cell death during *Salmonella* infection. For example, Hsu et al. reported that PKR knockout BMDMs are resistant to apoptosis induced by *S.* Typhimurium infection in comparison to wild-type macrophages (87) **(Table 1)**. Macrophages expressing a non-phosphorylatable mutant of EIF2α were also less susceptible to *Salmonella*-induced apoptosis, although a residual apoptotic response in these macrophages suggested the existence of another PKR-dependent pro-apoptotic pathway. The authors examined the levels of *Salmonella*-induced apoptosis in IRF3 knockout macrophages, and these macrophages were also resistant to *Salmonella*-induced apoptosis (87). As such, PKR may regulate two pro-apoptotic pathways during *Salmonella* infection, one involving EIF2α and the other involving IRF3. Interestingly, the apoptotic response to *Salmonella* was considerably reduced in BMDMs from TLR4-deficient mice, indicating that PKR is required for TLR4-dependent apoptosis during *Salmonella* infection (87). PKR is also reported to play a role in pyroptosis activation during *Salmonella* infection. Lu and colleagues observed that PKR deficiency in *S.* Typhimurium-infected murine peritoneal macrophages significantly inhibited caspase-1 activation, IL-1β cleavage, and HMGB1 secretion, as well as *Salmonella*-induced cell death (62) **(Table 1)**. PKR was shown to physically associate with inflammasomes in response to a variety of pyroptosis-inducing stimuli, and PKR expression was required for inflammasome activation. However, the specific mechanism of inflammasome activation by PKR remains unknown. Taken together, the findings from Hsu et al. and Lu et al. indicate that PKR is an important mediator of both apoptosis and pyroptosis in *Salmonella*-infected macrophages. However, the overall effect of PKR on bacterial survival remains to be elucidated.

Lastly, findings from Yeung and colleagues loosely suggest a role for PKR in the proper functioning of *Salmonella*-infected macrophages (109). The outcome of *Salmonella* infection is largely influenced by how the bacteria initially interact with macrophages, however the human macrophage factors required for *Salmonella* uptake are incompletely understood. A genome-scale CRISPR knockout library screening of THP-1 macrophages to identify loss-of-function mutations conferring resistance to *Salmonella* uptake identified NHLRC2, a gene involved in actin dynamics (109). NHLRC2 mutant macrophages were hyperinflammatory, unable to interact and phagocytose *S.* Typhimurium, and exhibited atypical morphology. Interestingly, PKR was shown to physically associate with NHLRC2, and NHLRC2 knockout macrophages had reduced PKR expression (109). Since PKR expression appears to be linked to NHLRC2 expression, and these two proteins physically interact, perhaps PKR contributes to NHLRC2-dependent uptake of *Salmonella* and the proper functioning of infected macrophages.

Escherichia coli

Escherichia coli is a Gram-negative bacterium that can either be harmless or pathogenic depending on the particular strain. Some strains of *E. coli* are part of the normal intestinal microbiota, whereas other strains can cause diarrhea, urinary tract infections, or other illnesses. There have been a few studies examining the effect of PKR deletion during *E. coli* infection both *in vitro* and in the mouse model. Lu et al. reported that PKR expression and phosphorylation is triggered in murine peritoneal macrophages following *E. coli* infection *in vitro* (62). It was observed that *E. coli*-induced pyroptosis was severely impaired in infected PKR knockout macrophages, as indicated by decreased cell death and impaired IL-1β production **(Table 1)**. Furthermore, transfection with *E. coli* RNA in BMDCs significantly activated capase-1 and stimulated IL-1β cleavage in wild-type cells but not PKR knockout cells (62) **(Table 1)**. Lu and colleagues also performed *in vivo* experiments and observed that serum IL-1β, IL-18, and HMGB1 levels were significantly reduced in *E. coli*-infected PKR knockout mice compared to control mice. Notably, PKR knockout mice had significantly lower titers of *E. coli* in the spleen and peritoneal cavity compared to control mice (62) **(Table 1)**. Altogether, the findings from this study suggest that PKR plays a role in inflammasome activation during *E. coli* infection, and PKR expression appears to be conducive for *E. coli* persistence. However, it is difficult to interpret the results from these *in vivo* studies since non-virulent *E. coli* was used, as reflected by $>10^9$ CFU challenge doses (62). In contrast, a recent study from the same group using virulent *E. coli* showed that genetic deficiency or pharmacological inhibition of PKR did not affect bacterial loads in *E. coli*-infected mice (90) **(Table 1)**. The discrepancy in findings between these two studies was suggested by the authors to be due to differences in the route of *E. coli* infection (90). In the first report, Lu et al. performed intraperitoneal infection, whereas the second study used intravenous infection (62, 90). Overall, more careful *in vivo* studies using virulent *E. coli* (typically reflected by dose challenges of 10^7 CFU or lower) must be performed before conclusions can be drawn.

A role for PKR in inflammasome activation was also reported by Poon and colleagues (91). This group observed that PKR knockout mice had diminished peripheral inflammatory responses following subcutaneous *E. coli* challenge. Indeed, PKR deficiency resulted in decreased IL-1β mRNA expression

in the livers of infected mice (91) **(Table 1)**. However, PKR deletion had no effect on the bacterial burden of *E. coli*-infected mice. Interestingly, while the core components of sickness (anorexia and motor impairments) were comparable between *E.coli*-infected wild-type and PKR knockout mice, the behavioural components of sickness – including reduced burrowing, exploratory activity deficits, and social withdrawal – were only observed in PKR knockout mice (91).

Finally, PKR might also regulate apoptotic cell death during *E. coli* infection. *E. coli* RNA was shown to activate PKR and induce apoptosis of cardiac cells, an effect that was blocked following pharmacological PKR inhibition (86) **(Table 1)**. Altogether, the findings from the studies discussed above suggest that PKR regulates cell death pathways such as pyroptosis and apoptosis during *E. coli* infection. However, the effect of PKR expression on bacterial burden remains unclear, as there are discrepancies between the current findings.

Yersinia pseudotuberculosis

Yersinia pseudotuberculosis is a Gram-negative, extracellular bacterium that causes Far East scarlet-like fever in humans. PKR is suggested to play a role in regulating inflammation and macrophage apoptosis during *Y. pseudotuberculosis* infection. Shrethsa and colleagues observed that EIF2α is phosphorylated in *Y. pseudotuberculosis*-infected RAW264.7 macrophages, and that phosphorylated EIF2α opposed bacterial invasion (103). Furthermore, phosphorylation of EIF2α was required for *Yersinia*-induced NF-κB activation and TNFα expression in MEFs. These findings indicated that PKR or another EIF2α kinase is involved in antibacterial defense against *Y. pseudotuberculosis*. Indeed, expression of the *Yersinia* virulence factor YopJ, which is known to inhibit EIF2α signaling in response to various stress stimuli, was also shown to inhibit PKR signalling in MEFs (103). This finding suggests that PKR is the kinase responsible for phosphorylating EIF2α during *Y. pseudotuberculosis* infection. PKR might also play a role in *Yersinia*-induced apoptosis, since deletion of PKR in infected BMDMs substantially impaired macrophage apoptosis when compared to wild-type macrophages (87) **(Table 1)**. The apoptotic response to *Y. pseudotuberculosis* was considerably reduced in BMDMs from TLR4-deficient mice, suggesting that PKR is required for TLR4-dependent apoptosis during *Yersinia* infection (103). The effect of PKR activity on the survival of *Y. pseudotuberculosis* has yet to be determined.

Chlamydia trachomatis

Chlamydia trachomatis is a Gram-negative, obligate intracellular bacterium that is the causative agent of chlamydia. There is growing evidence to suggest that PKR is involved in the immune response to *C. trachomatis*. Shrestha and colleagues first reported that expression of a non-phosphorylatable mutant of EIF2α increased *C. trachomatis* invasion in MEFs, indicating that PKR or another EIF2α kinase assists in antibacterial defense against *Chlamydia* (103). They later reported that PKR knockout MEFs had increased *C. trachomatis* invasion levels compared to wild-type cells, with invasion levels similar to the levels observed in cells expressing the non-phosphorylatable EIF2α mutant (92) **(Table 1)**. These findings indicate that PKR plays a role in the antibacterial response to *C. trachomatis*. Indeed, a later study revealed that *C. trachomatis* infection triggers phosphorylation of PKR in human monocyte-derived dendritic cells and murine BMDMs, and this activation of PKR is required for *C. trachomatis*-induced IFNβ production (93) **(Table 1)**. This suggests that PKR plays a role in regulating inflammation during *Chlamydia* infection, but whether this PKR-dependent induction of IFNβ is ultimately conducive or detrimental to bacterial survival was not explored. However, findings from Qiu et al. indicate that the type I IFN-inducing role of PKR is conducive for *C. trachomatis* infection (110). *IFNAR* knockout mice were more resistant to *Chlamydia* infection compared to wild-type mice, as indicated by a smaller decrease in body weight, lower bacterial burden, and milder lung pathology in infected mice. The increased resistance to *C. trachomatis* infection in the knockout mice was attributed to higher numbers of bactericidal macrophages in the lung resulting from decreased macrophage apoptosis. Notably, these knockout mice had lower expression of PKR. Since PKR plays a proapoptotic role during viral infection, the authors speculate that type I IFN indirectly promote *C. trachomatis* infection by activating PKR, thus resulting in macrophage apoptosis and increased bacterial persistence (110). Additional experimentation is required to assess whether PKR plays a proapoptotic role during *C. trachomatis* infection. Altogether, PKR is activated by *Chlamydia* infection, where it then induces IFNβ production and limits bacterial invasion. Further investigation is necessary to determine whether PKR activity in response to *Chlamydia* infection is ultimately beneficial or harmful to the host.

Legionella pneumophilia

Legionella pneumophilia is a Gram-negative, facultative intracellular bacterium that is the causative agent of Legionnaires' disease. To examine the role of PKR during *L. pneumophilia* infection, Mallama and colleagues generated PKR knockdown cells using the human U937 macrophage-like cell-line (94). PKR deficiency impaired IL-6 secretion in response to *L. pneumophilia* infection **(Table 1)**, a critical cytokine in antibacterial defense against this bacterium. As such, Mallama et al. concluded that PKR expression is required for an optimal cytokine response to *L. pneumophilia* infection (94). However, PKR deficiency did not affect the intracellular burden of *L. pneumophilia* in macrophages **(Table 1)**. As such, although PKR appears to regulate inflammation during *L. pneumophilia* infection, the kinase may be dispensable for bacterial control.

PKR IN MYCOBACTERIAL INFECTIONS

Mycobacterium tuberculosis Complex

Mycobacterium is a genus comprising over 190 species of bacteria. Mycobacteria possess an atypical outer membrane structure and organization comprised of mycolic acids, arabinogalactan, and numerous unique glycolipids (111). This unique cell wall contributes to the robustness of mycobacterial

species and their natural tolerance to many antibiotics (112). As such, mycobacteria do not stain Gram-positive or Gram-negative, which contributes to their phylogenetic ambiguity. Instead, mycobacterial species are classified as acid-fast bacteria due to their ability to resist acid or ethanol-based decolorization procedures during staining. The most notorious species of mycobacteria relevant for human disease is *Mycobacterium tuberculosis*, a facultative intracellular bacterium that causes tuberculosis (TB) disease. Mycobacteria can be broadly classified into three major groups: the *Mycobacterium tuberculosis* complex, which comprises mycobacteria that cause TB disease (e.g. *M. tuberculosis* and *Mycobacterium bovis*); *Mycobacterium leprae*, which causes leprosy; and non-tuberculosis mycobacteria, which includes all other mycobacteria that do not cause TB or leprosy. There is growing evidence that PKR plays a role in the immune response to mycobacteria. For example, one study revealed that PKR phosphorylation is triggered in human monocytes infected with bacillus Calmette-Guérin (BCG), a live attenuated form of *M. bovis* used for TB vaccination (95). Pharmacological inhibition of PKR decreased mRNA and protein levels of crucial anti-BCG cytokines in infected monocytes, including TNFα, IL-6, and IL-10 **(Table 1)**. PKR inhibition also prevented the binding of NF-κB to DNA and impaired downstream activation of the MAPK ERK1/2 in treated monocytes. As such, the authors speculate that PKR induces anti-BCG cytokine production *via* downstream activation of ERK1/2 and NF-κB (95). Other studies have shown that *EIF2AK2* mRNA increases during infection with BCG and *M. tuberculosis* (113, 114). The findings that PKR expression and activation is triggered by mycobacterial infections suggest that PKR plays a role in the immune response to mycobacteria. However, the effect of PKR on mycobacterial burden was not examined in these studies.

Since PKR plays a pro-apoptotic role during viral infection, Wu and colleagues examined the effect of PKR deletion on macrophage apoptosis and bacterial burden during *M. tuberculosis* infection (115). While they initially reported that PKR deficiency in mice enhances macrophage apoptosis and decreases *M. tuberculosis* burden in the lungs (115), there was a discrepancy between the genetic backgrounds of the mutant and control mice used in the study (116). A follow-up study led by Mundhra and colleagues using mutant and control mice from the same genetic background revealed that PKR deficiency had no effect on apoptosis or *M. tuberculosis* burden (96, 116) **(Table 1)**. Therefore, PKR was concluded to be dispensable during *M. tuberculosis* infection. In contrast, Ranjbar and colleagues demonstrated that PKR expression and activation is triggered during *M. tuberculosis* infection in THP-1 monocytes, and PKR deletion in *M. tuberculosis*-infected macrophages increased the bacterial burden (97) **(Table 1)**. Although Ranjbar and colleagues observed an effect of PKR modulation on *M. tuberculosis* burden, the specific mechanism regulated by PKR to restrict *M. tuberculosis* growth was not investigated. As such, our group sought to examine the effect of PKR modulation on the intracellular survival of *M. tuberculosis* and characterize the specific mechanism(s) involved. Consistent with the findings from Ranjbar and colleagues, we showed that PKR expression and activation is triggered in *M. tuberculosis*-infected THP-1 and primary human macrophages, and deletion of PKR increases intracellular *M. tuberculosis* survival compared to control macrophages (98) **(Table 1)**. Strikingly, we also observed that genetic overexpression of PKR decreases the intracellular survival of *M. tuberculosis* by nearly 80% compared to control macrophages **(Table 1)**. Immunological profiling of infected macrophages overexpressing PKR showed increased production of IP-10 and reduced production of IL-6, two cytokines that are reported to activate and inhibit IFNγ-dependent autophagy, respectively (117, 118). Indeed, we determined that the ability of PKR overexpression to limit intracellular *M. tuberculosis* survival is due to the induction of selective autophagy (98) **(Table 1)**. Although our group did not elucidate the events downstream of PKR activation that led to induction of autophagy, the mechanism is likely through the phosphorylation of EIF2α and downstream induction of ATF4. However, MAPK p38 and JNK have been shown to be important for induction of autophagy during *M. tuberculosis* infection, and IL-6 inhibits MAPK phosphorylation to block autophagy in *M. tuberculosis*-infected macrophages (118). Importantly, PKR activates p38 and JNK (25–27), and macrophages overexpressing PKR had reduced production of IL-6 (98). As such, it is possible that autophagy induction by PKR is dependent on a mechanism involving MAPK, whether by a direct effect of PKR on MAPK activation or an indirect effect from decreased IL-6 production. We did not observe an effect of PKR modulation on apoptosis or overall cell death of *M. tuberculosis*-infected macrophages (98), consistent with the findings from Mundhra and colleagues (96). Taken together, the results from these studies indicate that PKR plays a critical role in the antibacterial response to mycobacteria. The ability of PKR to limit the intracellular survival of *M. tuberculosis* in macrophages appears to be through selective autophagy induction, rather than by regulating apoptosis.

It is worth noting that the overall effect of PKR during *M. tuberculosis* infection may be context dependent. Although our findings and the results from Ranjbar et al. indicate that PKR limits *M. tuberculosis* survival *in vitro* (97, 98), a recent report using *sst1*-susceptible mice suggests that PKR contributes to macrophage necrosis in TB granulomas (119). *sst1*-susceptible mice develop necrotic inflammatory lung lesions similar to human TB granulomas, whereas their congenic B6 counterparts do not (120). PKR phosphorylation was increased in TNFα-treated macrophages extracted from *sst1*-susceptible mice compared to macrophages extracted from B6 mice (119). PKR-mediated phosphorylation of EIF2α led to hyperinduction of ATF3 and integrated stress response (ISR)-target genes in these macrophages. Importantly, pharmacological inhibition of the ISR prevented the development of necrosis in lung granulomas of *M. tuberculosis*-infected *sst1*-susceptible mice and reduced the bacterial burden (119). This finding suggests that PKR contributes to necrosis of granulomas and subsequent lung pathology during TB disease. Further investigation of the effects of PKR modulation *in vivo* is required to assess whether PKR activity is ultimately beneficial or harmful to the host during *M. tuberculosis* infection.

Non-Tuberculosis Mycobacteria

Non-tuberculosis mycobacteria (NTM) are mycobacteria that do not cause TB or leprosy. However, these mycobacteria can still cause illness in humans and animals, such as pulmonary disease resembling TB, lymphadenitis, and skin disease (121). NTM are mostly environmental bacteria and can be found in water and soil. Although most studies on PKR during mycobacterial infection used *M. tuberculosis* or BCG, there is limited evidence to indicate that PKR also plays a role during NTM infections. For instance, Madhvi et al. recently reported that *EIF2AK2* mRNA increases during infection with the non-pathogenic *Mycobacterium smegmatis* (114). In addition, there is evidence to loosely suggest that PKR plays a role in the immune response to *Mycobacterium ulcerans*, the causative agent of the tropical disease Buruli ulcer. *M. ulcerans* secretes an exotoxin virulence factor known as mycolactone, which triggers apoptosis of host cells (122). Cells that are exposed to mycolactone can persist for several days through the induction of autophagy before succumbing to apoptosis. However, chronic exposure to mycolactone causes cell death (123). Ogbechi and colleagues observed that MEFs with a deletion of both PERK and GCN2 ($Perk^{-/-}Gcn2^{-/-}$) succumbed to apoptosis faster than wild-type cells, which was attributed to an inability of these cells to induce autophagy (123). Furthermore, mycolactone treatment increased protein levels of ATF4 and CHOP and triggered phosphorylation of PKR, PERK, GCN2, and EIF2α. Taken together, these findings suggest that mycolactone triggers phosphorylation of EIF2α kinases to activate the EIF2α-ATF4-CHOP pathway, which results in induction of autophagy during short-term exposure to the exotoxin, and induction of apoptosis during chronic exposure. Although the effect of PKR deletion on mycolactone-induced autophagy and apoptosis was not examined, residual *Atf4* expression was observed in $Perk^{-/-}Gcn2^{-/-}$ MEFs (123). This suggests that PKR contributes to the phosphorylation of EIF2α and downstream induction of *Atf4* expression in response to mycolactone treatment. As such, it is possible that PKR plays a role in regulating autophagy and apoptosis during infection with *M. ulcerans*, although further experimentation using the live bacterium is required.

NON-CANONICAL ACTIVATORS OF PKR

Bacterial RNA

Although viral dsRNA is the canonical activator of PKR, recent studies have shown that PKR can also be activated by bacterial RNA. PKR was first suspected to be activated by bacteria when it was observed that purified PKR from *E. coli* cells is in a phosphorylated state and must be dephosphorylated to make the kinase responsive to RNA (124, 125). This suggested that endogenous bacterial products could trigger PKR activation. In 2012, Bleiblo and colleagues identified bacterial RNA as a ligand recognized by PKR (86). It was observed that total RNA extracted from *E. coli* and *S. aureus* potently activated PKR in cardiac cells in a dose-dependent manner, whereas human RNA did not. *In vitro* PKR binding assays showed that the bacterial RNA directly bound the purified PKR, suggesting that bacterial RNA possesses structural features that can directly activate PKR (86) **(Figure 2)**. A later study from the same group demonstrated that removal of the base-paired secondary structures of the bacterial RNA by RNase digestion hinders the activation of PKR, indicating that the double-stranded structures of bacterial RNA are required to fully activate PKR (126). More recently, Hull and colleagues investigated the specific features of bacterial RNA that can activate PKR (127, 128). The *Bacillus subtilis trp* 5'-UTR was identified as an activator of PKR. The *trp* 5'UTR has multiple structural RNA elements representative of many bacterial mRNAs, including a terminator, 5'-stem-loop, and Shine-Dalgarno hairpin. These elements were shown to potently activate PKR. In a follow-up study by Hull and colleagues, three more functional bacterial RNAs were tested for their ability to activate PKR: the Vc2 riboswitch from *Vibrio cholerae*, the *glmS* riboswitch-ribozyme from *B. anthracis*, and the twister ribozyme from *Clostridia bolteae* (128). Most constructs derived from these RNAs were able to activate PKR, provided they were long enough to form sufficient RNA structure. These findings demonstrate that PKR can be activated by numerous RNA elements from a wide range of bacteria, including both Gram-positive and Gram-negative bacteria.

DNA

The finding that PKR is required for AIM2 inflammasome activation in response to DNA transfection suggested that PKR can be activated by double-stranded DNA (dsDNA) (62), but PKR does not bind dsDNA or DNA/RNA hybrid strands (129). Nevertheless, DNA may activate PKR indirectly. Indeed, one study showed that transfection of HeLa cells with exogenous DNA led to phosphorylation of both PKR and EIF2α (130). This effect was dependent on recognition of dsDNA by the cytosolic DNA sensor cGAS. It was also observed that PKR and G3BP1, an RNA/DNA and RNA/RNA helicase, co-localize with cGAS following DNA transfection and are both required for cGAS sensing of intracellular vaccinia virus DNA. Interestingly, G3BP1 was required for PKR phosphorylation. As such, the authors of this study suggest that after interacting with DNA-bound cGAS, G3BP1 activates PKR (130) **(Figure 2)**. It is note-worthy that the cGAS/STING/TBK-1 axis stimulated by cytosolic dsDNA leads to activation of IRF3, which induces transcription of IFNβ (131). IFNβ triggers assembly and nuclear translocation of the transcription factor interferon-stimulated gene factor 3 (ISGF3), which regulates the PKR promoter at the ISRE (132). Therefore, it is also possible that the DNA-sensing pathway indirectly induces PKR transcription by triggering IFNβ production and downstream ISGF3 activation **(Figure 2)**. Altogether, we speculate that the cytosolic DNA sensing pathway is a potential mechanism that triggers PKR expression and phosphorylation during bacterial infection.

Toll-Like Receptor Signalling

Pathogens that are unable to perforate the phagosome, such as BCG and LLO-deficient *L. monocytogenes*, can trigger PKR phosphorylation and mRNA expression (89, 95). This suggests

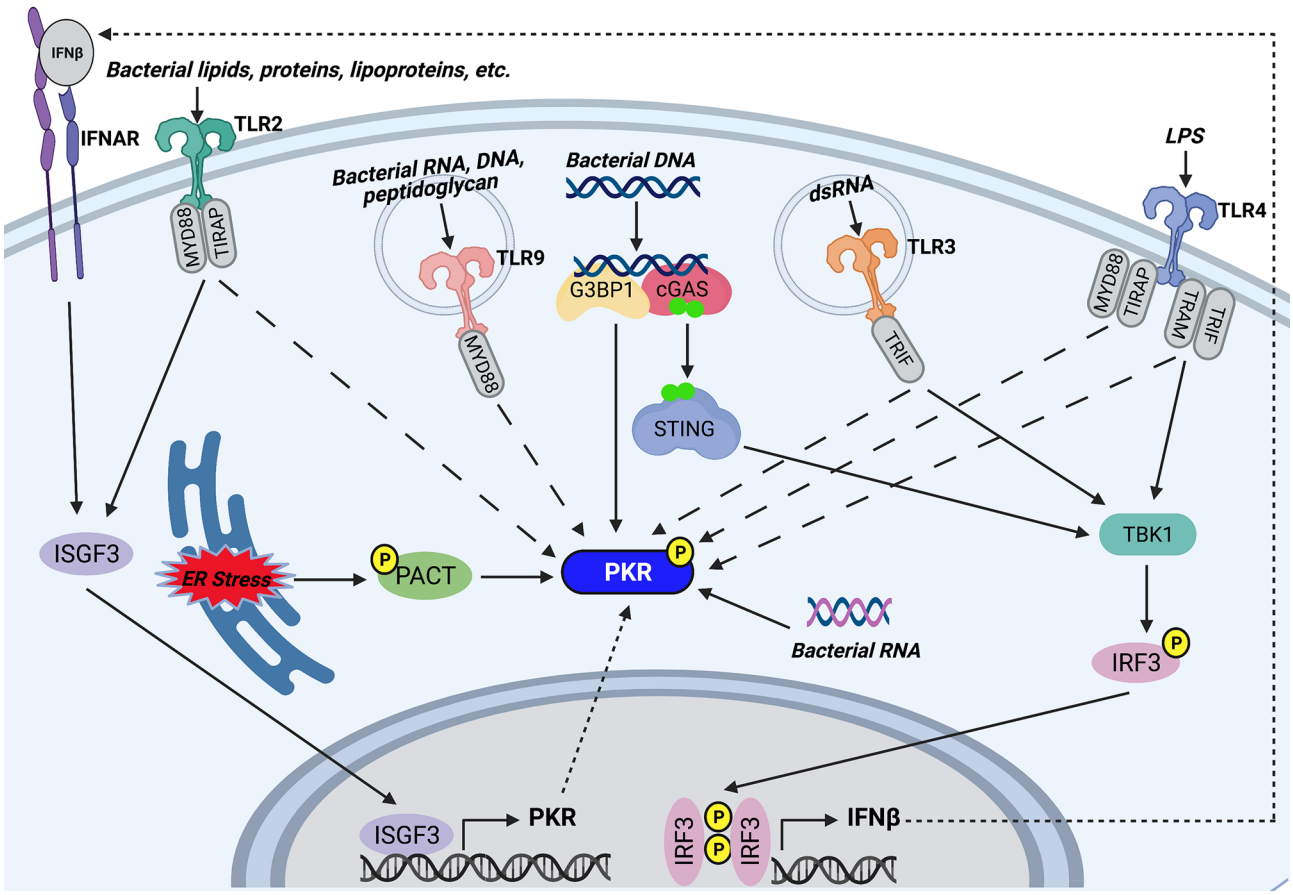


FIGURE 2 | Potential mechanisms of PKR activation during bacterial infections. TLR2 and TLR4 on the host cell surface recognize bacterial lipids, proteins, and lipoproteins, or lipopolysaccharide (LPS), respectively. Endosomal TLR9 recognizes CpG motifs found in bacterial RNA, DNA, and peptidoglycan, whereas endosomal TLR3 is activated by bacterial dsRNA. TLR2, TLR4, TLR9, and TLR3 trigger PKR phosphorylation by unknown mechanisms. Furthermore, TLR3 and TLR4 activate TBK1 by their adaptor proteins (TRIF for TLR3 and TRAM and TRIF for TLR4) which goes on to induce phosphorylation and dimerization of IRF3. IRF3 translocates to the nucleus and induces transcription of IFNβ. IFNβ signals through IFNAR to trigger assembly and nuclear translocation of ISGF3, which regulates the PKR promoter to induce transcription of PKR. TLR2 signaling also triggers association of ISGF3 with the PKR promoter. As such, TLR3, TLR4, and TLR2 may induce PKR transcription by downstream activation of ISGF3. Cytosolic bacterial DNA is recognized by cGAS, which associates with G3BP1. G3BP1 co-localizes with PKR and may directly phosphorylate the kinase. Recognition of bacterial DNA triggers cGAS to synthesize the secondary messenger cyclic GMP-AMP. GMP-AMP triggers activation and dimerization of STING, which in turn activates the TBK1-IRF3-IFNβ-ISGF3 axis to induce PKR transcription. In addition, certain bacteria induce ER stress, which triggers phosphorylation of PACT, a cellular activator of PKR. Phosphorylation of PACT enhances its association with PKR and leads to PKR activation. Finally, cytosolic bacterial RNA can directly bind PKR and trigger its activation. Created with BioRender.com.

that PKR can be activated/induced in the absence of cytosolic nucleic acids. Indeed, there is accumulating evidence to support that PKR is activated by TLR signaling. PKR is reported to be activated in response to TLR4 and TLR2, which are cell surface TLRs that mainly recognize microbial membrane components such as lipids, lipoproteins, and proteins. In 2001, Horng and colleagues observed that PKR is phosphorylated following treatment with LPS, a TLR4 agonist (133). Since then, there have been numerous reports of PKR activation occurring in a TLR4-dependent manner (87, 93, 134–138). TLR4 signaling has also been shown to increase *EIF2AK2* mRNA and protein levels (135). As such, we speculate that bacteria can trigger downstream PKR phosphorylation and expression by activating TLR4 signaling (**Figure 2**). Indeed, a link between TLR4 signaling and PKR activity has been reported during infection with bacteria such as *S.* Typhimurium, *Y. pseudotuberculosis*, *B. anthracis*, and *C. trachomatis* (87, 93). Importantly, both heat-treated and gamma-irradiated attenuated *C. trachomatis* can activate PKR to the same extent as live bacteria, indicating that intracellular bacterial replication or secretion of heat-labile bacterial products are not responsible for PKR activation (93). In contrast, inhibition of TLR4 prevented PKR activation (93). Altogether, these findings provide evidence that heat stable LPS is the likely bacterial product responsible for PKR activation during *C. trachomatis* infection. Indeed, heat-treating LPS did not impair its ability to activate PKR (93). Interestingly, PKR appears to be activated by different adaptor proteins depending on the specific TLR4 agonist (93, 133). *C. trachomatis* infection is unable to activate PKR in the presence of a MyD88 inhibitor but is unaffected by a TRIF inhibitor, whereas LPS is unable to

activate PKR in the presence of a TRIF inhibitor but is unaffected by a MyD88 inhibitor (93). TLR2 signaling can also trigger PKR phosphorylation **(Figure 2)**. Pam3CSK4, a TLR2 agonist, triggers PKR phosphorylation (134) in addition to increasing *PKR* mRNA and protein levels (135). Furthermore, PKR is activated in a TLR2-dependent manner following parasitic infection with *Leishmania amazonensis* (139).

PKR phosphorylation can also be triggered downstream of TLR3 and TLR9, which are endosomal TLRs that mainly recognize nucleic acids **(Figure 2)**. Indeed, a kinase-inactive PKR mutant inhibited poly(I:C)-induced TLR3-mediated activation of NF-κB, suggesting that PKR is a downstream component of TLR3 signaling (140). A later study confirmed that PKR is activated by TLR3 signaling, since poly(I:C)-induced phosphorylation of PKR in human neuroblastoma cells was impaired in TLR3-deficient cells (141). There is limited evidence to suggest that PKR is activated in response to TLR9 signaling. PKR was shown to be phosphorylated by CpG motifs present in bacterial DNA, dsRNA, and peptidoglycans (133). CpG engages the TLR9 receptor, indicating that PKR is activated downstream of TLR9 **(Figure 2)**. As such, TLR9 signaling could be yet another mechanism through which PKR indirectly senses bacterial DNA without a requirement for phagosome perforation. Overall, PKR appears to be a downstream component shared by at least four TLRs.

The specific mechanism of PKR activation downstream of TLR signaling remains unclear. However, Perkins and colleagues observed that TLR4 and TLR3 agonists trigger the phosphorylation of both PKR and IRF3 (138). IRF3 induces transcription of IFNβ, which triggers assembly and nuclear translocation of ISGF3. As mentioned in the previous section, ISGF3 regulates the PKR promoter (132); therefore, it is possible that TLR4 and TLR3 signaling induces PKR by triggering IFNβ production and downstream ISGF3 activation **(Figure 2)**. Furthermore, chromatin immunoprecipitation assays revealed that *L. amazonensis* infection, which activates PKR through TLR2 signaling, triggered binding of ISGF3 elements to the PKR promoter, an event that did not occur in TLR2 knockout macrophages (139). Therefore, ISGF3 may be a common link between TLR2-, TLR4-, and TLR3-dependent induction of PKR **(Figure 2)**.

ER Stress

There are numerous reports that PKR is activated in response to ER stress (142–144). Indeed, PKR has been shown to play a significant role in sustained ER stress-induced apoptosis (54). ER stress leads to downstream PKR activation by triggering the phosphorylation of PACT (54), a cellular activator of PKR that activates the kinase in the absence of dsRNA (55). Phosphorylation of PACT increases its association with PKR and leads to PKR activation. Certain bacteria, including *Pseudomonas aeruginosa*, *Helicobacter pylori*, and *Coxiella burnetti*, are reported to trigger ER stress in infected host cells (145–148). Although the phosphorylation state of PKR was not examined in these studies, PERK and EIF2α were shown to be phosphorylated in response to infection with these bacteria. It is possible that PKR is also activated in response to these bacteria and contributes to the phosphorylation of EIF2α. Indeed, one of the groups suggested that future work should assess whether PKR plays a role in the ER stress response during *C. burnetti* infection (146). As such, we speculate that infection with certain bacterial pathogens induces ER stress, which leads to PKR activation *via* PACT **(Figure 2)**.

PHARMACOLOGICAL MODULATION OF PKR

PKR Activators

Due to the emergence of antibiotic-resistant bacteria such as *M. tuberculosis* and *S. aureus*, the development of alternative therapies for certain bacterial infections is urgently required. Host-directed therapy (HDT) is a promising option, since this strategy aims to boost the host immune response to a particular bacterium rather than target the bacterium itself, thus circumventing the development of antibiotic resistance. Since there is growing evidence that PKR plays a role in the host immune response to bacterial pathogens, pharmacological modulation of PKR could be a promising strategy for HDT against various bacterial infections.

There are multiple pharmacological activators of PKR in various stages of development **(Table 2)**. Bozepinib is a small antitumor agent that both upregulates and activates PKR (149). Bozepinib has shown promise in pre-clinical studies since it induces apoptosis in breast and colon cancer cells (149, 150). Although the specific effects of bozepinib have not been assessed *in vivo*, it has been observed that bozepinib treatment does not cause acute toxicity in mice (150). The mechanism through which bozepinib induces and activates PKR remains unknown. Nitazoxanide (NTZ) is another drug that triggers PKR phosphorylation (151, 152). NTZ is an FDA-approved broad-spectrum antiparasitic drug. The typical use of NTZ is the treatment of cryptosporidiosis infection, however clinical trials have demonstrated efficacy and safety of NTZ in treating viral infections such as influenza and hepatitis C (188, 189). NTZ has been shown to deplete intracellular calcium stores, thereby raising levels of cytosolic calcium. This calcium mobilisation disrupts ER/Golgi glycoprotein trafficking and induces ER stress, thus triggering PKR phosphorylation (152). Several *in vivo* studies conducted in animal models have investigated the effects of NTZ in disease contexts such as viral infections, protozoan infections, cancer, Parkinson's disease, neuro-inflammation, and bacterial infections **(Table 2)** (153–166). Indeed, *in vivo* studies have shown that NTZ is effective in treating bacterial pathogens such as *C. difficile*, *E. coli*, *M. leprae*, and *M. tuberculosis* (153–156, 159). Interestingly, NTZ is reported to exert significant bactericidal activity directly against both replicating and non-replicating *M. tuberculosis* (190), and was recently evaluated for treatment of TB in a phase II clinical trial (191). In addition, Ranjbar and colleagues recently reported that NTZ treatment enhanced *M. tuberculosis*-induced *EIF2AK2* mRNA expression in THP-1 cells, and NTZ treatment reduced *M. tuberculosis* burden in THP-1 and human

TABLE 2 | Pharmacological modulators of PKR.

	Compound	Method of PKR modulation	Stage of development	Animal model	Disease context	Citation
Activators	Bozepinib	Unknown	Pre-clinical	N/A	N/A	(149, 150)
	Nitazoxanide	Depletes intracellular Ca^{2+} stores, resulting in ER stress and PKR phosphorylation	FDA approved	Rats, mice, hamsters	Microbial infections cancer, inflammation, neuropathic pain, Parkinson's disease	(151–166)
	BEPP	Unknown	Pre-clinical	N/A	N/A	(167)
	DHBDC	Unknown	Pre-clinical	N/A	N/A	(168)
Inhibitors	C16	Competitive inhibitor of ATP	Pre-clinical	Rats, mice	Neurodegeneration, hypertension, cancer, diabetes, rheumatoid arthritis, inflammation	(169–184)
	2-Aminopurine	Competitive inhibitor of ATP	Pre-clinical	Mice	Inflammation, diabetes	(170, 185–187)

N.A, not applicable.

peripheral blood mononuclear cells (97) **(Table 1)**. As such, NTZ is a PKR activator that holds promise for being repurposed as a host-directed antibacterial drug. The synthetic compound BEPP [1*H*-benzimidazole1-ethanol,2,3-dihydro-2-imino-*a*-(phenoxymethyl)-3-(phenylmethyl)-,monohydrochloride] is another PKR activator that increases PKR and EIF2α phosphorylation in a dose-dependent manner in MEFs (167). Interestingly, BEPP was shown to induce PKR-dependent apoptosis and effectively inhibited vaccinia virus replication in MEFs (167). However, the effects of BEPP have not been studied *in vivo*, and the mechanism of action of BEPP on PKR activity is unknown. Lastly, 3-(2,3-dihydrobenzo[b][1,4]dioxin-6-yl)-5,7-dihydroxy-4H-chromen-4-one (DHBDC) is a dual activator of PKR and PERK (168). DHBDC was shown to induce the phosphorylation of EIF2α, which was blocked by siRNAs targeting PKR and PERK. The mechanism by which DHBDC activates PKR remains unknown, and the effects of this compound have not been assessed *in vivo*. Both BEPP and DHBDC are commercially available for research use.

PKR Inhibitors

There are currently two pharmacological inhibitors of PKR being investigated in pre-clinical studies: imidazole-oxindole C16 and 2-aminopurine (2-AP) **(Table 2)**. Both C16 and 2-AP compete for ATP at the ATP binding site of PKR, thus inhibiting PKR autophosphorylation and kinase activity (169, 185). The most widely-used PKR inhibitor is C16, also known as PKRi or Imoxin (169). C16 has been shown to inhibit PKR phosphorylation *in vitro* and in the mouse model (169–171). The effects of this compound have been examined in numerous *in vitro* studies (5). Furthermore, several *in vivo* studies using mice and rats have examined the effect of C16 in disease contexts such as inflammation, neurodegeneration, obesity, hypertension, cancer, and diabetes (170–184) **(Table 2)**. Importantly, numerous groups have shown that C16 is protective of LPS-induced pathogenesis in mice, including acute lung injury, bone destruction, skeletal muscle atrophy, and acute kidney injury (177–181). Since LPS is a major cell wall component of Gram-negative bacteria, these findings suggest that C16 could protect against excessive inflammation and tissue damage during bacterial infections. However, it is also possible that the anti-inflammatory effect of C16 treatment could exacerbate disease progression in the context of live bacterial infections due to the dampening of the immune response. 2-AP is a less potent and less specific PKR inhibitor (185). In mouse models, 2-AP has been shown to prevent sepsis induced by cecal ligation puncture or endotoxin challenge (186, 187). Furthermore, 2-AP treatment reduces adipose tissue inflammation and improves insulin sensitivity in insulin-resistant obese mice (170). Since 2-AP has anti-inflammatory effects, this drug holds promise in treating bacterial infections where excessive inflammation is conducive for the pathogen. Both C16 and 2-AP are commercially available for research use.

Potential Challenges

There are numerous reports demonstrating that PKR plays an important role during bacterial infections **(Table 1)**, which suggests that pharmacological modulation of PKR could be a promising strategy for host-directed therapy. However, the vast majority of these studies were conducted *in vitro*. Out of the 14 studies listed in **Table 1**, only 4 studies were conducted *in vivo* (62, 90, 91, 96). Notably, these studies only examined the bacterial burden in organs of infected mice and did not assess the overall survival of the animals. Indeed, while there exist numerous pharmacological activators and inhibitors of PKR, only NTZ has been tested *in vivo* in the context of bacterial infections **(Table 2)**. As such, extensive *in vivo* experimentation must be conducted before promoting the use of pharmacological PKR modulation as a therapeutic intervention against bacterial pathogens. It will be critical to demonstrate that pharmacological modulation of PKR has the ability to improve host survival during bacterial infection in animal models. Furthermore, *in vivo* studies must be conducted to identify any limitations of using pharmacological modulators of PKR.

One potential challenge of inhibiting PKR is that interventions that dampen the inflammatory response can sometimes enhance the susceptibility of the host to lethal bacterial infection. For example, C3H/HeJ mice, which have a defective LPS response, are highly susceptible to *E. coli* and *S.* Typhimurium infection (192). Since PKR expression is demonstrated to be important for inflammasome activation and induction of pro-inflammatory cytokines in response to bacterial infections **(Table 1)**, it is possible that pharmacological inhibition of PKR would ultimately be disadvantageous for the host. Another concern is the fact that PKR activity affects many different signaling

pathways. This means that inhibiting or activating PKR-dependent pathways involved in the immune response to bacterial pathogens may also disrupt other PKR-dependent pathways that are essential for other functions. Indeed, dysregulation of PKR has been linked to numerous diseases, including neurodegeneration, cancer, and metabolic disorders (4–6). Furthermore, PKR regulates different immune functions depending on the context of the bacterial infection **(Table 1)**, which suggests that the kinase can play either a pro- or anti-host role during bacterial infection contingent on the specific bacterium involved. As such, it is possible that clinicians would be unable to administer pharmacological PKR modulators to patients until the specific pathogen was identified, thus delaying the initiation of host-directed therapy until it is potentially too late. Altogether, these potential challenges highlight the necessity of evaluating the effects of PKR modulators *in vivo*.

CONCLUDING REMARKS

There is growing evidence demonstrating that PKR plays key roles during infection with various bacterial pathogens **(Table 1)**. Indeed, current literature clearly demonstrates a role for PKR in regulating selective autophagy, cell death, and inflammation during bacterial infections. In response to both Gram-positive and Gram-negative bacterial infections, PKR expression has been shown to be important for inflammasome activation, pyroptosis, and apoptosis. In contrast, PKR is not observed to regulate cell death pathways during mycobacterial infection, but is instead reported to induce selective autophagy. PKR has also been shown to regulate cytokine production in response to mycobacteria, Gram-positive, and Gram-negative bacteria. We speculate that the varying functions of PKR during bacterial infections is due to the specific bacterium involved, since bacterial pathogens have methods of manipulating host immune responses to their advantage. For instance, PKR expression is required for macrophage apoptosis during *B. anthracis* infection (87), but PKR modulation does not impact apoptosis during *M. tuberculosis* infection (98, 116). This is likely explained by the fact that a major virulence mechanism of *B. anthracis* is to induce rapid cell death of host cells (193, 194), whereas *M. tuberculosis* inhibits macrophage apoptosis to allow it to persist undetected within the phagocyte (195). Most studies thus far have focused on the role of PKR in cell death during bacterial infection. Although it is important to investigate the function of PKR during cell death, we contend that this should not be the sole focus, since PKR has recently been shown to induce selective autophagy during bacterial and parasitic infection (77, 98). As such, it will be important for future studies to investigate the function of PKR in selective autophagy of intracellular bacteria such as *L. monocytogenes* and *S. enterica*, since autophagy is reported to play a role in antibacterial defense against these pathogens (196–198).

Although PKR has critical functions in bacterial defense, whether the kinase is ultimately protective or detrimental to the host remains to be clarified. For instance, deletion of PKR led to decreased bacterial burden in organs of *E. coli*-infected mice (62) but resulted in increased bacterial burden in *M. tuberculosis*-infected macrophages (97, 98). Whether PKR plays a pro- or anti-host role during bacterial infection is likely dependent on the specific bacterium involved, and whether the bacterium establishes acute *versus* chronic infection. For example, *S. enterica* causes acute infection, and a strong inflammatory response in the early stage of infection is generally considered to assist with bacterial clearance (199, 200). In contrast, *M. tuberculosis* establishes chronic infection, therefore excessive and prolonged inflammation during infection with this bacterium can be harmful to the host (201). As such, we speculate that the function of PKR in inflammasome activation would be beneficial to the host during *S. enterica* infection, but harmful to the host during *M. tuberculosis* infection. Similarly, PKR is established to induce IFNβ production, which can be a pro- or anti-host function depending on the bacterial context. Indeed, IFNβ production is detrimental to the host during *L. monocytogenes* infection due to its role in inducing macrophage apoptosis (202), but protective for the host during *L. pneumophilia* infection since it promotes itaconic acid production (203).

Unfortunately, most of the existing studies of PKR in the context of bacterial infections examined either the effect of PKR on a particular host signaling pathway, or the effect of PKR expression on bacterial burden, but rarely were both examined within the same study **(Table 1)**. Furthermore, only a limited number of studies have examined the effect of PKR modulation on bacterial burden, with only a select few that included *in vivo* experiments **(Table 1)**. *In vivo* studies will be critical in determining whether PKR is ultimately protective or detrimental to the host during infection with a given bacterium. Importantly, *in vivo* experimentation of PKR is feasible given that pharmacological approaches have been vetted in other disease models **(Table 2)** and both genetic overexpression and deletion of PKR is well-tolerated in mice (204, 205). Both inhibition and activation of PKR by pharmacological compounds **(Table 2)** should be actively pursued given that modulation in either direction could be specifically harnessed for treatment of specific bacterial diseases. As such, future studies should examine the effects of pharmacological modulation of PKR on bacterial burden, morbidity, and mortality of bacteria-infected mice to assess the suitability and feasibility of targeting PKR as a novel treatment strategy. At the same time, it will also be important to determine the specific mechanism regulated by PKR during bacterial infection, since it will link the specific functional pathway to whether PKR is ultimately protective or detrimental to the host.

There also exists a knowledge gap on the specific downstream effectors mediated by PKR in response to various bacteria. For example, although our group observed that PKR induces autophagic degradation of *M. tuberculosis*, the downstream pathway activated by PKR in this context was not elucidated (98). PKR is reported to mediate the activation of numerous downstream effectors, including MAPK, ATF2, NF-κB, IPS-1, IRF3, ATF4, and CHOP **(Figure 1)**. As such, there are many potential mechanisms controlled by PKR to regulate cellular processes such as autophagy, inflammation, and cell death in response to bacterial infections. Future studies should elucidate the specific downstream components regulated by PKR during the immune response to bacterial pathogens.

The upstream signaling events that trigger PKR activation during bacterial infection also need to be determined. Although the canonical activator of PKR is viral dsRNA, the ability of certain phagosome-restricted bacteria to activate PKR suggests the existence of alternative activating mechanisms (89, 95). In this review, we discussed non-canonical activators of PKR – including TLR signaling, ER stress, and bacterial nucleic acids – and speculated on potential mechanisms that trigger PKR activation during bacterial infection (**Figure 2**). However, although exogenous treatment of cells with TLR agonists, bacterial RNA, or chemical inducers of ER stress can activate PKR, there is a lack of evidence to show that live bacteria trigger PKR activation through these specific mechanisms. Future studies examining PKR activity during bacterial infection should strive to characterize the mechanism responsible for activating PKR in this context.

In summary, PKR undoubtedly plays key roles during bacterial infections, as multiple studies have shown that PKR regulates critical immune cell functions such as inflammation, apoptosis, pyroptosis, and autophagy. Increasing our knowledge on the role of PKR during bacterial infections is important since it could lead to the development of host-directed therapies for antibiotic-resistant bacteria. Regardless of whether PKR activity is ultimately beneficial or detrimental to the host, modulating its expression or activity holds promise as a novel treatment strategy for bacterial infections.

SUMMARY

- PKR regulates cell death in both Gram-positive and Gram-negative bacterial infections by inducing apoptosis and activating the inflammasome to trigger pyroptosis.
- PKR regulates the production of multiple cytokines with key roles in antibacterial defense, including Type I IFNs, IL-1β, IL-6, IL-10, IL-18, and TNFα.
- PKR induces selective autophagy during *M. tuberculosis* infection.
- Conflicting reports exist on whether PKR is protective or detrimental to the host. This is likely due to (i) different bacterial pathogens involved, (ii) the specific infection model used for each study, and (iii) the specific mechanistic pathway at play (i.e. cell death *vs*. autophagy).
- The mechanisms of PKR activation during bacterial infection remain to be elucidated, but may involve bacterial nucleic acids, TLR signaling, or ER stress.
- Pharmacological modulation of PKR holds promise as an alternative treatment strategy for bacterial infections, but extensive *in vivo* studies must be conducted to assess the effects of PKR modulation on host survival and identify potential off-target effects.

AUTHOR CONTRIBUTIONS

RS and JS wrote and edited the manuscript. All authors contributed to the article and approved the submitted version.

FUNDING

This work was supported by the Canadian Institutes of Health Research (CIHR) PJT-162424, the National Sanitarium Association Scholar's Program, and the Natural Sciences and Engineering Research Council of Canada (NSERC) RGPIN-2020-04032 to JS.

REFERENCES

1. Taniuchi S, Miyake M, Tsugawa K, Oyadomari M, Oyadomari S. Integrated Stress Response of Vertebrates Is Regulated by Four eIF2α Kinases. *Sci Rep* (2016) 6:1–11. doi: 10.1038/srep32886
2. Barber GN, Edelhoff S, Katze MG, Disteche CM. Chromosomal Assignment of the Interferon-Inducible Double-Stranded RNA-Dependent Protein Kinase (PRKR) to Human Chromosome 2p21-P22 and Mouse Chromosome 17 E2. *Genomics* (1993) 16:765–7. doi: 10.1006/geno.1993.1262
3. Meurs E, Chong K, Galabru J, Thomas NSB, Kerr IM, Williams BRG, et al. Molecular Cloning and Characterization of the Human Double-Stranded RNA-Activated Protein Kinase Induced by Interferon. *Cell* (1990) 62:379–90. doi: 10.1016/0092-8674(90)90374-N
4. García MA, Gil J, Ventoso I, Guerra S, Domingo E, Rivas C, et al. Impact of Protein Kinase PKR in Cell Biology: From Antiviral to Antiproliferative Action. *Microbiol Mol Biol Rev* (2006) 70:1032–60. doi: 10.1128/mmbr.00027-06
5. Gal-Ben-Ari S, Barrera I, Ehrlich M, Rosenblum K. PKR: A Kinase to Remember. *Front Mol Neurosci* (2019) 11:480. doi: 10.3389/fnmol.2018.00480
6. Watanabe T, Imamura T, Hiasa Y. Roles of Protein Kinase R in Cancer: Potential as a Therapeutic Target. *Cancer Sci* (2018) 109:919–25. doi: 10.1111/cas.13551
7. Galabru J, Hovanessians A. Autophosphorylation of the Protein Kinase Dependent on Double-Stranded RNA. *J Biol Chem* (1987) 262:15538–44. doi: 10.1016/S0021-9258(18)47759-9
8. Taniguchi T, Takaoka A. The Interferon-α/β System in Antiviral Responses: A Multimodal Machinery of Gene Regulation by the IRF Family of Transcription Factors. *Curr Opin Immunol* (2002) 14:111–6. doi: 10.1016/S0952-7915(01)00305-3
9. Kuhen KL, Samuel CE. Isolation of the Interferon-Inducible RNA-Dependent Protein Kinase Pkr Promoter and Identification of a Novel DNA Element Within the 5'-Flanking Region of Human and Mouse Pkr Genes. *Virology* (1997) 227:119–30. doi: 10.1006/viro.1996.8306
10. Das S, Ward SV, Tacke RS, Suske G, Samuel CE. Activation of the RNA-Dependent Protein Kinase PKR Promoter in the Absence of Interferon is Dependent Upon Sp Proteins. *J Biol Chem* (2006) 281:3244–53. doi: 10.1074/jbc.M510612200
11. Patel CV, Handy I, Goldsmith T, Patel RC. PACT, a Stress-Modulated Cellular Activator of Interferon-Induced Double-Stranded RNA-Activated Protein Kinase, PKR. *J Biol Chem* (2000) 275:37993–8. doi: 10.1074/jbc.M004762200
12. García MA, Meurs EF, Esteban M. The dsRNA Protein Kinase PKR: Virus and Cell Control. *Biochimie* (2007) 89:799–811. doi: 10.1016/j.biochi.2007.03.001
13. Kuhen KL, Shen X, Carlisle ER, Richardson AL, Weier HUG, Tanaka H, et al. Structural Organization of the Human Gene (PKR) Encoding an

Interferon- Inducible RNA-Dependent Protein Kinase (PKR) and Differences From its Mouse Homolog. *Genomics* (1996) 36:197–201. doi: 10.1006/geno.1996.0446
14. Dey M, Cao C, Dar AC, Tamura T, Ozato K, Sicheri F, et al. Mechanistic Link Between PKR Dimerization, Autophosphorylation, and eIF2α Substrate Recognition. *Cell* (2005) 122:901–13. doi: 10.1016/j.cell.2005.06.041
15. Lemaire PA, Lary J, Cole JL. Mechanism of PKR Activation: Dimerization and Kinase Activation in the Absence of Double-Stranded RNA. *J Mol Biol* (2005) 345:81–90. doi: 10.1016/j.jmb.2004.10.031
16. Zhang F, Romano PR, Nagamura-Inoue T, Tian B, Dever TE, Mathews MB, et al. Binding of Double-Stranded RNA to Protein Kinase PKR is Required for Dimerization and Promotes Critical Autophosphorylation Events in the Activation Loop. *J Biol Chem* (2001) 276:24946–58. doi: 10.1074/jbc.M102108200
17. Singh R, And R, London IM. Regulation of Protein Synthesis in Rabbit Reticulocyte Lysates: Purification and Initial Characterization of the Cyclic 3':5'-AMP Independent Protein Kinase of the Heme-Regulated Translational Inhibitor (Phosphorylation of Met-tRNAf Binding Factor). *Proc Natl Acad Sci USA* (1976) . 73:4349–54. doi: 10.1073/pnas.73.12.4349
18. Harding HP, Zhang Y, Ron D. Protein Translation and Folding are Coupled by an Endoplasmic- Reticulum-Resident Kinase. *Nature* (1999) 397:271–4. doi: 10.1038/16729
19. Dever TE, Feng L, Wek RC, Cigan AM, Donahue TF, Hinnebusch AG. Phosphorylation of Initiation Factor 2α by Protein Kinase GCN2 Mediates Gene-Specific Translational Control of GCN4 in Yeast. *Cell* (1992) 68:585–96. doi: 10.1016/0092-8674(92)90193-G
20. Sudhakar A, Ramachandran A, Ghosh S, Hasnain SE, Kaufman RJ, Ramaiah KVA. Phosphorylation of Serine 51 in Initiation Factor 2α (eIF2α) Promotes Complex Formation Between eIF2α(P) and eIF2B and Causes Inhibition in the Guanine Nucleotide Exchange Activity of eIF2B. *Biochemistry* (2000) 39:12929–38. doi: 10.1021/bi0008682
21. Gordiyenko Y, Llácer JL, Ramakrishnan V. Structural Basis for the Inhibition of Translation Through eIF2α Phosphorylation. *Nat Commun* (2019) 10:1–11. doi: 10.1038/s41467-019-10606-1
22. Liu Y, Wang M, Cheng A, Yang Q, Wu Y, Jia R, et al. The Role of Host eIF2α in Viral Infection. *Virol J* (2020) 17:112. doi: 10.1186/s12985-020-01362-6
23. Donnelly N, Gorman AM, Gupta S, Samali A. The eIF2α Kinases: Their Structures and Functions. *Cell Mol Life Sci* (2013) 70:3493–511. doi: 10.1007/s00018-012-1252-6
24. Dalet A, Gatti E, Pierre P. Integration of PKR-Dependent Translation Inhibition With Innate Immunity is Required for a Coordinated Anti-Viral Response. *FEBS Lett* (2015) 589:1539–45. doi: 10.1016/j.febslet.2015.05.006
25. Zhang P, Langland JO, Jacobs BL, Samuel CE. Protein Kinase PKR-Dependent Activation of Mitogen-Activated Protein Kinases Occurs Through Mitochondrial Adapter IPS-1 and is Antagonized by Vaccinia Virus E3L. *J Virol* (2009) 83:5718–25. doi: 10.1128/jvi.00224-09
26. Goh KC, DeVeer MJ, Williams BRG. The Protein Kinase PKR is Required for P38 MAPK Activation and the Innate Immune Response to Bacterial Endotoxin. *EMBO J* (2000) 19:4292–7. doi: 10.1093/emboj/19.16.4292
27. Silva AM, Whitmore M, Xu Z, Jiang Z, Li X, Williams BRG. Protein Kinase R (PKR) Interacts With and Activates Mitogen-Activated Protein Kinase Kinase 6 (MKK6) in Response to Double-Stranded RNA Stimulation. *J Biol Chem* (2004) 279:37670–6. doi: 10.1074/jbc.M406554200
28. Reimold AM, Kim J, Finberg R, Glimcher LH. Decreased Immediate Inflammatory Gene Induction in Activating Transcription Factor-2 Mutant Mice. *Int Immunol* (2001) 13:241–8. doi: 10.1093/intimm/13.2.241
29. Kirsch K, Zeke A, Tőke O, Sok P, Sethi A, Sebő A, et al. Co-Regulation of the Transcription Controlling ATF2 Phosphoswitch by JNK and P38. *Nat Commun* (2020) 11:1–15. doi: 10.1038/s41467-020-19582-3
30. Gil J, Alcamí J, Esteban M. Activation of NF-κB by the dsRNA-Dependent Protein Kinase, PKR Involves the IκB Kinase Complex. *Oncogene* (2000) 19:1369–78. doi: 10.1038/sj.onc.1203448
31. Bonnet MC, Weil R, Dam E, Hovanessian AG, Meurs EF. PKR Stimulates NF-κb Irrespective of its Kinase Function by Interacting With the IκB Kinase Complex. *Mol Cell Biol* (2000) 20:4532–42. doi: 10.1128/mcb.20.13.4532-4542.2000
32. Gil J, Alcamí J, Esteban M. Induction of Apoptosis by Double-Stranded-RNA-Dependent Protein Kinase (PKR) Involves the α Subunit of Eukaryotic Translation Initiation Factor 2 and NF-κB. *Mol Cell Biol* (1999) 19:4653–63. doi: 10.1128/mcb.19.7.4653
33. Yang YL, Reis LFL, Paylovic J, Aguzzi S, Schäfer R, Kumar A, et al. Deficient Signaling in Mice Devoid of Double-Stranded RNA-Dependent Protein Kinase. *EMBO J* (1995) 14:6095–106. doi: 10.1002/j.1460-2075.1995.tb00300.x
34. Zhang P, Samuel CE. Protein Kinase PKR Plays a Stimulus- and Virus-Dependent Role in Apoptotic Death and Virus Multiplication in Human Cells. *J Virol* (2007) 81:8192–200. doi: 10.1128/jvi.00426-07
35. Maran A, Maitra RK, Kumar A, Dong B, Xiao W, Li G, et al. Blockage of NF-κB Signaling by Selective Ablation of an mRNA Target by 2-5A Antisense Chimeras. *Science* (1994) 265:789–92. doi: 10.1126/science.7914032
36. Trinchieri G. Type I Interferon: Friend or Foe? *J Exp Med* (2010) 207:2053–63. doi: 10.1084/jem.20101664
37. Bolívar S, Anfossi R, Humeres C, Vivar R, Boza P, Muñoz C, et al. IFN-β Plays Both Pro- and Anti-Inflammatory Roles in the Rat Cardiac Fibroblast Through Differential STAT Protein Activation. *Front Pharmacol* (2018) 9:1368. doi: 10.3389/fphar.2018.01368
38. Kopitar-Jerala N. The Role of Interferons in Inflammation and Inflammasome Activation. *Front Immunol* (2017) 8:873. doi: 10.3389/fimmu.2017.00873
39. Jones JW, Kayagaki N, Broz P, Henry T, Newton K, O'Rourke K, et al. Absent in Melanoma 2 is Required for Innate Immune Recognition of Francisella Tularensis. *Proc Natl Acad Sci USA* (2010) 107:9771–6. doi: 10.1073/pnas.1003738107
40. Henry T, Brotcke A, Weiss DS, Thompson LJ, Monack DM. Type I Interferon Signaling is Required for Activation of the Inflammasome During Francisella Infection. *J Exp Med* (2007) 204:987–94. doi: 10.1084/jem.20062665
41. Broz P, Ruby T, Belhocine K, Bouley DM, Kayagaki N, Dixit VM, et al. Caspase-11 Increases Susceptibility to Salmonella Infection in the Absence of Caspase-1. *Nature* (2012) 490:288–91. doi: 10.1038/nature11419
42. Rathinam VAK, Vanaja SK, Waggoner L, Sokolovska A, Becker C, Stuart LM, et al. TRIF Licenses Caspase-11-Dependent NLRP3 Inflammasome Activation by Gram-Negative Bacteria. *Cell* (2012) 150:606–19. doi: 10.1016/j.cell.2012.07.007
43. Zhang P, Samuel CE. Induction of Protein Kinase PKR-Dependent Activation of Interferon Regulatory Factor 3 by Vaccinia Virus Occurs Through Adapter IPS-1 Signaling. *J Biol Chem* (2008) 283:34580–7. doi: 10.1074/jbc.M807029200
44. Munir M, Berg M. The Multiple Faces of Protein Kinase R in Antiviral Defense. *Virulence* (2013) 4:85–9. doi: 10.4161/viru.23134
45. Schulz O, Pichlmair A, Rehwinkel J, Rogers NC, Scheuner D, Kato H, et al. Protein Kinase R Contributes to Immunity Against Specific Viruses by Regulating Interferon mRNA Integrity. *Cell Host Microbe* (2010) 7:354–61. doi: 10.1016/j.chom.2010.04.007
46. Lee SB, Esteban M. The Interferon-Induced Double-Stranded RNA-Activated Protein Kinase Induces Apoptosis. *Virology* (1994) 199:491–6. doi: 10.1006/viro.1994.1151
47. Srivastava SP, Kumar KU, Kaufman RJ. Phosphorylation of Eukaryotic Translation Initiation Factor 2 Mediates Apoptosis in Response to Activation of the Double-Stranded RNA-Dependent Protein Kinase. *J Biol Chem* (1998) 273:2416–23. doi: 10.1074/jbc.273.4.2416
48. Der SD, Yang YL, Weissmann C, Williams BRG. A Double-Stranded RNA-Activated Protein Kinase-Dependent Pathway Mediating Stress-Induced Apoptosis. *Proc Natl Acad Sci USA* (1997) 94:3279–83. doi: 10.1073/pnas.94.7.3279
49. Williams BRG. PKR; A Sentinel Kinase for Cellular Stress. *Oncogene* (1999) 18:6112–20. doi: 10.1038/sj.onc.1203127
50. Kibler KV, Shors T, Perkins KB, Zeman CC, Banaszak MP, Biesterfeldt J, et al. Double-Stranded RNA is a Trigger for Apoptosis in Vaccinia Virus-Infected Cells. *J Virol* (1997) 71:1992–2003. doi: 10.1128/jvi.71.3.1992-2003.1997
51. Takizawa T, Ohashi K, Nakanishi Y. Possible Involvement of Double-Stranded RNA-Activated Protein Kinase in Cell Death by Influenza Virus Infection. *J Virol* (1996) 70:8128–32. doi: 10.1128/jvi.70.11.8128-8132.1996

52. Yeung MC, Chang DL, Camantigue RE, Lau AS. Inhibitory Role of the Host Apoptogenic Gene PKR in the Establishment of Persistent Infection by Encephalomyocarditis Virus in U937 Cells. *Proc Natl Acad Sci USA* (1999) 96:11860–5. doi: 10.1073/pnas.96.21.11860
53. Yeung MC, Liu J, Lau AS. An Essential Role for the Interferon-Inducible, Double-Stranded RNA-Activated Protein Kinase PKR in the Tumor Necrosis Factor-Induced Apoptosis in U937 Cells. *Proc Natl Acad Sci USA* (1996) 93:12451–5. doi: 10.1073/pnas.93.22.12451
54. Lee E-S, Yoon C-H, Kim Y-S, Bae Y-S. The Double-Strand RNA-Dependent Protein Kinase PKR Plays a Significant Role in a Sustained ER Stress-Induced Apoptosis. *FEBS Lett* (2007) 581:4325–32. doi: 10.1016/j.febslet.2007.08.001
55. Patel RC, Sen GC. PACT, a Protein Activator of the Interferon-Induced Protein Kinase, PKR. *EMBO J* (1998) 17:4379–90. doi: 10.1093/emboj/17.15.4379
56. Vattem KM, Wek RC. Reinitiation Involving Upstream ORFs Regulates ATF4 mRNA Translation in Mammalian Cells. *Proc Natl Acad Sci USA* (2004) 101:11269–74. doi: 10.1073/pnas.0400541101
57. Puthalakath H, O'Reilly LA, Gunn P, Lee L, Kelly PN, Huntington ND, et al. ER Stress Triggers Apoptosis by Activating BH3-Only Protein Bim. *Cell* (2007) 129:1337–49. doi: 10.1016/j.cell.2007.04.027
58. Wang XZ, Kuroda M, Sok J, Batchvarova N, Kimmel R, Chung P, et al. Identification of Novel Stress-Induced Genes Downstream of Chop. *EMBO J* (1998) 17:3619–30. doi: 10.1093/emboj/17.13.3619
59. Gil J, Esteban M. The Interferon-Induced Protein Kinase (PKR), Triggers Apoptosis Through FADD-Mediated Activation of Caspase 8 in a Manner Independent of Fas and TNF-α Receptors. *Oncogene* (2000) 19:3665–74. doi: 10.1038/sj.onc.1203710
60. Von Roretz C, Gallouzi IE. Protein Kinase RNA/FADD/caspase-8 Pathway Mediates the Proapoptotic Activity of the RNA-Binding Protein Human Antigen R (Hur). *J Biol Chem* (2010) 285:16806–13. doi: 10.1074/jbc.M109.087320
61. Balachandran S, Kim CN, Yeh WC, Mak TW, Bhalla K, Barber GN. Activation of the dsRNA-Dependent Protein Kinase, PKR, Induces Apoptosis Through FADD-Mediated Death Signaling. *EMBO J* (1998) 17:6888–902. doi: 10.1093/emboj/17.23.6888
62. Lu B, Nakamura T, Inouye K, Li J, Tang Y, Lundbäck P, et al. Novel Role of PKR in Inflammasome Activation and HMGB1 Release. *Nature* (2012) 488:670–4. doi: 10.1038/nature11290
63. Yim HCH, Wang D, Yu L, White CL, Faber PW, Williams BRG, et al. The Kinase Activity of PKR Represses Inflammasome Activity. *Cell Res* (2016) 26:367–79. doi: 10.1038/cr.2016.11
64. Kayagaki N, Warming S, Lamkanfi M, Vande WL, Louie S, Dong J, et al. Non-Canonical Inflammasome Activation Targets Caspase-11. *Nature* (2011) 479:117–21. doi: 10.1038/nature10558
65. He Y, Franchi L, Núñez G. The Protein Kinase PKR is Critical for LPS-Induced iNOS Production But Dispensable for Inflammasome Activation in Macrophages. *Eur J Immunol* (2013) 43:1147–52. doi: 10.1002/eji.201243187
66. Moraco AH, Kornfeld H. Cell Death and Autophagy in Tuberculosis. *Semin Immunol* (2014) 26:497–511. doi: 10.1016/j.smim.2014.10.001
67. Beckwith KS, Beckwith MS, Ullmann S, Sætra RS, Kim H, Marstad A, et al. Plasma Membrane Damage Causes NLRP3 Activation and Pyroptosis During Mycobacterium Tuberculosis Infection. *Nat Commun* (2020) 11:2270. doi: 10.1038/s41467-020-16143-6
68. Mishra BB, Rathinam VAK, Martens GW, Martinot AJ, Kornfeld H, Fitzgerald KA, et al. Nitric Oxide Controls the Immunopathology of Tuberculosis by Inhibiting NLRP3 Inflammasome-Dependent Processing of IL-1β. *Nat Immunol* (2013) 14:52–60. doi: 10.1038/ni.2474
69. Yonekawa T, Thorburn A. Autophagy and Cell Death. *Essays Biochem* (2013) 55:105–17. doi: 10.1042/BSE0550105
70. Nakagawa I, Amano A, Mizushima N, Yamamoto A, Yamaguchi H, Kamimoto T, et al. Autophagy Defends Cells Against Invading Group A Streptococcus. *Science* (2004) 306:1037–40. doi: 10.1126/science.1103966
71. Gutierrez MG, Master SS, Singh SB, Taylor GA, Colombo MI, Deretic V. Autophagy is a Defense Mechanism Inhibiting BCG and Mycobacterium Tuberculosis Survival in Infected Macrophages. *Cell* (2004) 119:753–66. doi: 10.1016/j.cell.2004.11.038
72. Andrade RM, Wessendarp M, Gubbels MJ, Striepen B, Subauste CS. CD40 Induces Macrophage Anti-Toxoplasma Gondii Activity by Triggering Autophagy-Dependent Fusion of Pathogen-Containing Vacuoles and Lysosomes. *J Clin Invest* (2006) 116:2366–77. doi: 10.1172/JCI28796
73. Singh SB, Davis AS, Taylor GA, Deretic V. Human IRGM Induces Autophagy to Eliminate Intracellular Mycobacteria. *Science* (2006) 313:1438–41. doi: 10.1126/science.1129577
74. Zhang Q, Sun J, Wang Y, He W, Wang L, Zheng Y, et al. Antimycobacterial and Anti-Inflammatory Mechanisms of Baicalin Via Induced Autophagy in Macrophages Infected With Mycobacterium Tuberculosis. *Front Microbiol* (2017) 8:2142. doi: 10.3389/fmicb.2017.02142
75. Tallóczy Z, Jiang W, Virgin HWIV, Leib DA, Scheuner D, Kaufman RJ, et al. Regulation of Starvation- and Virus-Induced Autophagy by the eIF2α Kinase Signaling Pathway. *Proc Natl Acad Sci USA* (2002) 99:190–5. doi: 10.1073/pnas.012485299
76. Tallóczy Z, Virgin HWIV, Levine B. PKR-Dependent Autophagic Degradation of Herpes Simplex Virus Type 1. *Autophagy* (2006) 2:24–9. doi: 10.4161/auto.2176
77. Ogolla PS, Portillo J-AC, White CL, Patel K, Lamb B, Sen GC, et al. The Protein Kinase Double-Stranded RNA-Dependent (PKR) Enhances Protection Against Disease Cause by a non-Viral Pathogen. *PloS Pathog* (2013) 9:e1003557. doi: 10.1371/journal.ppat.1003557
78. B'Chir W, Maurin AC, Carraro V, Averous J, Jousse C, Muranishi Y, et al. The eIF2α/ATF4 Pathway is Essential for Stress-Induced Autophagy Gene Expression. *Nucleic Acids Res* (2013) 41:7683–99. doi: 10.1093/nar/gkt563
79. Wei Y, An Z, Zou Z, Sumpter R, Su M, Zang X, et al. The Stress-Responsive Kinases MAPKAPK2/MAPKAPK3 Activate Starvation-Induced Autophagy Through Beclin 1 Phosphorylation. *Elife* (2015) 40:e05289. doi: 10.7554/eLife.05289
80. Pattingre S, Tassa A, Qu X, Garuti R, Xiao HL, Mizushima N, et al. Bcl-2 Antiapoptotic Proteins Inhibit Beclin 1-Dependent Autophagy. *Cell* (2005) 122:927–39. doi: 10.1016/j.cell.2005.07.002
81. Wei Y, Pattingre S, Sinha S, Bassik M, Levine B. JNK1-Mediated Phosphorylation of Bcl-2 Regulates Starvation-Induced Autophagy. *Mol Cell* (2008) 30:678–88. doi: 10.1016/j.molcel.2008.06.001
82. Kubica M, Guzik K, Koziel J, Zarebski M, Richter W, Gajkowska B, et al. A Potential New Pathway for Staphylococcus Aureus Dissemination: The Silent Survival of S. Aureus Phagocytosed by Human Monocyte-Derived Macrophages. *PloS One* (2008) 3:e1409. doi: 10.1371/journal.pone.0001409
83. Gresham HD, Lowrance JH, Caver TE, Wilson BS, Cheung AL, Lindberg FP. Survival of Staphylococcus Aureus Inside Neutrophils Contributes to Infection. *J Immunol* (2000) 164:3713–22. doi: 10.4049/jimmunol.164.7.3713
84. Mestre MB, Fader CM, Sola C, Colombo MI. α-Hemolysin is Required for the Activation of the Autophagic Pathway in Staphylococcus Aureus-Infected Cells. *Autophagy* (2010) 6:110–25. doi: 10.4161/auto.6.1.10698
85. Kloft N, Neukirch C, Bobkiewicz W, Veerachato G, Busch T, Von Hoven G, et al. Pro-Autophagic Signal Induction by Bacterial Pore-Forming Toxins. *Med Microbiol Immunol* (2010) 199:299–309. doi: 10.1007/s00430-010-0163-0
86. Bleiblo F, Michael P, Brabant D, Ramana CV, Tai TC, Saleh M, et al. Bacterial RNA Induces Myocyte Cellular Dysfunction Through the Activation of PKR. *J Thorac Dis* (2012) 4:114–25. doi: 10.3978/j.issn.2072-1439.2012.01.07
87. Hsu LC, Park JM, Zhang K, Luo JL, Maeda S, Kaufman RJ, et al. The Protein Kinase PKR is Required for Macrophage Apoptosis After Activation of Toll-Like Receptor 4. *Nature* (2004) 428:341–5. doi: 10.1038/nature02405
88. Hett EC, Slater LH, Mark KG, Kawate T, Monks BG, Stutz A, et al. Chemical Genetics Reveals a Kinase-Independent Role for Protein Kinase R in Pyroptosis. *Nat Chem Biol* (2013) 9:398–405. doi: 10.1038/nchembio.1236
89. Valderrama C, Clark A, Urano F, Unanue ER, Carrero JA. Listeria Monocytogenes Induces an Interferon-Enhanced Activation of the Integrated Stress Response That is Detrimental for Resolution of Infection in Mice. *Eur J Immunol* (2017) 47:830–40. doi: 10.1002/eji.201646856
90. Yang Y, Xie L, Zhong Y, Zhong X, Meng R, Xue Q, et al. Double-Stranded RNA Dependent Kinase R Regulates Antibacterial Immunity in Sepsis. *J Innate Immun* (2021) 13:26–37. doi: 10.1159/000507932
91. Poon DCH, Ho YS, You R, Tse HL, Chiu K, Chang RCC. PKR Deficiency Alters E. Coli-Induced Sickness Behaviors But Does Not Exacerbate Neuroimmune Responses or Bacterial Load. *J Neuroinflamm* (2015) 12:212. doi: 10.1186/s12974-015-0433-2

92. Shrestha N, Boucher J, Bahnan W, Clark ES, Rosqvist R, Fields KA, et al. The Host-Encoded Heme Regulated Inhibitor (HRI) Facilitates Virulence-Associated Activities of Bacterial Pathogens. *PloS One* (2013) 8:68754. doi: 10.1371/journal.pone.0068754
93. Webster SJ, Ellis L, O'Brien LM, Tyrrell B, Fitzmaurice TJ, Elder MJ, et al. Ire1α Mediates PKR Activation in Response to Chlamydia Trachomatis Infection. *Microbes Infect* (2016) 18:472–83. doi: 10.1016/j.micinf.2016.03.010
94. Mallama CA, McCoy-Simandle K, Cianciotto NP. The Type II Secretion System of Legionella Pneumophila Dampens the MyD88 and Toll-Like Receptor 2 Signaling Pathway in Infected Human Macrophages. *Infect Immun* (2017) 85:e00897–16. doi: 10.1128/IAI.00897-16
95. Cheung BKW, Lee DCW, Li JCB, Lau Y-L, Lau ASY. A Role for Double-Stranded RNA-Activated Protein Kinase PKR in Mycobacterium-Induced Cytokine Expression. *J Immunol* (2005) 175:7218–25. doi: 10.4049/jimmunol.175.11.7218
96. Mundhra S, Bryk R, Hawryluk N, Zhang T, Jiang X, Nathan CF. Evidence for Dispensability of Protein Kinase R in Host Control of Tuberculosis. *Eur J Immunol* (2018) 48:612–20. doi: 10.1002/eji.201747180
97. Ranjbar S, Haridas V, Nambu A, Jasenosky LD, Sadhukhan S, Ebert TS, et al. Cytoplasmic RNA Sensor Pathways and Nitazoxanide Broadly Inhibit Intracellular Mycobacterium Tuberculosis Growth. *iScience* (2019) 22:299–313. doi: 10.1016/j.isci.2019.11.001
98. Smyth R, Berton S, Rajabalee N, Chan T, Sun J. Protein Kinase R Restricts the Intracellular Survival of Mycobacterium Tuberculosis by Promoting Selective Autophagy. *Front Microbiol* (2021) 11:613963. doi: 10.3389/fmicb.2020.613963
99. Duesbery NS, Webb CP, Leppla SH, Gordon VM, Klimpel KR, Copeland TD, et al. Proteolytic Inactivation of MAP-Kinase-Kinase by Anthrax Lethal Factor. *Science* (1998) 280:734–7. doi: 10.1126/science.280.5364.734
100. Kang TJ, Basu S, Zhang L, Thomas KE, Vogel SN, Baillie L, et al. Bacillus Anthracis Spores and Lethal Toxin Induce IL-1β Via Functionally Distinct Signaling Pathways. *Eur J Immunol* (2008) 38:1574–84. doi: 10.1002/eji.200838141
101. Moayeri M, Martinez NW, Wiggins J, Young HA, Leppla SH. Mouse Susceptibility to Anthrax Lethal Toxin is Influenced by Genetic Factors in Addition to Those Controlling Macrophage Sensitivity. *Infect Immun* (2004) 72:4439–47. doi: 10.1128/IAI.72.8.4439-4447.2004
102. Skogberg K, Syrjanen J, Jahkola M, Renkonen O-V, Paavonen J, Ahonen J, et al. Clinical Presentation and Outcome of Listeriosis in Patients With and Without Immunosuppressive Therapy. *Clin Infect Dis* (1992) 14:815–21. doi: 10.1093/clinids/14.4.815
103. Shrestha N, Bahnan W, Wiley DJ, Barber G, Fields KA, Schesser K. Eukaryotic Initiation Factor 2 (eIF2) Signaling Regulates Proinflammatory Cytokine Expression and Bacterial Invasion. *J Biol Chem* (2012) 287:28738–44. doi: 10.1074/jbc.M112.375915
104. Namba T, Tanaka KI, Ito Y, Ishihara T, Hoshino T, Gotoh T, et al. Positive Role of CCAAT/enhancer-Binding Protein Homologous Protein, a Transcription Factor Involved in the Endoplasmic Reticulum Stress Response in the Development of Colitis. *Am J Pathol* (2009) 174:1786–98. doi: 10.2353/ajpath.2009.080864
105. Suyama K, Ohmuraya M, Hirota M, Ozaki N, Ida S, Endo M, et al. C/EBP Homologous Protein is Crucial for the Acceleration of Experimental Pancreatitis. *Biochem Biophys Res Commun* (2008) 367:176–82. doi: 10.1016/j.bbrc.2007.12.132
106. Park SH, Choi HJ, Yang H, Do KH, Kim J, Lee DW, et al. Endoplasmic Reticulum Stress-Activated C/EBP Homologous Protein Enhances Nuclear Factor-κB Signals Via Repression of Peroxisome Proliferator-Activated Receptor. *J Biol Chem* (2010) 285:35330–9. doi: 10.1074/jbc.M110.136259
107. Lebeaupin C, Proics E, De Bieville CHD, Rousseau D, Bonnafous S, Patouraux S, et al. ER Stress Induces NLRP3 Inflammasome Activation and Hepatocyte Death. *Cell Death Dis* (2015) 6:e1879–9. doi: 10.1038/cddis.2015.248
108. Shtrichman R, Heithoff DM, Mahan MJ, Samuel CE. Tissue Selectivity of Interferon-Stimulated Gene Expression in Mice Infected With Dam+ *Versus* Dam- Salmonella Enterica Serovar Typhimurium Strains. *Infect Immun* (2002) 70:5579–88. doi: 10.1128/IAI.70.10.5579-5588.2002
109. Yeung ATY, Choi YH, Lee AHY, Hale C, Ponstingl H, Pickard D, et al. A Genome-Wide Knockout Screen in Human Macrophages Idetified Host Factors Modulating Salmonella Infection. *MBio* (2019) 10:e02169–19. doi: 10.1128/mBio.02169-19
110. Qiu H, Fan Y, Joyee AG, Wang S, Han X, Bai H, et al. Type I Ifns Enhance Susceptibility to Chlamydia Muridarum Lung Infection by Enhancing Apoptosis of Local Macrophages. *J Immunol* (2008) 181:2092–102. doi: 10.4049/jimmunol.181.3.2092
111. Dulberger CL, Rubin EJ, Boutte CC. The Mycobacterial Cell Envelope — a Moving Target. *Nat Rev Microbiol* (2020) 18:47–59. doi: 10.1038/s41579-019-0273-7
112. Barkan D, Liu Z, Sacchettini JC, Glickman MS. Mycolic Acid Cyclopropanation is Essential for Viability, Drug Resistance, and Cell Wall Integrity of Mycobacterium Tuberculosis. *Chem Biol* (2009) 16:499–509. doi: 10.1016/j.chembiol.2009.04.001
113. Zhou X, Yang J, Zhang Z, Zhang L, Zhu B, Lie L, et al. Different Signaling Pathways Define Different Interferon-Stimulated Gene Expression During Mycobacteria Infection in Macrophages. *Int J Mol Sci* (2019) 20:663. doi: 10.3390/ijms20030663
114. Madhvi A, Mishra H, Chegou NN, Tromp G, Van Heerden CJ, Pietersen RD, et al. Distinct Host-Immune Response Toward Species Related Intracellular Mycobacterial Killing: A Transcriptomic Study. *Virulence* (2020) 11:170–82. doi: 10.1080/21505594.2020.1726561
115. Wu K, Koo J, Jiang X, Chen R, Cohen SN, Nathan C. Improved Control of Tuberculosis and Activation of Macrophages in Mice Lacking Protein Kinase R. *PloS One* (2012) 7:e30512. doi: 10.1371/journal.pone.0030512
116. Wu K, Koo J, Jiang X, Chen R, Cohen SN, Nathan C. Erratum: Improved Control of Tuberculosis and Activation of Macrophages in Mice Lacking Protein Kinase R (Plos One (2012) 7:E30512 Doi: 10.1371/Journal.Pone.0205424). *PloS One* (2018) 13:e0205424. doi: 10.1371/journal.pone.0205424
117. Chu LY, Hsueh YC, Cheng HL, Wu KK. Cytokine-Induced Autophagy Promotes Long-Term VCAM-1 But Not ICAM-1 Expression by Degrading Late-Phase IκBα. *Sci Rep* (2017) 7:12472. doi: 10.1038/s41598-017-12641-8
118. Dutta RK, Kathania M, Raje M, Majumdar S. IL-6 Inhibits IFN-γ Induced Autophagy in Mycobacterium Tuberculosis H37Rv Infected Macrophages. *Int J Biochem Cell Biol* (2012) 44:942–54. doi: 10.1016/j.biocel.2012.02.021
119. Bhattacharya B, Xiao S, Chatterjee S, Urbanowski M, Ordonez A, Ihms EA, et al. The Integrated Stress Response Mediates Necrosis in Murine Mycobacterium Tuberculosis Granulomas. *J Clin Invest* (2021) 131:e130319. doi: 10.1172/JCI130319
120. Pichugin AV, Yan BS, Sloutsky A, Kobzik L, Kramnik I. Dominant Role of the Sst1 Locus in Pathogenesis of Necrotizing Lung Granulomas During Chronic Tuberculosis Infection and Reactivation in Genetically Resistant Hosts. *Am J Pathol* (2009) 174:2190–201. doi: 10.2353/ajpath.2009.081075
121. Lai CC, Hsueh PR. Diseases Caused by Nontuberculous Mycobacteria in Asia. *Future Microbiol* (2014) 9:93–106. doi: 10.2217/fmb.13.138
122. George KM, Pascopella L, Welty DM, Small PLC. A Mycobacterium Ulcerans Toxin, Mycolactone, Causes Apoptosis in Guinea Pig Ulcers and Tissue Culture Cells. *Infect Immun* (2000) 68:877–83. doi: 10.1128/IAI.68.2.877-883.2000
123. Ogbechi J, Hall BS, Sbarrato T, Taunton J, Willis AE, Wek RC, et al. Inhibition of Sec61-Dependent Translocation by Mycolactone Uncouples the Integrated Stress Response From ER Stress, Driving Cytotoxicity Via Translational Activation of ATF4. *Cell Death Dis* (2018) 9:1–15. doi: 10.1038/s41419-018-0427-y
124. Matsui T, Tanihara K, Date T. Expression of Unphosphorylated Form of Human Double-Stranded RNA-Activated Protein Kinase in Escherichia Coli. *Biochem Biophys Res Commun* (2001) 284:798–807. doi: 10.1006/bbrc.2001.5039
125. Zheng X, Bevilacqua PC. Activation of the Protein Kinase PKR by Short Double-Stranded RNAs With Single-Stranded Tails. *RNA* (2004) 10:1934–45. doi: 10.1261/rna.7150804
126. Bleiblo F, Michael P, Brabant D, Ramana CV, Tai T, Saleh M, et al. JAK Kinases are Required for the Bacterial RNA and Poly I:C Induced Tyrosine Phosphorylation of PKR. *Int J Clin Exp Med* (2013) 6:16–25.
127. Hull CM, Bevilacqua PC. Mechanistic Analysis of Activation of the Innate Immune Sensor PKR by Bacterial Rna. *J Mol Biol* (2015) 427:3501–15. doi: 10.1016/j.jmb.2015.05.018
128. Hull CM, Anmangandla A, Bevilacqua PC. Bacterial Riboswitches and Ribozymes Potently Activate the Human Innate Immune Sensor PKR. *ACS Chem Biol* (2016) 11:1118–27. doi: 10.1021/acschembio.6b00081

129. Bevilacqua PC, Cech TR. Minor-Groove Recognition of Double-Stranded RNA by the Double-Stranded RNA-Binding Domain From the RNA-Activated Protein Kinase PKR. *Biochemistry* (1996) 35:9983–94. doi: 10.1021/bi9607259
130. Hu S, Sun H, Yin L, Li J, Mei S, Xu F, et al. PKR-Dependent Cytosolic cGAS Foci are Necessary for Intracellular DNA Sensing. *Sci Signal* (2019) 12: eaav7934. doi: 10.1126/scisignal.aav7934
131. Tanaka Y, Chen ZJ. STING Specifies IRF3 Phosphorylation by TBK1 in the Cytosolic DNA Signaling Pathway. *Sci Signal* (2012) 5:ra20. doi: 10.1126/scisignal.2002521
132. Ward SV, Samuel CE. Regulation of the Interferon-Inducible PKR Kinase Gene: The KCS Element is a Constitutive Promoter Element That Functions in Concert With the Interferon-Stimulated Response Element. *Virology* (2002) 296:136–46. doi: 10.1006/viro.2002.1356
133. Horng T, Barton GM, Medzhitov R. Tirap: An Adapter Molecule in the Toll Signaling Pathway. *Nat Immunol* (2001) 2:835–41. doi: 10.1038/ni0901-835
134. Cabanski M, Steinmüller M, Marsh LM, Surdziel E, Seeger W, Lohmeyer J. PKR Regulates TLR2/TLR4-Dependent Signaling in Murine Alveolar Macrophages. *Am J Respir Cell Mol Biol* (2008) 38:26–31. doi: 10.1165/rcmb.2007-0010OC
135. Sales PCM, Williams BRG, Silva AM. Regulation of Double-Stranded RNA Dependent Protein Kinase Expression and Attenuation of Protein Synthesis Induced by Bacterial Toll-Like Receptors Agonists in the Absence of Interferon. *J Interf Cytokine Res* (2012) 32:495–504. doi: 10.1089/jir.2012.0019
136. Faria MS, Calegari-Silva TC, De Carvalho Vivarini A, Mottram JC, Lopes UG, Lima APCA. Role of Protein Kinase R in the Killing of Leishmania Major by Macrophages in Response to Neutrophil Elastase and TLR4 Via TNFα: And IFNβ. *FASEB J* (2014) 28:3050–63. doi: 10.1096/fj.13-245126
137. Li W, Zhu S, Li J, D'Amore J, D'Angelo J, Yang H, et al. Serum Amyloid a Stimulates PKR Expression and HMGB1 Release Possibly Through TLR4/RAGE Receptors. *Mol Med* (2015) 21:515–25. doi: 10.2119/molmed.2015.00109
138. Perkins DJ, Qureshi N, Vogel SN. A Toll-Like Receptor-Responsive Kinase, Protein Kinase R, is Inactivated in Endotoxin Tolerance Through Differential K63/K48 Ubiquitination. *MBio* (2010) 1:e00239–10. doi: 10.1128/mBio.00239-10
139. Carvalho Vivarini Á, Meirelles Santos Pereira R, Teixeira KLD, Calegari-Silva TC, Bellio M, Laurenti MD, et al. Human Cutaneous Leishmaniasis: Interferon-Dependent Expression of Double-Stranded RNA-Dependent Protein Kinase (PKR). *via TLR2. FASEB J* (2011) 25:4162–73. doi: 10.1096/fj.11-185165
140. Jiang Z, Zamanian-Daryoush M, Nie H, Silva AM, Williams BRG, Li X. Poly (Di·Dc)-Induced Toll-Like Receptor 3 (TLR3)-Mediated Activation of Nfκb and MAP Kinase is Through an Interleukin-1 Receptor-Associated Kinase (IRAK)-Independent Pathway Employing the Signaling Components TLR3-TRAF6-TAK1-TAB2-PKR. *J Biol Chem* (2003) 278:16713–9. doi: 10.1074/jbc.M300562200
141. Chuang JH, Chuang HC, Huang CC, Wu CL, Du YY, Kung ML, et al. Differential Toll-Like Receptor 3 (TLR3) Expression and Apoptotic Response to TLR3 Agonist in Human Neuroblastoma Cells. *J BioMed Sci* (2011) 18:65. doi: 10.1186/1423-0127-18-65
142. Singh M, Fowlkes V, Handy I, Patel CV, Patel RC. Essential Role of PACT-Mediated PKR Activation in Tunicamycin-Induced Apoptosis. *J Mol Biol* (2009) 385:457–68. doi: 10.1016/j.jmb.2008.10.068
143. Nakamura T, Furuhashi M, Li P, Cao H, Tuncman G, Sonenberg N, et al. Double-Stranded RNA-Dependent Protein Kinase Links Pathogen Sensing With Stress and Metabolic Homeostasis. *Cell* (2010) 140:338–48. doi: 10.1016/j.cell.2010.01.001
144. Vaughn LS, Bragg DC, Sharma N, Camargos S, Cardoso F, Patel RC. Altered Activation of Protein Kinase PKR and Enhanced Apoptosis in Dystonia Cells Carrying a Mutation in PKR Activator Protein PACT. *J Biol Chem* (2015) 290:22543–57. doi: 10.1074/jbc.M115.669408
145. Akazawa Y, Isomoto H, Matsushima K, Kanda T, Minami H, Yamaghchi N, et al. Endoplasmic Reticulum Stress Contributes to Helicobacter Pylori VacA-Induced Apoptosis. *PloS One* (2013) 8:e82322. doi: 10.1371/journal.pone.0082322
146. Brann KR, Fullerton MS, Voth DE. Coxiella Burnetii Requires Host Eukaryotic Initiation Factor 2α Activity for Efficient Intracellular Replication. *Infect Immun* (2020) 88:e00096–20. doi: 10.1128/IAI.00096-20
147. Halder P, Datta C, Kumar R, Sharma AK, Basu J, Kundu M. The Secreted Antigen, HP0175, of Helicobacter Pylori Links the Unfolded Protein Response (UPR) to Autophagy in Gastric Epithelial Cells. *Cell Microbiol* (2015) 17:714–29. doi: 10.1111/cmi.12396
148. Bedi B, Lin KC, Maurice NM, Yuan Z, Bijli K, Koval M, et al. UPR Modulation of Host Immunity by Pseudomonas Aeruginosa in Cystic Fibrosis. *Clin Sci* (2020) 134:1911–34. doi: 10.1042/CS20200066
149. Marchal JA, Carrasco E, Ramirez A, Jiménez G, Olmedo C, Peran M, et al. Bozepinib, a Novel Small Antitumor Agent, Induces PKR-Mediated Apoptosis and Synergizes With IFNα Triggering Apoptosis, Autophagy and Senescence. *Drug Des Devel Ther* (2013) 7:1301–13. doi: 10.2147/DDDT.S51354
150. López-Cara LC, Conejo-García A, Marchal JA, MacChione G, Cruz-López O, Boulaiz H, et al. New (RS)-Benzoxazepin-Purines With Antitumour Activity: The Chiral Switch From (RS)-2,6-Dichloro-9-[1-(P-Nitrobenzenesulfonyl)-1,2,3,5-Tetrahydro-4,1- Benzoxazepin-3-Yl]-9h-Purine. *Eur J Med Chem* (2011) 46:249–58. doi: 10.1016/j.ejmech.2010.11.011
151. Elazar M, Liu M, McKenna SA, Liu P, Gehrig EA, Puglisi JD, et al. The Anti-Hepatitis C Agent Nitazoxanide Induces Phosphorylation of Eukaryotic Initiation Factor 2α Via Protein Kinase Activated by Double-Stranded RNA Activation. *Gastroenterology* (2009) 137:1827–35. doi: 10.1053/j.gastro.2009.07.056
152. Ashiru O, Howe JD, Butters TD. Nitazoxanide, an Antiviral Thiazolide, Depletes ATP-Sensitive Intracellular Ca2+ Stores. *Virology* (2014) 462–463:135–48. doi: 10.1016/j.virol.2014.05.015
153. Bolick DT, Roche JK, Hontecillas R, Bassaganya-Riera J, Nataro JP, Guerrant RL. Enteroaggregative Escherichia Coli Strain in a Novel Weaned Mouse Model: Exacerbation by Malnutrition, Biofilm as a Virulence Factor and Treatment by Nitazoxanide. *J Med Microbiol* (2013) 62:896–905. doi: 10.1099/jmm.0.046300-0
154. Gupta A, Meena J, Sharma D, Gupta P, Gupta UD, Kumar S, et al. Inhalable Particles for "Pincer Therapeutics" Targeting Nitazoxanide as Bactericidal and Host-Directed Agent to Macrophages in a Mouse Model of Tuberculosis. *Mol Pharm* (2016) 13:3247–55. doi: 10.1021/acs.molpharmaceut.6b00459
155. McVay CS, Rolfe RD. *In Vitro* and *In Vivo* Activities of Nitazoxanide Against Clostridium Difficile. *Antimicrob Agents Chemother* (2000) 44:2254–8. doi: 10.1128/AAC.44.9.2254-2258.2000
156. Warren CA, Van Opstal EJ, Riggins MS, Li Y, Moore JH, Kolling GL, et al. Vancomycin Treatment's Association With Delayed Intestinal Tissue Injury, Clostridial Overgrowth, and Recurrence of Clostridium Difficile Infection in Mice. *Antimicrob Agents Chemother* (2013) 57:689–96. doi: 10.1128/AAC.00877-12
157. Rossignol JF. Nitazoxanide: A First-In-Class Broad-Spectrum Antiviral Agent. *Antiviral Res* (2014) 110:94–103. doi: 10.1016/j.antiviral.2014.07.014
158. Hemphill A, Mueller J, Esposito M. Nitazoxanide, a Broad-Spectrum Thiazolide Anti-Infective Agent for the Treatment of Gastrointestinal Infections. *Expert Opin Pharmacother* (2006) 7:953–64. doi: 10.1517/14656566.7.7.953
159. Bailey MA, Na H, Duthie MS, Gillis TP, Lahiri R, Parish T. Nitazoxanide is Active Against Mycobacterium Leprae. *PloS One* (2017) 12:e0184107. doi: 10.1371/journal.pone.0184107
160. Wang X, Shen C, Liu Z, Peng F, Chen X, Yang G, et al. Nitazoxanide, an Antiprotozoal Drug, Inhibits Late-Stage Autophagy and Promotes ING1-Induced Cell Cycle Arrest in Glioblastoma. *Cell Death Dis* (2018) 9:1032. doi: 10.1038/s41419-018-1058-z
161. Kiehl IGA, Riccetto E, Salustiano ACC, Ossick MV, Ferrari KL, Assalin HB, et al. Boosting Bladder Cancer Treatment by Intravesical Nitazoxanide and Bacillus Calmette-Guérin Association. *World J Urol* (2021) 39:1187–94. doi: 10.1007/s00345-020-03294-w
162. Pal AK, Nandave M, Kaithwas G. Chemoprophylactic Activity of Nitazoxanide in Experimental Model of Mammary Gland Carcinoma in Rats. *3 Biotech* (2020) 10:338. doi: 10.1007/s13205-020-02332-z

163. Senkowski W, Zhang X, Olofsson MH, Isacson R, Höglund U, Gustafsson M, et al. Three-Dimensional Cell Culture-Based Screening Identifies the Anthelmintic Drug Nitazoxanide as a Candidate for Treatment of Colorectal Cancer. *Mol Cancer Ther* (2015) 14:1504–16. doi: 10.1158/1535-7163.MCT-14-0792
164. Ai N, Wood RD, Welsh WJ. Identification of Nitazoxanide as a Group I Metabotropic Glutamate Receptor Negative Modulator for the Treatment of Neuropathic Pain: An in Silico Drug Repositioning Study. *Pharm Res* (2015) 32:2798–807. doi: 10.1007/s11095-015-1665-7
165. Amireddy N, Puttapaka SN, Vinnakota RL, Ravuri HG, Thonda S, Kalivendi SV. The Unintended Mitochondrial Uncoupling Effects of the FDA-Approved Anti-Helminth Drug Nitazoxanide Mitigates Experimental Parkinsonism in Mice. *J Biol Chem* (2017) 292:15731–43. doi: 10.1074/jbc.M117.791863
166. Hong SK, Kim HJ, Song CS, Choi IS, Lee JB, Park SY. Nitazoxanide Suppresses IL-6 Production in LPS-Stimulated Mouse Macrophages and TG-Injected Mice. *Int Immunopharmacol* (2012) 13:23–7. doi: 10.1016/j.intimp.2012.03.002
167. Hu W, Hofstetter W, Wei X, Guo W, Zhou Y, Pataer A, et al. Double-Stranded RNA-Dependent Protein Kinase-Dependent Apoptosis Induction by a Novel Small Compound. *J Pharmacol Exp Ther* (2009) 328:866–72. doi: 10.1124/jpet.108.141754
168. Bai H, Chen T, Ming J, Sun H, Cao P, Fusco DN, et al. Dual Activators of Protein Kinase R (PKR) and Protein Kinase R-Like Kinase (PERK) Identify Common and Divergent Catalytic Targets. *ChemBioChem* (2013) 14:1255–62. doi: 10.1002/cbic.201300177
169. Jammi NV, Whitby LR, Beal PA. Small Molecule Inhibitors of the RNA-Dependent Protein Kinase. *Biochem Biophys Res Commun* (2003) 308:50–7. doi: 10.1016/S0006-291X(03)01318-4
170. Nakamura T, Arduini A, Baccaro B, Furuhashi M, Hotamisligil GS. Small-Molecule Inhibitors of PKR Improve Glucose Homeostasis in Obese Diabetic Mice. *Diabetes* (2014) 63:526–34. doi: 10.2337/db13-1019
171. Ingrand S, Barrier L, Lafay-Chebassier C, Fauconneau B, Page G, Hugon J. The Oxindole/Imidazole Derivative C16 Reduces *In Vivo* Brain PKR Activation. *FEBS Lett* (2007) 581:4473–8. doi: 10.1016/j.febslet.2007.08.022
172. Watanabe T, Ninomiya H, Saitou T, Takanezawa S, Yamamoto S, Imai Y, et al. Therapeutic Effects of the PKR Inhibitor C16 Suppressing Tumor Proliferation and Angiogenesis in Hepatocellular Carcinoma *In Vitro* and *In Vivo*. *Sci Rep* (2020) 10:5133. doi: 10.1038/s41598-020-61579-x
173. Kalra J, Bhat A, Jadhav KKB, Dhar A. Up-Regulation of PKR Pathway Contributes to L-NAME Induced Hypertension and Renal Damage. *Heliyon* (2020) 6:e05463. doi: 10.1016/j.heliyon.2020.e05463
174. Kalra J, Dasari D, Bhat A, Mangali S, Goyal SG, Jadhav KB, et al. PKR Inhibitor Imoxin Prevents Hypertension, Endothelial Dysfunction and Cardiac and Vascular Remodelling in L-NAME-Treated Rats. *Life Sci* (2020) 262:118436. doi: 10.1016/j.lfs.2020.118436
175. Wang WJ, Yin SJ, Rong RQ. PKR and HMGB1 Expression and Function in Rheumatoid Arthritis. *Genet Mol Res* (2015) 14:17864–70. doi: 10.4238/2015.December.22.11
176. Tronel C, Page G, Bodard S, Chalon S, Antier D. The Specific PKR Inhibitor C16 Prevents Apoptosis and IL-1β Production in an Acute Excitotoxic Rat Model With a Neuroinflammatory Component. *Neurochem Int* (2014) 64:73–83. doi: 10.1016/j.neuint.2013.10.012
177. Li R, Shang Y, Yu Y, Zhou T, Xiong W, Zou X. High-Mobility Group Box 1 Protein Participates in Acute Lung Injury by Activating Protein Kinase R and Inducing M1 Polarization. *Life Sci* (2020) 246:117415. doi: 10.1016/j.lfs.2020.117415
178. Li Y, Xiao J, Tan Y, Wang J, Zhang Y, Deng X, et al. Inhibition of PKR Ameliorates Lipopolysaccharide-Induced Acute Lung Injury by Suppressing NF-κB Pathway in Mice. *Immunopharmacol Immunotoxicol* (2017) 39:165–72. doi: 10.1080/08923973.2017.1303839
179. Teramachi J, Inagaki Y, Shinohara H, Okamura H, Yang D, Ochiai K, et al. PKR Regulates LPS-Induced Osteoclast Formation and Bone Destruction *In Vitro* and *In Vivo*. *Oral Dis* (2017) 23:181–8. doi: 10.1111/odi.12592
180. Zhou J, Zhang F, Lin H, Quan M, Yang Y, Lv Y, et al. The Protein Kinase R Inhibitor C16 Alleviates Sepsis-Induced Acute Kidney Injury Through Modulation of the NF-kB and NLR Family Pyrin Domain-Containing 3 (NLPR3) Pyroptosis Signal Pathways. *Med Sci Monit* (2020) 26:e926254. doi: 10.12659/MSM.926254
181. Valentine RJ, Jefferson MA, Kohut ML, Eo H. Imoxin Attenuates LPS-Induced Inflammation and MuRF1 Expression in Mouse Skeletal Muscle. *Physiol Rep* (2018) 6:e13941. doi: 10.14814/phy2.13941
182. Hwang KD, Bak MS, Kim SJ, Rhee S, Lee YS. Restoring Synaptic Plasticity and Memory in Mouse Models of Alzheimer's Disease by PKR Inhibition. *Mol Brain* (2017) 10:57. doi: 10.1186/s13041-017-0338-3
183. Xiao J, Tan Y, Li Y, Luo Y. The Specific Protein Kinase R (PKR) Inhibitor C16 Protects Neonatal Hypoxia-Ischemia Brain Damages by Inhibiting Neuroinflammation in a Neonatal Rat Model. *Med Sci Monit* (2016) 22:5074–81. doi: 10.12659/MSM.898139
184. Segev Y, Barrera I, Ounallah-Saad H, Wibrand K, Sporild I, Livne A, et al. PKR Inhibition Rescues Memory Deficit and Atf4 Overexpression in Apoe ϵ4 Human Replacement Mice. *J Neurosci* (2015) 35:12986–93. doi: 10.1523/JNEUROSCI.5241-14.2015
185. Hu Y, Conway TW. 2-Aminopurine Inhibits the Double-Stranded RNA-Dependent Protein Kinase Both *In Vitro* and *In Vivo*. *J Interferon Res* (1993) 13:323–8. doi: 10.1089/jir.1993.13.323
186. Supinski GS, Callahan LA. Double-Stranded RNA-Dependent Protein Kinase Activation Modulates Endotoxin-Induced Diaphragm Weakness. *J Appl Physiol* (2011) 110:199–205. doi: 10.1152/japplphysiol.01203.2009
187. Qiu CF, Wu JF, Pei F, Wang LH, Mei MH, Ouyang B, et al. Effect of Inhibiting the Activity of Double-Stranded RNA-Dependent Protein Kinase in Sepsis Mice. *Zhonghua Yi Xue Za Zhi* (2020) 100:1033–7. doi: 10.3760/cma.j.cn112137-20190825-01888
188. Rossignol JF, Elfert A, El-Gohary Y, Keeffe EB. Improved Virologic Response in Chronic Hepatitis C Genotype 4 Treated With Nitazoxanide, Peginterferon, and Ribavirin. *Gastroenterology* (2009) 136:856–62. doi: 10.1053/j.gastro.2008.11.037
189. Haffizulla J, Hartman A, Hoppers M, Resnick H, Samudrala S, Ginocchio C, et al. Effect of Nitazoxanide in Adults and Adolescents With Acute Uncomplicated Influenza: A Double-Blind, Randomised, Placebo-Controlled, Phase 2b/3 Trial. *Lancet Infect Dis* (2014) 14:609–18. doi: 10.1016/S1473-3099(14)70717-0
190. Shigyo K, Ocheretina O, Merveille YM, Johnson WD, Pape JW, Nathan CF, et al. Efficacy of Nitazoxanide Against Clinical Isolates of Mycobacterium Tuberculosis. *Antimicrob Agents Chemother* (2013) 57:2834–7. doi: 10.1128/AAC.02542-12
191. Walsh KF, McAulay K, Lee MH, Vilbrun SC, Mathurin L, Francois DJ, et al. Early Bactericidal Activity Trial of Nitazoxanide for Pulmonary Tuberculosis. *Antimicrob Agents Chemother* (2020) 64:e01956–19. doi: 10.1128/AAC.01956-19
192. Hagberg L, Briles DE, Edén CS. Evidence for Separate Genetic Defects in C3H/HeJ and C3HeB/FeJ Mice, That Affect Susceptibility to Gram-Negative Infections. *J Immunol* (1985) 134:4118–22.
193. Popov SG, Villasmil R, Bernardi J, Grene E, Cardwell J, Wu A, et al. Lethal Toxin of Bacillus Anthracis Causes Apoptosis of Macrophages. *Biochem Biophys Res Commun* (2002) 293:349–55. doi: 10.1016/S0006-291X(02)00227-9
194. Alileche A, Serfass ER, Muehlbauer SM, Porcelli SA, Brojatsch J. Anthrax Lethal Toxin-Mediated Killing of Human and Murine Dendritic Cells Impairs the Adaptive Immune Response. *PloS Pathog* (2005) 1:e19. doi: 10.1371/journal.ppat.0010019
195. Schaaf K, Smith SR, Duverger A, Wagner F, Wolschendorf F, Westfall AO, et al. Mycobacterium Tuberculosis Exploits the PPM1A Signaling Pathway to Block Host Macrophage Apoptosis. *Sci Rep* (2017) 7:42101. doi: 10.1038/srep42101
196. Birmingham CL, Smith AC, Bakowski MA, Yoshimori T, Brumell JH. Autophagy Controls Salmonella Infection in Response to Damage to the Salmonella-Containing Vacuole. *J Biol Chem* (2006) 281:11374–83. doi: 10.1074/jbc.M509157200
197. Py BF, Lipinski MM, Yuan J. Autophagy Limits Listeria Monocytogenes Intracellular Growth in the Early Phase of Primary Infection. *Autophagy* (2007) 3:117–25. doi: 10.4161/auto.3618
198. Matsuzawa T, Kim B-H, Shenoy AR, Kamitani S, Miyake M, MacMicking JD. Ifn-γ Elicits Macrophage Autophagy Via the P38 MAPK Signaling Pathway. *J Immunol* (2012) 189:813–8. doi: 10.4049/jimmunol.1102041
199. Raupach B, Peuschel SK, Monack DM, Zychlinsky A. Caspase-1-Mediated Activation of Interleukin-1β (Il-1β) and IL-18 Contributes to Innate Immune Defenses Against Salmonella Enterica Serovar Typhimurium Infection. *Infect Immun* (2006) 74:4922–6. doi: 10.1128/IAI.00417-06

200. Lara-Tejero M, Sutterwala FS, Ogura Y, Grant EP, Bertin J, Coyle AJ, et al. Role of the Caspase-1 Inflammasome in Salmonella Typhimurium Pathogenesis. *J Exp Med* (2006) 203:1407–12. doi: 10.1084/jem.20060206
201. Ravimohan S, Kornfeld H, Weissman D, Bisson GP. Tuberculosis and Lung Damage: From Epidemiology to Pathophysiology. *Eur Respir Rev* (2018) 27:170077. doi: 10.1183/16000617.0077-2017
202. Carrero JA, Calderon B, Unanue ER. Type I Interferon Sensitizes Lymphocytes to Apoptosis and Reduces Resistance to Listeria Infection. *J Exp Med* (2004) 200:535–40. doi: 10.1084/jem.20040769
203. Naujoks J, Tabeling C, Dill BD, Hoffmann C, Brown AS, Kunze M, et al. Ifns Modify the Proteome of Legionella-Containing Vacuoles and Restrict Infection Via IRG1-Derived Itaconic Acid. *PloS Pathog* (2016) 12: e1005408. doi: 10.1371/journal.ppat.1005408
204. Ladiges W, Morton J, Hopkins H, Wilson R, Filley G, Ware C, et al. Expression of Human PKR Protein Kinase in Transgenic Mice. *J Interf Cytokine Res* (2002) 22:329–34. doi: 10.1089/107999002753675758
205. Nakayama Y, Plisch EH, Sullivan J, Thomas C, Czuprynski CJ, Williams BRG, et al. Role of PKR and Type I Ifns in Viral Control During Primary and Secondary Infection. *PloS Pathog* (2010) 6:1000966. doi: 10.1371/journal.ppat.1000966

Conflict of Interest: The authors declare that the research was conducted in the absence of any commercial or financial relationships that could be construed as a potential conflict of interest.

Copyright © 2021 Smyth and Sun. This is an open-access article distributed under the terms of the Creative Commons Attribution License (CC BY). The use, distribution or reproduction in other forums is permitted, provided the original author(s) and the copyright owner(s) are credited and that the original publication in this journal is cited, in accordance with accepted academic practice. No use, distribution or reproduction is permitted which does not comply with these terms.

frontiers in Microbiology

ORIGINAL RESEARCH
published: 08 July 2021
doi: 10.3389/fmicb.2021.694081

Inhibitory Role of an *Aeromonas hydrophila* TIR Domain Effector in Antibacterial Immunity by Targeting TLR Signaling Complexes in Zebrafish

Huai-ping Tang[1], Chen Huang[1], Chong-bin Hu[1], Hao Li[1], Tong Shao[1], Jian-fei Ji[1], Jun Bai[1], Dong-dong Fan[1], Ai-fu Lin[1], Li-xin Xiang[1] and Jian-zhong Shao[1,2]**

[1] College of Life Sciences, Key Laboratory for Cell and Gene Engineering of Zhejiang Province, Zhejiang University, Hangzhou, China, [2] Laboratory for Marine Biology and Biotechnology, Qingdao National Laboratory for Marine Science and Technology, Qingdao, China

OPEN ACCESS

Edited by:
Karl Kuchler,
Medical University of Vienna, Austria

Reviewed by:
Birgit Strobl,
University of Veterinary Medicine Vienna, Austria
Catherine Ropert,
Federal University of Minas Gerais, Brazil

***Correspondence:**
Li-xin Xiang
xianglx@zju.edu.cn
Jian-zhong Shao
shaojz@zju.edu.cn

Specialty section:
This article was submitted to Microbial Immunology, a section of the journal Frontiers in Microbiology

Received: 12 April 2021
Accepted: 15 June 2021
Published: 08 July 2021

Citation:
Tang H-p, Huang C, Hu C-b, Li H, Shao T, Ji J-f, Bai J, Fan D-d, Lin A-f, Xiang L-x and Shao J-z (2021) Inhibitory Role of an Aeromonas hydrophila TIR Domain Effector in Antibacterial Immunity by Targeting TLR Signaling Complexes in Zebrafish. Front. Microbiol. 12:694081. doi: 10.3389/fmicb.2021.694081

The Toll/interleukin-1 receptor (TIR) domain is a structural unit responsible for the assembly of signal protein complexes in Toll-like receptor (TLR) and interleukin-1 receptor signaling pathways. TIR domain homologs are found in a considerable number of bacteria and enhance bacterial infection and survival in host organisms. However, whether TIR domain homologs exist in *Aeromonas hydrophila*, a ubiquitous waterborne bacterium in aquatic environments, remains poorly understood. In this study, a TIR domain protein (TcpAh) was identified from *A. hydrophila* JBN2301. TIR domain of TcpAh is highly homologous to the counterpart domains in TLRs and myeloid differentiation factor 88 (MyD88). The zebrafish infected with mutant *A. hydrophila* with *tcpAh* deletion had a remarkably lower mortality than those infected with the wild-type strain. This result suggests that TcpAh is a crucial virulence factor for *A. hydrophila* infection. TcpAh exhibited a strong ability to associate with MyD88, tumor necrosis factor receptor-associated factor 3 (TRAF3) and TRAF-associated NF-κB activator-binding kinase 1 (TBK1) in TIR–TIR, TIR–Death domain (DD), and other alternative interactions. This finding suggests that TcpAh extensively interferes with MyD88 and TIR domain-containing adapter inducing interferon (IFN)-β (TRIF) signaling pathways downstream of TLRs. Consequently, CD80/86 expression was suppressed by TcpAh via attenuating TLR-stimulated NF-κB activation, which ultimately led to the impairment of the major costimulatory signal essential for the initiation of adaptive humoral immunity against *A. hydrophila* infection. We believe that this study is the first to show a previously unrecognized mechanism underlying *A. hydrophila* evades from host antibacterial defense by intervening CD80/86 signal, which bridges innate and adaptive immunity. The mechanism will benefit the development of therapeutic interventions for *A. hydrophila* infection and septicemia by targeting TcpAh homologs.

Keywords: TIR domain effector, *A. hydrophila*, TLR signaling pathways, CD80/86, antibacterial immunity

INTRODUCTION

Toll-like receptors (TLRs) and interleukin-1 receptors (IL-1Rs) play crucial roles in an array of host immune responses (Tobias et al., 2000; Dunne and O'Neill, 2003). Signal transduction through these receptors leads to the activation of various transcription factors, such as NF-κB and activator protein 1 (AP-1) (Dunne and O'Neill, 2003). These two families of receptors share a conserved intracellular region with approximately 200 amino acids, known as the Toll/interleukin-1 receptor (TIR) domain (Slack et al., 2000; Akira and Takeda, 2004). This domain is also shared by the downstream signaling proteins, such as myeloid differentiation factor 88 (MyD88), TIR domain-containing adaptor protein (TIRAP), TIR domain-containing adapter inducing interferon (IFN)-β (TRIF) and TRIF-related adaptor molecule (TRAM), as a unit responsible for the signal-dependent assembly of protein complexes that enable the amplification and spatial propagation of a signal (O'Neill and Bowie, 2007). Site-directed mutagenesis and deletion analysis showed that the TIR domain is essential for TLR and IL-1R activities (Poltorak et al., 1998; Underhill et al., 1999). The TIR domain consists of three functional boxes of conserved residues set in a core sequence that ranges from 135 to 160 amino acids (Xu et al., 2000). Box 1 and 2 motifs participate in the association of proteins involved in signaling, whereas box 3 is involved in directing the localization of receptors (Slack et al., 2000; Xu et al., 2000). Two interfaces are responsible for mediating TIR domain interactions, which include receptor/adaptor oligomerization and the association between receptors and adaptors (Dunne et al., 2003). Crystal structure analysis showed that the TIR domains from human TLR1/2 contain a central five-stranded parallel β-sheet that is surrounded by five helices on both sides (Xu et al., 2000; Dunne et al., 2003). Conserved residues are located in the hydrophobic core and large insertions or deletions are present in several loop regions of different TIR domains. The BB loop, contains three highly conserved residues, protrudes from a large conserved surface patch, which is believed to mediate heterodimeric interactions with TIR domain-containing adaptor proteins (Xu et al., 2000; Dunne et al., 2003; Jin and Lee, 2008).

Among the numerous TIR domain-containing adaptors, MyD88 is the common adaptor recruited by all TLRs except TLR3 (Janssens and Beyaert, 2002). TIRAP is a unique adapter in TLR2 and TLR4 signaling and is associated with MyD88 for NF-κB activation (Horng et al., 2002). TRIF and TRAM activate IFN regulatory factor (IRF)-3, IRF-7, and NF-κB-dependent signaling pathways (Yamamoto et al., 2002; Oshiumi et al., 2003). TRIF functions downstream TLR3 and TLR4 signaling pathways, whereas TRAM is restricted to the TLR4 pathway (Yamamoto et al., 2003a,b). Some negative regulators, including single immunoglobulin IL-1 receptor related protein (SIGIRR), MyD88s, interleukin-1 receptor-associated kinase (IRAK)-M, Triad3A, and sterile alpha and TIR motif-containing protein (SARM), which block MyD88- or TRIF-dependent signaling pathways, co-evolve in host organisms to avoid excess inflammatory reactions (Kobayashi et al., 2002; Burns et al., 2003; O'Neill, 2003; Wald et al., 2003; Akira and Takeda, 2004; Carty et al., 2006; Fearns et al., 2006). The TIR domain in SIGIRR resembles MyD88 but lacks two amino acids needed for downstream signaling (O'Neill, 2003). In addition, the TIR–TIR interaction between SIGIRR and TLR4 prevents the recruitment of IRAK and tumor necrosis factor receptor-associated factor (TRAF) 6 to MyD88 (Wald et al., 2003). MyD88s is an alternatively spliced variant of MyD88 that lacks the intermediary domain; thus, it is unable to bind to IRAK4 and promote IRAK1 phosphorylation (Burns et al., 2003). IRAK-M prevents the dissociation of IRAK1–IRAK4 complex from MyD88 to prevent the formation of IRAK1–TRAF6 complex (Kobayashi et al., 2002). Triad3A interacts with the TIR domains of TLRs, TRIF, TIRAP and receptor-interacting protein 1 (RIP1); SARM blocks gene induction downstream of TRIF (Carty et al., 2006; Fearns et al., 2006). Interestingly, some of these negative regulatory strategies are imitated by bacterial TIR domain proteins to impair host TLR- and IL-1R-mediated signaling pathways and create a permissive environment facilitating bacterial infection and survival (Newman et al., 2006; Rosadini and Kagan, 2015). This observation implicates the complex evolutionary correlation between host and microbe.

Toll/interleukin-1 receptor domain proteins have been found in a considerable number of bacteria, such as *Salmonella enterica*, *Brucella melitensis*, *Escherichia coli* CFT073, *Yersinia pestis*, *Paracoccus denitrificans*, *Staphylococcus aureus* and *Pseudomonas aeruginosa* (Newman et al., 2006; Low et al., 2007; Cirl et al., 2008; Rana et al., 2011; Askarian et al., 2014; Imbert et al., 2017). These proteins include TlpA in *S. enterica*, TcpB in *B. melitensis*, TcpC in *E. coli* CFT073, YpTdp in *Y. pestis*, PdTLP in *P. denitrificans*, TirS in *S. aureus* and PumA in *P. aeruginosa*. These proteins enhance bacterial colonization and survival in host organisms. However, whether the TIR domain proteins exist in *Aeromonas hydrophila* remains poorly understood. *A. hydrophila* is one of the most ubiquitous waterborne bacteria in freshwater and brackish water environments. *A. hydrophila* shows wide host tropism, is frequently encountered in fish and other aquatic organisms, and is accountable for various infections, including severe aeromonad septicemia (Harikrishnan et al., 2003; Vivas et al., 2004). Therefore, understanding the associated mechanisms underlying *A. hydrophila* infection and pathogenesis has long been an attractive research topic waiting to be explored. In the present study, we identified a previously uncharacterized TIR domain protein (TcpAh) from *A. hydrophila* JBN2301 strain. TcpAh can strongly inhibit TLR signaling pathways by a wider association with MyD88, TRAF3 and TBK1 than previously known. TcpAh can also inhibit adaptive humoral immunity by downregulating CD80/86 costimulatory signal, which is essential for initiating $CD4^+$ T cell activation and downstream B cell proliferation and antibody production (Greenfield et al., 1998; Pasare and Medzhitov, 2004; Crotty, 2011). We believe that this study is the first to report the existence of TIR domain protein-mediated mechanisms underlying *A. hydrophila*

infection and adds a new member to the bacterial TIR domain protein family.

MATERIALS AND METHODS

Bacterial Strain and Culture

Aeromonas hydrophila JBN2301 strain (accession number CP013178.1) was kindly provided by Prof. Yang of Wuhan Polytechnic University, Hubei province of China. This *A. hydrophila* strain was routinely grown in Tryptic Soy Agar (TSA) plates or Tryptic Soy Broth (TSB) at 28°C. Antibiotics were added to the bacterial cultures, when appropriate, at the following concentrations: 100 μg/ml tetracycline (Tc), 100 μg/ml ampicillin (Amp) and 30 μg/ml Chloramphenicol (Cm). *Escherichia coli* was grown in Luria-Bertani (LB) medium and antibiotics were added when necessary at the following concentrations: 50 μg/ml kanamycin (Km) and 100 ug/ml ampicillin. To measure the growth curve, *A. hydrophila* strain cultures were diluted 1:500 in TSB and grown at 28°C for 12 h at 200 rpm after overnight cultivation. Samples were taken hourly and measured at OD_{600}. The bacterial experiments were performed followed by standard biosecurity and institutional safety procedures.

Experimental Fish and Embryo

Wild-type AB zebrafish (*Danio rerio*) of both sexes and with body weights of 0.5–1.0 g was raised in our laboratory in recirculating water at 26–28°C under standard conditions. The fish were fed with commercial pellets at a daily ration of 0.7% of their body weight and held for at least two weeks prior to use in experiments for the evaluation of their overall health. Only healthy fish, as determined by their normal appearance and level of activity, were used in the study. Zebrafish embryos were prepared according to previous protocols (Ma et al., 2018). The animal experiments were performed in accordance with legal regulations and approved by the Committee on Animal Care and Use and the Committee on the Ethic of Animal Experiments of Zhejiang University.

Bioinformatics Analysis

Genome location of the *tcpAh* gene was retrieved from the Genome Data Viewer in the National Center for Biotechnology Information (NCBI) database. Primers for gene cloning were predicted by the Primer-BLAST program. Multiple alignment of TIR domains were performed using Jalview/ClustalW and secondary structures were predicted by Jalview/Jpred. The 3D structures of TIR domains were predicted using Phyre server and figures were generated by PyMol.

Plasmid Constructions

The full coding sequence of *tcpAh* was inserted into pET28a (Invitrogen) between the *Eco*RI and *Xho*I sites to construct the prokaryotic expression vector pET28a-*tcpAh*. For the construction of plasmids pET28a-CP-*tcpAh*, the MTS sequence (GCAGCCGTTCTTCTCCCTGTTCTTCTTGCCGCACCC) (Rojas et al., 1998) were synthesized and ligated to the carboxyl-terminal of *tcpAh* and then inserted into the pET28a vector by *Eco*RI and *Xho*I sites. For the construction of eukaryotic expression plasmids, the sequence encoding the full length of *tcpAh* was subcloned into pRFP-C1 (constructed in this study) and pcDNA6-Myc/His (Sigma-Aldrich), to obtain pRFP-C1-*tcpAh* and pcDNA6-*tcpAh* vectors for expressing recombinant TcpAh proteins with RFP- and Myc-tag, respectively. The encoding sequences of zebrafish MyD88, MyD88-TIR, MyD88-DD and TRIF were subcloned into pcDNA3.1-EGFP/HA/His (Invitrogen). The encoding sequences of zebrafish TRIF, TRAF3, and TBK1 were subcloned into pEGFP-C1 or pCMV-tag2b-Flag (Invitrogen). For luciferase reporter assays, the *cd*80/86 promoter-luciferase reporter was constructed in our laboratory. The zebrafish IFNφ1 promoter-luciferase reporter (IFNφ1-Luc) was previously constructed in our laboratory and the zebrafish IFNφ2 promoter-luciferase reporter (IFNφ2-Luc) was kind gift of Li laboratory (Lu et al., 2016; Ma et al., 2018). The human NF-κB, IRF3, and IFN-β luciferase reporters and pRL-TK renilla luciferase reporter vectors were purchased from Clontech and Promega, respectively (Ma et al., 2018). The primers used for construction are listed in **Supplementary Table 2**. All constructs were sequenced to verify the correct sequences and orientations. Plasmids for transfection and microinjection were prepared free of endotoxin using an EZNA plasmid mini kit (Omega Bio-Tek).

Preparation of Recombinant Proteins

For eukaryotic expression of indicated proteins, the plasmid DNAs were transfected into HEK293T cells. For prokaryotic expression of soluble TcpAh or CP-TcpAh recombinant protein, the pET28a-*tcpAh* or pET28a-CP-*tcpAh* vectors were transformed into the BL21 (DE3) *E. coli* strain (Novagen). The freshly transformed cells were grown in LB Broth (supplemented with 50 μg/mL of kanamycin) until an OD_{600} of 0.8 was reached at 37°C. IPTG (0.2 mM) was added to induce protein expression for 16 h at 20°C. After ultrasonication, the supernatants were collected for purification. The recombinant TcpAh-His or CP-TcpAh-His proteins were purified by nickel–nitrilotriacetic acid agarose affinity chromatography (Qiagen), following the manufacturer's manual, and then detected by 12% SDS–PAGE.

Preparation of Polyclonal Antibody

Four-week-old male ICR mice (∼15 g) were immunized with the recombinant TcpAh protein (20 μg) each time in CFA (Sigma-Aldrich) initially and then in IFA (Sigma-Aldrich) for four times thereafter at biweekly intervals, as previously described (Shao et al., 2018). Seven days after the final immunization, serum samples were collected. Antibody against TcpAh were affinity purified by using Protein A agarose columns (Thermo Fisher Scientific), and their titers were examined by Enzyme-Linked Immunosorbent Assay (ELISA). The validity and specificity of the antibody were determined by Western blot analysis. The Abs against zebrafish MHC class II (MHC-II), mIgM, CD80/86, including rabbit anti-MHC-II, mouse anti-mIgM, rabbit anti-CD80/86, were produced in our previous studies (Shao et al., 2018).

Construction of *A. hydrophila* Δ*tcpAh* Mutant

To generate Δ*tcpAh* mutant, the upstream and downstream flanking sequences to *tcpAh* were amplified by PCR using two pairs of primers P1/P2 and P3/P4 as shown in **Supplementary Table 2**. In addition, a Tc^r gene cassette was amplified from the plasmid pBBR1MSC-3 (MiaoLing Plasmid Sharing Platform) using primers P5/P6 (**Supplementary Table 2**). The resulting 1148-, 1184- and 1267-bp DNA fragments were ligated together through overlap PCR and subcloned into pRE112 (MiaoLing Plasmid Sharing Platform) suicide vector at *Kpn*I restriction enzyme site using a Clone Express® II One Step Cloning Kit (Vazyme) to obtain a pRE112-Δ*tcpAh*Tc^r plasmid. Then, the pRE112-Δ*tcpAh*Tc^r was transformed into *E. coli* SM10 λpir (MiaoLing Plasmid Sharing Platform) for mobilization into wild-type *A. hydrophila* via conjugation. The resultant Δ*tcpAh* mutant strain was selected by tetracycline and sucrose resistance after allelic exchange between the chromosomal gene and the mutagenized plasmid copy by twice crossover event, and was verified by PCR and DNA sequencing and subjected to further analysis by Western blot analysis (Xie et al., 2018).

Challenge Assay

Wild-type *A. hydrophila* JBN2301 and Δ*tcpAh* mutant were collected from the logarithmic growth phase, and zebrafish were inoculated i.p. with the wild-type and mutant *A. hydrophila* at concentration of 5×10^6 CFU/fish (for 96 h challenge assay) or 2×10^4 CFU/fish (for 21 days challenge assay). In these cases, mock PBS was administered as negative control. Infection and mortality in each group was monitored for 96 h at one interval 12 h, or during the 21 days period at one interval 2 days. Kaplan–Meier survival curve was obtained using GraphPad Prism software version 8.0. Statistical differences between wild-type versus Δ*tcpAh A. hydrophila* infected groups were analyzed using log-rank test. Bacterial load was detected in gill, spleen, and kidney tissues of zebrafish in each group. For this, the tissues were collected and washed with sterilized PBS, homogenized, and centrifuged at 5,000 *g* at 4°C for 10 min. Bacterial load was calculated and expressed into colony forming unit (CFU) by counting the colonies appearing on the TSA plates as described (Saraceni et al., 2016).

In vivo Luciferase Reporter Assays

In vivo luciferase reporter assays were performed to examine MyD88-dependent TLR2- or TLR9-signaling activation and TRIF-dependent TLR3-signaling activation in zebrafish embryos through overexpression objective genes. For this, the one-cell-stage embryos were microinjected (2 nL) with 100 pg NF-κB-Luc or zebrafish IFNφ1/φ2-Luc reporter vectors, and 10 pg renilla luciferase reporter vectors with increasing amounts (0, 50, 100 pg) of pcDNA6-*tcpAh* vector. Empty control vector was added so that a total of 360 pg vector DNA was microinjected into each embryo. At 12 h post microinjection (hpm), embryos were stimulated with Pam3CSK4 (200 pg/embry; Invivogen), CpG-ODN (400 pg/embryo; Generay Biotechnology Company), TNF-α (10 pg/embryo; eBiosience), and poly (I:C) (200 pg/embryo; Invivogen) for 12 h, respectively. Plasmid DNAs were mixed in a microinjection buffer (0.5% phenol red, 240 mM KCl, and 40 mM HEPES, pH 7.4). Luciferase activity in total embryo lysates was detected with a Dual Luciferase Reporter Assay (Promega) at 24 hpm.

In vitro Luciferase Reporter Assays

In vitro luciferase reporter assays were performed to examine MyD88-mediated activation of NF-κB or *cd80/86* promoter and TRIF-mediated activation of IRF3 or IFN-β signaling in HEK293T cells. HEK293T cells were seeded in 12-well plates at a density of 5×10^5 cells/ml for 24 h and co-transfected with various indicated plasmids, luciferase reporter plasmid, and control reporter plasmid. pRL-TK vector was used as an internal control to normalize the expression level of the transfected plasmid. At 24 h post transfection, cells were stimulated with indicated stimulants for 12 h. Then cells were washed with PBS, lysed with Passive Lysis Buffer (Promega), and assayed for luciferase activities in a luminometer by the Dual-Luciferase Reporter Assay System (Promega). The luciferase reading of each sample was first normalized against that in the pRL-TK level, and the relative light unit was presented as the ratio of firefly luciferase to renilla luciferase. The results were obtained from three independent experiments (Ji et al., 2019).

Co-immunoprecipitation (Co-IP) and Western Blot Analysis

HEK293T cells were cultured in dishes with a diameter of 100 mm at 37°C in 5% CO_2 overnight. Cells were transiently transfected with 24 μL of PEI transfection reagent (Promega) containing a total of 6 μg plasmid DNAs, including pcDNA6-*tcpAh* plus pcDNA3.1-MyD88 or pcDNA3.1-MyD88-TIR or pcDNA3.1-MyD88-DD (at a ratio of 1:1); pcDNA6-*tcpAh* plus pCMV-TRIF or pCMV-TRAF3 or pCMV-TBK1 (at a ratio of 1:1) in different combinations, with the empty vector as control. After 48 h, the cells were washed with PBS and lysed for 30 min at 4°C in an ice-cold buffer containing 20 mM Tris–HCl (pH 7.5), 150 mM NaCl, 1 mM EDTA, 1% Triton X-100, and the cocktail protease inhibitor (Roche). Cell lysates were centrifuged at 4°C, 13,000 *g* for 10 min and the supernatants were incubated with mouse anti-Myc or anti-Flag tag mAb (Abmart; M20002M, M20008L) at 4°C overnight, followed by incubation with 50 μL protein A-agarose beads (Roche) for 3 h. Then, the beads were washed four times with lysis buffer. The precipitants were denatured in loading buffer for analysis by Western blot using 12% SDS–PAGE and transferred onto 0.22 μm polyvinylidene difluoride membranes (Bio-Rad). The blots were probed with mouse/rabbit anti-Myc (Abmart; M20002L, Sangon biotech; D110006-0200) or GFP (Abmart; M20004L, HuaBio; ET1607-31) or Flag (Abmart; M20008L, Sangon biotech; D110005-0200) tag Abs at 1:5,000 and HRP-conjugated goat anti-mouse/rabbit IgG (Abmart; M21001S, M21002S) at 1:8,000, and then incubated with ECL reagents (Millipore) according to the manufacturer's instructions. The emitted light was detected using a cooled CCD camera (LAS–1000; Fuji film) (Ma et al., 2018).

Fluorescence Localization Imaging

HEK293T cells were seeded into multiwell plates (Corning) and cultured in DMEM (HyClone Laboratories) supplemented with 10% FBS, 100 U/ml penicillin, and 100 μg/ml streptomycin at 37°C in 5% CO_2 to allow growth into 70–90% confluence. These cells were co-transfected with RFP tagged TcpAh plasmid DNA (500 ng) and a series of GFP tagged objective plasmid DNA (500 ng) using PEI in accordance with the manufacturer's instructions (Wan et al., 2016). At 24 h post transfection, the cells were washed with PBS and fixed in 4% paraformaldehyde for 10 min and stained with 100 ng/ml DAPI (Sigma) at room temperature for 10 min. For localization imaging in stimulated HEK293T cells, the cells were co-transfected with RFP tagged TcpAh plasmid DNA (500 ng) and a series of GFP tagged objective plasmid DNA (500 ng) together with TLR2 or TLR3 plasmids (50 ng) using PEI in accordance with the manufacturer's instructions. At 24 h post transfection, cells were stimulated with Pam3CSK4 or Poly(I:C) for 12 h, and then harvested as above described. Fluorescence images were obtained using a laser scanning confocal microscope (Zeiss LSM 710).

Flow Cytometric (FCM) Analysis

Cells under examination were blocked with 1% goat serum for 1 h at 4°C and then incubated with the defined primary Abs for 1 h at 4°C. Non-specific rabbit or mouse IgG was served as the negative control. After washing twice with D-Hank's buffer, the cells were incubated with secondary Abs (PE conjugated goat anti-mouse or FITC conjugated goat anti-rabbit) for 1 h at 4°C, and the fluorescence signals were determined using the flow cytometer (BD FACSCalibur). At least 10,000 cells were collected from the myelomonocyte or lymphocyte gate for analysis. Cell Quest software (BD Biosciences) and ModFit LT software were used for FCM analysis and T cell proliferation assays, respectively (Wan et al., 2016; Shao et al., 2018).

In vitro Assay for TcpAh on Lymphocyte Proliferation and Activation

Zebrafish were i.p. injected with sterile PBS, wild-type *A. hydrophila* (2×10^4 CFU/fish), Δ*tcpAh* mutant, or Δ*tcpAh* mutant supplemented with CP-TcpAh recombinant protein for 5 days before sacrificed. Leukocytes were sorted from spleen, head kidney, and peripheral blood through Ficoll-Hypaque density-gradient centrifugation as described (Wan et al., 2016). Leukocytes obtained from fish with infection of wild-type *A. hydrophila*, Δ*tcpAh* mutant, or Δ*tcpAh* mutant plus CP-TcpAh were subjected to MHC-II$^+$ antigen-presenting cells (APCs) isolation. For this, the cells were blocked with 1% goat serum for 1 h at 4°C and incubated with rabbit anti-MHC-II Ab for 2 h at 4°C. After the incubation, the cells were gently washed thrice with D-Hank's buffer, incubated with anti-rabbit IgG magnetic beads (Thermo Scientific) for 15 min at 4°C, and then applied to a magnetic separator to separate the MHC-II$^+$ cells. The MHC-II$^+$ cells were cultured in L-15 medium containing 10% FBS (Gibco), 100 U/mL penicillin, and 100 μg/mL streptomycin at 28°C overnight to detach the magnetic beads. In parallel, leukocytes from fish with stimulation of inactivated *A. hydrophila* were stained with 10 μM CFSE (Beyotime), and terminated by adding 10% FBS. Then, the MHC-II$^+$ APCs were cocultured with the CFSE-labeled leukocytes for 72 h. The proliferation and activation of lymphocytes were examined via FCM, and the expression of CD154 and LCK was detected using real-time PCR (Shao et al., 2018).

Real-Time PCR for Gene Expression Analysis

Total RNAs from leukocytes were isolated using TRIzol reagent (Invitrogen) and transcribed into first-strand cDNA with oligo(dT)18 (Takara Bio). Real-time PCR was performed using a Master cycler ep real plex instrument (Eppendorf) with a SYBR Premix Ex Taq kit (Takara Bio), following the manufacturer's instructions. Briefly, the reaction mixtures in a total volume of 10 μl were incubated for 2 min at 95°C, followed by 40 cycles of 15 s at 95°C, 15 s at 60°C, and 20 s at 68°C. The relative gene expression of *cd80/86* or other genes was calculated using the $2^{-\Delta\ cyclethreshold}$ and $2^{-\Delta\ \Delta\ cyclethreshold}$ methods with β-actin for normalization. In all cases, each PCR trial was performed with triplicate samples and repeated at least three times (Shao et al., 2018). The forward and reverse primers used were shown as in **Supplementary Table 2** in **Supplementary Material**.

Effect of TcpAh on B Cell Activation and IgM Production

For the B cell activation assay, zebrafish were i.p. injected with *A. hydrophila*, Δ*tcpAh* mutant or Δ*tcpAh* mutant supplemented with CP-TcpAh recombinant protein. After 5-day stimulation with indicated stains, leukocytes from the spleen, kidney, and peripheral blood were collected, and the proliferation and activation of B cells were examined as the increase of mIgM$^+$ cells through FCM with mouse anti-mIgM Ab. For the IgM production assay, fish were i.p. immunized with *A. hydrophila*, Δ*tcpAh* mutant or Δ*tcpAh* mutant plus CP-TcpAh. Serum samples were collected at 14 days after the immunization, and the level of IgM against heat-inactivated *A. hydrophila* was detected by ELISA (Wan et al., 2016; Xu et al., 2016). Briefly, the heat-inactivated *A. hydrophila* was used to coat 96-well ELISA plate overnight at 4°C. Then, the coated plate was treated with 2% BSA for 1 h at 37°C and washed with PBST (PBS with 0.05% Tween-20). Thereafter, the plate was loaded with serially diluted serum samples at 37°C. After incubation for 2 h, the plate was washed thrice with PBST and incubated with mouse anti-IgM Ab for 1 h at 37°C. Afterward, the plate was washed, and the HRP-conjugated goat anti-mouse-IgG Ab was added. Color was developed using tetramethylbenzidine and stopped with 2 mol/L H_2SO_4, and then measured at 450 nm on a Synergy H1 Hybrid Reader (BioTek Instruments). Ab titer is defined as the highest dilution of serum at which the A_{450} ratio (A_{450} of post-immunization sera/A_{450} of pre-immunization sera) is greater than 2.1 (Xu et al., 2016).

Statistical Analysis

Results were shown as mean ± SD from at least three independent experiments. Statistical evaluation of differences

between means of experimental groups was performed using ANOVA and Student's *t*-tests. Survival curve differences in the *A. hydrophila* challenge assay were assessed using log-rank test. Statistical significance was considered when $p < 0.05$ or $p < 0.01$ or $p < 0.001$. The sample number for each group of fish exceeded 10 and each group of zebrafish embryo exceeded 50.

RESULTS

Molecular Identification of TcpAh From *A. hydrophila*

A TIR domain protein (TcpAh)-encoding gene was retrieved from the genome database of *A. hydrophila* JBN2301 strain maintained by the National Center for Biotechnology Information (NCBI) through Basic Local Alignment Search Tool (BLAST) using a homologous sequence of *B. melitensis* TcpB as a query. This gene was named as *tcpAh* (accession number CP013178.1) because it originates from *A. hydrophila*. The *tcpAh* gene consists of 579 bp and located downstream a putative molecular chaperone Tir gene and upstream an unannotated sequence with 7.55 kb in length (**Figure 1A**). The *tcpAh* gene was predicted to encode TcpAh protein with 192 amino acids and molecular weight of 22 kDa. TcpAh contains a conserved TIR domain (38–184 aa) with 147 amino acids. The TIR domain of TcpAh is characterized by three functional boxes, namely, box 1 (F/Y) D–HS), box 2 (DW–VN) and box 3 (RG–NL), which also exist in other TIR domains from various bacterial Tcp proteins, as well as TLRs and adapters, such as MyD88 and TIRAP. Among the three boxes of TcpAh, box 1 shows the most similarity to those in other TIR domains. Box 1 contains several important residues, such as Phe/Tyr and Asp, which contribute to homodimer formation and are completely conserved in most TIR domains. By contrast, TcpAh lacks a well-defined box 2 region and some characteristic residues, such as the conserved Pro and Gly, which are critical for signaling in eukaryotic TIR domains. The box 3 region is also poorly conservative and lacks even the most highly conserved amino acid residues of the canonical TIR sequence (**Figure 1B**). Despite divergence in box 2 and box 3 regions, the secondary structure of TcpAh exhibits additional structure homologies in the BB and DD loops, which are functionally important for TIR domains (**Figures 1B,C**). In addition, tertiary architecture analysis showed that TcpAh shares considerable similarity with other TIR domains, particularly that of TLR5 (**Figure 1C**). The phylogenetic tree shows that TcpAh is clustered with other bacterial TIR domain proteins with high bootstrap probability, particularly with the YpTdp protein, which is a TIR domain protein in *Y. pestis* that inhibits NF-κB by interacting with MyD88 (**Figure 1D**). Notably, animal SARM is more closely related to bacterial TIR domain proteins than to other TIR domain proteins in animals, thus, an evolutionary correlation exists between SARM and bacterial TIR-domain proteins (**Figure 1D**). Importantly, TcpAh homologs were predicted in nine additional *A. hydrophila* strains with known genome sequences (**Supplementary Table 1**); and a number of highly conserved phage-signature sequences that encode site-specific integrases, coat and flagellar proteins were predicted in the regions flanking *tcpAh* homologous genes. These observations implied the possible phage-origin of the *tcpAh* homologs.

TcpAh Is Required for *A. hydrophila* Infection

A mutant *A. hydrophila* strain with *tcpAh* gene deletion (Δ*tcpAh*) was constructed by allelic replacement in wild-type (WT) JBN2301 strain to analyze the potential virulent activity of TcpAh in *A. hydrophila* infection. For this procedure, the up- and downstream flanking fragments of *tcpAh* in JBN2301 genomic DNA and a tetracycline resistance (Tc^r) gene cassette in pBBR1MCS-3 DNA were amplified by polymerase chain reaction (PCR) using the primers shown in **Supplementary Table 2**. The fusion of the three fragments was amplified by overlap PCR and then ligated into suicide plasmid (pRE112) at the *Kpn*I sites. The resulting plasmid (pRE112-Δ*tcpAh*Tc^r) was transformed into *E. coli* SM10 λpir for mobilization into JBN2301 via conjugation. The resultant Δ*tcpAh* mutant strain was selected by tetracycline and sucrose resistance after allelic exchange between the chromosomal gene and the mutagenized plasmid copy by twice crossover event (**Figure 2A**) and was verified by PCR and DNA sequencing (**Figure 2B**). The virulent activity of TcpAh was examined by a challenge assay in a well-established zebrafish infection model. Zebrafish were infected by intraperitoneal inoculation with wild-type *A. hydrophila* JBN2301 and Δ*tcpAh* mutant strains (5×10^6 CFU/fish) and observed for 96 h. The results showed that the wild-type strain caused a remarkable lethality (52%) within 24 h and displayed 100% lethality 72 hours after infection. However, the Δ*tcpAh* mutant strain caused a remarkably lower lethality during the same time period after inoculation, and the final lethality remained at 56%, which is lesser by 44% than that of the wild-type strain (**Figure 2E**). Although indiscriminate clinical signs, such as depression, gill hyperemia, and accumulated ascites, were observed in the two infection groups, the delay of clinical-symptom appearance and the extended survival time in the mutant infection group suggested that the mutation of *tcpAh* substantially weakened the virulence of *A. hydrophila*. For further clarification, a bacterial load assay was performed in the different tissues of zebrafish infected with wild-type and Δ*tcpAh*-mutant *A. hydrophila*. The result showed that Δ*tcpAh* mutant infected zebrafish showed a decreased bacterial load in gill, spleen, and kidney tissues compared with that in wild-type strain infected fish (**Figures 2F–H**). The differences in survival rate and bacterial load between zebrafish infected with wild-type and Δ*tcpAh*-mutant *A. hydrophila* were not likely due to the defect in the growth of the mutant strain and abnormal protein expression in wild-type strain, because a similar growth rate was observed between the two strains and a highly expressed TcpAh protein level was detected in wild-type *A. hydrophila* (**Figures 2D,C**). The results indicate that TcpAh is a crucial virulence-related factor required for *A. hydrophila* infection.

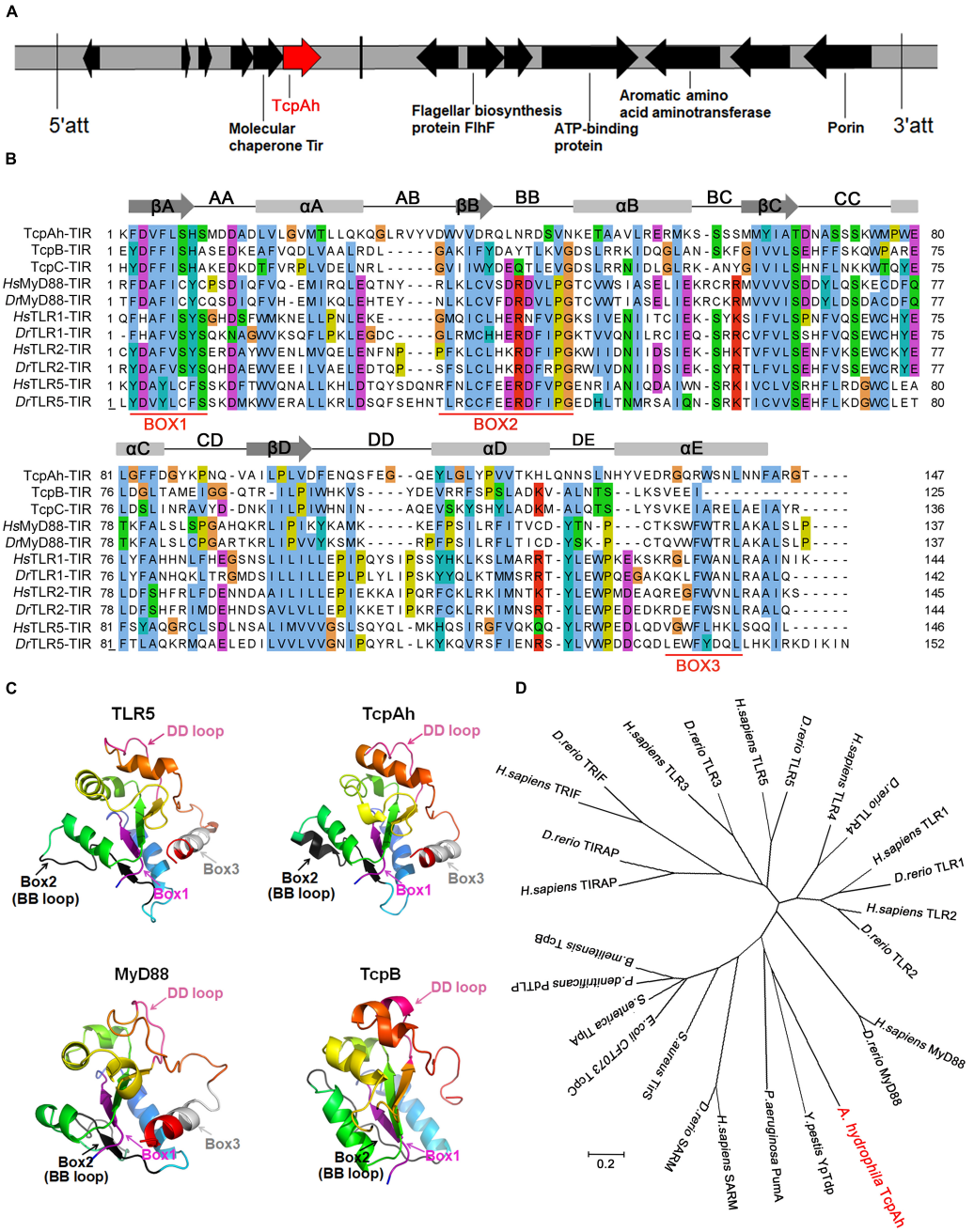


FIGURE 1 | Bioinformatic characterization of TcpAh-encoding gene and protein in *A. hydrophila* JBN2301 strain. **(A)** Localization of TcpAh-encoding gene in JBN2301 genome. The encoding sequence of TcpAh is indicated in red arrow and att means attachment site. **(B)** Sequence alignment of TIR domains using Jalview/ClustalW and ClustalX programs. Conserved functional motifs and amino acid residues are shaded in different colors. Secondary structures were predicted by Jalview/Jpred program. Gray boxes, gray arrows, and black lines denote alpha helices, beta-sheet areas, and connecting loops, respectively. **(C)** Prediction of the 3D structures of TIR domains using Phyre server and PyMol program. The TcpAh TIR domain (38–184 aa) was modeled with 100% confidence by the single highest scoring template as the TIR domain of TLR5 (PDB c3j0aA). Box 1 (purple), box 2 and BB loop (black), and box 3 and DD loop (hot pink) are indicated within the TIR domains. **(D)** Phylogenetic trees of the amino acid sequences of TcpAh and its homologs in other species constructed by neighbor-joining method using MEGA 7.0. The tree was drawn to scale, and branch lengths are in the same units as those of the evolutionary distances used to infer the phylogenetic tree. The evolutionary distances were computed using the p-distance method. The GenBank accession numbers of the sequences are as follows: *H. sapiens* MyD88, AAC50954.1; *D. rerio* MyD88, AAQ91324.1; *H. sapiens* TLR1, NP_891549.1; *D. rerio* TLR1, AAI63271.1; *H. sapiens* TLR2, AAY85648.1; *D. rerio* TLR2, NP_997977.1; *H. sapiens* TLR3, NP_003256.1; *D. rerio* TLR3, AAI07956.1; *H. sapiens* TLR4, NP_003257.1; *D. rerio* TLR4, NP_001315534.1; *H. sapiens* TLR5, NP_003259.2; *D. rerio* TLR5, NP_001124067.2; *H. sapiens* TRIF, AAH09860.2; *D. rerio* TRIF, NP_001038224.1; *H. sapiens* TRIAP, NP_001034750.1; *D. rerio* TRIAP, XP_002667158.2; *H. sapiens* SARM, NP_055892.2; *D. rerio* SARM, NP_001124068.1; *Y. pestis* YpTdp, WP_198249346.1; *A. hydrophila* TcpAh, WP_043158960; *P. aeruginosa* PumA, WP_012075302.1; *S. aureus* TirS, WP_000114516.1; *E. coli CFT073* TcpC, WP_000282336.1; *S. enterica* TlpA, WP_079786625.1; *P. denitrificans* PdTLP, QAR27511.1; *B. melitensis* TcpB, EPZ76643.1.

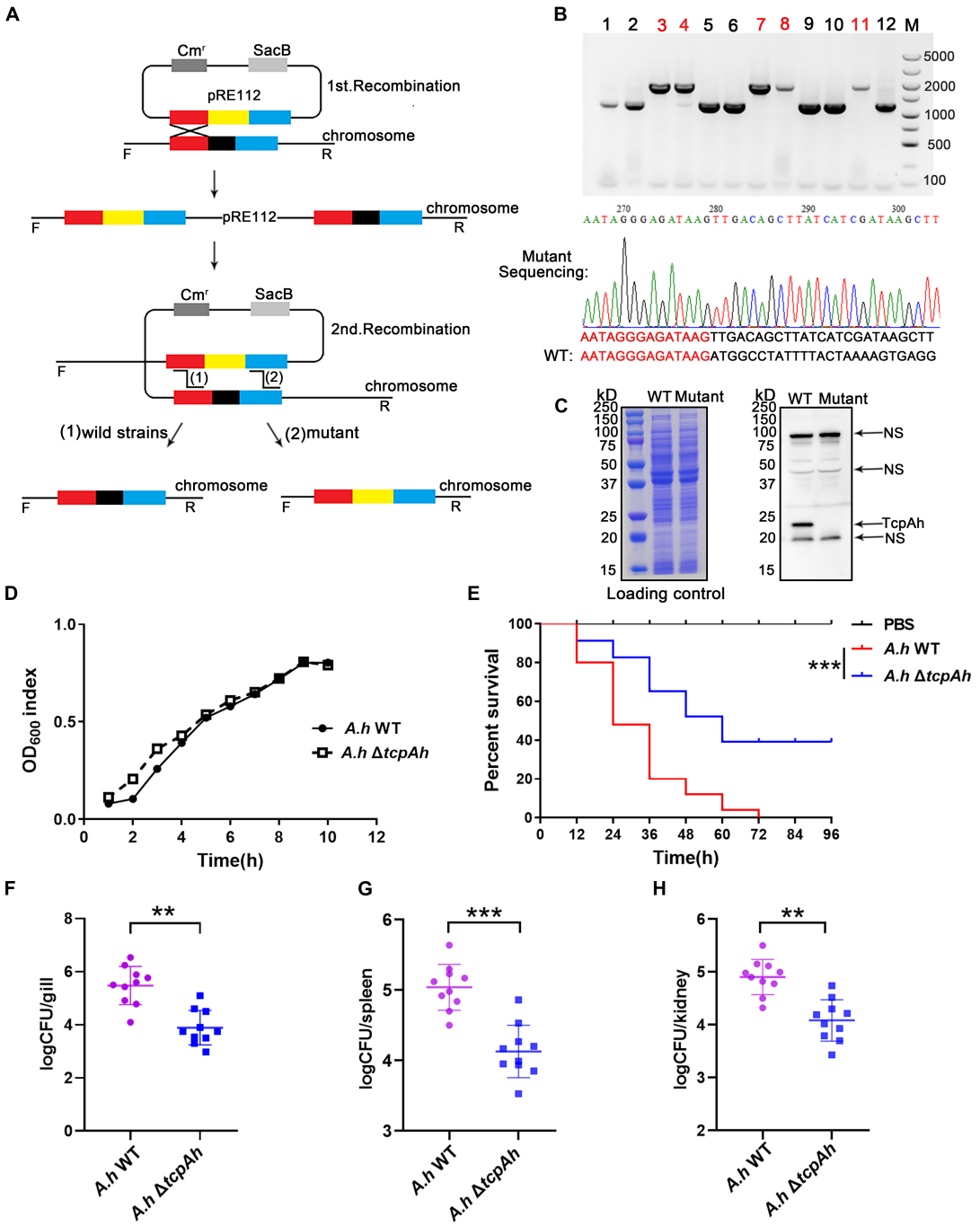


FIGURE 2 | Examination of the requirement of TcpAh for *A. hydrophila* infection. **(A)** Strategy for the deletion of the *tcpAh* gene in *A. hydrophila* JBN2301 strain by homologous recombination. The black block indicates the *tcpAh* gene; red and blue blocks indicate the left and right homologous sequences of the *tcpAh* gene, respectively; and the yellow block indicates the Tc^r gene. **(B)** PCR and sequencing identification of the mutant strain with *tcpAh* gene deletion (Δ*tcpAh*). The lanes with red number indicate the mutant strain; partial sequencing result is showed. **(C)** Western blot analysis of TcpAh protein in wild-type and mutant *A. hydrophila* JBN2301 strains in liquid cultures and NS means non-specific band. The total proteins of wild-type and Δ*tcpAh A. hydrophila* JBN2301 strains were separated by SDS-PAGE and stained with Coomassie brilliant blue R250 as a loading control. The TcpAh protein was detected by using a polyclonal rabbit anti-TcpAh antibody with an expected molecular weight of 22 kDa. **(D)** Growth curve of wild-type and Δ*tcpAh A. hydrophila* JBN2301 strains. **(E)** Zebrafish survival curve. Zebrafish were infected with wild-type *A. hydrophila* JBN2301 and Δ*tcpAh* mutant. Statistical differences between wild-type versus Δ*tcpAh A. hydrophila* infected groups were analyzed by log-rank test. $n = 25$. $^{***}p < 0.001$. Group of fish injected with mock PBS was used as a negative control. **(F–H)** Examination of bacterial load in the **(F)** gill, **(G)** spleen, and **(H)** kidney tissues of zebrafish infected with wild-type and Δ*tcpAh* mutant *A. hydrophila* JBN2301 strains. Non-parametric two-tailed Mann–Whitney test was carried out with **(F)** $^{**}p < 0.01$, **(G)** $^{***}p < 0.001$, and **(H)** $^{**}p < 0.01$.

TcpAh Inhibits MyD88 Signaling Pathway

Given that the TIR domains of TcpAh and zebrafish TLRs and adaptor proteins have structural homology, we propose that the potential regulatory function of TcpAh in zebrafish TLR signaling pathways is exerted through TIR–TIR homotypic interaction. An *in vivo* functional examination was performed using zebrafish embryo as a model to test this hypothesis. Zebrafish embryo was chosen because of its constitutive expression of various TLR signaling components during early development (2–24 hpf). For this procedure, one-cell-stage embryos were microinjected with NF-κB reporter vector in combination with different amounts of TcpAh-encoding plasmid and the stimulants Pam3CSK4, CpG-ODN and TNF-α for 12 h. As expected, the administration of TcpAh-encoding plasmid remarkably inhibited Pam3CSK4- and CpG-ODN-induced NF-κB activation in a dose-dependent manner (**Figures 3A,B**). By contrast, minimal alteration in NF-κB activity was detected in embryos exposed to TNF-α, whose signaling pathway is independent of TLRs and MyD88 (**Figure 3C**). These results indicated that TcpAh has a strong inhibitory effect on TLR signaling pathways, such as Pam3CSK4-induced TLR2 and CpG-ODN-induced TLR9 signaling pathways in this case, partially by association with MyD88 adaptor protein. Accordingly, TcpAh overexpression in HEK293T cells remarkably suppressed MyD88-induced NF-κB activation in a dose-dependent manner (**Figure 3D**). Furthermore, the expression of IL-1β and TNFα (two typical proinflammatory cytokines regulated by NF-κB signaling) in leukocytes was also dramatically impaired in wild-type *A. hydrophila*-infected zebrafish groups in comparison with those of Δ*tcpAh* mutant-infected groups (**Figures 3E,F**).

Next, the association of TcpAh with MyD88 was examined by the intracellular co-localization of RFP-TcpAh and EGFP-MyD88 proteins in resting HEK293T cells or TLR-stimulated HEK293T cells and evidenced by the co-immunoprecipitation (Co-IP) between EGFP-MyD88 and Myc-TcpAh proteins (**Figures 4A,B**; **Supplementary Figure 1A**). To examine which domains in MyD88 were potentially involved in the interaction with TcpAh, EGFP-tagged MyD88 DD (11–101 aa) or TIR domain (148–284 aa) expression vectors were generated and co-transfected with RFP-tagged TcpAh in HEK293T cells (**Figure 4C**). The results showed that the two MyD88 mutants displayed strong co-localization with TcpAh; hence, DD and TIR domain contributed to the TcpAh–MyD88 interaction (**Figure 4D**). This notion was confirmed by Co-IP assay (**Figure 4E**). Previous studies have shown that bacterial TIR domain proteins, such as TcpB and TcpC, are associated with MyD88 through TIR–TIR interaction. Our present study showed that TcpAh can also associate with MyD88 by TIR–DD interaction in addition to TIR–TIR interaction.

TcpAh Inhibits TRIF Signaling Pathway

Endocytosed TLRs, such as TLR3 and TLR4, trigger type-I IFN response in a TRIF-dependent manner. Recently, a TcpC protein from *E. coli* CFT073 was found to negatively regulate TRIF-dependent TLR signaling (Yadav et al., 2010). Zebrafish embryos were co-injected with an IFNφ1/φ2 (two typical type I interferon molecules in zebrafish) reporter vector and different amounts of TcpAh-encoding plasmid in combination with TLR3 agonist (PolyI:C) for 12 h to examine the potential role of TcpAh in TLR/TRIF-signaling axis. Results showed that TcpAh remarkably inhibited IFNφ1/φ2-reporter response to PolyI:C stimulation (**Figures 5A,B**). Similar results were also observed in HEK293T cells co-transfected with IRF3 or IFN-β reporter vector and zebrafish TRIF expression vector, and a mounting amount of TcpAh-Myc-encoding plasmid (**Figures 5C,D**). Furthermore, the expression of IFNφ1 and IFNφ2 in leukocytes was also dramatically impaired in wild-type *A. hydrophila*-infected zebrafish groups in comparison with those of Δ*tcpAh* mutant-infected groups (**Figures 5E,F**). These observations showed the ability of TcpAh to impair TRIF-mediated IFN signaling.

Given that TRIF is another TIR domain-containing protein that is potentially targeted by TcpAh; thus, an intracellular co-localization assay was performed to clarify this issue. Unexpectedly, minimal co-localization signal was detected between RFP-TcpAh and EGFP-TRIF by fluorescence imaging in resting HEK293T cells or TLR-stimulated HEK293T cells (**Figure 6A**; **Supplementary Figure 1B**), and no any interaction between Myc-TcpAh and Flag-TRIF was detected by Co-IP assay (**Figure 6B**). These results suggested that the ability of TcpAh to inhibit TRIF-mediated IFN signaling pathway was not by directly targeting TRIF itself, and was probably by association with TRAF3 and TBK1 downstream of the TRIF-mediated pathway. Expectedly, RFP-TcpAh was clearly co-localized with EGFP-TRAF3 or EGFP-TBK1 in resting HEK293T cells or TLR-stimulated HEK293T cells (**Figure 6C**; **Supplementary Figure 1B**). The associations of TcpAh with TRAF3 and TBK1 were further confirmed by Co-IP (**Figure 6D**). These data indicated that TcpAh inhibits the TRIF-signaling pathway through association with TRAF3 and TBK1. Next, we determined how TcpAh inhibits the TRIF-mediated IFN signaling pathway via association with TRAF3 and TBK1 through an IRF3 reporter assay. TRIF, TRAF3, TBK1, and TcpAh expression plasmids were co-transfected with IRF3 reporter vector into HEK293T cells in different combinations. The results showed that the co-transfection of TRIF and TRAF3, as well as the co-transfection of TBK1 and TRAF3, remarkably induced IRF3 promoter activity, and these reactions were remarkably inhibited in cells with TcpAh overexpression (**Figures 7A,B**). The outcomes suggested that TcpAh attenuated the TRIF-mediated signaling pathway by impairing TRIF–TRAF3 and TRAF3–TBK1 interactions. In support of this hypothesis, Co-IP assay clearly showed that the TRIF–TRAF3 and TRAF3–TBK1 interactions were both impaired by the intervention of TcpAh, and the TRIF–TRAF3 interaction was impaired much more seriously (**Figures 7C–E**). Altogether, TcpAh restrains TRIF-mediated signaling pathway by competitively interaction with TRAF3 and TBK1.

Inhibition of TcpAh in Host Defense Against Infection

As *A. hydrophila* TcpAh down-modulates TLR signaling activation, we next sought to investigate whether TcpAh could interfere with zebrafish adaptive immunity. CD80/86 reporter

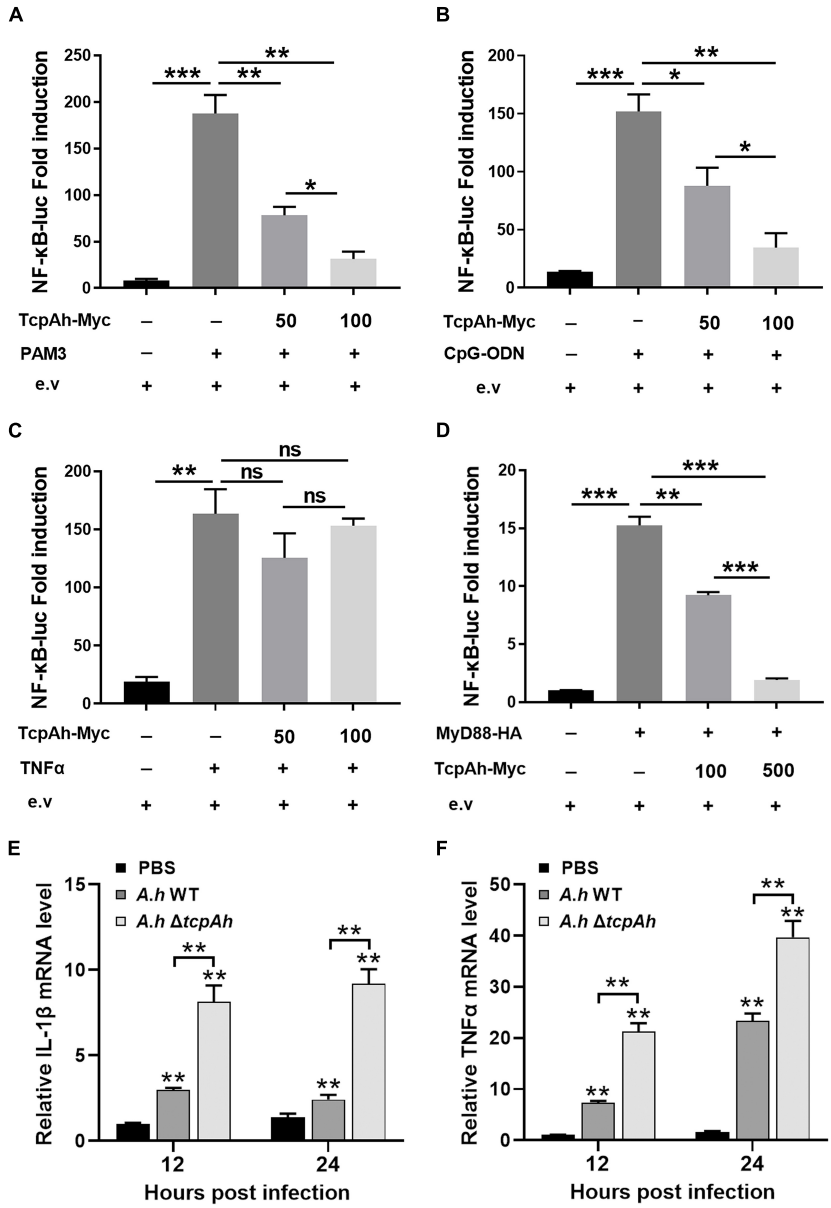


FIGURE 3 | Examination of the inhibitory role of TcpAh in MyD88 signaling pathway. **(A–C)** Activation of the NF-κB-binding promoters detected in zebrafish embryos microinjected with NF-κB luciferase reporter (NF-κB-Luc; 100 pg/embryo), renilla luciferase reporter (10 pg/embryo), and increasing amounts (0, 50, and 100 pg/embryo) of TcpAh expression vectors with stimulation of **(A)** Pam3CSK4 (200 pg/embryo), **(B)** CpG-ODN (400 pg/embryo), and **(C)** TNFα (10 pg/embryo) for 12 h. Data are the average luciferase activity ± SD (*$p < 0.05$; **$p < 0.01$; ***$p < 0.001$; ns, not significant). **(D)** Activation of the NF-κB-binding promoter detected in HEK293T cells transfected with NF-κB luciferase reporter (NF-κB-Luc; 150 ng/mL), renilla luciferase reporter (15 ng/mL), MyD88 expression vector (50 ng/mL), and increasing amounts (0, 100, and 500 ng/mL) of TcpAh expression vectors. Data are the average luciferase activity ± SD (**$p < 0.01$; ***$p < 0.001$). **(E,F)** Real-time PCR analysis for the expression of zebrafish IL-1β **(E)** and TNFα **(F)** in leukocytes, which were sorted from peripheral blood, spleen, and kidney tissues at indicated time after i.p. stimulation with PBS, wild-type *A. hydrophila* and Δ*tcpAh* mutant. Data are representative of three independent experiments as mean ± SD (**$p < 0.01$). Standard loading was indicated by β-actin expression.

assay clearly revealed that TcpAh suppressed the promotor activity of *cd80/86* gene by TLR2 or TLR9 or TLR3 signaling in HEK293T cells (**Figures 8A–C**). In addition, real-time PCR and flow cytometry analysis showed that zebrafish infected with Δ*tcpAh*-mutant *A. hydrophila* induced higher CD80/86 expression than those infected with wild-type strain at mRNA and protein levels (**Figures 8D,E**). This outcome suggested that TcpAh plays an inhibitory role in the expression of CD80/86 that is crucial for initiating adaptive immunity. We generated a cell-penetrating form of TcpAh (CP-TcpAh) with an appendant peptide for cell penetration at C-terminus to clarify this notion (**Supplementary Figure 2A**). This CP-TcpAh

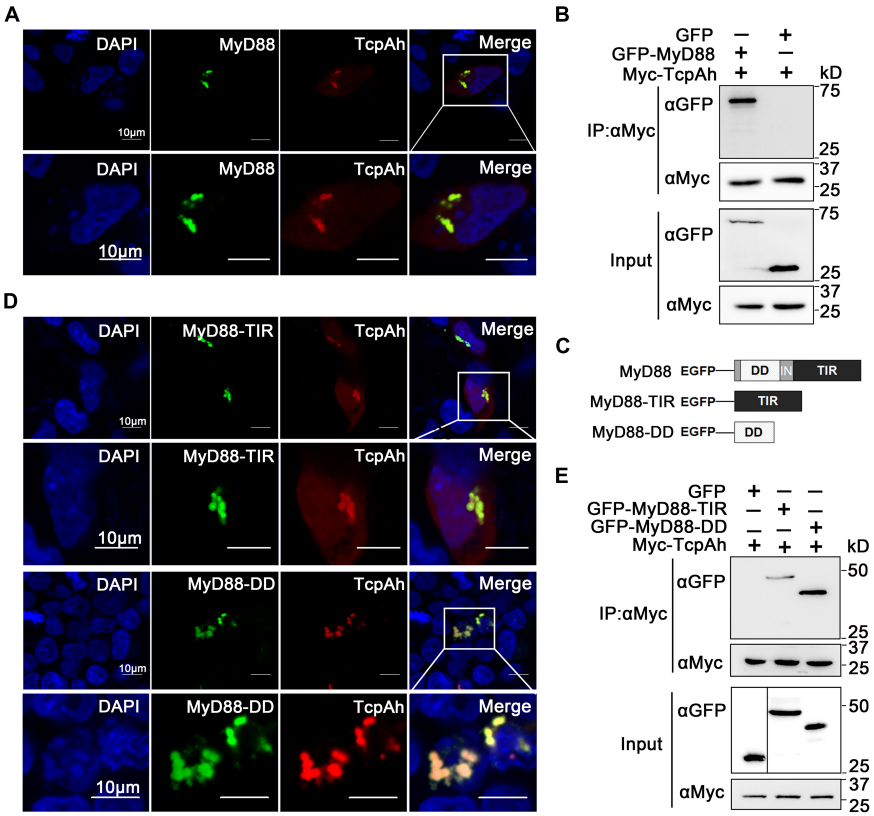


FIGURE 4 | Interaction between TcpAh and MyD88 by TIR–TIR and TIR–DD interactions. **(A)** Co-localization analysis of TcpAh and zebrafish MyD88 proteins in HEK293T cells by confocal microscopy (Zeiss LSM 710; original magnification, 630×). The nucleus was stained with DAPI. Scale bars correspond to 10 μm. **(B)** Co-IP analysis between TcpAh and zebrafish MyD88 proteins from HEK293T cells expressing Myc-TcpAh with GFP or GFP-MyD88. **(C)** Schematic diagram of wild-type and domain-truncated zebrafish MyD88 forms. **(D)** Co-localization analysis between TcpAh and truncated MyD88 proteins in HEK293T cells by confocal microscopy (Zeiss LSM 710; original magnification, 630×). The nucleus was stained with DAPI. Scale bars correspond to 10 μm. **(E)** Co-IP assay between TcpAh and MyD88-TIR domain (148–284 aa) or MyD88-DD domain (11–101 aa) as shown in **(B)**, except MyD88-TIR or MyD88-DD was used instead of full-length wild-type MyD88.

protein strongly inhibited NF-κB activity in HEK239T cells in a dose-dependent manner (**Supplementary Figure 2B**). The enhancement of CD80/86 expression induced by Δ*tcpAh* mutant in zebrafish was remarkably attenuated by the addition of CP-TcpAh protein (**Figures 8D,E**). Functionally, the Δ*tcpAh* mutant induced stronger T cell activation than wild-type *A. hydrophila in vitro* as determined by the higher cellular proliferation and transcriptional expression of LCK and CD154 in T cells upon Δ*tcpAh* mutant stimulation (**Figures 8F,H**). In this case, the enhanced T cell activation in response to Δ*tcpAh* mutant infection can be impaired by the restoration of CP-TcpAh (**Figures 8F,H**). The results implied that TcpAh inhibits the initiation of T cell activation by repressing CD80/86 expression on antigen-presenting cells, which potentially leads to the suppression of adaptive immunity against *A. hydrophila* infection. Thus, Ag-stimulated B cell activation and antibody (IgM) production were examined *in vivo*. Flow cytometric analysis showed that the percentage of B cells in Δ*tcpAh* mutant-administered groups (27.53% ± 0.85%) was dramatically upregulated ($p < 0.01$) in comparison with those of wild-type strain-infected groups (16.43% ± 0.91%) and mock PBS-treated control groups (8.46% ± 0.73%). The increased percentage of B cells in Δ*tcpAh* mutant-induced groups was remarkably decreased by administering CP-TcpAh protein (**Figure 8G**). Similar results were also detected in IgM production in various groups (**Figure 8I**). Furthermore, lethality declined in Δ*tcpAh*-mutant *A. hydrophila*-challenged zebrafish compared with that of the wild-type *A. hydrophila*-infected fish as shown by the survival rate increased from 20.0% to 64.0% ($p < 0.01$, log-rank test). The attenuated lethality of Δ*tcpAh*-mutant *A. hydrophila* was restored by the administration of CP-TcpAh protein in zebrafish and accompanied by the survival rate decreased from 64.0% to 32.0% (**Figure 8J**). The results suggested the inhibitory role of TcpAh in fish adaptive immune defense against infection and therefore uncovered a previously unrecognized strategy of *A. hydrophila* for immune evasion.

DISCUSSION

Aeromonas hydrophila is a group of Gram-negative bacteria that is widely distributed in aquatic environments (Lin et al., 2017).

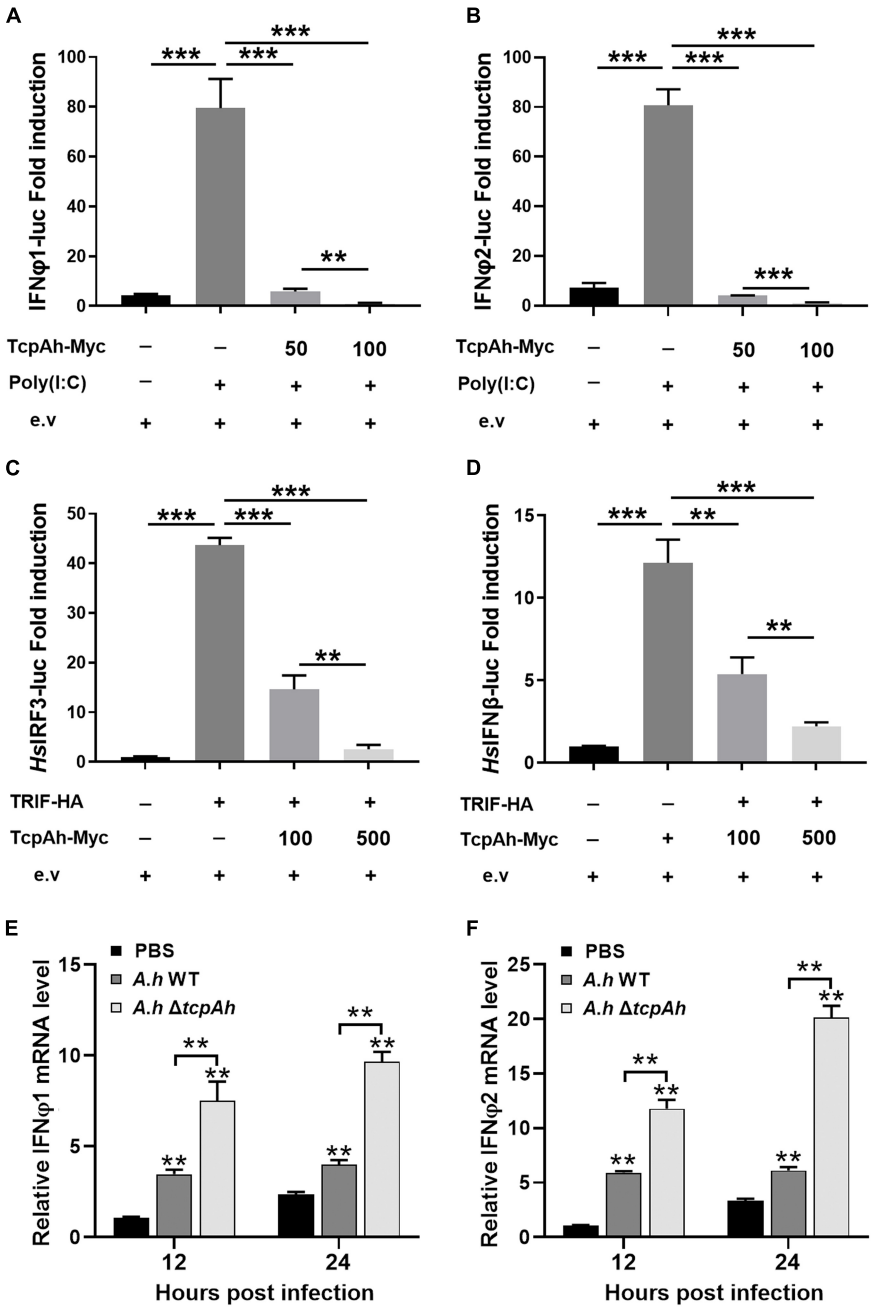


FIGURE 5 | Examination of the inhibitory role of TcpAh in TRIF signaling pathway. **(A,B)** Activation of zebrafish IFNφ1/IFNφ2 promoters detected in zebrafish embryos microinjected with IFNφ1 or IFNφ2 luciferase reporter (IFNφ1 or IFNφ2-Luc; 100 pg/embryo), renilla luciferase reporter (10 pg/embryo), and increasing amounts (0, 50, and 100 pg/embryo) of TcpAh expression vectors under stimulation with PolyI:C (200 pg/embryo) for 12 h. Data are the average luciferase activity ± SD (**$p < 0.01$; ***$p < 0.001$). **(C,D)** Activation of human IRF3 and IFN-β promoters in HEK293T cells transfected with human IRF3 or IFN-β luciferase reporter (IRF3-Luc or IFN-β-Luc; 200 ng/mL), renilla luciferase reporter (15 ng/mL), zebrafish TRIF expression vector (50 ng/mL), and increasing amounts (0, 100, and 500 ng/mL) of TcpAh expression vectors. Data are the average luciferase activity ± SD (**$p < 0.01$; ***$p < 0.001$). **(E,F)** Real-time PCR analysis for the expression of zebrafish IFNφ1 **(E)** and IFNφ2 **(F)** in leukocytes, which were sorted from peripheral blood, spleen, and kidney tissues at indicated time after i.p. stimulation with PBS, wild-type *A. hydrophila* and Δ*tcpAh* mutant. Data are representative of three independent experiments as mean ± SD (**$p < 0.01$). Standard loading was indicated by β-actin expression.

They are the causative agent of motile aeromonad septicemia (MAS) for a broad spectrum of host organisms, including mammals, amphibians, reptiles, and fish (Vivas et al., 2004). *A. hydrophila* causes disease outbreaks with high mortality in fish in aquaculture farms and severe economic losses to the aquaculture industry worldwide (Vivas et al., 2004;

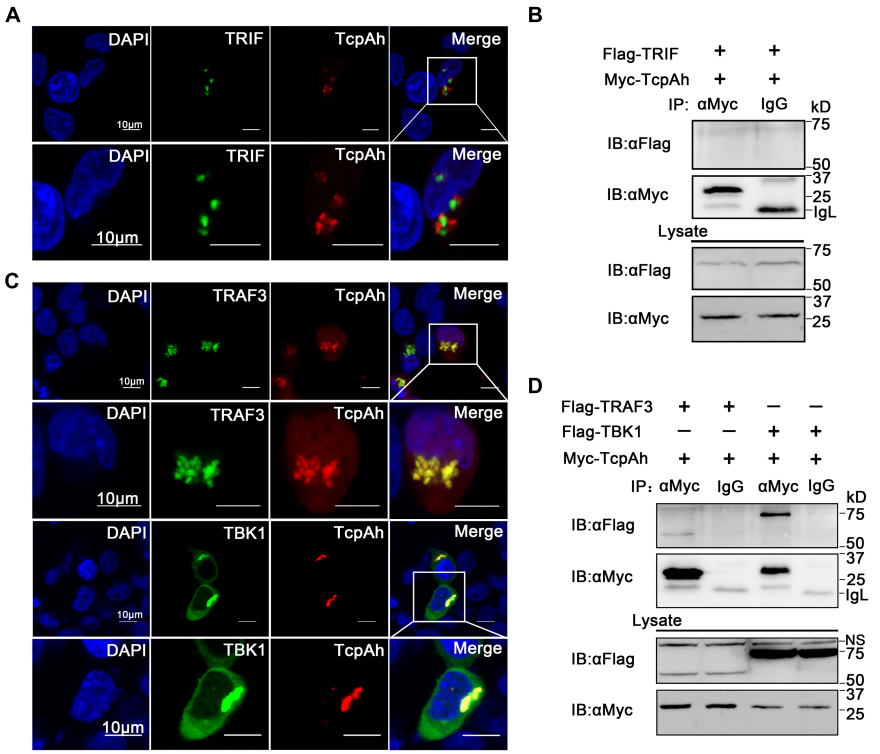


FIGURE 6 | Examination of the associations of TcpAh with TRAF3 and TBK1. **(A)** Co-localization analysis of TcpAh and zebrafish TRIF protein in HEK293T cells by confocal microscopy (Zeiss LSM 710; original magnification, 630×). The nucleus was stained with DAPI. Scale bars correspond to 10 μm. **(B)** Co-IP analysis between TcpAh and zebrafish TRIF proteins from HEK293T cells expressing Myc-TcpAh with Flag-TRIF. **(C)** Co-localization analysis of TcpAh and zebrafish TRAF3 or TBK1 proteins in HEK293T cells by confocal microscopy (Zeiss LSM 710; original magnification, 630×). The nucleus was stained with DAPI. Scale bars correspond to 10 μm. **(D)** Co-IP analysis between TcpAh and zebrafish TRAF3 or TBK1 proteins from HEK293T cells expressing Myc-TcpAh with Flag-TRAF3 or Flag-TBK1.

Jiang et al., 2017). Importantly, interest in the pathogenesis of *Aeromonas* now extends beyond the economic consequences to the fish farming industry, as members of this genus are increasingly implicated in intestinal and extraintestinal infections in humans (Thornley et al., 1997; Daskalov, 2006). *A. hydrophila* produces multiple virulence factors, including surface polysaccharides (such as capsule polysaccharide, lipopolysaccharide, and glucan), S-layers, iron-binding components, exotoxins, extracellular hydrolase, secretion complexes, fimbriae and other non-filamentous adhesins and flagella, which make the pathogenicity of this genus more complex (Alperi and Figueras, 2010; Tomas, 2012).

Although *A. hydrophila* possesses a variety of finely tuned pathogenic strategies that interfere with host defense against infection, TIR domain protein-mediated pathogenesis has not been reported in this species. In this study, we identified a TIR domain protein, namely TcpAh, from *A. hydrophila* JBN2301 strain, which is homologous to the TIR domains of TLRs. TcpAh ensures the efficient blockade of zebrafish immunity by interacting with MyD88, TRAF3, and TBK1, which are the three key components of TLR-mediated signaling pathways. Challenge assay showed that *tcpAh* deletion mutation substantially attenuated the virulence of *A. hydrophila* JBN2301 strain in zebrafish. Thus, TcpAh is a crucial virulence factor required for *A. hydrophila* infection. Importantly, nine additional highly virulent *A. hydrophila* strains were also predicted to contain such a TcpAh homolog. This finding suggests that TcpAh homologs ubiquitously exist in different *A. hydrophila* species. We believe that this study is the first to report the existence of a TIR domain protein-mediated pathogenic factor in *A. hydrophila*. Hence, this study uncovered a previously unrecognized virulence factor in this genus. TIR domain homologs have been found in many bacteria; these homologs include TlpA in *S. enterica*, TcpB in *B. melitensis*, TcpC in *E. coli*, YpTdp in *Y. pestis*, TirS in *S. aureus*, and PumA in *P. aeruginosa* (Newman et al., 2006; Cirl et al., 2008; Rana et al., 2011; Askarian et al., 2014; Imbert et al., 2017). Mechanistically, most of these TIR domain proteins function as inhibitors of host innate immunity by association with MyD88 or TIRAP through TIR–TIR interaction even though their molecular mode of action remains elusive (Rana et al., 2013). For example, *B. melitensis* TcpB, described as a molecular mimicry of TIRAP, can bind with MyD88 and TIRAP via TIR–TIR interaction to promote the ubiquitin-mediated degradation of TIRAP during bacterial infection (Cirl et al., 2008; Radhakrishnan et al., 2009). Our study showed that TcpAh can also interact with MyD88 through TIR–TIR interaction. More importantly, TIR–DD interaction, as an alternative binding manner, was utilized by TcpAh to associate with MyD88; thus,

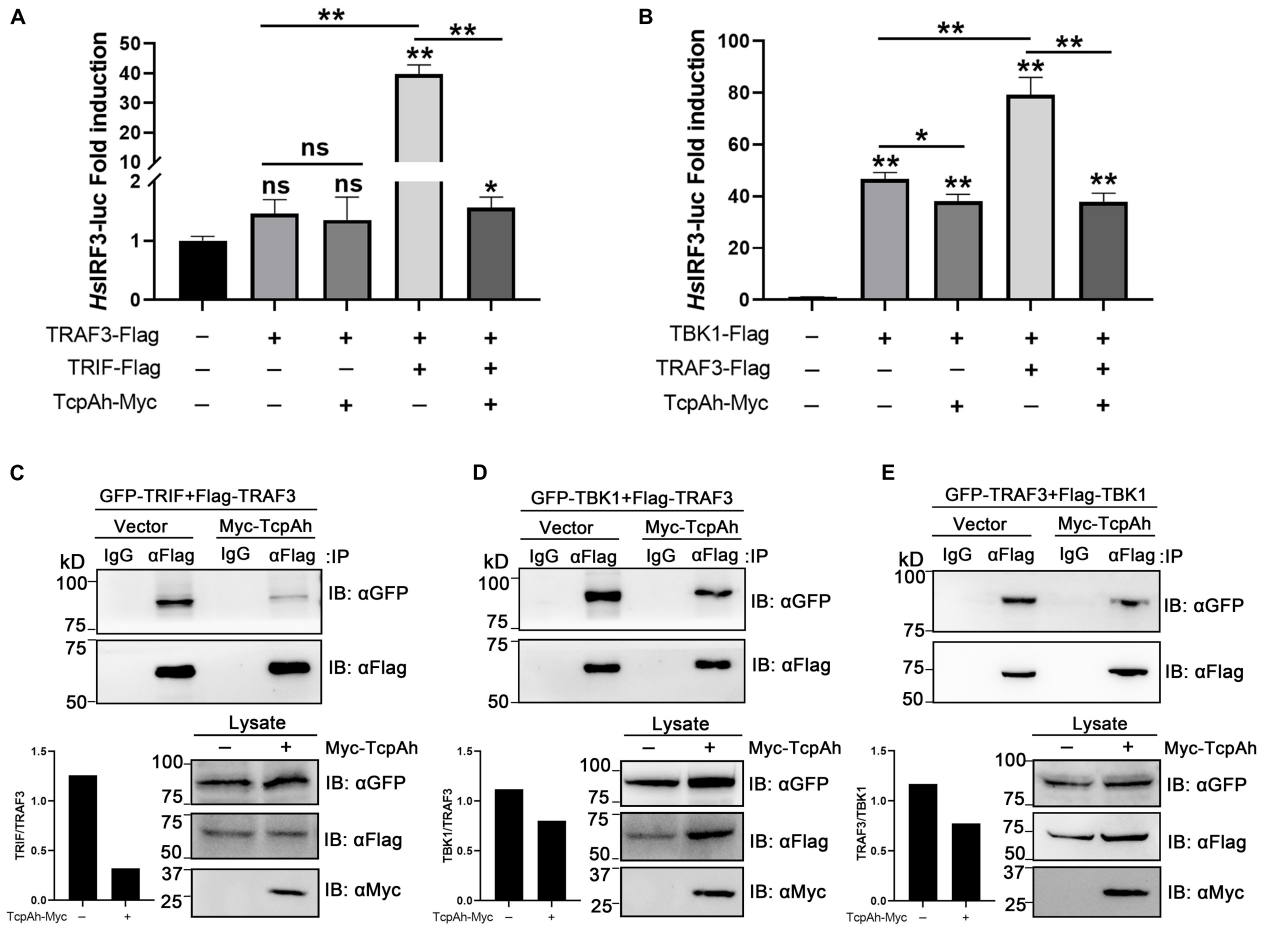


FIGURE 7 | Examination of the functional role of TcpAh in preventing TRIF–TRAF3 and TRAF3–TBK1 interactions. **(A,B)** Activation of human IRF3 promoter in HEK293T cells transfected with human IRF3 luciferase reporter (*Hs*IRF3-Luc; 200 ng/mL), renilla luciferase reporter (15 ng/mL), and **(A)** zebrafish TRAF3 expression vector (50 ng/mL) alone or in combination with zebrafish TRIF expression vector (50 ng/mL) with or without TcpAh expression vector (500 ng/mL) or **(B)** zebrafish TBK1 expression vector (50 ng/mL) alone or in combination with a zebrafish TRAF3 expression vector (50 ng/mL) with or without TcpAh expression vector (500 ng/mL). Data are the average luciferase activity ± SD (*$p < 0.05$; **$p < 0.01$; ns, not significant). **(C–E)** Co-IP analysis showing the inhibition of TRIF–TRAF3 and TRAF3–TBK1 interactions by TcpAh in HEK293T cells transfected with plasmids in indicated combinations.

TcpAh may have a stronger binding activity to MyD88 than other TIR domain proteins by possessing additional TIR–DD interaction. This unconventional interaction also exists between TcpB and MyD88 (Chaudhary et al., 2012). Hence, the interaction between bacterial TIR-domain proteins and their targets are not always restricted to TIR–TIR interaction. Remarkably, we found that TcpAh can also associate with TRAF3 and TBK1, which are two critical components downstream of TRIF-dependent TLR signaling pathway. We believe that this study is the first to show that TRAF3 and TBK1 are the cellular targets of a bacterial TIR domain protein. This finding indicated that TcpAh has a broad spectrum of target proteins in innate immune signaling pathways in addition to its interaction with MyD88 to interfere with MyD88-dependent TLR signaling. The multiple associations of TcpAh with MyD88, TRAF3, and TBK1 endow this TIR domain protein a powerful pathogenic activity in the inhibition of host immunity against *A. hydrophila* infection at extensive levels, including MyD88- and TRIF-dependent immune responses. However, the precise mechanisms underlying the associations among TcpAh, MyD88, TRAF3 and TBK1 independent of the canonical TIR–TIR interaction remain to be further clarified. Additionally, the current interpretation of the intervention of bacterial TIR domain proteins to host immune defense largely focused on innate immunity; whether bacterial TIR domain proteins have an influence on host adaptive immunity remains poorly understood. In the present study, we found that TcpAh plays an inhibitory role in adaptive humoral immunity against *A. hydrophila* infection in zebrafish as determined by an enhanced activation of T and B cells and an increased production of IgM Abs in fish upon Δ*tcpAh* mutant infection. This enhancement can be impaired by administering a recombinant TcpAh protein tagged with a cell penetration peptide (CP-TcpAh). In addition, TcpAh remarkably suppressed CD80/86 activation by attenuating NF-κB signaling as examined by an *in vitro* reporter assay. Infection with Δ*tcpAh* mutant *A. hydrophila* dramatically upregulated CD80/86 expression

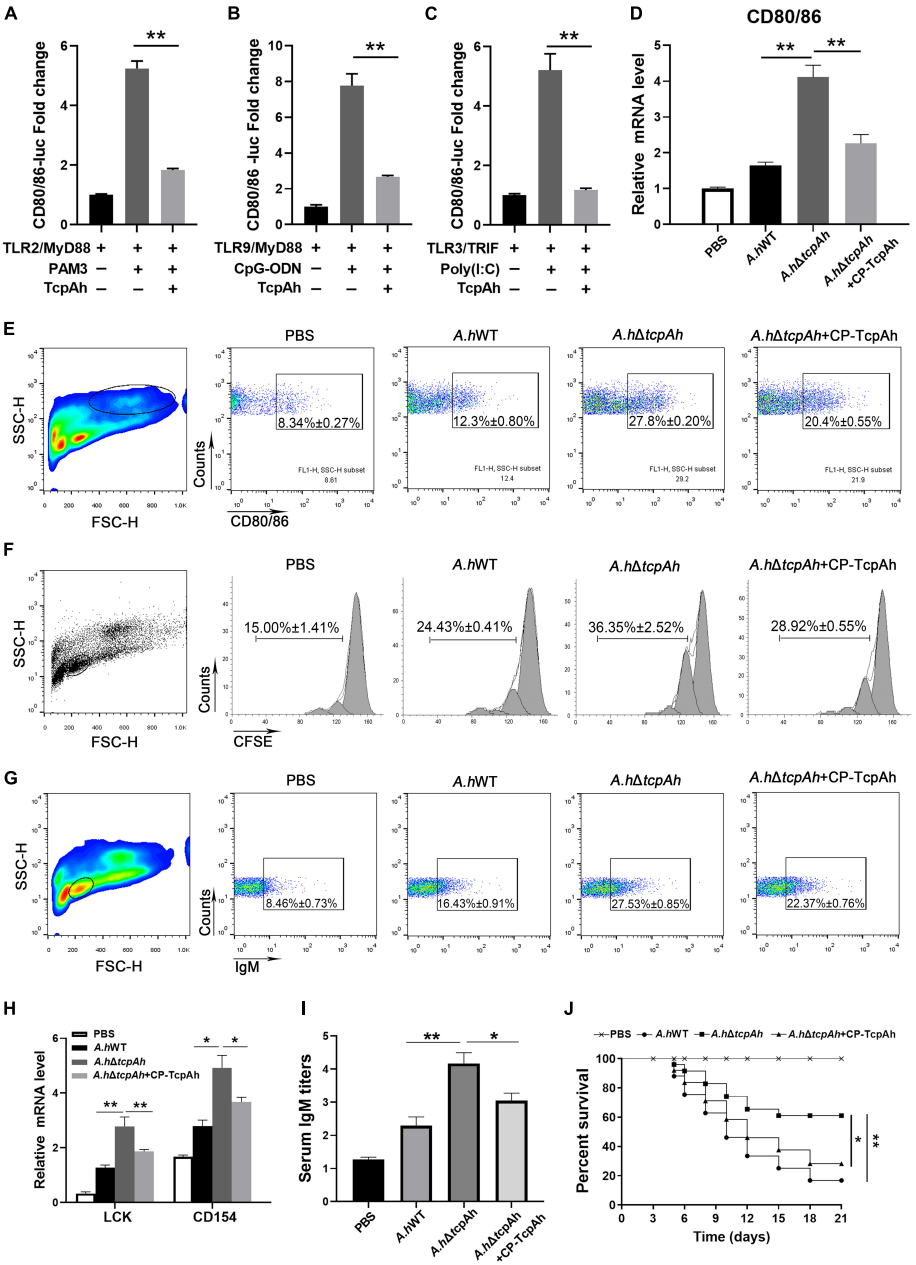


FIGURE 8 | Examination of the inhibitory role of TcpAh in zebrafish adaptive humoral immunity against infection by repressing CD80/86 expression. **(A–C)** Activation of zebrafish CD80/86 promoter in HEK293T cells transfected with CD80/86 luciferase reporter (CD80/86-Luc; 200 ng/mL), renilla luciferase reporter (15 ng/mL) and expression vectors for zebrafish TLR2 or TLR9 or TLR3 (20 ng/mL) in combination with MyD88 or TRIF (20 ng/mL) with or without TcpAh expression vector (250 ng/mL). After 24 h, the HEK293T cells were stimulated with PAM3 or CpG-ODN or Poly(I:C) for 12 h. Data are the average luciferase activity ± SD (**$p < 0.01$; ***$p < 0.001$). **(D)** Real-time PCR analysis for the expression of zebrafish *cd80/86* in leukocytes, which were sorted from peripheral blood, spleen, and kidney tissues 2 days after i.p. stimulation with PBS, wild-type *A. hydrophila*, Δ*tcpAh* mutant, or Δ*tcpAh* mutant complemented with CP-TcpAh protein. Data are representative of three independent experiments as mean ± SD (*$p < 0.05$; **$p < 0.01$). **(E)** Flow cytometric analysis of CD80/86 expression level on MHC-II$^+$ antigen-presenting cells (APCs) of each *in vivo* treatment group. Data are representative of three independent experiments as mean ± SD (*$p < 0.05$; **$p < 0.01$). **(F)** Proliferation of lymphocytes determined by CFSE dilution through flow cytometry under the indicated experimental treatment. **(G)** Proliferation of IgM$^+$ B cells determined by flow cytometry under the indicated experimental treatment. Data are representative of three independent experiments as mean ± SD (*$p < 0.05$; **$p < 0.01$). **(H)** Real-time PCR analysis of the expression levels of zebrafish LCK and CD154 of each *in vitro* treatment group. Data are representative of three independent experiments as mean ± SD (*$p < 0.05$; **$p < 0.01$). **(I)** Examination of the inhibitory role of TcpAh in IgM production in response to *A. hydrophila* infection in each treatment group by ELISA. Data are representative of three independent experiments as mean ± SD (n = 20; *$p < 0.05$; **$p < 0.01$). **(J)** Examination of the inhibitory role of TcpAh in zebrafish defense against *A. hydrophila* infection. Zebrafish were infected with *A. hydrophila* Δ*tcpAh* or with wild-type *A. hydrophila* or with *A. hydrophila* Δ*tcpAh* complement with CP-TcpAh. Differences were analyzed using log-rank test (*$p < 0.05$; **$p < 0.01$). Group of fish injected with mock PBS was used as a negative control.

in fish, and this outcome was attenuated by supplementing CP-TcpAh protein. These observations suggested that TcpAh plays an inhibitory role in adaptive humoral immunity through the attenuation of CD80/86 costimulatory signal, which is an important connection between innate and adaptive immunities and a crucial initiator of the activation of adaptive immunity.

In conclusion, our study identified a TIR domain protein (TcpAh) from *A. hydrophila*, which can be considered a new member of the bacterial TIR domain protein family. TcpAh acts as a strong virulence effector by extensively targeting MyD88, TRAF3, and TBK1 downstream of TLR signaling pathways, which leads to the inhibition of CD80/86 costimulatory signal essential for the activation of adaptive immunity. Thus, our findings uncovered a previously unrecognized mechanism underlying *A. hydrophila* evades from host immune defense, which will benefit the development of therapeutic interventions for *A. hydrophila* infection. Particularly, TcpAh can become a promising target for drug therapy because of its great potential use in *A. hydrophila*-elicited diseases, such as motile aeromonad septicemia in fish and other species.

DATA AVAILABILITY STATEMENT

The raw data supporting the conclusions of this article will be made available by the authors, without undue reservation.

ETHICS STATEMENT

The animal study was reviewed and approved by the Committee on Animal Care and Use and the Committee on the Ethic of Animal Experiments of Zhejiang University.

AUTHOR CONTRIBUTIONS

J-ZS, H-PT, and L-XX conceived and designed the experiments. H-PT, CH, HL, and C-BH performed the experiments. H-PT, CH, J-FJ, JB, TS, and A-FL analyzed the data. L-XX, D-DF, and J-ZS contributed reagents, materials, and analysis tools. H-PT, CH, and J-ZS wrote the manuscript. All authors contributed to the article and approved the submitted version.

FUNDING

This work was supported by grants from the National Key Research and Development Program of China (2018YFD0900505, 2018YFD0900503), the National Natural Science Foundation of China (31630083), and the Open Funding Project of the State Key Laboratory of Bioreactor Engineering.

ACKNOWLEDGMENTS

We thank Shun Li for the gifts of the zebrafish IFNφ2 promoter-luciferase reporter vector and Wu-ming Yang for the gifts of the *A. hydrophila* JBN2301 strain.

SUPPLEMENTARY MATERIAL

The Supplementary Material for this article can be found online at: https://www.frontiersin.org/articles/10.3389/fmicb.2021.694081/full#supplementary-material

REFERENCES

Akira, S., and Takeda, K. (2004). Toll-like receptor signalling. *Nat. Rev. Immunol.* 4, 499–511.

Alperi, A., and Figueras, M. J. (2010). Human isolates of Aeromonas possess Shiga toxin genes (stx1 and stx2) highly similar to the most virulent gene variants of *Escherichia coli*. *Clin. Microbiol. Infec.* 16, 1563–1567. doi: 10.1111/j.1469-0691.2010.03203.x

Askarian, F., van Sorge, N. M., Sangvik, M., Beasley, F. C., Henriksen, J. R., Sollid, J. U., et al. (2014). A Staphylococcus aureus TIR domain protein virulence factor blocks TLR2-mediated NF-kappaB signaling. *J. Innate Immun.* 6, 485–498. doi: 10.1159/000357618

Burns, K., Janssens, S., Brissoni, B., Olivos, N., Beyaert, R., and Tschopp, J. (2003). Inhibition of interleukin 1 receptor/toll-like receptor signaling through the alternatively spliced, short form of MyD88 is due to its failure to recruit IRAK-4. *J. Exp. Med.* 197, 263–268. doi: 10.1084/jem.20021790

Carty, M., Goodbody, R., Schroder, M., Stack, J., Moynagh, P. N., and Bowie, A. G. (2006). The human adaptor SARM negatively regulates adaptor protein TRIF-dependent Toll-like receptor signaling. *Nat. Immunol.* 7, 1074–1081. doi: 10.1038/ni1382

Chaudhary, A., Ganguly, K., Cabantous, S., Waldo, G. S., Micheva-Viteva, S. N., Nag, K., et al. (2012). The Brucella TIR-like protein TcpB interacts with the death domain of MyD88. *Biochem. Biophys. Res. Commun.* 417, 299–304. doi: 10.1016/j.bbrc.2011.11.104

Cirl, C., Wieser, A., Yadav, M., Duerr, S., Schubert, S., Fischer, H., et al. (2008). Subversion of Toll-like receptor signaling by a unique family of bacterial Toll/interleukin-1 receptor domain-containing proteins. *Nat. Med.* 14, 399–406. doi: 10.1038/nm1734

Crotty, S. (2011). Follicular helper CD4 T cells (TFH). *Annu. Rev. Immunol.* 29, 621–663. doi: 10.1146/annurev-immunol-031210-101400

Daskalov, H. (2006). The importance of Aeromonas hydrophila in food safety. *Food Control.* 17, 474–483. doi: 10.1016/j.foodcont.2005.02.009

Dunne, A., Ejdeback, M., Ludidi, P. L., O'Neill, L. A. J., and Gay, N. J. (2003). Structural complementarity of Toll/interleukin-1 receptor domains in toll-like receptors and the adaptors Mal and MyD88. *J. Biol. Chem.* 278, 41443–41451. doi: 10.1074/jbc.m301742200

Dunne, A., and O'Neill, L. A. (2003). The interleukin-1 receptor/Toll-like receptor superfamily: signal transduction during inflammation and host defense. *Sci. STKE* 2003:re3. doi: 10.1126/stke.2003.171.re3

Fearns, C., Pan, Q., Mathison, J. C., and Chuang, T. H. (2006). Triad3A regulates ubiquitination and proteasomal degradation of RIP1 following disruption of Hsp90 binding. *J. Biol. Chem.* 281, 34592–34600. doi: 10.1074/jbc.m604019200

Greenfield, E. A., Nguyen, K. A., and Kuchroo, V. K. (1998). CD28/B7 costimulation: a review. *Crit. Rev. Immunol.* 18, 389–418. doi: 10.1615/critrevimmunol.v18.i5.10

Harikrishnan, R., Rani, M. N., and Balasundaram, C. (2003). Hematological and biochemical parameters in common carp, Cyprinus carpio, following herbal treatment for Aeromonas hydrophila infection. *Aquaculture* 221, 41–50. doi: 10.1016/s0044-8486(03)00023-1

Horng, T., Barton, G. M., Flavell, R. A., and Medzhitov, R. (2002). The adaptor molecule TIRAP provides signalling specificity for Toll-like receptors. *Nature* 420, 329–333. doi: 10.1038/nature01180

Imbert, P. R., Louche, A., Luizet, J. B., Grandjean, T., Bigot, S., Wood, T. E., et al. (2017). A *Pseudomonas aeruginosa* TIR effector mediates immune evasion by targeting UBAP1 and TLR adaptors. *EMBO J.* 36, 1869–1887. doi: 10.15252/embj.201695343

Janssens, S., and Beyaert, R. (2002). A universal role for MyD88 in TLR/IL-1R-mediated signaling. *Trends Biochem. Sci.* 27, 474–482. doi: 10.1016/s0968-0004(02)02145-x

Ji, J., Liao, Z., Rao, Y., Li, W., Yang, C., Yuan, G., et al. (2019). Thoroughly Remold the Localization and Signaling Pathway of TLR22. *Front. Immunol.* 10:3003. doi: 10.3389/fimmu.2019.03003 eCollection 2019

Jiang, Q. L., Chen, W. B., Qin, Y. X., Huang, L. X., Xu, X. J., Zhao, L. M., et al. (2017). AcuC, a histone deacetylase, contributes to the pathogenicity of Aeromonas hydrophila. *Microbiologyopen* 6:e00468. doi: 10.1002/mbo3.468

Jin, M. S., and Lee, J. O. (2008). Structures of the toll-like receptor family and its ligand complexes. *Immunity* 29, 182–191. doi: 10.1016/j.immuni.2008.07.007

Kobayashi, K., Hernandez, L. D., Galan, J. E., Janeway, C. A., Medzhitov, R., and Flavell, R. A. (2002). IRAK-M is a negative regulator of toll-like receptor signaling. *Cell* 110, 191–202. doi: 10.1016/s0092-8674(02)00827-9

Lin, G. F., Chen, W. B., Su, Y. Q., Qin, Y. X., Huang, L. X., and Yan, Q. P. (2017). Ribose operon repressor (RbsR) contributes to the adhesion of Aeromonas hydrophila to Anguilla japonica mucus. *Microbiologyopen* 6:e00451.

Low, L. Y., Mukasa, T., Reed, J. C., and Pascual, J. (2007). Characterization of a TIR-like protein from Paracoccus denitrificans. *Biochem. Biophys. Res. Commun.* 356, 481–486. doi: 10.1016/j.bbrc.2007.03.003

Lu, L. F., Li, S., Lu, X. B., LaPatra, S. E., Zhang, N., Zhang, X. J., et al. (2016). Spring Viremia of Carp Virus N Protein Suppresses Fish IFNphi1 Production by Targeting the Mitochondrial Antiviral Signaling Protein. *J. Immunol.* 196, 3744–3753. doi: 10.4049/jimmunol.1502038

Ma, J. X., Li, J. Y., Fan, D. D., Feng, W., Lin, A. F., Xiang, L. X., et al. (2018). Identification of DEAD-Box RNA Helicase DDX41 as a Trafficking Protein That Involves in Multiple Innate Immune Signaling Pathways in a Zebrafish Model. *Front. Immunol.* 9:1327. doi: 10.3389/fimmu.2018.01327 eCollection 2018

Newman, R. M., Salunkhe, P., Godzik, A., and Reed, J. C. (2006). Identification and characterization of a novel bacterial virulence factor that shares homology with mammalian Toll/interleukin-1 receptor family proteins. *Infect. Immun.* 74, 594–601. doi: 10.1128/iai.74.1.594-601.2006

O'Neill, L. A. (2003). SIGIRR puts the brakes on Toll-like receptors. *Nat. Immunol.* 4, 823–824. doi: 10.1038/ni0903-823

O'Neill, L. A. J., and Bowie, A. G. (2007). The family of five: tIR-domain-containing adaptors in Toll-like receptor signalling. *Nat. Rev. Immunol.* 7, 353–364. doi: 10.1038/nri2079

Oshiumi, H., Matsumoto, M., Funami, K., Akazawa, T., and Seya, T. (2003). TICAM-1, an adaptor molecule that participates in Toll-like receptor 3-mediated interferon-beta induction. *Nat. Immunol.* 4, 161–167. doi: 10.1038/ni886

Pasare, C., and Medzhitov, R. (2004). Toll-like receptors: linking innate and adaptive immunity. *Microb. Infect.* 6, 1382–1387. doi: 10.1016/j.micinf.2004.08.018

Poltorak, A., He, X. L., Smirnova, I., Liu, M. Y., Van Huffel, C., Du, X., et al. (1998). Defective LPS signaling in C3H/HeJ and C57BL/10ScCr mice: mutations in Tlr4 gene. *Science* 282, 2085–2088. doi: 10.1126/science.282.5396.2085

Radhakrishnan, G. K., Yu, Q., Harms, J. S., and Splitter, G. A. (2009). Brucella TIR Domain-containing Protein Mimics Properties of the Toll-like Receptor Adaptor Protein TIRAP. *J. Biol. Chem.* 284, 9892–9898. doi: 10.1074/jbc.m805458200

Rana, R. R., Simpson, P., Zhang, M., Jennions, M., Ukegbu, C., Spear, A. M., et al. (2011). Yersinia pestis TIR-domain protein forms dimers that interact with the human adaptor protein MyD88. *Microb. Pathog.* 51, 89–95. doi: 10.1016/j.micpath.2011.05.004

Rana, R. R., Zhang, M., Spear, A. M., Atkins, H. S., and Byrne, B. (2013). Bacterial TIR-containing proteins and host innate immune system evasion. *Med. Microbiol. Immunol.* 202, 1–10. doi: 10.1007/s00430-012-0253-2

Rojas, M., Donahue, J. P., Tan, Z. J., and Lin, Y. Z. (1998). Genetic engineering of proteins with cell membrane permeability. *Nat. Biotechnol.* 16, 370–375. doi: 10.1038/nbt0498-370

Rosadini, C. V., and Kagan, J. C. (2015). Microbial strategies for antagonizing Toll-like-receptor signal transduction. *Curr. Opinion Immunol.* 32, 61–70. doi: 10.1016/j.coi.2014.12.011

Saraceni, P. R., Romero, A., Figueras, A., and Novoa, B. (2016). Establishment of Infection Models in Zebrafish Larvae (Danio rerio) to Study the Pathogenesis of Aeromonas hydrophila. *Front. Microbiol.* 7:1219. doi: 10.3389/fmicb.2016.01219

Shao, T., Shi, W., Zheng, J. Y., Xu, X. X., Lin, A. F., Xiang, L. X., et al. (2018). Costimulatory Function of Cd58/Cd2 Interaction in Adaptive Humoral Immunity in a Zebrafish Model. *Front. Immunol.* 9:1204. doi: 10.3389/fimmu.2018.01204 eCollection 2018

Slack, J. L., Schooley, K., Bonnert, T. P., Mitcham, J. L., Qwarnstrom, E. E., Sims, J. E., et al. (2000). Identification of two major sites in the type I interleukin-1 receptor cytoplasmic region responsible for coupling to pro-inflammatory signaling pathways. *J. Biol. Chem.* 275, 4670–4678. doi: 10.1074/jbc.275.7.4670

Thornley, J. P., Shaw, J. G., Gryllos, I. A., and Eley, A. (1997). Virulence properties of clinically significant Aeromonas species: evidence for pathogenicity. *Rev. Med. Microbiol.* 8, 61–72. doi: 10.1097/00013542-199704000-00002

Tobias, P. S., Lee, H. K., Orr, S., Soldau, K., and Tapping, R. (2000). Innate immune system recognition of microbial pathogens. *Immunol. Res.* 21, 341–343. doi: 10.1385/ir:21:2-3:341

Tomas, J. M. (2012). The main Aeromonas pathogenic factors. *ISRN Microbiol.* 2012:256261.

Underhill, D. M., Ozinsky, A., Hajjar, A. M., Stevens, A., Wilson, C. B., Bassetti, M., et al. (1999). The Toll-like receptor 2 is recruited to macrophage phagosomes and discriminates between pathogens. *Nature* 401, 811–815. doi: 10.1038/44605

Vivas, J., Carracedo, B., Riano, J., Razquin, B. E., Lopez-Fierro, P., Acosta, F., et al. (2004). Behavior of an Aeromonas hydrophila aroA live vaccine in water microcosms. *Appl. Environ. Microb.* 70, 2702–2708. doi: 10.1128/aem.70.5.2702-2708.2004

Wald, D., Qin, J. Z., Zhao, Z. D., Qian, Y. C., Naramura, M., Tian, L. P., et al. (2003). SIGIRR, a negative regulator of Toll-like receptor-interleukin 1 receptor signaling. *Nat. Immunol.* 4, 920–927. doi: 10.1038/ni968

Wan, F., Hu, C. B., Ma, J. X., Gao, K., Xiang, L. X., and Shao, J. Z. (2016). Characterization of γδ T Cells from Zebrafish Provides Insights into Their Important Role in Adaptive Humoral Immunity. *Front. Immunol.* 7:675. doi: 10.3389/fimmu.2016.00675 eCollection 2016

Xie, Q., Mei, W., Ye, X., Zhou, P., Islam, M. S., Elbassiony, K. R. A., et al. (2018). The two-component regulatory system CpxA/R is required for the pathogenesis of Aeromonas hydrophila. *FEMS Microbiol. Lett.* 1:365.

Xu, X. G., Hu, J. F., Ma, J. X., Nie, L., Shao, T., Xiang, L. X., et al. (2016). Essential Roles of TIM-1 and TIM-4 Homologs in Adaptive Humoral Immunity in a Zebrafish Model. *J Immunol* 196, 1686–1699. doi: 10.4049/jimmunol.1501736

Xu, Y. W., Tao, X., Shen, B. H., Horng, T., Medzhitov, R., Manley, J. L., et al. (2000). Structural basis for signal transduction by the Toll/interleukin-1 receptor domains. *Nature* 408, 111–115. doi: 10.1038/35040600

Yadav, M., Zhang, J., Fischer, H., Huang, W., Lutay, N., Cirl, C., et al. (2010). Inhibition of TIR domain signaling by TcpC: myD88-dependent and independent effects on *Escherichia coli* virulence. *PLoS Pathog.* 6:e1001120. doi: 10.1371/journal.ppat.1001120

Yamamoto, M., Sato, S., Hemmi, H., Hoshino, K., Kaisho, T., Sanjo, H., et al. (2003a). Role of adaptor TRIF in the MyD88-independent toll-like receptor signaling pathway. *Science* 301, 640–643. doi: 10.1126/science.1087262

Yamamoto, M., Sato, S., Hemmi, H., Uematsu, S., Hoshino, K., Kaisho, T., et al. (2003b). TRAM is specifically involved in the Toll-like receptor 4-mediated MyD88-independent signaling pathway. *Nat. Immunol.* 4, 1144–1150. doi: 10.1038/ni986

Yamamoto, M., Sato, S., Mori, K., Hoshino, K., Takeuchi, O., Takeda, K., et al. (2002). Cutting edge: a novel toll/IL-1 receptor Domain containing adapter that preferentially activates the IFN-beta promoter in the toll-like receptor signaling. *J. Immunol.* 169, 6668–6672. doi: 10.4049/jimmunol.169.12.6668

Conflict of Interest: The authors declare that the research was conducted in the absence of any commercial or financial relationships that could be construed as a potential conflict of interest.

Copyright © 2021 Tang, Huang, Hu, Li, Shao, Ji, Bai, Fan, Lin, Xiang and Shao. This is an open-access article distributed under the terms of the Creative Commons Attribution License (CC BY). The use, distribution or reproduction in other forums is permitted, provided the original author(s) and the copyright owner(s) are credited and that the original publication in this journal is cited, in accordance with accepted academic practice. No use, distribution or reproduction is permitted which does not comply with these terms.

frontiers in Microbiology

ORIGINAL RESEARCH
published: 04 August 2021
doi: 10.3389/fmicb.2021.692474

Paeonol Attenuates Quorum-Sensing Regulated Virulence and Biofilm Formation in *Pseudomonas aeruginosa*

Dan Yang[1†], Suqi Hao[1†], Ling Zhao[1], Fei Shi[1], Gang Ye[1], Yuanfeng Zou[1], Xu Song[1], Lixia Li[1], Zhongqiong Yin[1], Xiaoli He[2], Shiling Feng[3], Helin Chen[1], Yu Zhang[1], Yuanze Gao[1], Yinglun Li[1] and Huaqiao Tang[1]**

[1] College of Veterinary Medicine, Sichuan Agricultural University, Chengdu, China, [2] College of Science, Sichuan Agricultural University, Chengdu, China, [3] College of Life Science, Sichuan Agricultural University, Yaan, China

OPEN ACCESS

Edited by:
Alina Maria Holban,
University of Bucharest, Romania

Reviewed by:
Faizan Abul Qais,
Aligarh Muslim University, India
Wen-Ru Li,
Guangdong Institute of Microbiology, Guangdong Academy of Science, China
Arunachalam Kannappan,
Shanghai Jiao Tong University, China

***Correspondence:**
Yinglun Li
liyinglun02@163.com
Huaqiao Tang
turtletang@163.com

[†] These authors share first authorship

Specialty section:
This article was submitted to Microbial Immunology, a section of the journal Frontiers in Microbiology

Received: 08 April 2021
Accepted: 23 June 2021
Published: 04 August 2021

Citation:
Yang D, Hao S, Zhao L, Shi F, Ye G, Zou Y, Song X, Li L, Yin Z, He X, Feng S, Chen H, Zhang Y, Gao Y, Li Y and Tang H (2021) Paeonol Attenuates Quorum-Sensing Regulated Virulence and Biofilm Formation in Pseudomonas aeruginosa. Front. Microbiol. 12:692474. doi: 10.3389/fmicb.2021.692474

With the prevalence of multidrug-resistant bacteria and clinical -acquired pathogenic infections, the development of quorum-sensing (QS) interfering agents is one of the most potential strategies to combat bacterial infections and antibiotic resistance. Chinese herbal medicines constitute a valuable bank of resources for the identification of QS inhibitors. Accordingly, in this research, some compounds were tested for QS inhibition using indicator strains. Paeonol is a phenolic compound, which can effectively reduce the production of violacein without affecting its growth in *Chromobacterium violaceum* ATCC 12472, indicating its excellent anti-QS activity. This study assessed the anti-biofilm activity of paeonol against Gram-negative pathogens and investigated the effect of paeonol on QS-regulated virulence factors in *Pseudomonas aeruginosa*. A *Caenorhabditis elegans* infection model was used to explore the anti-infection ability of paeonol *in vivo*. Paeonol exhibited an effective anti-biofilm activity against Gram-negative bacteria. The ability of paeonol to interfere with the AHL-mediated quorum sensing systems of *P. aeruginosa* was determined, found that it could attenuate biofilm formation, and synthesis of pyocyanin, protease, elastase, motility, and AHL signaling molecule in a concentration- and time-dependent manner. Moreover, paeonol could significantly downregulate the transcription level of the QS-related genes of *P. aeruginosa* including *lasI/R, rhlI/R, pqs/mvfR*, as well as mediated its virulence factors, *lasA, lasB, rhlA, rhlC, phzA, phzM, phzH,* and *phzS*. *In vivo* studies revealed that paeonol could reduce the pathogenicity of *P. aeruginosa* and enhance the survival rate of *C. elegans*, showing a moderate protective effect on *C. elegans*. Collectively, these findings suggest that paeonol attenuates bacterial virulence and infection of *P. aeruginosa* and that further research elucidating the anti-QS mechanism of this compound *in vivo* is warranted.

Keywords: paeonol, quorum sensing, *Pseudomonas aeruginosa*, anti-virulence, biofilm

INTRODUCTION

Quorum sensing (QS) is a type of density-dependent cell-to-cell communication mechanism used by bacteria to detect community density. QS coordinates its clustering behavior by producing and sensing signaling molecules called autoinducers (AIS) and their receptors (Swift et al., 1996; Davies et al., 1998). Three different types of AIs have been discovered: *N*-acyl L-homoserine lactone (AHLs) exploited by Gram-negative species, small peptide signals exploited by Gram-positive species and autoinducer-2 for inter-species communication (Ng and Bassler, 2009). Once the bacterial population density reaches a critical threshold, the QS system activates the expression of virulence-associated genes to control a vast set of relevant phenotypes including biofilm-formation, motility, exopolysaccharide production, virulence factors, motility, and bioluminescence (Bassler et al., 1993; Miller and Bassler, 2001).

The excessive and indiscriminate use of antibiotics has eventually led to the emergence of multidrug-resistant bacteria that are difficult to control using conventional antibiotics, as most evident in the ESKAPE-pathogens (*Enterococcus faecium*, *Staphylococcus aureus*, *Klebsiella pneumoniae*, *Acinetobacter baumannii*, *Pseudomonas aeruginosa*, and *Enterobacter* spp.; Tacconelli et al., 2002; Boucher et al., 2009; MacPherson et al., 2009). Biofilm is a barrier system, which can protect the bacteria from the immune reaction of the host, prevent the entry of disinfectants and antibiotics, make the bacteria develop multi-drug resistance, and lead to clinical infection which is difficult to cure (Dunne, 2002). About 80% of all microbial-induced infections are biofilm-based. Quorum sensing has known to play a crucial role in biofilm formation of many pathogenic bacteria, serving as biofilm quorum-sensing molecules (Fuqua and Greenberg, 2002). *Pseudomonas aeruginosa* (*P. aeruginosa*) is a pervasive Gram-negative organism and an opportunistic pathogen in humans capable of causing multiple diseases including chronic panbronchiolitis, cystic fibrosis (CF), and chronic urinary tract infections (Lyczak et al., 2002; Hassett et al., 2009). The QS networks in *P. aeruginosa* comprise four distinct interwoven circuits, namely *las*, *rhl*, *pqs*, and *iqs*, with the *las* system positively at the upstream position regulating both the *rhl* and *pqs* systems, which also cross-regulate in a complex manner (Schuster and Greenberg, 2006; Welsh et al., 2015; Huang et al., 2019). The QS system is essential for the production of different signaling molecules including *P. aeruginosa* autoinducer 1 [*N*-(3-oxododecanoyl-homoserine lactones) or 3-oxo-C12-HSL], *Pseudomonas* autoinducer 2 (*N*-butyryl-homoserine lactones or C4-HSL), and PQS (2-heptyl-3-hydroxy-4-quinolone), each of which acts as an autoinducer of a specific sensing and responding system (Williams and Camara, 2009; Ismail et al., 2016). Once these signals reach a threshold, the collective behavior changes by activating the sensor or modulating the protein (Ilangovan et al., 2013). The QS system in *P. aeruginosa* regulates biofilm formation, motility, and the expression of virulence-associated factors such as pyocyanin, proteolytic enzymes, extracellular proteases, and rhamnolipids (Parsek and Greenberg, 2000). Therefore, *P. aeruginosa* has become the typical model organism for assessment of antibacterial, anti-QS and anti-biofilm activity.

Given the essential role of QS in bacterial pathogenicity and virulence, it is considered a novel and potential therapeutic strategy for coping with bacterial infections and antibiotic resistance (Packiavathy et al., 2014; Hernando-Amado et al., 2019). Natural products obtained from plants, microorganisms, and marine organisms have shown promise in inhibiting QS signaling and biofilm formation rather than targeting bacterial growth (Valdez et al., 2005; Khan et al., 2009; Glamoclija et al., 2015). *Chromobacterium violaceum* is a QS biosensor strain that produces the pigment, violacein, in response to QS-related gene expression, and is, thus, widely used to research QS activities (Singh et al., 2009). Paeonol is one of the main compounds present in traditional Chinese medicine, including Moutan cortex, *Cynanchum paniculatum*, and *Paeonia lactiflora* Pal. Paeonol is known to exert multiple pharmacological effects, immunomodulation, and liver and kidney protection, antitumor, antipyretic, analgesic, anti-inflammatory, and antibacterial and has been widely used as a nutrient supplement (Zhang et al., 2019; Tsai et al., 2020).

However, to the best of our knowledge, there are no studies showing the anti-biofilm and anti-QS activity of paeonol. Thus, in this study, we preliminary evaluated the effect of paeonol on bacterial biofilm formation. Further, we investigated the mechanism of paeonol *in vitro* against *P. aeruginosa*-based anti-QS by detecting the virulence phenotypes, biofilm-formation, and related gene expression. The protective effect of paeonol on the pathogenicity of *P. aeruginosa* was determined *in vivo* using a nematode model.

MATERIALS AND METHODS

Bacterial Strains, Chemicals, and Culture Conditions

Pseudomonas aeruginosa (PAO1, ATCC 27853, and ATCC 9027), *P. aeruginosa* clinically isolated stains (PAO3401, isolated from Chinchilla and identified in the laboratory), *C. violaceum* (ATCC 12472 and CV026), *A. baumannii* 17978, *Escherichia coli* (ATCC 25922 and OP50), *Salmonella typhimurium* 14028 and MRSA TCH1516 that were stored in our laboratory were used in this study. The cryopreserved *P. aeruginosa* (PAO1, ATCC 27853, ATCC 9027, and PAO3401), *A. baumannii* 17978, *E. coli* (ATCC 25922 and OP50), *S. typhimurium* 14028 and MRSA TCH1516 were cultured overnight in Luria-Bertani (LB) broth in a rotator shaker with agitation at 180 rpm at 37°C. *C. violaceum* (ATCC 12472 and CV026) were cultured overnight at 30°C aerobically in LB broth in a rotator shaker with agitation 180 rpm. The test compounds were dissolved in dimethyl sulfoxide (DMSO), including protocatechuic aldehyde, aniseed aldehyde, paeonol, carvacrol, polydatin, saikosaponin A, atractylenolide, gallate, calycosin-7-glucoside, veratric acid, myristic acid, ellagic acid, glycyrrhiza acid, aurantiamarin, baicalin, rutin, puerarin, and sophocarpidine (Yuanye Bio-Technology Co., Shanghai, China). DMSO and fresh LB broth were used as controls. The chemicals and reagents used in this study

was analytical grade. For each experiment, the bacteria were cultured overnight and re-inoculated at 1:1,000 dilution (approximately 5×10^5 CFU/mL) in fresh LB broth. Cell growth was determined based on the optical density that was measured at a wavelength of 600 nm using microplate reader (Thermo Fisher Scientific, Waltham, MA, United States). Then, *C. elegans* N2 cultures and *E. coli* OP50 were maintained on nematode growth medium (NGM) as a food source at 20°C. IPEC-J2 cells were cultured in DMEM medium (Gibco, Grand Island, New York, United States) supplemented with 10% fetal bovine serum (Gibco, Oshima, New York, United States) and 1% penicillin/chain (Solarbio, Beijing, China) at 37°C with 5% CO_2 in the incubator.

Preliminary Screening of AI-1 Quorum Sensing Inhibitors

A quantitative assay for violacein was carried out as previously described with few modifications (Blosser and Gray, 2000). Briefly, 200 μL of *C. violaceum* ATCC 12472 (approximately 5×10^5 CFU/mL) was incubated individually with different concentrations of chemical compounds at 30°C for 18 h and OD_{600} was measured by microplate reader. After incubation, the violacein from 200 μL of the bacterial culture was extracted using 100 μL of 10% SDS and 400 μL of *n*-butanol. After centrifugation at 8,900×*g* for 5 min, 200 μL the organic layer was taken in a 96-well plate. The absorbance was determined at 595 nm to quantify the violacein in the supernatant.

Chromobacterium violaceum ATCC 12472 was cultured in LB medium at 30°C with shaking at 180 rpm, diluted in a 1:100 ratio with LB solid medium, and poured into Petri dishes (McLean et al., 2004). Then, 20 μL of the test compounds at a concentration of 20 mg/mL were added to the wells of the plates and incubated at 30°C for 24 h. Due to a loss of violacein pigmentation, the anti-QS activity was evaluated by the production of a colorless and opaque but turbid halo around the well, and was measured from the outer edge of the disk to the edge of the anti-QS inhibition zone.

Minimum Inhibitory Concentration Assay and Growth Curves

Various concentrations of paeonol were examined against the selected bacteria strains and their inhibitory activity was determined using a modified broth microdilution method as stated in the Clinical and Laboratory Standards Institute (2012). Twofold dilutions of paeonol were prepared using LB broth in a 96-well plate with final concentrations ranging from 16 to 2,048 μg/mL. A suspension of bacteria strains at a final test concentration of about 5×10^5 CFU/mL was added to each well and incubated at 37°C for 24 h. The MIC was defined as the minimum concentration of paeonol that inhibited the growth of the selected microorganisms (Clinical and Laboratory Standards Institute, 2012).

A growth-curve analysis was performed for the PAO1 strain to determine the impact of the sub-inhibitory concentrations of paeonol on growth (Jorgensen, 1993). Overnight grown cultures of PAO1 were prepared using LB broth and supplemented with paeonol (0, 128, 256, and 512 μg/mL). LB medium and the same concentration of DMSO were used as negative controls. The conical flask was cultured in a rotator shaker while being agitated at 180 rpm and 37°C. The optical density was determined at 600 nm every hour for up to 36 h.

Anti-biofilm Activity Assay of Paeonol

Anti-biofilm Formation Quantitative Assay

For observing the inhibitory effect of paeonol on bacterial biofilm, we incubated the bacterial suspension of *C. violaceum* 12472, *P. aeruginosa* (PAO1, ATCC 27853, ATCC 9027, and PAO3401), *A. baumannii* 17978, *E. coli* 25922, *S. typhimurium* 14028, and MRSA TCH1516. The biofilm-forming ability of selected bacteria was determined using the crystal violet method (Lee et al., 2011). Briefly, 200 μL of the bacteria culture (approximately 5×10^5 CFU/mL) was taken in a 96-well plate and incubated with different concentrations of paeonol at 37°C for 24 and 36 h. After incubation, the biofilm was washed with sterile phosphate-buffered saline (PBS) for three times and fixed with 200 μL of methanol (99%) for 15 min. The supernatant was discarded, and the biofilm was stained with 200 μL of 0.1% crystal violet and dissolved in 33% acetic acid for 15 min. The absorbance was measured at 595 nm to quantify biofilm formation.

Microscopy Analysis of Paeonol Against *P. aeruginosa*

The method of biofilm formation was conducted as described previously (Murphy et al., 2014). Briefly, biofilms were cultured for 36 h on a glass coverslip using 24 well plates with paeonol (0–512 μg/mL) treated and untreated cultures of PAO1. The total biofilm biomass was determined by washing the glass coverslip with PBS three times, drying at 60°C, staining with 0.1% crystal violet, and then observing under the light microscope. Scanning electron microscopy (SEM) was further applied to visualize biofilm architecture. The coverslips were washed for non-adhered bacteria three with PBS and fixed overnight at 4°C in 2.5% (v/v) glutaraldehyde, then processed for SEM using standard protocol.

Flagellar Motility Assay of Paeonol Against *P. aeruginosa*

Bacterial motility was assayed on agar plates after treatment with different concentrations of paeonol (0, 128, 256, and 512 μg/mL). *P. aeruginosa* (PAO1, ATCC 27853, ATCC 9027, and PAO3401) were cultured in LB broth overnight at 37°C at constant shaking at 180 rpm. Next, 1 μL of *P. aeruginosa* cells was added to the center of the swarming solid medium (1.0% peptone, 0.5% sodium chloride, 0.5% glucose, and 0.5% agar) and swimming soft medium (1.0% peptone, 0.5% sodium chloride, and 0.3% agar). The plates were inoculated at 37°C for 24 h, and the flagellar motility was determined by measuring the diameter (cm) of the traveled cells on the surface of the agar plate (Rashid and Kornberg, 2000).

Analysis Virulence Phenotypes of *P. aeruginosa*

Pyocyanin Quantitative Assay

Pyocyanin production was determined using different concentrations of paeonol in PB medium (2% tryptone, 1%

K_2SO_4, and 0.14% $MgCl_2$) by the chloroform-HCl extraction method (Chong et al., 2011). A volume of 2 mL of the PAO1 culture (approximately 5×10^5 CFU/mL) was incubated with different concentrations of paeonol (0–512 μg/mL) at 37°C for 48 h in a 24-well plate. After centrifugation at 10,000×*g* for 10 min, the supernatant of the PAO1 culture was extracted with 0.75 mL of chloroform and 0.2 M HCl (0.25 mL) was added to the chloroform layer. After centrifugation, the HCl was removed and pyocyanin was quantified at 520 nm.

Proteolytic Activity Assay

A protease quantitative analysis was performed according to a previously published method (Hentzer et al., 2002) with minor modifications. Briefly, 2 mL of PAO1 culture (approximately 5×10^5 CFU/mL) was incubated with different concentrations of paeonol (0–512 μg/mL) at 37°C for 24 h. After centrifugation, the filter-sterilized supernatant (150 μL each) of PAO1 treated with paeonol was added with 250 μL of 2% azocasein (w/v)-*Tris*/HCl solution (pH 7.8). Next, the azocasein-treated solutions were incubated at 4°C for 4 h and the reaction was terminated by the addition of trichloroacetic acid (10%, 1.2 mL) for 15 min. After centrifugation at 10,000×*g* for 10 min, the supernatant was added to 1 M NaOH (1.4 mL). Protease activity was determined by measuring the absorbance at a wavelength of 440 nm.

Elastase Activity Assay

The elastasse qualitative analysis was monitored according to previously reported methods (Adonizio et al., 2008). Briefly, 2 mL of PAO1 cultures (approximately 5×10^5 CFU/mL) were incubated with different concentrations of paeonol (0–512 μg/mL) at 37°C for 24 h. The cultures were centrifuged for 10 min at 10,000 rpm and filter-purified by a 0.22 μm nylon filter, 100 μL supernatant were added to 400 μl of ECR buffer (100 mM *Tris*, 1 mM $CaCl_2$, pH 7.2) containing 20 mg ECR. Then, the mixture was incubated at 37°C for 16 h with shaking (200 rpm). The insoluble ECR was removed by centrifugation, and the absorbance of the supernatant at 495 nm was measured to evaluate elastase activity.

Rhamnolipids Quantitative Assay

Rhamnolipids of *P. aeruginosa* were cultured in PPGAS medium (20 mM KCl, 20 mM NH_4Cl, 0.5% glucose, 1.6 mM $MgSO_4$, 120 mM *Tris*–HCl, and 1.0% peptone) according to a previously published method (Grosso-Becerra et al., 2016). Briefly, 2 mL of the PAO1 cells (approximately 5×10^5 CFU/mL) were allowed to grow in the presence and absence of paeonol at 37°C for 24 h. After centrifugation, the supernatants were extracted twice with ethyl acetate; the organic layers were combined and evaporated to dryness overnight at 50°C. The solid product was dissolved in 500 μL of sterile distilled water. Next, 100 μL of the sample was added to 0.19% orcinol in 53% concentrated sulfuric acid (900 μL) and incubated in a water bath at 80°C for 30 min. After cooling to room temperature (18–25°C), the absorbance of the samples was measured spectrophotometrically at 421 nm.

AHL Synthesis Activity Assay of Paeonol Against *P. aeruginosa*

The levels of AHL in the PAO1 supernatants were measured after treatment with paeonol by assessing the violacein production by CV026. About 2 mL of the PAO1 culture (approximately 5×10^5 CFU/mL) was incubated with different concentrations of paeonol (0–512 μg/mL) at 37°C for 24 h. After centrifugation, the supernatants were extracted twice with ethyl acetate. The organic layers were combined and evaporated to dryness overnight at 40°C. The yellow precipitate was resuspended in 200 μL of DMSO, and 20 μL was added into the wells of the fresh agar plates containing CV026. The plates were inoculated at 30°C for 24 h. The production of AHL was monitored by measuring the zone of clearance around each well (Ravn et al., 2001).

Expression of QS Genes on *P. aeruginosa*

Fluorescence real-time PCR was used to detect the expression of the QS genes of PAO1 in the presence of paeonol (0, 128, 256, and 512 μg/mL). **Table 1** shows the primers that were used to amplify *lasI, lasR, rhlI, rhlR, pqsA, pqsR, lasA, lasB, rhlA, rhlC, phzm, phzM, phzH, phzS, and pvdQ* (reference gene). Total RNA was then extracted using TRIzol Reagent (Songon Biotech, Shanghai, China) according to the manufacturer's instructions. Next, the samples were reverse-transcribed to single-stranded cDNA in a 20-μL volume of the reaction mixture using Maxima H Minus First Strand cDNA Synthesis kit (Thermo Fisher Scientific, Waltham, MA, United States). Then, real-time PCR was performed in a 10-μL reaction volume, containing 5 μL of PerfectStartTM Green qPCR SuperMix (TransGen Biotech, Beijing, China), 2 μL of the template cDNA, 1 μL of primers (Shenzhen Huada Gene Research Institute, Shenzhen, China), and 2 μL of DNase/RNase-free water (Tiangen Biotech, Beijing, China). The pvdQ gene was chosen as a reference gene and used to normalize the quantitative PCR data and calculate the relative differences in mRNA expression using the $2^{-\Delta\Delta CT}$ method.

TABLE 1 | PCR primers of *Pseudomonas aeruginosa* for analysis of gene expression.

Genes	Primer sequences (5′–3′)	
lasI	F: CGCACATCTGGGAACTCA	R: CGGCACGGATCATCATCT
lasR	F: CTGTGGATGCTCAAGGACTAC	R: AACTGGTCTTGCCGATGG
rhlI	F: GTAGCGGGTTTGCGGATG	R: CGGCATCAGGTCTTCATCG
rhlR	F: GCCAGCGTCTTGTTCGG	R: CGGTCTGCCTGAGCCATC
pqsA	F: GACCGGCTGTATTCGATTC	R: GCTGAACCAGGGAAAGAAC
pqsR	F: CTGATCTGCCGGTAATTGG	R: ATCGACGAGGAACTGAAGA
lasA	F: CTGTGGATGCTCAAGGACTAC	R: AACTGGTCTTGCCGATGG
lasB	F: AACCGTGCGTTCTACCTGTT	R: CGGTCCAGTAGTAGCGGTTG
rhlA	F: TGGCCGAACATTTCAACGT	R: GATTTCCACCTCGTCGTCCTT
rhlC	F: GCCATCCATCTCGACGGAC	R: CGCAGGCTGTATTCGGTG
phzM	F: ACGGCTGTGGCGGTTTA	R: CCGTGACCGTCGCATT
phzA	F: AACGGTCAGCGGTACAGGGAAC	R: AACGGTCAGCGGTACAGG GAAAC
phzH	F: GCTCATCGACAATGCCGAACT	R: GCGGATCTCGCCGAACATCAG
phzS	F: CCGAAGGCAAGTCGCTGGTGA	R: GGTCCCAGTCGGCGAAGAACG
pvdQ	F: GCCGAGGAGATCGTCACC	R: CAGGCGTAGAAGATGTCGGA

Anti-infection Activity of Paeonol on *C. elegans*

The *C. elegans* population was synchronized according to a method reported previously (Tan et al., 1999b), with some modifications. Briefly, 200 μL of the broth culture of *P. aeruginosa* was spread evenly on NGM agar plates containing paeonol (0, 128, and 256 μg/mL) and cultured for 18 h at 37°C to create a bacterial lawn. Plates coated with *E. coli* OP50 were used as negative controls. Then, 40 synchronized nematodes (L4 stage) of the wild type *C. elegans* N2 strain were selected and suspended onto the plates and counted every 24 h using a stereomicroscope. In the experiment, the nematodes were considered dead when immobilized. The number of surviving nematodes was tabulated and a survival curve was constructed.

Cell Proliferation Assay

The CCK-8 assay was performed to determine the number of viable cells according to the manufacturer's protocol. IPEC-J2 cells in logarithmic growth were seeded in 96-well plates (1×10^5 per well) and cultured in DMEM medium supplemented with 10% FBS for 12 h, and then treated with a series of concentrations of paeonol (0, 16, 32, 64,128, 256, 512, and 1,024 μg/ml) for 24 h. Then, 10 μl CCK-8 solution was added to each well of the plates. After incubation at 37°C for another 3 h, the absorbance at 450 nm was detected to determine the number of viable cells.

Statistical Analysis

All data were processed using SPSS 22.0 (IBM Corporation, Armonk, NY, United States) and are presented as mean ± SD. Graphs were constructed using GraphPad Prism 8.0.1 (GraphPad Software, La Jolla, CA, United States). ANOVA was used to determine significance, and $p < 0.05$ was considered statistically significant.

RESULTS

Screening of AI-1 QS Inhibitors

Screening assays, based on QS-mediated violacein production and viability, were performed in broth and agar plates to identify non-bactericidal QS inhibitors (QSIs). Three concentrations of the compound were selected for violacein quantitative assay such that they did not affect the growth of *C. violaceum*. **Table 2** shows the effect of test compounds on violacein production in *C. violaceum* 12472, our results indicated that protocatechualdehyde, anisic aldehyde, carvacrol, paeonol, polydatin, saikosaponin A, atractylenolide gallate, veratric

TABLE 2 | Inhibition of *Chromobacterium violaceum* (CV12472) pigments by different compounds.

Test compounds	Selected concentration (μg/mL)	Inhibition rate (%)	Test compounds	Selected concentration (μg/mL)	Inhibition rate (%)
Protocatechuic aldehyde	12.5	16.28 ± 1.85**	Veratric acid	128	5.24 ± 0.37*
	25	27.39 ± 1.60**		256	13.29 ± 2.56**
	50	55.23 ± 5.92**		512	29.76 ± 1.46**
Aniseed aldehyde	12.5	21.41 ± 0.96**	Myristic acid	128	12.93 ± 0.73**
	25	21.56 ± 0.48**		256	12.93 ± 1.46**
	50	31.99 ± 2.22**		512	27.56 ± 3.66**
Paeonol	12.5	18.70 ± 1.96**	Ellagic acid	200	9.27 ± 1.46
	25	23.77 ± 0.79**		400	8.17 ± 6.22
	50	37.81 ± 1.99**		800	15.12 ± 9.51*
	12.5	21.48 ± 1.46**	Glycyrrhiza acid	128	3.78 ± 1.6
Carvacrol	25	31.06 ± 0.31**		256	−4.23 ± 7.25
	50	54.99 ± 0.56**		512	22.27 ± 1.43**
	25	24.81 ± 11.36**	Aurantiamarin	120	−18.94 ± 3.01*
Polydatin	50	10.13 ± 0.44		240	−29.00 ± 9.15**
	100	12.66 ± 2.64*		480	−31.27 ± 10.7**
	6.25	17.41 ± 3.28**	Baicalin	128	−29.74 ± 3.83**
Saikosaponin A	12.5	12.77 ± 3.23**		256	−20.25 ± 2.30**
	25	17.92 ± 1.74**		512	−25.82 ± 3.67**
	128	15.40 ± 3.74**	Rutin	128	−8.22 ± 6.49
Atractylenolide	256	18.79 ± 2.38**		256	−19.80 ± 3.59**
	512	39.86 ± 1.70**		512	−13.32 ± 4.96*
Gallate	64	12.93 ± 1.46**	Puerarin	150	−19.28 ± 14.68*
	128	18.41 ± 4.02**		300	−11.52 ± 3.36
	256	25.73 ± 1.83**		600	0.14 ± 6.27
Calycosin-7-glucoside	128	−0.21 ± 4.80	Sophocarpidine	64	4.88 ± 1.46
	256	11.86 ± 1.78**		128	3.78 ± 1.10
	512	18.25 ± 1.87**		256	−1.71 ± 5.12

*$p < 0.05$; **$p < 0.01$ vs. Control. Values represent means ± SD ($n = 3$).*

acid, and myristic acid inhibited violacein production, and aurantiamarin, baicalin, and rutin promoted violacein production. The other compounds were found to be less effective. A turbid halo around the well on the purple pigmented agar plates was observed for protocatechualdehyde, anisic aldehyde, carvacrol, and paeonol (**Table 3** and **Figure 1**), which indicated a significant inhibition in violacein production without any growth inhibition. Paeonol was selected for further study owing to its excellent anti-QS activity.

In vitro Antimicrobial Activity of Paeonol

The antimicrobial activity of paeonol was evaluated by the MIC microdilution method. Gram negative strains are as follows: *C. violaceum*12472, *E. coli* 25922, *S. typhimurium* 14028, *A. baumannii* 17978, and *P. aeruginosa* PAO1. The MICs of paeonol against these strains were 512, 2,048, 1,024, 512, and 2,048 μg/mL, respectively. Paeonol exhibited an effective anti-bacteria activity against Gram-negative. But no obvious antibacterial effect on MRSA TCH1516. The sub-MIC concentration was selected to evaluate the anti-biofilm and anti-QS activity. Paeonol showed no growth-inhibition activity on *P. aeruginosa* when used at concentrations of 128–512 μg/mL, as determined using the growth curves (**Figure 2**).

Anti-biofilm Activity of Paeonol

Effect of Paeonol on Biofilm Formation

The results of the inhibitory effects of paeonol on biofilm formation on selected microorganisms are demonstrated in **Table 4**. Our results indicated that paeonol could decrease the biofilm-forming of Gram-negative bacteria *in vitro,* and the ability in the suppression of biofilm formation was as follows: *C. violaceum* 12472 > *P. aeruginosa* PAO1 > *S. typhimurium* 14028 > *A. baumannii* 17978 > *E. coli* 25922. The sub-MIC concentrations of paeonol were found to have a significant inhibitory effect on the biofilm formation at 36 h. The rates of inhibition also obtained using high concentration of paeonol were 73.75, 74.70, 29.22, 43.32, and 27.18% at 36 h, respectively, compared with the control group. Compared to the effects of selected concentrations on biofilm formation of four *P. aeruginosa* strains, 32.73–74.70, 31.04–67.94, 25.33–30.85, and 57.31–72.52% reduction in biofilm-forming were measured treated with paeonol against PAO1, ATCC 27853, ATCC 9027, and PAO3401, respectively. This study showed that paeonol inhibited the biofilm formation, thus reducing the resistance of bacterials to clinical antibiotics. There was no significant inhibitory effect on biofilm formation against *E. coli* 25922 and MRSA TCH1516. Based on the violacein inhibition and anti-biofilm of the pathogenic bacteria, paeonol was found to be an interesting ingredient against *P. aeruginosa* PAO1.

TABLE 3 | Anti-QS activity of compounds against *C. violaceum* 12472.

Test compounds	Zone of inhibition against *C. violaceum* ATCC 12472 (CV12472) (cm)		
	Total inhibition (d1)	Growth inhibition (d2)	Pigment inhibition (d1–d2)
Paeonol	2.33 ± 0.09	1.19 ± 0.03	1.14 ± 0.12
Aniseed aldehyde	2.53 ± 0.09	0.87 ± 0.09	1.67 ± 0.09
Protocatechuic aldehyde	2.93 ± 0.09	1.47 ± 0.09	1.47 ± 0.09
Carvacrol	5.47 ± 0.19	2.60 ± 0.16	2.87 ± 0.34

Values represent means ± SD (n = 3).

Effect of Paeonol on Biofilm Development of *P. aeruginosa*

The above anti-biofilm activity was further tested by light microscope and SEM. In the control experiment, the *P. aeruginosa* cells were not treated with the paeonol and a thick biofilm was found. However, compared with the control group, the concentrations of 128,256 and 512 μg/mL paeonol on the glass surface showed a significant reduction in microbial attachment (**Figure 3A**). The biofilm of *P. aeruginosa* showed a compact surface covered with intact rod-shaped cells. The bacterial cells treated with 128 and 256 μg/mL paeonol also showed normal morphology with clear and complete inner and outer membranes and thin and uniform periplasmic space. But the biofilm is significantly destroyed, which eliminates the basis for pathogenicity (**Figure 3B**). Based on these results, we concluded that paeonol could effectively inhibit the biofilm formation of *P. aeruginosa* PA01 without interfering its growth in the concentration range of 128–512 μg/mL.

Effect of Paeonol on Flagellar Motility Against *P. aeruginosa*

Swarming and swimming motility of *P. aeruginosa* was inhibited by paeonol at concentrations from 128 to 512 μg/mL. An increase in paeonol concentration led to a significant inhibitory effect on *P. aeruginosa* flagellar motility (**Figure 4**). 55.20, 52.88, 36.39, and 28.77% decrease in swarming motility was determined in the presence of 512 μg/mL paeonol against PAO1, ATCC 27853, ATCC 9027, and PAO3401, respectively. Treatment with paeonol (512 μg/ml) caused significant reduction of swimming motility (51.19, 68.52, 60.71, and 57.69%, respectively) against PAO1, ATCC 27853, ATCC 9027, and PAO3401 (**Figures 4A–F**). In this study, a dose-dependent decrease was observed in pyocyanin pigment on swarming and swimming motility plates of *P. aeruginosa* ATCC 27853. Interestingly, the outcome of biofilm reduction interrelated definitely with swarming and swimming inhibition, as motility plays a critical role in biofilm adhesion and development.

Effect of Paeonol on the Virulence Phenotypes of *P. aeruginosa*

Pyocyanin

The inhibitory effect of paeonol on the production of pyocyanin by *P. aeruginosa* was investigated. Pyocyanin production was significantly decreased by paeonol treatment in a concentration- and time-dependent manner. Paeonol at a concentration of 512 μg/mL was found to have the strongest inhibitory effect on pyocyanin; the rate of inhibition of pyocyanin at 18, 24, and 36 h were 37.19, 52.20, and 43.80%, respectively (**Figure 5**). Paeonol

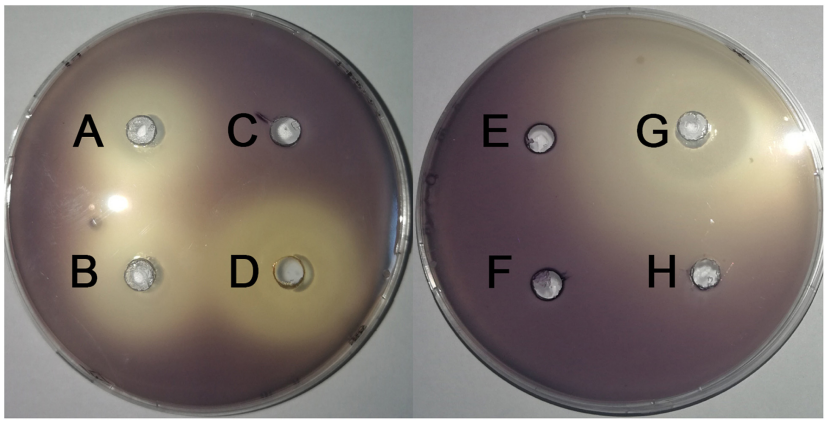


FIGURE 1 | Effects of compounds on the inhibition the violacein production on LB plates. **(A)** paeonol, **(B)** anisic aldehyde, **(C)** polydatin, **(D)** protocatechualdehyde, **(E)** gallate, **(F)** rutin, **(G)** carvacrol, and **(H)** DMSO.

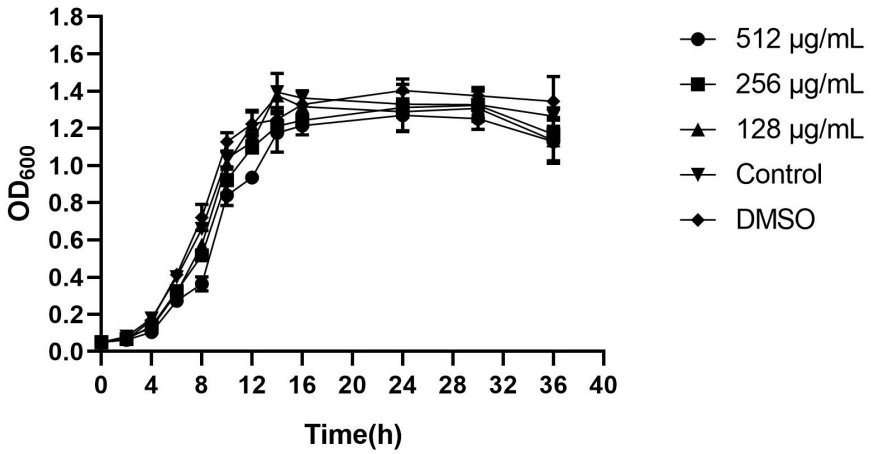


FIGURE 2 | Effects of paeonol on the growth of *Pseudomonas aeruginosa* (PAO1) at different concentrations. All data were expressed as means ± SD (n = 3).

exhibited relatively weak inhibitory effects on the production of pyocyanin at a concentration of 128 μg/mL.

Protease

The inhibitory ability of paeonol for QS-dependent protease activity was assessed. The extent of protease activity decreased with increasing concentrations of paeonol (128, 256, and 512 μg/mL). Compared with the control group, the rate of inhibition of the proteolytic enzymes with paeonol (512 μg/mL) was determined to be 33.43, 29.80, and 23.85% at 12, 18, and 24 h, respectively, and the inhibitory effect of paeonol was found to decrease over time (**Figure 6**).

Elastase

In the elastase activity assay, paeonol significantly inhibited the elastase production of PAO1 on all tested concentrations and the inhibitory effect of paeonol decreased over time. When the concentration of paeonol was 128–512 μg/mL, the elastase activity decreased by 22.59, 55.05, and 68.02% at 18 h, and by 16.48, 26.79, and 59.16% at 24 h, respectively. The results indicated a significantly inhibiting effect of paeonol on elastase activity of *P. aeruginosa* in a concentration- and time-dependent manner (**Figure 7**).

Rhamnolipids

Results from the quantitative analysis indicated that paeonol significantly inhibited rhamnolipid production by PAO1 at all tested concentrations in a concentration-dependent manner. In the presence of 128, 256, and 512 μg/mL paeonol, the levels of rhamnolipids decreased by 37.41, 60.50, and 66.27% at 24 h. At a paeonol concentration of 512 μg/mL, the inhibitory rates of rhamnolipids at 12, 18, and 24 h were 28.20, 52.25, and 66.27%, respectively, suggesting that the paeonol treatment resulted in the strongest inhibitory effect on rhamnolipids at 24 h (**Figure 8**).

Effect of Paeonol on AHL Synthesis Activity Against *P. aeruginosa*

N-acyl L-homoserine lactone-induced violacein from *C. violaceum* 026 was extracted from PAO1 culture that

TABLE 4 | Effect of sub-MICs of paeonol on inhibition of biofilm formation in bacterial microorganisms.

Bacterial microorganisms	Concentration (μg/mL)	Inhibition rate at 24 h (%)	Inhibition rate at 36 h (%)
Chromobacterium violaceum 12472	8	68.84 ± 2.21**	61.83 ± 5.46**
	16	73.10 ± 5.42**	71.33 ± 4.21**
	32	74.75 ± 3.10**	73.75 ± 1.28**
	128	40.43 ± 0.72**	32.73 ± 5.88**
Pseudomonas aeruginosa PAO1	256	56.49 ± 2.94**	59.04 ± 6.64**
	512	56.84 ± 3.36**	74.70 ± 4.00**
	128	33.06 ± 15.10**	31.04 ± 17.35**
Pseudomonas aeruginosa ATCC 27853	256	40.02 ± 9.06**	44.24 ± 1.99**
	512	46.08 ± 6.62**	67.94 ± 0.49**
	128	24.66 ± 7.88**	25.33 ± 13.31*
Pseudomonas aeruginosa ATCC 9027	256	31.79 ± 9.92**	30.27 ± 3.20*
	512	46.73 ± 9.02**	30.85 ± 11.36**
	128	8.34 ± 0.87**	57.31 ± 9.63**
PAO3401	256	22.40 ± 3.14**	67.34 ± 4.86**
	512	33.07 ± 2.93**	72.52 ± 0.84**
	32	36.81 ± 6.65**	23.55 ± 5.06**
Acinetobacter baumannii 17978	64	37.68 ± 4.85**	23.40 ± 5.55**
	128	54.08 ± 6.88**	29.22 ± 5.03**
	64	14.85 ± 1.59	24.78 ± 3.86**
Escherichia coli 25922	128	17.06 ± 6.89	23.39 ± 11.28**
	256	16.47 ± 7.92	27.18 ± 8.14**
	32	26.36 ± 3.55**	34.06 ± 11.32**
Salmonella typhimurium 14028	64	39.17 ± 0.68**	39.54 ± 7.00**
	128	45.27 ± 4.48**	43.32 ± 11.05**
	128	2.40 ± 7.14	10.35 ± 7.96
MRSA TCH1516	256	15.21 ± 8.42	12.11 ± 8.36
	512	26.31 ± 6.03**	17.88 ± 9.68

*$P < 0.05$; **$P < 0.01$ vs. Control. Values represent means ± SD ($n = 3$).

was treated with different concentrations of paeonol. The purple shades of signal molecules at different drug concentrations and various time periods were compared, AHL-mediated production and activity of purple pigment in CV026 were lower in the presence of paeonol, and an obvious inhibition in pigment production was observed upon treatment with paeonol at 18 and 24 h (**Figures 9A,B**). Quorum sensing signal increased over time was observed, thus, paeonol could effectively inhibit the formation of PAO1 signal molecules in a concentration- and time-dependent manner (**Figure 9C**). These results indicated paeonol interfered with QS mediated virulence expression of *P. aeruginosa* by reducing the synthesis of AHLs.

Effect of Paeonol on the Expression of *P. aeruginosa* QS-Regulated Genes

Fluorescence real-time PCR was used to determine the expression of QS-regulated genes in *P. aeruginosa* to elucidate the QS-regulating effect of paeonol at the transcriptional level. Our findings indicated that QS-related genes were downregulated. The rates of inhibition in the presence of paeonol (512 μg/mL) at 18 h were as follows: *lasI* 56.60%, *lasR* 49.61%, *rhlI* 35.91%, *rhlR* 38.97%, *pqsA* 42.95%, and *pqsR* 52.65%, *lasA* 57.83%, *lasB* 52.52%, *rhlA* 44.82%, *rhlC* 43.57%, *phzA* 37.01%, *phzM* 33.60%, *phzH* 41.30%, and *phzS* 25.86% (**Figures 10A,B**). These results indicated that the paeonol-treated group had the strongest inhibitory effect on QS-related gene expression at 18 h, and that the inhibitory effect of paeonol reduced over time. With the increase of the concentration of paeonol, the inhibition of QS target genes (*lasI*, *lasR*, *rhlI*, *rhlR*, *pqsA*, and *pqsR*) and their mediated virulence factors (*lasA*, *lasB*, *rhlA*, *rhlC*, *phzA*, *phzM*, *phzH*, and *phzS*) of *las*, *rhl*, and *pqs* system was enhanced, while 128 μg/mL paeonol resulted in the most significant reduction in *pqs* system at 18 h. The inhibitory effect of paeonol on PAO1 was in concentration- and time-dependent manner, and it may attenuate virulence by interfering with the QS pathway of *P. aeruginosa*.

Effect of Paeonol on the Survival of *P. aeruginosa* Infected *C. elegans*

Pseudomonas aeruginosa accumulates and produces virulence factors in the gut of *C. elegans* to kill nematodes. The protective

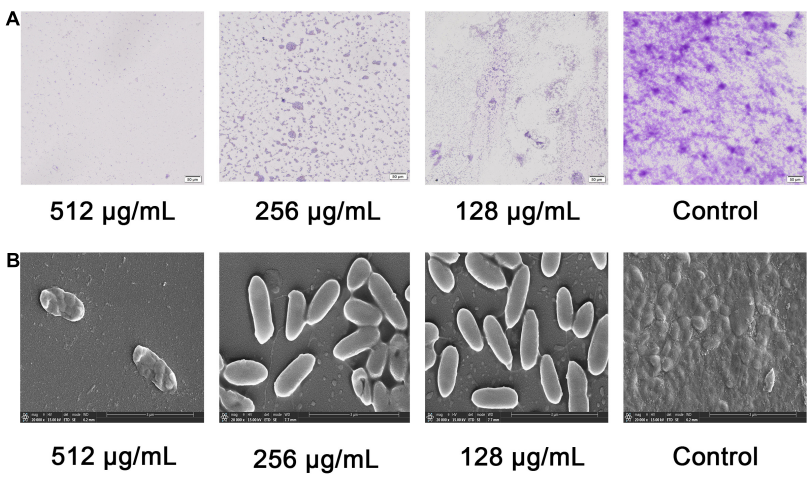


FIGURE 3 | Effects of paeonol on biofilm formation of *P. aeruginosa* (PAO1) at different concentrations. **(A)** Light microscopic images and **(B)** SEM images.

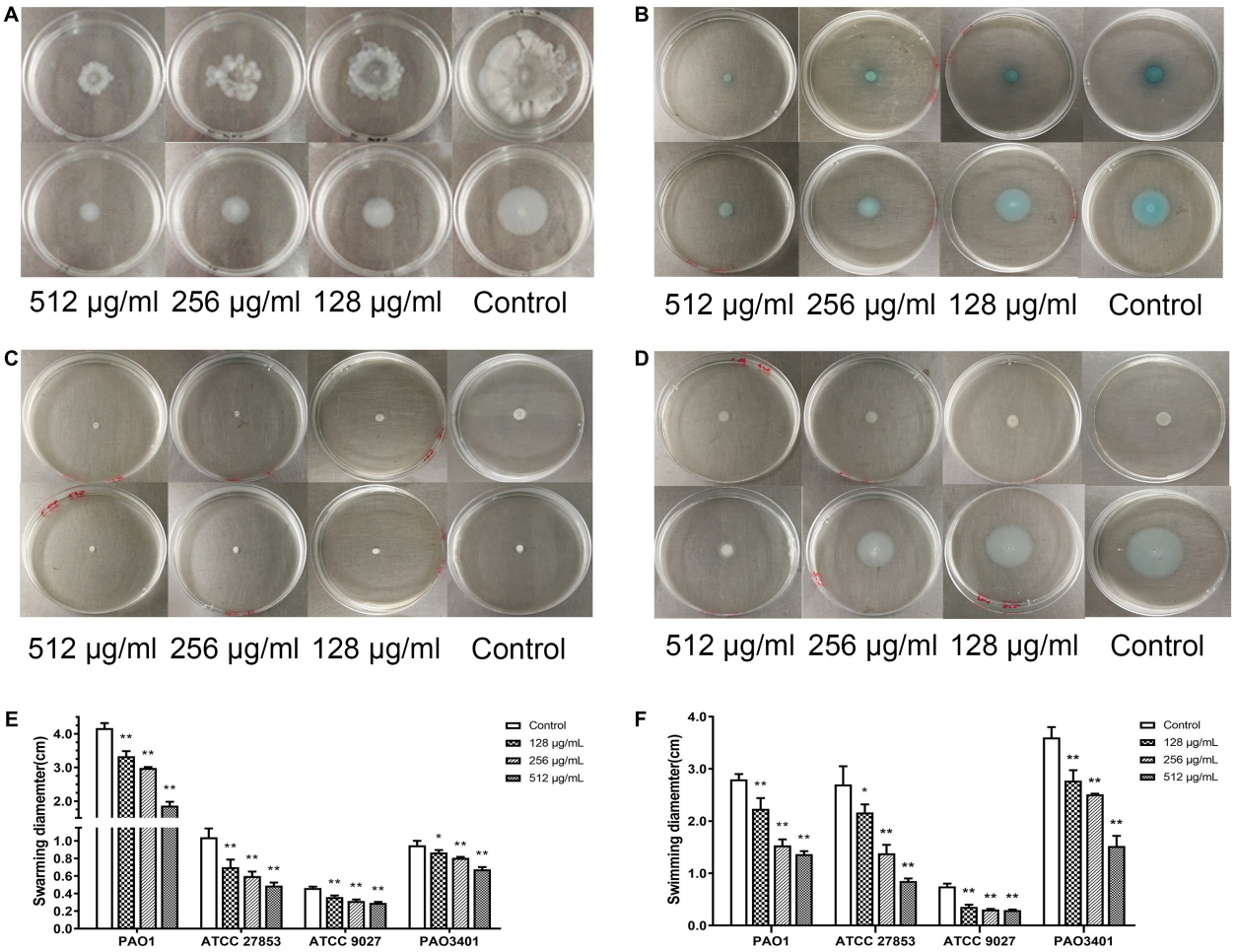


FIGURE 4 | Effect of sub-MICs of paeonol on inhibition of motility in *P. aeruginosa*. *P. aeruginosa* was spotted on a plate supplemented with different concentration paeonol for 24 h by analyzing the swarming motility and swimming motility of PAO1 **(A)**, ATCC 27853 **(B)**, ATCC 9027 **(C)**, and PAO3401 **(D)**, the swarming and swimming diameter statistics **(E,F)**. All data were expressed as means ± SD ($n = 3$). *$p < 0.05$ and **$p < 0.01$ versus the control group.

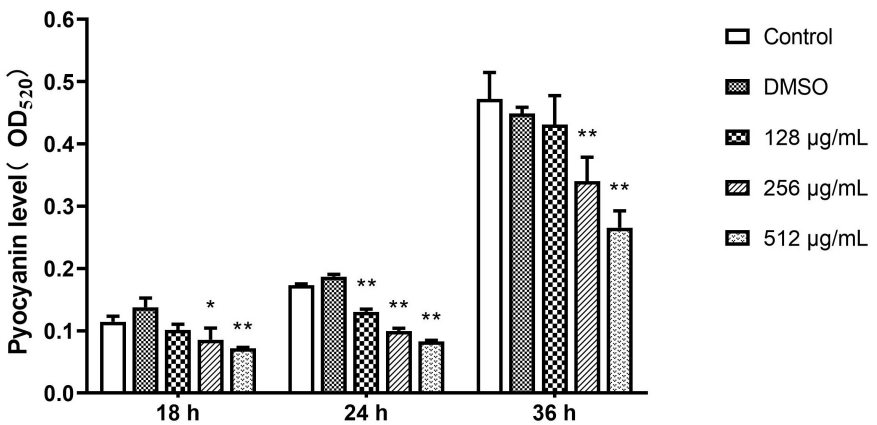


FIGURE 5 | Effect of sub-MICs of paeonol on inhibition of pyocyanin production in *P. aeruginosa* (PAO1). All data were expressed as means ± SD ($n = 3$). *$p < 0.05$ and **$p < 0.01$ versus the control group.

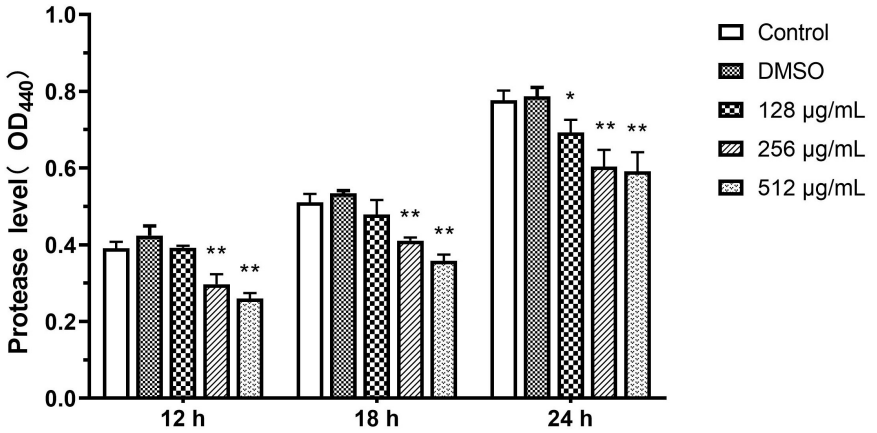


FIGURE 6 | Effect of sub-MICs of paeonol on inhibition of protease activity in *P. aeruginosa* (PAO1). All data were expressed as means ± SD ($n = 3$). $^{*}p < 0.05$ and $^{**}p < 0.01$ versus the control group.

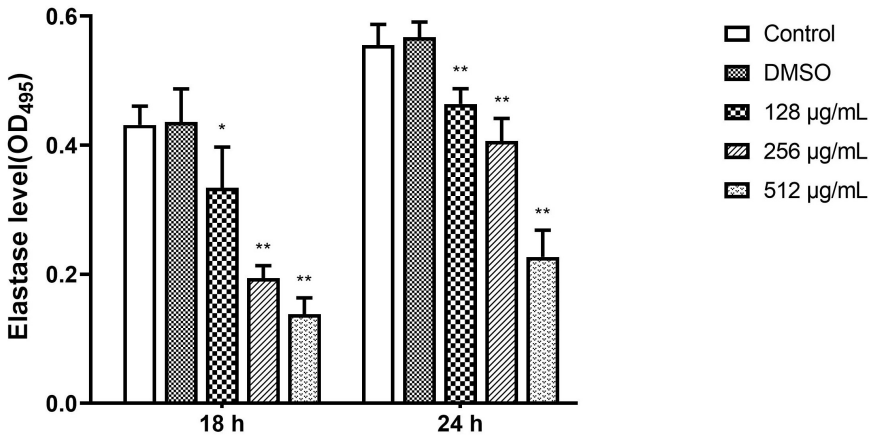


FIGURE 7 | Effect of sub-MICs of paeonol on inhibition of elastase activity in *P. aeruginosa* (PAO1). Elastase activity in *P. aeruginosa* (PAO1) cultured in LB and LB supplemented with different concentration paeonol for 18 h and 24 h were measured by elastin congo red. All data were expressed as means ± SD ($n = 3$). $^{*}p < 0.05$ and $^{**}p < 0.01$ versus the control group.

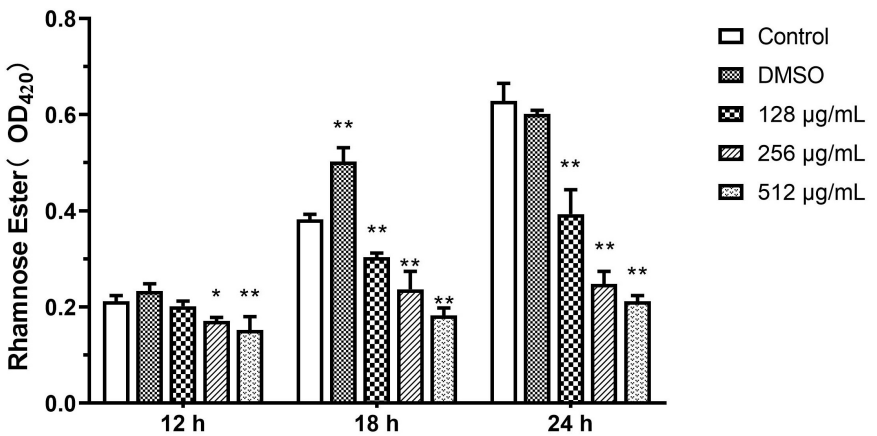


FIGURE 8 | Effect of sub-MICs of paeonol on inhibition of rhamnolipids production in *P. aeruginosa* (PAO1). All data were expressed as means ± SD ($n = 3$). $^{*}p < 0.05$ and $^{**}p < 0.01$ versus the control group.

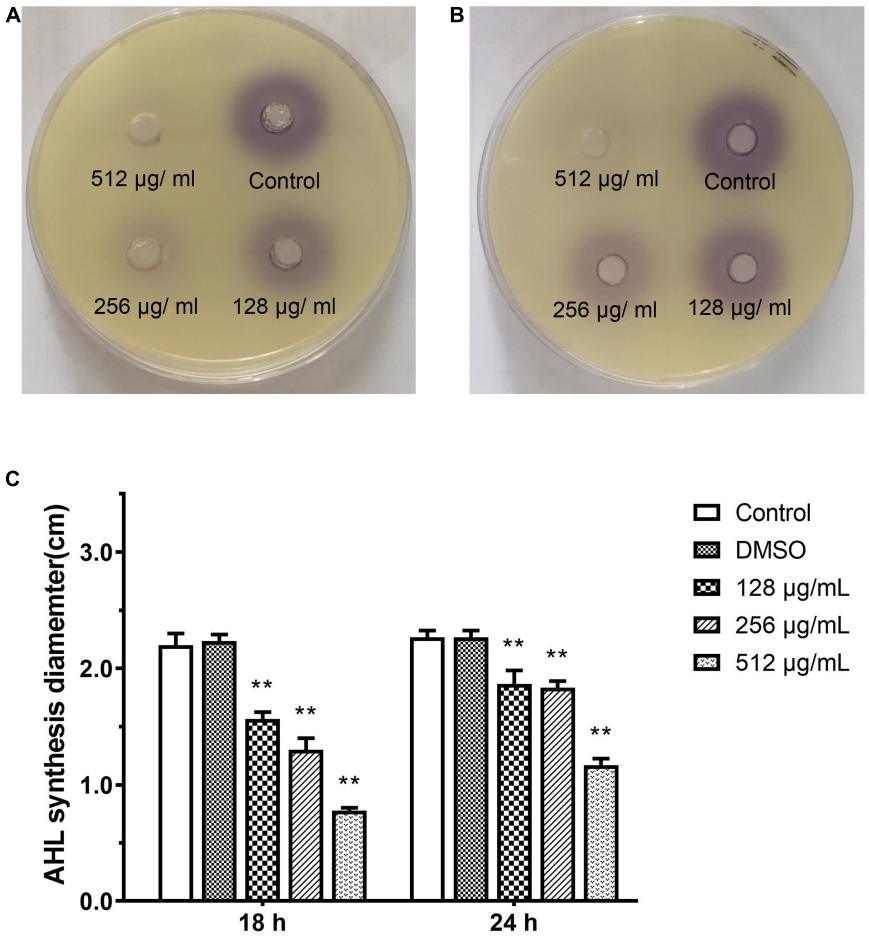


FIGURE 9 | Effect of sub-MICs of paeonol on inhibition of AHL synthesis activity in *P. aeruginosa* (PAO1). Assessment of AHL synthesis activity in *P. aeruginosa* (PAO1) cultured in LB and LB supplemented with different concentration paeonol for 18 h **(A)** and 24 h **(B)** the AHL synthesis diameter statistics **(C)**. All data were expressed as means ± SD ($n = 3$). $^{**}p < 0.01$ versus the control group.

effect of paeonol on *P. aeruginosa* infection model of *C. elegans* was further studied. In comparison, *C. elegans* infected by *P. aeruginosa* after treatment with paeonol could significantly improve their survival. In the absence of paeonol, the mortality of *C. elegans* reached 100% after 7 days of PAO1 pathogenicity. The survival rate of *C. elegans* infected with PAO1 were increased about 23.02 and 32.48% when treated by paeonol at the concentrations of 128 and 256 μg/mL. In particular, after 6 days of incubation with paeonol at a concentration of 256 μg/mL, the rate of survival of *C. elegans* N2 was the highest and was found to increase by 38.14% (**Figure 11A**). Paeonol did not affect the growth of *C. elegans* at the experimental concentrations.

Paeonol Affect the Viability of IPEC-J2 Cells

For assessing the cytotoxicity of paeonol on IPEC-J2 cells, CCK-8 assay was performed to determine their appearance following treatment with different doses (0, 16, 32, 64, 128, 256, 512, and 1,024 μg/ml) of paeonol for 24 h. Paeonol inhibited the proliferation of cells dose-dependently. The results showed that at the highest concentrations of paeonol (1,024 μg/mL), IPEC-J2 cells viability was 63.08% compared with control. At the lowest concentrations tested (0–256 μg/mL), IPEC-J2 cell viability was unaltered by paeonol (**Figure 11B**).

DISCUSSION

Many bacteria sense and communicate with each other through quorum sensing, a gene regulatory mechanism that depends on cell density (Waters and Bassler, 2005). Several naturally occurring compounds have been screened for their anti-QS and anti-biofilm activities in *C. violaceum* (Paczkowski et al., 2017; Zhong et al., 2020). Some potential compounds with anti-QS activity were identified in the preliminary screening, including protocatechualdehyde, anisic aldehyde, carvacrol, and paeonol. Paeonol showed no inhibition in the growth of *C. violaceum* at concentrations of 12.5–50 μg/mL, and production of the AHL-dependent pigment was reduced by nearly 38% at 50 μg/mL, which indicated that paeonol interfered with the QS pathway.

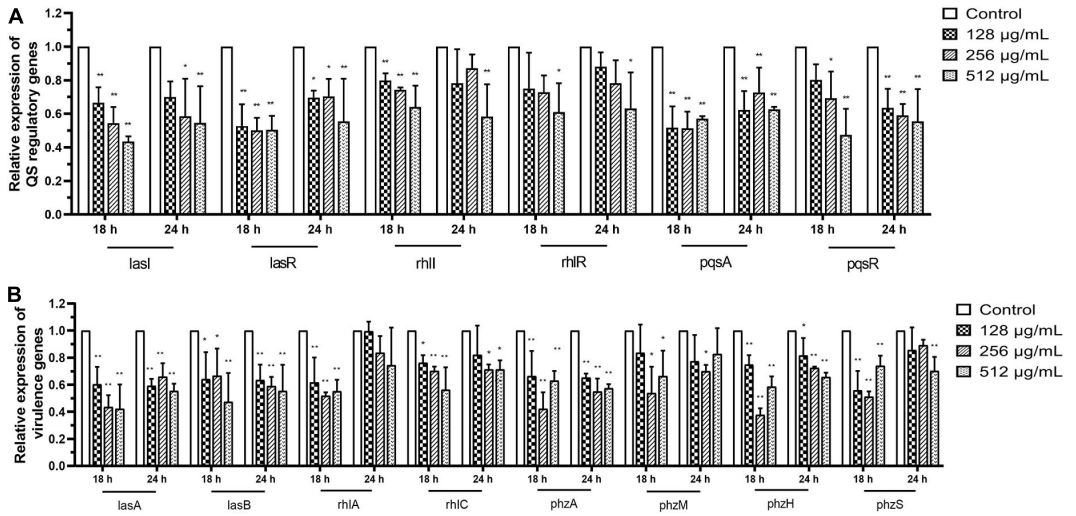


FIGURE 10 | Transcriptional levels of the QS-related **(A)** and virulence genes **(B)** in *P. aeruginosa* with different concentrations paeonol for compared with untreated control at 18 and 24 h were detected by q-PCR. All data were expressed as means ± SD ($n = 3$). $^{*}p < 0.05$ and $^{**}p < 0.01$ versus the control group.

Snoussi et al. (2018) have reported that the essential oils and phenolics of *Carum copticum* inhibit violacein production. Similar results also have been reported for the phenolic compounds from plants (Mostafa et al., 2020). There are three QS systems in bacteria: the LuxR/I-type systems, typically used by Gram-negative species, in which the signaling molecule is an *N*-acyl L-homoserine lactone (AI-1); the small oligopeptides (AIP) systems, typically used by Gram-positive species; and the LuxS/furanone metabolites (AI-2) interspecies signaling systems (Galloway et al., 2011; Hawver et al., 2016). Paeonol had shown antibacterial activity against Gram-negative bacteria and interesting disruptive properties against biofilm formation in pathogenic bacterial strains: *C. violaceum*, *P. aeruginosa*, and *A. baumannii*. AHL-mediated quorum sensing is known to play an important role in the formation, development and maturation of biofilms. Therefore, paeonol may penetrate bacterial biofilm interferes with cell signaling and inhibits the QS of most biofilm-related cells. Paeonol reduced the AHL dependent production of violacein and biofilm formation revealed that it interfered with QS systems of Gram-negative pathogens containing various AHL molecules, exhibiting broad-spectrum anti-QS activity. Lv et al. (2020) reported that paeonol could treat *S. typhimurium* infection through the type III secretion system. It was found that paeonol had anti-biofilm-forming activity in *S. typhimurium*, which could be a potential target for anti-infected. Jiao et al. (2016) confirmed that the PDMS surface of paeonol coating showed excellent antibacterial and anticancer activity against Gram-negative and Gram-positive bacteria. The results showed that paeonol could be used as a potential coating material against bacterial biofilm in the industrial environment and on the surface of medical instruments.

Pseudomonas aeruginosa is a prevalent hospital-acquired opportunistic pathogen that causes cystic fibrosis. Its pathogenic mechanism is associated with the production of QS-regulated virulence factors and biofilm formation (Sadikot et al., 2005; Ciofu et al., 2015; Azam and Khan, 2019). Compared with that in the untreated PAO1 group, paeonol treatment (128–512 μg/mL) in the experimental group did not result in a direct bactericidal effect, but significantly inhibited the biofilm formation, virulence phenotypes and motility in a concentration- and time-dependent manner. Previous studies have confirmed that phenolic compounds from plants, such as eugenol, tea polyphenols, and thymol, can inhibit the production of virulence-associated factors and biofilm formation in *P. aeruginosa* (Yin et al., 2015; Walsh et al., 2019; Antunes et al., 2021). Scanning electron microscopy results further demonstrated that paeonol decreased biofilm formation against *P. aeruginosa*, possibly interfered with the subsequent steps of surface adhesion or biofilm formation (Pederson et al., 2018; Liu et al., 2019). Additionally, the motility of *P. aeruginosa* is a complex process that is co-regulated by the *las* and *rhl* systems to promote the formation and spread of biofilms (Glessner et al., 1999). *In vitro* studies demonstrated that different concentration of paeonol influenced not only motility of *P. aeruginosa* but also the capability to form biofilm. The results of biofilm formation and flagellar motility demonstrated that paeonol had differences in terms of activity with respect to different strains of *P. aeruginosa*. Our findings indicated that paeonol significantly inhibited the motility of *P. aeruginosa*, suggesting that its inhibitory effect was likely by interfering with QS or by directly acting on the flagella and Type IV pili (Anyan et al., 2014).

Pyocyanin production is controlled by two QS pathways (*rhl* and *pqs*) in *P. aeruginosa* and can interfere with various cellular functions such as chelated iron absorption and respiration (Diggle et al., 2003; Chang et al., 2014). Similarly, paeonol inhibited pyocyanin production in a dose-dependent manner, and the highest inhibition rate was found to be 52.20% at a concentration of 512 μg/mL. Similar inhibitory effects were observed on its QS-regulated gene *rhlI/R* and *pqsA/R*. Protease and elastase are regulated by *lasA* and *lasB* genes, respectively, for

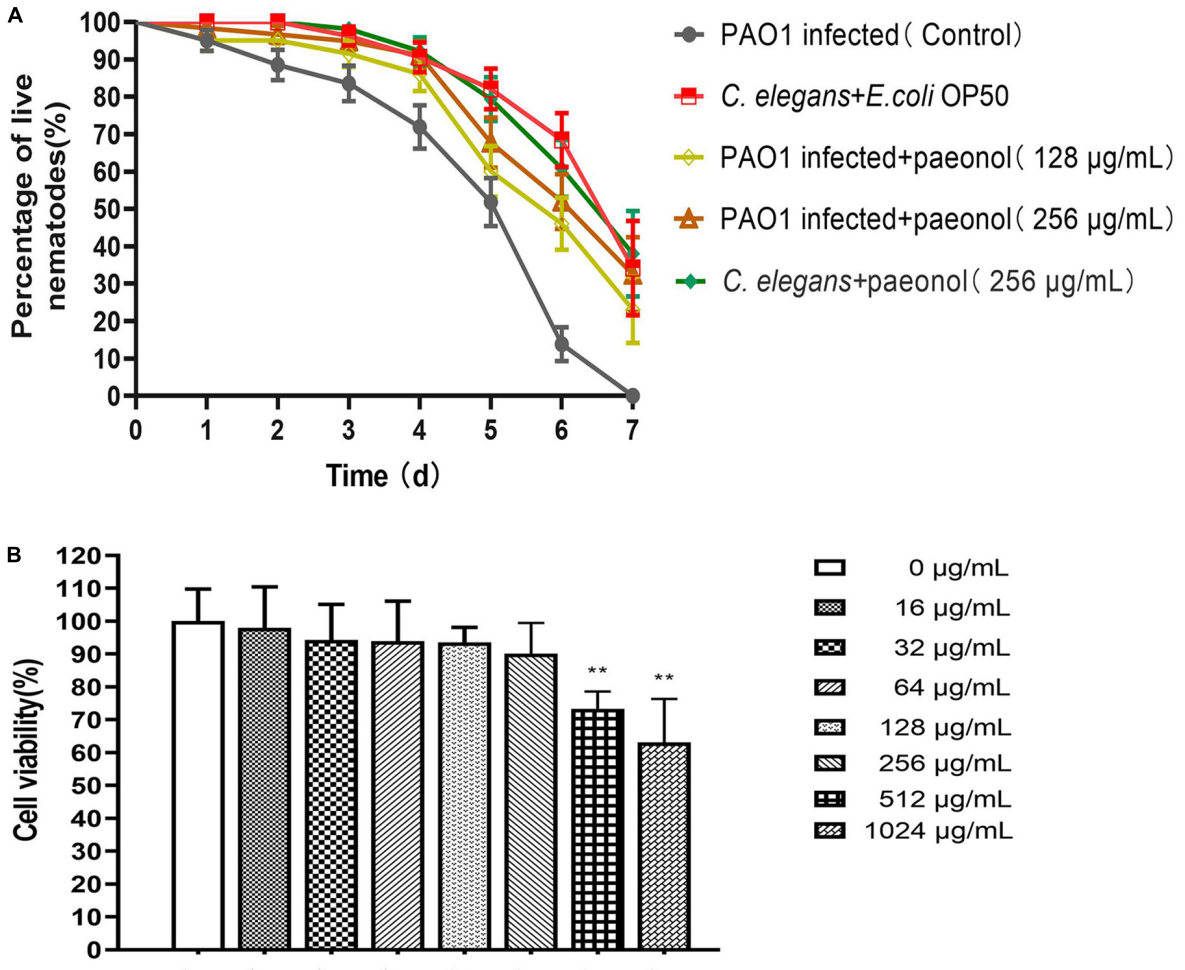


FIGURE 11 | The effect of paeonol on the survival of C. elegans infected with *P. aeruginosa* **(A)**. Effect of different concentrations (0–1,024 μg/mL) of paeonol on IPEC-J2 cell viability activity **(B)**. All data were expressed as means ± SD ($n = 3$). $^{**}p < 0.01$ versus the control group.

the growth and invasion of *P. aeruginosa*, and play an important role in different stages of bacterial colonization and pathogenicity (Husain et al., 2017). With an increase in incubation time, the rate of inhibition of *lasA* protease using 512 μg/mL of paeonol was 23.85–33.43%, whereas that of *lasB* protease was 59.16–68.02%. Rhamnolipids that are synthesized by rhamnolipid synthases *rhlA* and *rhlB* promote the formation and diffusion of biofilms and also kill the polymorphonuclear white blood cells in patients with CF (Bazire and Dufour, 2014). With an increase in culture time, the rate of inhibition of rhamnose achieved using 512 μg/mL of paeonol ranged from 28.20 to 66.27%.

Results from the AHL activity assay showed that the anti-QS activity of paeonol against *P. aeruginosa* may likely result from the binding between AHL and the receptor protein (Smith and Iglewski, 2003; Kaufmann et al., 2006). The QS mechanism on expression at the gene level was further explored, the outcome revealed that paeonol had an obvious inhibitory effect on the QS-related genes, *lasI/R, rhlI/R, pqs/mvfR*, and their mediated virulence factors, *lasA, lasB, rhlA, rhlC, phzA, phzM, phzH, and phzS*. Thus, Paeonol could inhibit the major lactones (C4-HSL, 3-oxo-C12-HSLs, and PQS) that regulated the expression of virulence factors produced by *P. aeruginosa*. These data corroborated with the previous literature where, virulence phenotypes, QS-related genes and biofilm formation of *P. aeruginosa* was descreaced to varying levels by plant-derived compounds and phenolic compounds (Rudrappa and Bais, 2008; Vandeputte et al., 2010; Mok et al., 2020; Rather et al., 2021). The reason may be attributed to the fact that *P. aeruginosa* has a complex QS regulating network, including three main QS circuits, and *las*, the master regulator that induces the expression of both *rhl* and *pqs* (Deziel et al., 2004). The results indicated that paeonol may play a role in multiple targets through QS interference.

Previous research had shown that QS inhibitors block the virulence and biofilm formation of *P. aeruginosa*, protecting *C. elegans* and human lung epithelial cells (O'Loughlin et al., 2013). Therefore, *C. elegans* was used to assess the protective effects of paeonol *in vivo* against *P. aeruginosa* because of the susceptibility to different virulent phenotypes of this bacterium (Tan et al., 1999a; Martin et al., 2017). *P. aeruginosa*

accumulates and produces virulence factors, such as pyocyanin, in the intestines of nematodes, which is lethal. Although our research showed that 512 μg/mL paeonol had the most anti-quorum sensing activity on PAO1 *in vitro*, the QS inhibitory concentration is too high when it reaches the clinical treatment level *in vivo*. Therefore, 128–256 μg/ml of paeonol was selected to evaluate the protection of C. elegans infected with PAO1. Paeonol exhibited a significant protective effect at a dose of 256 μg/mL, and the survival rate of the nematodes increased by 38.14% on day 6, shown its anti-infected ability. These results demonstrated paeonol (128–256 μg/mL) could attenuate some virulence factors of *P. aeruginosa* and reduce the pathogenicity of *P. aeruginosa* to improve the survival rate of infected nematodes. In cytotoxicity study, paeonol inhibited IPEC-J2 viability in a dependent manner but had no cytotoxicity in the range of 0–256 μg/mL. Previous studies demonstrated that intragastric LD_{50} value of paeonol in mice is 3,430 mg/kg, which indicated that the toxicity of paeonol is relatively low (Harada and Yamashita, 1969). But the recommended dose of paeonol for the treatment of clinical *P. aeruginosa* infection is 128–256 μg/mL based on the result of viability of IPEC-J2 cells. The anti-virulence mechanism of paeonol against *P. aeruginosa* should be conducted and evaluated if higher doses are more effective *in vivo* by animal experiments in future studies. Its clinical application requires considerable safety and efficacy data.

CONCLUSION

In the present study, protocatechualdehyde, anisic aldehyde, carvacrol, and paeonol displayed excellent anti-QS activity. The preliminary screening compounds results provide a platform for exploring QS inhibitors. Taken together, paeonol downregulated the virulence phenotypes by regulating the expression of QS related genes in *P. aeruginosa*. Paeonol attenuated the virulence of *P. aeruginosa* and increased the survival of *C. elegans in vivo*. In addition, paeonol exhibited significant anti-biofilm activity against Gram-negative species including *C. violaceum, P. aeruginosa,* and *A. baumannii*, further demonstrating the potential clinical importance. Hence, paeonol is a promising QSI to be developed a novel and extremely effective anti-virulence and anti-infective drugs. Further research is necessary to elucidate the clinical utility of paeonol against other multi-drug resistance bacteria.

DATA AVAILABILITY STATEMENT

The raw data supporting the conclusions of this article will be made available by the authors, without undue reservation.

AUTHOR CONTRIBUTIONS

DY and HT designed the experimental approach and wrote the manuscript. SH, LZ, FS, GY, YZ, XS, LL, SF, and ZY refined the experimental protocols. DY, SH, and HT performed the animal experiments, physicochemical analyses of particle suspensions. DY prepared the draft. YL and HT made some revision. All authors reviewed and approved the final manuscript.

FUNDING

The following grants information was disclosed by the authors: Sichuan Science and Technology Program: 2020YFH0143 and Traditional Chinese Veterinary Medicine Laboratory of the National Ethnic Affairs Commission [2020] 03.

ACKNOWLEDGMENTS

We want to thank Sichuan Agricultural University provide necessary materials used for experiments.

REFERENCES

Adonizio, A., Kong, K., and Mathee, K. (2008). Inhibition of quorum sensing-controlled virulence factor production in *Pseudomonas aeruginosa* by South Florida plant extracts. *Antimicrob. Agents Chemother.* 52, 198–203.

Antunes, J. C., Tavares, T. D., Teixeira, M. A., Teixeira, M. O., Homem, N. C., Amorim, M., et al. (2021). Eugenol-containing essential oils loaded onto chitosan/polyvinyl alcohol blended films and their ability to eradicate *Staphylococcus aureus* or *Pseudomonas aeruginosa* from infected microenvironments. *Pharmaceutics* 13:195. doi: 10.3390/pharmaceutics13020195

Anyan, M. E., Amiri, A., Harvey, C. W., Tierra, G., Morales-Soto, N., Driscoll, C. M., et al. (2014). Type IV pili interactions promote intercellular association and moderate swarming of *Pseudomonas aeruginosa*. *Proc. Natl. Acad. Sci. U.S.A.* 111, 18013–18018. doi: 10.1073/pnas.1414661111

Azam, M. W., and Khan, A. U. (2019). Updates on the pathogenicity status of *Pseudomonas aeruginosa*. *Drug Discov. Today* 24, 350–359. doi: 10.1016/j.drudis.2018.07.003

Bassler, B. L., Wright, M., Showalter, R. E., and Silverman, M. R. (1993). Intercellular signalling in *Vibrio harveyi*: sequence and function of genes regulating expression of luminescence. *Mol. Microbiol.* 9, 773–786. doi: 10.1111/j.1365-2958.1993.tb01737.x

Bazire, A., and Dufour, A. (2014). The *Pseudomonas aeruginosa* rhlG and rhlAB genes are inversely regulated and RhlG is not required for rhamnolipid synthesis. *BMC Microbiol.* 14:160. doi: 10.1186/1471-2180-14-160

Blosser, R. S., and Gray, K. M. (2000). Extraction of violacein from *Chromobacterium violaceum* provides a new quantitative bioassay for N-acyl homoserine lactone autoinducers. *J. Microbiol. Methods* 40, 47–55. doi: 10.1016/s0167-7012(99)00136-0

Boucher, H. W., Talbot, G. H., Bradley, J. S., Edwards, J. E., Gilbert, D., Rice, L. B., et al. (2009). Bad bugs, no drugs: no ESKAPE! An update from the infectious diseases society of America. *Clin. Infect. Dis.* 48, 1–12. doi: 10.1086/595011

Chang, C. Y., Krishnan, T., Wang, H., Chen, Y., Yin, W. F., Chong, Y. M., et al. (2014). Non-antibiotic quorum sensing inhibitors acting against N-acyl homoserine lactone synthase as druggable target. *Sci. Rep.* 4:7245. doi: 10.1038/srep07245

Chong, Y. M., Yin, W. F., Ho, C. Y., Mustafa, M. R., Hadi, A. H., Awang, K., et al. (2011). Malabaricone C from *Myristica cinnamomea* exhibits anti-quorum sensing activity. *J. Nat. Prod.* 74, 2261–2264. doi: 10.1021/np100872k

Ciofu, O., Tolker-Nielsen, T., Jensen, P. O., Wang, H., and Hoiby, N. (2015). Antimicrobial resistance, respiratory tract infections and role of biofilms in lung infections in cystic fibrosis patients. *Adv. Drug Deliv. Rev.* 85, 7–23. doi: 10.1016/j.addr.2014.11.017

Clinical and Laboratory Standards Institute (2012). *Methods for Dilution Antimicrobial Susceptibility Tests for Bacteria That Grow Aerobically*, 9th Edn. Wayne, PA: CLSI.

Davies, D. G., Parsek, M. R., Pearson, J. P., Iglewski, B. H., Costerton, J. W., and Greenberg, E. P. (1998). The involvement of cell-to-cell signals in the development of a bacterial biofilm. *Science* 280, 295–298. doi: 10.1126/science.280.5361.295

Deziel, E., Lepine, F., Milot, S., He, J., Mindrinos, M. N., Tompkins, R. G., et al. (2004). Analysis of *Pseudomonas aeruginosa* 4-hydroxy-2-alkylquinolines (HAQs) reveals a role for 4-hydroxy-2-heptylquinoline in cell-to-cell communication. *Proc. Natl. Acad. Sci. U.S.A.* 101, 1339–1344. doi: 10.1073/pnas.0307694100

Diggle, S. P., Winzer, K., Chhabra, S. R., Worrall, K. E., Camara, M., and Williams, P. (2003). The *Pseudomonas aeruginosa* quinolone signal molecule overcomes the cell density-dependency of the quorum sensing hierarchy, regulates rhl-dependent genes at the onset of stationary phase and can be produced in the absence of LasR. *Mol. Microbiol.* 50, 29–43. doi: 10.1046/j.1365-2958.2003.03672.x

Dunne, W. M. J. (2002). Bacterial adhesion: seen any good biofilms lately? *Clin. Microbiol. Rev.* 15, 155–166.

Fuqua, C., and Greenberg, E. P. (2002). Listening in on bacteria: acyl-homoserine lactone signalling. *Nat. Rev. Mol. Cell Biol.* 3, 685–695.

Galloway, W. R. J. D., Hodgkinson, J. T., Bowden, S. D., Welch, M., and Spring, D. R. (2011). Quorum sensing in Gram-negative bacteria: small-molecule modulation of AHL and AI-2 quorum sensing pathways. *Chem. Rev.* 111, 28–67. doi: 10.1021/cr100109t

Glamoclija, J., Stojkovic, D., Nikolic, M., Ciric, A., Reis, F. S., Barros, L., et al. (2015). A comparative study on edible *Agaricus* mushrooms as functional foods. *Food Funct.* 6, 1900–1910. doi: 10.1039/c4fo01135j

Glessner, A., Smith, R. S., Iglewski, B. H., and Robinson, J. B. (1999). Roles of *Pseudomonas aeruginosa* las and rhl quorum-sensing systems in control of twitching motility. *J. Bacteriol.* 181, 1623–1629. doi: 10.1128/JB.181.5.1623-1629.1999

Grosso-Becerra, M. V., Gonzalez-Valdez, A., Granados-Martinez, M. J., Morales, E., Servin-Gonzalez, L., Mendez, J. L., et al. (2016). *Pseudomonas aeruginosa* ATCC 9027 is a non-virulent strain suitable for mono-rhamnolipids production. *Appl. Microbiol. Biotechnol.* 100, 9995–10004. doi: 10.1007/s00253-016-7789-9

Harada, M., and Yamashita, A. (1969). Pharmacological studies on the root bark of paeonia moutan. I. Central effects of paeonol. *Yakugaku zasshi* 89, 1205–1211. doi: 10.1248/yakushi1947.89.9_1205

Hassett, D. J., Sutton, M. D., Schurr, M. J., Herr, A. B., Caldwell, C. C., and Matu, J. O. (2009). *Pseudomonas aeruginosa* hypoxic or anaerobic biofilm infections within cystic fibrosis airways. *Trends Microbiol.* 17, 130–138. doi: 10.1016/j.tim.2008.12.003

Hawver, L. A., Jung, S. A., and Ng, W. (2016). Specificity and complexity in bacterial quorum-sensing systems. *FEMS Microbiol. Rev.* 40, 738–752. doi: 10.1093/femsre/fuw014

Hentzer, M., Riedel, K., Rasmussen, T. B., Heydorn, A., Andersen, J. B., Parsek, M. R., et al. (2002). Inhibition of quorum sensing in *Pseudomonas aeruginosa* biofilm bacteria by a halogenated furanone compound. *Microbiology* 148(Pt 1), 87–102. doi: 10.1099/00221287-148-1-87

Hernando-Amado, S., Sanz-Garcia, F., and Martinez, J. L. (2019). Antibiotic resistance evolution is contingent on the quorum-sensing response in *Pseudomonas aeruginosa*. *Mol. Biol. Evol.* 36, 2238–2251. doi: 10.1093/molbev/msz144

Huang, H., Shao, X., Xie, Y., Wang, T., Zhang, Y., Wang, X., et al. (2019). An integrated genomic regulatory network of virulence-related transcriptional factors in *Pseudomonas aeruginosa*. *Nat. Commun.* 10:2931. doi: 10.1038/s41467-019-10778-w

Husain, F. M., Ahmad, I., Al-Thubiani, A. S., Abulreesh, H. H., AlHazza, I. M., and Aqil, F. (2017). Leaf extracts of mangifera indica l. Inhibit quorum sensing – regulated production of virulence factors and biofilm in test bacteria. *Front. Microbiol.* 8:727. doi: 10.3389/fmicb.2017.00727

Ilangovan, A., Fletcher, M., Rampioni, G., Pustelny, C., Rumbaugh, K., Heeb, S., et al. (2013). Structural basis for native agonist and synthetic inhibitor recognition by the *Pseudomonas aeruginosa* quorum sensing regulator PqsR (MvfR). *PLoS Pathog.* 9:e1003508. doi: 10.1371/journal.ppat.1003508

Ismail, A. S., Valastyan, J. S., and Bassler, B. L. (2016). A host-produced autoinducer-2 mimic activates bacterial quorum sensing. *Cell Host Microbe* 19, 470–480. doi: 10.1016/j.chom.2016.02.020

Jiao, J., Sun, L., Guo, Z., Hou, S., Holyst, R., Lu, Y., et al. (2016). Antibacterial and anticancer PDMS surface for mammalian cell growth using the Chinese herb extract paeonol(4-methoxy-2-hydroxyacetophenone). *Sci. Rep.* 6:38973. doi: 10.1038/srep38973

Jorgensen, J. H. (1993). Antimicrobial susceptibility testing of bacteria that grow aerobically. *Infect. Dis. Clin. North Am.* 7, 393–409.

Kaufmann, G. F., Sartorio, R., Lee, S. H., Mee, J. M., Altobell, L. R., Kujawa, D. P., et al. (2006). Antibody interference with N-acyl homoserine lactone-mediated bacterial quorum sensing. *J. Am. Chem. Soc.* 128, 2802–2803. doi: 10.1021/ja0578698

Khan, M. S., Zahin, M., Hasan, S., Husain, F. M., and Ahmad, I. (2009). Inhibition of quorum sensing regulated bacterial functions by plant essential oils with special reference to clove oil. *Lett. Appl. Microbiol.* 49, 354–360. doi: 10.1111/j.1472-765X.2009.02666.x

Lee, J. H., Cho, M. H., and Lee, J. (2011). 3-Indolylacetonitrile decreases *Escherichia coli* O157:H7 biofilm formation and *Pseudomonas aeruginosa* virulence. *Environ. Microbiol.* 13, 62–73. doi: 10.1111/j.1462-2920.2010.02308.x

Liu, Y., Jiang, Y., Zhu, J., Huang, J., and Zhang, H. (2019). Inhibition of bacterial adhesion and biofilm formation of sulfonated chitosan against *Pseudomonas aeruginosa*. *Carbohyd. Polym.* 206, 412–419. doi: 10.1016/j.carbpol.2018.11.015

Lv, Q., Li, S., Wei, H., Wen, Z., Wang, Y., Tang, T., et al. (2020). Identification of the natural product paeonol derived from peony bark as an inhibitor of the *Salmonella enterica* serovar Typhimurium type III secretion system. *Appl. Microbiol. Biotechnol.* 104, 1673–1682. doi: 10.1007/s00253-019-10290-7

Lyczak, J. B., Cannon, C. L., and Pier, G. B. (2002). Lung infections associated with cystic fibrosis. *Clin. Microbiol. Rev.* 15, 194–222. doi: 10.1128/cmr.15.2.194-222.2002

MacPherson, D. W., Gushulak, B. D., Baine, W. B., Bala, S., Gubbins, P. O., Holtom, P., et al. (2009). Population mobility, globalization, and antimicrobial drug resistance. *Emerg. Infect. Dis.* 15, 1727–1732.

Martin, N., Singh, J., and Aballay, A. (2017). Natural genetic variation in the *Caenorhabditis elegans* response to *Pseudomonas aeruginosa*. *G3* 7, 1137–1147. doi: 10.1534/g3.117.039057

McLean, R. J., Pierson, L. R., and Fuqua, C. (2004). A simple screening protocol for the identification of quorum signal antagonists. *J. Microbiol. Methods* 58, 351–360. doi: 10.1016/j.mimet.2004.04.016

Miller, M. B., and Bassler, B. L. (2001). Quorum sensing in bacteria. *Annu. Rev. Microbiol.* 55, 165–199. doi: 10.1146/annurev.micro.55.1.165

Mok, N., Chan, S. Y., Liu, S. Y., and Chua, S. L. (2020). Vanillin inhibits PqsR-mediated virulence in *Pseudomonas aeruginosa*. *Food Funct.* 11, 6496–6508. doi: 10.1039/d0fo00046a

Mostafa, I., Abbas, H. A., Ashour, M. L., Yasri, A., El-Shazly, A. M., Wink, M., et al. (2020). Polyphenols from salix tetrasperma impair virulence and inhibit quorum sensing of *Pseudomonas aeruginosa*. *Molecules* 25:1341. doi: 10.3390/molecules25061341

Murphy, K., Park, A. J., Hao, Y., Brewer, D., Lam, J. S., and Khursigara, C. M. (2014). Influence of O polysaccharides on biofilm development and outer membrane vesicle biogenesis in *Pseudomonas aeruginosa* PAO1. *J. Bacteriol.* 196, 1306–1317. doi: 10.1128/JB.01463-13

Ng, W., and Bassler, B. L. (2009). Bacterial quorum-sensing network architectures. *Annu. Rev. Genet.* 43, 197–222. doi: 10.1146/annurev-genet-102108-134304

O'Loughlin, C. T., Miller, L. C., Siryaporn, A., Drescher, K., Semmelhack, M. F., and Bassler, B. L. (2013). A quorum-sensing inhibitor blocks *Pseudomonas aeruginosa* virulence and biofilm formation. *Proc. Natl. Acad. Sci. U.S.A.* 110, 17981–17986. doi: 10.1073/pnas.1316981110

Packiavathy, I. A., Priya, S., Pandian, S. K., and Ravi, A. V. (2014). Inhibition of biofilm development of uropathogens by curcumin – an anti-quorum sensing agent from *Curcuma longa*. *Food Chem.* 148, 453–460. doi: 10.1016/j.foodchem.2012.08.002

Paczkowski, J. E., Mukherjee, S., McCready, A. R., Cong, J. P., Aquino, C. J., Kim, H., et al. (2017). Flavonoids suppress *Pseudomonas aeruginosa* virulence through allosteric inhibition of quorum-sensing receptors. *J. Biol. Chem.* 292, 4064–4076. doi: 10.1074/jbc.M116.770552

Parsek, M. R., and Greenberg, E. P. (2000). Acyl-homoserine lactone quorum sensing in gram-negative bacteria: a signaling mechanism involved in

associations with higher organisms. *Proc. Natl. Acad. Sci. U.S.A.* 97, 8789–8793. doi: 10.1073/pnas.97.16.8789

Pederson, D. B., Dong, Y., Blue, L. B., Smith, S. V., and Cao, M. (2018). Water-soluble cranberry extract inhibits *Vibrio cholerae* biofilm formation possibly through modulating the second messenger 3′, 5′ – cyclic diguanylate level. *PLoS One* 13:e207056. doi: 10.1371/journal.pone.0207056

Rashid, M. H., and Kornberg, A. (2000). Inorganic polyphosphate is needed for swimming, swarming, and twitching motilities of *Pseudomonas aeruginosa*. *Proc. Natl. Acad. Sci. U.S.A.* 97, 4885–4890. doi: 10.1073/pnas.060030097

Rather, M. A., Gupta, K., and Mandal, M. (2021). Inhibition of biofilm and quorum sensing-regulated virulence factors in *Pseudomonas aeruginosa* by *Cuphea* carthagenensis (Jacq.) J. F. Macbr. Leaf extract: an in vitro study. *J. Ethnopharmacol.* 269:113699. doi: 10.1016/j.jep.2020.113699

Ravn, L., Christensen, A. B., Molin, S., Givskov, M., and Gram, L. (2001). Methods for detecting acylated homoserine lactones produced by Gram-negative bacteria and their application in studies of AHL-production kinetics. *J. Microbiol. Methods* 44, 239–251. doi: 10.1016/s0167-7012(01)00217-2

Rudrappa, T., and Bais, H. P. (2008). Curcumin, a known phenolic from *Curcuma longa*, attenuates the virulence of *Pseudomonas aeruginosa* PAO1 in whole plant and animal pathogenicity models. *J. Agric. Food Chem*. 56, 1955–1962. doi: 10.1021/jf072591j

Sadikot, R. T., Blackwell, T. S., Christman, J. W., and Prince, A. S. (2005). Pathogen-host interactions in *Pseudomonas aeruginosa* pneumonia. *Am. J. Respir. Crit. Care Med*. 171, 1209–1223. doi: 10.1164/rccm.200408-1044SO

Schuster, M., and Greenberg, E. P. (2006). A network of networks: quorum-sensing gene regulation in *Pseudomonas aeruginosa*. *Int. J. Med. Microbiol.* 296, 73–81. doi: 10.1016/j.ijmm.2006.01.036

Singh, B. N., Singh, B. R., Singh, R. L., Prakash, D., Dhakarey, R., Upadhyay, G., et al. (2009). Oxidative DNA damage protective activity, antioxidant and anti-quorum sensing potentials of *Moringa oleifera*. *Food Chem. Toxicol.* 47, 1109–1116. doi: 10.1016/j.fct.2009.01.034

Smith, R. S., and Iglewski, B. H. (2003). *P. Aeruginosa* quorum-sensing systems and virulence. *Curr. Opin. Microbiol.* 6, 56–60.

Snoussi, M., Noumi, E., Punchappady-Devasya, R., Trabelsi, N., Kanekar, S., Nazzaro, F., et al. (2018). Antioxidant properties and anti-quorum sensing potential of *Carum copticum* essential oil and phenolics against *Chromobacterium violaceum*. *J. Food Sci. Technol.* 55, 2824–2832. doi: 10.1007/s13197-018-3219-6

Swift, S., Throup, J. P., Williams, P., Salmond, G. P., and Stewart, G. S. (1996). Quorum sensing: a population-density component in the determination of bacterial phenotype. *Trends Biochem. Sci.* 21, 214–219.

Tacconelli, E., Tumbarello, M., Bertagnolio, S., Citton, R., Spanu, T., Fadda, G., et al. (2002). Multidrug-resistant *Pseudomonas aeruginosa* bloodstream infections: analysis of trends in prevalence and epidemiology. *Emerg. Infect. Dis.* 8, 220–221. doi: 10.3201/eid0802.010121

Tan, M. W., Mahajan-Miklos, S., and Ausubel, F. M. (1999a). Killing of *Caenorhabditis elegans* by *Pseudomonas aeruginosa* used to model mammalian bacterial pathogenesis. *Proc. Natl. Acad. Sci. U.S.A.* 96, 715–720.

Tan, M. W., Rahme, L. G., Sternberg, J. A., Tompkins, R. G., and Ausubel, F. M. (1999b). *Pseudomonas aeruginosa* killing of *Caenorhabditis elegans* used to identify *P. Aeruginosa* virulence factors. *Proc. Natl. Acad. Sci. U.S.A.* 96, 2408–2413. doi: 10.1073/pnas.96.5.2408

Tsai, C. F., Su, H. H., Chen, K. M., Liao, J. M., Yao, Y. T., Chen, Y. H., et al. (2020). Paeonol protects against myocardial Ischemia/Reperfusion-induced injury by mediating apoptosis and autophagy crosstalk. *Front. Pharmacol.* 11:586498. doi: 10.3389/fphar.2020.586498

Valdez, J. C., Peral, M. C., Rachid, M., Santana, M., and Perdigon, G. (2005). Interference of *Lactobacillus plantarum* with *Pseudomonas aeruginosa* in vitro and in infected burns: the potential use of probiotics in wound treatment. *Clin. Microbiol. Infect.* 11, 472–479. doi: 10.1111/j.1469-0691.2005.01142.x

Vandeputte, O. M., Kiendrebeogo, M., Rajaonson, S., Diallo, B., Mol, A., El, J. M., et al. (2010). Identification of catechin as one of the flavonoids from *Combretum albiflorum* bark extract that reduces the production of quorum-sensing-controlled virulence factors in *Pseudomonas aeruginosa* PAO1. *Appl. Environ. Microbiol.* 76, 243–253. doi: 10.1128/AEM.01059-09

Walsh, D. J., Livinghouse, T., Goeres, D. M., Mettler, M., and Stewart, P. S. (2019). Antimicrobial activity of naturally occurring phenols and derivatives against biofilm and planktonic bacteria. *Front. Chem.* 7:653. doi: 10.3389/fchem.2019.00653

Waters, C. M., and Bassler, B. L. (2005). Quorum sensing: cell-to-cell communication in bacteria. *Annu. Rev. Cell Dev. Biol.* 21, 319–346.

Welsh, M. A., Eibergen, N. R., Moore, J. D., and Blackwell, H. E. (2015). Small molecule disruption of quorum sensing cross-regulation in *pseudomonas aeruginosa* causes major and unexpected alterations to virulence phenotypes. *J. Am. Chem. Soc.* 137, 1510–1519. doi: 10.1021/ja5110798

Williams, P., and Camara, M. (2009). Quorum sensing and environmental adaptation in *Pseudomonas aeruginosa*: a tale of regulatory networks and multifunctional signal molecules. *Curr. Opin. Microbiol.* 12, 182–191. doi: 10.1016/j.mib.2009.01.005

Yin, H., Deng, Y., Wang, H., Liu, W., Zhuang, X., and Chu, W. (2015). Tea polyphenols as an antivirulence compound disrupt quorum-sensing regulated pathogenicity of *Pseudomonas aeruginosa*. *Sci. Rep*. 5:16158. doi: 10.1038/srep16158

Zhang, L., Li, D. C., and Liu, L. F. (2019). Paeonol: pharmacological effects and mechanisms of action. *Int. Immunopharmacol.* 72, 413–421. doi: 10.1016/j.intimp.2019.04.033

Zhong, L., Ravichandran, V., Zhang, N., Wang, H., Bian, X., Zhang, Y., et al. (2020). Attenuation of *pseudomonas aeruginosa* quorum sensing by natural products: virtual screening, evaluation and biomolecular interactions. *Int. J. Mol. Sci.* 21:2190. doi: 10.3390/ijms21062190

Conflict of Interest: The authors declare that the research was conducted in the absence of any commercial or financial relationships that could be construed as a potential conflict of interest.

Publisher's Note: All claims expressed in this article are solely those of the authors and do not necessarily represent those of their affiliated organizations, or those of the publisher, the editors and the reviewers. Any product that may be evaluated in this article, or claim that may be made by its manufacturer, is not guaranteed or endorsed by the publisher.

Copyright © 2021 Yang, Hao, Zhao, Shi, Ye, Zou, Song, Li, Yin, He, Feng, Chen, Zhang, Gao, Li and Tang. This is an open-access article distributed under the terms of the Creative Commons Attribution License (CC BY). The use, distribution or reproduction in other forums is permitted, provided the original author(s) and the copyright owner(s) are credited and that the original publication in this journal is cited, in accordance with accepted academic practice. No use, distribution or reproduction is permitted which does not comply with these terms.

frontiers in Microbiology

ORIGINAL RESEARCH
published: 05 August 2021
doi: 10.3389/fmicb.2021.705712

Dual Transcriptomic Analyses Unveil Host–Pathogen Interactions Between *Salmonella enterica* Serovar Enteritidis and Laying Ducks (*Anas platyrhynchos*)

Yu Zhang[1,2], Lina Song[1,2], Lie Hou[2], Zhengfeng Cao[2], Wanwipa Vongsangnak[3], Guoqiang Zhu[1], Qi Xu[1,2] and Guohong Chen[1,2]*

[1] Joint International Research Laboratory of Agriculture and Agri-Product Safety, The Ministry of Education, Yangzhou University, Yangzhou, China, [2] College of Animal Science and Technology, Yangzhou University, Yangzhou, China, [3] Department of Zoology, Faculty of Science, Kasetsart University, Bangkok, Thailand

OPEN ACCESS

Edited by:
Alina Maria Holban, University of Bucharest, Romania

Reviewed by:
Devendra H. Shah, Washington State University, United States
Regan Hayward, Helmholtz Institute for RNA-based Infection Research (HIRI), Germany
Michael Kogut, Agricultural Research Service, United States Department of Agriculture, United States

***Correspondence:**
Qi Xu
xuqi@yzu.edu.cn

Specialty section:
This article was submitted to Microbial Immunology, a section of the journal Frontiers in Microbiology

Received: *06 May 2021*
Accepted: *13 July 2021*
Published: *05 August 2021*

Citation:
Zhang Y, Song L, Hou L, Cao Z, Vongsangnak W, Zhu G, Xu Q and Chen G (2021) Dual Transcriptomic Analyses Unveil Host–Pathogen Interactions Between Salmonella enterica Serovar Enteritidis and Laying Ducks (Anas platyrhynchos). Front. Microbiol. 12:705712. doi: 10.3389/fmicb.2021.705712

Salmonella enteritidis (SE) is a pathogen that can readily infect ovarian tissues and colonize the granulosa cell layer such that it can be transmitted via eggs from infected poultry to humans in whom it can cause food poisoning. Ducks are an important egg-laying species that are susceptible to SE infection, yet the host–pathogen interactions between SE and ducks have not been thoroughly studied to date. Herein, we performed dual RNA-sequencing analyses of these two organisms in a time-resolved infection model of duck granulosa cells (dGCs) by SE. In total, 10,510 genes were significantly differentially expressed in host dGCs, and 265 genes were differentially expressed in SE over the course of infection. These differentially expressed genes (DEGs) of dGCs were enriched in the cytokine–cytokine receptor interaction pathway via KEGG analyses, and the DEGs in SE were enriched in the two-component system, bacterial secretion system, and metabolism of pathogen factors pathways as determined. A subsequent weighted gene co-expression network analysis revealed that the cytokine–cytokine receptor interaction pathway is mostly enriched at 6 h post-infection (hpi). Moreover, a number of pathogenic factors identified in the pathogen–host interaction database (PHI-base) are upregulated in SE, including genes encoding the pathogenicity island/component, type III secretion, and regulators of systemic infection. Furthermore, an intracellular network associated with the regulation of SE infection in ducks was constructed, and 16 cytokine response-related dGCs DEGs (including *IL15*, *CD40*, and *CCR7*) and 17 pathogenesis-related factors (including *sseL*, *ompR*, and *fliC*) were identified, respectively. Overall, these results not only offer new insights into the mechanisms underlying host–pathogen interactions between SE and ducks, but they may also aid in the selection of potential targets for antimicrobial drug development.

Keywords: transcriptomics, dual RNA-seq, host–pathogen interactions, *Salmonella* enteritidis, duck

INTRODUCTION

Salmonellosis is an important foodborne illness that primarily occurs as a consequence of consuming eggs contaminated with *Salmonella* enteritidis (SE) (Gantois et al., 2009; Pijnacker et al., 2019) with more than 75% of SE outbreaks being linked to eggs or products derived therefrom (Braden, 2006). For example, an egg-linked international outbreak of SE infection has been occurring in the European Union for many years, posing a significant risk to consumer health and socioeconomic outcomes (Pijnacker et al., 2019). Although efforts to control SE outbreaks by vaccination and related interventional strategies to date have been made, these approaches have not completely prevented SE prevalence amid poultry flocks. Therefore, better strategies need to be further explored to control SE infection.

During SE infection, both the SE and the host mobilize all available resources to win the life-and-death struggle (Aprianto et al., 2016). One the one hand, SE encodes a number of pathogenic factors, such as PAMPs, including components of the bacterial cell wall–peptidoglycans, lipopolysaccharide, flagellin, and secretion system effectors to attack host innate immune (LaRock et al., 2015). Moreover, SE manipulates the cellular mechanisms of host organisms via pathogen–host interactions (PHIs) in order to take advantage of the capabilities of host cells, leading to infections; subsequently, transovarial transmission to offspring results in the spread of SE through the production of contaminated eggs and fecal matter (Gantois et al., 2009; Jennings et al., 2017). On the other hand, the host response to infection depends on innate immunity in which intrinsic mechanisms are responsible for recognizing and responding to SE challenge. The *NFKBIA*, *IL1B*, *IL8*, and *CCL4* genes were consistently induced after endotoxin treatment in chicken (Ciraci et al., 2010). Besides this, the *AVD*, *EXFABP*, *IRG1*, *AH221*, *TRAP6*, *SAA*, and all immunoglobulin genes also played important roles in the course of SE infection in chickens (Matulova et al., 2012). These findings only revealed the mechanism of *Salmonella* in the process of infection from host or pathogen. However, pathogen infection is a complex process involving the interaction between pathogen and host. Understanding of the host–SE interactions may reveal the underlying mechanism of SE infection, which will lay the theoretical foundation for better strategies to control the SE pathogen.

Ducks, especially Shaoxing and Pekin ducks, are an economically important poultry species, which are susceptible to SE infection (Yan et al., 2008; Cha et al., 2013; Zhang et al., 2019a). Notably, SE has recently grown to be the most common *Salmonella* serotype to be isolated from laying ducks throughout the world, and its prevalence in countries such as China and the United Kingdom have led to major economic losses while threatening human health and contaminating water (Martelli et al., 2016; Yang et al., 2019; Wang et al., 2020). SE is known to readily infect ovarian tissues and to colonize the granulosa cell layer in poultry (Thiagarajan et al., 1994). However, the PHIs between SE and duck granulosa cells (dGCs) have not been effectively defined. As such, we herein generated a time-resolved model of the SE infection of dGCs to simultaneously assess dynamic changes in gene expression in both duck and SE cells via a dual RNA-seq approach, enabling us to characterize the interactions between these two species and to identify key duck immune genes and SE virulence genes related to these responses.

MATERIALS AND METHODS

Ethics Statement

The Institutional Animal Care and Use Committee of Yangzhou University (Jiangsu, China) approved all animal studies conducted herein, which were consistent with experimental animal use guidelines and regulations. All ducks were housed in a standard facility that met the requirements outlined in the Laboratory Animal Requirements of Environment and Housing Facilities (GB 14925-2001) publication, and all protocols were consistent with the Jiangsu Administration Rules for Laboratory Animal Use.

Experimental Model Animals and Bacterial Strains

Healthy Shaoxing ducks (*Anas platyrhynchos*, Chinese native breed, 26 weeks old) that were free of *Salmonella* were obtained from the National Waterfowl Conservation Farm (Taizhou, China). SE (No. MY1, phage type 4) was isolated from ducks and maintained by the Key Laboratory of Animal Disease and Human Health of Sichuan Province (Deng et al., 2008). The National Center for Medical Culture Collection (Beijing, China) established the phage type and serotype of SE isolates.

dGCs Isolation and SE Infection

Duck granulosa cells were isolated and cultured as in prior studies (Gilbert et al., 1977; Zhang et al., 2019b). Briefly, 10–15 adult prehierarchical follicles were collected from egg-laying ducks under sterile conditions. Yolks and vitelline membranes were removed by rinsing these follicles with Ca^{2+}- and Mg^{2+}-free PBS, after which tissues were minced into 1–2 mm^3 pieces and digested with type II collagenase (1 mg/mL; Sigma, St. Louis, MO, United States) for 5 min at 37°C. Samples were then passed through a 200-μm nylon filter, centrifuged twice for 5 min at 67 × *g*, washed with M199 media to remove the remaining collagenase and cell debris, followed by resuspension in 3 mL of 50% Percoll, centrifugation at 421 × *g* for 15 min, and cell layer isolation. The dGCs were then suspended in M199 media (5% fetal calf serum, 2 mmol/L L-glutamine, 5 μg/mL transferrin, 10 μg/mL insulin, 1.75 mM HEPES [4-(2-hydroxyerhyl) piperazine-1-erhanesulfonic acid]) and counted with 0.1% trypan blue being added to assess viability. Only samples with >90% cell survival were used for subsequent experiments. Cells were allowed to adhere in tissue culture flasks for 24 h prior to experimental utilization, after which purity was initially determined by indirect immunofluorescence assay (IFA) to detect follicle granulosa cell-specific receptor, follicle-stimulating hormone receptor (FSHR) expression using anti-FSHR antibodies (1:500, Proteintech, Rosemont, IL, United States, L594-22665).

Invasion Assays

Invasion assays were conducted as in prior reports (Jouve et al., 1997; Lane and Mobley, 2007). Briefly, bacteria were cultured in LB broth to an OD_{600} of 2.0 (at mid logarithmic phase) at 37°C. dGCs were added to 96-well plates (1×10^5/well) for 24 h, after which they were washed thrice with PBS (pH 7.2) prior to the addition to each well of 100 μL of SE in Dulbecco's modified Eagle medium (DMEM) at a multiplicity of infection (MOI) of 10 with DMEM being added to control wells. Plates were then cultured 37°C for 1 h, after which PBS supplemented with 50 μg/mL gentamicin was added to kill any non-invasive bacteria. Cells were then incubated for an additional 1 h period and then lysed by 0.5% Triton X-100 (Solarbio, Beijing, China) for 30 min before vigorous pipetting. Samples were removed, diluted, and plated on LB agar to determine the number of colony forming units (CFU) per monolayer. Samples were assessed in triplicate.

Salmonella enteritidis infection was confirmed via an IFA approach as detailed previously (Zhang et al., 2019c). Briefly, medium was removed, and cells were washed three times with 0.01 M PBS, fixed with 4% paraformaldehyde, permeabilized with 0.1% Triton X-100, and blocked for 1 h with 10% FBS in PBS. After a 2-h incubation with an anti-*Salmonella* antibody (1:2000, Abcam, Cambridge, MA, United States, ab69253), cells were washed thrice with PBS, stained with DAPI (0.2 mg/mL) for 15 min at 37°C, and imaged via fluorescence microscopy (Leica, Wetzlar, Germany).

RNA-Sequencing

TRIzol (Invitrogen, Carlsbad, CA, United States) was used based on provided directions to extract RNA from 0, 3, 6, and 9 hpi groups ($n = 3$, respectively) with 1% agarose gel electrophoresis being used to assess RNA quality and contamination. A NanoPhotometer spectrophotometer (IMPLEN, Westlake Village, CA, United States) was also used to assess RNA purity, and a Qubit RNA Assay Kit and a Qubit 2.0 Fluorometer (Life Technologies, Carlsbad, CA, United States) were used to measure RNA concentrations. An RNA Nano 6000 Assay Kit and a Bioanalyzer 2100 system (Agilent Technologies, Santa Clara, CA, United States) were then used to assess RNA integrity. Next, a strand-specific library was constructed followed by the previous method (Parkhomchuk et al., 2009; Borodina et al., 2011). Briefly, oligo (dT) beads were used to enrich for eukaryotic RNA in each sample first, then prokaryotic mRNA was enriched via the removal of rRNA with a Ribo-Zero Magnetic Kit (Epicentre) and Quick-RNA^{TM} Fungal/Bacterial Microprep (Zymo Research). After enrichment, fragmentation buffer was used to fragment mRNA into short segments, after which first-strand DNA synthesis was conducted using random hexamer primers. Second-strand cDNA synthesis was then performed with DNA polymerase I, RNase H, dNTPs, and an appropriate buffer. A QiaQuick PCR extraction kit was then used for cDNA isolation, followed by end repair, polyadenylation, and Illumina sequencing adapter ligation. Ligation product size selection was then performed via agarose gel electrophoresis, followed by PCR amplification and sequencing runs of paired-end 150 bp with an Illumina HiSeq 2500 instrument at Major BioTech Co., Ltd. (Shanghai, China).

Raw reads were trimmed and subjected to quality control using Sickle[1] and SeqPrep[2] with default settings. After cleaning, data were mapped to the duck [NCBI: IASCAAS_PekingDuck_PBH1.5 (GCF_003850225.1)] and SE (NC_011294.1) reference genomes using TopHat2 and Bowtie2, respectively (Trapnell et al., 2010; Langmead and Salzberg, 2012). The "MarkDuplicate" tools of Picard[3] were used removed the reads that mapped to both organisms. Relationships among samples were assessed with the gmodels R package[4].

Differentially Expressed Gene (DEG) Analyses

The gene abundances were quantified by software RSEM, and the gene expression level was normalized by using the fragments per kilobase of transcript per million mapped reads method (Li and Dewey, 2011). Differentially expressed genes (DEGs) among samples were identified with the edgeR package (Robinson et al., 2010). DEGs were defined as those genes with a $|\log2FC| \geq 2$ and a false discovery rate (FDR) < 0.05. After identification, Blast2GO (Conesa and Götz, 2008) was utilized for the GO annotation of these genes (Conesa et al., 2005), and the KEGG program was utilized for KEGG pathway enrichment analyses (Kanehisa and Goto, 2000). The weighted gene co-expression network analysis (WGCNA) R package was used to conduct a WGCNA of gene expression patterns across samples (Langfelder and Horvath, 2008). Following pair-wise correlation matrix calculation, an adjacency matrix was calculated by raising the correlation matrix based on a power value (β) that had been selected based upon scale-free topology criteria (scale-free topology criteria $R^2 \geq 0.85$). Topological overlap was then assessed. A cluster tree branch gene co-expression module was constructed based upon average linkage hierarchical clustering. Module eigengenes were statistically classified (dynamicTreeCut algorithm, parameters deepSplit = 2, minModulesize = 30) (Langfelder et al., 2008), after which very similar modules were merged, leading to the identification of key host genes associated with responses to SE infection at different time points. Clusterprofiler and DAVID were used for KEGG and GO enrichment analysis, respectively (Huang et al., 2009; Yu et al., 2012).

Interaction Network Construction and Prediction of the Regulation of Pathogenicity-Associated Genes

Genes involved in PHIs were identified by using BLASTp to compare potentially relevant genes against the PHI-base version 4.8 database (September 2019) (Urban et al., 2020).

[1]https://github.com/najoshi/sickle

[2]https://github.com/jstjohn/SeqPrep

[3]http://broadinstitute.github.io/picard/

[4]https://cran.r-project.org/web/packages/gmodels/index.html

Network-based inferences necessitating a gene expression profile is centralized and standardized using the min-max normalization method (Zhu et al., 2019). Gene expression pattern analysis is used to cluster genes of similar expression patterns for multiple samples. To examine the expression pattern of DEGs, the expression data of each sample (in the order of treatment) were normalized to 0, log2 (v1/v0), log2 (v2/v0), and then clustered by Short Time-series Expression Miner software (STEM) (Ernst and Bar-Joseph, 2006). Host dGCs DEGs (euk-DEGs) and prokaryotic SE-associated DEGs (pro-DEGs) were then selected to predict associations between key virulence genes and host genes via an expression correlation analysis. Interaction networks of euk-DEGs and corresponding pro-DEGs were constructed using Cytoscape (Shannon et al., 2003). To improve network visibility, the edges (connections) were filtered to show only those with a degree cutoff = 2, a node score cutoff = 0.2, k-core = 2, and max depth = 100. The two significant networks were then calculated with the MCODE plug-in (Bader and Hogue, 2003).

qPCR-Based Result Validation

In order to validate RNA-seq results via qPCR, 12 duck genes (*IL15*, *CCR7*, *IL18R1*, *CD40*, *IL23R*, *IL20RA*, *TNFRSF8*, *TNFRSF13B*, *TNFRSF4*, *CSF3R*, *IL2RG*, *TNFRSF18*) and 17 SE virulence-associated genes (*sseL*, *sseE*, *invE*, *ssaM*, *ssaN*, *ssaP*, *spiC*, *slyA*, *spaR*, *aroA*, *sipB*, *prgH*, *hilD*, *ompR*, *fruR*, *fliC*, *sipA*) were selected for analysis with *GAPDH* and *gyrA* being used for the respective normalization of duck and SE transcript expression levels. Primers were designed with the Primer 5 software (Premier, Canada) based upon sequencing data (**Table 1**), and were synthesized by Sangon Biotech (Shanghai, China). TRIzol (Takara, Dalian, China) was used based on provided directions to extract RNA from prepared samples. All qPCR reactions were conducted with an ABI 7500 instrument (Applied Biosystems, Foster City, CA, United States) with individual reactions being composed of 10 μL 2 × SYBR Premix Ex Taq II (Takara), 0.4 μL of each primer (10 μM), 0.4 μL 50 × ROX Reference Dye II (Takara), 2 μL cDNA, and ddH_2O to a final volume of 20 μL. Thermocycler settings were 95°C for 30 s, 40 cycles of 95°C for 5 s, 60°C for 34 s. The thermal program for RT-qPCR was 98°C for 30 s, followed by 40 cycles of 98°C for 10 s and 60°C for 30 s. All samples were conducted with three technical replications. The $2^{-\Delta\Delta CT}$ method (Kenneth and Thomas, 2002) was used to assess relative gene expression levels.

Statistical Analyses

Data are means ± standard deviation (SD), and experiments were repeated at least three times. Data were analyzed with SPSS 26.0 (Chicago, IL, United States) via one-way ANOVAs with Dunnett's test, with $p < 0.05$ as the significance threshold.

Data Access

RNA-seq data from the present study have been deposited in the Short Read Archive of the National Center for Biotechnology Information (NCBI) under the bio-project number PRJNA721551.

TABLE 1 | Primers of genes used in RT-qPCR.

Primer	Sequences (5′-3′)	Accession number	Size (bp)
IL15	F: TGTTGTTCCCACCCTC R: AGCATCTTGCCTCCTG	XM_013109782.3	150
CCR7	F: CTGGCATCAAAGTATCC R: TGACGCTGTTGTAGGG	XM_005030336.5	186
IL18R1	F: TCATTGCCGTGGTTATCG R: AAGCAGGCCAGCGTGTA	XM_038173244.1	154
CD40	F: CAGGGCTTTGGGTTTG R: TAGCACGGCTCGGTTT	XM_027442951.2	110
IL23R	F: TCACCTACATCCAAGAAGACA R: CCCATTCCCAGGTAAACTC	XM_038183055.1	181
IL20RA	F: CAAACCTGGTATGGCACT R: GCACTTCTTTTGGAGGC	XM_027454461.2	207
TNFRSF8	F: ACAGCCATCGCTCACCT R: GCTTTTGGGATTCTTCGT	XM_013102263.4	188
TNFRSF13B	F: GCATCGGAGGGATAAGG R: TGGTCGGTGCAGTTGTT	XM_013099438.3	208
TNFRSF4	F: ATTTGGTGGGGACGGT R: GCGACTTCTCATCCTTTCA	XM_013102273.4	189
CSF3R	F: GAAGAGCATCAGCAAGGC R: TGCTTCACCCTCCCATT	XM_038167306.1	360
IL2RG	F: CAGGACCTCGTGAAACC R: GCTGGGGAAGGAGAAGAT	XM_027464860.2	192
TNFRSF18	F: CAGAAATCAAGGACACGG R: AGTCAATAATGCCACGCT	XM_013103783.4	129
GAPDH	F: TGCTAAGCGTGTCATCATCT R: AGTGGTCATAAGACCCTCCA	XM_038180584.1	60
sseL	F: GAATCAGCCCAATAGGATAG R: ACCAGTTCGCTCAGACAGA	AM933172.1	153
sseE	F: AGCCATGCTACGCAGGAAA R: GATGCTCGGCGGATAAAACT	AM933172.1	101
invE	F: TCCCGGCAGACATCTCAT R: AAGCCTCATCCTCCAGCAC	AM933172.1	226
ssaM	F: TCTGGCGGCAAGGACAATA R: GAAAGAGGTGGAGAACAAC	AM933172.1	205
ssaN	F: CTTTGGTCGTCCCCTTGA R: TACCCACTCGTTGCCCTTC	AM933172.1	167
ssaP	F: GTTGAGGGAAGTCTTGGGTT R: ATGGGTAATGCCTGGTGC	AM933172.1	104
spiC	F: ATGCTGGCAGTTTTAAAAGGCATTC R: CATAGGCAAGACAAGGCT	AM933172.1	181
slyA	F: CATCGCCTCAAGCCTCT R: CGCTTTCTCGGTCAGTT	AM933172.1	225
spaR	F: CTCCGCAAATGAACGCTT R: CCTCGCTCGTAAAACCAACT	AM933172.1	154
aroA	F: CGAACCACCACTACCAACAA R: GAAAATAGGACGCTGACGAG	AM933172.1	102
sipB	F: TGGAAGGATTAGGCGTCG R: CCTGGGTAAAGAGTTTGCTG	AM933172.1	234
prgH	F: GCTGTGAGTTTCCATTGCTG R: CCGACCTGTATTGGCGTATT	AM933172.1	241
hilD	F: CAGACTCAGCAGGTTACCATCA R: GTCGTTGCGTCGGTATCTC	AM933172.1	217
ompR	F: GATTCTGGTGGTTGATGACG R: GATGGAAAGATTCACGGGTC	AM933172.1	134
fruR	F: AGCATCCCTTCTATCAGCG R: GCCCAAATAAAGCACCGT	AM933172.1	170
fliC	F: ATTGAGCGTCTGTCCTCTGG R: GATTTCATTCAGCGCACCTT	AM933172.1	170
sipA	F: CCATTCGACTAACAGCAGCA R: CGGTCGTACCGGCTTTATTA	AM933172.1	449
gyrA	F: GCATGACTTCGTCAGAACCA R: GGTCTATCAGTTGCCGGAAG	MG995181.1	278

RESULTS

Evaluation of dGC Invasion by SE

After isolation, dGCs exhibited a rounded or ovoid shape and were fully adherent to tissue culture flasks within 24 h of

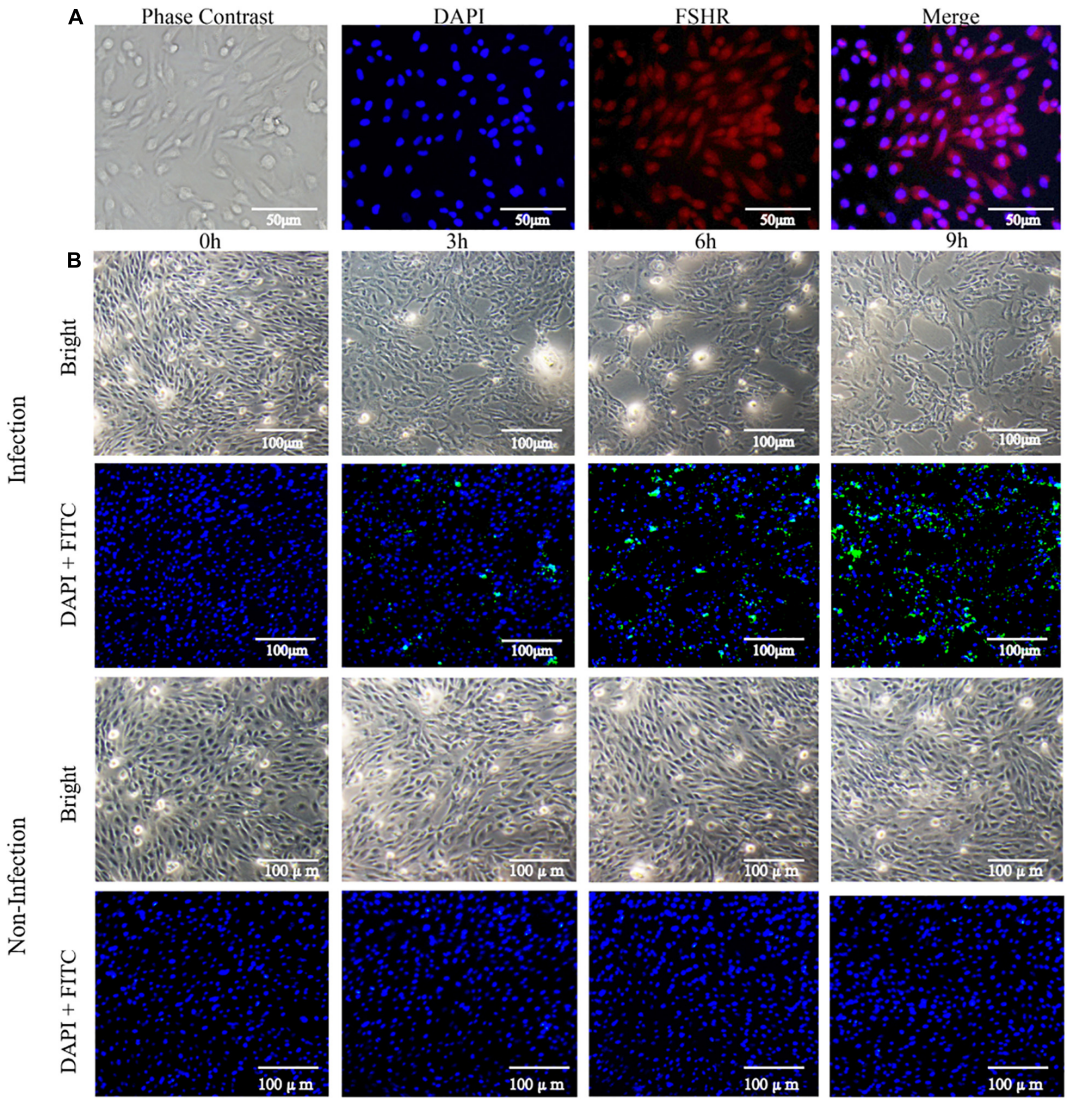


FIGURE 1 | Isolation of dGCs and challenge with SE. **(A)** Isolation and identification of dGCs. Diagram of a dGC (400×), DAPI staining of cell nucleus, and fluorescent image of FSHR. **(B)** The changes of morphology and indirect immunofluorescent staining and DAPI staining of dGCs infected at an MOI of 10 at different times post-infection. The row represents 0, 3, 6, and 9 hpi, respectively.

culture at which point they were spread out in a pebble-like manner. These cells reached 100% confluence within 3–5 days, at which time granular material was evident in the cytoplasm. DAPI was used to stain dGCs nuclei, and the cytoplasm of the FSHRs was stimulated to emit red fluorescence for detection by IFA (**Figure 1A**). After treatment with bacterial suspensions and gentamicin-containing growth media, changes in cell morphology and numbers of invasive SE were assessed at different time points post-infection. At 3 hpi, cells appeared swollen and rounded or irregular in shape with some evidence of vacuolation. At 6 hpi, infected cells were increasingly non-adherent with some blue or black particles, cellular deformation, and clumping in strip-like aggregates. At 9 hpi, some cells had broken down and dissolved with increases in the presence of dark blue particles within dGCs. The media also appeared increasingly flocculated at this time point due to cell exfoliation. IFA staining of the SE in these samples revealed that the degree of bacterial invasion increased significantly over time such that relatively few bacteria were detectable at 3 hpi, whereas these bacterial numbers had expanded significantly by 6 hpi and had invaded most cells by 9 hpi (**Figure 1B**). The intracellular CFU counts of SE at each time point are listed in **Supplementary Table 1**.

Profiling of Gene Expression Patterns Associated With HPIs

To examine dGCs and SE gene expression profiles over the course of this infection process, we conducted a dual RNA-seq time-course analysis of both dGCs and SE cells at 0, 3, 6, and 9 hpi (**Supplementary Table 2**). This RNA-seq approach

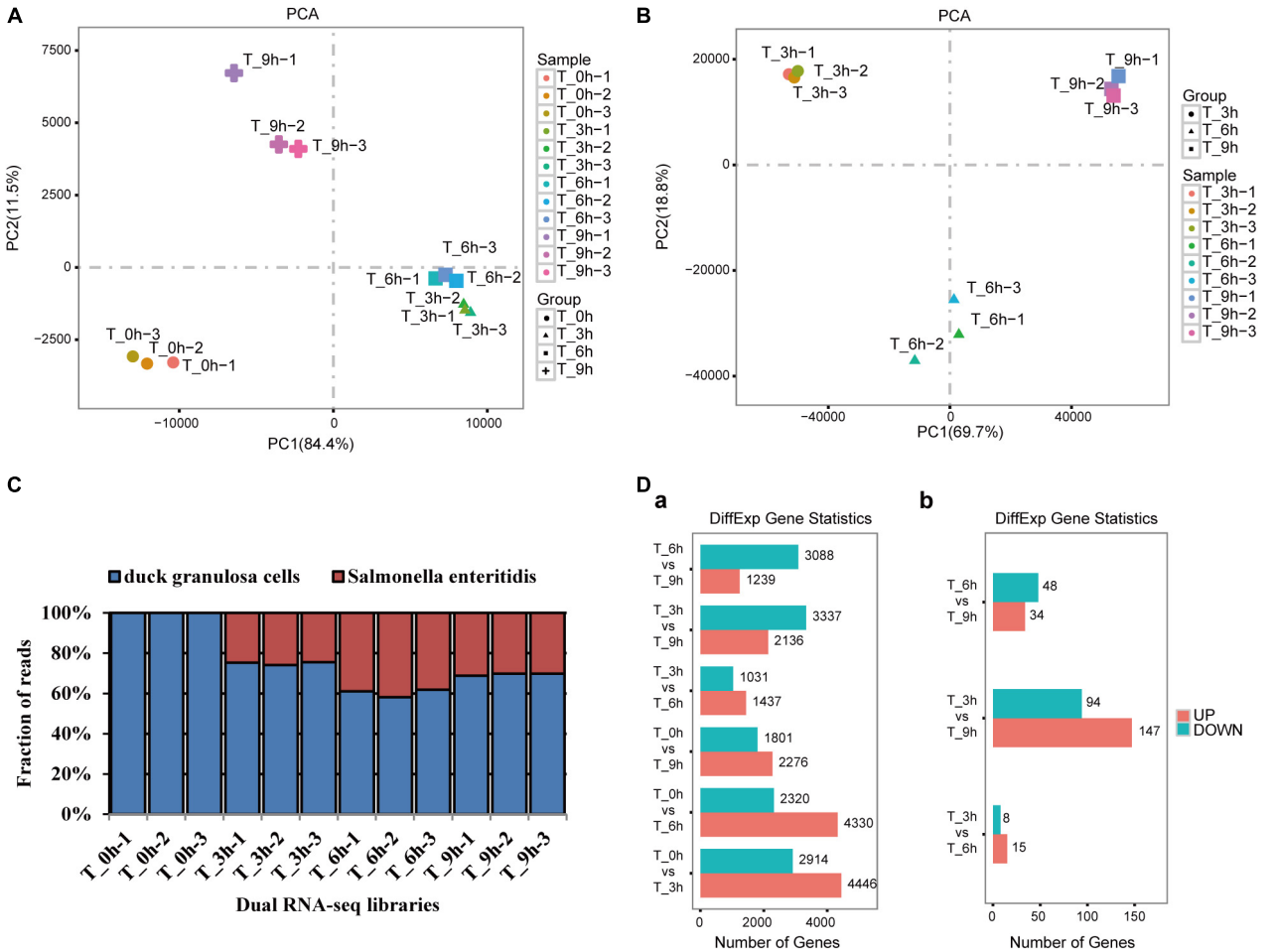


FIGURE 2 | Dual RNA-seq generates high-quality data sets suitable for probing host–pathogen transcriptomes. Principal component analysis was performed separately for dGCs and SE libraries. Biological duplicates clustered closely to each other in host **(A)** and pathogen **(B)** libraries (see sample duplicates). Variability within samples was mainly dependent on the infection time points but not sequencing batch of the samples; 78.6 million reads per library: 76.2% of the reads aligned to the duck reference genome and 23.8% to the SE P125109 reference genomes **(C)**, the DEG statistics at different specific stage of dGCs (a) and SE (b) interaction **(D)**.

yielded high-quality yields with an appropriately balanced base distribution and a reasonable N% (>10%) consistent with these data being of sufficient quality to permit downstream analyses (**Supplementary Table 3**). Average base error rate distributions in these sequencing reads were <0.1% and were, thus, considered acceptable. Principal component analysis clustering was then conducted to confirm sample distribution and biological reproducibility (**Figures 2A,B**). The gmodels R package was used to evaluate the relationships among samples (**Supplementary Figure 1**). On average, this analysis yielded 78.6 million reads per library with 76.2% of these reads aligning to the duck reference genome and 23.8% aligning to the SE P125109 reference genome (**Supplementary Table 4** and **Figure 2C**). The edgeR package (Robinson et al., 2010) was used to assess gene expression profiles and to identify significant DEGs that met the defined criteria (FDR < 0.05 and $|\log2FC| > 1$) at different time points in both dGCs and SE cells (**Figure 2D**). For further details regarding DEGs and virulence-associated genes between the 0, 3, 6, and 9 hpi time points and associated biological functions, see **Supplementary Tables 5, 6**.

Enrichment Analysis of Pathways and GO Terms for DEGs in SE and dGCs

GO analyses of identified DEGs in dGCs and SE were conducted (**Supplementary Tables 7, 8**), revealing these genes to be associated with GO terms mainly enriched in host immune function, including *immune system process* (GO: 0002376), *regulation of cytokine production* (GO: 0001817), *positive regulation of biological process* (GO: 0001819), and *regulation of cellular metabolic process* (GO: 0031323). Bacterial DEGs were additionally associated with bacterial virulence–related protein secretion, such as *the metabolic process* (GO: 0008152), *peptide biosynthetic process* (GO: 0043043), and *regulation of gene expression* (GO: 0010468) GO terms (**Supplementary Figure 2**). In addition, the top 20 enriched KEGG pathways associated

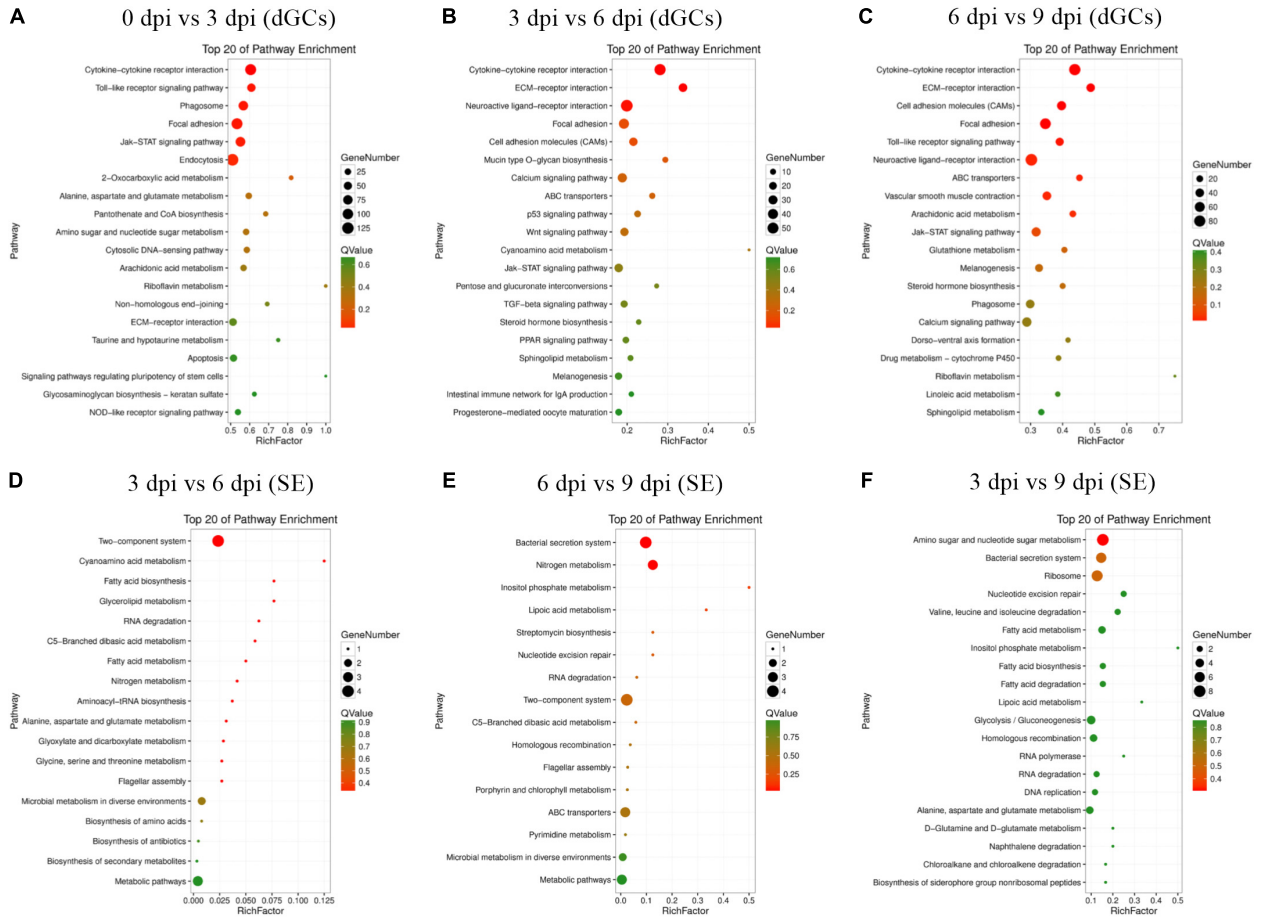


FIGURE 3 | Top 20 enriched KEGG pathways for difference expression genes between the different stages of the SE infection. All DEGs in specific stage infection were analyzed by KEGG enrichment. Fold change > 2 and FDR < 0.01 was set as the cutoff values: 0 vs. 3 hpi **(A)**, 3 vs. 6 hpi **(B)**, 6 vs. 9 hpi **(C)** of dGCs in different contrasts, respectively. 3 vs. 6 hpi **(D)**, 6 vs. 9 hpi **(E)**, 3 vs. 9 hpi **(F)** of SE in different contrasts, respectively.

with genes that were differentially expressed during different stages of the SE infection process were assessed (**Figure 3**). These pathways included the cytokine–cytokine receptor interaction, Toll-like receptor signaling, JAK-STAT signaling, ECM-receptor interaction, and p53 signaling pathways, which play key roles in immune, signal transduction, and transcription-related processes. Statistical analyses suggest that the cytokine–cytokine receptor interaction pathway in dGCs was significantly altered during SE infection as were the two-component system and bacterial secretion system pathways in SE (**Table 2**). For further details regarding the DEGs associated with the cytokine–cytokine receptor interaction, two-component system, and bacterial secretion system pathways in this experimental system, see **Table 3**.

Identification of Key Genes Associated With dGC Responses to Infection and SE Pathogenicity

A WGCNA analysis was conducted to assess relationships between particular genes during a given stage of the infection process, grouping similarly expressed genes into modules via average linkage clustering (based on the weighted correlation coefficients of genes, genes are classified according to their expression patterns, and genes with similar patterns are grouped into one module). Herein, a power value of $\beta = 9$ (scale-free $R^2 = 0.85$) was utilized for oft-thresholding to ensure a scale-free network (**Figure 4A**), leading to the identification of 12 modules (**Figure 4B**). Module connectivity was assessed based upon Pearson's correlation coefficient values (cor.geneModuleMembership > 0.8) with clinical trait relationships similarly being measured based upon absolute Pearson's correlation coefficient values (cor.geneTraitSignificance > 0.4). As the identification of modules significantly associated with clinical features was considered to be of biological importance, module–feature relationships were assessed at different pathological stages, revealing that the most closely associated modules at the 0, 3, 6, and 9 hpi time points were the blue, dark red, black, and light cyan modules, respectively (**Figures 4C,D** and **Supplementary Table 9**). These four modules were, thus, selected as modules of interest with clinical features worthy of

TABLE 2 | Top 2 significantly changed pathways in different group contrasts and specific modules.

Class	Group/module	Term	Count	Percent (%)	*p*-Value	*Q*-Value
dGCs	0 vs. 3 hpi	Cytokine-cytokine receptor interaction Toll-like receptor signaling pathway	11253	5.882.78	9.34×10^{-8}1.93 × 10^{-4}	1.62×10^{-5}1.34 × 10^{-2}
	3 vs. 6 hpi	Cytokine-cytokine receptor interaction ECM-receptor interaction	5227	8.934.64	8.42×10^{-9}7.64 × 10^{-7}	1.17×10^{-6}5.31 × 10^{-5}
	6 vs. 9 hpi	Cytokine-cytokine receptor interaction ECM-receptor interaction	8139	7.973.84	1.85×10^{-11}1.17 × 10^{-7}	3.05×10^{-9}9.68 × 10^{-6}
dGCs	Blue (0 hpi)	Metabolic pathways Biosynthesis of amino acids	23721	28.402.51	2.20×10^{-3}1.40 × 10^{-3}	0.160.16
	Darkred (3 hpi)	Valine, leucine and isoleucine degradation Tryptophan metabolism	97	3.412.65	1.20×10^{-3}7.05 × 10^{-3}	0.160.26
	Black (6 hpi)	Cytokine-cytokine receptor interaction Wnt signaling pathway	4831	7.234.67	2.15×10^{-5}1.22 × 10^{-3}	3.6×10^{-3}0.10
	Lightcyan (9 hpi)	Cell cycle DNA replication	3115	7.403.58	6.07×10^{-8}2.71 × 10^{-8}	4.13×10^{-6}3.68 × 10^{-6}
SE	3 vs. 6 hpi	Two-component system Cyanoamino acid metabolism	41	40.0010.00	1.88×10^{-2}5.18 × 10^{-2}	0.300.30
	6 vs. 9 hpi	Bacterial secretion system Nitrogen metabolism	43	19.0514.29	1.99×10^{-3}3.87 × 10^{-3}	0.030.03
	3 vs. 9 hpi	Amino sugar and nucleotide sugar metabolism Bacterial secretion system	86	10.007.50	4.83×10^{-3}1.84 × 10^{-2}	0.310.50

KEGG pathway analysis was performed with DAVID.
p-value < 0.05 was considered to be statistically significant.

examination in subsequent analyses. Genes in these significant modules at the 0, 3, 6, and 9 hpi time points were associated with metabolic pathways, the MAPK and JAK-STAT signaling pathways, the cytokine–cytokine receptor interaction pathway, and the cell cycle and p53 signaling pathways, respectively (**Table 2** and **Supplementary Figure 3**). The key genes in the cytokine–cytokine receptor interaction pathway within the black modules are additionally listed in **Table 4**. To further understand SE pathogen-related factor expression over the course of the infection process, identified genes were subjected to a BLAST analysis and annotation of high-abundance genes (expression > 10) using the PHI database with identified pathogenicity-associated factors being listed in **Table 4**.

Co-expression Analysis of DEGs in SE and dGCs

Fuzzy c-means clustering (Bezdek, 1992) and expression correlation analyses were next used to evaluate the expression matrices of DEGs from dGCs and SE cells (**Supplementary Figures 4,5**). This led to the identification of 16 host genes associated with the cytokine–cytokine receptor interaction pathway that exhibited high fold-change expression patterns during the infection process as well as 17 pathogenicity-associated factors that were primarily associated with functions including regulators of systemic infection, pathogenicity island/component, and type III secretion system components (<0.05, $P_{x,y} > 0.6$) (**Figure 5**). In **Figure 5**, host and pathogen DEGs are, respectively, represented by circles and inverted triangles. The expression levels of most host cytokines were positively correlated with the expression of bacterial virulence factors, particularly the type III secretion-related proteins; bacterial virulence factors *ompR*, *fliC*, and *ssaU* were the negative regulators to the expression of host response genes; and *sseL*, *ttrB*, and *ompR* interact throughout the higher cooperative diversity in the regulatory network.

qPCR-Based Validation of Hub Genes and Pathogenicity-Associated Factors

Last, a qPCR approach was used to validate the DEGs identified in the above RNA-seq analysis. In total, 12 hub genes (*IL15*, *CCR7*, *IL18R1*, *CD40*, *IL23R*, *IL20RA*, *TNFRSF8*, *TNFRSF13B*, *TNFRSF4*, *CSF3R*, *IL2RG*, and *TNFRSF18*) and 17 pathogenicity-associated factors (*sseL*, *sseE*, *invE*, *ssaM*, *ssaN*, *ssaP*, *spiC*, *slyA*, *spaR*, *aroA*, *sipB*, *prgH*, *hilD*, *ompR*, *fruR*, *fliC*, and *sipA*) were selected for validation. Subsequent qPCR results appeared similar to the outcomes of the dual RNA-seq analysis, thus confirming the validity of these RNA-Seq results (**Figure 6**).

TABLE 3 | The significantly changed pathways and enrichment different expression genes of host and bacteria during SE infection.

Class	DEGs	Function
dGCs	*IL22RA1*, *IL23R*, *TNFSF4*, *IL7*, *IL18*, *TNFRSF13B*, *TNFRSF8*, *CCL19*, *IL15*, *TNFRSF4*, *TNFSF8*, *TNFRSF1B*, *CCR7*, *TNFSF11*, *IL20RA*, *TNFRSF18*, *CSF3R*, *TNFRSF19*, *IL2RG*, *NGFR*, *IL13RA1*, *IL18R1*, *IL1R2*, *IL6*, *IL21R*, *TNFSF15*, *CD40*, *IL7R*, *AMH*, *TNFRSF9*, *TNFRSF11B*, *TNFSF10*, *CCL20*, *CXCL14*	Cytokine–cytokine receptor interaction
SE	*fliC*, *ttrB*, *pagC*, *ompR*, *pagO*, *narG*, *ssrA*, *ssrB*, *pagC*, *htrA*, *ompC*, *pids*	Two-component system
	ssaU, *yscR*, *ssaV*, *ssaJ*, *ssaC*, *tolC*, *BPSS1504*, *ssaL*, *ssaK*, *sseD*, *sseC*, *ssaI*	Bacterial secretion system

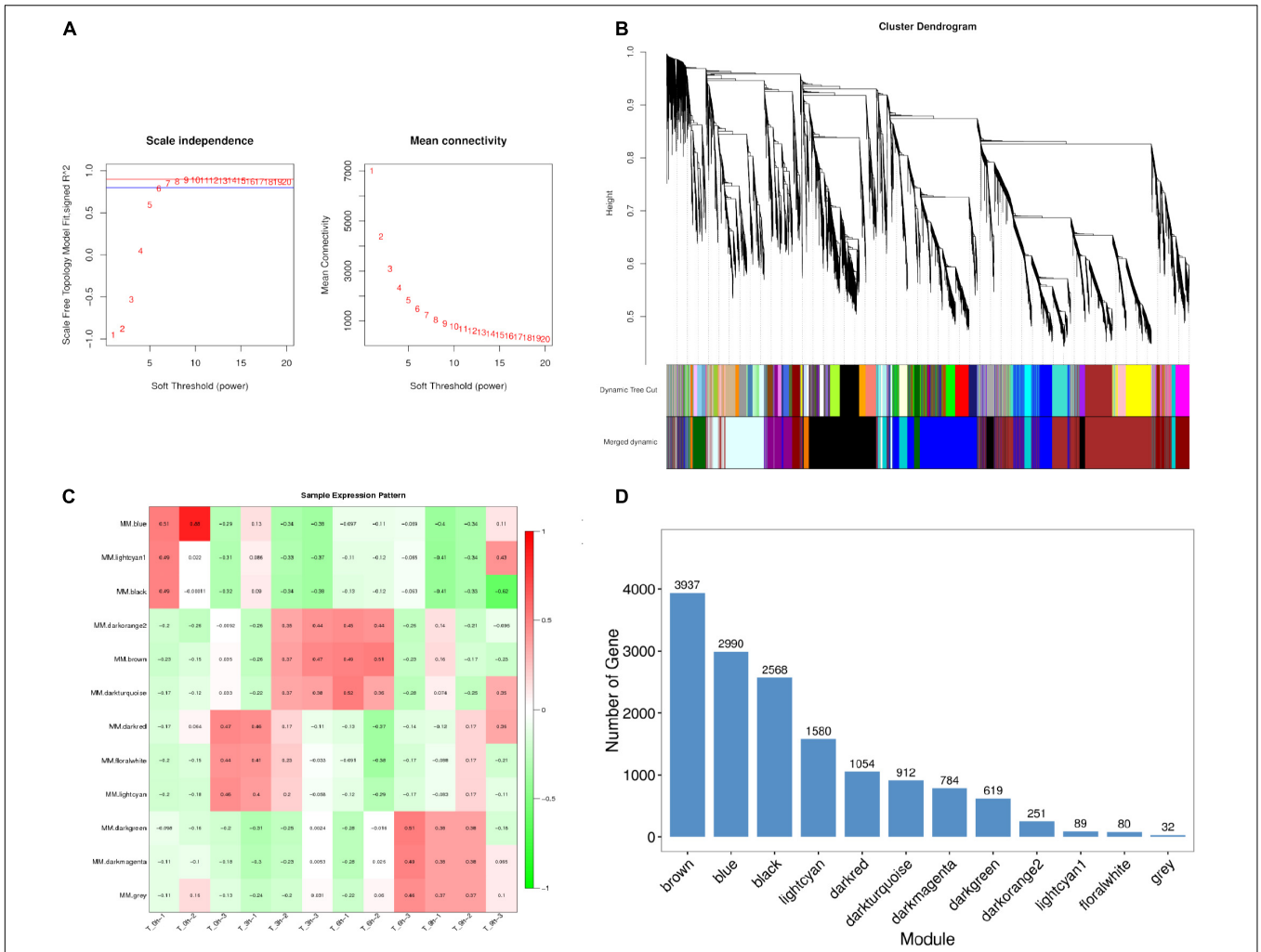


FIGURE 4 | Identification and visualization of stage-specific modules based on WGCNA. **(A)** Analysis of the scale-free fit index for soft-thresholding powers (β) and the mean connectivity for soft-thresholding powers. **(B)** Clustering dendrogram of genes showing module membership in colors. **(C)** Heat map of correlations between module and specific infection stage. The colors ranging from green through white to red indicate low through intermediate to high correlations, respectively. MM, the first principal component of the standardized expression profiles of a given module (absolute correlation greater than 0.4 and *p*-value less than 0.01) are indicated significant. **(D)** Distribution of average gene significance in the modules associated with the stage-specific modules.

TABLE 4 | The key genes and pathologic factors based on pattern expression of specific module and PHI database.

Class	Key genes/pathologic factors	Function
dGCs	*TNFRSF1A*, *CD40*, *CCR5*, *CCR7*, *CXCR4*, *EGF*, *EGFR*, *PDGFRA*, *IL1R1*, *TGFBR2*, *ACVR2A*, *TNFRSF10A_B*, *IL1RAP*, *CSF2RB*, *CSF3R*, *IL23R*, *CSF2RA*, *IL2RB*, *IL2RG*, *CSF1R*, *IL10RA*, *IL20RA*, *IL22RA1*, *IL22RA2*, *IFNLR1*, *TNFRSF1B*, *TNFRSF4*, *TNFRSF6B*, *TNFRSF8*, *TNFRSF13B*, *TNFRSF18*, *TNFRSF21*, *IL18R1*, *IL12B*, *IL15*, *IL19*, *TNFSF8*, *CCL19*, *CXCL13*, *CCL5*, *CCL4*, *CCL21*	Cytokine–cytokine receptor interaction
SE	*slyA*, *ssrB*, *hfq*, *csrA*, *smpB*, *ssrA*, *rpoE*, *himD*, *crp*, *hnr*, *envZ*, *ompR*, *fruR*, *hilD*, *hnr*, *ropS*	Regulators of systemic infection
	sseL, *sseB*, *spiC*, *ssaM*, *ssaV*, *purA*, *aroA*, *ttrB*, *fliC*, *BPSS1504*	Pathogenicity island/component
	ssaJ, *sseC*, *ssaC*, *ssaL*, *ssaK*, *ssaT*, *sseE*, *ssaE*, *ssaS*, *ssaU*, *ssaN*, *ssaQ*, *sseD*, *ssaP*, *ssaI*, *sseF*, *sscB*, *lon*, *invE*, *sifA*, *spaR*, *sipB*, *prgK*, *prgH*, *sipA*, *yscR*	Type III secretion

DISCUSSION

Salmonella enteritidis is a zoonotic pathogen that can readily colonized the granulosa cell layer of ovarian tissues (Gantois et al., 2009). Clarifying HPIs will help reveal the mechanism for regulating the virulence of pathogenic bacteria. In this study, the 10,510 DEGs in host dGCs and 265 in SE were identified during SE infection, and 16 cytokine response-related dGCs DEGs (including *IL15*, *CD40*, and *CCR7*) and 17 pathogenesis-related factors (including *sseL*, *ompR*, and *fliC*) were identified.

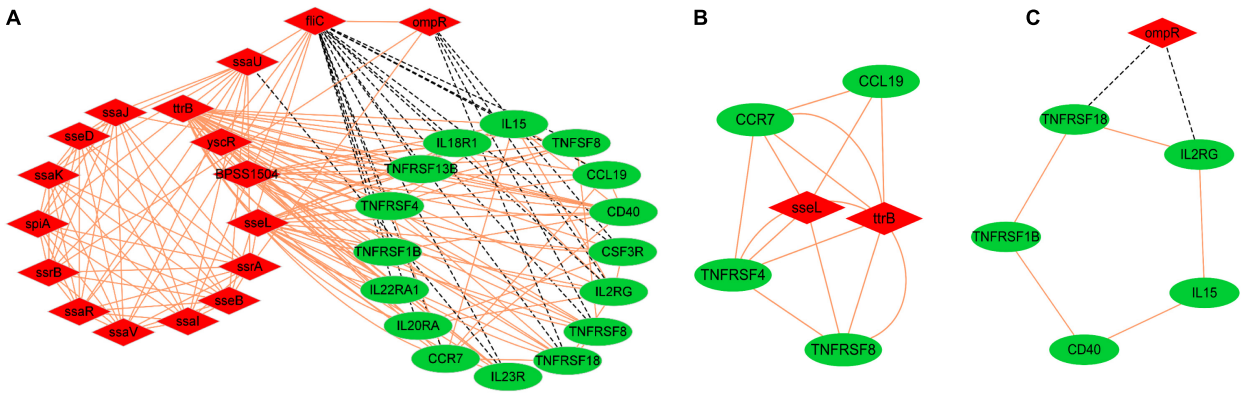


FIGURE 5 | The interaction relationships among the host DEGs of cytokine–cytokine receptor interaction pathways and the pathogenic expression genes of SE. Sixteen host genes interaction with 17 pathogenicity-associated factors during infection **(A)**, Degree cutoff = 2, node score cutoff = 0.2, k-core = 2, and max. depth = 100 as the criteria two significant modules were selected by using plug-in MCODE, Score = 4.8 **(B)**, Score = 2.4 **(C)**, p-value < 0.05, $P_{x,y} > 0.6$. Red and green color represent bacteria and host, respectively, red solid lines represent positive relationship, and black dashed lines represent negative relationship.

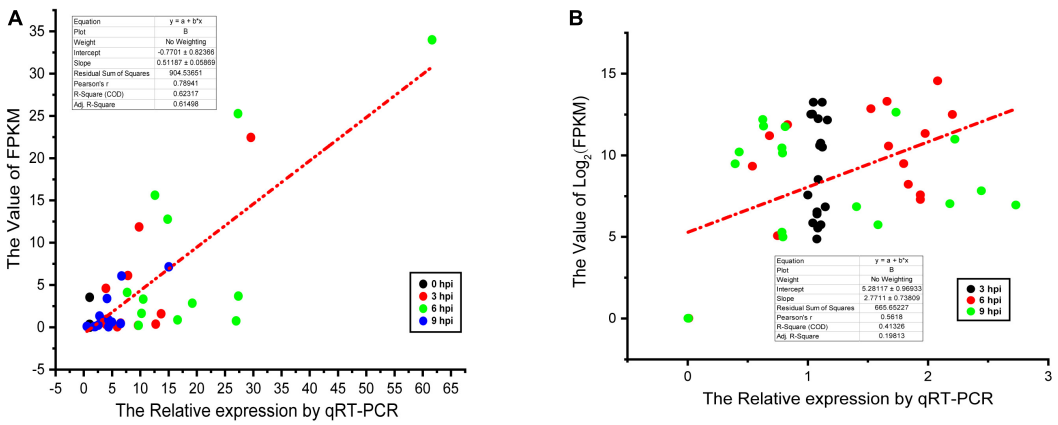


FIGURE 6 | Linear regression fitted for Log_2 fold change of selected genes determined via qPCR and RNA-seq. The selected genes in each comparison were used for linear regression analysis. Log_2FC in RNA-seq equals $2^{-\Delta\Delta Ct}$ in qPCR for each comparison. **(A)** The results of dGCs. **(B)** The results of SE.

These results were similar to those of chicken granulosa cells or duck ovary tissues challenged by SE (Tsai et al., 2010; Babu et al., 2016; Zhang et al., 2019a). Other genes, including *IAP1*, *CD28*, *TGFβ2-4*, *Gal11-13*, *TRAIL*, *PSAP*, *CASP1*, *AVD*, *EXFABP*, *IRG1*, and *AH221*, et al., played an important role of anti-SE immune regulation in cecum and spleen (Calenge and Beaumont, 2012; Matulova et al., 2012, 2013). Together, these data suggest that the immune response of host immune genes were different in different tissues and organs during SE infection. *Salmonella*, as a pathogen of vertical transmission through the ovary, should establish an ovary-specific immune response during the infection process.

Furthermore, the cytokine–cytokine receptor interaction pathway, two-component system, and bacterial secretion system were enriched to involve HPIs. Results of the present study were not in agreement with the findings of Huang et al. (2016) and Wang et al. (2019), who demonstrate that the IgA production signaling pathway and TLR4-FOS/JUN pathway contributed to the protection of chicken from *Salmonella* invasion, respectively. The reason for these different pathways might be due to sequencing methods. In the present study, the dual transcriptomic analyses were performed to unveil HPIs. Westermann and Vogel (2018) prove that dual RNA sequencing is an effective strategy to reveal the pathogenic mechanisms and the host immune response although the RNA sequencing could only reflect the immune response of the pathogen or host. In this sense, the cytokine–cytokine receptor interaction pathway, two-component system, and bacterial secretion system are more likely to be involved in the immune response during *Salmonella* infection.

Evaluating host–SE interactions not only helps uncover the pathogenesis of SE infections, but also has the potential to develop to antimicrobial drug targeting. For example, sMtb-RECON was established by a combination model of bacteria *Mycobacterium tuberculosis* (Mtb) and human macrophage-like cell line THP-1 metabolic processes used as the elucidation of metabolic drug responses in a manner that has the potential to reduce antibiotic abuse (Rienksma et al., 2019). In another

study, a dual RNA-sequencing time-course approach was used to monitor transcriptomic responses in both *Salmonella typhimurium* and infected HeLa cells, revealing a link between the *S. typhimurium* PinT virulence gene and the induction of immune signaling responses in HeLa cells via JAK-STAT signaling pathways (Westermann et al., 2016). In the present study, we find that *BPSS1504* was involved in SE infection, which served as a Type VI secretion system (T6SS) component capable of influencing hemolysin-coregulated protein Hcp1 secretion and T6SS apparatus integrity (Hopf et al., 2014). The interaction between *BPSS1504* and T6SS might be a potential target to develop an antimicrobial drug for SE clearance.

CONCLUSION

In conclusion, the 10,510 euk-DEGs and 265 pro-DEGs were screened during duck SE challenge using dual RNA-seq, which enriched in the host cytokine–cytokine receptor interaction pathway and bacterial two-component/secretion system throughout the process, respectively. Also, a number of PHIs between cytokine–cytokine receptors and virulence-associated genes were found in this process based on WGCNA. Furthermore, the intracellular network associated with the regulation of SE infection in ducks was constructed, and 16 cytokine response–related dGC DEGs (including *IL15*, *CD40*, and *CCR7*, et al.) and 17 pathogenesis-related factors (including *sseL*, *ompR*, and *fliC*, et al.) were identified. Also, the interaction between *BPSS1504* and T6SS might be involved in immune regulation during SE infection. These data offer novel insights into the complex HPIs that occur upon SE infection of ducks, and unveil novel potential targets for SE infection diagnosis and antimicrobial drug development.

DATA AVAILABILITY STATEMENT

The datasets presented in this study can be found in online repositories. The names of the repository/repositories and accession number(s) can be found below: Short Read Archive (SRA), PRJNA721551.

ETHICS STATEMENT

The animal study was reviewed and approved by The Institutional Animal Care and Use Committee (IACUC) of Yangzhou University (Jiangsu, China).

AUTHOR CONTRIBUTIONS

QX and GC conceived and designed the experiments. GZ assisted in experimental design. YZ and LS performed the experiments. LH, ZC, and WV analyzed the data. YZ wrote the manuscript. All authors contributed to the article and approved the submitted version.

FUNDING

This study was supported by the National Natural Science Foundation of China (31702107) and the Open Project Program of Joint International Research Laboratory of Agriculture and Agri-Product Safety, the Ministry of Education of China, Yangzhou University (JILAR-KF202018).

ACKNOWLEDGMENTS

We thank the personnel of Jiangsu Waterfowl Conservation Farm (Taizhou, China) for their cooperation.

SUPPLEMENTARY MATERIAL

The Supplementary Material for this article can be found online at: https://www.frontiersin.org/articles/10.3389/fmicb.2021.705712/full#supplementary-material

Supplementary Figure 1 | Sample cluster map of dGCs and SE. **(A)** The results of dGCs. **(B)** The results of SE.

Supplementary Figure 2 | Visualization of GO enrichment analysis of difference expression genes between 0, 3, 6, and 9 hpi during SE infection. All DEGs in specific-stage infection were analyzed by KEGG enrichment. Fold change > 2 and FDR < 0.01 were set as cutoff values. 0 vs. 3 hpi **(A)**, 3 vs. 6 hpi **(B)**, 6 vs. 9 hpi **(C)** of dGCs in different contrasts, respectively. 3 vs. 6 hpi **(D)**, 6 vs. 9 hpi **(E)**, 3 vs. 9 hpi **(F)** of SE in different contrasts, respectively.

Supplementary Figure 3 | Visualization of gene expression levels and KEGG enrichment analysis of significant modules. Clustering heat map and bar plot represent gene expression levels of each module. In the heat maps, the colors range from green to red, indicating low to high expression levels, respectively. Panels **(A–D)** and panels **(E–H)** represent blue, dark red, black, and light cyan modules.

Supplementary Figure 4 | dGC clustering of dDEGs (scaled and centered log2 values) over the time course of the infection. Gray lines represent the expression of individual genes; black lines are shown the variance; p-value < 0.05.

Supplementary Figure 5 | SE clustering of DEGs (scaled and centered log2 values) over the time course of the infection. Gray lines represent the expression of individual genes; black lines are shown the variance; p-value < 0.05.

Supplementary Table 1 | Intracellular CFU counts of SE at 0, 3, 6, and 9 h post-infection.

Supplementary Table 2 | Summary of dual RNA sequencing for the samples.

Supplementary Table 3 | Base information statistics before and after filtering.

Supplementary Table 4 | Reads aligning to the SE and duck reference.

Supplementary Table 5 | Analysis of dGCs differentially expressed mRNAs between 0, 3, 6, and 9 h post-infection.

Supplementary Table 6 | Analysis of SE differentially expressed mRNAs between 3, 6, and 9 h post-infection.

Supplementary Table 7 | GO enrichment analysis of dGCs difference expression genes between 0, 3, 6, and 9 h post-infection.

Supplementary Table 8 | GO enrichment analysis of SE difference expression genes between 3, 6, and 9 h post-infection.

Supplementary Table 9 | Identification of stage-specific modules based on weighted gene co-expression network analysis.

REFERENCES

Aprianto, R., Slager, J., Holsappel, S., and Veening, J. W. (2016). Time-resolved dual RNA-seq reveals extensive rewiring of lung epithelial and pneumococcal transcriptomes during early infection. *Genome Biol.* 17:198. doi: 10.1186/s13059-016-1054-5

Babu, U. S., Harrison, L. M., Patel, I. R., Ramirez, G. A., Williams, K. M., Pereira, M., et al. (2016). Differential antibacterial response of chicken granulosa cells to invasion by *Salmonella* serovars. *Poultry Sci.* 95, 1370–1379. doi: 10.3382/ps/pew050

Bader, G. D., and Hogue, C. W. (2003). An automated method for finding molecular complexes in large protein interaction networks. *BMC Bioinform.* 4:2. doi: 10.1186/1471-2105-4-2

Bezdek, J. C. (1992). "Clustering in banach spaces", in *Fuzzy Approach to Reasoning and Decision-Making*, ed. V. Novák (Dordrecht: Springer), 173–184. doi: 10.1007/978-94-011-2753-0_15

Borodina, T., Adjaye, J., and Sultan, M. (2011). A strand-specific library preparation protocol for RNA sequencing. *Methods Enzymol.* 500, 79–98. doi: 10.1016/B978-0-12-385118-5.00005-0

Braden, C. R. (2006). *Salmonella enterica* serotype Enteritidis and eggs: a national epidemic in the United States. *Clin. Infect. Dis.* 43, 512–517. doi: 10.1086/505973

Calenge, F., and Beaumont, C. (2012). Toward integrative genomics study of genetic resistance to *Salmonella* and *Campylobacter* intestinal colonization in fowl. *Front. Genet.* 3:261. doi: 10.3389/fgene.2012.00261

Cha, S. Y., Kang, M., Yoon, R. H., Park, C. K., Moon, O. K., and Jang, H. K. (2013). Prevalence and antimicrobial susceptibility of *Salmonella* isolates in Pekin ducks from South Korea. *Comp. Immuno. Microbiol. Infect. Dis.* 36, 473–479. doi: 10.1016/j.cimid.2013.03.004

Ciraci, C., Tuggle, C. K., Wannemuehler, M. J., Nettleton, D., and Lamont, S. J. (2010). Unique genome-wide transcriptome profiles of chicken macrophages exposed to *Salmonella*-derived endotoxin. *BMC Genom.* 11:545. doi: 10.1186/1471-2164-11-545

Conesa, A., and Götz, S. (2008). Blast2GO: A comprehensive suite for functional analysis in plant genomics. *Int. J. Plant Genom.* 2008:619832. doi: 10.1155/2008/619832

Conesa, A., Gotz, S., Garcia-Gomez, J. M., Terol, J., Talon, M., and Robles, M. (2005). Blast2GO: a universal tool for annotation, visualization and analysis in functional genomics research. *Bioinformatics.* 21, 3674–3676. doi: 10.1093/bioinformatics/bti610

Deng, S. X., Cheng, A. C., Wang, M. S., and Cao, P. (2008). Serovar-specific real-time quantitative detection of *Salmonella* enteritidis in the gastrointestinal tract of ducks after oral challenge. *Avian Dis.* 52, 88–93. doi: 10.1637/8102-090107-Reg

Ernst, J., and Bar-Joseph, Z. (2006). STEM: a tool for the analysis of short time series gene expression data. *BMC Bioinform.* 7:191. doi: 10.1186/1471-2105-7-191

Gantois, I., Ducatelle, R., Pasmans, F., Haesebrouck, F., Gast, R., Humphrey, T. J., et al. (2009). Mechanisms of egg contamination by *Salmonella* Enteritidis. *FEMS Microbiol. Rev.* 33, 718–738. doi: 10.1111/j.1574-6976.2008.00161.x

Gilbert, A. B., Evans, A. J., Perry, M. M., and Davidson, M. H. (1977). A method for separating the granulosa cells, the basal lamina and the theca of the preovulatory ovarian follicle of the domestic fowl (Gallus domesticus). *J. Reprod. Fertil.* 50, 179–181. doi: 10.1530/jrf.0.0500179

Hopf, V., Göhler, A., Eske-Pogodda, K., Bast, A., Steinmetz, I., and Breitbach, K. (2014). BPSS1504, a cluster 1 type VI secretion gene, is involved in intracellular survival and virulence of Burkholderia pseudomallei. *Infect. Immun.* 82, 2006–2015. doi: 10.1128/IAI.01544-14

Huang, D. W., Sherman, B. T., and Lempicki, R. A. (2009). Bioinformatics enrichment tools: paths toward the comprehensive functional analysis of large gene lists. *Nucleic Acids Res.* 37, 1–13. doi: 10.1093/nar/gkn923

Huang, H. B., Liu, A., Wu, H., Ansari, A. R., Wang, J. X., Huang, X. Y., et al. (2016). Transcriptome analysis indicated that *Salmonella* lipopolysaccharide-induced thymocyte death and thymic atrophy were related to TLR4-FOS/JUN pathway in chicks. *BMC Genom.* 17:322. doi: 10.1186/s12864-016-2674-6

Jennings, E., Thurston, T. L. M., and Holden, D. W. (2017). *Salmonella* SPI-2 type III secretion system effectors: molecular mechanisms and physiological consequences. *Cell. Host Microb.* 22, 217–231. doi: 10.1016/j.chom.2017.07.009

Jouve, M., Garcia, M. I., Courcoux, P., Labigne, A., Gounon, P., and Le Bouguénec, C. (1997). Adhesion to and invasion of HeLa cells by pathogenic *Escherichia coli* carrying the afa-3 gene cluster are mediated by the AfaE and AfaD proteins, respectively. *Infect. Immun.* 65, 4082–4089. doi: 10.1128/iai.65.10.4082-4089.1997

Kanehisa, M., and Goto, S. (2000). KEGG: kyoto encyclopedia of genes and genomes. *Nucleic Acids Res.* 28, 27–30. doi: 10.1093/nar/28.1.27

Kenneth, J. L., and Thomas, D. S. (2002). Analysis of relative gene expression data using real-time quantitative PCR and the 2-ΔΔCT method. *Methods* 25, 402–408. doi: 10.1006/meth.2001.1262

Lane, M. C., and Mobley, H. L. T. (2007). Role of P-fimbrial-mediated adherence in pyelonephritis and persistence of uropathogenic *Escherichia coli* (UPEC) in the mammalian kidney. *Kidney Int.* 72, 19–25. doi: 10.1038/sj.ki.5002230

Langfelder, P., and Horvath, S. (2008). WGCNA: an R package for weighted correlation network analysis. *BMC Bioinform.* 9:559. doi: 10.1186/1471-2105-9-559

Langfelder, P., Zhang, B., and Horvath, S. (2008). Defining clusters from a hierarchical cluster tree: the dynamic tree cut package for R. *Bioinformatics.* 24, 719–720. doi: 10.1093/bioinformatics/btm563

Langmead, B., and Salzberg, S. L. (2012). Fast gapped-read alignment with Bowtie 2. *Nat. Methods.* 9, 357–359. doi: 10.1038/nmeth.1923

LaRock, D. L., Chaudhary, A., and Miller, S. I. (2015). *Salmonella*e interactions with host processes. *Nat. Rev. Microbiol.* 13, 191–205. doi: 10.1038/nrmicro3420

Li, B., and Dewey, C. N. (2011). RSEM: accurate transcript quantification from RNA-Seq data with or without a reference genome. *BMC Bioinform.* 12:323. doi: 10.1186/1471-2105-12-323

Martelli, F., Birch, C., and Davies, R. H. (2016). Observations on the distribution and control of *Salmonella* in commercial duck hatcheries in the UK. *Avian Pathol.* 45, 261–266. doi: 10.1080/03079457.2016.1146820

Matulova, M., Rajova, J., Vlasatikova, L., Volf, J., Stepanova, H., Havlickova, H., et al. (2012). Characterization of chicken spleen transcriptome after infection with *Salmonella enterica* Serovar Enteritidis. *PloS One.* 7:e48101. doi: 10.1371/journal.pone.0048101

Matulova, M., Varmuzova, K., Sisak, F., Havlickova, H., Babak, V., Stejskal, K., et al. (2013). Chicken innate immune response to oral infection with *Salmonella enterica* serovar Enteritidis. *Vet. Res.* 44:37. doi: 10.1186/1297-9716-44-37

Parkhomchuk, D., Borodina, T., Amstislavskiy, V., Banaru, M., Hallen, L., Krobitsch, S., et al. (2009). Transcriptome analysis by strand-specific sequencing of complementary DNA. *Nucleic Acids Res.* 37:e123. doi: 10.1093/nar/gkp596

Pijnacker, R., Dallman, T. J., Tijsma, A. S. L., Hawkins, G., Larkin, L., Kotila, S. M., et al. (2019). An international outbreak of *Salmonella enterica* serotype Enteritidis linked to eggs from Poland: a microbiological and epidemiological study. *Lancet Infect. Dis.* 19, 778–786. doi: 10.1016/S1473-3099(19)30047-7

Rienksma, R. A., Schaap, P. J., dos Santos, V. A. P. M., and Suarez-Diez, M. (2019). Modeling host-pathogen interaction to elucidate the metabolic drug response of intracellular *Mycobacterium tuberculosis*. *Front. Cell. Infect. Microbiol.* 9:144. doi: 10.3389/fcimb.2019.00144

Robinson, M. D., McCarthy, D. J., and Smyth, G. K. (2010). edgeR: a Bioconductor package for differential expression analysis of digital gene expression data. *Bioinformatics.* 26, 139–140. doi: 10.1093/bioinformatics/btp616

Shannon, P., Markiel, A., Ozier, O., Baliga, N. S., Wang, J. T., Ramage, D., et al. (2003). Cytoscape: A software environment for integrated models of biomolecular interaction networks. *Genome Res.* 13, 2498–2504. doi: 10.1101/gr.1239303

Thiagarajan, D., Saeed, A. M., and Asem, E. K. (1994). Mechanism of transovarian transmission of *Salmonella* enteritidis in laying hens. *Poult. Sci.* 73, 89–98. doi: 10.3382/ps.0730089

Trapnell, C., Williams, B. A., Pertea, G., Mortazavi, A., Kwan, G., van Baren, M. J., et al. (2010). Transcript assembly and quantification by RNA-Seq reveals unannotated transcripts and isoform switching during cell differentiation. *Nat. Biotech.* 28, 511–515. doi: 10.1038/nbt.1621

Tsai, H. J., Chiu, C. H., Wang, C. L., and Chou, C. H. (2010). A time-course study of gene responses of chicken granulosa cells to *Salmonella* Enteritidis infection. *Vet. Microbiol.* 144, 325–333. doi: 10.1016/j.vetmic.2010.01.004

Urban, M., Cuzick, A., Seager, J., Wood, V., Rutherford, K., Venkatesh, S. Y., et al. (2020). PHI-base: the pathogen-host interactions database. *Nucleic Acids Res.* 48, D613–D620. doi: 10.1093/nar/gkz904

Wang, F., Zhang, J., Zhu, B., Wang, J., Wang, Q., Zheng, M. Q., et al. (2019). Transcriptome analysis of the Cecal Tonsil of Jingxing yellow chickens revealed the mechanism of differential resistance to *Salmonella*. *Genes* 10:979. doi: 10.3390/genes10120979

Wang, J., Li, J. X., Liu, F. L., Cheng, Y. Y., and Su, J. L. (2020). Characterization of *Salmonella enterica* Isolates from diseased poultry in Northern China between 2014 and 2018. *Pathogens* 9:95. doi: 10.3390/pathogens9020095

Westermann, A. J., Forstner, K. U., Amman, F., Barquist, L., Chao, Y. J., Schulte, L. N., et al. (2016). Dual RNA-seq unveils noncoding RNA functions in host-pathogen interactions. *Nature* 529, 496–501. doi: 10.1038/nature16547

Westermann, A. J., and Vogel, J. (2018). Host-pathogen transcriptomics by dual RNA-Seq. *Methods Mol. Biol.* 1737, 59–75. doi: 10.1007/978-1-4939-7634-8_4

Yan, B., Cheng, A. C., Wang, M. S., Deng, S. X., Zhang, Z. H., Yin, N. C., et al. (2008). Application of an indirect immunofluorescent staining method for detection of *Salmonella* enteritidis in paraffin slices and antigen location in infected duck tissues. *World J. Gastroenterol.* 14, 776–781. doi: 10.3748/wjg.14.776

Yang, J., Ju, Z., Yang, Y., Zhao, X., Jiang, Z., and Sun, S. (2019). Serotype, antimicrobial susceptibility and genotype profiles of *Salmonella* isolated from duck farms and a slaughterhouse in Shandong province, China. *BMC Microbiol.* 19:202. doi: 10.1186/s12866-019-1570-z

Yu, G. C., Wang, L. G., Han, Y. Y., and He, Q. Y. (2012). clusterProfiler: an R Package for comparing biological themes among gene clusters. *Omics* 16, 284–287. doi: 10.1089/omi.2011.0118

Zhang, Y., Chen, Y., Gu, T., Xu, Q., Zhu, G., and Chen, G. (2019a). Effects of *Salmonella enterica* serovar enteritidis infection on egg production and the immune response of the laying duck *Anas platyrhynchos*. *PeerJ.* 7:e6359. doi: 10.7717/peerj.6359

Zhang, Y., Gu, T., Chen, Y., Zhu, G., Vongsangnak, W., Xu, Q., et al. (2019b). Screening and identification of SipC-interacting proteins in *Salmonella* enteritidis using Gal4 yeast two-hybrid system in duck. *PeerJ* 7:e7663. doi: 10.7717/peerj.7663

Zhang, Y., Gu, T. T., Chen, Y., Huang, Y., Du, J. P., Lu, L. Z., et al. (2019c). Comparative transcriptome analysis reveals PERP upregulated during *Salmonella* Enteritidis challenge in laying ducks. *J. Cell. Physiol.* 234, 11330–11347. doi: 10.1002/jcp.27790

Zhu, X. L., Fu, B. F., Yang, Y. D., Ma, Y., Hao, J. Y., Chen, S. Q., et al. (2019). Attention-based recurrent neural network for influenza epidemic prediction. *BMC Bioinform.* 20:575. doi: 10.1186/s12859-019-3131-8

Conflict of Interest: The authors declare that the research was conducted in the absence of any commercial or financial relationships that could be construed as a potential conflict of interest.

Publisher's Note: All claims expressed in this article are solely those of the authors and do not necessarily represent those of their affiliated organizations, or those of the publisher, the editors and the reviewers. Any product that may be evaluated in this article, or claim that may be made by its manufacturer, is not guaranteed or endorsed by the publisher.

Copyright © 2021 Zhang, Song, Hou, Cao, Vongsangnak, Zhu, Xu and Chen. This is an open-access article distributed under the terms of the Creative Commons Attribution License (CC BY). The use, distribution or reproduction in other forums is permitted, provided the original author(s) and the copyright owner(s) are credited and that the original publication in this journal is cited, in accordance with accepted academic practice. No use, distribution or reproduction is permitted which does not comply with these terms.

frontiers in Microbiology

ORIGINAL RESEARCH
published: 30 August 2021
doi: 10.3389/fmicb.2021.723152

Respiratory Microbiota Profiles Associated With the Progression From Airway Inflammation to Remodeling in Mice With OVA-Induced Asthma

Jun Zheng[1], Qian Wu[1], Ya Zou[2], Meifen Wang[3], Li He[1] and Sheng Guo[4]**

[1] Department of Traditional Chinese Medicine, Shanghai Children's Hospital, Shanghai Jiao Tong University, Shanghai, China, [2] Department of Emergency Medicine, Putuo Hospital, Shanghai University of Traditional Medicine, Shanghai, China, [3] Department of Pediatrics, Sanmen People's Hospital, Taizhou, China, [4] Department of Endocrine, Genetics and Metabolism, Shanghai Children's Hospital, Shanghai Jiao Tong University, Shanghai, China

OPEN ACCESS

Edited by:
Alina Maria Holban,
University of Bucharest, Romania

Reviewed by:
Gurupreet S. Sethi,
La Jolla Institute for Immunology (LJI), United States
Nabijan Mohammadtursun,
Huashan Hospital, Fudan University, China
Joan Cook-Mills,
Indiana University Bloomington, United States

***Correspondence:**
Li He
hel@shchildren.com.cn
Sheng Guo
guosheng@shchildren.com.cn

Specialty section:
This article was submitted to Microbial Immunology, a section of the journal Frontiers in Microbiology

Received: 10 June 2021
Accepted: 27 July 2021
Published: 30 August 2021

Citation:
Zheng J, Wu Q, Zou Y, Wang M, He L and Guo S (2021) Respiratory Microbiota Profiles Associated With the Progression From Airway Inflammation to Remodeling in Mice With OVA-Induced Asthma. Front. Microbiol. 12:723152. doi: 10.3389/fmicb.2021.723152

Background: The dysbiosis of respiratory microbiota plays an important role in asthma development. However, there is limited information on the changes in the respiratory microbiota and how these affect the host during the progression from acute allergic inflammation to airway remodeling in asthma.

Objective: An ovalbumin (OVA)-induced mouse model of chronic asthma was established to explore the dynamic changes in the respiratory microbiota in the different stages of asthma and their association with chronic asthma progression.

Methods: Hematoxylin and eosin (H&E), periodic acid-schiff (PAS), and Masson staining were performed to observe the pathological changes in the lung tissues of asthmatic mice. The respiratory microbiota was analyzed using 16S rRNA gene sequencing followed by taxonomical analysis. The cytokine levels in bronchoalveolar lavage fluid (BALF) specimens were measured. The matrix metallopeptidase 9 (MMP-9) and vascular endothelial growth factor (VEGF-A) expression levels in lung tissues were measured to detect airway remodeling in OVA-challenged mice.

Results: Acute allergic inflammation was the major manifestation at weeks 1 and 2 after OVA atomization stimulation, whereas at week 6 after the stimulation, airway remodeling was the most prominent observation. In the acute inflammatory stage, *Pseudomonas* was more abundant, whereas *Staphylococcus* and *Cupriavidus* were more abundant at the airway remodeling stage. The microbial compositions of the upper and lower respiratory tracts were similar. However, the dominant respiratory microbiota in the acute inflammatory and airway remodeling phases were different. Metagenomic functional prediction showed that the pathways significantly upregulated in the acute inflammatory phase and airway remodeling phase were different. The cytokine levels in BALF and

the expression patterns of proteins associated with airway remodeling in the lung tissue were consistent with the metagenomic function results.

Conclusion: The dynamic changes in respiratory microbiota are closely associated with the progression of chronic asthma. Metagenomic functional prediction indicated the changes associated with acute allergic inflammation and airway remodeling.

Keywords: asthma, respiratory microbiota, airway inflammation, airway remodeling, metagenomic functional prediction

INTRODUCTION

Bronchial asthma is one of the most common chronic respiratory diseases globally. At present, it affects more than 300 million individuals worldwide, and its incidence continues to increase (Huang et al., 2019). According to estimates, the global medical cost of asthma is as high as US $100 billion per year (Rothenberg, 2016). While asthma affects all age groups, it is frequently diagnosed in children. The major symptoms of asthma include coughing, wheezing, shortness of breath, and chest tightness, which are associated with variable expiratory airflow impairment due to bronchoconstriction, increased mucus production, and airway remodeling.

Asthma occurrence and development are related to several factors, including genetic predisposition, immunity, and environmental factors, among others. Although the pathogenesis of asthma is yet to be fully understood, allergic airway inflammation is considered one of the leading causes of allergic asthma (Xiao et al., 2021). Lymphocytes, particularly helper T lymphocytes, are known to play an important role in airway inflammation in asthma (Tumes et al., 2017). To date, most studies have shown that an imbalance in the Th1/Th2 and CD4 + CD25 + Treg/Th17 cell counts is closely related with the occurrence and development of asthma. An increase in the levels of Th2 cytokines (IL-4, IL-5, and IL-13, among others) and Th17 cytokines (IL-17 and IL-6, among others) was observed in both patients with asthma and animal models of asthma (Gandhi et al., 2020). Furthermore, Treg cytokines (IL-10 and TGF-β, among others) were reduced in patients with asthma and animal models of asthma (Boonpiyathad et al., 2019). As the inflammatory response persists in asthma, it eventually leads to airway remodeling. The primary characteristics of airway remodeling are subepithelial collagen deposition, hyperplasia and hypertrophy of airway smooth muscles, angiogenesis under the mucosa, and hyperplasia of mucus glands, which eventually lead to the thickening of the airway wall and narrowing of the functional cavity (Fehrenbach et al., 2017).

In recent years, with the development of high-throughput sequencing technology, the relationship between changes in the human microbiota and asthma has attracted increasing attention. The "hygiene hypothesis" was the first theory to suggest a link between microbes and allergy (Strachan, 1989). Th2 cell-mediated airway inflammation in ovalbumin (OVA)-stimulated germ-free mice was considerably stronger than that in mice colonized with symbiotic microorganisms. The alterations in the immune response driven by microbes indicate that microbial exposure affects the risk of asthma. Dysbiosis and the subsequent dysregulation of microbiota-related immunological processes affect the onset of the disease, its clinical characteristics, and treatment responses (Barcik et al., 2020). For a long time, the lower respiratory tract (LRT) was considered to be sterile; hence, studies on the link between microbes and asthma have mostly focused on the gut microbiota. However, in recent years, several studies have shown that the respiratory microbiome is also closely associated with the occurrence and development of asthma (Budden et al., 2019). The predominant respiratory microbial phyla are Proteobacteria, Firmicutes, Bacteroidetes, and Actinobacteria. Proteobacteria, the most common respiratory microbes in patients with asthma, can promote neutrophil aggregation and are closely associated with airway hyperresponsiveness (AHR) and airway inflammation (Huang et al., 2011, 2015). Previous studies have shown that at the genus level, the abundance of *Haemophilus*, *Neisseria*, and *Fusobacterium* increased significantly in the respiratory tract of patients with asthma (Durack et al., 2017). A 16S rRNA gene sequencing study on the nasal microbiota of children aged less than 5 years showed that the increased abundance of *Streptococcus*, *Haemophilus*, and *Moraxella* was an important risk factor for predicting wheezing in preschoolers that persisted till a school-going age (Teo et al., 2018). *In vitro*, the epithelial damage and inflammatory cytokine expression (IL-33 and IL-8) induced by *Moraxella catarrhalis* were considerably greater than that induced by dominant nasal bacterial isolates (McCauley et al., 2019). *Bifidobacterium* polysaccharides can inhibit Th17-related inflammation in the lungs (Schiavi et al., 2016). *Haemophilus influenzae* is the most common pathogen detected in patients with asthma (Wood et al., 2010). The P38 MAPK pathway was found to be activated when macrophages isolated from bronchoalveolar lavage fluid (BALF) specimens collected from patients with asthma were cultured with *Haemophilus parainfluenza in vitro* (Goleva et al., 2013). In addition, some lung microbes also produce metabolites (such as short-chain fatty acids) and play a specific biological role (Remot et al., 2017; Segal et al., 2017).

However, only a limited number of studies have investigated the association between the dynamic changes in respiratory microbiota and the chronic progression of asthma or whether the changes in respiratory microbiota may trigger asthma progression. In this study, an OVA-induced mouse model of chronic asthma was established

to investigate the differences in respiratory microbiota at different stages of asthma development and their association with the chronic progression of asthma using metagenomic functional prediction; we believe the findings will help identify new strategies for the prevention and treatment of asthma in the future.

MATERIALS AND METHODS

Reagents

Ovalbumin was purchased from Sigma Chemical Co. (OVA; grade V; St. Louis, MO, United States). Imject Alum was obtained from Thermo Fisher Scientific (Rockford, IL, United States). Mouse IL-4, IL-6, IL-10, and IL-17A ELISA kits were purchased from R&D Systems (Minneapolis, MN, United States). Mouse total IgE and OVA-specific IgE ELISA kits were purchased from BioLegend (San Diego, CA, United States). Antibodies against matrix metallopeptidase 9 (MMP-9) and vascular endothelial growth factor (VEGF-A) were obtained from Abcam Co. (Cambridge, MA, United States).

Animal Experiments

Female BALB/c mice (n = 30) aged 4–6 weeks and weighing 17–20 g were obtained from Shanghai Sippr-BK Laboratory Animal Co. Ltd. (Shanghai, China). All mice were maintained in a specific-pathogen-free environment under controlled conditions with a 12 h light/dark cycle at an appropriate temperature and humidity. All animal experiments were conducted in accordance with the institutional guidelines for animal research. The experimental protocol was approved by the Center for Laboratory Animals, Shanghai Children's Hospital, Shanghai Jiao Tong University, Shanghai, China (approval no. 2017Y003).

The mouse model of OVA-induced chronic asthma was established as described previously with minor modifications (Temelkovski et al., 1998). Briefly, the 30 mice were divided into two groups: the control group and OVA group. The mice in the OVA group were sensitized by intraperitoneally injecting with 200 μL of a solution composed of 20 μg OVA dissolved in 100 μL sterile saline and 100 μL Imject Alum [containing 4 mg aluminum hydroxide (net weight)] on days 0, 7, and 14. For the OVA challenge, the mice were exposed to an OVA aerosol [2.5% (wt/vol) OVA solution in sterile saline administered using a PARI PRONEB Ultra compressor (Pari Proneb, Midlothian, WA, United States)] for 30 min on days 21–24 and 28–31, followed by exposure two times per week for an additional 4 weeks. Mice in the control group (n = 6) were injected intraperitoneally with saline and an Imject Alum emulsion and then exposed to an aerosol of sterile saline without OVA according to the same schedule. Six mice in the OVA group were sacrificed in the first (OVA1W), second (OVA2W), fourth (OVA4W), and sixth weeks (OVA6W), and the mice in the control group were sacrificed at the end of the experiment. The mice were sacrificed within 24 h of the final nebulization. After the mice were euthanized, BALF, nasal lavage fluid (NLF), and the left lower lung tissues were collected and preserved. The sensitization-challenge protocols used in this study are summarized in **Figure 1**.

Histological Analysis and Immunofluorescence Staining of Lung Tissue

We first ligated the left lower lung and removed it after complete bronchoalveolar lavage washing. The lungs were harvested, infused with 4% paraformaldehyde, and maintained for 24 h. Sections (4 μm-thick) were embedded in paraffin and then subjected to hematoxylin and eosin (H&E), periodic acid-schiff (PAS), and Masson's trichrome staining to evaluate airway inflammation, mucus production, and collagen deposition in the lung tissues. Pathological changes were observed using a light microscope at 200× magnification. To grade the extent of lung inflammation, goblet cell hyperplasia and collagen fiber deposition semiquatitative scoring system was used as previously described (Kujur et al., 2015; Kubo et al., 2019). Pathological scoring was performed by three different individuals blinded to the experimental methods.

Immunofluorescent staining was performed to measure MMP-9 and VEGF-A expression in the lung tissue specimens. The paraffin-embedded sections were cut and mounted. The sections were deparaffinized and rehydrated using a standard protocol. Next, the tissue sections were treated with a citric acid antigenic repair solution for antigenic repair and washed with PBS three times after cooling. The sections were permeabilized by treatment with 0.5% Triton X-100 for 30 min at room temperature. Then, the sections were incubated with 3% BSA for 30 min at room temperature, followed by immunostaining with primary antibodies (anti-MMP-9 antibody, 1:250; anti-VEGF-A antibody, 1:200) overnight at 4°C. IgG isotype controls were used for each group of tissue samples at the same concentration. The slides were washed with PBS and labeled with fluorescent tagged goat anti-rabbit secondary antibody (1:1,000) for 1 h in the dark at room temperature. The slides were then treated with DAPI (1:200), a fluorescent nuclear stain for improved protein localization. The slides were washed three times with PBS, rinsed with PBS, mounted, sealed, and evaluated within 2 h of staining under an epifluorescence microscope. Representative fluorescent images of each slide were acquired at 200× for morphometric and comparative analysis.

Collection of BALF and NLF

After the mice were sedated with low doses of 10% chloral hydrate, and euthanized by cervical dislocation, their lungs were washed four times by endotracheal intubation to the LRT with cold sterile saline (0.5 mL in each round) to collect BALF specimens. Then, a sterile leather hose was re-inserted to rinse the nasal cavity with normal saline (0.5 mL in each round) for 3–4 times and to collect the NLF. The BALF and NLF were filtered once using a 0.22 μm filter. The filtered BALF was centrifuged at 1,000 × g for 15 min, and the supernatants were collected for cytokine detection. The membrane of the filter was used for subsequent DNA extraction. All specimens were temporarily stored at –80°C.

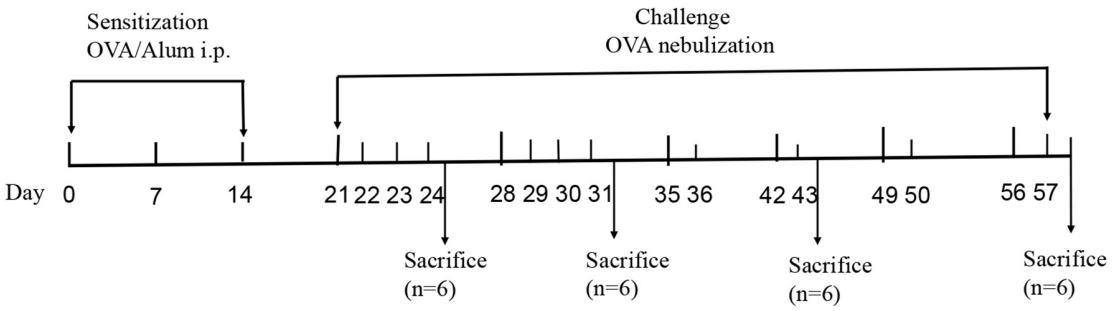


FIGURE 1 | Sensitization-challenge protocols for mice with OVA-induced asthma.

Cytokine and IgE Measurement

The BALF specimens were collected as described above. The levels of IL-4, IL-6, IL-10, IL-17A, total IgE, and OVA-specific IgE in BALF were measured using ELISA kits according to the manufacturer's instructions.

16S rRNA Gene Sequencing and Bioinformatics Analysis

To explore the association between the dynamic changes in respiratory microbiota and the progression of chronic asthma, 16S rRNA gene sequencing was performed using NLF and BALF specimens from control, OVA1W, OVA2W, and OVA6W asthmatic mice.

Total genomic DNA was extracted using the OMEGA Soil DNA Kit (Omega Bio-Tek, Norcross, GA, United States) according to the manufacturer's instructions and stored at –80°C before further analysis. PCR amplification of the V3–V4 region of bacterial 16S rRNA genes was performed using the forward primer 338F (5′-ACTCCTACGGGAGGCAGCA-3′) and the reverse primer 806R (5′-GGACTACHVGGGTWTCTAAT-3′). Sample-specific barcodes were incorporated into the primers for multiplex sequencing. The PCR mixture contained 5 μL of reaction buffer (5×), 0.25 μL of Fast Pfu DNA Polymerase (5 U/μL), 2 μL (2.5 mM) of dNTPs, 1 μL (10 μM) each of the forward and reverse primers, 1 μL of the DNA template, and 14.75 μL of ddH_2O. The thermal cycling conditions were as follows: initial denaturation for 2 min at 98°C, 25 cycles of denaturation for 15 s at 98°C, annealing for 30 s at 55°C, extension for 30 s at 72°C, and a final extension step of 5 min at 72°C. The PCR amplicons were purified using Vazyme VAHTSTM DNA Clean Beads (Vazyme, Nanjing, China) and measured using the Quant-iT PicoGreen dsDNA Assay Kit (Invitrogen, Carlsbad, CA, United States). After the individual quantification step, the amplicons were pooled in equal quantities, and paired-end sequencing (2 × 300 bp) was performed using Illumina MiSeq (Illumina, San Diego, CA, United States) at Shanghai Personal Biotechnology Co., Ltd. (Shanghai, China).

Microbiome bioinformatics analysis was performed using QIIME 2 2020.11 (Hall and Beiko, 2018) with minor modifications (recommended in the official tutorials). Briefly, raw sequence data were demultiplexed using the demux plugin, followed by primer cutting with the cutadapt plugin. The sequences were subjected to quality filtering, denoising, and merging, and the chimera were removed using the DADA2 plugin (Callahan et al., 2016). Non-singleton amplicon sequence variants were aligned using MAFFT and used to construct a phylogeny with FastTree (Price et al., 2009). We used the q2-diversity plugin for computing different α diversity metrics using Shannon's diversity index and β diversity metrics using weighted UniFrac distance matrices. Principal coordinates analysis (PCoA) with weighted UniFrac distance matrices was used to study the community composition. Taxonomy was assigned using a Naive Bayes classifier pre-trained on the Greengenes 13_8_99% OTUs 16S rRNA gene full-length sequences and the q2-feature-classifier plugin (Bokulich et al., 2018). Linear discriminant analysis effect size (LEfSe; Segata et al., 2011) was used to detect differentially abundant taxa across groups using the default parameters. The PICRUSt software package (Langille et al., 2013) was used for metagenomic functional prediction analysis. Kyoto Encyclopedia of Genes and Genomes (KEGG) pathways (Kanehisa et al., 2004) were used to identify the metagenomic contents. LEfSe and PICRUSt analysis were performed using the resource available at http://huttenhower.sph.harvard.edu/galaxy/. The STAMP software (Parks et al., 2014) was used to analyze the predicted metagenome and identify pathways associated with asthma.

Statistical Analysis

The expression levels of IgE, inflammatory factors, and airway remodeling-related proteins were compared by analysis of variance using SPSS 24.0 and GraphPad Prism 8.0. In case of statistical significance, the two groups were compared using a least significant difference *t*-test. The Kruskal–Wallis test was used to estimate intergroup differences for α diversity metrics, β diversity metrics, and LEfSe analysis. The Wilcoxon test was used for comparison between subclasses. The predicted metagenome was analyzed using White's non-parametric *t*-test for comparison between two groups. Statistical tests used in the study were two-sided, and a P value ≤ 0.05 was considered to indicate statistical significance.

RESULTS

While the Increase in Airway Inflammation Is Not Obvious, Airway Remodeling Increases Gradually in Mice With OVA-Induced Chronic Asthma

As indicated by the H&E, compared to the control mice, OVA-challenged mice showed obvious inflammatory cell infiltration around the small airways, bronchial wall thickening, and constricted, even occluded, lumen. As the time period of the OVA challenge increased, there were no significant increases in the signs of allergic inflammation (**Figure 2** and **Supplementary Figure 1A**). PAS staining showed that the number of mucus-secreting goblet cells increased gradually from OVA2W to OVA6W mice (**Figure 2** and **Supplementary Figure 1B**). We observed that collagen fiber deposition around the small airways increased gradually and significantly in the OVA-challenged mice (starting with OVA2W mice) compared to that in control mice, as indicated by Masson's trichome staining (**Figure 2** and **Supplementary Figure 1C**). This indicated the increase in the degree of pulmonary fibrosis and the gradual progression of airway remodeling.

Diversity of the Respiratory Microbiota in Mice With OVA-Induced Chronic Asthma

The shape of the alpha rarefaction curve indicated that the sequencing depth in this study was sufficient (**Figures 3A,B**). The α diversity indicates the richness, diversity, and evenness of the species in a locally homogeneous habitat. The upper respiratory tract (URT) microbiota (NLF samples) of the OVA-induced mice had a significantly higher α diversity ($P < 0.05$) than that of the control mice, as determined using the Shannon index (**Figure 3C**). However, there were no significant differences between the Shannon indices of LRT microbiota (BALF samples) from the control and OVA-induced asthmatic mice ($P > 0.05$) (**Figure 3D**).

The β diversity among the different groups was evaluated using the weighted UniFrac distance. The scatter plot based on the PCoA scores showed the clear separation of the community composition between the control and OVA-induced groups. PCoA revealed significant differences in the diversity of the respiratory microbiota of the OVA-induced and control mice (**Figures 3E,F**).

Modifications in the Composition of the Respiratory Microbiota in Mice With OVA-Induced Chronic Asthma

To understand the differences between the respiratory microbiota in normal mice and OVA-induced asthmatic mice, we analyzed the microbial composition at the phylum and genus levels. We found that Proteobacteria, Firmicutes, Actinobacteria, and Bacteroidetes formed the four dominant phyla in all groups. At the phylum level, Actinobacteria were predominant in normal mice, whereas Proteobacteria, Firmicutes, and Bacteroidetes were the top three phyla in asthmatic mice (in both URT and LRT samples). There were no significant differences in the three dominant phyla in asthmatic mice at different time periods (**Figures 4A,B**).

At the genus level, the top three genera in the respiratory microbiota were *Micrococcaceae*, *Cupriavidus*, and *Pseudomonas*. *Micrococcaceae* had the highest abundance in control mice, whereas *Cupriavidus* and *Pseudomonas* were more abundant in asthmatic mice (**Figures 4C,D**).

Interestingly, the predominant respiratory tract microbiota in the OVA-induced mice varied at different time points. To identify the differences in the bacterial community composition in different groups, we analyzed the different abundances of bacterial communities using LEfSe (**Figure 5**). The analysis of microbial composition at the genus level using LEfSe revealed that among URT microbiota, *Micrococcaceae* from Actinobacteria were most abundant in the control group, *Pseudomonas* from Proteobacteria in the OVA1W and OVA2W groups, and both *Cupriavidus* from Proteobacteria and *Staphylococcus* from Firmicutes in the OVA6W group. Among LRT microbiota, *Micrococcaceae* were most abundant in the control group, *Pseudomonas* in the OVA1W and OVA2W groups, and *Cupriavidus* in the OVA6W group. The results showed that the composition of the URT and LRT microbiota was similar; however, the composition of respiratory microbiota differed significantly at different stages of asthma.

Metagenomic Functional Prediction of the Respiratory Microbiota of Mice With OVA-Induced Chronic Asthma

To understand whether the dynamic changes in the respiratory microbiota contribute to the progression of OVA-induced chronic asthma, we performed bacterial metagenomic function prediction analyses using the PICRUSt program. We explored the differences in bacterial metagenomic functional prediction among different groups at KEGG Level 3.

The following trends were observed in the URT samples. The pathways "MAPK signaling pathway-yeast" and "NOD-like receptor signaling pathway" (both associated with immune inflammation), "antigen processing and presentation," and "two-component system" (associated with allergy) were significantly upregulated in the OVA1W and OVA2W group than in the control group (**Figures 6A,B**). Compared to the control group, "secretion system," "replication, recombination and repair proteins," and "cell division" were upregulated in the OVA6W group (**Figure 6C**). Comparison of the OVA1W and OVA2W groups with the OVA6W group (**Figures 6D,E**) showed that the immune inflammation-related pathways, such as "MAPK signaling pathway-yeast" and "RIG-I-like receptor signaling pathway," were significantly upregulated in the OVA1W and OVA2W groups, whereas "replication, recombination and repair proteins" was upregulated in the OVA6W group.

The results predicted for the URT and LRT samples from the OVA and control groups at different time points were similar (**Figures 6F–H**). In the LRT samples, relative to the OVA6W group, "RIG-I-like receptor signaling pathway" was upregulated

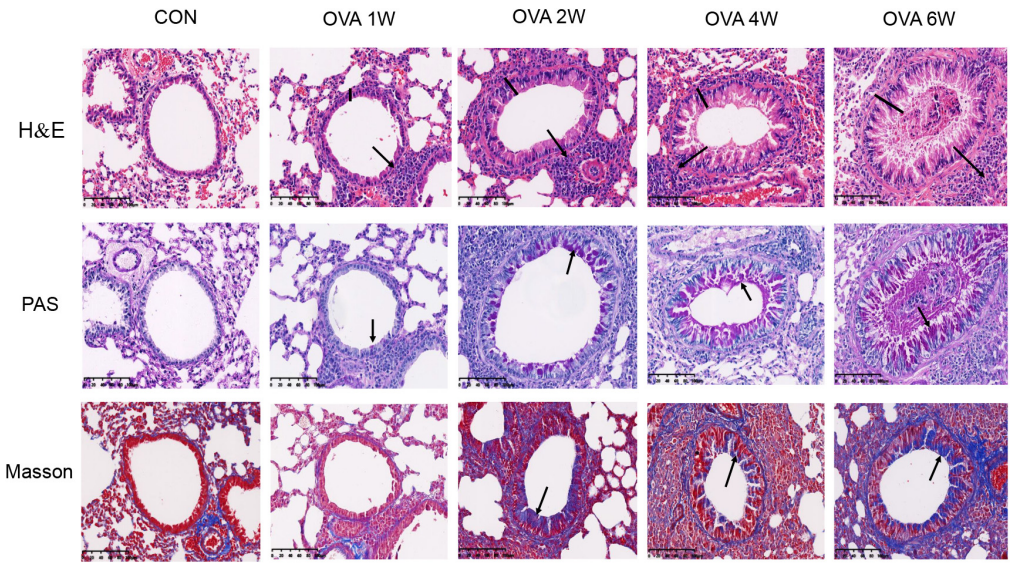


FIGURE 2 | Changes in the pulmonary pathology of mice with OVA-induced chronic asthma. Representative hematoxylin and eosin (H&E)-stained lung sections showing inflammatory cell infiltration around the small airways, bronchial wall thickening, and constriction (200×; the black arrows indicate the aggregation of inflammatory cells, and the black vertical line indicates the airway wall thickness). PAS staining indicating the mucus-producing goblet cells around the small airways (200×; similar to the purple area indicated by the black arrow). Masson's trichome staining indicating collagen fiber deposition around small airways (200×; similar to the blue area indicated by the black arrow).

in the OVA1W group and "MAPK signaling pathway-yeast" was upregulated in the OVA2W group, whereas the pathway "cell division," which is involved in recombination and repair, was upregulated in the OVA6W group (**Figures 6I, J**).

Levels of IgE and Inflammatory Cytokines in BALF of Mice With OVA-Induced Chronic Asthma

Metagenomic functional prediction revealed that the pathways associated with immune inflammation were significantly upregulated in the OVA1W and OVA2W groups; the total IgE, OVA-specific IgE, IL-4, IL-17A, IL-6, and IL-10 levels in BALF were measured using ELISA to confirm the results (**Figure 7**). Compared to the control group, the OVA group had significantly high levels of total IgE (**Figure 7A**) and OVA-specific IgE (**Figure 7B**) in BALF ($P < 0.01$), with the highest level recorded in the OVA2W group. After the OVA challenge, the trends observed in the changes in IL-4 (**Figure 7C**) and IgE levels were similar; however, there was no significant difference between the values obtained in the OVA1W and OVA2W groups. Among OVA-challenged mice, the IL-6 (**Figure 7D**) levels increased gradually from that in OVA2W mice and peaked in OVA6W mice ($P < 0.01$); however, there was no difference between the OVA1W and control groups. With the exception of the OVA1W group, the other OVA groups showed a significant increase in IL-17A (**Figure 7E**) levels compared to the control group ($P < 0.01$), with the highest value obtained in the OVA2W group; however, there was no significant difference among the OVA2W, OVA4W, and OVA6W groups. The IL-10 (**Figure 7F**) level was significantly reduced in OVA-challenged mice compared to that in the control group ($P < 0.01$); the OVA1W mice were an exception.

Expression of MMP-9 and VEGF-A Proteins in Lung Tissues of Mice With OVA-Induced Chronic Asthma

Metagenomic functional prediction showed that the "replication, recombination and repair proteins" pathway was more frequently upregulated in the OVA6W group, and the expression levels of MMP-9 and VEGF-A in the lung tissues were measured using immunofluorescence to confirm this result. MMP-9 and VEGF-A are among the various mediators activated in airway remodeling. Compared to wild-type mice, MMP-9-deficient mice exhibited low levels of peribronchial fibrosis and lower total lung collagen content (Lim et al., 2006). VEGF-A transgenic mice exhibited an asthma-like phenotype with inflammation, vascular remodeling, mucus metaplasia, and AHR (Lee et al., 2004). Compared to the control mice, mice with OVA-induced asthma showed a significantly higher expression of MMP-9 protein around the small airways ($P < 0.05$). However, the expression of MMP-9 protein decreased gradually in these mice (**Figures 8A,B**). Compared to that in control mice, the expression of VEGF-A protein increased significantly in the lung tissues of OVA-challenged mice ($P < 0.05$), and the expression increased with time (**Figures 8C,D**).

DISCUSSION

In the present study, we explored the dynamic changes in the respiratory microbiota and their association with the

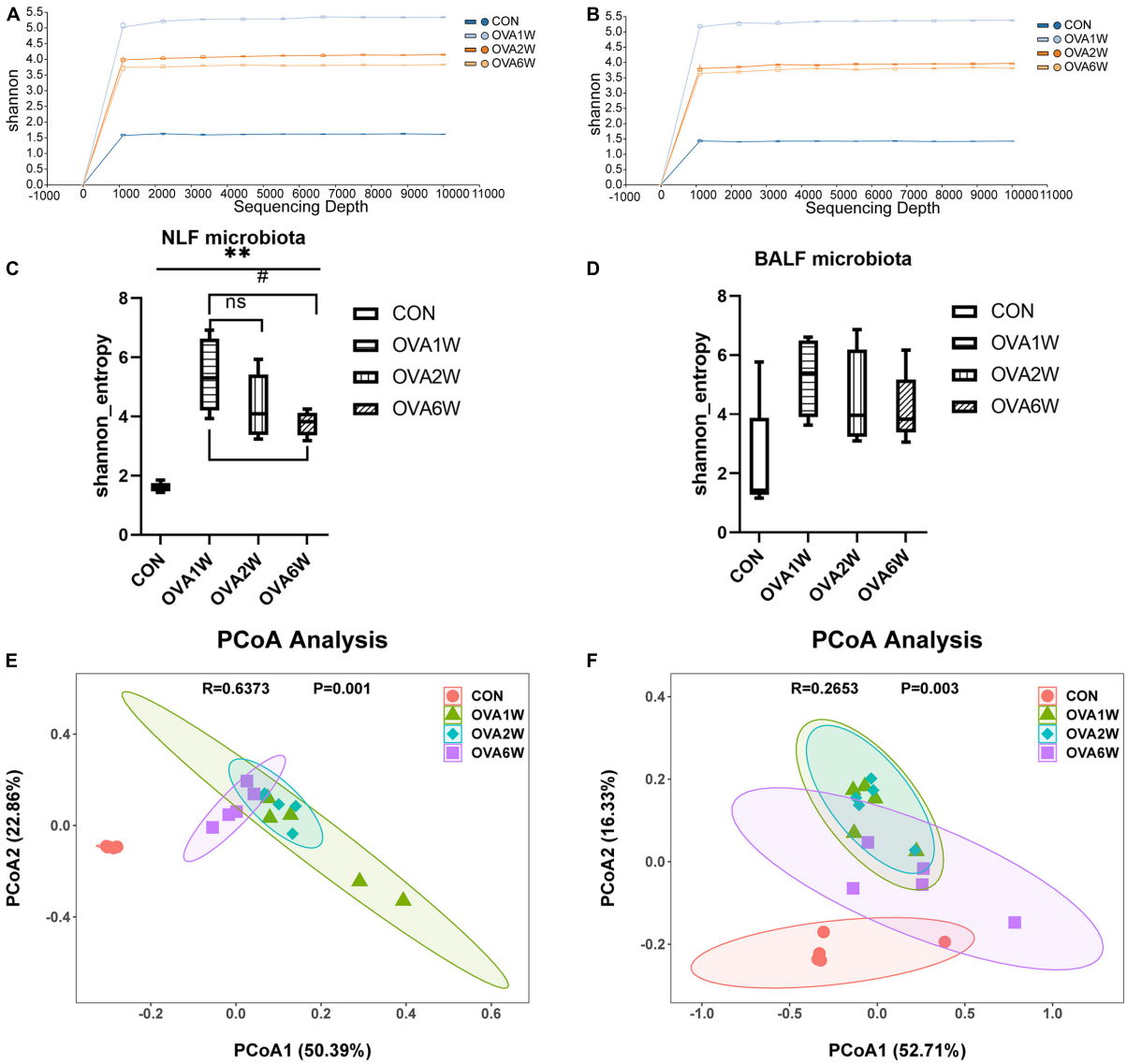


FIGURE 3 | Diversity of the respiratory microbiota in mice with OVA-induced chronic asthma. **(A)** The alpha rarefaction curve in NLF microbiota; **(B)** The alpha rarefaction curve in BALF microbiota; **(C)** α diversity analysis (using Shannon index) of the NLF microbiota; **(D)** α diversity analysis (using Shannon index) of the BALF microbiota; **(E)** PCoA plot showing the β diversity of NLF microbiota ($P = 0.001$); **(F)** PCoA plot showing the β diversity of BALF microbiota ($P = 0.003$). PCoA of all samples using weighted UniFrac distance. PCoA, principal coordinates analysis. ($n = 5$ in each group).

progression of chronic asthma in a mouse model of OVA-induced chronic asthma. In previous studies on the respiratory microbiome, many differences were reported between patients with asthma and healthy people and between patients with different clinical types of asthma (Huang et al., 2011, 2015; Fazlollahi et al., 2018). However, there are no reports on the dynamic changes in the respiratory microbiota in patients with asthma or in animal models during disease progression. We first observed the dynamic changes in the lung pathology of the OVA-induced mice. At the early stage of asthma, the OVA-induced mice exhibited signs of inflammatory cell aggregation around the small airways. From the second week of nebulizing stimulation, small airway wall thickening and stenosis were increased gradually in the OVA-induced mice, following which the number of mucus-secreting goblet cells and collagen fibers increased; however, airway inflammation did not increase significantly. Airway remodeling was the major observation during the sixth week after atomization, whereas airway inflammation was the primary pathological change observed at the early stage of atomization stimulation in mice with OVA-induced chronic asthma. Since the lung pathology changes dynamically in OVA-induced mice, does the composition of the respiratory microbiota also change accordingly? We performed 16S rRNA gene sequencing to study the dynamic changes in the URT and LRT microbiota for the first time.

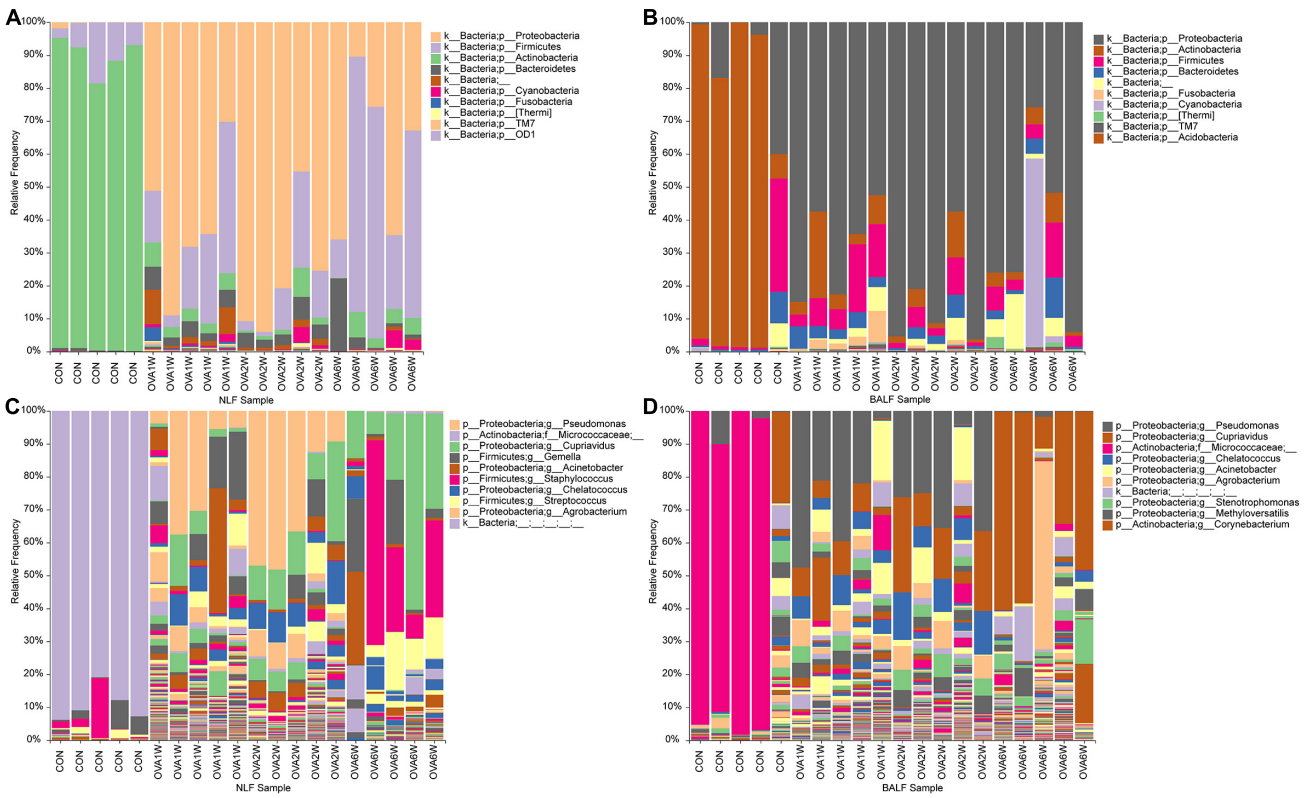


FIGURE 4 | Microbial composition in the URT and LRT at the phylum and genus levels. **(A)** The composition of URT microbiota (NLF samples) at the phylum level. **(B)** The composition of LRT microbiota (BALF samples) at the phylum level. **(C)** The composition of URT microbiota (NLF samples) at the genus level. **(D)** The composition of the LRT microbiota (BALF samples) at the genus level (n = 5 in each group; only the top 10 legends with high abundance are shown).

The microbial diversity analysis revealed that the α diversity, which represents the diversity of microbial groups in the model, increased drastically in the URT, whereas it remained unchanged in the LRT. However, the findings of most studies on the α diversity of respiratory microbiota are inconsistent (Goleva et al., 2013; Budden et al., 2019). β diversity analysis indicated the effect of OVA on the microbial diversities in different groups of mice. The results revealed the significant differences between the respiratory microbiota of OVA-induced mice at the acute airway inflammation and airway remodeling stages and that of control mice.

The β diversity indicated the differences in the respiratory microbiota of OVA-induced mice at different time points and that of normal mice; based on this finding, we studied the microbiota composition. The URT and LRT microbiota were similar at the phylum level, with Proteobacteria being the most abundant phylum and having a significantly higher abundance in OVA-induced mice than in normal mice at the acute inflammation and airway remodeling stages. Previous studies have shown that Proteobacteria have the highest abundance in both URT and LRT microbiota in patients with asthma (Huang et al., 2015; Li et al., 2017). Although the URT and LRT microbiota were shown to be highly consistent, Wypych et al. (2019) reported that URT samples do not accurately reflect the interactions that occur in the LRT, as the microbes present in the LRT depend on the balance between microbes that enter through the URT and those eliminated by host immunity. However, in our study, URT microbiota composition indicates the LRT microbiota composition at the phylum level to some extent. Proteobacteria were the predominant phylum in both URT and LRT specimens of OVA-induced asthmatic mice.

Since the phylum-level microbiota of OVA-induced mice was similar at different time periods, we analyzed the respiratory microbiota composition at the genus level. Among the URT microbiota, *Pseudomonas* was most abundant at the acute inflammatory stage, and *Staphylococcus* and *Cupriavidus* were most abundant at the airway remodeling stage. *Pseudomonas* was shown to be associated with the occurrence of asthma in several studies (Jung et al., 2016; Dimakou et al., 2018). Ferri et al. (2020) showed that the presence of *Pseudomonas* in sputum is an important risk factor for the persistence and frequent exacerbation of asthma. The abundance of *Staphylococcus* in the URT was shown to be significantly high in patients with asthma (Durack et al., 2018). Boutin et al. (2017) showed that the abundance of *Staphylococcus* was significantly higher in patients with pulmonary cystic fibrosis than in patients with asthma. This suggested that *Staphylococcus* may be more closely related to pulmonary fibrosis. *Cupriavidus* acts as an opportunistic pathogen in soil, and its association with asthma has been shown in previous studies. Zhao et al. (2020) showed

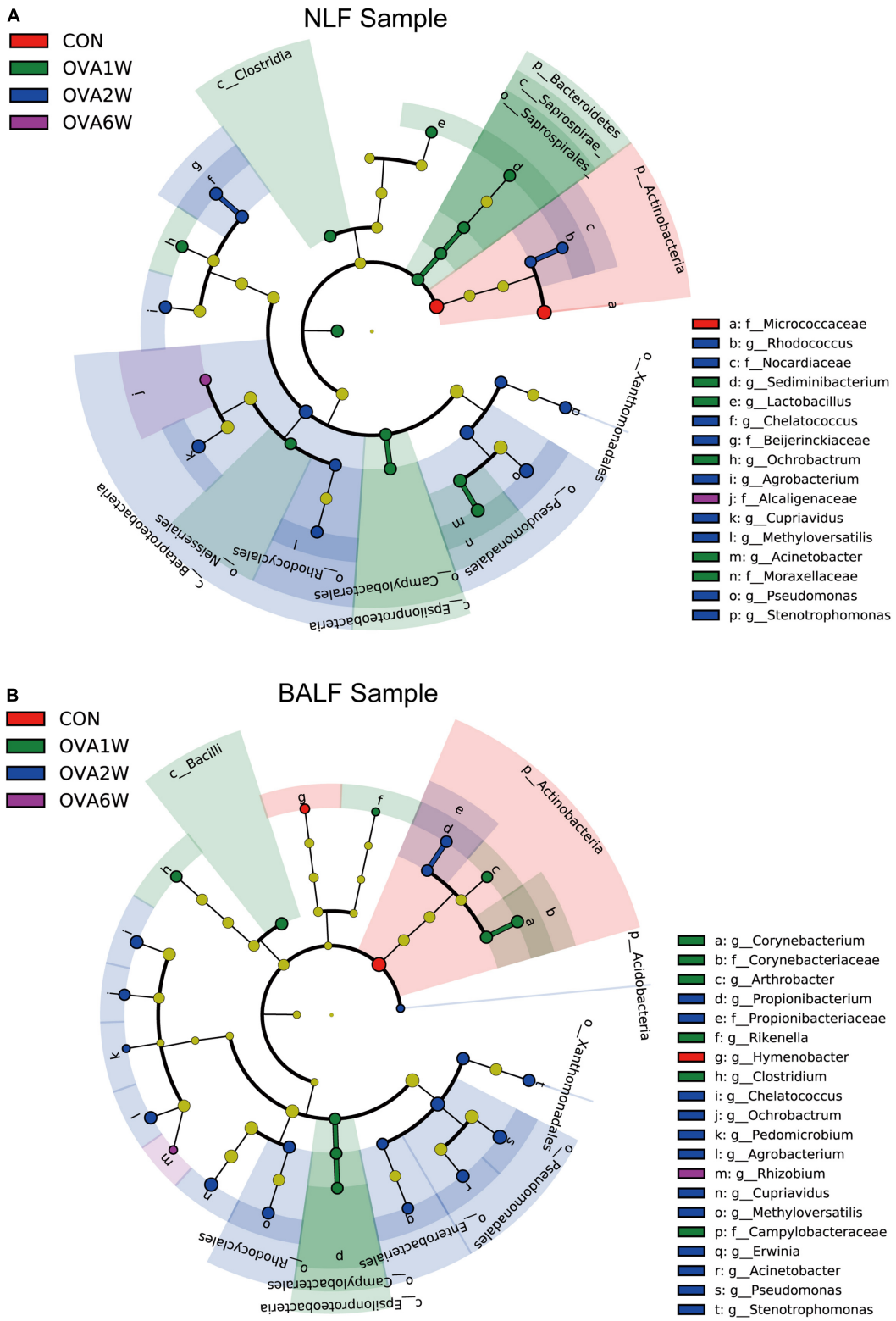


FIGURE 5 | Different abundances of bacterial communities in the respiratory samples, as indicated in LEfSe analysis. The differences are indicated by the color of over-represented taxa: red indicating control mice, green indicating OVA1W mice, blue indicating OVA2W mice and purple indicating OVA6W mice. **(A)** Different abundances of bacterial communities in the URT (NLF samples) with LDA scores > 2.6. **(B)** Different abundances of bacterial communities in the LRT (BALF samples) with LDA scores > 2.5. The circles represent phylogenetic levels from phylum (innermost circle) to genera (outermost circle). $n = 5$ in each group; adjusted P values ≤ 0.05.

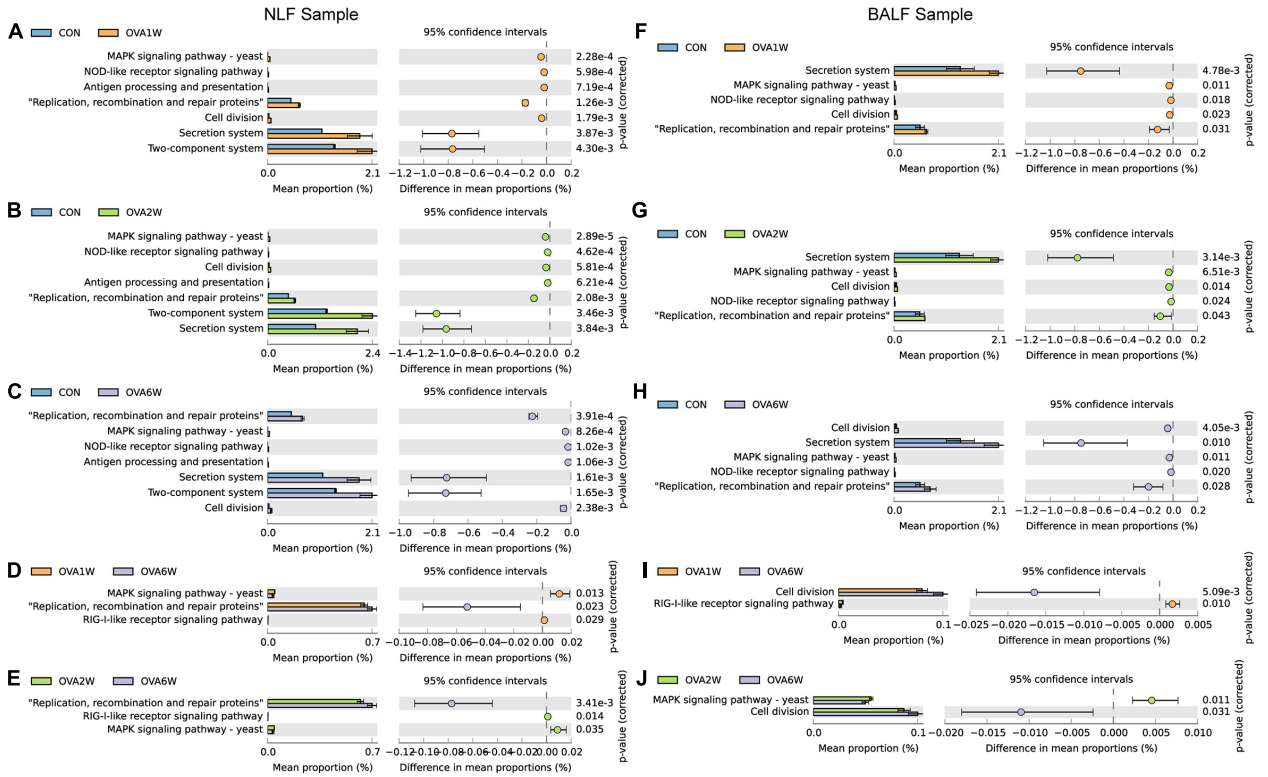


FIGURE 6 | Metagenomic functional prediction of the respiratory microbiota using PICRUSt. Bacterial metagenomic functional categories were derived from level 3 KEGG pathways. Gene functions with a significant difference (corrected *P* value < 0.05) and parts of the pathways associated with asthma are shown. **(A)** Control group vs OVA1W group in URT samples. **(B)** Control group vs OVA2W group in URT samples. **(C)** Control group vs OVA6W group in URT samples. **(D)** OVA1W group vs OVA6W group in URT samples. **(E)** OVA2W group vs OVA6W group in URT samples. **(F)** Control group vs OVA1W group in LRT samples. **(G)** Control group vs OVA2W group in LRT samples. **(H)** Control group vs OVA6W group in LRT samples. **(I)** OVA1W group vs OVA6W group in LRT samples. **(J)** OVA2W group vs OVA6W group in LRT samples.

that the abundance of *Cupriavidus* increased significantly in the URT of patients with asthma that were exposed to high concentrations of PM2.5 particulates. In the acute inflammatory phase, the bacteria with high abundance in the LRT and URT were similar, and only *Cupriavidus* was more abundant at the airway remodeling stage in the LRT. In general, we observed a high degree of similarity in the URT and LRT microbiota of OVA-induced mice. *Pseudomonas* was abundant at the acute inflammatory stage, whereas *Staphylococcus* and *Cupriavidus* were abundant at the airway remodeling stage. These results indicate that the predominant microbiota of the respiratory tract was different at different stages of asthma. *Pseudomonas* may play an important role in airway allergic inflammation, while *Staphylococcus* and *Cupriavidus* are closely related to the progress of airway remodeling.

To determine how the differences in microbiota composition influence the occurrence and development of airway inflammation and remodeling, we performed metagenomic function prediction. In both URT and LRT samples, the pathways associated with immune inflammation, including "MAPK signaling pathway-yeast," "NOD-like receptor signaling pathway," and "RIG-I-like receptor signaling pathway" were significantly upregulated during the acute inflammatory phase. The "antigen processing and presentation" and "two-component system" pathways associated with allergies were also upregulated at this stage. MAPK signaling was shown to be involved in airway inflammation and hyper-responsiveness in asthma (Bao et al., 2017; Sun X. et al., 2020; Sun Y. et al., 2020). The members of the NOD-like receptor family promote inflammatory cell recruitment and regulate immune responses in different tissues, such as lung tissues (Donovan et al., 2020). RIG-I was first shown to be associated with the innate immune response, and RIG-I-like receptor-induced signaling was shown to promote NF-κB and MAPK activation (Heine, 2011; Quicke et al., 2017; Lefkopoulos et al., 2020). The two-component system is a common and important signal transmission system in bacteria and is also a regulatory system for gene expression. It targets genes that encode proteins with bacteria-specific functions, including the hrp gene, which is an allergic response gene (Li et al., 2014; Piqué et al., 2015). At the airway remodeling stage, "secretion system" and "replication, recombination and repair proteins" were primarily upregulated, along with pathways related to recombination and repair, such as "cell division." Previous metagenomic function prediction studies have only suggested significant differences in cellular processes, metabolism, genetic information processing, and human disease pathways between

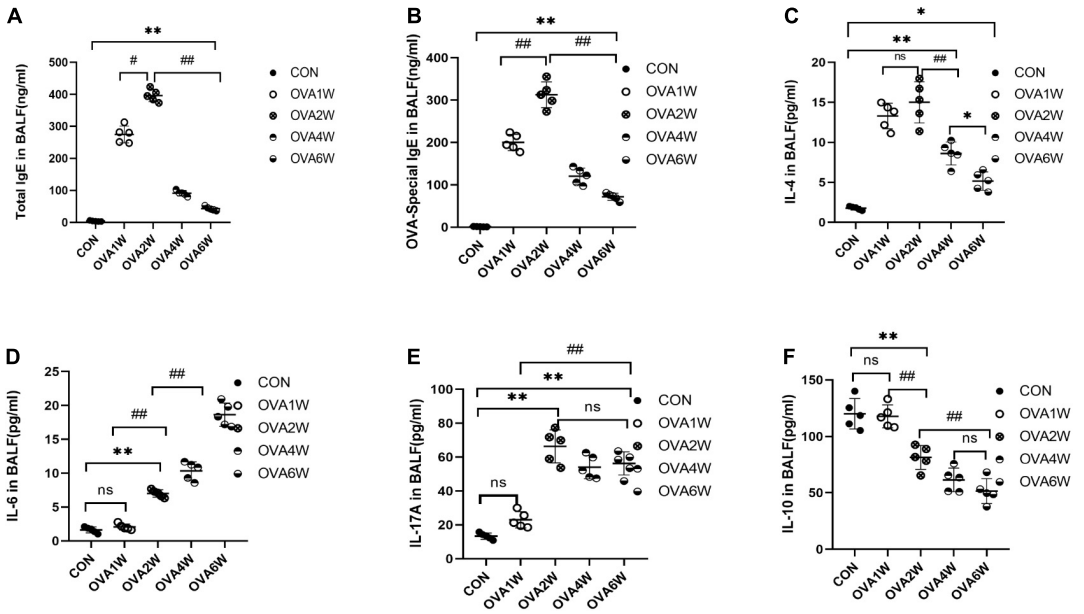


FIGURE 7 | Levels of IgE and inflammatory cytokines in BALF samples. BALF was collected from control mice and OVA-challenged asthmatic mice to measure the levels of total IgE **(A)**, OVA-specific IgE **(B)**, IL-4 **(C)**, IL-6 **(D)**, IL-17A **(E)**, and IL-10 **(F)** using ELISA. Data are expressed as mean ± SD, tested using one-way ANOVA. $n = 5$, $^{*}P \leq 0.05$ vs the control group, $^{**}P \leq 0.01$ vs the control group; $^{\#}P \leq 0.05$ vs group OVA2W, $^{\#\#}P \leq 0.01$ vs group OVA2W. ns: no difference.

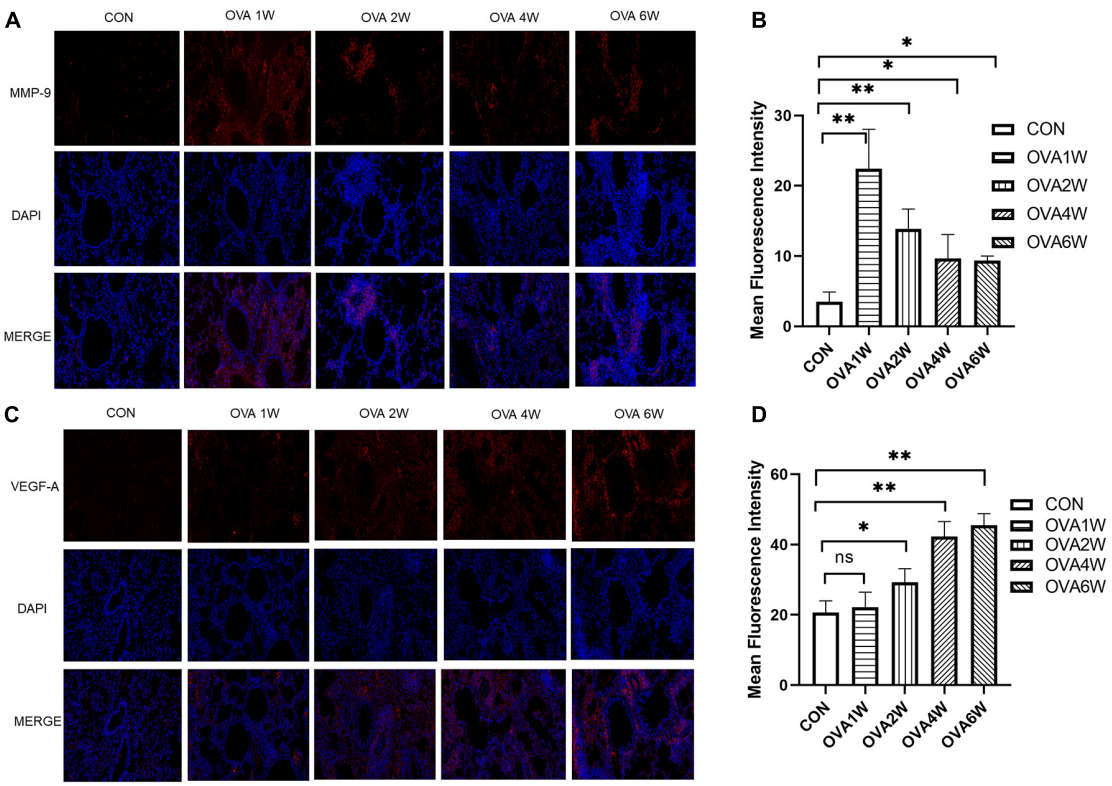


FIGURE 8 | Expression of MMP-9 and VEGF-A proteins in lung tissues. **(A)** Immunofluorescent staining of MMP-9 (200×, red: MMP-9; blue: DAPI). **(B)** Mean fluorescence intensity of MMP-9. Each bar represents the mean ± SD ($n = 6$, $^{*}P \leq 0.05$ vs the control group; $^{**}P \leq 0.01$ vs the control group). **(C)** Immunofluorescent staining of VEGF-A (200×, red: VEGF-A; blue: DAPI). **(D)** Mean fluorescence intensity of VEGF-A. Each bar represents the mean ± SD ($n = 6$, $^{*}P \leq 0.05$ vs the control group; $^{**}P \leq 0.01$ vs the control group; ns: no difference).

patients with asthma and healthy individuals (Millares et al., 2017). However, the metagenomic function prediction analysis of respiratory microflora at KEGG level 3 in animal models of asthma has not been reported. At a more in-depth level, our study confirmed the differences in metagenomic function prediction due to the differences in respiratory microbiota composition.

To confirm the predictions for respiratory microbiota, we measured the levels of total IgE, OVA-specific IgE, IL-4, IL-17A, IL-6, and IL-10 in BALF and the levels of airway remodeling-associated proteins in the lung tissues. The levels of total IgE, OVA-specific IgE, and IL-4 in BALF which represent levels of eosinophilic inflammation increased significantly during acute allergic inflammation. The levels of IL-6 and IL-17A in BALF and VEGF-A in lung tissues increased gradually. Previous studies have shown that IL-6 and IL-17A are associated with airway remodeling in asthma (Camargo et al., 2020; Hudey et al., 2020). The level of MMP-9 also increased significantly compared to that in normal mice, and the minor reduction in the MMP-9 level observed in the late stage could be attributed to the increased MMP-9 utilization during airway remodeling. The expression levels of these cytokines and proteins at different stages of asthma development were consistent with the metagenomic function prediction of respiratory microbiota.

This study had certain limitations. First, our findings are based on a small sample size study. Therefore, validity of the results will have to be confirmed in a larger sample size. Second, sample collection from the control mice and OVA-induced mice was not conducted at the same time points, and we were unable to eliminate the influence of age-related changes in the respiratory microbiota of the mice. Furthermore, the study duration was considerably short. Additionally, the atomization stimulation process was conducted in adult mice, and the mice had not entered senescence; hence, the bacterial and immune status in the mice did not change considerably. Thevaranjan et al. (2017) showed that senescent mice exhibited increased inflammation and changes in microbiota composition.

In conclusion, we established a mouse model of asthma from the onset of acute inflammation to the induction of airway remodeling, and observed the dynamic changes in respiratory microbiota for the first time. The dominant microbiota in the acute inflammatory and airway remodeling phases were different. The pathways associated with immune inflammation were significantly upregulated during the acute inflammatory phase. In contrast, different pathways, including "replication, recombination and repair proteins," were upregulated at the airway remodeling stage. The cytokine levels in BALF and the concentration of airway remodeling-associated proteins in the lung tissues were consistent with the bacterial metagenomic function prediction. Although the precise relationship between airway inflammation and airway remodeling in patients with asthma is is not clear, these are important pathological mechanisms in the development of asthma (Banno et al., 2020). Our findings showed that in the progression of chronic asthma, the dominant microbiota at different stages are different, which may affect the pathophysiological processes in the host. These findings could form the basis for novel methods of asthma prevention and treatment.

DATA AVAILABILITY STATEMENT

The raw sequences of 20 female mice have been submitted to NCBI Project under accession number PRJNA730096 with NCBI Sequence Read Archive under accession number SRP320140.

ETHICS STATEMENT

The animal study was reviewed and approved by Shanghai Children's Hospital, Shanghai Jiao Tong University, Shanghai, China.

AUTHOR CONTRIBUTIONS

LH and SG conceived and designed the study, critically revised the manuscript, and were responsible for funding. JZ, QW, YZ, and MW completed animal experiments, acquired and interpreted the data, and drafted and critically revised the manuscript. All authors read and approved the final manuscript.

FUNDING

This study was financially supported by two grants from the National Natural Science Foundation of China (Nos. 81774365 and 81973902).

ACKNOWLEDGMENTS

We are grateful to Xiao-yong Fan (TB Center, Shanghai Emerging and Reemerging Infectious Disease Institute, Shanghai) for his help with the experimental techniques. We are also grateful to TianTian Liu (School of Life Sciences and Biotechnology, Shanghai Jiao Tong University) for her help with the statistical analyses.

SUPPLEMENTARY MATERIAL

The Supplementary Material for this article can be found online at: https://www.frontiersin.org/articles/10.3389/fmicb.2021.723152/full#supplementary-material

Supplementary Figure 1 | The pathological score in the mice with OVA-induced chronic asthma. **(A)** Inflammation scores are based on H&E staining; **(B)** The PAS scores indicating the mucus-producing goblet cells around the small airways; **(C)** Masson staining score indicating collagen fiber deposition around small airways. Data are expressed as mean ± SD. n=5, $^{*}P \leq 0.05$ vs the control group, $^{**}P \leq 0.01$ vs the control group; $^{\#}P \leq 0.05$ between the two groups, $^{\#\#}P \leq 0.01$ between the two groups, ns: no difference.

Supplementary Figure 2 | The leukocyte cell type counts in BALF samples. The BALF was centrifuged and the precipitated cells were counted after staining by Wright-Giemsa. Data are expressed as mean ± SD. n=5, $^{*}P \leq 0.05$ vs the control group, $^{**}P \leq 0.01$ vs the control group; $^{\#}P \leq 0.05$ between the two groups, $^{\#\#}P \leq 0.01$ between the two groups, ns: no difference.

REFERENCES

Banno, A., Reddy, A. T., Lakshmi, S. P., and Reddy, R. C. (2020). Bidirectional interaction of airway epithelial remodeling and inflammation in asthma. *Clin. Sci.* 134, 1063–1079. doi: 10.1042/cs20191309

Bao, A., Yang, H., Ji, J., Chen, Y., Bao, W., Li, F., et al. (2017). Involvements of p38 MAPK and oxidative stress in the ozone-induced enhancement of AHR and pulmonary inflammation in an allergic asthma model. *Respir. Res.* 18:216. doi: 10.1186/s12931-017-0697-4

Barcik, W., Boutin, R. C. T., Sokolowska, M., and Finlay, B. B. (2020). The Role of Lung and Gut Microbiota in the Pathology of Asthma. *Immunity* 52, 241–255. doi: 10.1016/j.immuni.2020.01.007

Bokulich, N. A., Dillon, M. R., Bolyen, E., Kaehler, B. D., Huttley, G. A., and Caporaso, J. G. (2018). q2-sample-classifier: machine-learning tools for microbiome classification and regression. *J. Open Res. Softw.* 3:934. doi: 10.21105/joss.00934

Boonpiyathad, T., Satitsuksanoa, P., Akdis, M., and Akdis, C. A. (2019). Il-10 producing T and B cells in allergy. *Semin. Immunol.* 44:101326. doi: 10.1016/j.smim.2019.101326

Boutin, S., Depner, M., Stahl, M., Graeber, S. Y., Dittrich, S. A., Legatzki, A., et al. (2017). Comparison of Oropharyngeal Microbiota from Children with Asthma and Cystic Fibrosis. *Mediators Inflamm.* 2017:5047403. doi: 10.1155/2017/5047403

Budden, K. F., Shukla, S. D., Rehman, S. F., Bowerman, K. L., Keely, S., Hugenholtz, P., et al. (2019). Functional effects of the microbiota in chronic respiratory disease. *Lancet Respir. Med.* 7, 907–920. doi: 10.1016/s2213-2600(18)30510-1

Callahan, B. J., Mcmurdie, P. J., Rosen, M. J., Han, A. W., Johnson, A. J., and Holmes, S. P. (2016). DADA2: high-resolution sample inference from Illumina amplicon data. *Nat. Methods* 13, 581–583. doi: 10.1038/nmeth.3869

Camargo, L. D. N., Dos Santos, T. M., De Andrade, F. C. P., Fukuzaki, S., Dos Santos Lopes, F., De Arruda Martins, M., et al. (2020). Bronchial Vascular Remodeling Is Attenuated by Anti-IL-17 in Asthmatic Responses Exacerbated by LPS. *Front. Pharmacol.* 11:1269. doi: 10.3389/fphar.2020.01269

Dimakou, K., Gousiou, A., Toumbis, M., Kaponi, M., Chrysikos, S., Thanos, L., et al. (2018). Investigation of bronchiectasis in severe uncontrolled asthma. *Clin. Respir. J.* 12, 1212–1218. doi: 10.1111/crj.12653

Donovan, C., Liu, G., Shen, S., Marshall, J. E., Kim, R. Y., Alemao, C. A., et al. (2020). The role of the microbiome and the NLRP3 inflammasome in the gut and lung. *J. Leukoc. Biol.* 108, 925–935. doi: 10.1002/jlb.3mr0720-472rr

Durack, J., Huang, Y. J., Nariya, S., Christian, L. S., Ansel, K. M., Beigelman, A., et al. (2018). Bacterial biogeography of adult airways in atopic asthma. *Microbiome* 6:104. doi: 10.1186/s40168-018-0487-3

Durack, J., Lynch, S. V., Nariya, S., Bhakta, N. R., Beigelman, A., Castro, M., et al. (2017). Features of the bronchial bacterial microbiome associated with atopy, asthma, and responsiveness to inhaled corticosteroid treatment. *J. Allergy Clin. Immunol.* 140, 63–75. doi: 10.1016/j.jaci.2016.08.055

Fazlollahi, M., Lee, T. D., Andrade, J., Oguntuyo, K., Chun, Y., Grishina, G., et al. (2018). The nasal microbiome in asthma. *J. Allergy Clin. Immunol.* 142, 834–843.e2. doi: 10.1016/j.jaci.2018.02.020

Fehrenbach, H., Wagner, C., and Wegmann, M. (2017). Airway remodeling in asthma: what really matters. *Cell Tissue Res.* 367, 551–569. doi: 10.1007/s00441-016-2566-8

Ferri, S., Crimi, C., Campisi, R., Cacopardo, G., Paoletti, G., Puggioni, F., et al. (2020). Impact of asthma on bronchiectasis severity and risk of exacerbations. *J. Asthma* [Epub Online ahead of print]. doi: 10.1080/02770903.2020.1857395

Gandhi, G. R., Leão, G. C. S., Calisto, V., Vasconcelos, A. B. S., Almeida, M. L. D., Quintans, J. S. S., et al. (2020). Modulation of interleukin expression by medicinal plants and their secondary metabolites: a systematic review on anti-asthmatic and immunopharmacological mechanisms. *Phytomedicine* 70:153229. doi: 10.1016/j.phymed.2020.153229

Goleva, E., Jackson, L. P., Harris, J. K., Robertson, C. E., Sutherland, E. R., Hall, C. F., et al. (2013). The effects of airway microbiome on corticosteroid responsiveness in asthma. *Am. J. Respir. Crit. Care Med.* 188, 1193–1201. doi: 10.1164/rccm.201304-0775OC

Hall, M., and Beiko, R. G. (2018). 16S rRNA Gene Analysis with QIIME2. *Methods Mol. Biol.* 1849, 113–129. doi: 10.1007/978-1-4939-8728-3_8

Heine, H. (2011). TLRs, NLRs and RLRs: innate sensors and their impact on allergic diseases–a current view. *Immunol. Lett.* 139, 14–24. doi: 10.1016/j.imlet.2011.04.010

Huang, K., Yang, T., Xu, J., Yang, L., Zhao, J., Zhang, X., et al. (2019). Prevalence, risk factors, and management of asthma in China: a national cross-sectional study. *Lancet* 394, 407–418. doi: 10.1016/s0140-6736(19)31147-x

Huang, Y. J., Nariya, S., Harris, J. M., Lynch, S. V., Choy, D. F., Arron, J. R., et al. (2015). The airway microbiome in patients with severe asthma: associations with disease features and severity. *J. Allergy Clin. Immunol.* 136, 874–884. doi: 10.1016/j.jaci.2015.05.044

Huang, Y. J., Nelson, C. E., Brodie, E. L., Desantis, T. Z., Baek, M. S., Liu, J., et al. (2011). Airway microbiota and bronchial hyperresponsiveness in patients with suboptimally controlled asthma. *J. Allergy Clin. Immunol.* 127, 372–381.e3. doi: 10.1016/j.jaci.2010.10.048

Hudey, S. N., Ledford, D. K., and Cardet, J. C. (2020). Mechanisms of non-type 2 asthma. *Curr. Opin. Immunol.* 66, 123–128. doi: 10.1016/j.coi.2020.10.002

Jung, J. W., Choi, J. C., Shin, J. W., Kim, J. Y., Park, I. W., Choi, B. W., et al. (2016). Lung Microbiome Analysis in Steroid-Na^{i}ive Asthma Patients by Using Whole Sputum. *Tuberc. Respir. Dis.* 79, 165–178. doi: 10.4046/trd.2016.79.3.165

Kanehisa, M., Goto, S., Kawashima, S., Okuno, Y., and Hattori, M. (2004). The KEGG resource for deciphering the genome. *Nucleic Acids Res.* 32, D277–D280. doi: 10.1093/nar/gkh063

Kubo, F., Ariestanti, D. M., Oki, S., Fukuzawa, T., Demizu, R., Sato, T., et al. (2019). Loss of the adhesion G-protein coupled receptor ADGRF5 in mice induces airway inflammation and the expression of CCL2 in lung endothelial cells. *Respir. Res.* 20:11. doi: 10.1186/s12931-019-0973-6

Kujur, W., Gurram, R. K., Haleem, N., Maurya, S. K., and Agrewala, J. N. (2015). Caerulomycin A inhibits Th2 cell activity: a possible role in the management of asthma. *Sci. Rep.* 5:15396. doi: 10.1038/srep15396

Langille, M. G., Zaneveld, J., Caporaso, J. G., Mcdonald, D., Knights, D., Reyes, J. A., et al. (2013). Predictive functional profiling of microbial communities using 16S rRNA marker gene sequences. *Nat. Biotechnol.* 31, 814–821. doi: 10.1038/nbt.2676

Lee, C. G., Link, H., Baluk, P., Homer, R. J., Chapoval, S., Bhandari, V., et al. (2004). Vascular endothelial growth factor (VEGF) induces remodeling and enhances TH2-mediated sensitization and inflammation in the lung. *Nat. Med.* 10, 1095–1103. doi: 10.1038/nm1105

Lefkopoulos, S., Polyzou, A., Derecka, M., Bergo, V., Clapes, T., Cauchy, P., et al. (2020). Repetitive Elements Trigger RIG-I-like Receptor Signaling that Regulates the Emergence of Hematopoietic Stem and Progenitor Cells. *Immunity* 53, 934–951.e9. doi: 10.1016/j.immuni.2020.10.007

Li, N., Qiu, R., Yang, Z., Li, J., Chung, K. F., Zhong, N., et al. (2017). Sputum microbiota in severe asthma patients: relationship to eosinophilic inflammation. *Respir. Med.* 131, 192–198. doi: 10.1016/j.rmed.2017.08.016

Li, R. F., Lu, G. T., Li, L., Su, H. Z., Feng, G. F., Chen, Y., et al. (2014). Identification of a putative cognate sensor kinase for the two-component response regulator HrpG, a key regulator controlling the expression of the hrp genes in *Xanthomonas campestris* pv. *campestris*. *Environ. Microbiol.* 16, 2053–2071. doi: 10.1111/1462-2920.12207

Lim, D. H., Cho, J. Y., Miller, M., Mcelwain, K., Mcelwain, S., and Broide, D. H. (2006). Reduced peribronchial fibrosis in allergen-challenged MMP-9-deficient mice. *Am. J. Physiol. Lung. Cell. Mol. Physiol.* 291, L265–L271. doi: 10.1152/ajplung.00305.2005

McCauley, K., Durack, J., Valladares, R., Fadrosh, D. W., Lin, D. L., Calatroni, A., et al. (2019). Distinct nasal airway bacterial microbiotas differentially relate to exacerbation in pediatric patients with asthma. *J. Allergy Clin. Immunol.* 144, 1187–1197. doi: 10.1016/j.jaci.2019.05.035

Millares, L., Bermudo, G., Pérez-Brocal, V., Domingo, C., Garcia-Nuñez, M., Pomares, X., et al. (2017). The respiratory microbiome in bronchial mucosa and secretions from severe IgE-mediated asthma patients. *BMC Microbiol.* 17:20. doi: 10.1186/s12866-017-0933-6

Parks, D. H., Tyson, G. W., Hugenholtz, P., and Beiko, R. G. (2014). STAMP: statistical analysis of taxonomic and functional profiles. *Bioinformatics* 30, 3123–3124. doi: 10.1093/bioinformatics/btu494

Piqué, N., Miñana-Galbis, D., Merino, S., and Tomás, J. M. (2015). Virulence Factors of Erwinia amylovora: a Review. *Int. J. Mol. Sci.* 16, 12836–12854. doi: 10.3390/ijms160612836

Price, M. N., Dehal, P. S., and Arkin, A. P. (2009). FastTree: computing large minimum evolution trees with profiles instead of a distance matrix. *Mol. Biol. Evol.* 26, 1641–1650. doi: 10.1093/molbev/msp077

Quicke, K. M., Diamond, M. S., and Suthar, M. S. (2017). Negative regulators of the RIG-I-like receptor signaling pathway. *Eur. J. Immunol.* 47, 615–628. doi: 10.1002/eji.201646484

Remot, A., Descamps, D., Noordine, M. L., Boukadiri, A., Mathieu, E., Robert, V., et al. (2017). Bacteria isolated from lung modulate asthma susceptibility in mice. *ISME J.* 11, 1061–1074. doi: 10.1038/ismej.2016.181

Rothenberg, M. E. (2016). Humanized Anti-IL-5 Antibody Therapy. *Cell* 165:509. doi: 10.1016/j.cell.2016.04.020

Schiavi, E., Gleinser, M., Molloy, E., Groeger, D., Frei, R., Ferstl, R., et al. (2016). The Surface-Associated Exopolysaccharide of Bifidobacterium longum 35624 Plays an Essential Role in Dampening Host Proinflammatory Responses and Repressing Local TH17 Responses. *Appl. Environ. Microbiol.* 82, 7185–7196. doi: 10.1128/aem.02238-16

Segal, L. N., Clemente, J. C., Wu, B. G., Wikoff, W. R., Gao, Z., Li, Y., et al. (2017). Randomised, double-blind, placebo-controlled trial with azithromycin selects for anti-inflammatory microbial metabolites in the emphysematous lung. *Thorax* 72, 13–22. doi: 10.1136/thoraxjnl-2016-208599

Segata, N., Izard, J., Waldron, L., Gevers, D., Miropolsky, L., Garrett, W. S., et al. (2011). Metagenomic biomarker discovery and explanation. *Genome Biol.* 12:R60. doi: 10.1186/gb-2011-12-6-r60

Strachan, D. P. (1989). Hay fever, hygiene, and household size. *BMJ* 299, 1259–1260. doi: 10.1136/bmj.299.6710.1259

Sun, X., Hou, T., Cheung, E., Iu, T. N., Tam, V. W., Chu, I. M., et al. (2020). Anti-inflammatory mechanisms of the novel cytokine interleukin-38 in allergic asthma. *Cell. Mol. Immunol.* 17, 631–646. doi: 10.1038/s41423-019-0300-7

Sun, Y., Shi, Z., Liu, B., Li, X., Li, G., Yang, F., et al. (2020). YKL-40 mediates airway remodeling in asthma via activating FAK and MAPK signaling pathway. *Cell Cycle* 19, 1378–1390. doi: 10.1080/15384101.2020.1750811

Temelkovski, J., Hogan, S. P., Shepherd, D. P., Foster, P. S., and Kumar, R. K. (1998). An improved murine model of asthma: selective airway inflammation, epithelial lesions and increased methacholine responsiveness following chronic exposure to aerosolised allergen. *Thorax* 53, 849–856. doi: 10.1136/thx.53.10.849

Teo, S. M., Tang, H. H. F., Mok, D., Judd, L. M., Watts, S. C., Pham, K., et al. (2018). Airway Microbiota Dynamics Uncover a Critical Window for Interplay of Pathogenic Bacteria and Allergy in Childhood Respiratory Disease. *Cell Host Microbe* 24, 341–352.e5. doi: 10.1016/j.chom.2018.08.005

Thevaranjan, N., Puchta, A., Schulz, C., Naidoo, A., Szamosi, J. C., Verschoor, C. P., et al. (2017). Age-Associated Microbial Dysbiosis Promotes Intestinal Permeability, Systemic Inflammation, and Macrophage Dysfunction. *Cell Host Microbe* 21, 455–466.e4. doi: 10.1016/j.chom.2017.03.002

Tumes, D. J., Papadopoulos, M., Endo, Y., Onodera, A., Hirahara, K., and Nakayama, T. (2017). Epigenetic regulation of T-helper cell differentiation, memory, and plasticity in allergic asthma. *Immunol. Rev.* 278, 8–19. doi: 10.1111/imr.12560

Wood, L. G., Simpson, J. L., Hansbro, P. M., and Gibson, P. G. (2010). Potentially pathogenic bacteria cultured from the sputum of stable asthmatics are associated with increased 8-isoprostane and airway neutrophilia. *Free Radic. Res.* 44, 146–154. doi: 10.3109/10715760903362576

Wypych, T. P., Wickramasinghe, L. C., and Marsland, B. J. (2019). The influence of the microbiome on respiratory health. *Nat. Immunol.* 20, 1279–1290. doi: 10.1038/s41590-019-0451-9

Xiao, Q., He, J., Lei, A., Xu, H., Zhang, L., Zhou, P., et al. (2021). PPARγ enhances ILC2 function during allergic airway inflammation via transcription regulation of ST2. *Mucosal Immunol.* 14, 468–478. doi: 10.1038/s41385-020-00339-6

Zhao, H., Liu, J., Zhu, J., Yang, F., Wu, H., Ba, Y., et al. (2020). Bacterial composition and community structure of the oropharynx of adults with asthma are associated with environmental factors. *Microb. Pathog.* 149:104505. doi: 10.1016/j.micpath.2020.104505

Conflict of Interest: The authors declare that the research was conducted in the absence of any commercial or financial relationships that could be construed as a potential conflict of interest.

Publisher's Note: All claims expressed in this article are solely those of the authors and do not necessarily represent those of their affiliated organizations, or those of the publisher, the editors and the reviewers. Any product that may be evaluated in this article, or claim that may be made by its manufacturer, is not guaranteed or endorsed by the publisher.

Copyright © 2021 Zheng, Wu, Zou, Wang, He and Guo. This is an open-access article distributed under the terms of the Creative Commons Attribution License (CC BY). The use, distribution or reproduction in other forums is permitted, provided the original author(s) and the copyright owner(s) are credited and that the original publication in this journal is cited, in accordance with accepted academic practice. No use, distribution or reproduction is permitted which does not comply with these terms.

frontiers in Immunology

ORIGINAL RESEARCH
published: 01 September 2021
doi: 10.3389/fimmu.2021.715559

Cytotoxic T-Cell Trafficking Chemokine Profiles Correlate With Defined Mucosal Microbial Communities in Colorectal Cancer

Jiali Zhang[1,2], Ji Tao[1], Ruo-Nan Gao[1], Zhi-Yuan Wei[1], Yu-Shan He[1], Chun-Yan Ren[1], Qi-Chun Li[1], Yan-Shan Liu[1], Ke-Wei Wang[1,3], Gong Yang[2,4], Chengjia Qian[5] and Jian-Huan Chen[1]**

[1] Laboratory of Genomic and Precision Medicine, Wuxi School of Medicine, Jiangnan University, Wuxi, China, [2] Central Laboratory, The Fifth People's Hospital of Shanghai Fudan University, Shanghai, China, [3] Department of Hospital Infection, Affiliated Hospital of Jiangnan University, Wuxi, China, [4] Cancer Institute, Fudan University Shanghai Cancer Center, Shanghai, China, [5] Department of General Surgery, Affiliated Hospital of Jiangnan University, Wuxi, China

OPEN ACCESS

Edited by:
Monica Cartelle Gestal,
Louisiana State University Health Shreveport, United States

Reviewed by:
Sandra J. Van Vliet,
Vrije Universiteit Amsterdam, Netherlands
Graciela Alicia Cremaschi,
Consejo Nacional de Investigaciones Científicas y Técnicas (CONICET), Argentina

***Correspondence:**
Jian-Huan Chen
cjh_bio@hotmail.com
Chengjia Qian
qianchengjia85@hotmail.com

Specialty section:
This article was submitted to Microbial Immunology, a section of the journal Frontiers in Immunology

Received: 27 May 2021
Accepted: 29 July 2021
Published: 01 September 2021

Citation:
Zhang J, Tao J, Gao R-N, Wei Z-Y, He Y-S, Ren C-Y, Li Q-C, Liu Y-S, Wang K-W, Yang G, Qian C and Chen J-H (2021) Cytotoxic T-Cell Trafficking Chemokine Profiles Correlate With Defined Mucosal Microbial Communities in Colorectal Cancer. Front. Immunol. 12:715559. doi: 10.3389/fimmu.2021.715559

The involvement of gut microbiota in T-cell trafficking into tumor tissue of colorectal cancer (CRC) remains to be further elucidated. The current study aimed to evaluate the expression of major cytotoxic T-cell trafficking chemokines (CTTCs) and chemokine-associated microbiota profiles in both tumor and adjacent normal tissues during CRC progression. We analyzed the expression of chemokine C-X-C motif ligands 9, 10, and 11 (*CXCL9*, *CXCL10*, and *CXCL11*), and C-C motif ligand 5 (*CCL5*), characterized gut mucosa-associated microbiota (MAM), and investigated their correlations in CRC patients. Our results showed that the expression of *CXCL9, CXCL10*, and *CXCL11* was significantly higher in tumor than in adjacent normal tissues in 136 CRC patients. Notably, the high expression of *CXCL9* in tumor tissues was associated with enhanced $CD8^+$ T-cell infiltration and improved survival. Moreover, the MAM in tumor tissues showed reduction of microbial diversity and increase of oral bacteria. Microbial network analysis identified differences in microbial composition and structure between tumor and adjacent normal tissues. In addition, stronger associations between oral bacteria and other gut microbes were observed. Furthermore, the correlation analysis between the defined MAM and individual CTTCs showed that the CTTCs' correlated operational taxonomic units (OTUs) in tumor and adjacent normal tissues rarely overlap with each other. Notably, all the enriched OTUs were positively correlated with the CTTCs in either tumor or adjacent normal tissues. Our findings demonstrated stronger interactions between oral bacteria and gut microbes, and a shifted correlation pattern between MAM and major CTTCs in tumor tissues, underlining possible mechanisms of gut microbiota–host interaction in CRC.

Keywords: T cell trafficking, mucosa-associated bacteria, tumor, adjacent normal tissues, colorectal cancer, chemokines

INTRODUCTION

Colorectal cancer (CRC) accounts for the third most commonly diagnosed cancer and the second leading cause of cancer-related death worldwide (1). High infiltration with cytotoxic T cells (CTCs) correlates with improved relapse-free and overall survival (OS) in patients with CRC (2–4). Therefore, recent therapeutic strategies for cancer such as immunotherapies focus on CTC trafficking to the tumor site (5–8). Different from the remarkable treatment responses of adoptive immunotherapy in patients affected by advanced melanoma and hematologic malignancy, the effect of immunotherapy against CRCs has been more moderate (9). One of the major challenges is to effectively traffic CTCs to the tumor microenvironment (10, 11).

The expression of chemokine receptors in CTCs, as well as the expression of their ligands in tumor tissues, is essential for localizing CTCs to tumor tissue (5, 12, 13). It has been reported that CTCs with higher CXCR3 expression can be recruited to the tumor site by ligands, including CXCL9, CXCL10, and CXCL11, which are known as IFNγ-inducible chemokines (12, 13). Additionally, studies have identified CCL5 and its receptor (C-C motif) receptor 5 (CCR5) as another critical component of T-cell chemotaxis that is closely associated with CTC infiltration and better survival (12). Therefore, expression of specific chemokines in tumors could be potentially correlated with the presence of CTCs, which might serve as useful targets for anti-cancer therapies.

The gut mucosa is a dynamic interface between host cells and microbiota (14). Progress of colorectal neoplasia has been linked to interactions between tumor microenvironment and mucosal microbiota barrier, whose process can be reversed by interfering the microbiota (15–17). In mouse models, mixture of microbes enhances anti-cancer immunity through inducing interferon-γ-producing CTCs in the tumor tissues (18), pointing to plausible evidence for the use of gut microbiota as a therapeutic target. Additionally, it has recently been demonstrated that bacteria isolated from CRC tissues could upregulate expression of most types of CTTCs in CRC cell lines *in vitro* (19). However, it remains to be elucidated the change of microbiome profiles during the transition from normal mucosae to malignant lesions, and the correlation between CTTCs and defined microbial communities in the CRC tumor microenvironment. Although enrichment of *Fusobacterium* and its regulation of tumor microenvironment have been demonstrated in CRC (20, 21), increasing evidence suggests that microbiota work as a community with nonnegligible contribution from various microbes (22–24), which remains to be clarified. Herein, we investigated the microbial transition in the tumor mucosae and adjacent normal mucosae, and the association between bacterial colonization and CTTCs in CRC patients.

MATERIALS AND METHODS

Patient Recruitment and Sample Collection

A total of 136 CRC patients scheduled for a primary resection of their tumor at the Affiliated Hospital of Jiangnan University between 2016 and 2019 were recruited in the study. The participants did not receive chemo-radiotherapy before the resection and were not treated with antibiotics in the month prior to surgery but were administered antibiotics intravenously within a few hours of the resection. After surgery, there were 136 pairs of fresh tissues from colorectal tumor or as far away from the tumor as possible (adjacent tissue) collected. Biopsies were snap-frozen in a cryovial immediately with liquid nitrogen and then stored at −80°C until DNA extraction. Histopathological and clinical features were scored according to the International Union Against Cancer (UICC)–TNM staging system. This study was approved by the Ethics Committee of Jiangnan University and was conducted in accordance with the Declaration of Helsinki. Informed consent was obtained from all of the participants after explanation of the nature of the study.

DNA Extraction and 16S rRNA Gene Sequencing

Paired mucosae samples from tumor and adjacent normal tissues were subjected to DNA extraction. Mucosal DNA was extracted using the AllPrep DNA/RNA extraction kit. Total DNA was purified from tumor and paired normal adjacent tissue samples. MAM was analyzed based on 16S rRNA gene sequencing. 16S rRNA gene amplicon sequencing was carried out employing the 16S rRNA gene Sequencing Library Preparation protocol developed by Illumina (San Diego, California, USA). Briefly, 200 ng of mucosal DNA was amplified from each sample using the primers 515F (5′ GTGCCAGCMGCCGCGGTAA 3′) with Titanium Adaptor B and 806R (5′ GGACTACHVGGGTWT CTAAT 3′) with Titanium Adaptor A and a sample-specific barcode sequence targeting the V4 hypervariable region of the 16S rRNA gene using FastStart Taq DNA Polymerase (Roche, USA).

RNA Isolation, mRNA Expression, and Quantitative PCR

Total RNA was isolated from CRC tumor tissues and paired normal adjacent tissue using Trizol (Invitrogen, USA). The obtained RNA was used to synthesize cDNA by Superscript III Reverse Transcriptase (Promega, USA). Real-time PCR reaction mixes were prepared using SYBR Green (TaKaRa, Japan) and run on the LightCycler® 480 II Real-time PCR System (Roche, USA) with the following conditions: 95°C for 5 min, 95°C for 5 s, and 60°C for 30 s, for 40 cycles. The relative expression level of CTTC mRNA was calculated using the $2^{-\Delta Ct}$ (dCt) method. The ΔCt value was calculated by subtracting the Ct value of the housekeeping gene [glyceraldehyde-3-phosphate dehydrogenase (GAPDH)] from that of the target genes. The primers used were as follows: *CXCL9*, forward primer (5′ AAGC AGCCAAGTCGGTTAGT 3′) and reverse primer (5′ CAGCAGTGTGAGCAGTGATTC 3′); *CXCL10*, forward primer (5′ AGCAGAGGAACCTCCAGTCT 3′) and reverse primer (5′ AGGTACTCCTTGAATGCCACT 3′); *CXCL11*, forward primer (5′ GAGTGTGAAGGGCATGGCTA 3′) and reverse primer (5′ CCTTGAACA 3′); *CCL5*, forward primer (5′ CAGTCGTCCACAGGTCAAGG 3′) and reverse

primer (5′ CTTGTTCAGCCGGGAGTCAT 3′); *GAPDH*, forward primer (5′ TGACTTCAACAGCGACACCCA 3′) and reverse primer (5′ CACCCTGTTGCTGTAGCCAAA 3′). Experiments were repeated in triplicate.

Immunohistochemistry and Immunofluorescence Staining and Image Analysis

Specimens used for immunohistochemistry and immunofluorescence staining were obtained immediately after surgical resection and fixed in 10% neutral formalin, paraffin-embedded, and used for histological assays as previously described (25). Immunohistochemistry of paraffin sections was carried out using a two-step protocol. Briefly, 5-μm paraffin sections were first deparaffinized and hydrated, and endogenous peroxidase activity was blocked by incubating the slides in 0.3% H_2O_2. Antigen retrieval was performed by microwave treatment in citrate buffer, pH 6.0. Sections were blocked with normal sera from the same species from which the secondary antibodies were derived. After overnight incubation at 4°C with antibodies against human CD8 (1:300 dilution, Abcam, ab101500), CXCR3 (1:300 dilution, ABclonal, A2939), or control antibodies (Rabbit monoclonal IgG, Abcam, ab172730), we applied Envision System HRP-labeled polymer anti-rabbit (for CD8 and CXCR3) (Dako Cytomation) for 30 min and diaminobenzidine (5 min) and hematoxylin counterstain (1 min). Slides were scanned by an automated scanning microscope (Pannoramic Digital Slide Scanners, 3DHISTECH). The 3DHISTECH software (CaseViewer) was used to count the number of positive signals in each tissue core. We calculated the average density (cells/mm^2) of each tumor-infiltrating $CD8^+$ T-cell subset or $CXCR3^+$ subset.

For multiple-color immunofluorescence staining, formalin-fixed, paraffin-embedded sections were deparaffinized and rehydrated. Antigen retrieval was performed by microwave treatment in citrate buffer, pH 6.0, and blockage of non-specific antibody binding was carried out with 5% BSA. Sections were then incubated with anti-human CXCR3 and CD3 overnight at 4°C, followed by specimen-paired immunofluorescence secondary antibodies. Negative controls were generated by replacing primary antibodies with isotype-matched antibodies. Slides were analyzed on a fluorescent imaging microscope.

Bioinformatics Analysis

The Quantitative Insights into Microbial Ecology version 2 (QIIME2) software (subversion 2019.1) was used for quality filtering of DNA sequences, demultiplexing, taxonomic assignment, and calculating α- and β-diversity. For details, selected sequences were clustered into OTUs with USEARCH (version 11, http://drive5.com/uparse/), with a threshold sequence identity of 99%. The reads were aligned to the Greengenes Core Set reference alignment using PyNAST. The Greengenes taxonomies were used to generate summaries of the taxonomic distributions of OTUs across different levels (phylum, order, family, genus, and species). A phylogenetic tree was built with FastTree and used for estimates of α-diversity (Rarefaction curves, Chao1, Shannon diversity) and β-diversity (using unweighted UniFrac). Metagenomic content of the microbiota samples was predicted from the 16S rRNA profiles, and KEGG pathway functions were categorized at Levels 1–3 using the phylogenetic investigation of communities by reconstruction of unobserved states (PICRUSt) tool (26).

Statistical Methods

All data were summarized as means ± SEM and analyzed with SPSS software (Version 22). Comparisons between CTTC groups were performed by Student's *t*-test. Correlations between continuous variables were determined by Pearson correlation analysis. Survival was estimated by the Kaplan–Meier method and compared by the log-rank test. Multivariate analysis of prognostic factors for OS was performed using the Cox proportional hazards model. The χ^2 test was used to test for relationships between categorical variables. Values of $p < 0.05$ (two-tailed) were considered significant.

For microbiota, differential abundance analyses were performed using paired Wilcoxon signed-rank test to identify significant changed features between tumor and adjacent normal mucosae. Using the R implementation of Random Forests 10-fold cross-validations with 100 iterations, we selected a minimum set of bacterial taxa that maximally discriminated against each Dukes stage, different patients' survival state, and lymph node metastasis state; the variable importance of a microbial taxon was determined by 100 iterations of the algorithm with 3,000 trees and the default mtry of $p^{1/2}$, where p is the number of input phylotypes.

RESULTS

Expression of CTTCs in CRC Tissues and Their Association With Disease Progression

CTTC mRNA expression in tumor and adjacent normal tissues from 136 CRC patients was analyzed using quantitative PCR. The expression of *CXCL9*, *CXCL10*, and *CXCL11* except for *CCL5* was significantly higher in the tumor compared with the adjacent normal tissues (**Figures 1A–D**; $p = 0.0707$, $p = 0.0001$, $p < 0.0001$, and $p = 0.4207$). Correlation analysis showed that several chemokines were significantly associated with one another in adjacent normal tissues but not tumor tissues, indicating that different chemokines might be regulated simultaneously in adjacent normal tissues during tumor progression (**Figure 1E**).

In CRC, the expression level of CTTCs in tissues can significantly impact the distribution of CTCs and then the patients' clinical outcome (2–4). Therefore, we further examined the expression level of CTTCs from patients at different stages of CRC. In tumor, the expression level of chemokine *CXCL9* and *CXCL11* was significantly decreased in advanced stage CRC patients (stages IV, $n = 11$; $p = 0.02$ and $p = 0.045$; **Figure 1F**) compared to those in early stages (stages I,

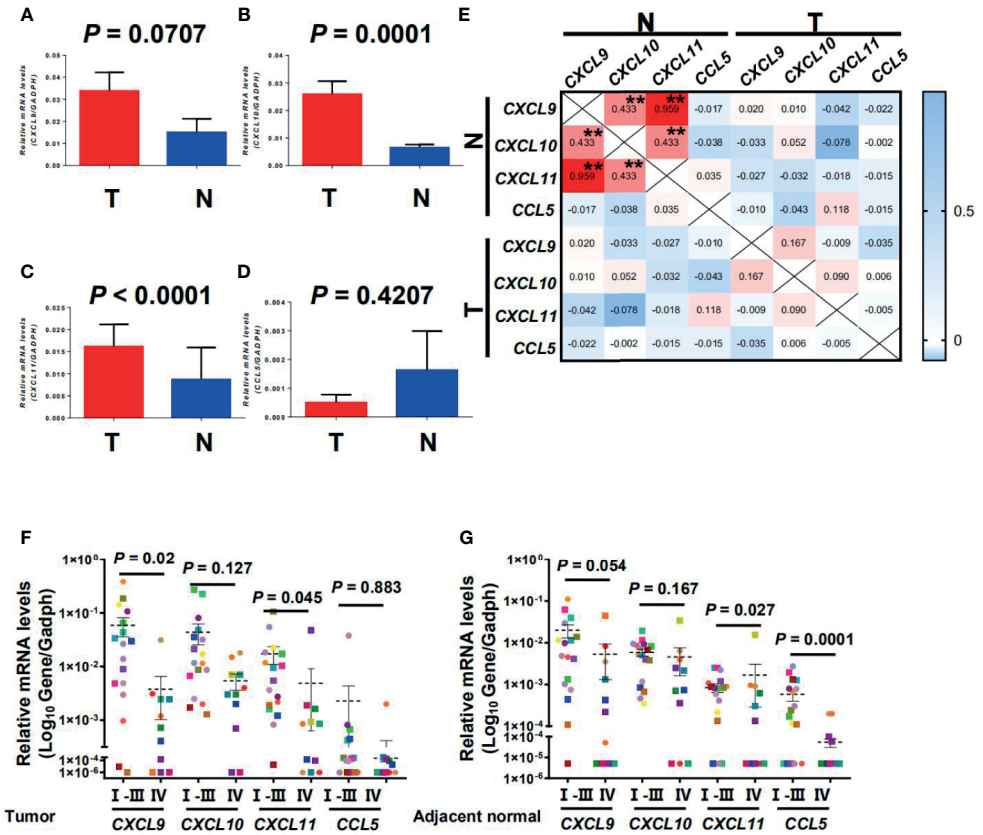


FIGURE 1 | *CXCL9, CXCL10, CXCL11*, and *CCL5* were selectively regulated in tumor and adjacent normal tissues and decreased with progressive stages in CRC patients. Quantitative real-time polymerase chain reaction (qPCR) results of gene expression are shown for *CXCL9, CXCL10, CXCL11*, and *CCL5* in tumor and adjacent normal tissues (n = 136) **(A–D)**. T, Tumor; N, Adjacent normal. Results are expressed as means ± SEM. **(E)** Correlation between the relative expression level of CTTCs in tumor and adjacent normal tissues. Pearson correlation coefficients calculated from the relative expression of CTTCs are shown. $^{**}p < 0.001$. **(F, G)** Representative dot plots of at least three individuals from more than three independent experiments; the continuous and dashed horizontal bars in **(F, G)** represent median values.

II and III, n = 18). Moreover, the expression level of chemokine *CXCL11* and *CCL5* in the adjacent normal tissues was significantly lower in advanced stage CRC (stages IV, n = 11; p = 0.027 and p = 0.0001; **Figure 1G**) than those in early stages (stages I, II, and III, n = 18). In addition, no significant difference was observed in the expression level of *CXCL10* in the tumor or adjacent normal tissues between patients in advanced stage and those in early stages (p = 0.127 for tumor and p = 0.167 for adjacent normal; **Figures 1F, G**). Collectively, the results indicated that the three CTTCs (*CXCL9, CXCL11*, and *CCL5*) were selectively regulated in tumor or adjacent normal tissues and decreased with progressive stages in CRC patients.

Association Between CTTC Expression and Local CD8$^+$ T-Cell Infiltration

The CRC patients were then categorized into two groups according to the expression level of CTTCs (*CXCL9*, *CXCL10*, *CXCL11*, and *CCL5*) in tumor. To evaluate the potential role of these chemokines in the localization of immune cells, immunofluorescence staining was applied to examine the *in situ* infiltration of CXCR3$^+$ and CD3$^+$ cells in CRC patients. CXCR3$^+$ cells were enriched in tumor tissues from *CXCL9*^{high} patients, which also was the hotspot for CXCR3$^+$ CD3$^+$ cells (**Figure 2A**). Additionally, the infiltration density of CD8$^+$ T cells in tumor and adjacent normal tissues was assessed and compared between patients with high and low CTTC expression (**Figures 2B–D**). We found that the density of CTCs was significantly higher in tumors in the *CXCL9*^{high} group than that in the *CXCL9*^{low} group (**Figure 2C**). In adjacent normal tissues, the density of CTCs was higher in the *CCL5*^{high} group than in the *CCL5*^{low} group (**Figure 2D**). Taken together, the results showed that the *CXCL9*^{high} group in tumor or *CCL5*^{high} group in adjacent normal tissues exhibited relatively higher CTC infiltration than the matched chemokine low group, implicating altered anti-tumor immune activity.

Prognostic Significance of CTTCs in CRC Patients

To address whether CTTC expression was associated with CRC progression, we analyzed the correlation between relevant

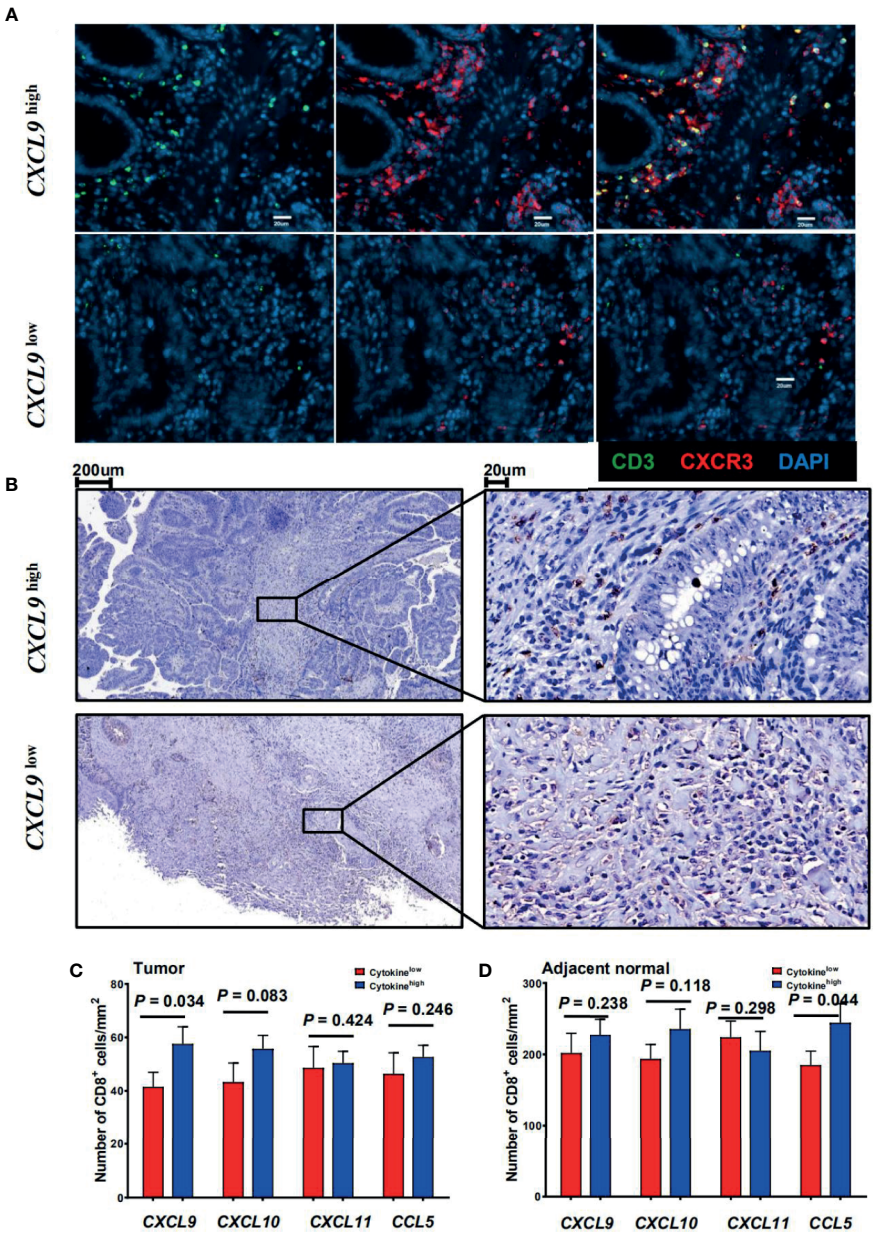


FIGURE 2 | Association between the cytotoxic T-cell trafficking chemokine expression and local $CD8^+$ T-cell infiltration. **(A)** Immunofluorescence microscopy of CRC tissue sections from CRC patients with high or low *CXCL9* expression levels, and stained with anti-CD3 (green) and anti-CXCR3 (red) monoclonal antibodies. **(B)** CD8 (brown) immunostaining of tumor tissues from CRC patients. Representative images of low (upper panel) or high (lower panel) CD8 score are shown. **(C, D)** Comparison of the mean (± SEM) of $CD8^+$ cell densities in high (blue bars) and low (red bars) expression levels of individual chemokines within the tumor (left) or adjacent normal tissues (right) from CRC patients (n = 29).

clinical features and the expression level of these chemokines in tumor or adjacent normal tissues from 136 patients. Using the median value (50–50 division), the expression level of *CXCL9, CXCL10, CXCL11*, and *CCL5* in tumor or adjacent normal tissues allowed the stratification of patients into groups. We first determined if any significant associations existed between clinical characteristics and these chemokines. The results showed that in tumor, the expression of *CXCL9* negatively correlated with tumor stage, nodal and distant metastases, and Dukes' stage (p = 0.01, p = 0.005, p = 0.005; **Table 1**), but not with the other three chemokines (data not shown).

Kaplan–Meier survival curves further showed positive correlations between *CXCL9* expression level and OS (p = 0.048) and disease-free survival (DFS) (p = 0.032) in tumor tissues, but not with the other three chemokines in tumor or adjacent normal tissues (**Figures 3A, B** and **Table 2**).

TABLE 1 | Association of *CXCL9* mRNA expression levels in tumor with clinicopathologic characteristics.

Variables	No. of patients (%)		*p*
	Low	High	
Age, years			0.583
≤64	22	19	
>64	29	30	
Gender			0.509
Male	32	28	
Female	19	21	
Tumor (T) stage			0.494
pTis + pT1 + pT2 + pT3	16	9	
pT4	35	40	
Nodal (N) status			**0.010**
Negative	18	28	
Positive	33	21	
Distant metastases (M)			**0.005**
Negative	43	49	
Positive	7	1	
Dukes' stage			**0.005**
A + B	17	44	
C + D	34	5	
Differentiation			0.894
Low	32	30	
High + Moderate	19	19	
Vascular invasion			0.465
Absent	12	9	
Present	39	40	
MSI status			0.494
MSS/MSI-low	48	45	
MSI-high	3	4	
Location			0.622
Colon	38	26	
Rectal	13	23	

The bold face indicates p-values of variables with significance in either univariate or multivariate analyses.

Multivariate Cox proportional hazards analysis was then performed, with variables associated with survival in univariate analysis adopted as covariates. In multivariate analysis shown in **Table 2**, the *CXCL9* expression level in tumor could not emerge as an independent prognostic factor of both OS (HR, 0.205; 95% CI, 0.043–0.988; $p = 0.062$) and DFS (HR, 0.443; 95% CI, 0.265–0.742; $p = 0.065$). These results suggested that chemokine *CXCL9* was significantly associated with CRC progression, but might not serve as a powerful predictor of CRC survival alone.

Difference of MAM Between Tumor and Adjacent Normal Mucosae

As gut MAM could serve as stimulation that impacted the chemokine expression, we next continued to identify MAM in tumors and paired adjacent normal mucosae from the CRC patients. To investigate how MAM changed in tumors compared with adjacent normal tissues, we compared paired tumor and adjacent normal tissues from 101 patients in our CRC cohort (**Table 3**). Wilcoxon signed-rank tests showed that alpha-diversity indices, including the Shannon and Simpson indices and Pielou's evenness, were significantly decreased in tumors ($p < 0.0001$, $p = 0.0041$ and $p = 0.0014$, respectively, **Figures 4A–C**), while richness indices, such as ACE, Chao, and phylogenetic diversity (PD) whole tree, were also decreased in tumors ($p < 0.0001$, $p < 0.0001$, and $p < 0.0001$, **Figures 4D–F**) compared with paired adjacent normal tissues. As for beta-diversity, principal coordinate analysis (PCoA) could not separate the microbiomes from tumor and adjacent normal mucosae into different clusters, which could be due to significant inter-individual variation (data not shown).

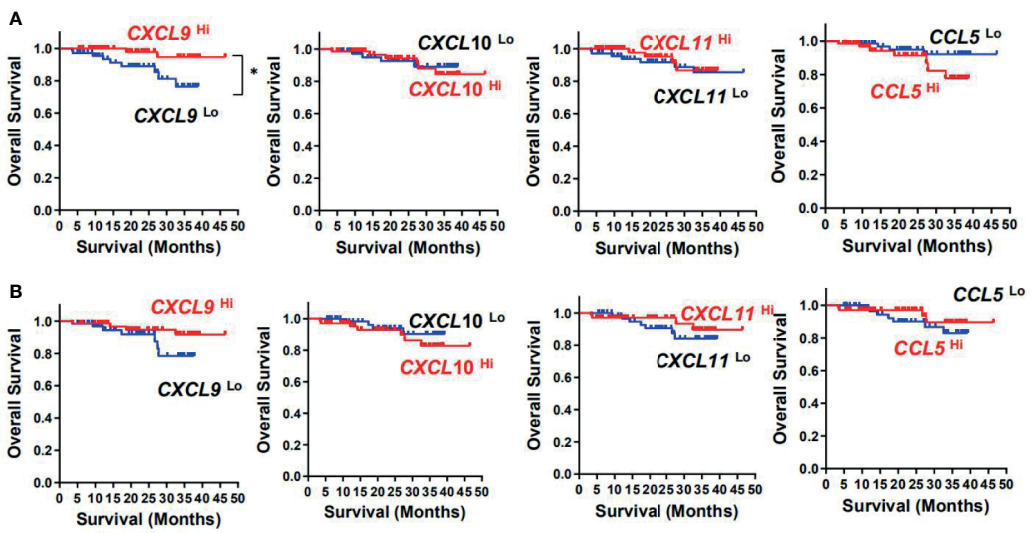


FIGURE 3 | Prognostic significance of *CXCL9, CXCL10, CXCL11*, and *CCL5* in CRC patients. Cumulative OS times were calculated by the Kaplan–Meier method and analyzed by the log-rank test. The patients were divided into two groups according to the median value of *CXCL9, CXCL10, CXCL11*, and *CCL5* in tumor **(A)** or adjacent normal tissues **(B)**.

TABLE 2 | Univariate and multivariate analyses of factors associated with survival and recurrence.

Variables	OS				DFS			
	Univariate *p*	Multivariate			Univariate *p*	Multivariate		
		HR	95% CI	*p*		HR	95% CI	*p*
Age, years (>58/≤58)	0.764			NA	0.971			NA
Gender (female/male)	0.724			NA	0.601			NA
Tumor stage (pT4/pTis + pT1 + pT2 + pT3)	0.133			NA	0.114			NA
Nodal status (pN1 + pN2/pN0)	0.997			NA	0.997			NA
Distant metastases (Pos/Neg)	**0.002**	9.633	2.269–40.895	**0.001**	**<0.0001**	14.048	1.489–6.933	**<0.0001**
Differentiation(H + M/L)	0.535			NA	0.086			NA
$CXCL9_{high}/CXCL9_{low}$ tumor	**0.048**	0.205	0.043–.988	**0.062**	**0.032**	0.443	0.265–.742	**0.065**
$CXCL10_{high}/CXCL10_{low}$ tumor	0.715			NA	0.957			NA
$CXCL11_{high}/CXCL11_{low}$ tumor	0.377			NA	0.256			NA
$CCL5_{high}/CCL5_{low}$ tumor	0.326			NA	0.957			NA
$CXCL9_{high}/CXCL9_{low}$ peri-tumor	0.377	0.205	0.043–.988	NA	0.092			NA
$CXCL10_{high}/CXCL10_{low}$ peri-tumor	0.326			NA	0.957			NA
$CXCL11_{high}/CXCL11_{low}$ peri-tumor	0.377			NA	0.256			NA
$CCL5_{high}/CCL5_{low}$ peri-tumor	0.357			NA	0.092			NA
Location (rectal/colon)	0.564			NA	0.630			NA

Cox proportional hazards regression model; variables associated with survival by univariate analysis were adopted as covariates in multivariate analyses.
OS, overall survival; DFS, disease-free survival; HR, hazard ratio; CI, confidence interval; NA, not applicable; Pos, positive; Neg, negative.
The bold face indicates p-values of variables with significance in either univariate or multivariate analyses.

TABLE 3 | Characteristics of Patients.

Patient characteristics	Group 1	Group 2	Group 3
No. of patients	136	29	101
Age, years (median, range)	64, 21–88	64, 29–79	64, 21–88
Gender (male/female)	81/55	19/10	58/43
Tumor (T) stage (pTis + pT1 +pT2 + pT3/pT4)	43/93	19/10	28/73
Nodal (N) status (Negative/Positive/Nx)	61/74/1	18/11	46/54/1
Distant metastases (M) (None detected/Present)	125/11	18/11	94/7
Dukes' stage (A + B/C + D)	60/76	17/12	46/55
No. of lymph nodes analyzed (median, range)	10, 1–27	14, 4–26	15, 0–40
Differentiation (Well/Moderate/Poor)	3/81/52	3/15/11	2/56/43
MSI status (MSS+MSI-low/MSI-high)	126/10	27/2	95/6
Location (right side of colon/transverse colon/left side of colon/sigmoid colon/rectum)	15/12/35/26/48	6/1/4/5/13	27/10/15/16/33
Mucinous (colloid) adenocarcinoma (No/Yes)	0/136	0/29	0/101

Nx, Nodal status cannot be assessed in one patient.
Group 2 patients are included in immunohistochemistry and immunofluorescence analysis.
Group 3 patients are included in gut microbiota analysis.
Both Group 2 and Group 3 are included in Group 1, the total patient group.

In our CRC cohort, abundance changes of operational taxonomic units (OTUs) were found at multiple taxonomic levels between the tumor and paired adjacent normal mucosae (**Figures 5A, B**; **Supplementary Figure S2** and **Additional Files 1–6**). At the phylum level, significant changes were found between the tumor and paired adjacent normal mucosae [false discovery rate (FDR) $q \leq 0.1$], with enrichment of Fusobacteria and Synergistetes, and decrease of Cyanobacteria, Actinobacteria, Gemmatimonadetes, Acidobacteria, TM7, Chlorobi, Verrucomicrobia, Chloroflexi, OD1, Armatimonadetes, OP3, [Thermi], Nitrospirae, WPS-2, Elusimicrobia, BRC1, GOUTA4, Deferribacteres, Fibrobacteres, GN02, Planctomycetes, SR1, WS4, and AC1 in the tumor mucosae (**Figures 5A, B** and **Additional File 6**). In general, 225 gut microbiota OTUs (grouped at 99% sequence identity) were differentially abundant between tumor and adjacent normal mucosae (FDR $q \leq 0.1$; **Additional File 1**). Most of the differentially abundant OTUs (19/225) were less abundant in the tumor than in the adjacent normal mucosae. Of note, taxa that were detected in over 90% of the patients and were enriched in tumors included *Fusobacterium*, *Bacteroides*, *Stenotrophomonas*, *Lactobacillus*, and *Parvimonas* genera (**Supplementary Figures S2A–D**). The widely distributed tumor microbiomes showed decreased abundances of taxa within the order *Streptophyta* and *Bacteroidales*, also the family *S24-7* and *Rikenellaceae*, as well as species, namely, *Parabacteroides distasonis, Bacteroides uniformis, Akkermansia muciniphila*, and *Clostridium ramosum*, and species in *Turicibacter* genus (**Figures S2E–J** and **Additional File 1**).

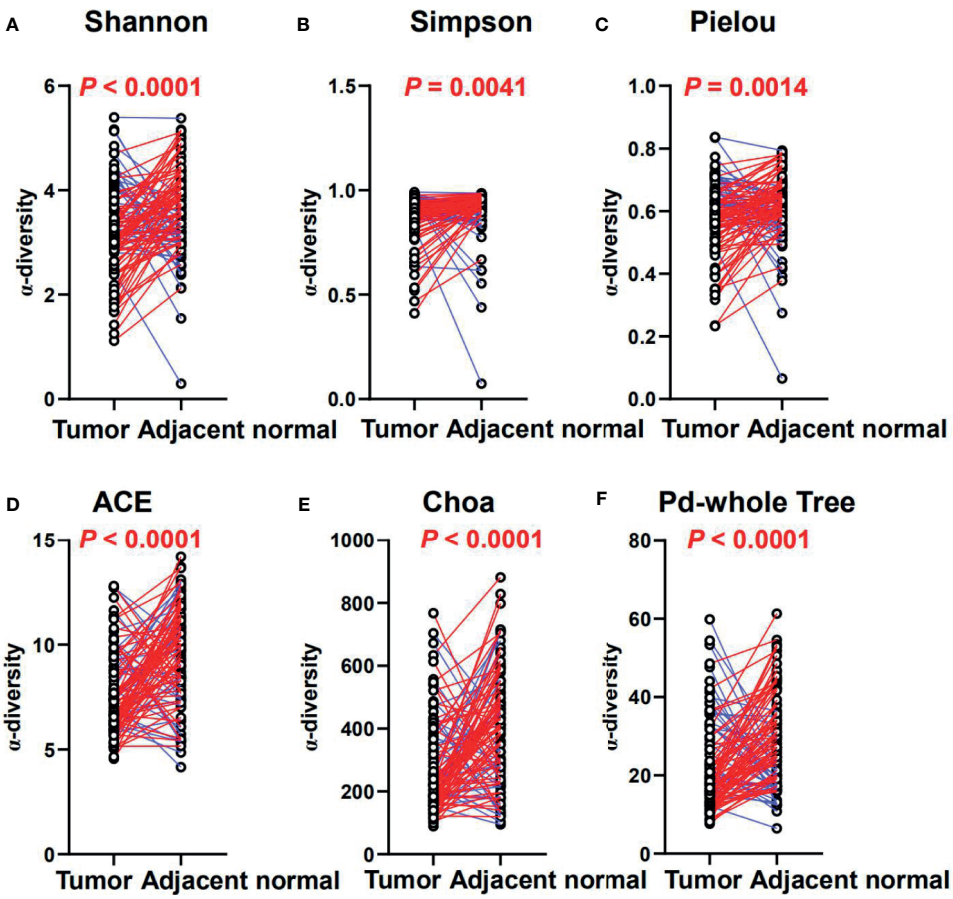


FIGURE 4 | The diversity and richness of the MAM in tumor and adjacent normal mucosae. The diversity indices, such as Shannon **(A)**, Simpson **(B)**, and Heip evenness **(C)**, and the richness indices, such as ACE **(D)**, Choa **(E)**, and PD whole tree **(F)**, are used to evaluate the overall structure of the mucosae microbiota in the CRC patients. *p*-values are derived from two-sided Wilcoxon signed rank tests. The colors indicate increase (blue) or reduction (red) of the diversity indices in tumor compared with adjacent normal tissues.

Large Centralities of Oral Bacteria in CRC MAM Network

The structure change of the mucosae microbiota is the result of dynamic interactions between community members. The SparCC algorithm was employed to construct microbial interaction networks. Here, we observed both co-occurrence and co-excluding interactions of significantly different OTUs between the tumor and adjacent normal mucosae (**Figures 6A, B** and **Supplementary Figures S3A, B**). As shown in **Figure 6A**, the microbial network interactions in tumors mainly occurred among genera belonging to phyla Firmicutes and Proteobacteria. Notably, co-occurrence interactions among oral bacteria *Fusobacterium*, *Peptostreptococcus*, *Parvimonas*, *Gemellaceae*, and *Campylobacter*, and between *Fusobacterium* and *Clostridium* were observed in both tumor and adjacent normal network. In addition, co-occurrence interactions between oral bacteria *Fusobacterium* and *Lachnoanaerobaculum*, between *Fusobacterium* and *Bulleidia*, and between *Lachnoanaerobaculum* and *Selenomonas* were exclusively observed in tumors. The mucosae microbiota in adjacent normal tissues was also dominated by Firmicutes and Proteobacteria and consisted mainly of the six phyla observed in the tumor group (**Figure 6B**). However, the richer interaction network incorporated more commensal bacteria, with interactions among the family *S24-7, Streptophyta*, and *Acinetobacter* presented in adjacent normal tissues.

Weighted node connectivity (WNC) scores were calculated to determine hub microbes with significant roles in CRC microbial ecological network. To prioritize differentially abundant taxa, we next focused on OTUs with large WNC scores, which indicated large centralities and importance in the CRC MAM interaction network. These taxa with large centralities included genera *Peptostreptococcus, Fusobacterium, Parvimonas, Bulleidia, Rhodoplanes, Candidatus Solibacter, Dialister, Lachnoanaerobaculum*, and *Selenomonas* in tumors (**Figure 6A**). Species-level identification of these OTUs included *Clostridium aldenense, Lachnoanaerobaculum orale, Bacteroides fragilis, Ruminococcus bromii, Bacteroides uniformis*, and *Parabacteroides distasonis* (**Supplementary Figure S3A**). Their centralities suggested that they can form a backbone of niche-specific relationships and might exhibit significant influence on the tumor microbial ecology.

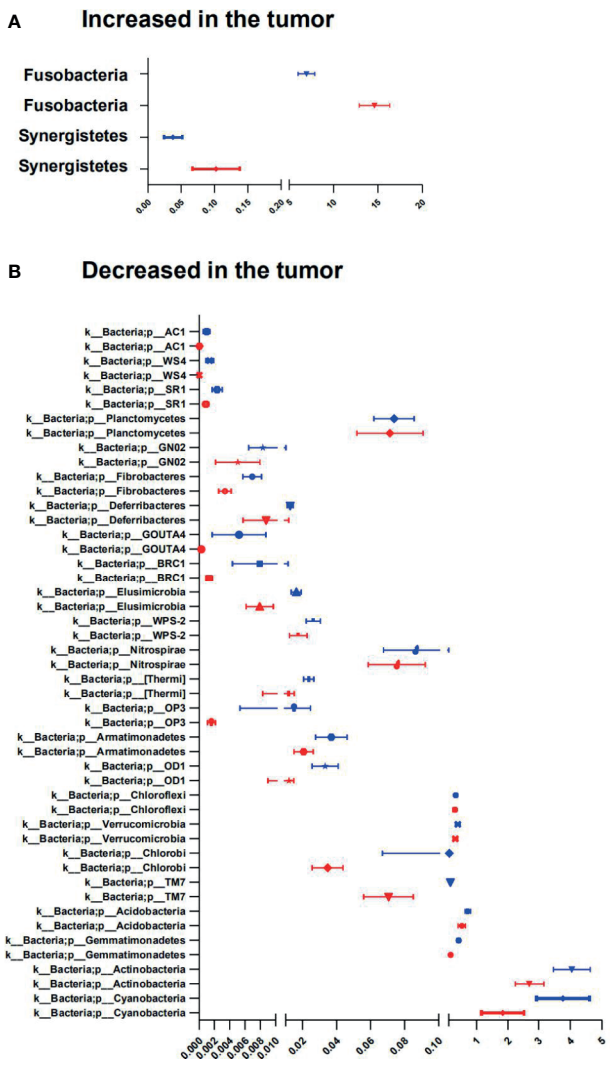


FIGURE 5 | Phyla involved in tumor-associated signature with CRC. **(A, B)** Relative abundance of significantly different phyla between tumor and adjacent normal tissues. The two-sided Wilcoxon signed rank test was used to evaluate the importance of comparisons. Tumor (red bars), Adjacent normal (blue bars).

Altered MAM Functions in Tumors

To determine the potential functional impact of taxonomic changes in CRC MAM, microbial functions associated with CRC in MAM were then predicted by using Phylogenetic Investigation of Communities by Reconstruction of Unobserved States (PICRUSt). Results from Kyoto Encyclopedia of Genes and Genomes (KEGG) pathways showed 18 differentially altered functions at the L2 level between tumor and adjacent normal mucosae with a threshold of Benjamini-Hochberg p-values <0.05 (**Supplementary Figure S4**). Functions enriched in adjacent normal tissues compared to tumors at the L3 level such as pathogenic *Escherichia coli* infection, Fc gamma R-mediated phagocytosis, and p53 signaling pathway (**Supplementary Figure S5**). In contrast, 18 pathways at the L3 level were enriched in tumors compared to adjacent normal tissues, such as MAPK signaling pathway, Fc epsilon RI signaling pathway, Carbohydrate digestion and absorption, Lipopolysaccharide biosynthesis, Nucleotide metabolism, D-Alanine metabolism, Epithelial cell signaling in *Helicobacter pylori* infection, Bacterial toxins, Amino acid metabolism, and Antigen processing and presentation.

Distinctive CTTC Expression Profiles Were Associated With MAM

To assess the correlations between the relative abundance of defined MAM and the expression of individual CTTCs in CRC, correlation was analyzed between the expression of CTTCs and the abundance of differently enriched OTUs in tumor compared to adjacent normal mucosal tissues. CTTCs including *CXCL9, CXCL10, CXCL11*, and *CCL5*, which were differentially expressed between tumor and adjacent normal tissues (**Figures 1A–D**), were significantly correlated with the abundance of several OTUs (**Figures 7A–H** and **Additional File 7**). In particular, abundance of several OTUs, mainly including *Acinetobacter lwoffii*, species in *Wautersiella* genus, and *Desulfobacteraceae* family, was significantly correlated with expression of at least two kinds of CTTCs in tumor tissues. It has been reported that *Methylobacteriaceae* was associated with all prognostically favorable T-cell markers and most corresponding recruiting chemokines (19). In line with this, *Methylobacterium adhaesivum* was associated with the high expression of *CXCL10* in tumor tissues. Moreover, *Streptomyces mirabilis*, *Psychrobacter marincola*, *Acinetobacter johnsonii*, *Psychrobacter sanguinis*, and species in *Photobacterium* and *Acinetobacter* genus and *SHA-31* family were significantly correlated with expression of at least two kinds of CTTCs in adjacent normal tissues. Although for each of the CTTCs, their correlated OTUs in tumor and adjacent normal tissues rarely overlap with each other, we still found several OTUs that were correlated with CTTCs in both tumor and adjacent tissues such as *Desulfosporosinus meridiei*, *Rothia mucilaginosa*, and *Haemophilus parasuis*, and species in *B-42* and *Catonella* genus, *Neisseriaceae* and *ML1228J-1* family, and *Spirobacillales* and *GN03* order (**Figures 7A–H**). Notably, taxa that have been reported to be associated with CRC progression (22), such as species in *Fusobacterium* and *Parvimonas* genus, were only positively correlated with the CTTCs in tumor (**Figures 7A–D**). Notably, taxa that have been reported to be associated with CRC progression (22), such as species in *Fusobacterium* and *Parvimonas* genus, were only positively correlated with the CTTCs in tumors (**Figures 7A–D**).

We then analyzed how the MAM was altered during CRC progression. Changes in the microbial communities were identified by comparing the patients at low Dukes' stages (stages I–II) with those at high Dukes' stages (stages III–IV) and linear discriminant analysis (LDA) effect size (LEfSe) to compare the taxonomic abundance. In addition, we added the chemokine levels into the risk index to generate the ROC curves (**Supplementary Figures S6A–D**). Our results showed that the changes in abundances of specific taxa in tumor or adjacent normal mucosae can be used as a classifier that distinguishes

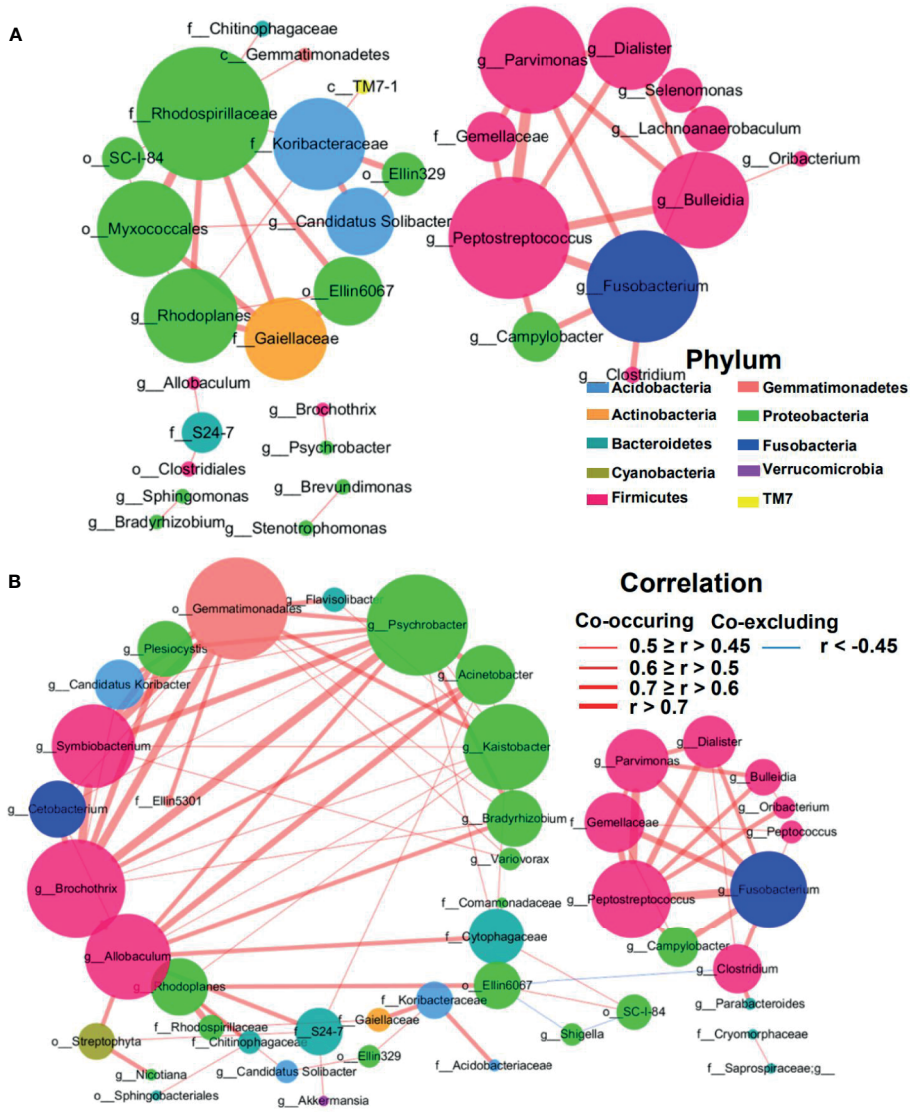


FIGURE 6 | Correlation network of differential MAM in tumor **(A)** and adjacent normal mucosae **(B)**. The correlation coefficients were calculated with the Sparse Correlations for Compositional data algorithm (SparCC). A subset of significant correlations with strengths of at least 0.45 in the mucosae commensals at the genera level were selected for visualization using Cytoscape version 3.6. The size of the nodes corresponds to weighted node connectivity (WNC) scores. Red and green lines represent positive and negative correlations, respectively.

between low/high Dukes' stage at a fixed specificity of 81.1% and 81.4% (**Addition File 7**). Besides, the addition of CTTC levels into the risk index would slightly improve the specificity at 83.0% and 88.3%.

DISCUSSION

In the present study, we aimed to explore the chemotactic factors associated with CRC prognosis and to profile MAM of CRC patients and to investigate the relationship between mucosae microbiota and chemokines involved in CTC recruitment during CRC progression. Based on existing reported clinical data and evidence, we explored major chemokines (including *CCL5*, *CXCL9*, *CXCL10*, and *CXCL11*) associated with recruitment of CTCs into CRC tissues (5, 12, 27–29).

In our current cohort, significant positive correlations between expression of *CXCL9*, *CXCL10*, and *CXCL11* were detected in adjacent normal tissues, suggesting that these chemokines, targeting the same chemokine receptor, may be concomitantly induced and regulated, pointing to their co-expression in normal tissues. Notably, such co-expression was dramatically weakened in tumors, indicating dysregulation of the CTTCs in the tumor microenvironment. Particularly, we found that in tumors, the expression of *CXCL9* negatively correlated with tumor stage, nodal and distant metastases, and Dukes' stage,

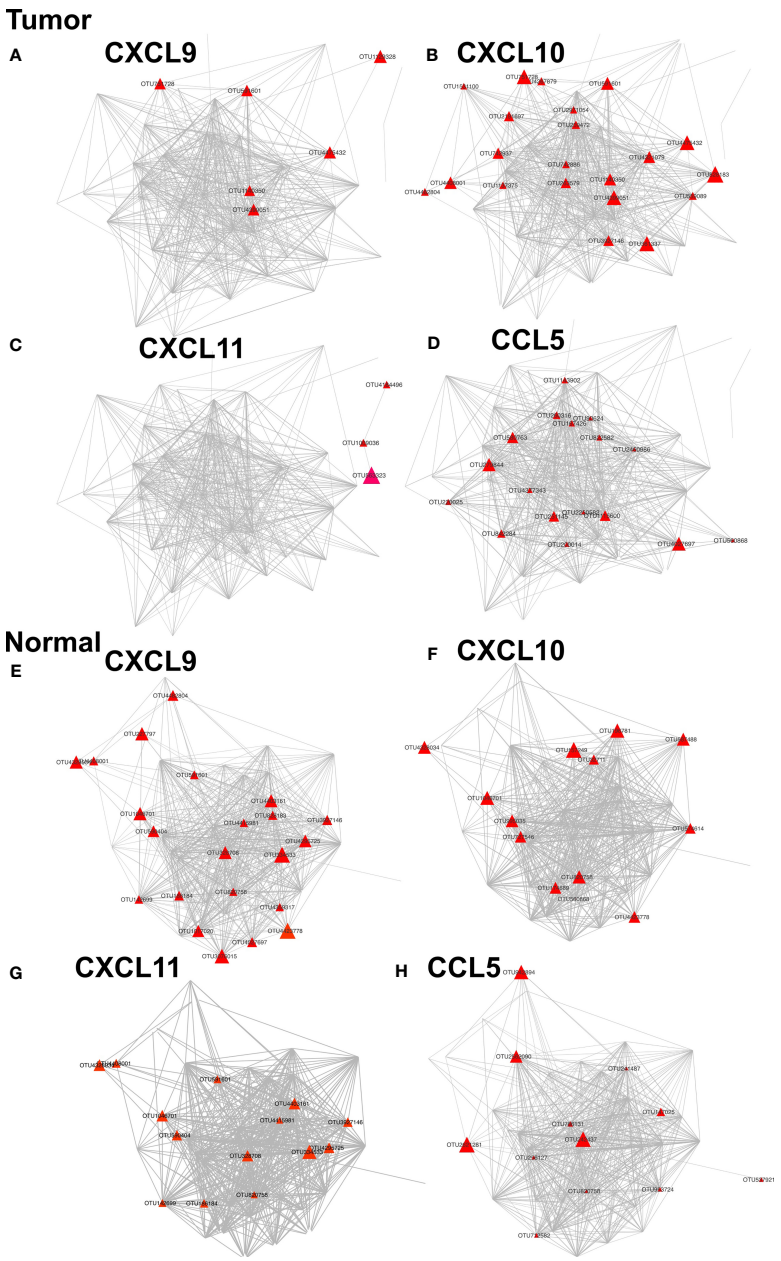


FIGURE 7 | Networks of OTUs associated with CTTCs in tumor and adjacent normal tissues. Each node represents an OTU. Nodes (OTUs) are shown if the abundance of the OTU is significantly correlated with the expression of *CXCL9*, *CXCL10*, *CXCL11*, or *CCL5* in either tumors **(A–D)** or adjacent normal mucosae **(E–H)** ($p < 0.05$). The color and size of nodes denote the *P* value and correlation coefficients (*r*) of correlation between OTUs and CTTCs.

and predictive of favorable clinical outcome. Due to the limitation of follow-up time, we could only evaluate the impact on identified chemokines on patients' 3-year survival instead of 5-year survival in our cohort. Therefore, more follow-up work needs to be completed in the future in order to assess the prognostic value of these CTTCs on the long-term survival and DFS of patients. Previous reports showed that the positive prognostic significance of these chemokines could rely on their capacity to attract the T-cell populations with receptors into tumor tissues (5, 12, 13). In consistent with previous findings, our data also showed that tumors with high *CXCL9* expression level or adjacent normal tissues with high *CCL5* expression level were infiltrated with a higher number of CTCs. It should be noted that a higher-level infiltration of CD8+ T cells does not directly confirm a higher immune activity before further functional validation. Nevertheless, patients with better prognosis outcome might benefit from higher levels of CTTCs within CRC tissues, and more CTC infiltration could possibly be

linked to tumor suppression. Recently, Yu et al. observed an increased exhaustion phenotype of intratumoral $CD8^+$ T cells that were hyper stimulated by several bacterial species to promote chronic inflammation and consequently tumor development (30), indicating that certain bacterial species could be useful microenvironmental stimuli and dynamically regulate $CD8^+$ T-cell function. These findings, taken together, underscore the possibility of $CD8^+$ T cells' functional recovery by gut bacteria intervention, as well as the importance of potential mechanisms on how the microbiome may alter anti-tumor response by $CD8^+$ T cells *via* the chemokine–chemokine receptor axis.

Our CRC patients showed heterogeneous CTTC expression and its dysregulation in tumors compared to adjacent normal tissues. Such changes might reflect distinct genetic backgrounds and/or exposure to different microorganisms in the tumor microenvironment. Recent studies reported that stimulation by gut commensal bacteria induced upregulation or *de novo* expression of multiple chemokines in tumor cell lines (18, 19). However, specific microbes in MAM correlated to high chemokine expression, and immune cell infiltration in human CRC samples was not evaluated by far. In the current study, the gut MAM in tumor and adjacent normal tissues showed distinct taxonomic composition, with decreased diversity and richness in tumor tissues. Our findings in CRC are thus in line with a previous hypothesis that altered microbial diversity can be recognized as a feature of disease status, including inflammatory diseases and cancer (31–33).

In addition to confirmation of previously reported association between microbes and CRC, our MAM analysis also revealed novel taxonomic changes in the disease. At the phylum level, *Fusobacteria* was substantially enriched in tumor MAM in our CRC patients, in consistent with previous reports (34–37). Notably, *Synergistetes* could be a novel phylum significantly enriched in tumors, although its abundance was much lower compared with that of *Fusobacteria* in the CRC patients. *Synergistetes* has not previously been reported as a tumor-enriched phylum in gut microbiome studies with European and American CRC cohorts (22, 22, 35), suggesting that this phylum might be a characteristic in our local Chinese CRC cohort. At the genus level, *Fusobacterium* has been reported as the most abundant genus, which resides in the oral cavity as commensals, but can be an opportunistic pathogen for colon carcinogenesis *via* alterations in signaling pathways or impairment of antitumor immune functions (20). In addition, it has been demonstrated that *Fusobacterium nucleatum* plays a role in the development and progression of colon cancer (20, 38–40), and it has also been detected in patient samples with nodal and distant metastasis (41–44). In our current study, we also confirmed a significantly increased abundance of *Fusobacterium* in tumor compared with adjacent normal tissues and in advanced stage CRC patients compared with early-stage CRC patients, suggesting it as an important and dominant candidate pathogen in both occurrence and development of CRC. Moreover, *B. fragilis* was shown in our data to be detected in 95% of CRC tumor tissues, and it could possibly stimulate an inflammatory status that can promote carcinogenesis *via* induction of proinflammatory toxins as reported (45).

It is noteworthy that our findings demonstrate substantial alteration of MAM microbial functions in CRC patients. Pathways related to genetic information processing and bacterial toxin biosynthesis were also found at higher abundance in tumor, which was in line with the increase of bacteria that could synthesize proinflammatory toxins, such as *B. fragilis*. In contrast, microbial pathways associated with metabolism were downregulated in tumor. Such findings, in line with a previous report in other cohorts (22), indicate that during CRC progression, altered microbiome could be involved in shifted host immune response and metabolism, which were key components of carcinogenesis and the maintenance of local microenvironment of CRC.

Previous reports showed that CTTCs might predict favorable outcome in CRC patients (3, 4). However, our data showed that CTTCs could not serve as a powerful predictor of patient survival. Moreover, our results revealed that a set of defined microbes positively associated with the expression of CTTCs in CRC patients, suggesting that intervention of gut microbiota might be useful in targeting the balance of the tumor microenvironment of CRC. Notably, a group of defined microbes in tumor and adjacent normal mucosae were associated with expression of CTTC genes, possibly indicating their capacity to promote recruitment of CTC populations. Most of the correlations between OTUs and CTTCs in tumor and adjacent normal tissues were not found in the other tissue types, in line with the dysregulation of CTTCs in tumors. Interestingly, *Methylobacteriaceae* was positively correlated with *CXCL10* in both tumor and adjacent normal mucosa in our CRC patients, and it has been reported to be associated with prognostically favorable T-cell markers and most corresponding recruiting chemokines (19). The results suggested that in view of the complex tumor microenvironment, both cancer-promoting and cancer-suppressing factors could co-exist in MAM. Considering that species in *Fusobacterium* genus was one of the mucosal bacteria that promoted tumor development, this could partially explain why the chemokine *CXCL9* could not serve as a powerful independent predictor of our CRC patient survival. Importantly, among the microbes positively associated with CTTCs such as *CXCL9*, there were a set of gram-negative bacteria. The enriched gram-negative bacteria in tumors could possibly stimulate an inflammatory state, induce the increase of CTTCs in the tumor microenvironment, and affect the progression and prognosis of CRC patients. Such findings might improve our understanding of the microbiota dynamics along CRC progression and provide new insight into the development of treatment strategies with immune therapy. Further studies are thus warranted to clarify the species-level or strain-level impact of MAM microbes on chemokine secretion in tumor tissues and T-cell infiltration.

In conclusion, the current study reveals the significant correlation between cytotoxic trafficking chemokines and gut MAM in CRC patients and improved prognosis. This knowledge might eventually pave the way towards development of innovative

treatments by modifying gut microbiota to promote cytotoxic T-cell infiltration for the favorable prognostic significance.

DATA AVAILABILITY STATEMENT

Our data has been successfully deposited to NCBI. The accession number is: PRJNA669258.

ETHICS STATEMENT

The studies involving human participants were reviewed and approved by Medical Ethics Committee of Jiangnan University. The ethics committee waived the requirement of written informed consent for participation.

AUTHOR CONTRIBUTIONS

JZ and J-HC designed the study, analyzed the data, and wrote the paper. CQ and R-NG developed the clinical sample cohorts, and JT, C-YR, R-NG, and Q-CL managed collection of clinical samples and information, DNA extraction, and quantification. JZ analyzed the NGS data. JZ and K-WW performed the statistical analysis. GY, Y-SL, and J-HC, in addition to all other co-authors, reviewed the manuscript, provided feedback, and approved the manuscript in its final form. All authors contributed to the article and approved the submitted version.

FUNDING

This study was supported in part by grants from the National Natural Science Foundation of China (No. 31671311), the Chinese Postdoctoral Science Foundation (No. 2019M651713), Jiangsu Planned Projects for Postdoctoral Research Funds (No. 2018K239C), the Youth Foundation of Jiangsu Natural Science Foundation (No. BK20180617), Guangdong Basic and Applied Basic Research Foundation (No. 2019A1515012062), the Fundamental Research Funds for the Central Universities (JUSRP51712B and JUSRP1901XNC), the Program for High-Level Entrepreneurial and Innovative Talents Introduction of Jiangsu Province, Guangdong High-level Personnel of Special Support Program, Yangfan Plan of Talents Recruitment Grant, the Taihu Lake Talent Plan, Research Program of Public Health Research Center, Jiangnan University (JUPH201827), Youth Research Program of Wuxi Health Commission (Q202011) and Wuxi Institute of Translational Medicine.

ACKNOWLEDGMENTS

We are grateful to the participants that have made this research possible.

SUPPLEMENTARY MATERIAL

The Supplementary Material for this article can be found online at: https://www.frontiersin.org/articles/10.3389/fimmu.2021.715559/full#supplementary-material

Supplementary Figure 1 | Differential enrichment of representative species between tumor and adjacent normal mucosae microbiomes. Representative dot plots of each tumor tissue with corresponding paired adjacent normal tissue indicating the relative abundances of representative microbes that are presented in over 90% of the patients and are differentially abundant between tumor and adjacent tissues **(A–N)**. The continuous and dashed horizontal bars denotes median abundance. Results are expressed as means ± SEM.

Supplementary Figure 2 | Multiple taxonomic levels involved in tumor associated-signature with CRC. **(A–J)** Relative abundance of significantly different taxa between tumor and adjacent normal tissues. The two-sided Wilcoxon signed rank test is used to evaluate the importance of comparisons. Tumor (Red Bars), Adjacent normal (Blue Bars).

Supplementary Figure 3 | Correlation network of differential MAM in tumor **(A)**, adjacent normal mucosae **(B)**. The correlation coefficients are calculated with the Sparse Correlations for Compositional data algorithm (SparCC). A subset of significant correlations with strengths of at least 0.4 in the mucosae commensals at the OTU level are selected for visualization. The size of the nodes corresponds to weighted node connectivity (WNC) scores. Cytoscape version 3.6.1 is used for network construction. Red and green lines represent positive and negative correlations, respectively.

Supplementary Figure 4 | Representative KEGG pathways **(A)** and level 2 COG **(B)** of MAM that are enriched in tumor or adjacent normal mucosae. PiCRUSt-based CRC MAM functions are analyzed in tumor and adjacent normal tissues. The microbial functions between the two groups are compared based on two-sided Welch's t-test. The Benjamini-Hochberg method was used for multiple testing correction based on the false discovery rate (FDR) by STAMP.

Supplementary Figure 5 | Summary cladogram of differentially abundant KEGG (level3) modules imputed in MAM. Node sizes represent the tumor to adjacent normal relative abundance ratios. Clades and nodes are annotated in a clockwise manner. Functional categories at level 1and 2 are distinguished by respective node shapes and lower-case letters. Node colors represent enriched functions in tumor (red) and those in adjacent normal tissues (blue). The letters on annotation, I and D stands for increased and decreased function in tumors, respectively.

Supplementary Figure 6 | ROC curves analysis to evaluate the discriminatory potential of mucosal microbial community combined with CCTC levels in Ducks' stage identification. **(A)** Microbial community at the tumor mucosal classify Low- Ducks' stage (stages 1–2) from high- Ducks' stage (stages 3–4). **(B)** Microbial community combined with CCTC at the tumor mucosal classify Low- Ducks' stage (stages 1–2) from high-Ducks' stage (stages 3–4). **(C)** Microbial community at the adjacent normal mucosal classify low-Ducks' stage (stages 1–2) from high-Ducks' stage (stages 3–4). **(D)** Microbial community combined with CCTC at the adjacent normal mucosal classify low-Ducks' stage (stages 1–2) from high-Ducks' stage (stages 3–4).

REFERENCES

1. Siegel RL, Miller KD, Jemal A. Cancer Statistics, 2020. *CA Cancer J Clin* (2020) 70(1):7–30. doi: 10.3322/caac.21590
2. Fridman WH, Pagès F, Sautès-Fridman C, Galon J. The Immune Contexture in Human Tumours: Impact on Clinical Outcome. *Nat Rev Cancer* (2012) 12 (4):298–306. doi: 10.1038/nrc3245
3. Galon J, Costes A, Sanchez-Cabo F, Kirilovsky A, Mlecnik B, Lagorce-Pagès C, et al. Type, Density, and Location of Immune Cells Within Human Colorectal Tumors Predict Clinical Outcome. *Science* (2006) 313 (5795):1960–4. doi: 10.1126/science.1129139
4. Pagès F, Berger A, Camus M, Sanchez-Cabo F, Costes A, Molidor R, et al. Effector Memory T Cells, Early Metastasis, and Survival in Colorectal Cancer. *N Engl J Med* (2005) 353(25):2654–66. doi: 10.1056/NEJMoa051424

5. Tokunaga R, Zhang W, Naseem M, Puccini A, Berger MD, Soni S, et al. CXCL9, CXCL10, CXCL11/CXCR3 Axis for Immune Activation - A Target for Novel Cancer Therapy. *Cancer Treat Rev* (2018) 63:40–7. doi: 10.1016/j.ctrv.2017.11.007
6. House IG, Savas P, Lai J, Chen AXY, Oliver AJ, Teo ZL, et al. Macrophage-Derived CXCL9 and CXCL10 Are Required for Antitumor Immune Responses Following Immune Checkpoint Blockade. *Clin Cancer Res* (2020) 26(2):487–504. doi: 10.1158/1078-0432.CCR-19-1868
7. Spranger S, Dai D, Horton B, Gajewski TF. Tumor-Residing Batf3 Dendritic Cells Are Required for Effector T Cell Trafficking and Adoptive T Cell Therapy. *Cancer Cell* (2017) 31(5):711–23.e4. doi: 10.1016/j.ccell.2017.04.003
8. Hong M, Puaux AL, Huang C, Loumagne L, Tow C, Mackay C, et al. Chemotherapy Induces Intratumoral Expression of Chemokines in Cutaneous Melanoma, Favoring T-Cell Infiltration and Tumor Control. *Cancer Res* (2011) 71(22):6997–7009. doi: 10.1158/0008-5472.CAN-11-1466
9. Ribas A, Wolchok JD. Cancer Immunotherapy Using Checkpoint Blockade. *Science* (2018) 359(6382):1350–5. doi: 10.1126/science.aar4060
10. Jobin C. Precision Medicine Using Microbiota. *Science* (2018) 359(6371):32–4. doi: 10.1126/science.aar2946
11. Gopalakrishnan V, Spencer CN, Nezi L, Reuben A, Andrews MC, Karpinets TV, et al. Gut Microbiome Modulates Response to Anti-PD-1 Immunotherapy in Melanoma Patients. *Science* (2018) 359(6371):97–103. doi: 10.1126/science.aan4236
12. Zumwalt TJ, Arnold M, Goel A, Boland CR. Active Secretion of CXCL10 and CCL5 From Colorectal Cancer Microenvironments Associates With GranzymeB+ CD8+ T-Cell Infiltration. *Oncotarget* (2015) 6(5):2981–91. doi: 10.18632/oncotarget.3205
13. Ding Q, Lu P, Xia Y, Ding S, Fan Y, Li X, et al. CXCL9: Evidence and Contradictions for Its Role in Tumors Progression. *Cancer Med* (2016) 5(11):3246–59. doi: 10.1002/cam4.934
14. Louis P, Hold GL, Flint HJ. The Gut Microbiota, Bacterial Metabolites and Colorectal Cancer. *Nat Rev Microbiol* (2014) 12(10):661–72. doi: 10.1038/nrmicro3344
15. Sanchez-Alcoholado L, Ramos-Molina B, Otero A, Laborda-Illanes A, Ordóñez R, Sanchez-Alcoholado L, et al. The Role of the Gut Microbiome in Colorectal Cancer Development and Therapy Response. *Cancers (Basel)* (2020) 12(6):1406. doi: 10.3390/cancers12061406
16. Singh A, Nayak N, Rathi P, Verma D, Sharma R, Chaudhary A, et al. Microbiome and Host Crosstalk: A New Paradigm to Cancer Therapy. *Semin Cancer Biol* (2020) 70:71–84. doi: 10.1016/j.semcancer.2020.05.014.
17. McQuade JL, Daniel CR, Helmink BA, Wargo JA. Modulating the Microbiome to Improve Therapeutic Response in Cancer. *Lancet Oncol* (2019) 20(2):e77–91. doi: 10.1016/S1470-2045(18)30952-5
18. Tanoue T, Morita S, Plichta DR, Skelly AN, Suda W, Sugiura Y, et al. A Defined Commensal Consortium Elicits CD8 T Cells and Anti-Cancer Immunity. *Nature* (2019) 565(7741):600–5. doi: 10.1038/s41586-019-0878-z
19. Cremonesi E, Governa V, Garzon JFG, Mele V, Amicarella F, Muraro MG, et al. Gut Microbiota Modulate T Cell Trafficking Into Human Colorectal Cancer. *Gut* (2018) 67(11):1984–94. doi: 10.1136/gutjnl-2016-313498
20. Yang Y, Weng W, Peng J, Hong L, Yang L, Toiyama Y, et al. Fusobacterium Nucleatum Increases Proliferation of Colorectal Cancer Cells and Tumor Development in Mice by Activating Toll-Like Receptor 4 Signaling to Nuclear Factor-Kappab, and Up-Regulating Expression of MicroRNA-21. *Gastroenterology* (2017) 152(4):851–66.e24. doi: 10.1053/j.gastro.2016.11.018
21. Kostic AD, Gevers D, Gevers CS, Michaud M, Duke F, Earl AM, et al. Genomic Analysis Identifies Association of Fusobacterium With Colorectal Carcinoma. *Genome Res* (2012) 22(2):292–8. doi: 10.1101/gr.126573.111
22. Yachida S, Mizutani S, Shiroma H, Shiba S, Nakajima T, Sakamoto T, et al. Metagenomic and Metabolomic Analyses Reveal Distinct Stage-Specific Phenotypes of the Gut Microbiota in Colorectal Cancer. *Nat Med* (2019) 25(6):968–76. doi: 10.1038/s41591-019-0458-7
23. Chiu CY, Miller SA. Clinical Metagenomics. *Nat Rev Genet* (2019) 20(6):341–55. doi: 10.1038/s41576-019-0113-7
24. Allen J, Sears CL. Impact of the Gut Microbiome on the Genome and Epigenome of Colon Epithelial Cells: Contributions to Colorectal Cancer Development. *Genome Med* (2019) 11(1):11. doi: 10.1186/s13073-019-0621-2
25. Yachida S, Mizutani S, Shiroma H, Shiba S, Nakajima T, Sakamoto T, et al. CD169 Identifies an Activated CD8(+) T Cell Subset in Regional Lymph Nodes That Predicts Favorable Prognosis in Colorectal Cancer Patients. *Oncoimmunology* (2016) 5(7):e1177690. doi: 10.1080/2162402X.2016.1177690
26. Langille MG, Zaneveld J, Caporaso JG, McDonald D, Knights D, Reyes JA, et al. Predictive Functional Profiling of Microbial Communities Using 16S rRNA Marker Gene Sequences. *Nat Biotechnol* (2013) 31(9):814–21. doi: 10.1038/nbt.2676
27. Bedognetti D, Spivey TL, Zhao Y, Uccellini L, Tomei S, Dudley ME, et al. CXCR3/CCR5 Pathways in Metastatic Melanoma Patients Treated With Adoptive Therapy and Interleukin-2. *Br J Cancer* (2013) 109(9):2412–23. doi: 10.1038/bjc.2013.557
28. Cani PD. Human Gut Microbiome: Hopes, Threats and Promises. *Gut* (2018) 67(9):1716–25. doi: 10.1136/gutjnl-2018-316723
29. Angell HK, Bruni D, Barrett JC, Herbst R, Galon J. The Immunoscore: Colon Cancer and Beyond. *Clin Cancer Res* (2020) 26(2):332–9. doi: 10.1158/1078-0432.CCR-18-1851
30. Yu AI, Zhao L, Eaton KA, Ho S, Chen J, Poe S, et al. Gut Microbiota Modulate CD8 T Cell Responses to Influence Colitis-Associated Tumorigenesis. *Cell Rep* (2020) 31(1):107471. doi: 10.1016/j.celrep.2020.03.035
31. Franzosa EA, Sirota-Madi A, Avila-Pacheco J, Fornelos N, Haiser HJ, Reinker S, et al. Gut Microbiome Structure and Metabolic Activity in Inflammatory Bowel Disease. *Nat Microbiol* (2019) 4(2):293–305. doi: 10.1038/s41564-018-0306-4
32. Gong D, Gong X, Wang L, Yu X, Dong Q. Involvement of Reduced Microbial Diversity in Inflammatory Bowel Disease. *Gastroenterol Res Pract 2016* (2016) p:6951091. doi: 10.1155/2016/6951091
33. Cheng WY, Wu CY, Yu J. The Role of Gut Microbiota in Cancer Treatment: Friend or Foe? *Gut* (2020) 69(10):1867–76. doi: 10.1136/gutjnl-2020-321153
34. Gao R, Kong C, Huang L, Li H, Qu X, Liu Z, et al. C Microbiota Signature in Colorectal Cancer. *Eur J Clin Microbiol Infect Dis* (2017) 36(11):2073–83. doi: 10.1007/s10096-017-3026-4
35. Flemer B, Warren RD, Barrett MP, Cisek K, Das A, Jeffery IB, et al. The Oral Microbiota in Colorectal Cancer is Distinctive and Predictive. *Gut* (2018) 67(8):1454–63. doi: 10.1136/gutjnl-2017-314814
36. Omar Al-Hassi H, Ng O, Brookes M. Tumour-Associated and non-Tumour-Associated Microbiota in Colorectal Cancer. *Gut* (2018) 67(2):395. doi: 10.1136/gutjnl-2017-314219
37. Chen XH, Wang A, Chu AN, Gong YH, Yuan Y. Mucosa-Associated Microbiota in Gastric Cancer Tissues Compared With Non-Cancer Tissues. *Front Microbiol* (2019) 10:1261. doi: 10.3389/fmicb.2019.01261
38. Rubinstein MR, Wang X, Liu W, Hao Y, Cai G, Han YW. Fusobacterium Nucleatum Promotes Colorectal Carcinogenesis by Modulating E-Cadherin/Beta-Catenin Signaling *via* its FadA Adhesin. *Cell Host Microbe* (2013) 14(2):195–206. doi: 10.1016/j.chom.2013.07.012
39. Gur C, Ibrahim Y, Isaacson B, Yamin R, Abed J, Gamliel M, et al. Binding of the Fap2 Protein of Fusobacterium Nucleatum to Human Inhibitory Receptor TIGIT Protects Tumors From Immune Cell Attack. *Immunity* (2015) 42(2):344–55. doi: 10.1016/j.immuni.2015.01.010
40. Bullman S, Pedamallu CS, Sicinska E, Clancy TE, Zhang X, Cai D, et al. Analysis of Fusobacterium Persistence and Antibiotic Response in Colorectal Cancer. *Science* (2017) 358(6369):1443–8. doi: 10.1126/science.aal5240
41. Yu T, Guo F, Yu Y, Sun T, Ma D, Han J, et al. Fusobacterium Nucleatum Promotes Chemoresistance to Colorectal Cancer by Modulating Autophagy. *Cell* (2017) 170(3):548–63.e16. doi: 10.1016/j.cell.2017.07.008
42. Chen Y, Chen Y, Zhang J, Cao P, Su W, Deng Y, et al. Fusobacterium Nucleatum Promotes Metastasis in Colorectal Cancer by Activating Autophagy Signaling *via* the Upregulation of CARD3 Expression. *Theranostics* (2020) 10(1):323–39. doi: 10.7150/thno.38870
43. Chen S, Su T, Zhang Y, Lee A, He J, Ge Q, et al. Fusobacterium Nucleatum Promotes Colorectal Cancer Metastasis by Modulating KRT7-As/Krt7. *Gut Microbes* (2020) 11(3):511–25. doi: 10.2139/ssrn.3405559
44. Li YY, Ge QX, Cao J, Zhou YJ, Du YL, Shen B, et al. Association of Fusobacterium Nucleatum Infection With Colorectal Cancer in Chinese Patients. *World J Gastroenterol* (2016) 22(11):3227–33. doi: 10.3748/wjg.v22.i11.3227
45. Chung L, Orberg ET, Geis AL, Chan JL, Fu K, DeStefano Shields CE, et al. Bacteroides Fragilis Toxin Coordinates a Pro-Carcinogenic Inflammatory

Cascade via Targeting of Colonic Epithelial Cells. *Cell Host Microbe* (2018) 23 (3):421. doi: 10.1016/j.chom.2018.02.004

Conflict of Interest: The authors declare that the research was conducted in the absence of any commercial or financial relationships that could be construed as a potential conflict of interest.

Publisher's Note: All claims expressed in this article are solely those of the authors and do not necessarily represent those of their affiliated organizations, or those of the publisher, the editors and the reviewers. Any product that may be evaluated in this article, or claim that may be made by its manufacturer, is not guaranteed or endorsed by the publisher.

Copyright © 2021 Zhang, Tao, Gao, Wei, He, Ren, Li, Liu, Wang, Yang, Qian and Chen. This is an open-access article distributed under the terms of the Creative Commons Attribution License (CC BY). The use, distribution or reproduction in other forums is permitted, provided the original author(s) and the copyright owner(s) are credited and that the original publication in this journal is cited, in accordance with accepted academic practice. No use, distribution or reproduction is permitted which does not comply with these terms.

frontiers in Immunology

ORIGINAL RESEARCH
published: 14 September 2021
doi: 10.3389/fimmu.2021.715098

Lactobacillus rhamnosus GR-1 Prevents *Escherichia coli*-Induced Apoptosis Through PINK1/Parkin-Mediated Mitophagy in Bovine Mastitis

*Yanan Li, Yaohong Zhu, Bingxin Chu, Ning Liu, Shiyan Chen and Jiufeng Wang**

Department of Veterinary Medicine, China Agricultural University, Beijing, China

Escherichia coli is one of the most important pathogens that cause clinical mastitis in dairy cattle worldwide and lead to severe economic losses. Antibiotics are often used to treat this inflammatory disease; however, antimicrobial resistance and environmental pollution cannot be ignored. Probiotic is the best alternative; however, its mechanisms of action to prevent mastitis remain unclear. Moreover, the role of probiotics in regulating mitophagy, a selective autophagy that maintains mitochondrial quality, needs to be explored. *E. coli* infection induced NOD-like receptor family member pyrin domain-containing protein 3 (NLRP3) inflammasome assembly, Caspase-1 activation, and apoptosis in MAC-T cells. Infection also resulted in mitochondrial damage and subsequent increase in reactive oxygen species (ROS) production. Moreover, inhibition of ROS release by scavenger N-acetyl-L-cysteine (NAC) abrogated the importance of ROS in NLRP3 assembly and apoptosis in MAC-T cells. Pretreatment with *Lactobacillus rhamnosus* GR-1 (LGR-1), a probiotic, alleviated *E. coli*-induced NLRP3 inflammasome activation and apoptosis *via* ROS inhibition. Besides, *E. coli* infection inhibited mitophagy while LGR-1 pretreatment augmented PINK1/Parkin–mediated mitophagy activation, which further blocked ROS generation. To explore the effect of LGR-1 *in vivo*, a mouse mastitis model was established. The results showed that LGR-1 pretreatment had preventive and protective effects on *E. coli* induced mastitis, and could reduce cytokines levels such as IL-1β and TNF-α. In accordance with the results *in vitro*, *E. coli* can inhibit mitophagy and activate NLRP3 inflammasome and apoptosis, while LGR-1 can weaken the effect of *E. coli*. Taken together, our data indicated that LGR-1 pretreatment induced PINK1/Parkin-mediated mitophagy that eliminated damaged mitochondria and reduced ROS production and NLRP3 inflammasome activation, which subsequently decreased *E. coli*-induced apoptosis. To conclude, our study suggests that therapeutic strategies aiming at the upregulation of mitophagy under *E. coli*-induced mastitis may preserve mitochondrial function and provide theoretical support for the application of probiotics in bovine mastitis.

Keywords: mastitis, *Escherichia coli*, mitophagy, NLRP3 inflammasome, ROS, *Lactobacillus rhamnosus*

OPEN ACCESS

Edited by:
Alina Maria Holban, University of Bucharest, Romania

Reviewed by:
Qiang Zhang, Tianjin Medical University General Hospital, China
Zhongjun Du, Shandong First Medical University, China

***Correspondence:**
Jiufeng Wang
jiufeng_wang@hotmail.com

Specialty section:
This article was submitted to Microbial Immunology, a section of the journal Frontiers in Immunology

Received: *26 May 2021*
Accepted: *27 August 2021*
Published: *14 September 2021*

Citation:
Li Y, Zhu Y, Chu B, Liu N, Chen S and Wang J (2021) Lactobacillus rhamnosus GR-1 Prevents Escherichia coli-Induced Apoptosis Through PINK1/Parkin-Mediated Mitophagy in Bovine Mastitis. Front. Immunol. 12:715098. doi: 10.3389/fimmu.2021.715098

INTRODUCTION

Mastitis, mainly caused by a microbial infection, is the inflammation of the breast parenchyma associated with lactation (1). In dairy cattle, mastitis, which causes swelling and pain in the udder and systemic inflammatory injuries, seriously affects animal health and reduces milk yield and quality, leading to considerable economic losses worldwide (2). Clinical bovine mastitis caused by *Escherichia coli* (*E. coli*) leads to endotoxin shock and death in extreme cases (3, 4). Although many countries have improved farm management practices and reduced the incidence, mastitis caused by *E. coli* has proven difficult to solve (5). So far, antibiotics have been used to treat mastitis. However, this approach often leads to environmental pollution, bacterial resistance, and antibiotic residues, which affect human health, increase veterinary care costs, and result in premature slaughter (6, 7). Therefore, it is necessary to find a target and a new drug or any other alternative to prevent and treat mastitis in dairy cattle.

Probiotics have gained special attention as an alternative to antibiotics. They are defined as "live microorganisms which when administered in adequate amounts confer a health benefit on the host" (8). Microbes recognized as intestinal probiotics include Lactobacillus, Bifidobacterium, Streptococcus, and few *E. coli* strains (9). Many studies have demonstrated Lactobacillus and Bifidobacterium's antioxidant activities that help defend against pathogen infection (10–12). *Lactobacillus rhamnosus* GG inhibited autophagy induced by *Salmonella enterica serovar* Infantis though promoting EGFR-mediated Akt activation (13). Several studies have analyzed probiotics for the treatment of gastrointestinal infections; however, few studies are more interested in the application of probiotics in breast. A study indicated that intestinal microbiota dysbiosis may be one of the causes of mastitis, and probiotics can improve the symptoms of mastitis (14). Meanwhile, our previous study showed that *Lactobacillus rhamnosus* GR-1 (LGR-1) reduced excessive NOD-like receptor family member pyrin domain-containing protein 3 (NLRP3) inflammasome activation induced *by E. coli*, thereby reducing interleukin-1 beta (IL-1β) secretion (15). However, the mechanism employed by LGR-1 to attenuate the NLRP3 signaling pathway activation in *E. coli*-induced bovine mastitis needs to be elucidated.

During a microbial infection, the host immune system gets activated. Increasing evidence has shown autophagy's role in regulating this immune response and inflammation to resist microbial infection (16, 17). The deletion of autophagic protein Beclin-1 in macrophages isolated from the mouse lead to the activation of NLRP3 inflammasome and the increased secretion of IL-1β and interleukin-18 (IL-18) (18). Autophagy activation inhibited the secretion of IL-1β and enhanced the degradation of inflammasome (19). These findings indicated that autophagy negatively regulates inflammasome activation. Mitophagy, the selective autophagy of mitochondria, reduces the production of free radicals, adjusts the dynamic balance of mitochondria, and maintains cell survival (20). Although the correlation between mitophagy and NLRP3 inflammasome activation is unclear, mitochondria-derived reactive oxygen species (ROS) are known to participate in NLRP3 inflammasome activation (21). When mitophagy function is impaired, the damaged mitochondria-induced the excessive accumulation of ROS (mtROS) causes NLRP3 inflammasome activation and leads to an inflammatory cascade (22). NLRP3 inflammasome has been proved to play a key role in the host defense against microbial infections (23, 24). Studies have shown that NLRP3 can identify *Salmonella typhimurium* infections in macrophages and promote Caspase-1-dependent cell death and IL-1β production (25). Researchers also observed NLRP3 inflammasome activation induced by *E. coli* (15), *C. rodentium* (26) and *Staphylococcus aureus* (27) infection in macrophages. These studies indicated that the activation of NLRP3 inflammasome was very closely related to the interaction between host and bacteria. In our previous study, LGR-1 attenuate *E. coli*-induced NLRP3 inflammasomes activation, however, mechanism is not yet known. Moreover, during infection, *E. coli* decreases mitochondrial transmembrane potential, increase depolarization rate (28), and reactive oxygen species (ROS) levels (29) and subsequently results in cell apoptosis. However, the role of mitochondrial damage and mitophagy in *E. coli*-induced bovine mastitis is not known. The protective role of mitophagy pathway during LGR-1 action needs to be explored.

Therefore, we hypothesize that LGR-1 probiotic inhibits *E. coli*-induced cell apoptosis NLRP3 inflammasome assembly and by blocking ROS production and mediating mitophagy activation. In the present study, we examine the correlation between probiotics and mitophagy and its role in defense against the pathogen, specifically during coliform mastitis.

RESULTS

LGR-1 Alleviates Mitophagy Inhibition in *E. coli*-Infected MAC-T Cells

Autophagy is a host defense system that plays a vital role in resisting bacterial infections. First, we explored the correlation between *E. coli* infection and autophagy. After 8 h, *E. coli* infection reduced LC3II, ATG5, and Beclin1 expression levels and LC3II to LC3I ratio compared with the control, while LGR-1 pretreatment alleviated this reduction (**Figure 1A**). In contrast, *E. coli* infection increased p62 expression, a common autophagy substrate, indicating autophagic flux blockage, while LGR-1 pretreatment attenuated this increase (**Figure 1A**). Confocal laser scanning confirmed the inhibition of autophagy in MAC-T cells (**Figure 1B**). Besides, *E. coli* infection significantly decreased LC3 puncta while LGR-1 pretreatment increased LC3 puncta (**Figure 1B**). These results suggest that *E. coli* inhibits autophagy, and LGR-1 alleviates this inhibition. Interestingly, *E. coli* significantly reduced PINK1 and Parkin protein levels, and LGR-1 pretreatment prevented this reduction (**Figure 1A**). Furthermore, immunofluorescence revealed colocalized Parkin and MitoTracker in LGR-1 pretreated MAC-T cells, indicating the formation of mitophagosomes (**Figure 1C**). Consistent with the immunofluorescence results,

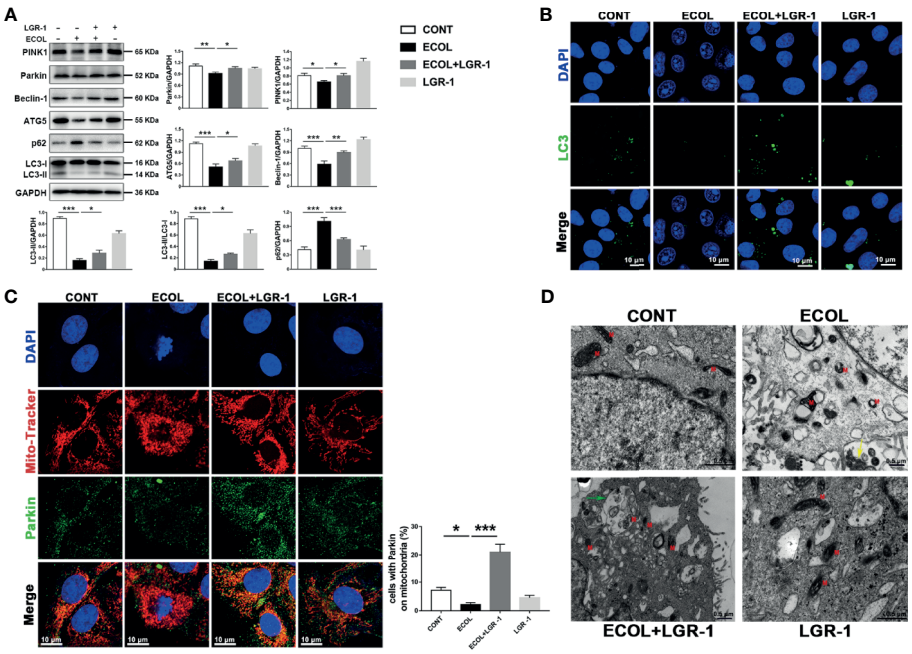


FIGURE 1 | LGR-1 alleviates *Escherichia coli*-induced inhibition of mitophagy in MAC-T cells. **(A)** Western blot analysis of PINK1, Parkin, Beclin-1, ATG5, p62, and LC3. The lower right panel shows the protein quantification using ImageJ software (version 1.50). **(B)** Representative immunofluorescence images of LC3 (green). DAPI (Blue) stains the nucleus. Scale bar, 10 μm. **(C)** Representative images and quantification of immunofluorescence double-labelling Parkin (Green) and mitochondrial marker (MitoTracker, red). DAPI (Blue) stains the nucleus. Scale bar, 10 μm. **(D)** Representative TEM images of mitochondria and autophagosomes. Red M, mitochondria; Green arrows, autophagosome; Yellow arrows, *E coli*. Scale bar, 0.5 μm. Confluent MAC-T cell were pretreated with LGR-1 (10^5 CFU/mL, MOI = 1) for 3 h, washed three times with PBS, and exposed to *E coli* (10^7 CFU/mL, MOI = 66). Cells were analyzed 8 h after *E coli* infection. Data presented are mean ± SEM; n = 3. $^*p < 0.05$, $^{**}p < 0.01$, $^{***}p < 0.001$.

TEM showed mitophagosomes in LGR-1 pretreated MAC-T cells (**Figure 1D**). TEM results also showed that *E. coli* can cause mitochondria swell, mitochondrial cristae disappear and vacuolization (**Figure 1D**). Collectively, our findings indicate PINK1/Parkin–mediated mitophagy was inhibited in MAC-T cells infected with *E. coli*.

In order to further verify the relationship between LGR-1, *E. coli* and mitophagy, we used promoter and inhibitor for positive and negative verification respectively. MAC-T cells were incubated with 3-MA before exposure to LGR-1 and Rapa for 12 h before exposure to *E. coli*. Immunoblot analysis of PINK1, Parkin, p62, LC3, ATG5, and Beclin-1 showed that mitophagy was inhibited by 3-MA and activated by Rapa. The increased levels of PINK1, Parkin and LC3II proteins, proved that Rapa promoted mitophagy. The decreased levels of PINK1, Parkin and LC3II proteins, proved that 3-MA inhibited mitophagy. *E. coli* decreased PINK1, Parkin, p62, LC3, ATG5, and Beclin-1 expression levels and increased p62 expression level even with Rapa pretreatment (**Figure 2A**). On the contrary, LGR-1 increased PINK1, Parkin, p62, LC3, ATG5, and Beclin-1 expression levels and decreased p62 expression level even with 3-MA pretreatment (**Figure 2B**). Similarly, *E. coli* significantly reduced the number of LC3 puncta (**Figure 2D**). Furthermore, the colocalization of Parkin and MitoTracker was reduced (**Figure 2E**) after *E. coli* infection in cells pretreated with Rapa compared with Rapa control. MitoTracker staining showed mitochondria with a clear outline and a network structure in Rapa-pretreated MAC-T cells compared with the *E. coli* group (**Figure 2E**). TEM also showed mitophagosomes and normal mitochondria in Rapa-pretreated MAC-T cells before exposure to *E. coli* (**Figure 2C**). These findings suggest that the promotion of mitophagy in MAC-T cells reduced the mitochondrial damage by *E. coli* and LGR-1 may play a certain protective role by reducing the inhibition of *E. coli* on mitophagy.

LGR-1 Activates Mitophagy to Suppress *E. coli*-Induced NLRP3 Inflammasome Activation and Apoptosis

Further, we investigated the regulatory role of mitophagy on NLRP3 inflammasome and apoptosis. Immunoblot analysis showed an increase in NLRP3, ASC, and Caspase-1 p10, indicating NLRP3 inflammasome activation in cells infected with *E. coli*, and LGR-1 reduced this increase (**Figure 3A**). Chromatin deep staining and nuclear fragmentation, the apoptosis-related events, were observed after *E. coli* infection (**Figures 1B, C**). *E. coli* infection increased BAX and Caspase-3 p17 expression levels and BAX to Bcl-2 ratio and decreased Bcl-2 expression level; LGR-1 pretreatment reversed these phenomena (**Figure 3B**). These data suggest that LGR-1 can reduce the NLRP3 inflammasome activation and apoptosis induced by *E. coli*.

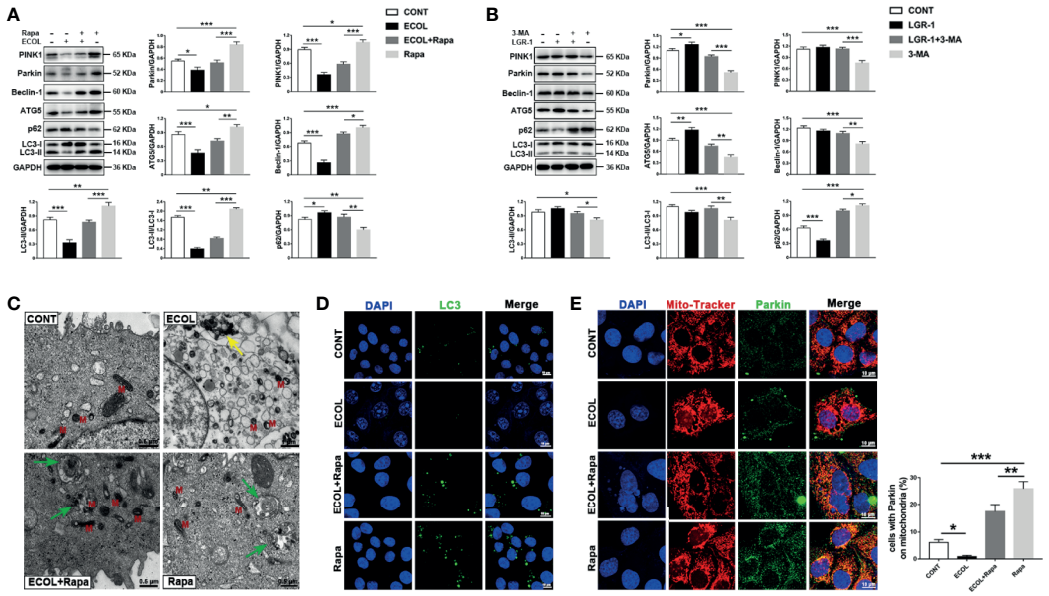


FIGURE 2 | LGR-1 reduces the inhibitory effect of *Escherichia coli* on mitophagy in MAC-T cells. **(A, B)** Western blot analysis of PINK1, Parkin, Beclin-1, ATG5, p62, and LC3. The lower right panel shows the protein quantification using ImageJ software (version 1.50). **(C)** Representative TEM images of mitochondria and autophagosomes. Red M, mitochondrial; Green arrows, autophagosome; Yellow arrows, *E coli*. Scale bar, 0.5 μm and 1 μm. **(D)** Representative immunofluorescence images of LC3 (Green). DAPI (Blue) stains the nucleus. Scale bar, 10 μm. **(E)** Representative images and quantification of immunofluorescence double-labelling Parkin (green) and mitochondrial marker (MitoTracker, Red). DAPI (Blue, nucleus). Scale bar, 10 μm. MAC-T cells were pretreated with 3-methyladenine (3-MA, 5 mM) for 12 h and then treated with LGR-1 (MOI = 1) for 3 h or pretreated with rapamycin (Rapa, 2 μM) for 12 h and then treated with *E coli* (MOI = 66) for 8 (h) Data presented are mean ± SEM; n = 3. $^{*}p < 0.05$, $^{**}p < 0.01$, $^{***}p < 0.001$.

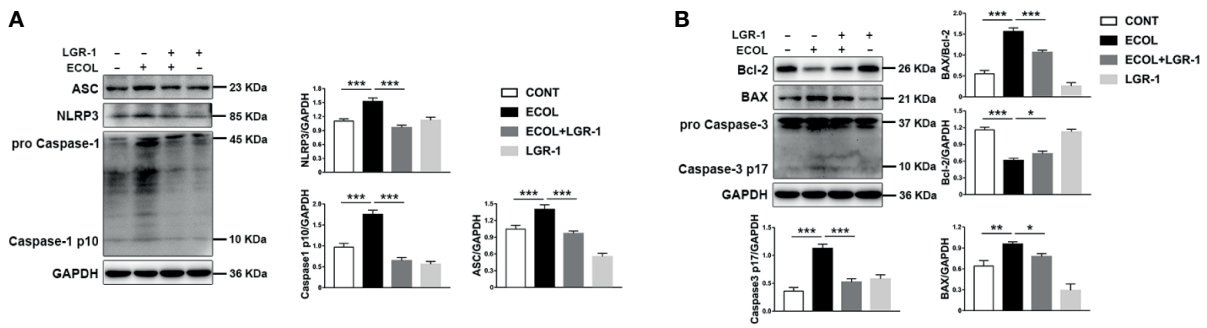


FIGURE 3 | LGR-1 alleviates *Escherichia coli*-induced NLRP3 inflammasome activation and apoptosis in MAC-T cells. **(A, B)** Western blot analysis of ASC, NLRP3, Caspase-1, BAX, Bcl-2, and Caspase-3. The lower right panel shows the protein quantification using ImageJ software (version 1.50) Confluent MAC-T cell were pretreated with LGR-1 (10^5 CFU/mL, MOI = 1) for 3 h, washed three times with PBS, and exposed to *E coli* (10^7 CFU/mL, MOI = 66). Cells were analyzed 8 h after *E coli* infection. Data presented are mean ± SEM; n = 3. $^{*}p < 0.05$, $^{**}p < 0.01$, $^{***}p < 0.001$.

Autophagy negatively regulates NLRP3 inflammasome activation and apoptosis. In order to try to clarify the effect of *E. coli*/LGR-1 on mitophagy in MAC-T cells without considering other factors, and try to simulate the protective mechanism of LGR-1, Rapa and 3-MA were introduced. LGR-1 pretreatment prior to *E. coli* infection improved cell state by promoting mitophagy. Rapa displayed a potent inhibitory effect on NLRP3 and Caspase-1 activation in *E. coli* challenged cells (**Figure 4A**). In *E. coli*-infected MAC-T cells, Caspase-3 p17 and BAX expression levels and BAX to Bcl-2 ratio decreased and Bcl-2 expression level decreased by Rapa pretreatment (**Figure 4A**). Similarly, the state of the nucleus in Rapa-pretreated cells was better than in the cells infected with *E. coli* after Rapa pretreatment (**Figure 4B**). In the presence of the autophagy inhibitor 3-MA, NLRP3 inflammasome and apoptosis were activated, and LGR-1 pretreatment alleviated this situation (**Figure 4C**). These data indicate that activated mitophagy suppresses *E. coli*-induced NLRP3 inflammasome activation and apoptosis.

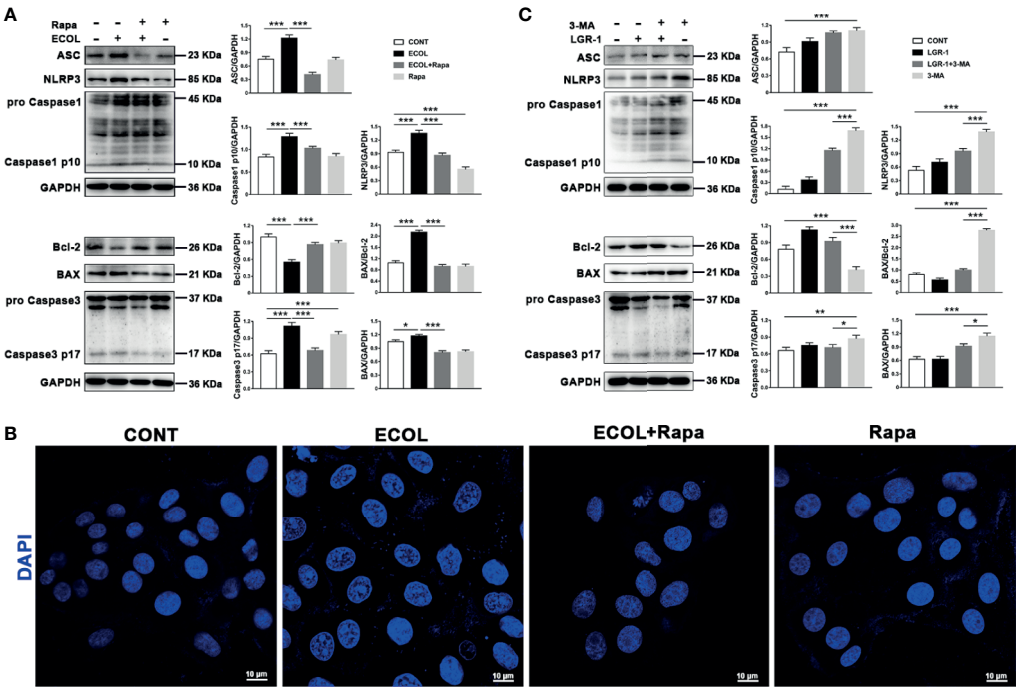


FIGURE 4 | LGR-1 alleviates *Escherichia coli*-induced inhibition of mitophagy to suppress NLRP3 inflammasome activation and apoptosis in MAC-T cells. **(A, C)** Western blot analysis of ASC, NLRP3, Caspase-1, BAX, Bcl-2, and Caspase-3. The right panel shows the protein quantification by ImageJ software (version 1.50). **(B)** Cell apoptosis was detected by staining the nucleus with DAPI (Blue). Scale bar, 10 μm. MAC-T cells were pretreated with LGR-1 (MOI = 1) for 3 h and then treated with 3-methyladenine (3-MA, 5 mM) for 12 h or pretreated with rapamycin (Rapa, 2 μM) for 12 h and then treated with *E coli* (MOI = 66) for 8 (h) Data presented are mean ± SEM; n = 3. $^{*}p < 0.05$, $^{**}p < 0.01$, $^{***}p < 0.001$.

LGR-1 Alleviates *E. coli*-Induced ROS Production and Mitochondrial Damage in MAC-T Cells

Furthermore, we analyzed the mitochondria in the MAC-T cells. TOM20 staining showed evenly distributed linear or short, rod-shaped, straight or curved mitochondria with clear outlines, forming a network structure throughout the cytoplasm (**Figure 5A**). Mitochondria were fragmented in the cells infected with *E. coli*, and LGR-1 pretreatment returned mitochondria to normal. TEM also showed severe mitochondrial damage, manifested as mitochondrial swelling, loss of cristae, and vacuolization, in cells infected with *E. coli*; LGR-1 alleviated the damage (**Figure 1D**). We further measured the T-AOC and ROS and SOD levels in the cells. *E. coli* decreased T-AOC and SOD level and increased ROS levels, and LGR-1 pretreatment alleviated these trends (**Figure 5B**). Collectively, our findings indicate that *E. coli* activates NLRP3 inflammasome and apoptosis by causing mitochondrial damage and oxidative stress and LGR-1 alleviates these effects.

LGR-1 Eliminates *E. coli*-Induced ROS to Suppress NLRP3 Inflammasome Activation and Apoptosis

E. coli induced mitochondrial damage led to the accumulation of ROS, which stimulate NLRP3 and apoptosis. MAC-T cells infected by *E. coli* showed high ROS levels (**Figure 5B**). Meanwhile, the ROS levels in *E. coli*-infected cells pretreated with the ROS scavenger-NAC were similar to those in the control cells (**Figure 6C**). Furthermore, LGR-1 pretreatment prevented ROS production in response to *E. coli* infection (**Figure 5B**), showing the effective ROS scavenging activity of LGR-1. The ROS scavenging effect of LGR-1 was further demonstrated in H_2O_2-induced MAC-T cells (**Figure 8D**). We tested the activation of NLRP3 inflammasome and apoptosis after adding NAC. Accompanying the decrease in ROS, NLRP3, Caspase-1 p10, and Caspase-3 p17 levels (**Figure 6A**) due to *E. coli* infection was mitigated by NAC, which indicated that *E. coli*-induced NLRP3 inflammasome and apoptosis activation required ROS production. Therefore, after NAC treatment, the ability of *E. coli* to induce ROS production is weakened, and ROS levels return to normal levels. The increase in NLRP3, ASC, Caspase-1 p10, BAX, and Caspase-3 p17 levels and BAX to Bcl-2 ratio and the decrease in Bcl-2 level in H_2O_2-treated cell suggest that H_2O_2 activates NLRP3 inflammasome and apoptosis by producing ROS (**Figure 6B**). Meanwhile, LGR-1 showed an effect similar to NAC; LGR-1 alleviated H_2O_2-induced NLRP3 inflammasome activation and apoptosis (**Figure 6B**). Flow cytometry showed less Annexin V-positive MAC-T cells after LGR-1 pretreatment compared with H_2O_2 (**Figure 8C**). Meanwhile, LGR-1 pretreatment decreased the ROS levels in cells compared with H_2O_2-induced cells (**Figure 8D**). Based on these data, we speculate that LGR-1 eliminates ROS to relieve *E. coli*-induced NLRP3 inflammasome activation and apoptosis.

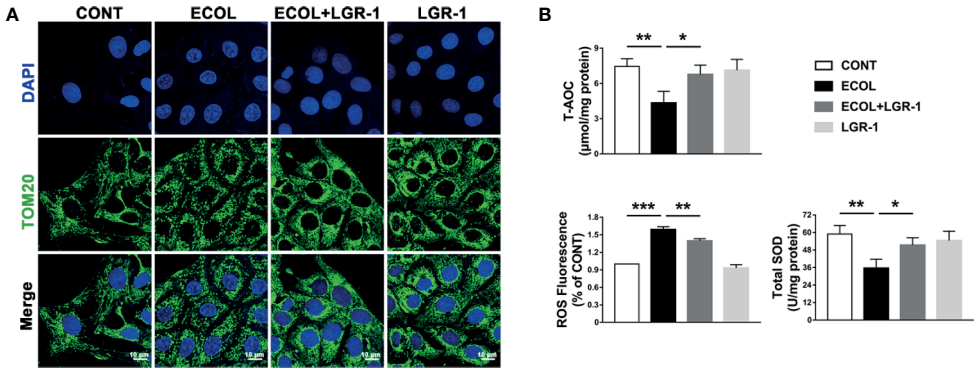


FIGURE 5 | LGR-1 alleviates *Escherichia coli*-induced ROS production, mitochondrial damage in MAC-T cells. **(A)** Representative immunofluorescence images of TOM20 (Green). DAPI (Blue, nucleus). Scale bar, 10 μm. **(B)** T-AOC and SOD and ROS levels. Confluent MAC-T cell were pretreated with LGR-1 (10^5 CFU/mL, MOI = 1) for 3 h, washed three times with PBS, and exposed to *E coli* (10^7 CFU/mL, MOI = 66). Cells were analyzed 8 h after *E coli* infection. Data presented are mean ± SEM; n = 3. *$p < 0.05$, **$p < 0.01$, ***$p < 0.001$.

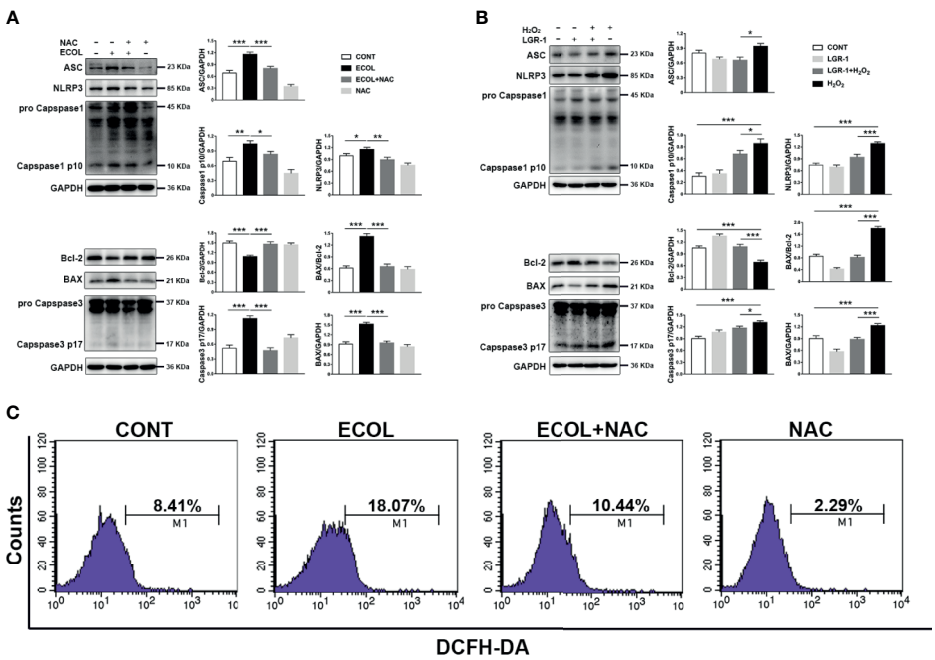


FIGURE 6 | *Escherichia coli*-induced NLRP3 inflammasome activation and apoptosis requires ROS production in MAC-T cells. **(A, B)** Western blot analysis of ASC, NLRP3, Caspase-1, BAX, Bcl-2, and Caspase-3. The right panel shows the protein quantification using ImageJ software (version 1.50). **(C)** Flow cytometry analysis of ROS. M1 represents the proportion of cells stained with DCFH-DA. MAC-T cells were pretreated with *N-acetyl-L-cysteine* (NAC, 5 mM) for 2 h and then exposed to *E coli* (MOI = 66) for 8 h or pretreated with LGR-1 for 3 h and then exposed to hydrogen peroxide (H_2O_2, 0.5 mM) for 0.5 (h) Data presented are mean ± SEM; n = 3. *$p < 0.05$, **$p < 0.01$, ***$p < 0.001$.

LGR-1 Inhibits NLRP3 Inflammasome Activity to Reduce *E. coli*-Induced Apoptosis

LGR-1 attenuated NLRP3 inflammasome activation and apoptosis induced by *E. coli*; therefore, we explored the relationship between NLRP3 inflammasomes and apoptosis. Immunoblot analysis showed an increase in the pro-apoptotic protein (BAX and Caspase3) and decrease in the anti-apoptotic protein (Bcl-2) with *E. coli* exposure (**Figures 3B**, **4A**, **6A** and **7A**). MCC950, an NLRP3 inflammasome inhibitor, was used to pretreat MAC-T cells before exposure to *E. coli* to inhibit NLRP3 inflammasome activation and explore the correlation between NLRP3 inflammasome and *E. coli*-induced apoptosis. MCC950 abolished *E. coli*-induced apoptosis, which was demonstrated by the decrease in BAX, BAX/Bcl-2 ratio

and Caspase-3 p17 level and an increased in Bcl-2 level in immunoblot analysis (**Figure 7A**). Flow cytometry also showed less Annexin V-positive MAC-T cells after MCC950 pretreatment (**Figure 7B**). Collectively, our findings indicate that LGR-1 inhibits NLRP3 inflammasome activity to protect MAC-T cells from *E. coli*-induced apoptosis.

Silencing PINK1 Blocks the Inhibitory Effect of LGR-1 on ROS, NLRP3 Inflammasome, and Apoptosis

To verify whether LGR-1 eliminates ROS production through mitophagy mediated by PINK1/Parkin to inhibit the activation of NLRP3 inflammasome and apoptosis, we applied siRNA interference technology to knock down the PINK1 protein expression in MAC-T cells. Immunoblot analysis confirmed that siRNA effectively suppressed PINK1 expression (**Figure 8A**). We further added H_2O_2 as a positive control to increase ROS production and activate NLRP3 inflammasome and apoptosis. LGR-1 could not reduce H_2O_2-induced NLRP3, ASC, and Caspase-1 p10 levels after PINK1 was knocked down (**Figure 8B**). Besides, LGR-1 could not alleviate H_2O_2-apoptosis, manifested by the increase in BAX, BAX/Bcl-2 ratio, and cleaved-Caspase-3, and the decrease in Bcl-2 (**Figure 8B**). Knocking down PINK1 inhibited the ROS scavenging effect of LGR-1 (**Figure 8C**). Flow cytometry showed more Annexin V-positive MAC-T cells after silencing PINK1 compared with the H_2O_2-induced cells pretreated with LGR-1 (**Figure 8D**). These results indicate that LGR-1 exerts a beneficial effect through PINK/Parkin-mediated mitophagy.

LGR-1 Alleviates *E. coli*-Induced Mitophagy Inhibition, NLRP3 Inflammasome Activation, and Apoptosis in Mice Mammary Gland

In order to verify whether LGR-1 has obvious protective effect *in vivo*, we successfully established a mouse mastitis model. First, we observed the morphological and histological changes of mammary gland tissue by H&E staining. There was no significant change in the mammary glands of the CONT group and LGR-1 group. In ECOL group, the wall of mammary acinus was obviously thickened, the stroma was congested, and the acinus was filled with inflammatory cells (**Figure 9A**). And LGR-1 could significantly improve the histopathological changes caused by *E. coli*. Further detection of cytokines expression showed that *E. coli* could significantly increase IL-1 β and TNF- α, whereas LGR-1 can inhibit the production of these inflammatory factors in the breast (**Figure 9B**). Then, in order to detect whether LGR-1 can affect mitophagy, NLRP3 inflammasome and apoptosis, we detected the changes of related proteins by Western blotting. In line with the results of *in vitro*, *E. coli* can inhibit mitophagy related protein (PINK1, Parkin, ATG5, Beclin-1 and LC3II/LC3I), increase the expression of NLRP3 inflammasome (NLRP3, ASC and Caspase1 p10), and cause apoptosis, while LGR-1 can reduce these effects of *E. coli* (**Figures 9C–E**). Finally, TUNEL staining was performed to further explore the effect on apoptosis. The results showed that *E. coli* induced the accumulation of TUNEL-positive cells in the epithelial cells of breast tissue, while LGR-1 could significantly reduce the proportion of TUNEL-positive cells (**Figure 9F**).

DISCUSSION

E. coli is the main causative agent of clinical mastitis in dairy cattle, which is difficult to cure and results in huge economic losses. During bacterial infection, many pathogen-associated molecular patterns (30), such as type III secretion system and lipopolysaccharides, get expressed on the cell wall, which activate inflammasomes, including NLRP3 inflammasome. The NLRP3 inflammasome has been known to play a role in many inflammatory diseases (31, 32), and its excessive activation induces intestinal and breast inflammation and tissue damage (3, 33). Consistent with the previous studies (34),

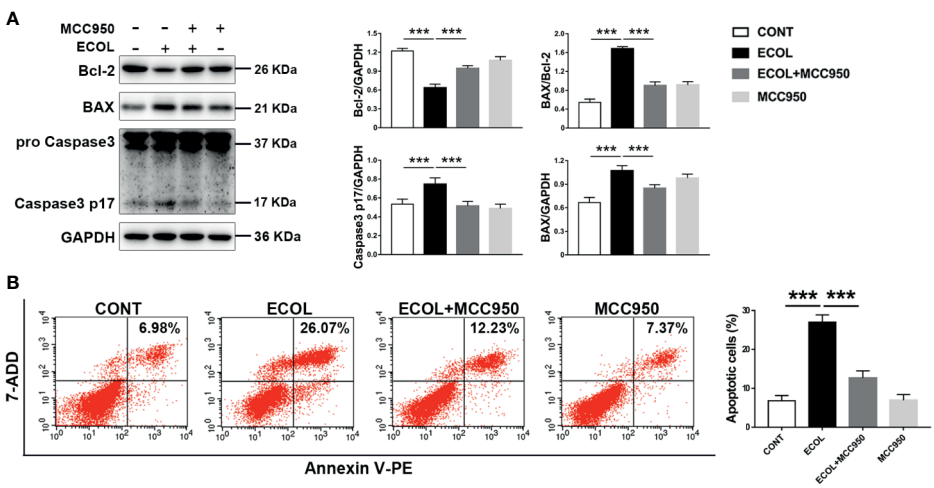


FIGURE 7 | Inhibition of NLRP3 inflammasome activation reduces *Escherichia coli*-induced apoptosis in MAC-T cells. **(A)** Western blot analysis of BAX, Bcl-2, and Caspase-3. The right panel shows the protein quantification using ImageJ software (version 1.50). **(B)** Flow cytometry analysis of the percentage of apoptotic cells. MAC-T cells were pretreated with MCC950 (100 nM) for 0.5 h and then exposed to *E coli* (MOI = 66) for 8 (h) Data presented are mean ± SEM; n = 3. ***$p < 0.001$.

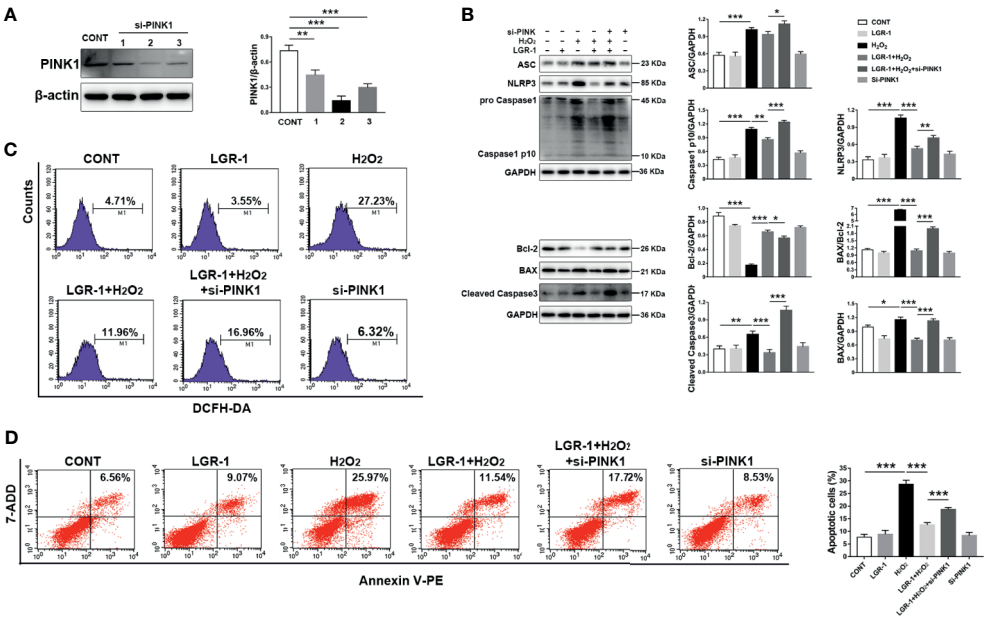


FIGURE 8 | Silencing PINK1 blocks the inhibitory effect of LGR-1 on *Escherichia coli*-induced ROS release, NLRP3 inflammasome activation, and apoptosis in MAC-T cells. **(A)** Western blot analysis of PINK1 in MAC-T cells after PINK1silencing (si-PINK1). The right panel shows the protein quantification using ImageJ software (version 1.50). **(B)** Western blot analysis ASC, NLRP3, Caspase-1, BAX, Bcl-2, and Caspase-3 in MAC-T cells after PINK1silencing (si-PINK1). The right panel shows the protein quantification using ImageJ software (version 1.50). **(C)** Flow cytometry analysis of ROS. M1 represents the proportion of cells stained with DCFH-DA. **(D)** Flow cytometry analysis of the percentage of apoptotic cells. The si-PINK1-MAC-T cells pretreated with LGR-1 for 3 h and then exposed to hydrogen peroxide (H_2O_2, ROS inducer; 0.5 mM) for 0.5 (h) Data presented are mean ± SEM; n = 3. $^*p < 0.05$, $^{**}p < 0.01$, $^{***}p < 0.001$.

our study confirms that *E. coli* can activate NLRP3 inflammasome in mammary epithelial cells also (**Figure 1**). Besides, mitophagy, a host defense mechanism, prevents excessive activation of NLRP3 inflammasome (18, 21, 35). Therefore, a balance between these two is vital to prevent microbial response and maintain immunity and health. However, the mechanism *via* which mitophagy regulates the NLRP3 inflammasome in breast diseases, especially during mastitis, remains unknown. Our study for the first time showed that mitophagy mediated by PINK1/Parkin was inhibited in *E. coli*-induced mastitis (**Figure 10**).

Probiotics, as an alternative to antibiotics, have attracted scientific interest in mastitis treatment. *Lactobacillus rhamnosus* induced STAT3 and JNK activation through granulocyte colony-stimulating factor and consequently inhibited tumor necrosis factor production in lipopolysaccharide-or *E. coli*-activated macrophages (36). Similarly, *Lactobacillus johnsonii* L531 inhibited *Salmonella* Infantis-induced activation of NLRP3 inflammasome (33). Meanwhile, our previous study showed that LGR-1 attenuated NLRP3 inflammasome activation induced by *E. coli*. These studies collectively indicate the beneficial effects of probiotics; however, the specific mechanism of LGR-1 in inhibiting NLRP3 inflammation activation to prevent mastitis remains unclear. We found that LGR-1 inhibited pathogen infection by triggering mitophagy to inhibit ROS production, NLRP3 inflammasome activation and apoptosis in breast epithelial cells (**Figure 10**), which provides an understanding of the mechanism *via* which probiotics demonstrate antimicrobial effects and maintain breast health. A study showed that blocking NLRP3 activation provided protection against lethal influenza A virus (IAV) (37). Consistent with that study, we found that LGR-1 diminished *E. coli*-induced NLRP3 assembly and pro-Caspase-1 cleavage. Thus, the study confirms the selective inhibition of NLRP3 inflammasome by LGR-1 to rescue cellular damage caused by pathogens.

Recently, many studies have proven the key role of mitochondria in innate immune response (38, 39). However, mitochondrial damage can lead to the accumulation of ROS, which can activate NLRP3 inflammasome and apoptosis (18, 40). In MAC-T cells, *E. coli* infection led to massive ROS release and severe mitochondrial damage (**Figures 1**, **2** and **5**). *E. coli* induced chromatic agglutination and karyopyknosis, increased BAX and cleaved-Caspase-3 expression levels, and decreased Bcl-2 expression level, indicating apoptosis (**Figure 3**). In view of this, we speculate that ROS is necessary for *E. coli* to induce NLRP3 inflammasome activation and apoptosis. Therefore, we explored the importance of ROS for *E. coli*-induced NLRP3 inflammasome activation and apoptosis by treating cells with NAC (a ROS scavenger). The results showed that NAC prevented *E. coli*-induced the activation of NLRP3 inflammasome and apoptosis in MAC-T cells (**Figure 6A**). The observation indicated that the activation of *E. coli*-induced NLRP3 requires ROS release. Parallelly, LGR-1 can attenuate ROS activation and apoptosis induced by *E. coli* (**Figures 3** and **5**). Thus, we speculate that lgr-1 has the ability to

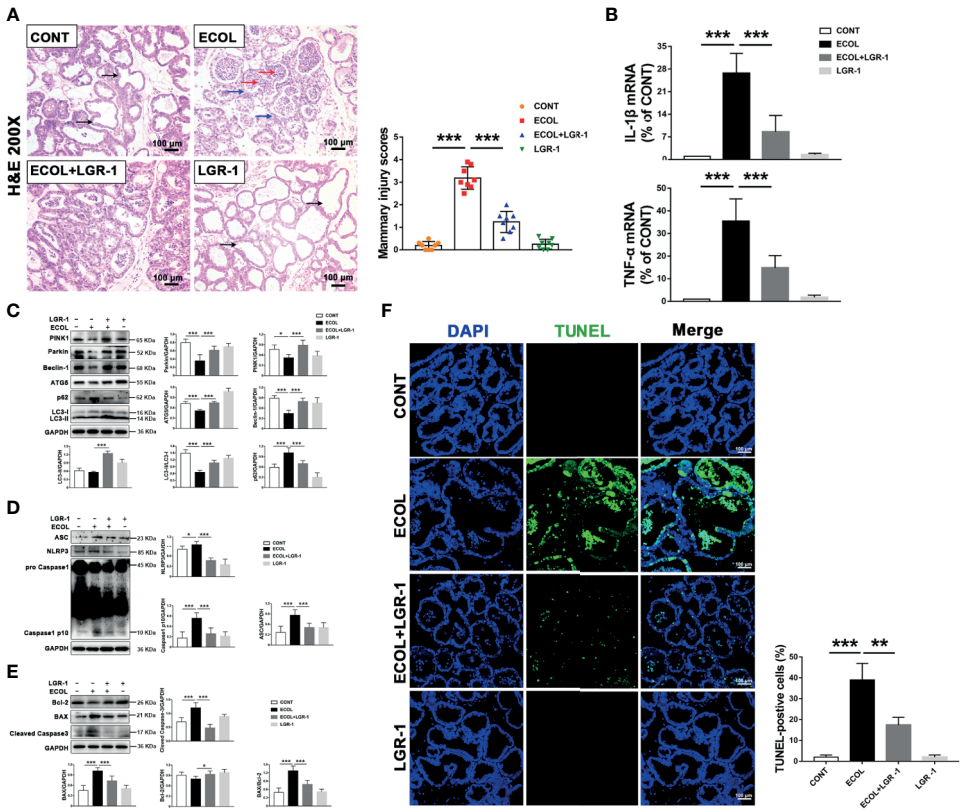


FIGURE 9 | LGR-1 alleviates *E coli*-induced mitophagy inhibition, NLRP3 inflammasome activation, and apoptosis in mice mammary gland. **(A)** Mammary gland tissue sections were stained with H & **(E)** The black arrow was the normal tissues. The red arrow was the infiltration of inflammatory cells. The blue arrow was the hyperplastic of alveolar wall. The scoring criteria are varying from 0 points to 4 points in no injury, mild injury, moderate injury, severe injury, and extreme injury, respectively. Scale bar, 100 μm. **(B)** The mRNA levels of IL-1β and TNF-α in mammary tissue homogenate. **(C, D, E)** Western blot analysis of PINK1, Parkin, Beclin-1, ATG5, p62, LC3, ASC, NLRP3, Caspase-1, BAX, Bcl-2, and cleaved Caspase-3. The right and lower panel shows the protein quantification using ImageJ software (version 1.50). **(F)** Apoptosis was accessed by TUNEL staining of mammary and quantification of TUNEL-positive cells. DAPI (Blue, nucleus). Scale bar, 100 μm. LGR-1 was given by gavage (2.5×10^8 CFU/200 μL saline, 7 consecutive days, once a day), and then *E coli* (1×10^6 CFU/30 μL saline) was injected into mammary duct to establish a mouse mastitis model (24 hours later, the mice were euthanized and mammary tissue was collected). Data presented are mean ± SEM; n = 8. $^*p < 0.05$, $^{***}p < 0.001$.

clear ROS. To verify the role of LGR-1 in reducing ROS production, H_2O_2, a ROS stimulant, was introduced to the cell culture. As shown in **Figure 6B**, LGR-1 alleviated the increase of NLRP3 protein and pro-apoptotic protein, and the decrease of anti-apoptotic protein induced by H_2O_2, suggesting the anti-ROS, anti-inflammatory, and antiapoptotic effects of LGR-1.

Furthermore, mitochondrial damage was associated with NLRP3 inflammasome activation and apoptosis induced by *E. coli*. Widespread mitochondrial damage was detected when autophagy was inhibited. Therefore, eliminating the damaged mitochondria by autophagy is necessary to prevent excessive activation of NLRP3 inflammasome (18, 21, 35). Mitophagy, a selective autophagy in mitochondria, is a crucial process for regulating NLRP3 inflammasome activation by removing damaged mitochondria. PINK1/Parkin pathway has been reported to regulate mitophagy. In normal conditions, PINK1 is imported into mitochondria, anchored in inner mitochondrial membrane, and degraded by mitochondrial proteases. However, when mitochondria are damaged, PINK1 does not get imported into inner mitochondrial membrane, but aggregates on outer mitochondrial membrane (41), recruits and activates Parkin, binds with LC3 on the autophagosome, and promotes damaged mitochondria degradation (39). In a variety of inflammatory diseases, moderate regulation of mitophagy is important for maintaining mitochondrial homeostasis. In autophagy/mitophagy-deficient macrophages, NLRP3 activators increased the accumulation of damaged mitochondria, accompanied by ROS production. Consistent with this, *E. coli* reduced PINK1, Parkin, LC3II, ATG5, and Beclin-1 expression levels and Mito-Tracker/Parkin colocalization and increased p62 expression level, ROS production (**Figures 1**, **2**, and **5**), NLRP3 inflammasome activation, and apoptosis (**Figures 3** and **4**) in MAC-T cell. These findings together suggest that *E. coli* can inhibits mitophagy. However, LGR-1 can reverse the inhibitory effect of *E. coli* on mitophagy. In order to verify the regulatory effects of *E. coli* and LGR-1 on mitophagy, mitophagy promoter and inhibitor were

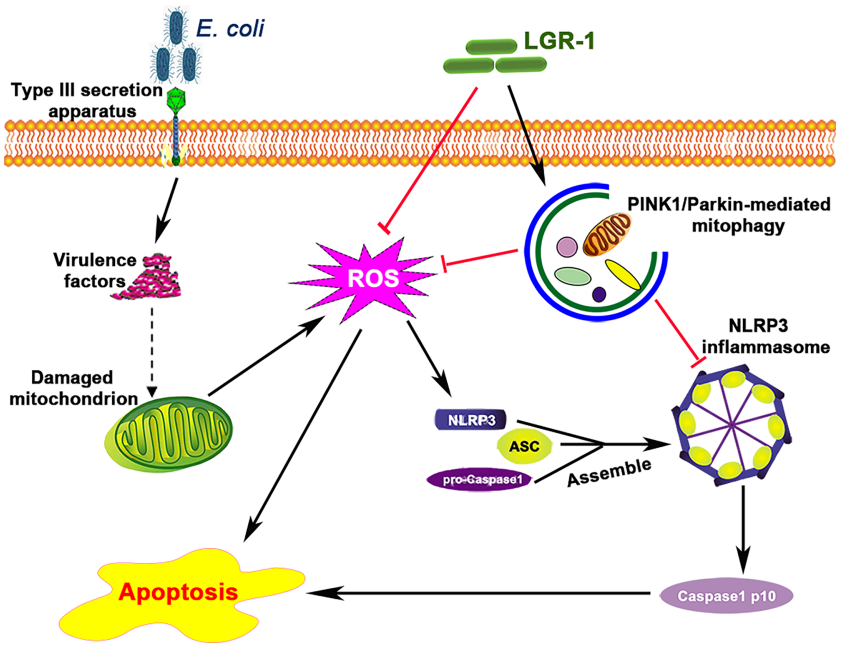


FIGURE 10 | *Lactobacillus rhamnosus* GR-1 prevents *Escherichia coli*-induced cell apoptosis through PINK1/Parkin-mediated mitophagy by inhibiting ROS production and NLRP3 inflammasome activation. *E. coli* secretes virulence factors *via* the type III secretion system and causes mitochondrial dysfunction. The damaged mitochondrion produces excessive reactive oxidative species (ROS), which induces NLRP3 inflammasome activation and subsequently causes apoptosis. LGR-1 has anti-ROS function and inhibits ROS production. LGR-1 pretreatment induces mitophagy that eliminates ROS and inhibits NLRP3 inflammasome activation. The solid arrows indicate demonstrated effects, the dashed arrow indicates the potential effects, and the red lines indicate negative effects.

introduced for verification. As shown in **Figure 4**, the results were consistent with the above speculation. Hence, LGR-1 alleviated the inhibitory effect of *E. coli* on mitophagy and weakened NLRP3 inflammasome activation and apoptosis in MAC-T cells.

Studies have proven the protective role of mitophagy mediated by PINK1/Parkin in apoptosis (42, 43). And study has found that increasing the expression of SESN2 to promote mitophagy can protect the host from sepsis (44). However, the specific pathway of mitophagy that regulates apoptosis is not yet reported in in mastitis induced by *E. coli*. This study elucidates the protective role of mitophagy mediated by PINK1/Parkin under *E. coli*-induced mastitis in MAC-T cells using 3-MA and Rapa (**Figures 2** and **4**). Besides, pretreatment of cells with NAC (ROS scavenger) and MCC950 (NLRP3 inhibitor) showed that apoptosis was inhibited through decreased ROS production and NLRP3 inflammasome activation in MAC-T cells (**Figures 6** and **7**). Then, in order to verify the importance of the PINK1/Parkin pathway in the protection of LGR-1, the PINK1 protein was knocked down. When the PINK1 protein is knocked down, LGR-1 cannot attenuate the accumulation of ROS, the NLRP3 inflammasome activation and apoptosis, thus cannot exert its protective effect. (**Figure 8**). Our findings collectively indicate that PINK1/Parkin-mediated mitophagy is one of the self-limiting pathways *via* which LGR-1 protects cells from excessive inflammation and apoptosis.

All of the above are our application of breast epithelial cells as an *in vitro* infection model to explore the protective effect of LGR-1 in mastitis. However, whether LGR-1 still has a protective effect *in vivo* is still unknown. Therefore, we established a mouse model of mastitis to explore the effects of LGR-1 *in vivo*. These results indicated that LGR-1 alleviated the inhibitory effect of *E. coli* on mitophagy and reduced the apoptosis and the increase of inflammatory factors induced by *E. coli* in mouse mastitis (**Figure 9**). Consequently, these data indicate that LGR-1 pretreatment has a preventive and protective effect in *E. coli*-induced mastitis (**Figure 9**). It has been reported that probiotics such as *clostridium tyrobutyricum* can significantly reduce the symptoms of mastitis induced by *Staphylococcus aureus*, which may be related to changes in gut microbiota and short-chain fatty acids in the intestine (14). We also used the same way of intragastric administration of probiotics, which may also change the state of gut microbiota in mice, and increase the content of probiotics such as lactic acid bacteria and short-chain fatty acids, so as to prevent mastitis. However, the application and effect of LGR-1 as a probiotic in bovine need to be further explored.

In summary, *E. coli* inhibited mitophagy and enhanced NLRP3 inflammasome activation and apoptosis, both *in vivo* and *vitro*. LGR-1 pretreatment induced PINK1/Parkin-mediated mitophagy, cleared the damaged mitochondria, and reduced ROS production, NLRP3 inflammasome activation and apoptosis under *E. coli* infection. These findings deepen understanding of probiotics' immune protection and contribute to its application in bovine mastitis prevention and treatment. However, the protective mechanisms in bovine and the probiotic administration route

need to be investigated. To conclude, our study suggests that therapeutic strategies aiming at the upregulation of mitophagy under *E. coli*-induced mastitis may preserve mitochondrial function in bovine mastitis.

MATERIALS AND METHODS

Animals

Thirty-two females (8-10 week old) specific-pathogen-free pregnant Crl: CD1 (ICR) mice were purchased from Charles River (Beijing, China). Mice were reared in a sterile environment with 12h light and dark cycle. and ad libitum access to food and water.

Ethics Statement

This study is approved by the Animal Ethics Committee of China Agricultural University, and all animal care and experimental procedures are under the supervision of this committee.

Establishment of Mouse Mastitis Model

In order to verify the protective effect of LGR-1 on *E. coli* induced mastitis, we established a mouse mastitis model. This mouse mastitis model was induced by *E. coli* as previously described (14). In short, offspring were removed 4h before intramammary inoculation. The mice were anesthetized with Zoletil 50 (55mgkg, WK001, Virbac, France) and placed in supine position under the stereoscope. Disinfect the fourth pair of mammary glands and expose the mammary duct by cutting the tip of the nipple. *E. coli* dissolved in 30 μL physiologic saline was slowly intraductal injected through a 100-μL syringe with a 30-gauge blunt needle. Four groups (n = 8 per group) of mice were allocated: (1) a negative control group (CONT group); (2) *E. coli* group (ECOL group); (3) *E. coli* + LGR-1 group (ECOL + LGR-1 group); (4) LGR-1 group (LGR-1 group). Before *E. coli* infection, mice in the ECOL + LGR-1 and LGR-1 group were inoculated with LGR-1 (2.5×10^8 CFU/200 μL saline) by oral gavage for 7 consecutive days, once a day; mice in the CONT and ECOL groups were administered an equal volume of sterile physiologic saline at 10:00 AM daily. At 10:00 AM on Day 8, ECOL and ECOL + LGR-1 group mice were intraductal injected *E. coli* (1×10^6 CFU/30 μL saline), whereas mice in the CONT and LGR-1 group received equal volume of sterile physiologic saline. After 24 hours of *E. coli* infection, all mice were euthanized and the mammary glands tissue were collected and frozen at -80 °C until use.

Bacterial Strains and Growth Conditions

Lactobacillus rhamnosus GR-1 (LGR-1, ATCC 55826; American Type Culture Collection, Manassas, VA, United States) was grown in De Man, Rogosa, and Sharpe (MRS) broth (Oxoid, Hampshire, United Kingdom) under microaerophilic conditions at 37°C for 24 h. After overnight incubation, LGR-1 was diluted (1:1000) in fresh MRS broth and grown for approximately 12 h until mid-log phase (OD600 = 0.6).

Escherichia coli strain (serotype O111:K58, CVCC1450, the China Institute of Veterinary Drug Center, Beijing, China) was grown in Luria–Bertani (LB) broth (Oxoid, Hampshire, United Kingdom). After overnight incubation, *E. coli* was diluted (1:1000) in fresh LB at 37°C for 8h and 200rpm until mid-log phase (OD600 = 0.6).

Cell Culture and Infection

MAC-T cells (a kind gift from Dr. Ying Yu in China Agricultural University) were seeded in 6- or 12-well plates (3×10^5 and 3×10^4 cells per well, respectively) and cultured in DMEM/Ham's F-12 (1:1) (GE Healthcare Life Sciences HyClone Laboratories, Utah, USA) supplemented with 10% FBS (ThermoFish Scientific, Rockford, USA) and penicillin (100 Units/mL)/streptomycin (100 μg/mL) at 37°C in a 5% CO_2 incubator for 24 h. MAC-T cells were pretreated with LGR-1 (10^5 CFU/mL; multiplicity of infection, MOI = 1) for 3 h. Then cells were washed three times with PBS and exposed to *E. coli* (10^7 CFU/mL, MOI = 66). After 8 h, MAC-T cells were collected for further analysis.

Drug Treatments

MAC-T cells were treated as follows to verify the role of autophagy in LGR-1 defense against *E. coli* infection: MAC-T cells were (1) pretreated with 3-methyladenine (3-MA, 5 mM, S2767, autophagy inhibitor from Selleck Chemicals, Houston, USA) for 12 h washed three times with PBS, and treated with LGR-1 (MOI = 1) for 3 h, or (2) pretreated with rapamycin (Rapa, 2 μM, S1039, autophagy activator from Selleck Chemicals, Houston, USA) for 12 h, washed three times with PBS, and challenge with *E. coli* (MOI = 66) for 8 h.

MAC-T cells were treated as follows to verify whether ROS is the target of LGR-1 in the defense against *E. coli* infection: MAC-T cells were (1) pretreated with N-acetyl-L-cysteine (NAC, 5 mM, S0077, ROS scavenger from Beyotime Biotechnology, Shanghai, China) for 2 h, washed three times with PBS, and exposed to *E. coli* (MOI = 66) for 8 h or (2) pretreated with LGR-1 for 3 h, washed three times with PBS, and exposed to hydrogen peroxide (H_2O_2, ROS inducer; 0.5 mM) for 0.5 h.

MAC-T cells were treated as follows to verify the correlation between NLRP3 inflammasome activation and cell apoptosis during *E. coli* infection: MAC-T cells were pretreated with MCC950 (100 nM, HY-12815A, NLRP3 inhibitor from MedChemExpress, New Jersey, USA) for 0.5 h, washed three times with PBS, and exposed to *E. coli* (MOI = 66) for 8 h.

In this study, MAC-T cells in all control groups were not treated, only washed with PBS synchronously. Both untreated and treated cells were collected for protein analysis.

Histopathologic Scoring

The mammary tissues were fixed with 4% paraformaldehyde for at least 24h. The paraffin embedded tissues were sliced into 3 μm thick slices and stained with hematoxylin and eosin (H&E) staining to observe the pathological changes. The level of mammary inflammation was scored as described previously (45).

RNA Interference

To verify the importance of PINK1/Parkin mediated-mitophagy pathway in the protection of LGR-1, we performed gene silencing to knocked down PINK. MAC-T cells were seeded in

24 well plates. When the cells grew to 60%-80% confluence, PINK1-siRNA (si-PINK1, sense 5'-GGAGCGGUCACUG ACAGAATT-3'; antisense 5'-UUCUGUCAGUGACCG CUCCTT-3', GenePharma, Suzhou, China) diluted with Lipofectamine™ RNAiMAX (13778075, a transfection reagent from ThermoFish Scientific, Rockford, USA) was transfected into the cells. At 5h after transfection, media were removed, supplemented with DMEM and incubated at 37°C for 48 h.

Transmission Electron Microscopy

At 8 h after *E. coli* challenged, MAC-T cells were harvested and fixed in 3% glutaraldehyde (pH = 7.4) for 48 h. Samples were treated following the standard TEM procedure (15, 46).

Immunofluorescence

MAC-T cells were cultivated on cell climbing sheets for staining and treated as described above (47). For labeling the mitochondria, Mito-Tracker Red CMXRos (CMXRos, C1035, Beyotime Biotechnology, Shanghai, China) was added to living MAC-T cells at 37°C for 30 min. The treated MAC-T cells were fixed with 4% paraformaldehyde for 10 min, then incubated with 1% Triton-X-100 (T8787, Sigma-Aldrich, St. Louis, USA) for 15 min at room temperature to permeate the cell membrane, and blocked with 2% bovine serum albumin for 1.5 h at room temperature. The cells were incubated with anti-Parkin (1:200, 14060-1-AP, Proteintech Group Inc, Rosemont, IL 60018, USA) or anti-TOM 20 (1:300, 11802-1-AP, Proteintech Group Inc), at 4°C overnight. Then cells were incubated with Alexa Fluor 488 goat anti-rabbit secondary antibody (Beyotime Biotechnology, Shanghai, China) at room temperature for 1 h. DAPI (C0060, Solarbio Science&Technology Co., Ltd, Beijng, China) was used to stain cell nuclei. The cells were observed and images captured under a confocal laser scanning microscope (Nikon A1); MitoTracker Red CMXRos was detected at 555 nm, and secondary antibodies at their corresponding wavelengths (488 nm/555 nm).

Detection of Total Anti-Oxidation Capacity and Superoxide Dismutase Level

The T-AOC (S0121, Beyotime Biotechnology, Shanghai, China) and SOD (S0101S, Beyotime Biotechnology, Shanghai, China) level were determined using the commercial kits, following the manufacturers' instructions.

Measurement of Intracellular ROS

Intracellular ROS levels were measured by the 2,7-dichlorofluorescein diacetate (DCFH-DA, S0033S, cell-permeable fluorescent probe from Beyotime Biotechnology, Shanghai, China). Fluorescence was directly assessed by a fluorescence plate reader (BioTek Synergy H1). All the values were normalized using control. Flow cytometry was performed using a FACS Calibur system (BD Biosciences), and data were analyzed using FlowJO software (version 10.0.7).

Quantitative Real-Time PCR

Total RNA was extracted from mice mammary tissue by using RNAiso Plus (9108, TaKaRa, Japan), and RNA transcription was performed adopting the PrimeScriptTM RT Reagent Kit (RR047A, TaKaRa, Japan). Quantitative real-time RT-PCR was performed through using a SYBR Green PCR Master Mix (LS2062, Promega, USA). The mRNA expression of IL-1β and TNF-α was normalized to the mRNA expression of β-actin. The primer sequences are demonstrated in **Table S1** and the gene expression levels were analyzed with the $2^{-\Delta\Delta CT}$.

Western Blotting

MAC-T cells were lysed in RIPA buffer containing a protease/phosphatase inhibitor cocktail on ice for 30 min.). Protein (equal amounts, 20 μg) were loaded on 10% or 12% SDS-polyacrylamide gels and transferred to polyvinylidene difluoride (PVDF) membranes (Roche). After blocking with 5% skim milk at 37°C for 1 h and the membranes were incubated with the following primary antibodies at 4°C overnight: anti-LC3 I/II (1:1000, #4108) and anti-cleaved-Caspase-3 (1:1000, #9664) from Cell Signaling Technology (Danvers, USA); anti-ATG5 (1:750, 10181-2-AP), anti-Beclin-1 (1:1000, 11036-1-AP), anti-p62/SQSTM1 (1:1000, 18420-1-AP), anti-ASC (1:1000, 10500-1-AP), anti-BAX (1:1000, 50599-2-Ig), anti-Bcl-2 (1:1000, 12789-1-AP), anti-Caspase-3 (1:1000), anti-PINK1 (1:1000, 23274-1-AP), anti-Parkin (1:1000, 14060-1-AP), anti-GAPDH (1:5000, 60004-1-AP) and anti-β-Actin (1:5000, 60008-1-AP) from Proteintech Group Inc (Rosemont, IL 60018, USA); anti-NLRP3 (1:500, AF2155) from Beyotime Biotechnology (Shanghai, China) and anti-Caspase-1 (1:1000, ab179515) from Abcam (Cambridge, UK). The immunoreactive bands were visualized with an ECL detection system (Tanon 6200 chemiluminescence imaging workstation, Tanon Science & Technology Co., Ltd. Shanghai, China). The protein bands were quantified by densitometry using ImageJ software (version 1.50).

Flow Cytometry Assessment of Apoptosis

Cell apoptosis was measured by the Annexin V-PE/7-AAD apoptosis detection kit (A213-01, Vazyme Biotech, Nanjing, China). MAC-T cells were harvested, and softly re-suspended in 1× binding buffer (100 μL). Then Annexin V-PE (5 μL) and 7-ADD (5 μL) were added to each group and incubated in the dark for 15 min. Approximately 10,000 or 20,000 cells from each group were used to analyze on a FACS Calibur system (BD Biosciences) and evaluated with the FlowJo software (version 10.0.7).

TUNEL Assay

The paraffin embedded tissues were sliced into 3 μm thick slices, dewaxed and dehydrated, and then TUNEL staining (A112, Vazyme, Nanjing, China) was performed according to the manufacturer's instructions. Briefly, the slices were washed with PBS and reacted with TdT enzyme/buffer at 37°C for 1 h, followed by DAPI (C0060, Solarbio Science&Technology Co., Ltd, Beijng, China) staining at room temperature for 5 min. Then the slices were observed and images were captured at x400 magnification using a confocal laser scanning microscope (Nikon A1).

Data Analysis

Using Prism 7 (GraphPad) to perform statistical analysis. Qualitative data were expressed as means ± standard error of

the mean (SEM; n = 3 or 6). One-way analysis of variance (ANOVA) was applied to analyze statistically significant differences at $p < 0.05$, followed by Tukey's test.

DATA AVAILABILITY STATEMENT

The original contributions presented in the study are included in the article/**Supplementary Material**. Further inquiries can be directed to the corresponding author.

ETHICS STATEMENT

All animals were treated in strict accordance with the Guidelines for Laboratory Animal Use and Care from the Chinese Center for Disease Control and Prevention and the Rules for Medical Laboratory Animals (1998) from the Chinese Ministry of Health, under protocol CAU20161016- 1, which was approved by the Animal Ethics Committee of China Agricultural University.

AUTHOR CONTRIBUTIONS

YL: Conceptualization, methodology, validation, formal analysis, investigation, writing-original draft, supervision, and project administration. YZ: Methodology and funding acquisition. BC: Methodology and validation. NL: Validation and investigation. SC: Investigation. JW: Writing-review and editing, and funding acquisition. All authors contributed to the article and approved the submitted version.

FUNDING

This work was supported from the following funds: the National Key R&D Program of China (Project No. 2017YFD0502200), the program for the Beijing Dairy Industry Innovation Team and the National Natural Science Foundation of China (Project No. 31873034).

ACKNOWLEDGMENTS

We would like to acknowledge the reviewers for their helpful comments on this paper.

SUPPLEMENTARY MATERIAL

The Supplementary Material for this article can be found online at: https://www.frontiersin.org/articles/10.3389/fimmu.2021.715098/full#supplementary-material

REFERENCES

1. Omaleki L, Browning GF, Allen JL, Markham PF, Barber SR. Molecular Epidemiology of an Outbreak of Clinical Mastitis in Sheep Caused by Mannheimia Haemolytica. *Vet Microbiol* (2016) 191:82–7. doi: 10.1016/j.vetmic.2016.06.005
2. Castilho IG, Dantas STA, Langoni H, Araujo JP Jr, Fernandes A Jr, Alvarenga FCL, et al. Host-Pathogen Interactions in Bovine Mammary Epithelial Cells and HeLa Cells by *Staphylococcus Aureus* Isolated From Subclinical Bovine Mastitis. *J Dairy Sci* (2017) 100:6414–21. doi: 10.3168/jds.2017-12700
3. Bhattarai D, Worku T, Dad R, Rehman ZU, Gong X, Zhang S. Mechanism of Pattern Recognition Receptors (PRRs) and Host Pathogen Interplay in Bovine Mastitis. *Microb Pathog* (2018) 120:64–70. doi: 10.1016/j.micpath.2018.04.010
4. Hagiwara S, Mori K, Nagahata H. Predictors of Fatal Outcomes Resulting From Acute *Escherichia Coli* Mastitis in Dairy Cows. *J Vet Med Sci* (2016) 78:905–8. doi: 10.1292/jvms.15-0400
5. Blum SE, Goldstone RJ, Connolly JPR, Reperant-Ferter M, Germon P, Inglis NF, et al. Postgenomics Characterization of an Essential Genetic Determinant of Mammary Pathogenic *Escherichia Coli*. *mBio* (2018) 9:e00423–18. doi: 10.1128/mBio.00423-18
6. Smith GW, Lyman RL, Anderson KL. Efficacy of Vaccination and Antimicrobial Treatment to Eliminate Chronic Intramammary *Staphylococcus Aureus* Infections in Dairy Cattle. *J Am Vet Med Assoc* (2006) 228:422–5. doi: 10.2460/javma.228.3.422
7. Ziesch M, Wente N, Zhang Y, Zaremba W, Engl S, Kromker V. Noninferiority Trial Investigating the Efficacy of a Nonantibiotic Intramammary Therapy in the Treatment of Mild-to-Moderate Clinical Mastitis in Dairy Cows With Longer Lasting Udder Diseases. *J Vet Pharmacol Ther* (2018) 41:11–21. doi: 10.1111/jvp.12415
8. Pineiro M, Stanton C. Probiotic Bacteria: Legislative Framework–Requirements to Evidence Basis. *J Nutr* (2007) 137:850S–3S. doi: 10.1093/jn/137.3.850S
9. Eckburg PB, Bik EM, Bernstein CN, Purdom E, Dethlefsen L, Sargent M, et al. Diversity of the Human Intestinal Microbial Flora. *Science* (2005) 308:1635–8. doi: 10.1126/science.1110591
10. Lebeer S, Vanderleyden J, De Keersmaecker SC. Genes and Molecules of Lactobacilli Supporting Probiotic Action. *Microbiol Mol Biol Rev* (2008) 72:728–64. doi: 10.1128/MMBR.00017-08
11. Candela M, Perna F, Carnevali P, Vitali B, Ciati R, Gionchetti P, et al. Interaction of Probiotic Lactobacillus and *Bifidobacterium* Strains With Human Intestinal Epithelial Cells: Adhesion Properties, Competition Against Enteropathogens and Modulation of IL-8 Production. *Int J Food Microbiol* (2008) 125:286–92. doi: 10.1016/j.ijfoodmicro
12. Shen Q, Shang N, Li P. In Vitro and *In Vivo* Antioxidant Activity of *Bifidobacterium* Animalis 01 Isolated From Centenarians. *Curr Microbiol* (2011) 62:1097–103. doi: 10.1007/s00284-010-9827-7
13. Zhang W, Zhu YH, Yang GY, Liu X, Xia B, Hu X, et al. *Lactobacillus Rhamnosus* GG Affects Microbiota and Suppresses Autophagy in the Intestines of Pigs Challenged With *Salmonella* Infantis. *Front Microbiol* (2017) 8:2705. doi: 10.3389/fmicb.2017.02705
14. Hu X, Guo J, Zhao C, Jiang P, Maimai T, Yanyi L. The Gut Microbiota Contributes to the Development of Staphylococcus Aureus-Induced Mastitis in Mice. *ISME J* (2020) 14:1897–910. doi: 10.1038/s41396-020-0651-1
15. Wu Q, Zhu YH, Xu J, Liu X, Duan C, Wang MJ, et al. *Lactobacillus Rhamnosus* GR-1 Ameliorates *Escherichia Coli*-Induced Activation of NLRP3 and NLRC4 Inflammasomes With Differential Requirement for ASC. *Front Microbiol* (2018) 9:1661. doi: 10.3389/fmicb.2018.01661
16. Deretic V, Levine B. Autophagy, Immunity, and Microbial Adaptations. *Cell Host Microbe* (2009) 5:527–49. doi: 10.1016/j.chom.2009.05.016
17. Levine B, Mizushima N, Virgin HW. Autophagy in Immunity and Inflammation. *Nature* (2011) 469:323–35. doi: 10.1038/nature09782
18. Nakahira K, Haspel JA, Rathinam VA, Lee SJ, Dolinay T, Lam HC, et al. Autophagy Proteins Regulate Innate Immune Responses by Inhibiting the Release of Mitochondrial DNA Mediated by the NALP3 Inflammasome. *Nat Immunol* (2011) 12:222–30. doi: 10.1038/ni.1980
19. Shi CS, Shenderov K, Huang NN, Kabat J, Abu-Asab M, Fitzgerald KA, et al. Activation of Autophagy by Inflammatory Signals Limits IL-1beta Production by Targeting Ubiquitinated Inflammasomes for Destruction. *Nat Immunol* (2012) 13:255–63. doi: 10.1038/ni.2215
20. Cao S, Shrestha S, Li J, Yu X, Chen J, Yan F, et al. Melatonin-Mediated Mitophagy Protects Against Early Brain Injury After Subarachnoid

Hemorrhage Through Inhibition of NLRP3 Inflammasome Activation. *Sci Rep* (2017) 7:2417. doi: 10.1038/s41598-017-02679-z
21. Zhou R, Yazdi AS, Menu P, Tschopp J. A Role for Mitochondria in NLRP3 Inflammasome Activation. *Nature* (2011) 469:221–5. doi: 10.1038/nature09663
22. Kim MJ, Yoon JH, Ryu JH. Mitophagy: A Balance Regulator of NLRP3 Inflammasome Activation. *BMB Rep* (2016) 49:529–35. doi: 10.5483/bmbrep.2016.49.10.115
23. Franchi L, Munoz-Planillo R, Nunez G. Sensing and Reacting to Microbes Through the Inflammasomes. *Nat Immunol* (2012) 13:325–32. doi: 10.1038/ni.2231
24. Wu J, Fernandes-Alnemri T, Alnemri ES. Involvement of the AIM2, NLRC4, and NLRP3 Inflammasomes in Caspase-1 Activation by Listeria Monocytogenes. *J Clin Immunol* (2010) 30:693–702. doi: 10.1007/s10875-010-9425-2
25. Broz P, Newton K, Lamkanfi M, Mariathasan S, Dixit VM, Monack DM. Redundant Roles for Inflammasome Receptors NLRP3 and NLRC4 in Host Defense Against *Salmonella*. *J Exp Med* (2010) 207:1745–55. doi: 10.1084/jem.20100257
26. Rathinam VA, Vanaja SK, Waggoner L, Sokolovska A, Becker C, Stuart LM, et al. TRIF Licenses Caspase-11-Dependent NLRP3 Inflammasome Activation by Gram-Negative Bacteria. *Cell* (2012) 150:606–19. doi: 10.1016/j.cell.2012.07.007
27. Mariathasan S, Weiss DS, Newton K, McBride J, O'Rourke K, Roose-Girma M, et al. Cryopyrin Activates the Inflammasome in Response to Toxins and ATP. *Nature* (2006) 440:228–32. doi: 10.1038/nature04515
28. Wang F, Zuo Z, Yang Z, Chen K, Fang J, Cui H, et al. Delayed Pulmonary Apoptosis of Diet-Induced Obesity Mice Following *Escherichia Coli* Infection Through the Mitochondrial Apoptotic Pathway. *Oxid Med Cell Longev* (2019) 2019:1968539. doi: 10.1155/2019/1968539
29. Zheng L, Xu Y, Lu J, Liu M, Bin D, Miao J, et al. Variant Innate Immune Responses of Mammary Epithelial Cells to Challenge by Staphylococcus Aureus, *Escherichia Coli* and the Regulating Effect of Taurine on These Bioprocesses. *Free Radic Biol Med* (2016) 96:166–80. doi: 10.1016/j.freeradbiomed.2016.04.022
30. Akira S, Uematsu S, Takeuchi O. Pathogen Recognition and Innate Immunity. *Cell* (2006) 124:783–801. doi: 10.1016/j.cell.2006.02.015
31. Coll RC, Robertson AA, Chae JJ, Higgins SC, Munoz-Planillo R, Inserra MC, et al. A Small-Molecule Inhibitor of the NLRP3 Inflammasome for the Treatment of Inflammatory Diseases. *Nat Med* (2015) 21:248–55. doi: 10.1038/nm.3806
32. Abderrazak A, Syrovets T, Couchie D, El Hadri K, Friguet B, Simmet T, et al. NLRP3 Inflammasome: From a Danger Signal Sensor to a Regulatory Node of Oxidative Stress and Inflammatory Diseases. *Redox Biol* (2015) 4:296–307. doi: 10.1016/j.redox.2015.01.008
33. Xia B, Yu J, He T, Liu X, Su J, Wang M, et al. *Lactobacillus Johnsonii* L531 Ameliorates Enteritis *via* Elimination of Damaged Mitochondria and Suppression of SQSTM1-Dependent Mitophagy in a *Salmonella* Infantis Model of Piglet Diarrhea. *FASEB J* (2019) 34:2821–39. doi: 10.1096/fj.201901445RRR
34. Ma M, Pei Y, Wang X, Feng J, Zhang Y, Gao MQ. LncRNA XIST Mediates Bovine Mammary Epithelial Cell Inflammatory Response *via* NF-Kappab/NLRP3 Inflammasome Pathway. *Cell Prolif* (2018) 52:e12525. doi: 10.1111/cpr.12525:e12525
35. Harris J, Hartman M, Roche C, Zeng SG, O'Shea A, Sharp FA, et al. Autophagy Controls IL-1beta Secretion by Targeting Pro-IL-1beta for Degradation. *J Biol Chem* (2011) 286:9587–97. doi: 10.1074/jbc.M110.202911
36. Kim SO, Sheikh HI, Ha SD, Martins A, Reid G. G-CSF-Mediated Inhibition of JNK Is a Key Mechanism for *Lactobacillus Rhamnosus*-Induced Suppression of TNF Production in Macrophages. *Cell Microbiol* (2006) 8:1958–71. doi: 10.1111/j.1462-5822.2006.00763.x
37. Tate MD, Ong JDH, Dowling JK, McAuley JL, Robertson AB, Latz E, et al. Reassessing the Role of the NLRP3 Inflammasome During Pathogenic Influenza A Virus Infection *via* Temporal Inhibition. *Sci Rep* (2016) 6:27912. doi: 10.1038/srep27912
38. Gurung P, Lukens JR, Kanneganti TD. Mitochondria: Diversity in the Regulation of the NLRP3 Inflammasome. *Trends. Mol Med* (2015) 21:193–201. doi: 10.1016/j.molmed.2014.11.008
39. Lazarou M. Keeping the Immune System in Check: A Role for Mitophagy. *Immunol Cell Biol* (2015) 93:3–10. doi: 10.1038/icb.2014.75
40. Shimada K, Crother TR, Karlin J, Dagvadorj J, Chiba N, Chen S, et al. Oxidized Mitochondrial DNA Activates the NLRP3 Inflammasome During Apoptosis. *Immunity* (2012) 36:401–14. doi: 10.1016/j.immuni.2012.01.009
41. Jin SM, Lazarou M, Wang C, Kane LA, Narendra DP, Youle RJ. Mitochondrial Membrane Potential Regulates PINK1 Import and Proteolytic Destabilization by PARL. *J Cell Biol* (2010) 191:933–42. doi: 10.1083/jcb.201008084
42. Park YS, Choi SE, Koh HC. PGAM5 Regulates PINK1/Parkin-Mediated Mitophagy *via* DRP1 in CCCP-Induced Mitochondrial Dysfunction. *Toxicol Lett* (2018) 284:120–8. doi: 10.1016/j.toxlet.2017.12.004
43. Wang Y, Tang C, Cai J, Chen G, Zhang D, Zhang Z, et al. PINK1/Parkin-Mediated Mitophagy Is Activated in Cisplatin Nephrotoxicity to Protect Against Kidney Injury. *Cell Death Dis* (2018) 9:1113. doi: 10.1038/s41419-018-1152-2
44. Kim MJ, Bae SH, Ryu JC, Kwon Y, Oh JH, Kwon J, et al. SESN2/sestrin2 Suppresses Sepsis by Inducing Mitophagy and Inhibiting NLRP3 Activation in Macrophages. *Autophagy* (2016) 12:1272–91. doi: 10.1080/15548627.2016.1183081
45. Ran X, Yan Z, Yang Y, Hu G, Liu J, Hou S, et al. Dioscin Improves Pyroptosis in LPS-Induced Mice Mastitis by Activating AMPK/Nrf2 and Inhibiting the NF-KappaB Signaling Pathway. *Oxid Med Cell Longev* (2020) 2020:8845521. doi: 10.1155/2020/8845521
46. Liu G, Wang ZK, Wang ZY, Yang DB, Liu ZP, Wang L. Mitochondrial Permeability Transition and Its Regulatory Components Are Implicated in Apoptosis of Primary Cultures of Rat Proximal Tubular Cells Exposed to Lead. *Arch Toxicol* (2016) 90:1193–209. doi: 10.1007/s00204-015-1547-0
47. Chu B, Zhu Y, Su J, Xia B, Zou Y, Nie J, et al. Butyrate-Mediated Autophagy Inhibition Limits Cytosolic *Salmonella* Infantis Replication in the Colon of Pigs Treated With a Mixture of *Lactobacillus* and *Bacillus*. *Vet Res* (2020) 51:99. doi: 10.1186/s13567-020-00823-8

Conflict of Interest: The authors declare that the research was conducted in the absence of any commercial or financial relationships that could be construed as a potential conflict of interest.

Publisher's Note: All claims expressed in this article are solely those of the authors and do not necessarily represent those of their affiliated organizations, or those of the publisher, the editors and the reviewers. Any product that may be evaluated in this article, or claim that may be made by its manufacturer, is not guaranteed or endorsed by the publisher.

Copyright © 2021 Li, Zhu, Chu, Liu, Chen and Wang. This is an open-access article distributed under the terms of the Creative Commons Attribution License (CC BY). The use, distribution or reproduction in other forums is permitted, provided the original author(s) and the copyright owner(s) are credited and that the original publication in this journal is cited, in accordance with accepted academic practice. No use, distribution or reproduction is permitted which does not comply with these terms.

frontiers in Immunology

REVIEW
published: 11 October 2021
doi: 10.3389/fimmu.2021.742449

Microbiota–Gut–Brain Axis and Epilepsy: A Review on Mechanisms and Potential Therapeutics

*Manqiu Ding, Yue Lang, Hang Shu, Jie Shao and Li Cui**

Department of Neurology, First Hospital of Jilin University, Changchun, China

The gut–brain axis refers to the bidirectional communication between the gut and brain, and regulates intestinal homeostasis and the central nervous system *via* neural networks and neuroendocrine, immune, and inflammatory pathways. The development of sequencing technology has evidenced the key regulatory role of the gut microbiota in several neurological disorders, including Parkinson's disease, Alzheimer's disease, and multiple sclerosis. Epilepsy is a complex disease with multiple risk factors that affect more than 50 million people worldwide; nearly 30% of patients with epilepsy cannot be controlled with drugs. Interestingly, patients with inflammatory bowel disease are more susceptible to epilepsy, and a ketogenic diet is an effective treatment for patients with intractable epilepsy. Based on these clinical facts, the role of the microbiome and the gut–brain axis in epilepsy cannot be ignored. In this review, we discuss the relationship between the gut microbiota and epilepsy, summarize the possible pathogenic mechanisms of epilepsy from the perspective of the microbiota gut–brain axis, and discuss novel therapies targeting the gut microbiota. A better understanding of the role of the microbiota in the gut–brain axis, especially the intestinal one, would help investigate the mechanism, diagnosis, prognosis evaluation, and treatment of intractable epilepsy.

Keywords: epilepsy, gut–brain axis, microbiota, pathogenesis, therapy

OPEN ACCESS

Edited by:
Monica Cartelle Gestal,
Louisiana State University Health Shreveport, United States

Reviewed by:
Francesca Ronchi,
University of Bern, Switzerland
Shan Liang,
Institute of Microbiology (CAS), China

***Correspondence:**
Li Cui
lcui@jlu.edu.cn

Specialty section:
This article was submitted to Microbial Immunology, a section of the journal Frontiers in Immunology

Received: *16 July 2021*
Accepted: *17 September 2021*
Published: *11 October 2021*

Citation:
Ding M, Lang Y, Shu H, Shao J and Cui L (2021) Microbiota–Gut–Brain Axis and Epilepsy: A Review on Mechanisms and Potential Therapeutics. Front. Immunol. 12:742449. doi: 10.3389/fimmu.2021.742449

1 INTRODUCTION

Epilepsy is a chronic neurological disorder that affects >70 million people worldwide (1) with a considerable social and economic burden. Characterized by relapses and unprovoked spontaneous seizures (2), its mechanisms are complicated, and 60% of cases are idiopathic (3). In clinical practice, a diagnosis of epilepsy is challenging. If patients have infrequent seizures, the electrical markers for diagnosis may not be present, and epileptiform discharges may occasionally occur in patients who do not have seizures. The most common antiepileptic treatments are pharmaceutical, including low-cost medications and new drugs. However, in >30% of patients with epilepsy, seizures cannot be controlled with drug therapy, a phenomenon known as refractory epilepsy (4). The *ad hoc* Task Force of the International League Against Epilepsy (ILAE) defined drug resistance as "failure of adequate trials of two tolerated, appropriately chosen and used antiepileptic drug schedules (whether as monotherapies or in combination) to achieve sustained seizure freedom" (5). Despite alternative treatments such as dietary control, nerve stimulation, and surgery, still some patients do not improve. Although the effectiveness of seizure focus resection is high, not all patients benefit from it, some exhibit obvious

adverse effects, and surgery alone may not be sufficient, due to the complex etiology of epilepsy (6, 7). Therefore, there is a need to develop more effective protocols for the diagnosis and treatment of epilepsy.

Epileptic patients often have gastrointestinal symptoms, while patients with inflammatory bowel disease have a higher susceptibility to epilepsy (8). Ketogenic diet (KD) has been used for a long time as a non-pharmacological therapy in drug-resistant epileptic patients not suitable for surgery—especially in children—with good curative effects (9). These clinical phenomena support a relationship between the gut and epilepsy. Recent advances in sequencing technology have allowed studies on the composition and function of microbiota in neurology. In recent years, some studies have suggested statistical differences in fecal microbial composition between epileptic patients and healthy people, as well as between epileptic patients before and after KD treatment, and in animal models (10–21). The intestinal microbiota may shape brain function through a variety of pathways and systems, including the central nervous system (CNS), the hypothalamic–pituitary–adrenal (HPA) axis, immune and inflammatory systems, and neuromodulators, and could therefore also be involved in epilepsy (**Figure 1**). Remodeling intestinal microbiota through individualized diet, probiotics, antibiotics, and even fecal microbiota transplantation (FMT) may become the future standard treatment of refractory epilepsy. Herein, we review the latest knowledge on the correlation between the gut microbiota (GM) and epilepsy.

2 CLASSIC ANIMAL MODELS OF EPILEPSY

Epilepsy is a complex syndrome with a complicated etiology (structural, genetic, infectious, metabolic, immune, and unknown) and diverse clinical manifestations (1, 22). Due to its complexity, in 2017, the ILAE developed a three-level classification, including seizure types, epilepsy types, and epilepsy syndromes (22). Epilepsy can be divided into four categories: focal epilepsy, generalized epilepsy, combined generalized and focal epilepsy, and unknown epilepsy (22). According to its responsiveness to antiepileptic drugs, epilepsy can be divided into drug-sensitive and refractory epilepsy. Together, the complex etiology, clinical signs, and classification of epilepsy determines the lack of a specific animal model reflecting all of its characteristics. Classical animal models of epilepsy include the following categories. The maximal electroshock model and pentylenetetrazol (PTZ) models are classical ones that simulate acute epilepsy (23). The kindling model simulates the characteristics of progressive development and long-term recurrence through repeated electrical and chemical stimulation of the thalamus, amygdala, hippocampus,

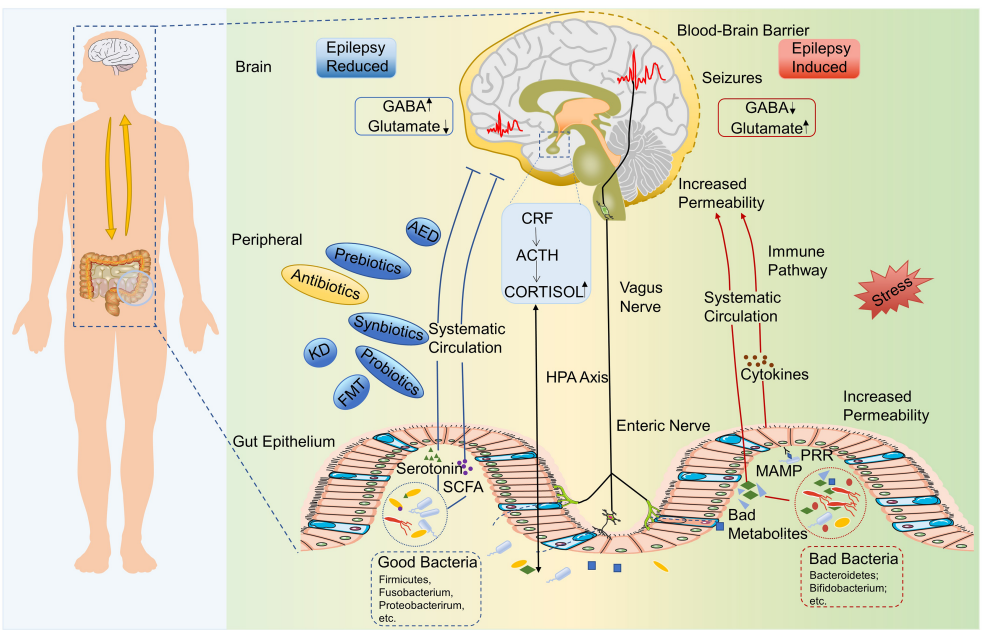


FIGURE 1 | The microbiota–gut–brain axis in epilepsy. Bad gut microbiota could upregulate the production of epilepsy-promoting metabolites, the secretion of inflammatory factors, and so on, which lead to abnormal GABA/glutamate ratio and then induce the epilepsy. Chronic stress may be a trigger for this process. Healthy gut microbiota could produce good metabolites, such as SCFAs and serotonin, which could inhibit the occurrence of epilepsy. HPA axis, enteric nervous system, and vagus nervous system are also involved in the interaction between gut microbiota and epilepsy. ACTH, Adrenocorticotropic hormone; AED, Antiepileptic drug; CRF, Corticotrophin-releasing factor; HPA, Hypothalamic–pituitary–adrenal; GABA, γ-aminobutyric acid; KD, Ketogenic diet; MAMP, Microbe-associated molecular pattern; SCFA, Short-chain fatty acid; PRR, Pattern recognition receptor.

and other regions, while continuous stimulation could induce status epilepticus. The WAG/Rij rat model is used for the study of hereditary absence epilepsy (24). In addition, animal models of epilepsy with a special etiology can be prepared by microbial infection, trauma, ischemia, and hypoxia. Chemical kindling models induced by li-pilocarpine (25) or kainic acid (26, 27), amygdala electrical kindling models (28), and genetic models have been used to construct animal models of refractory epilepsy (29). These models are important for exploring the pathogenesis of intractable epilepsy and screening and identifying new antiepileptic drugs.

3 THE CLOSE RELATIONSHIP BETWEEN INTESTINAL MICROBIOTA AND EPILEPSY

The microbiota, a wide variety of microorganisms populating the gut, including 50 bacterial phyla, is 10 times more abundant than the somatic and germ line cells of the human body (30). Firmicutes, Bacteroidetes, Actinobacteria, Proteobacteria, Fusobacteria, Verrucomicrobia, and Cyanobacteria are the seven dominant bacterial phyla in the human gastrointestinal tract, among which Bacteroidetes and Firmicutes constitute >90% (31–33). Although the overall distribution of GM in healthy people remains constant, temporal and spatial differences still exist. GM influences human health by regulating the metabolism and the host immune response. It has been reported that the species of GM in individuals with neuropsychiatric and neurodegenerative disorders differ from those in healthy people, but there are few reports on the correlation between epilepsy and GM (34). With the wide spread of 16S/18S rDNA sequencing, recent studies have reported that individuals with refractory epilepsy show altered GM composition (34). We elaborate on the relationship between the GM and epilepsy in humans and murine and discuss the dietary intervention for epilepsy *via* modulation of GM.

3.1 Human Microbiota and Epilepsy

Only a few population-based studies revealed GM differences between the epilepsy group and healthy controls (HC) in a relatively limited sample size (**Table 1**) (10–15). Xie et al. compared the GM of 14 patients with refractory epilepsy and 30 HCs and found a higher GM diversity in HCs (15). At the phylum level, Bacteroidetes was the main GM in the HC group, followed by Firmicutes, while Firmicutes predominated in patients (15). At the genus level, the GM was also significantly different between these two groups (15). Peng et al. demonstrated differences in GM diversity and composition between the drug-resistant (DR), drug-sensitive (DS), and HC groups, and that

TABLE 1 | Summary of previous studies on the intestinal microbiota in patients with epilepsy (drug-resistant/drug-sensitive).

Author	Year	Type of experimental design	Patient Group	Age	Key Findings
Gong et al. (35)	2020	Cross-sectional study	Exploration Cohort (n=55 EP and *n* = 46 HC) and Validation Cohort (*n* = 13 EP and *n* = 10 HC)	EP: 26.33± 12.05 HC: 28.5 ± 4.27	HC: a typical human diversity profile EP: lower alpha diversity; Phylum:↑Actinobacteria and Verrucomicrobia;↓Proteobacteria Genus:↑*Prevotella_9*, *Blautia*, *Bifidobacterium* DRE: Phylum: ↑Actinobacteria, Verrucomicrobia, and Nitrospirae Genus:↑*Blautia*, *Bifidobacterium*, *Subdoligranulum*, *Dialister*, and *Anaerostipes*
Şafak et al. (36)	2020	Cross-sectional study	Idiopathic focal epilepsy (*n* = 30) and HC (*n* = 10)	EP: 41.3 ± 12.2 HC: 1.7± 6.8	HC:↑Firmicutes (*Blautia*, *Coprococcus*, *Faecalibacterium*, and *Ruminococcus*), Bacteroidetes (*Bacteroides* and *Parabacteroides*), Actinobacteria (*Bifidobacterium* and *Collinsellagenus*) EP:↑Proteobacteria (*Campylobacter*, *Delftia*, *Haemophilus*, *Lautropia*, *Neisseria*), Fusobacteria
Peng et al. (37)	2018	Cross-sectional study	DRE (*n* = 42), DSE (*n* = 49), HC (*n* = 65)	DRE: 28.4 ± 12.4 DSE: 5.1 ± 14.6 HC: 29.4 ± 13.8	DSE and HC: ↑Bacteroidetes; DRE group: ↓ Bacteroidetes, ↑Firmicutes, and ↑Verrucomicrobia
Lee et al. (38)	2020	Prospective study	Intractable epilepsy (*n* = 8), HC (*n* = 32)	EP: 3.49 ± 1.76	EP:↓Bacteroidetes, Proteobacteria;↑Actinobacteria ↓Microbiota richness indices Biomarkers for intractable epilepsy:↑*E. faecium*, *B. longum, E. lenta;*↑ABCT
Lee et al. (39)	2021	Prospective study	DRE (*n* = 23) *vs*. DSE (*n* = 21)	DSE: 44 ± 17.2 DRE: 41 ± 13.6	DSE:↑*Bacteroides finegoldii*, *Ruminococcus_g2* DRE:↑*Negativicutes* Alpha and beta diversities: no significant difference between the two groups Epilepsy patients with a normal EEG: ↑*Bifidobacterium* Epilepsy patients with a normal MRI: ↑*Bacteroides finegoldii*
Xie et al. (40)	2017	Prospective observational study	Refractory epilepsy (*n* = 14) *vs.* HC (*n* = 30)	EP: 1.95 ± 3.10 HC: aged up to 3 years	HC:↑Bacteroidetes,↑Actinobacteria EP:↑Proteobacteria,↑Firmicutes

DRE, drug-resistant epilepsy; DSE, drug-sensitive epilepsy; EP, patients with epilepsy; HC, health control group.
Patients age was expressed as the mean ± SD according to the normality of distribution.

epilepsy frequency and GM were correlated (12). The alpha-diversity of the DR group was higher than that of the DS and HC groups, and similar between the HC and DS groups (12). Alpha-diversity in patients with ≤4 seizures per year was similar to that of HC, while patients with >4 seizures had significantly higher alpha-diversity (12). At the phylum level, DS and HC had similar GM composition, with Bacteroidetes as the largest phylum and Firmicutes as the second (12), while in the DR group, Firmicutes was the largest group, followed by Bacteroidetes (12). At the genus level, differences between the DS and DR groups still existed (12). *Bifidobacteria* and *Lactobacillus* were lower in patients with >4 seizures per year than in patients with ≤4 seizures per year (12). Bacterial function analysis showed that glucose- and lipid-associated metabolic pathways were all downregulated in the epileptic group and ABC (ATP-binding cassette) transporter-associated metabolic pathways elevated in the DR group compared to the DS group (12). Gong et al. investigated GM structure and composition in an exploratory cohort (epilepsy patients, n = 55; HC, n = 46) and validated the GM as a biomarker for epilepsy in a validation cohort (epilepsy patients, n = 13; HCs, n = 10) (10). A much lower GM alpha-diversity was observed in patients than in HCs (10). Actinobacteria and Verrucomicrobia increased and Proteobacteria decreased at the phylum level, while at the genus level, *Prevotella_9*, *Blautia*, *and Bifidobacterium* increased in patients with epilepsy (10). They further constructed a random forest model based on the GM and verified its value as a biomarker to discriminate epilepsy from HCs or drug-resistant epilepsy (DRE) *vs.* drug-sensitive epilepsy (DSE) (10). Safak et al. performed a contrast analysis of the fecal microbiome between idiopathic focal epilepsy (n = 30) and the HC group (n = 10), finding that Proteobacteria and Fusobacteria, which could cause autoimmune diseases, were significantly higher in the idiopathic focal epilepsy group than in the HC group, and Bacteroidetes and Actinobacteria, which have a positive effect on the immune system, were significantly lower (11). This study indicated the possible roles of autoimmune mechanisms and inflammation in the etiology of epilepsy. However, they did not perform a GM diversity analysis. Lee et al. conducted a study on the GM of eight children with intractable epilepsy and 32 HCs (13). Microbiota richness was lower in the epilepsy group than in the HC group (13). Actinobacteria was higher in the epilepsy group than in HCs, whereas Bacteroidetes was lower (13). They identified 17 and 18 species of bacteria strongly related to epilepsy and the HC group, respectively (13). *Enterococcus faecium*, *Bifidobacterium longum*, and *Eggerthella lenta* were the strongest potential biomarkers in the intractable epilepsy group (13). They also suggested the ABC transporter as a functional biomarker of intractable epilepsy, consistent with the results of Peng et al. (12, 13). Forty-four adult epilepsy patients were classified into the DRE (n =23) and DSE groups (n = 21) in a 2021 study (14). Alpha- and beta-diversity analyses showed no significant differences between patients in these two groups, but GM composition differences were related to patients' response to epileptic drugs, magnetic resonance imaging (MRI), and electroencephalogram (EEG) (14). *Bacteroides finegoldii* and *Ruminococcus_g2* were more abundant, and *negativicutes* decreased in the DRE group; *B. finegoldii* was more abundant in patients with normal MRI, and *Bifidobacterium* was more abundant in patients with normal EEG (14). Taken together, these six clinical studies evaluated GM diversity, composition, and function in patients with epilepsy, but with partially inconsistent results. All these studies indicated GM dysbiosis in patients with epilepsy, showing the potential value of GM for epilepsy diagnosis and treatment, especially in refractory epilepsy, but there are still some contradictions. Most studies indicated a higher alpha-diversity in the HC group than in the epilepsy group (10, 13–15); however, a study suggested the opposite result (12). GM changes in patients with epilepsy are not completely consistent. However, given the many variables that could affect the gut microbiome, such as differences in study design, age, diet, and living environment, efforts are needed to conduct larger sample analyses based on reasonably controlled variables.

3.2 Murine Microbiota and Epilepsy

The susceptibility to PTZ-induced epilepsy was increased in rats with 2,4,6-trinitro-benzene-sulfonic acid (TNBS)-induced colitis (41). In a mouse model of PTZ-induced seizures, intestinal inflammation increases convulsive activity and decreases the effectiveness of antiepileptic drugs. Further, alleviation of intestinal inflammation has a specific antiepileptic effect (8). In addition, a reversible inflammatory response characterized by microglial activation and an increase in tumor necrosis factor alpha (TNFα) was observed in the hippocampus of TNBS-treated rats, suggesting that gut inflammation may increase CNS excitability by inducing CNS inflammation (41); however, the underlying mechanism is still unknown. Medel-Matus et al. revealed that chronic stress can facilitate seizure development by perturbing the GM (42). GM transplantation from stress donors to sham-stressed subjects increased seizure kindling rate and duration after kindling of the basolateral amygdala, while the proconvulsant effects of chronic stress were prevented by GM transplantation from sham stress donors (42). In WAG/Rij rats, a genetic model of absence epilepsy, GM was altered with a lower Bacteroidetes/Firmicutes ratio at the age of 1 month and before the onset of epilepsy, and a further reduced Bacteroidetes/Firmicutes ratio with a large number of absence seizures was observed at 4 months (16). Short-chain fatty acids (SCFAs) are messengers between the gut and brain, and butyrate has an anti-epileptic effect in rats (43). SCFAs were reduced in WAG/Rij rats (16). Furthermore, FMT altered the number of absence seizures in rats with concomitant GM remodeling (16). This model suggests that the GM is involved in the initiation and maintenance of hereditary absence seizures. In conclusion, both human and murine studies have shown that the GM is closely related to the occurrence of multiple types of epilepsy.

3.3 Dietary Intervention for Epilepsy *via* Modulation of GM

Diet is a major factor in shaping GM composition (44, 45). Zmora et al. concluded in their review that nutrients in food

could shape the GM in a variety of ways: (1) directly interact and regulate microorganisms, (2) indirectly by influencing host metabolism, and (3) by passively introducing microbiota (46). Researchers analyzed fecal microbiota by applying next-generation sequencing technology and classified enterotypes into *Bacteroides*, *Prevotella*, and *Enterobacteriaceae*, which could be correlated with dietary habits (47). Long-term intake of animal protein and fat was beneficial to the growth of the *Bacteroides* enterotype, while carbohydrate-enriched diet enriched *Prevotella* (48). A classic Western diet (rich in fats or proteins) results in the reduction of beneficial butyrate-producing bacteria, *Bifidobacteria*, and *Eubacterium*. Most of the carbon and energy of the GM originate from dietary fiber (49, 50). Dietary protein is an essential source of nitrogen for GM growth, but high-protein diets are related to high levels of harmful metabolites in feces, cancer, and inflammatory bowel disease (50, 51). GM composition can be adjusted by altering the proportion of dietary fiber, protein, and fat (52). Therefore, a healthy diet and lifestyle are both important in GM formation.

KD indeed has a role in reducing the frequency of seizures, especially in refractory epilepsy; however, the underlying mechanisms need to be further elucidated. The existing mechanisms mainly involve neurotransmitters, brain energy metabolism, oxidative stress, and ion channels (53, 54). KD can induce GABA synthesis by upregulating glutamic acid and inhibiting GABA degradation by altering GABA transaminase activity (55, 56). Aspartate is a known glutamate decarboxylase inhibitor whose reduction can theoretically promote GABA synthesis. Aspartate levels were reduced in astrocytes exposed to ketone bodies, and similar declines were found in the forebrain and cerebellum of mice fed with KD (57). Ketosis increases the conversion of glutamate to glutamine in astrocytes (57). Glutamine then enters the neurons, eventually converting to GABA and increasing the inhibition of neurons. Barañano et al. reported that KD could prevent neuronal overexcitation *via* changes in brain pH, directly inhibit channels, and contribute to the conversion of the stimulatory glutamate to the inhibitory GABA (58) which could be secreted by certain *Lactobacillus* and *Bifidobacterium* strains (59). KD also promotes the production of fatty acids, particularly PUFAs, which may activate peroxisome proliferator-activated receptors that regulate anti-inflammatory, antioxidant, and mitochondrial genes, leading to enhanced energy reserves, synaptic function stabilization, and hyperexcitability restriction (60).

KD induces GM alteration and it is therefore involved in this treatment of epilepsy. At present, only four clinical studies suggest that KD may play a protective role in epilepsy patients by adjusting the GM (**Table 2**) (15, 17–19). Xie et al. performed successive KD therapy for ≥1 week in 14 infants with refractory epilepsy, after which the clinical occurrence of epilepsy was largely alleviated. *Proteobacteria* and *Cronobacter* decreased, and *Prevotella* and *Bifidobacterium* significantly increased after KD treatment (15). Zhang et al. further explored the changes in GM after KD in children ($n = 20$) and linked these changes to the differential efficacy of KD treatment (17). A lower alpha-diversity of the GM was observed after 6 months of KD (17). The abundance ratio of Bacteroidetes significantly increased, while that of Firmicutes and Actinobacteria significantly decreased during KD intervention (17). Bacteroides can regulate the secretion of 6–17 interleukins in dendritic cells, which are connected with seizures and can break down dietary fiber into SFCAs, which are beneficial for patients with epilepsy (64). Several gut bacteria (*Clostridiales*, *Ruminococcaceae*, *Rikenellaceae*, *Lachnospiraceae*, and *Alistipes*) were enriched in the non-responsive group, which makes them potential biomarkers and therapeutic targets in patients with non-reactive epilepsy (17). Lindefeldt et al. offered 12 children with therapy-resistant epilepsy 3-month KD and observed differences in bacterial taxa and functional structures (18). Compared with baseline, fecal microbial profiles showed an approximately identical alpha-diversity after KD therapy and a relatively decreased abundance of *Bifidobacteria*, *E. rectale*, and *Dialister* and increased abundance of *E. coli* (18). Functional analysis revealed a decline in seven pathways associated with

TABLE 2 | Summary of previous study on intestinal microbiota in epileptic patients with KD treatment.

Author	Patient Group	Age	Epilepsy Type	Intervention	Key Finding
Xie et al. (40)	EP ($n = 14$) *vs.* HC ($n = 30$)	EP: 1.95 ± 3.10 HC: aged up to 3 years	Refractory epilepsy	KD for 1 week	Healthy group: ↑Bacteroidetes;↑Actinobacteria Refractory group: ↑ Proteobacteria,↑Firmicutes KD treated group: ↑Bacteroidetes;↓Proteobacteria, *Cronobacter*
Zhang et al. (61)	EP ($n = 20$)	EP: median age is 4.3 years	Refractory epilepsy	KD for 6 months	After KD treatment: ↓Alpha diversity;↑Bacteroidetes,↓Firmicutes In the non-responsive group: specific gut microbiota is enriched
Lindefeldt et al. (62)	Children with epilepsy ($n = 12$) *vs.* parents ($n = 11$)	EP: 2–17 years	Refractory epilepsy	KD for 3 months	Parents group:↑Bacteroidetes, Proteobacteria;↓Actinobacteria, Firmicutes, After KD treatment: ↑Proteobacteria (*E. coli*);↓Actinobacteria, *Dialister*, *Bifidobacteria*, and *E. rectale;* Alpha diversity does not change significantly Function: Changes in 29 SEED subsystems
Gong et al. (63)	EP ($n = 12$) *vs.* HC ($n = 12$)	EP: 2–8 years	Refractory epilepsy	KD for 6 months	DR group: ↑Alpha diversity;↑Actinobacteria, *Enterococcus*, *Anaerostipes*, *Bifidobacterium*, *Bacteroides*, and *Blautia* After KD: ↑*Subdoligranulum*, *Dialister*, *Alloprevotella;* ↓*Bifidobacterium*, *Akkermansia*, *Enterococcaceae*, *Actinomyces* In the non-responsive group: some taxa are more prevalent

KD, ketogenic diet; EP, patients with epilepsy; HC, health control group.

carbohydrate metabolism after KD (18). Gong et al. treated 12 drug-resistant epileptic children during 6 months with KD and observed changes in GM composition and metabolites (19). The abundance of eight epilepsy-associated genera of GM significantly changed with decreases in *Bifidobacterium*, *Akkermansia muciniphila*, *Enterococcaceae*, and *Actinomyces* and increases in *Subdoligranulum*, *Dialister*, and *Alloprevotella*, which were more prevalent in patients with an inadequate response to KD than in those with an adequate response (19). In these four studies, the epileptic symptoms were alleviated to different degrees after KD treatment, and GM composition and function changed to some extent after KD treatment.

Olson et al. studied two mouse models of refractory epilepsy and found that KD could increase the GABA/glutamate ratio in the colonic lumen, serum, and hippocampus by modulating key bacterial species, resulting in seizure reduction (20). This is the first study to verify the role of GM in the antiseizure effects of KD treatment in a mouse model. The protective effect of KD was abrogated in GF or Abx-treated SPF mice, while recolonization with KD-associated bacteria restored the epilepsy protection of KD treatment to normal levels (20). This phenomenon suggests the essential role of the GM in the epileptic protective mechanism mediated by KD. Further, this study revealed the possible underlying cellular and molecular pathways by which specific GM interact with each other to modulate peripheral metabolites and then impact the levels of hippocampal neurotransmitters (20). In a recent animal study, the abundance of Firmicutes was increased, and *Acetatifactor*, *Anaerotaenia*, *Escherichia*, *Flintibacter*, *Oscillibacter*, and *Erysipelatoclostridium* were higher in the KD group than in the ND group. The GM with increased abundance was related to the production of SCFAs and GABA (21). Although KD has specific value in the treatment of epilepsy and neurodegenerative diseases, it increases the risk of glucose and lipid metabolism disorders. The glucose intolerance and lipid accumulation induced by KD are closely related to the source and proportion of fat in the diet, which could be associated with alterations in GM composition (65).

There are still some questions on the mechanism whereby KD could protect epileptic patients from seizures. For example, how does modulation of bacterial species affect changes in membrane potential of hippocampal neurons? Is modulation of GABA/glutamate levels the main pathway? How can changes in bacterial species modulate GABA/glutamate levels? These questions should be the subject of future research.

4 MECHANISM OF THE CORRELATION OF MICROBIOTA–GUT–BRAIN AXIS AND EPILEPSY

4.1 Immune and Inflammation Pathways

The pathogenesis of epilepsy is linked to neuroimmunity and neuroinflammation (66). Accumulating evidence has demonstrated that immune and inflammatory pathways in the brain–gut axis may be involved in the pathogenesis of epilepsy. Microglia and astrocytes are the main inflammatory cells in the CNS, and their inflammatory state promotes the occurrence of epilepsy (67, 68).

4.1.1 Gut Immunity

The lymphoid tissue of the intestinal mucosa contains 70%–80% of all immune cells in the body (69). The GM affects immune cells; for example, germ-free (GF) mice show immune abnormalities with a decreased population of T and B cells and a reduced cytokine production (70). Further, the GM appears as one of the most important factors for the maturation of microglial cells, as well as the astrocyte activation (71), which is age- and sex-dependent (72). The GM regulates innate immunity, adaptive immunity, and inflammatory mechanisms to modulate the development of epilepsy.

4.1.2 Gut Barrier and Blood–Brain Barrier

The intestinal mucosal barrier and blood–brain barrier (BBB) work together to prevent GM and its secretions from entering the brain. "Leaky gut" syndrome is characterized by increased intestinal permeability, which allows bacteria, toxic metabolites, and small molecules to translocate into the bloodstream (73). Under gut inflammation, bacteria can directly release factors into the systemic circulation, which activates peripheral immune cells, alters BBB integrity and thus transport rates, and can even induce "leaky brain" (74). Stress can increase intestinal mucosal permeability, and lipopolysaccharides and other cytokines in the lumen enter the blood circulation stimulating toll-like receptors, producing inflammatory cytokines that could increase BBB permeability and damage the brain (75, 76).

4.1.3 Neuroimmunity

Astrocytes are the most abundant glial cells in the brain and have a variety of functions, including regulating the integrity of the BBB, the recycling of neurotransmitters, and participating in immune responses (77). Microglial cells are the resident macrophages of the CNS, mediating the innate immune response (78). Microglia with a larger, less ramified, amoeboid morphology can promote inflammation, neuronal activity regulation, phagocytic neuron clearance, and chronic seizures (79). Microglia and astrocytes are involved in the pathogenesis of epilepsy by releasing excess cytokines (67), and interact with each other: microglia can modulate astrocytes' phenotype and function (80), while mouse microglia can regulate astrocytes' behavior through, for example, VEGF-B, which promotes the pathogenic response and inflammatory response of astrocytes, and TGF-α, which promotes the opposite (81). Gut microbes metabolize dietary tryptophan into aryl hydrocarbon receptor agonists and interact with its receptor to control microglial activation and TGF-α and VEGF-B expression, thereby modulating astrocyte pathogenic activity (81, 82). Inflammatory cytokines and chemokines released by astrocytes enhance microglial activities, including migration, phagocytosis of apoptotic cells, and synaptic pruning (83). The interaction between astrocytes and microglia leads to increased pro-inflammatory cytokine production and BBB permeability, which results in the infiltration of peripheral blood immune cells and cytokines into the CNS, and subsequent chronic neuroinflammation (84). GF and antibiotic-treated (Abx-treated) animals have also altered microglial morphology and defects in

maturation, activation, and differentiation, resulting in an inadequate immune response to a variety of pathogens, which could be repaired after GM recolonization, which suggests that intestinal microbial diversity is critical for microglial and CNS function (85). In addition to glial cells residing in the CNS, peripheral immune cells, such as T cells and monocytes invading the brain tissue, are also involved in epilepsy's morbidity. Monocytes can differentiate into macrophages and invade the brain, where they differentiate into "microglia-like cells" and contribute to epilepsy (86). As the organ with the largest population of immune cells, the gut is likely to play a role in this process, but the exact mechanism requires further investigation.

The GM can induce epilepsy through the innate immune pathway. BBB permeability increases throughout the life of GF mice related to the decreased expression of occludin and claudin-5 proteins in the endothelium (87). GM dysbiosis decreases claudin production and increases the permeability of the intestinal lining, leading to the escape of microorganisms, metabolites, and toxins from the intestinal lumen (88). GM dysbiosis also reduces SCFAs, which increases BBB permeability and promotes neuroinflammation (89). If these two barriers are broken, the immune cells and factors released by the microbiota enter the brain and induce seizures. Peptidoglycan (PGN) is a component of the bacterial cell wall that mainly exists in the human intestinal tract (90). PGN, as a driver of chronic encephalitis, has also been detected in brain microglia (90). Chronic inflammation, such as sclerosis-related temporal lobe epilepsy, is also a cause of epilepsy (91). Therefore, we conclude that PGN may translocate from the gut to the CNS by promoting gut leakage and brain leakage, leading to chronic inflammation and contributing to the occurrence of epilepsy.

The GM also contributes to epilepsy generation by inducing adaptive immunity. The GM can induce immune cells to produce cytokines that enter the brain through the intestinal mucosa and BBB and activate brain immune cells to participate in the immune response. T helper cell 17 (Th 17) cells are a proinflammatory CD4+ T cell subtype and key components of adaptive immunity (92). IL-17 is a cytokine produced by Th 17 cells, which can be modulated by specific GM phyla, such as Bacteroidetes (92, 93). As recently shown, both in the CSF and in the peripheral blood of patients with epilepsy, IL-17 levels were higher than in controls, and highly correlated with the frequency and severity of seizures (94–97). Therefore, the GM can influence the occurrence of epilepsy by mediating IL-17. GM metabolites, such as SCFAs, can affect the synthesis and secretion of immunoglobulins by regulating B lymphocyte differentiation (98, 99). The absence of commensal microbiota downregulates IgA and IgG1, and upregulates IgE, which leads to increased susceptibility to diseases (100, 101).

Therefore, GM can induce an immune response through the gut–brain axis, which leads to epileptogenesis. However, only a few studies have directly focused on the relationship between the gut, immune responses, and epilepsy, and many issues remain to be explored.

4.2 Nervous System

One of the most important pathways for transmitting information between the brain and the gut is *via* autonomic nerve fibers (102). Oral inoculation of *Campylobacter jejuni* to a mouse model leads to increased c-fos expression in the sensory ganglia and primary sensory relay nucleus of the vagus nerve in the brainstem, suggesting that gut stimulation can modulate brain activity *via* the autonomic nervous system (103). Vagus nerve stimulation (VNS) has become a normal therapy for epilepsy since being first reported in 1988 (104). Ressler et al. reported that electrical stimulation of vagal afferent fibers could modify brain concentrations of serotonin, GABA, and glutamate, thus explaining its use in epilepsy (105). VN goes through all intestinal layers, except the epithelial one, so it cannot directly interact with the GM (106). Enteroendocrine cells (EECs) can detect signals released from the luminal microbiota through different receptors. Previously, gut endocrine cells and the cranial nerve were thought to communicate only through hormones (107); however, Kaelberer et al. found that EECs named neuropod cells could synapse with vagal neurons to transduce gut luminal signals to connect the intestinal lumen to the brainstem using glutamate as a neurotransmitter (107). The discovery of neuropod cells provides a strong theoretical support for the treatment of neurological diseases by regulating the GM.

4.3 Enteroendocrine Signaling and Microbial Metabolites: Neurotransmitters and Short-Chain Fatty Acids

4.3.1 Enteroendocrine Signaling and Neurotransmitters

Neurotransmitter imbalance is closely related to epilepsy. Neurotransmitter imbalance exists in epileptic foci, such as GABA with hypoactivity and glutamate with hyperactivity, dopamine and norepinephrine (NE) with hyperactivity, and serotonin with hypoactivity (108). In the gastrointestinal tract, neurotransmitters can be secreted directly by the GM or produced by gastrointestinal cells under the stimulation of GM metabolites. Different GM can produce different neurotransmitters (*Enterococcus* spp., *Streptococcus* spp., and *Escherichia* spp. produce serotonin; *Lactobacillus* spp. and *Bifidobacterium* spp. produce GABA, *Escherichia* spp. and *Bacillus* spp. produce NE and dopamine). The various neurotransmitters produced by the GM can pass through the intestinal mucosa but rarely through the BBB, with the exception of GABA (109). In hippocampal injury, or epileptic status, GABA produced by GM can lead to an imbalance between the GABA and glutamate systems, causing seizures. Sun et al. showed that the relative abundance of the genera *Coprococcus, Ruminococcus*, and *Turicibacter* was positively correlated with glutamate and glutamine levels (110). The GM can affect the glutamine–glutamate–GABA cycle, produce neurotransmitters, and mediate the expression of GABA and NMDA receptors in specific brain regions (hippocampus, amygdala, and locus coeruleus) (111). *A. mucinophilia* and *Parabacteroides* colonization could alter the level of amino acids in the serum and gut lumen to modulate the levels of seizure-associated neurotransmitters, such as GABA and glutamate, in the hippocampus, thus providing protective anti-seizure effects in mice (20, 112). Enterochromaffin cells (ECs) produce approximately 90% of 5-hydroxytryptamine (5-HT) (113). In GF mice, certain intestinal microbiota, such as spore-forming clostridia taxa, can promote 5-HT biosynthesis in the gut by upregulating colonic tryptophan hydroxylase 1, a rate-limiting enzyme for 5-HT

production (114, 115). Previous studies have shown that patients with temporal lobe epilepsy have a 5-HT deficiency. A drug combination that increases 5-HT, such as selective serotonin reuptake inhibitors, may improve seizure control in patients with epilepsy (116). The 5-HT decrease induced by reserpine appears to increase susceptibility to minimal electroshock seizures in rats (117). However, changes in intestinal 5-HT levels could not directly affect the brain, as 5-HT cannot cross the BBB (118). Chemotherapeutic drugs often cause nausea and vomiting, caused by the release of large amounts of 5-HT in the intestine and the subsequent activation of vagal afferents (119). 5-HT released by ECs may have a potential impact on brain–gut axis signal transduction by regulating intestinal vagal afferent activity (120) and inflammatory responses (121). Alterations in 5-HT signaling are associated with irritable bowel syndrome (122). Therefore, we speculate that a change in 5-HT levels in the intestine may be related to epilepsy, but there is no evidence to support this. N-acetyl aspartic acid (NAA) levels are reduced in patients with epilepsy, and in the epileptic suckling pig model, Austin et al. found that low NAA levels were associated with fecal *Ruminococcus*, and this process may be mediated by serum cortisol (123). NE has a double effect on epilepsy onset depending on its amount, NE at low doses has pro-epileptic effects, while high doses could inhibit epilepsy (124). Dopamine, serotonin, and acetylcholine are closely correlated with epilepsy and could indirectly affect brain function through the enteric nervous system, the vagus nervous system, and by regulating the expression of peripheral receptors (125).

4.3.2 SCFAs

SCFAs, including acetate, propionate, and butyrate, can be produced by some gut bacteria (mainly Bacteroides and Firmicutes) through the fermentation of insoluble dietary fibers (126). SCFAs play an essential role in microglial maturation, the gut–brain nervous system, BBB permeability, and stress responses through direct or indirect pathways, all closely related to epilepsy (127). As mentioned earlier, SCFAs were reduced in WAG/Rij rats, and butyrate had an anti-absence seizure effect (16). The protective effects and mechanisms of different SCFAs in epilepsy were further studied in a PTZ-induced epileptic mouse model (8, 128, 129). Sodium butyrate may exhibit antiepileptic effects in PTZ-induced epileptic mice by alleviating intestinal inflammation and oxidative stress (8). Butyrate also ameliorates mitochondrial dysfunction and protects brain tissue from oxidative stress and neuronal apoptosis through the Keap/Nrf2/HO-1 pathway, thereby increasing seizure threshold and reducing seizure intensity (129). Propionate treatment may alleviate seizure intensity and prolong the incubation period of seizures by reducing mitochondrial damage, hippocampal apoptosis, and neurological deficits (128). These studies show that SCFAs are reduced in epilepsy models and their protective effect on epilepsy through different mechanisms.

4.4 The HPA Axis

Stress can promote the induction of epilepsy, and epileptic patients have higher glucocorticoid levels (130). The HPA axis is central to stress responses, including the secretion of corticotrophin-releasing factor, adrenocorticotropic hormone, and subsequent release of glucocorticoids (e.g., cortisol, corticosterone, deoxycorticosterone, and corticotrophin) and catecholamine downstream pathways (131). The HPA axis is regulated either by the negative feedback of glucocorticoids or by input from numerous different brain regions, including the prefrontal cortex, hippocampus, amygdala, and the bed nucleus of the stria terminalis (132). Different hormones may have different effects; for example, most deoxycorticosterones are anticonvulsants, whereas corticotropin-releasing hormone and corticosterone could induce seizure activity (133, 134). Despite the correlation between the HPA axis and GM, the specific mechanism has not been elucidated (135). Chronic stress could upregulate glucocorticoids, which could enhance glutamatergic signaling and induce seizures (136). GM can affect the function of the hypothalamus by changing circulating cytokine levels or other pathways, thereby regulating the HPA axis (137). Stress responses in both SPF and GF mice suggest that the GM modulates stress-dependent pituitary and adrenal activation and alters the expression of genes regulating the corticotropin-releasing hormone pathway in the colon (138). We hypothesized that chronic stress may affect the HPA axis through the GM and promote epilepsy; however, the specific relationship among the HPA axis, GM, and epilepsy still needs to be further investigated.

5 BRAIN–GUT AXIS AS POTENTIAL DIAGNOSTIC AND THERAPEUTIC TARGET FOR EPILEPSY

5.1 The GM Perspective in Differential Diagnosis of Epilepsy

The GM differences between healthy people and patients with different types of epilepsy make it a potential biomarker for differential diagnosis, prognosis, and treatment monitoring in epilepsy. Fecal microbiota may not accurately reflect GM situation because of possible pollution, and although colonoscopy is more accurate than fecal GM, its invasiveness limits its clinical application. In addition, the GM is affected by age, diet, living environment, and other factors, the sample size in these studies was small, and there were some contradictory results. Therefore, the GM needs to be further studied in larger patient samples and under strictly controlled variables.

5.2 The Value of the Brain–Gut Axis in the Treatment of Epilepsy

Modulation of the GM may be a potential therapeutic approach for intractable epilepsy. On the one hand, regulation of GM could reduce the occurrence of seizures by adjusting the mechanisms related to epilepsy. On the other hand, drugs can be converted into metabolites by GM through direct or indirect ways to exert therapeutic efficacy or cause toxic side effects (139). For DRE patients, adjusting the composition of the gut microbiome may promote drug metabolism and absorption and increase their responsiveness to antiepileptic drugs. In this section, we will review the effects of dietary intervention,

antibiotics, probiotics, prebiotics, synbiotics, antiepileptic drugs, and fecal transplantation on epilepsy (**Figure 2**).

5.2.1 Dietary Intervention

Diet, especially KD, could regulate the occurrence of epilepsy by shaping GM as discussed in detail in *Section 3*. KD is a high-fat, low-carbohydrate, and adequate protein diet used since 1921 in patients with refractory epilepsy (140). KD also has positive effects on other neurological diseases, such as multiple sclerosis, Parkinson's disease, Alzheimer's disease, and migraine (141–143). The classic ratio of fat to protein and carbohydrates in KD is 4:1 (18), which triggers a metabolic pattern shift from glucose metabolism toward the metabolism of fatty acids (53). The classic KD could relieve epilepsy by multiple pathways, including modulation of neurotransmitters, brain energy metabolism, oxidative stress, ion channels, and GM (53, 54, 144).

In addition to the classical form, several modified KD diets have arisen, including the modified Atkins diet, medium-chain triglyceride diet, low-glycemic index treatment, and modified Mediterranean ketogenic diet (MMKD), with various composition ratios of fat, protein, and carbohydrates (145). In medium-chain triglyceride diet, medium-chain triglycerides are used instead of long-chain triglycerides (145). MMKD is characterized by olive oil as a source of monounsaturated fatty acids (146). Olive oil contains antioxidant molecules such as monounsaturated fatty acids and polyphenols, which have beneficial effects on inflammation, cardiovascular disease, and oxidative status of the body (147). MMKD can regulate the GM of patients with mild cognitive impairment, especially fungal flora (146). A 12-month KD based on olive oil could alleviate symptoms in 83.1% of patients with refractory epilepsy, comparable to the effect of a traditional KD treatment (147). However, there is no comparative study between MMKD and traditional KD on the efficacy and side effects on refractory epilepsy. At present, most KDs are individualized modified KDs balanced between ketogenic effect and palatability.

In KD, saturated fat has always been the prominent fat used (148); however, animal and human studies have demonstrated the anti-epileptic effects of polyunsaturated fatty acids (PUFAs), especially omega-3(n-3) PUFAs (149). Dietary n-3 PUFAs are found in flaxseed, nuts, marine fish, and marine mammals. N-6 PUFAs are mainly derived from animal products and vegetable oils and constitute the majority of PUFAs in the modern Western diet (149). Docosahexaenoic acid (DHA, 22:6n-3), the primary n-3 PUFA in the brain, participates in the regulation of neural function through a variety of pathways, such as interaction with ion channels and neurotransmitter release (150, 151). A case–control study indicated a lower serum omega 3/omega 6 ratio in children with epilepsy than in healthy children (152). Both *in vitro* and *in vivo* studies demonstrated that a diet rich in n-3 fatty acids is

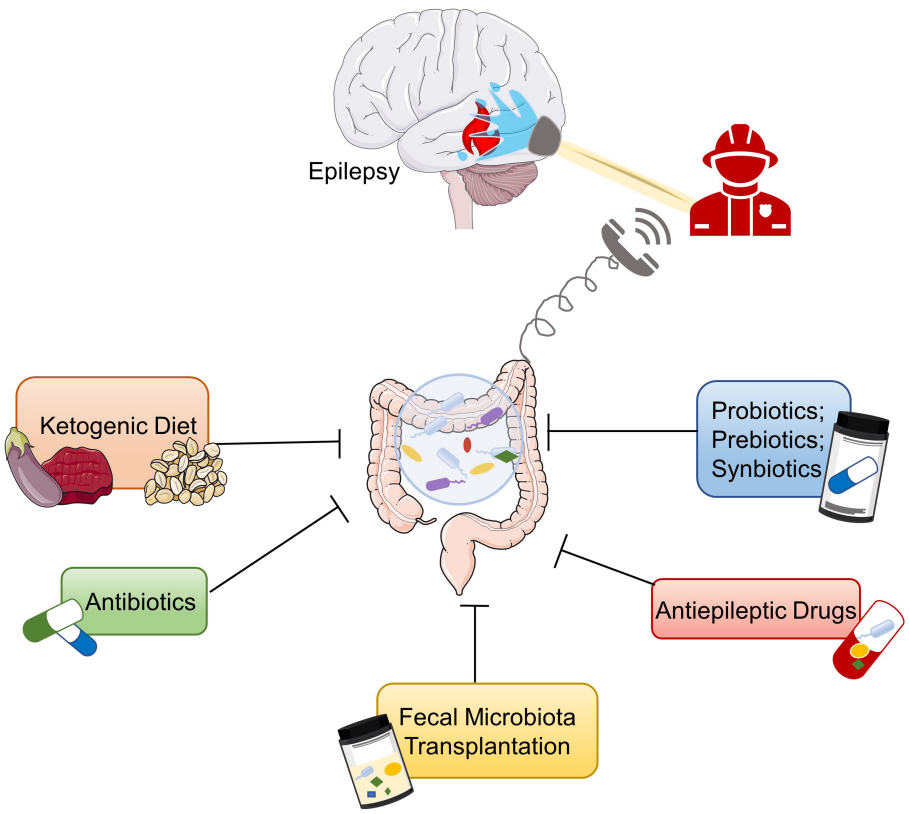


FIGURE 2 | Potential therapies for epilepsy based on gut microbiota. Ketogenic diet, antiepileptic drugs, probiotics, prebiotics, synbiotics, antibiotics, and fecal microbiota transplantation are potential treatments for epilepsy based on the microbiota–gut–brain axis.

beneficial for epilepsy control, but the results of clinical studies are somewhat contradictory (149). A meta-analysis of seven clinical trial studies in 2021 indicated that omega-3 supplementation significantly reduced seizure frequency and was more effective in adults than in children (153). Therefore, adjustment of dietary n-3/n-6 levels could be associated with seizure control. A recent study indicated that a high [fat]:[carbohydrate + protein] ratio is not indispensable for the treatment of epilepsy (154). A new combined diet with low [fat]:[proteins + carbohydrates] ratio, including medium-chain triglycerides, PUFAs, low glycemic index carbohydrates, and a high branched-chain amino acids/aromatic amino acids ratio also reduces excitatory drive and protects against seizures in rodent models (154). Although only tested on animals, it is a promising diet with fewer side effects.

Dietary intervention is an effective and perspective way to control epilepsy, and further research on the bacterial–gut–brain axis would contribute to develop the more effective dietotherapy.

5.2.2 Probiotics/Prebiotics/Synbiotics

Probiotics are living microorganisms that, at the appropriate dose, are beneficial to the host health (155). Most common probiotics include *Bifidobacterium* and *Lactobacillus* (156). In 2020, the International Scientific Association for Probiotics and Prebiotics defined prebiotics as a "substrate selectively utilized by host microorganisms conferring a health benefit" (157). Synbiotics has been defined as "a mixture comprising live microorganisms and substrate(s) selectively utilized by host microorganisms that confers a health benefit on the host" consisting of two subsets: synergistic synbiotic (the prebiotic is selectively utilized by the co-administered live microorganisms) and complementary synbiotic (each component works independently) (157). In a prospective study, the frequency of seizures was reduced by ≥50% in 28.9% of DRE patients treated with a probiotic mixture for 4 months, and 76.9% of these improved patients maintained a lower seizure frequency 4 months after discontinuation (158). This study indicated that adjuvant probiotics reduced the frequency of seizures and could be used as a complementary treatment to antiepileptic therapy (158). In the PTZ-induced chemical kindling mouse model, the probiotic supplementation group did not show full kindling, and GABA increased in mouse brain tissue, which indicated that probiotic supplementation could substantially reduce seizure severity (159).When treating PTZ-induced seizures in mice with KD, synbiotics or *Lactobacillus fermentum* MSK 408 could reduce the side effects of KD without disturbing its antiepileptic effects (21, 160). Both KD and MSK 408 increase GABA metabolism by regulating the GM (160). Several SCFAs, such as propionate and butyrate, have antiepileptic effects. After a month of intervention with the classic KD, the total SCFAs were significantly reduced, especially acetate, propionate, and butyrate, which may be due to a reduction in the intake of fermentable carbohydrates or a reduction in fermenting bacteria by KD (161). Synbiotics can lead to GM enrichment associated with SCFAs (21). MSK 408 could influence SCFAs and restore serum lipid profile and tight junction protein mRNA expression in the gut and brain independently by modulating the GM (160).

These studies are preliminary observations of supplementary probiotics in the treatment of DRE, and further theoretical validation and mechanism exploration in larger placebo-controlled trials and more rigorous animal experiments should be conducted. Probiotics have the potential to be a complementary treatment for refractory epilepsy and can be used in combination with KD therapy to reduce side effects.

5.2.3 Antibiotics

Antibiotics can have either good or negative effects on the treatment of inflammatory bowel disease, irritable bowel syndrome, hepatic encephalopathy, and other diseases (162). Despite the little evidence on the link between the use of antibiotics and seizures, a retrospective study of six refractory epileptic patients treated with antibiotics showed that certain antibiotics could reduce the frequency of seizures in the short term (163). They hypothesized that antibiotics might induce seizure freedom or decrease seizure frequency by interfering with the intestinal flora and the gut–brain axis (163). However, certain antibiotics can also induce epilepsy; for example, lactam antibiotics, including penicillin, cephalosporins, and carbapenems, are most likely to cause seizures (164). Unsubstituted penicillin, like fourth-generation cephalosporins, imipenem, and ciprofloxacin in combination with renal dysfunction, brain lesions, and epilepsy could lead to an increased risk of symptomatic seizures. Therefore, serum levels and EEG should be closely monitored when using antibiotics in these patients (165). Antibiotic application exerts short- or long-term effects on GM composition in both humans and animals (162). Although some antibiotics can disrupt the balance of intestinal microorganisms and cause diseases, others increase the abundance of beneficial microorganisms and play a positive role in the GM (162). Different antibiotics lead to different patterns of GM alteration; for example, macrolides induce the reduction of Actinobacteria (mainly *Bifidobacteria*) (166, 167), oral vancomycin reduces Firmicutes and increases Proteobacteria (168), whereas penicillin only has a weak effect on the human microbiota (168). The extent of amoxicillin-induced epilepsy is not parallel to GM changes, which is contradictory to the hypothesis that GM acts as a bridge in antibiotic-induced epilepsy. However, the influence of antibiotics on GM is also related to the initial GM composition (169) and habits of the host (170). In the future, multi-center cooperation is needed to further clarify the specific effects and mechanisms of various antibiotics on epilepsy.

5.2.4 Antiepileptic Drugs and GM

The GM contains a rich variety of drug-metabolizing enzymes that influence their pharmacology, resulting in interpersonal differences in drug efficacy and toxicity (171). For example, clonazepam is an anticonvulsant and anti-anxiety drug reduced and metabolized by the GM, resulting in drug toxicity (172). Non-antibiotic drugs alter the GM to some extent. In a large study involving the effects of 1,197 non-antibiotic drugs on 40 GM, 24% of the drugs with human targets inhibited the growth of ≥1 strain *in vitro* (173). Antiepileptic drugs, such as carbamazepine, valproic acid, and lamotrigine affect GM composition (174, 175). Valproic acid treatment during pregnancy in mice resulted in altered fecal microbiota (176, 177), with increased Firmicutes and decreased Bacteroidetes (178), which may be associated with ASD-like behavior in offspring (176, 177). Lamotrigine might decrease the growth of *E. coli* by inhibiting bacterial ribosome biogenesis (179). Further research on the relationship between antiepileptic drugs and gut

microorganisms will help to develop new antiepileptic drugs based on the principle of GM regulation. Adjusting GM composition could alter the metabolic process of antiepileptic drugs to improve their efficacy and reduce side effects.

5.2.5 FMT

FMT has been proven to be an extremely effective treatment for recurrent or refractory *Clostridium difficile* infections (176, 177, 180, 181). Moreover, FMT has been extensively studied as a potential treatment for GM-related diseases. Its effectiveness has been demonstrated in a range of diseases, such as ulcerative colitis (182), hepatic encephalopathy (183), irritable bowel syndrome (184), obesity (185), and even neurological disorders (186, 187). Recent studies have revealed a correlation between epilepsy and GM; thus, the value of FMT administration in patients with epilepsy has been further investigated. FMT has been shown to prevent the recurrence of epilepsy after discontinuation of antiepileptic drugs in patients with Crohn's disease and a long history of epilepsy (188). In a rat model of epilepsy with basolateral amygdala kindling following chronic stress, GM transplantation from chronically stressed rats to sham-stressed rats accelerated the kindling epileptogenesis process, whereas transplantation from sham-stressed group to stressed rats reduced the pro-epileptic effects of stress (42). Olson et al. observed an increased seizure threshold in a GF temporal lobe epilepsy mouse model after transplantation with microbiota from KD-treated mice or long-term administration of microbiota associated with KD treatment (20). However, there are still some challenges to the FMT process. Currently, FMT is performed by placing small amounts of liquefied or filtered feces directly into the colon or through a feeding tube, enema, or capsule (189). Therefore, FMT may result in the transmission of bacteria, viruses, or diseases that cannot be detected by screening (189, 190). Furthermore, FMT may disrupt the baseline microbiota diversity, resulting in the breakdown of colonization resistance to a broad spectrum of harmful microorganisms (190). Therefore, more long-term follow-up studies are needed to determine the efficacy and safety of FMT in patients with epilepsy before large-scale clinical application.

6 GUT–BRAIN PSYCHOLOGY AND EPILEPSY

In addition to epilepsy, current research have linked the brain–gut axis to the development of many other neuropsychiatric disorders, such as neurodegenerative diseases and mental disorders (191, 192). Psychiatric diseases are often comorbid with epilepsy (193, 194). Patients with epilepsy have an increased risk of mental illness, which increases their disability and mortality rates (193, 194). Depression is the most common comorbidity in patients with epilepsy (195). Patients with epilepsy have a twofold increased risk of depression compared to the standard population (196). Mental disorders, such as depression, anxiety, dipolar disorder, and schizophrenia, could be rooted in abnormal GM (192, 197). Though gut–brain axis in psychology has been rapidly developed over the decades (192), the conception of "gut–brain psychology" was firstly proposed by Jin et al. in 2018: the discipline of studying the relationship between the gut–brain and mind (192). Neuroinflammation, HPA axis hyperactivity, and altered neurotransmitters (such as 5-HT) are common mechanisms for epilepsy and comorbid depression, and involved in the gut–brain axis (117, 198, 199). KD, a well-known treatment for epilepsy, has been shown to play a role in psychiatric disorders (200). Other than KD, antibiotics, FMT, probiotics, and prebiotics also have potential in regulating both mood and epilepsy (158, 163, 188, 192). Therefore, in the process of studying the relationship between epilepsy and brain–gut axis, the gut–brain psychology should be considered. In the future, it may be possible to treat neuropsychiatric diseases and improve brain and mental health by manipulating the microbiome and the gut–brain axis.

CONCLUSION

Advances in sequencing techniques have deepened our understanding of GM, and an increasing number of studies have indicated the indispensable role that the brain–gut axis plays in epilepsy. The autonomic nervous system, enteric nervous system, neuroendocrine system, and neuroimmune system all contribute to communication between the brain and the gut. KD has been long used in the clinical practice as an effective treatment for intractable epilepsy. The involvement of the brain–gut axis further clarifies the potential mechanism behind this treatment method. In addition, controlling GM by probiotics, prebiotics, synbiotics, antibiotics, or FMT could reduce the frequency of seizures and improve the threshold of epilepsy. Gut–brain psychology should be considered in the study of gut–brain axis in epilepsy. At present, research on the relationship between the brain–gut axis and epilepsy is still at the preliminary stage. Future research will help identify new diagnostic and therapeutic targets for refractory epilepsy in relation with the gut–brain axis.

AUTHOR CONTRIBUTIONS

MD and YL conceived the topic and designed the outline of this review. MD, YL, HS, and JS contributed to the manuscript writing. MD prepared the figures and tables. LC critically revised the manuscript. All authors contributed to the article and approved the submitted version.

FUNDING

This work was supported by a grant from the National Natural Science Foundation of China (82071351).

ACKNOWLEDGMENTS

Several graphical elements (human figure, brain, gut, bottle, etc.) in **Figures 1**, **2** are provided by Servier Medical Art (https://smart.Servier.com) under CC BY 3.0 license.

REFERENCES

1. Thijs RD, Surges R, O'Brien TJ, Sander JW. Epilepsy in Adults. *Lancet* (2019) 393:689–701. doi: 10.1016/S0140-6736(18)32596-0
2. Beghi E, Giussani G, Sander JW. The Natural History and Prognosis of Epilepsy. *Epileptic Disord* (2015) 17:243–53. doi: 10.1684/epd.2015.0751
3. Beghi E, Giussani G, Abd-Allah FA, Abdela J, Abdelalim A, Abraha HN, et al.Global, Regional, and National Burden of Epilepsy, 1990-2016: A Systematic Analysis for the Global Burden of Disease Study 2016. *Lancet Neurol* (2019) 18:357–75. doi: 10.1016/S1474-4422(18)30454-X
4. Kobow K, Blümcke I. Epigenetics in Epilepsy. *Neurosci Lett* (2018) 667:40–6. doi: 10.1016/j.neulet.2017.01.012
5. Kwan P, Arzimanoglou A, Berg AT, Brodie MJ, Allen Hauser W, Mathern G, et al. Definition of Drug Resistant Epilepsy: Consensus Proposal by the Ad Hoc Task Force of the ILAE Commission on Therapeutic Strategies. *Epilepsia* (2010) 51:1069–77. doi: 10.1111/j.1528-1167.2009.02397.x
6. Engel J Jr. The Current Place of Epilepsy Surgery. *Curr Opin Neurol* (2018) 31:192–7. doi: 10.1097/WCO.0000000000000528
7. Sheng J, Liu S, Qin H, Li B, Zhang X. Drug-Resistant Epilepsy and Surgery. *Curr Neuropharmacol* (2018) 16:17–28. doi: 10.2174/1570159X15666170504123316
8. De Caro C, Leo A, Nesci V, Ghelardini C, di Cesare Mannelli L, Striano P, et al. Intestinal Inflammation Increases Convulsant Activity and Reduces Antiepileptic Drug Efficacy in a Mouse Model of Epilepsy. *Sci Rep* (2019) 9:13983. doi: 10.1038/s41598-019-50542-0
9. López González FJ, Rodríguez Osorio X, Gil-Nagel Rein A, Carreño Martínez M, Serratosa Fernández J, Villanueva Haba V, et al. Drug-Resistant Epilepsy: Definition and Treatment Alternatives. *Neurologia* (2015) 30:439–46. doi: 10.3389/fmicb.2020.517797
10. Gong X, et al. Alteration of Gut Microbiota in Patients With Epilepsy and the Potential Index as a Biomarker. *Front Microbiol* (2020) 11:517797. doi: 10.3389/fmicb.2020.517797
11. Şafak B, Altunan B, Topçu B, Eren Topkaya A. The Gut Microbiome in Epilepsy. *Microb Pathog* (2020) 139:103853. doi: 10.1016/j.micpath.2019.103853
12. Peng A, Qiu X, Lai W, Li W, Zhang L, Zhu X, et al. Altered Composition of the Gut Microbiome in Patients With Drug-Resistant Epilepsy. *Epilepsy Res* (2018) 147:102–7. doi: 10.1016/j.eplepsyres.2018.09.013
13. Lee K, Kim N, Shim JO, Kim GH. Gut Bacterial Dysbiosis in Children With Intractable Epilepsy. *J Clin Med* (2020) 10(1):5. doi: 10.3390/jcm10010005
14. Lee H, Lee S, Lee DH, Kim DW. A Comparison of the Gut Microbiota Among Adult Patients With Drug-Responsive and Drug-Resistant Epilepsy: An Exploratory Study. *Epilepsy Res* (2021) 172:106601. doi: 10.1016/j.eplepsyres.2021.106601
15. Xie G, Zhou Q, Qiu CZ, Dai WK, Wang HP, Li YH, et al. Ketogenic Diet Poses a Significant Effect on Imbalanced Gut Microbiota in Infants With Refractory Epilepsy. *World J Gastroenterol* (2017) 23:6164–71. doi: 10.3748/wjg.v23.i33.6164
16. Citraro R, Lembo F, De Caro C, Tallarico M, Coretti L, Iannone LF, et al. First Evidence of Altered Microbiota and Intestinal Damage and Their Link to Absence Epilepsy in a Genetic Animal Model, the WAG/Rij Rat. *Epilepsia* (2021) 62:529–41. doi: 10.1111/epi.16813
17. Zhang Y, Zhou S, Zhou Y, Yu L, Zhang L, Wang Y, et al. Altered Gut Microbiome Composition in Children With Refractory Epilepsy After Ketogenic Diet. *Epilepsy Res* (2018) 145:163–8. doi: 10.1016/j.eplepsyres.2018.06.015
18. Lindefeldt M, Eng A, Darban H, Bjerkner A, Zetterström CK, Allander T, et al. The Ketogenic Diet Influences Taxonomic and Functional Composition of the Gut Microbiota in Children With Severe Epilepsy. *NPJ Biofilms Microbiomes* (2019) 5:5. doi: 10.1038/s41522-018-0073-2
19. Gong X, Cai Q, Liu X, An D, Zhou D, Luo R, et al. Gut Flora and Metabolism Are Altered in Epilepsy and Partially Restored After Ketogenic Diets. *Microb Pathog* (2021) 155:104899. doi: 10.1016/j.micpath.2021.104899
20. Olson CA, Vuong HE, Yano JM, Liang QY, Nusbaum DJ, Hsiao EY. The Gut Microbiota Mediates the Anti-Seizure Effects of the Ketogenic Diet. *Cell* (2018) 173:1728–41.e1713. doi: 10.1016/j.cell.2018.04.027
21. Eor JY, Son YJ, Kim JY, Kang HC, Youn SE, Kim JH, et al. Neuroprotective Effect of Both Synbiotics and Ketogenic Diet in a Pentylenetetrazol-Induced Acute Seizure Murine Model. *Epilepsy Res* (2021) 174:106668. doi: 10.1016/j.eplepsyres.2021.106668
22. Scheffer IE, Berkovic S, Capovilla G, Connolly MB, French J, Guilhoto L, et al. ILAE Classification of the Epilepsies: Position Paper of the ILAE Commission for Classification and Terminology. *Epilepsia* (2017) 58:512–21. doi: 10.1111/epi.13709
23. Góra M, Czopek A, Rapacz A, Gębska A, Wójcik-Pszczoła K, Pękala E, et al. Synthesis, Anticonvulsant, and Antinociceptive Activity of New 3-(2-Chlorophenyl)- and 3-(3-Chlorophenyl)-2,5-Dioxo-Pyrrolidin-1-Yl-Acetamides. *Molecules* (2021) 26:1564. doi: 10.3390/molecules26061564
24. Russo E, Citraro R, Constanti A, Leo A, Lüttjohann A, van Luijtelaar G, et al. Upholding WAG/Rij Rats as a Model of Absence Epileptogenesis: Hidden Mechanisms and a New Theory on Seizure Development. *Neurosci Biobehav Rev* (2016) 71:388–408. doi: 10.1016/j.neubiorev.2016.09.017
25. Kim JE, Cho KO. The Pilocarpine Model of Temporal Lobe Epilepsy and EEG Monitoring Using Radiotelemetry System in Mice. *J Vis Exp* (2018) (132):56831. doi: 10.3791/56831
26. Lévesque M, Avoli M. The Kainic Acid Model of Temporal Lobe Epilepsy. *Neurosci Biobehav Rev* (2013) 37:2887–99. doi: 10.1016/j.neubiorev.2013.10.011
27. Leite JP, Garcia-Cairasco N, Cavalheiro EA. New Insights From the Use of Pilocarpine and Kainate Models. *Epilepsy Res* (2002) 50:93–103. doi: 10.1016/S0920-1211(02)00072-4
28. Zhang Q, Wu ZC, Yu JT, Zhong XL, Xing YY, Tian Y, et al. Anticonvulsant Effect of Unilateral Anterior Thalamic High Frequency Electrical Stimulation on Amygdala-Kindled Seizures in Rat. *Brain Res Bull* (2012) 87:221–6. doi: 10.1016/j.brainresbull.2011.11.023
29. Löscher W. Animal Models of Intractable Epilepsy. *Prog Neurobiol* (1997) 53:239–58. doi: 10.1016/S0301-0082(97)00035-X
30. Adak A, Khan MR. An Insight Into Gut Microbiota and Its Functionalities. *Cell Mol Life Sci* (2019) 76:473–93. doi: 10.1007/s00018-018-2943-4
31. Bäckhed F, Roswall J, Peng Y, Feng Q, Jia H, Kovatcheva-Datchary P, et al. Dynamics and Stabilization of the Human Gut Microbiome During the First Year of Life. *Cell Host Microbe* (2015) 17:690–703. doi: 10.1016/j.chom.2015.04.004
32. Khanna S, Tosh PK. A Clinician's Primer on the Role of the Microbiome in Human Health and Disease. *Mayo Clin Proc* (2014) 89:107–14. doi: 10.1016/j.mayocp.2013.10.011
33. O'Toole PW, Jeffery IB. Gut Microbiota and Aging. *Science* (2015) 350:1214–5. doi: 10.1126/science.aac8469
34. Lum GR, Olson CA, Hsiao EY. Emerging Roles for the Intestinal Microbiome in Epilepsy. *Neurobiol Dis* (2019) 135:104576–6. doi: 10.1016/j.nbd.2019.104576
35. Gong X, Liu X, Chen C, Lin J, Li A, Guo K, et al. Alteration of Gut Microbiota in Patients With Epilepsy and the Potential Index as a Biomarker. *Front Microbiol* (2020) 11:517797. doi: 10.3389/fmicb.2020.517797
36. Şafak B, Altunan B, Topçu B, Eren Topkaya A. The Gut Microbiome in Epilepsy. *Microb Pathog* (2020) 139:103853. doi: 10.1016/j.micpath.2019.103853
37. Peng A, Qiu X, Lai W, Li W, Zhang L, Zhu X, et al. Altered Composition of the Gut Microbiome in Patients With Drug-Resistant Epilepsy. *Epilepsy Res* (2018) 147:102–7. doi: 10.1016/j.eplepsyres.2018.09.013
38. Lee K, Kim N, Shim JO, Kim G-H. Gut Bacterial Dysbiosis in Children With Intractable Epilepsy. *J Clin Med* (2020) 10(1):5. doi: 10.3390/jcm10010005
39. Lee H, Lee S, Lee DH, Kim DW. A Comparison of the Gut Microbiota Among Adult Patients With Drug-Responsive and Drug-Resistant Epilepsy: An Exploratory Study. *Epilepsy Res* (2021) 172:106601. doi: 10.1016/j.eplepsyres.2021.106601
40. Xie G, Zhou Q, Qiu C-Z, Dai WK, Wang HP, Li YH, et al. Ketogenic Diet Poses a Significant Effect on Imbalanced Gut Microbiota in Infants With Refractory Epilepsy. *World J Gastroenterol* (2017) 23(33):6164–71. doi: 10.3748/wjg.v23.i33.6164
41. Riazi K, Galic MA, Kuzmiski JB, Ho W, Sharkey KA, Pittman QJ. Microglial Activation and TNFalpha Production Mediate Altered CNS Excitability Following Peripheral Inflammation. *Proc Natl Acad Sci USA* (2008) 105:17151–6. doi: 10.1073/pnas.0806682105
42. Medel-Matus JS, Shin D, Dorfman E, Sankar R, Mazarati A. Facilitation of Kindling Epileptogenesis by Chronic Stress may be Mediated by Intestinal Microbiome. *Epilepsia Open* (2018) 3:290–4. doi: 10.1002/epi4.12114

43. Citraro R, Leo A, De Caro C, Nesci V, Gallo Cantafio ME, Amodio N, et al. Effects of Histone Deacetylase Inhibitors on the Development of Epilepsy and Psychiatric Comorbidity in WAG/Rij Rats. *Mol Neurobiol* (2020) 57:408–21. doi: 10.1007/s12035-019-01712-8
44. Falony G, Joossens M, Vieira-Silva S, Wang J, Darzi Y, Faust K, et al. Population-Level Analysis of Gut Microbiome Variation. *Science (New York N.Y.)* (2016) 352:560–4. doi: 10.1126/science.aad3503
45. David LA, Maurice CF, Carmody RN, Gootenberg DB, Button JE, Wolfe BE, et al. Diet Rapidly and Reproducibly Alters the Human Gut Microbiome. *Nature* (2014) 505:559–63. doi: 10.1038/nature12820
46. Zmora N, Suez J, Elinav E. You Are What You Eat: Diet, Health and the Gut Microbiota. *Nat Rev Gastroenterol Hepatol* (2019) 16:35–56. doi: 10.1038/s41575-018-0061-2
47. Liang C, Tseng HC, Chen HM, Wang WC, Chiu CM, Chang JY, et al. Diversity and Enterotype in Gut Bacterial Community of Adults in Taiwan. *BMC Genomics* (2017) 18:932. doi: 10.1186/s12864-016-3261-6
48. Wu GD, Chen J, Hoffmann C, Bittinger K, Chen YY, Keilbaugh SA, et al. Linking Long-Term Dietary Patterns With Gut Microbial Enterotypes. *Science* (2011) 334:105–8. doi: 10.1126/science.1208344
49. Tan J, McKenzie C, Vuillermin PJ, Goverse G, Vinuesa CG, Mebius RE, et al. Dietary Fiber and Bacterial SCFA Enhance Oral Tolerance and Protect Against Food Allergy Through Diverse Cellular Pathways. *Cell Rep* (2016) 15:2809–24. doi: 10.1016/j.celrep.2016.05.047
50. Zhang N, Ju Z, Zuo T. Time for Food: The Impact of Diet on Gut Microbiota and Human Health. *Nutrition* (2018) 51-52:80–5. doi: 10.1016/j.nut.2017.12.005
51. Yao CK, Muir JG, Gibson PR. Review Article: Insights Into Colonic Protein Fermentation, Its Modulation and Potential Health Implications. *Aliment Pharmacol Ther* (2016) 43:181–96. doi: 10.1111/apt.13456
52. Sonnenburg ED, Sonnenburg JL. Starving Our Microbial Self: The Deleterious Consequences of a Diet Deficient in Microbiota-Accessible Carbohydrates. *Cell Metab* (2014) 20:779–86. doi: 10.1016/j.cmet.2014.07.003
53. Ułamek-Kozioł M, Czuczwar SJ, Januszewski S, Pluta R. Ketogenic Diet and Epilepsy. *Nutrients* (2019) 11:2510. doi: 10.3390/nu11102510
54. Barzegar M, Afghan M, Tarmahi V, Behtari M, Rahimi Khamaneh S, Raeisi S, et al. Ketogenic Diet: Overview, Types, and Possible Anti-Seizure Mechanisms. *Nutr Neurosci* (2021) 24:307–16. doi: 10.1080/1028415X.2019.1627769
55. Cheng CM, Hicks K, Wang J, Eagles DA, Bondy CA. Caloric Restriction Augments Brain Glutamic Acid Decarboxylase-65 and -67 Expression. *J Neurosci Res* (2004) 77:270–6. doi: 10.1002/jnr.20144
56. Suzuki Y, Takahashi H, Fukuda M, Hino H, Kobayashi K, Tanaka J, et al. Beta-Hydroxybutyrate Alters GABA-Transaminase Activity in Cultured Astrocytes. *Brain Res* (2009) 1268:17–23. doi: 10.1016/j.brainres.2009.02.074
57. Yudkoff M, Daikhin Y, Nissim I, Lazarow A, Nissim I. Brain Amino Acid Metabolism and Ketosis. *J Neurosci Res* (2001) 66:272–81. doi: 10.1002/jnr.1221
58. Barañano KW, Hartman AL. The Ketogenic Diet: Uses in Epilepsy and Other Neurologic Illnesses. *Curr Treat Options Neurol* (2008) 10:410–9. doi: 10.1007/s11940-008-0043-8
59. Barrett E, Ross RP, O'Toole PW, Fitzgerald GF, Stanton C. γ-Aminobutyric Acid Production by Culturable Bacteria From the Human Intestine. *J Appl Microbiol* (2012) 113:411–7. doi: 10.1111/j.1365-2672.2012.05344.x
60. Bough KJ, Rho JM. Anticonvulsant Mechanisms of the Ketogenic Diet. *Epilepsia* (2007) 48:43–58. doi: 10.1111/j.1528-1167.2007.00915.x
61. Zhang Y, Zhou S, Zhou Y, Yu L, Zhang L, Wang Y. Altered Gut Microbiome Composition in Children With Refractory Epilepsy After Ketogenic Diet. *Epilepsy Res* (2018) 145:163–8. doi: 10.1016/j.eplepsyres.2018.06.015
62. Lindefeldt M, Eng A, Darban H, Bjerkner A, Zetterström CK, Allander T, et al. The Ketogenic Diet Influences Taxonomic and Functional Composition of the Gut Microbiota in Children With Severe Epilepsy. *NPJ Biofilms Microbiomes* (2019) 5(1):5–5. doi: 10.1038/s41522-018-0073-2
63. Gong X, Cai Q, Liu X, An D, Zhou D, Luo R, et al. Gut Fora and Metabolism Are Altered in Epilepsy and Partially Restored After Ketogenic Diets. *Microb Pathog* (2021) 155:104899. doi: 10.1016/j.micpath.2021.104899
64. Arumugam M, Raes J, Pelletier E, Le Paslier D, Yamada T, Mende DR, et al. Enterotypes of the Human Gut Microbiome. *Nature* (2011) 473:174–80. doi: 10.1038/nature09944
65. Li Y, Yang X, Zhang J, Jiang T, Zhang Z, Wang Z, et al. Ketogenic Diets Induced Glucose Intolerance and Lipid Accumulation in Mice With Alterations in Gut Microbiota and Metabolites. *mBio* (2021) 12:e03601–20. doi: 10.1128/mBio.03601-20.
66. Yamanaka G, Morichi S, Takamatsu T, Watanabe Y, Suzuki S, Ishida Y, et al. Links Between Immune Cells From the Periphery and the Brain in the Pathogenesis of Epilepsy: A Narrative Review. *Int J Mol Sci* (2021) 22:4395. doi: 10.3390/ijms22094395.
67. Devinsky O, Vezzani A, Najjar S, De Lanerolle NC, Rogawski MA. Glia and Epilepsy: Excitability and Inflammation. *Trends Neurosci* (2013) 36:174–84. doi: 10.1016/j.tins.2012.11.008
68. Sanz P, Garcia-Gimeno MA. Reactive Glia Inflammatory Signaling Pathways and Epilepsy. *Int J Mol Sci* (2020) 21(11):4096. doi: 10.3390/ijms21114096.
69. Tlaskalova-Hogenova H, Tuckova L, Mestecky J, Kolinska J, Rossmann P, Stepankova R, et al. Interaction of Mucosal Microbiota With the Innate Immune System. *Scand J Immunol* (2005) 62 Suppl:1, 106–113. doi: 10.1111/j.1365-3083.2005.01618.x
70. Smith K, McCoy KD, Macpherson AJ. Use of Axenic Animals in Studying the Adaptation of Mammals to Their Commensal Intestinal Microbiota. *Semin Immunol* (2007) 19:59–69. doi: 10.1016/j.smim.2006.10.002
71. de Theije CGM, Wu J, da Silva SL, Kamphuis PJ, Garssen J, Korte SM, et al. Pathways Underlying the Gut-to-Brain Connection in Autism Spectrum Disorders as Future Targets for Disease Management. *Eur J Pharmacol* (2011) 668:S70–80. doi: 10.1016/j.ejphar.2011.07.013
72. Thion MS, Low D, Silvin A, Chen J, Grisel P, Schulte-Schrepping J, et al. Microbiome Influences Prenatal and Adult Microglia in a Sex-Specific Manner. *Cell* (2018) 172:500–16.e516. doi: 10.1016/j.cell.2017.11.042
73. Obrenovich MEM. Leaky Gut, Leaky Brain? *Microorganisms* (2018) 6. doi: 10.3390/microorganisms6040107
74. Logsdon AF, Erickson MA, Rhea EM, Salameh TS, Banks WA. Gut Reactions: How the Blood-Brain Barrier Connects the Microbiome and the Brain. *Exp Biol Med (Maywood)* (2018) 243:159–65. doi: 10.1177/1535370217743766
75. Ait-Belgnaoui A, Durand H, Cartier C, Chaumaz G, Eutamene H, Ferrier L, et al. Prevention of Gut Leakiness by a Probiotic Treatment Leads to Attenuated HPA Response to an Acute Psychological Stress in Rats. *Psychoneuroendocrinology* (2012) 37:1885–95. doi: 10.1016/j.psyneuen.2012.03.024
76. McCusker RH, Kelley KW. Immune-Neural Connections: How the Immune System's Response to Infectious Agents Influences Behavior. *J Exp Biol* (2013) 216:84–98. doi: 10.1242/jeb.073411
77. Khakh BS, Sofroniew MV. Diversity of Astrocyte Functions and Phenotypes in Neural Circuits. *Nat Neurosci* (2015) 18:942–52. doi: 10.1038/nn.4043
78. Ginhoux F, Lim S, Hoeffel G, Low D, Huber T. Origin and Differentiation of Microglia. *Front Cell Neurosci* (2013) 7:45. doi: 10.3389/fncel.2013.00045
79. Bosco DB, Tian DS, Wu LJ. Neuroimmune Interaction in Seizures and Epilepsy: Focusing on Monocyte Infiltration. *FEBS J* (2020) 287:4822–37. doi: 10.1111/febs.15428
80. Liddelow SA, Guttenplan KA, Clarke LE, Bennett FC, Bohlen CJ, Schirmer L, et al. Neurotoxic Reactive Astrocytes Are Induced by Activated Microglia. *Nature* (2017) 541:481–7. doi: 10.1038/nature21029
81. Rothhammer V, Borucki DM, Tjon EC, Takenaka MC, Chao CC, Ardura-Fabregat A, et al. Microglial Control of Astrocytes in Response to Microbial Metabolites. *Nature* (2018) 557:724–8. doi: 10.1038/s41586-018-0119-x
82. Rothhammer V, Mascanfroni ID, Bunse L, Takenaka MC, Kenison JE, Mayo L, et al. Type I Interferons and Microbial Metabolites of Tryptophan Modulate Astrocyte Activity and Central Nervous System Inflammation via the Aryl Hydrocarbon Receptor. *Nat Med* (2016) 22:586–97. doi: 10.1038/nm.4106
83. Yang L, Zhou Y, Jia H, Qi Y, Tu S, Shao A, et al. Affective Immunology: The Crosstalk Between Microglia and Astrocytes Plays Key Role? *Front Immunol* (2020) 11:1818. doi: 10.3389/fimmu.2020.01818
84. Moradi K, Ashraf-Ganjouei A, Tavolinejad H, Bagheri S, Akhondzadeh S. The Interplay Between Gut Microbiota and Autism Spectrum Disorders: A Focus on Immunological Pathways. *Prog Neuropsychopharmacol Biol Psychiatry* (2021) 106:110091. doi: 10.1016/j.pnpbp.2020.110091
85. Erny D, Hrabě de Angelis AL, Jaitin D, Wieghofer P, Staszewski O, David E, et al. Host Microbiota Constantly Control Maturation and Function of Microglia in the CNS. *Nat Neurosci* (2015) 18:965–77. doi: 10.1038/nn.4030

86. Djukic M, Mildner A, Schmidt H, Czesnik D, Brück W, Priller J, et al. Circulating Monocytes Engraft in the Brain, Differentiate Into Microglia and Contribute to the Pathology Following Meningitis in Mice. *Brain* (2006) 129:2394–403. doi: 10.1093/brain/awl206
87. Braniste V, Al-Asmakh M, Kowal C, Anuar F, Abbaspour A, Tóth M, et al. The Gut Microbiota Influences Blood-Brain Barrier Permeability in Mice. *Sci Transl Med* (2014) 6:263ra158–263ra158. doi: 10.1126/scitranslmed.3009759
88. Amasheh S, Fromm M, Günzel D. Claudins of Intestine and Nephron - a Correlation of Molecular Tight Junction Structure and Barrier Function. *Acta Physiol (Oxf)* (2011) 201:133–40. doi: 10.1111/j.1748-1716.2010.02148.x
89. Welcome MO. Gut Microbiota Disorder, Gut Epithelial and Blood-Brain Barrier Dysfunctions in Etiopathogenesis of Dementia: Molecular Mechanisms and Signaling Pathways. *Neuromolecular Med* (2019) 21:205–26. doi: 10.1007/s12017-019-08547-5
90. Laman JD, t Hart BA, Power C, Dziarski R. Bacterial Peptidoglycan as a Driver of Chronic Brain Inflammation. *Trends Mol Med* (2020) 26:670–82. doi: 10.1016/j.molmed.2019.11.006
91. Gales JM, Prayson RA. Chronic Inflammation in Refractory Hippocampal Sclerosis-Related Temporal Lobe Epilepsy. *Ann Diagn Pathol* (2017) 30:12–6. doi: 10.1016/j.anndiagpath.2017.05.009
92. Chow J, Mazmanian SK. Getting the Bugs Out of the Immune System: Do Bacterial Microbiota "Fix" Intestinal T Cell Responses? *Cell Host Microbe* (2009) 5:8–12. doi: 10.1016/j.chom.2008.12.006
93. Ivanov II, Frutos Rde L, Manel N, Yoshinaga K, Rifkin DB, Sartor RB, et al. Specific Microbiota Direct the Differentiation of IL-17-Producing T-Helper Cells in the Mucosa of the Small Intestine. *Cell Host Microbe* (2008) 4:337–49. doi: 10.1016/j.chom.2008.09.009
94. Burfeind KG, Kashama JK, Bora BK, Murchison CF, Ramos-Crawford AL, Nseka MT, et al. Baseline Characterization of Epilepsy in an Onchocerciasis Endemic Area of the Democratic Republic of Congo. *Brain Res Bull* (2019) 145:45–52. doi: 10.1016/j.brainresbull.2018.11.009
95. Han Y, Yang L, Liu X, Feng Y, Pang Z, Lin Y, et al. HMGB1/CXCL12-Mediated Immunity and Th17 Cells Might Underlie Highly Suspected Autoimmune Epilepsy in Elderly Individuals. *Neuropsychiatr Dis Treat* (2020) 16:1285–93. doi: 10.2147/NDT.S242766
96. Mao LY, Ding J, Peng WF, Ma Y, Zhang YH, Fan W, et al. Interictal Interleukin-17A Levels Are Elevated and Correlate With Seizure Severity of Epilepsy Patients. *Epilepsia* (2013) 54:e142–5. doi: 10.1111/epi.12337
97. Lee YK, Menezes JS, Umesaki Y, Mazmanian SK. Proinflammatory T-Cell Responses to Gut Microbiota Promote Experimental Autoimmune Encephalomyelitis. *Proc Natl Acad Sci USA* (2011) 108 Suppl 1:4615–22. doi: 10.1073/pnas.1000082107
98. Honda K, Littman DR. The Microbiota in Adaptive Immune Homeostasis and Disease. *Nature* (2016) 535:75–84. doi: 10.1038/nature18848
99. Kim M, Qie Y, Park J, Kim CH. Gut Microbial Metabolites Fuel Host Antibody Responses. *Cell Host Microbe* (2016) 20:202–14. doi: 10.1016/j.chom.2016.07.001
100. Gensollen T, Iyer SS, Kasper DL, Blumberg RS. How Colonization by Microbiota in Early Life Shapes the Immune System. *Science* (2016) 352:539–44. doi: 10.1126/science.aad9378
101. McCoy KD, Ronchi F, Geuking MB. Host-Microbiota Interactions and Adaptive Immunity. *Immunol Rev* (2017) 279:63–9. doi: 10.1111/imr.12575
102. Gaman A, Kuo B. Neuromodulatory Processes of the Brain-Gut Axis. *Neuromodulation* (2008) 11:249–59. doi: 10.1111/j.1525-1403.2008.00172.x
103. Goehler LE, Gaykema RP, Opitz N, Reddaway R, Badr N, Lyte M. Activation in Vagal Afferents and Central Autonomic Pathways: Early Responses to Intestinal Infection With Campylobacter Jejuni. *Brain Behav Immun* (2005) 19:334–44. doi: 10.1016/j.bbi.2004.09.002
104. Attenello F, Amar AP, Liu C, Apuzzo MLJ. Theoretical Basis of Vagus Nerve Stimulation. *Prog Neurol Surg* (2015) 29:20–8. doi: 10.1159/000434652
105. Ressler KJ, Mayberg HS. Targeting Abnormal Neural Circuits in Mood and Anxiety Disorders: From the Laboratory to the Clinic. *Nat Neurosci* (2007) 10:1116–24. doi: 10.1038/nn1944
106. Wang F-B, Powley TL. Vagal Innervation of Intestines: Afferent Pathways Mapped With New En Bloc Horseradish Peroxidase Adaptation. *Cell Tissue Res* (2007) 329:221–30. doi: 10.1007/s00441-007-0413-7
107. Kaelberer MM, Buchanan KL, Klein ME, Barth BB, Montoya MM, Shen X, et al. A Gut-Brain Neural Circuit for Nutrient Sensory Transduction. *Science* (2018) 361:eaat5236. doi: 10.1126/science.aat5236
108. Werner F-M, Coveñas R. Classical Neurotransmitters and Neuropeptides Involved in Generalized Epilepsy in a Multi-Neurotransmitter System: How to Improve the Antiepileptic Effect? *Epilepsy Behav* (2017) 71:124–9. doi: 10.1016/j.yebeh.2015.01.038
109. Takanaga H, Ohtsuki S, Hosoya K-I, Terasaki T. GAT2/BGT-1 as a System Responsible for the Transport of γ-Aminobutyric Acid at the Mouse Blood–Brain Barrier. *J Cereb Blood Flow Metab* (2001) 21:1232–9. doi: 10.1097/00004647-200110000-00012
110. Sun Y, Su Y, Zhu W. Microbiome-Metabolome Responses in the Cecum and Colon of Pig to a High Resistant Starch Diet. *Front Microbiol* (2016) 7:779–9. doi: 10.3389/fmicb.2016.00779
111. De Caro C, Iannone LF, Citraro R, Striano P, De Sarro G, Constanti A, et al. Can We 'Seize' the Gut Microbiota to Treat Epilepsy? *Neurosci Biobehav Rev* (2019) 107:750–64. doi: 10.1016/j.neubiorev.2019.10.002
112. Galland L. The Gut Microbiome and the Brain. *J Med Food* (2014) 17:1261–72. doi: 10.1089/jmf.2014.7000
113. Lu Y, Zhang Z, Tong L, Zhou X, Liang X, Yi H, et al. Mechanisms Underlying the Promotion of 5-Hydroxytryptamine Secretion in Enterochromaffin Cells of Constipation Mice by Bifidobacterium and Lactobacillus. *Neurogastroenterol Motil* (2021) 33:e14082. doi: 10.1111/nmo.14082
114. Reigstad CS, Salmonson CE, JH S, DR L, JL S, et al. Gut Microbes Promote Colonic Serotonin Production Through an Effect of Short-Chain Fatty Acids on Enterochromaffin Cells. *FASEB J* (2015) 29:1395–403. doi: 10.1096/fj.14-259598
115. Yano JM, Yu K, Donaldson GP, Shastri GG, Ann P, Ma L, et al. Indigenous Bacteria From the Gut Microbiota Regulate Host Serotonin Biosynthesis. *Cell* (2015) 161:264–76. doi: 10.1016/j.cell.2015.02.047
116. Specchio LM, Iudice A, Specchio N, La Neve A, Spinelli A, Galli R, et al. Citalopram as Treatment of Depression in Patients With Epilepsy. *Clin Neuropharmacol* (2004) 27:133–6. doi: 10.1097/00002826-200405000-00009
117. Wenger GR, Stitzel RE, Craig CR. The Role of Biogenic Amines in the Reserpine-Induced Alteration of Minimal Electroshock Seizure Thresholds in the Mouse. *Neuropharmacology* (1973) 12:693–703. doi: 10.1016/0028-3908(73)90122-6
118. Donovan MH, Tecott LH. Serotonin and the Regulation of Mammalian Energy Balance. *Front Neurosci* (2013) 7:36. doi: 10.3389/fnins.2013.00036
119. Gale JD. Serotonergic Mediation of Vomiting. *J Pediatr Gastroenterol Nutr* (1995) 21 Suppl:1, S22–28. doi: 10.1097/00005176-199501001-00008
120. Hagbom M, Hellysaz A, Istrate C, Nordgren J, Sharma S, de-Faria FM, et al. The 5-HT(3) Receptor Affects Rotavirus-Induced Motility. *J Virol* (2021) 95:e0075121. doi: 10.1128/JVI.00751-21
121. Shajib MS, Baranov A, Khan WI. Diverse Effects of Gut-Derived Serotonin in Intestinal Inflammation. *ACS Chem Neurosci* (2017) 8:920–31. doi: 10.1021/acschemneuro.6b00414
122. Mawe GM, Coates MD, Moses PL. Review Article: Intestinal Serotonin Signalling in Irritable Bowel Syndrome. *Aliment Pharmacol Ther* (2006) 23:1067–76. doi: 10.1111/j.1365-2036.2006.02858.x
123. Mudd AT, Berding K, Wang M, Donovan SM, Dilger RN. Serum Cortisol Mediates the Relationship Between Fecal Ruminococcus and Brain N-Acetylaspartate in the Young Pig. *Gut Microbes* (2017) 8:589–600. doi: 10.1080/19490976.2017.1353849
124. Jurgens CWD, Boese SJ, King JD, Pyle SJ, Porter JE, Doze VA. Adrenergic Receptor Modulation of Hippocampal CA3 Network Activity. *Epilepsy Res* (2005) 66:117–28. doi: 10.1016/j.eplepsyres.2005.07.007
125. Mittal R, Debs LH, Patel AP, Nguyen D, Patel K, O'Connor G, et al. Neurotransmitters: The Critical Modulators Regulating Gut–Brain Axis. *J Cell Physiol* (2017) 232:2359–72. doi: 10.1002/jcp.25518
126. den Besten G, van Eunen K, Groen AK, Venema K, Reijngoud DJ, Bakker BM. The Role of Short-Chain Fatty Acids in the Interplay Between Diet, Gut Microbiota, and Host Energy Metabolism. *J Lipid Res* (2013) 54:2325–40. doi: 10.1194/jlr.R036012
127. De Caro C, Iannone LF, Citraro R, Striano P, De Sarro G, Constanti A, et al. Can We 'Seize' the Gut Microbiota to Treat Epilepsy? *Neurosci Biobehav Rev* (2019) 107:750–64. doi: 10.1016/j.neubiorev.2019.10.002

128. Cheng Y, Mai Q, Zeng X, Wang H, Xiao Y, Tang L, et al. Propionate Relieves Pentylenetetrazol-Induced Seizures, Consequent Mitochondrial Disruption, Neuron Necrosis and Neurological Deficits in Mice. *Biochem Pharmacol* (2019) 169:113607. doi: 10.1016/j.bcp.2019.08.009
129. Li D, Bai X, Jiang Y, Cheng Y. Butyrate Alleviates PTZ-Induced Mitochondrial Dysfunction, Oxidative Stress and Neuron Apoptosis in Mice via Keap1/Nrf2/HO-1 Pathway. *Brain Res Bull* (2021) 168:25–35. doi: 10.1016/j.brainresbull.2020.12.009
130. Cano-López I, González-Bono E. Cortisol Levels and Seizures in Adults With Epilepsy: A Systematic Review. *Neurosci Biobehav Rev* (2019) 103:216–29. doi: 10.1016/j.neubiorev.2019.05.023
131. Miller WL. The Hypothalamic-Pituitary-Adrenal Axis: A Brief History. *Horm Res Paediatr* (2018) 89:212–23. doi: 10.1159/000487755
132. Jacobson L. Hypothalamic-Pituitary-Adrenocortical Axis Regulation. *Endocrinol Metab Clin North Am* (2005) 34:271–vii. doi: 10.1016/j.ecl.2005.01.003
133. Reddy DS, Rogawski MA. Stress-Induced Deoxycorticosterone-Derived Neurosteroids Modulate GABA(A) Receptor Function and Seizure Susceptibility. *J Neurosci* (2002) 22:3795–805. doi: 10.1523/JNEUROSCI.22-09-03795.2002
134. Baram TZ, Schultz L. Corticotropin-Releasing Hormone Is a Rapid and Potent Convulsant in the Infant Rat. *Brain Res Dev Brain Res* (1991) 61:97–101. doi: 10.1016/0165-3806(91)90118-3
135. Rea K, Dinan TG, Cryan JF. The Microbiome: A Key Regulator of Stress and Neuroinflammation. *Neurobiol Stress* (2016) 4:23–33. doi: 10.1016/j.ynstr.2016.03.001
136. Moghaddam B, Bolinao ML, Stein-Behrens B, Sapolsky R. Glucocorticoids Mediate the Stress-Induced Extracellular Accumulation of Glutamate. *Brain Res* (1994) 655:251–4. doi: 10.1016/0006-8993(94)91622-5
137. de Weerth C. Do Bacteria Shape Our Development? Crosstalk Between Intestinal Microbiota and HPA Axis. *Neurosci Biobehav Rev* (2017) 83:458–71. doi: 10.1016/j.neubiorev.2017.09.016
138. Vodička M, Ergang P, Hrnčíř T, Mikulecká A, Kvapilová P, Vagnerová K, et al. Microbiota Affects the Expression of Genes Involved in HPA Axis Regulation and Local Metabolism of Glucocorticoids in Chronic Psychosocial Stress. *Brain Behav Immun* (2018) 73:615–24. doi: 10.1016/j.bbi.2018.07.007
139. Javdan B, Lopez JG, Chankhamjon P, Lee YJ, Hull R, Wu Q, et al. Personalized Mapping of Drug Metabolism by the Human Gut Microbiome. *Cell* (2020) 181:1661–79.e1622. doi: 10.1016/j.cell.2020.05.001
140. Pluta R, Jablonski M. The Ketogenic Diet for Epilepsy Therapy in Children: Quo Vadis? *Nutr (Burbank Los Angeles County Calif.)* (2011) 27:615–6. doi: 10.1016/j.nut.2010.12.015
141. Choi IY, Piccio L, Childress P, Bollman B, Ghosh A, Brandhorst S, et al. A Diet Mimicking Fasting Promotes Regeneration and Reduces Autoimmunity and Multiple Sclerosis Symptoms. *Cell Rep* (2016) 15:2136–46. doi: 10.1016/j.celrep.2016.05.009
142. Barbanti P, Fofi L, Aurilia C, Egeo G, Caprio M. Ketogenic Diet in Migraine: Rationale, Findings and Perspectives. *Neurol Sci* (2017) 38:111–5. doi: 10.1007/s10072-017-2889-6
143. Włodarek D. Role of Ketogenic Diets in Neurodegenerative Diseases (Alzheimer's Disease and Parkinson's Disease). *Nutrients* (2019) 11(1):169. doi: 10.3390/nu11010169.
144. Fan Y, Wang H, Liu X, Zhang J, Liu G. Crosstalk Between the Ketogenic Diet and Epilepsy: From the Perspective of Gut Microbiota. *Mediators Inflamm* (2019) 2019:8373060. doi: 10.1155/2019/8373060
145. Verrotti A, Iapadre G, Di Francesco L, Zagaroli L, Farello G. Diet in the Treatment of Epilepsy: What We Know So Far. *Nutrients* (2020) 12(9):2645. doi: 10.3390/nu12092645.
146. Mahapatra S, Nagpal R, Marya CM, Taneja P, Kataria S. Gut Mycobiome and Its Interaction With Diet, Gut Bacteria and Alzheimer's Disease Markers in Subjects With Mild Cognitive Impairment: A Pilot Study. *EBioMedicine* (2020) 59:102950. doi: 10.1016/j.ebiom.2020.102950
147. Guzel O, Uysal U, Arslan N. Efficacy and Tolerability of Olive Oil-Based Ketogenic Diet in Children With Drug-Resistant Epilepsy: A Single Center Experience From Turkey. *Eur J Paediatr Neurol* (2019) 23:143–51. doi: 10.1016/j.ejpn.2018.11.007
148. Kim DY, Rho JM. The Ketogenic Diet and Epilepsy. *Curr Opin Clin Nutr Metab Care* (2008) 11:113–20. doi: 10.1097/MCO.0b013e3282f44c06
149. Taha AY, Burnham WM, Auvin S. Polyunsaturated Fatty Acids and Epilepsy. *Epilepsia* (2010) 51:1348–58. doi: 10.1111/j.1528-1167.2010.02654.x
150. Xiao YF, Kang JX, Morgan JP, Leaf A. Blocking Effects of Polyunsaturated Fatty Acids on Na+ Channels of Neonatal Rat Ventricular Myocytes. *Proc Natl Acad Sci USA* (1995) 92:11000–4. doi: 10.1073/pnas.92.24.11000
151. Zimmer L, Delpal S, Guilloteau D, Aïoun J, Durand G, Chalon S. Chronic N-3 Polyunsaturated Fatty Acid Deficiency Alters Dopamine Vesicle Density in the Rat Frontal Cortex. *Neurosci Lett* (2000) 284:25–8. doi: 10.1016/S0304-3940(00)00950-2
152. Bahagat KA, Elhady M, Aziz AA, Youness ER, Zakzok E. Omega-6/Omega-3 Ratio and Cognition in Children With Epilepsy. *Pediatr (Engl Ed)* (2019) 91:88–95. doi: 10.1016/j.anpedi.2018.07.015
153. Sohouli MH, Razmpoosh E, Zarrati M, Jaberzadeh S. The Effect of Omega-3 Fatty Acid Supplementation on Seizure Frequency in Individuals With Epilepsy: A Systematic Review and Meta-Analysis. *Nutr Neurosci* (2021)0) 30:1–10. doi: 10.1080/1028415X.2021.1959100
154. Dallérac G, Moulard J, Benoist JF, Rouach S, Auvin S, Guilbot A, et al. Non-Ketogenic Combination of Nutritional Strategies Provides Robust Protection Against Seizures. *Sci Rep* (2017) 7:5496. doi: 10.1038/s41598-017-05542-3
155. Hill C, Guarner F, Reid G, Gibson GR, Merenstein DJ, Pot B, et al. Expert Consensus Document. The International Scientific Association for Probiotics and Prebiotics Consensus Statement on the Scope and Appropriate Use of the Term Probiotic. *Nat Rev Gastroenterol Hepatol* (2014) 11:506–14. doi: 10.1038/nrgastro.2014.66
156. Yan F, Polk DB. Probiotics and Probiotic-Derived Functional Factors-Mechanistic Insights Into Applications for Intestinal Homeostasis. *Front Immunol* (2020) 11:1428. doi: 10.3389/fimmu.2020.01428
157. Swanson KS, Gibson GR, Hutkins R, Reimer RA, Reid G, Verbeke K, et al. The International Scientific Association for Probiotics and Prebiotics (ISAPP) Consensus Statement on the Definition and Scope of Synbiotics. *Nat Rev Gastroenterol Hepatol* (2020) 17:687–701. doi: 10.1038/s41575-020-0344-2
158. Gómez-Eguílaz M, Ramón-Trapero JL, Pérez-Martínez L, Blanco JR. The Beneficial Effect of Probiotics as a Supplementary Treatment in Drug-Resistant Epilepsy: A Pilot Study. *Benef Microbes* (2018) 9:875–81. doi: 10.3920/BM2018.0018
159. Bagheri S, Heydari A, Alinaghipour A, Salami M. Effect of Probiotic Supplementation on Seizure Activity and Cognitive Performance in PTZ-Induced Chemical Kindling. *Epilepsy Behav* (2019) 95:43–50. doi: 10.1016/j.yebeh.2019.03.038
160. Eor JY, Tan PL, Son YJ, Kwak MJ, Kim SH. Gut Microbiota Modulation by Both Lactobacillus Fermentum MSK 408 and Ketogenic Diet in a Murine Model of Pentylenetetrazole-Induced Acute Seizure. *Epilepsy Res* (2021) 169:106506. doi: 10.1016/j.eplepsyres.2020.106506
161. Ferraris C, Meroni E, Casiraghi MC, Tagliabue A, De Giorgis V, Erba D. One Month of Classic Therapeutic Ketogenic Diet Decreases Short Chain Fatty Acids Production in Epileptic Patients. *Front Nutr* (2021) 8:613100. doi: 10.3389/fnut.2021.613100
162. Ianiro G, Tilg H, Gasbarrini A. Antibiotics as Deep Modulators of Gut Microbiota: Between Good and Evil. *Gut* (2016) 65:1906–15. doi: 10.1136/gutjnl-2016-312297
163. Braakman HMH, van Ingen J. Can Epilepsy be Treated by Antibiotics? *J Neurol* (2018) 265:1934–6. doi: 10.1007/s00415-018-8943-3
164. Imani S, Buscher H, Marriott D, Gentili S, Sandaradura I. Too Much of a Good Thing: A Retrospective Study of β-Lactam Concentration–Toxicity Relationships. *J Antimicrobial Chemotherapy* (2017) 72:2891–7. doi: 10.1093/jac/dkx209
165. Sutter R, Ruegg S, Tschudin-Sutter S. Seizures as Adverse Events of Antibiotic Drugs: A Systematic Review. *Neurology* (2015) 85:1332–41. doi: 10.1212/WNL.0000000000002023
166. Jakobsson HE, Jernberg C, Andersson AF, Sjölund-Karlsson M, Jansson JK, Engstrand L. Short-Term Antibiotic Treatment has Differing Long-Term Impacts on the Human Throat and Gut Microbiome. *PLoS One* (2010) 5: e9836. doi: 10.1371/journal.pone.0009836
167. Korpela K, Salonen A, Virta LJ, Kekkonen RA, Forslund K, Bork P, et al. Intestinal Microbiome Is Related to Lifetime Antibiotic Use in Finnish Pre-School Children. *Nat Commun* (2016) 7:10410. doi: 10.1038/ncomms10410
168. Vrieze A, Out C, Fuentes S, Jonker L, Reuling I, Kootte RS, et al. Impact of Oral Vancomycin on Gut Microbiota, Bile Acid Metabolism, and Insulin Sensitivity. *J Hepatol* (2014) 60:824–31. doi: 10.1016/j.jhep.2013.11.034

169. Raymond F, Ouameur AA, Déraspe M, Iqbal N, Gingras H, Dridi B, et al. The Initial State of the Human Gut Microbiome Determines Its Reshaping by Antibiotics. *ISME J* (2016) 10:707–20. doi: 10.1038/ismej.2015.148
170. Jeffery IB, Lynch DB, O'Toole PW. Composition and Temporal Stability of the Gut Microbiota in Older Persons. *Isme J* (2016) 10:170–82. doi: 10.1038/ismej.2015.88
171. Zimmermann M, Zimmermann-Kogadeeva M, Wegmann R, Goodman AL. Separating Host and Microbiome Contributions to Drug Pharmacokinetics and Toxicity. *Science* (2019) 363. doi: 10.1126/science.aat9931
172. Takeno S, Sakai T. Involvement of the Intestinal Microflora in Nitrazepam-Induced Teratogenicity in Rats and Its Relationship to Nitroreduction. *Teratology* (1991) 44:209–14. doi: 10.1002/tera.1420440209
173. Maier L, Pruteanu M, Kuhn M, Zeller G, Telzerow A, Anderson EE, et al. Extensive Impact of Non-Antibiotic Drugs on Human Gut Bacteria. *Nature* (2018) 555:623–8. doi: 10.1038/nature25979
174. Vasiliadou IA, Molina R, Martinez F, Melero JA, Stathopoulou PM, Tsiamis G. Toxicity Assessment of Pharmaceutical Compounds on Mixed Culture From Activated Sludge Using Respirometric Technique: The Role of Microbial Community Structure. *Sci Total Environ* (2018) 630:809–19. doi: 10.1016/j.scitotenv.2018.02.095
175. Sgritta M, Dooling SW, Buffington SA, Momin EN, Francis MB, Britton RA, et al. Mechanisms Underlying Microbial-Mediated Changes in Social Behavior in Mouse Models of Autism Spectrum Disorder. *Neuron* (2019) 101:246–59.e246. doi: 10.1016/j.neuron.2018.11.018
176. van Nood E, Vrieze A, Nieuwdorp M, Fuentes S, Zoetendal EG, de Vos WM, et al. Duodenal Infusion of Donor Feces for Recurrent Clostridium Difficile. *N Engl J Med* (2013) 368:407–15. doi: 10.1056/NEJMoa1205037
177. Drekonja D, Reich J, Gezahegn S, Greer N, Shaukat A, MacDonald R, et al. Fecal Microbiota Transplantation for Clostridium Difficile Infection: A Systematic Review. *Ann Intern Med* (2015) 162:630–8. doi: 10.7326/M14-2693
178. de Theije CGM, Wopereis H, Ramadan M, van Eijndthoven T, Lambert J, Knol J, et al. Altered Gut Microbiota and Activity in a Murine Model of Autism Spectrum Disorders. *Brain Behavior Immun* (2014) 37:197–206. doi: 10.1016/j.bbi.2013.12.005
179. Stokes JM, Davis JH, Mangat CS, Williamson JR, Brown ED. Discovery of a Small Molecule That Inhibits Bacterial Ribosome Biogenesis. *Elife* (2014) 3: e03574. doi: 10.7554/eLife.03574
180. Lee CH, Steiner T, Petrof EO, Smieja M, Roscoe D, Nematallah A, et al. Frozen *vs* Fresh Fecal Microbiota Transplantation and Clinical Resolution of Diarrhea in Patients With Recurrent Clostridium Difficile Infection: A Randomized Clinical Trial. *JAMA* (2016) 315:142–9. doi: 10.1001/jama.2015.18098
181. Fischer M, Sipe B, Cheng YW, Phelps E, Rogers N, Sagi S, et al. Fecal Microbiota Transplant in Severe and Severe-Complicated Clostridium Difficile: A Promising Treatment Approach. *Gut Microbes* (2017) 8:289–302. doi: 10.1080/19490976.2016.1273998
182. Costello SP, Soo W, Bryant RV, Jairath V, Hart AL, Andrews JM. Systematic Review With Meta-Analysis: Faecal Microbiota Transplantation for the Induction of Remission for Active Ulcerative Colitis. *Aliment Pharmacol Ther* (2017) 46:213–24. doi: 10.1111/apt.14173
183. Bajaj JS, Kassam Z, Fagan A, Gavis EA, Liu E, Cox IJ, et al. Fecal Microbiota Transplant From a Rational Stool Donor Improves Hepatic Encephalopathy: A Randomized Clinical Trial. *Hepatology* (2017) 66:1727–38. doi: 10.1002/hep.29306
184. Johnsen PH, Hilpüsch F, Cavanagh JP, Leikanger IS, Kolstad C, Valle PC, et al. Faecal Microbiota Transplantation *Versus* Placebo for Moderate-to-Severe Irritable Bowel Syndrome: A Double-Blind, Randomised, Placebo-Controlled, Parallel-Group, Single-Centre Trial. *Lancet Gastroenterol Hepatol* (2018) 3:17–24. doi: 10.1016/S2468-1253(17)30338-2
185. Jayasinghe TN, Chiavaroli V, Holland DJ, Cutfield WS, O'Sullivan JM. The New Era of Treatment for Obesity and Metabolic Disorders: Evidence and Expectations for Gut Microbiome Transplantation. *Front Cell Infect Microbiol* (2016) 6:15. doi: 10.3389/fcimb.2016.00015
186. Ruggiero M. Fecal Microbiota Transplantation and the Brain Microbiota in Neurological Diseases. *Clin Endosc* (2016) 49:579. doi: 10.5946/ce.2016.098
187. Vendrik KEW, Ooijevaar RE, de Jong PRC, Laman JD, van Oosten BW, van Hilten JJ, et al. Fecal Microbiota Transplantation in Neurological Disorders. *Front Cell infection Microbiol* (2020) 10:98–8. doi: 10.3389/fcimb.2020.00098
188. He Z, Cui BT, Zhang T, Li P, Long CY, Ji GZ, et al. Fecal Microbiota Transplantation Cured Epilepsy in a Case With Crohn's Disease: The First Report. *World J Gastroenterol* (2017) 23:3565–8. doi: 10.3748/wjg.v23.i19.3565
189. Gupta A, Khanna S. Fecal Microbiota Transplantation. *JAMA* (2017) 318:102–2. doi: 10.1001/jama.2017.6466
190. McKenney PT, Pamer EG. From Hype to Hope: The Gut Microbiota in Enteric Infectious Disease. *Cell* (2015) 163:1326–32. doi: 10.1016/j.cell.2015.11.032
191. Singh A, Dawson TM, Kulkarni S. Neurodegenerative Disorders and Gut-Brain Interactions. *J Clin Invest* (2021) 131(13):e143775. doi: 10.1172/JCI143775.
192. Liang S, Wu X, Jin F. Gut-Brain Psychology: Rethinking Psychology From the Microbiota-Gut-Brain Axis. *Front Integr Neurosci* (2018) 12:33. doi: 10.3389/fnint.2018.00033
193. Salpekar JA, Basu T, Thangaraj S, Maguire J. The Intersections of Stress, Anxiety and Epilepsy. *Int Rev Neurobiol* (2020) 152:195–219. doi: 10.1016/bs.irn.2020.02.001
194. Kanner AM, Balabanov A. Depression and Epilepsy: How Closely Related Are They? *Neurology* (2002) 58:S27–39. doi: 10.1212/WNL.58.8_suppl_5.S27
195. Grover S. Depressive Symptoms in Persons With Epilepsy: Methodological Issues. *J Neurosci Rural Pract* (2017) 8:S3–4. doi: 10.4103/jnrp.jnrp_215_17
196. Shaikh MF, Lee CY, Chen WN, Shaikh FA. The Gut-Brain-Axis on the Manifestation of Depressive Symptoms in Epilepsy: An Evidence-Driven Hypothesis. *Front Pharmacol* (2020) 11:465. doi: 10.3389/fphar.2020.00465
197. Yang J, Zheng P, Li Y, Wu J, Tan X, Zhou J, et al. Landscapes of Bacterial and Metabolic Signatures and Their Interaction in Major Depressive Disorders. *Sci Adv* (2020) 6(49):eaba8555. doi: 10.3390/ijms22169015.
198. Ślifirski G, Król M, Turło J. 5-HT Receptors and the Development of New Antidepressants. *Int J Mol Sci* (2021) 22(16):9015. doi: 10.3390/ijms22169015.
199. Singh T, Goel RK. Epilepsy Associated Depression: An Update on Current Scenario, Suggested Mechanisms, and Opportunities. *Neurochem Res* (2021) 46:1305–21. doi: 10.1007/s11064-021-03274-5
200. Palmer CM, Gilbert-Jaramillo J, Westman EC. The Ketogenic Diet and Remission of Psychotic Symptoms in Schizophrenia: Two Case Studies. *Schizophr Res* (2019) 208:439–40. doi: 10.1016/j.schres.2019.03.019

Conflict of Interest: The authors declare that the research was conducted in the absence of any commercial or financial relationships that could be construed as a potential conflict of interest.

Publisher's Note: All claims expressed in this article are solely those of the authors and do not necessarily represent those of their affiliated organizations, or those of the publisher, the editors and the reviewers. Any product that may be evaluated in this article, or claim that may be made by its manufacturer, is not guaranteed or endorsed by the publisher.

Copyright © 2021 Ding, Lang, Shu, Shao and Cui. This is an open-access article distributed under the terms of the Creative Commons Attribution License (CC BY). The use, distribution or reproduction in other forums is permitted, provided the original author(s) and the copyright owner(s) are credited and that the original publication in this journal is cited, in accordance with accepted academic practice. No use, distribution or reproduction is permitted which does not comply with these terms.

frontiers in Microbiology

MINI REVIEW
published: 11 October 2021
doi: 10.3389/fmicb.2021.729717

Uncovering the Oral Dysbiotic Microbiota as Masters of Neutrophil Responses in the Pathobiology of Periodontitis

*Zsombor Prucsi[1], Alicja Płonczyńska[1], Jan Potempa[1,2] and Maja Sochalska[1]**

[1] Department of Microbiology, Faculty of Biochemistry, Biophysics and Biotechnology, Jagiellonian University, Krakow, Poland, [2] Department of Oral Immunity and Infectious Diseases, University of Louisville School of Dentistry, Louisville, KY, United States

OPEN ACCESS

Edited by:
Carmen Mariana Chifiriuc, University of Bucharest, Romania

Reviewed by:
Geetha Parthasarathy, Tulane University, United States
Eugenia Bezirtzoglou, Democritus University of Thrace, Greece
Youngnim Choi, Seoul National University, South Korea

***Correspondence:**
Maja Sochalska
maja.sochalska@uj.edu.pl

Specialty section:
This article was submitted to Microbial Immunology, a section of the journal Frontiers in Microbiology

Received: *06 July 2021*
Accepted: *14 September 2021*
Published: *11 October 2021*

Citation:
Prucsi Z, Płonczyńska A, Potempa J and Sochalska M (2021) Uncovering the Oral Dysbiotic Microbiota as Masters of Neutrophil Responses in the Pathobiology of Periodontitis. Front. Microbiol. 12:729717. doi: 10.3389/fmicb.2021.729717

Numerous bacterial species participate in the shift of the oral microbiome from beneficial to dysbiotic. The biggest challenge lying ahead of microbiologists, immunologists and dentists is the fact that the bacterial species act differently, although usually synergistically, on the host immune cells, including neutrophils, and on the surrounding tissues, making the investigation of single factors challenging. As biofilm is a complex community, the members interact with each other, which can be a key issue in future studies designed to develop effective treatments. To understand how a patient gets to the stage of the late-onset (previously termed chronic) periodontitis or develops other, in some cases life-threatening, diseases, it is crucial to identify the microbial composition of the biofilm and the mechanisms behind its pathogenicity. The members of the red complex (*Porphyromonas gingivalis*, *Treponema denticola*, and *Tannerella forsythia*) have long been associated as the cause of periodontitis and stayed in the focus of research. However, novel techniques, such as 16S clonal analysis, demonstrated that the oral microbiome diversity is greater than ever expected and it opened a new era in periodontal research. This review aims to summarize the current knowledge concerning bacterial participation beyond *P. gingivalis* and the red complex in periodontal inflammation mediated by neutrophils and to spread awareness about the associated diseases and pathological conditions.

Keywords: periodontitis, neutrophils (PMNs), innate immunity, virulence factor, inflammation

Abbreviations: TLR, Toll-like receptor; MMPs, Matrix metalloproteinases; NET, Neutrophil extracellular trap; Msp, major outer sheath protein; eATP, extracellular adenosine triphosphate; NOD-like receptors, nucleotide-binding oligomerization domain-like receptors; HNP-1, Human Neutrophil Peptide-1; hDFSCs, Human dental follicle stem cells; PMNs, polymorphonuclear leukocytes; GSDs, Glycogen storage diseases; S-layer, surface layer; MAPK, mitogen-activated protein kinase; MK2, MAPK-activated protein kinase 2; ROS, reactive oxygen species; IL, interleukin; SCFAs, short-chain fatty acids; Spp., Species; LtxA, leukotoxin A; NE, Neutrophil elastase; CDT, cytolethal distending toxin; MOI, Multiplicity of infection; TNFα, tumor necrosis factor alpha; OSCC, oral squamous cell carcinoma; NF-κB, nuclear factor-κB; NO, nitrite oxide; PG, prostaglandin; LPS, lipopolysaccharide; DHMDT, Daehwangmokdantang; ERK, extracellular signal-regulated kinases.

BIOFILM IMPACT ON NEUTROPHILS IN THE DEVELOPMENT OF THE PERIODONTAL DISEASE

The innate immune system is the first line of defense against pathogenic invasion. The response begins with the recruitment of immune cells. In the oral cavity, the most abundant contributors are neutrophils. The mechanism of the immune system involves the promotion of inflammation, recruitment of other immune cell types and use of neutrophil-specific defense mechanisms (**Figure 1**). The coordinated attack against pathogens involves the formation of Neutrophil extracellular traps (NETs), a web-like structure destined to capture and eliminate, the internalization (a.k.a. phagocytosis) and the release of the diverse granule content (Scott and Krauss, 2012; Vladimer et al., 2013; Li et al., 2020). In response to the biofilm microbiome, e.g., Fusobacterium nucleatum a significant change in neutrophil gene expression is observed (Wright et al., 2011).

Within the oral biofilm, pathogens have developed countless sophisticated strategies to bypass elimination and turn an inflamed environment in their favor, such as manipulation of neutrophil survival, prolonged inflammatory responses or subversion of anti-microbial properties (White et al., 2014; Olsen and Yilmaz, 2016). Throughout the shift of the microbial composition of the oral cavity, also known as the development of periodontitis, some pathogens act as bridging species between early and late contributors. During the progression of the infection, a strong manipulation of the neutrophil function by the biofilm pathogens can be identified (**Table 1**). Research-wise, it is highly challenging to reveal the interaction between multi-species biofilms and neutrophils. The first step is to identify pathogen-specific effects.

PATHOGEN-SPECIFIC EFFECTS ON NEUTROPHIL FUNCTIONS

Fusobacterium nucleatum

Fusobacterium nucleatum is recognized as a master species in the development of periodontitis, with many strain-specific functions. In order to enhance the multiplication of late colonizers, it is crucial to create favorable conditions with priority to decrease neutrophil efficiency. This is carried out by decreasing superoxide generation and apoptosis induction, limiting the number of counter-attacking immune cells (Kurgan et al., 2017). The production and release of reactive oxygen species (ROS) is part of the pathogen elimination strategies and can be induced by the phagocytosis of the invaders (El-Benna et al., 2016; Zeng et al., 2019). In contrast to well-characterized pathogens, the amount of *F. nucleatum* differs within the timeline of disease progression in accordance with its bridging-specie nature (Tomšič et al., 2021). Moreover, it has been proved that *F. nucleatum* exaggerates NET formation in comparison to other bacterial species, such as *P. gingivalis*, in strong connection with NOD-like receptors (Alyami et al., 2019). Triggering NETosis, instead of phagocytosis, as a neutrophil defense mechanism is probably associated with the huge size of the pathogen (Urban et al., 2006). Another antimicrobial mechanism strongly exploited by *F. nucleatum* is the release of Human Neutrophil Peptide-1 (HNP-1) (Musrati et al., 2016). Increased concentrations of HNP-1 peptide trigger epithelial cell death and bacterial attachment to keratinocytes (Gursoy et al., 2013). Exposure of *F. nucleatum* to defensins, a class of antimicrobial peptides released for instance by neutrophils, can result in decreased bacterial membrane permeability and elevated dental plaque biofilm formation. These strategies are destined to aid the resistance against the membrane disruption and lysis caused by the above-mentioned proteins. As a consequence, the proliferation level is secured (Keskin et al., 2014; Xu and Lu, 2020). Importantly, secreted serine protease fusolisin degrades extracellular matrix proteins as well as cleaves the most abundant immunoglobulin at the mucosal surface (IgA), contributing to the inactivation of the host defense and disease progression (Bachrach et al., 2004; Doron et al., 2014). To add insult to injury, observed tissue environment modulation can give rise to other pathological conditions, such as colorectal cancer (Luo et al., 2019).

Prevotella intermedia and *Tannerella forsythia*

Pathogens can also have an indirect effect on the function of neutrophils. In the case of *Prevotella intermedia* and *Tannerella forsythia*, it has been proved that they can adhere to and internalize into human dental follicle stem cells (hDFSCs). This infection modulates the environment and diminishes the expression of cytokines, however, it does not change hDFSC differentiation capacity. Consequently, a reduced release of IL-8 can contribute to limited chemotaxis of polymorphonuclear leukocytes (PMNs). Moreover, in the presence of infected hDFSCs neutrophil phagocytic activity and NET formation are also decreased, which gives pathogens enough time for gingival colonization (Hieke et al., 2016). Importantly, a challenge with *T. forsythia* induces a strong immune response as indicated by the number of immune cells accumulated at the lesion of administration in a murine model. These *in vivo* experiments showed, that unlike in the presence of *P. gingivalis*, the neutrophil migration is not inhibited (Gosling et al., 2005). However, some comorbidity, such as glycogen storage diseases (GSDs), can in few cases further enhance gingival tissue destruction. A case report of a GSD patient manifesting with the subversion of the neutrophil chemotaxis and neutropenia described an evident *T. forsythia*-mediated intraoral bone loss (Ma et al., 2018).

Interestingly, Ksiazek et al. discovered that *T. forsythia* expresses a serpin (protease inhibitor) called miropin that can contribute to its survival and ability to avoid protease activity of neutrophils (Ksiazek et al., 2015). Strikingly, another newly discovered metalloproteinase called ***miro***lysin together with the previously characterized, secreted metalloproteinase called karilysin, represent important virulence factors of *T. forsythia*. Both proteinases show a synergistic inhibitory effect on many pathways in the host immune system. Significantly,

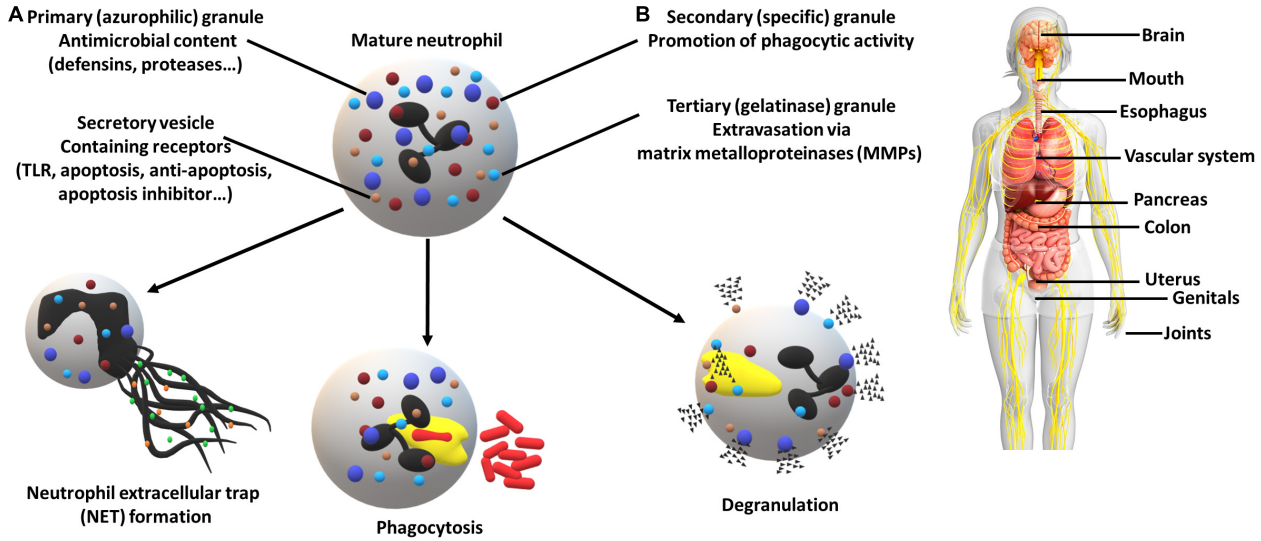


FIGURE 1 | Neutrophil defense mechanisms **(A)** and associated diseases **(B). (A)** Neutrophils can employ numerous strategies in order to eliminate pathogens, including the formation of neutrophil extracellular traps, destined to capture and eliminate, internalization (phagocytosis) and the release of a high variety of granule contents (e.g., receptors, proteases and enzymes). The utilization of secretory vesicles provides an easy to mobilize source of receptors crucial for pathogen recognition (TLRs) and cell fate determination (apoptosis regulators). **(B)** Periodontal pathogens have been associated with multiple other diseases which resulted in increased attention. Affected organs and systems (non-exhaustive): brain (Alzheimer's disease), mouth (periodontitis, oral squamous cell carcinoma, peri-implantitis), esophagus (esophageal cancer), vascular system (aortitis, atherosclerosis), pancreas (pancreatic cancer), colon (colorectal cancer), uterus (preterm birth), genitals (bacterial vaginosis), joints (rheumatoid arthritis).

TABLE 1 | Identified prevalent pathogens associated with periodontitis (non-exhaustive).

Name & Gram staining [+/−]	Use of oxygen	Virulence factor	Effect on neutrophil function	Association with other disease	Sources
Porphyromonas gingivalis −	Anaerobic	Gingipain	Abolish pro-inflammatory signaling	Alzheimer's disease	Popadiak et al., 2007; Ilievski et al., 2018
Treponema denticola −	Anaerobic	Major outer sheath protein (Msp)	Distract neutrophil chemotaxis	Oral squamous cell carcinoma (OSCC)	Jones et al., 2017; Fitzsimonds et al., 2020
Tannerella forsythia −	Anaerobic	Miropin	Neutrophil protease inhibitor	Atherosclerotic lesions	Honma et al., 2009; Lee et al., 2014; Ksiazek et al., 2015
Fusobacterium nucleatum −	Anaerobic	Serine protease	Degrade extracellular matrix proteins	Colorectal cancer	Signat et al., 2011; Han, 2015
Prevotella intermedia −	Anaerobic	nucA/D	Degrade neutrophil extracellular traps (NETs)	Aortitis	Nambu et al., 2015; Boersma et al., 2017; Doke et al., 2017
Aggregatibacter actinomycetemcomitans −	Anaerobic	Extracellular adenosine triphosphate (eATP)	Recruitment of immune cells	Rheumatoid arthritis	Ding et al., 2016; Konig et al., 2016
Peptoanaerobacter stomatis +	Anaerobic	Neutrophil-derived chemokines	Induced chemotaxis of both neutrophils and monocytes.	Unknown	Sizova et al., 2015; Vashishta et al., 2019
Filifactor alocis +	Anaerobic	High tolerance against oxidative stress	Avoid oxygen-dependent defense mechanism	Peri-implantitis	Aruni et al., 2011, 2015

T. forsythia with a mutation in the expression of these enzymes presented with a strongly diminished survival rate (Jusko et al., 2012, 2015). Apart from proteinases, an outer surface layer (S-layer) is a *T. forsythia*-associated virulence factor that can contribute to serum resistance and has a significant role in coaggregation with other oral pathogens, such as *P. gingivalis*. The S-layer significantly reduces the deposition of C3b on the bacterial surface, which would

act as a tag for phagocytosis (Shimotahira et al., 2013). Strikingly, a bacterial glycan found linked to the S-layer can modulate dendritic cells and suppress T helper 17 response (Settem et al., 2013). As an anaerobic bacteria, *T. forsythia* lacks a complex enzymatic system against oxidative stress. However, the genome of this pathogen encodes an oxidative stress response sensor protein (OxyR) homolog, that acts as a positive regulator for antioxidant gene expression. This can contribute to the resistance of the bacterial community to oxidative stress in the aerobic oral cavity and protect against oxidative burst in leukocytes, which is essential in the dental plaque biofilm formation (Honma et al., 2009; Moriguchi et al., 2017).

The main component of NETs is DNA (Brinkmann et al., 2004). Among other species (*P. gingivalis*, *F. nucleatum* and *Aggregatibacter actinomycetemcomitans*), *P. intermedia* has the highest nuclease activity, enabling it to block the capture and subsequent phagocytosis by neutrophils. Two genes have been identified as responsible for this feature, *nucA* and *nucD*, encoding enzymes that require cations for their activity (Doke et al., 2017). Still, this strategy itself cannot be considered unique, as numerous pathogens associated with periodontal disease are able to express such enzymes, including members of the red and the orange complexes (Palmer et al., 2012). Bacteria species are grouped based on chronological coexistence during diseases progression. Members of the red complex (*Porphyromonas gingivalis*, *Treponema denticola* and *Tannerella forsythia*) are late colonizers and the multiplication of them relies on, and is tightly connected to the conquest of the members of the orange complex (e.g., *Fusobacterium nucleatum*, *Prevotella intermedia*) (Mohanty et al., 2019).

Aggregatibacter actinomycetemcomitans

Secreted extracellular adenosine triphosphate (eATP) is a distinctive virulence factor characterized in *A. actinomycetemcomitans*. eATP is predominantly an intracellular signaling molecule involved in the recruitment of immune cells (Ding et al., 2016). However, in periodontitis, eATP secreted by *A. actinomycetemcomitans* induces an upregulation of cytokine expression, resulting in the massive recruitment of inflammatory cells via mainly the p38 mitogen-activated protein kinase (MAPK) and MAPK-activated protein kinase 2 (MK2) pathways (Herbert et al., 2017). Therefore, would be of great importance to investigate the effects of eATP on p38 or MK2 kinases not only in macrophages, but also in neutrophils Interestingly, macrophages challenge with *A. actinomycetemcomitans* induced autophagic influx, restricting the expression of the proinflammatory cytokine IL-1β and ROS production, which ensure protection for this pathogen (Lee et al., 2020). Of importance, bacterial metabolites, such as short-chain fatty acids (SCFAs), are widely spread among different species and connected to a great number of immunological disorders (Ferreira et al., 2014). During bacterial infection, *A. actinomycetemcomitans*-associated SCFAs can also alter neutrophil effector mechanisms by downregulating cytokine production and phagocytic activity (Corrêa et al., 2017).

Leukotoxins are virulence factors expressed e.g., by some *Staphylococcus spps*. or by *Mannheimia haemolytica*, altering both the innate and the adaptive immune system (Futagawa-Saito et al., 2004; Aulik et al., 2010). Strikingly, leukotoxin A (LtxA) secreted by *A. actinomycetemcomitans* triggers a dysregulation in neutrophils, resulting in the release of citrullinated proteins (Konig et al., 2016). The hypercitrullination of host proteins, on one hand leads to diminished functions, such as in the case of histone proteins embedded in NETs can be responsible for decreased anti-microbial activity (Li et al., 2010). On the other hand, the development of rheumatoid arthritis (RA) is the consequence of an elevated level of citrullinated proteins, that leads to the hyperactivity of the immune system resulting in the destruction of the host tissue (Kuhn et al., 2006). The link between RA and periodontitis has long been under the scope of scientific research due to the numerous shared immune-pathological similarities, including overall disease progression, cytokine profile and risk factors (Koziel et al., 2014; de Molon et al., 2019). As these two diseases can present with similar symptoms, some approaches can be applied in both cases to control disease manifestations, i.e., the melanocortin agonism can be a potential way to overcome excessive oral inflammation (Madeira et al., 2016). Melanocortin proteins upon receptor biding elevate the resolution of inflammation by reducing the amount of released pro-inflammatory cytokines and induce efferocytosis, the clearance of neutrophils by macrophages (Montero-Melendez et al., 2011). Besides the induction of citrullinating enzymes in neutrophils, LtxA has a strong toxic effect on leukocytes and induces NET formation in a dose-dependent manner. Additionally, the activity of neutrophil elastase (NE), a principal proteinase in bacterial defense, is exploited. Normally, NE is localized in the cytoplasm, however, upon LtxA exposure, neutrophil lysis is triggered, followed by the release of high amounts of elastase. As a consequence, human gingival epithelial cells and fibroblasts detach and die (Madeira et al., 2016; Hiyoshi et al., 2019).

Of note, *A. actinomycetemcomitans* activates many more neutrophil defense mechanisms, such as ROS production, the release of proteases and the already mentioned NET formation that can be considered a successful defense strategy in the absence of bacterial nuclease activity (Mikolai et al., 2021). Although, the coin has two sides, the overactivation of the above-mentioned mechanisms results in the destruction of the host tissues. Among other virulence factors, this pathogen produces a toxin called the Cytolethal Distending Toxin (CDT), which causes cell cycle arrest *in vitro* and *in vivo* as well as blocks proliferation of the target cells. These disease-promoting effects of CTD are noted towards the periodontal epithelial cells in the rat model (Ohara et al., 2011). Unfortunately, amoxicillin, azithromycin, and metronidazole show an attenuated efficiency against *A. actinomycetemcomitans*, while phagocytosis of the pathogen is only effective at a lower MOI (Multiplicity of Infection) (Ardila and Bedoya-García, 2020). Fortunately, when neutrophils are highly outnumbered by bacterial cells,

internalized azithromycin significantly increases the phagocytic elimination efficiency of PMNs (Lai et al., 2015).

Peptoanaerobacter stomatis and *Filifactor alocis*

Peptoanaerobacter stomatis is a newly characterized member of the destructive oral microbiome. In contrast to well-characterized periodontal pathogens, this one is Gram-positive (Sizova et al., 2015). Infection with this pathogen promotes migration of not just neutrophils, but also monocytes, which additionally strongly fuel inflammation, along with the vigorously induced granule content exocytosis (Vashishta et al., 2019). Furthermore, a significant induction of NET formation is observed upon neutrophil challenge with this pathogen (Armstrong et al., 2018). Moreover, *P. stomatis* is relatively resistant to phagocytosis, while ROS production is significantly increased. These types of defense mechanisms are a double-edged sword, because they simultaneously induce the degradation of the host gingival tissue and periodontitis progression (Flores et al., 2017).

Another Gram-positive member of the community is *Filifactor alocis* that shows an extraordinary resilience to oxidative stress as mentioned in **Table 1**. This provides a substantial colonization advantage over the host defense system and competing pathogens. Similar to other victorious pathogens, *F. alocis* manipulates the neutrophil immune responses. The analysis of global changes in the transcriptome of neutrophils challenged with *F. alocis* reveals strong effects on the PMNs. A delayed apoptosis is accompanied by a prolonged inflammatory response and activated migration through the MAPK cascade and the TNF-α signaling pathways (Miralda et al., 2020). Strikingly, *F. alocis* fails to induce NET formation, but doesn't influence the *P. stomatis*-mediated NETosis. In contrast, an earlier challenge of neutrophils with *F. alocis* decreases NET formation triggered by PMA (Armstrong et al., 2018).

BEYOND PERIODONTITIS

Recently, periodontal pathogens have started being linked to other, often life-threatening diseases, such as atherosclerosis, cardiovascular diseases or rheumatoid arthritis, as mentioned above (Baetta and Corsini, 2010; Steyers and Miller, 2014). *Campylobacter rectus* in addition to inhibit neutrophil elastase by ecotin, has been associated with hypertension (Pietropaoli et al., 2019; Thomas et al., 2020). *P. gingivalis* is the most abundant pathogen of all the detected species (Mougeot et al., 2017). Notwithstanding the fact that inflammation is an essential part of the defense of the immune system, in the case of chronic inflammation, the effect is the opposite. In the oral cavity, a dysbiotic and proinflammatory environment can accelerate the development of gum disease or can even lead to oral cancer. Accordingly, *P. gingivalis, F. nucleatum*, and *Treponema denticola* are the most frequently identified enriched species in patients with oral squamous cell carcinoma (OSCC) (Fitzsimonds et al., 2020). As indicated in **Table 1**, *T. denticola* can alter neutrophil migration as well as trigger a strong inflammatory response, mediated by the elevated expression of Oncostatin M (Jones et al., 2020). The identification of *P. gingivalis* and the secreted virulence factor (protease gingipain) in the brains of patients has been an important milestone in the research of Alzheimer's disease. *In vivo* models demonstrated the pathogen's ability to translocate from the oral cavity to the brain (Ilievski et al., 2018). By applying this knowledge, neurodegeneration can be reduced using specific gingipain inhibitors, which may be a promising treatment (Dominy et al., 2019). Of note, in rare cases, *F. nucleatum* was isolated from immunocompromised patients with pyogenic liver abscesses. However, this might be a slight contribution based on negligible case numbers (Collins and Diamond, 2021).

SUMMARY AND FUTURE REMARKS

The scope of this article included anaerobic bacterial species. However, it has to be mentioned that also aerobic species (*Streptococcus* and *Staphylococcus*) avoid killing by neutrophils and can be found among other microorganisms leading to periodontal disease (Daniluk et al., 2006). As mentioned and summarized in **Table 1**, such pathogens start to be linked to other severe disorders and accelerated disease progressions. As a result of emerging detection methods, both the list of pathogens and the linked diseases will grow constantly, providing not just a better understanding, but also powerful diagnostic tools based on biomarkers in the long term (Han et al., 2021). Although it is almost impossible to list all the pathways and virulence factors, **Table 1** presents the variety of bacterial adaptation mechanisms. The most abundant virulence factors are the proteases, but they are usually specific for the individual bacterial species. Therefore. such peculiarities hinder the development of new therapeutic approaches.

The shift of the oral microbiome and the emerging inflammation are the results of complex bacterial interactions and biofilm formation. Through the mentioned examples, it is demonstrated that pathogens develop an arsenal of functions to generate a favorable environment and to avoid killing by the most abundant immune cell type found in the oral cavity, the neutrophil. There are still many pathways to be discovered in the future and it cannot be ignored that this is not just a localized problem. **Figure 1** illustrates that pathogens can use body fluids as highways to reach other parts of the body and promote inflammation. This might be the key information in some of the adverse pregnancy outcomes, where the placental microbiome shows an incredible resemblance to its assumed origin, the mouth (Fischer et al., 2019).

Interestingly, an investigation of ancient and traditional medications is still as beneficial as at the dawn of modern medicine. Daehwangmokdantang (DHMDT) is a polyherbal mixture known in ancient Korea. Another potential medicament can be an extract from a shrub called border forsythia (in Latin: *Forsythia x intermedia*) known in ancient China. Active lignans from its leaves or flowers have a similar anti-inflammatory effect through the MAPK/ERK pathway (Michalak et al., 2018).

Therefore, the review of the underlying molecular mechanisms can bring us closer to efficient treatments (Máthé, 2020). The nuclear factor-κB (NF-κB) is the major transcription factor during inflammation that controls the expression of many pro-inflammatory factors, such as nitrite oxide (NO), prostaglandin (PG)E2, TNF-α and IL-1β (Li and Verma, 2002). Bacterial lipopolysaccharide (LPS) induces the translocation of NF-κB from the cytoplasm to the nucleus. In the presence of DHMDT, the process is inhibited and the expression of the mentioned pro-inflammatory substances is significantly reduced (Lee et al., 2017).

Statins are a class of widely used lipid-lowering medications that also have antimicrobial properties. A novel study by the group of dr Piotr Mydel (Kamińska et al., 2019), aiming to analyze statin effects on a dysbiotic oral microbiome *in vitro*, included different pathogens, such as *P. gingivalis, F. nucleatum*, *Actinomyces naeslundii*, *T. forsythia*, and *Streptococcus gordonii.* Results indicate high effectiveness against *P. gingivalis* without killing the commensal microbiota, which is a side effect of broad-spectrum antibiotics.

In summary, the future of periodontal medicine undoubtedly lies in a personalized approach as the microbial composition shows a huge variation between patients. An essential step along the way is the identification of contributing pathogens, their distinct biomarkers and the development of specific diagnostic tools (Van der Weijden et al., 2021).

AUTHOR CONTRIBUTIONS

ZP wrote and revised the manuscript, prepared figures, and tables. AP wrote and revised the manuscript. MS wrote, corrected, and revised the manuscript. JP corrected the manuscript. All authors contributed to the article and approved the submitted version.

FUNDING

This work was supported by funding grants from the Foundation for Polish Science (First Team/2017-4/40, POIR.04.04.00-00-42FE/17) to MS, US NIH/NIDCR (DE026280) to JP and International Visegrad Fund (#51910968) to ZP.

ACKNOWLEDGMENTS

The authors acknowledge the financial support from the Foundation for Polish Science grant FIRST TEAM. The FIRST TEAM program is co-financed by the European Union under the European Regional Development Fund. The open-access publication of this article was funded by the Priority Research Area BioS as part of the program "Excellence Initiative – Research University" at the Jagiellonian University in Krakow, Poland.

REFERENCES

Alyami, H. M., Finoti, L. S., Teixeira, H. S., Aljefri, A., Kinane, D. F., and Benakanakere, M. R. (2019). Role of NOD1/NOD2 receptors in *Fusobacterium nucleatum* mediated NETosis. *Microb. Pathog.* 131, 53–64. doi: 10.1016/j.micpath.2019.03.036

Ardila, C. M., and Bedoya-García, J. A. (2020). Antimicrobial resistance of *Aggregatibacter actinomycetemcomitans*, *Porphyromonas gingivalis* and *Tannerella forsythia* in periodontitis patients. *J. Glob. Antimicrob. Resist.* 22, 215–218. doi: 10.1016/J.JGAR.2020.02.024

Armstrong, C. L., Klaes, C. K., Vashishta, A., Lamont, R. J., and Uriarte, S. M. (2018). *Filifactor alocis* manipulates human neutrophils affecting their ability to release neutrophil extracellular traps induced by PMA. *Innate Immun.* 24, 210–220. doi: 10.1177/1753425918767507

Aruni, A. W., Mishra, A., Dou, Y., Chioma, O., Hamilton, B. N., and Fletcher, H. M. (2015). Filifactor alocis–a new emerging periodontal pathogen. *Microbes Infect.* 17, 517–530. doi: 10.1016/j.micinf.2015.03.011

Aruni, A. W., Roy, F., and Fletcher, H. M. (2011). *Filifactor alocis* has virulence attributes that can enhance its persistence under oxidative stress conditions and mediate invasion of epithelial cells by porphyromonas gingivalis. *Infect. Immun.* 79, 3872–3886. doi: 10.1128/IAI.05631-11

Aulik, N. A., Hellenbrand, K. M., Klos, H., and Czuprynski, C. J. (2010). *Mannheimia haemolytica* and its leukotoxin cause neutrophil extracellular trap formation by bovine neutrophils. *Infect. Immun.* 78, 4454–4466. doi: 10.1128/IAI.00840-10

Bachrach, G., Haake, S. K., Glick, A., Hazan, R., Naor, R., Andersen, R. N., et al. (2004). Characterization of the novel *Fusobacterium nucleatum* plasmid pKH9 and evidence of an addiction system. *Appl. Environ. Microbiol.* 70, 6957–6962. doi: 10.1128/AEM.70.12.6957-6962.2004

Baetta, R., and Corsini, A. (2010). Role of polymorphonuclear neutrophils in atherosclerosis: current state and future perspectives. *Atherosclerosis* 210, 1–13. doi: 10.1016/J.ATHEROSCLEROSIS.2009.10.028

Boersma, C., Kampschreur, L. M., Buter, H., Doorenbos, B. M., Klinkert, P., and Koning, G. G. (2017). *Prevotella intermedia* infection causing acute and complicated aortitis-a case report. *Int. J. Surg. Case Rep.* 32, 58–61. doi: 10.1016/j.ijscr.2017.02.015

Brinkmann, V., Reichard, U., Goosmann, C., Fauler, B., Uhlemann, Y., Weiss, D. S., et al. (2004). Neutrophil extracellular traps kill bacteria. *Science* 303, 1532–1535. doi: 10.1126/SCIENCE.1092385

Collins, L., and Diamond, T. (2021). *Fusobacterium nucleatum* causing a pyogenic liver abscess: a rare complication of periodontal disease that occurred during the COVID-19 pandemic. *BMJ Case Reports* 14, e240080. doi: 10.1136/bcr-2020-240080

Corrêa, R. O., Vieira, A., Sernaglia, E. M., Lancellotti, M., Vieira, A. T., Avila-Campos, M. J., et al. (2017). Bacterial short-chain fatty acid metabolites modulate the inflammatory response against infectious bacteria. *Cell. Microbiol.* 19:e12720. doi: 10.1111/CMI.12720

Daniluk, T., Tokajuk, G., Cylwik-Rokicka, D., Rozkiewicz, D., Zaremba, M. L., and Stokowska, W. (2006). Aerobic and anaerobic bacteria in subgingival and supragingival plaques of adult patients with periodontal disease. *Adv. Med. Sci.* 51(Suppl. 1), 81–85.

de Molon, R. S., Rossa, C. Jr., Thurlings, R. M., Cirelli, J. A., and Koenders, M. I. (2019). Linkage of periodontitis and rheumatoid arthritis: current evidence and potential biological interactions. *Int. J. Mol. Sci.* 20, 4541. doi: 10.3390/ijms20184541

Ding, Q., Quah, S. Y., and Tan, K. S. (2016). Secreted adenosine triphosphate from *Aggregatibacter actinomycetemcomitans* triggers chemokine response. *Mol. Oral Microbiol.* 31, 423–434. doi: 10.1111/omi.12143

Doke, M., Fukamachi, H., Morisaki, H., Arimoto, T., Kataoka, H., and Kuwata, H. (2017). Nucleases from *Prevotella intermedia* can degrade neutrophil extracellular traps. *Mol. Oral Microbiol.* 32, 288–300. doi: 10.1111/omi.12171

Dominy, S. S., Lynch, C., Ermini, F., Benedyk, M., Marczyk, A., Konradi, A., et al. (2019). *Porphyromonas gingivalis* in Alzheimer's disease brains: evidence for disease causation and treatment with small-molecule inhibitors. *Sci. Adv.* 5:eaau3333. doi: 10.1126/sciadv.aau3333

Doron, L., Coppenhagen-Glazer, S., Ibrahim, Y., Eini, A., Naor, R., Rosen, G., et al. (2014). Identification and characterization of fusolisin, the *Fusobacterium nucleatum* autotransporter serine protease. *PLoS One* 9:e111329. doi: 10.1371/journal.pone.0111329

El-Benna, J., Hurtado-Nedelec, M., Marzaioli, V., Marie, J.-C., Gougerot-Pocidalo, M.-A., and Dang, P. M.-C. (2016). Priming of the neutrophil respiratory burst: role in host defense and inflammation. *Immunol. Rev.* 273, 180–193. doi: 10.1111/imr.12447

Ferreira, C. M., Vieira, A. T., Vinolo, M. A. R., Oliveira, F. A., Curi, R., and Martins, F. D. S. (2014). The central role of the gut microbiota in chronic inflammatory diseases. *J. Immunol. Res.* 2014, 1–12. doi: 10.1155/2014/689492

Fischer, L. A., Demerath, E., Bittner-Eddy, P., and Costalonga, M. (2019). Placental colonization with periodontal pathogens: the potential missing link. *Am. J. Obstet. Gynecol.* 221, 383–392.e3. doi: 10.1016/j.ajog.2019.04.029

Fitzsimonds, Z. R., Rodriguez-Hernandez, C. J., Bagaitkar, J., and Lamont, R. J. (2020). From beyond the pale to the pale riders: the emerging association of bacteria with oral cancer. *J. Dental Res.* 99, 604–612. doi: 10.1177/0022034520907341

Flores, E. J., Tian, S., Sizova, M., Epstein, S. S., Lamont, R. J., and Uriarte, S. M. (2017). *Peptoanaerobacter stomatis* primes human neutrophils and induces granule exocytosis. *Infect. Immun.* 85:e01043-16. doi: 10.1128/IAI.01043-16

Futagawa-Saito, K., Sugiyama, T., Karube, S., Sakurai, N., Ba-Thein, W., and Fukuyasu, T. (2004). Prevalence and characterization of leukotoxin-producing *Staphylococcus intermedius* in isolates from dogs and pigeons. *J. Clin. Microbiol.* 42, 5324–5326. doi: 10.1128/JCM.42.11.5324-5326.2004

Gosling, P. T., Gemmell, E., Carter, C. L., Bird, P. S., and Seymour, G. J. (2005). Immunohistological analysis of *Tannerella forsythia*-induced lesions in a murine model. *Oral Microbiol. Immunol.* 20, 25–30. doi: 10.1111/j.1399-302X.2004.00188.x

Gursoy, U. K., Könönen, E., Luukkonen, N., and Uitto, V.-J. (2013). Human neutrophil defensins and their effect on epithelial cells. *J. Periodontol.* 84, 126–133. doi: 10.1902/jop.2012.120017

Han, P., Bartold, P. M., Salomon, C., and Ivanovski, S. (2021). Salivary outer membrane vesicles and dna methylation of small extracellular vesicles as biomarkers for periodontal status: a pilot study. *Int. J. Mol. Sci.* 22, 1–15. doi: 10.3390/ijms22052423

Han, Y. W. (2015). *Fusobacterium nucleatum*: a commensal-turned pathogen. *Curr. Opin. Microbiol.* 23, 141–147. doi: 10.1016/j.mib.2014.11.013

Herbert, B. A., Steinkamp, H. M., Gaestel, M., and Kirkwood, K. L. (2017). Mitogen-activated protein kinase 2 signaling shapes macrophage plasticity in *Aggregatibacter actinomycetemcomitans*-induced bone loss. *Infect. Immun.* 85:e00552-16. doi: 10.1128/IAI.00552-16

Hieke, C., Kriebel, K., Engelmann, R., Müller-Hilke, B., Lang, H., and Kreikemeyer, B. (2016). Human dental stem cells suppress PMN activity after infection with the periodontopathogens *Prevotella intermedia* and *Tannerella forsythia*. *Sci. Rep.* 6:39096. doi: 10.1038/srep39096

Hiyoshi, T., Domon, H., Maekawa, T., Nagai, K., Tamura, H., Takahashi, N., et al. (2019). *Aggregatibacter actinomycetemcomitans* induces detachment and death of human gingival epithelial cells and fibroblasts via elastase release following leukotoxin−dependent neutrophil lysis. *Microbiol. Immunol.* 63, 100–110. doi: 10.1111/1348-0421.12672

Honma, K., Mishima, E., Inagaki, S., and Sharma, A. (2009). The OxyR homologue in *Tannerella forsythia* regulates expression of oxidative stress responses and biofilm formation. *Microbiology* 155, 1912–1922. doi: 10.1099/mic.0.027920-0

Ilievski, V., Zuchowska, P. K., Green, S. J., Toth, P. T., Ragozzino, M. E., Le, K., et al. (2018). Chronic oral application of a periodontal pathogen results in brain inflammation, neurodegeneration and amyloid beta production in wild type mice. *PLoS One* 13:e0204941. doi: 10.1371/journal.pone.0204941

Jones, M. M., Vanyo, S. T., Ibraheem, W., Maddi, A., and Visser, M. B. (2020). *Treponema denticola* stimulates Oncostatin M cytokine release and de novo synthesis in neutrophils and macrophages. *J. Leukocyte Biol.* 108, 1527–1541. doi: 10.1002/JLB.4MA0620-072RR

Jones, M. M., Vanyo, S. T., and Visser, M. B. (2017). The C-terminal region of the major outer sheath protein of *Treponema denticola* inhibits neutrophil chemotaxis. *Mol. Oral Microbiol.* 32, 375–389. doi: 10.1111/omi.12180

Jusko, M., Potempa, J., Karim, A. Y., Ksiazek, M., Riesbeck, K., Garred, P., et al. (2012). A metalloproteinase karilysin present in the majority of *Tannerella forsythia* isolates inhibits all pathways of the complement system. *J. Immunol.* 188, 2338–2349. doi: 10.4049/jimmunol.1101240

Jusko, M., Potempa, J., Mizgalska, D., Bielecka, E., Ksiazek, M., Riesbeck, K., et al. (2015). A metalloproteinase mirolysin of *Tannerella forsythia* inhibits all pathways of the complement system. *J. Immunol.* 195, 2231–2240. doi: 10.4049/jimmunol.1402892

Kamińska, M., Aliko, A., Hellvard, A., Bielecka, E., Binder, V., Marczyk, A., et al. (2019). Effects of statins on multispecies oral biofilm identify simvastatin as a drug candidate targeting *Porphyromonas gingivalis*. *J. Periodontol.* 90, 637–646. doi: 10.1002/JPER.18-0179

Keskin, M., Könönen, E., Söderling, E., Isik, G., Firatli, E., Uitto, V.-J., et al. (2014). Increased proliferation and decreased membrane permeability as defense mechanisms of *Fusobacterium nucleatum* against human neutrophilic peptide-1. *Anaerobe* 30, 35–40. doi: 10.1016/j.anaerobe.2014.08.001

Konig, M. F., Abusleme, L., Reinholdt, J., Palmer, R. J., Teles, R. P., Sampson, K., et al. (2016). *Aggregatibacter actinomycetemcomitans*-induced hypercitrullination links periodontal infection to autoimmunity in rheumatoid arthritis. *Sci. Transl. Med.* 8:369ra176. doi: 10.1126/scitranslmed.aaj1921

Koziel, J., Mydel, P., and Potempa, J. (2014). The link between periodontal disease and rheumatoid arthritis: an updated review. *Curr. Rheumatol. Rep.* 16:408. doi: 10.1007/s11926-014-0408-9

Ksiazek, M., Mizgalska, D., Enghild, J. J., Scavenius, C., Thogersen, I. B., and Potempa, J. (2015). Miropin, a novel bacterial serpin from the periodontopathogen *Tannerella forsythia*, inhibits a broad range of proteases by using different peptide bonds within the reactive center loop. *J. Biol. Chem.* 290, 658–670. doi: 10.1074/jbc.M114.601716

Kuhn, K. A., Kulik, L., Tomooka, B., Braschler, K. J., Arend, W. P., Robinson, W. H., et al. (2006). Antibodies against citrullinated proteins enhance tissue injury in experimental autoimmune arthritis. *J. Clin. Invest.* 116, 961–973. doi: 10.1172/JCI25422

Kurgan, Ş, Kansal, S., Nguyen, D., Stephens, D., Koroneos, Y., Hasturk, H., et al. (2017). Strain-specific impact of *Fusobacterium nucleatum* on neutrophil function. *J. Periodontol.* 88, 380–389. doi: 10.1902/jop.2016.160212

Lai, P.-C., Schibler, M. R., and Walters, J. D. (2015). Azithromycin enhances phagocytic killing of *Aggregatibacter actinomycetemcomitans* Y4 by human neutrophils. *J. Periodontol.* 86, 155–161. doi: 10.1902/jop.2014.140183

Lee, H. A., Park, M. H., Song, Y., Na, H. S., and Chung, J. (2020). Role of *Aggregatibacter actinomycetemcomitans*− induced autophagy in inflammatory response. *J. Periodontol.* 91, 1682–1693. doi: 10.1002/JPER.19-0639

Lee, H. R., Jun, H. K., and Choi, B. K. (2014). *Tannerella forsythia* BspA increases the risk factors for atherosclerosis in ApoE$^{-/-}$ mice. *Oral Dis.* 20, 803–808. doi: 10.1111/odi.12214

Lee, M., Hong, S., Park, C., Han, M., Kim, S., Hong, S., et al. (2017). Anti-inflammatory effects of Daehwangmokdantang, a traditional herbal formulation, in lipopolysaccharide-stimulated RAW 264.7 macrophages. *Exp. Ther. Med.* 14, 5809–5816. doi: 10.3892/etm.2017.5296

Li, P., Li, M., Lindberg, M. R., Kennett, M. J., Xiong, N., and Wang, Y. (2010). PAD4 is essential for antibacterial innate immunity mediated by neutrophil extracellular traps. *J. Exp. Med.* 207, 1853–1862. doi: 10.1084/jem.20100239

Li, Q., and Verma, I. M. (2002). NF-κB regulation in the immune system. *Nat. Rev. Immunol.* 2, 725–734. doi: 10.1038/nri910

Li, T., Zhang, Z., Li, X., Dong, G., Zhang, M., Xu, Z., et al. (2020). Neutrophil extracellular traps: signaling properties and disease relevance. *Mediators Inflamm.* 2020, 1–14. doi: 10.1155/2020/9254087

Luo, K., Zhang, Y., Xv, C., Ji, J., Lou, G., Guo, X., et al. (2019). *Fusobacterium nucleatum*, the communication with colorectal cancer. *Biomed. Pharmacother.* 116:108988. doi: 10.1016/j.biopha.2019.108988

Ma, R., Moein Vaziri, F., Sabino, G., Sarmast, N., Zove, S., Iacono, V., et al. (2018). Glycogen storage disease Ib and severe periodontal destruction: a case report. *Dent. J.* 6:53. doi: 10.3390/dj6040053

Madeira, M. F. M., Queiroz−Junior, C. M., Montero−Melendez, T., Werneck, S. M. C., Corrêa, J. D., Soriani, F. M., et al. (2016). Melanocortin agonism as a viable strategy to control alveolar bone loss induced by oral infection. *FASEB J.* 30, 4033–4041. doi: 10.1096/fj.201600790R

Máthé, Á (2020). *Medicinal and Aromatic Plants of North America*, Vol. 6. Cham: Springer, 1–342. doi: 10.1007/978-3-030-44930-8

Michalak, B., Filipek, A., Chomicki, P., Pyza, M., Woźniak, M., Żyżyńska-Granica, B., et al. (2018). Lignans from forsythia x intermedia leaves and flowers attenuate the pro-inflammatory function of leukocytes and their interaction with endothelial cells. *Front. Pharmacol.* 9:401. doi: 10.3389/fphar.2018.00401

Mikolai, C., Branitzki-Heinemann, K., Ingendoh-Tsakmakidis, A., Stiesch, M., von Köckritz-Blickwede, M., and Winkel, A. (2021). Neutrophils exhibit an individual response to different oral bacterial biofilms. *J. Oral Microbiol.* 13:1856565. doi: 10.1080/20002297.2020.1856565

Miralda, I., Vashishta, A., Rogers, M. N., Rouchka, E. C., Li, X., Waigel, S., et al. (2020). Whole transcriptome analysis reveals that filifactor alocis modulates TNFα-stimulated MAPK activation in human neutrophils. *Front. Immunol.* 11:497. doi: 10.3389/fimmu.2020.00497

Mohanty, R., Asopa, S., Joseph, M. D., Singh, B., Rajguru, J., Saidath, K., et al. (2019). Red complex: polymicrobial conglomerate in oral flora: a review. *J. Fam. Med. Prim. Care* 8, 3480. doi: 10.4103/jfmpc.jfmpc_759_19

Montero-Melendez, T., Patel, H. B., Seed, M., Nielsen, S., Jonassen, T. E. N., and Perretti, M. (2011). The melanocortin agonist AP214 exerts anti-inflammatory and proresolving properties. *Am. J. Pathol.* 179, 259–269. doi: 10.1016/J.AJPATH.2011.03.042

Moriguchi, K., Hasegawa, Y., Higuchi, N., Murakami, Y., Yoshimura, F., Nakata, K., et al. (2017). Energy dispersive spectroscopy-scanning transmission electron microscope observations of free radical production in human polymorphonuclear leukocytes phagocytosing non-opsonized *Tannerella forsythia*. *Microsc. Res. Tech.* 80, 555–562. doi: 10.1002/jemt.22819

Mougeot, J.-L. C., Stevens, C. B., Paster, B. J., Brennan, M. T., Lockhart, P. B., and Mougeot, F. K. B. (2017). *Porphyromonas gingivalis* is the most abundant species detected in coronary and femoral arteries. *J. Oral Microbiol.* 9:1281562. doi: 10.1080/20002297.2017.1281562

Musrati, A. A., Fteita, D., Paranko, J., Könönen, E., and Gürsoy, U. K. (2016). Morphological and functional adaptations of *Fusobacterium nucleatum* exposed to human neutrophil Peptide-1. *Anaerobe* 39, 31–38. doi: 10.1016/j.anaerobe.2016.02.008

Nambu, T., Yamane, K., Maruyama, H., Mashimo, C., and Yamanaka, T. (2015). Complete genome sequence of *Prevotella intermedia* strain 17-2. *Genome Announc.* 3:e00951-15. doi: 10.1128/genomeA.00951-15

Ohara, M., Miyauchi, M., Tsuruda, K., Takata, T., and Sugai, M. (2011). Topical application of *Aggregatibacter actinomycetemcomitans* cytolethal distending toxin induces cell cycle arrest in the rat gingival epithelium in vivo. *J. Periodontal Res.* 46, 389–395. doi: 10.1111/j.1600-0765.2011.01348.x

Olsen, I., and Yilmaz, Ö (2016). Modulation of inflammasome activity by *Porphyromonas gingivalis* in periodontitis and associated systemic diseases. *J. Oral Microbiol.* 8:30385. doi: 10.3402/jom.v8.30385

Palmer, L. J., Chapple, I. L. C., Wright, H. J., Roberts, A., and Cooper, P. R. (2012). Extracellular deoxyribonuclease production by periodontal bacteria. *J. Periodontal Res.* 47, 439–445. doi: 10.1111/j.1600-0765.2011.01451.x

Pietropaoli, D., Del Pinto, R., Ferri, C., Ortu, E., and Monaco, A. (2019). Definition of hypertension-associated oral pathogens in NHANES. *J. Periodontol.* 90, 866–876. doi: 10.1002/JPER.19-0046

Popadiak, K., Potempa, J., Riesbeck, K., and Blom, A. M. (2007). Biphasic effect of gingipains from *Porphyromonas gingivalis* on the human complement system. *J. Immunol.* 178, 7242–7250. doi: 10.4049/jimmunol.178.11.7242

Scott, D. A., and Krauss, J. (2012). Neutrophils in periodontal inflammation. *Front. Oral Biol.* 15:56–83. doi: 10.1159/000329672

Settem, R. P., Honma, K., Nakajima, T., Phansopa, C., Roy, S., Stafford, G. P., et al. (2013). A bacterial glycan core linked to surface (S)-layer proteins modulates host immunity through Th17 suppression. *Mucosal Immunol.* 6, 415–426. doi: 10.1038/mi.2012.85

Shimotahira, N., Oogai, Y., Kawada-Matsuo, M., Yamada, S., Fukutsuji, K., Nagano, K., et al. (2013). The surface layer of *Tannerella forsythia* contributes to serum resistance and oral bacterial coaggregation. *Infect. Immun.* 81, 1198–1206. doi: 10.1128/IAI.00983-12

Signat, B., Roques, C., Poulet, P., and Duffaut, D. (2011). *Fusobacterium nucleatum* in periodontal health and disease. *Curr. Issues Mol. Biol.* 13, 25–36. doi: 10.21775/cimb.013.025

Sizova, M. V., Chilaka, A., Earl, A. M., Doerfert, S. N., Muller, P. A., Torralba, M., et al. (2015). High-quality draft genome sequences of five anaerobic oral bacteria and description of *Peptoanaerobacter stomatis* gen. nov., sp. nov., a new member of the family Peptostreptococcaceae. *Stand. Genomic Sci.* 10:37. doi: 10.1186/s40793-015-0027-8

Steyers, C., and Miller, F. (2014). Endothelial dysfunction in chronic inflammatory diseases. *Int. J. Mol. Sci.* 15, 11324–11349. doi: 10.3390/ijms150711324

Thomas, C., Nothaft, H., Yadav, R., Fodor, C., Alemka, A., Oni, O., et al. (2020). Characterization of ecotin homologs from *Campylobacter rectus* and *Campylobacter showae*. *PLoS One* 15:e0244031. doi: 10.1371/journal.pone.0244031

Tomšič, K., Rodič, K., Sotošek, A., Videmšek, P., Seme, K., Herrera, D., et al. (2021). Do differences in cultivable subgingival species exist between different periodontitis stages and grades? *Oral Health Prev. Dentistry* 19, 15–24. doi: 10.3290/j.ohpd.b875525

Urban, C. F., Reichard, U., Brinkmann, V., and Zychlinsky, A. (2006). Neutrophil extracellular traps capture and kill *Candida albicans* yeast and hyphal forms. *Cell. Microbiol.* 8, 668–676. doi: 10.1111/j.1462-5822.2005.00659.x

Van der Weijden, F., Rijnen, M., and Valkenburg, C. (2021). Comparison of three qPCR-based commercial tests for detection of periodontal pathogens. *Sci. Rep.* 11:6141. doi: 10.1038/s41598-021-85305-3

Vashishta, A., Jimenez-Flores, E., Klaes, C., Tian, S., Miralda, I., Lamont, R., et al. (2019). Putative periodontal pathogens, *Filifactor alocis* and *Peptoanaerobacter stomatis*, induce differential cytokine and chemokine production by human neutrophils. *Pathogens* 8:59. doi: 10.3390/pathogens8020059

Vladimer, G. I., Marty-Roix, R., Ghosh, S., Weng, D., and Lien, E. (2013). Inflammasomes and host defenses against bacterial infections. *Curr. Opin. Microbiol.* 16, 23–31. doi: 10.1016/j.mib.2012.11.008

White, P., Cooper, P., Milward, M., and Chapple, I. (2014). Differential activation of neutrophil extracellular traps by specific periodontal bacteria. *Free Radic. Biol. Med.* 75(Suppl. 1):S53. doi: 10.1016/j.freeradbiomed.2014.10.827

Wright, H. J., Chapple, I. L. C., Matthews, J. B., and Cooper, P. R. (2011). *Fusobacterium nucleatum* regulation of neutrophil transcription. *J. Periodontal Res.* 46, 1–12. doi: 10.1111/j.1600-0765.2010.01299.x

Xu, D., and Lu, W. (2020). Defensins: a double-edged sword in host immunity. *Front. Immunol.* 11:764. doi: 10.3389/fimmu.2020.00764

Zeng, M. Y., Miralda, I., Armstrong, C. L., Uriarte, S. M., and Bagaitkar, J. (2019). The roles of NADPH oxidase in modulating neutrophil effector responses. *Mol. Oral Microbiol.* 34, 27–38. doi: 10.1111/omi.12252

Conflict of Interest: The authors declare that the research was conducted in the absence of any commercial or financial relationships that could be construed as a potential conflict of interest.

Publisher's Note: All claims expressed in this article are solely those of the authors and do not necessarily represent those of their affiliated organizations, or those of the publisher, the editors and the reviewers. Any product that may be evaluated in this article, or claim that may be made by its manufacturer, is not guaranteed or endorsed by the publisher.

Copyright © 2021 Prucsi, Płonczyńska, Potempa and Sochalska. This is an open-access article distributed under the terms of the Creative Commons Attribution License (CC BY). The use, distribution or reproduction in other forums is permitted, provided the original author(s) and the copyright owner(s) are credited and that the original publication in this journal is cited, in accordance with accepted academic practice. No use, distribution or reproduction is permitted which does not comply with these terms.

frontiers in Microbiology

PERSPECTIVE
published: 11 October 2021
doi: 10.3389/fmicb.2021.727430

Can Salivary Innate Immune Molecules Provide Clue on Taste Dysfunction in COVID-19?

*Aaron Ermel[1,2], Thankam Paul Thyvalikakath[3,4,5], Tatiana Foroud[2,6], Babar Khan[2,5,7] and Mythily Srinivasan[8]**

[1] Division of Infectious Diseases, Department of Internal Medicine, Indiana University Purdue University at Indianapolis, Indianapolis, IN, United States, [2] Indiana University School of Medicine, Indiana University Purdue University at Indianapolis, Indianapolis, IN, United States, [3] Department of Cariology, Operative Dentistry and Dental Public Health, Indiana University Purdue University at Indianapolis, Indianapolis, IN, United States, [4] Indiana University School of Dentistry, Indiana University Purdue University at Indianapolis, Indianapolis, IN, United States, [5] Regenstrief Institute, Inc., Indianapolis, IN, United States, [6] Department of Medical and Molecular Genetics, Indiana University Purdue University at Indianapolis, Indianapolis, IN, United States, [7] Division of Pulmonary, Critical Care, Sleep and Occupational Medicine, Department of Medicine, Indiana University School of Medicine, Indianapolis, IN, United States, [8] Department of Oral Pathology, Medicine and Radiology, Indiana University Purdue University at Indianapolis, Indianapolis, IN, United States

Emerging concerns following the severe acute respiratory syndrome coronavirus-2 (SARS-CoV2) pandemic are the long-term effects of coronavirus disease (COVID)-19. Dysgeusia in COVID-19 is supported by the abundant expression of the entry receptor, angiotensin-converting enzyme-2 (ACE2), in the oral mucosa. The invading virus perturbs the commensal biofilm and regulates the host responses that permit or suppress viral infection. We correlated the microbial recognition receptors and soluble ACE2 (sACE2) with the SARS-CoV2 measures in the saliva of COVID-19 patients. Data indicate that the toll-like receptor-4, peptidoglycan recognition protein, and sACE2 are elevated in COVID-19 saliva and correlate moderately with the viral load.

Keywords: saliva, COVID-19, innate, receptor, taste, health informatics

OPEN ACCESS

Edited by:
Alina Maria Holban, University of Bucharest, Romania

Reviewed by:
Marlus Pedrosa, University of São Paulo, Brazil
Kenneth Lundstrom, PanTherapeutics, Switzerland

****Correspondence:***
Mythily Srinivasan
mysriniv@iu.edu

Specialty section:
This article was submitted to Infectious Diseases, a section of the journal Frontiers in Microbiology

Received: *18 June 2021*
Accepted: *25 August 2021*
Published: *11 October 2021*

Citation:
Ermel A, Thyvalikakath TP, Foroud T, Khan B and Srinivasan M (2021) Can Salivary Innate Immune Molecules Provide Clue on Taste Dysfunction in COVID-19? Front. Microbiol. 12:727430. doi: 10.3389/fmicb.2021.727430

INTRODUCTION

The coronavirus disease (COVID-19) pandemic caused by the novel severe acute respiratory syndrome coronavirus-2 (SARS-CoV2) has taken a toll on global health and economy, infecting 197 million people and causing over four million deaths worldwide as of July 30, 2021. While most individuals with symptomatic illness recover completely by 4 weeks, a significant proportion of individuals experience long-term symptoms (Centre for disease control and prevention, 2021). Fatigue, headaches, difficulties in concentrating/mental fog, change/loss of taste, change/loss of smell, sleep disorders, and dyspnea constitute the most frequent symptoms in long COVID-19 (Estiri et al., 2021). The SARS-CoV2 virus encodes four major structural proteins, including the spike protein, the membrane protein, the envelope protein, and the nucleocapsid protein. The spike protein of the viral envelope binds the angiotensin-converting enzyme 2 (ACE2) on the surface of target cells for host cell entry. Following ACE2 binding, the spike protein is cleaved by the host protease, transmembrane protease serine 2 (TMPRSS-2), facilitating the intracellular release of viral RNA. A second host protease, the tumor necrosis factor α-converting enzyme (TACE), cleaves the ACE2 protein at the transmembrane helix and releases the ectodomain as a soluble protein (sACE2) (Heurich et al., 2014).

Complex symbiotic relationships between members of the commensal microflora, which is site specific, contribute to the maintenance of human health (Li et al., 2019). The host microbiome could either be neutral or hinder or facilitate viral infection (Wilks et al., 2013). Perturbations in microbiome following viral invasion have been shown to trigger host innate immune responses by signaling *via* pattern recognition receptors such as toll-like receptors (TLR)—for example, while inflammation and cytokine secretion induced by the influenza virus promotes pneumococcal infection, co-infection with *Echinacea purpurea* suppresses influenza A infection by inhibiting TLR-4 and NF-κB activation (Wilks et al., 2013). In COVID-19, a review of clinical case series suggests that bacterial co-infection or superinfection correlates positively with disease severity and poor outcomes (Feldman and Anderson, 2021). Pertinently, emerging evidence suggests that, in addition to ACE2, the SARS-CoV2 could use TLR-2 or TLR-4 for host cell entry (Gadanec et al., 2021). Furthermore, the observations of TLR upregulation by the damage-associated molecular patterns in COVID-19 clinical samples as well as the proposed models of direct binding of SARS-CoV2 spike protein with TLRs1, 4, and 6 suggest specific roles for these TLRs in facilitating viral entry and/or pathology (Sohn et al., 2020; Gadanec et al., 2021). Among the TLRs, TLR-4 has been shown to exhibit the strongest protein–protein interaction with the spike protein of COV-2 (Choudhury and Mukherjee, 2020). Furthermore, it has been suggested that the CoV2/TLR-4 binding induced an increased expression of interferon-stimulated gene expression, and the resultant upregulation of ACE-2 represents a mechanistic link between TLR-4 and CoV2 cellular entry (Gadotti et al., 2020).

Much like the nasopharynx, the oral mucosa is also a portal for entry of airborne virus, including SARS-CoV2. The oral epithelial cells have been shown to express abundantly the SARS-CoV2 receptor, ACE2, and the associated metalloproteases TMPRSS-2 and TACE (Hirayama et al., 2017; Srinivasan et al., 2020). Additionally, the expression of TLR-2 and TLR-4 in the oral epithelium could contribute to SARS-CoV2 entry (Gadanec et al., 2021). The virus has been consistently detected in saliva, and some studies have suggested that the SARS-CoV2 load is higher in saliva than that in the nasopharyngeal swabs. Since the SARS-CoV2 and host interactions within the oral cavity could contribute to the symptoms and the pathology of COVID-19, we hypothesized that the pattern recognition receptors that recognize the oral flora will be upregulated in SARS-CoV2-infected individuals.

Whole saliva is a mixture of secretions (from salivary glands, passive diffusion from blood, and from cells lining the oral mucosa) and cellular components that include corpuscles, exfoliated epithelial cells, and the oral microbiome. Hence, salivary proteome and transcriptome are recognized as excellent resources for investigating the markers for oral and systemic diseases (Lee et al., 2011). Previously, we and others have reported that the salivary TLR-2 and TLR-4 are upregulated in inflammatory diseases of the oral cavity. Here we assessed the expression of TLR-2, TLR-4, and peptidoglycan recognition protein (PGRP)-4 and evaluated the association of changes in these markers as it related to SARS-COV-2 infection in the saliva of hospitalized patients with COVID-19.

METHODS

Study Cohort and Samples

The study cohort included 30 symptomatic, non-ventilated patients with COVID-19 diagnosed by RT-PCR SARS-CoV2 testing from nasopharyngeal swabs and admitted to the IU Health hospital system between September 2020 and December 2020. Unstimulated whole saliva (UWS) was collected within 48 h of admission to the hospital with the help of the Indiana Biobank and in accordance with the institutional review board (IRB protocol # 1105005445). The UWS was collected using the ORA-100 ORAcollect RNA kit following the instructions of the manufacturer (DNA Genotex, ON, Canada). The control UWS included archived saliva bank samples from the salivary research laboratory at Indiana University School of Dentistry that predated the COVID-19 pandemic. All UWS samples were processed at the Infectious Disease Laboratory of the Indiana University School of Medicine. SARS-CoV2 was detected qualitatively by RT-PCR amplifying the RdRp and N genes on the Abbott m2000 Real Time System (Abbott Laboratories, Chicago, IL, United States). Quantitative viral load testing was performed by RT-qPCR targeting the N-gene utilizing the N1 primers from the 2019-nCoV CDC kit against a six-point standard.

The sACE2 activity in each UWS was determined using the CoviDrop^{TM} SARS-CoV-2 Spike-ACE2 binding activity/inhibition assay kit (Epigentek, Farmingdale, NY, United States). The binding activity was calculated according to the equation binding activity = (sample OD− blank OD)/(slope × sample volume, μl) × 1,000, where OD is optical density, blank is the negative control, and slope is calculated from the linear regression of ACE2 standards of known concentration.

The saliva RNA was reverse-transcribed using the iScript cDNA synthesis kit (Biorad, Austin, TX, United States), and an equal quantity of cDNA was amplified for TLR-2, TLR-4, PGPR-4, IFN-γ, and β-actin as a house-keeping gene using the SYBR green/ROX qPCR master mix (SA Biosciences, Frederick, MD, United States) on ABI PRISM^{TM} 7000 Sequence Detection Systems (Thermo Fisher Scientific, United States). The primers used are as follows: βactin-F: 5′-GCCAACCGCGAGAAGATGA-3′, βactin-R: 5′-CATCACGATG CCAGTGGTA-3′; TLR-2F: 5′-ACCTGTGTGACTCTCCATCC-3′, TLR 2R: 5′-GCAGCATCA TTGTTCTCTC-3′; TLR-4F: 5′-TTCCTCTCCTGCGTGAGAC -3′, TLR-4R: 5′-TTCATAGGGTTCAGGGACAG-3′; IFN-γ: 5′-AGTGCCAGCAGAAATATCCTCC-3′, IFNγR: 5′-GAACG AGGTGAGCCAAATATCC-3′, and peptidoglycan recognition protein (PGRP)-4F: 5′-TTTTGCCCTCCTCCCCTGCCA-3′, PGRP-4R: 5′-ATGAGGTTTGGAGGCCCTTGG-A-3′. The relative expression (Ct value) of the TLR-2, TLR-4, PGRP-4, and IFN-γ gene was normalized with βactin by subtracting the latter from the former. Because the level of gene expression is inversely proportional to the Ct and the amount of the product

doubles with each cycle of the RT-PCR, fold change in the gene expression was calculated by the $2^{-\Delta ct}$ method.

Statistics

Differences in sACE2 binding activity and in the measures of the transcripts amplified between the COVID-19 and control samples were determined by Student's *t*-test and Mann–Whitney *U*-test. The value of $p < 0.05$ was considered significant. A correlation between the measures of SARS-CoV2 and the sACE2 or the transcripts in saliva was determined by Spearman correlation.

RESULTS

Clinical Data of the COVID-19 Cohort

Among the 30 COVID-19-positive individuals recruited for this study, unstimulated whole saliva samples from 25 individuals were assessed, as five samples were discarded due to contamination and insufficient collection. The highest incidence of COVID-19 was observed in the seventh decade (36%) of life and a female to male ratio of 1.5:1 in our cohort (see **Figure 1A**). Shortness of breath was the most common symptom (72%), and 20% of individuals experienced loss of taste.

SARS-CoV2 and Its Receptor in COVID-19 Saliva

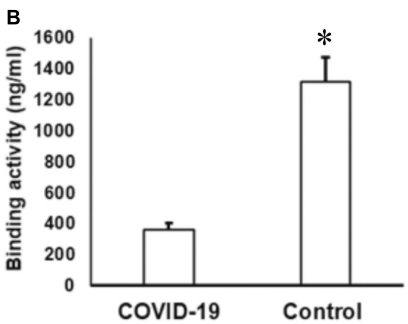
The Ct values for SARS-CoV2 in the UWS samples ranged from 13.60 to 30.47 based on the CN value reported by the Abbott SARS-CoV-2 Real Time Assay. The viral load was calculated in nine samples and ranged from 1.6 to 678 copies/ml. We quantitated the salivary sACE2 binding to the plate-bound spike protein as a measure of sACE2 concentration (**Figure 1A**). The sACE-2 was significantly lower in the UWS of COVID-19 patients than that in the control cohort (**Figure 1B**). Interestingly, the sACE2 exhibited a strong correlation to the viral load ($r_s = -0.5$ with the SARS-CoV2 Ct value) (**Figure 1C**). Significantly, in the nine samples with viral load available, there was a strong positive correlation with sACE2, $r_s = 0.9$. Although the sample numbers are few, these observations support reports of potential oral mucosal infection by SARS-CoV2 (**Figure 1C**).

Pattern Recognition Receptors in COVID-19 Saliva

Molecular docking studies have demonstrated significant binding of the native spike protein of SARS−CoV−2 to TLR1, TLR4, and TLR6, with TLR4 exhibiting the strongest interaction (Choudhury and Mukherjee, 2020). Previously, inflammation by a respiratory virus such as the influenza virus has been shown to enhance host receptors that either facilitate or suppress bacterial co-infection and modulate the disease (Keynan et al., 2011). Several studies have investigated the transcriptome of cell-free and supernatant saliva for biomarkers of oral and systemic diseases (Lee et al., 2011). Here we investigated the salivary transcripts of microbial pattern recognition receptors that recognize the normal oral flora in COVID-19 patients. The fold change or relative expression of TLR-2, TLR-4, and PGRP-4

A

Demographic data and clinical features		
Age (years) distribution		
	<50	1
	50-60	5
	60-70	9
	>70	7
	>80	3
Sex	Females	15
	Males	10
Presenting symptoms		
	Shortness of breath, cough	18
	Fever, fatigue	10
	Bleeding (nasal, hemoptysis, GI)	4
	Loss of smell	3
	Loss of taste	5
Co-morbidity		
	Diabetes	10
	Hypertension	15
	Diabetes and Hypertension	9



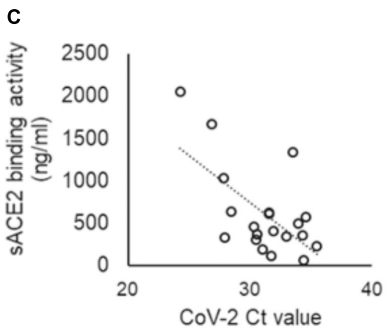


FIGURE 1 | Demographic data of the COVID-19 cohort and sACE2 in saliva. **(A)** The age and sex distribution as well as the presenting symptoms of the COVID-19 cohort included in the study are provided. **(B,C)** The sACE-2 is lower in COVID-19 saliva. **(B)** Unstimulated whole saliva samples collected from hospitalized COVID-19 patients were assessed for sACE2 by ELISA as described in the "Methods" section; $*p < 0.05$. **(C)** Spearman correlation (r_s) for the relationship between the sACE-2 and the SARS-CoV2 ct value.

was significantly higher in COVID-19 saliva as compared to that in the control saliva (**Figures 2A–C**).

Dysregulated immune responses and elevated cytokines, in particular, the higher levels of IFN-γ, were related to a poorer prognosis in COVID-19 (Gadotti et al., 2020). Since our cohort included hospitalized COVID-19 individuals, we measured IFN-γ in saliva samples. The fold change in IFN-γ was higher in COVID-19 saliva than that of control saliva, although the difference did not reach a significant level. While the Δct of PGRP-4 exhibited a strong correlation (r_s = 0.65) with the viral load, that of TLR-4 exhibited a moderate correlation (r_s = 0.44) with the ct value of CoV2 in COVID-19 saliva (**Figure 2D**). No definitive correlation was observed between the CoV2 measures and TLR-2 or IFN-γ transcripts (**Figure 2D**).

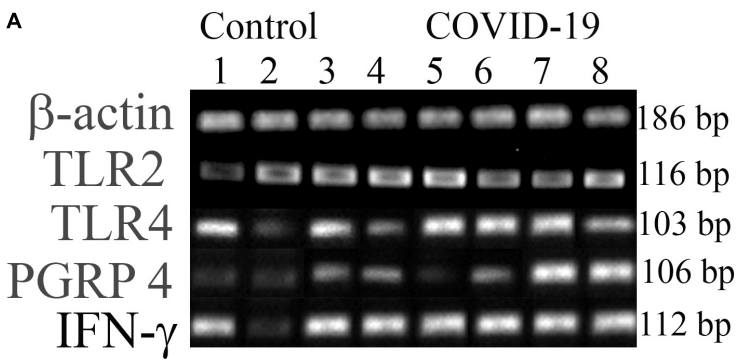
DISCUSSION

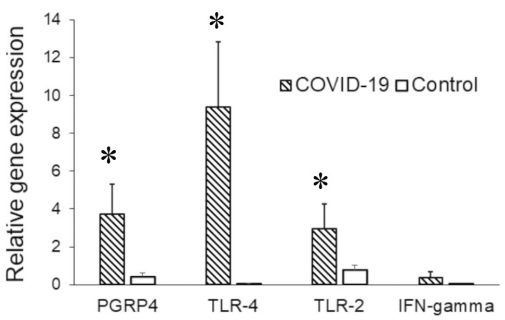
Saliva is an excellent biospecimen not only for the detection of SARS-CoV2 but also for the identification of biomarkers of disease severity in COVID-19 (Silva et al., 2021). Here we observed that the CoV2 load is directly correlated with the concentration of sACE2 and that the innate immune and inflammatory markers are upregulated in the saliva of hospitalized COVID-19 patients.

Membrane-bound ACE2 is the port of entry for SARS-CoV2 into the target cells. Several human tissues express ACE2, and the density of expression contributes to the diverse clinical symptoms of COVID-19 (Heurich et al., 2014; Gadanec et al., 2021). A positive feedback loop between the SARS-CoV2-bound ACE2 endocytosis, ACE2 ectodomain shedding, and the associated inflammation-induced ACE2 expression in bystander cells leads to sustained tissue injury in COVID-19. Elevated plasma sACE2 activity that remained high for over 3 months has been reported in symptomatic COVID-19 patients (Patel et al., 2021). We and others have shown that Ace-2 is expressed in the lining mucosa of the oral cavity, including the dorsum of the tongue. The high expression of ACE2 has also been reported in the glandular and ductal epithelial cells of the salivary glands (Pascolo et al., 2020). These observations suggest the active infection of oral mucosa by SARS-CoV2 and support the clinical symptoms of xerostomia and dysgeusia in COVID-19.

Our observation of reduced sACE2 in COVID-19 patients is seemingly paradoxical since SARS-CoV-2 infection of oral epithelial cells should increase TACE-mediated cleavage of the extracellular domain of ACE2. Since we investigated the saliva of hospitalized COVD-19 patients and there is considerable evidence that the SARS-CoV2 load is higher, if not equivalent, to that in the nasopharyngeal swabs, the reduced sACE2 could be attributed to quenching by the virus. Pertinently, the sACE2 has been shown to bind the spike protein of CoV2, and recombinant sACE2 has been suggested as a potential therapeutic for COVID-19 (Monteil et al., 2020).

Together with the nasopharynx, the oral mucosa is the site of first encounter for SARS-CoV2. The oral epithelial cells at the host/viral interface respond to the exposure by chemokine secretion, upregulating TLR-mediated signaling, increasing inflammatory cytokines, and accelerating exfoliation.





C

			Student's t-test		Mann Whitney's test	
	COVID-19	Control	t value	p value	Z value	p value
PGRP4	3.75	0.43	2.5306	0.00687	-2.6941	0.00714
TLR-4	9.41	0.059	3.18861	0.001388	-4.9681	0.00001
TLR-2	2.96	0.77	1.75804	0.0457	-1.10584	0.1335
IFN-gamma	0.36	0.002	1.23006	0.113963	-2.136	0.01618

D

Paramaters	Spearman rs	pvalue
Δct CoV2:sACE2	-0.48	0.08083
Δct CoV2:TLR-4	0.44625	0.4259
Δct CoV2:TLR-2	0.118	0.72928
Δct CoV2:PGRP4	-0.012	0.926
Viral load: sACE2	0.92	0.0005
Viral load: Δct PGRP	0.65	0.05807

FIGURE 2 | The transcripts for pattern recognition receptors are higher in COVID-19 saliva. Unstimulated whole saliva (UWS) collected from hospitalized COVID-19 patients and archived UWS were assessed for the indicated gene. **(A)** Gel electrophoresis images of the genes of representative samples. **(B)** Mean gene expression normalized to beta actin. **(C)** The table shows the *t*-value, *z*-value, and *p*-value for each transcript assessed. **(D)** The table shows the Spearman correlation (rho) value for the pairs of parameters indicated. *$p < 0.05$.

Transcripts from cellular sediments and cell-free clarified saliva have been assessed for biomarkers for oral and systemic diseases (Lee et al., 2011). Previously, we have shown that the TLR-4 transcript is elevated in chronic oral mucosa inflammatory conditions (Swaminathan et al., 2013). Our observations of higher TLR-4 transcript in the saliva of COVID-19 patients is in alignment with its potential role as a receptor for SARS-CoV2. In this context, it is intriguing to note that TLR-4 signaling and elevated IFN-γ in taste bud epithelial cells have been associated with dysgeusia (Wang et al., 2007).

A recent preprint has reported that the microbiome is distinctly different in COVID-19 saliva samples with a disproportionate increase in select bacterial species (*Veillonella*, *Prevotella*, and *Capnocytophaga*) that are recognized by the peptidoglycan recognition protein including PGRP4 (Iebba et al., 2020). In this context, it is pertinent to note that the transcript for PGRP-4 was higher in the COVID-19 saliva than that in the control samples.

CONCLUSION

The CDC and the COVID-19-Associated Hospitalization Surveillance Network (COVID-NET) report that a significant proportion of individuals experience a variety of post-COVID conditions, including long-term smell and taste dysfunctions (Centre for disease control and prevention, 2021). Pathologically, this could be attributed to either a persistent viral load (albeit at a low titer) or progressive cellular/functional alterations. The oral epithelial expressions of ACE2 and TLR-4 support their function as potential reservoirs of CoV-2. Interestingly, the specialized sensory taste bud epithelial cells in the dorsum of the tongue express TLR-4, and inflammation has been shown to activate IFN-γ signaling in these cells. Our data demonstrate an association of an increase in specific microbe recognition receptors and increasing SARS-CoV-2 viral load relative to the control saliva. The limitation of this study is the small sample size and the lack of a control group of individuals who are hospitalized for reasons other than COVID-19. However, this study does demonstrate that these measurements can be performed from saliva in a prospective manner and warrant a further study of the interaction between SARS-CoV-2 and the inflammasome of the oral cavity.

DATA AVAILABILITY STATEMENT

The original contributions presented in the study are included in the article/supplementary material, further inquiries can be directed to the corresponding author/s.

ETHICS STATEMENT

The studies involving human participants were reviewed and approved by Institutional Review Board, Indiana University Purdue University at Indianapolis. The patients/participants provided their written informed consent to participate in this study.

AUTHOR CONTRIBUTIONS

MS: concept, analysis, and writing. TT: concept and review. AE: sample testing, analysis, and review. BK: review and discussion. TF: sample collection and review. All authors contributed to the article and approved the submitted version.

FUNDING

This work was supported by a Cross Center Collaboration Grant from Regenstrief Institute grant from Regenstrief Institute, Inc., (Indianapolis, IN, United States) and the Indiana University Clinical and Translational Sciences Institute the Indiana Clinical and Translational Sciences Institute which is funded in part by Award Number UL1TR002529 from the National Institutes of Health, National Center for Advancing Translational Sciences, Clinical and Translational Sciences Award. The content is solely the responsibility of the authors and does not necessarily represent the official views of the National Institutes of Health.

REFERENCES

Centre for disease control and prevention (2021). *COVID-19-Associated Hospitalization Surveillance Network (COVID-NET)*. Available online at: https://www.cdc.gov/coronavirus/2019-ncov/covid-data/covid-net/ (accessed June 10, 2021).

Choudhury, A., and Mukherjee, S. (2020). In silico studies on the comparative characterization of the interactions of SARS-CoV-2 spike glycoprotein with ACE-2 receptor homologs and human TLRs. *J. Med. Virol.* 92, 2105–2113. doi: 10.1002/jmv.25987

Estiri, H., Strasser, Z. H., Brat, G. A., Semenov, Y. R., Patel, C. J., and Murphy, S. N. (2021). Evolving phenotypes of non-hospitalized patients that indicate long covid. *Medrxiv*. [Preprint] doi: 10.1101/2021.04.25.21255923

Feldman, C., and Anderson, R. (2021). The role of co-infections and secondary infections in patients with COVID-19. *Pneumonia* 13:5.

Gadanec, L. K., McSweeney, K. R., Qaradakhi, T., Ali, B., Zulli, A., and Apostolopoulos, V. (2021). Can SARS-CoV-2 virus use multiple receptors to enter host cells? *Int. J. Mol. Sci.* 22:992. doi: 10.3390/ijms22030992

Gadotti, A. C., de Castro Deus, M., Telles, J. P., Wind, R., Goes, M., Garcia Charello Ossoski, R., et al. (2020). IFN-gamma is an independent risk factor associated with mortality in patients with moderate and severe COVID-19 infection. *Virus Res.* 289:198171. doi: 10.1016/j.virusres.2020.198171

Heurich, A., Hofmann-Winkler, H., Gierer, S., Liepold, T., Jahn, O., and Pohlmann, S. (2014). TMPRSS2 and ADAM17 cleave ACE2 differentially and only proteolysis by TMPRSS2 augments entry driven by the severe acute respiratory syndrome coronavirus spike protein. *J. Virol.* 88, 1293–1307. doi: 10.1128/jvi.02202-13

Hirayama, A., Awano, S., Seta, Y., and Ansai, T. (2017). ADAM17 regulates TNF-alpha expression upon lipopolysaccharide stimulation in oral keratinocytes. *Biomed. Res.* 38, 157–165. doi: 10.2220/biomedres.38.157

Iebba, V., Zanotta, N., Campisciano, G., Zerbato, V., Di Bella, S., Cason, C., et al. (2020). Profiling of oral microbiota and cytokines in COVID-19 patients. *Biorxiv*. [Preprint] doi: 10.1101/2020.12.13.422589

Keynan, Y., Fowke, K., Ball, T., and Meyers, A. (2011). Toll-like receptors dysregulation after influenza virus infection: insights into pathogenesis of subsequent bacterial pneumonia. *Int. Sch. Res. Notices* 2011:142518.

Lee, Y. H., Zhou, H., Reiss, J. K., Yan, X., Zhang, L., Chia, D., et al. (2011). Direct saliva transcriptome analysis. *Clin. Chem.* 57, 1295–1302. doi: 10.1373/clinchem.2010.159210

Li, N., Ma, W. T., Pang, M., Fan, Q. L., and Hua, J. L. (2019). The commensal microbiota and viral infection: a comprehensive review. *Front. Immunol.* 10:1551. doi: 10.3389/fimmu.2019.01551

Monteil, V., Kwon, H., Prado, P., Hagelkruys, A., Wimmer, R. A., Stahl, M., et al. (2020). Inhibition of SARS-CoV-2 infections in engineered human tissues using clinical-grade soluble human ACE2. *Cell* 181, 905–913. doi: 10.1016/j.cell.2020.04.004

Pascolo, L., Zupin, L., Melato, M., Tricarico, P. M., and Crovella, S. (2020). TMPRSS2 and ACE2 coexpression in SARS-CoV-2 salivary glands infection. *J. Dent. Res.* 99, 1120–1121. doi: 10.1177/0022034520933589

Patel, S. K., Juno, J. A., Lee, W. S., Wragg, K. M., Hogarth, P. M., Kent, S. J., et al. (2021). Plasma ACE2 activity is persistently elevated following SARS-CoV-2 infection: implications for COVID-19 pathogenesis and consequences. *Eur. Respir. J.* 57:2003730. doi: 10.1183/13993003.03730-2020

Silva, J., Lucas, C., Sundaram, M., Israelow, B., Wong, P., Klein, J., et al. (2021). Saliva viral load is a dynamic unifying correlate of COVID-19 severity and mortality. *Medrxiv*. [Preprint] doi: 10.1101/2021.01.04.21249236

Sohn, K. M., Lee, S. G., Kim, H. J., Cheon, S., Jeong, H., Lee, J. I, et al. (2020). COVID-19 patients upregulate toll-like receptor 4-mediated inflammatory signaling that mimics bacterial sepsis. *J. Korean Med. Sci.* 35:e343.

Srinivasan, M., Zunt, S. L., and Goldblatt, L. I. (2020). Oral epithelial expression of angiotensin converting enzyme-2: implications for COVID-19 diagnosis and prognosis. *Biorxiv*. [Preprint] doi: 10.1101/2020.06.22.165035

Swaminathan, V., Prakasam, S., Puri, V., and Srinivasan, M. (2013). Role of salivary epithelial toll-like receptors 2 and 4 in modulating innate immune responses in chronic periodontitis. *J. Periodontal Res.* 48, 757–765. doi: 10.1111/jre.12066

Wang, H., Zhou, M., Brand, J., and Huang, L. (2007). Inflammation activates the interferon signaling pathways in taste bud cells. *J. Neurosci* 27, 10703–10713. doi: 10.1523/jneurosci.3102-07.2007

Wilks, J., Beilinson, H., and Golovkina, T. V. (2013). Dual role of commensal bacteria in viral infections. *Immunol. Rev.* 255, 222–229. doi: 10.1111/imr.12097

Conflict of Interest: The authors declare that the research was conducted in the absence of any commercial or financial relationships that could be construed as a potential conflict of interest.

Publisher's Note: All claims expressed in this article are solely those of the authors and do not necessarily represent those of their affiliated organizations, or those of the publisher, the editors and the reviewers. Any product that may be evaluated in this article, or claim that may be made by its manufacturer, is not guaranteed or endorsed by the publisher.

Copyright © 2021 Ermel, Thyvalikakath, Foroud, Khan and Srinivasan. This is an open-access article distributed under the terms of the Creative Commons Attribution License (CC BY). The use, distribution or reproduction in other forums is permitted, provided the original author(s) and the copyright owner(s) are credited and that the original publication in this journal is cited, in accordance with accepted academic practice. No use, distribution or reproduction is permitted which does not comply with these terms.

frontiers in Microbiology

ORIGINAL RESEARCH
published: 12 October 2021
doi: 10.3389/fmicb.2021.719601

Oral Microbiota Analysis of Tissue Pairs and Saliva Samples From Patients With Oral Squamous Cell Carcinoma – A Pilot Study

Ke Yang[1,2†], Yuezhu Wang[3,4†], Shizhou Zhang[1], Dongsheng Zhang[1], Lihua Hu[1], Tengda Zhao[1] and Huajun Zheng[3]**

[1] Department of Oral and Maxillofacial Surgery, Shandong Provincial Hospital Affiliated to Shandong First Medical University, Jinan, China, [2] Department of Health Management Center, Shandong Provincial Hospital Affiliated to Shandong First Medical University, Jinan, China, [3] NHC Key Lab of Reproduction Regulation, Shanghai Institute for Biomedical and Pharmaceutical Technologies, Fudan University, Shanghai, China, [4] Shanghai-MOST Key Laboratory of Health and Disease Genomics, Chinese National Human Genome Center at Shanghai and Shanghai Institute for Biomedical and Pharmaceutical Technologies, Shanghai, China

OPEN ACCESS

Edited by:
Alina Maria Holban, University of Bucharest, Romania

Reviewed by:
Nezar Al-Hebshi, Temple University, United States
Tomasz M. Karpiński, Poznań University of Medical Sciences, Poland

***Correspondence:**
Tengda Zhao
zhaotengda@sdfmu.edu.cn
Huajun Zheng
zhenghj@chgc.sh.cn

† These authors have contributed equally to this work

Specialty section:
This article was submitted to Infectious Agents and Disease, a section of the journal Frontiers in Microbiology

Received: *02 June 2021*
Accepted: *23 September 2021*
Published: *12 October 2021*

Citation:
Yang K, Wang Y, Zhang S, Zhang D, Hu L, Zhao T and Zheng H (2021) Oral Microbiota Analysis of Tissue Pairs and Saliva Samples From Patients With Oral Squamous Cell Carcinoma – A Pilot Study. Front. Microbiol. 12:719601. doi: 10.3389/fmicb.2021.719601

Oral microbiota dysbiosis is associated with the occurrence and progression of oral cancer. To investigate the association between the microbiota and risk of oral squamous cell carcinoma (OSCC), we identified the microbial composition of paired tumor (TT)/normal paracancerous tissues (NPT) and saliva (TS) samples in OSCC patients through 16S rRNA gene sequencing. A total of 22 phyla, 321 genera, and 869 species were identified in the oral samples. Paired comparisons revealed significant differences between TT, NPT, and TS groups, with the genus *Filifactor* significantly enriched in TT. The phylum Actinobacteria; genus *Veillonella*; and species *Granulicatella adiacens*, *Streptococcus sanguinis*, and *Veillonella rogosae* were significantly enriched in NPT, while the phylum Bacteroidetes; genera *Capnocytophaga*, *Haemophilus*, and *Prevotella*; and seven species, including *Capnocytophaga* sp., *Haemophilus* sp., and *Neisseria* sp., were significantly enriched in TS. In TTs, the abundance of *Prevotella intermedia* was profoundly higher in the gingiva, while *Capnocytophaga gingivalis* and *Rothia mucilaginosa* were enriched in the lining mucosa and tongue. Increasing in abundance from the early tumor stage to the late stage, *Solobacterium moorei* in TT and *Campylobacter* sp. *strain HMT 044* in TS were positively correlated with OSCC development, suggesting that bacteria were selected by different microenvironments. The correlation between 11 microbial species and 17 pathway abundances was revealed, indicating the potential function of low-abundance bacteria. Overall, our analysis revealed that multiple oral bacterial taxa are associated with a subsequent risk of OSCC and may be used as biomarkers for risk prediction and intervention in oral cancers.

Keywords: oral microbiota, 16S rRNA, *Rothia mucilaginosa*, *Prevotella intermedia*, oral squamous cell carcinoma

INTRODUCTION

Annually, more than 447,000 new diagnoses of and nearly 228,000 deaths due to oral cancer are reported worldwide, over 90% of which can be attributed to squamous cell carcinoma (SCC) (Bray et al., 2018). SCC is defined as an epithelial malignancy with poor prognosis that originates from the buccal mucosa, tongue, mouth floor, gingiva, and oropharynx, with a 5-year relative survival rate of less than 65% (Siegel et al., 2020). Environmental triggers, such as tobacco, alcohol consumption, and betel quid chewing, along with human papillomavirus infection, specifically identified in the oropharynx, are major risk factors for oral cancer. In addition, poor oral hygiene and periodontal disease, which affect bacterial ecology, have been epidemiologically and independently linked to oral cancer (Healy and Moran, 2019).

Specific bacteria have been implicated in cancer development. A typical example of a bacterial carcinogen is *Helicobacter pylori*, which is known to promote gastric cancer (Amieva and Peek, 2016). In the human oral cavity, more than 700 different bacterial species have been identified, and dysbiosis of these species results in significant and distant effects in patients with gastrointestinal, hepatobiliary, pancreatic, and colorectal tumors (Mascitti et al., 2019). It has been suggested that the oral microbiota plays an important role in carcinogenesis by stimulating chronic inflammation, producing carcinogenic substances, or inhibiting cell apoptosis (Karpinski, 2019).

Oral bacteria are most likely linked to oral squamous cell carcinoma (OSCC) (Whitmore and Lamont, 2014). Four common inhabitants of the oral cavity, *Porphyromonas gingivalis*, *Fusobacterium nucleatum*, *Treponema denticola*, and *Streptococcus anginosus*, have been identified as potential etiologic agents of OSCC (Zhang W.L. et al., 2019). Bacterial culture demonstrated that significantly higher levels of *Veillonella, Porphyromonas*, and *Fusobacterium* are harbored by tumor surface of OSCC than healthy mucosa (Nagy et al., 1998). Mager et al. (2005) revealed that the levels of three species (*Capnocytophaga gingivalis*, *Prevotella melaninogenica*, and *Streptococcus mitis*) were elevated in the saliva of patients with OSCC. *S. anginosus*, a pathogen that occurs frequently in OSCC tissue specimens, was detected in the dental plaque but not in the saliva of patients (Sasaki et al., 2005). By comparing OSCC tissues and adjacent non-tumor mucosa, Pushalkar et al. (2012) revealed that *Streptococcus* sp. (*S. salivarius*, *S. gordonii*, and *S. parasanguinis*), *Gemella* sp. (*G. haemolysans* and *G. morbillorum*), *Johnsonella ignava*, and *Peptostreptococcus stomatis* were prevalent in tumor sites, whereas *Granulicatella adiacens* was prevalent in non-tumor sites.

With the advent of 16S rRNA high-throughput sequencing, there is growing interest in the possible relationships between changes in the oral microbiota and the risk of oral cancer (Guerrero-Preston et al., 2016). Lee et al. (2017) found that five genera (*Bacillus*, *Enterococcus*, *Parvimonas*, *Peptostreptococcus*, and *Slackia*) exhibited significant differences in saliva between epithelial precursor lesions and OSCC patients, and the genera *Cloacibacillus*, *Gemmiger*, *Oscillospira*, and *Roseburia* were 20 times more abundant in OSCC patients than in healthy controls. Yang et al. compared oral mouthwash samples from OSCC patients and healthy controls and found that the abundances of *Fusobacterium periodonticum* and *Streptococcus constellatus* were positively correlated with the development of OSCC, whereas *S. mitis*, *Haemophilus parainfluenzae*, and *Porphyromonas pasteri* were negatively correlated (Yang et al., 2018). Zhao et al. (2017) and Zhang L. et al. (2019) compared the epithelial samples collected from tumor sites and normal tissues of patients with OSCC using swabs. Zhang L. et al. (2019) found that 10 species (including *F. nucleatum* and *Prevotella intermedia*) and genes involved in bacterial chemotaxis, flagellar assembly, and lipopolysaccharide (LPS) biosynthesis were significantly increased in the tumor sites. Zhao et al. (2017) observed that a group of periodontitis-correlated taxa, including *Fusobacterium* and *Dialister*, was significantly enriched in tumor sites. By comparing fresh OSCC biopsies and epithelial samples of healthy controls collected by swab, Al-Hebshi et al. (2017) reported that some specific species in tumor tissues (TTs), such as *F. nucleatum* and *Pseudomonas aeruginosa*, were related to OSCC. Chang et al. (2019) revealed that *P. gingivalis* and *F. nucleatum* were present at higher levels in cancer tissue than in normal tissues of patients with OSCC and were correlated with subgingival plaques. By comparing OSCC tissue, saliva, and mouthwash samples from the same subjects, Zhang Z. et al. (2019) revealed that the genera *Acinetobacter* and *Campylobacter* were enriched in OSCC tissues, while *Streptococcus* and *Prevotella* were enriched in saliva and mouthwash.

According to a growing number of studies, over 30 genera and a panel of bacterial species have been associated with OSCC (Sami et al., 2020). However, we could see variations in OSCC-associated bacteria among the above-mentioned studies, which might be caused by different bacterial detection techniques and sample types. Traditional methods used in OSCC bacterial studies, such as bacterial culture (Nagy et al., 1998), DNA–DNA hybridization (Mager et al., 2005), PCR (Sasaki et al., 2005), immunohistochemical staining (Katz et al., 2011), and denaturing gradient gel electrophoresis (DGGE) (Pushalkar et al., 2012), usually focus on certain species, while high-throughput sequencing has higher sensitivity. The oral ecosystem has several significantly different niches, including saliva, oral mucosa, and teeth surfaces, each having a unique microbiota (Zhang et al., 2018). A recent study reported that the structure and function of the bacteriome on the surface of oral cancer is significantly different from that within the tumor, suggesting that different types of sample collection (swab, tissue, or saliva) and controls (adjacent mucosa or healthy people) might yield inconsistent conclusions (Gopinath et al., 2021).

To date, comparisons among paired tumor/paracancerous tissues and saliva samples from the same OSCC patients have not been performed. In the current pilot study, we aimed to investigate the association between microbiota and the risk of developing OSCC, as well as to establish the connection between the changes in the microbiota in TT, normal paracancerous

tissue (NPT), and saliva (TS). Twenty-three patients with OSCC from Northern China were recruited, and the overall microbiota composition and abundance of specific bacterial taxa in TT, NPT, and TS were identified through 16S rRNA gene sequencing. Furthermore, phylogenetic investigation of communities by reconstruction of unobserved states (PICRUSt2) (Langille et al., 2013) was used to infer the underlying pathways associated with oral cancer. Our study will add new information on OSCC-associated oral microbiota from both saliva and cancer tissue, and provide a target for the diagnosis and treatment of OSCC.

MATERIALS AND METHODS

Subject Enrollment and Sample Collection

The subjects were recruited from 2018 to 2020 with the approval of the Chinese Clinical Trial Registry (ChiCTR2000032543). All participants were not administered any antibiotics 3 months before the study. Written informed consent was obtained from all participants before sample collection. In total, 23 patients with OSCC who had not undergone any treatment, including chemotherapy and/or radiotherapy were enrolled. TNM staging and data on age, sex, alcohol intake, cigarette smoking, oral hygiene, and periodontal status were assessed. Saliva samples were successfully collected from 19 out of the 23 OSCC patients before breakfast without stimulation. Furthermore, TT samples were dissected from the deep site of the tumor during surgery, and the diameter of each sample was larger than 3.0 mm. Concurrently, paired NPT samples harvested at least 2.0 cm away from the tumor edge were also obtained under aseptic conditions. Finally, saliva and tissue samples were aseptically transferred into a screw-cap vial and stored at −80°C immediately after collection.

To characterize the differences in the microbiota composition in different tissue and saliva samples, 65 samples were classified into three groups as follows: TT, NPT, and TS.

Genomic DNA Extraction, PCR, and 16S rRNA Gene Sequencing

Total genomic DNA was extracted using the TIANamp Swab DNA Kit (TIANGEN, Beijing, China) after TS samples were vortexed with glass beads and TT/NPT samples were liquid nitrogen-ground. To eliminate any contamination caused by blood stains on the surface of the sterile tissues, surface decontamination of the samples was achieved by washing with PBS. Amplification of the 16S rRNA gene V3–4 region was performed with primers 338F and 806R (Huse et al., 2007) using TransStart Fastpfu DNA Polymerase (TransGen, Beijing, China). Cycling conditions were as follows: denaturation at 95°C for 2 min; 20 cycles of 45 s at 95°C, 30 s at 55°C, and 30 s at 72°C; and extension at 72°C for 5 min. PCR amplification was performed for each sample in triplicate, and the samples were purified using the AxyPrep DNA Gel Extraction kit (Axygen Scientific Inc., Union City, CA, United States) and assessed via spectrophotometry (QuantiFluor-ST, Promega). Equivalent pooled 16S rRNA PCR amplicons were sequenced on an Illumina MiSeq instrument with 2 × 300 bp paired-end sequencing.

Bioinformatics and Statistical Analysis

Raw paired FASTQ files were imported into QIIME 2 (Bolyen et al., 2019), and the DADA2 plugin was used for further sequence quality control and chimera removal with default parameters. The merged high-quality sequences were used to produce amplicon sequence variants (ASVs) with 100% sequence identity. The taxonomic affiliation assignments were based on the Ribosomal Database Project (Cole et al., 2009) using default parameters (80% threshold). The representative sequence of each ASV was used as a query sequence to define species through BlastN against the Human Oral Microbiome Database (HOMD) RefSeq V15.22 (Escapa et al., 2018) and the online NCBI database with more than 99% identity and the highest total score.

Differences among the groups were assessed using analysis of similarities (ANOSIM). Microbiome functions were predicted using PICRUSt2 (Langille et al., 2013). Significant differences in taxa (species/ASVs, genus, and phylum) and microbiome functional profiles between TT, NPT, and TS groups were first

TABLE 1 | Clinical characteristics of SCC subjects participating in the study.

Characteristics	Patients (*n* = 23)	
	Tissues (23)	Saliva (19)
Age (years)	61.9 ± 12.3	62.7 ± 12.1
Sex		
Male	11	10
Female	12	9
Clinical stage		
I–II	15	13
III–IV	8	6
Tumor sites		
Tongue	6	6
Bucca	3	3
Gingiva	11	7
Mouth floor	3	3
Tumor Grade*		
Well-differentiated	6	5
Moderately differentiated	14	12
Poorly differentiated	3	2
Smoking status		
Never	17	13
Former	3	3
Current	3	3
Alcohol consumption		
Never	17	13
Former	1	1
Current	5	5
Oral hygiene		
Fair	11	9
Bad	12	10
Periodontitis status		
No or mild	13	11
Moderate or severe	10	8

**The criteria of clinical stage are based on the AJCC Cancer Staging Manual. Values were displayed as mean ± SD.*

determined by paired Wilcoxon signed-rank tests (Wilcoxon, 1946), and then the Benjamini–Hochberg false discovery rate (FDR) (Benjamini and Hochberg, 1995) was applied to adjust *p*-values for multiple tests in *R*. Significantly different features (FDR < 0.05) were further validated using linear discriminant analysis effect size (LEfSe) (Segata et al., 2011), and only features with an LDA score >2.0 were retained. The differences in taxa and microbiome functional profiles among different tumor sites and clinical stages were analyzed using LEfSe, and p values were adjusted using Benjamini–Hochberg FDR for multiple tests. The coefficient relationship between significantly changed taxa in different tumor sites or clinical stages and the corresponding microbial pathways of these groups were calculated using the Spearman correlation algorithm. The correlation parameters were set as coefficient >0.68 or <-0.68 and FDR < 0.05.

RESULTS

Bacterial Populations of Different Oral Sites in Oral Squamous Cell Carcinoma

We collected 65 samples from 23 patients, including 23 TT, 23 NPT, and 19 saliva samples from the patients (**Table 1**). A total of 4,414,145 (23,645–174,760) high-quality 16S rRNA genes were obtained via high-throughput DNA sequencing. To normalize the data and avoid statistical bias, 23,645 16S rRNA genes from each sample were chosen to produce ASVs. A total of 4,164 ASVs were obtained. Good's coverage was over 99.9% for each sample, suggesting that the sequencing depth was sufficient for microbiota investigation.

In patients with OSCC, the evenness (Simpsoneven index) of the TS group was significantly different from that of the TT and NPT groups (**Figures 1A–C** and **Supplementary Table 1**). Principal coordinates analysis showed that the TS groups were significantly separated from the other groups ($P_{ANOSIM} < 0.01$, **Figure 1D**).

A total of 22 phyla, 321 genera, and 869 species were identified in the oral samples, with the major taxa displayed in **Figure 2**. Firmicutes (27.93%), Proteobacteria (20.38%), Fusobacteria (19.67%), Bacteroidetes (17.73%), Campilobacterota (4.69%), Actinobacteria (4.17%), Spirochaetes (3.24%), and Candidatus Saccharibacteria (1.07%) were the eight major phyla identified in all samples ($>1\%$). A total of 21 major genera (proportion $>1\%$), such as *Fusobacterium* (15.99%), *Neisseria* (7.9%), *Streptococcus* (6.92%), *Porphyromonas* (5.66%), and *Haemophilus* (4.78%) were identified in the oral samples (**Supplementary Table 2**). Among these taxa, 12 phyla ($>99.71\%$ of all the samples), 115 genera ($>97.98\%$), and 420 species ($>97.49\%$) were consistently found in all samples.

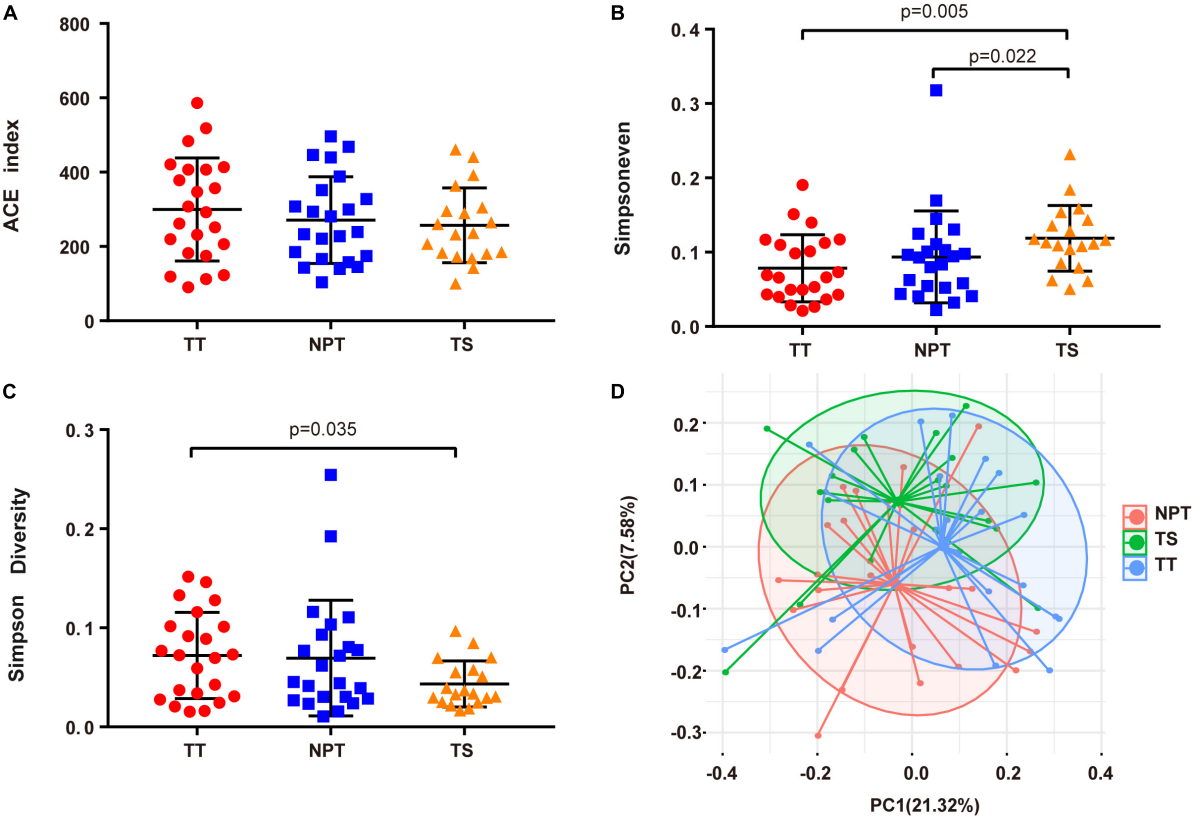


FIGURE 1 | Comparison of alpha and beta diversity in TT, NPT, and TS groups. **(A)** ACE index, **(B)** Simpsoneven, **(C)** Simpson diversity, and **(D)** Principal Coordinate Analysis (PCoA) based on weighted UniFrac distance metrics.

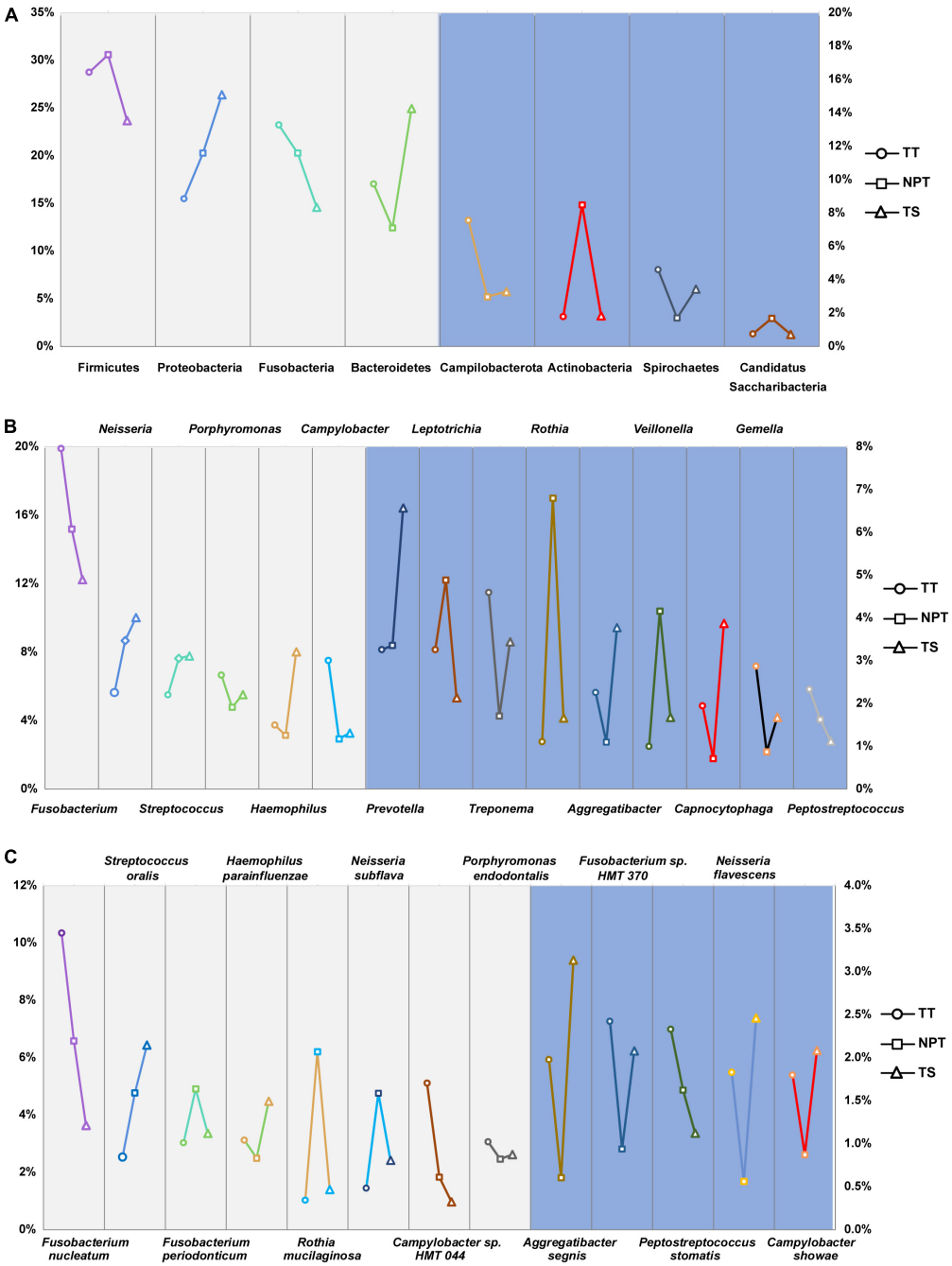


FIGURE 2 | The proportion of major phyla **(A)**, genera **(B)**, and species **(C)** in the TT, NPT, and TS of OSCC patients. The relative abundance of taxa labeled in light gray was indicated by the left ordinate, and that labeled in light blue was indicated by the right ordinate.

Bacterial Diversity Analysis of Tumor Tissue and Normal Paracancerous Tissue of Oral Squamous Cell Carcinoma Patients

The microbiota composition between TT (2,473 ASVs) and NPT (2,625 ASVs) from the same patients showed diversity (P_{ANOSIM} = 0.103, **Figure 1D**). The phylum Actinobacteria was significantly enriched in NPT, and the phylum Campilobacterota was significantly enriched in TT (**Figure 3**). The genera *Veillonella* and *Granulicatella* were highly enriched (proportion difference >0.5%) in NPT, and the genera *Campylobacter*, *Gemella*, *Filifactor*, and *Catonella* were highly enriched in TT (**Figure 2**). The species *Rothia mucilaginosa*, *G. adiacens*, *Streptococcus sanguinis*, and *Veillonella rogosae* were highly enriched (proportion difference >0.5%) in

NPT, and *Aggregatibacter segnis*, *Campylobacter showae*, and *G. morbillorum* were highly enriched in TT (**Figure 3**).

Changes in the composition of the bacterial community altered the microbial functional profile. Through PICRUSt2 analysis, we found that only two pathways (Bifidobacterium shunt and heterolactic fermentation) were significantly enriched in TT compared with NPT (FDR < 0.05, proportions ratio >2) (**Supplementary Table 3**).

Discrepancy Between the Tumor Tissue and Saliva Samples

The microbiota composition between the TT and TS of the same patient showed significant diversity ($P_{ANOSIM} < 0.01$, **Figure 1D**). The phyla Bacteroidetes and Proteobacteria were significantly enriched in TS samples (**Figure 4**). Four genera were highly enriched (proportion difference $>0.5\%$) in TS samples, and the genera *Filifactor* and *Peptostreptococcus* were highly enriched in TT (**Figure 4**). Nine species were highly enriched (proportion difference $>0.5\%$) in TS samples, including *Streptococcus oralis* and *Neisseria macacae*, and three species were enriched in TT (**Figure 4**), including *Neisseria flavescens*, *Fusobacterium naviforme*, and *S. stomatis*.

Thirty-seven and one pathways were separately enriched in TT and TS, respectively (FDR < 0.05, proportion ratio >2, **Supplementary Table 4**). Compared with TS, the function of aromatic compound degradation was highly enriched in TT, such as gallate degradation I (proportion ratio = 179).

Discrepancy Between the Normal Paracancerous Tissue and Saliva Samples

A comparison between NPT and TS samples also revealed significantly different taxa. Two phyla (Actinobacteria and Synergistetes), 6 genera, and 5 species were significantly enriched

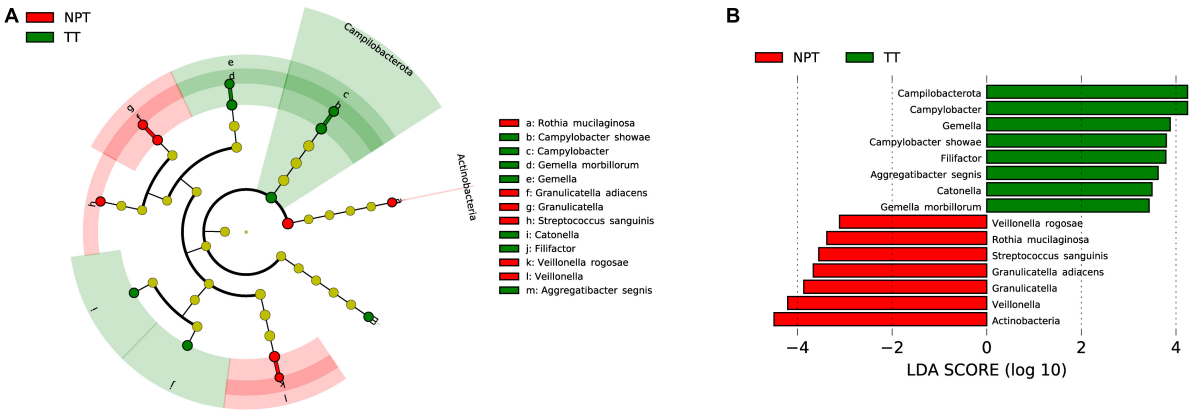


FIGURE 3 | Comparative taxonomic profile of TT and NPT groups. **(A)** The cladogram showed differently enriched taxa. **(B)** LDA scores computed for differentially abundant taxa between TT and NPT groups (Log10 LDA scores >2). The phyla, genera, and species with significant richness differences (FDR < 0.05) between the two groups are shown.

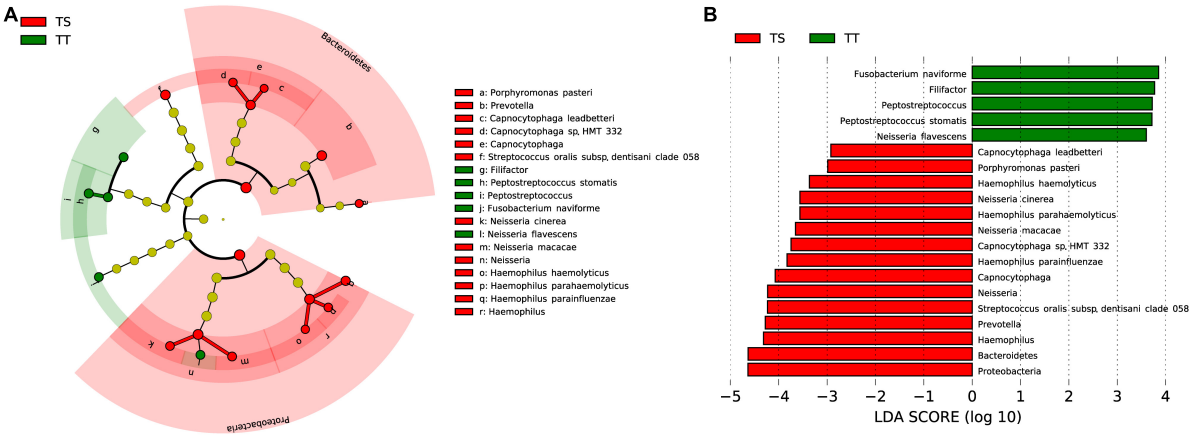


FIGURE 4 | Comparative taxonomic profile of TT and TS groups. **(A)** The cladogram showed differently enriched taxa. **(B)** LDA scores computed for differentially abundant taxa between TT and TS groups (Log10 LDA scores >2). The phyla, genera, and species with significant richness differences (FDR < 0.05) between the two groups are shown.

in NPT, while the phylum Bacteroidetes, 5 genera, and 13 species were significantly enriched in TS (**Figure 5**), including the three species highly enriched in TT relative to NPT.

Twenty-eight and two pathways were separately enriched in NPT and TS (FDR < 0.05, proportion ratio >2, **Supplementary Table 5**). Compared with TS, the function of amine and polyamine degradation was highly enriched in NPT, such as the superpathway of phenylethylamine degradation (proportion ratio = 343).

Microbiota Diversity Analysis of Tissues at Different Tumor Sites

All TT samples were collected from different sites involved in three types of oral mucosa, including the masticatory mucosa (gingiva), lining mucosa (bucca and mouth floor), and specialized mucosa (tongue). Four genera and 13 species were observed to be separately enriched in each of the three types of tumor mucosa (**Figure 6A**). *C. gingivalis, R, mucilaginosa*, and *P. intermedia* were significantly enriched in the lining mucosa, tongue, and gingiva, respectively. Although no significant differences were found in pathways among the three tumor sites, the correlation analysis of the pathway and species showed that the abundance changes of the three species were strongly related ($R > 0.68$) with seven different pathways (**Figure 6C** and **Supplementary Table 6**).

In addition, NPT samples from the three sites were more diverse, with two phyla (Actinobacteria and Synergistetes) and 10 genera and 16 species separately enriched in each of the three sites (**Figure 6B**). Most of these taxa were different from those observed in TT samples, indicating a different microenvironment between TTs and NPTs. The correlation analysis of the pathway and species showed that the abundance changes of the three species were strongly related ($R > 0.68$) with four different pathways (**Figure 6D** and **Supplementary Table 7**).

Microbiota Diversity Analysis of Oral Cancer Stage

We further analyzed the relationship between oral microbiota and the clinical stage (I–IV) of oral cancer. In the early tumor stage (I/II), both TT and NPT had higher abundances of *Treponema* sp. and *Leptotrichia* sp., while *Prevotella* sp. and *Capnocytophaga* sp. were enriched in TS (**Figures 7A–C**). In the late tumor stage (III/IV), *Solobacterium moorei* and *Slackia exigua* were separately enriched in TT and NPT, while *Campylobacter* sp. *HMT 044* was enriched in TS (**Figures 7A–C**). The correlation analysis showed that only six pathways were positively associated with five significantly changed species in different clinical stages (**Figures 7D,E** and **Supplementary Table 8**); for example, *S. moorei* was positively related to peptidoglycan biosynthesis V.

DISCUSSION

Oral cancer is a highly complex, multifactorial disease associated with the dysbiosis of the oral microbiota. A comprehensive study of the oral microbiota is essential for understanding

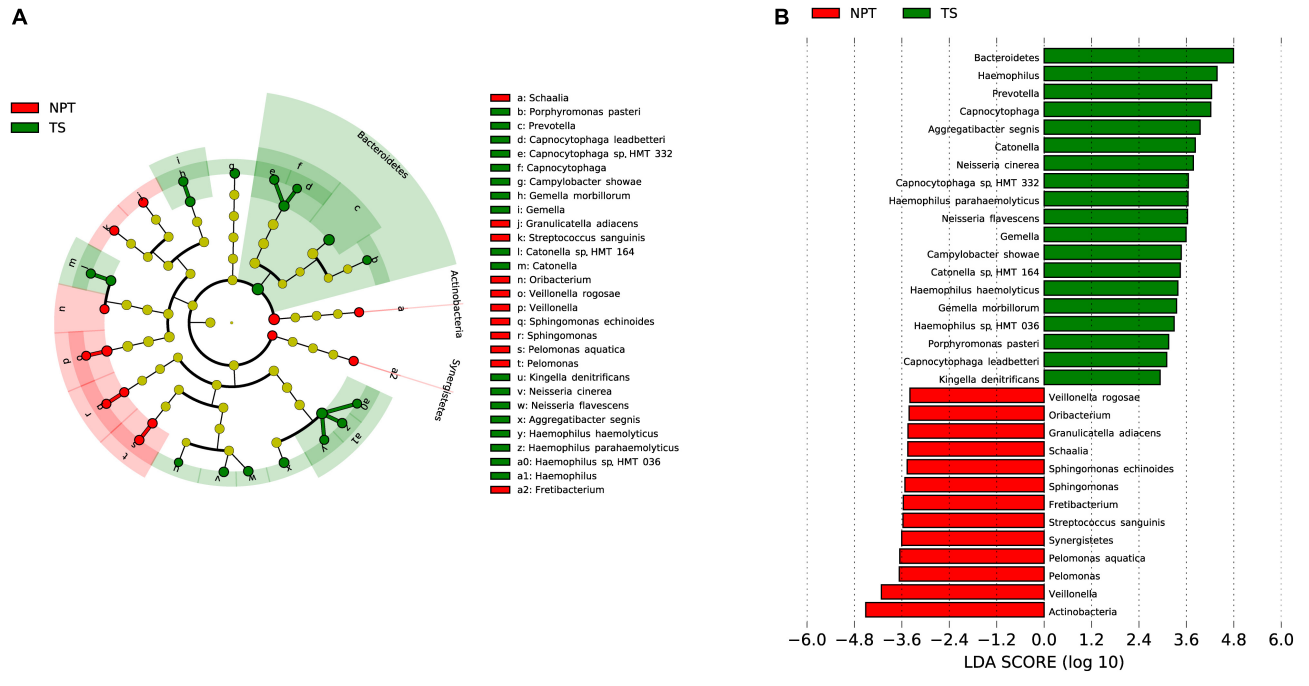


FIGURE 5 | Comparative taxonomic profile of NPT and TS groups. **(A)** The cladogram showed differently enriched taxa. **(B)** LDA scores computed for differentially abundant taxa between TT and TS groups (Log10 LDA scores >2). The phyla, genera, and species with significant richness differences (FDR < 0.05) between the two groups are shown.

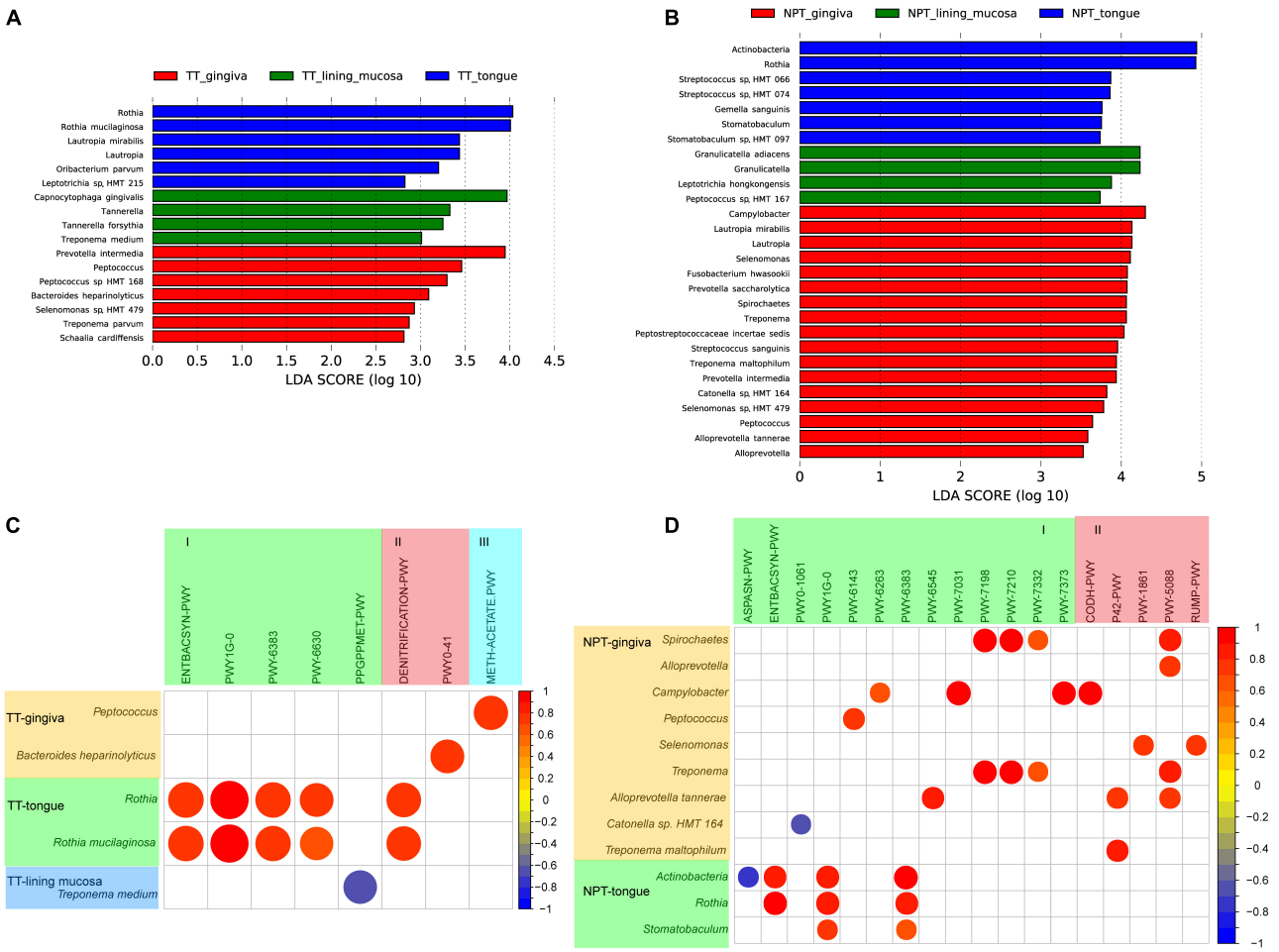


FIGURE 6 | Comparative taxonomic profile and association with pathways of different tumor sites of OSCC. **(A)** LDA scores computed for differentially abundant taxa of TT among the tumor sites (Log10 LDA scores >2). **(B)** LDA scores computed for differentially abundant taxa of NPT among the tumor sites (Log10 LDA scores >2). **(C)** Correlation coefficient among different taxa and minipaths of TT samples among the different tumor sites. **(D)** Correlation coefficient among different taxa and minipaths of NPT samples among the different tumor sites. I, biosynthesis; II, degradation/utilization/assimilation; III, generation of precursor metabolites and energy.

the pathogenesis of oral cancer. Previous studies have shown higher alpha diversity in saliva (Takahashi et al., 2019) and tissue biopsy samples (Zhang L. et al., 2019) of patients with oral cancer than that in healthy controls, and a recent study reported that TT has significantly lower richness and diversity than TS in patients with oral cancer (Zhang Z. et al., 2019). Here, we explored the oral microbiota composition of paired tumor/paracancerous tissues and saliva samples from patients with OSCC. Beta diversity analysis revealed a significant difference among TT, NPT, and TS samples, indicating that oral microbiota dysbiosis might be involved in the progression of OSCC (**Figure 1**).

Upon microbiota composition assessment between paired TT and NPT samples, in contrast with previous studies that reported increased Firmicutes abundance in TT compared to NPT (48 vs. 40%, respectively; $p = 0.004$) (Mukherjee et al., 2017), we did not find a significant change in the abundance of Firmicutes. The abundance of Actinobacteria was markedly decreased in TT (1.78% in TT vs. 8.48% in NPT, FDR < 0.01), coinciding with a previous report that the abundance of Actinobacteria decreased significantly with cancer progression (Yang et al., 2018), whereas the abundance of Campilobacterota was significantly increased in NPT (2.98% in NPT vs. 7.56% in TT, FDR < 0.05). At the species level, *R. mucilaginosa, F. periodonticum*, and *S. oralis* were among the most abundant taxa in the NPT, which is consistent with previous findings (Hooper et al., 2007; Moritani et al., 2015; Zhao et al., 2017). Furthermore, we identified *A. segnis*, *C. showae*, and *G. morbillorum* as significantly overrepresented species in both TT and TS (**Figures 2**, **3**, **5**). *A. segnis* is part of the oral microbiota, particularly in dental plaque (Norskov-Lauritsen and Kilian, 2006), and the aggregative nature of the pathogen in genus *Aggregatibacter* is crucial to its involvement in human disease (Norskov-Lauritsen et al., 2019). *C. showae*, a commensal species of the human oral cavity, has been associated with periodontitis (Lugonja et al., 2016), Crohn's disease (Zhang et al., 2009), and colorectal

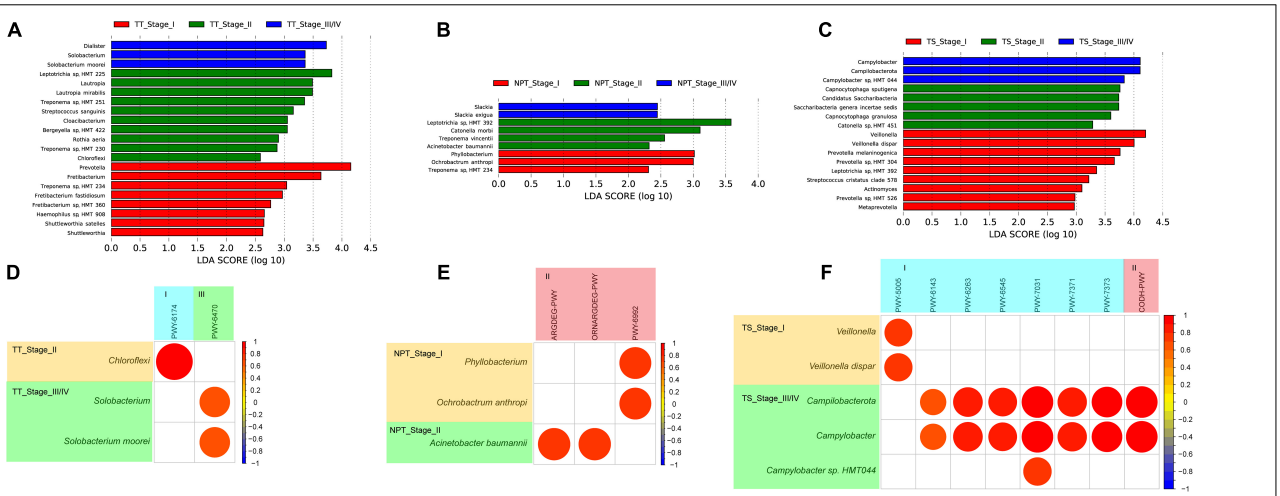


FIGURE 7 | LDA scores computed for differentially abundant taxa among different clinical stages of TT **(A)**, NPT **(B)**, and TS **(C)** samples, and correlation coefficient among different species and minipaths in different clinical stages of TT **(D)**, NPT **(E)**, and TS **(F)** samples. I, biosynthesis; II, degradation/utilization/assimilation; III, generation of precursor metabolites and energy.

cancer (Warren et al., 2013). *G. morbillorum* has been found to be relevant to the progression of periodontitis (Ai et al., 2017) and is highly associated with tumor site in patients with OSCC (Pushalkar et al., 2012). Therefore, these relatively abundant species may act as triggers for tumor initiation and progression.

Because the transient fluidity of surface TS differs from the stable environment of deep TT, the existing enriched oral microbiota could be distinguished in a site-specific manner. Interestingly, the comparison between TT and TS samples from the same patient revealed distinct microbial patterns associated with OSCC. We noted that the abundance of Proteobacteria (15.49% in TT vs. 26.40% in TS, FDR < 0.01) and Bacteroidetes (17.05% in TT vs. 24.95% in TS, FDR < 0.01) was remarkably higher in TS samples (**Figure 4**). Consistent with previous findings (Li et al., 2020), *Peptostreptococcus* and *Filifactor* were enriched in TT samples. At the species level, we confirmed that *F. naviforme*, *P. stomatis*, and *N. flavescens* were significantly enriched in TT. *F. naviforme* is known to be associated with the development and progression of OSCC (Fujiwara et al., 2020). Two reports have indicated that the abundance of *P. stomatis* is significantly higher in TT than in NPT (Pushalkar et al., 2012; Zhang L. et al., 2019). Additionally, nine species were observed in relatively higher proportions in TS samples, including *Neisseria cinerea* and *N. macacae*. As a high producer of the carcinogen acetaldehyde, a high abundance of *Neisseria* species in the saliva of patients with OSCC might play an important role in alcohol-related carcinogenesis (Muto et al., 2000). These findings indicate that unique pathogenic bacteria prefer inhabiting the inside/surrounding tumor sites, where the environment is different from the oral cavity.

The microbiota of different tumor sites in OSCC patients showed a homogenous population at a certain phylogenetic distance. Regarding the relative abundance of taxa, Zhang Z. et al. (2019) recently reported a greater abundance of *Prevotella*, *Acinetobacter*, *Pseudomonas*, and *Fusobacterium* in the tongue, oropharynx, gingiva, and bucca of patients with oral cancer. Here, our results revealed that in TTs, *Lautropia* and *Rothia* were enriched in the tongue, while *Peptococcus* and *Tannerella* were separately enriched in the gingiva and lining mucosa (**Figure 6A**). In NPTs, *Rothia* was enriched in the tongue, and *Lautropia* and *Peptococcus* were enriched in the gingiva (**Figure 6B**). The level of *P. intermedia* in the gingiva was significantly higher than that in the tongue and lining mucosa. As a periodontitis-related pathogen, *P. intermedia* is associated with an increased OSCC risk (Hsiao et al., 2018) and can release nuclease-degrading neutrophil extracellular traps (Doke et al., 2017). Increased abundance of *R. mucilaginosa* has been observed in oral leukoplakias from the tongue (Amer et al., 2017), and *R. mucilaginosa* can produce acetaldehyde comparable to that produced by *Neisseria mucosa* (Amer et al., 2020). *C. gingivalis* is thought to play an essential role in carcinogenesis (Karpinski, 2019) and may be a diagnostic indicator of OSCC (Mager et al., 2005). These findings indicate that the specific distribution of cancer-associated microbiota at different sites may be associated with the subsequent risk of OSCC.

The microbiota composition shown in the present study revealed differentially enriched species in TT, NPT, and TS samples of different OSCC stages (**Figure 7**). From the early stage to the late stage, the relative abundance of *S. moorei* in TT was significantly increased, and it is known to produce hydrogen sulfide and be associated with oral halitosis (Haraszthy et al., 2008). In addition, it is positively related to the pathway conferring pathogen beta-lactam resistance (**Supplementary Table 8**). We found that the relative abundances of *Veillonella dispar*, *Catonella morbi*, and *Leptotrichia* sp. *HMT 392* in both TT and TS microbiota were negatively correlated with the progression of OSCC, and that of *Campylobacter* sp. *HMT 044* was positively correlated. These differentially enriched species may be used as new biomarkers to predict OSCC progression.

At very low colonization levels, *P. gingivalis* can induce changes in oral commensal microbiota leading to periodontitis (Hajishengallis et al., 2011), which supports the "keystone pathogen" hypothesis (Hajishengallis et al., 2012). Therefore, we postulated that some low-abundance oral bacteria might also contribute to OSCC, although no significant changes were observed in the present study. To evaluate the possible functional changes caused by these low-abundance bacteria, we analyzed the functional relationship between species and pathways and found a correlation between 11 microbial species and 17 pathway abundances (**Supplementary Tables 6–8**). Since oral bacteria can interact through multiple pathways (Lamont et al., 2018), we postulated that significantly changed pathways, such as heterolactic fermentation, etc. (**Supplementary Tables 3–5**), might affect the growth of certain bacteria and lead to oral microbiota dysbiosis, thus finally inducing OSCC.

CONCLUSION

In conclusion, the comparison analysis revealed that microbiota colonizing TT, NPT, and TS samples showed significant differences. The genus *Filifactor* and *Peptostreptococcus* showed the highest abundance in TT and the lowest abundance in TS samples, whereas *Neisseria* showed the opposite trend. At the species level, the abundance of *P. stomatis* decreased in the order of TT, NPT, and TS, while that of *S. oralis*, *N. macacae*, and *Capnocytophaga* sp. *HMT 332* increased in the same order. In addition, microbial communities showed variations in different tumor sites and clinical stages. The abundance of *P. intermedia* was profoundly higher in gingival tumor sites, whereas *C. gingivalis* and *R. mucilaginosa* were enriched in the lining mucosa and tongue. *S. moorei* in TT and *Campylobacter* sp. *strain HMT 044* in TS were positively correlated with the progression of OSCC. All these newly identified bacteria in the tissue surface or tumor microenvironment might be used as biomarkers to predict OSCC.

DATA AVAILABILITY STATEMENT

All the data generated or analyzed during this study are included in this published article and its **Supplementary Material**. The sequencing data from this study have been deposited in the National Omics Data Encyclopedia (NODE, https://www.biosino.org/node/index) under accession number OEX003132.

ETHICS STATEMENT

The studies involving human participants were reviewed and approved by the Chinese Clinical Trial Registry (ChiCTR2000032543). The patients/participants provided their written informed consent to participate in this study.

AUTHOR CONTRIBUTIONS

TZ and HZ designed the study. KY, SZ, DZ, LH, and TZ collected all the saliva and tissue samples. YW and HZ performed the measurements and data analysis. KY, TZ, and HZ wrote and edited the manuscript. All authors read and approved the final manuscript.

FUNDING

This work was supported by the Natural Science Foundation (Grant Nos. ZR2016HQ25 and ZR2017BH069), Medical and Health Science and Technology Development project (Grant No. 2017WS097), and the Study Abroad Program (Grant No. 201803053) of Shandong Province.

ACKNOWLEDGMENTS

We would like to highly appreciate the help of Huijun Xie of Shandong University on the initiation of this research.

SUPPLEMENTARY MATERIAL

The Supplementary Material for this article can be found online at: https://www.frontiersin.org/articles/10.3389/fmicb.2021.719601/full#supplementary-material

Supplementary Table 1 | The microbiota diversity evaluations of all groups.

Supplementary Table 2 | Major abundant genera of all groups.

Supplementary Table 3 | The different pathways between TT and NPT of OSCC patients.

Supplementary Table 4 | The different pathways between TT and TS of OSCC patients.

Supplementary Table 5 | The different pathways between NPT and TS of OSCC patients.

Supplementary Table 6 | The correlation between significantly enriched TT species in different tumor sites and predicted microbial pathway (FDR < 0.05 and $R > 0.68$).

Supplementary Table 7 | The correlation between significantly enriched NPT species in TT of different tumor grades and predicted microbial pathways (FDR < 0.05 and $R > 0.68$).

Supplementary Table 8 | The correlation between significantly enriched species of different tumor clinical stages and predicted microbial pathways (FDR < 0.05 and $R > 0.68$).

REFERENCES

Ai, D., Huang, R., Wen, J., Li, C., Zhu, J., and Xia, L. C. (2017). Integrated metagenomic data analysis demonstrates that a loss of diversity in oral microbiota is associated with periodontitis. *BMC Genomics* 18:1041. doi: 10.1186/s12864-016-3254-5

Al-Hebshi, N. N., Nasher, A. T., Maryoud, M. Y., Homeida, H. E., Chen, T., Idris, A. M., et al. (2017). Inflammatory bacteriome featuring *Fusobacterium*

nucleatum and *Pseudomonas aeruginosa* identified in association with oral squamous cell carcinoma. *Sci. Rep.* 7:1834.

Amer, A., Galvin, S., Healy, C. M., and Moran, G. P. (2017). The Microbiome of Potentially Malignant Oral Leukoplakia Exhibits Enrichment for Fusobacterium, Leptotrichia, Campylobacter, and Rothia Species. *Front. Microbiol.* 8:2391. doi: 10.3389/fmicb.2017.02391

Amer, A., Whelan, A., Al-Hebshi, N. N., Healy, C. M., and Moran, G. P. (2020). Acetaldehyde production by Rothia mucilaginosa isolates from patients with oral leukoplakia. *J. Oral Microbiol.* 12:1743066. doi: 10.1080/20002297.2020.1743066

Amieva, M., and Peek, R. M. Jr. (2016). Pathobiology of *Helicobacter pylori*-Induced Gastric Cancer. *Gastroenterology* 150, 64–78. doi: 10.1053/j.gastro.2015.09.004

Benjamini, Y., and Hochberg, Y. (1995). Controlling the False Discovery Rate: a Practical and Powerful Approach to Multiple Testing. *J. R. Stat. Soc. Series B Stat. Methodol.* 57, 289–300. doi: 10.1111/j.2517-6161.1995.tb02031.x

Bolyen, E., Rideout, J. R., Dillon, M. R., Bokulich, N. A., Abnet, C. C., Al-Ghalith, G. A., et al. (2019). Reproducible, interactive, scalable and extensible microbiome data science using QIIME 2. *Nat. Biotechnol.* 37, 852–857.

Bray, F., Ferlay, J., Soerjomataram, I., Siegel, R. L., Torre, L. A., and Jemal, A. (2018). Global cancer statistics 2018: GLOBOCAN estimates of incidence and mortality worldwide for 36 cancers in 185 countries. *CA Cancer J. Clin.* 68, 394–424. doi: 10.3322/caac.21492

Chang, C., Geng, F., Shi, X., Li, Y., Zhang, X., Zhao, X., et al. (2019). The prevalence rate of periodontal pathogens and its association with oral squamous cell carcinoma. *Appl. Microbiol. Biotechnol.* 103, 1393–1404. doi: 10.1007/s00253-018-9475-6

Cole, J. R., Wang, Q., Cardenas, E., Fish, J., Chai, B., Farris, R. J., et al. (2009). The Ribosomal Database Project: improved alignments and new tools for rRNA analysis. *Nucleic Acids Res.* 37, D141–D145.

Doke, M., Fukamachi, H., Morisaki, H., Arimoto, T., Kataoka, H., and Kuwata, H. (2017). Nucleases from Prevotella intermedia can degrade neutrophil extracellular traps. *Mol. Oral Microbiol.* 32, 288–300. doi: 10.1111/omi.12171

Escapa, I. F., Chen, T., Huang, Y., Gajare, P., Dewhirst, F. E., and Lemon, K. P. (2018). New Insights into Human Nostril Microbiome from the Expanded Human Oral Microbiome Database (eHOMD): a Resource for the Microbiome of the Human Aerodigestive Tract. *mSystems* 3, e00187–18.

Fujiwara, N., Kitamura, N., Yoshida, K., Yamamoto, T., Ozaki, K., and Kudo, Y. (2020). Involvement of Fusobacterium Species in Oral Cancer Progression: a Literature Review Including Other Types of Cancer. *Int. J. Mol. Sci.* 21:6207. doi: 10.3390/ijms21176207

Gopinath, D., Menon, R. K., Wie, C. C., Banerjee, M., Panda, S., Mandal, D., et al. (2021). Differences in the bacteriome of swab, saliva, and tissue biopsies in oral cancer. *Sci. Rep.* 11:1181.

Guerrero-Preston, R., Godoy-Vitorino, F., Jedlicka, A., Rodriguez-Hilario, A., Gonzalez, H., Bondy, J., et al. (2016). 16S rRNA amplicon sequencing identifies microbiota associated with oral cancer, human papilloma virus infection and surgical treatment. *Oncotarget* 7, 51320–51334. doi: 10.18632/oncotarget.9710

Hajishengallis, G., Darveau, R. P., and Curtis, M. A. (2012). The keystone-pathogen hypothesis. *Nat. Rev. Microbiol.* 10, 717–725. doi: 10.1038/nrmicro2873

Hajishengallis, G., Liang, S., Payne, M. A., Hashim, A., Jotwani, R., Eskan, M. A., et al. (2011). Low-abundance biofilm species orchestrates inflammatory periodontal disease through the commensal microbiota and complement. *Cell Host Microbe* 10, 497–506.

Haraszthy, V. I., Gerber, D., Clark, B., Moses, P., Parker, C., Sreenivasan, P. K., et al. (2008). Characterization and prevalence of Solobacterium moorei associated with oral halitosis. *J. Breath Res.* 2:017002. doi: 10.1088/1752-7155/2/1/017002

Healy, C. M., and Moran, G. P. (2019). The microbiome and oral cancer: more questions than answers. *Oral Oncol.* 89, 30–33. doi: 10.1016/j.oraloncology.2018.12.003

Hooper, S. J., Crean, S. J., Fardy, M. J., Lewis, M. A. O., Spratt, D. A., Wade, W. G., et al. (2007). A molecular analysis of the bacteria present within oral squamous cell carcinoma. *J. Med. Microbiol.* 56, 1651–1659. doi: 10.1099/jmm.0.46918-0

Hsiao, J. R., Chang, C. C., Lee, W. T., Huang, C. C., Ou, C. Y., Tsai, S. T., et al. (2018). The interplay between oral microbiome, lifestyle factors and genetic polymorphisms in the risk of oral squamous cell carcinoma. *Carcinogenesis* 39, 778–787.

Huse, S. M., Huber, J. A., Morrison, H. G., Sogin, M. L., and Welch, D. M. (2007). Accuracy and quality of massively parallel DNA pyrosequencing. *Genome Biol.* 8:R143.

Karpinski, T. M. (2019). Role of Oral Microbiota in Cancer Development. *Microorganisms* 7:20. doi: 10.3390/microorganisms7010020

Katz, J., Onate, M. D., Pauley, K. M., Bhattacharyya, I., and Cha, S. (2011). Presence of Porphyromonas gingivalis in gingival squamous cell carcinoma. *Int. J. Oral Sci.* 3, 209–215.

Lamont, R. J., Koo, H., and Hajishengallis, G. (2018). The oral microbiota: dynamic communities and host interactions. *Nat. Rev. Microbiol.* 16, 745–759. doi: 10.1038/s41579-018-0089-x

Langille, M. G., Zaneveld, J., Caporaso, J. G., Mcdonald, D., Knights, D., Reyes, J. A., et al. (2013). Predictive functional profiling of microbial communities using 16S rRNA marker gene sequences. *Nat. Biotechnol.* 31, 814–821. doi: 10.1038/nbt.2676

Lee, W. H., Chen, H. M., Yang, S. F., Liang, C., Peng, C. Y., Lin, F. M., et al. (2017). Bacterial alterations in salivary microbiota and their association in oral cancer. *Sci. Rep.* 7:16540.

Li, Y., Tan, X., Zhao, X., Xu, Z., Dai, W., Duan, W., et al. (2020). Composition and function of oral microbiota between gingival squamous cell carcinoma and periodontitis. *Oral Oncol.* 107:104710. doi: 10.1016/j.oraloncology.2020.104710

Lugonja, B., Yeo, L., Milward, M. R., Smith, D., Dietrich, T., Chapple, I. L., et al. (2016). Periodontitis prevalence and serum antibody reactivity to periodontal bacteria in primary Sjogren's syndrome: a pilot study. *J. Clin. Periodontol.* 43, 26–33. doi: 10.1111/jcpe.12485

Mager, D. L., Haffajee, A. D., Devlin, P. M., Norris, C. M., Posner, M. R., and Goodson, J. M. (2005). The salivary microbiota as a diagnostic indicator of oral cancer: a descriptive, non-randomized study of cancer-free and oral squamous cell carcinoma subjects. *J. Transl. Med.* 3:27.

Mascitti, M., Togni, L., Troiano, G., Caponio, V. C. A., Gissi, D. B., Montebugnoli, L., et al. (2019). Beyond Head and Neck Cancer: the Relationship Between Oral Microbiota and Tumour Development in Distant Organs. *Front. Cell. Infect. Microbiol.* 9:232. doi: 10.3389/fcimb.2019.00232

Moritani, K., Takeshita, T., Shibata, Y., Ninomiya, T., Kiyohara, Y., and Yamashita, Y. (2015). Acetaldehyde production by major oral microbes. *Oral Dis.* 21, 748–754. doi: 10.1111/odi.12341

Mukherjee, P. K., Wang, H., Retuerto, M., Zhang, H., Burkey, B., Ghannoum, M. A., et al. (2017). Bacteriome and mycobiome associations in oral tongue cancer. *Oncotarget* 8, 97273–97289. doi: 10.18632/oncotarget.21921

Muto, M., Hitomi, Y., Ohtsu, A., Shimada, H., Kashiwase, Y., Sasaki, H., et al. (2000). Acetaldehyde production by non-pathogenic Neisseria in human oral microflora: implications for carcinogenesis in upper aerodigestive tract. *Int. J. Cancer* 88, 342–350. doi: 10.1002/1097-0215(20001101)88:3<342::aid-ijc4>3.0.co;2-i

Nagy, K. N., Sonkodi, I., Szoke, I., Nagy, E., and Newman, H. N. (1998). The microflora associated with human oral carcinomas. *Oral Oncol.* 34, 304–308. doi: 10.1016/s1368-8375(98)80012-2

Norskov-Lauritsen, N., Claesson, R., Birkeholm Jensen, A., Aberg, C. H., and Haubek, D. (2019). Aggregatibacter Actinomycetemcomitans: clinical Significance of a Pathobiont Subjected to Ample Changes in Classification and Nomenclature. *Pathogens* 8:243. doi: 10.3390/pathogens8040243

Norskov-Lauritsen, N., and Kilian, M. (2006). Reclassification of Actinobacillus actinomycetemcomitans, Haemophilus aphrophilus, Haemophilus paraphrophilus and Haemophilus segnis as Aggregatibacter actinomycetemcomitans gen. nov., comb. nov., Aggregatibacter aphrophilus comb. nov. and Aggregatibacter segnis comb. nov., and emended description of Aggregatibacter aphrophilus to include V factor-dependent and V factor-independent isolates. *Int. J. Syst. Evol. Microbiol.* 56, 2135–2146. doi: 10.1099/ijs.0.64207-0

Pushalkar, S., Ji, X., Li, Y., Estilo, C., Yegnanarayana, R., Singh, B., et al. (2012). Comparison of oral microbiota in tumor and non-tumor tissues of patients with oral squamous cell carcinoma. *BMC Microbiol.* 12:144. doi: 10.1186/1471-2180-12-144

Sami, A., Elimairi, I., Stanton, C., Ross, R. P., and Ryan, C. A. (2020). The Role of the Microbiome in Oral Squamous Cell Carcinoma with Insight into the Microbiome-Treatment Axis. *Int. J. Mol. Sci.* 21:8061. doi: 10.3390/ijms21218061

Sasaki, M., Yamaura, C., Ohara-Nemoto, Y., Tajika, S., Kodama, Y., Ohya, T., et al. (2005). Streptococcus anginosus infection in oral cancer and its infection route. *Oral Dis.* 11, 151–156. doi: 10.1111/j.1601-0825.2005.01051.x

Segata, N., Izard, J., Waldron, L., Gevers, D., Miropolsky, L., Garrett, W. S., et al. (2011). Metagenomic biomarker discovery and explanation. *Genome Biol.* 12:R60.

Siegel, R. L., Miller, K. D., and Jemal, A. (2020). Cancer statistics, 2020. *CA Cancer J. Clin.* 70, 7–30.

Takahashi, Y., Park, J., Hosomi, K., Yamada, T., Kobayashi, A., Yamaguchi, Y., et al. (2019). Analysis of oral microbiota in Japanese oral cancer patients using 16S rRNA sequencing. *J. Oral Biosci.* 61, 120–128. doi: 10.1016/j.job.2019.03.003

Warren, R. L., Freeman, D. J., Pleasance, S., Watson, P., Moore, R. A., Cochrane, K., et al. (2013). Co-occurrence of anaerobic bacteria in colorectal carcinomas. *Microbiome* 1:16.

Whitmore, S. E., and Lamont, R. J. (2014). Oral bacteria and cancer. *PLoS Pathog.* 10:e1003933. doi: 10.1371/journal.ppat.1003933

Wilcoxon, F. (1946). Individual comparisons of grouped data by ranking methods. *J. Econ. Entomol.* 39:269. doi: 10.1093/jee/39.2.269

Yang, C. Y., Yeh, Y. M., Yu, H. Y., Chin, C. Y., Hsu, C. W., Liu, H., et al. (2018). Oral Microbiota Community Dynamics Associated With Oral Squamous Cell Carcinoma Staging. *Front. Microbiol.* 9:862. doi: 10.3389/fmicb.2018.00862

Zhang, L., Liu, Y., Zheng, H. J., and Zhang, C. P. (2019). The Oral Microbiota May Have Influence on Oral Cancer. *Front. Cell. Infect. Microbiol.* 9:476. doi: 10.3389/fcimb.2019.00476

Zhang, W. L., Wang, S. S., Wang, H. F., Tang, Y. J., Tang, Y. L., and Liang, X. H. (2019). Who is who in oral cancer?. *Exp. Cell Res.* 384:111634.

Zhang, Z., Yang, J., Feng, Q., Chen, B., Li, M., Liang, C., et al. (2019). Compositional and Functional Analysis of the Microbiome in Tissue and Saliva of Oral Squamous Cell Carcinoma. *Front. Microbiol.* 10:1439. doi: 10.3389/fmicb.2019.01439

Zhang, L., Man, S. M., Day, A. S., Leach, S. T., Lemberg, D. A., Dutt, S., et al. (2009). Detection and isolation of Campylobacter species other than C. jejuni from children with Crohn's disease. *J. Clin. Microbiol.* 47, 453–455. doi: 10.1128/jcm.01949-08

Zhang, Y., Wang, X., Li, H., Ni, C., Du, Z., and Yan, F. (2018). Human oral microbiota and its modulation for oral health. *Biomed. Pharmacother.* 99, 883–893. doi: 10.1016/j.biopha.2018.01.146

Zhao, H., Chu, M., Huang, Z., Yang, X., Ran, S., Hu, B., et al. (2017). Variations in oral microbiota associated with oral cancer. *Sci. Rep.* 7:11773.

Conflict of Interest: The authors declare that the research was conducted in the absence of any commercial or financial relationships that could be construed as a potential conflict of interest.

Publisher's Note: All claims expressed in this article are solely those of the authors and do not necessarily represent those of their affiliated organizations, or those of the publisher, the editors and the reviewers. Any product that may be evaluated in this article, or claim that may be made by its manufacturer, is not guaranteed or endorsed by the publisher.

Copyright © 2021 Yang, Wang, Zhang, Zhang, Hu, Zhao and Zheng. This is an open-access article distributed under the terms of the Creative Commons Attribution License (CC BY). The use, distribution or reproduction in other forums is permitted, provided the original author(s) and the copyright owner(s) are credited and that the original publication in this journal is cited, in accordance with accepted academic practice. No use, distribution or reproduction is permitted which does not comply with these terms.

frontiers in Microbiology

ORIGINAL RESEARCH
published: 14 October 2021
doi: 10.3389/fmicb.2021.738047

Induction of Apoptotic Cell Death by Oral Streptococci in Human Periodontal Ligament Cells

Ok-Jin Park[1†], A Reum Kim[1†], Yoon Ju So[1], Jintaek Im[1], Hyun Jung Ji[2], Ki Bum Ahn[2], Ho Seong Seo[2], Cheol-Heui Yun[3,4] and Seung Hyun Han[1]*

[1]*Department of Oral Microbiology and Immunology and Dental Research Institute, School of Dentistry, Seoul National University, Seoul, South Korea,* [2]*Research Division for Radiation Science, Korea Atomic Energy Research Institute, Jeongeup, South Korea,* [3]*Department of Agricultural Biotechnology, Research Institute of Agriculture and Life Sciences, Seoul National University, Seoul, South Korea,* [4]*Institute of Green Bio Science and Technology, Seoul National University, Pyeongchang, South Korea*

OPEN ACCESS

Edited by:
Alina Maria Holban, University of Bucharest, Romania

Reviewed by:
Guya Diletta Marconi, University of Studies G. d'Annunzio Chieti and Pescara, Italy
Jens Kreth, Oregon Health and Science University, United States

***Correspondence:**
Seung Hyun Han
shhan-mi@snu.ac.kr

†These authors have contributed equally to this work and share first authorship

Specialty section:
This article was submitted to Microbial Immunology, a section of the journal Frontiers in Microbiology

Received: *08 July 2021*
Accepted: *16 September 2021*
Published: *14 October 2021*

Citation:
Park O-J, Kim AR, So YJ, Im J, Ji HJ, Ahn KB, Seo HS, Yun C-H and Han SH (2021) Induction of Apoptotic Cell Death by Oral Streptococci in Human Periodontal Ligament Cells. Front. Microbiol. 12:738047. doi: 10.3389/fmicb.2021.738047

Initiation and progression of oral infectious diseases are associated with streptococcal species. Bacterial infection induces inflammatory responses together with reactive oxygen species (ROS), often causing cell death and tissue damage in the host. In the present study, we investigated the effects of oral streptococci on cytotoxicity and ROS production in human periodontal ligament (PDL) cells. *Streptococcus gordonii* showed cell cytotoxicity in a dose- and time-dependent manner. The cytotoxicity might be due to apoptosis since *S. gordonii* increased annexin V-positive cells, and the cytotoxicity was reduced by an apoptosis inhibitor, Z-VAD-FMK. Other oral streptococci such as *Streptococcus mitis*, *Streptococcus sanguinis*, and *Streptococcus sobrinus* also induced apoptosis, whereas *Streptococcus mutans* did not. All streptococci tested except *S. mutans* triggered ROS production in human PDL cells. Interestingly, however, streptococci-induced apoptosis appears to be ROS-independent, as the cell death induced by *S. gordonii* was not recovered by the ROS inhibitor, resveratrol or *n*-acetylcysteine. Instead, hydrogen peroxide (H_2O_2) appears to be important for the cytotoxic effects of streptococci since most oral streptococci except *S. mutans* generated H_2O_2, and the cytotoxicity was dramatically reduced by catalase. Furthermore, streptococcal lipoproteins are involved in cytotoxicity, as we observed that cytotoxicity induced by the lipoprotein-deficient *S. gordonii* mutant was less potent than that by the wild-type and was attenuated by anti-TLR2-neutralizing antibody. Indeed, lipoproteins purified from *S. gordonii* alone were sufficient to induce cytotoxicity. Notably, *S. gordonii* lipoproteins did not induce H_2O_2 or ROS but cooperatively induced cell death when co-treated with H_2O_2. Taken together, these results suggest that most oral streptococci except *S. mutans* efficiently induce damage to human PDL cells by inducing apoptotic cell death with bacterial H_2O_2 and lipoproteins, which might contribute to the progression of oral infectious diseases such as apical periodontitis.

Keywords: apoptosis, streptococcal species, human periodontal ligament cells, hydrogen peroxide, lipoproteins, reactive oxygen species

INTRODUCTION

Streptococci are commensal Gram-positive aerobic bacteria found in human body such as skin, oral cavity, and intestine (Abranches et al., 2018). At the same time, they can act as opportunistic pathogens causing infectious diseases such as apical periodontitis, pneumonia, sepsis, and skin infections (Parks et al., 2015). Among them, oral streptococci including *S. gordonii*, *S. mutans*, *S. mitis*, and *S. sanguinis* are commonly found in the human oral cavity (Abranches et al., 2018). They have been demonstrated to cause systemic diseases such as bacteremia, sepsis, and infective endocarditis (Park et al., 2020). Oral streptococci, as early colonizers of the oral cavity, have been isolated from infected root canals of patients with apical periodontitis (Chavez de Paz et al., 2005) and are known to cause inflammation and tissue destruction in periapical lesions (Kutlu et al., 2003). Metagenomic analysis showed that *Streptococcus* is a predominant genus in patients with gingivitis (Park et al., 2015). Oral streptococci have been shown to induce macrophage cell death through hydrogen peroxide (H_2O_2) production (Okahashi et al., 2013). We previously reported that *S. gordonii* efficiently produces nitric oxide and proinflammatory cytokines in macrophages and induces bone destruction by stimulating osteoclastogenesis while inhibiting osteoblastogenesis (Kim et al., 2017b, 2018; Park et al., 2019).

Bacterial infections in the oral cavity induce inflammatory responses that often cause destruction of tissues such as the periodontal ligament (PDL), pulp, and alveolar bone (Cekici et al., 2014). The PDL, a type of connective tissue between teeth and alveolar bone, includes fibroblasts (the most predominant cells), epithelial cells, and osteoblasts (Jonsson et al., 2011). It is well known that PDL cells interact with bacteria in the periodontal pocket and periapical lesions and are associated with inflammatory responses (Cekici et al., 2014). For example, periodontopathic bacteria such as *Porphyromonas gingivalis* have been reported to induce inflammatory cytokines including IL-1β, IL-8, and TNF-α in PDL cells (Yamamoto et al., 2006). We also previously reported increase in IL-8 expression in PDL cells treated with *S. gordonii* (Kim et al., 2017a) or *Aggregatibacter actinomycetemcomitans* lipopolysaccharide (LPS) (Im et al., 2015). In addition, PDL cells treated with *P. gingivalis* LPS exhibit increased production of reactive oxygen species (ROS) (Golz et al., 2014). Furthermore, it has been reported that the upregulation of receptor activator of NF-kappa B ligand (RANKL) by *A. actinomycetemcomitans* LPS in PDL cells contributes to the pathogenesis of periodontitis (Tiranathanagul et al., 2004). Therefore, effector molecules produced during the interactions between pathogenic bacteria and PDL cells seem to be important for the development of periodontitis.

ROS are induced by reduction of molecular oxygen in the mitochondria under normal physiological conditions (Circu and Aw, 2010). ROS include free radicals such as superoxide anion and hydroxyl radical and non-radicals such as H_2O_2 and singlet oxygen (Li et al., 2016). ROS contribute to cell proliferation, differentiation, and inflammation through regulation of intracellular signaling (Circu and Aw, 2010). Moderate ROS production induces inflammatory responses for host defense (Wang et al., 2014). In contrast, excessive ROS production by the inflammatory lesion can damage nucleic acids, proteins, and lipids and eventually lead to tissue injury *via* cellular damage and apoptosis (Circu and Aw, 2010; Mittal et al., 2014). ROS-independent apoptosis has been also reported (Seong and Lee, 2018). It has been suggested that hyper-production of ROS is associated with pathologies in various diseases including cancer, atherosclerosis, and diabetes (Brieger et al., 2012; Kehrer and Klotz, 2015). Periodontitis often induces excessive ROS in periodontal tissues (Akalin et al., 2007), but the underlying molecular mechanism is not clear. Therefore, in this study, we investigated the effects of various oral streptococci on cytotoxicity and ROS production in PDL cells.

MATERIALS AND METHODS

Reagents and Chemicals

S. gordonii CH1 and *S. mitis* SF100 were used as previously described (Seo et al., 2010; Kim et al., 2017a). *S. mutans* KCTC3065 and *S. sanguinis* KCTC3284 were obtained from the Korean Collection for Type Cultures (Jeongeup, Korea). *S. sobrinus* NIDR 6715-7 was provided by Prof. Bong-Kyu Choi (Seoul National University, Seoul, Korea). Lipoprotein-deficient (*Δlgt*) and lipoteichoic acid (LTA)-deficient (*ΔltaS*) *S. gordonii* and lipoproteins were prepared from *S. gordonii* CH1 as previously described (Kim et al., 2017b). Todd–Hewitt broth, brain heart infusion (BHI), and yeast extract were purchased from BD Biosciences (San Diego, CA, United States). Minimum Essential Medium, alpha modification (α-MEM), Dulbecco's Modified Eagle's Medium (DMEM), and phosphate-buffered saline (PBS) were obtained from WelGENE (Daegu, Korea). Penicillin/streptomycin was purchased from HyClone (Logan, UT, United States). Fetal bovine serum (FBS), trypsin–EDTA, and trypan blue were purchased from Gibco-BRL (Carlsbad, CA, United States). 2',7'-Dichlorofluorescin diacetate (DCF-DA), resveratrol, *n*-acetylcysteine (NAC), and catalase were purchased from Sigma-Aldrich (St. Louis, MO, United States). Z-VAD-FMK was purchased from InvivoGen (San Diego, CA, United States). Dead cell apoptosis kit was purchased from Invitrogen (Carlsbad, CA, United States).

Bacteria Culture

Wild-type *S. gordonii* CH1, lipoprotein-deficient (*Δlgt*) *S. gordonii*, LTA-deficient (*ΔltaS*) *S. gordonii* in Todd-Hewitt broth with 5% yeast extract (THY), and *S. mutans*, *S. mitis*, *S. sobrinus*, and *S. sanguinis* in BHI were grown at 37°C under static condition. The bacteria were diluted 1:100 in fresh medium, cultured to mid-log phase, and then washed with PBS. The cells were grown in α-MEM containing 10% FBS and 1% penicillin/streptomycin at 37°C in a 5% CO_2 incubator.

Isolation and Culture of PDL Cells

All experiments using healthy human PDL cells were approved by the Institutional Review Board at Seoul National University. The wisdom teeth were obtained from young adults (two males and one female, average 23 years old) at the Dental Hospital of Seoul National University, Korea. PDL tissue was removed from

the root surface of teeth and chopped into the small pieces. The tissue was digested with 0.25% trypsin and 1 mM EDTA in PBS for 1 h at 37°C and vortexed every 10 min. To obtain the single cells, the digested tissue suspension was passed through a 70-μm cell strainer (BD Falcon, Franklin Lakes, NJ, United States). The cells were collected by centrifugation and cultured in DMEM containing 10% heat-inactivated FBS, 100 U/ml penicillin, and 100 μg/ml streptomycin at 37°C in a 5% CO_2 humidified incubator. The PDL cells were treated with streptococci at various multiplicities of infection (MOI) for 1, 3, or 6 h in the complete culture media without antibiotics. Primary human PDL cells at passages four to nine were used in this study.

Cell Viability Test

Human PDL cells (3×10^5 cells/ml, 2 ml) were plated onto 60-mm dishes and stimulated with *S. gordonii* at MOI 1:10, 100, or 1,000 for 1, 3, or 6 h. In separate experiments, the cells were pre-treated with Z-VAD-FMK or resveratrol for 1 h and then stimulated with *S. gordonii* for 3 h. The cells were washed with PBS, detached using trypsin–EDTA, and stained with trypan blue. Live (unstained) and dead (stained) cells were enumerated under light microscopy. The cells were counted within 5 min after the mixing with trypan blue.

Cell Apoptosis Assay

Cell death staining was conducted according to the manufacturer's instructions (Invitrogen). Briefly, human PDL cells (3×10^5 cells/ml, 2 ml) were plated onto 60-mm dishes and stimulated with *S. gordonii* at MOI of 1,000 for 30, 60, or 180 min. Then, the cells were treated with EDTA for 5 min, detached with a scraper, and harvested. After washing twice with PBS, the cells were stained with FITC-annexin V and propidium iodide (PI) in the dark for 15 min. The staining of cells was analyzed by flow cytometer (BD Biosciences) using Flow Jo software (Tree Star, San Carlos, CA).

Intracellular ROS Detection

Intracellular ROS were detected using DCF-DA as described previously (Song et al., 2021). Briefly, human PDL cells (3×10^5 cells/ml, 2 ml) were plated onto 60-mm dishes. The cells were detached with trypsin–EDTA, washed with PBS, and treated with 10 μM of DCF-DA for 30 min at 37°C. DCF-DA-treated cells were washed twice with PBS, followed by stimulation with *S. gordonii* at MOI of 1:10, 100, or 1,000 for 3 h. After washing, the ROS levels were analyzed using a flow cytometer (BD Biosciences).

H_2O_2 Measurement

Human PDL cells (3×10^5 cells/ml, 2 ml) were plated onto 60-mm dishes and treated with oral streptococci for 1 h. The supernatants were harvested by centrifugation at $10{,}000 \times g$ for 5 min. Level of H_2O_2 in the supernatant was assayed according to the manufacturer's instructions (EZ-hydrogen peroxide/peroxidase assay kit, DoGenBio, Seoul, Korea). H_2O_2 was quantified by measuring the absorbance at 560 nm using a microplate reader (Molecular Devices, San Jose, CA, United States).

Statistical Analysis

All experiments were performed three to five times. All data are expressed as mean ± standard deviation (SD) of triplicate samples. Statistical significance was examined with a nonparametric Mann–Whitney test. An asterisk (*) indicates a significant difference, defined as $p < 0.05$.

RESULTS

S. gordonii Exhibits Cytotoxicity to Human Periodontal Ligament Cells

We examined the effect of *S. gordonii* on the viability of human PDL cells. The cells treated with live *S. gordonii* exhibited morphological changes typical of dying cells and were detached from the culture dish (**Figure 1A**). Cytotoxicity was dose- and

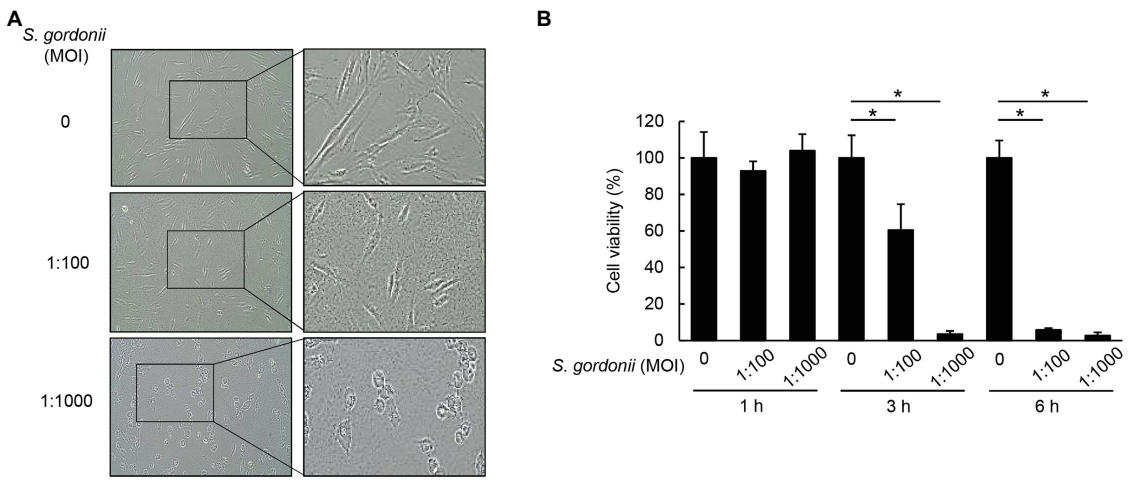


FIGURE 1 | *S. gordonii* induces cytotoxicity of periodontal ligament (PDL) cells. *S. gordonii* was cultured to mid-log phase in THY media at 37°C. PDL cells were treated with *S. gordonii* at multiplicities of infection (MOI) 1:10, 1:100, or 1:1,000 for 1, 3, or 6 h. Trypan blue assay was used to determine the number of viable PDL cells. The cells were photographed **(A)** and counted **(B)**. One of three similar results is shown. *$p < 0.05$.

time-dependent (**Figure 1B**). In addition, *S. gordonii* efficiently induced cell death in primary PDL cells taken from different donors (**Supplementary Figure 1**). These results suggest that *S. gordonii* induces damage in human PDL cells to result in cell death.

S. gordonii Induces Apoptotic Cell Death Through ROS-Independent Pathways

Next, annexin V/PI staining was performed to determine whether cell death induced by *S. gordonii* was due to apoptosis or necrosis. As shown in **Figure 2A**, *S. gordonii* increased annexin V-positive cells (apoptotic cells) and annexin V/PI double-positive cells (both late apoptotic and necrotic cells) but decreased annexin V/PI double-negative cells (viable cells) in a time-dependent manner. However, when the cells were pre-treated with Z-VAD-FMK, an apoptosis inhibitor, *S. gordonii* did not inhibit cell viability (**Figure 2B**). These results indicate that *S. gordonii*-induced PDL cell death is mediated through apoptosis. On the other hand, excessive ROS production can lead to cell apoptosis (Circu and Aw, 2010) Thus, we hypothesized that *S. gordonii* induces ROS-mediated apoptosis in PDL cells. When the cells were treated with *S. gordonii*, ROS production of PDL cells was increased in a dose-dependent manner (**Figure 3A**). However, ROS inhibitor resveratrol or *n*-acetylcysteine did not affect

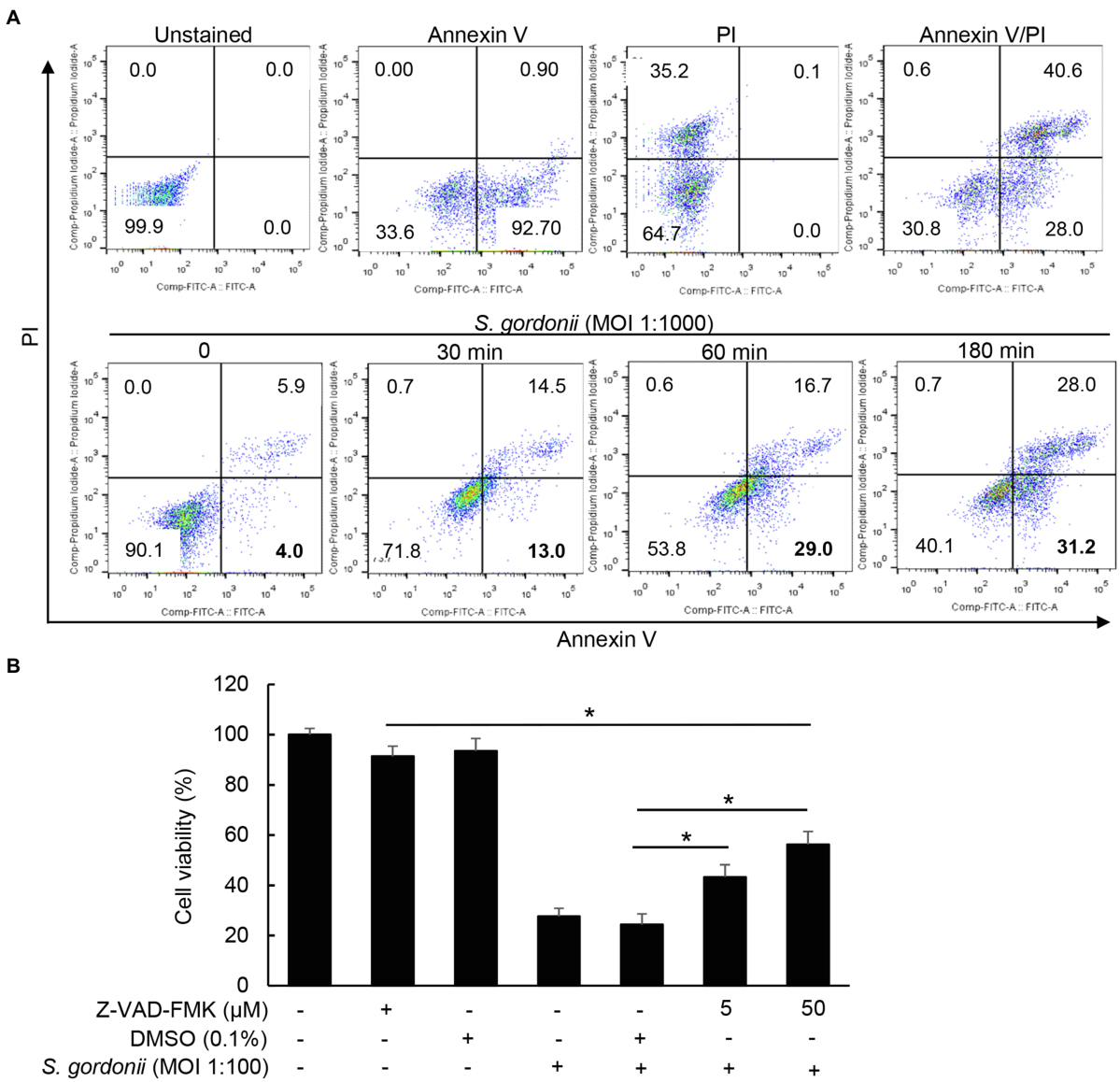


FIGURE 2 | Cytotoxicity by *S. gordonii* is mediated through apoptosis in PDL cells. *S. gordonii* was cultured to mid-log phase in THY media at 37°C. **(A)** PDL cells were treated with *S. gordonii* at MOI 1:1,000 for 30, 60, or 180 min. The cells were stained with annexin V and PI and then analyzed using flow cytometry. Numbers indicate the percentage of cells in each panel. **(B)** PDL cells were pre-treated with Z-VAD-FMK (0, 5, or 50 μM) for 1 h, followed by treatment with *S. gordonii* at MOI 1:100 for 3 h. Trypan blue assay was used to determine the number of viable PDL cells. The cells were counted. One of three similar results is shown. *$p < 0.05$.

cytotoxicity of PDL cells by *S. gordonii* (**Figures 3B,C**). These results suggest that *S. gordonii* induces ROS generation but is not related to PDL cell death.

Other Streptococcal Species Except *S. mutans* Also Induce Apoptosis and ROS Production of Human PDL Cells

To examine whether other streptococci can also induce apoptosis, human PDL cells were treated with *S. gordonii*, *S. mitis*, *S. mutans*, *S. sanguinis*, and *S. sobrinus* for 3 h. Interestingly, *S. gordonii*, *S. mitis*, *S. sanguinis*, and *S. sobrinus* induced PDL cell cytotoxicity (**Figure 4A**) and annexin V-positive cell population (**Figure 4B**). However, such effects were not observed in PDL cells treated with *S. mutans* under the same conditions (**Figures 4A,B**). Concordant with their cytotoxic effect on human PDL cells, *S. gordonii*, *S. mitis*, *S. sanguinis*, and *S. sobrinus* but not *S. mutans* induced ROS production (**Figure 4C**). These results suggest that most streptococcal species, except *S. mutans*, induce apoptotic cell death and ROS generation in human PDL cells.

Streptococci-Induced PDL Cell Cytotoxicity Is Mediated Through H_2O_2 Production

Oral streptococci have been reported to induce cell death of macrophages *via* production of H_2O_2 (Okahashi et al., 2013). Thus, we examined whether the reduction of PDL cell viability was due to the cytotoxicity of streptococci-produced H_2O_2. As shown in **Figure 5A**, *S. gordonii* induced H_2O_2, which was completely inhibited by catalase treatment. When human PDL cells were treated with *S. gordonii* in the presence of catalase, *S. gordonii*-induced PDL cytotoxicity was reversed substantially (**Figure 5B**). Likewise, *S. mitis*, *S. sanguinis*, and *S. sobrinus* also produced H_2O_2, but *S. mutans* did not (**Figure 5C**). The reduction of cell viability by H_2O_2-producing streptococci was recovered by catalase treatment (**Figures 5D–F**), suggesting that oral streptococci induce the death of human PDL cells *via* H_2O_2 production. In addition, when human PDL cells were co-treated with *S. gordonii* and catalase, ROS was still produced in human PDL cells (**Figure 5G**). These results suggest that *S. gordonii*-produced H_2O_2 does not significantly affect the generation of ROS in PDL cells.

Streptococcus gordonii Lipoproteins Are Partially Involved in the Cytotoxicity of Human PDL Cells

Lipoproteins are a major virulence factor of Gram-positive bacteria (Kim et al., 2018), and over-activation of toll-like receptor 2 (TLR2) by sensing bacterial lipoproteins often results in cytotoxicity (Aliprantis et al., 2000). Indeed, bacterial lipoproteins have been shown to induce cell death *via* TLR2 in

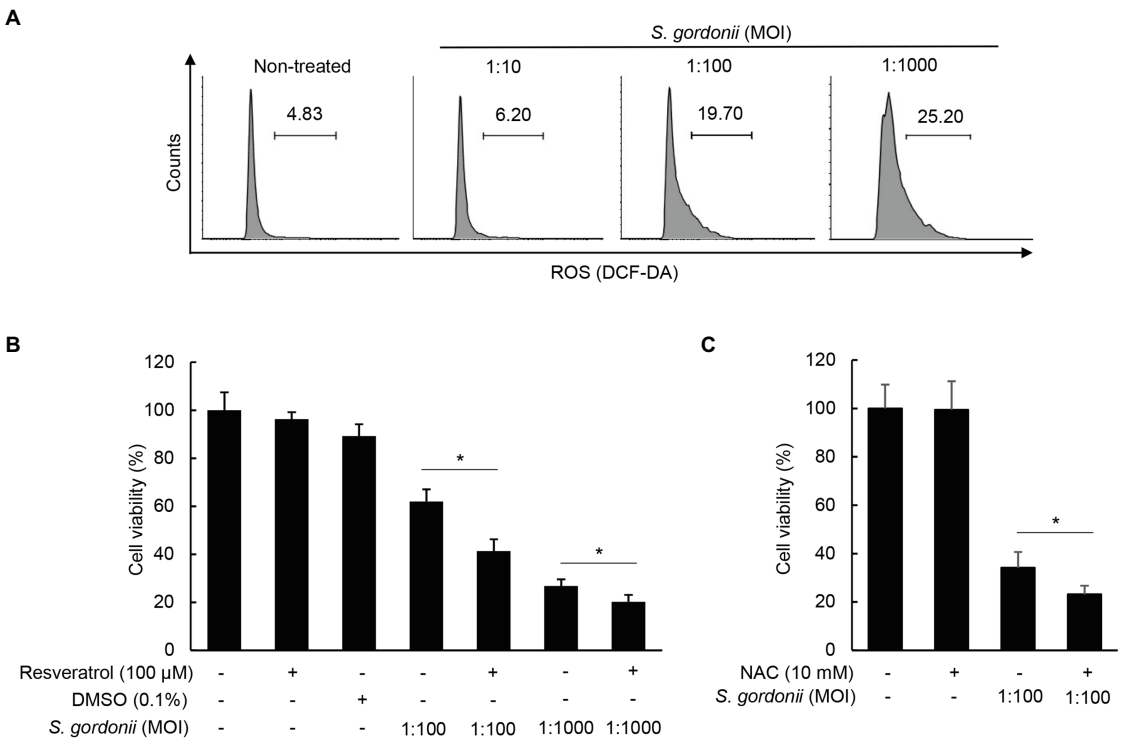


FIGURE 3 | *S. gordonii* induces reactive oxygen species (ROS) production regardless of its cytotoxic effects in PDL cells. **(A)** PDL cells were treated with 10 μM of DCF-DA for 30 min at 37°C. After washing with PBS, the DCF-DA-labeled cells were treated with *S. gordonii* at MOI 1:10, 1:100, or 1:1,000 for 3 h. Fluorescent intensity was analyzed by flow cytometry. **(B)** PDL cells were pre-treated with 100 μM of resveratrol for 1 h, followed by treatment with *S. gordonii* at MOI 1:100 or 1:1,000 for 3 h. **(C)** PDL cells were pre-treated with 10 mM NAC for 1 h, followed by treatment with *S. gordonii* at MOI 1:100 for 3 h. Trypan blue assay was used to determine the number of viable cells. One of three similar results is shown. $^*p < 0.05$.

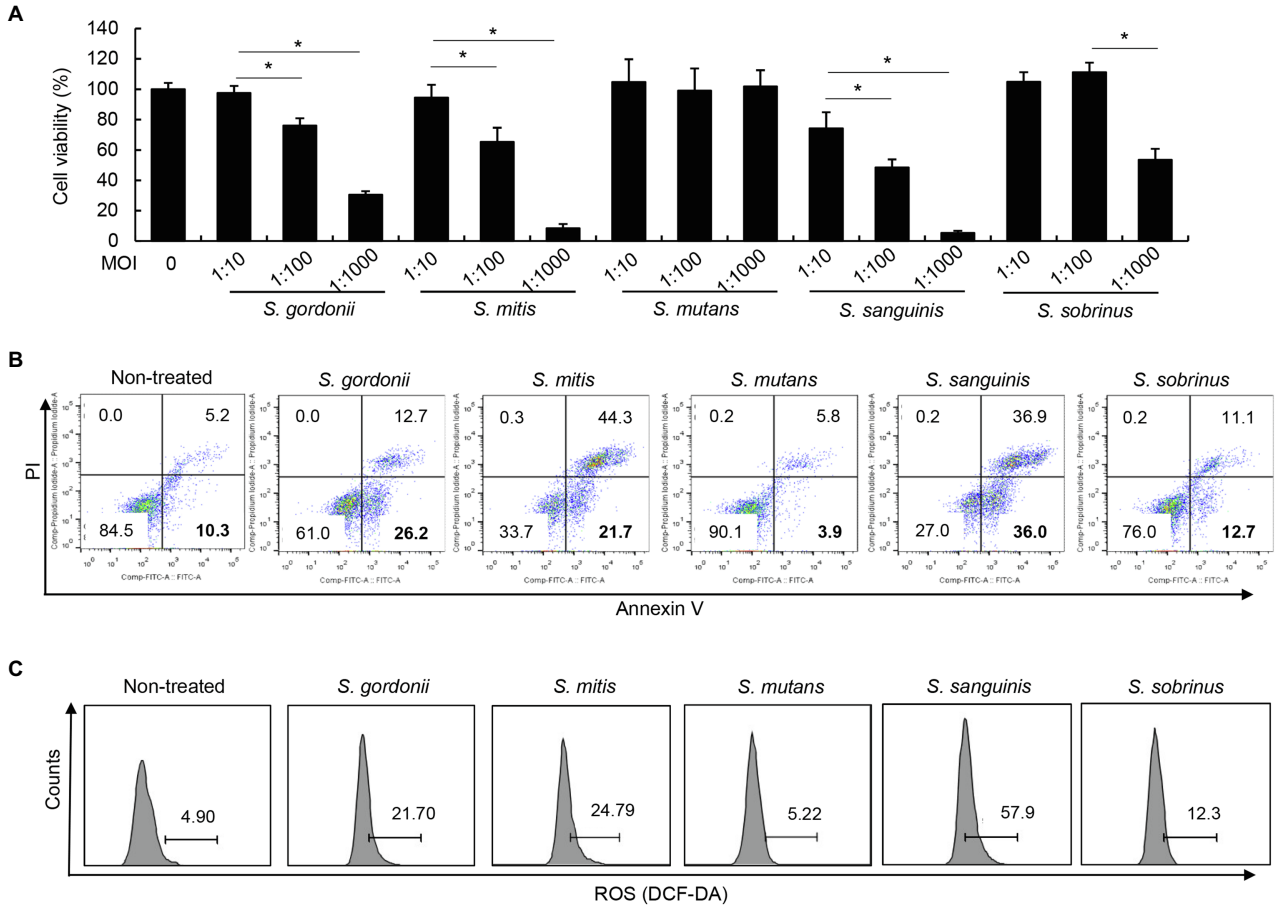


FIGURE 4 | Various streptococcal species differ in induction of apoptosis and ROS in human PDL cells. **(A)** PDL cells were treated with *S. gordonii*, *S. mitis*, *S. mutans*, *S. sanguinis*, and *S. sobrinus* at MOI 1:10, 1:100, or 1:1,000 for 3 h. Trypan blue assay was used to determine the number of viable cells. **(B)** PDL cells were treated with *S. gordonii*, *S. mitis*, *S. mutans*, *S. sanguinis*, and *S. sobrinus* at MOI 1:1,000 for 1 h. The cells were strained with annexin V and PI and then analyzed using flow cytometry. **(C)** PDL cells were treated with 10 μM of DCF-DA for 30 min at 37°C. The DCF-DA-treated cells were washed with PBS and then treated with *S. gordonii*, *S. mitis*, *S. mutans*, *S. sanguinis*, and *S. sobrinus* at MOI 1:1,000 for 3 h in a CO_2 incubator. Fluorescent intensity was analyzed by flow cytometry. One of three similar results is shown. $^*p < 0.05$.

THP-1 cells (Aliprantis et al., 1999). Thus, we examined whether bacterial lipoproteins also contribute to streptococci-induced PDL cell cytotoxicity with *Δlgt*. As shown in **Figure 6A**, *Δlgt S. gordonii* showed decreased cytotoxicity in PDL cells compared to wild-type *S. gordonii*. In contrast, *ΔltaS S. gordonii*-treated cells showed even higher cytotoxicity than wild-type *S. gordonii*. In addition, treatment with lipoproteins purified from *S. gordonii* also decreased the viability of PDL cells. When cells were co-treated with *Δlgt S. gordonii* and lipoproteins purified from *S. gordonii*, the extent of cytotoxicity was comparable to that induced by wild-type *S. gordonii* (**Figure 6B**). Moreover, when PDL cells were pre-treated with anti-human TLR2 neutralizing antibody, *S. gordonii*-decreased cell viability was recovered substantially (**Figure 6C**). However, such recovery was not seen in the presence of isotype control antibody. These results suggest that TLR2 is a critical factor for inhibition of cell viability by *S. gordonii*. On the other hand, *S. gordonii* lipoproteins are unable to induce H_2O_2 (**Figure 6D**) or ROS (**Figure 6E**) generation, indicating that lipoprotein-induced cytotoxicity is independent of H_2O_2 or ROS. In addition, *S. gordonii* lipoproteins and H_2O_2 cooperatively induced PDL cell cytotoxicity (**Figure 6F**). Collectively, these results suggest that *S. gordonii* lipoproteins contribute to the cytotoxicity of PDL cells in cooperation with H_2O_2.

DISCUSSION

Apical periodontitis is characterized by inflammation and tissue injury in the lesion (Nair, 2004). Since PDL cells play critical roles in the support of teeth in the alveolar bone (Jonsson et al., 2011), damage to PDL cells might contribute to the pathogenesis of apical periodontitis. *S. gordonii* is a medically important bacterium that enters the bloodstream through oral cavity and causes systemic diseases (Park et al., 2020). In this study, we demonstrated that most oral streptococcal species including *S. gordonii* could damage PDL

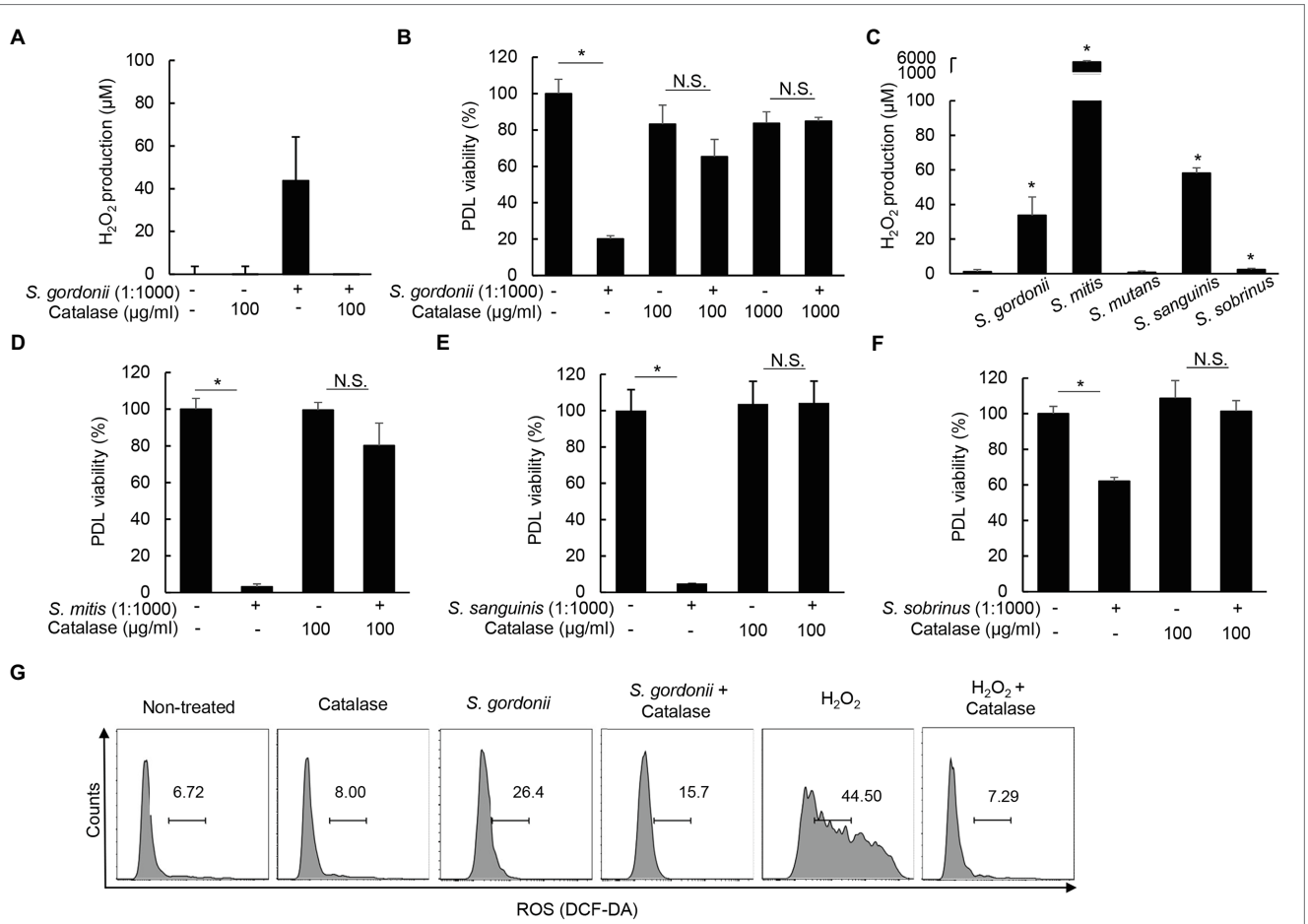


FIGURE 5 | *Streptococci*-induced cytotoxicity of PDL cells is mediated through production of H_2O_2. **(A)** PDL cells were treated with *S. gordonii* at MOI 1:1,000 in the presence or absence of catalase (100 μg/ml) for 1 h. The level of H_2O_2 in the supernatant was determined using a hydrogen peroxide assay kit. **(B)** PDL cells were treated with *S. gordonii* at MOI 1:1,000 in the presence or absence of catalase (100 or 1,000 μg/ml) for 3 h. Trypan blue assay was used to determine the number of viable cells. **(C)** PDL cells were treated with *S. gordonii, S. mitis, S. mutans, S. sanguinis,* or *S. sobrinus* at MOI 1:1,000 for 1 h. The level of H_2O_2 in the supernatant was determined using a hydrogen peroxide assay kit. **(D–F)** PDL cells were treated with *S. mitis, S. sanguinis,* or *S. sobrinus* in the presence or absence of catalase for 3 h. Trypan blue assay was used to determine the number of viable cells. **(G)** PDL cells were treated with 10 μM of DCF-DA for 30 min at 37°C. DCF-DA-treated cells were washed with PBS and then treated with *S. gordonii* at MOI 1:1,000 or H_2O_2 in the presence or absence of catalase for 3 h. Fluorescent intensity was analyzed by flow cytometry. One of three similar results is shown. *$p < 0.05$.

cells by inducing apoptotic cell death. Mechanism studies suggest that streptococcal H_2O_2 generation is crucial for PDL cytotoxicity, while cell death was independent of ROS production. In addition, streptococcal lipoproteins also contribute to cytotoxic effects on PDL cells. Considering that streptococcal species are found predominantly in the initial stage of periodontal damage (Park et al., 2015) and refractory apical periodontitis (Chavez de Paz et al., 2005), the current results demonstrate that *S. gordonii* plays an important role in the early stage of inflammation by inducing cytotoxicity in PDL cells.

We found that *S. gordonii* induces apoptotic cell death of human PDL cells, as demonstrated by pre-treatment with apoptosis inhibitor attenuating *S. gordonii*-induced apoptosis. In fact, bacteria-induced host cell damage *via* apoptosis is not uncommon in apical periodontitis. For example, *Enterococcus faecalis*, which is associated with refractory apical periodontitis (Wang et al., 2012a), has been shown to induce apoptosis and pyroptosis in human osteoblastic MG63 cells (Ran et al., 2019), suggesting that *E. faecalis* infection in periapical lesions contributes to delay in periapical repair. In addition, diabetic rats treated with oral administration of *A. actinomycetemcomitans* exhibit increased numbers of apoptotic cells in the PDL adjacent to the bone and lining on the bone surface. However, when *A. actinomycetemcomitans*-inoculated diabetic rats receive the apoptosis inhibitor ZDEVD-FMK, bone destruction is decreased *via* increased osteoblast numbers in PDL (Pacios et al., 2013). Since PDL cells play a critical role in tooth attachment to the surrounding alveolar bone (Jonsson et al., 2011), apoptosis of PDL cells is likely to contribute to tooth loss *via* apical periodontitis.

We observed that H_2O_2 production by various streptococci is critical for cell death of human PDL cells. In this study,

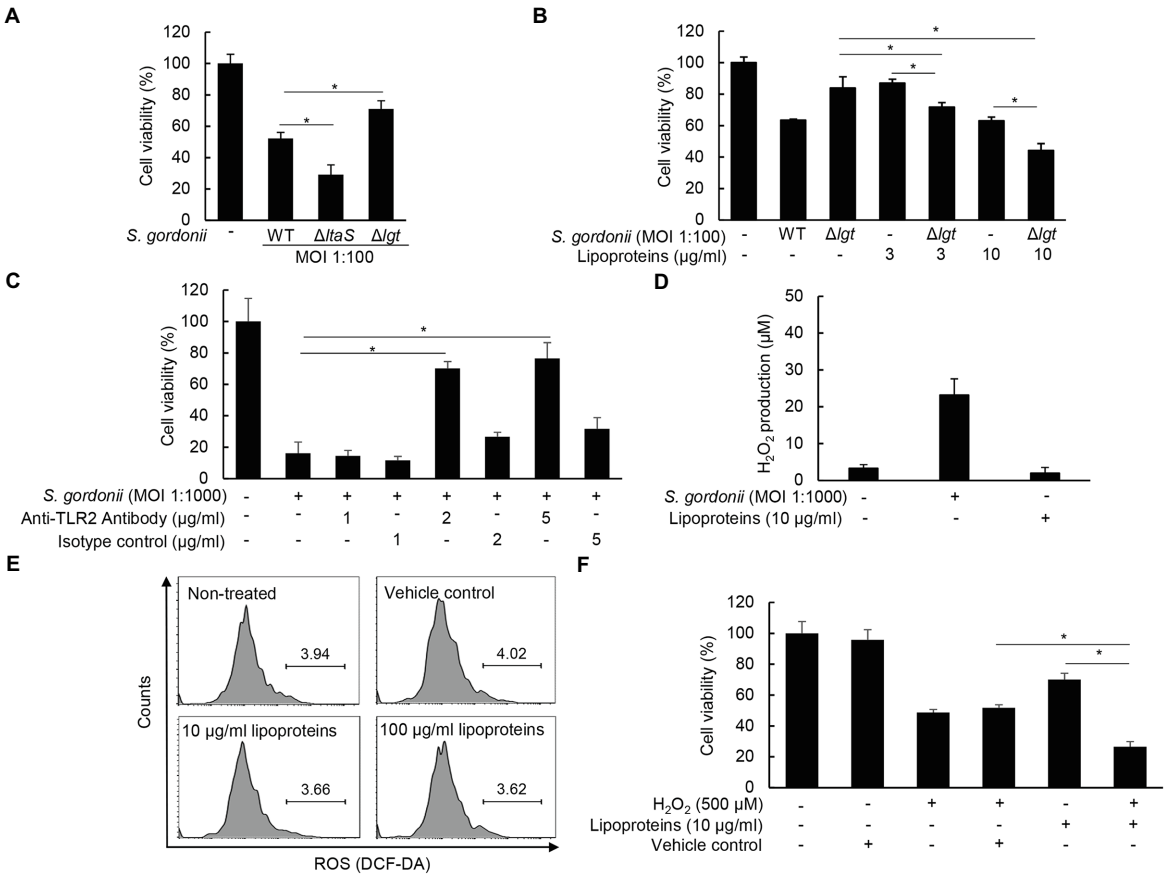


FIGURE 6 | *S. gordonii* lipoproteins contribute to the cytotoxicity of PDL cells in cooperation with H_2O_2. **(A)** PDL cells were treated with *S. gordonii* wild-type, its *ΔltaS*, and *Δlgt* at MOI 1:100 for 3 h. **(B)** PDL cells were treated with *S. gordonii* wild-type or its *Δlgt* at MOI 1:100 in the presence or absence of *S. gordonii* lipoproteins (3 or 10 μg/ml) for 3 h. **(C)** PDL cells were pre-treated with anti-TLR2 antibody (0, 1, 2, or 5 μg/ml) for 1 h, followed by treatment with *S. gordonii* at MOI 1:1000 for 3 h. Trypan blue assay was used to determine the number of viable cells. **(D)** PDL cells were treated with *S. gordonii* at MOI 1:1000 or S. gordonii lipoproteins (10 μg/ml) for 1 h. The level of H_2O_2 in the supernatant was determined using a hydrogen peroxide assay kit. **(E)** PDL cells were treated with 10 μM of DCF-DA for 30 min at 37°C. The DCF-DA-treated cells were washed with PBS and then treated with *S. gordonii* lipoproteins (10 or 100 μg/ml) for 3 h in a CO_2 incubator. Fluorescent intensity was analyzed by flow cytometry. **(F)** PDL cells were treated with *S. gordonii* lipoproteins (10 μg/ml) in the presence or absence of H_2O_2 for 3 h. Trypan blue assay was used to determine the number of viable cells. One of three similar results is shown. *$p < 0.05$.

when the cells were co-treated with catalase and H_2O_2-producing streptococci, the reduction of cell viability by streptococci was recovered almost completely. As in the present study, oral streptococci have been shown to induce macrophage cell death through H_2O_2 generation (Okahashi et al., 2013), and streptococci-induced H_2O_2 is independent of inflammatory responses. It is well known that exogenous H_2O_2 induces apoptosis of various host cells including rat primary neuronal cell culture and human pulmonary artery smooth muscle cells (Whittemore et al., 1995; Park, 2016). Rai et al. reported that H_2O_2 produced by *Streptococcus pneumoniae* contributes to acute pneumonia *via* DNA damage and apoptosis of lung cells (Rai et al., 2015). Therefore, the cytotoxicity of H_2O_2 by oral streptococci can contribute to the pathogenicity in infectious diseases *via* tissue damage. In addition, because streptococcus pyruvate oxidase (spxB) is critical for the induction of H_2O_2 by oral streptococci (Zhu et al., 2014), further studies using spxB mutant *S. gordonii* are needed to clearly understand the role of H_2O_2 produced by *S. gordonii* on cell death.

In our study, *S. gordonii*, like many other bacteria previously reported, increased ROS production in PDL cells. For example, under physiological conditions, commensal gut microbiota induce ROS in intestinal epithelial cells (Jones et al., 2012). *E. faecalis* increases ROS production in gastric carcinoma cell line MKN74 (Strickertsson et al., 2013). *P. gingivalis* and *A. actinomycetemcomitans* induce ROS in gingival epithelial cells and macrophages, respectively (Wang et al., 2014; Okinaga et al., 2015). However, under excessive stress, host cells produce high amounts of ROS, often leading to cell death (He et al., 2017). ROS induction by *Streptococcus oralis* and *Staphylococcus aureus* has been shown to cause host cell death (Okahashi et al., 2013; Deplanche et al., 2019). We found that *S. gordonii*-induced ROS production is not associated

with apoptosis of PDL cells. Thus, further studies are needed to determine the ROS requirements for apoptosis by bacterium. On the other hand, Marconi et al. reported the protective effect of ascorbic acid in primary culture of human periodontal ligament stem cells (PDLSCs) exposed to *P. gingivalis* LPS through down-regulation of inflammatory pathway and ROS induction (Marconi et al., 2021). It would be necessary to study streptococci-induced cytotoxicity in other cell types including PDLSCs and human dental pulp stem cells.

In the present study, we demonstrated that all streptococci do not affect the viability of PDL cells to similar extents. *S. gordonii*, *S. mitis*, *S. sanguinis*, and *S. sobrinus* but not *S. mutans* induced apoptosis of PDL cells. In general, it is well known that *S. mutans* induces dental caries (Forssten et al., 2010). Since *S. mutans* is an early colonizer that converts sucrose into sticky glucan and causes other bacteria to adhere to it (Ren et al., 2016), its action seems to be largely limited to hard tissues such as teeth. Instead, accompanying bacteria that arrive after *S. mutans* can more efficiently enter the pulp and consequently cause inflammation by inducing cell cytotoxicity. Nevertheless, *S. mutans* LTA has been shown to induce apoptosis in human dental pulp cells (Wang et al., 2001). Since LTA can be released by Gram-positive bacteria (Ginsburg, 2002), bacterial components derived from streptococcal species including *S. mutans* can contribute to host cell damage or inflammatory responses, although the bacteria do not directly contribute. On the other hand, cell tropism in differential responses to bacteria might be another reason for the variation in results. For example, *S. gordonii* does not induce apoptosis in gingival keratinocytes (Li et al., 2013) even though it induced apoptotic cell death in human PDL cells in the current study. Although further studies are required to clarify our observations, most oral streptococci might contribute to apical periodontitis through death of PDL cells.

We demonstrated that lipoproteins are involved at least partially in PDL cell cytotoxicity by *S. gordonii via* TLR2 activation, although lipoproteins have weak cytotoxic effects compared to H_2O_2. The strong TLR2 signaling caused by high doses of lipoproteins might be cytotoxic to a level similar to that of H_2O_2. TLR2 activation seems to be a positive modulator of apoptosis. Aliprantis et al. reported that a synthetic lipopeptide, Pam3CSK4, mimicking bacterial lipoproteins induces apoptosis of THP-1 cells through activation of TLR2/MyD88-NF-κB and a Fas-associated death domain protein/caspase 8 pathway (Aliprantis et al., 1999, 2000). Additionally, *Propionibacterium acnes* has been shown to induce the apoptosis of nucleus pulposus cells isolated from human intervertebral discs by the TLR2/c-Jun *N*-terminal kinase pathway (Lin et al., 2018). Indeed, lipoproteins of streptococci are important inflammatory components, based on the previous studies in which we found that lipoprotein-deficient *S. gordonii* weakly stimulates the induction of inflammatory mediators compared with the wild-type strain, and purified lipoproteins are sufficient to induce inflammatory responses in macrophages and PDL cells (Kim et al., 2017a, 2018). Therefore, streptococcal lipoproteins together with H_2O_2 appear to be major factors underlying damage to human PDL cells caused by streptococcal species. Furthermore, macrophages infected by *E. faecalis* produce 4-hydroxynonenal (4-HNE; Wang et al., 2012b) likely *via* lipid oxidation. 4-HNE, on the other hand, is known to induce apoptotic cell death (Dalleau et al., 2013). Therefore, it is seemingly necessary to determine whether indirect effects *via* macrophages can affect oral streptococci-induced apoptosis.

In conclusion, we demonstrate that *S. gordonii* induces apoptosis *via* H_2O_2 production in PDL cells. *S. gordonii* lipoproteins are involved in the death of human PDL cells. *S. gordonii* is an opportunistic bacterium, commonly found in apical lesions of patients with apical periodontitis. Therefore, apoptotic cell death of PDL cells due to tissue damage caused by *S. gordonii* could influence the development of apical periodontitis.

DATA AVAILABILITY STATEMENT

The original contributions presented in the study are included in the article/**Supplementary Material**, further inquiries can be directed to the corresponding author.

ETHICS STATEMENT

All experiments using healthy human PDL cells were approved by the Institutional Review Board at Seoul National University. The patients/participants provided their written informed consent to participate in this study.

AUTHOR CONTRIBUTIONS

SHH conceived the study. SHH and O-JP designed the experiments. O-JP, ARK, YJS, JI, HJJ, KBA, and SHH performed the experiments and interpreted the data. HSS and C-HY provided critical comments. All authors contributed to the article and approved the submitted version.

FUNDING

This work was supported by grants from the National Research Foundation of Korea, which is funded by the Korean government (NRF-2019R1A2C2007041, NRF-2018R1A5A2024418, and NRF-2019R1I1A1A01060952).

SUPPLEMENTARY MATERIAL

The Supplementary Material for this article can be found online at: https://www.frontiersin.org/articles/10.3389/fmicb.2021.738047/full#supplementary-material

REFERENCES

Abranches, J., Zeng, L., Kajfasz, J. K., Palmer, S. R., Chakraborty, B., Wen, Z. T., et al. (2018). Biology of oral streptococci. *Microbiol. Spectr.* 6, 1–18. doi: 10.1128/microbiolspec.GPP3-0042-2018

Akalin, F. A., Baltacioglu, E., Alver, A., and Karabulut, E. (2007). Lipid peroxidation levels and total oxidant status in serum, saliva and gingival crevicular fluid in patients with chronic periodontitis. *J. Clin. Periodontol.* 34, 558–565. doi: 10.1111/j.1600-051X.2007.01091.x

Aliprantis, A. O., Yang, R. B., Mark, M. R., Suggett, S., Devaux, B., Radolf, J. D., et al. (1999). Cell activation and apoptosis by bacterial lipoproteins through toll-like receptor-2. *Science* 285, 736–739. doi: 10.1126/science.285.5428.736

Aliprantis, A. O., Yang, R. B., Weiss, D. S., Godowski, P., and Zychlinsky, A. (2000). The apoptotic signaling pathway activated by toll-like receptor-2. *EMBO J.* 19, 3325–3336. doi: 10.1093/emboj/19.13.3325

Brieger, K., Schiavone, S., Miller, F. J. Jr., and Krause, K. H. (2012). Reactive oxygen species: from health to disease. *Swiss Med. Wkly.* 142:w13659. doi: 10.4414/smw.2012.13659

Cekici, A., Kantarci, A., Hasturk, H., and Van Dyke, T. E. (2014). Inflammatory and immune pathways in the pathogenesis of periodontal disease. *Periodontol.* 64, 57–80. doi: 10.1111/prd.12002

Chavez de Paz, L., Svensater, G., Dahlen, G., and Bergenholtz, G. (2005). Streptococci from root canals in teeth with apical periodontitis receiving endodontic treatment. *Oral Surg. Oral Med. Oral Pathol. Oral Radiol. Endod.* 100, 232–241. doi: 10.1016/j.tripleo.2004.10.008

Circu, M. L., and Aw, T. Y. (2010). Reactive oxygen species, cellular redox systems, and apoptosis. *Free Radic. Biol. Med.* 48, 749–762. doi: 10.1016/j.freeradbiomed.2009.12.022

Dalleau, S., Baradat, M., Gueraud, F., and Huc, L. (2013). Cell death and diseases related to oxidative stress: 4-hydroxynonenal (HNE) in the balance. *Cell Death Differ.* 20, 1615–1630. doi: 10.1038/cdd.2013.138

Deplanche, M., Mouhali, N., Nguyen, M. T., Cauty, C., Ezan, F., Diot, A., et al. (2019). *Staphylococcus aureus* induces DNA damage in host cell. *Sci. Rep.* 9:7694. doi: 10.1038/s41598-019-44213-3

Forssten, S. D., Bjorklund, M., and Ouwehand, A. C. (2010). *Streptococcus mutans*, caries and simulation models. *Nutrients* 2, 290–298. doi: 10.3390/nu2030290

Ginsburg, I. (2002). Role of lipoteichoic acid in infection and inflammation. *Lancet Infect. Dis.* 2, 171–179. doi: 10.1016/S1473-3099(02)00226-8

Golz, L., Memmert, S., Rath-Deschner, B., Jager, A., Appel, T., Baumgarten, G., et al. (2014). LPS from *P. gingivalis* and hypoxia increases oxidative stress in periodontal ligament fibroblasts and contributes to periodontitis. *Mediat. Inflamm.* 2014:986264. doi: 10.1155/2014/986264

He, L., He, T., Farrar, S., Ji, L., Liu, T., and Ma, X. (2017). Antioxidants maintain cellular redox homeostasis by elimination of reactive oxygen species. *Cell. Physiol. Biochem.* 44, 532–553. doi: 10.1159/000485089

Im, J., Baik, J. E., Kim, K. W., Kang, S. S., Jeon, J. H., Park, O. J., et al. (2015). *Enterococcus faecalis* lipoteichoic acid suppresses *Aggregatibacter actinomycetemcomitans* lipopolysaccharide-induced IL-8 expression in human periodontal ligament cells. *Int. Immunol.* 27, 381–391. doi: 10.1093/intimm/dxv016

Jones, R. M., Mercante, J. W., and Neish, A. S. (2012). Reactive oxygen production induced by the gut microbiota: pharmacotherapeutic implications. *Curr. Med. Chem.* 19, 1519–1529. doi: 10.2174/092986712799828283

Jonsson, D., Nebel, D., Bratthall, G., and Nilsson, B. O. (2011). The human periodontal ligament cell: a fibroblast-like cell acting as an immune cell. *J. Periodontal Res.* 46, 153–157. doi: 10.1111/j.1600-0765.2010.01331.x

Kehrer, J. P., and Klotz, L. O. (2015). Free radicals and related reactive species as mediators of tissue injury and disease: implications for health. *Crit. Rev. Toxicol.* 45, 765–798. doi: 10.3109/10408444.2015.1074159

Kim, A. R., Ahn, K. B., Kim, H. Y., Seo, H. S., Kum, K. Y., Yun, C. H., et al. (2017a). *Streptococcus gordonii* lipoproteins induce IL-8 in human periodontal ligament cells. *Mol. Immunol.* 91, 218–224. doi: 10.1016/j.molimm.2017.09.009

Kim, H. Y., Baik, J. E., Ahn, K. B., Seo, H. S., Yun, C. H., and Han, S. H. (2017b). *Streptococcus gordonii* induces nitric oxide production through its lipoproteins stimulating toll-like receptor 2 in murine macrophages. *Mol. Immunol.* 82, 75–83. doi: 10.1016/j.molimm.2016.12.016

Kim, H. Y., Kim, A. R., Seo, H. S., Baik, J. E., Ahn, K. B., Yun, C. H., et al. (2018). Lipoproteins in *Streptococcus gordonii* are critical in the infection and inflammatory responses. *Mol. Immunol.* 101, 574–584. doi: 10.1016/j.molimm.2018.08.023

Kutlu, B., Cardozo, A. K., Darville, M. I., Kruhoffer, M., Magnusson, N., Orntoft, T., et al. (2003). Discovery of gene networks regulating cytokine-induced dysfunction and apoptosis in insulin-producing INS-1 cells. *Diabetes* 52, 2701–2719. doi: 10.2337/diabetes.52.11.2701

Li, S., Dong, G., Moschidis, A., Ortiz, J., Benakanakere, M. R., Kinane, D. F., et al. (2013). *P. gingivalis* modulates keratinocytes through FOXO transcription factors. *PLoS One* 8:e78541. doi: 10.1371/journal.pone.0085815

Li, R., Jia, Z., and Trush, M. A. (2016). Defining ROS in biology and medicine. *React. Oxyg. Species (Apex)* 1, 9–21. doi: 10.20455/ros.2016.803

Lin, Y., Jiao, Y., Yuan, Y., Zhou, Z., Zheng, Y., Xiao, J., et al. (2018). *Propionibacterium acnes* induces intervertebral disc degeneration by promoting nucleus pulposus cell apoptosis via the TLR2/JNK/mitochondrial-mediated pathway. *Emerg. Microbes Infect.* 7:1. doi: 10.1038/s41426-017-0002-0

Marconi, G. D., Fonticoli, L., Guarnieri, S., Cavalcanti, M., Franchi, S., Gatta, V., et al. (2021). Ascorbic acid: a new player of epigenetic regulation in LPS-*gingivalis* treated human periodontal ligament stem cells. *Oxid. Med. Cell Longev.* 2021:6679708. doi: 10.1155/2021/6679708

Mittal, M., Siddiqui, M. R., Tran, K., Reddy, S. P., and Malik, A. B. (2014). Reactive oxygen species in inflammation and tissue injury. *Antioxid. Redox Signal.* 20, 1126–1167. doi: 10.1089/ars.2012.5149

Nair, P. N. (2004). Pathogenesis of apical periodontitis and the causes of endodontic failures. *Crit. Rev. Oral Biol. Med.* 15, 348–381. doi: 10.1177/154411130401500604

Okahashi, N., Nakata, M., Sumitomo, T., Terao, Y., and Kawabata, S. (2013). Hydrogen peroxide produced by oral streptococci induces macrophage cell death. *PLoS One* 8:e62563. doi: 10.1371/journal.pone.0062563

Okinaga, T., Ariyoshi, W., and Nishihara, T. (2015). *Aggregatibacter actinomycetemcomitans* invasion induces interleukin-1beta production through reactive oxygen species and cathepsin B. *J. Interf. Cytokine Res.* 35, 431–440. doi: 10.1089/jir.2014.0127

Pacios, S., Andriankaja, O., Kang, J., Alnammary, M., Bae, J., De Brito Bezerra, B., et al. (2013). Bacterial infection increases periodontal bone loss in diabetic rats through enhanced apoptosis. *Am. J. Pathol.* 183, 1928–1935. doi: 10.1016/j.ajpath.2013.08.017

Park, W. H. (2016). Exogenous H_2O_2 induces growth inhibition and cell death of human pulmonary artery smooth muscle cells via glutathione depletion. *Mol. Med. Rep.* 14, 936–942. doi: 10.3892/mmr.2016.5307

Park, O. J., Kim, J., Kim, H. Y., Kwon, Y., Yun, C. H., and Han, S. H. (2019). *Streptococcus gordonii* induces bone resorption by increasing osteoclast differentiation and reducing osteoblast differentiation. *Microb. Pathog.* 126, 218–223. doi: 10.1016/j.micpath.2018.11.005

Park, O. J., Kwon, Y., Park, C., So, Y. J., Park, T. H., Jeong, S., et al. (2020). *Streptococcus gordonii*: pathogenesis and host response to its cell wall components. *Microorganisms* 8:1852. doi: 10.3390/microorganisms8121852

Park, O. J., Yi, H., Jeon, J. H., Kang, S. S., Koo, K. T., Kum, K. Y., et al. (2015). Pyrosequencing analysis of subgingival microbiota in distinct periodontal conditions. *J. Dent. Res.* 94, 921–927. doi: 10.1177/0022034515583531

Parks, T., Barrett, L., and Jones, N. (2015). Invasive streptococcal disease: a review for clinicians. *Br. Med. Bull.* 115, 77–89. doi: 10.1093/bmb/ldv027

Rai, P., Parrish, M., Tay, I. J., Li, N., Ackerman, S., He, F., et al. (2015). *Streptococcus pneumoniae* secretes hydrogen peroxide leading to DNA damage and apoptosis in lung cells. *Proc. Natl. Acad. Sci. U. S. A.* 112, E3421–E3430. doi: 10.1073/pnas.1424144112

Ran, S., Chu, M., Gu, S., Wang, J., and Liang, J. (2019). *Enterococcus faecalis* induces apoptosis and pyroptosis of human osteoblastic MG63 cells via the NLRP3 inflammasome. *Int. Endod. J.* 52, 44–53. doi: 10.1111/iej.12965

Ren, Z., Chen, L., Li, J., and Li, Y. (2016). Inhibition of *Streptococcus mutans* polysaccharide synthesis by molecules targeting glycosyltransferase activity. *J. Oral Microbiol.* 8:31095. doi: 10.3402/jom.v8.31095

Seo, H. S., Xiong, Y. Q., Mitchell, J., Seepersaud, R., Bayer, A. S., and Sullam, P. M. (2010). Bacteriophage lysin mediates the binding of *Streptococcus mitis* to human platelets through interaction with fibrinogen. *PLoS Pathog.* 6:e1001047. doi: 10.1371/journal.ppat.1001047

Seong, M., and Lee, D. G. (2018). Reactive oxygen species-independent apoptotic pathway by gold nanoparticles in *Candida albicans*. *Microbiol. Res.* 207, 33–40. doi: 10.1016/j.micres.2017.11.003

Song, J., Jung, K. J., Yang, M. J., Han, S. C., and Lee, K. (2021). Assessment of acute and repeated pulmonary toxicities of oligo(2-(2-ethoxy)ethoxyethyl) guanidium chloride in mice. *Toxicol. Res.* 37, 99–113. doi: 10.1007/s43188-020-00058-x

Strickertsson, J. A., Desler, C., Martin-Bertelsen, T., Machado, A. M., Wadstrom, T., Winther, O., et al. (2013). *Enterococcus faecalis* infection causes inflammation, intracellular oxphos-independent ROS production, and DNA damage in human gastric cancer cells. *PLoS One* 8:e63147. doi: 10.1371/journal.pone.0063147

Tiranathanagul, S., Yongchaitrakul, T., Pattamapun, K., and Pavasant, P. (2004). *Actinobacillus actinomycetemcomitans* lipopolysaccharide activates matrix metalloproteinase-2 and increases receptor activator of nuclear factor-kappaB ligand expression in human periodontal ligament cells. *J. Periodontol.* 75, 1647–1654. doi: 10.1902/jop.2004.75.12.1647

Wang, P. L., Shirasu, S., Daito, M., and Ohura, K. (2001). *Streptococcus mutans* lipoteichoic acid-induced apoptosis in cultured dental pulp cells from human deciduous teeth. *Biochem. Biophys. Res. Commun.* 281, 957–961. doi: 10.1006/bbrc.2001.4451

Wang, X., Yang, Y., Moore, D. R., Nimmo, S. L., Lightfoot, S. A., and Huycke, M. M. (2012b). 4-hydroxy-2-nonenal mediates genotoxicity and bystander effects caused by *Enterococcus faecalis*-infected macrophages. *Gastroenterology* 142, 543.e547–551.e547. doi: 10.1053/j.gastro.2011.11.020

Wang, Q. Q., Zhang, C. F., Chu, C. H., and Zhu, X. F. (2012a). Prevalence of *Enterococcus faecalis* in saliva and filled root canals of teeth associated with apical periodontitis. *Int. J. Oral Sci.* 4, 19–23. doi: 10.1038/ijos.2012.17

Wang, H., Zhou, H., Duan, X., Jotwani, R., Vuddaraju, H., Liang, S., et al. (2014). *Porphyromonas gingivalis*-induced reactive oxygen species activate JAK2 and regulate production of inflammatory cytokines through c-Jun. *Infect. Immun.* 82, 4118–4126. doi: 10.1128/IAI.02000-14

Whittemore, E. R., Loo, D. T., Watt, J. A., and Cotman, C. W. (1995). A detailed analysis of hydrogen peroxide-induced cell death in primary neuronal culture. *Neuroscience* 67, 921–932. doi: 10.1016/0306-4522(95)00108-U

Yamamoto, T., Kita, M., Oseko, F., Nakamura, T., Imanishi, J., and Kanamura, N. (2006). Cytokine production in human periodontal ligament cells stimulated with *Porphyromonas gingivalis*. *J. Periodontal Res.* 41, 554–559. doi: 10.1111/j.1600-0765.2006.00905.x

Zhu, L., Xu, Y., Ferretti, J. J., and Kreth, J. (2014). Probing oral microbial functionality–expression of spxB in plaque samples. *PLoS One* 9:e86685. doi: 10.1371/journal.pone.0115087

Conflict of Interest: The authors declare that the research was conducted in the absence of any commercial or financial relationships that could be construed as a potential conflict of interest.

Publisher's Note: All claims expressed in this article are solely those of the authors and do not necessarily represent those of their affiliated organizations, or those of the publisher, the editors and the reviewers. Any product that may be evaluated in this article, or claim that may be made by its manufacturer, is not guaranteed or endorsed by the publisher.

Copyright © 2021 Park, Kim, So, Im, Ji, Ahn, Seo, Yun and Han. This is an open-access article distributed under the terms of the Creative Commons Attribution License (CC BY). The use, distribution or reproduction in other forums is permitted, provided the original author(s) and the copyright owner(s) are credited and that the original publication in this journal is cited, in accordance with accepted academic practice. No use, distribution or reproduction is permitted which does not comply with these terms.

frontiers in Microbiology

ORIGINAL RESEARCH
published: 01 November 2021
doi: 10.3389/fmicb.2021.725483

Glucocorticoids Elevate *Pseudomonas aeruginosa* Binding to Airway Epithelium by Upregulating Syndecan-1 Expression

*Dong Liu[1,2], Ying-Ying Zeng[3], Meng-Meng Shi[1] and Jie-Ming Qu[1]**

[1] Department of Respiratory and Critical Care Medicine, Ruijin Hospital, Shanghai Jiao Tong University School of Medicine, Shanghai, China, [2] Department of Respiratory and Critical Care Medicine, Huadong Hospital, Shanghai Medical College, Fudan University, Shanghai, China, [3] Department of Respiratory and Critical Care Medicine, Zhongshan Hospital, Shanghai Medical College, Fudan University, Shanghai, China

Glucocorticoids are commonly used for the treatment of asthma and chronic obstructive pulmonary disease (COPD). Inhaled corticosteroids are associated with a significantly increased risk of pneumonia. Syndecan-1 (SDC1) located in the cell membrane of airway epithelial cell is the crucial molecule mediating infections by *P. aeruginosa* (PA). In the present study, we found that SDC1 expression was upregulated and the adhesion of PA to human bronchial epithelial (HBE) cells increased to 125 and 138%, respectively, after stimulation by dexamethasone or budesonide. The HBE cells knocking down SDC1 showed lower affinity to PA compared with control. CCAAT-enhancer-binding protein β (C/EBP β) and its phosphorylated form participated in the regulation of glucocorticoid to SDC1 for interfering C/EBP β or inhibiting phosphorylation of C/EBP β by LiCl and BIO, which are inhibitors of glycogen synthase kinase 3β (GSK-3β), and could prevent glucocorticoids from upregulating SDC1 expression. One should be cautious in administering glucocorticoids in chronic lung disease because of their property of increasing the expression of SDC1 and PA binding to the airway epithelium.

Keywords: ***Pseudomonas aeruginosa*, airway epithelium, bacteria binding, syndecan-1, glucocorticoids**

OPEN ACCESS

Edited by:
Monica Cartelle Gestal,
Louisiana State University Health Shreveport, United States

Reviewed by:
Jessica Scoffield,
University of Alabama at Birmingham, United States
Sebastián A. Riquelme,
Columbia University Irving Medical Center, United States

****Correspondence:***
Jie-Ming Qu
jmqu0906@163.com

Specialty section:
This article was submitted to Infectious Agents and Disease, a section of the journal Frontiers in Microbiology

Received: *15 June 2021*
Accepted: *15 September 2021*
Published: *01 November 2021*

Citation:
Liu D, Zeng Y-Y, Shi M-M and Qu J-M (2021) Glucocorticoids Elevate Pseudomonas aeruginosa Binding to Airway Epithelium by Upregulating Syndecan-1 Expression. Front. Microbiol. 12:725483. doi: 10.3389/fmicb.2021.725483

INTRODUCTION

Administration of glucocorticoids (GCs) provides substantial clinical benefit to patients with asthma and chronic obstructive pulmonary disease (COPD). However, more and more clinical studies indicate that inhaled corticosteroids (ICS) were associated with a significantly increased risk of pneumonia (Singh et al., 2009). The risk was particularly elevated with high doses and shorter durations (Drummond et al., 2008). Another study comprised a large cohort of over 160,000 patients with COPD followed for a mean of 5 years with the conclusion that the risk of serious pneumonia was sustained with long-term use but declined after discontinuation. Both inhaled budesonide (BUDE) and fluticasone increased the risk of pneumonia with a more significant risk with fluticasone (Suissa et al., 2013). Administration of GCs is a predisposing factor of lung

Abbreviations: DEX, dexamethasone; BUDE, budesonide; SDC1, syndecan-1; GR, glucocorticoid-receptor; ICS, inhaled corticosteroids; HSPGs, heparan sulfate proteoglycans; MOI, multiplicity of infection; GAPDH, glyceraldehyde 3-phosphate-dehydrogenase; C/EBP β, CCAAT-enhancer-binding protein β;GSK-3β, glycogen synthase kinase 3β; PA, *Pseudomonas aeruginosa.*

infection, but the exact mechanism is unclear. Stolberg and their colleagues carried out one animal study to target this question. Their research showed that ICS significantly increased the uptake of apoptotic cells by alveolar macrophages, which could inhibit pulmonary pneumococcal clearance (Stolberg et al., 2015). Although their identification offers a possible explanation for the molecular basis of this epidemiological association, the issue is far from settled.

Heparan sulfate proteoglycans (HSPGs) are glycoproteins, with the common characteristic of containing one or more covalently attached heparan sulfate (HS) chains, a type of glycosaminoglycan (GAG). There are three groups according to their location: membrane HSPGs, such as syndecans and glypicans, the secreted extracellular matrix HSPGs (agrin, perlecan, and type XVIII collagen), and the secretory vesicle proteoglycan, serglycin (Sarrazin et al., 2011). Park et al. (2001) reported 7-day-old syndecan-$1^{-/-}$ ($SDC1^{-/-}$) mice markedly resisted infection by intranasally inoculated *Pseudomonas aeruginosa* (PA). This result gives a strong proof to indicate that SDC1 is the crucial molecule mediating infection by PA, a clinically important Gram-negative bacterium in pneumonia and possibly in other infections in which the bacteria first encounter the host's epithelia—a cell type whose predominant HSPG is SDC1. Peggy Benad-Mehner reported that dexamethasone (DEX) time- and dose-dependently increased SDC1 expression up to fourfold in breast cancer cell lines (Benad-Mehner et al., 2014). All these above studies provide adequate justification to develop the hypothesis that administration of GCs may influence the expression of SDC1 and its interaction with PA in airway epithelial cells.

In order to verify our hypothesis, we investigated the influence of DEX and BUDE to SDC1 expression *in vitro* and to the ability of binding PA to human airway epithelia cell line as well. The related molecular mechanism was further investigated. From the available data, we are unaware of any published reports involving the underlying molecular control of transcriptional interactions between GCs and SDC1. However, it was reported that CCAAT-enhancer-binding protein β (C/EBP β) was a key transcriptive factor regulating SDC1 expression (Larabee et al., 2011). C/EBP β mediated the effect of fluticasone propionate in host defense gene expression in BEAS-2B cells (Kimura et al., 2001; Zhang et al., 2007). Therefore, we explored whether GCs regulated SDC1 through transcription factor C/EBP β and its phosphorylation. Previous studies have proved that GSK-3β could interact with and phosphorylate C/EBP β (Lee et al., 2010). The phosphorylated C/EBP β by GSK-3β transactivated the subsequent gene expression (Tang et al., 2005). The rise in cellular cAMP augmented the activity of GSK-3β (Larabee et al., 2008). Thus, whether or not GCs could influence the cellular cAMP level in human bronchial epithelial (HBE) cells was also discussed in this study.

MATERIALS AND METHODS

Airway Epithelial Cell Culture

The transformed 16-HBE cell line was kindly provided by Dr. Lin Shi of the central lab of Zhongshan Hospital, Fudan University and cultured at 37°C in RPMI (Hyclone) containing fetal calf serum 10% and antibiotics. To assess the effects of GCs, 90% confluent cells were exposed to DEX (Sigma-Aldrich) in various concentrations (10^{-5} M to 10^{-7} M). The concentration of BUDE (Sigma-Aldrich) was ranged from 2.3×10^{-6} M to 2.3×10^{-9} M (1 μg/ml to 1 ng/ml). To antagonize the effects of GCs, mifepristone (RU-486, Sigma-Aldrich) was used at a concentration of 10^{-5} M. 6MB-cAMP (Biolog Life Science Institute, Cat. No. M003) was used at a concentration of 10^{-3} M.

Bacterial Strains

Pseudomonas aeruginosa strain O1 (PAO1) was obtained from the ATCC (ATCC 15692). GFP-labeled *P. aeruginosa* (GFP-PA) was kindly provided by Prof. Yuan-Lin Song, Zhongshan Hospital, Fudan University. Individual strain was routinely grown with shaking overnight in Luria-Bertani broth (LB broth) at 37°C, washed, and diluted to the appropriate concentration in Hanks' balanced salt solution. Bacterial concentrations were determined by densitometry and confirmed by serial dilution followed by viable plate counts on appropriate agar media.

Bacterial Binding Assay

Pseudomonas aeruginosa strain O1 or GFP-PA cells grown overnight in LB broth to stationary phase were diluted in 50 μl of serum-free RPMI and added to cells at a multiplicity of infection (MOI) of 20. After 1 h of infection at 37°C, adhesion assays were performed as described previously (Bucior et al., 2010). Briefly, cells were washed in PBS to remove non-adherent bacteria and were lysed in 1 ml of Ca^{2+}- and Mg^{2+}-free PBS with 0.25% Triton X-100 (Sigma-Aldrich) for 30 min. After lysis, cells were removed from the 96-well plates by gentle scraping. Bacteria were enumerated by plating serial dilutions of cell lysates on LB plates and counting the CFU.

RNA Isolation and Real-Time PCR

RNA was isolated using RNAiso Plus (Takara Bio Inc., Dalian) according to the manufacturer's protocol. Five hundred nanograms of RNA was reverse transcribed using PrimeScript™ RT reagent Kit with gDNA Eraser (Takara Bio Inc., Dalian) and subsequently used for SYBR green-based real-time PCR using a standard protocol (Takara Bio Inc., Dalian). Primers (Sangon, Shanghai, China) used for gene expression: GAPDH (glyceraldehyde 3-phosphate-dehydrogenase) (NCBI GenBank: NM_002046): AGAAGGCTGGGGCTCATTG/AGGGGCCATCCACAGTCT TC; SDC1 (NCBI GenBank:NM_001006946): CTCTGGCT CTGGCTGTGC/GGTCTGCTGTGACAAGGTGA; C/EBP β (NCBI GenBank:NM_001285879.1): ACAGCGACGAGTA CAAGATCC/TGCTTGAACAAGTTCCGCAG.

PCR conditions were 95°C for 10 s followed by 40 cycles with 95°C for 5 s and 60°C for 34 s. The results were calculated applying the ΔΔCT method and were presented in percentage increase relative to control.

Protein Analysis

Cells were lysed with RIPA buffer (10 mM Tris–HCl, pH 7.4, 150 mM NaCl, 1 mM EDTA, 0.1% SDS, 1% Triton X-100,

and 1% sodium deoxycholate) containing Complete Protease Inhibitor (Cell Signaling Technology) and PhosphoSTOP (Roche) for phosphoprotein detection. Protein concentration was determined by using the BCA Protein Assay Kit (Thermo Fisher Scientific), and equal amounts of proteins were separated by electrophoresis in 6% SDS-polyacrylamide gel for SDC1 and 12% gel for other proteins and resolved by electrophoresis (Mini Protean II apparatus; Bio-Rad) at 100 V in a buffer containing 2.5 mM Tris base (pH 8.3), 192 mM glycine, and 0.1% SDS. After electrophoresis, the proteins were transferred to a PVDF membrane (Millipore) with a 300-mA current for 90 min. Membranes were blocked by TBST with 5% milk for 1 h in room temperature. After blocking, the membranes were incubated in a 1:1,000 dilution of the primary antibody at 4°C overnight. The membranes were washed and then incubated in a 1:5,000 dilution of secondary horseradish peroxidase-conjugated goat (anti-rabbit/mouse) IgG (Santa Cruz) in blocking solution. Membranes were again washed and processed for detection of target protein by incubation in an appropriate substrate solution containing a luminol compound (SuperSignal Substrate; Thermo Fisher Scientific) for chemiluminescent signal development.

The following primary and secondary antibodies for western blot were used for detection of SDC1 (AbD Serotec), glucocorticoid-receptor (GR; Cell Signal Technology), C/EBP β (Abcom), Phospho-C/EBP β (Cell Signal Technology), and Glycogen synthase kinase 3β (GSK-3β; Cell Signal Technology).

Cell Surface Syndecan-1 Was Detected by Immunofluorescence

Cells were seeded into 12-well Culture Slide at 3×10^4 cells per well and fixed in 100% cold methanol on ice for 10 min followed by 4% paraformaldehyde at room temperature for 2 min. Cells were blocked with 2.5% goat serum and 2% BSA in TBS for 1 h at room temperature, then incubated with 1:400 primary antibodies for SDC1 (AbD Serotec) in 2% BSA in TBST overnight at 4°C. Secondary antibodies (Alexa Fluor 488 goat anti-mouse IgG or Alexa Fluor 568 or 594 goat anti-mouse IgG, 1:500, Thermo Fisher Scientific) were applied in 2% BSA in TBST for 1 h at room temperature. Cell nucleus was stained with DAPI for 5 min. Slides were cover-slipped using Fluoromount-G (eBioscience) and images were captured with inverted microscope (Leica Microsystems).

Confocal Microscope Images for Adhesion of *Pseudomonas aeruginosa* to Human Bronchial Epithelial

Human bronchial epithelial cells were seeded into 12-well Culture Slide at 3×10^4 cells per well. GFP-PA grown overnight in LB broth to stationary phase were diluted in 50 μl of serum-free RPMI and added to cells at a MOI of 20:1. After 1 h of infection at 37°C, cells were washed in PBS to remove non-adherent bacteria and then fixed in 100% cold methanol on ice for 10 min followed by 4% paraformaldehyde at room temperature for 2 min. The following steps are the same as the immunofluorescence detection. Images were captured with confocal microscope (Zeiss LSM 800).

siRNA Transfection

siRNA targeting SDC1 or C/EBP β was transfected into HBE cells with the transfection reagent TianFect (Tiangen) using the manufacturer's protocol. Briefly, 1.2×10^5 cells were plated into each well of a 24-well plate. Twelve hours after plating the cells, the transfection mixture containing 6 μl of TianFect and 100 nmol siRNA was prepared in 50 μl of Opti-MEM (Thermo Fisher Scientific). After 10 min of incubation, the transfection mixture was added to the cells, bringing the volume to 400 μl. After a 6-h exposure, the medium was removed and replaced with fresh RPMI containing 10% FBS. The sequence of the siRNAs against SDC1 was ggagacagcatcagggtta. The siRNAs against C/EBP β (Cat. stB0005928C-1-5, Ribobio, Guangzhou, China) contains a pool of three to four target-specific siRNAs. As a negative control, cells were transfected with a scrambled sequence not targeting any known gene.

Lentivirus Packaging and Stable Transfection Cell Line Generation

Lentiviral constructs were designed by the HANYINBT (Shanghai). The HBE cells were stably transfected with hU6-MCS-CMV-ZsGreen 1-PGK-Puro negative control vectors and lentivirus (SH-SDC1) for knocking down SDC1. Target cells (1×10^5) were transfected at a lentivirus/medium ratio of 1:50 in the presence of 5 μg/ml polybrene. Puromycin (2 μg/ml) was used to screen the stable transfected HBE cells (SH-HBE). Real-time qPCR and immunofluorescence were used to assess the efficiency of knocking down SDC1 expression in HBE.

Cellular cAMP Measuring

Cellular cAMP was measured as the manufacturer's protocol (Neweast Bioscience, Cat. No. 80203). Briefly, 3×10^4 cells in 100 μl of RPMI with 10% FBS were plated into each well of a 96-well plate. When the confluence reaches about 90%, HBE cells were treated with DEX (10^{-5} M) or BUDE (2.3×10^{-6} M, 1 μg/ml) for 1 h in the presence or absence of RU-486 (10^{-5} M) simultaneously. Cellular cAMP was measured by ELISA method.

Co-immunoprecipitation

Co-immunoprecipitation was performed with a nuclear extraction kit (Active Motif). The nuclear extracts containing 200 μg of proteins were incubated overnight at 4°C with 2 μg of anti-GR antibody (Cell Signal Technology) in 500 μl of NP-40 lysis buffer. Protein A/G beads (60 μl, Thermo Scientific) were added to the mixture and incubated for an additional hour with rocking. The immunocomplexes were then washed six times with NP-40 lysis buffer. The immunoprecipitated proteins were dissolved in 60 μl of 2× Laemmli buffer and boiled for 5 min before analysis by western blotting.

Statistical Analysis

Data are expressed as means ± SD (standard deviation). Statistical significance was estimated by Student's *t*-test using SPSS (19.0 version). Differences were considered to be significant at $p < 0.05$.

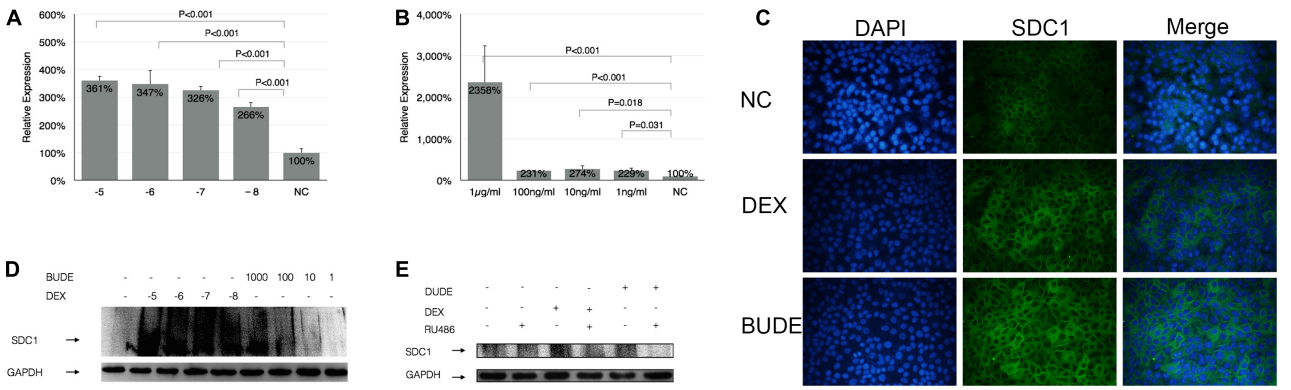


FIGURE 1 | Glucocorticoid enhanced the expression of SDC1. DEX or BUDE increased SDC1 expression by qPCR **(A,B)**, by immunofluorescence staining **(C)**, and by western blot **(D)**. SDC1 is displayed in green (Alexa Fluor 488) and the nucleus is shown in blue (DAPI) in **(C)**. The receptor antagonist RU-486 inhibited SDC1 expression triggered by DEX or BUDE by western blot **(E)**. Student's *t*-test was used to analyze the different groups. Six replications and three independent experiments. Magnification: 400× **(C)**.

RESULTS

Expression of Syndecan-1 Gene Was Influenced by Glucocorticoids

As shown by **Figures 1A,B**, SDC1 expression was dose dependently induced 4 h later by GCs administration *in vitro*. Both DEX and BUDE increased SDC1 expression with a large concentration span from 10^{-5} M to 10^{-7} M of DEX and 2.3×10^{-6} M to 2.3×10^{-9} M (1 μg/ml to 1 ng/ml) of BUDE. The expression even soared more than 23-fold compared to those without stimulation of BUDE. Immunofluorescence staining (**Figure 1C**) and western blot (**Figure 1D**) verified the results from real-time quantitative PCR. SDC1 was mainly located at the HBE cell surface. SDC1 expression was observed in control HBE cells with a significant increase after 24 h stimulation by DEX (10^{-5} M) or BUDE (2.3×10^{-6}, 1 μg/ml) (**Figure 1C**). The DEX- or BUDE-dependent induction of SDC1 was inhibited by the GR antagonist RU-486 (10^{-5} M, incubation for 24 h) (**Figure 1E**). From **Figure 1**, we could see that SDC1 expression was increased by glucocorticoid treatment, which was GR dependent.

Upregulated Syndecan-1 Increased Adhesion of *Pseudomonas aeruginosa* to Human Bronchial Epithelial

The binding experiments were carried out to show the relationship between the SDC1 expression level and the adhesion of PA to HBE. As shown by **Figure 2A**, the adhesion of PA to HBE increased to 125 and 138%, respectively, after stimulation by DEX (10^{-5} M) or BUDE (2.3×10^{-6}, 1 μg/ml) assessed by bacterial binding assay *in vitro* (CFU counting). RU-486 (10^{-5} M) could reverse this function of GCs partially. The confocal microscope was used to show the affinity of PA to HBE cells. From **Figure 2B**, DEX or BUDE increased the fluorescence intensity significantly (red for SDC1). At the same time, the adhesion of PA was upregulated by DEX or BUDE compared with normal control group. RU486, the inhibitor of GR, reversed these functions.

Knocking Down of Syndecan-1 Decreased the *Pseudomonas aeruginosa* Adhesion to Human Bronchial Epithelial

In order to study whether the adhesion level of PA to HBE is associated with the expression of SDC1, the HBE cells knocking down SDC1 were established by lentivirus (SH-HBE). When we established the lentiviral-mediated knockdown of SDC1 in HBE cells, three sequences were used to select the most effective one (data not shown). From **Figure 3A**, the expression of SDC1 stained by red fluorescence was downregulated in the cells transfected by SDC1-SH vectors compared with that of NC-GFP and Blank groups. In **Figure 3B**, quantitative real-time PCR results showed that the SDC1 was downregulated to 23% in SH-HBE compared with that in NC-HBE. The adhesion of PA was decreased to 73% (**Figure 3C**) in the SH-HBE in which SDC1 was downregulated to 23% (**Figure 3B**). These results showed that the adhesion of PA to HBE was positively correlated with the expression level of SDC1.

Syndecan-1 Expression by Glucocorticoids Associated With CCAAT-Enhancer-Binding Protein β

It was reported that C/EBP β was a key transcriptive factor regulating SDC1 expression. In this section, we discussed whether C/EBP β influenced the SDC1 expression. **Figures 4A,B** show the time course of SDC1 and C/EBP β expression stimulated by DEX or BUDE. The expression patterns of SDC1 and C/EBP β were very consistent. C/EBP β expression was earlier than SDC1 for it increased statistically significantly at half an hour (BUDE, 2.3×10^{-6}, 1 μg/ml) or 1 h (DEX, 10^{-5} M) after the stimulation of GCs while SDC1 did not.

CCAAT-Enhancer-Binding Protein β protein expression and its phosphorylation increased after GC stimulation (**Figure 4C**) and this process was GR dependent for RU486 (10^{-5} M)-inhibited C/EBP β expression and its phosphorylation.

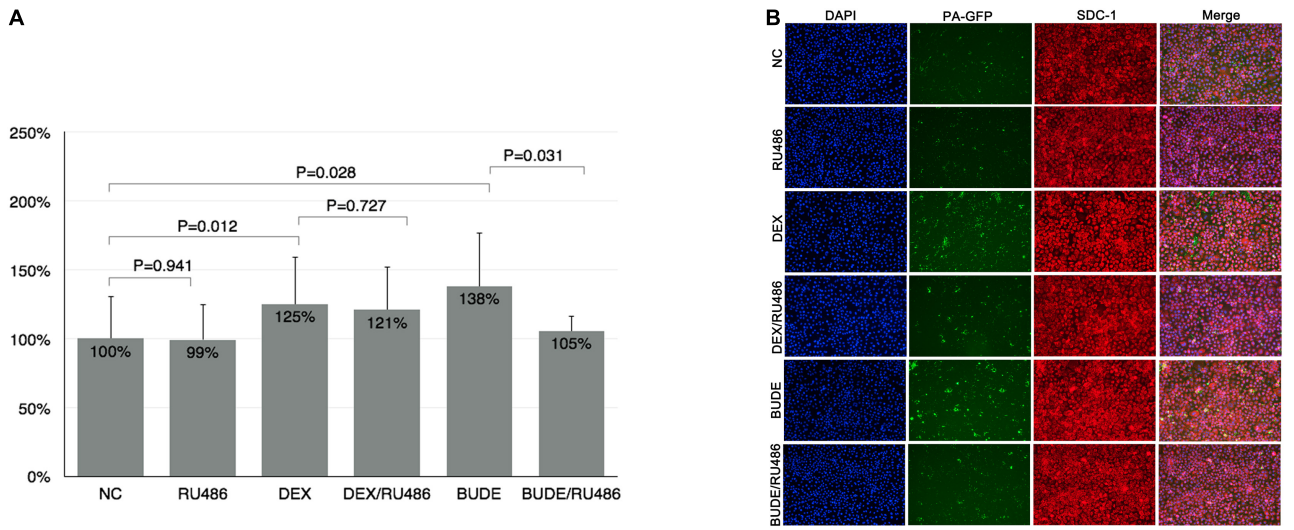


FIGURE 2 | Glucocorticoids enhanced the adhesion of PA to HBE. DEX or BUDE increased the adhesion of PA to HBE assessed by CFU counting **(A)** and by confocal microscopy experiment **(B)**. RU486 inhibited the effects of glucocorticoids. SDC1 was stained by red (Alexa Fluor 568). PA was labeled by GFP (green). The nucleus was stained by DAPI (blue). Student's *t*-test was used to analyze the different groups. Six replications and three independent experiments. Magnification: 400× **(B)**.

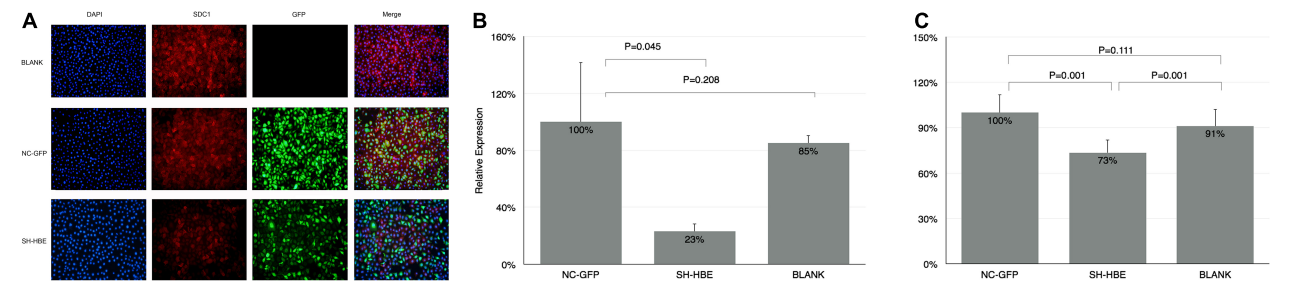


FIGURE 3 | The adhesion of PA was reduced in the SDC1 knockdown HBE. **(A)** SDC1 was successfully downregulated by lentivirus vector carrying SH-RNA (SDC1-SH) assessed by immunofluence method. SDC1 was stained by red (Alexa Fluor 568). Both NC vector and SDC1-SH vector were labeled by GFP (green). The nucleus was stained by DAPI (blue). The qPCR was used to verify the knocking down of SDC1 **(B)**. The adhesion of PA to the knocking down SDC1 HBE cells assessed by CFU counting was decreased compared with that to control HBE cells **(C)**. Student's *t*-test was used to analyze the different groups. Eight replications and three independent experiments. Magnification: 400× **(A)**.

We designed three siRNAs for interfering C/EBP β and the most efficient one could decrease C/EBP β to 23 or 47% with the exposure of DEX (10^{-5} M) or BUDE (2.3×10^{-6}, 1 μg/ml) by qPCR (**Figure 4D**) or western blot (**Figure 4E**). **Figure 4F** shows that the increase of SDC1 with GC exposure was inhibited by C/EBP β siRNA analyzed by qPCR. When the C/EBP β was downregulated by siRNA, the increased adhesion of PA stimulated by GCs decreased compared with that in the group of NC-siRNA for C/EBP β assessed by CFU counting (**Figure 4G**) and confocal microscopy (**Figure 4H**).

CCAAT-Enhancer-Binding Protein β Phosphorylation Was Dependent on Glycogen Synthase Kinase 3β

Glycogen synthase kinase 3β (GSK-3β) is a serine-threonine kinase in the classic Wnt cell signal. GSK-3β was demonstrated to participate into the C/EBP β phosphorylation in a previous study (Lee et al., 2010). The phosphorylated C/EBP β by GSK-3β acquired DNA-binding function and transactivated the subsequent gene expression (Tang et al., 2005). We hypothesized that GSK-3β may be involved in the phosphorylation of C/EBP β at Thr-235 in GC-exposed HBE. To examine this possibility, the ability of GCs to induce C/EBP β phosphorylation was examined in HBE exposed to GSK-3 inhibitors. In **Figure 5A**, GC exposures lead to increased levels of GSK-3β, and RU486 reduced GSK-3β expression with GCs. In **Figure 5B**, the GC-induced phosphorylation of C/EBP β at Thr-235 was reduced by two different GSK-3 inhibitors, LiCl and BIO. These data suggest that GSK-3β was critical for the phosphorylation of C/EBP β at Thr-235 during GC stimulation (**Figure 5C**). The RT-qPCR results indicated that SDC1 was decreased in HBE cells with GSK-3 inhibitors, LiCl and BIO, which further suggests that inhibiting phosphorylation of C/EBP β by controlling of kinase activity of

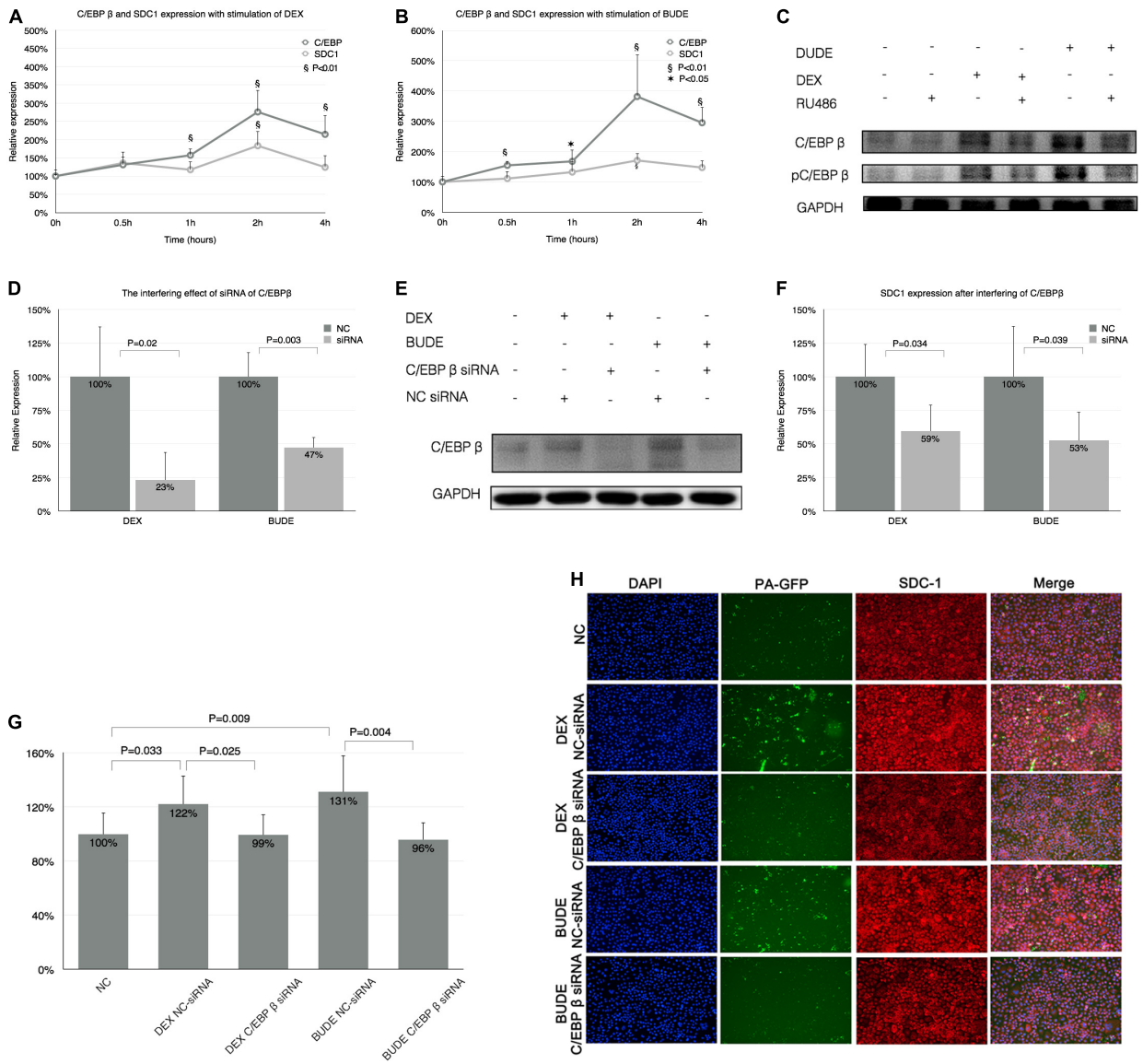


FIGURE 4 | Syndecan-1 expression by GCs associated with C/EBP β. **(A,B)** The time course of SDC1 and C/EBP β expression after stimulation of DEX (10^{-5} M) or BUDE (2.3×10^{-6} M, 1 μg/ml) by qPCR. "*" indicates $p < 0.05$, "§" indicates $p < 0.01$. **(C)** C/EBP β protein and its phosphorylation increased with exposure of GCs and RU-486 (10^{-5} M) reversed these processes analyzed by western blot. C/EBP β was downregulated by C/EBP β siRNA in HBE cells with incubation of DEX or BUDE assessed by qPCR **(D)** and western blot **(E)**. Silencing C/EBP β decreased SDC1 expression assessed by qPCR **(F)** and reversed augmented adhesion of PA stimulated by GCs assessed by CFU counting **(G)** and confocal microscopy **(H)**. SDC1 was displayed in red (Alexa Fluor 594) and the nucleus in blue (DAPI). Magnification: 400× **(H)**. Student's *t*-test was used to analyze the different groups. Four replications for qPCR, eight replications for CFU counting and three independent experiments.

GSK-3β downregulated expression of SDC1, the critical binding protein of PA. Consequently, it is reasonable to speculate that the inhibition of SDC1 expression during the stimulation of GCs by GSK-3β inhibitors can reduce the adhesion of PA to respiratory epithelial cells.

Glucocorticoids upregulates SDC1 expression mainly by genomic signaling. However, RU486 did not reverse the function of BUDE or DEX completely (**Figure 1E**), which may imply the non-genomic effects of glucocorticoids. It was reported that the rise in cellular cAMP augmented the activity of GSK-3β by reducing the phosphorylation at Ser-9 (Larabee et al., 2008). Thus, we planned to detect whether or not GCs could increase the cellular cAMP in HBE cells. As shown in **Figure 6A**, BUDE (2.3×10^{-6} M, 1 μg/ml) incubation for 1 h increased cellular cAMP, which was not RU486 dependent. The cells treated by DEX (10^{-5} M) trended to increase but did not reach statistical significance. SDC1 expression triggered by 6MB-cAMP increased, but not as significant as GC incubation, which indicated that the genomic effect of GCs was the major factor triggering SDC1 expression. When the HBE cell was

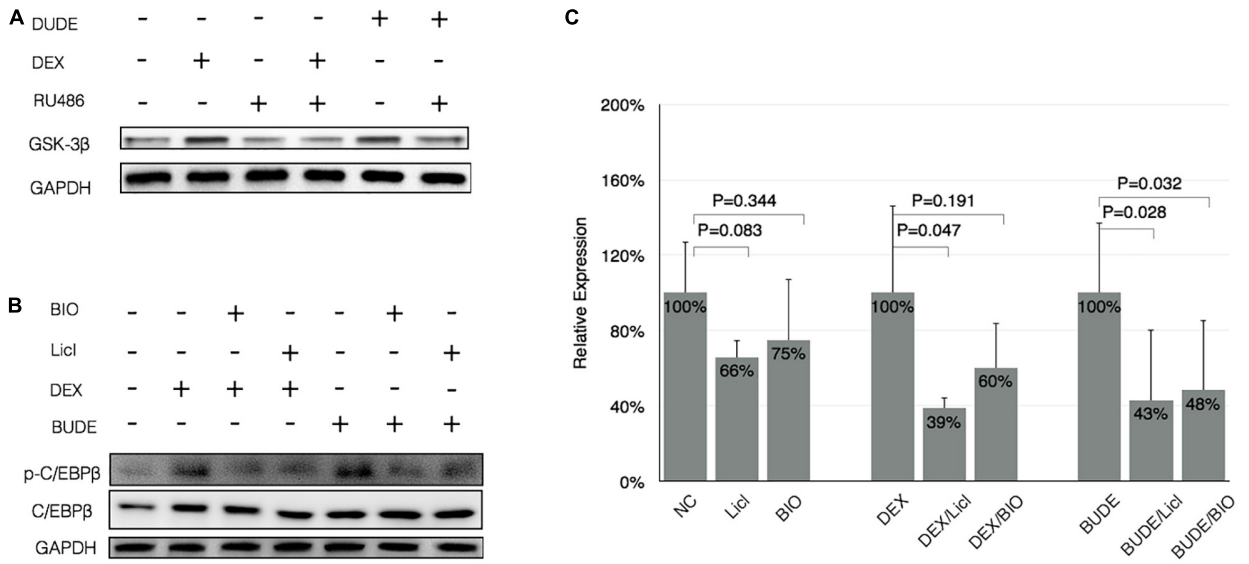


FIGURE 5 | CCAAT-enhancer-binding protein β phosphorylation was dependent on GSK-3β. **(A)** DEX (10^{-5} M) or BUDE (2.3×10^{-6} M, 1 μg/ml) exposure increased expression of GSK-3β assessed by western blot, and the addition of RU-486 reduced levels of GSK-3β in GCs-exposed HBE. **(B)** GSK-3 inhibitors (20 mM LiCl or 5 μM BIO) reduced the GCs-induced phosphorylation of C/EBP β. **(C)** GSK-3 inhibitors reduced the expression of SDC1 with or without GC incubation assessed by real-time qPCR. Student's *t*-test was used to analyze the different groups. Four replications for qPCR and three independent experiments.

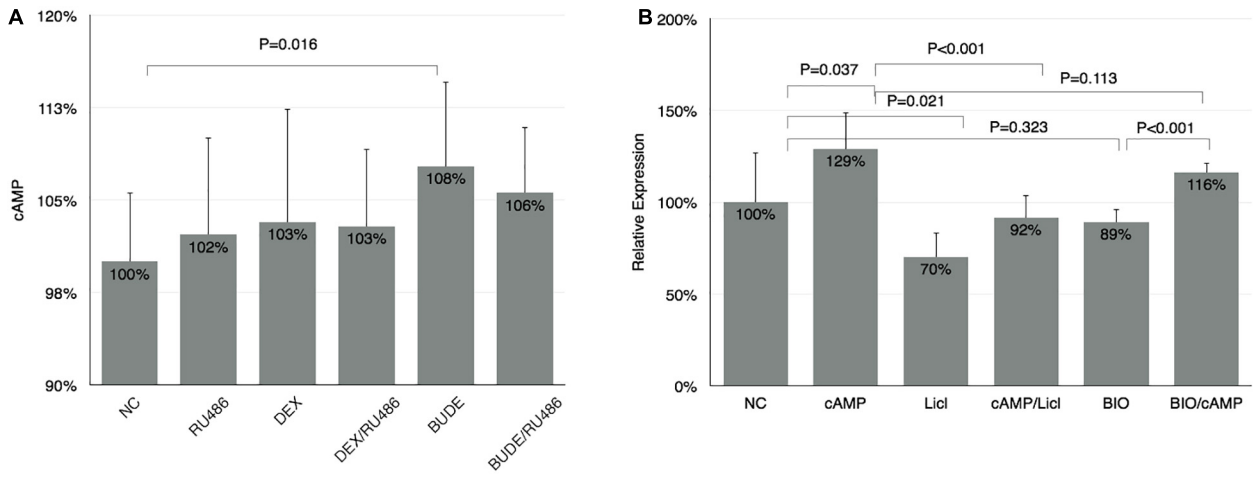


FIGURE 6 | The non-genomic effect of GCs on SDC1 expression. **(A)** BUDE (2.3×10^{-6} M, 1 μg/ml) incubation increased cellular cAMP. RU-486 (10^{-5} M) did not reverse the effect of BUDE. Cellular cAMP was measured by ELISA method. **(B)** 6MB-cAMP triggered SDC1 expression up compared with control analyzed by qPCR. Student's *t*-test was used to analyze the different groups. Four replications for qPCR and ELISA and three independent experiments.

treated with a membrane-permeable analog of cAMP (6MB-cAMP), SDC1 expression increased to 129% compared with control (**Figure 6B**). GSK-3β inhibitors reversed the rising function of 6MB-cAMP to SDC1 in HBE partly. GSK-3β was important for maintaining SDC1 expression at a physiological level in HBE for that the GSK-3β inhibitor (LiCl or BIO) alone downregulated SDC1 expression (**Figure 6B**). GSK-3β inhibitor exposure reversing the function of 6MB-cAMP to SDC1 further verified that cAMP could activate GSK-3β and stimulate subsequent target gene expression. The above results show that although cAMP did not play a major role in the regulation of SDC1 expression, it still contributed to the process to a certain extent, which affected the affinity of PA to epithelial cells.

Glucocorticoid Combined With CCAAT-Enhancer-Binding Protein β Regulated Expression of Syndecan-1

The co-immunoprecipitation experiment was performed to examine whether GR interacted with C/EBP β during its transactivation of SDC1. HBE cells were exposed to DEX (10^{-5} M) or BUDE (2.3×10^{-6} M, 1 μg/ml) for 4 or 24 h.

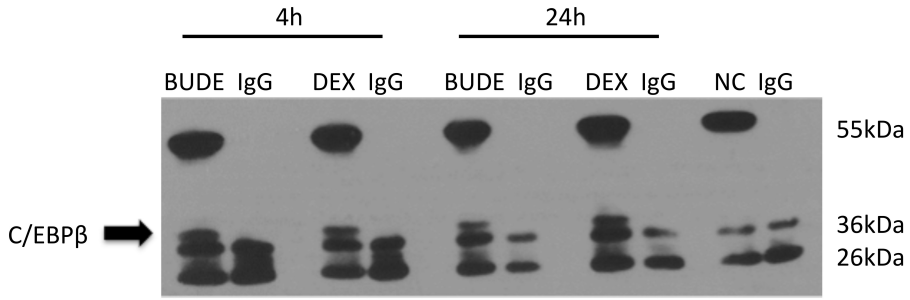


FIGURE 7 | Glucocorticoid receptor combined with C/EBP β regulated expression of SDC1. HBE cells were exposed to Dex (10^{-5} M) or BUDE (2.3×10^{-6} M, 1 μg/ml) for 4 h or 24 h. In the immunoprecipitates of GR, C/EBP β was detectable in GC-treated cells but not in control cells.

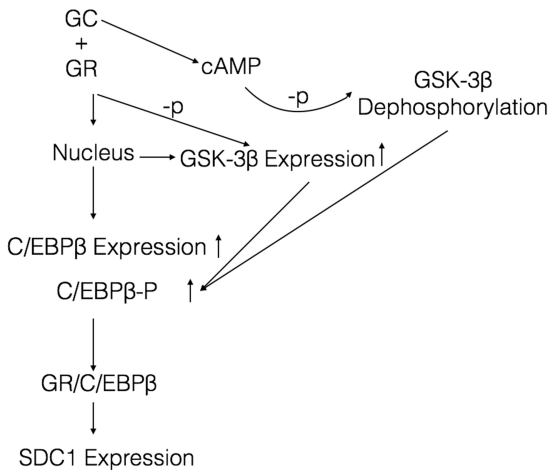


FIGURE 8 | Proposed model depicting a signaling mechanism of GCs to activate SDC1 expression in HBE. Once GCs are delivered to the cytoplasm, GCs bind to GR and enter the nucleus to active the expression of C/EBP β and GSK-3β. GCs also increase the generation of cellular cAMP, which augments the activity of GSK-3β by reducing the phosphorylation. The increased GSK-3β enhances phosphorylation of C/EBP β. The activated C/EBP β binds to GR and induces SDC1 expression.

In the immunoprecipitates of GR, C/EBP β was detectable in GC-treated cells but not in vehicle-treated cells (**Figure 7**). This result indicates the interaction of the GR and C/EBP β for GCs action.

DISCUSSION

The adhesion of PA to HBE increased significantly after GC stimulation assessed by bacterial binding assay and confocal microscopy images. C/EBP β and its phosphorylated form participated in the regulation of glucocorticoid to SDC1 for interfering C/EBP β or inhibiting phosphorylation of C/EBP β by LiCl and BIO, which are inhibitors of GSK-3β, and prevented glucocorticoids from upregulating SDC1 expression. Our study may give a clue to explain why using glucocorticoids are associated with a significantly increased risk of pneumonia. To our knowledge, the present study is the first one to target this issue from a bacterial binding aspect.

Epithelial cells are lined on the mucosal surfaces of respiratory tracts and serve as the primary barrier against the entry of most infectious agents. PA is a ubiquitous opportunistic pathogen of humans and it chronically colonizes the lungs of patients with cystic fibrosis (CF) or other chronic lung diseases, leading to severe pulmonary damage and death.

Syndecan-1 is mainly expressed in placenta and bronchial epithelial cells (Su et al., 2004). SDC1 was reported to mediate PA binding to the airway epithelium through a flagella- and pili-dependent (Bucior et al., 2012) and –independent manner (Plotkowski et al., 2001; Imberty et al., 2004; Chemani et al., 2009; Bucior et al., 2010). SDC1 is preferentially expressed on the basolateral surface of polarized epithelium (Bishop et al., 2007). Chronic inflammation leads to epithelial injury and the exposure of the basolateral surface to the bacteria. Our results proved that GC administration increased the expression of SDC1 significantly. The upregulated SDC1 lead increased PA adhesion to HBE. Knockdown of SDC1 in HBE showed low affinity to PA, which highlights that SDC1 plays a critical role during PA adhesion. SDC1 is also known to mediate binding of various bacterial and viral pathogens besides PA (Freissler et al., 2000; Surviladze et al., 2012). Freissler et al. (2000) showed that overexpression of SDC1 and SDC4 leads to a three- and sevenfold increase in *Neisseria gonorrhoeae* invasion, respectively. *Streptococcus bovis*, *Streptococcus agalactiae*, *Streptococcus pyogenes*, *Staphylococcus aureus*, and *Staphylococcus epidermidis* showed increased adhesion to transfected ARH-77 cells with high expression of SDC1 (Henry-Stanley et al., 2005). Accordingly, it can be speculated that its increase has specific importance in pneumonia after giving GCs.

Glucocorticoid treatment causes robust changes in gene expression. We are unaware of any published reports involving the underlying molecular control of transcriptional interactions between GCs and SDC1. Our results showed that the upregulation of SDC1 was GR dependent for RU486, the inhibitor of GR, and reversed SDC1 increase by GCs.

Glucocorticoid modulates transcription of a few target genes in a unique way that requires the receptor to dimerize with itself or other transcription factors. It was reported that C/EBP β was a key transcriptive factor regulating SDC1 expression

(Larabee et al., 2011). Therefore, we explored the mechanism whether GCs regulate SDC1 through the transcription factor C/EBP β. From our results, we found that GCs upregulated the expression of C/EBP β in a time-dependent way. The increase of C/EBP β was earlier than SDC1. Knockdown of C/EBP β by siRNA significantly blocked the expression of SDC1 triggered by GCs. Phosphorylation of C/EBP β at Thr-235 by GSK-3β was also involved in the SDC1 expression in GC-exposed HBE. These results support the notion that C/EBP β and its phosphorylation level promote the transcription of SDC1 regulated by GCs. Our data are consistent with the literature showing that C/EBP β mediates the effect of fluticasone propionate in host defense gene expression in BEAS-2B cells (Kimura et al., 2001; Zhang et al., 2007). GSK-3β is a serine-threonine kinase in the classic Wnt cell signal. Previous studies have proved that GSK-3β can interact with and phosphorylate C/EBP β, supporting the present results (Lee et al., 2010). The phosphorylated C/EBP β by GSK-3β acquired DNA-binding function and transactivated the subsequent gene expression (Tang et al., 2005). Immunoprecipitate results showed that GR combined with C/EBP β regulated expression of SDC1 (**Figure 7**). Taken together, these results suggest a model where GCs trigger expression of GSK-3β and C/EBP β, leading the phosphorylation of C/EBP β on Thr-235 by GSK-3β and enhancing the ability of C/EBP β to combine GR and activate SDC1 transcription (**Figure 8**).

Our results verified that GCs increased cellular cAMP slightly and SDC1 expression increase was triggered by cAMP mimics (6MB-cAMP). cAMP regulated the expression of SDC1 by GSK-3β in that GSK-3β inhibitors' exposure reversed the function of 6MB-cAMP to SDC1, which further verified that cAMP could activate GSK-3β and stimulate subsequent target gene expression. Kaur et al. (2008) reported that cAMP-elevating agents and a cAMP mimetic could enhance simple GRE-dependent transcription *via* the classical cAMP–PKA pathway. Further studies are needed to demonstrate whether or not the cAMP–PKA pathway is associated with cAMP activating GSK-3β.

It is important to point out that only one human airway epithelial cell line and one strain of PA were used in this study. Though fluticasone propionate upregulated C/EBP β expression in BEAS-2B cells (Kimura et al., 2001), just as we found in this study, it is appropriate to extrapolate our data cautiously in other experiment conditions. Secondly, the data were derived from the *in vitro* experiments, and the *in vivo* environment is much more complex. Additional experiments with pertinent animal models will be needed to confirm this speculation.

CONCLUSION

In summary, our work established a new aspect for better understanding the predilection to infections by PA with the treatment of GCs in chronic lung disease. Administrating GCs increased the interaction between PA and the host airway epithelium by upregulating the expression of SDC1. The strategies based on inhibiting SDC1 upregulation when giving GCs may provide new therapeutic approaches to correct the risk of pneumonia that occurs in administrating GCs in chronic lung disease.

DATA AVAILABILITY STATEMENT

The original contributions presented in the study are included in the article/supplementary material, further inquiries can be directed to the corresponding author/s.

ETHICS STATEMENT

This study was approved by the Ethics Committee of Ruijin Hospital. Neither samples from patients nor animal experiments were involved in this study.

AUTHOR CONTRIBUTIONS

DL contributed to the experimental design, study conduct, data analysis, and manuscript preparation. Y-YZ and M-MS contributed to the experiment conduct. J-MQ contributed to the experimental design, data analysis, and revision of the manuscript. All authors had full access to all study data and had final responsibility for the decision to submit for publication. All authors have reviewed the manuscript and approved the final version for submission.

FUNDING

This study was supported by the National Innovative Research Team of High-level Local Universities in Shanghai and Shanghai Key Laboratory of Emergency Prevention, Diagnosis and Treatment of Respiratory Infectious Diseases (20dz2261100).

REFERENCES

Benad-Mehner, P., Thiele, S., Rachner, T. D., Gobel, A., Rauner, M., and Hofbauer, L. C. (2014). Targeting syndecan-1 in breast cancer inhibits osteoclast functions through up-regulation of osteoprotegerin. *J. Bone Oncol.* 3, 18–24. doi: 10.1016/j.jbo.2013.11.001

Bishop, J. R., Schuksz, M., and Esko, J. D. (2007). Heparan sulphate proteoglycans fine-tune mammalian physiology. *Nature* 446, 1030–1037. doi: 10.1038/nature05817

Bucior, I., Mostov, K., and Engel, J. N. (2010). *Pseudomonas aeruginosa*-mediated damage requires distinct receptors at the apical and basolateral surfaces of the polarized epithelium. *Infect. Immun.* 78, 939–953. doi: 10.1128/iai.01215-09

Bucior, I., Pielage, J. F., and Engel, J. N. (2012). *Pseudomonas aeruginosa* pili and flagella mediate distinct binding and signaling events at the apical and basolateral surface of airway epithelium. *PLoS Pathog.* 8:e1002616. doi: 10.1371/journal.ppat.1002616

Chemani, C., Imberty, A., de Bentzmann, S., Pierre, M., Wimmerova, M., Guery, B. P., et al. (2009). Role of LecA and LecB lectins in *Pseudomonas aeruginosa*-induced lung injury and effect of carbohydrate ligands. *Infect. Immun.* 77, 2065–2075. doi: 10.1128/iai.01204-08

Drummond, M. B., Dasenbrook, E. C., Pitz, M. W., Murphy, D. J., and Fan, E. (2008). Inhaled corticosteroids in patients with stable chronic obstructive pulmonary disease: a systematic review and meta-analysis. *JAMA* 300, 2407–2416. doi: 10.1001/jama.2008.717

Freissler, E., Meyer auf der Heyde, A., David, G., Meyer, T. F., and Dehio, C. (2000). Syndecan-1 and syndecan-4 can mediate the invasion of OpaHSPG-expressing *Neisseria gonorrhoeae* into epithelial cells. *Cell. Microbiol.* 2, 69–82. doi: 10.1046/j.1462-5822.2000.00036.x

Henry-Stanley, M. J., Hess, D. J., Erlandsen, S. L., and Wells, C. L. (2005). Ability of the heparan sulfate proteoglycan syndecan-1 to participate in bacterial translocation across the intestinal epithelial barrier. *Shock* 24, 571–576. doi: 10.1097/01.shk.0000184286.95493.78

Imberty, A., Wimmerova, M., Mitchell, E. P., and Gilboa-Garber, N. (2004). Structures of the lectins from *Pseudomonas aeruginosa*: insight into the molecular basis for host glycan recognition. *Microbes Infect.* 6, 221–228. doi: 10.1016/j.micinf.2003.10.016

Kaur, M., Chivers, J. E., Giembycz, M. A., and Newton, R. (2008). Long-acting beta2-adrenoceptor agonists synergistically enhance glucocorticoid-dependent transcription in human airway epithelial and smooth muscle cells. *Mol. Pharmacol.* 73, 203–214.

Kimura, T., Chowdhury, S., Tanaka, T., Shimizu, A., Iwase, K., Oyadomari, S., et al. (2001). CCAAT/enhancer-binding protein beta is required for activation of genes for ornithine cycle enzymes by glucocorticoids and glucagon in primary-cultured hepatocytes. *FEBS Lett.* 494, 105–111. doi: 10.1016/s0014-5793(01)02320-1

Larabee, J. L., DeGiusti, K., Regens, J. L., and Ballard, J. D. (2008). *Bacillus anthracis* edema toxin activates nuclear glycogen synthase kinase 3beta. *Infect. Immun.* 76, 4895–4904. doi: 10.1128/iai.00889-08

Larabee, J. L., Shakir, S. M., Hightower, L., and Ballard, J. D. (2011). Adenomatous polyposis coli protein associates with C/EBP beta and increases *Bacillus anthracis* edema toxin-stimulated gene expression in macrophages. *J. Biol. Chem.* 286, 19364–19372. doi: 10.1074/jbc.m111.224543

Lee, S. H., Krisanapun, C., and Baek, S. J. (2010). NSAID-activated gene-1 as a molecular target for capsaicin-induced apoptosis through a novel molecular mechanism involving GSK3beta, C/EBPbeta and ATF3. *Carcinogenesis* 31, 719–728. doi: 10.1093/carcin/bgq016

Park, P. W., Pier, G. B., Hinkes, M. T., and Bernfield, M. (2001). Exploitation of syndecan-1 shedding by *Pseudomonas aeruginosa* enhances virulence. *Nature* 411, 98–102. doi: 10.1038/35075100

Plotkowski, M. C., Costa, A. O., Morandi, V., Barbosa, H. S., Nader, H. B., de Bentzmann, S., et al. (2001). Role of heparan sulphate proteoglycans as potential receptors for non-piliated *Pseudomonas aeruginosa* adherence to non-polarised airway epithelial cells. *J. Med. Microbiol.* 50, 183–190. doi: 10.1099/0022-1317-50-2-183

Sarrazin, S., Lamanna, W. C., and Esko, J. D. (2011). Heparan sulfate proteoglycans. *Cold Spring Harb. Perspect. Biol.* 3:a004952.

Singh, S., Amin, A. V., and Loke, Y. K. (2009). Long-term use of inhaled corticosteroids and the risk of pneumonia in chronic obstructive pulmonary disease: a meta-analysis. *Arch. Intern. Med.* 169, 219–229. doi: 10.1001/archinternmed.2008.550

Stolberg, V. R., McCubbrey, A. L., Freeman, C. M., Brown, J. P., Crudgington, S. W., Taitano, S. H., et al. (2015). Glucocorticoid-augmented efferocytosis inhibits pulmonary pneumococcal clearance in mice by reducing alveolar macrophage bactericidal function. *J. Immunol.* 195, 174–184. doi: 10.4049/jimmunol.1402217

Su, A. I., Wiltshire, T., Batalov, S., Lapp, H., Ching, K. A., Block, D., et al. (2004). A gene atlas of the mouse and human protein-encoding transcriptomes. *Proc. Natl. Acad. Sci. U.S.A.* 101, 6062–6067. doi: 10.1073/pnas.0400782101

Suissa, S., Patenaude, V., Lapi, F., and Ernst, P. (2013). Inhaled corticosteroids in COPD and the risk of serious pneumonia. *Thorax* 68, 1029–1036. doi: 10.1136/thoraxjnl-2012-202872

Surviladze, Z., Dziduszko, A., and Ozbun, M. A. (2012). Essential roles for soluble virion-associated heparan sulfonated proteoglycans and growth factors in human papillomavirus infections. *PLoS Pathog.* 8:e1002519. doi: 10.1371/journal.ppat.1002519

Tang, Q. Q., Gronborg, M., Huang, H., Kim, J. W., Otto, T. C., Pandey, A., et al. (2005). Sequential phosphorylation of CCAAT enhancer-binding protein beta by MAPK and glycogen synthase kinase 3beta is required for adipogenesis. *Proc. Natl. Acad. Sci. U.S.A.* 102, 9766–9771. doi: 10.1073/pnas.0503891102

Zhang, N., Truong-Tran, Q. A., Tancowny, B., Harris, K. E., and Schleimer, R. P. (2007). Glucocorticoids enhance or spare innate immunity: effects in airway epithelium are mediated by CCAAT/enhancer binding proteins. *J. Immunol.* 179, 578–589. doi: 10.4049/jimmunol.179.1.578

Conflict of Interest: The authors declare that the research was conducted in the absence of any commercial or financial relationships that could be construed as a potential conflict of interest.

Publisher's Note: All claims expressed in this article are solely those of the authors and do not necessarily represent those of their affiliated organizations, or those of the publisher, the editors and the reviewers. Any product that may be evaluated in this article, or claim that may be made by its manufacturer, is not guaranteed or endorsed by the publisher.

Copyright © 2021 Liu, Zeng, Shi and Qu. This is an open-access article distributed under the terms of the Creative Commons Attribution License (CC BY). The use, distribution or reproduction in other forums is permitted, provided the original author(s) and the copyright owner(s) are credited and that the original publication in this journal is cited, in accordance with accepted academic practice. No use, distribution or reproduction is permitted which does not comply with these terms.

frontiers in Immunology

ORIGINAL RESEARCH
published: 05 November 2021
doi: 10.3389/fimmu.2021.757909

Salmonella Infantis Delays the Death of Infected Epithelial Cells to Aggravate Bacterial Load by Intermittent Phosphorylation of Akt With *SopB*

Bing-Xin Chu, Ya-Nan Li, Ning- Liu, Lan-Xin Yuan, Shi-Yan Chen, Yao-Hong Zhu and Jiu-Feng Wang*

Department of Veterinary Clinical Sciences, College of Veterinary Medicine, China Agricultural University, Beijing, China

OPEN ACCESS

Edited by:
Mario Alberto Flores-Valdez, Centro de Investigación y Asistencia en Tecnología y Diseño del Estado de Jalisco (CIATEJ), Mexico

Reviewed by:
Felix Ngosa Toka, Ross University School of Veterinary Medicine, Saint Kitts and Nevis
Kendal Galbraith Cooper, Rocky Mountain Laboratories (NIAID), United States

***Correspondence:**
Jiu-Feng Wang
jiufeng_wang@hotmail.com

Specialty section:
This article was submitted to Microbial Immunology, a section of the journal Frontiers in Immunology

Received: *13 August 2021*
Accepted: *19 October 2021*
Published: *05 November 2021*

Citation:
Chu B-X, Li Y-N, Liu N-, Yuan L-X, Chen S-Y, Zhu Y-H and Wang J-F (2021) Salmonella Infantis Delays the Death of Infected Epithelial Cells to Aggravate Bacterial Load by Intermittent Phosphorylation of Akt With SopB. Front. Immunol. 12:757909. doi: 10.3389/fimmu.2021.757909

Salmonella Infantis has emerged as a major clinical pathogen causing gastroenteritis worldwide in recent years. As an intracellular pathogen, *Salmonella* has evolved to manipulate and benefit from the cell death signaling pathway. In this study, we discovered that *S*. Infantis inhibited apoptosis of infected Caco-2 cells by phosphorylating Akt. Notably, Akt phosphorylation was observed in a discontinuous manner: immediately 0.5 h after the invasion, then before peak cytosolic replication. Single-cell analysis revealed that the second phase was only induced by cytosolic hyper-replicating bacteria at 3–4 hpi. Next, Akt-mediated apoptosis inhibition was found to be initiated by *Salmonella SopB.* Furthermore, Akt phosphorylation increased mitochondrial localization of Bcl-2 to prevent Bax oligomerization on the mitochondrial membrane, maintaining the mitochondrial network homeostasis to resist apoptosis. In addition, *S*. Infantis induced pyroptosis, as evidenced by increased caspase-1 (p10) and GSDMS-N levels. In contrast, cells infected with the Δ*SopB* strain displayed faster but less severe pyroptosis and had less bacterial load. The results indicated that *S*. Infantis *SopB*–mediated Akt phosphorylation delayed pyroptosis, but aggravated its severity. The wild-type strain also caused more severe diarrhea and intestinal inflammatory damage than the Δ*SopB* strain in mice. These findings revealed that *S*. Infantis delayed the cells' death by intermittent activation of Akt, allowing sufficient time for replication, thereby causing more severe inflammation.

Keywords: *Salmonella* Infantis, Akt, *SopB*, apoptosis, pyroptosis, inflammation, host-pathogen interactions

INTRODUCTION

For decades, non-typhoidal salmonella (NTS) has been one of the most common foodborne zoonosis pathogens worldwide that cause host gastroenteritis. There are more than 2,600 known *Salmonella enterica* serovars, with *Salmonella enterica* serovar Infantis (*S.* Infantis) the third most prevalent serovar of human NTS infections in Europe (1, 2). It is mainly transmitted through contaminated food, such as broiler chicken and pork (3–5). Worryingly, *S.* Infantis infection has been frequently reported in many countries recently, indicating that *S.* Infantis is an emerging pathogen causing gastroenteritis worldwide (6, 7).

Salmonella is a Gram-negative facultative intracellular pathogen that possesses two functionally distinct T3SSs (T3SS1 and T3SS2) encoded in *Salmonella* pathogenicity islands 1 and 2 (SPI1 and SPI2), respectively (8). In epithelial cells, approximately 10–30% of *Salmonella* can escape from the *Salmonella*-containing vacuole (SCV) to the cytoplasm after internalization and replicate there (9). Cytosolic *Salmonella* proliferates faster than SCV bacteria, a phenomenon known as hyper-replication (defined as >20 bacteria/cell) (10, 11). Hyper-replicating *Salmonella* proliferates geometrically within several hours in host cells, causing cell death and extrusion and releasing invasive bacteria into the gastrointestinal tract (11).

Salmonella appears to have evolved to benefit from host cell signaling pathways involved in regulating cell proliferation and death (12–14). Apoptosis is a highly conserved and gene-regulated physiological programmed cell death mechanism. An increasing body of evidence indicated that the pathogenic mechanism of bacteria involves the regulation of apoptosis. The manipulation of apoptosis by *Salmonella* depends on the type of host cell and the stage of infection. Multiple apoptotic pathways are found to be rapidly activated during *Salmonella* infection of macrophages (15–17). In contrast, the apoptosis of infected epithelial cells is inhibited by *Salmonella* (18–20). It is beneficial for *Salmonella* to prolong the lifespan of infected cells, enabling bacteria to gain sufficient time for intracellular replication. *Salmonella* then induces the assembly of inflammasomes when the intracellular bacterial load increases (11, 13). Caspase-1 is subsequently activated, which converts gasdermin D (GSDMD) and the precursors of IL-1β and IL-18 to their active forms. The N-terminal fragment of GSDMD accumulates on the cell membrane, forming a polymeric pore and inducing pyroptosis, which results in the release of the intracellular bacteria and inflammatory cytokines, all of which contribute to inflammation (21–23). During an enteric infection, the induction of inflammation may be conducive to the spread of *Salmonella* in the gastrointestinal tract through the induction of rapid inflammatory pyroptosis. *Salmonella* can effectively escape from infected host cells, infect adjacent normal cells, and eliminate host immunocytes, leading to a weakened immune response (24).

In the battle between the host and *Salmonella*, two pivotal biological processes that occur are apoptosis and pyroptosis. For *Salmonella*, the regulation of cell death is also dependent on the serotype. Interestingly, *Salmonella* Typhi can replicate in macrophages without inducing cytotoxicity, while *Salmonella* Typhimurium causes severe cytotoxicity in macrophages (25). Most studies have focused on the interaction between *S.* Typhimurium and macrophages or other phagocytes, and little is known about the role of programmed cell death in controlling the pathogenesis of *S.* Infantis in epithelial cells. Furthermore, intestinal epithelial cells represent the first point of contact for *Salmonella* with the host after invasion (20, 26). In addition, there are significant differences in SPI-1 expression between *S.* Infantis and *S.* Typhimurium (27). In this study, we revealed that cytosolic *S.* Infantis phosphorylated Akt in a discontinuous manner through *SopB* to delay apoptosis and pyroptosis in infected Caco-2 cells. *S.* Infantis gained sufficient time to proliferate by prolonging the lifespan of infected cells, eventually causing pyroptosis, which was accompanied by the release of inflammatory factors and bacteria. This created favorable conditions for the spread and infection of *S.* Infantis.

MATERIALS AND METHODS

Reagents and Antibodies

The reagents and antibodies used in the study are shown in **Table 1**.

Bacterial Strains

The *S.* Infantis wild-type strain CAU1508 was isolated from the intestinal contents of diarrhea piglets. *S.* Infantis with the pFPV-mCherry plasmid has been previously described (12). The *SopB* mutant strain was derived from the parental *S.* Infantis wild-type strain CAU1508 and constructed using the λ-Red homologous recombination system.

Host Cell Infection and Enumeration of Intracellular Bacteria

Caco-2 cells were purchased from Kunming Cell Bank of Chinese Academy of Sciences. The Caco-2 cells were cultured in DMEM/High Glucose media supplemented with 10% FBS and 1% penicillin streptomycin at 37°C in a 5% CO_2 incubator. Cells were seeded in six-well (1×10^6 cells per well) or 24-well culture plates (1×10^5 cells per well) and infected when the cell density reached 60% (this is to ensure that bacteria can infect as many cells as possible). *Salmonella* was grown in LB medium overnight with shaking at 200 rpm and 37°C, then subcultured in 10 ml fresh LB medium (1:40) with shaking under the same conditions for 4 h. Following that, the bacteria were centrifuged at 4,000 g for 15 min at room temperature and resuspended in PBS. The entire infection was according to the experimental procedure of the gentamicin protection assay. The monolayers were infected at an MOI of ~50 for 15 min and washed three times with PBS supplemented with gentamicin (100 μg/ml) to remove extracellular bacteria. Cells were then incubated in fresh growth medium containing gentamicin (100 mg/ml) for 2 h, followed by growth medium supplemented with gentamicin (10 μg/ml) until the infection was complete. After 15 min of *Salmonella* invasion, the time was 0 hpi (hours post-infection), and the infection lasted for 8 h in total. For groups that required treatment with MK2206 (1 μM) and SC79 (25 μM), both drugs

TABLE 1 | Reagents and antibodies.

Reagents and antibodies	Catalog number	Company/Brand	Origin
Mito-Tracker Red CMXRos	C1035	Beyotime Biotechnology	Shanghai, China
Hoechst 33342	C1025	Beyotime Biotechnology	Shanghai, China
SC79	SF2730	Beyotime Biotechnology	Shanghai, China
MK2206	SF2712	Beyotime Biotechnology	Shanghai, China
Cell Mitochondria Isolation Kit	C3601	Beyotime Biotechnology	Shanghai, China
Enhanced Cell Counting Kit-8	C0042	Beyotime Biotechnology	Shanghai, China
Alexa Fluor 488-labeled Goat Anti-Rabbit IgG(H+L)	A0423	Beyotime Biotechnology	Shanghai, China
4',6'-diamidino-2-phenylindole (DAPI) solution	C0060	Beijing Solarbio Science & Technology Co., Ltd.	Beijing, China
Calcein-AM/PI	CA1630	Beijing Solarbio Science & Technology Co., Ltd.	Beijing, China
Gentamycin Sulfate	G8170	Beijing Solarbio Science & Technology Co., Ltd.	Beijing, China
Carbonyl cyanide 3-chlorophenylhydrazone (CCCP)	C6700	Beijing Solarbio Science & Technology Co., Ltd.	Beijing, China
Chlorquine diphosphate salt	C6628	Sigma-Aldrich	St. Louis, USA
Triton X-100	T8787	Sigma-Aldrich	St. Louis, USA
Dulbecco's Modified Eagle Medium (DMEM)/High Glucose	SH30022.01	GE Healthcare Life Sciences HyClone Laboratories	Utah, USA
Phosphate buffered saline (PBS)	SH30256.01	GE Healthcare Life Sciences HyClone Laboratories	Utah, USA
Fetal bovine serum (FBS)	10099141	Thermo Fisher Scientific	Rockford, USA
Annexin V-PE/7-AAD Apoptosis Detection Kit	A213	Vazyme Biotech Co., Ltd	Jiangsu, China
TUNEL FITC Apoptosis Detection Kit	A111-01	Vazyme Biotech Co., Ltd	Jiangsu, China
Rabbit Anti-LAMP 1 polyclonal antibody	21997-1-AP	Proteintech Group Inc	Rosemont, USA
Rabbit Anti-Occludin polyclonal antibody	27260-1-AP	Proteintech Group Inc	Rosemont, USA
Rabbit Anti-Claudin-1 polyclonal antibody	13050-1-AP	Proteintech Group Inc	Rosemont, USA
Rabbit Anti-Caspase 9/p35/p10 polyclonal antibody	10380-1-AP	Proteintech Group Inc	Rosemont, USA
Rabbit Anti-Bax polyclonal antibody	50599-2-Ig	Proteintech Group Inc	Rosemont, USA
Rabbit Anti-Bcl-2 polyclonal antibody	12789-1-AP	Proteintech Group Inc	Rosemont, USA
Rabbit Anti-VDAC1 polyclonal antibody	55259-1-AP	Proteintech Group Inc	Rosemont, USA
Rabbit Anti-Phospho-Caspase-9 (Ser196) polyclonal antibody	28794-1-AP	Proteintech Group Inc	Rosemont, USA
Rabbit Anti-Cytochrome c monoclonal antibody	66264-1-Ig	Proteintech Group Inc	Rosemont, USA
Mouse Anti-Beta ACTIN monoclonal antibody	60008-1-Ig	Proteintech Group Inc	Rosemont, USA
HRP-conjugated Affinipure Goat Anti-Rabbit IgG(H+L)	SA00001-2	Proteintech Group Inc	Rosemont, USA
HRP-conjugated Affinipure Goat Anti-Mouse IgG(H+L)	SA00001-1	Proteintech Group Inc	Rosemont, USA
Rabbit Anti-Cleaved Caspase-3 monoclonal antibody	9661T	Cell Signaling Technology	Danvers, USA
Mouse Anti-Cleaved PARP monoclonal antibody	9548T	Cell Signaling Technology	Danvers, USA
Rabbit Anti-Phospho-Akt (Ser473) monoclonal antibody	4060T	Cell Signaling Technology	Danvers, USA
Rabbit Anti-Phospho-Akt (Thr308) monoclonal antibody	13038T	Cell Signaling Technology	Danvers, USA
Rabbit Anti- Caspase-1 monoclonal antibody	24232S	Cell Signaling Technology	Danvers, USA
Rabbit Anti-ZO-1 polyclonal antibody	40-2300	Thermo Fisher Scientific	Rockford, USA
Rabbit Anti-Phospho-Bad (Ser136) polyclonal antibody	ab15098	Abcam	Cambridge, UK
Rabbit Anti GSDMD-N monoclonal antibody	ab215203	Abcam	Cambridge, UK

were added 2 h before infection, and their concentrations remained unchanged in the medium until the end of the experiment. For the positive control of apoptosis, cells treated with CCCP (Carbonyl cyanide 3-chlorophenylhydrazone, an apoptosis inducer, 50 μM) for 1 h before other experiments were carried out (immunoblotting or immunofluorescence).

Cell Viability Assay

Cell viability was determined using the Cell Counting Kit-8. Cells were seeded in 96-well culture plates. At the end of each treatment, the medium was removed and replaced with 100 μl medium containing 10 μl fresh CCK-8 solution, then incubated at 37°C for 2 h. Following that, absorbance was measured at 450 nm. Experiments were performed six times on each group to ensure the authenticity of the results.

Enumeration of Intracellular Bacteria

In order to quantify viable intracellular bacteria, monolayers in six-well plates were washed three times with PBS containing gentamicin (100 mg/ml) for 5 min each time before being lysed in 1 ml of 0.3% (v/v) Triton X-100. Serial dilutions were plated on LB agar plates. For quantification of intracellular cytosolic bacteria, cells were co-incubated with media containing chloroquine (700 μM) for 1 h before being solubilized in 1 ml of 1% (v/v) Triton X-100, then plated on LB agar plates.

Apoptosis Assay

After *Salmonella* infection, Caco-2 cells were collected, washed twice with PBS, suspended in 100 μl 1× binding buffer, and stained with the Annexin V-PE/7-AAD Apoptosis Detection Kit. Next, 5 μl each of Annexin V-PE and 7-ADD were added to each sample and incubated in the dark for 15 min. Flow cytometry analysis was performed using a BD FACSVerse™ Flow Cytometer.

Calcein-AM/PI Assay

Cells were seeded into 24-well plates. After 8 h of *Salmonella* infection, media was removed and the cells were washed with PBS. Following that, 2 ml of 1× assay buffer supplemented with Calcein-AM (2 μM) and PI (4.5 μM) was added to the cells and

incubated at 37°C for 15 min. The samples were then examined with a fluorescence microscope under a 490 ± 10 nm excitation filter.

Western Blotting

Total protein of Caco-2 cells was extracted using RIPA buffer (Solarbio, Beijing, China) containing a protease/phosphatase inhibitor cocktail (Cell Signaling Technology, USA) on ice for 30 min. Protein concentration was quantified using the BCA Protein Assay kit (23227, ThermoFisher Scientific). SDS-PAGE was used to separate protein samples, which were then transferred to polyvinylidene fluoride membranes. After incubation with 5% skim milk, the membranes were incubated with primary antibodies. Further details about the primary antibodies are described in the **Table 2**. Next, the membranes were incubated with secondary antibodies, then coated with ECL immunoblotting substrate. Images were captured using a Tanon 6200 chemiluminescence imaging workstation.

Immunofluorescence

Cells were fixed with 4% paraformaldehyde and permeabilized with 1% (v/v) Triton X-100. Following that, the samples were blocked with 2% bovine serum albumin at room temperature. The samples were then incubated with anti-LAMP1 (1:100); anti-Cleaved-caspase-3 (1:100); anti-Cytochrome c (1:50); anti-Phospho-Akt (Thr308) (1:800); anti-Tom-20 (1:200) at 4°C overnight. The Mito-Tracker Red CMXRos was used to label mitochondria. Next, the samples were incubated with secondary antibodies at room temperature. Either DAPI or Hoechst 33342 was used to stain the DNA. Images were taken using a Nikon A1 confocal laser scanning microscope.

Mitochondrial Network Morphology Assay

Mitochondria were labeled with Tom-20 and imaged using confocal microscopy. The Mitochondrial Network Analysis (MiNA) toolset, which consists of a relatively simple pair of macros using existing ImageJ plug-ins, was used to analyze the mitochondrial networks.

Animal Infection Experiment

All animal work was performed in accordance with the Guidelines for Laboratory Animal Use and Care of the Chinese Center for Disease Control and Prevention and the Rules for Medical Laboratory Animals (1998) of the Chinese Ministry of Health. A total of 36 six-week-old male C57BL/6 mice were obtained from Charles River Laboratory Animal Technology Co., Ltd (Beijing, China). Mice were provided food and water *ad libitum* throughout the entire experiment. All mice were administered a single dose of streptomycin (15 mg per mouse) *via* gastric gavage before being infected *via* gavage 24 h later (2×10^6 *Salmonella* in 200 μl of PBS). Control mice were orally fed an equal volume of PBS. The mice were then euthanized, and their ileum tissues were harvested 3 days after infection. Mice feces were homogenized in 1 ml of PBS, and serial dilutions were plated on LB agar plates to quantify bacterial burdens.

Assessment of Diarrhea Degree

The severity of diarrhea was evaluated using the fecal score and the dry/wet weight of fecal pellets. The fecal scoring criteria were as follows: 1 (normal stool); 2 (slightly wet, soft stool and formed stool); 3 (wet and unformed stool with mucus); 4 (watery stool). In order to determine the fecal dry/wet weight ratio, mice were separately placed in a clean cage, without food or water. Next, 0.5 g of feces was collected and weighed. Following that, the feces were placed in a 60°C oven for 24 h until the weight change was less than 1% before being weighed. The dry/wet weight ratio was then calculated.

Histopathologic Section

In order to evaluate ileal pathology, the mid-segments of the ileum were excised, rinsed with saline, then fixed with 4% paraformaldehyde for 48 h. Paraffin-embedded tissue samples

TABLE 2 | The dilution ratio of primary antibodies.

Antibody	Dilution rate
Rabbit Anti-LAMP 1 polyclonal antibody	1:2,000
Rabbit Anti-Occludin polyclonal antibody	1:1,500
Rabbit Anti-Claudin-1 polyclonal antibody	1:2,000
Rabbit Anti-Caspase 9/p35/p10 polyclonal antibody	1:500
Rabbit Anti-Bax polyclonal antibody	1:5,000
Rabbit Anti-Bcl-2 polyclonal antibody	1:1,000
Rabbit Anti-VDAC1 polyclonal antibody	1:1,000
Rabbit Anti-Phospho-Caspase-9 (Ser196) polyclonal antibody	1:1,000
Rabbit Anti-Cytochrome c monoclonal antibody	1:5,000
Mouse Anti-Beta ACTIN monoclonal antibody	1:5,000
Rabbit Anti-Cleaved Caspase-3 monoclonal antibody	1:1,000
Mouse Anti-Cleaved PARP monoclonal antibody	1:1,000
Rabbit Anti-Phospho-Akt (Ser473) monoclonal antibody	1:2,000
Rabbit Anti-Phospho-Akt (Thr308) monoclonal antibody	1:2,000
Rabbit Anti- Caspase-1 monoclonal antibody	1:1,000
Rabbit Anti-ZO-1 polyclonal antibody	1:500
Rabbit Anti-Phospho-Bad (Ser136) polyclonal antibody	1:500
Rabbit Anti GSDMD-N monoclonal antibody	1:1,000

were sectioned (3 μm) and stained with hematoxylin and eosin. A neutral resin was used for sealing. Tissue sections were observed and imaged using an Olympus CX23 microscope equipped with an imaging system.

Real-Time Quantitative PCR

For gene expression analysis, total RNA was extracted from ileal tissues using the Trizol reagent (Invitrogen, Carlsbad, CA, USA). RNA transcription was performed using the PrimeScriptTM RT Reagent Kit according to the manufacturer's instructions (RR047A, TaKaRa, Japan). Quantitative real-time RT-PCR was performed using the SYBR Green PCR Master Mix (LS2062, Promega, USA). The cycle threshold (CT) values of target genes were normalized to the CT value of hypoxanthine gene hypoxanthine phosphoribosyl-transferase. The results were presented as fold-change using the $2^{-\Delta\Delta CT}$ method. Primer sequences for PCR are listed in **Table 3**.

Statistical Analysis

All statistical analysis was performed using GraphPad Prism 7 with a one-way ANOVA or a t-test with Bonferroni correction. Data were presented as means ± SEM. $P < 0.05$ was considered statistically significant.

RESULTS

S. Infantis Can Hyper-Replicate in Caco-2 Cells

The curves showed that the bacterial load began to rapidly increase at 4 hpi and peaked at 8 hpi (**Figure 1A**). We discovered two bacterial subpopulations in the cell by adding chloroquine (used to selectively kill vacuolar bacteria): one in the SCV and the other free in the cytoplasm. The bacterial load was mainly contributed by cytosolic bacteria (**Figure 1A**). Next, we used mCherry-*S.* Infantis to infect the cells and LAMP-1 to label SCV for confirmation. Confocal microscopy images revealed that cytosolic *S.* Infantis was the absolute dominant subpopulation (**Figure 1B**).

S. Infantis Infection Does Not Induce Apoptosis of Caco-2 Cells

The cell survival rate significantly decreased at 6 hpi and remained almost unchanged after 8 hpi (**Figure 1C**). Therefore, we focused on the 0–8 hpi period, which encompasses the peak of cytosolic replication and the low phase of cell viability. The results showed that Caspase-9, Cleaved-caspase-3, and Cleaved-PARP were not activated during *S.* Infantis infection (**Figure 1D**). Morphological analysis of apoptosis revealed that *S.* Infantis infection did not result in apoptotic characteristics of the nucleus (**Figures 1B, E**). These findings indicated that cytosolic *S.* Infantis hyper-replicated in Caco-2 cells without inducing apoptosis.

Cytosolic *S.* Infantis Inhibits Apoptosis by Intermittently Phosphorylating Akt

Akt regulates cell survival and suppresses apoptosis *via* phosphorylation at Thr308 and Ser473 sites (27–29). Several studies have found that Akt is constantly phosphorylated after *S.* Typhimurium invades epithelial cells (18, 20). In this study, we hypothesized that continuous Akt phosphorylation contributes to the inhibition of apoptosis. As seen in **Figure 2A**, phosphorylation of Akt occurred in a discontinuous manner during *S.* Infantis infection. The first phase occurred at 0.5 hpi and rapidly decreased to near the background level. The second phase was observed at 3–4 hpi, with the expression of p-Akt higher than in the first phase. The levels of Cleaved-caspase-3 and Cleaved-PARP significantly increased after Akt phosphorylation was inhibited by MK2206, an Akt inhibitor that inhibits Akt phosphorylation at Thr 308 and Ser 473 (**Figures 2B, C**).

Next, we explored which parts of the bacteria induced Akt phosphorylation. At 0.5 hpi, Akt phosphorylation was observed in all infected cells (**Figure 2D**). Images at 4 hpi revealed high levels of p-Akt in cells containing cytosolic hyper-replicating *S.* Infantis (bacteria number >20), which were not observed at 8 hpi (**Figure 2E**). In infected cells without cytosolic bacteria, phosphorylation of p-Akt was not detected at 4 and 8 hpi (**Figure 2F**). These results demonstrated that *S.* Infantis-

TABLE 3 | Real-time PCR primers.

Primer name	Direction[a]	Sequence (5′→3′)
TNF-α	F	CCTGTAGCCCACGTCGTAG
	R	GGGAGTAGACAAGGTACAACCC
IL-6	F	TCTATACCACTTCACAAGTCGGA
	R	GAATTGCCATTGCACAACTCTTT
IL-1β	F	GAAATGCCACCTTTTGACAGTG
	R	TGGATGCTCTCATCAGGACAG
IL-18	F	TGTTGAGCATGAAAAGCCTCTAT
	R	AGGTCTCCCGAATTGGAAAGG
IL-22	F	ATGAGTTTTTCCCTTATGGGGAC
	R	GCTGGAAGTTGGACACCTCAA
IFN-γ	F	ATGAACGCTACACACTGCATC
	R	CCATCCTTTTGCCAGTTCCTC
β-Actin	F	CTACCTCATGAAGATCCTGACC
	R	CACAGCTTCTCTTTGATGTCAC

[a]*F, forward; R, reverse.*

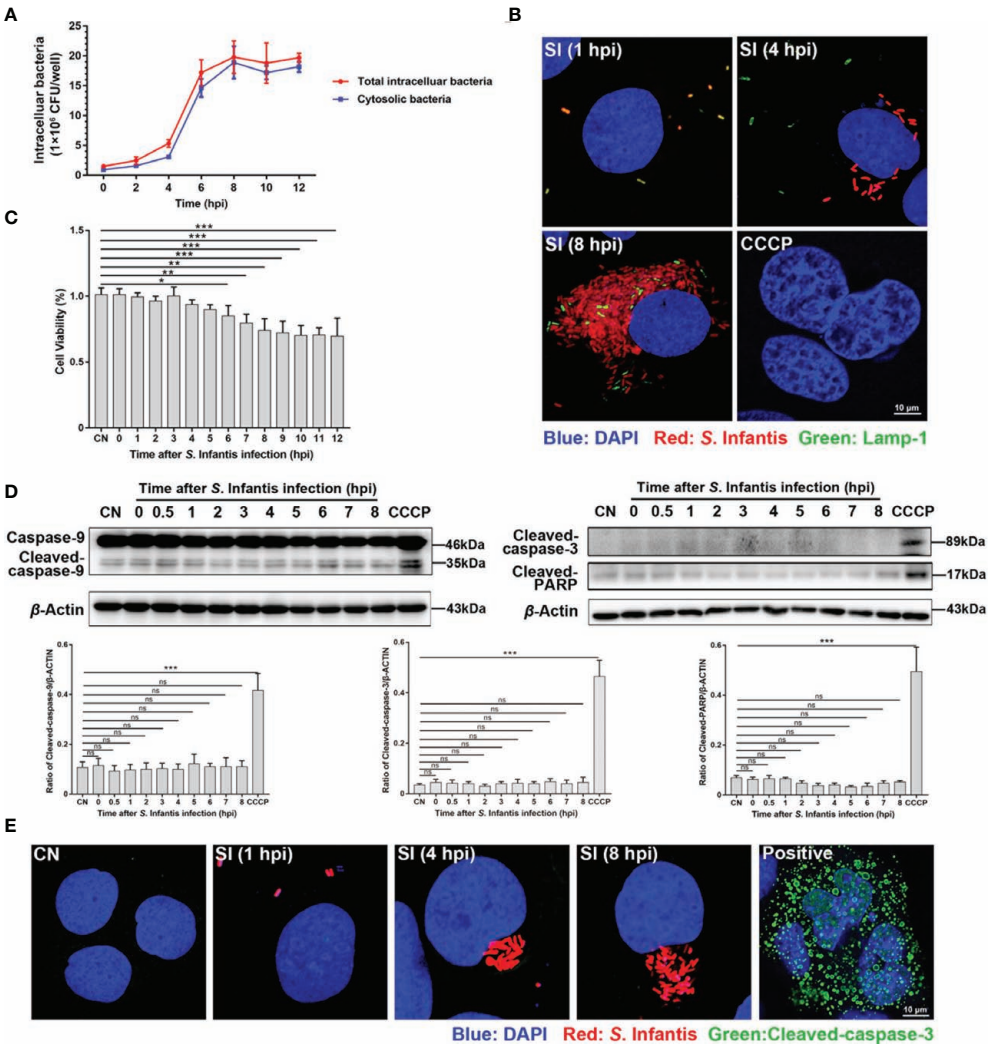


FIGURE 1 | Infected cells containing hyper-replicating cytosolic *S*. Infantis did not undergo apoptosis. **(A)** Detection of intracellular bacterial load using the gentamicin protection assay, without (total intracellular bacteria, red curve) or with (cytosolic bacteria, blue curve) chloroquine. Data were obtained from three independent replicates of each sample at 0, 2, 4, 6, 8, 10, and 12 hpi. **(B)** Detection of the distribution and proportion of two subpopulations in Caco-2 cells by immunofluorescence staining. SI, *S*. Infantis. Red: *Salmonella*. Green: Lamp-1. Blue: DAPI. Scale bar, 10 μm. **(C)** Cell viability assay of Caco-2 cells infected with *S*. Infantis within 12 h. CN, control. **(D)** Western blot analysis of Caspase-9, Cleaved-caspase-3, and Cleaved-PARP protein expression levels within 12 h after bacterial infection. A total of 10 time points were set for sampling: 0, 0.5, 1, 2, 3, 4, 5, 6, 7, 8 hpi. CN, control. ns, no significant difference. **(E)** Immunofluorescence staining analysis of Cleaved-caspase-3 in Caco-2 cells. Samples were treated at 1, 4, and 8 hpi, respectively. CN, control; SI, *S*. Infantis. Red: *S*. Infantis. Green: Cleaved-caspase-3. Blue: DAPI. Scale bar, 10 μm. CCCP was the apoptosis-positive control group. Data were presented as the mean ± SEM from three independent experiments (n = 3). $^{*}P < 0.05$, $^{**}P < 0.01$, $^{***}P < 0.001$.

induced Akt phosphorylation occurred in two distinct phases. The first phase is widely induced after the invasion and rapidly depleted within 30 min, whereas the second phase is only induced by cytosolic bacteria at 3–4 hpi. Both phases of Akt phosphorylation inhibited apoptosis of the infected cells.

Inhibition of Apoptosis by Akt Intermittent Phosphorylation Is Mediated by Cytosolic *S*. Infantis *SopB*

Notably, the SPI1 effector *SopB*, which contributes to invasion and SCV maturation, has 4-phosphatase activity, which can induce Akt activation during *S*. Typhimurium infection (18, 20). As expected, the p-Akt level was almost completely diminished in cells infected with the *ΔSopB* mutant (**Figures 3A, C**). Interestingly, LY294002 (Ly, a pan Akt inhibitor) completely inhibited Akt phosphorylation, but there was a certain expression of p-Akt after Wortmannin (Wor, a PI3K/Akt inhibitor) treatment (**Figure 3B**). Furthermore, infection with the *SopB* mutant induced apoptosis, as demonstrated by nuclear chromatin condensation and increase of Cleaved-caspase-3 and Cleaved-PARP levels (**Figures 3C, D**). The SC79 (an Akt phosphorylation activator) was used to

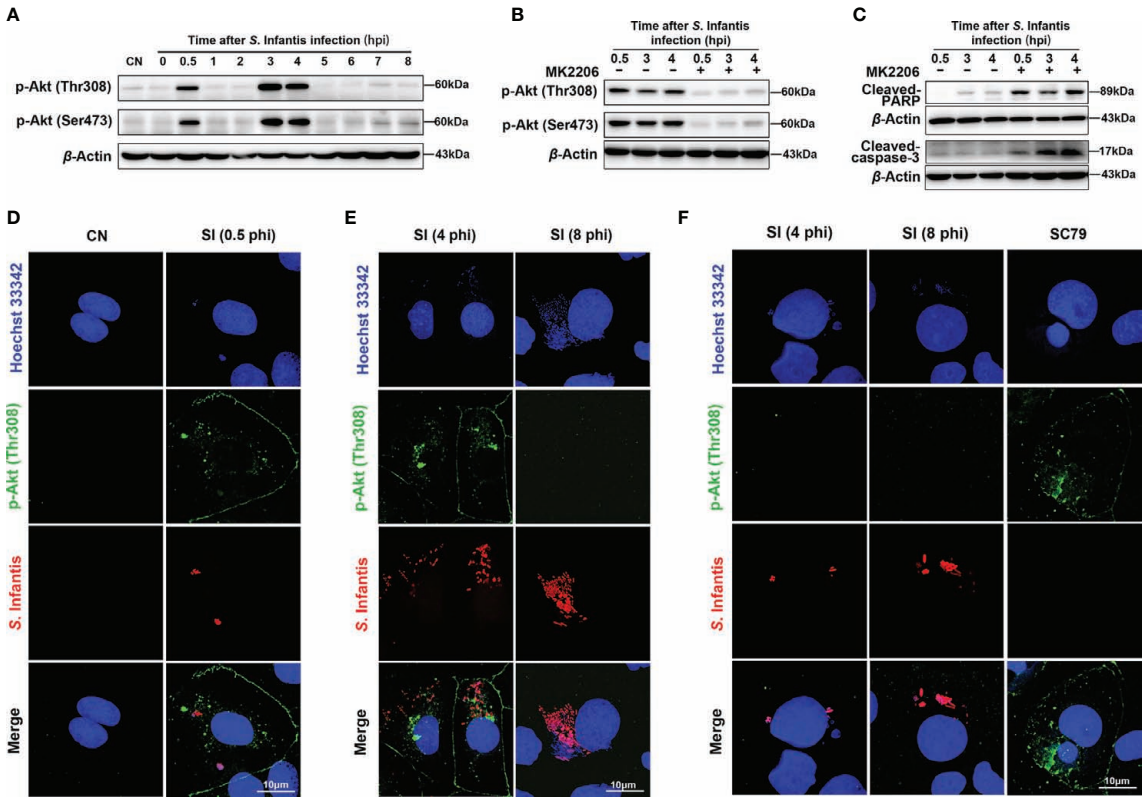


FIGURE 2 | Cytosolic hyper-replicating *S*. Infantis inhibited apoptosis by intermittently phosphorylating Akt. **(A)** Western blot analysis of p-Akt (Ser473) and p-Akt (Thr308) protein expression levels at 0, 0.5, 1, 2, 3, 4, 5, 6, 7, 8 hpi, respectively. CN, control. **(B)** Immunoblotting verified the inhibitory effect of MK2206 on p-Akt (Ser473) and p-Akt (Thr308) protein expression levels at 0.5, 3, and 4 hpi. **(C)** Western blot analysis of Cleaved-caspase-3 and Cleaved-PARP protein expression levels at 0.5, 3, and 4 hpi after after p-Akt was suppressed by MK2206. **(D–F)** Immunofluorescence staining analysis p-Akt (Thr308) distribution. CN, control; SI, *S*. Infantis. **(D)** Distribution of p-Akt (Thr308) in all infected cells at 0.5 hpi. **(E)** Expression of p-Akt (Thr308) in infected cells containing cytosolic hyper-replicating *S*. Infantis at 4 and 8 hpi. **(F)** Expression of p-Akt (Thr308) in infected cells without cytosolic hyper-replicating *S*. Infantis at 4 and 8 hpi. At least 100 cells were counted for each group. Red: *S*. Infantis. Green: p-Akt (Thr308). Blue: Hoechst 333342. Data were presented as the mean ± SEM from three independent experiments (n = 3).

activate Akt (**Figure 3E**), with findings confirming that *SopB*-mediated Akt intermittent phosphorylation inhibited apoptosis of infected cells (**Figures 3F, G**). Importantly, wild-type (WT) *S*. Infantis had enough time for intracellular replication, resulting in increased bacterial load by inhibiting apoptosis (**Figure 3H**).

SopB Mediated Akt Phosphorylation Inhibits Apoptosis by Maintaining Mitochondrial Dynamic Network Homeostasis

The mitochondrion is the primary control organelle responsible for endogenous apoptosis. In normal cells, individual mitochondria connect to form tubules and shape dynamic networks through continuous division and fusion (30). Therefore, we evaluated the morphology of the infected cells' mitochondrial network. At 4 hpi, the mitochondria of WT *S*. Infantis–infected cells still maintained an abundant network structure, but infection with the *SopB* mutant disrupted the mitochondrial network (**Figure 4A**). The mitochondrial cavity also appeared to be expanding, as evidenced by the ring-shaped structure (yellow arrows) (**Figure 4A**). Morphological analysis of the mitochondrial network revealed that infection with the WT strain had no discernible effect on the dynamics of the mitochondrial network (**Figure 4B**).

The key events of mitochondria-mediated apoptosis are the opening of mitochondrial permeability transition pore (MPTP) and the release of cytochrome c (31, 32). In the WT group, cytochrome c and mitochondria remained co-localized, while mk2206 treatment resulted in cytochrome c translocation from the mitochondria to the cytoplasm (**Figures 4C, D**). Infection with the *SopB* mutant resulted in massive cytochrome c release into cytoplasm, which was reversed by the addition of SC79, partially restoring the mitochondrial network (**Figures 4C, D**). Interestingly, co-localization of cytochrome c and mitochondria was also restored by the addition of CSA (a MPTP blocker) (**Figure 4C**). The mitochondrial membrane permeability may be affected by p-Akt induced by *SopB*, and the Bcl-2 family regulates the permeability of the mitochondrial outer membrane by inhibiting Bax translocation from the cytosol to the mitochondria (33, 34). We extracted mitochondrial protein

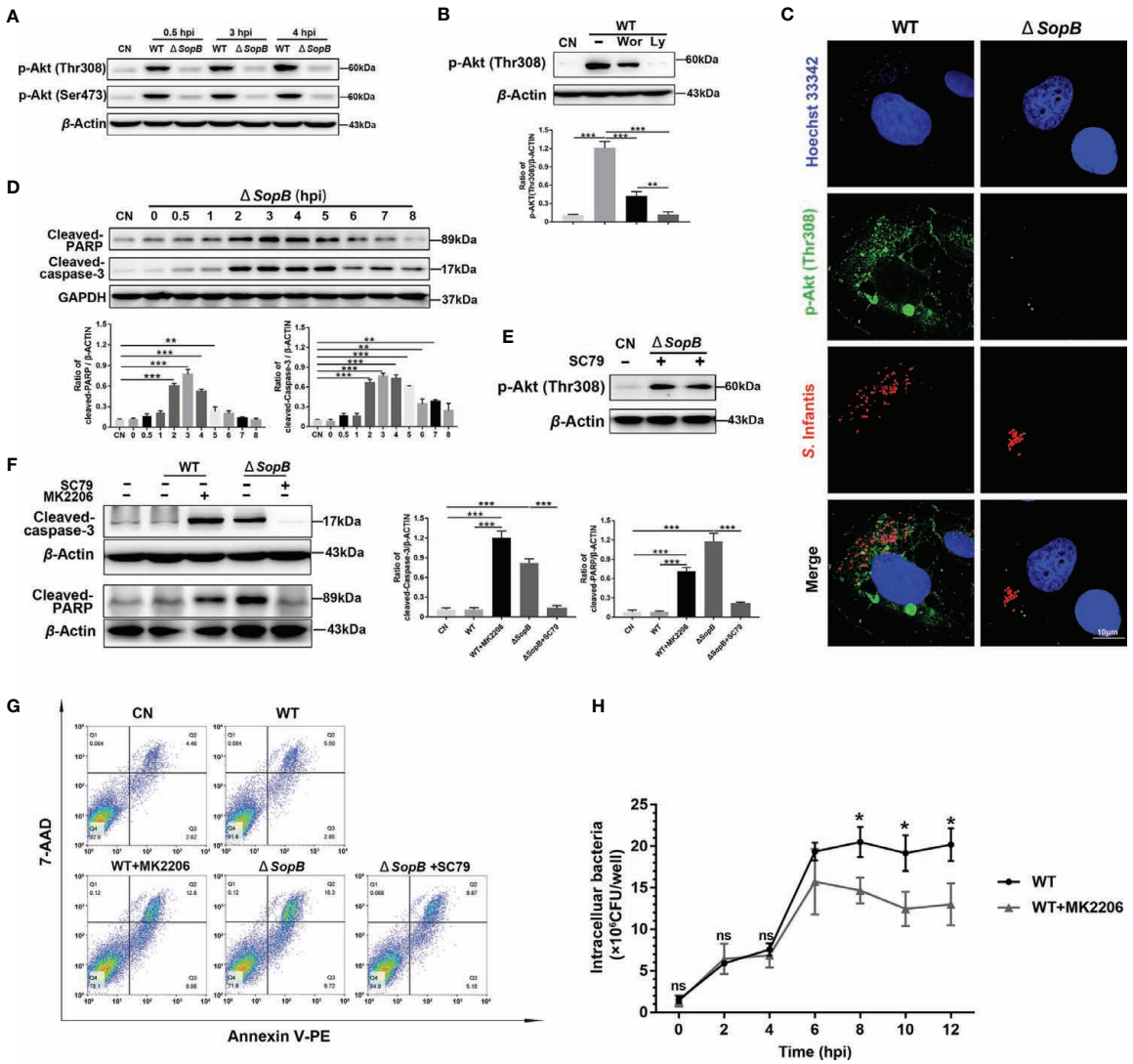


FIGURE 3 | Inhibition of apoptosis by intermittent Akt phosphorylation was mediated by Cytosolic *S*. Infantis *SopB*. **(A)** Western blot analysis of p-Akt (Ser473) and p-Akt (Thr308) protein expression levels after WT *S*. Infantis or *SopB* mutant infection at 0.5, 3, and 4 hpi. CN, control. **(B)** Immunoblotting verified the repressive effects of Ly294002 (Ly) and Wortmannin (Wor) on p-Akt (Thr308) protein expression levels after infection with WT *S*. Infantis. CN, control. **(C)** Immunofluorescence staining of p-Akt (Thr308) after infection with WT *S*. Infantis or the *SopB* mutant at 4 hpi. Red: *S*. Infantis. Green: p-Akt (Thr308). Blue: Hoechst 333342. **(D)** Western blot analysis of Cleaved-caspase-3 and Cleaved-PARP protein expression levels within 8 h after *SopB* mutant infection. CN, control. **(E)** Immunoblotting verified the activation of SC79 on p-Akt (Thr308) protein expression level after *SopB* mutant infection at 4 hpi. CN, control. **(F, G)** Apoptosis was evaluated after infection with WT *S*. Infantis or the *SopB* mutant at 4 hpi. In the process of bacterial infection, the phosphorylation level of Akt was regulated by the addition of MK2206 or SC79. **(F)** The protein levels of Cleaved-caspase-3 and Cleaved-PARP were analyzed using Western blotting. **(G)** The proportion of apoptotic cells was detected using flow cytometry. **(H)** Detection of intracellular bacterial load using the gentamicin protection assay without (total intracellular bacteria, black curve) or with (total intracellular bacteria, gray curve) MK2206. ns, no significant difference. Data were presented as the mean ± SEM from three independent experiments (n = 3). $^{*}P < 0.05$, $^{**}P < 0.01$, $^{***}P < 0.001$.

and detected the distribution of Bcl-2 and Bax. As shown in **Figure 4D**, WT *S*. Infantis infection significantly increased the distribution of Bcl-2 in the mitochondria, while the addition of mk2206 decreased Bcl-2 and increased the distribution of Bax in the mitochondria. Infection with the *SopB* mutant also resulted in the decrease of Bcl-2 and the increase of Bax in mitochondria, which could be reversed by adding SC79. In addition, WT *S*. Infantis infection could phosphorylate Bad and Caspase-9 (**Figure 4E**), which enhanced the inhibition of apoptosis. In summary, *S*. Infantis-mediated Akt phosphorylation by *SopB* maintained mitochondrial dynamic network homeostasis, hence suppressing the apoptosis in infected cells.

SopB-Mediated Akt Phosphorylation Delays Pyroptosis by Inhibiting Caspase-1

Flow cytometry results showed that the proportion of 7-ADD^{+}/Annexin-V PE^{+} cells significantly increased during 6–8 hpi, and the cells entered later stage of apoptosis without the early phase

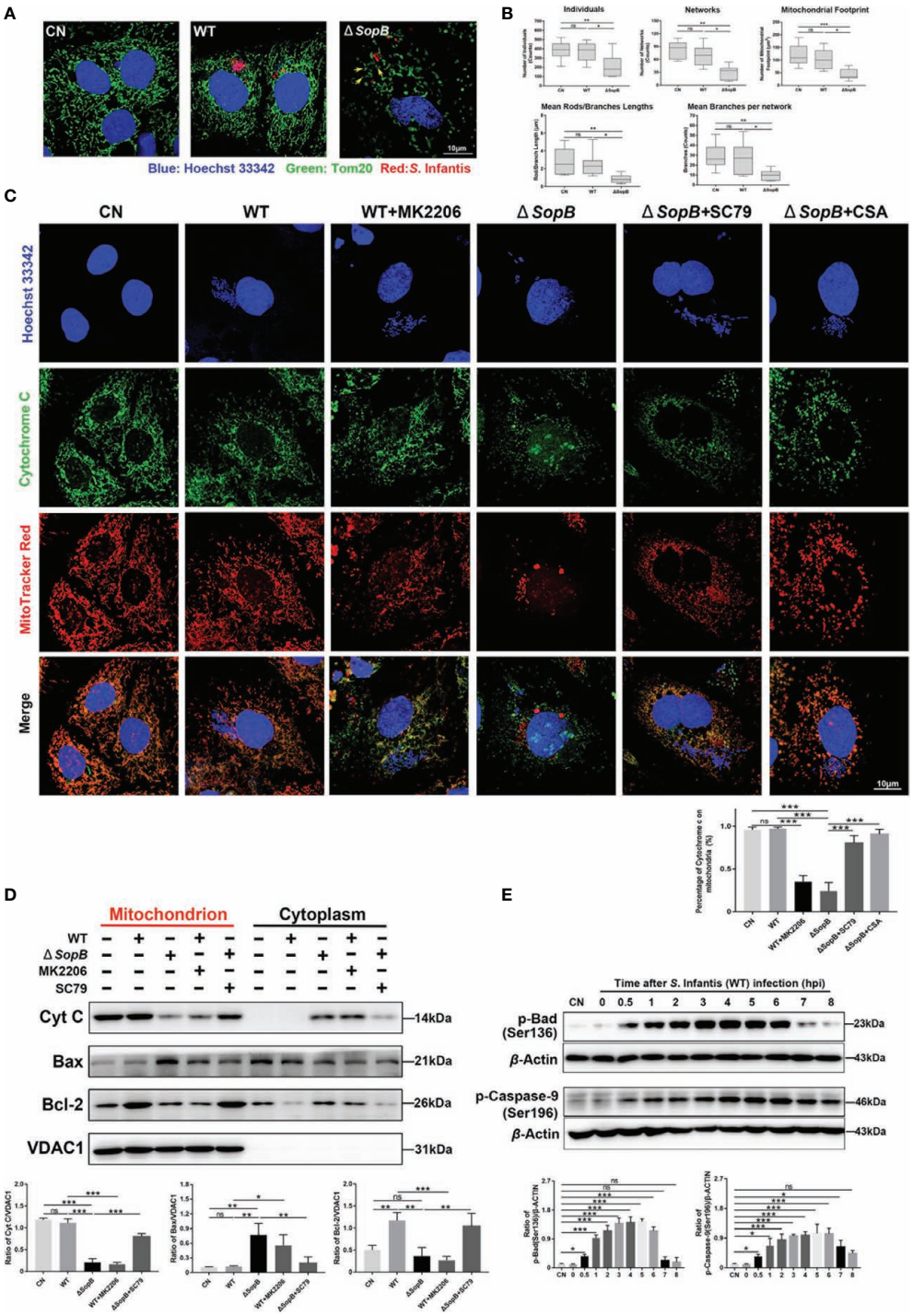


FIGURE 4 | *SopB*-mediated Akt phosphorylation inhibited apoptosis by maintaining mitochondrial dynamic network homeostasis. In **(A–D)**, all cell samples were collected and processed at 4 hpi after infection with *S*. Infantis. Immunofluorescence analysis of mitochondrial network after infection with WT *S*. Infantis or the *SopB* mutant. Red: *Salmonella*; Green: Tom20 (mitochondria); Blue: Hoechst 333342. **(B)** Mitochondrial network analysis using the MiNA toolset of Image (J) **(C)** Co-localization of cytochrome c and mitochondria was detected using immunofluorescence. In the bacterial infection process, the phosphorylation level of Akt was regulated by the addition of MK2206 or SC79. CSA was used to inhibit the opening of the mitochondrial permeability transition pore (MPTP) Red: Mitochondria; Green: Cytochrome c; Blue: Hoechst 333342 (Nucleus and bacteria). **(D)** Detection of Cytochrome c, Bcl-2, and Bax protein levels in mitochondrial and cytoplasmic protein after infection with WT *S*. Infantis or the *SopB* mutant. In the bacterial infection process, the phosphorylation level of Akt was regulated by the addition of MK2206 or SC79. **(E)** Western blot analysis of p-Caspase-9 (Ser136) and p-Bad (Ser196) protein expression levels within 8 h after infection with *S*. Infantis. Data were presented as the mean ± SEM from three independent experiments (n = 3). $^{*}P < 0.05$, $^{**}P < 0.01$, $^{***}P < 0.001$. CN, control. ns, no significant difference.

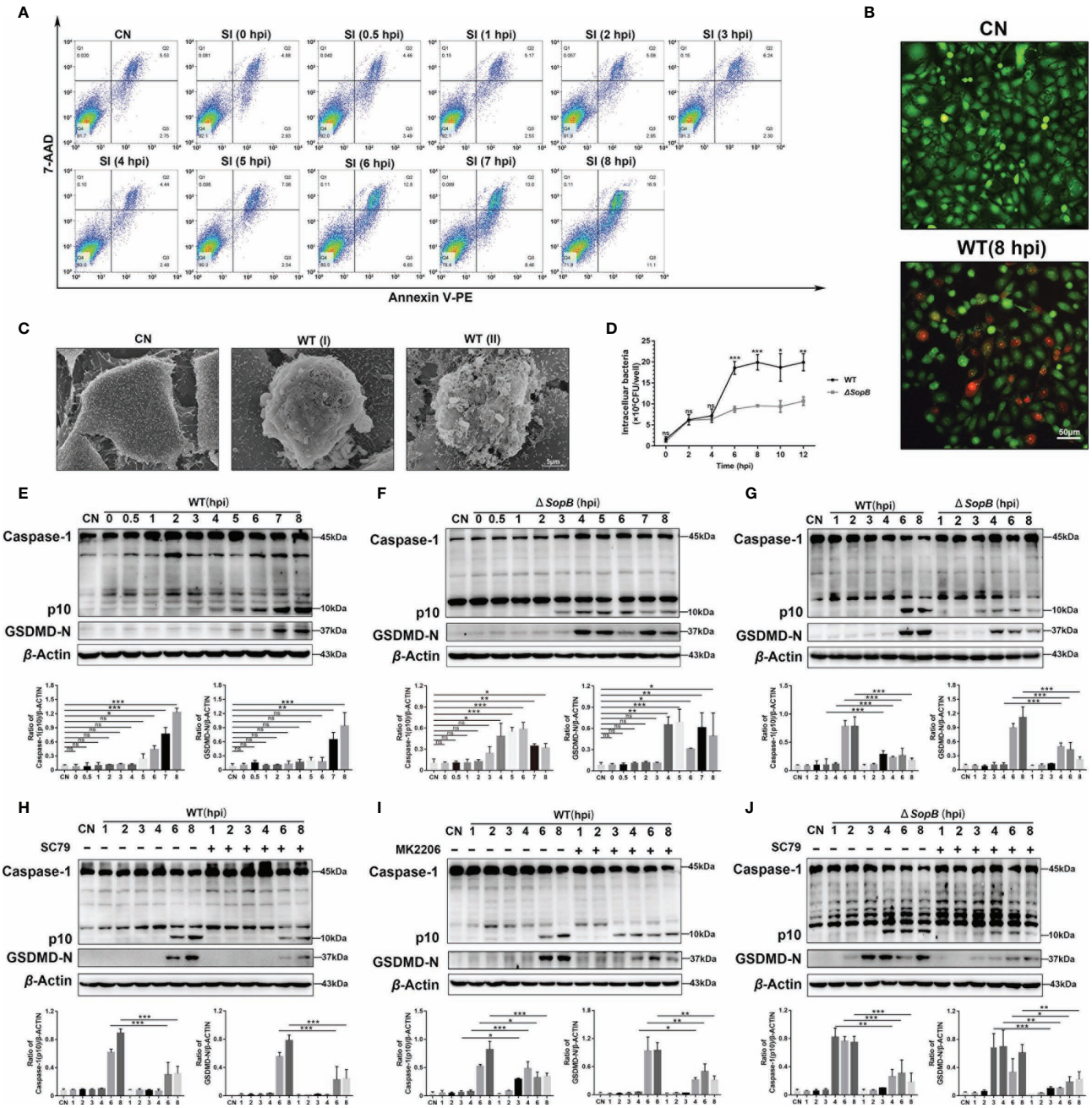


FIGURE 5 | *SopB*-mediated Akt phosphorylation delayed pyroptosis. **(A)** The proportion of apoptotic cells within 8 h after infection with WT *S*. Infantis was detected using flow cytometry. **(B)** Calcein-AM/PI was used to evaluate cell membrane permeability after 8 h of infection with WT *S*. Infantis. Green: Calcein-AM; Red: PI. **(C)** Observation of the apical surface of Caco-2 cell monolayer ultrastructure using scanning electron microscopy. WT (I) (6 hpi) and WT (II) (8 hpi) showed that the WT *S*. Infantis–infected cell was bacteria-laden, which were extruded from the monolayer. **(D)** Detection of intracellular bacterial load using the gentamicin protection assay at 0, 2, 4, 6, 8, 10, and 12 hpi after infection (Black curve: WT *S*. Infantis; Gray curve: *SopB* mutant). **(E–J)** Western blot analysis of Caspase-1 and GSDMD-N protein levels after infection with WT *S*. Infantis or the *SopB* mutant within 8 h. **(E)** Infection with WT *S*. Infantis; **(F)** infection with the *SopB* mutant; **(G)** comparison of WT *S*. Infantis and the *SopB* mutant; **(H)** infection with WT *S*. Infantis in the presence of SC79; **(I)** infection with WT *S*. Infantis in the presence of MK2206; **(J)** infection with the *SopB* mutant infection in the presence of SC79. Data were presented as the mean ± SEM from three independent experiments (n = 3). $^{*}P < 0.05$, $^{**}P < 0.01$, $^{***}P < 0.001$. CN, control; SI, *S*. Infantis. ns, no significant difference.

(**Figure 5A**). This indicated that there was a change in the membrane permeability of infected cells. In order to validate this conjecture, we performed double staining with Calcein-AM and PI during infection with *S.* Infantis. Images revealed that a subset of cells in the *S.* Infantis infection group had been damaged, as evidenced by PI-positive staining (**Figure 5B**). The scanning electron microscope images revealed that plasmalemma was destroyed and bacteria had been drilled out along the pores (**Figure 5C**), suggesting the occurrence of pyroptosis.

Next, the protein markers of pyroptosis, caspase-1 (p10), and GSDMD-N were examined. Infection with WT *S.* Infantis significantly activated pyroptosis (**Figure 5E**). Surprisingly, the *ΔSopB* strain induced caspase-1 (p10) and GSDMD-N activation 2 h earlier than WT *S.* Infantis (**Figure 5F**). However, the *SopB* mutant induced lower levels of caspase-1 (p10) and GSDMD-N compared to the WT strain, indicating a weaker degree of pyroptosis induced by the *SopB* mutant (**Figure 5G**). A recent study reported that p-Akt suppressed inflammasome activation in *Salmonella*-infected macrophages (35). Pyroptosis can be regulated by *S.* Infantis through p-Akt. MK2206 significantly reduced the levels of caspase-1 (p10) and GSDMD-N induced by WT *S.* Infantis, while SC79 treatment caused the WT strain to display a similar regulation as the *ΔSopB* strain (**Figures 5H, I**). Furthermore, SC79 treatment resulted in a significant decrease in caspase-1 (p10) and GSDMD-N levels during infection with the *ΔSopB* strain (**Figure 5J**), indicating that Akt phosphorylation both delayed pyroptosis and aggravated the severity of pyroptosis of infected Caco-2 cells. Intracellular bacterial load detection revealed that the number of bacteria in cells infected with the WT strain was much higher than in cells infected with the *ΔSopB* strain (**Figure 5D**). This may explain the two phenotypes of *S.* Infantis causing varying degrees of pyroptosis: the WT strain has a greater bacterial load and stimulates the inflammasome more strongly.

WT *S.* Infantis Causes More Severe Intestinal Inflammatory Damage Than the *ΔSopB* Strain

In order to verify our findings *in vivo*, we infected the C57BL/6 mouse model with *Salmonella*. The severity of diarrhea was determined by fecal score and the dry/wet weight of fecal pellets. The results revealed that WT *S.* Infantis caused more severe diarrhea than the *ΔSopB* strain (**Figures 6A, B**). In addition, the fecal bacterial load in the WT group was also significantly higher than the *ΔSopB* group (**Figure 6C**). Since *Salmonella* infection can cause severe ileal injury, the pathological changes in the ileum were examined. Infection with WT *S.* Infantis resulted in more severe ileal damage than infection with the *ΔSopB* strain (**Figures 6D, E**). Consistent with the *in vitro* results, p-Akt (Ser473 and Thr308) was found to be highly expressed in the WT group (**Figure 6F**). As shown in **Figure 6G**, infection with WT *S.* Infantis significantly increased the mRNA level of inflammatory factors, while the mRNA level of inflammatory factors induced by the *ΔSopB* strain was lower compared to WT *S.* Infantis. In combination with the detection of caspase-1 level (**Figure 6H**), we discovered that the infection with WT strain led to more severe intestinal inflammatory injury. Furthermore, immunoblotting and the TUNEL fluorescence assay showed that the *ΔSopB* strain caused more severe apoptosis of intestinal cells than the WT stain (**Figures 6I, J**). Intestinal cells infected with the *ΔSopB* strain may shed rapidly from the epithelium through apoptosis and be eliminated from the body, reducing the gut *Salmonella* load and inflammatory response.

In conclusion, *S.* Infantis delayed the death of infected Caco-2 cells through intermittent activation of Akt mediated by *SopB*, allowing intracellular cytosolic bacteria sufficient time for replication and resulting in more severe intestinal inflammation.

DISCUSSION

Many pathogenic bacteria that are closely related to public health reproduce intracellularly, enhancing their virulence. Invasion and colonization in epithelial cells are crucial processes in *Salmonella* pathogenesis (36). The replication of cytosolic *Salmonella* is key to the early establishment of the infection (10, 11). In this study, we elucidated the mechanism by which cytosolic *S.* Infantis delayed the death of infected epithelial cells *via* intermittent Akt phosphorylation mediated by *SopB*.

Salmonella utilizes *SopB* to activate Akt, suggesting that it plays an important role in regulating host cell survival (18, 19). However, the distribution of *SopB*-dependent Akt phosphorylation in epithelial cells remained unclear. A single-cell approach was used to evaluate the relationship between *SopB* and Akt phosphorylation. Because *SopB* was transported to cells to play a role in mediating both actin-dependent and myosin II-dependent bacterial invasion, we attributed the induction of the first wave of Akt phosphorylation to its residual activity. The second wave of Akt phosphorylation activity only occurred at 3–4 hpi, with Akt phosphorylation only strongly induced in infected cells containing hyper-replicating cytosolic bacteria. Notably, there was no Akt phosphorylation at any other time in all infected cells. We hypothesized that the second wave of Akt activation was due to the residual SPI-1 activity of bacteria escaping from the SCV. This was similar to Akt phosphorylation by *S.* Typhimurium: the first stage was widely induced during invasion, and the second stage was induced only in the infected cells containing cytosolic *Salmonella* (20). However, there were some differences between the two types of *Salmonella*: the first phase of Akt phosphorylation induced by *S.* Typhimurium was largely depleted by 3 hpi, whereas the first phase of Akt phosphorylation induced by *S.* Infantis induced was almost depleted at 1 hpi. The second stage of Akt activation induced by *S.* Infantis induction was occurred at 3–4 hpi, while *S.* Typhimurium-induced Akt activation was later at 6 hpi (20). Previous studies have shown that *S.* Infantis was less invasive and induced considerably weaker enteritis than *S.* Typhimurium (37). These differences were attributed to the low expression of SPI-1 in *S.* Infantis than that in *S.* Typhimurium (37).

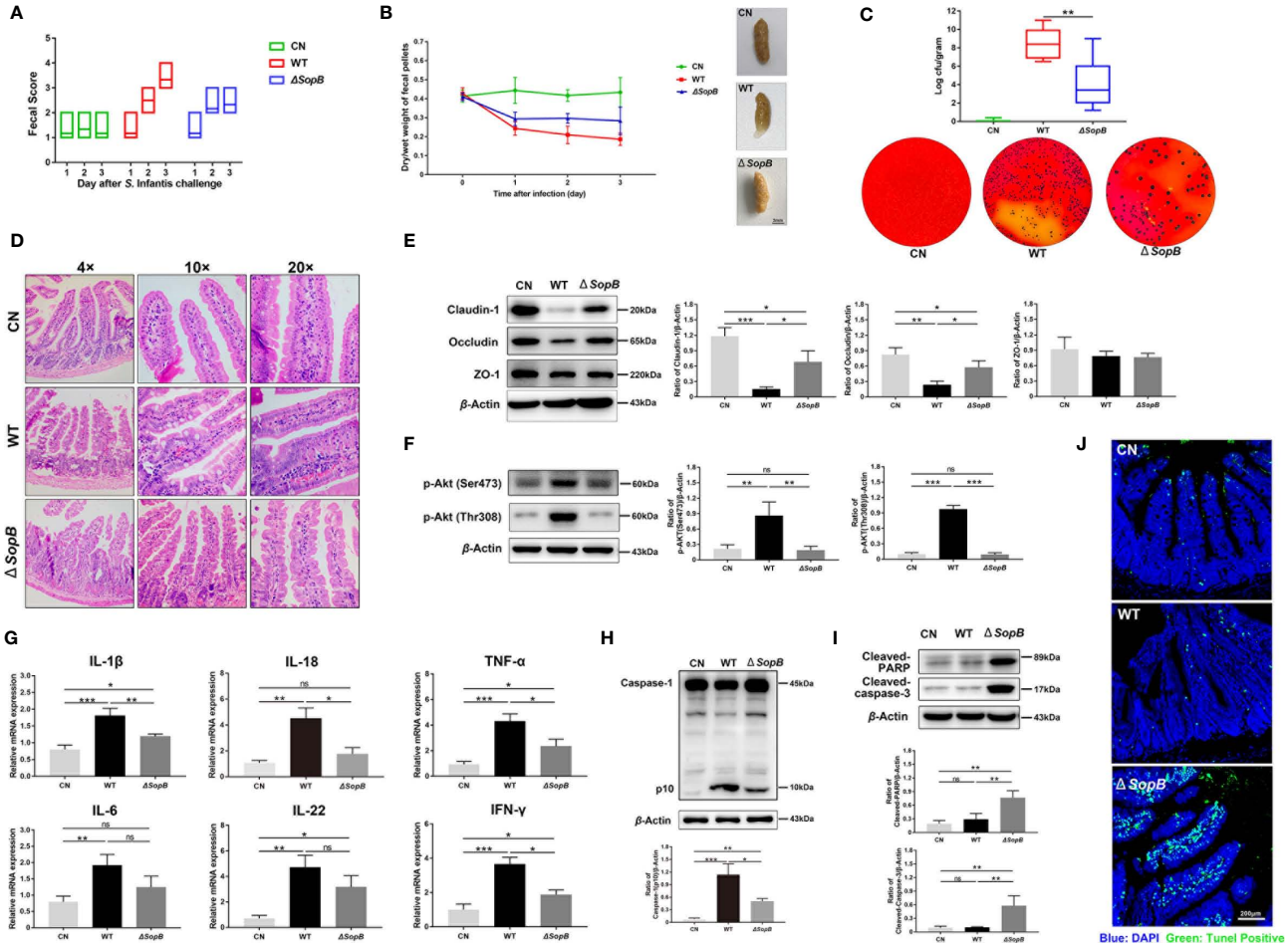


FIGURE 6 | WT *S.* Infantis caused more severe intestinal inflammatory damage to the C57BL/6 mice gut than the Δ*SopB* mutant. **(A)** The fecal score curve of mice in three groups after *Salmonella* infection. The fecal status of mice was scored daily. **(B)** Results of the dry/wet weight ratio of feces. The starting day of the experiment was considered as day 0 (24 h after streptomycin gavage). Three representative feces images of each group are shown on the right side of the curve. **(C)** Quantification of fecal bacterial burdens on day 3. Three representative plots of bacterial colonies images in each group are below the curve. **(D)** Ileum representative photomicrographs of sections stained with H&E. **(E, F)** Western blot analysis of Claudin-1, Occludin, p-Akt (Ser473), and p-Akt (Thr308) protein levels of three groups. **(G)** Expression of IL-1β, IL-18, IL-6, IL-22, TNF-α, and IFN-γ mRNA in ileal tissues. **(H, I)** Western blot analysis of Caspase-1, Cleaved-caspase-3, and Cleaved-PARP protein levels of three groups. **(J)** The representative images of TUNEL fluorescence staining in ileum tissue pathological sections. Blue: DAPI; Green: TUNEL positive cells. Data were presented as mean ± SEM. (n = 6). Data were presented as the mean ± SEM from three independent experiments (n = 3). **P* < 0.05, ***P* < 0.01, ****P* < 0.001. CN, control. ns, no significant difference.

SopB delayed the inevitable and rapid apoptosis of intestinal epithelial cells. For *Salmonella*, the most obvious advantage gained by inhibiting apoptosis is time, which allows *Salmonella* to establish an intracellular stronghold to rapidly proliferate, as well as regulate its and the host's gene expression to prepare for the spread of infection in the gut. The mitochondrion is the primary organelle for endogenous apoptosis (30). In this study, we discovered that cytosolic *S.* Infantis phosphorylated Akt through *SopB* to (i) reposition Bcl-2 to regulate the permeability of the mitochondrial outer membrane by inhibiting Bax translocation from cytosol to the mitochondria; (ii) maintain mitochondrial dynamic network homeostasis; (iii) phosphorylate Bad and Caspase-9 to inhibit apoptosis of infected cells, thereby maintaining the mitochondrial membrane and network homeostasis to suppress the apoptosis of infected cells.

Importantly, we discovered that *SopB*-mediated Akt phosphorylation delayed the pyroptosis of infected cells. Recently, it has been reported that *SopB* inhibited the activation of NLRC4 inflammasome in BMDMs through an Akt signal-dependent process (35). Another study found that *SopB* promoted YAP phosphorylation through Akt in B cells, thereby inhibiting the assembly of the inflammasome (38). The activation of the inflammasome is a crucial step in inducing of pyroptosis. Our findings demonstrated that *SopB*-mediated Akt phosphorylation also delayed the activation of caspase-1 and pyroptosis in Caco-2 cells. Compared to apoptosis, pyroptosis occurs faster and is accompanied by the release of pro-inflammatory factors, such as IL-1β and IL-18 (21–23). Inflammatory factors increase the number of inflammatory cells and aggravate the inflammatory response, which is a vital

defense mechanism for the host to combat pathogenic microorganism infection (39). Although the inflammatory response accelerates the elimination of pathogens, it also alters the intestinal environment by disrupting gut microbiota and causing a burst of intestinal electron acceptors (40, 41). An alteration in the intestinal ecosystem provides variables for pathogens to gain a growth advantage to spread infection. In this study, *S.* Infantis rapidly induced the pyroptosis within 2 h after Akt phosphorylation diminished. The WT *S.* Infantis caused more severe intestinal inflammation *in vivo* than the *SopB* mutant (**Figure 6**). We hypothesized that *SopB* contributes to the rapid proliferation of bacteria in the intestinal infection phase of *S.* Infantis, which leads to inflammatory response, intestinal damage, and other intestinal environmental variables, as well as provides favorable conditions for the subsequent establishment of long-term colonization infection in the gut.

In conclusion, this study demonstrated that the *S.* Infantis SPI-1 effector *SopB* acts as a pro-survival factor in epithelial cells by inhibiting apoptosis and delaying pyroptosis. *S.* Infantis gained sufficient time to proliferate through the regulation of host cell death, which resulted in inflammation and suitable conditions for the spread and colonization of pathogens in the gut. As it is interesting that bacterial pathogens can manipulate host cell death mechanisms to enhance pathogen survival and spread infection, further studies focusing on how *S.* Infantis regulates different types of host cell death to cause enteritis will be performed. This study also provides a solid theoretical basis as well as potential drug targets for the treatment of salmonellosis.

DATA AVAILABILITY STATEMENT

The raw data supporting the conclusions of this article will be made available by the authors, without undue reservation.

ETHICS STATEMENT

The animal study was reviewed and approved by the Guidelines for Laboratory Animal Use and Care from the Chinese Center for Disease Control and Prevention and the Rules for Medical Laboratory Animals (1998) from the Chinese Ministry of Health, under the approval of the Animal Ethics Committee of the China Agricultural University.

AUTHOR CONTRIBUTIONS

B-XC designed and performed the experiments. Y-NL, N-L, and Y-HZ participated and assisted in the experiments as well as provided advice during the procedure. L-XY and S-YC contributed to data analysis. B-XC drafted the manuscript, and J-FW critically revised the manuscript. J-FW was responsible for obtaining funding and overseeing the project. All authors contributed to the article and approved the submitted version.

FUNDING

This work was supported by the National Key R&D Program of China (Project No. 2017YFD0502200).

ACKNOWLEDGMENTS

We thank the fund for support in this work: The National Key R&D Program of China (Project No. 2017YFD0502200). We are very grateful to Drs. Ning Xie and Jin Hui Su for technical support.

REFERENCES

1. Centers for Disease Control and Prevention (CDC). *National Salmonella Surveillance Annual Report — Appendices, 2010*. Atlanta, Georgia: US Department of Health and Human Services, CDC, (2013).
2. Gili A, Katherine TS, Natalie S, Mali SD, Antje C, Galia R, et al. A Unique Megaplasmid Contributes to Stress Tolerance and Pathogenicity of an Emergent Salmonella Enterica Serovar Infantis Strain. *Environ Microbiol* (2014) 16:977–94. doi: 10.1111/1462-2920.12351
3. European Food Safety Authority. European Centre for Disease Prevention and Control. The European Union Summary Report on Antimicrobial Resistance in Zoonotic and Indicator Bacteria From Humans, Animals and Food in 2015. *EFSA J* (2017) 15:e04694. doi: 10.2903/j.efsa.2017.4694
4. European Food Safety Authority. European Centre for Disease Prevention and Control-. *EFSA J* (2017) 15:e05077. doi: 10.2903/j.efsa.2017.5077
5. European Food Safety Authority. European Centre for Disease Prevention and Control. The European Union Summary Report on Antimicrobial Resistance in Zoonotic and Indicator Bacteria From Humans, Animals and Food in 2017. *EFSA J* (2019) 17:e05598. doi: 10.2903/j.efsa.2019.5598
6. Hauser E, Tietze E, Helmuth R, Junker E, Prager R, Schroeter A, et al. Clonal Dissemination of Salmonella Enterica Serovar Infantis in Germany. *Foodborne Pathog Dis* (2012) 9:352–60. doi: 10.1089/fpd.2011.1038
7. Shahada F, Sugiyama H, Chuma T, Sueyoshi M, Okamoto K. Genetic Analysis of Multi-Drug Resistance and the Clonal Dissemination of Beta-Lactam Resistance in Salmonella Infantis Isolated From Broilers. *Vet Microbiol* (2010) 140:136–41. doi: 10.1016/j.vetmic.2009.07.007
8. LaRock DL, Chaudhary A, Miller SI. *Salmonellae* Interactions With Host Processes. *Nat Rev Microbiol* (2015) 13:191–205. doi: 10.1038/nrmicro3420
9. Knodler LA, Nair V, Steele-Mortimer O. Quantitative Assessment of Cytosolic Salmonella in Epithelial Cells. *PloS One* (2014) 9:e84681. doi: 10.1371/journal.pone.0084681
10. Malik-Kale P, Winfree S, Steele-Mortimer O. The Bimodal Lifestyle of Intracellular Salmonella in Epithelial Cells: Replication in the Cytosol Obscures Defects in Vacuolar Replication. *PloS One* (2012) 7:e38732. doi: 10.1371/journal.pone.0038732
11. Knodler LA, Vallance BA, Celli J, Winfree S, Hansen B, Montero M, et al. Dissemination of Invasive Salmonella *via* Bacterial-Induced Extrusion of Mucosal Epithelia. *Proc Natl Acad Sci USA* (2010) 107:17733–8. doi: 10.1073/pnas.1006098107
12. Chu BX, Zhu YH, Su JH, Xia B, Zou YJ, Nie JW. Butyrate-Mediated Autophagy Inhibition Limits Cytosolic Salmonella Infantis Replication in the Colon of Pigs Treated With a Mixture of Lactobacillus and Bacillus. *Vet Res* (2020) 51:99. doi: 10.1186/s13567-020-00823-8
13. Yu HB, Croxen MA, Marchiando AM, Ferreira RBR, Cadwell K, Foster LJ, et al. Autophagy Facilitates Salmonella Replication in Hela Cells. *mBio* (2014) 5:e00865–14. doi: 10.1128/mBio.00865-14
14. Huang J, Birmingham CL, Shahnazari S, Shiu J, Zheng YT, Smith AC, et al. Antibacterial Autophagy Occurs at PI(3)P-Enriched Domains of the

Endoplasmic Reticulum and Requires Rab1 GTPase. *Autophagy* (2011) 7:17–26. doi: 10.4161/auto.7.1.13840
15. Yrlid U, Wick MJ. Salmonella-Induced Apoptosis of Infected Macrophages Results in Presentation of a Bacteria-Encoded Antigen After Uptake by Bystander Dendritic Cells. *J Exp Med* (2000) 191:613–24. doi: 10.1084/jem.191.4.613
16. Wu S, Li Y, Xu Y, Li Q, Chu Y, Huang R, et al. A Salmonella Enterica Serovar Typhi Plasmid Induces Rapid and Massive Apoptosis in Infected Macrophages. *Cell Mol Immunol* (2010) 7:271–8. doi: 10.1038/cmi.2010.17
17. Takaya A, Suzuki A, Kikuchi Y, Eguchi M, Isogai E, Tomoyasu T, et al. Derepression of Salmonella Pathogenicity Island 1 Genes Within Macrophages Leads to Rapid Apoptosis *via* Caspase-1 and Caspase-3-Dependent Pathways. *Cell Microbiol* (2010) 7:79–90. doi: 10.1111/j.1462-5822.2004.00435.x
18. Knodler LA, Finlay BB, Steele-Mortimer O. The Salmonella Effector Protein Sopb Protects Epithelial Cells From Apoptosis by Sustained Activation of Akt. *J Biol Chem* (2005) 280:9058–64. doi: 10.1074/jbc.M412588200
19. Ruan H, Zhang Z, Tian L, Wang S, Hu S, Qiao JJ. The Salmonella Effector Sopb Prevents Ros-Induced Apoptosis of Epithelial Cells by Retarding Traf6 Recruitment to Mitochondria. *Biochem Biophys Res Commun* (2016) 478:618–23. doi: 10.1016/j.bbrc.2016.07.116
20. Finn CE, Chong A, Cooper KG, Starr T, Steele-Mortimer O. A Second Wave of Salmonella T3ss1 Activity Prolongs the Lifespan of Infected Epithelial Cells. *PloS Pathog* (2017) 13:e1006354. doi: 10.1371/journal.ppat.1006354
21. Shi J, Gao W, Feng S. Pyroptosis: Gasdermin-Mediated Programmed Necrotic Cell Death. *Trends Biochem Sci* (2016) 42:245–54. doi: 10.1016/j.tibs.2016.10.004
22. Martinon F, Tschopp J. Inflammatory Caspases and Inflammasomes: Master Switches of Inflammation. *Cell Death Differ* (2007) 14:10–2. doi: 10.1038/sj.cdd.4402038
23. Miao EA, Leaf IA, Treuting PM, Mao DP, Dors M, Sarkar A, et al. Caspase-1-Induced Pyroptosis Is an Innate Immune Effector Mechanism Against Intracellular Bacteria. *Nat Immunol* (2010) 11:1136–42. doi: 10.1038/ni.1960
24. Knodler LA, Finlay BB. Salmonella and Apoptosis: To Live or Let Die. *Microbes Infect* (2001) 3:1321–6. doi: 10.1016/S1286-4579(01)01493-9
25. Schwan WR, Huang XZ, Hu L, Kopecko DJ. Differential Bacterial Survival, Replication, and Apoptosis-Inducing Ability of Salmonella Serovars Within Human and Murine Macrophages. *Infect Immun* (2000) 68:1005–13. doi: 10.1128/IAI.68.3.1005-1013.2000
26. Geiser P, Martino M, Ventayol PS, Eriksson J, Sellin ME, Al-Saffar AK, et al. Salmonella Enterica Serovar Typhimurium Exploits Cycling Through Epithelial Cells to Colonize Human and Murine Enteroids. *mBio* (2021) 12:e02684–20. doi: 10.1128/mBio.02684-20
27. Liang J, Slingerland JM. Multiple Roles of the PI3K/PKB (Akt) Pathway in Cell Cycle Progression. *Cell Cycle* (2014) 2:336–42. doi: 10.4161/cc.2.4.433
28. Sarbassov DD, Guertin DA, Ali SM, Sabatini DM. Phosphorylation and Regulation of Akt/PKB by the rictor-mTOR Complex. *Science* (2005) 307:1098–101. doi: 10.1126/science.1106148
29. Song G, Ouyang GL, Bao SD. The Activation of Akt/PKB Signaling Pathway and Cell Survival. *J Cell Mol Med* (2005) 1:59–71. doi: 10.1111/j.1582-4934.2005.tb00337.x
30. Green DR, Kroemer G. The Pathophysiology of Mitochondrial Cell Death. *Science* (2004) 305:626–9. doi: 10.1126/science.1099320
31. Jason K, Onur K, Brody MJ, Sargent MA, Michael DM, Molkentin JD, et al. Necroptosis Interfaces With Momp and the Mptp in Mediating Cell Death. *PloS One* (2015) 10:e0130520. doi: 10.1371/journal.pone.0130520
32. Halestrap AP. What Is the Mitochondrial Permeability Transition Pore? *J Mol Cell Cardiol* (2009) 46:821–31. doi: 10.1016/j.yjmcc.2009.02.021
33. Edlich F, Banerjee S, Suzuki M, Cleland M, Arnoult D, Wang C, et al. Bcl-X(L) Retrotranslocates Bax From the Mitochondria Into the Cytosol. *Cell* (2011) 145:104–16. doi: 10.1016/j.cell.2011.02.034
34. Mikhailov V, Mikhailova M, Pulkrabek DJ, Dong Z, Venkatachalam MA, Saikumar P. Bcl-2 Prevents Bax Oligomerization in the Mitochondrial Outer Membrane. *J Biol Chem* (2001) 276:18361–74. doi: 10.1074/jbc.M100655200
35. Hu GQ, Song PX, Chen W, Qi S, Yu SX, Du CT. Cirtical Role for Salmonella Effector SopB in Regulating Inflammasome Activation. *Mol Immunol* (2017) 90:280–6. doi: 10.1016/j.molimm.2017.07.011
36. Haraga A, Ohlson MB, Miller SI. Salmonellae Interplay With Host Cells. *Nat Rev Microbiol* (2008) 6:53–66. doi: 10.1038/nrmicro1788
37. Gili A, Antje C, Maya D, Helit C, Abdulhadi S, Alibek G, et al. Differences in the Expression of SPI-1 Genes Pathogenicity and Epidemiology Between the Emerging Salmonella Enterica Serovar Infantis and the Model Salmonella Enterica Serovar Typhimurium. *J Infect Dis* (2019) 6:1071–81. doi: 10.1093/infdis/jiz235
38. Abraham G, Carlos S, Araceli P, Nava P, Ortiz-Navarrete V. SopB Activates the Akt-YAP Pathway to Promote Salmonella Survival Within B Cells. *Virulence* (2018) 9:1390–402. doi: 10.1080/21505594.2018.1509664
39. Crowley SM, Knodler LA, Vallance BA. Salmonella and the Inflammasome: Battle for Intracellular Dominance. *Curr Top Microbiol Immunol* (2016) 397:43–67. doi: 10.1007/978-3-319-41171-2_3
40. Winter SE, Thiennimitr P, Winter MG, Butler BP, Huseby DL, Crawford RW. Gut Inflammation Provides a Respiratory Electron Acceptor for Salmonella. *Nature* (2010) 467:426–9. doi: 10.1038/nature09415
41. Hakansson A, Molin G. Gut Microbiota and Inflammation. *Nutrients* (2011) 3:637–82. doi: 10.3390/nu3060637

Conflict of Interest: The authors declare that the research was conducted in the absence of any commercial or financial relationships that could be construed as a potential conflict of interest.

Publisher's Note: All claims expressed in this article are solely those of the authors and do not necessarily represent those of their affiliated organizations, or those of the publisher, the editors and the reviewers. Any product that may be evaluated in this article, or claim that may be made by its manufacturer, is not guaranteed or endorsed by the publisher.

Copyright © 2021 Chu, Li, Liu, Yuan, Chen, Zhu and Wang. This is an open-access article distributed under the terms of the Creative Commons Attribution License (CC BY). The use, distribution or reproduction in other forums is permitted, provided the original author(s) and the copyright owner(s) are credited and that the original publication in this journal is cited, in accordance with accepted academic practice. No use, distribution or reproduction is permitted which does not comply with these terms.

frontiers in Microbiology

ORIGINAL RESEARCH
published: 17 November 2021
doi: 10.3389/fmicb.2021.742255

Long-Term Efficacy of Low-Intensity Single Donor Fecal Microbiota Transplantation in Ulcerative Colitis and Outcome-Specific Gut Bacteria

*Rongrong Ren[1†], Xuefeng Gao[2,3†], Yichao Shi[1], Jianfeng Li[1], Lihua Peng[1], Gang Sun[1], Zikai Wang[1], Bin Yan[1], Junli Zhi[1] and Yunsheng Yang[1]**

[1] Department of Gastroenterology and Hepatology, The First Medical Center, Chinese PLA General Hospital, Beijing, China, [2] Department of Gastroenterology and Hepatology, Shenzhen University General Hospital, Shenzhen, China, [3] Central Laboratory, Shenzhen Key Laboratory of Precision Medicine for Hematological Malignancies, Shenzhen University General Hospital, Shenzhen, China

OPEN ACCESS

Edited by:
Monica Cartelle Gestal,
Louisiana State University Health Sciences Center Shreveport, United States

Reviewed by:
Guillaume Sarrabayrouse, Université de Paris, France
Nikhil Pai, McMaster University, Canada

***Correspondence:**
Yunsheng Yang
sunnyddc@plagh.org

† These authors have contributed equally to this work and share first authorship

Specialty section:
This article was submitted to Infectious Agents and Disease, a section of the journal Frontiers in Microbiology

Received: 15 July 2021
Accepted: 07 October 2021
Published: 17 November 2021

Citation:
Ren R, Gao X, Shi Y, Li J, Peng L, Sun G, Wang Z, Yan B, Zhi J and Yang Y (2021) Long-Term Efficacy of Low-Intensity Single Donor Fecal Microbiota Transplantation in Ulcerative Colitis and Outcome-Specific Gut Bacteria. Front. Microbiol. 12:742255. doi: 10.3389/fmicb.2021.742255

Aims: To assess the long-term efficacy and safety of single-donor, low-intensity fecal microbiota transplantation (FMT) in treating ulcerative colitis (UC), and to identify the outcome-specific gut bacteria.

Design: Thirty-one patients with active UC (Mayo scores $\geq$ 3) were recruited, and all received FMT twice, at the start of the study and 2∼3 months later, respectively, with a single donor and a long-term follow-up. The fecal microbiome profile was accessed via 16S rRNA sequencing before and after FMT.

Results: After the first FMT, 22.58% (7/31) of patients achieved clinical remission and endoscopy remission, with the clinical response rate of 67.74% (21/31), which increased to 55% (11/20) and 80% (16/20), respectively, after the second FMT. No serious adverse events occurred in all patients. During 4 years of follow-up, the mean remission period of patients was 26.5 $\pm$ 19.98 m; the relapse rate in the 12 remission patients was 33.33% within 1 year, and 58.3% within 4 years. At baseline, UC patients showed an enrichment in some proinflammatory microorganisms compared to the donor, such as *Bacteroides fragilis*, *Clostridium difficile*, and *Ruminococcus gnavus*, and showed reduced amounts of short-chain fatty acid (SCFA) producing bacteria especially *Faecalibacterium prausnitzii.* FMT induced taxonomic compositional changes in the recipient gut microbiota, resulting in a donor-like state. Given this specific donor, UC recipients with different outcomes showed distinct gut microbial features before and after FMT. In prior to FMT, relapse was characterized by higher abundances of *Bacteroides fragilis* and *Lachnospiraceae incertae sedis*, together with lower abundances of *Bacteroides massiliensis*, *Roseburia*, and *Ruminococcus*; *Prevotella copri* was more abundant in the non-responders (NR); and the patients with sustained remission (SR) had a higher abundance of *Bifidobacterium breve*. After FMT,

the NR patients had a lower level of *Bifidobacterium* compared to those with relapse (Rel) and SR, while a higher level of *Bacteroides* spp. was observed in the Rel group.

Conclusion: Low-intensity single donor FMT could induce long remission in active UC. The gut microbiota composition in UC patients at baseline may be predictive of therapeutic response to FMT.

Keywords: ulcerative colitis, low-intensity FMT, long-term efficacy, gut bacteria, 16s rRNA

INTRODUCTION

Ulcerative colitis (UC) is a chronic idiopathic inflammatory bowel disorder, which is difficult to cure and easy to relapse. It has become a global disease with a high prevalence in western countries, and the growing incidence in newly industrialized countries (Ng et al., 2018). The exact pathogenesis of UC is thought to be a multi-factor disease, which is a result of the interaction between host susceptibility genes, environment, diet, immunity, intestinal barrier, and gut microbiota (Ramos and Papadakis, 2019). A large body of evidence has revealed the intestinal microbiome playing a critical role in the pathogenesis of UC, and has shown major shifts of intestinal flora in UC patients, such as reduced bacterial diversity, higher abundance of Proteobacteria and lower abundance of Firmicutes (Sokol and Seksik, 2010; Lane et al., 2017; Franzosa et al., 2019). However, the perturbation of specific microbes involved in UC pathogenesis have not been identified.

Several clinical trials have been performed to treat UC by manipulating the intestinal microbiota through probiotics, prebiotics, synbiotics, and antibiotics (Ghouri et al., 2014; Asto et al., 2019; Xi et al., 2021). However, evidence supporting significant therapeutic effects for UC remains limited. Fecal microbiota transplantation (FMT) is a powerful way to manipulate gut microbiota, which has been proven to be an effective treatment for *Clostridium difficile* infection (CDI). So far, only five randomized controlled trials (RCTs) studies were published regarding FMT treatment for UC (**Supplementary Table 1**), including four for adult patients and one for pediatric patients, and three of which reported higher remission rates [24%(Moayyedi et al., 2015), 27%(Paramsothy et al., 2017), and 32%(Costello et al., 2019)] in patients received high-intensity FMT compared to placebo (5, 8, and 9%, respectively). The pediatric RCT study also showed a higher composite clinical outcome of FMT group versus placebo group (91.7% vs. 50% at 6 weeks) (Pai and Popov, 2017; Pai et al., 2021). One RCT study reported a negative result in treating UC, with remission rates 30.4% vs. 20.0% compared to the control ($p = 0.51$) (Rossen et al., 2015). The uniform protocols of FMT administration have not been achieved, and there is a paucity of data on the long-term durability and safety of FMT in patients with active UC especially those with moderate to severe disease. In addition, most previous studies including RCTs performed FMT with high intensities, which increases the practical barriers. In this study, we assessed the long-term efficacy and safety of single-donor, low-frequency FMT in the treatment of UC, and analyzed the intestinal microbiota characteristics associated with different therapeutic outcomes.

MATERIALS AND METHODS

Trial Design

This was a single-center, historical control trial of FMT for the treatment of active UC. Patients received the initial (F0) and second (F1) treatments with time interval of 2 months. The follow-up clinical and endoscopy examinations were performed at F1 and 4 months after F0, which were marked as F2.

Enrollment

Eligible patients fulfilled the following criteria: established UC according to clinical symptoms, colonoscopy, and pathology; Mayo scores $\geq$ 3; Mayo endoscopic scores $\geq$ 2; initial onset cases without any treatment, or, subjects refractory or intolerant to the existing treatments including 5-ASA, glucocorticoids, immunosuppressants and biologics; a 1-week washout period before treatment if the patients were exposed to antibiotics, probiotics or other medicines that could influence intestinal flora; and the ability to provide informed consent. Patients were excluded if they underwent long-term prokinetic treatment to control diarrheal symptom, had a history of colectomy or other intestinal surgery, had a concomitant *C. difficile* infection or infection with another enteric pathogen, had severe congenital or acquired immunodeficiency disease, had a progressive severe disease except for UC that required hospitalization, or were pregnant or lactating.

The Cohort

The enrolled patients completed general questionnaires for demographic information including age, gender, weight, body mass index, and Inflammatory Bowel Disease Questionnaire score (IBDQ, a validated disease-specific quality of life measure; scores range from 0 to 224 with a higher score indicating better quality of life) (Guyatt et al., 1989). Clinical syndromes were recorded, including body temperature, daily defecation frequency, hematochezia, stool consistency, abdominal pain, abdominal distension, etc. Lab test included hemoglobin (Hb), number of leukocytes, erythrocyte sedimentation rate (ESR), c-reactive protein (CRP), platelet count, etc., were examined. Endoscopic performance, baseline Mayo scores, clinical Mayo scores and endoscopic Mayo scores were documented.

Donor

We screened self-perceived healthy volunteers heavily to acquire eligible donors via a preliminary screening questionnaire, laboratory examinations. These donor candidates reported their medical history and lifestyle habits via questionnaires to exclude any exposure to infectious agents or risky behaviors (e.g., sexual preference). They underwent serology screening tests for HIV, hepatitis A, B, C, and E, syphilis, Epstein–Barr virus, cytomegalovirus, rotavirus. Stool culturing was performed for enteric pathogens including *Escherichia coli O157*, *Salmonella* spp., *Shigella* spp., *Campylobacter* spp., *Staphylococcus aureus*, *Yersinia*, *Vibrio parahaemolyticus*, *Vibrio cholerae*, *Candida albicans*, *Clostridium difficile* toxin A/B, as well as ova and parasites. In addition, physical examination, electrocardiogram, chest X-ray, urea breath test, as well as blood tests were also performed to exclude gastrointestinal, or non-gastrointestinal disorders. All eligible donors had negative results for these tests and examinations. Among the donor candidates we selected, one 12-years old boy showed outstanding therapeutic outcomes in treating UC patients in our previous report (Ren et al., 2015). In order to further define beneficial donor-specific and microbial content-specific effects, we only used the material from this "super-donor" candidate for FMT in this study. The donor has signed informed consent for each donation.

Fecal Microbiota Transplantation Interventions and Follow-Up

The donor did not use antibiotics, probiotics or other agents that could influence intestinal flora and had no travel history during the feces donation time, and he was requested to repeat screening every 3 months. Donor feces were collected on the day of treatment into a sterile medical container in a special bathroom and stored on ice, then sent to the laboratory within 1 h. Then, a total of 350 to 400 ml filtered stool suspension was obtained from a mixture of 100 g specimen stool and 500 ml sterile saline solution and immediately transferred to the endoscopy center on ice for later use. FMT was administrated via colonoscopy or colonoscopy combined with gastroscopy. Patients were pretreated with 2L bowel lavage solution (polyethylene glycol electrolyte disperses) on the morning of the treatment. Patients underwent a routine colonoscopy examination, during which biopsy specimens were obtained. An endoscopic spray tube (model:AF-2416PB, Olympus, Japan) was inserted into the ileum through the biopsy channel of the colonoscope, and then approximately 300 ml of stool suspension was infused with a syringe into the tube as the colonoscope was slowly retracted. If a combined gastroscopic approach was applied, the tube was placed in the duodenal descending portion to deliver the stool suspension (approximately 80∼100 ml). After delivery, patients stayed in bed for at least 45 to 60 min.

Measures and Outcomes

The clinical syndromes, lab indexes, IBDQ, Mayo scores (MS) and endoscopic Mayo scores (EMS) were recorded at F0, F1, and F2. Adverse effects were recorded after each FMT and during the follow-up period.

The primary end points of the study included clinical remission [defined as a total Mayo score ≤ 2, with no individual sub-score >1 (Rutgeerts et al., 2005; D'Haens et al., 2007; Carbonnel et al., 2016)], clinical response [defined as a decrease in the Mayo score of at least 3 points and at least 30%, with an accompanying decrease in the sub-score for rectal bleeding of at least 1 point or an absolute rectal-bleeding sub-score of 0 or 1 (Rutgeerts et al., 2005; D'Haens et al., 2007; Carbonnel et al., 2016)], and endoscopy remission [defined as an absolute sub-score for endoscopy of 0 or 1 (Rutgeerts et al., 2005; D'Haens et al., 2007; Paul et al., 2013)] at the end of the follow-up period. Patients were followed for up to 2∼5 years after inclusion and long-term clinical remission (or sustained remission) was defined as clinical remission without the need of rescue therapy at or more than 2 years. All the remission and response here were steroid-free.

The secondary end points included adverse events, changes in IBDQ score, CRP, ESR, Hb, weight, BMI, as well as relapse rate during long-term follow-up. The relapse rate was defined as the proportion of relapsed patients in patients with remission during long-term follow-up.

Specimen Collection and Microbiota Profiling

Fecal samples were collected from patients at three time points and from the corresponding donor on the day of treatment. Samples were divided into sterile tubes, stored in a −20°C freezer immediately after production and subsequently transferred to −80°C within 24 h. DNA was isolated using QIAamp® DNA Stool Mini Kit (Qiagen, Valencia, CA, United States) from fecal samples, and then its concentration was measured by Nanodrop2000 instrument (Thermo Scientific, United States) and molecular size was estimated by agarose gel electrophoresis. 16S rRNA genes of V3-V4 regions were amplified and raw sequencing data were processed with the Illumina MiSeq platform as described previously (Ren et al., 2018).

USEARCH pipeline was applied to denoise the raw sequences, remove chimeras, and produce operational taxonomic units (OTUs) (Edgar, 2010). Sequences were assembled using *–fastq_mergepairs* command with default parameters, and quality trimmed using *–fastq_filter* command with a *–fastq_maxee* set at 1.0. The assembled sequences were clustered into zero-radius OTUs by using unoise3 (Edgar, 2013) algorithm with the minimum abundance cut-off (*–minsize*) set at 8. Taxonomic assignments to the OTUs were performed using SINTAX with Ribosomal Database Project (RDP) 16S training set as the reference database (Cole et al., 2014).

Statistical Analysis

The clinical data were analyzed by GraphPad Prism v7.0 (GraphPad Software Inc., CA, United States) or SPSS v23.0 software (SPSS, Chicago, IL, United States). Categorical data were analyzed using Pearson's χ^2 or Fisher's exact test. Continuous data were analyzed using t tests with significance defined as $p < 0.05$.

Statistical analysis of the microbiota profiles was performed by using Calypso (v 8.6.4) (Zakrzewski et al., 2017). Taxa that have less than 3,000 read counts or 2% relative abundance across all samples were excluded from analysis. In order to account for the non-normal distribution of taxonomic counts data, the sequences of OTUs were normalized via Cumulative-sum scaling (CSS) followed by log2 transformation. Alpha diversity was quantified at the OTU level using the Shannon' and Chao1 indexes indices, testing for significant differences with analysis of variance (ANOVA) followed by Tukey *post hoc* test. For beta diversity, we performed principal coordinates analysis (PCoA) using Bray-Curtis dissimilarity at the OTU level, and determined significant differences among groups using permutational multivariate analysis of variance (PERMANOVA). Three or more group-wise comparisons were performed by Kruskal–Wallis testing on the relative abundance of fecal bacteria. Further pairwise Mann-Whitney test was carried out between all groups to assess relevant signatures.

RESULTS

Patients

An overview of the recruitment process is shown in **Figure 1**. From November 2014 to May 2017, 33 patients diagnosed with active UC were recruited. Two patients were excluded in the subsequent analysis due to glucocorticoids administration after the first FMT. Eleven patients did not receive the last examination after the second FMT. The baseline characteristics of the enrolled patients are presented in **Table 1**. The 31 enrolled patients included 19 males and 12 females, with an average age of 36 ± 12.39 years (range 14 to 62 years) and an average disease course of 4.44 ± 4.52 years (range 2 months to 20 years). Among all of the UC patients according to the Montreal classification (Saidani et al., 2019), 77.4% (24 cases) had extensive UC (E3, pancolitis), 16.1% (5 cases) had left sided UC (E2, distal UC), and 6.5% (2 cases) had ulcerative proctitis (E1) (Satsangi et al., 2006). Three treatment-naïve patients with new-onset UC, and the rest had a medication history including the use of mesalamine, glucocorticoids, immunosuppressants (azathioprine) or tumor necrosis factor antagonists (infliximab). Each patient received FMT treatment twice with an interval of 2–3 months. The medications of the UC patients before and after FMT are presented in **Supplementary Tables 2, 3**.

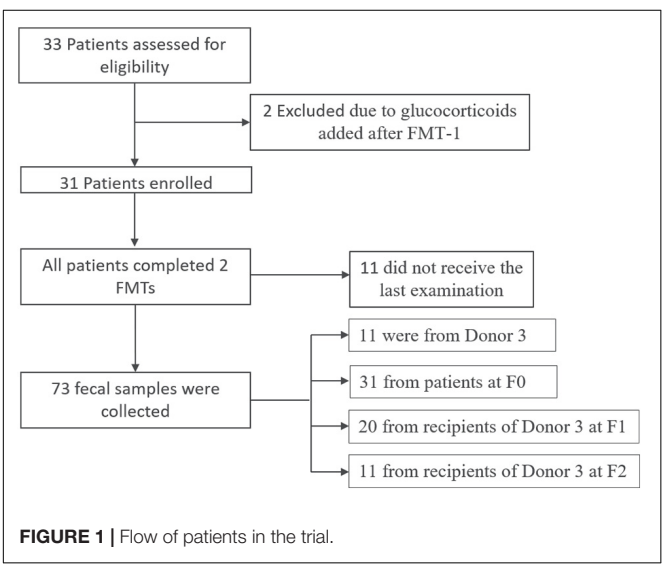


FIGURE 1 | Flow of patients in the trial.

TABLE 1 | Baseline characteristics of enrolled UC patients.

Characteristic	Patients (*n* = 31)
Gender, n (male/female)	19/12
Age, mean ± SD (range)	36 ± 12.39 (14∼62)
Disease course (year)	4.44 ± 4.52
Height, mean ± SD (m)	1.70 ± 0.11
Weight, mean ± SD (kg)	56.69 ± 12.73
BMI, mean ± SD	19.76 ± 3.59
Montreal classification *, n (E1/E2/E3)	2/5/24
Mayo scores, mean ± SD	9.58 ± 2.63
Severity, n (mild/moderate/severe)	3/12/16

**E3, extensive UC (pancolitis); E2, left sided UC (distal UC); E1, ulcerative proctitis; according to the Montreal classification.*

Responses

Overall, the Mayo scores and endoscopic Mayo scores significantly decreased in UC patients compared to the baseline ($p < 0.05$) (**Figures 2A,B**). After the first FMT (FMT-1), the clinical remission rate and endoscopic remission rate were 22.58% (7/31), and the clinical response rate was 67.74% (21/31). After the second FMT (FMT-2), only 20 patients received the last examination after the second FMT, and the clinical remission rate and endoscopic remission rate rose to 60% (12/20), and the clinical response rate increased to 80% (16/20).

The efficacy of FMT was diverse in patients with different symptom severity showed. After two FMT treatments, the clinical remission rate and response rate of moderate UC were much higher than mild and severe UC. It is worth mentioning that all the moderate UC patients were responded to FMT treatment (**Table 2**). Of all the patients, 11 were administrated in the route of colonoscopy combined with gastroscopy, and 20 were delivered only through colonoscopy. After two FMT treatments, the clinical remission rates and clinical response rates were 27.3% (3/11) vs. 45% (9/20), and 63.6% (7/11) vs. 70% (14/20) (**Table 2**). The intestinal mucosa lesions and histopathological images of patients improved to different extents after two FMT treatments (**Supplementary Figure 1**). The clinical responses of E3 (pancolitis), E2 (distal UC), and E1 (ulcerative proctitis) patients were 83.3% (20/24), 80% (4/5), and 50% (1/2), respectively (**Table 2**). There was an interesting phenomenon that the lesions in the rectum and/or sigmoid colon persisted in some E3 patients.

Fecal microbiota transplantation treatment significantly decreased the defecation frequency, improved hematochezia, and increased the body weight and BMI of the UC patients after FMT-1 (**Table 3**). ESR, CRP and platelets decreased significantly after FMT-1 and FMT-2 ($p < 0.05$); there was no significant difference

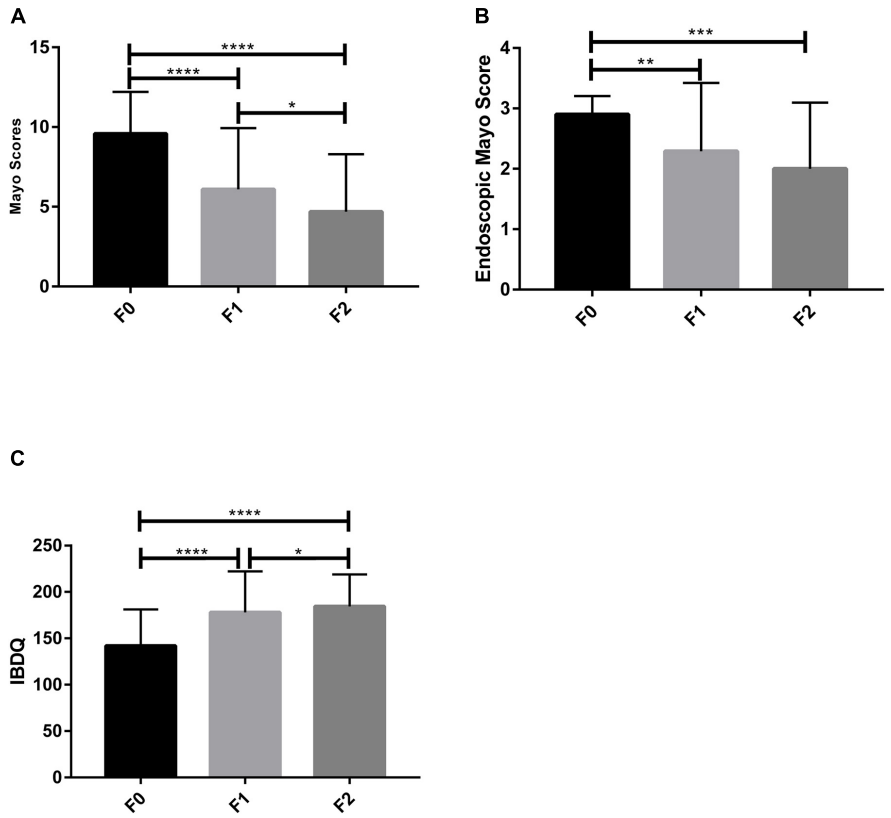


FIGURE 2 | Clinical indexes of patients. **(A)** Mayo score, **(B)** Endoscopic Mayo score, and **(C)** IBDQ score were measured to evaluate the FMT therapeutic outcomes. F0, before FMT; F1, 2∼3 months after the first FMT, or before the second FMT; F2, 2∼3 months after the second FMT. $^{*}p < 0.05$, $^{**}p < 0.01$, $^{***}p < 0.001$, $^{****}p < 0.0001$ (Paired *t*-test with GraphPad Prism 7.00).

in Hb before and after FMT, though it had an increasing trend (**Table 3**). The total IBDQ score increased significantly after FMT ($p < 0.0001$) (**Figure 2C**).

During a 4-year follow-up, the mean remission duration was 26.5 ± 19.98 m (3 m∼48 m). Among 12 patients with remission after FMT, 4 patients (33.33%) relapsed within one year, and 6 patients (50%) relapsed within two years. Notably, four participants remained in remission for four years without receiving medication even mesalamine.

TABLE 2 | Clinical efficacy after two FMT treatments under different conditions.

Clinical conditions		Clinical remission rates	Clinical response rates
severity	Mild UC	33.3% (1/3)	33.3% (1/3)
	Moderate UC	58.3% (7/12)	100% (12/12)
	Severe UC	25% (4/16)	75% (12/16)
Administration routes	Colonoscopy combined with gastroscopy (*n* = 11)	27.3% (3/11)	63.6% (7/11)
	Colonoscopy only (*n* = 20)	45% (9/20)	70% (14/20)
Montreal classification	E3 (*n* = 24)	41.7% (10/24)	83.3% (20/24)
	E2 (*n* = 5)	40% (2/5)	80% (4/5)
	E1 (*n* = 2)	0	50% (1/2)

In this table, the 11 patients who did not receive the examination at F2, were analyzed based on the assessments at F1.

Adverse Events

A portion of patients experienced mild adverse events shortly after FMT. Low fever was the most common side effect (27.4%, 17/62), followed by abdominal pain (9.7%, 6/62) and transient abdominal distension (9.7%, 6/62) (**Table 4**). Most adverse events were transient and disappeared spontaneously within hours.

Bacterial Analysis

Seventy-three fecal samples were collected, 11 of which were from the single donor (Donor 3), 31 from the UC patients at F0, 20 from the corresponding recipients at F1, and 11 were from the corresponding recipients at F2. The bacterial alpha diversity (measured by Simpson's index and Shannon index) of UC patients was significantly lower compared to the donor at baseline (F0), but increased to the donor level after FMT treatment (**Figures 3A,B**). The results of principal component analysis (PCoA) analysis suggested that the microbial community composition and structure of UC patients were shifted toward a

TABLE 3 | Clinical variables before and after FMT.

Clinical variables	F0 (*n* = 31)	F1 (*n* = 31)	F2 (*n* = 17)	*p* value
Hematochezia scores	2.19 ± 1.11	1 ± 1.13****	0.53 ± 1.007****	< 0.0001
Stool frequency	8.23 ± 6.17	4.29 ± 4.31**	2.82 ± 2.68**	0.0005
ESR (mm/h)	22.56 ± 19.69	15.48 ± 17.2	14.88 ± 15.55	0.256
CRP (mg/dl)	1.83 ± 2.09	1.23 ± 1.84	0.67 ± 0.71*	0.116
High ESR, % (n/30)	46.43% (13/28)	28.57% (8/28)	23.53% (4/17)	0.211
High CRP, % (n/30)	51.61% (16/31)	29.03% (9/31)*	23.53% (4/17)*	0.081
Platelet	335.6 ± 136.2	316.5 ± 122.9	276.9 ± 93.82*	0.312
Hb	111.9 ± 18.4	116.7 ± 24.78	116.4 ± 24.68	0.664
Weight (kg)	56.69 ± 12.73	58.86 ± 13.19**	58.32 ± 13.97**	0.802
BMI	19.76 ± 3.59	20.49 ± 3.67**	20.76 ± 3.93**	0.608
IBDQ	142 ± 39.19	178 ± 44.24****	184.4 ± 34.51****	0.0010

*All values are mean ± SD unless high ESR and high CRP. High ESR > 20 mm/h; High CRP > 0.8 mg/dl. *p < 0.05, **p < 0.01, ****p < 0.0001 (Paired t test with GraphPad Prism 7.00 and Chi-Square Test with IBM SPSS Statistics 23 versus F0).*

TABLE 4 | Safety assessment of 31 patients with 62 FMTs.

Adverse effects	Proportion	Duration	Treatment	Notes
Fever	27.4% (17/62)	A few hours ∼1 day	Spontaneous relief or physical cooling	The body temperature was approximately 37.5°C, the highest temperature was 39°C, which decreased to normal level the second day without chills.
Abdominal pain	9.7% (6/62)	A few hours	One patient had persistent abdominal cramps after administration via gastroscopy and achieved remission after the administration of intramuscular anisodamine. The others had mild symptoms.	
Abdominal distension	9.7% (6/62)	1∼3 days	Spontaneous relief	Mostly mild
Nausea	1.6% (1/62)	A few hours	Spontaneous relief	
Furuncle in the leg	1.6% (1/62)	1 week	No diffusion, scab without treatment	

donor-like state after the first FMT, and this transformation was enhanced after the second FMT (**Figure 3C**).

Among the top 100 most abundant OTUs in the fecal samples of UC patients at the baseline, the relative abundances 55 OTUs were significantly different from that of the donor (Mann Whitney *U* test $p < 0.05$; **Supplementary Table 4**). Among the UC-enriched taxa, we observed some potential pathogens that reported to induce/exacerbate inflammation in IBD, such as *Bacteroides fragilis* (Rabizadeh et al., 2007), *Clostridium difficile* (Negron et al., 2016), and *Ruminococcus gnavus* (Hall et al., 2017). In contrast, multiple short-chain fatty acid (SCFA) producing Firmicutes taxa were significantly depleted in UC such as *Eubacterium hallii*, *Faecalibacterium prausnitzii*, and *Roseburia* spp. (Louis and Flint, 2017). The composition of the gut bacterial community significantly changed in the patients after FMT treatment (**Figure 4**; **Supplementary Table 5**). Among the FMT-increased OTUs, six belong to *Faecalibacterium prausnitzii*, five to genus *Bifidobacterium*, and four to *Bacteroides plebeius*. Moreover, some potential pathogenic microorganisms such as *Clostridium difficile* and *Ruminococcus gnavus* were substantially decreased after FMT (**Supplementary Table 5**).

To further analyze the associations of the fecal microbiota with different therapeutic outcomes, we performed Spearman correlations between the relative abundance of fecal bacteria and some clinical variables including Mayo score, IBDQ, stool frequency, erythrocyte sedimentation rate (ESR), C-reactive protein (CRP), white blood count (WBC), and neutrophil (**Supplementary Table 6**). The relative abundance of *g__Bifidobacterium_OTU1617* was inversely correlated with the Mayo score, stool frequency, ESR, and neutrophil, indicating its pleiotropic effect in improving the UC symptoms. In contrast, *s__Nocardia_coeliaca_OTU2421* was found to be positively correlated with the Mayo score, stool frequency, and neutrophil, implicating a its pathogenic potential for UC.

Based on the therapeutic outcomes, we classified the UC patients into the SR (SR, sustained remission patients without relapse in 4 years), Res (Res, responders to FMT without relapse in 4 years), Rel (remission or response patients relapsed within 4 years), and NR (NR, patients with no response) groups. In prior to FMT (F0), NR and Rel patients showed a lower microbial alpha diversity (measured in Shannon's index) than Res and SR patients, albeit significance was not achieved (**Supplementary Figures 2A,C**). In addition, the Rel patients were characterized by higher abundances of *Bacteroides fragilis* and *Lachnospiraceae incertae sedis*, together with lower abundances of *Bacteroides massiliensis*, *Roseburia*, and *Ruminococcus*; *Prevotella copri* was more abundant in the NR patients; and the SR patients had a higher abundance of *Bifidobacterium breve* (**Figure 5A**).

After FMT, the alpha diversity reached similar levels across the groups with different therapeutic response

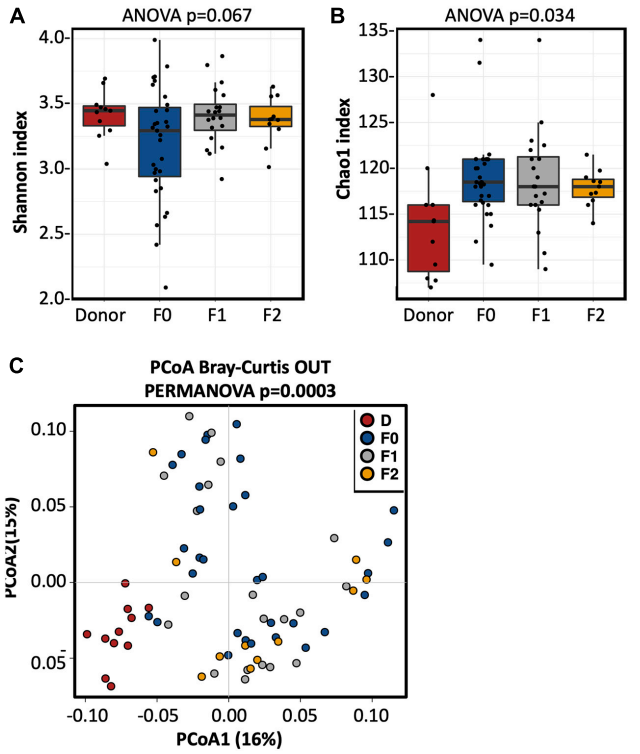


FIGURE 3 | The fecal microbiota alpha diversity increased in the UC patients after FMT. **(A)** Shannon index and **(B)** Chao1 index of the fecal microbiota in UC patients prior and after FMT treatments. ANOVA is performed to evaluate alpha diversity among the different groups. **(C)** PCoA analysis of the fecal microbiota in donor and UC patients prior and after FMT. Statistical significance of distances among the four groups was assessed using PERMANOVA. D, donor; F0, before FMT; F1, 2∼3 months after the first FMT, or before the second FMT; F2, 2∼3 months after the second FMT.

(**Supplementary Figures 2B,D**). NR patients had a lower level of *Bifidobacterium* compared to other response groups (**Figure 5B**). A higher level of multiple *Bacteroides* spp. (including OTU232, OTU397, OTU1349 and OTU2371) was observed in the Rel patient group, while the SR patients had a lower level of *Bacteroides finegoldii*, and a higher level of some *Blautia* (OTU1900). In addition, a reduced level of taxon (OTU1641) belonging to Clostridiales order was observed in the Res patients.

DISCUSSION

Differences in FMT procedures might cause different therapeutic effects in various studies. Most previous studies including RCTs performed FMT with high intensities (pooled donors and frequent treatments over a short duration). FMT with a single donor and long interval between administrations could be considered as a low intensity regimen. Although UC patients benefit from FMT, concerns about the efficacy, safety, and durability of low-intensity FMT for UC treatment remains to be addressed. In this study, we performed FMT using stool suspensions from a single donor with time interval of 2 months for all UC patients, and achieved a remission rate of 22.58% (7/31) after the first FMT and 60% (12/20) after the second FMT. All the clinical indicators including Mayo scores, Endoscopic mayo scores, hematochezia scores, stool frequency, IBDQ were improved after the two FMT treatments. Thus, our results suggested that a low-intensity single donor FMT can lead to positive therapeutic results.

The long-term outcomes and health consequences of FMT remain to be established, with most studies reporting mixed results and without showing a sustained benefit of FMT (Brandt et al., 2012; Kump et al., 2013; Vermeire et al., 2016). Analysis with 109 UC patients received FMT from two clinical trials (NCT01790061, NCT02560727), 21.1% (23/109) and 25.7% (28/109) of patients maintained clinical response at 6 months after single FMT, and step multiple FMTs, respectively (Ding et al., 2019). In another study (Sood et al., 2019a), that the primary outcome of maintenance of clinical remission at 48 weeks was achieved in 27/31 [87.1%] patients who received FMT via colonoscopy every 8 weeks. In the present study, the longest remission time was 6 years which continued till this article was completed, and in 8 of the 12 patients (66.7%) in clinical remission, the results remained in remission at 1-year follow up, 50% (6/12) at 2-year follow up and 41.7% (5/12) at 4-year follow up, without continued fecal infusion. Nevertheless, UC patients also have recurrence issues after FMT treatment or other therapies, and some studies reported maintenance FMT administration could sustain clinical efficacy either by capsule or colonoscopy (Sood et al., 2019a; Steube et al., 2019). Long-term maintenance treatment is necessary for some patients.

In one retrospective study regarding the long-term safety of FMT to treat UC, new-onset urticaria, arthritis, depression, and so on, were found in the long-term follow-up, while abdominal discomfort, flatulence, low-grade fever were the most common short-term adverse events (Sood et al., 2019b). Besides, one study reported a serious adverse event of myasthenia gravis in 1 month after FMT treatment (Ding et al., 2019). In our study, all the patients treated with FMT were observed for 4 years, with a maximum of 6.5 years. During the follow-up period, short-term adverse effects were consistent with previous studies by and large, but no long-term adverse reactions caused by FMT were found. Nevertheless, a remarkable adverse event was that one 14-year-old girl underwent furuncle in her legs after the first FMT treatment, though the furuncles scabbed in 1 week without any treatment. The risk of infectious disease transmission for FMT needs to be investigated with more cases collected. On June 13, 2019, the US FDA issued a safety alert regarding two immunocompromised adults who acquired Extended Spectrum Beta-Lactamase (ESBL)-producing *E. coli* infections following FMT, resulting in one death. Hence, the donor screening protocols for FMT should be further improved by excluding use of stool that tests positive for multi-drug resistant organisms.

Diverse administration routes of FMT have been observed to have similar efficacy in the studies of FMT for the treatment of CDI (Postigo and Kim, 2012; Furuya-Kanamori et al., 2017). We used a combination of colonoscopy and endoscopy as the route of FMT for 11 patients with a clinical response rate 63.6%, and the next 20 patients underwent only a colonoscopy

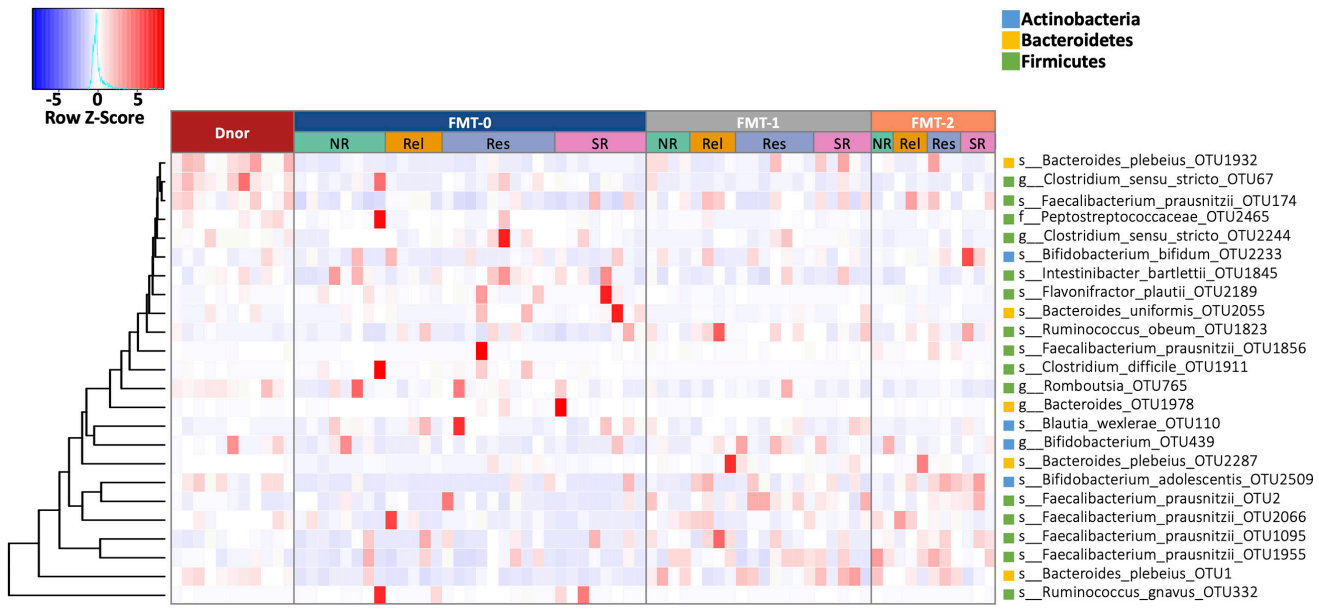


FIGURE 4 | The fecal microbiota composition of UC patients shifted by FMT. OTUs that were statistically different in abundance between F0 and F1, and between F0 and F2 (Wilcoxon rank-sum test $p < 0.01$). Heatmap is color-coded based on row z-scores. D, donor; F0, before FMT; F1, 2∼3 months after the first FMT, or before the second FMT; F2, 2∼3 months after the second FMT.

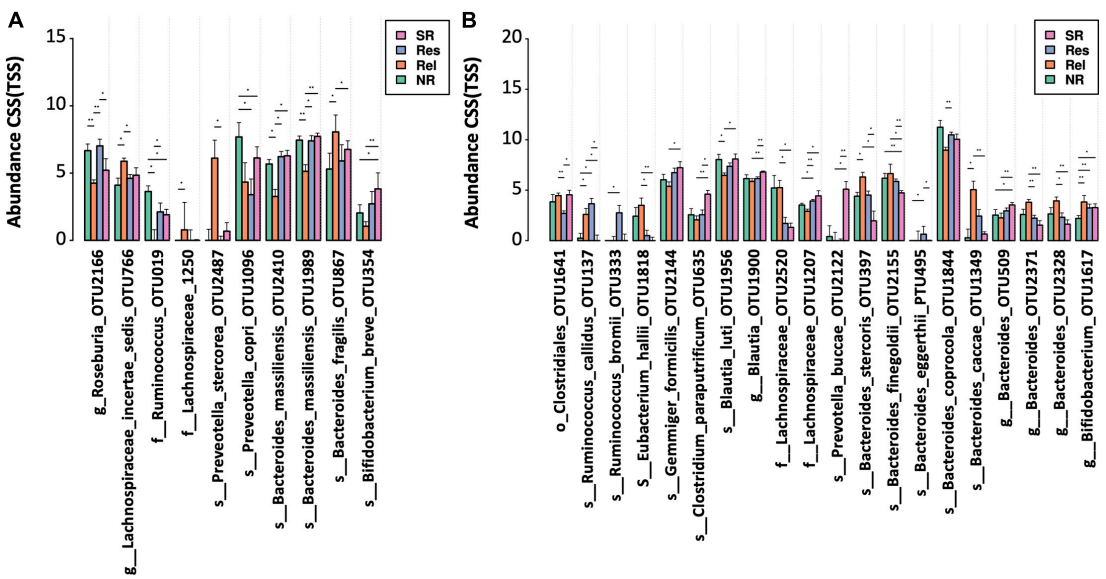


FIGURE 5 | Bacterial taxa associated with different FMT outcomes. OTUs were compared among the patient with different therapeutic outcomes **(A)** before and **(B)** after FMT. Significance was determined by Kruskal-Wallis test ($p < 0.05$) and confirmed by pairwise Mann-Whitney *U* test (*$p < 0.05$ and **$p < 0.01$) NR, no response; Rel, relapse; Res, responders; SR, sustained remission.

approach, who also experienced good efficacy with a clinical response rate 70%. In the studies of FMT treatment for UC, colonoscopy approach, enema and nasogastric tube are the most common methods of administration. In the five RCT studies, four obtained positive results by conducting under lower GI tract administration (Moayyedi et al., 2015; Paramsothy et al., 2017; Costello et al., 2019), and one obtained negative results by using upper gastrointestinal tract route (Rossen et al., 2015). It is speculated that the upper gastrointestinal administration might be one of the reasons leading to the treatment failure, and FMT via colonoscopy route may be a better choice for UC.

Previous studies mainly focused on mild to moderate UC, including the above-mentioned RCT studies. A few cohort studies have reported the efficacy of FMT on moderate to severe

UC (Angelberger et al., 2013; Kump et al., 2013; Ding et al., 2019), and showed only marginally clinical responses. In our study, patients with moderate UC had the highest responses to FMT, followed by, in turn, severe and mild UC. It is worth noting that the FMT treatment was more effective in patients with extensive UC, followed by distal UC. And patients with proctitis had poor responses to FMT, while some patients with extensive and distal UC responded to FMT but were more likely to leave behind lesions in rectum and/or left-sided colon. These findings suggest that lesions confined to distal colon, especially proctitis, had less responsive to FMT and may require more long-term treatment (persistent therapy). It was recently suggested that CD patients with a low microbial load presented a better response to FMT (Sarrabayrouse et al., 2020). Moreover, oral decontamination with antibiotics such as colistin or aminoglycosides has been proposed to enhance the efficacy of FMT (Huttner et al., 2019; Saidani et al., 2019). Thus, an initial low microbial load or reducing the microbial load in UC patients may promote the colonization of donor microbiota thereby enhancing the efficacy of FMT. In fact, the bacterial load various at different location of the GI tract, with a higher bacteria load in the distal colon ($\sim 10^{10}$ CFU/ml) than the ileum ($\sim 10^{6}$ CFU/ml), which give rise to different degrees of colonization resistance. Therefore, an intensive FMT regime may be required to efficiently modulate the microbiome for UC patients with the distal colitis.

The gut microbiota profile analysis demonstrated similar results as reported in previous studies of FMT (Costello et al., 2019; Paramsothy et al., 2019). For instance, a lower gut microbiota diversity was observed in the UC patients compared with the healthy donor, which was increased after FMT treatments. The composition of the gut bacterial community was shifted by FMT to a donor-like state and was enhanced after the second administration. These results suggest that repeated FMT treatments enhance the colonization of donor-derived microbiota in UC patients leading to improvement in clinical symptoms. In particular, *Faecalibacterium prausnitzii*, *Bacteroides plebeius*, and *Bifidobacterium* spp. were significantly increased in UC patients receiving FMT, agreeing with some previous studies (Lopez-Siles et al., 2017; Nishino et al., 2018; Lloyd-Price et al., 2019). Interestingly, an increased level of some *Bifidobacterium* spp. was closely correlated with a reduction in Mayo score, stool frequency, ESR, and neutrophil, indicating a pleiotropic of *Bifidobacterium* for UC symptoms improvement (Jakubczyk et al., 2020).

As one of the main butyrate producers in the gut, *Faecalibacterium prausnitzii* is able to induce secretion of anti-inflammatory cytokines, thereby producing energy to the colonocytes and enhancing the intestinal barrier (Sokol et al., 2008; Louis and Flint, 2009; Ferreira-Halder et al., 2017; Lopez-Siles et al., 2017). Hence, the relative abundances of *Faecalibacterium prausnitzii* increased in UC patients after FMT treatments, suggesting a potential contribution in suppressing inflammation. In addition, we found that a high abundance of *Blautia* in UC patients at baseline was associated with sustained remission, and an enrichment of *Roseburia* was particularly associated with therapeutic responses. These results were consistent with previous studies (Paramsothy et al., 2019; Lloyd-Price et al., 2019).

Data about the correlation between *Bacteroidetes* spp. abundance and UC activity was controversial. In fact, different *Bacteroides* spp. may have different influences on the disease development in UC patients. For example, *Bacteroides plebeius* showed a significant therapeutic effect in UC patients from our study, whereas their nearest recognized species *Bacteroides vulgatus* (Kitahara et al., 2005) was considered as a pathobiont in human gut (Kootte et al., 2017)with a potential of driving injury in the small intestine (Ramanan et al., 2014). From our data, a combination of reduced *Bacteroides massiliensis* and enriched *Bacteroides fragilis* seemed to augur a relapse in UC after FMT. *Bacteroides fragilis* was shown to play a protective role from intestinal inflammation via Toll-like receptor 2 signaling, inducing production of polysaccharide A (PSA) and anti-inflammatory cytokine IL-10 (Mazmanian et al., 2008; Honda and Littman, 2016; Lee et al., 2018). Nevertheless, strains of enterotoxigenic *Bacteroides fragilis* have functions of tissue invasion and induce severe intestinal inflammation in humans and animals (Zamani et al., 2017). Moreover, a lower level of *Bacteroides finegoldii* after FMT characterized the patients with sustained remission. In contrast, Paramsothy et al. (2019) found that an increased abundance of *Bacteroides finegoldii* in donor stool may be associated with observed remission in UC patients receiving FMT. Thus, close species may have significantly distinct characteristics and the same species may contain various strains with different functions. Moreover, our data indicated that *Blautia* spp. and *Ruminococcus bromii* were predictors of achieving the sustained remission, which is in line with the findings in Paramsothy et al. (2017, 2019).

Preveotella copri was found to be more abundant in the non-responders at baseline. In a previous study (Paramsothy et al., 2019), *P. copri* was also found in higher abundance in UC patients who experienced therapeutic failure after FMT. The relative abundance of *P. copri* presents more stable in the population with IBD than non-IBD populations (Lloyd-Price et al., 2019). It was postulated that *Prevotella* has an antagonistic relationship with *Bacteroides* (Ley, 2016). Thus, the response of FMT might be partially impeded by *P. copri* resisting the colonization of the donor bacteria such as *Bacteroides*. Moreover, *P. copri* was suggested to play an immune-modulatory role in human rheumatoid arthritis (RA). About 32% of patients with RA were found to have serum immunoglobulin A (IgA) antibodies specific for *P. copri* (Larsen, 2017), which was almost absent in healthy subjects. Secretory IgA is the dominant immunoglobulin at the mucosal surface, and it plays a critical role in interacting with the microbiota and maintaining intestinal homeostasis. It was suggested that IgA coating identifies colitogenic bacteria in IBD patients and is associated with treatment outcomes (Palm et al., 2014; Shapiro et al., 2021). Therefore, *P. copri*-specific IgA may be related to poor response to FMT for UC patients, which deserves further investigation.

This is a series study with only 31 cases at baseline, which were further reduced at the points of F1 ($n = 20$). Therefore, this small cohort size and samples limited the strength of our conclusions. In addition, there was a loss of endoscopic examination in the long-term follow-up.

Collectively, our study demonstrated that low-intensity single donor FMT treatment is effective and safe for mild to severe UC,

and a repeated FMT provides a beneficial efficacy for disease improvement, with a considerable long-term efficacy and safety. The abundances of *Faecalibacterium prausnitzii*, *Bacteroides plebeius* and *Bifidobacterium* spp. increased significantly after FMT treatments in UC patients. The gut microbial composition of UC with different FMT therapeutic outcomes was distinguishable at baseline. In particular, a higher level of *Bacteroides fragilis* together with lower levels of *Bacteroides massiliensis* and *Roseburia* genus might be indicators of relapse given this particular donor. Moreover, an enrichment of *Blautia* spp. and *Ruminococcus bromii* together with a reduced *Bacteroides finegoldii* were associated with long-term remission. Further investigations to identify specific species/strains associated with clinical remission may shed a light for precise treatment, and a donor-recipient matching approach based on the gut microbiota compositions may increase the remission rate in long term.

DATA AVAILABILITY STATEMENT

The original contributions presented in the study are included in the article/**Supplementary Material**, further inquiries can be directed to the corresponding author/s.

ETHICS STATEMENT

The studies involving human participants were reviewed and approved by the Chinese PLA General Hospital Ethics Committee. Written informed consent to participate in this study was provided by the participants' legal guardian/next of kin. Written informed consent was obtained from the individual(s), and minor(s)' legal guardian/next of kin, for the publication of any potentially identifiable images or data included in this article.

AUTHOR CONTRIBUTIONS

YY responsible for the study concept and design. RR analysis and interpretation of the clinical data and drafted the manuscript. XG analysis and interpretation of the microbiome data and critical revision of the manuscript. YS, JL, LP, GS, ZW, BY, and JZ performance of the FMT and revision of the manuscript. All authors had access to the study data and have reviewed and approved the final manuscript.

FUNDING

This work was supported by the National High-tech Research and Development Projects (863, No. 2015AA020702), the National Natural Science Foundation of China (No. 81900474), Science and Technology Commission of the Central Military Commission (Grant No. 17-163-12-ZT-002-048-01), Shenzhen Key Laboratory Foundation (No. ZDSYS20200811143757022), and the Military Translational Medicine Fund of Chinese PLA General Hospital (No. ZH19001).

ACKNOWLEDGMENTS

We would like to acknowledge the staff of the colonoscopy unit at the Chinese PLA General Hospital and all the patients involved in the study.

SUPPLEMENTARY MATERIAL

The Supplementary Material for this article can be found online at: https://www.frontiersin.org/articles/10.3389/fmicb.2021.742255/full#supplementary-material

Supplementary Figure 1 | Improvement of intestinal mucosa lesions and histopathological images of PUC2 after two FMT treatments. F0, before FMT; F1, 2 months after the first FMT; F2, 5 months after the first FMT. PUC2, 40y, male, disease course: 15 years, extensive UC (E3), glucocorticoids (60 mg) for 2 weeks combined with mesalamine (4 g) more than 4 weeks did not respond well.

Supplementary Figure 2 | Comparisons of alpha diversity among UC patients with different FMT outcomes. Shannon index and Chao1 index are compared among UC patients **(A,B)** at baseline as well as **(C,D)** post-FMT with one-way ANOVA. NR, no response; Rel, relapse; Res, responders; SR, sustained remission.

REFERENCES

Angelberger, S., Reinisch, W., Makristathis, A., Lichtenberger, C., Dejaco, C., Papay, P., et al. (2013). Temporal bacterial community dynamics vary among ulcerative colitis patients after fecal microbiota transplantation. *Am. J. Gastroenterol.* 108, 1620–1630. doi: 10.1038/ajg.2013.257

Asto, E., Mendez, I., Audivert, S., Farran-Codina, A., and Espadaler, J. (2019). The Efficacy of Probiotics, Prebiotic Inulin-Type Fructans, and Synbiotics in Human Ulcerative Colitis: a Systematic Review and Meta-Analysis. *Nutrients* 11:293. doi: 10.3390/nu11020293

Brandt, L. J., Aroniadis, O. C., Mellow, M., Kanatzar, A., Kelly, C., Park, T., et al. (2012). Long-term follow-up of colonoscopic fecal microbiota transplant for recurrent Clostridium difficile infection. *Am. J. Gastroenterol.* 107, 1079–1087. doi: 10.1038/ajg.2012.60

Carbonnel, F., Colombel, J. F., Filippi, J., Katsanos, K. H., Peyrin-Biroulet, L., Allez, M., et al. (2016). Methotrexate Is Not Superior to Placebo for Inducing Steroid-Free Remission, but Induces Steroid-Free Clinical Remission in a Larger Proportion of Patients With Ulcerative Colitis. *Gastroenterology* 150, 380–8.e4. doi: 10.1053/j.gastro.2015.10.050

Cole, J. R., Wang, Q., Fish, J. A., Chai, B., McGarrell, D. M., Sun, Y., et al. (2014). Ribosomal Database Project: data and tools for high throughput rRNA analysis. *Nucleic Acids Res.* 42, D633–D642. doi: 10.1093/nar/gkt1244

Costello, S. P., Hughes, P. A., Waters, O., Bryant, R. V., Vincent, A. D., Blatchford, P., et al. (2019). Effect of Fecal Microbiota Transplantation on 8-Week Remission in Patients With Ulcerative Colitis: a Randomized Clinical Trial. *JAMA* 321, 156–164. doi: 10.1001/jama.2018.20046

D'Haens, G., Sandborn, W. J., Feagan, B. G., Geboes, K., Hanauer, S. B., Irvine, E. J., et al. (2007). A review of activity indices and efficacy end points for clinical trials of medical therapy in adults with ulcerative colitis. *Gastroenterology* 132, 763–786. doi: 10.1053/j.gastro.2006.12.038

Ding, X., Li, Q., Li, P., Zhang, T., Cui, B., Ji, G., et al. (2019). Long-Term Safety and Efficacy of Fecal Microbiota Transplant in Active Ulcerative Colitis. *Drug Saf.* 42, 869–880. doi: 10.1007/s40264-019-00809-2

Edgar, R. C. (2010). Search and clustering orders of magnitude faster than BLAST. *Bioinformatics* 26, 2460–2461. doi: 10.1093/bioinformatics/btq461

Edgar, R. C. (2013). UPARSE: highly accurate OTU sequences from microbial amplicon reads. *Nat Methods* 10, 996–998. doi: 10.1038/nmeth.2604

Ferreira-Halder, C. V., Faria, A. V. S., and Andrade, S. S. (2017). Action and function of Faecalibacterium prausnitzii in health and disease. *Best Pract. Res. Clin. Gastroenterol.* 31, 643–648. doi: 10.1016/j.bpg.2017.09.011

Franzosa, E. A., Sirota-Madi, A., Avila-Pacheco, J., Fornelos, N., Haiser, H. J., Reinker, S., et al. (2019). Gut microbiome structure and metabolic activity in inflammatory bowel disease. *Nat. Microbiol.* 4, 293–305. doi: 10.1038/s41564-018-0306-4

Furuya-Kanamori, L., Doi, S. A., Paterson, D. L., Helms, S. K., Yakob, L., McKenzie, S. J., et al. (2017). Upper Versus Lower Gastrointestinal Delivery for Transplantation of Fecal Microbiota in Recurrent or Refractory Clostridium difficile Infection: a Collaborative Analysis of Individual Patient Data From 14 Studies. *J. Clin. Gastroenterol.* 51, 145–150. doi: 10.1097/MCG.0000000000000511

Ghouri, Y. A., Richards, D. M., Rahimi, E. F., Krill, J. T., Jelinek, K. A., and DuPont, A. W. (2014). Systematic review of randomized controlled trials of probiotics, prebiotics, and synbiotics in inflammatory bowel disease. *Clin. Exp. Gastroenterol.* 7, 473–487. doi: 10.2147/CEG.S27530

Guyatt, G., Mitchell, A., Irvine, E. J., Singer, J., Williams, N., Goodacre, R., et al. (1989). A new measure of health status for clinical trials in inflammatory bowel disease. *Gastroenterology* 96, 804–810.

Hall, A. B., Yassour, M., Sauk, J., Garner, A., Jiang, X., Arthur, T., et al. (2017). A novel Ruminococcus gnavus clade enriched in inflammatory bowel disease patients. *Genome Med.* 9, 103. doi: 10.1186/s13073-017-0490-5

Honda, K., and Littman, D. R. (2016). The microbiota in adaptive immune homeostasis and disease. *Nature* 535, 75–84. doi: 10.1038/nature18848

Huttner, B. D., Galperine, T., Kapel, N., and Harbarth, S. (2019). 'A five-day course of oral antibiotics followed by faecal transplantation to eradicate carriage of multidrug-resistant *Enterobacteriaceae*' - Author's reply. *Clin. Microbiol. Infect.* 25, 914–915. doi: 10.1016/j.cmi.2019.02.001

Jakubczyk, D., Leszczynska, K., and Gorska, S. (2020). The Effectiveness of Probiotics in the Treatment of Inflammatory Bowel Disease (IBD)-A Critical Review. *Nutrients* 12:1973. doi: 10.3390/nu12071973

Kitahara, M., Sakamoto, M., Ike, M., Sakata, S., and Benno, Y. (2005). *Bacteroides* plebeius sp. nov. and *Bacteroides* coprocola sp. nov., isolated from human faeces. *Int. J. Syst. Evol. Microbiol.* 55, 2143–2147. doi: 10.1099/ijs.0.63788-0

Kootte, R. S., Levin, E., Salojarvi, J., Smits, L. P., Hartstra, A. V., Udayappan, S. D., et al. (2017). Improvement of Insulin Sensitivity after Lean Donor Feces in Metabolic Syndrome Is Driven by Baseline Intestinal Microbiota Composition. *Cell Metab.* 26, 611–9.e6. doi: 10.1016/j.cmet.2017.09.008

Kump, P. K., Grochenig, H. P., Lackner, S., Trajanoski, S., Reicht, G., Hoffmann, K. M., et al. (2013). Alteration of intestinal dysbiosis by fecal microbiota transplantation does not induce remission in patients with chronic active ulcerative colitis. *Inflamm. Bowel. Dis.* 19, 2155–2165. doi: 10.1097/MIB.0b013e31829ea325

Lane, E. R., Zisman, T. L., and Suskind, D. L. (2017). The microbiota in inflammatory bowel disease: current and therapeutic insights. *J. Inflamm. Res.* 10, 63–73. doi: 10.2147/JIR.S116088

Larsen, J. M. (2017). The immune response to Prevotella bacteria in chronic inflammatory disease. *Immunology* 151, 363–374. doi: 10.1111/imm.12760

Lee, Y. K., Mehrabian, P., Boyajian, S., Wu, W. L., Selicha, J., Vonderfecht, S., et al. (2018). The Protective Role of *Bacteroides* fragilis in a Murine Model of Colitis-Associated Colorectal Cancer. *Msphere* 3, e00587–18. doi: 10.1128/mSphere.00587-18

Ley, R. E. (2016). Gut microbiota in 2015: Prevotella in the gut: choose carefully. *Nat. Rev. Gastroenterol. Hepatol.* 13, 69–70. doi: 10.1038/nrgastro.2016.4

Lloyd-Price, J., Arze, C., Ananthakrishnan, A. N., Schirmer, M., Avila-Pacheco, J., Poon, T. W., et al. (2019). Multi-omics of the gut microbial ecosystem in inflammatory bowel diseases. *Nature* 569, 655–662. doi: 10.1038/s41586-019-1237-9

Lopez-Siles, M., Duncan, S. H., Garcia-Gil, L. J., and Martinez-Medina, M. (2017). Faecalibacterium prausnitzii: from microbiology to diagnostics and prognostics. *ISME J.* 11, 841–852. doi: 10.1038/ismej.2016.176

Louis, P., and Flint, H. J. (2009). Diversity, metabolism and microbial ecology of butyrate-producing bacteria from the human large intestine. *FEMS Microbiol. Lett.* 294, 1–8. doi: 10.1111/j.1574-6968.2009.01514.x

Louis, P., and Flint, H. J. (2017). Formation of propionate and butyrate by the human colonic microbiota. *Environ. Microbiol.* 19, 29–41. doi: 10.1111/1462-2920.13589

Mazmanian, S. K., Round, J. L., and Kasper, D. L. (2008). A microbial symbiosis factor prevents intestinal inflammatory disease. *Nature* 453, 620–625. doi: 10.1038/nature07008

Moayyedi, P., Surette, M. G., Kim, P. T., Libertucci, J., Wolfe, M., Onischi, C., et al. (2015). Fecal Microbiota Transplantation Induces Remission in Patients With Active Ulcerative Colitis in a Randomized Controlled Trial. *Gastroenterology* 149, 102–109.e6. doi: 10.1053/j.gastro.2015.04.001

Negron, M. E., Rezaie, A., Barkema, H. W., Rioux, K., De Buck, J., Checkley, S., et al. (2016). Ulcerative Colitis Patients With Clostridium difficile are at Increased Risk of Death, Colectomy, and Postoperative Complications: a Population-Based Inception Cohort Study. *Am. J. Gastroenterol.* 111, 691–704. doi: 10.1038/ajg.2016.106

Ng, S. C., Shi, H. Y., Hamidi, N., Underwood, F. E., Tang, W., Benchimol, E. I., et al. (2018). Worldwide incidence and prevalence of inflammatory bowel disease in the 21st century: a systematic review of population-based studies. *Lancet* 390, 2769–2778. doi: 10.1016/S0140-6736(17)32448-0

Nishino, K., Nishida, A., Inoue, R., Kawada, Y., Ohno, M., Sakai, S., et al. (2018). Analysis of endoscopic brush samples identified mucosa-associated dysbiosis in inflammatory bowel disease. *J. Gastroenterol.* 53, 95–106. doi: 10.1007/s00535-017-1384-4

Pai, N., and Popov, J. (2017). Protocol for a randomised, placebo-controlled pilot study for assessing feasibility and efficacy of faecal microbiota transplantation in a paediatric ulcerative colitis population: pediFETCh trial. *BMJ Open* 7:e016698. doi: 10.1136/bmjopen-2017-016698

Pai, N., Popov, J., Hill, L., Hartung, E., Grzywacz, K., Moayyedi, P., et al. (2021). Results of the First Pilot Randomized Controlled Trial of Fecal Microbiota Transplant In Pediatric Ulcerative Colitis: lessons, Limitations, and Future Prospects. *Gastroenterology* 161, 388–393.e3. doi: 10.1053/j.gastro.2021.04.067

Palm, N. W., de Zoete, M. R., Cullen, T. W., Barry, N. A., Stefanowski, J., Hao, L., et al. (2014). Immunoglobulin A coating identifies colitogenic bacteria in inflammatory bowel disease. *Cell* 158, 1000–1010. doi: 10.1016/j.cell.2014.08.006

Paramsothy, S., Kamm, M. A., Kaakoush, N. O., Walsh, A. J., van den Bogaerde, J., Samuel, D., et al. (2017). Multidonor intensive faecal microbiota transplantation for active ulcerative colitis: a randomised placebo-controlled trial. *Lancet* 389, 1218–1228. doi: 10.1016/S0140-6736(17)30182-4

Paramsothy, S., Nielsen, S., Kamm, M. A., Deshpande, N. P., Faith, J. J., Clemente, J. C., et al. (2019). Specific Bacteria and Metabolites Associated With Response to Fecal Microbiota Transplantation in Patients With Ulcerative Colitis. *Gastroenterology* 156, 1440–1454.e2. doi: 10.1053/j.gastro.2018.12.001

Paul, S., Del Tedesco, E., Marotte, H., Rinaudo-Gaujous, M., Moreau, A., Phelip, J. M., et al. (2013). Therapeutic drug monitoring of infliximab and mucosal healing in inflammatory bowel disease: a prospective study. *Inflamm. Bowel Dis.* 19, 2568–2576. doi: 10.1097/MIB.0b013e3182a77b41

Postigo, R., and Kim, J. H. (2012). Colonoscopic versus nasogastric fecal transplantation for the treatment of Clostridium difficile infection: a review and pooled analysis. *Infection* 40, 643–648. doi: 10.1007/s15010-012-0307-9

Rabizadeh, S., Rhee, K. J., Wu, S., Huso, D., Gan, C. M., Golub, J. E., et al. (2007). Enterotoxigenic *bacteroides* fragilis: a potential instigator of colitis. *Inflamm. Bowel Dis.* 13, 1475–1483. doi: 10.1002/ibd.20265

Ramanan, D., Tang, M. S., Bowcutt, R., Loke, P., and Cadwell, K. (2014). Bacterial sensor Nod2 prevents inflammation of the small intestine by restricting the expansion of the commensal *Bacteroides* vulgatus. *Immunity* 41, 311–324. doi: 10.1016/j.immuni.2014.06.015

Ramos, G. P., and Papadakis, K. A. (2019). Mechanisms of Disease: inflammatory Bowel Diseases. *Mayo. Clin. Proc.* 94, 155–165. doi: 10.1016/j.mayocp.2018.09.013

Ren, R., Sun, G., Yang, Y., Peng, L., Zhang, X., Wang, S., et al. (2015). [A pilot study of treating ulcerative colitis with fecal microbiota transplantation]. *Zhonghua Nei. Ke. Za. Zhi.* 54, 411–415.

Ren, R., Wang, Z., Sun, H., Gao, X., Sun, G., Peng, L., et al. (2018). The gastric mucosal-associated microbiome in patients with gastric polyposis. *Sci. Rep.* 8:13817. doi: 10.1038/s41598-018-31738-2

Rossen, N. G., Fuentes, S., van der Spek, M. J., Tijssen, J. G., Hartman, J. H., Duflou, A., et al. (2015). Findings From a Randomized Controlled Trial of

Fecal Transplantation for Patients With Ulcerative Colitis. *Gastroenterology* 149, 110–118.e4. doi: 10.1053/j.gastro.2015.03.045

Rutgeerts, P., Sandborn, W. J., Feagan, B. G., Reinisch, W., Olson, A., Johanns, J., et al. (2005). Infliximab for induction and maintenance therapy for ulcerative colitis. *N. Engl. J. Med.* 353, 2462–2476. doi: 10.1056/NEJMoa050516

Saidani, N., Lagier, J. C., Cassir, N., Million, M., Baron, S., Dubourg, G., et al. (2019). Faecal microbiota transplantation shortens the colonisation period and allows re-entry of patients carrying carbapenamase-producing bacteria into medical care facilities. *Int. J. Antimicrob. Agents*53, 355–361. doi: 10.1016/j.ijantimicag.2018.11.014

Sarrabayrouse, G., Landolfi, S., Pozuelo, M., Willamil, J., Varela, E., Clark, A., et al. (2020). Mucosal microbial load in Crohn's disease: a potential predictor of response to faecal microbiota transplantation. *Ebiomedicine.* 51:102611. doi: 10.1016/j.ebiom.2019.102611

Satsangi, J., Silverberg, M. S., Vermeire, S., and Colombel, J. F. (2006). The Montreal classification of inflammatory bowel disease: controversies, consensus, and implications. *Gut* 55, 749–753. doi: 10.1136/gut.2005.082909

Shapiro, J. M., de Zoete, M. R., Palm, N. W., Laenen, Y., Bright, R., Mallette, M., et al. (2021). Immunoglobulin A targets a unique subset of the microbiota in inflammatory bowel disease. *Cell Host Microbe* 29, 83–93.e3. doi: 10.1016/j.chom.2020.12.003

Sokol, H., and Seksik, P. (2010). The intestinal microbiota in inflammatory bowel diseases: time to connect with the host. *Curr. Opin. Gastroenterol.* 26, 327–331. doi: 10.1097/MOG.0b013e328339536b

Sokol, H., Pigneur, B., Watterlot, L., Lakhdari, O., Bermudez-Humaran, L. G., Gratadoux, J. J., et al. (2008). Faecalibacterium prausnitzii is an anti-inflammatory commensal bacterium identified by gut microbiota analysis of Crohn disease patients. *Proc. Natl. Acad. Sci. U. S. A.* 105, 16731–16736. doi: 10.1073/pnas.0804812105

Sood, A., Mahajan, R., Singh, A., Midha, V., Mehta, V., Narang, V., et al. (2019a). Role of Faecal Microbiota Transplantation for Maintenance of Remission in Patients With Ulcerative Colitis: a Pilot Study. *J. Crohns Colitis.* 13, 1311–1317. doi: 10.1093/ecco-jcc/jjz060

Sood, A., Singh, A., Mahajan, R., Midha, V., Mehta, V., Gupta, Y. K., et al. (2019b). Acceptability, tolerability, and safety of fecal microbiota transplantation in patients with active ulcerative colitis (AT&S Study). *J. Gastroenterol Hepatol.* 35, 418–424. doi: 10.1111/jgh.14829

Steube, A., Vital, M., Grunert, P., Pieper, D. H., and Stallmach, A. (2019). Long-term Multidonor Faecal Microbiota Transfer by Oral Capsules for Active Ulcerative Colitis. *J. Crohns Colitis.* 13, 1480–1481. doi: 10.1093/ecco-jcc/jjz073

Vermeire, S., Joossens, M., Verbeke, K., Wang, J., Machiels, K., Sabino, J., et al. (2016). Donor species richness determines faecal microbiota transplantation success in inflammatory bowel disease. J. Crohns Colitis 10, 387–394. doi: 10.1093/ecco-jcc/jjv203

Xi, W., Li, Z., Ren, R., Sai, X. Y., Peng, L., and Yang, Y. (2021). Effect of antibiotic therapy in patients with ulcerative colitis: a meta-analysis of randomized controlled trials. *Scand. J. Gastroenterol.* 56, 162–170. doi: 10.1080/00365521.2020.1858958

Zakrzewski, M., Proietti, C., Ellis, J. J., Hasan, S., Brion, M. J., Berger, B., et al. (2017). Calypso: a user-friendly web-server for mining and visualizing microbiome-environment interactions. *Bioinformatics* 33, 782–783. doi: 10.1093/bioinformatics/btw725

Zamani, S., Hesam Shariati, S., Zali, M. R., Asadzadeh Aghdaei, H., Sarabi Asiabar, A., Bokaie, S., et al. (2017). Detection of enterotoxigenic *Bacteroides* fragilis in patients with ulcerative colitis. *Gut Pathog.* 9:53. doi: 10.1186/s13099-017-0202-0

Conflict of Interest: The authors declare that the research was conducted in the absence of any commercial or financial relationships that could be construed as a potential conflict of interest.

Publisher's Note: All claims expressed in this article are solely those of the authors and do not necessarily represent those of their affiliated organizations, or those of the publisher, the editors and the reviewers. Any product that may be evaluated in this article, or claim that may be made by its manufacturer, is not guaranteed or endorsed by the publisher.

Copyright © 2021 Ren, Gao, Shi, Li, Peng, Sun, Wang, Yan, Zhi and Yang. This is an open-access article distributed under the terms of the Creative Commons Attribution License (CC BY). The use, distribution or reproduction in other forums is permitted, provided the original author(s) and the copyright owner(s) are credited and that the original publication in this journal is cited, in accordance with accepted academic practice. No use, distribution or reproduction is permitted which does not comply with these terms.

frontiers in Immunology

ORIGINAL RESEARCH
published: 29 November 2021
doi: 10.3389/fimmu.2021.774233

The Role of Flagellin B in *Vibrio anguillarum*-Induced Intestinal Immunity and Functional Domain Identification

Quanxin Gao[2†], Shaokui Yi[2†], Yang Li[2†], Jinping Luo[2], Qianqian Xing[2], Xia Yang[2], Ming Zhao[1], Minghua Min[1], Qian Wang[1], Yabing Wang[1], Lingbo Ma[1] and Shiming Peng[1]*

[1] Key Laboratory of Marine and Estuarine Fisheries, Ministry of Agriculture, East China Sea Fisheries Research Institute, Chinese Academy of Fishery Sciences, Shanghai, China, [2] Zhejiang Provincial Key Laboratory of Aquatic Resources, Conservation and Development, Key Laboratory of Aquatic Animal Genetic Breeding and Nutrition, Chinese Academy of Fishery Sciences, College of Life Science, Huzhou University, Huzhou, China

OPEN ACCESS

Edited by:
Alina Maria Holban, University of Bucharest, Romania

Reviewed by:
Lihua Song, Beijing University of Chemical Technology, China
C Gopi Mohan, Amrita Vishwa Vidyapeetham University, India

***Correspondence:**
Shiming Peng
pengsm2008@163.com

[†]These authors have contributed equally to this work

Specialty section:
This article was submitted to Microbial Immunology, a section of the journal Frontiers in Immunology

Received: *11 September 2021*
Accepted: *11 November 2021*
Published: *29 November 2021*

Citation:
Gao Q, Yi S, Li Y, Luo J, Xing Q, Yang X, Zhao M, Min M, Wang Q, Wang Y, Ma L and Peng S (2021) The Role of Flagellin B in Vibrio anguillarum-Induced Intestinal Immunity and Functional Domain Identification. Front. Immunol. 12:774233. doi: 10.3389/fimmu.2021.774233

Vibrio anguillarum, an opportunistic pathogen of aquatic animals, moves using a filament comprised of polymerised flagellin proteins. Flagellins are essential virulence factors for *V. anguillarum* infection. Herein, we investigated the effects of flagellins (*flaA*, *flaB*, *flaC*, *flaD* and *flaE*) on cell apoptosis, TLR5 expression, and production of IL-8 and TNF-α. *FlaB* exhibited the strongest immunostimulation effects. To explore the functions of *flaB* in infection, we constructed a *flaB* deletion mutant using a two-step recombination method, and *in vitro* experiments showed a significant decrease in the expression of TLR5 and inflammatory cytokines compared with wild-type cells. However in the *in vivo* study, expression of inflammatory cytokines and intestinal mucosal structure showed no significant differences between groups. Additionally, *flaB* induced a significant increase in TLR5 expression based on microscopy analysis of fluorescently labelled TLR5, indicating interactions between the two proteins, which was confirmed by native PAGE and yeast two-hybrid assay. Molecular simulation of interactions between *flaB* and TLR5 was performed to identify the residues involved in binding, revealing two binding sites. Then, based on molecular dynamics simulations, we carried out thirteen site-directed mutations occurring at the amino acid sites of Q57, N83, N87, R91, D94, E122, D152, N312, R313, N320, L97, H316, I324 in binding regions of *flaB* protein by TLR5, respectively. Surface plasmon resonance (SPR) was employed to compare the affinities of *flaB* mutants for TLR5, and D152, D94, I324, N87, R313, N320 and H316 were found to mediate interactions between *flaB* and TLR5. Our comprehensive and systematic analysis of *V. anguillarum* flagellins establishes the groundwork for future design of flagellin-based vaccines.

Keywords: *Vibrio anguillarum*, flagellin, *flaB*, TLR5, structure-activity relationship, protein-protein interaction

INTRODUCTION

Vibrio anguillarum, one of the most common bacteria in the marine environment, is widely distributed in coastal and estuarine seawater (1). *V. anguillarum* is a representative opportunistic bacterial pathogen that causes disease in marine fish. It causes vibriosis in both wild and farmed fish and other aquatic animals, resulting in huge losses to aquaculture (2). Therefore, *V. anguillarum* is considered a significant threat to commercial production in marine aquaculture. At least 50 species of fish can be infected with *V. anguillarum*, including pacific salmon, Atlantic salmon, rainbow trout, turbot, perch, sea carp, striped bass, codfish and Japanese flounder (3, 4). In view of the wide host range and economic losses caused by this devastating pathogen, elucidating its infection mechanism is vital for the development of control methods.

During the initial stages of pathogenesis, *V. anguillarum* uses flagellum-mediated motility to infect and colonise the surface and gut of fish hosts. Flagella are involved in both motility and virulence (5). Flagellin, the main protein of bacterial flagella, is the only known agonist of toll-like receptor 5 (TLR5), and it stimulates intestinal inflammation by activating the TLR5 signalling pathway (6, 7). Normally, this activation triggers an immunological cascade that stimulates both innate and adaptive immune responses, contributing to a reduction in bacterial multiplication in the gut. Therefore, flagellin-TLR5 interaction plays an important role in infection of pathogenic bacteria (8). However, interactions between flagellin and TLR5 in different bacteria and hosts are complex and can differ significantly, making it challenging to assess their relative contributions to pathology. Surprisingly, flagellin from a minority of bacteria cannot induce the activation of TLR5, which is critical for the survival of these bacteria at mucosal sites in hosts, and raises the intriguing possibility that flagellin receptors provided the selective force to drive the evolution of these unique subclasses of bacterial flagellins (9, 10).

To better understand bacterial flagellins, their domains, which are critical for immune activation, have been intensively investigated. Flagellin proteins contain four structural domains, D0, D1, D2 and D3, arranged in a boomerang-like structure (11). The N- and C-terminal regions that form the D0-D1 domains are highly conserved among flagellins of different bacterial species, whereas amino acid sequences of D2 and D3 show greater variability in sequence and structure (12). The D0 and D1 domains form the inner core of the filament, while the variable D2 and D3 domains form the surface. The conserved D1 domain necessary for filament assembly can be recognised by TLR5 and induces the production and release of pro- and anti-inflammatory cytokines (13). Structural and functional studies have identified many residues in the D1 domain as the interaction site with TLR5 (14), and the D0 domain also contributes to TRL5 activation (15).

Several studies have shown that *V. anguillarum flaB* and its D1 domain can activate TLR receptor pathways, and significantly upregulate tumour necrosis factor α (TNF-α) and proinflammatory cytokines (16–18). Despite increased knowledge of the structural and functional roles of flagellins in *V. anguillarum*, the molecular interactions between TLR5 and flagellins remain unclear. In this study, we examined the interaction characteristics between flagellins from *V. anguillarum* and TLR5 from silvery pomfret (*Pampus argenteus*), an economically important fish in China that is regarded a delicacy by Chinese consumers due to its favourable meat properties. Unfortunately, infectious diseases occur frequently when rearing silvery pomfret, and *V. anguillarum* is one of the main pathogens, causing huge economic losses. We speculate that flagellin-induced TLR5 activation plays an important role in the host response to infection with *V. anguillarum*. Thus, we constructed a *flaB* deletion strain and investigated the virulence of the δ*flaB* mutant *via in vivo* and *in vitro* assays. The mechanism of interaction between TLR5 and *flaB* through were also investigated, and molecular dynamics simulation and surface plasmon resonance (SPR) experiments were carried to identify the functional domains of *flaB* at the amino acid sequence level.

MATERIALS AND METHODS

Bacterial Strains and Growth Conditions

V. anguillarum cells were isolated from diseased farmed fish, cultured in LB broth at 28°C, and stored in 30% glycerol at -80°C.

Expression and Purification of Flagellins

Full-length flagellin A–E genes from *V. anguillarum* (*flaA–E*) were obtained by PCR using primers listed in **Table 1**. PCR products were purified from a 1.5% agarose gels and cloned into the pET28 expression vector using GeneArt Seamless Cloning and Assembly Enzyme Mix (Invitrogen). Competent *E. coli* (DE3) cells were separately transformed with pET28-*flaA–E* constructs, and transformants were cultured in LB medium (50 μg/mL kanamycin) at 37°C, then in SOC medium (50 μg/mL kanamycin) at 37°C for another 2–3 h to OD_{600} 0.5–0.6. IPTG was added to a final concentration of 0.5 mM to induce expression of flagellins, and bacteria were collected and resuspended in phosphate-buffered saline (PBS) with 1% Triton X-100.

Bacteria were lysed by sonication (200–300 W) and bacterial lysates were centrifuged at 12,000 rpm for 10 min at 4°C Supernatants and precipitates were separated and analysed by sodium dodecyl sulphate-polyacrylamide gel electrophoresis (SDS-PAGE). Recombinant proteins in soluble supernatants were purified from inclusion bodies under denaturing conditions using Ni-NTA Agarose (Qiagen). Protein concentration was determined using a BCA protein assay kit according to the manufacturer's instructions (Beyotime).

Isolation, Culture and Stimulation of Primary Fish Intestinal Epithelial Cells (FIECs)

Fish intestinal epithelial cells (FIECs) were isolated from silvery pomfret as an *in vitro* model, and prepared and cultured according to our previous studies (19). FIECs were allowed to attach to and grow in 24-well tissue culture plates (Costar) for 48 h. Before stimulation assays, all flagellins were resuspended in

TABLE 1 | Sequences of primers used for cloning and expression of flagellins and TLR5.

Primer name		Sequence (5'–3')
FlaA	*FlaA*-F	ACAGCAAATGGGTCGCGGATCCACCATTACAGTAAATACTAACGTC (BamHI)
	FlaA-R	GCAAGCTTGTCGACGGAGCTCTTACTGCAATAGTGACATTGCAG (SacI)
FlaB	*FlaB*-F	ACAGCAAATGGGTCGCGGATCCGCAATTAATGTAAGCACTAACGTG (BamHI)
	FlaB-R	GCAAGCTTGTCGACGGAGCTCTTAACCCAATAGACTAAGAGCTG (SacI)
FlaC	*FlaC*-F	ACAGCAAATGGGTCGCGGATCCGCGGTTAATGTAAACACTAACGTT (BamHI)
	FlaC-R	GCAAGCTTGTCGACGGAGCTCTTAACCAAGCAAACCAAGAGCAG (SacI)
FlaD	*FlaC*-F	ACAGCAAATGGGTCGCGGATCCGCAGTTAATGTAAATACCAACGTA (BamHI)
	FlaC-R	GCAAGCTTGTCGACGGAGCTCTTAGCCAAGTAAGCTAAGTGCCG (SacI)
FlaE	*FlaC*-F	ACAGCAAATGGGTCGCGGATCCGCAATTACCGTTAATACCAATGTT (BamHI)
	FlaC-R	GCAAGCTTGTCGACGGAGCTCCTAGCGAAGTAAGGCCAATGCTA (SacI)
TLR5	TLR5-F	ACAGCAAATGGGTCGCGGATCCACGTCGCTGGTTCTTCACTTG (BamHI)
	TLR5-R	GCAAGCTTGTCGACGGAGCTCTTAGTTTTCTTCAAGTTTGAGAAAGTG (SacI)

The meaning of the gray shadings is the restriction sites, and the restriction sites are in the brackets.

DMEM medium at a concentration of 1 μg/mL. FIECs were incubated with *flaA*–*flaE* in 5% CO_2 at 28°C After incubation for 30, 60, 120 and 150 min, the culture medium and cells were collected for ELISA, real-time PCR analysis, and assessment of apoptotic and necrotic cells (20).

Assessment of Apoptotic and Necrotic Cells

Apoptosis and necrosis of FIECs were assessed using an Annexin V-FITC apoptosis detection kit (BD, USA). After stimulation with flagellins, cells were stained with Anexin V-fluorescein isothiocyanate (Annexin V-FITC) and propidium iodide (PI) for analysis by flow cytometry (FCM). Annexin V-FITC and PI fluorescence levels were measured at 530 nm and 585 nm emission wavelengths, respectively. The positioning of quadrants on Annexin V/PI dot plots was used to distinguish between living cells (Annexin V^-/PI^-), early apoptotic cells (Annexin V^+/PI^-), late apoptotic cells (Annexin V^+/PI^+) and necrotic cells (Annexin V^-/PI^+). Therefore, the total apoptotic proportions among cells with fluorescent Annexin were V^+/PI^- and V^+/PI^+.

ELISA

Protein concentration was assayed by ELISA using a Protein Assay kit (Nanjing Jiancheng Bioengineering Institute, Nanjing, China). ELISA results were quantified using an iMark Microplate Reader (Bio-Rad) at 450 nm. Absorbance was measured and protein concentration was calculated according to the relevant standard curve constructed from proteins in ELISA kits (20).

Construction of the *flaB* Deletion Mutant Strain

Construction of the *flaB* deletion mutant strain was performed as described in our previous study (21). Briefly, the upstream homologous arm fragment (593 bp) and the downstream homologous arm fragment (545 bp) of *flaB* were amplified, and the fusion fragment (1138 bp) was obtained by overlapping PCR using the two fragments as templates. The purified PCR product was cloned into the suicide vector Plp12 and transformed into *E. coli* DH5α, yielding a positive clone of 1388 bp, which was verified by PCR and DNA sequencing. The recombinant Plp12-*flaB* plasmid was extracted and transformed into wild-type *V. anguillarum* by electro transformation. After two cycles of homologous recombination, the *flaB* deletion mutant strain was constructed and verified by PCR and DNA sequencing (1413 bp).

Bacterial Infection

In vivo and *in vitro* experiments were conducted to study infection by the *δflaB* mutant. In the *in vitro* experiment, FIECs were isolated and cultured. Before stimulation of bacteria, *δflaB* mutant and wild-type strains were collected and resuspended in antibiotic-free DMEM medium at a density of 1×10^8 CFU/mL. FIECs were coincubated with DMEM medium, *δflaB* mutant, and wild-type strains in 5% CO_2 at 28°C for 2 h, respectively. After incubation, the culture medium and cells were collected for ELISA and real-time PCR analysis.

In the *in vivo* experiment, 450 silver pomfret juveniles (body weight 12–16 g) bred by artificial fertilisation were assessed. The *δflaB* mutant and wild-type strains were first cultured in LB medium for ~24 h at 28°C, centrifuged at 8000×g for 10 min, and resuspended at 1×10^{10} CFU/mL in sterile saline. Bacterial diets were prepared by gently spraying the bacterial suspension on the basal diet followed by mixing thoroughly to obtain a final cell density of 1×10^8 CFU/mL. The bacterial feeding experiment was carried out in nine cement pools (length 6 m, width 4 m, height 1.5 m). Each pool was randomly stocked with 50 fish, and three tanks of fish were assigned to each treatment (**Figure 1**). Three fishes were sampled at 0, 12, 24 and 48 h after bacterial feeding. All fish were anaesthetised, and intestinal samples were collected for ELISA and real-time PCR analysis. At the end of the experiment, the same part of midgut of each animal was fixed in 2.5% glutaraldehyde solution (4°C) for transmission electron microscopy (TEM) analysis.

Real-Time PCR Analysis

The methods for RNA extraction, cDNA synthesis and real-time PCR were performed according to our previous study (22).

TEM Analysis

The method used for TEM examination was described in a previous study (23). Briefly, samples were fixed in 2.5% glutaraldehyde solution, then in 1% osmium tetroxide (O_sO_4)

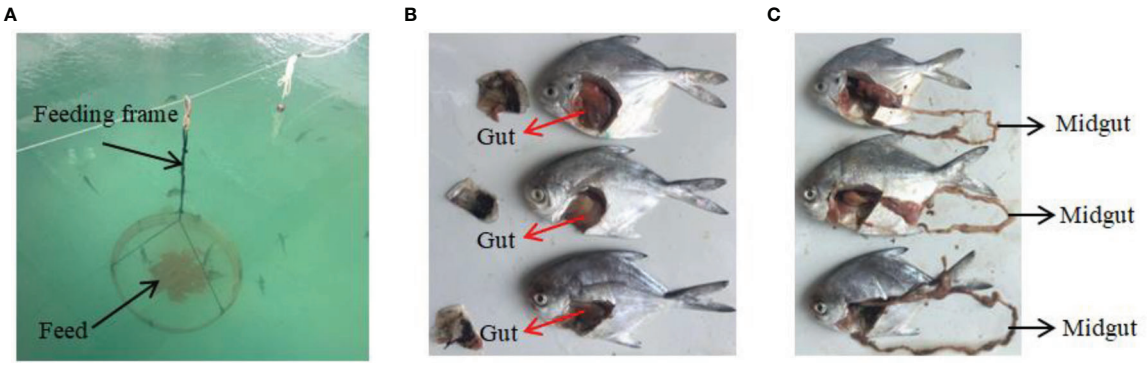


FIGURE 1 | *In vivo* experiments and sampling. **(A)** Feeding device for silvery pomfret. **(B, C)** Experimental fish and sampling of intestine.

for 1 h, dehydrated in a graded series of ethyl alcohol, and embedded in resin. Ultrathin sections were placed on copper grids, stained with uranyl acetate, and observed under a TECNAI 10 TEM instrument (Philips).

Native PAGE Analysis

The method used to obtain the extracellular region of the TLR5 protein (erTLR5) was the same as that used for expression and purification of flagellins, and primers are listed in **Table 1**. Purified *flaB* and erTLR5 proteins were incubated at 18°C for 30 min and complex formation was analysed. Native PAGE was performed using polyacrylamide gels separated at room temperature at a voltage of 200 V. After electrophoresis, gels were stained with Coomassie Brilliant Blue.

Fluorescence Observation

Green fluorescent protein (GFP)-tagged TLR5 was used to assess the effect of *flaB* on expression of TLR5. TLR5 forward primer TCTCGAGCTCAAGCTTCGAATTCGCCACCATGACG TCGCTGGTTCTTCACTT (*Eco*RI) and reverse primer GGTACCGTCGACTGCAGAATTCGTTTTCTTCAAG TTTGAGAAAGTG (*Eco*RI) were employed for construction of erTLR5-PEGFP-N2 using GeneArt Seamless Cloning and Assembly Enzyme Mix (Invitrogen). Zebrafish embryo fibroblast cells (ZF4) were grown in DMED supplemented with 10% foetal bovine serum (FBS) and cultured in 6-well tissue culture plates (Costar) for about 24–48 h. The cell density reached 60–80% confluency prior to transfection. The erTLR5-pEGFP-N2 plasmid encoding GFP-erTLR5 was transfected into ZF4 cells using Lipo2000 (Thermo Fisher) according to the manufacturer's instructions. The *flaB* protein was then added to 6-well plates and incubated at 28°C for 2 h. After incubation, laser scanning confocal microscopy (LSCM) was employed to observe the location and immunofluorescence expression of GFP-erTLR5.

Yeast Two-Hybrid Analysis

The primers listed in **Table 2** were used to amplify the sequences of *flaB* (1128 bp) and *TLR5* (1770 bp). The purified *flaB* and *TLR5* sequences were ligated into pGADT7 and pGBKT7 vectors, respectively, and recombinant pGADT7-*flaB* and pGBKT7-erTLR5 vectors were simultaneously transformed into yeast strain AH109. Transformants were grown on synthetic dropout medium lacking amino acids leucine and tryptophan (SD/–Leu/–Trp), synthetic dropout medium lacking adenine and amino acids histidine, leucine and tryptophan (SD/–Ade/–His/–Leu/–Trp) and SD/–Ade/–His/–Leu/–Trp/X-α-Gal (40 μg/mL X-α-Gal) on agar plates at 30°C for 3–5 days to assess growth.

Modelling of *flaB* Interaction With TLR5 Using PROCHECK and Rosetta

The 3J0A and 3K8W proteins served as templates for homology modelling of TLR5 and *flaB* proteins, respectively, using Modeller v9.19. The two models were then subjected to molecular mechanics optimisation, and PROCHECK was used to evaluate the optimised protein models. Analysis of the Ramachandran plot showed that 99.1% and 99.3% of non-glycine residues of TLR5 and *flaB* were in the 'most favoured or allowed' regions. Finally, we used Rosetta to carry out *flaB*-TLR5 docking.

In Vitro Mutagenesis

The amino acid sites selected for mutation are shown in **Table 3**. KOD FX DNA polymerase (Toyobo) was applied to construct the mutated genes from the wild-type pET28-*flaB* template *via* thermal cycling at 95°C for 3 min followed by 25 cycles at 95°C for 15 s, 62°C for 15 s, 68°C for 1 min, and a final extension at 72°C for 5 min. FastDigest *Dpn*I (Thermo Fisher) was added to the PCR product and incubated in a 37°C water bath for 2 h. The mixture was purified using a PCR Clean-Up Kit and transformed into DMT competent cells. Transformants were selected for sequencing using T7 promoter and T7 terminator primers.

Surface Plasmon Resonance (SPR) Analysis

Prokaryotic expression and purification of mutant *flaB* was performed as described above. The TLR5 gene was inserted into the pGEX-6p-1 vector, and after its transformation into BL21(DE3) strain and induction by IPTG, recombinant protein

was expressed in BL21 cells and purified using glutathione S-transferase (GST) affinity chromatography. The GST-His*10-TEV-TLR5 fusion protein was digested by tobacco etch virus (TEV) protease to remove the GST tag, and purified TLR5 protein was obtained.

Analysis of ligand binding kinetics was performed on a BIAcore S200 SPR instrument (GE Healthcare, USA) according to methods reported previously (24). In brief, TLR5 protein was immobilised onto the SA sensor chip surface. *FlaB* mutant proteins were injected into wells at a flow rate of 30 μL/min in PBS-P running buffer. After 5 min of dissociation, TLR5 and bound analytes were removed by a 60 s wash with 10 mmol/mL glycine-HCl at a flow rate of 30 mL/min. After subtraction of appropriate controls, data were analysed by fitting to a 1:1 Langmuir binding model using the BIAcore S200 evaluation software.

RESULTS

In Vitro Analysis of Flagellins in Infection

To gain insight into the functions of flagellins, we expressed and purified the *flaA–E* and investigated their effects on cell apoptosis and necrosis. All five flagellins were shown to be capable of inducing apoptosis and necrosis in FICEs in a time-dependent manner through the observation of cells at 0, 30, 60, 120 and 150 min (**Figure 2**). After the final incubation at 28°C for 150 min, the *flaB* markedly increased early (Annexin V+/P-) and late (Annexin V+/PI+) apoptosis rates to 10.3 and 81.8, respectively. Among the flagellins, *flaB* was ranked most effective at inducing cell apoptosis (92.1%), followed by *flaA* and *flaE* (59.2% and 45.1%, respectively). Cell apoptosis induced by *flaC* and *flaD* showed the same trend, albeit with lower rates of 29.7% and 27.7%, respectively. Overall, here was a notable difference in the sensitivity of FICEs to different flagellins, and *flaB* was the most capable of inducing apoptosis.

Following cell apoptosis analysis, expression of TLR5, IL-8 and TNF-α was measured. As shown in **Figure 3**, all five flagellins increased the expression of TLR5 significantly and in a time-dependent manner. After incubation for 120 min, *flaB* -induced TLR5 expression was more significant than that of other flagellins (p <0.05). Similar to TLR5 gene expression, secretion levels of IL-8 and TNF-α proteins from FICEs were increased significantly after infection with flagellins (p <0.05). Significantly higher production of IL-8 was observed in the *flaB* treatment group than the other flagellin groups. Unlike other groups, IL-8 expression in the *flaE* treatment group increased significantly at 30 min, peaked at 60 min, and decreased significantly at 120 min (p <0.05). Except for *flaD*, TNF-α expression varied in a time-dependent manner after treatment with flagellins; *flaB* and *flaE* had the strongest stimulatory effects on the expression of TNF-α (p <0.05), and there was no significant difference between these two groups.

In Vivo Analysis of Infection

Among the five flagellins, *flaB* was the most capable of inducing TLR5-meditated inflammatory responses, hence we knocked out the *flaB* gene in *V. anguillarum* and tested the infection ability of the mutant to explore the function and mechanism of *flaB*. A time course of TLR5 expression was performed by real-time PCR in FICEs after treatment with the *flaB* mutant. As shown in **Figure 4**, significantly lower expression of TLR5 was observed in the mutant group in comparison with the wild-type group at all time points. However, in the *in vivo* experiment, only at 48 h of exposure to bacteria were TLR5 mRNA expression levels in the mutant group lower than in the wild-type group; at other time points levels were comparable in the two groups.

Following analysis of TLR5 expression, production of IL-8 and TNF-α was evaluated (**Figure 4**). The results showed that expression of IL-8 at 60 min and TNF-α at 30 min was significantly lower in the mutant group than in the wild-type group in *in vitro* experiments. However, in *in vivo* experiments there was no significant difference in IL-8 and TNF-α protein abundance between the two groups. The reason for the inconsistent *in vivo* and *in vitro* results might be because the fish gut microbiome is a complex ecosystem that can mediate interaction of the fish host with *V. anguillarum*. Therefore, we conducted TEM examination of intestinal mucosal samples. As shown in **Figure 5**, the intestinal mucosa in the control group remained intact, the epithelium was normal, and the columnar epithelium in the mucosa had an ordered arrangement. However, in wild-type and mutant *V. anguillarum* treatment groups, microvilli on the surface of epithelial cells of the intestine were sparse or distributed irregularly, the mucosal folds were flattened, and the mucosa layer was thin. Overall, there was little difference between the two treatment groups in terms of changes in the intestinal mucosal structure.

Native PAGE and Size Exclusion Chromatography Analyses

To confirm that *flaB* -mediated TLR5 activation occurs through direct interaction between *flaB* and erTLR5, the formation of the *flaB* -erTLR5 complex was monitored by native PAGE. As shown in **Figures 6A, B**, *flaB* and erTLR5 proteins were expressed and purified, and further validated by western blotting (**Figures 6C, D**).

TABLE 2 | Sequences of primers used for yeast two-hybrid analysis.

Primer name		Sequence (5'–3')
FlaB	*FlaB*-F	GCCATGGAGGCCAGTGAATTCATGGCCATTAACGTTT (EcoRI)
	FlaB-R	TGCAGCTCGAGCTCGATGGATCCACCCAACAAAGACAAA (BamHI)
erTLR5	erTLR5-F	GCATATGGCCATGGAGGCCGAATTCATGACGTCGCTGGTTCTTCACTTG (EcoRI)
	erTLR5-R	GCGGCCGCTGCAGGTCGACGGATCCTCAGTTTTCTTCAAGTTTGAGAAAGTG (BamHI)

The meaning of the gray shadings is the restriction sites, and the restriction sites are in the brackets.

TABLE 3 | Sequences of primers used for site-directed mutagenesis of *flaB*.

FlaB	Abbreviation	Amino acid mutation	Sequence (mutation sites are shaded grey)
Q57	F1	Gln—Ala	F: 5' CGTCAGCAAGCCGTGGCTTAG 3' R: 5' GCCACGGCTTGCTGACGTTAAAC 3'
N83	F2	Asn—Ala	F: 5' GGTGCAATGGCTGAAACCACCAA 3' R: 5' GATATTGGTGGTTTCAGCCATTG 3'
N87	F3	Asn—Ala	F: 5' CCACCGCTATCTTGCAACGTATG 3' R: 5' CGTTGCAAGATAGCGGTGGTTTC 3'
R91	F4	Arg—Ala	F: 5' CTTGCAAGCTATGCGAGATCTTTC 3' R: 5' GATCTCGCATAGCTTGCAAGATA 3'
D94	F5	Asp—Ala	F: 5' CGTATGCGAGCTCTTTCTTTG 3' R: 5' GCAAAGAAAGAGCTCGCATA 3'
E122	F6	Glu—Ala	F: 5' GATGCATTAAACCGTATTGCTGAA 3' R: 5' GCAATACGGTTTAATGCATCATTG 3'
D152	F7	Asp—Ala	F: 5' GGTGCCGCCTCTGGTGAA 3' R: 5' CTTCACCAGAGGCGGCACCAAT 3'
N312	F8	Asn—Ala	F: 5' CCAGGCCCGTTTCGGTCATG 3' R: 5' GACCGAAACGGGCCTGGAATG 3'
R313	F9	Arg—Ala	F: 5' CCAGAACGCTTTCGGTCAT 3' R: 5' GACCGAAAGCGTTCTGGAATG 3'
N320	F11	Asn—Ala	F: 5' GCCATCAGTGCCCTTGATAAC 3' R: 5' CAAGGGCACTGATGGCATGA 3'
L97	F12	Leu—Asn	F: 5' GAGATCTTTCTAACCAATCAGCA 3' R: 5' CGTTTGCTGATTGGTTAGAAAG 3'
H316	F13	His—Ala	F: 5' CGTTTCGGTGCTGCCATCAGTA 3' R: 5' GGTTACTGATGGCAGCACCGAAA 3'
I324	F14	Ile—Asn	F: 5' GATAACAACAACGAGAACGTCAA 3' R: 5' CGTTCTCGTTGTTGTTATCAAGGT 3'

In the native PAGE analysis, *flaB* altered erTLR5 mobility, and the mobility shift was complete at a molar ratio of 1:1 (**Figure 6E**). These results imply a relatively strong interaction between *flaB* and erTLR5.

Fluorescence Observations

In order to observe the *flaB* -induced expression of TLR5 protein directly, GFP was used to label erTLR5. As shown in **Figure 7A**, GFP was expressed in the cytoplasm in the empty plasmid transfection group. In the erTLR5-pEGFP-N2 transfection group, GFP fluorescence was observed on the cell surface of ZF4 cells (**Figure 7B**), indicating that TLR5 protein was efficiently transported to the plasma membrane. Because TLR5 is a Type I membrane protein, GFP-erTLR5 proteins can be transported to the cell membrane, consistent with our observations. Furthermore, our results showed that treatment with *flaB* induced the expression of GFP-erTLR5 protein (**Figure 7C**), which further demonstrated an interaction between *flaB* and TLR5.

Yeast Two-Hybrid Analysis

Yeast two-hybrid screening methods are an effective means for the detection of protein-protein interactions. Therefore, yeast two-hybrid analysis was conducted to determine if the TLR5 protein interacts directly with *flaB*. As shown in **Figure 8**, yeast transfected with pGADT7-*flaB* and pGBKT7-erTLR5 vectors could be grown on SD/–Leu/–Trp plates, indicating the successful co-transformation of the AH109 yeast strain. Additionally, growth on SD/–Ade/–His/–Leu/–Trp and SD/–Ade/–His/–Leu/–Trp/X-α-Gal medium plates (blue clones) indicated a direct interaction between *flaB* and erTLR5 (**Figure 8**).

The Binding Interface of the *flaB* -TLR5 Complex

We docked *flaB* and TLR5 proteins, and took the highest I_sc (interface score) as representative of binding between TLR5 and *flaB*. I_sc can be used to describe the strength of the interaction between two proteins, and I_sc generally ranges from -2 to -10. Our results showed that the I_sc of the final docking result was -9.561, which confirmed that the TLR5- *flaB* complex was compatible in terms of shape and energy.

As shown in **Figure 9**, we analysed hydrogen bonds between the binding sites of TLR5 and *flaB*. The binding area includes two main regions (Interface A and Interface B) located in the middle part and N-terminus of the TLR5 protein structure, respectively. The amino acid residues involved in binding between *flaB* and TLR5 are shown in **Table 3**. Most of the amino acids that interact with each other can do so *via* hydrogen bonds, indicating that hydrogen bonds play important roles in TLR5 recognition of *flaB*. In addition, we speculate that hydrophobic amino acids on the interface may further enhance the interactions between *flaB* and TLR5.

In order to better understand the *flaB* -TLR5 interaction, the binding interfaces and interacting amino acids in Interface A and Interface B are shown in **Figure 9**. The amino acids from *flaB* and TLR5 interact *via* numerous hydrogen bonds and hydrophobic interactions (**Figure 9C**), resulting in a strong affinity between the two proteins. According to the results of protein docking, it can be inferred that the mechanism of *flaB* -induced activation of TLR5 may involve *flaB* binding to TLR5, which leads to TLR dimerisation and conformational changes, resulting in signal transduction.

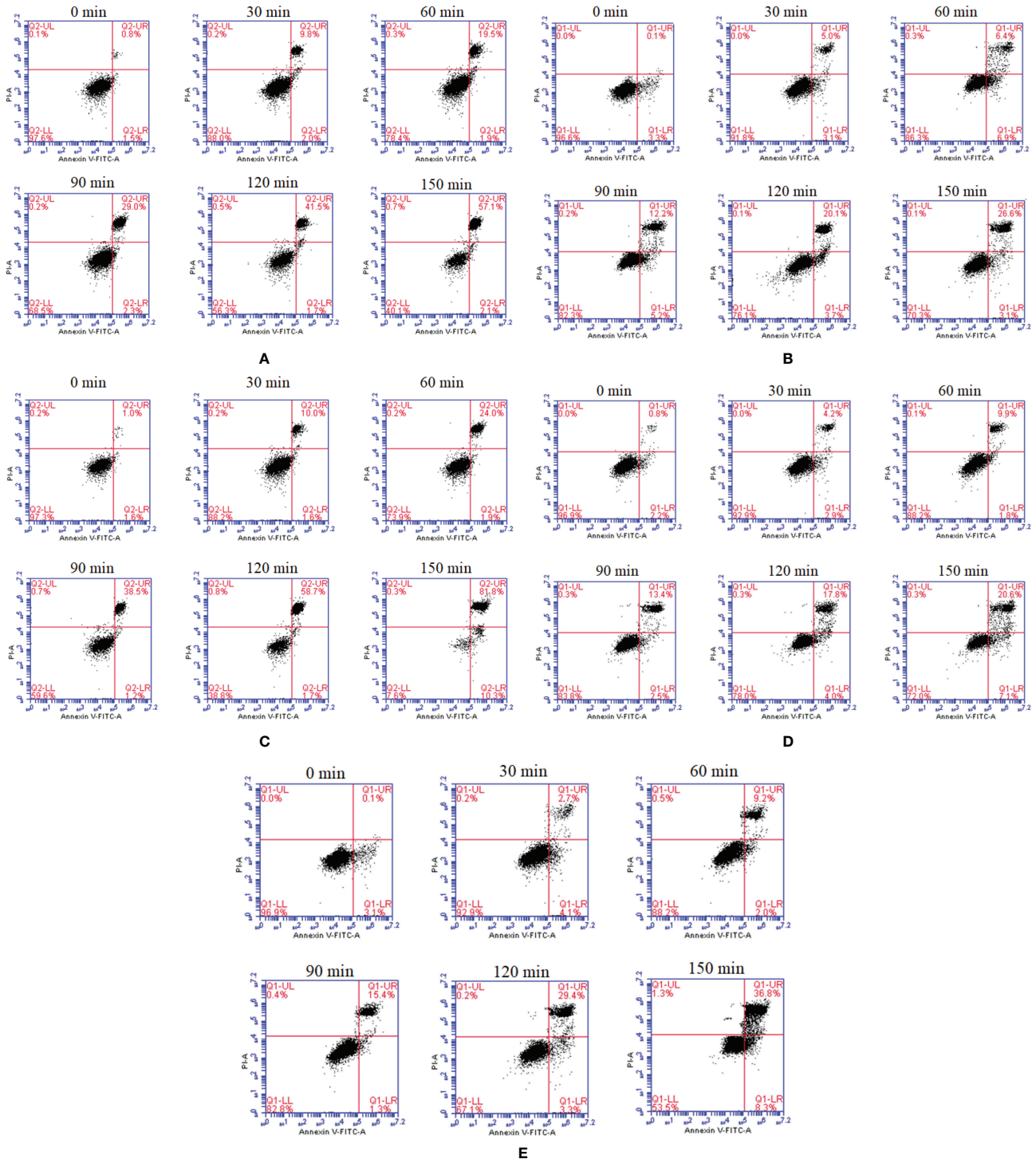


FIGURE 2 | *In vitro* dynamic monitoring of FIECs infected with flagellins by flow cytometry. The *flaA* **(A)**, *flaB* **(B)**, *flaC* **(C)**, *flaD* **(D)** and *flaE* **(E)** genes were separately added into FIECs. At definite time intervals of 30, 60, 120 and 150 min, cells were collected, stained with Annexin V-fluorescein and PI, and analysed by flow cytometry. LL, living cells; LR, early apoptotic cells; UR, late apoptotic cells; UL, necrotic cells.

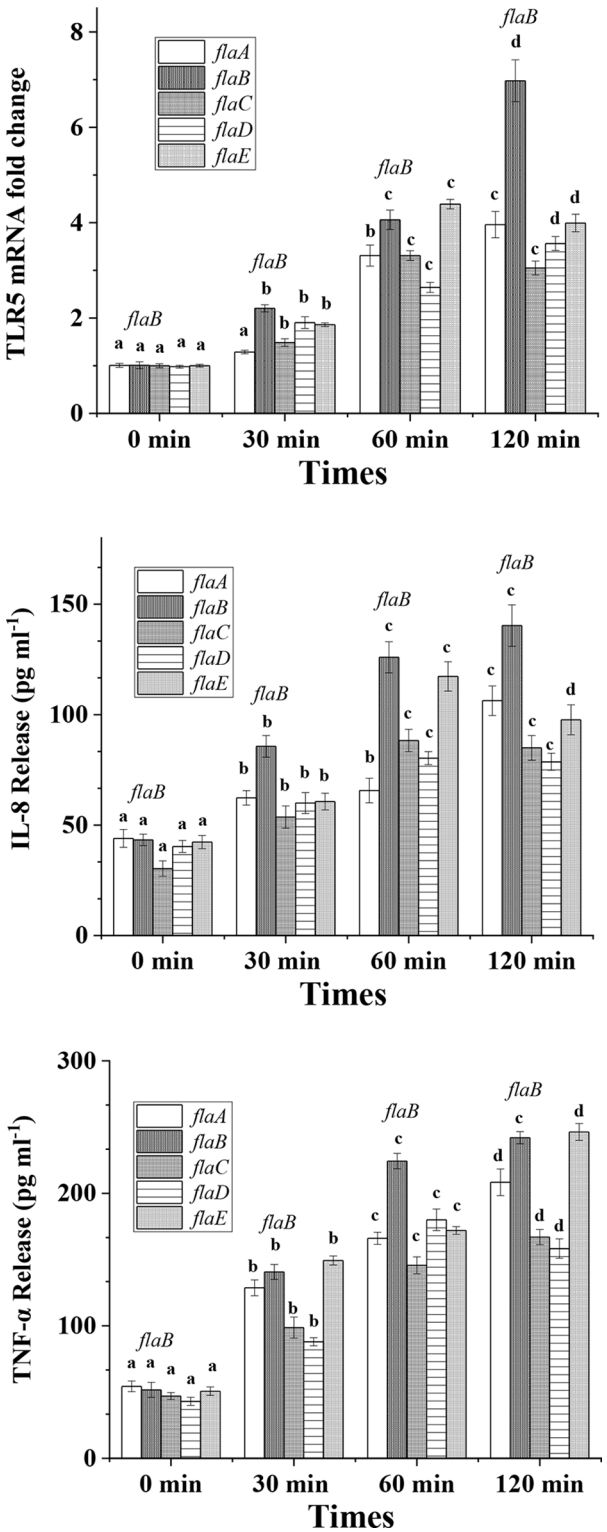


FIGURE 3 | TLR5, IL-8 and TNF-α expression in cultured FIECs after addition of flagellins. Cells were exposed to *flaA*, *flaB*, *flaC*, *flaD* and *flaE* for 30, 60 and 120 min. After incubation, cells were harvested for quantitative real-time PCR to determine TLR5 expression levels. Supernatants were collected and TNF-α and IL-8 concentrations in the supernatant were measured by ELISA. Results are means ± standard errors of the means for three independent experiments. Different lowercase letters indicate significant differences between different time points within the same treatment.

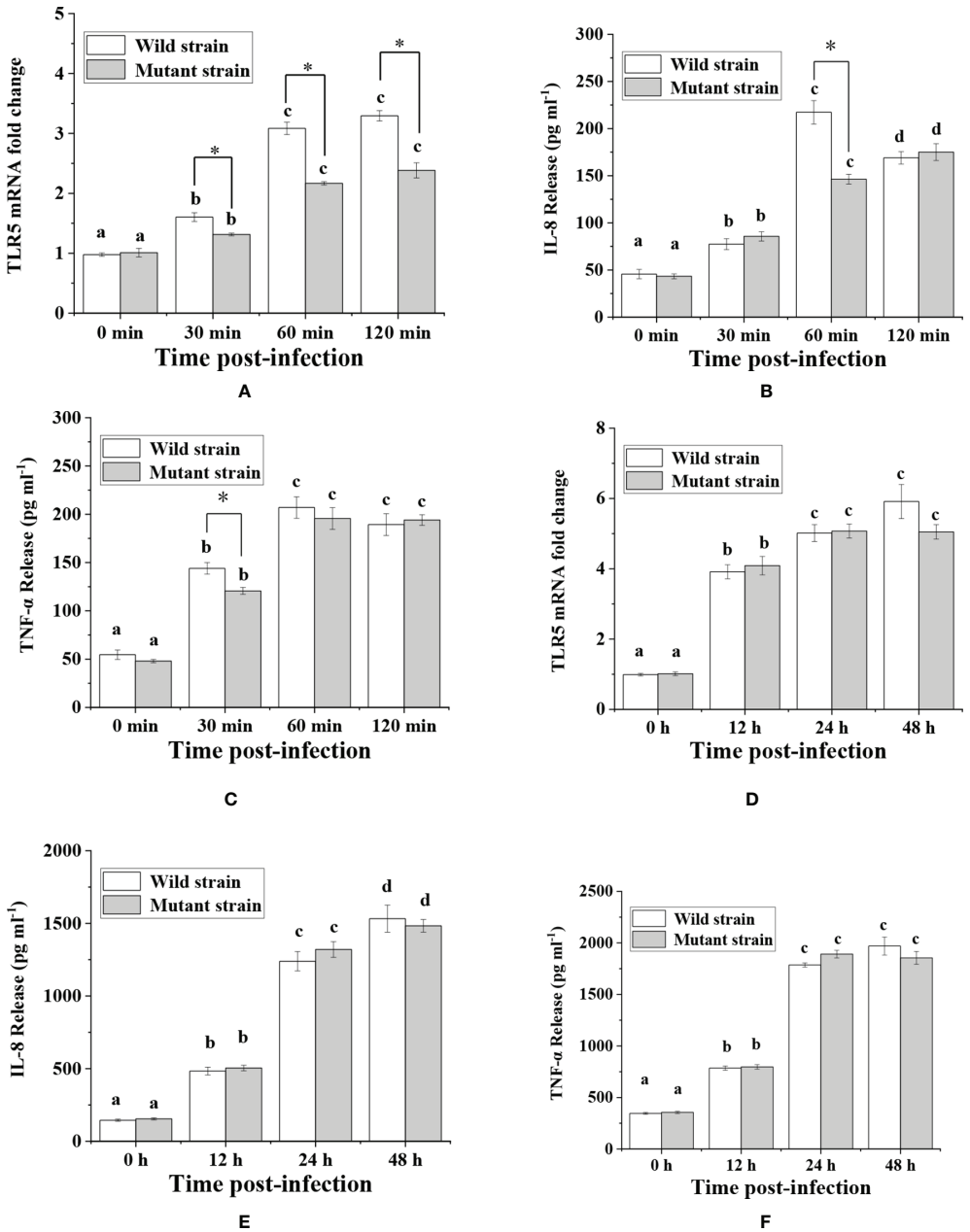


FIGURE 4 | Analysis of TLR5, IL-8 and TNF-α expression in response to V. *anguillarum* and its mutant challenge. Time-lag experiments were performed to explore *in vitro* **(A–C)** and *in vivo* **(D–F)** infection with bacteria. The production of IL-8 and TNF-α proteins was measured by ELISA, and mRNA expression levels of TLR5 were measured by real-time PCR. Different lowercase letters indicate significant differences between different time points within the same treatment. * indicate significant differences between the two groups at the same time point.

Site-Directed Mutagenesis and Expression and Purification of *flaB* Mutant Proteins and TLR5

To identify the predicted functional domains in *flaB*, we performed site-directed mutagenesis and SPR experiments. Firstly, we performed site-directed mutagenesis of amino acids predicted to be involved in TLR5- *flaB* interactions. The TLR5 and *flaB* mutant proteins were successfully expressed and purified using a prokaryotic expression system. Distinct bands with molecular masses of ~39.5 kDa (**Figure 10A**) and ~64.4 kDa (**Figure 10B**) were observed, consistent with the predicted molecular masses of *flaB* and TLR5.

Our enhanced SPR assay was then applied to assess the impact of the various *flaB* profiles (F1–F14 mutants) upon

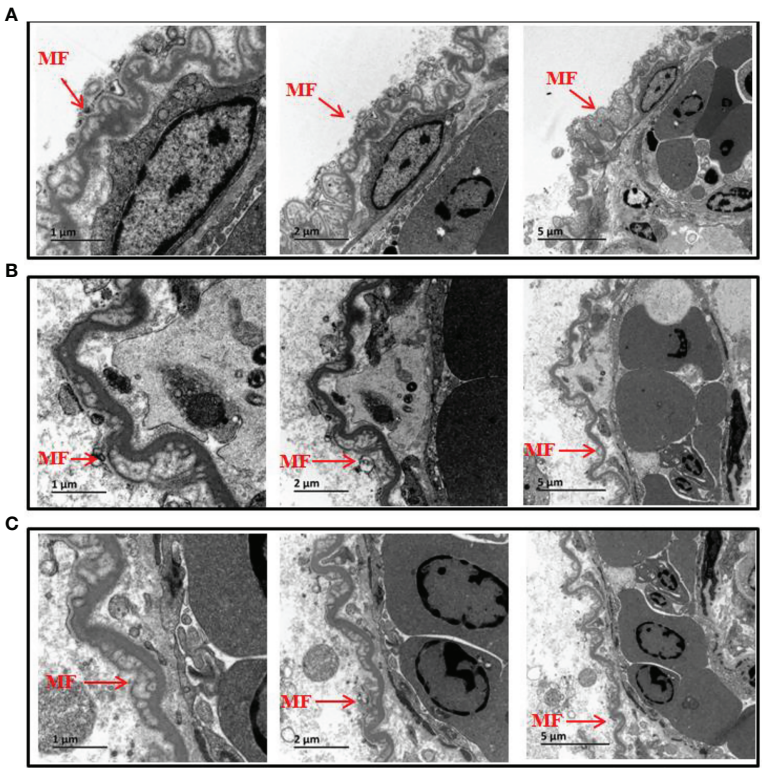


FIGURE 5 | Electron microscopic structure of the intestine epithelium of silver pomfret juveniles fed with *δflaB* mutant and wild-type strains. **(A)** Controls. **(B)** Wild-type treatment. **(C)** *δflaB* mutant treatment. MF, mucosal folds. Arrows indicate the epithelium layer.

binding to TLR5. As shown in **Figure 11** and **Table 4**, Kd values of F1, F2, F4 and F12 decreased, while Kd values of the other *flaB* mutants increased, compared with wild-type controls. Kd values of F7, F5, F14, F3, F9, F11 and F13 increased by 21.8-, 14.1-, 8.3-, 7.9-, 4.4-, 3.9- and 2.2-fold respectively compared with controls, indicating that amino acids D152, D94, I324, N87, R313, N320 and H316 play key roles in the spatial interaction between *flaB* and TLR5.

DISCUSSION

V. anguillarum is one of the most serious pathogenic bacteria affecting global aquaculture of various fish species. Due to its high morbidity and mortality rates, a substantial amount of research has been carried out to elucidate the virulence mechanisms of this pathogen, and to develop rapid detection techniques and effective disease-prevention strategies (25). It is well known that the flagella of pathogens are important for both bacterial motility and virulence. Furthermore, flagella are novel and effective adjuvants for vaccines (12, 26). However, to our knowledge, few studies have focused on the flagella of *V. anguillarum*. In the present study, constructs of flagellin gene deletion mutants revealed the roles of flagellin proteins in *V. anguillarum* infection. Additionally, interactions between flagellin proteins and TLR5 were comprehensively explored at the protein structure level.

Importantly, flagellins are usually species-specific (27), and there are significant differences in the immune properties of flagellins from different bacterial sources (28). Even from the same bacteria, the immunogenicities of different flagellins can differ markedly (29). Flagellins do not contribute equally to the virulence of pathogenic bacteria. Thus, in order to obtain a clearer picture of the roles of flagellins in *V. anguillarum*, their immune characteristics should be thoroughly investigated. In the present study, *in vitro* experiments showed that *flaB* induced the strongest immune response among the flagellins. Studies by Gonzalez-Stegmaier et al. (2019 and 2021) reported similar findings (16, 30). However, these previous studies did not delve further into the immune function mechanisms of *flaB*, hence further research is required to deepen our understanding in this area.

Knocking out flagellin genes can reduce bacterial pathogenicity, but it may also promote infection (31). Although flagellins contribute to intestinal inflammation by activating TLR5, the absence of flagellins in pathogenic bacteria can assist their ability to escape from the animal tract by avoiding triggering the proinflammatory response during invasion, thus favouring the development of systemic infection (32). Our *in vitro* experiments showed that deletion of *flaB* significantly decreased *V. anguillarum*-induced expression of TLR5, IL-8 and TNF-α. It has been reported that mutants of some flagellins have little or no effect, and only by deletion of the most influential components can bacterial infectivity

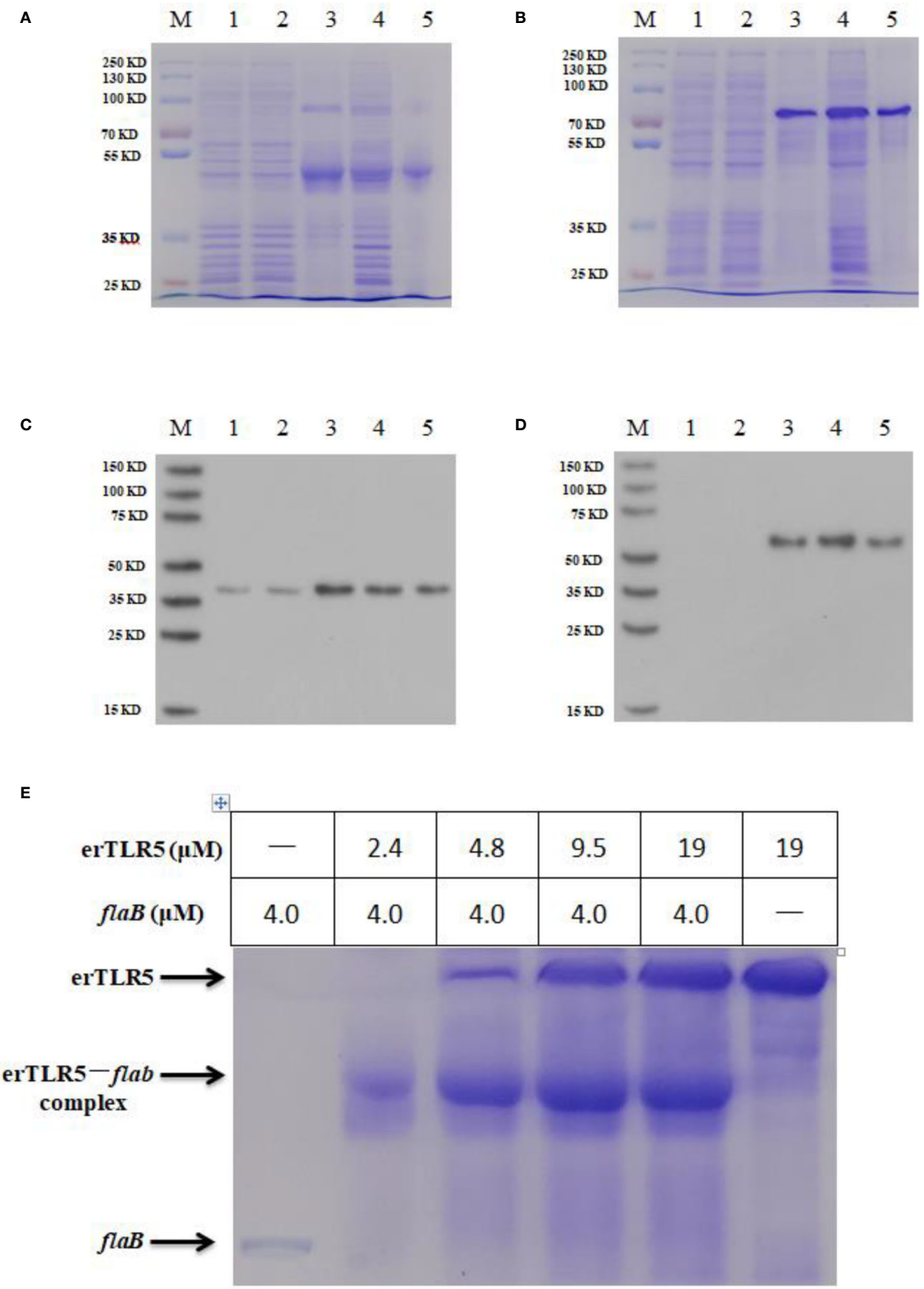


FIGURE 6 | Native PAGE analysis of the direct interaction between *flaB* and erTLR5. *FlaB* **(A)** and erTLR5 **(B)** production was assessed by SDS-PAGE. *FlaB* **(C)** and erTLR5 **(D)** proteins were further validated by western blotting. Lane M, markers; lane 1, empty plasmid control; lane 2, no IPTG control; lane 3, inclusion bodies; lane 4, supernatant; lane 5, purified protein. **(E)** Native PAGE (upper panel) and size exclusion chromatography (lower panel) reveal the formation of a 1:1 erTLR5-*flaB* heterodimer.

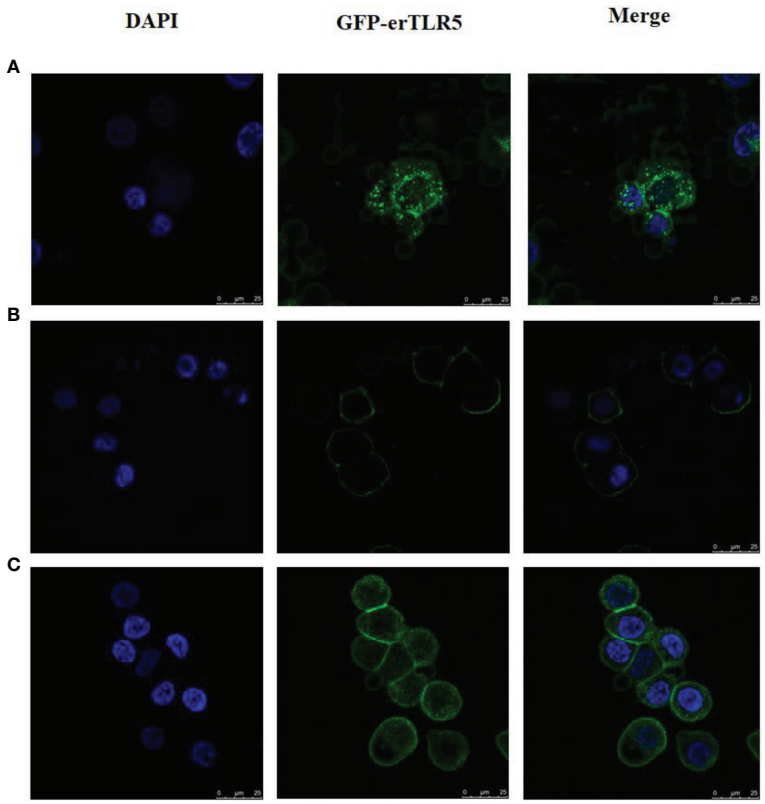


FIGURE 7 | Observation and analysis of enhanced GFP-erTLR5 expression induced by *flaB* in ZF4 cells using LSCM. **(A)** Transfection of empty plasmid (pEGFP-N2). **(B)** Transfection of erTLR5-pEGFP-N2. **(C)** *FlaB* treatment. Left, staining with DAPI; middle, GFP-erTLR5; right, merge of the two images.

be reduced (29). Based on our current experimental data and other studies, we can conclude that *flaB* is an important virulence factor. However, *in vivo* experiments showed that the *flaB* mutant displayed similar immune characteristics to the wild-type strain. We speculate that the inconsistency between *in vivo* and *in vitro* results might be due to the complexity of fish gut microbes. A large number of diverse microorganisms live in the gut of fish and other animals, and these microorganisms can work together with the host to fight against the invasion of pathogenic bacteria to maintain the stability of the living environment (33). Thus, commensal microbes may help the fish host alleviate immune stimulation caused by *flaB* during infection with *V. anguillarum*.

FlaB-induced TLR5 expression was visualised directly using fluorescent labelling, which confirmed that *flaB* induced TLR5 activation. Additionally, for the first time, we confirmed the interaction effects between *flaB* and TLR5 using native PAGE and yeast two-hybrid analysis. It is almost certain that *flaB* binds directly to TLR5 expressed on cultured cells, which consequently induces cytokine expression. Many studies have proved that TLR5 recognises flagellins *via* the extracellular domain, which leads to the expression of a variety of genes. However, due to variation in the sequences and domains of flagellins, flagellins from diverse bacterial species use different TLR5 recognition mechanisms (34). For activation, the receptor must undergo a ligand-induced conformational change (27). In the present study, we aimed to identify the specific ligand-binding sites on the surface of ligand-receptor complexes. Through a detailed examination of our refined docking model and its experimental validation using point mutants, we identified *flaB* residues at two different interfaces that are important for flagellin recognition, and are therefore candidates for participation in an extended TLR5 interaction site.

Successful vaccine preparations have to properly activate immune cells to induce a long-term memory protective immunity. Together with antigens of pathogen, adjuvants strongly contribute to the effectiveness of a vaccine. A number of studies have clearly demonstrated that that flagellin is a strong candidate for an engineered vaccine scaffold as it is known to provide adjuvant activity through its TLR5 and inflammasome activation (35, 36). So far, flagellin has been developed as an important versatile adjuvant applicable to wide spectrum of vaccines and immunotherapies adjuvant with great success (37, 38). It is generally known that *V. anguillarum* is a highly pathogenic bacterium of aquatic species worldwide, hence its flagellins could be actively explored as vaccine adjuvants and carriers. Compared to other flagellins, *flaB* has the strongest immunostimulatory activity, thus *flaB* is recommended for adjuvanted vaccines in order to strengthen the efficacy of the

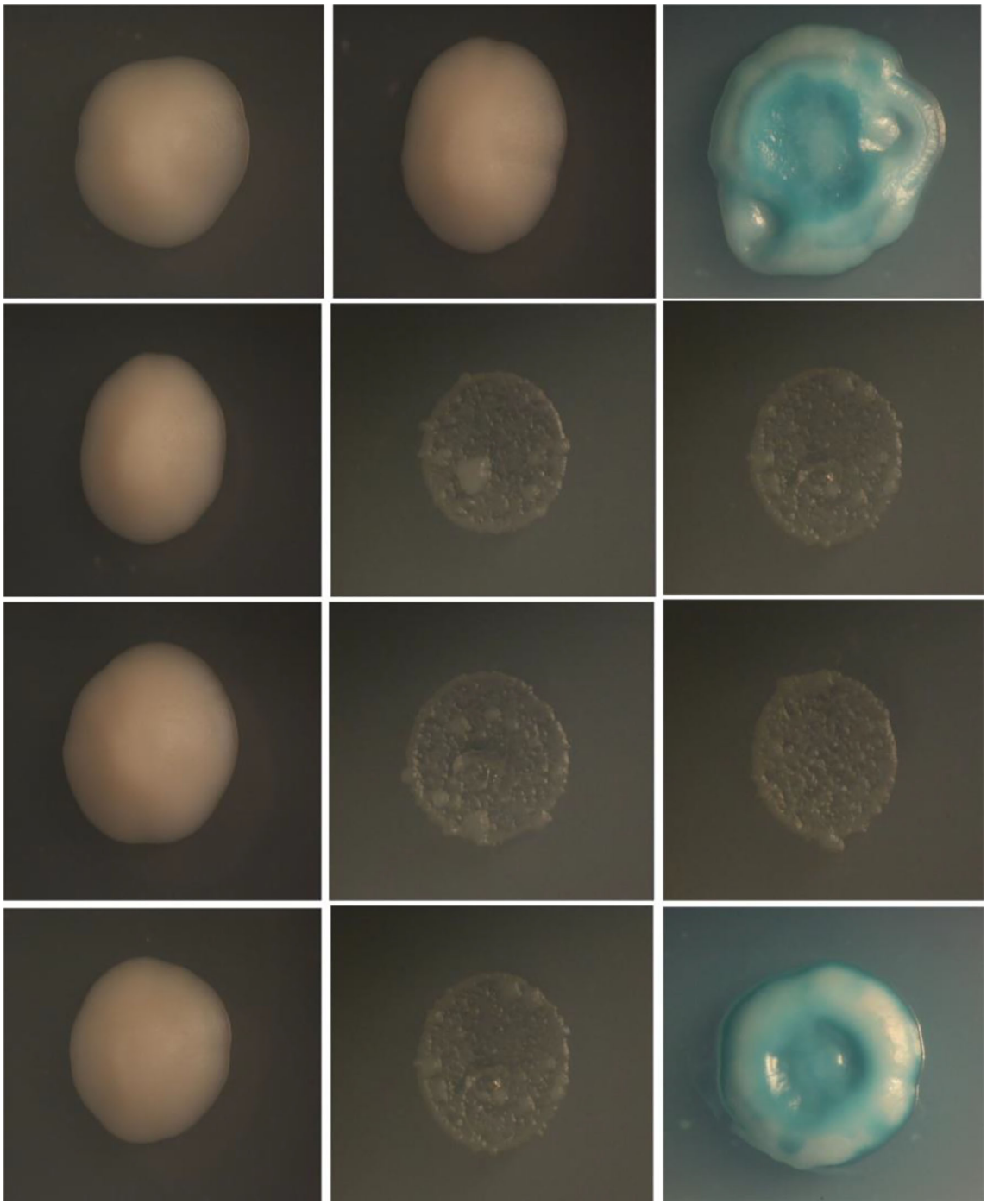
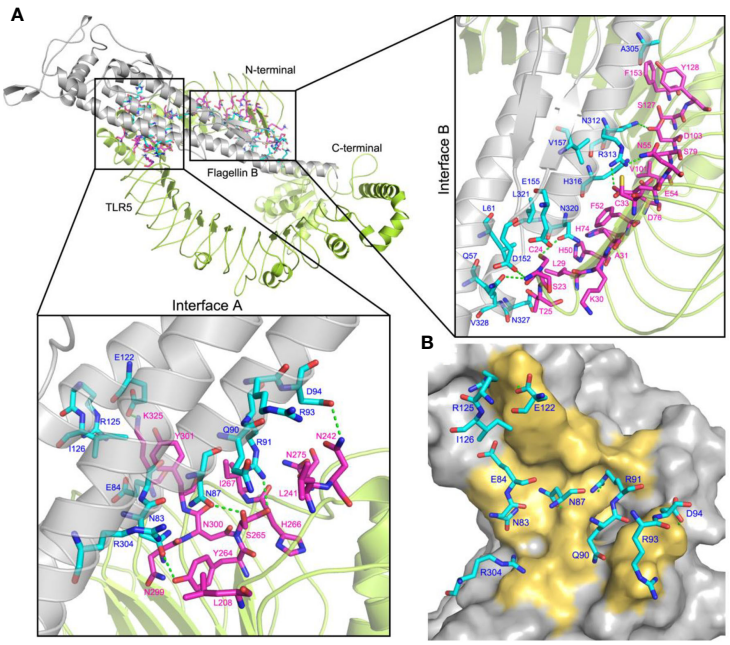


FIGURE 8 | Yeast-two-hybrid screening for interaction between *flaB* and erTLR5. First column, SD-Leu-Trp medium; second column, SD/–Ade/–His/–Leu/–Trp medium; third column, SD/–Ade/–His/–Leu/–Trp/X-α-Gal medium. Fist line, positive control; second line, negative control; third line, self-activated control; fourth line, experimental group.

vaccine. The *flaB* adjuvants might allow more effective flagellin-based vaccines to enter clinical trials.

It is widely accepted that as an adjuvant, flagellin can help induce more potent antigen-specific immune response. However, if the functional domains of flagellins are disrupted during vaccine adjuvant production, their immunity effects may be lowered or lost (39). Therefore, structure-guided fusion-protein design using flagellin as vaccine adjuvant has been one of the research hotspots in the world scope (36). That makes it possible to avoid destroying the functional area of flagellin in the



C

Hydrogen bond interaction			
Abbreviate	*FlaB*	Hydrogen bond	TLR5
F1	Q57	——	S23
F2	N83	——	Y264
F3	N87	——	S265
F4	R91	——	S265
F5	D94	——	N242
FL	E122	——	K325
FL	D152	——	S23
FL	N312	——	D103
F9	R313	——	E54
F10	R313	——	S79
F11	N320	——	C24

Hydrophobic interaction		
Abbreviate	*FlaB*	TLR5
F12	L97	Leu29, Phe52, Tyr264, Leu241 and Leu276
F13	H316	
F14	I324	

FIGURE 9 | The binding model of *flaB* and TLR5 protein docking. **(A)** TLR5 is shown in cyan ribbon representation and *flaB* is shown in grey ribbon representation. Amino acid residues involved in the interaction between TLR5 and *flaB* are shown in purple and blue ribbons, respectively. The green dotted line represents hydrogen bonding between the two proteins. **(B)** The TLR5 surface (grey). Amino acid residues of *flaB* are colored blue, and amino acids of TLR5 that interact with *flaB* are colored yellow. **(C)** Amino acids involved in protein interactions.

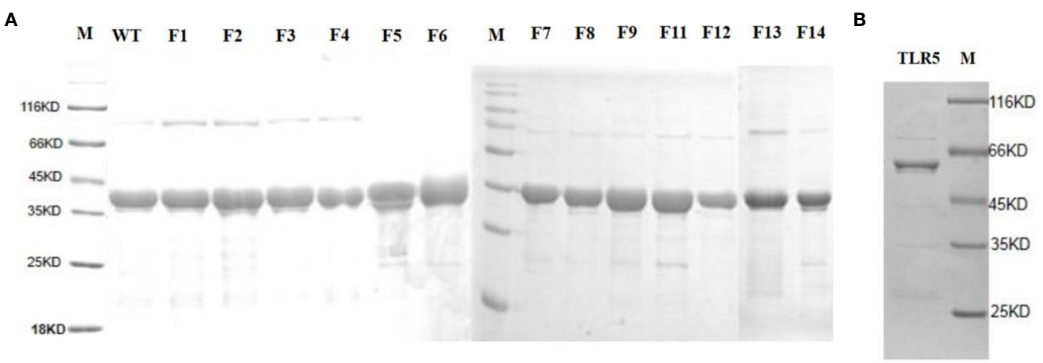


FIGURE 10 | SDS-PAGE analysis of TLR5 and *flaB* mutant proteins. Lane M: protein molecular standard (kDa). **(A)** *FlaB* mutant proteins. **(B)** TLR5 protein. Lane M, protein molecular standards (kDa).

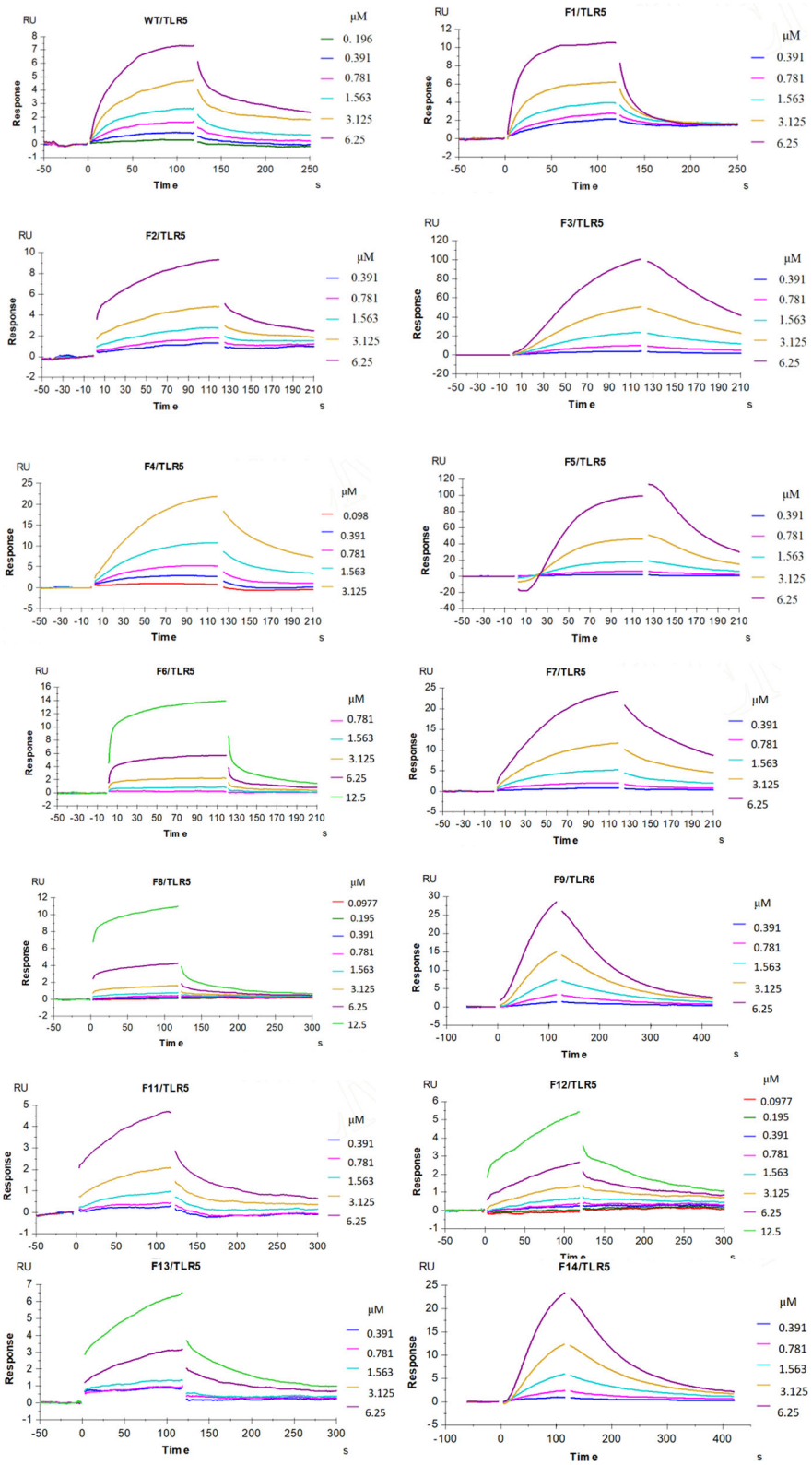


FIGURE 11 | Influence of *flaB* gene site mutation upon binding to TLR5. Multiple concentrations of the indicated *flaB* mutant and wild-type proteins were passed over TLR5 immobilised on the surface of the SA sensor chip. The binding response is shown as response units (RU) and was assessed at a flow rate of 30 μL/min at 25°C.

TABLE 4 | Calculated dissociation constant (Kd) values *flaB* mutants binding to TLR5 protein inferred by SPR.

FLAB	Ligand/receptor	Dissociation constant(Kd, μM)
WT	WT/TLR5	3.283
F1	F1/TLR5	0.4314
F2	F2/TLR5	0.4472
F3	F3/TLR5	26.23
F4	F4/TLR5	2.571
F5	F5/TLR5	46.34
F6	F6TLR5	4.403
F7	F7/TLR5	71.68
F8	F8/TLR5	3.796
F9	F9/TLR5	14.76
F11	F11/TLR5	12.96
F12	F12/TLR5	2.411
F13	F13/TLR5	7.29
F14	F14/TLR5	27.48

process of vaccine preparation, so as to ensure the efficacy of the vaccine (40). Therefore, the study of functional structure of *flaB* has important practical significance. In this study, according to the results of molecular simulations, SPR assays were further performed to determine the binding affinity between TLR5 and *flaB* mutant proteins generated by site-directed mutagenesis, and we identified several key amino acid residues that mediate binding of *flaB* to TLR5, which might be important for exploitation and utilization of flagellins from *V. anguillarum* (41). In order to effectively prevent and control *V. anguillarum*, development of effective vaccines is paramount, and our current research on the functional domains of flagellins will contribute toward the development of innovative vaccines against *V. anguillarum*.

In summary, we present the first comprehensive and in-depth study of flagellins in *V. anguillarum*. We performed flow cytometry, PCR and ELISA to compare the immunostimulatory effects of different flagellins in *V. anguillarum*, and *flaB* displayed the strongest ability to induce apoptosis and inflammatory responses. To further dissect the functions of *flaB* in infection, we constructed a *flaB* deletion mutant using a two-step recombination technique and found that this mutant exhibited dramatically decreased virulence in FICEs in *in vitro* experiments. Through native PAGE, yeast two-hybrid and fluorescence analyses, we further confirmed the physical interaction between *flaB* and TLR5. Finally, we analysed the functional domains and key amino acids, and revealed the roles of these amino acids in interactions between *flaB* and TLR5 using site-directed mutagenesis and SPR analyses. Our results help to reveal the properties of bacterial flagellins, and provide a basis for development of vaccines.

DATA AVAILABILITY STATEMENT

The original contributions presented in the study are included in the article/supplementary material. Further inquiries can be directed to the corresponding author.

ETHICS STATEMENT

The animal study was reviewed and approved by Chinese Academy of Fishery Sciences.

AUTHOR CONTRIBUTIONS

QG, SY, and YL participated in the design of experiments, analyzed verification results and wrote the manuscript. SP, JL, and QX assisted in laboratory work. MZ, YW, QW, and MM were involved in sampling and mRNA extraction. LM and XY designed and supervised the work, plus they edited the paper. All authors contributed to the article and approved the submitted version.

FUNDING

This work was supported by grants from the Natural Science Foundation of Shanghai (No.19ZR1470000), National Natural Science Foundation of China (31772870); the Central Nonprofit Basic Scientific Research Project for the Scientific Research Institutes of China (2420-2019).

REFERENCES

1. Lages MA, Balado M, Lemos ML. The Expression of Virulence Factors in Vibrio Anguillarum Is Dually Regulated by Iron Levels and Temperature. *Front Microbiol* (2019) 10:2335. doi: 10.3389/fmicb.2019.02335
2. Ning X, Sun L. Gene Network Analysis Reveals a Core Set of Genes Involved in the Immune Response of Japanese Flounder (Paralichthys Olivaceus) Against Vibrio Anguillarum Infection. *Fish Shellfish Immunol* (2020) 98:800–9. doi: 10.1016/j.fsi.2019.11.033
3. Fauzi IA, Haga Y, Kondo H, Hirono I, Satoh S. Dietary Citrulline Improves Survival of Rainbow Trout Oncorhynchus Mykiss Juveniles Challenged With Vibrio Anguillarum. *Aquaculture* (2020) 528:735491. doi: 10.1016/j.aquaculture.2020.735491
4. Akter T, Lindegaard M, Pedersen K, Strube ML, Ronco T, Dalsgaard I. Sequence Analysis of Plasmids in Vibrio Anguillarum From Different Fish and Locations. *J Aquat Anim Health* (2020) 32:21–7. doi: 10.1002/aah.10093
5. Hung NB, Ramkumar G, Bhattacharyya D, Lee YH. Elucidation of the Functional Role of Flagella in Virulence and Ecological Traits of

Pseudomonas Cichorii Using Flagella Absence (Δflij) and Deficiency (Δflii) Mutants. *Res Microbiol* (2016) 167:262–71. doi: 10.1016/j.resmic.2016.01.006
6. Senevirathne A, Hewawaduge C, Park J-Y, Park S, Lee JH. Parenteral Immunization of Salmonella Typhimurium Ghosts With Surface-Displayed Escherichia Coli Flagellin enhancesTLR-5 Mediated Activation of Immune Responses That Protect the Chicken Against Salmonella Infection. *Microbial Pathogenesis* (2020) 147:104252. doi: 10.1016/j.micpath.2020.104252
7. Sharma P, Levy O, Dowling DJ. The TLR5 Agonist Flagellin Shapes Phenotypical and Functional Activation of Lung Mucosal Antigen Presenting Cells in Neonatal Mice. *Front Immunol* (2020) 11:171. doi: 10.3389/fimmu.2020.00171
8. Yang J, Hwang I, Lee E, Shin SJ, Lee E-J, Rhee JH, et al. Bacterial Outer Membrane Vesicle-Mediated Cytosolic Delivery of Flagellin Triggers Host NLRC4 Canonical Inflammasome Signaling. *Front Immunol* (2020) 11:581165. doi: 10.3389/fimmu.2020.581165
9. Dickey AK, Chantratita N, Tandhavanant S, Ducken D, Lovelace-Macon L, Seal S, et al. Flagellin-Independent Effects of a Toll-Like Receptor 5 Polymorphism in the Inflammatory Response to Burkholderia Pseudomallei. *PloS neglected Trop Dis* (2019) 13:e0007354–e0007354. doi: 10.1371/journal.pntd.0007354
10. Andersen-Nissen E, Smith KD, Strobe KL, Barrett SLR, Cookson BT, Logan SM, et al. Evasion of Toll-Like Receptor 5 by Flagellated Bacteria. *Proc Natl Acad Sci United States America* (2005) 102:9247–52. doi: 10.1073/pnas.0502040102
11. Kaliamurthi S, Selvaraj G, Chinnasamy S, Wang Q, Nangraj AS, Cho WC, et al. Exploring the Papillomaviral Proteome to Identify Potential Candidates for a Chimeric Vaccine Against Cervix Papilloma Using Immunomics and Computational Structural Vaccinology. *Viruses* (2019) 11:63. doi: 10.3390/v11010063
12. Doan TD, Wang HY, Ke GM, Cheng LT. N-Terminus of Flagellin Fused to an Antigen Improves Vaccine Efficacy Against Pasteurella Multocida Infection in Chickens. *Vaccines (Basel)* (2020) 8:823. doi: 10.3390/vaccines8020283
13. Il Kim M, Lee C, Park J, Jeon BY, Hong M. Crystal Structure of Bacillus Cereus Flagellin and Structure-Guided Fusion-Protein Designs. *Sci Rep* (2018) 8:5814. doi: 10.1038/s41598-018-24254-w
14. Ivičak-Kocjan K, Panter G, Benčina M, Jerala R. Determination of the Physiological 2:2 TLR5:flagellin Activation Stoichiometry Revealed by the Activity of a Fusion Receptor. *Biochem Biophys Res Commun* (2013) 435:40–5. doi: 10.1016/j.bbrc.2013.04.030
15. Lee C, Kim MI, Park J, Jeon B-Y, S-i Y, Hong M. Crystal Structure of the Flagellar Chaperone FliS From Bacillus Cereus and an Invariant Proline Critical for FliS Dimerization and Flagellin Recognition. *Biochem Biophys Res Commun* (2017) 487:381–7. doi: 10.1016/j.bbrc.2017.04.070
16. González-Stegmaier R, Aguirre I, Villarroel-Espíndola F, Enríquez R, Figueroa J. Recombinant Flagellin B and Its ND1 Domain From Vibrio Anguillarum Promote *In Vivo* Overexpression of IL-1β and IL-8 Cytokines in Salmo Salar. *Fish Shellfish Immunol* (2019) 91:412–3. doi: 10.1016/j.fsi.2019.04.133
17. González-Stegmaier R, Guzmán F, Albericio F, Villarroel-Espíndola F, Romero A, Mulero V, et al. A Synthetic Peptide Derived From the D1 Domain of Flagellin Induced the Expression of Proinflammatory Cytokines in Fish Macrophages. *Fish Shellfish Immunol* (2015) 47:239–44. doi: 10.1016/j.fsi.2015.09.016
18. González-Stegmaier R, Romero A, Estepa A, Montero J, Mulero V, Mercado L. Effects of Recombinant Flagellin B and Its ND1 Domain From Vibrio Anguillarum on Macrophages From Gilthead Seabream (Sparus Aurata L.) and Rainbow Trout (Oncorhynchus Mykiss, W.). *Fish Shellfish Immunol* (2015) 42:144–52. doi: 10.1016/j.fsi.2014.10.034
19. Gao Q, Gao Q, Min M, Zhang C, Peng S, Shi Z. Ability of Lactobacillus Plantarum Lipoteichoic Acid to Inhibit Vibrio Anguillarum-Induced Inflammation and Apoptosis in Silvery Pomfret (Pampus Argenteus) Intestinal Epithelial Cells. *Fish Shellfish Immunol* (2016) 54:573–9. doi: 10.1016/j.fsi.2016.05.013
20. Gao Q, Xiao Y, Zhang C, Min M, Peng S, Shi Z. Molecular Characterization and Expression Analysis of Toll-Like Receptor 2 in Response to Bacteria in Silvery Pomfret Intestinal Epithelial Cells. *Fish Shellfish Immunol* (2016) 58:1–9. doi: 10.1016/j.fsi.2016.08.057
21. Gao Q, Yi S, Luo J, Xing Q, Lv J, Wang P, et al. Construction of a Vibrio Anguillarum Flagellin B Mutant and Analysis of Its Immuno-Stimulation Effects on Macrobrachium Rosenbergii. *Int J Biol Macromolecules* (2021) 174:457–65. doi: 10.1016/j.ijbiomac.2021.01.146
22. Gao Q, Yin F, Zhang C, Yue Y, Sun P, Min M, et al. Cloning, Characterization, and Function of MyD88 in Silvery Pomfret (Pampus Argenteus) in Response to Bacterial Challenge. *Int J Biol Macromolecules* (2017) 103:327–37. doi: 10.1016/j.ijbiomac.2017.05.039
23. Xie S, Liu Y, Tian L, Niu J, Tan B. Low Dietary Fish Meal Induced Endoplasmic Reticulum Stress and Impaired Phospholipids Metabolism in Juvenile Pacific White Shrimp, Litopenaeus Vannamei. *Front Physiol* (2020) 11:1024. doi: 10.3389/fphys.2020.01024
24. Chen H, Wang M, Zhang H, Wang H, Lv Z, Zhou L, et al. An LRR-Domain Containing Protein Identified in Bathymodiolus Platifrons Serves as Intracellular Recognition Receptor for the Endosymbiotic Methane-Oxidation Bacteria. *Fish Shellfish Immunol* (2019) 93:354–60. doi: 10.1016/j.fsi.2019.07.032
25. Frans I, Michiels CW, Bossier P, Willems KA, Lievens B, Rediers H. Vibrio Anguillarum as a Fish Pathogen: Virulence Factors, Diagnosis and Prevention. *J Fish Dis* (2011) 34:643–61. doi: 10.1111/j.1365-2761.2011.01279.x
26. Zhao Y, Li Z, Zhu X, Cao Y, Chen X. Improving Immunogenicity and Safety of Flagellin as Vaccine Carrier by High-Density Display on Virus-Like Particle Surface. *Biomaterials* (2020) 249:120030. doi: 10.1016/j.biomaterials.2020.120030
27. Ivičak-Kocjan K, Forstnerič V, Panter G, Jerala R, Benčina M. Extension and Refinement of the Recognition Motif for Toll-Like Receptor 5 Activation by Flagellin. *J Leukoc Biol* (2018) 104:767–76. doi: 10.1002/jlb.3vma0118-035r
28. Steimle A, Menz S, Bender A, Ball B, Weber ANR, Hagemann T, et al. Flagellin Hypervariable Region Determines Symbiotic Properties of Commensal Escherichia Coli Strains. *PloS Biol* (2019) 17:e3000334. doi: 10.1371/journal.pbio.3000334
29. Kim SY, Thanh XTT, Jeong K, Kim SB, Pan SO, Jung CH, et al. Contribution of Six Flagellin Genes to the Flagellum Biogenesis of Vibrio Vulnificus and *In Vivo* Invasion. *Infection Immun* (2014) 82:29–42. doi: 10.1128/iai.00654-13
30. González-Stegmaier R, Peña A, Villarroel-Espíndola F, Aguila P, Oliver C, MacLeod-Carey D, et al. Full Recombinant Flagellin B From Vibrio Anguillarum (rFLA) and Its Recombinant D1 Domain (Rnd1) Promote a Pro-Inflammatory State and Improve Vaccination Against P. Salmonis in Atlantic Salmon (S. Salar). *Dev Comp Immunol* (2021) 117:103988. doi: 10.1016/j.dci.2020.103988
31. de Oliveira Barbosa F, de Freitas Neto OC, Rodrigues Alves LB, Benevides VP, de Souza AIS, da Silva Rubio M, et al. Immunological and Bacteriological Shifts Associated With a Flagellin-Hyperproducing Salmonella Enteritidis Mutant in Chickens. *Braz J Microbiol [publication Braz Soc Microbiology]* (2021) 52:419–29. doi: 10.1007/s42770-020-00399-7
32. Freitas Neto O, Setta A, Imre A, Bukovinski A, Elazomi A, Kaiser P, et al. A Flagellated Motile Salmonella Gallinarum Mutant (SG Fla+) Elicits a Pro-Inflammatory Response From Avian Epithelial Cells and Macrophages and is Less Virulent to Chickens. *Veterinary Microbiol* (2013) 165:425–33. doi: 10.1016/j.vetmic.2013.04.015
33. Westermann AJ, Vogel J. Cross-Species RNA-Seq for Deciphering Host–Microbe Interactions. *Nat Rev Genet* (2021) 22:361–78. doi: 10.1038/s41576-021-00326-y
34. Xu M, Xie Y, Tan M, Zheng K, Xiao Y, Jiang C, et al. The N-Terminal D1 Domain of Treponema Pallidum Flagellin Binding to TLR5 is Required But Not Sufficient in Activation of TLR5. *J Cell Mol Med* (2019) 23:7490–504. doi: 10.1111/jcmm.14617
35. Gries CM, Mohan RR, Morikis D, Lo DD. Crosslinked Flagella as a Stabilized Vaccine Adjuvant Scaffold. *BMC Biotechnol* (2019) 19:48–8. doi: 10.1186/s12896-019-0545-3
36. Zhao B, Yang J, He B, Li X, Yan H, Liu S, et al. A Safe and Effective Mucosal RSV Vaccine in Mice Consisting of RSV Phosphoprotein and Flagellin Variant. *Cell Rep* (2021) 36:109401. doi: 10.1016/j.celrep.2021.109401
37. Cui B, Liu X, Fang Y, Zhou P, Zhang Y, Wang Y. Flagellin as a Vaccine Adjuvant. *Expert Rev Vaccines* (2018) 17:335–49. doi: 10.1080/14760584.2018.1457443
38. Reis ECD, Leal VNC, Soares J, Fernandes FP, Souza de Lima D, de Alencar BC, et al. Flagellin/NLRC4 Pathway Rescues NLRP3-Inflammasome Defect in Dendritic Cells From HIV-Infected Patients: Perspective for New Adjuvant in Immunocompromised Individuals. *Front Immunol* (2019) 10:1291. doi: 10.3389/fimmu.2019.01291
39. Song WS, Jeon YJ, Namgung B, Hong M, Yoon S. A Conserved TLR5 Binding and Activation Hot Spot on Flagellin. *Sci Rep* (2017) 7:40878. doi: 10.1038/srep40878

40. Li Q, Peng O, Wu T, Xu Z, Huang L, Zhang Y, et al. PED Subunit Vaccine Based on COE Domain Replacement of Flagellin Domain D3 Improved Specific Humoral and Mucosal Immunity in Mice. *Vaccine* (2018) 36:1381–8. doi: 10.1016/j.vaccine.2018.01.086
41. Biedma ME, Cayet D, Tabareau J, Rossi AH, Ivičak-Kocjan K, Moreno G, et al. Recombinant Flagellins With Deletions in Domains D1, D2, and D3: Characterization as Novel Immunoadjuvants. *Vaccine* (2019) 37:652–63. doi: 10.1016/j.vaccine.2018.12.009

Conflict of Interest: The authors declare that the research was conducted in the absence of any commercial or financial relationships that could be construed as a potential conflict of interest.

Publisher's Note: All claims expressed in this article are solely those of the authors and do not necessarily represent those of their affiliated organizations, or those of the publisher, the editors and the reviewers. Any product that may be evaluated in this article, or claim that may be made by its manufacturer, is not guaranteed or endorsed by the publisher.

Copyright © 2021 Gao, Yi, Li, Luo, Xing, Yang, Zhao, Min, Wang, Wang, Ma and Peng. This is an open-access article distributed under the terms of the Creative Commons Attribution License (CC BY). The use, distribution or reproduction in other forums is permitted, provided the original author(s) and the copyright owner(s) are credited and that the original publication in this journal is cited, in accordance with accepted academic practice. No use, distribution or reproduction is permitted which does not comply with these terms.

frontiers in Immunology

ORIGINAL RESEARCH
published: 29 November 2021
doi: 10.3389/fimmu.2021.728723

Fecal Microbiota Transplantation Controls Progression of Experimental Autoimmune Hepatitis in Mice by Modulating the TFR/TFH Immune Imbalance and Intestinal Microbiota Composition

Ma Liang[1,2†], Zhang Liwen[3†], Song Jianguo[2†], Dai Juan[1], Ding Fei[1], Zhang Yin[1], Wu Changping[1] and Chen Jianping[1*]*

[1] Department of Gastroenterology, The First People's Hospital of Changzhou, The Third Affiliated Hospital of Soochow University, Changzhou, China, [2] Department of Gastroenterology, The People's Hospital of Wuqia, Xinjiang, China, [3] Department of Pediatrics, the Second People's Hospital of Changzhou, Affiliate Hospital of Nanjing Medical University, Changzhou, China

Intestinal microbiota (IM) dysbiosis contributes to the development of autoimmune hepatitis (AIH). This study aimed to investigate the potential effect of fecal microbiota transplantation (FMT) in a murine model of experimental AIH (EAH), a condition more similar to that of AIH patients. Changes in the enteric microbiome were determined in AIH patients and EAH mice. Moreover, we established an experimental model of secondary EAH mice harboring dysbiosis (ABx) to analyze the effects of therapeutic FMT administration on follicular regulatory T (TFR) and helper T (TFH) cell imbalances and IM composition *in vivo*. Alterations of the IM composition and bacterial translocation occurred in AIH patients compared to nonalcoholic fatty liver disease patients and healthy controls (HCs). Therapeutic FMT significantly attenuated liver injury and bacterial translocation and improved the imbalance between splenic TFR cells and TFH cells in ABx EAH mice. Furthermore, therapeutic FMT also partially reversed the increasing trend in serum liver enzymes (ALT and AST) of CXCR5−/−EAH mice on the 28th day. Finally, therapeutic FMT could effectively restore antibiotic-induced IM dysbiosis in EAH mice. Taken together, our findings demonstrated that FMT was capable of controlling hepatitis progression in EAH mice, and the associated mechanism might be involved in the regulation of the TFR/TFH immune imbalance and the restoration of IM composition.

Keywords: fecal microbiota transplantation, TFR cells, TFH cells, AIH, EAH

OPEN ACCESS

Edited by:
Gee W. Lau, University of Illinois at Urbana–Champaign, United States

Reviewed by:
Sergio Serrano-Villar, Ramón y Cajal University Hospital, Spain
Debbie Shawcross, King's College London, United Kingdom

***Correspondence:**
Wu Changping
wuchangping123abc@163.com
Chen Jianping
chenjianping123abc@163.com

†These authors have contributed equally to this work

Specialty section:
This article was submitted to Microbial Immunology, a section of the journal Frontiers in Immunology

Received: *21 June 2021*
Accepted: *04 November 2021*
Published: *29 November 2021*

Citation:
Liang M, Liwen Z, Jianguo S, Juan D, Fei D, Yin Z, Changping W and Jianping C (2021) Fecal Microbiota Transplantation Controls Progression of Experimental Autoimmune Hepatitis in Mice by Modulating the TFR/TFH Immune Imbalance and Intestinal Microbiota Composition. Front. Immunol. 12:728723. doi: 10.3389/fimmu.2021.728723

INTRODUCTION

Autoimmune hepatitis (AIH) is a chronic, progressive, and immunologically mediated inflammatory liver disease (1, 2). At present, the pathophysiology of AIH is not fully unknown. Several hypotheses have been proposed that genetic susceptibility with environment factors led to the breakdown of the hepatic immune homeostasis (3), which in collaboration induce follicular helper T (TFH) cell immune-mediated necroinflammation and tissue destruction of the liver (4, 5). Our previous study also confirmed that TFH cell has been detected in the peripheral circulation, and the excessive activation of TFH cells are associated with hypergammaglobulinemia, which accelerated the immunopathological process of AIH (6). In addition, our own previous work demonstrated that follicular regulatory T (TFR) cell could inhibit the secretion of autoantibody by indirectly inhibiting the activation of TFH cells *via* the coreceptor CTLA-4. Further research found that dysregulation between TFR and TFH cells might cause excessive production of autoantibodies and destruction of the immune homeostasis, leading to the immunopathological process in AIH, suggesting that reversing the disorder between TFR and TFH cell will provide new perspectives for the treatment of AIH (6). However, recent research found that the defensive mechanism maintaining the hepatic immune homeostasis mainly depended on the intestinal microbiota (IM) and their metabolic byproducts constituting a reservoir of foreign antigens (7–10). This intimate relationship existing between the gut and liver was called "gut–liver axis", which played a critical role in the pathogenesis initiation and progression of many types of liver diseases (11–13). There was evidence that alterations in the composition of the intestinal microbiome (dysbiosis) were found in AIH, including a reduction in microbial diversity and a reduced number of anaerobes such as *Bifidobacterium* and *Lactobacillus* (7). Furthermore, germ-free mice are resistant to concanavalin A (ConA)-induced liver injury (14), further confirming the necessity of IM in the initiation of AIH. Therefore, remodeling the homeostasis between the host and intestinal microorganisms and reversing the disorder between TFR and TFH cell will provide new perspectives for the treatment of AIH.

Corticosteroids and immunosuppressants are the main therapeutic methods for alleviating symptoms and prolonging life in AIH patients (15). Although the efficacy of these therapy are satisfactory in most patients, 10%–20% of cases with AIH still progress to end-stage liver disease and require liver transplantation (16). Furthermore, side effects of the drug—such as moon face, central obesity, and osteoporosis—might severely interrupt patients' quality of life (17). Therefore, the development of new safe and effective therapies is an urgent need for patients with AIH.

Fecal microbiota transplantation (FMT) is a treatment method in which the functional bacteria from a healthy donor feces is transferred into another patient's gastrointestinal tract through different routes of administration, so as to reconstitute of a healthy microbial ecosystem in the gut (18, 19). The initial purpose of FMT is used to treat intestinal-associated diseases, such as refractory and recurrent *Clostridium difficile* infections (CDI) (20). Lately, therapeutic application of FMT can improve insulin sensitivity in patients suffering from metabolic syndrome (21). Furthermore, recent studies have suggested that FMT can increase intestinal microbial diversity and modulate intestinal immune response towards control of intestinal inflammation in patients with inflammatory bowel disease, such as ulcerative colitis (UC) (22). Specifically, a recent study showed supplement sodium butyrate, a metabolite of intestinal flora, attenuated liver injury and prevented migration of intestinal pathobionts into the liver in a mouse model of AIH (10). Moreover, FMT can increase the concentration of intestinal butyrate (23). Taken together, these studies indicate that FMT may be a promising method for managing AIH. However, whether FMT can control hepatitis progression of AIH or not requires further research.

Here, the present ongoing study aims to evaluate whether FMT regulate TFR/TFH cell disorders and affect colonization of intestinal flora, so as to clarify the beneficial mechanism of action of FMT in AIH.

MATERIALS AND METHODS

Participants

A total of 32 newly diagnosed patients with AIH were enrolled into this study at the Department of Inpatient Clinic of the Department of Gastroenterology, the First People's Hospital of Changzhou. According to the international criteria for the definitive diagnosis of AIH type I (3), all patients were diagnosed in an active disease state, as defined by an alanine aminotransferase (ALT) value or aspartate aminotransferase (AST) value >50 U/ml. Individuals were excluded if she/he had a history of another autoimmune disease, recent infection, or received immune suppressive or glucocorticoid therapies within the past 6 months. For comparison, another 20 age-, gender-, and ethnicity-matched nonalcoholic fatty liver disease (NAFLD) patients without other disease and 20 age-, gender-, and ethnicity-matched healthy controls (HCs) without any disease were recruited from the Department of Medical Examination Center of the First People's Hospital of Changzhou during the same period. An informed consent was written from individual participants, and the experimental protocol was approved by the Ethical Committee of the First People's Hospital of Changzhou.

Clinical Index Assay

The clinical data of each subject were collected from the hospital records. These data included age, sex, and laboratory tests. Individual subjects were subjected to routine laboratory tests for full blood cell counts, and the concentrations of total bilirubin (TBIL), albumin (ALB), IgG, IgM, IgA, and antinuclear and smooth muscle antibody (ANA/SMA) by a biochemistry automatic analyzer (Roche Diagnostics, Branchburg, USA) and scattered turbidimetry on a Siemens special protein analysis instrument (Siemens Healthcare Diagnostics Products, GmbH, Germany).

Animals

Specific pathogen-free (SPF)-class female C57BL/6 mice (6–8 weeks of age, 18–22 g) and CXCR5-deficient (CXCR5−/−) mice (6 weeks of age, 16–20 g) were obtained from Nanjing Experimental Animal Center (Jiangsu, China). All animal experiments had been approved by the Laboratory Animal Ethics Committee of the First People's Hospital of Changzhou, and the Guide for the Care and Use of Laboratory Animals were observed.

Induction of Experimental Autoimmune Hepatitis (EAH)

According to the previously mature method of establishing autoimmune hepatitis (EAH) mouse model (5, 6), owning to AIH occurring more frequently in women, SPF class female C57BL/6 mice were selected and induced into EAH model mice, a condition more similar to that of AIH patients. Liver antigens were always prepared freshly as described previously from C57BL/6 female mice after perfusion of livers with phosphate-buffered saline (PBS). Livers were homogenized on ice, and the nuclei and remaining intact cells were centrifuged at 150*g* for 10 min. Subsequently, the supernatants were centrifuged for 1 h at 100,000*g*, and the remaining supernatants were used for immunization (called S100). Induction of experimental EAH was achieved by intraperitoneal injection of the mice with freshly prepared S-100 antigen at a dose of 0.5–2 mg/ml in 0.5 ml PBS that had been emulsified in an equal volume of complete Freund's adjuvant (CFA) on day 0. A booster dose was given on day 7 as well (5, 6, 20). Disease severity was assessed histologically on day 28 when the peak of disease activity was observed. Disease severity was graded on a scale of 0–3 by a researcher who was blinded to the sample identity, as follows: grade 0, none; grade 1, mild–scattered foci of lobular-infiltrating lymphocytes; grade 2, moderate–numerous foci of lobular-infiltrating lymphocytes; and grade 3, severe–extensive pan-lobular-infiltrating lymphocytes.

Mouse Model of Intestinal Dysbiosis Induced by Ceftriaxone Sodium

In order to counteract physiological colonization resistance, secondary mice harboring IM dysbiosis were generated as described previously (24). In brief, secondary EAH mice harboring dysbiosis (ABx) were administered 0.2 ml of ceftriaxone sodium (400 mg/ml) orally twice a day at an interval of 6 h for 7 days.

Fecal Microbiota Transplantation

In brief, 50 g of fresh murine fecal samples was collected from 10 age- and sex-matched SPF-class C57BL/6 mice, pooled, dissolved in 250 ml sterile PBS, and the supernatant used as murine donor suspension under anaerobic conditions. Anesthetized EAH mice were treated with 0.3 ml of murine donor suspension *via* anus. Mock control mice were treated with 0.3 ml of PBS *via* anus.

Histological Evaluation

Liver tissues from sacrificed animals were fixed with 4% (v/v) PFA, dehydrated through a graded series of sucrose, frozen in an optimal cutting temperature (OCT) compound (Tissue TCK, Miles Elkhart, IN, USA), and stored at −80°C. Five-micrometer cryostat sections were stained with hematoxylin and eosin (HE) to reveal and estimate the degree of inflammatory cell infiltration. Liver histology of EAH mice was scored using light microscopy and a modified Scheuer scoring scale, assigning scores for lobular inflammation (0, none; 1, mild-scattered foci of lobular-infiltrating lymphocytes; 2, moderate–numerous foci of lobular-infiltrating lymphocytes; and 3, severe–extensive pan-lobular-infiltrating lymphocytes).

Flow Cytometric Analysis

Spleen mononuclear cells (SMNCs) were isolated from EAH mice by density-gradient centrifugation using Ficoll–Paque Plus (Amersham Biosciences, Little Chalfont, UK). To detect TFR/TFH cell subsets, SMNCs (1×10^6/tube) were stained with BV510-anti-CD4 (0.2 mg/ml), PerCP-Cy5.5-anti-CXCR5 (0.1 mg/ml), and FITC–anti-GITR (0.1 mg/ml) in the dark at 4°C for 30 min. After being washed with PBS, the frequency of CD4+ CXCR5+GITR+TFR and CD4+CXCR5+GITR-TFH in EAH mice were determined by flow cytometry analysis (LSR II Instrument BD Biosciences). The cells were gated on living lymphocytes and then gated on CD4+CXCR5+ T cells, and at least 20,000 events were analyzed by FlowJo software (v5.7.2).

Enzyme-Linked Immunosorbent Assay

The concentrations of serum lipopolysaccharide (LPS) in AIH patients and the concentrations of serum endotoxin (ET) and diamine oxidase (DAO) in EAH mice were determined by ELISA. The levels of cytokines in the supernatant of normalized hepatic tissue weight (mice) were measured by ELISA using commercially available interleukin-10 (IL-10), transforming growth factor beta 1 (TGF-β1), and IL-22 ELISA kits (Boster, Wuhan, China) according to the manufacturer's instructions.

Real-Time PCR

Total RNA was acquired from the hepatic tissue at each time point from EAH mice. The expressions of transcriptional repressor Foxp3 and IL-21 were then measured through real-time quantitative RT-PCR. Total RNA was extracted from the hepatic tissue using the acid guanidinium thiocyanate-phenol-chloroform method. Total RNA of 2 μg was reverse transcribed with hexamer and M-MuLV reverse transcriptase (New England Biolabs, Ipswich, MA) according to the manufacturer's instructions (R&D Systems). cDNA corresponding to 25 ng of total RNA was subjected to quantitative PCR (qPCR) using primer sets and TaqMan probes corresponding to murine Foxp3 and IL-21 with qPCR Mastermix. All estimated messenger RNA (mRNA) values were normalized to glyceraldehyde 3-phosphate dehydrogenase (GAPDH) mRNA levels. The sequences of the primers and TaqMan probes were as follows:

FOXP3, forward: 5′-ATGGAGTCTGCAAGTGGCCT-′3; reverse: 5′-TCTGCTTGGCAGTGCTTGAG-′3

Probe sequences, 5′-ACTCTTCTGGTCCTCGAAGACC TTCTCA-′3

IL-21, forward: 5′-AAGATTCCTGAGGATCCGAGAAG-′3; reverse: 5′-GCATTCGTGAGCGTCTATAGTGTC-′3

Probe sequences, 5′-TTCCCGAGGACTGAGGAGACGCC-′3

GAPDH, forward: 5′-GCTCTGGCTCCTAGCACCAT-′3; reverse: 5′-GATCCACACAGAGTACTTGCGC-′3

Probe sequences, 5′-AGATCAAGATCATTGCTCC-′3

Cycling conditions were 95°C for15 s, 95°C for 15 s, and 95°C for 15 s.

Real-Time PCR of Intestinal Microbiome

Total DNA in fecal pellets of EAH mice was isolated using the QIAamp fast DNA stool mini kit (Qiagen) following the manufacturer's protocol (R&D Systems). Moreover, the target bacteria 16S rRNA were amplified by using specific primers and a thermocycler PCR system (GeneAmp 9700, ABI, USA).

Quantitative real-time polymerase chain reaction (qRT-PCR) primers were used for amplification:

Bifidobacterium, forward: 5′-TCTGGCTCAGGATGAACGC-′3; reverse: 5′-CACCGTTACACCGGGAATTC-′3

Lactobacillus, forward: 5′-TGGAAACAGRTGCTAATACCG-′3; reverse: 5′-GTCCATTGTGGAAGATTCCC-′3

Clostridium leptum, forward: 5′-GCACAAGCAGTGGAGT-′3; reverse: 5′-CTTCCTCCGTTTTGTCAA-′3

Escherichia coli, forward: 5′-CGGACTTTCTGCGTGC TAAGA-′3; reverse: 5′-CAATTGGATTTTTGACTTCTG-′3

Cycling conditions were 95°C for 15 s; 60°C for 1 h, 60°C for 30 s, and 95°C for 40 s.

Statistical Analysis

The difference between two independent groups was analyzed by the Kruskal–Wallis nonparametric test or Fisher's exact test using the SPSS 18.0 software (SPSS, Inc., Chicago, IL, USA). A two-sided $p < 0.05$ was considered statistically significant.

RESULTS

Intestinal Microbiota Dysbiosis in AIH Patients

To assess whether or not the intestinal flora has changed, 32 AIH patients, 20 NAFLD patients, and 20 healthy subjects were recruited. As summarized in **Table 1**, there were no significant differences in the distribution of age and gender among the different groups of patients. As expected, the levels of serum liver enzymes (ALT, AST, γ-GT, and ALP) and serum immunoglobulin (IgG, IgM, and IgA) were significantly higher in AIH patients than those in NAFLD and HC patients. Moreover, 23 of 32 patients had cirrhosis. Furthermore, the majority of patients with new onset AIH were seropositive for anti-ANAs and anti-SMA antibodies. These results indicate that AIH patient displayed active disease and hypergammaglobulinemia.

Next, the major enteric bacteria in the fecal samples were quantitatively analyzed using the real-time PCR method. The quantity of *Bifidobacteria*, *Lactobacillus*, *Bacteroides*, and *C. leptum* in AIH patients were significantly lower than those in the NAFLD patients and HCs, while the quantity of *Escherichia coli* in the AIH patients were significantly higher than those in the NAFLD patients and HCs (**Figure 1A**). We further assessed the presence of bacterial translocation and found that the levels of serum LPS in AIH patients were significantly higher than those in the NAFLD patients and HCs (**Figure 1B**). These results indicate that IM dysbiosis occurred in AIH and NAFLD patients but not in healthy control group.

TABLE 1 | The demographic and clinical characteristics of subjects.

Parameters	AIH	NAFLD	HC
No.	32	20	20
Age (years)	48 (37–76)	45 (35–66)	51 (41–74)
Gender/female/male	24/8	13/7	14/6
ALT (U/L)	125.9 ± 108.3*	57 ± 7.3#	27.2 ± 8.2
AST (U/L)	101.1 ± 53.7*	62 ± 6.8#	22.7 ± 5.7
γ-GT (U/L)	89.1 ± 30.3*	29.3 ± 6.5	25.1 ± 7.4
ALP (U/L)	133.4 ± 37.1*	90.5 ± 16.3	89.5 ± 23.6
Bilirubin (μmol/L)	12.5 ± 8.1*	9.8 ± 7.6	10.8 ± 6.8
Albumin (g/L)	23.8 ± 5.7	20.3 ± 5.5	25.3 ± 4.8
PT-INR	1.0 ± 0.9	1.0 ± 0.5	1.1 ± 0.6
Cirrhosis	25/32 (78.1%)*	–	–
Anti-ANA (+)	23/32 (71.8%)*	0/20 (0%)	0/20 (0%)
Anti-ANA titer	1:640 (1:80–1:10,000)	–	–
Anti-SMA (+)	2/32 (6.25%)	0/20 (0%)	0/20 (0%)
Anti-SMA titer	1:1,000 (1:160–1:3,200)	–	–
IgG (g/L)	15.9 ± 3.7*	5.8 ± 3.4	7.8 ± 2.3
IgM (g/L)	6.9 ± 1.9*	2.08 ± 1.03	2.64 ± 0.87
IgA (g/L)	4.07 ± 2.3*	1.2 ± 0.9	1.6 ± 1.1
WBC (*10^9/L)	7.93 (5.6–11.2)*	4.55 (4.3–8.8)	5.08 (3.9–9.2)

Data shown are real case number or mean ± SD. Normal values: alanine aminotransferase (ALT), 5-40 U/L; aspartate transaminase (AST), 5–40 U/L; gamma glutamyl transferase (γ-GT), 10–60 μ/L; alkaline phosphatase (ALP), 45–125 μ/L; bilirubin, 3.4–20.5 μmol/L; albumin, 35–53 g/L; antinuclear antibody (ANA), <1:80; antimitochondrial antibodies (SMA), <1:80; IgG, 7–16 g/L; IgM, 0.7–4.6 g/L; IgA, 0.4–2.3 g/L.

HC, healthy control; AIH, autoimmune hepatitis.

**$p < 0.05$ vs. HC/NAFLD.*

#$p < 0.05$ vs. HC.

Impaired Liver Function and Imbalance of TFR/TFH Cell Were More Serious in EAH Mice Harboring IM Dysbiosis

Next, we employed S100/FCA-induced EAH model treated with broad-spectrum antibiotics (ABx) to investigate the effects of IM dysbiosis on liver functions and TFR/TFH balance. Successful alterations of the IM composition was confirmed as described previously (24). Compared with the control group and the EAH group, ABx EAH mice had obvious liver injury evidenced by liver edema with a rising liver index and elevated serum levels of ALT, AST, and TBIL and decreased serum levels of albumin (**Figures 2A**–**E**). Splenocytes were collected from mice at each time point, and flow cytometry was performed to analyze the percentages of CD4+CXCR5+GITR+TFR and CD4+CXCR5 +GITR-TFH cells (**Figure 2F**). We observed that CD4+CXCR5 +GITR+TFR cells in the ABx EAH group significantly decreased on the days of post-EAH induction. On the other hand, CD4 +CXCR5+GITR-TFH cells in the ABx EAH gradually increased from 7th to 14th days of post-EAH induction compared to the control group and the EAH group (**Figure 2G**). These results indicated that treatment with broad-spectrum antibiotics might not only induce IM dysbiosis but also aggravate liver inflammation and TFR/TFH cell disorder in EAH mice.

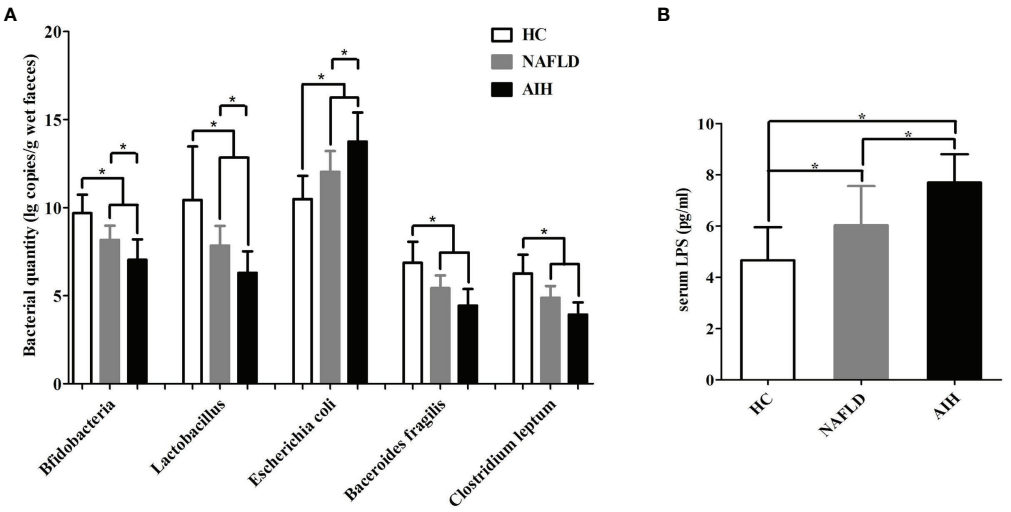


FIGURE 1 | Changes in the enteric microbiome and serum LPS levels of AIH patients compared to NAFLD patients and controls. **(A)** The levels of fecal *Bifidobacteria*, *Lactobacillus*, *Bacteroides*, *Escherichia coli*, and *Clostridium leptum* l g copies/g wet feces (copies per gram of wet feces); **(B)** the levels of serum LPS. The data are presented as the mean ± SD. *p < 0.05.

Therapeutic FMT Attenuated Liver Injury, Hypergammaglobulinemia, and Bacterial Translocation in EAH Mice Harboring IM Dysbiosis

To evaluate if FMT might exert beneficial effects in a chronic autoimmune-related liver inflammation similar to that observed in human AIH patients, ABx EAHs were subjected to murine fecal microbiota transplantation (mFMT) for 28 consecutive days starting at day 10 antibiotic treatment. Three days before mFMT transplantation, the antibiotic cocktail was replaced by autoclaved tap water (**Figure 3A**). During the course of the treatment, the elevated serum liver enzymes (ALT and AST) of FMT-treated ABx EAH and EAH group significantly decreased on the 7th, 14th, and 28th day compared with those in the control group (**Figures 3B, C**). The histological score was also similar among FMT-treated and untreated group (**Figure 3D**). In addition, the elevated serum IgG of FMT-treated ABx EAH and EAH group significantly decreased on the 28th day compared with those in the control group (*p < 0.05). Next, we further evaluated the effect of FMT on bacterial translocation and found that the serum ET and DAO of FMT-treated ABx EAH and EAH group significantly decreased on the 28th day compared with those in the control group (**Figures 3E, F**). Thus, our results showed that therapeutic FMT might attenuate liver injury and bacterial translocation in settings that more closely resemble human AIH pathology.

Therapeutic FMT Regulated TFR/TFH Cell Imbalances in EAH Mice Harboring IM Dysbiosis

To evaluate the effect of FMT on the expression of TFR/TFH cell, we further examined the impact of therapeutic FMT administration on the frequency of CD4+CXCR5+GITR+TFR and CD4+CXCR5+GITR-TFH cells in the spleen tissue of ABx EAH and EAH group. We observed that CD4+CXCR5+GITR+ TFR cells and TFR/TFH ratio in the FMT-treated ABx EAH and EAH group significantly increased, while TFH cells were significantly decreased on the 28th day compared with those in the control group (**Figures 4A, B**). Furthermore, our data also showed that the liver levels of IL-10, TGF-β, and FoxP3-mRNA on the 28th day of FMT administration were statistically higher in the ABx EAH and EAH group than in the control group. Conversely, the liver levels of IL-21 and IL-21 mRNA obviously decreased on the 28th day of FMT administration compared with those in the control group (**Figures 4C–G**). Taken together, these data indicated that therapeutic FMT might regulate TFR/TFH cell imbalances in settings that more closely resemble human AIH pathology.

Therapeutic FMT Attenuated Liver Injury in CXCR5−/−EAH Mice

To explore whether the role of FMT in controlling hepatitis progression was achieved by regulating TFR/TFH cell balance, we employed CXCR5-deficient mice, which failed to develop discrete primary follicles. We observed that the levels of serum liver enzymes (ALT and AST) were significantly higher in PBS-treated CXCR5−/−EAH group than those in the PBS-treated control group on the 28th day. Furthermore, our data also showed that the levels of serum liver enzymes (ALT and AST) did not significantly decrease until the 28th day in the FMT-treated CXCR5−/−EAH group but decreased significantly on the 7th day in the FMT-treated EAH group (**Figures 5A, B**). These data indicated that the FMT might control hepatitis progression by regulating TFR and TFH cell imbalances, but it is not entirely dependent on this pathway.

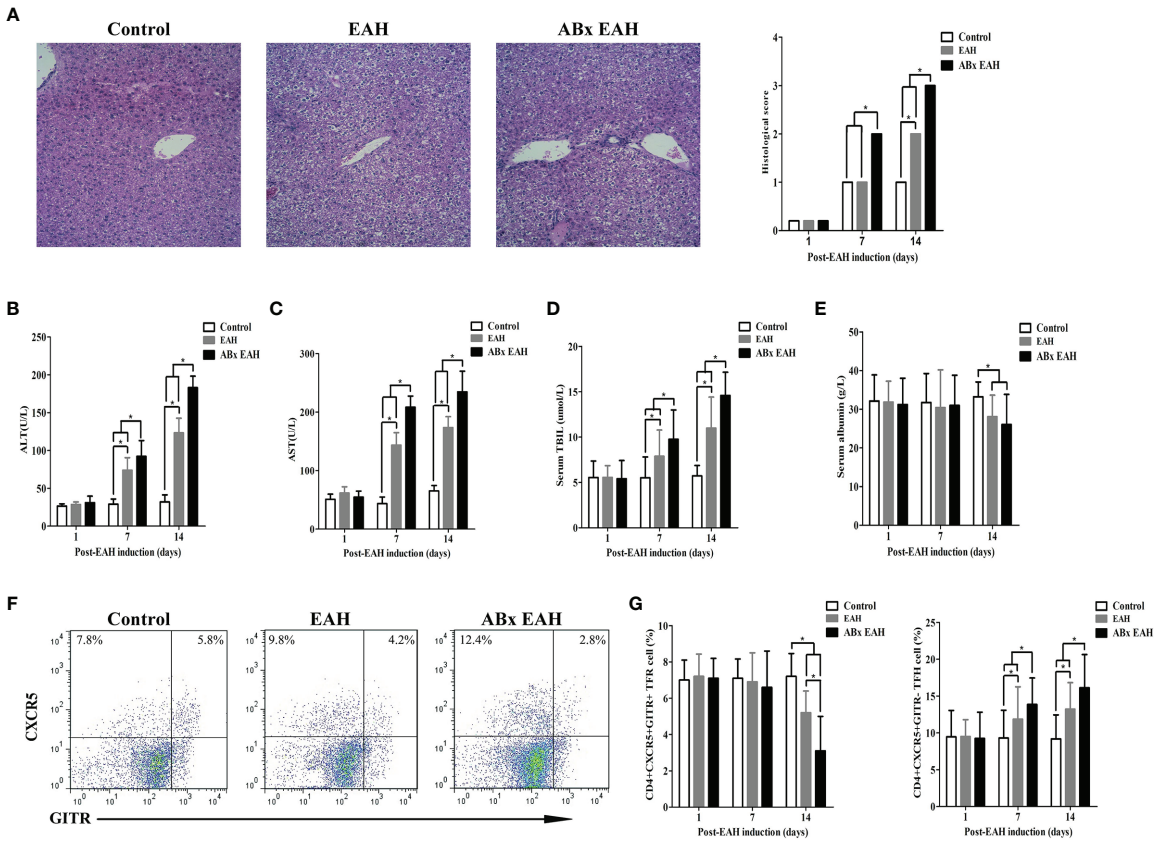


FIGURE 2 | Flow cytometry of TFR/TFH cells in SMNC. Fifteen mice (five from the EAH group, five from the ABxEAH group, and five from the control group) were killed at each time point (1, 7, and 14 days). **(A)** Representative histological picture of liver lesions in animals after standard induction of ABx-EAH, EAH, and controls on the 14th day (magnification, 200×); **(B–E)** the levels of serum ALT, AST, TBIL, and ANA in mice after standard induction of ABx EAH and EAH mice with S100 and control mice with PBS; **(F)** flow cytometry analysis of TFR and TFH cells from the spleen on the 14th day; **(G)** percentages of TFR and TFH cells at each time point from ABx EAH, EAH, and control mice were analyzed by FACS. The horizontal lines indicate the mean values of the different groups. *p < 0.05.

Therapeutic FMT Restored Antibiotic-Induced IM Dysbiosis in EAH Mice

To assess whether the reduction in liver damage in FMT-treated mice was associated with changes in the IM composition, fecal samples of untreated and FMT-treated mice were analyzed by the real-time PCR method. Compared with the control group, the quantitative amounts of *Bifidobacterium* and *Lactobacillus* were significantly increased, and *Escherichia coli* was significantly reduced on the 28th day in the FMT-treated group (**Figures 6A–C**). Furthermore, the quantitative amounts of *C. leptum* of the FMT-treated group did not differ from that of EAH group (**Figure 6D**). Taken together, these data indicated that the beneficial effects of FMT might originate from the functional reshuffling of the entire IM composition alterations towards anti-inflammatory activities.

DISCUSSION

IM dysbiosis has been associated with the pathogenesis of many autoimmune diseases, such as and diabetes mellitus type 1 (T1DM), systemic lupus erythematosus (SLE), and inflammatory bowel disease (IBD) (25, 26). Besides, various studies have also provided evidence that the liver–gut axis play an important role in the pathogenesis of chronic hepatitis, such as NAFLD and primary biliary cirrhosis (PBC) (11–13, 27). In this study, our findings revealed that the IM was disordered in AIH patients undergoing an active state. These patients had fewer *Bifidobacteria*, *Lactobacillus*, and *Bacteroides* in their intestines, suggesting that these IMs might have a preventive role in the pathogenesis of AIH. These findings were consistent with some of the results of previous studies (7), but part of the difference were that these patients had fewer *Escherichia coli* in their intestines, indicating that *Escherichia coli* might have a negative effect in the pathogenesis of AIH. Conflicting results might be due to the uncontrolled effects of factors, such as environment and eating habits. Moreover, these inconsistencies are partly due to the methodological issues that include variations in sample size and use of different techniques for the determination of the IM composition. In addition, recent studies have reported that *C. leptum* were a risk factor for the

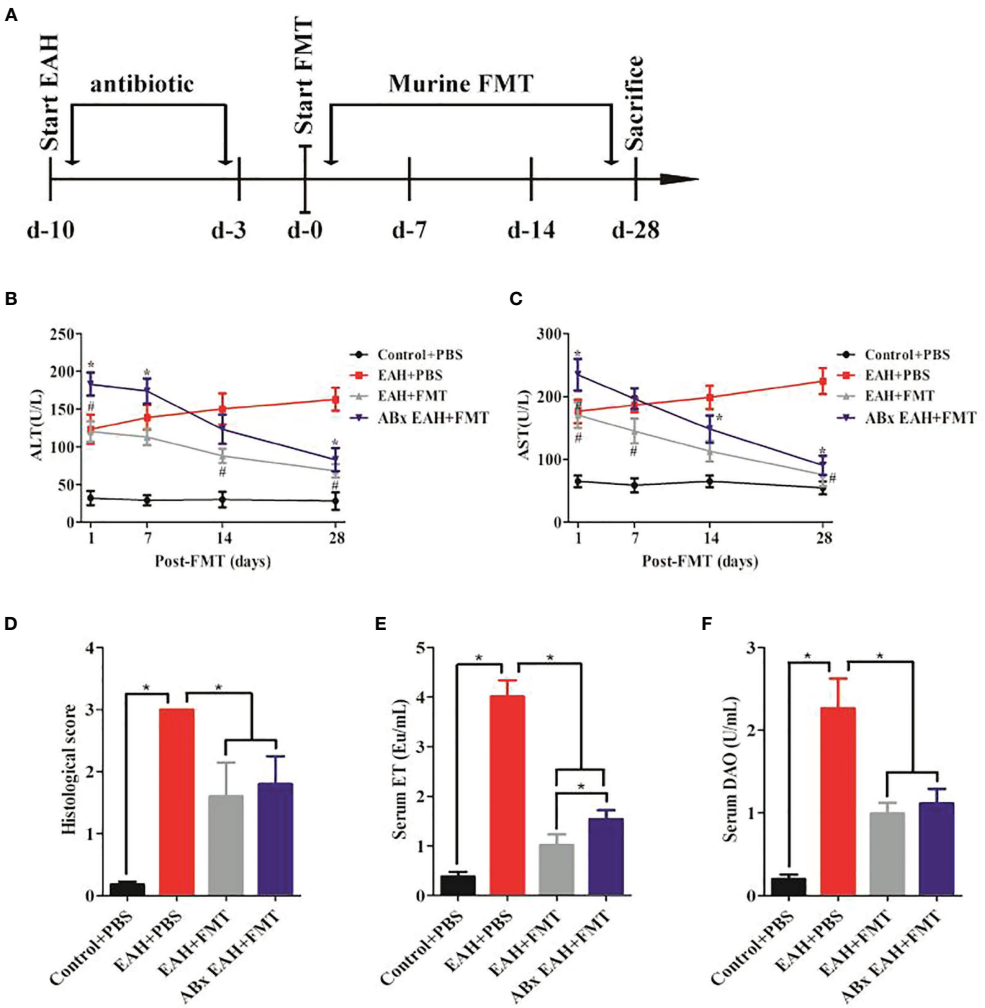


FIGURE 3 | FMT attenuated liver injury and bacterial translocation. **(A)** Experimental setup. Secondary EAH mice harboring dysbiosis (ABx) mice were generated by broad-spectrum antibiotic treatment for 7 days. Three days before FMT, the antibiotic cocktail was replaced by sterile tap water to guarantee antibiotic washout. ABx EAH mice were then subjected to FMT on 28 consecutive days; **(B, C)** serum ALT/AST levels; **(D)** histological score of liver lesions; **(E)** serum ET levels; **(F)** serum DAO levels. The horizontal lines indicate the mean values of the different groups. *$p < 0.05$.

development of various autoimmune diseases, such as pulmonary immunosuppression (28) and inflammatory bowel disease (29). However, the role of *C. leptum* in AIH is still unclear. Hence, we further found lower levels of *C. leptum* in the intestines of AIH patients, indicating that their absence might be related to the pathogenesis of AIH. More importantly, consistent with previous studies (7), our data showed a high expression level of serum LPS, which are a hallmark of bacterial translocation (30), suggesting that bacteria-derived LPS translocated into the bloodstream may contribute to the progression of liver damage and fibrosis (31). Taken together, these findings support the concept that AIH might be associated with IM dysbiosis and translocation of gut-derived microbial products into the systemic circulation.

Our previous study that established an experimental EAH model in mice with S100/FCA revealed obvious liver injury evidenced by liver edema with a rising liver index and elevated serum levels of ALT, AST, and TBIL similar to that observed in human AIH (5, 6). Furthermore, our study showed that TFR and TFH cells, which were important for the maintenance of immune tolerance (32), were dysregulated in EAH mice, which was consistent with our previous studies that imbalance of TFR-to-TFH ratios promoted the pathogenesis of EAH (6). More notably, IM dysbiosis by broad-spectrum antibiotic treatment resulted in more severe liver injury and TFR/TFH imbalance in EAH mice, which further confirmed previous findings that IM disorders might play an important role in the pathogenesis of AIH (7). Therefore, the reconstruction of IM balance through administration of FMT may be a potential treatment for AIH.

In this study, we found that the onset of AIH may be also related to IM alterations. In addition, the "gut–liver axis" was widely described in various chronic liver diseases, including AIH

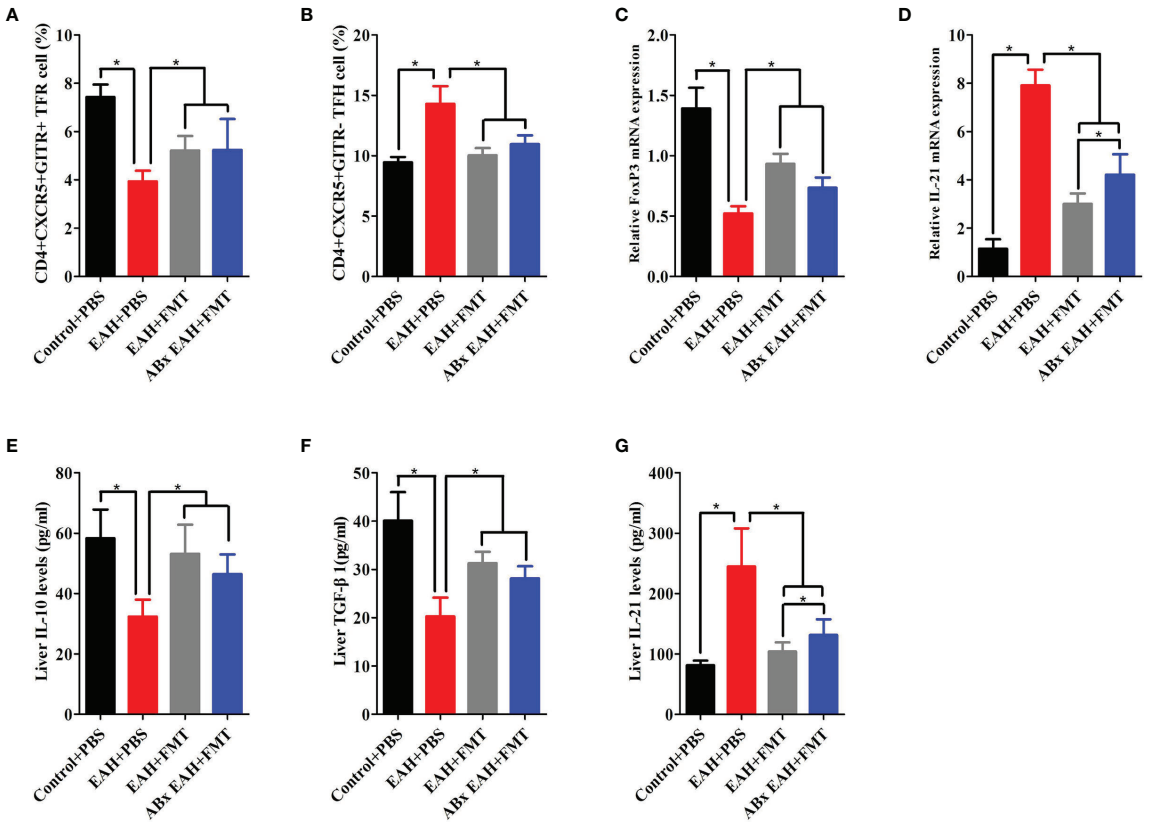


FIGURE 4 | FMT-regulated TFR/TFH cell imbalances. Fifteen mice (five from the EAH group, five from the ABxEAH group, and five from the control group) were killed at each time point (1, 7, 14, and 28 days) after therapeutic FMT. **(A, B)** Percentages of TFR and TFH cells in SMNCs on the 28th day were analyzed. **(C, D)** The mRNA levels of FoxP3 and IL-21 on the 28th day were analyzed. **(E–G)** Liver IL-10, TGF-β, and IL-21 levels on the 28th day were analyzed. The horizontal lines indicate the mean values of the different groups. *$p < 0.05$.

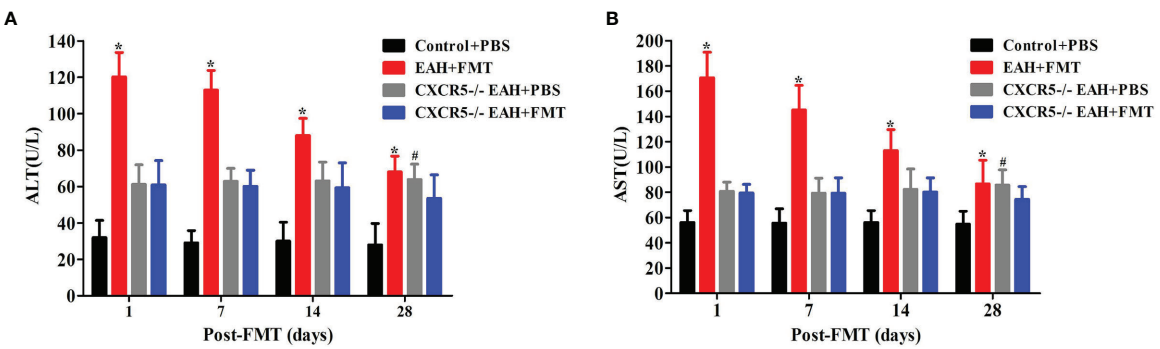


FIGURE 5 | FMT attenuated liver injury *in CXCR5–/–EAH mice*. **(A, B)** Serum ALT/AST levels progressively downregulated from 1 to 28 days in EAH and CXCR5–/–EAH mice after therapeutic FMT. The horizontal lines indicate the mean values of the different groups. *$p < 0.05$ vs. control+PBS/CXCR5–/–EAH+PBS/CXCR5–/–EAH+FMT; #$p < 0.05$ vs. control+PBS/CXCR5–/–EAH+FMT.

(10). Therefore, these studies supported this concept that FMT might be a promising treatment for AIH. Here, we found that histological score of liver lesions were altered in EAH mice, and serum levels of AST and ALT in EAH mice with and without antibiotics were restored upon therapeutic FMT. Moreover, the serum ET and DAO, which are hallmarks of bacterial translocation (30, 33), were also similarly improved in EAH mice upon therapeutic FMT. Taken together, our results

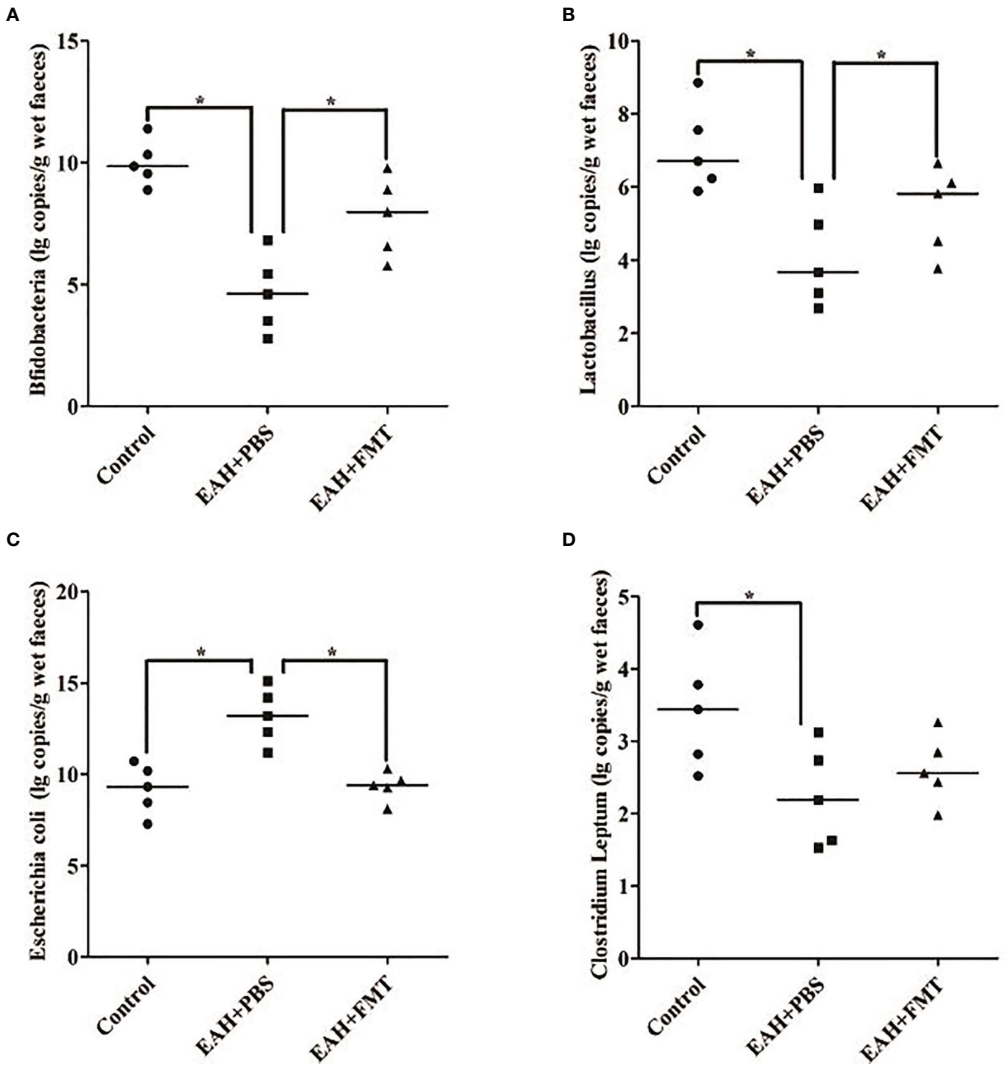


FIGURE 6 | FMT restored antibiotic-induced IM dysbiosis. Fecal samples on the 28th day of untreated and FMT-treated EAH mice are analyzed by the real-time PCR method. **(A)** Amounts of fecal *Bifidobacteria*; **(B)** amounts of fecal *Lactobacillus*; **(C)** amounts of fecal *Escherichia coli*; **(D)** amounts of fecal *Clostridium leptum*. The horizontal lines indicate the mean values of the different groups. *$p < 0.05$.

suggested a potential role of FMT in the amelioration of hepatic inflammatory indexes and protection of gut barrier integrity in the development of AIH.

Given that TFR/TFH cell disorder might promote the progress of AIH (6), we found that ABx EAH mice treated with broad-spectrum antibiotics exacerbated the TFR/TFH imbalance. This possible underlying mechanism of microbiota change to TFR/TFH balance is attributed to the fact that elevated LPS, a metabolite of intestinal flora, activates Toll-like receptor 4 (TLR4)/MyD88 signaling pathway, which leads to the inhibition of TFR cells and the activation of TFH cells (25). We further set out to evaluate the effect of FMT on TFR/TFH cell balance in EAH mice. Our data demonstrated dynamically elevated TFR cells and decreased TFH cells in EAH mice with and without antibiotics, indicating that the restore of IM dysbiosis induced by FMT positively promoted immune tolerance through induction of TFR cell and suppression of TFH cell. Subsequently, we employed CXCR5-deficient mice to assess whether the role of FMT in controlling hepatitis progression was achieved by regulating TFR/TFH cell balance and found that FMT was able to improve liver inflammation in CXCR5-deficient EAH mice but later than EAH mice. Collectively, our findings indicated that FMT might control hepatitis progression by regulating TFR/TFH cell balance, but it was not entirely dependent on this pathway.

Next, we found changes in the levels of *Bifidobacterium*, *Lactobacillus*, *Escherichia coli*, and *Clostridium leptum* in EAH mice, which more closely resembles the clinical features observed in AIH patients (5, 6). These findings provide strong evidence supporting the correlation between IM dysbiosis and AIH (7). However, their dysbiosis in EAH mice were partially restored

upon therapeutic FMT, indicating that FMT might be beneficial to reconstruct the composition of the intestinal flora in EAH mice.

Taken together, the presented data described the IM dysbiosis in AIH patients. In addition, our study also showed that FMT might control hepatitis progression by reversing TFR/TFH cell disorders and restoring the antibiotic-induced IM dysbiosis in EAH mice. These data revealed important information that FMT might be an effective method for the treatment of AIH. However, we recognized the limitations of our study, such as a relative small sample size, variable of water content in individual stools, and the lack of mechanism research of FMT regulating TFR/TFH cell balance in the pathogenesis of AIH. Hence, we are interested in further exploring the aggregate mechanism of FMT regulating TFR/TFH cell balance in the pathogenesis of AIH with a bigger population.

DATA AVAILABILITY STATEMENT

The datasets presented in this study can be found in online repositories. The names of the repository/repositories and accession number(s) can be found in the article/supplementary material.

ETHICS STATEMENT

The studies involving human participants were reviewed and approved by the Department of Medical Examination Center of the First People's Hospital of Changzhou. The patients/participants provided their written informed consent to participate in this study. The animal study was reviewed and approved by the Ethical Committee of the First People's Hospital of Changzhou.

AUTHOR CONTRIBUTIONS

ML, ZL, and SJ contributed equally to this work. CJ and ZL designed the experiments and analyzed data. ML wrote the main manuscript text. ML, ZY, and DJ performed the experiments and prepared the figures. WC provided samples. SJ and DF provided conceptual and technical advices. All authors contributed to the article and approved the submitted version.

FUNDING

This study was supported by grants from the Changzhou Sci&Tech Program (Grant Nos. CZQM2020011 and CZQM2020079), Natural Science Foundation of Xinjiang Uygur Autonomous Region (2021D01F64), Xinjiang Kirgiz Autonomous Prefecture Medical and Health Technology Project (Grant Nos. 39 and 41), the National Natural Science Foundation of China (Nos. 81700500 and 81700575), the Applied Basic Research Programs of Science, Technology Department of Changzhou City (CJ20160031, CJ20190095 and CJ20210109), the Research Project of Jiangsu Province Commission of Health and Family Planning (No. H201547), the Major Scientific and Technological Project of Changzhou City Commission of Health and Family Planning (No. ZD201612), and the Scientific and Technological Project of Nanjing medical University (No. 2017NJMU042).

ACKNOWLEDGMENTS

We thank WC and the staff of the animal research facility of the Suzhou University for excellent technical assistance and animal breeding.

REFERENCES

1. Heneghan MA, Yeoman AD, Verma S, Smith AD, Longhi MS. Autoimmune Hepatitis. *Lancet* (2013) 382:1433–44. doi: 10.1016/S0140-6736(12)62163-1
2. Oliveira LC, Porta G, Marin ML, Bittencourt PL, Kalil J, Goldberg AC. Autoimmune Hepatitis, HLA and Extended Haplotypes. *Autoimmun Rev* (2011) 10:189–93. doi: 10.1016/j.autrev.2010.09.024
3. Podhorzer A, Paladino N, Cuarterolo ML, Fainboim HA, Paz S, Theiler G, et al. The Early Onset of Type 1 Autoimmune Hepatitis has a Strong Genetic Influence: Role of HLA and KIR Genes. *Genes Immun* (2016) 17:187–92. doi: 10.1038/gene.2016.7
4. Ma L, Qin JJ, Ji HF, Zhao PW and Jiang YF. Tfh and Plasma Cells are Correlated With Hypergamaglobulinaemia in Patients With Autoimmune Hepatitis. *Liver Int* (2013) 34:405–15. doi: 10.1111/liv.12245
5. Ma L, Zhang L, Zhuang Y, Ding Y, Chen J-P. Exploration the Significance of Tfh and Related Molecules on C57BL/6 Mice Model of Experimental Autoimmune Hepatitis. *J Microbiol Immunol Infect* (2019) 54:221–7. doi: 10.1016/j.jmii.2019.06.007
6. Ma L, Zhang L, Dai J, Zhuang Y, Ding Y, Chen J. Dysregulated TFR and TFH Cells Correlate With B Cell Differentiation and Antibody Production in Autoimmune Hepatitis. *J Cell Mol Med* (2020) 24:3948–57. doi: 10.1111/jcmm.14997
7. Rui L, Lu Z, Jie Z, Bangmao W. Abnormal Intestinal Permeability and Microbiota in Patients With Autoimmune Hepatitis. *Int J Clin Exp Pathol* (2015) 8:5153–60. doi: 10.1007/s003840050236
8. Czaja AJ. Factoring the Intestinal Microbiome Into the Pathogenesis of Autoimmune Hepatitis. *World J Gastroenterol* (2016) 22:9257–78. doi: 10.3748/wjg.v22.i42.9257
9. Wangfeng C, Ying R, Li Y, Bangmao W, Lu Z. Intestinal Microbiome and Permeability in Patients With Autoimmune Hepatitis. *Best Pract Res Clin Gastroenterol* (2017) 31:669–73. doi: 10.1016/j.bpg.2017.09.013
10. Jinlu W, Jiayun Z, Ende H, Dazhi C, Lu C, Fengbin L, et al. Sodium Butyrate Ameliorates S100/FCA-Induced Autoimmune Hepatitis Through Regulation of Intestinal Tight Junction and Toll-Like Receptor 4 Signaling Pathway. *Immunol Lett* (2017) 190:169–76. doi: 10.1016/j.imlet.2017.08.005
11. Brandi G, De Lorenzo S, Candela M, Pantaleo MA, Bellentani S, Tovoli F, et al. Microbiota, NASH, HCC and the Potential Role of Probiotics. *Carcinog* (2017) 38:231–40. doi: 10.1093/carcin/bgx007
12. Saltzman ET, Palacios T, Thomsen M, Vitetta L. Intestinal Microbiome Shifts, Dysbiosis, Inflammation, and Non-Alcoholic Fatty Liver Disease. *Front Microbiol* (2018) 9:61. doi: 10.3389/fmicb.2018.00061
13. Schnabl B, Brenner DA. Interactions Between the Intestinal Microbiome and Liver Diseases. *Gastroenterol* (2014) 146:1513–24. doi: 10.1053/j.gastro.2014.01.020
14. Wei Y, Zeng B, Chen J, Cui G, Lu C, Wu W, et al. Enterogenous Bacterial Glycolipids are Required for the Generation of Natural Killer T Cells Mediated Liver Injury. *Sci Rep* (2016) 6:36365. doi: 10.1038/srep36365
15. Chapman RW, Aspinall RJ, Trivedi P, Wright G, Heneghan M. Challenges in the Use of Corticosteroids in the Management of Autoimmune Hepatitis. *Br J Hosp Med (Lond)* (2019) 80:594–9. doi: 10.12968/hmed.2019.80.10.594

16. Czaja. Diagnosis AJ. And Management of Autoimmune Hepatitis: Current Status and Future Directions. *Gut Liver* (2016) 10:177–203. doi: 10.5009/gnl15352
17. Sciveres M, Nastasio S, Maggiore G. Novel Diagnostic and Therapeutic Strategies in Juvenile Autoimmune Hepatitis. *Front Pediatr* (2019) 7:382. doi: 10.3389/fped.2019.00382
18. Yadav V, Varum F, Bravo R, Furrer E, Bojic D, Basit Abdul W. Inflammatory Bowel Disease: Exploring Gut Pathophysiology for Novel Therapeutic Targets. *Transl Res* (2016) 176:38–68. doi: 10.1016/j.trsl.2016.04.009
19. Li D, Wang P, Wang P, Hu X, Chen F. The Gut Microbiota: A Treasure for Human Health. *Biotechnol Adv* (2016) 34:1210–24. doi: 10.1016/j.biotechadv.2016.08.003
20. Van NE, Speelman P, Kuijper EJ, Keller JJ. Struggling With Recurrent Clostridium Difficile Infections: Is Donor Faeces the Solution? *Euro Surveill* (2009) 14:19316. doi: 10.2807/ese.14.34.19316-en
21. De Groot PF, Frissen MN, de Clercq NC, Nieuwdorp M. Fecal Microbiota Transplantation in Metabolic Syndrome: History, Present and Future. *Gut Microbes* (2017) 8:253–67. doi: 10.1080/19490976.2017.1293224
22. Chen H-T, Huang H-L, Xu H-M, Luo Q-L, He J, Li Y-Q, et al. Fecal Microbiota Transplantation Ameliorates Active Ulcerative Colitis. *Exp Ther Med* (2020) 19:2650–60. doi: 10.3892/etm.2020.8512
23. Xu M-Q, Cao H-L, Wang W-Q, Wang S, Cao X-C, Yan F, et al. Fecal Microbiota Transplantation Broadening its Application Beyond Intestinal Disorders. *World J Gastroenterol* (2015) 21:102–11. doi: 10.3748/wjg.v21.i1.102
24. Li M, Li W, Wen S, Liu Y, Tang L. Effects of Ceftriaxone-Induced Intestinal Dysbacteriosis on Dendritic Cells of Small Intestine in Mice. *Microbiol Immunol* (2013) 57:561–8. doi: 10.1016/j.intimp.2018.05.003
25. Levy M, Kolodziejczyk AA, Thaiss CA, Elinav E. Dysbiosis and the Immune System. *Nat Rev Immunol* (2017) 17:219–32. doi: 10.1038/nri.2017.7
26. Hevia A, Milani C, Lopez P, Cuervo A, Arboleya S, Duranti S. Intestinal Dysbiosis Associated With Systemic Lupus Erythematosus. *Mbio* (2014) 5:1514–48. doi: 10.1128/mBio.01548-14
27. Lemoinne S, Kemgang A, Ben BK, Straube M, Jegou S, Corpechot C, et al. Fungi Participate in the Dysbiosis of Gut Microbiota in Patients With Primary Sclerosing Cholangitis. *Gut* (2020) 69:92–102. doi: 10.1136/gutjnl-2018-317791
28. Huang F, Qiao H, Yin J, Gao Y, Ju Y, Li Y. Early-Life Exposure to Clostridium Leptum Causes Pulmonary Immunosuppression. *PloS One* (2015) 10(11): e0141717. doi: 10.1371/journal.pone.0141717
29. Jayakanthan K, Vijayalakshmi S, Srinivasan P, Balakrishnan SR. Clostridium Leptum Group Bacteria Abundance and Diversity in the Fecal Microbiota of Patients With Inflammatory Bowel Disease: A Case-Control Study in India. *Int J Clin Exp Pathol* (2013) 109(3):201–7. doi: 10.1186/1471-230X-13-20
30. Othman M, Aguero R, Lin HC. Alterations in Intestinal Microbial Flora and Human Disease. *Curr Opin Gastroenterol* (2008) 24:11–6. doi: 10.1097/mog.0b013e3282f2b0d7
31. Gabbard SL, Lacy BE, Levine GM, Crowell MD. The Impact of Alcohol Consumption and Cholecystectomy on Small Intestinal Bacterial Overgrowth. *Dig Dis Sci* (2014) 59:638–44. doi: 10.1007/s10620-013-2960-y
32. Sage PT, Sharpe AH. T Follicular Regulatory Cells in the Regulation of B Cell Responses. *Trends Immunol* (2015) 36:410–8. doi: 10.1016/j.it.2015.05.005
33. Tsunooka N, Maeyama K, Nakagawa H, Doi T, Horiuchi A, Katsutoshi M, et al. Localization and Changes of Diamine Oxidase During Cardiopulmonary Bypass in Rabbits. *J Surg Res* (2006) 131:58–63. doi: 10.1016/j.jss.2005.10.004

Conflict of Interest: The authors declare that the research was conducted in the absence of any commercial or financial relationships that could be construed as a potential conflict of interest.

Publisher's Note: All claims expressed in this article are solely those of the authors and do not necessarily represent those of their affiliated organizations, or those of the publisher, the editors and the reviewers. Any product that may be evaluated in this article, or claim that may be made by its manufacturer, is not guaranteed or endorsed by the publisher.

Copyright © 2021 Liang, Liwen, Jianguo, Juan, Fei, Yin, Changping and Jianping. This is an open-access article distributed under the terms of the Creative Commons Attribution License (CC BY). The use, distribution or reproduction in other forums is permitted, provided the original author(s) and the copyright owner(s) are credited and that the original publication in this journal is cited, in accordance with accepted academic practice. No use, distribution or reproduction is permitted which does not comply with these terms.

frontiers in Microbiology

ORIGINAL RESEARCH
published: 01 December 2021
doi: 10.3389/fmicb.2021.745299

Lacticaseibacillus casei Strain T21 Attenuates *Clostridioides difficile* Infection in a Murine Model Through Reduction of Inflammation and Gut Dysbiosis With Decreased Toxin Lethality and Enhanced Mucin Production

Wimonrat Panpetch[1], Pornpimol Phuengmaung[1], Thanya Cheibchalard[2], Naraporn Somboonna[2,3], Asada Leelahavanichkul[1,4*†] and Somying Tumwasorn[1,3*†]

[1] Department of Microbiology, Faculty of Medicine, Chulalongkorn University, Bangkok, Thailand, [2] Department of Microbiology, Faculty of Science, Chulalongkorn University, Bangkok, Thailand, [3] Microbiome Research Unit for Probiotics in Food and Cosmetics, Chulalongkorn University, Bangkok, Thailand, [4] Department of Microbiology, Faculty of Medicine, Center of Excellence in Immunology and Immune-Mediated Diseases, Bangkok, Thailand

Clostridioides difficile is a major cause of diarrhea in patients with antibiotic administration. *Lacticaseibacillus casei* T21, isolated from a human gastric biopsy, was tested in a murine *C. difficile* infection (CDI) model and colonic epithelial cells (Caco-2 and HT-29). Daily administration of *L. casei* T21 [1 × 10^8 colony forming units (CFU)/dose] for 4 days starting at 1 day before *C. difficile* challenge attenuated CDI as demonstrated by a reduction in mortality rate, weight loss, diarrhea, gut leakage, gut dysbiosis, intestinal pathology changes, and levels of pro-inflammatory cytokines [interleukin (IL)-1β, tumor necrosis factor (TNF)-α, macrophage inflammatory protein 2 (MIP-2), and keratinocyte chemoattractant (KC)] in the intestinal tissue and serum. Conditioned media from *L. casei* T21 exerted biological activities that fight against *C. difficile* as demonstrated in colonic epithelial cells by the following: (i) suppression of gene expression and production of IL-8, an important chemokine involved in *C. difficile* pathogenesis, (ii) reduction in the expression of *SLC11A1* (solute carrier family 11 member 1) and *HuR* (human antigen R), important genes for the lethality of *C. difficile* toxin B, (iii) augmentation of intestinal integrity, and (iv) up-regulation of *MUC2*, a mucosal protective gene. These results supported the therapeutic potential of *L. casei* T21 for CDI and the need for further study on the intervention capabilities of CDI.

Keywords: *Lacticaseibacillus casei* T21, probiotics, proinflammatory cytokines, *Clostridioides difficile*, gut dysbiosis, inflammation, toxin lethality

OPEN ACCESS

Edited by:
Axel Cloeckaert, Institut National de Recherche pour l'Agriculture, l'Alimentation et l'Environnement (INRAE), France

Reviewed by:
Marjorie Pizarro-Guajardo, Texas A&M University, United States
Maria de los Angeles Serradell, Consejo Nacional de Investigaciones Científicas y Técnicas (CONICET), Argentina

****Correspondence:***
Asada Leelahavanichkul
aleelahavanit@gmail.com
Somying Tumwasorn
somying.T@chula.ac.th

† These authors have contributed equally to this work

Specialty section:
This article was submitted to Infectious Agents and Disease, a section of the journal Frontiers in Microbiology

Received: *21 July 2021*
Accepted: *02 November 2021*
Published: *01 December 2021*

Citation:
Panpetch W, Phuengmaung P, Cheibchalard T, Somboonna N, Leelahavanichkul A and Tumwasorn S (2021) Lacticaseibacillus casei Strain T21 Attenuates Clostridioides difficile Infection in a Murine Model Through Reduction of Inflammation and Gut Dysbiosis With Decreased Toxin Lethality and Enhanced Mucin Production. Front. Microbiol. 12:745299. doi: 10.3389/fmicb.2021.745299

INTRODUCTION

Clostridioides difficile, an anaerobic Gram-positive spore-forming bacillus (Kachrimanidou and Malisiovas, 2011), is one of the important causative organisms of diarrhea in hospitalized patients who receive antibiotics (Kelly et al., 1994b; Bartlett, 2002; Aslam et al., 2005). Clinical symptoms of *C. difficile* infection (CDI) vary from mild diarrhea (usually self-limited) to pseudomembranous colitis with severe sepsis (Mylonakis et al., 2001) and/or toxic megacolon (Kuehne et al., 2011). The pathogenesis of CDI is associated with antibiotic-induced gut dysbiosis that facilitates *C. difficile* colonization and toxin production (Mooyottu et al., 2017). Two protein exotoxins referred to as toxin A (TcdA) and toxin B (TcdB) are the major virulence factors contributing to CDI (Lyerly et al., 1988; Voth and Ballard, 2005; Kuehne et al., 2011). Binding of TcdA and TcdB to specific receptors on the surface of intestinal epithelial cells stimulates the secretion of several pro-inflammatory cytokines and chemokines (Hodges and Gill, 2010). Both toxins cause the loss of intestinal epithelial barrier function (gut leakage) by glucosylating Rho GTPases, which causes actin cytoskeleton rearrangement, tight junction disruption, and enterocyte cell death (Pothoulakis, 2000; Aktories and Barbieri, 2005; Jank and Aktories, 2008; Kuehne et al., 2011; Chen et al., 2015). In addition, binary toxin (*C. difficile* transferase, CDT) is observed in some *C. difficile* strains that cause severe CDI. This toxin is an ADP-ribosyltransferase that causes depolymerization of F-actin and rearrangement of the actin cytoskeleton (Gerding et al., 2014; Aktories et al., 2018).

The pathogenic effects of TcdA and TcdB have been studied extensively. Epithelial cells demonstrate a decrease in transepithelial electrical resistance (TEER) and an increase in paracellular permeability after toxin activation, indicating that *C. difficile* toxins disrupt gut tight junctions (Hecht et al., 1988; Nusrat et al., 2001; Zemljic et al., 2010). Toxin-activated intestinal epithelial chemotactic mediators, such as interleukin (IL)-8, cause an accumulation of neutrophils and lymphocytes (inflammatory colitis) and other clinical signs of infectious diarrhea (such as white blood cell in feces) (Viswanathan et al., 2009; Sun et al., 2010). CDI not only causes local intestinal inflammation but also induces systemic inflammation from gut leakage-induced bacteremia. Disruption of gut tight junctions also allows for the transfer of intestinal contents, including TcdA and TcdB from *C. difficile*, into the circulation, resulting in the activation of various immune cells in the bloodstream (Viswanathan et al., 2009; Sun et al., 2010). Subsequently, the activated immune cells systemically secrete several pro-inflammatory cytokines, which lead to systemic inflammatory responses and sepsis. In addition to bacterial factors, host factors also contribute to the severity of CDI. Notably, a previous report identified solute carrier family 11 member 1 gene (*SLC11A1*), which enhances TcdB lethality by the increased Rho GTPase glucosylation, and the suppression of *SLC11A1* resulted in reduced toxin sensitivity. In addition, the up-regulation of *SLC11A1* requires the RNA-binding protein HuR or human antigen R (encoded in *HuR)* to stabilize the mRNA (Feng and Cohen, 2013).

Probiotics are live microorganisms that, when administered in adequate amounts, confer a health benefit on the host (FAO and WHO, 2001; Hill et al., 2014). Probiotics have been a popular approach for the prevention and improvement of treatment efficacy of human diseases. Several meta-analyses suggest that probiotics, mainly *Lactobacillus*, are effective for preventing *C. difficile*-associated diarrhea (Ritchie and Romanuk, 2012; Goldenberg et al., 2017; Shen et al., 2017). It has been suggested that probiotic administration counteracts gut dysbiosis caused by antibiotics or infections (Reid et al., 2011), resulting in the restoration of gut microbiota diversity, which plays a crucial role in the prevention of CDI (Kachrimanidou and Tsintarakis, 2020). Specific strains of *Lactobacillus* spp. effectively inhibit the pathogenicity of *C. difficile* both *in vitro* (Banerjee et al., 2009; Trejo et al., 2010; Spinler et al., 2017) and *in vivo* (Leelahavanichkul et al., 2016) and secrete several anti-inflammatory substances that attenuate enterocyte injury from several insults (Boonma et al., 2014; Panpetch et al., 2016, 2018).

Despite a variety of probiotics, we speculated that indigenous probiotic strains derived from a specific population might be more suitable for a specific ethnic group. Accordingly, *Lacticaseibacillus casei* (formerly *Lactobacillus casei*) strain T21 isolated from a human gastric biopsy might be suitable for use as a probiotic for populations in Southeast Asia. An investigation of the effect of *L. casei* T21 on *C. difficile* infection in a mouse model and in colonic epithelial cells was conducted.

MATERIALS AND METHODS

Bacterial Strains and Culture Conditions

L. casei strain T21 was obtained from the stock culture of the Department of Microbiology, Faculty of Medicine, Chulalongkorn University. Bacterial stock culture was maintained in deMan Rogosa Sharpe (MRS) broth (Oxoid, Hampshire, United Kingdom) containing 20% (vol/vol) glycerol at −80°C. *L. casei* T21 was cultured on MRS agar under anaerobic conditions using gas generation sachets (Anaero Pack-Anaero, Mitsubishi Gas Chemical, Japan) at 37°C for 48 h. *C. difficile* ATCC BAA1870 (ATCC, Manassas, VA, United States) was cultured anaerobically on Brucella agar (Becton Dickinson, France) supplemented with 5% (vol/vol) sheep blood at 37°C for 48 h.

C. difficile Infection Mouse Model and *L. casei* T21 Intervention

The experimental protocol in accordance with the US National Institutes of Health standards (NIH publication no. 85–23, revised 1985) was approved by the Institutional Animal Care and Use Committee of the Faculty of Medicine, Chulalongkorn University (SST006/2560). Male 8-week-old C57BL/6 mice were purchased from the Nomura Siam International Co., Ltd. (Lumphini, Pathumwan, Bangkok, Thailand). CDI mouse model as previously developed (Chen et al., 2008) and recently published (Panpetch et al., 2019) was performed with modifications. Briefly, 500 μL of the antibiotic cocktail (Sigma-Aldrich, St. Louis, MO, United States) containing gentamicin (3.5 mg/kg), colistin

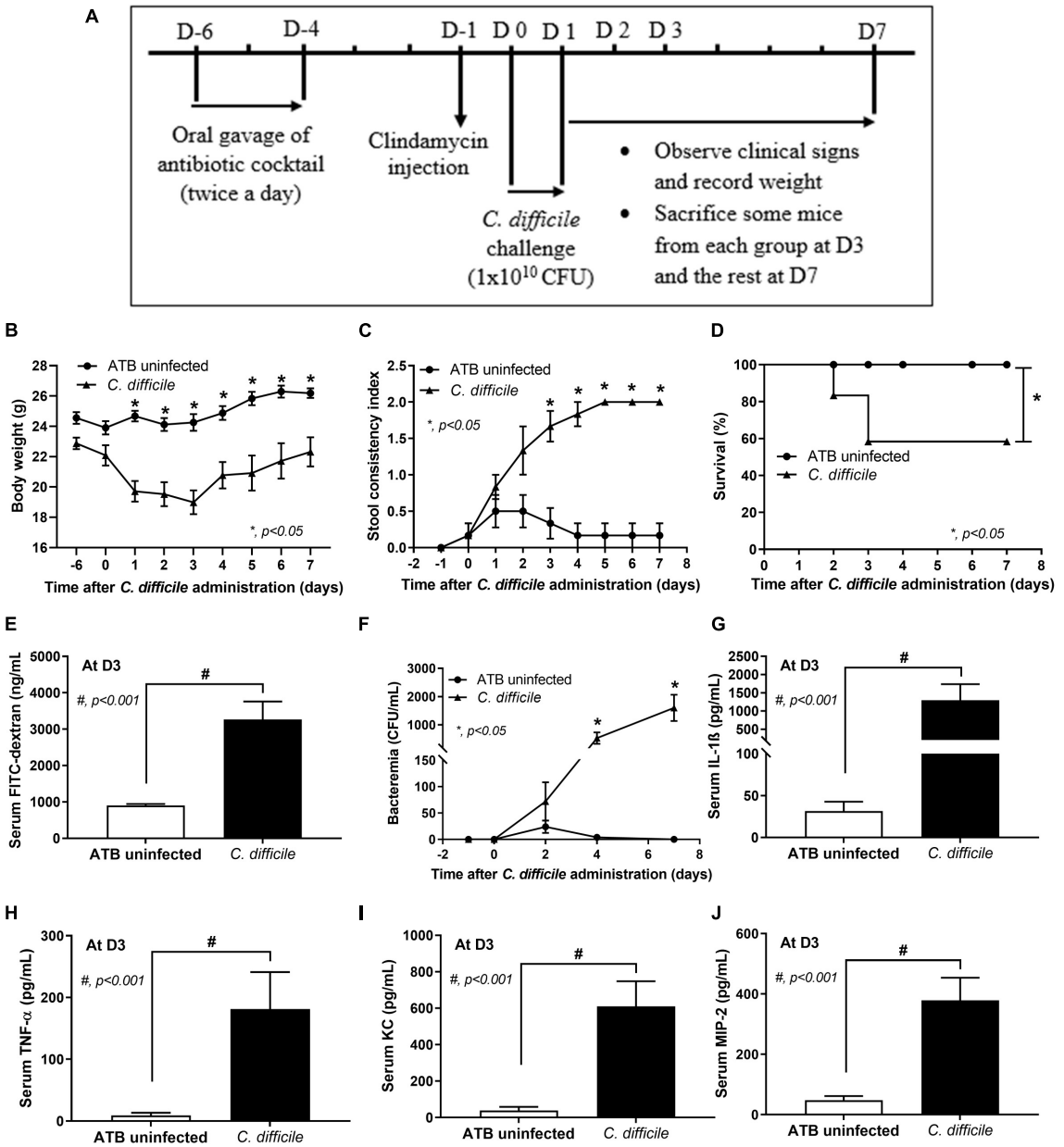


FIGURE 1 | Murine model of *C. difficile* infection. Mice in the antibiotic-administered uninfected group (ATB uninfected group; $n = 12$) and *C. difficile*-infected group (*C. difficile* group; $n = 24$) were used in the experiment as in the schematic presentation **(A)**. The severity of *C. difficile* infection in mice is manifested by weight loss (n = number of mice/group or survivors) **(B)**; stool consistency index (n = number of mice/group or survivors) **(C)**; survival rate **(D)**; bacteremia (n = number of mice/group or survivors) **(E)**; gut leakage by serum FITC-dextran assay monitored at day 3 ($n = 8$) **(F)**; and levels of serum pro-inflammatory cytokines IL-1β **(G)**, TNF-α **(H)**, KC **(I)**, and MIP-2 **(J)** at day 3 ($n = 8$). $^{*}p < 0.05$; $^{\#}p < 0.001$. FITC, fluorescein isothiocyanate; IL, interleukin; TNF, tumor necrosis factor; KC, keratinocyte chemoattractant; MIP-2, macrophage inflammatory protein 2.

(4.2 mg/kg), metronidazole (21.5 mg/kg), and vancomycin (4.5 mg/kg) was administered by oral gavage twice a day from day −6 to day −4 before *C. difficile* infection (D-6–D-4) (**Figure 1A**). Mice were free from antibiotic administration for 2 days and received an intraperitoneal injection of a single dose of clindamycin (10 mg/kg) at 1 day before infection (D-1). After the treatment with antibiotics (ATB), mice were gavaged with either 0.5 ml of normal saline solution (NSS) in the ATB-administered uninfected group (ATB uninfected group; $n = 12$) or 1×10^{10} colony forming units (CFU) of *C. difficile* vegetative cells in 0.5 ml of NSS once daily for 2 days (D0 and D1) in the *C. difficile* group ($n = 24$). Mice were observed and monitored daily for weight, stool consistency, and survival until D7. Blood was collected through tail vein nicking for enumeration of bacteria at D2, D4, and D7. According to our pilot study, *C. difficile*-infected mice developed severe symptoms

for 3 days, some succumbed to infection, and the survivors gradually recovered from CDI. At D3, mice from each group (n = 8) were then tested for gut leakage and sacrificed with cardiac puncture under isoflurane anesthesia for determining CDI severity by using serum pro-inflammatory cytokines as markers. The stool consistency was semi-quantitatively evaluated using the following scoring; 0, normal; 1, soft or loose; and 2, diarrhea, as previously published (Kim et al., 2012).

For *Lacticaseibacillus* treatment in the CDI mouse model, mice were randomly divided into three groups: ATB uninfected group (n = 18), *C. difficile*-infected mice treated with NSS (NSS group; n = 24), and *C. difficile*-infected mice treated with *L. casei* T21 (T21 group; n = 20), which received 1×10^8 CFU of *L. casei* T21 in 0.5 ml of NSS once daily for 4 days from D-1 (started at 6 h after clindamycin injection), D0 and D1 (together with *C. difficile*), and D2 (**Figure 2A**). Mice were observed and monitored daily until D7 as described above. Feces were collected for microbiome analysis at D-6 for baseline and D-1 (before clindamycin injection and gavage with *L. casei* T21) as time of post-ATB administration. At D3, some mice from each group (n = 8) were tested for gut leakage and sacrificed for determining the parameters of CDI severity. Blood samples and cecal and ascending colonic tissues were collected for the assessment of cytokine levels, which represented systemic and local inflammation, respectively. Cecal and ascending colonic tissues were also used for histopathologic evaluation, while luminal content including feces in the cecum and colon were used for quantitation of *C. difficile* and microbiome analysis. All mice were sacrificed on D7 at the end of experiment.

Mouse Sample Analysis

The pro-inflammatory cytokines as previously described (Leffler and Lamont, 2015), including IL-1β, tumor necrosis factor (TNF)-α, macrophage inflammatory protein 2 (MIP-2), and keratinocyte chemoattractant (KC), in serum and homogenized tissue of the cecum and colon were measured by an enzyme-linked immunosorbent assay (ELISA) (PeproTech, NJ, United States). For determining tissue pro-inflammatory cytokines, tissue samples (approximately 100 mg) were weighed and homogenized using an Ultra-Turrax homogenizer (IKA, Staufen, Germany) in 500 μL of phosphate-buffered saline (PBS, pH 7.4) containing protease inhibitor and centrifuged at 12,000 × g for 15 min at 4°C to separate the supernatant for analysis.

For quantitation of *C. difficile* in luminal content including feces, quantitative real-time polymerase chain reaction (qPCR) was performed as previously published (Panpetch et al., 2019). Briefly, genomic DNA of *C. difficile* was extracted from cecum and colon contents using the High Pure PCR Template Preparation Kit (Roche, NJ, United States), quantified by NanoDrop™ 1000 Spectrophotometer (Thermo Fisher Scientific, Inc., United States), and amplified with *tcdB* (*C. difficile* toxin B) primers (forward, 5′-GGAAAAGAGAATGGTTTTATTAA-3′ and reverse, 5′-ATC TTTAGTTATAACTTTGACATCTTT-3′) as previously described (Lemee et al., 2004) in the QuantStudio 5 Real-Time PCR System (Thermo Fisher Scientific, Inc., United States) using the QuantiNova® SYBR® Green PCR Kit (QIAGEN, Hilden, Germany). The standard curve was created by using 10-fold serially diluted plasmids containing 1–10^9 copies of *tcdB*. The number of *C. difficile* was calculated using the standard curve and shown as bacterial copy number.

Histopathological analysis was performed by fixing the sample in 10% buffered formalin, embedding in paraffin, sectioning, and staining with hematoxylin and eosin (H&E) before grading (score 0–4) as previously published (Reeves et al., 2011; Erikstrup et al., 2015) based upon epithelial damage, edema, and cellular infiltration by two pathologists in a blinded manner.

Microbiome Analysis

Gut microbiota composition was determined as previously reported (Panpetch et al., 2020). Feces collected at D-6 as baseline, D-1 as time of post-ATB administration, and luminal content including feces at D3 as time of sacrifice were used for microbiome analysis. Briefly, fecal samples or luminal content (0.25 g/mouse; three mice/group) were extracted for total DNA with the DNeasy PowerSoil Kit (Qiagen GmbH, Hilden, Germany). The quality and concentration of the extracted DNA were monitored by agarose gel electrophoresis and NanoDrop spectrophotometry. Libraries of the V4 hypervariable region of 16S rRNA gene were amplified by PCR using primers 515F (forward; 5′-GTGCCAGCMGCCGCGGTAA-3′) and 806R (reverse; 5′-GGACTACHVGGGTWTCTAAT-3′), modified with the Illumina adapter and Golay barcode sequences as previously described (Caporaso et al., 2012). PCR was run in triplicate, and the products from the triplicate reactions were pooled and visualized on agarose gel. Amplicons of approximately 381 base pairs were purified by PureDireX PCR Clean-Up & Gel Extraction Kit (BIO-HELIX Co., Ltd., Keelung City, Taiwan) and quantified using PicoGreen fluorescence with the Qubit dsDNA HS assay kit (Invitrogen, Eugene, OR, United States). The amplicon pool was sequenced with the Illumina MiSeq300 platform (Illumina, San Diego, CA, United States) (Caporaso et al., 2012). Sequences were analyzed with Mothur version 1.3 (Schloss et al., 2009). Briefly, quality filtering and trimming were performed to remove low-quality bases and short reads from the raw sequences. Quality-filtered sequences were then aligned to each other and binned into operational taxonomic units (OTUs) with a minimum of 97% similarity. Each representative OTU sequence was compared to the SILVA rDNA sequence database (version 1.32) and assigned a taxonomical annotation. Alpha diversity (total OTUs, Chao1 index, and Shannon diversity) and beta diversity (non-metric multidimensional scaling) were calculated using Mothur (Schloss et al., 2009). The 16S rDNA sequences in this study were deposited in an NCBI open access Sequence Read Archive database with accession number SRP336496.

Gut Leakage Measurement and Enumeration of Bacteria in the Blood

Intestinal epithelial permeability defect (gut leakage) was determined using a single oral administration of 12.5 mg fluorescein isothiocyanate–dextran (FITC-dextran; molecular

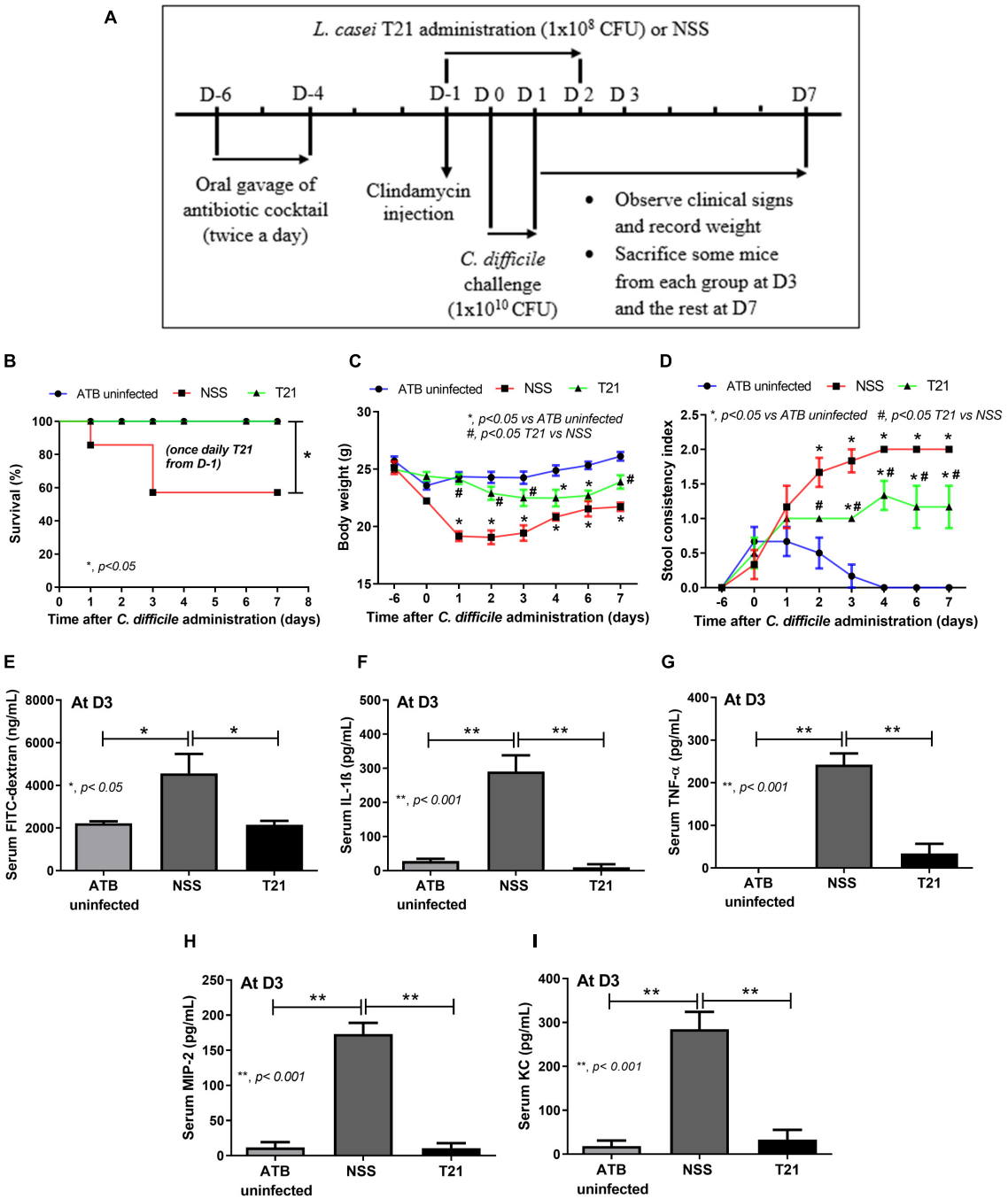


FIGURE 2 | *Lacticaseibacillus casei* T21 effectively attenuated *C. difficile*-induced severity in mice. Mice were randomly assigned to three groups: ATB uninfected group (n = 18), NSS group (n = 24), and T21 group (n = 20) as described in the text and used in the experiment **(A)**. The reduction of severity was demonstrated by survival rate **(B)**; body weight (n = number of mice/group or survivors) **(C)**; stool consistency index (n = number of mice/group or survivors) **(D)**; gut leakage by serum FITC-dextran assay monitored at day 3 (n = 8) **(E)**; and levels of serum pro-inflammatory cytokines IL-1β **(F)**, TNF-α **(G)**, MIP-2 **(H)**, and KC **(I)** at day 3 (n = 8). $^{*}p < 0.05$; $^{**}p < 0.001$; $^{\#}p < 0.05$.

weight 4.4 kDa) (Sigma-Aldrich, St. Louis, MO, United States), a non-intestinal-absorbable marker, before the determination in serum at 3 h later as previously described (Leelahavanichkul et al., 2016; Panpetch et al., 2018). Serum FITC-dextran was measured by the fluorospectrometry (Thermo Fisher Scientific, Wilmington, DE, United States) with the excitation and emission wavelengths at 485 and 523 nm, respectively, against a standard curve of serially diluted FITC-dextran. For the enumeration of live bacteria, blood (25 μL) was collected through tail vein nicking and spread directly onto blood agar (Oxoid, Hampshire,

United Kingdom) and incubated at 37°C for 24 h before counting bacterial colonies.

The Immunomodulatory Effect of *L. casei* T21 on *C. difficile*-Stimulated Colonic Epithelial Cells

The conditioned medium of *L. casei* T21 was tested for immunomodulation of IL-8 production in colonic epithelial cell lines as previously described (Panpetch et al., 2016, 2018). In brief, *Lacticaseibacillus*-conditioned medium (LCM) was prepared by growing *L. casei* T21 with an OD_{600} of 0.1 in MRS broth anaerobically for 48 h. The supernatant was collected and subjected to filtration with a 0.22-μm membrane (Minisart, Sartorius Stedim Biotech GmbH, Goettingen, Germany), concentrated by speed vacuum drying, resuspended in cell culture medium with equal volume, and stored at −20°C until use. In parallel, human colonic epithelial cell lines Caco-2 (ATCC HTB-37) and HT-29 (ATCC HTB-38) were maintained (5×10^4 cells/well) in supplemented Dulbecco's Modified Eagle Medium (DMEM) and McCoy's 5A modified medium, respectively. Colonic epithelial cells were then incubated with viable cells of *C. difficile* ATCC BAA1870 at multiplicity of infection (MOI) 1:300 either alone or with 5% (vol/vol) LCM for 24 h in 5% CO_2 at 37°C. Subsequently, the supernatant was collected by centrifugation ($125 \times g$, 4°C for 7 min), and the levels of IL-8 were measured by using a Human CXCL8/IL-8 ELISA kit (R&D Systems, Minneapolis, MN) according to the manufacturer's instructions.

In addition, colonic epithelial cells at 2 and 4 h from the incubation time were collected for performing quantitative reverse transcription-polymerase chain reaction (qRT-PCR) as previously described (Panpetch et al., 2018). In short, the total RNA of treated colonic epithelial cells was extracted by TRIzol reagent (Invitrogen, United States), prepared for complementary DNA (cDNA) from total RNA (50 ng) by SuperScript® VILO™ cDNA Synthesis Kit (Invitrogen), and subjected to qPCR measurement in a QuantStudio™ Design & Analysis Software v1.4.3 (Thermo Fisher Scientific) with the following primers: IL-8 (forward 5′-ACACTGCGCCAACACAGAAATTA-3′, reverse 5′-ACACTGCGCCAACACAGAAATTA-3′) and human glyceraldehyde-3-phosphate dehydrogenase (GAPDH) (forward 5′-GCACCGTCAAGGCTGAGAAC-3′, reverse 5′-ATGGTGGTGAAGACGCCAGT-3′) (Imaoka et al., 2008; Panpetch et al., 2016). The expression of *IL-8* relative to *GAPDH* was calculated according to the $2^{-\Delta\Delta Cp}$ method (Pfaffl, 2001).

The Effect of *L. casei* T21 on the Expression of *SLC11A1, HuR, and MUC2 in C. difficile*-Stimulated Colonic Epithelial Cells

The conditioned medium of *L. casei* T21 was tested for its effect on the expression of *C. difficile*-activated host genes *SLC11A1*, *HuR*, and *MUC2* by using qRT-PCR as described above with the following primers: SLC11A1 (forward 5′-CTGGACGAATCCCACTCTGG-3′, reverse 5′-CGCGCCACCACATACTCAT-3′), HuR (forward 5′-GCTTGGGCTATGGCTTTGTGAACT-3′, reverse 5′-CGCTG ATGTACAAGTTGGCGTCTT-3′) (Feng and Cohen, 2013), and mucin2 (MUC2) (forward 5′-CCTGCCGACACCTGCTGCAA-3′, reverse 5′-ACACCAGTAGAAGGGACAGCACCT-3′) (Xue et al., 2014). In parallel, the pH of cell culture medium was measured at multiple time points using a pH meter (Orion 4-star, Benchtop pH/Conductivity, Thermo Fisher Scientific).

The Effect of *L. casei* T21 on Transepithelial Electrical Resistance of Caco-2 Cells

TEER was performed according to a previous report (Gao et al., 2017). In short, Caco-2 cells (ATCC HTB-37) at 5×10^4 cells per well were seeded onto the upper compartment of a 24-well Boyden chamber transwell using high-glucose DMEM supplemented with 20% fetal bovine serum (FBS), 1% HEPES, 1% sodium pyruvate, and 1.3% penicillin/streptomycin under 5% CO_2 at 37°C for 15 days with daily medium replacement to establish the confluent monolayer. The cells were then treated with 5% (vol/vol) LCM of *L. casei* T21 or medium alone together with viable *C. difficile* cells (5×10^6 CFU/well) with MOI at 1:100 for 24 h. Next, TEER was measured by an EMOM^2 Epithelial Volt/Ohm Meter with a chopstick electrode (World Precision Instruments, Inc., Sarasota, United States) that was placed at a 90° angle with one tip in supernatant at the basolateral chamber and another tip at the apical chamber. The TEER value in control media without cells was used as a baseline subtracted from all measurements. The value of TEER was reported as ohm (Ω) × cm^2.

Statistical Analysis

Mean ± standard error of mean (SEM) was used for data presentation. The difference between groups was examined for statistical significance by one-way analysis of variance (ANOVA) followed by Tukey's analysis or unpaired *t* tests for comparisons of multiple groups or two groups, respectively. Survival analysis was performed by log-rank test. All statistical analyses were performed with GraphPad Prism version 9.0 software (La Jolla, CA, United States). A p-value of < 0.05 was considered statistically significant.

RESULTS

Disease Progression and Severity of Murine *C. difficile* Infection Model

In the CDI murine model (**Figure 1A**), *C. difficile*-infected mice began to develop CDI symptoms such as weight loss and soft stool on day 1 after the first oral gavage with *C. difficile* on day 0. After the second oral gavage on day 1, CDI symptoms became worse on day 2, and mice were moribund on day 3 with maximum weight loss (**Figure 1B**) and significant diarrhea (loose stools) as compared with the ATB uninfected group (**Figure 1C**). By day 3, 41.67% (10/24) of mice succumbed to infection (58.33% survival rate) (**Figure 1D**). Eight mice were

sacrificed on day 3, and the remaining six mice gradually gained weight while still having diarrhea and surviving until the end of the experiment (**Figures 1B,C**). Additionally, *C. difficile* damaged intestinal integrity as demonstrated by the increased serum FITC-dextran levels (**Figure 1E**), causing gut leakage-induced bacteremia (**Figure 1F**) that enhanced the production of systemic inflammatory cytokines (serum IL-1β, TNF-α, KC, and MIP-2 levels as markers) (**Figures 1G–J**). In contrast, mice in the ATB uninfected group demonstrated loose stools for a few days (days 1–3) without weight loss, death, gut leakage, bacteremia, or systemic inflammation (**Figures 1B–J**).

L. casei Strain T21 Reduced Mortality, Clinical Symptoms, and Disease Severity of *C. difficile*-Infected Mice

For the treatment of *L. casei* T21 in the murine model of CDI, *C. difficile*-infected mice in the T21 group received 1×10^8 CFU of *L. casei* T21 once daily for 4 days (D-1–D-2), whereas infected mice in the NSS group received NSS (**Figure 2A**). All mice in the T21 and the ATB uninfected group survived, while only 54.17% (13/24) of the NSS group survived by day 3 (**Figure 2B**). Compared to the NSS group, the T21 group had significantly lesser weight loss (except at days 4 and 5) (**Figure 2C**) and diarrhea (**Figure 2D**), which were monitored for 7 days. The average weight at each day (except at days 4 and 5) between the T21 group and the ATB uninfected group showed no significant difference (**Figure 2C**). However, mice in the T21 group still had soft stool with a stool consistency index significantly different from the ATB uninfected group (**Figure 2D**). Treatment with T21 also reduced gut leakage and systemic inflammation. The T21 group had significantly decreased levels of FITC-dextran (**Figure 2E**) and pro-inflammatory cytokines IL-1β, TNF-α, MIP-2, and KC in sera (**Figures 2F–I**). Likewise, *L. casei* T21 also attenuated intestinal injury in the cecum and colon as evaluated by histopathology (**Figures 3A,B**) and reduced the levels of pro-inflammatory cytokines in the intestinal tissue (**Figures 3C–F**). Notably, *C. difficile*-infected mice without T21 treatment (NSS group) demonstrated several characteristics of severe intestinal injury, including loss of villi, villous edema, numerous neutrophil infiltration (**Figure 3A**), and neutrophils in feces (data not shown). In addition, T21 treatment reduced the abundance of *C. difficile* in the intestinal content. The analysis of luminal content including feces by q-PCR of the *tcdB* gene demonstrated that the T21 group had significantly decreased copies compared to the NSS group (**Figure 3G**). Moreover, the absence of the *tcdB* gene in the ATB uninfected mice (**Figure 3G**) revealed the reliability of the experiment.

L. casei T21 Slightly Attenuated Gut Dysbiosis in *C. difficile*-Infected Mice

Gut dysbiosis of the model was evaluated by a fecal microbiome analysis of mice in the ATB uninfected, NSS, and T21 groups at multiple time points. Alpha diversity measures used in this study included total OTUs (the simplest measure of richness), Chao1 (a measure of richness that gives more weight to rare taxon), and Shannon (a measure of richness and evenness). Antibiotic cocktail treatment significantly reduced the diversity of fecal bacteria as the values of the total OTUs (**Figure 4A**) and Chao1 index (**Figure 4B**) were significantly lower in all groups of mice at post-ATB compared to baseline. After clindamycin injection, antibiotic-induced dysbiosis worsened at day 3 of the experiment as determined by total OTUs (**Figure 4A**), but not by Chao1 index (**Figure 4B**). *C. difficile* infection did not lead to a significant decrease of bacterial diversity as demonstrated by total OTUs (**Figure 4A**) and Chao1 index (**Figure 4B**). Surprisingly, T21 treatment did not increase the diversity of fecal bacteria as the values of total OTUs (**Figure 4A**) and Chao1 index (**Figure 4B**) of the NSS and T21 groups were not significantly different. The T21 group did show an increased Chao1 index, although the value was not significantly different from that of the NSS group. The values of Chao1 index were also not significantly different in the T21 and ATB uninfected groups (**Figure 4B**). Notably, the bacterial diversity in all groups of mice at day 3, post-ATB, and baseline was not significantly different as determined by the Shannon index (**Figure 4C**). To examine the beta diversity, non-metric multidimensional scaling (NMDS) based on Thetayc dissimilarity was performed. The NMDS (**Figure 4D**) demonstrated similar results in all groups at baseline (D-6) (blue-colored symbols at the upper left quadrant) and at post-ATB (D-1) (red-colored symbols at the lower right quadrant). In contrast, there were some differences at D3 from the experiments between groups of mice with or without *L. casei* T21 (green-colored symbols of the NSS and T21 groups), suggesting a possible impact of *L. casei* T21 on gut microbiota. The ATB uninfected and T21 groups showed similar results.

To characterize the microbiome composition in each group of mice, the relative taxa abundances at each time point were compared. The gut microbiome of mice at baseline was predominated by Bacteriodetes, followed by Firmicutes and Proteobacteria, as shown by the average relative abundances of microbiota at the phylum level in each group of mice (**Figure 5A**) and the relative abundances of Bacteroidetes (**Figure 5D**), Firmicutes (**Figure 5E**), and Proteobacteria (**Figure 5F**) at each time point. In contrast, antibiotic cocktail treatment induced a significant decrease in the relative abundance of Bacteriodetes and Firmicutes and a significant increase in the abundance of Proteobacteria and Verrucomicrobia at D-1 (**Figures 5A,D–G**). Antibiotic pre-conditioning of the model thus caused fecal dysbiosis as indicated by a decrease in Firmicutes and Bacteroidetes together with an increase in Proteobacteria and Verrucomicrobia. By day 3, microbiota composition at the phylum level almost turned to the baseline without T21 treatment. The relative abundance of Bacteroidetes (**Figure 5D**), Firmicutes (**Figure 5E**), and Verrucomicrobia (**Figure 5G**) in the ATB uninfected group and the NSS group was not significantly different from the baseline, whereas the abundance of Proteobacteria was still significantly different from the baseline (**Figure 5F**). *L. casei* T21 treatment led to an increase in the relative abundance of Firmicutes in the T21 group with a significant difference compared to post-ATB, but not from the NSS group (**Figure 5E**). In addition, T21 treatment resulted in a significant decrease in the relative abundance of Verrucomicrobia in the T21 group compared

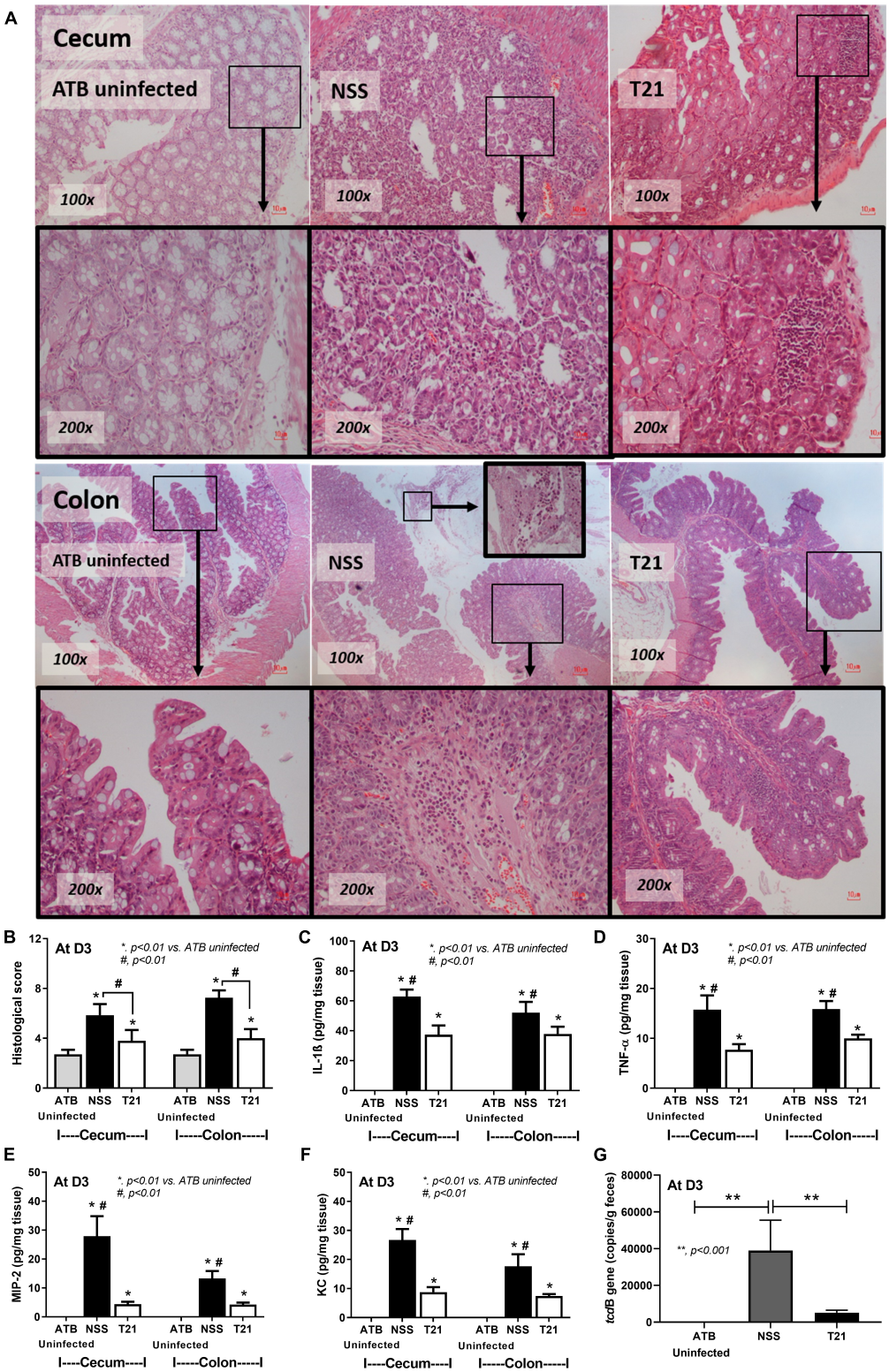


FIGURE 3 | *Lacticaseibacillus casei* T21 attenuated *C. difficile*-induced cecal and colonic tissue damage. Three groups of mice (n = 8 for each group) as described in **Figure 2** were sacrificed at day 3 and examined for histopathology and local inflammation. Representative image of hematoxylin and eosin (H&E) staining sections **(A)**, histological scores **(B)**, and levels of intestinal pro-inflammatory cytokines **(C–F)** are shown. The copy number of *tcdB*, which represents *C. difficile* abundance in each group of mice, is demonstrated **(G)**. $^{*}p < 0.01$; $^{**}p < 0.001$; $^{\#}p < 0.01$.

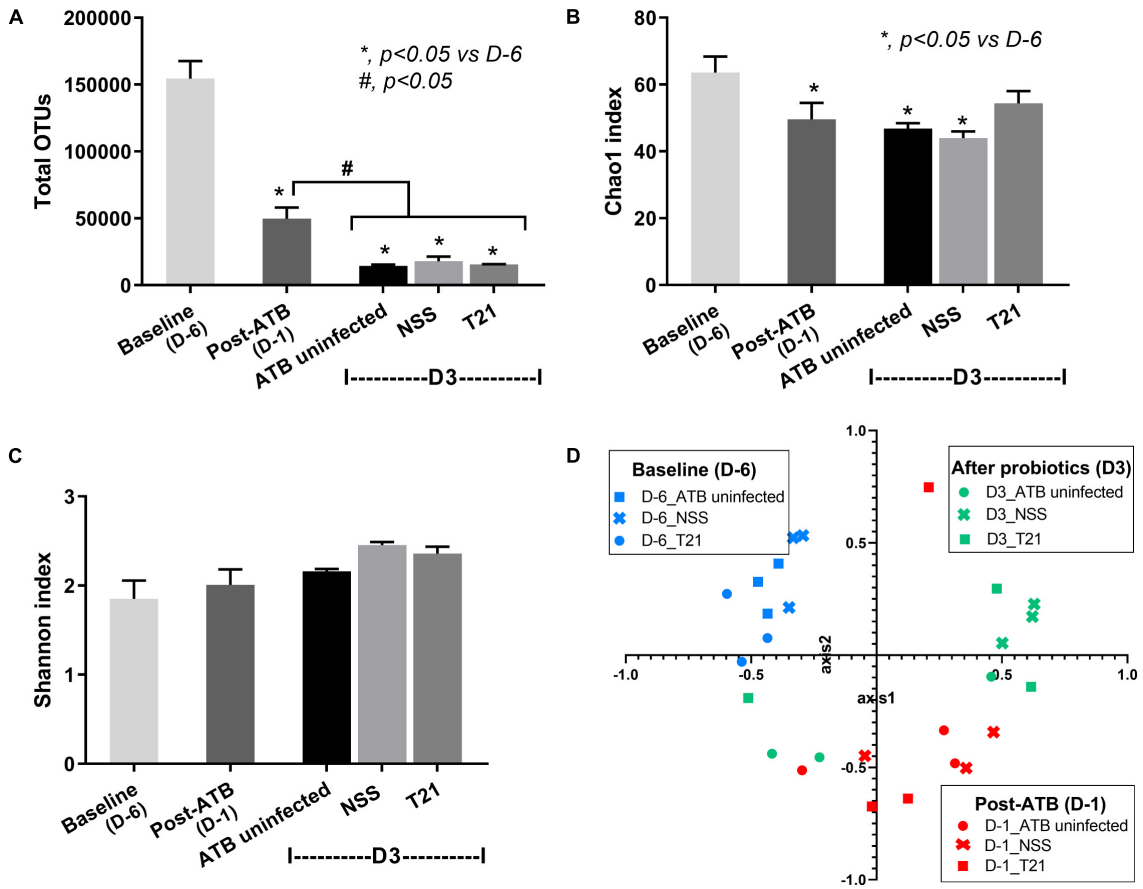


FIGURE 4 | Diversity of gut microbiota in each group of mice at multiple time points. Fecal microbiome data of the ATB uninfected, NSS, and T21 groups (n = 3/group) at baseline, post-ATB, and at sacrifice were calculated for microbial diversity and presented as total operational taxonomic units (OTUs) **(A)**, Chao1 index **(B)**, Shannon index **(C)**, and the non-metric multidimensional scaling (NMDS) based on Thetayc dissimilarity **(D)**. Independent triplicate experiments were performed. $^{*}p < 0.05$ vs. D-6, $^{\#}p < 0.05$.

to the NSS group and post-ATB, and the abundance of Verrucomicrobia in the T21 group was not significantly different from the baseline (**Figure 5G**). Although the relative abundance of Proteobacteria in the T21 group significantly decreased compared to post-ATB, this change also occurred in the NSS group (**Figure 5F**).

The analysis of microbiome at the lower taxon levels (class, order, family, genus, and species) was performed. The average relative abundances of microbiota at baseline, post-ATB, and among groups of mice at sacrifice (day 3) are shown at the class level (**Figure 5B**) and the genus level (**Figure 5C**). There were significant changes in class Clostridia (**Figure 5H**) and family *Enterobacteriaceae* (**Figure 5I**) in the T21 group at sacrifice (D3) as compared with mice at post-ATB. Although the NSS group had changes in the relative abundance of these taxa as compared with mice at post-ATB, the differences were not statistically significant. Microorganisms of interest in class Clostridia (phylum Firmicutes) were the families *Lachnospiraceae* and *Ruminococcaceae* (**Figure 5C**) that have been reported to protect *C. difficile* colonization (Reeves et al., 2012; Lee et al., 2017). The relative abundances of the family *Lachnospiraceae* (**Figure 5J**) were not significantly different among the ATB uninfected, the NSS, and the T21 groups, while there was a slight increase in the abundance of the family *Ruminococcaceae* in the T21 group compared to the NSS group, although the difference was not statistically significant (**Figure 5K**). The relative abundances of other taxa (at the class and genus levels) were also not significantly different among these groups of mice at sacrifice (data not shown). Data on the relative abundances of microbiota from individual mouse are shown at the levels of phylum (**Supplementary Figure 1**), class (**Supplementary Figure 2**), and genus (**Supplementary Figure 3**) in **Supplementary Material**.

L. casei T21 Suppressed IL-8 Production, Modulated Host Gene Expression, and Increased Transepithelial Electrical Resistance of *C. difficile*-Activated Colonic Epithelial Cells

Probiotic bacteria, such as *Lactobacillus* spp., have been reported to produce biologically active compounds that can suppress

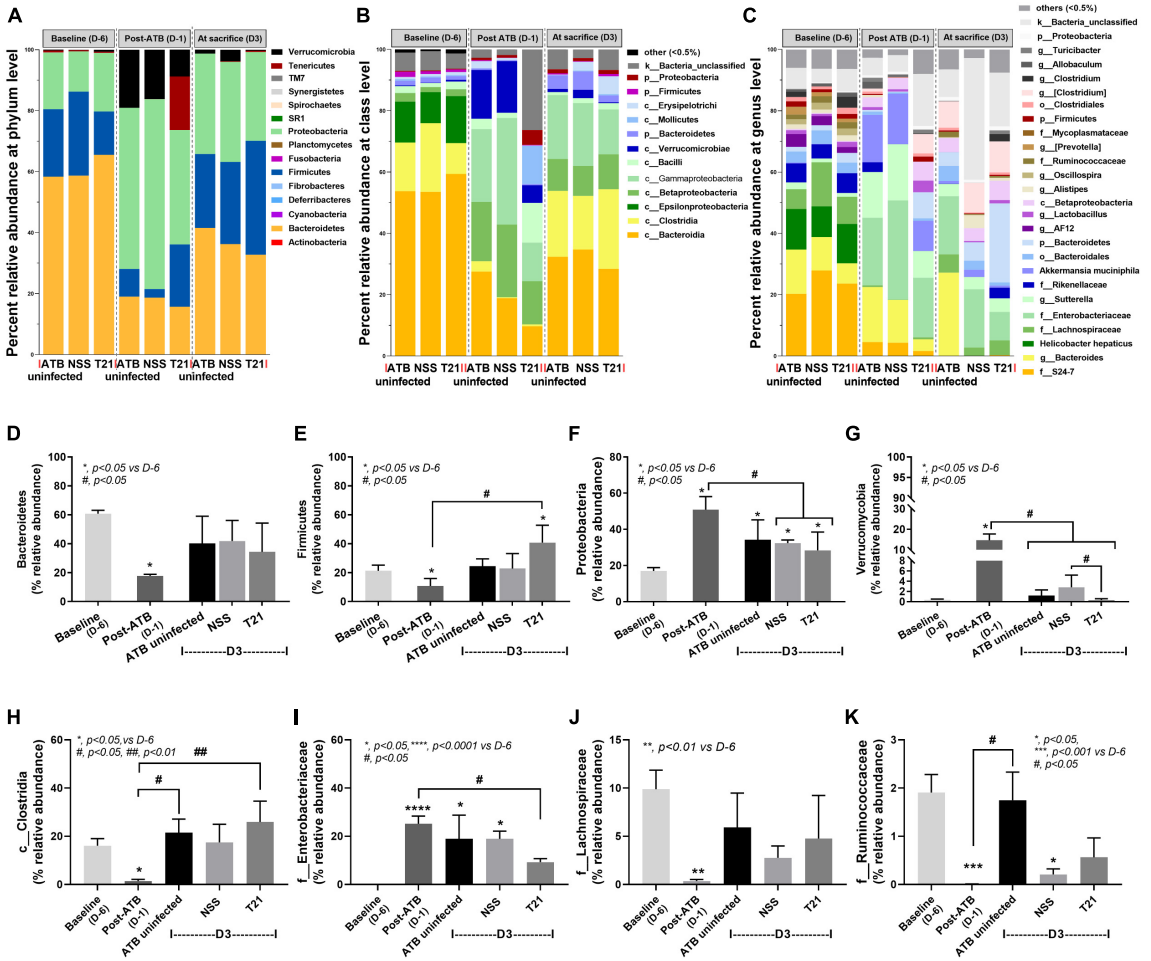


FIGURE 5 | *Lacticaseibacillus casei* T21 slightly attenuated gut dysbiosis in *C. difficile*-infected mice. Gut dysbiosis of the *C. difficile* infection (CDI) model was evaluated by fecal microbiome analysis of mice in the ATB uninfected, NSS, and T21 groups at multiple time points. The average relative abundances of microbiota at the phylum level **(A)**, class level **(B)**, and genus level **(C)** are demonstrated. The average relative abundances of individual taxon are shown: Bacteroidetes **(D)**, Firmicutes **(E)**, Proteobacteria **(F)**, Verrucomicrobia **(G)**, Clostridia **(H)**, *Enterobacteriaceae* **(I)**, *Lachnospiraceae* **(J)**, and *Ruminococcaceae* **(K)**. Notably, data of all mice at day –6 (D-6) and day –1 (D-1) of the experiments are combined into baseline and post-antibiotic administration (post-ATB), respectively, due to the non-different procedures in these mice. $^{*}p < 0.05$; $^{**}p < 0.01$; $^{***}p < 0.001$; $^{****}p < 0.0001$; $^{\#}p < 0.01$; $^{\#\#}p < 0.01$.

inflammation (Thomas et al., 2012, 2016; Panpetch et al., 2016, 2018). To strengthen the beneficial effects of *L. casei* T21 in the murine model of CDI, the LCM of T21 was tested for its ability to attenuate inflammation and modulate the expression of important host genes involved in the pathogenesis of CDI in colonic epithelial cell lines. The LCM of T21 suppressed the production of IL-8 (**Figures 6A,B**) and down-regulated the expression of *IL-8* (**Figures 6C,D**) in *C. difficile*-stimulated Caco-2 and HT-29 colonic epithelial cells, respectively. In *C. difficile*-stimulated Caco-2 cells, the LCM of T21 down-regulated the expression of associated genes of toxin lethality *SLC11A1* (**Figure 6E**) and *HuR* (**Figure 6F**) while up-regulated a mucosal protective gene *MUC2* (**Figure 6G**). Similar benefits exerted by the LCM of T21 were also demonstrated in HT-29 cells (**Figures 6H–J**). Additionally, the LCM of T21 strengthened mucosal integrity as shown by TEER values in *C. difficile*-stimulated differentiated Caco-2 cells (**Figure 6K**). However, TEER could not be determined in the HT-29 cell line due to limitation in the generation of polarized monolayers (Le Bivic et al., 1988). Since the enhanced mucin production by enterocytes is also influenced by the acidity in gut content (Velcich and Augenlicht, 1993; Shekels et al., 1996), lactic acid produced from *L. casei* T21 might stimulate the up-regulation of *MUC2* expression. To determine whether the up-regulated *MUC2* could be attributable to the acidity, the pH of the cell culture medium (McCoy's 5A modified medium) was measured at multiple time points. The LCM of T21 did not significantly reduce the pH of the cell culture medium at 2 and 4 h after incubation with HT-29 cells as compared to controls (**Figure 6L**). A simple acidification of the cell culture medium with lactic acid also did not upregulate *MUC2* expression (data not shown). This suggested that mucin production was induced by other substances produced by *L. casei* T21.

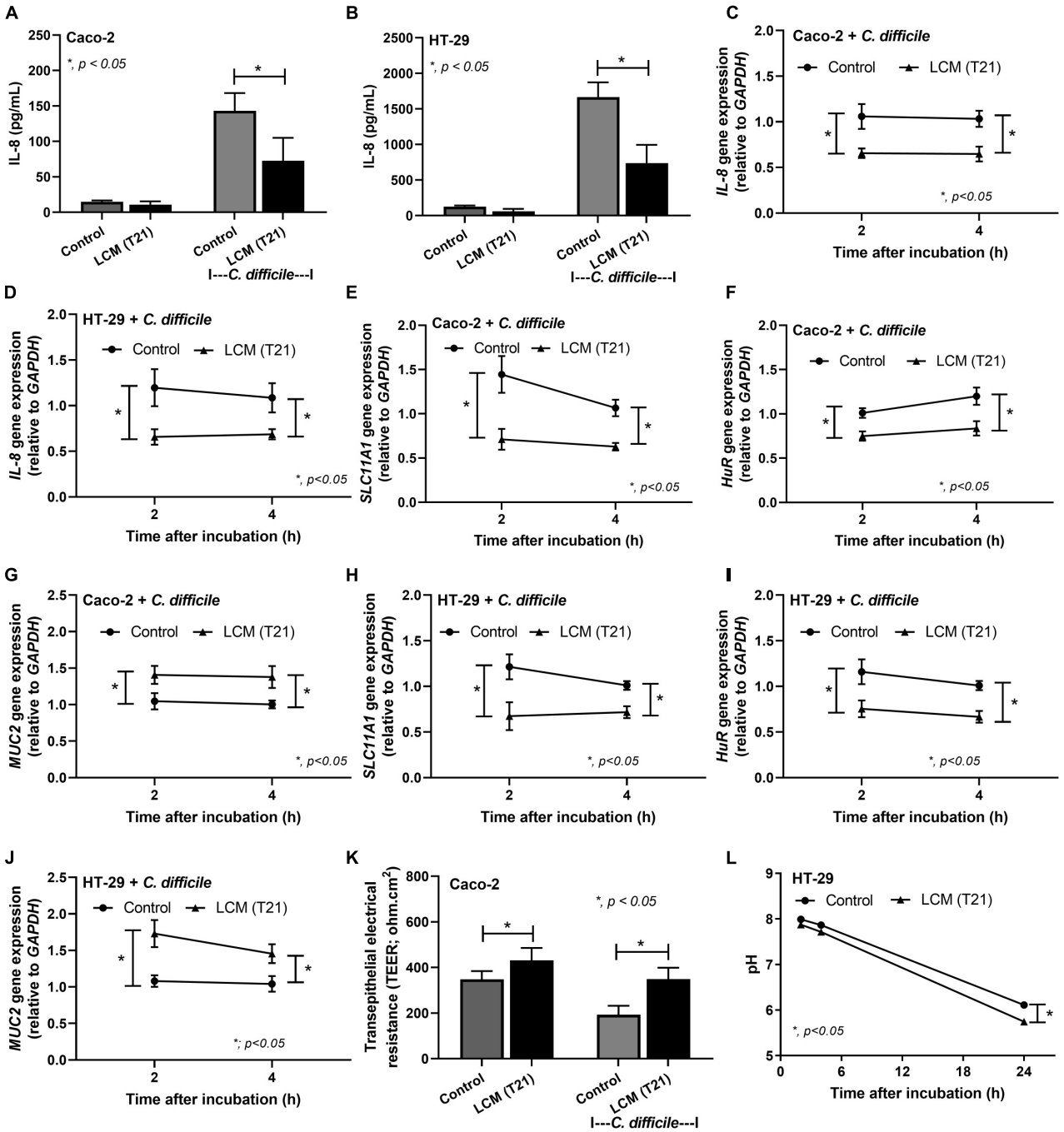


FIGURE 6 | The *Lacticaseibacillus casei*-conditioned medium (LCM) of *L. casei* T21 attenuated *C. difficile*-induced IL-8 production, host gene expression, and increased transepithelial electrical resistance of *C. difficile*-stimulated colonic epithelial cells. The results are shown as IL-8 production in Caco-2 and HT-29 cells, respectively **(A,B)**; IL-8 gene expression (relative to *GAPDH*) in Caco-2 and HT-29 cells, respectively **(C,D)**; the expression of *SLC11A1*, *HuR*, and *MUC-2* in Caco-2 cells, respectively **(E–G)**; the expression of *SLC11A1*, *HuR*, and *MUC-2* in HT-29 cells, respectively **(H–J)**; the transepithelial electrical resistance (TEER) values of Caco-2 cells **(K)**; and the pH of cell culture medium (McCoy's 5A modified medium for HT-29 cells) **(L)**. The results were from three independent experiments each in triplicate and expressed as the mean ± SEM. *$p < 0.05$.

DISCUSSION

In this study, the effect of *L. casei* T21 treatment on CDI was investigated in a murine model of *C. difficile* infection with antibiotic pre-conditioning before *C. difficile* oral gavage. The clinical features of CDI are primarily mediated by TcdA and TcdB, which are the major virulence factors of *C. difficile* (Voth and Ballard, 2005; Sun et al., 2010). Clinical symptoms including

less weight loss and diarrhea in *L. casei* T21-treated mice are correlated with mild intestinal pathology characterized by decreased epithelial damage, edema, and neutrophil infiltration. Due to the importance of intestinal neutrophil accumulation in *C. difficile* pathogenesis, the anti-inflammatory properties of probiotics is of utmost importance for the alleviation of CDI symptoms. Neutrophil infiltration, which leads to the congestion and edema of colonic mucosa and epithelial cell damage (Kelly et al., 1994a; Castagliuolo et al., 1998), results from the stimulation by pro-inflammatory cytokines secreted from *C. difficile* toxin-induced intestinal epithelial cells and immune cells (Kim et al., 2002; Savidge et al., 2003; Sun et al., 2010). Interestingly, *L. casei* T21 administration markedly reduced the levels of IL-1β, TNF-α, MIP-2, and KC (mouse homolog of IL-8) in the colon and cecum of mice as well as in sera. The anti-inflammatory properties of *L. casei* T21was also supported by *in vitro* results that found the conditioned medium of *L. casei* T21 suppressed gene expression and production of IL-8 in *C. difficile*-stimulated colonic epithelial cells Caco-2 and HT-29. Our findings were consistent with other reports showing that the administration of specific strains of probiotics ameliorates intestinal pathology with the reduction in the levels of pro-inflammatory cytokines in tissue and/or sera in animal models of CDI (Koon et al., 2016; Roychowdhury et al., 2018; Wei et al., 2018; Xu et al., 2018). The production of anti-inflammatory substances from lactobacilli is well known (Thomas et al., 2012, 2016; Boonma et al., 2014; Panpetch et al., 2016, 2018), although the nature of the substances varies depending on the strain of probiotic bacteria.

Our microbiome results regarding antibiotic-induced dysbiosis is in agreement with findings from previous reports (Mooyottu et al., 2017; Xu et al., 2018; Li et al., 2019) that showed antibiotic treatment induced a decrease in the dominant bacterial phyla Firmicutes and Bacteroidetes and an increase in phylum Proteobacteria. Although the influence of *L. casei* T21 on gut dysbiosis attenuation was subtle, with an increase in members of phylum Firmicutes (class Clostridia) and a decrease in family *Enterobacteriaceae* (phylum Proteobacteria), the abundance of *C. difficile* in cecum and colon luminal content was decreased as determined by quantitative analysis of *C. difficile* toxin B gene (*tcdB*). Members of class Clostridia, which have been reported to protect *C. difficile* colonization, include the family *Lachnospiraceae* (Reeves et al., 2012; Lee et al., 2017) and the family *Ruminococcaceae* (Lee et al., 2017; Li et al., 2019). However, our results showed only a slight increase in *Ruminococcaceae* in mice treated with *L. casei* T21. We speculate that members of class Clostridia either alone or in combination might mediate colonization resistance against *C. difficile*.

Since *C. difficile* toxins are mainly responsible for the pathogenesis of CDI, an interference in toxin effect might be another mechanism to be considered for *C. difficile* attenuation (Kolling et al., 2012; Panpetch et al., 2019; Yong et al., 2019). *C. difficile* toxins inactivate Rho GTPases resulting in gut leakage, intestinal inflammation, and cell death (Chen et al., 2015). The interference with the expression of toxin lethality-associated genes *SLC11A1* and *HuR* may lead to the reduction of gut leakage, inflammation, and mortality in *C. difficile*-infected mice treated with *L. casei* T21. While *L. casei* T21 reduced the toxin effect by down-regulation of the expression of *SLC11A1* and *HuR*, which enhances TcdB action, other probiotics interfere with the activity of *C. difficile* toxins by other mechanisms. For example, *Saccharomyces boulardii* interferes the binding between the toxins and intestinal brush borders (Castagliuolo et al., 1999), *L. delbrueckii* directly inhibits the cytotoxicity (Banerjee et al., 2009), and *Streptococcus thermophilus* reduced toxin production through potent lactic acid generation (Kolling et al., 2012).

L. casei T21 was found to up-regulate the expression of *MUC2*, which codes for mucin, an intestinal mucosal protective factor, referred to as "mucin barrier" (Dharmani et al., 2009; Paone and Cani, 2020), which can promote gut integrity. Similarly, *Lactobacillus plantarum* induces the expression of *MUC2* and *MUC3* that inhibit *Escherichia coli* adherence to intestinal epithelium cells (Mack et al., 1999). The mucin-binding protein in several strains of lactobacilli also implies an association between lactobacilli and intestinal mucin (Cornick et al., 2015). Although the enterocyte stimulation by lactic acid might theoretically enhance mucin production (Shekels et al., 1996), the direct incubation of lactic acid-containing cell culture medium with HT-29 cell line did not result in the up-regulation of *MUC2* expression. Other substances produced by *L. casei* T21 are possibly associated with *MUC2* gene up-regulation. More studies on this topic are required. Our findings revealed that *L. casei* T21 had a protective effect against *C. difficile* infection and suggested a great potential of *L. casei* T21 as a probiotic for humans, especially in Southeast Asian populations.

CONCLUSION

Our study demonstrated that *L. casei* strain T21 attenuated *C. difficile* infection in mice through anti-inflammation, attenuation of gut leakage and dysbiosis, interference with toxin lethality by down-regulation of the toxin enhancer gene, and augmentation of mucin production by up-regulation of mucin-producing gene.

DATA AVAILABILITY STATEMENT

The datasets presented in this study can be found in online repositories. The names of the repository/repositories and accession number(s) can be found below: NCBI (accession: SRP336496).

ETHICS STATEMENT

The animal study was reviewed and approved by the experimental protocol in accordance with the US National Institutes of Health standards (NIH publication No. 85-23, revised 1985) was approved by the Institutional Animal Care and Use Committee of the Faculty of Medicine, Chulalongkorn University (SST006/2560).

AUTHOR CONTRIBUTIONS

ST, AL, and WP designed the study. WP performed *in vitro* and *in vivo* experiments. PP performed *in vitro* experiments. WP, TC, and NS designed and performed the microbiome analysis. WP, AL, and ST analyzed the data, discussed the results, and wrote the manuscript. All authors contributed to the article and approved the submitted version.

FUNDING

This research was funded by the Thai Government Research Budget for Fiscal years 2016 and 2017 from the National Research Council of Thailand (GB-B_60_080_30_24) to ST, the Fundamental Fund 2565, Program Management Unit for Human Resources and Institutional Development Research and Innovation-CU (Global Partnership B16F630071 and Flagship B05F630073), TSRI Fund (CU_FRB640001_01_23_1) to AL, and the National Research Council of Thailand (NRCT5-RGJ63001). WP was supported by Rachadapisek Sompote Fund for Postdoctoral Fellowship, Chulalongkorn University.

ACKNOWLEDGMENTS

We would like to express their gratitude to the Translational Research in Inflammation and Immunology Research Unit (TRIRU), Department of Microbiology, Chulalongkorn University, Bangkok, Thailand.

SUPPLEMENTARY MATERIAL

The Supplementary Material for this article can be found online at: https://www.frontiersin.org/articles/10.3389/fmicb.2021.745299/full#supplementary-material

REFERENCES

Aktories, K., and Barbieri, J. T. (2005). Bacterial cytotoxins: targeting eukaryotic switches. *Nat. Rev. Microbiol.* 3, 397–410.

Aktories, K., Papatheodorou, P., and Schwan, C. (2018). Binary *Clostridium difficile* toxin (CDT) - A virulence factor disturbing the cytoskeleton. *Anaerobe* 53, 21–29. doi: 10.1016/j.anaerobe.2018.03.001

Aslam, S., Hamill, R. J., and Musher, D. M. (2005). Treatment of *Clostridium difficile*-associated disease: old therapies and new strategies. *Lancet Infect. Dis.* 5, 549–557. doi: 10.1016/S1473-3099(05)70215-2

Banerjee, P., Merkel, G. J., and Bhunia, A. K. (2009). *Lactobacillus delbrueckii* ssp. bulgaricus B-30892 can inhibit cytotoxic effects and adhesion of pathogenic *Clostridium difficile* to Caco-2 cells. *Gut Pathog.* 1:8. doi: 10.1186/1757-4749-1-8

Bartlett, J. G. (2002). Clinical practice. Antibiotic-associated diarrhea. *N. Engl. J. Med.* 346, 334–339.

Boonma, P., Spinler, J. K., Venable, S. F., Versalovic, J., and Tumwasorn, S. (2014). *Lactobacillus rhamnosus* L34 and *Lactobacillus casei* L39 suppress *Clostridium difficile*-induced IL-8 production by colonic epithelial cells. *BMC Microbiol.* 14:177. doi: 10.1186/1471-2180-14-177

Caporaso, J. G., Lauber, C. L., Walters, W. A., Berg-Lyons, D., Huntley, J., Fierer, N., et al. (2012). Ultra-high-throughput microbial community analysis on the Illumina HiSeq and MiSeq platforms. *ISME J.* 6, 1621–1624.

Castagliuolo, I., Keates, A. C., Wang, C. C., Pasha, A., Valenick, L., Kelly, C. P., et al. (1998). *Clostridium difficile* toxin A stimulates macrophage-inflammatory protein-2 production in rat intestinal epithelial cells. *J. Immunol.* 160, 6039–6045.

Castagliuolo, I., Riegler, M. F., Valenick, L., Lamont, J. T., and Pothoulakis, C. (1999). *Saccharomyces boulardii* protease inhibits the effects of *Clostridium difficile* toxins A and B in human colonic mucosa. *Infect. Immun.* 67, 302–307. doi: 10.1128/IAI.67.1.302-307.1999

Chen, S., Sun, C., Wang, H., and Wang, J. (2015). The role of Rho GTPases in toxicity of *Clostridium difficile* toxins. *Toxins (Basel)* 7, 5254–5267. doi: 10.3390/toxins7124874

Chen, X., Katchar, K., Goldsmith, J. D., Nanthakumar, N., Cheknis, A., Gerding, D. N., et al. (2008). A mouse model of *Clostridium difficile*-associated disease. *Gastroenterology* 135, 1984–1992. doi: 10.1053/j.gastro.2008.09.002

Cornick, S., Tawiah, A., and Chadee, K. (2015). Roles and regulation of the mucus barrier in the gut. *Tissue Barriers* 3:e982426.

Dharmani, P., Srivastava, V., Kissoon-Singh, V., and Chadee, K. (2009). Role of intestinal mucins in innate host defense mechanisms against pathogens. *J. Innate Immun.* 1, 123–135.

Erikstrup, L. T., Aarup, M., Hagemann-Madsen, R., Dagnaes-Hansen, F., Kristensen, B., Olsen, K. E., et al. (2015). Treatment of *Clostridium difficile* infection in mice with vancomycin alone is as effective as treatment with vancomycin and metronidazole in combination. *BMJ Open Gastroenterol.* 2:e000038. doi: 10.1136/bmjgast-2015-000038

FAO and WHO (2001). *Report of a Joint FAO/WHO Expert Consultation on Evaluation of Health and Nutritional Properties of Probiotics in Food Including Powder Milk With Live Lactic Acid Bacteria*. Rome: Food and Agriculture Organization of the United Nations, World Health Organization.

Feng, Y., and Cohen, S. N. (2013). Upregulation of the host SLC11A1 gene by *Clostridium difficile* toxin B facilitates glucosylation of Rho GTPases and enhances toxin lethality. *Infect. Immun.* 81, 2724–2732. doi: 10.1128/IAI.01177-12

Gao, Y., Li, S., Wang, J., Luo, C., Zhao, S., and Zheng, N. (2017). Modulation of intestinal epithelial permeability in differentiated Caco-2 cells exposed to Aflatoxin M1 and Ochratoxin A individually or collectively. *Toxins (Basel)* 10:13.

Gerding, D. N., Johnson, S., Rupnik, M., and Aktories, K. (2014). *Clostridium difficile* binary toxin CDT: mechanism, epidemiology, and potential clinical importance. *Gut Microbes* 5, 15–27. doi: 10.4161/gmic.26854

Goldenberg, J. Z., Yap, C., Lytvyn, L., Lo, C. K., Beardsley, J., Mertz, D., et al. (2017). Probiotics for the prevention of *Clostridium difficile*-associated diarrhea in adults and children. *Cochrane Datab. Syst. Rev.* 12:CD006095.

Hecht, G., Pothoulakis, C., Lamont, J. T., and Madara, J. L. (1988). *Clostridium difficile* toxin A perturbs cytoskeletal structure and tight junction permeability of cultured human intestinal epithelial monolayers. *J. Clin. Invest.* 82, 1516–1524. doi: 10.1172/JCI113760

Hill, C., Guarner, F., Reid, G., Gibson, G. R., Merenstein, D. J., Pot, B., et al. (2014). Expert consensus document. The international scientific association for probiotics and prebiotics consensus statement on the scope and appropriate use of the term probiotic. *Nat. Rev. Gastroenterol. Hepatol.* 11, 506–514. doi: 10.1038/nrgastro.2014.66

Hodges, K., and Gill, R. (2010). Infectious diarrhea: cellular and molecular mechanisms. *Gut Microbes* 1, 4–21. doi: 10.4161/gmic.1.1.11036

Imaoka, A., Shima, T., Kato, K., Mizuno, S., Uehara, T., Matsumoto, S., et al. (2008). Anti-inflammatory activity of probiotic *Bifidobacterium*: enhancement of IL-10 production in peripheral blood mononuclear cells from ulcerative colitis patients and inhibition of IL-8 secretion in HT-29 cells. *World J. Gastroenterol.* 14, 2511–2516. doi: 10.3748/wjg.14.2511

Jank, T., and Aktories, K. (2008). Structure and mode of action of clostridial glucosylating toxins: the ABCD model. *Trends Microbiol.* 16, 222–229. doi: 10.1016/j.tim.2008.01.011

Kachrimanidou, M., and Malisiovas, N. (2011). *Clostridium difficile* infection: a comprehensive review. *Crit. Rev. Microbiol.* 37, 178–187.

Kachrimanidou, M., and Tsintarakis, E. (2020). Insights into the role of human gut microbiota in *Clostridioides difficile* infection. *Microorganisms* 8:200.

Kelly, C. P., Pothoulakis, C., and Lamont, J. T. (1994b). *Clostridium difficile* colitis. *N. Engl. J. Med.* 330, 257–262.

Kelly, C. P., Keates, S., Siegenberg, D., Linevsky, J. K., Pothoulakis, C., and Brady, H. R. (1994a). IL-8 secretion and neutrophil activation by HT-29 colonic epithelial cells. *Am. J. Physiol.* 267, G991–G997.

Kim, J. J., Shajib, M. S., Manocha, M. M., and Khan, W. I. (2012). Investigating intestinal inflammation in DSS-induced model of IBD. *J. Vis. Exp.* 3678.

Kim, J. M., Kim, J. S., Jun, H. C., Oh, Y. K., Song, I. S., and Kim, C. Y. (2002). Differential expression and polarized secretion of CXC and CC chemokines by human intestinal epithelial cancer cell lines in response to *Clostridium difficile* toxin A. *Microbiol. Immunol.* 46, 333–342. doi: 10.1111/j.1348-0421.2002.tb02704.x

Kolling, G. L., Wu, M., Warren, C. A., Durmaz, E., Klaenhammer, T. R., Timko, M. P., et al. (2012). Lactic acid production by *Streptococcus thermophilus* alters *Clostridium difficile* infection and *in vitro* toxin A production. *Gut Microbes* 3, 523–529. doi: 10.4161/gmic.21757

Koon, H. W., Su, B., Xu, C., Mussatto, C. C., Tran, D. H., Lee, E. C., et al. (2016). Probiotic *Saccharomyces boulardii* CNCM I-745 prevents outbreak-associated *Clostridium difficile*-associated cecal inflammation in hamsters. *Am. J. Physiol. Gastrointest. Liver Physiol.* 311, G610–G623. doi: 10.1152/ajpgi.00150.2016

Kuehne, S. A., Cartman, S. T., and Minton, N. P. (2011). Both, toxin A and toxin B, are important in *Clostridium difficile* infection. *Gut Microbes* 2, 252–255. doi: 10.4161/gmic.2.4.16109

Le Bivic, A., Hirn, M., and Reggio, H. (1988). HT-29 cells are an *in vitro* model for the generation of cell polarity in epithelia during embryonic differentiation. *Proc. Natl. Acad. Sci. U.S.A.* 85, 136–140. doi: 10.1073/pnas.85.1.136

Lee, Y. J., Arguello, E. S., Jenq, R. R., Littmann, E., Kim, G. J., Miller, L. C., et al. (2017). Protective factors in the intestinal microbiome against *Clostridium difficile* infection in recipients of allogeneic hematopoietic stem cell transplantation. *J. Infect. Dis.* 215, 1117–1123. doi: 10.1093/infdis/jix011

Leelahavanichkul, A., Panpetch, W., Worasilchai, N., Somparn, P., Chancharoenthana, W., Nilgate, S., et al. (2016). Evaluation of gastrointestinal leakage using serum (1–>3)-beta-D-glucan in a *Clostridium difficile* murine model. *FEMS Microbiol. Lett.* 363:fnw204. doi: 10.1093/femsle/fnw204

Leffler, D. A., and Lamont, J. T. (2015). *Clostridium difficile* infection. *N. Engl. J. Med.* 372, 1539–1548.

Lemee, L., Dhalluin, A., Testelin, S., Mattrat, M. A., Maillard, K., Lemeland, J. F., et al. (2004). Multiplex PCR targeting tpi (triose phosphate isomerase), tcdA (Toxin A), and tcdB (Toxin B) genes for toxigenic culture of *Clostridium difficile*. *J. Clin. Microbiol.* 42, 5710–5714. doi: 10.1128/JCM.42.12.5710-5714.2004

Li, X., Chu, Q., Huang, Y., Xiao, Y., Song, L., Zhu, S., et al. (2019). Consortium of probiotics attenuates colonization of *Clostridioides difficile*. *Front. Microbiol.* 10:2871. doi: 10.3389/fmicb.2019.02871

Lyerly, D. M., Krivan, H. C., and Wilkins, T. D. (1988). *Clostridium difficile*: its disease and toxins. *Clin. Microbiol. Rev.* 1, 1–18. doi: 10.1128/CMR.1.1.1

Mack, D. R., Michail, S., Wei, S., Mcdougall, L., and Hollingsworth, M. A. (1999). Probiotics inhibit enteropathogenic *E. coli* adherence *in vitro* by inducing intestinal mucin gene expression. *Am. J. Physiol.* 276, G941–G950.

Mooyottu, S., Flock, G., Upadhyay, A., Upadhyaya, I., Maas, K., and Venkitanarayanan, K. (2017). Protective effect of Carvacrol against gut dysbiosis and *Clostridium difficile* associated disease in a mouse model. *Front. Microbiol.* 8:625. doi: 10.3389/fmicb.2017.00625

Mylonakis, E., Ryan, E. T., and Calderwood, S. B. (2001). *Clostridium difficile*–associated diarrhea: a review. *Arch. Intern. Med.* 161, 525–533.

Nusrat, A., Von Eichel-Streiber, C., Turner, J. R., Verkade, P., Madara, J. L., and Parkos, C. A. (2001). *Clostridium difficile* toxins disrupt epithelial barrier function by altering membrane microdomain localization of tight junction proteins. *Infect. Immun.* 69, 1329–1336. doi: 10.1128/IAI.69.3.1329-1336.2001

Panpetch, W., Chancharoenthana, W., Bootdee, K., Nilgate, S., Finkelman, M., Tumwasorn, S., et al. (2018). *Lactobacillus rhamnosus* L34 attenuates gut translocation-induced bacterial sepsis in murine models of leaky gut. *Infect. Immun.* 86, e700–e717. doi: 10.1128/IAI.00700-17

Panpetch, W., Hiengrach, P., Nilgate, S., Tumwasorn, S., Somboonna, N., Wilantho, A., et al. (2020). Additional *Candida albicans* administration enhances the severity of dextran sulfate solution induced colitis mouse model through leaky gut-enhanced systemic inflammation and gut-dysbiosis but attenuated by *Lactobacillus rhamnosus* L34. *Gut Microbes* 11, 465–480. doi: 10.1080/19490976.2019.1662712

Panpetch, W., Somboonna, N., Palasuk, M., Hiengrach, P., Finkelman, M., Tumwasorn, S., et al. (2019). Oral *Candida* administration in a *Clostridium difficile* mouse model worsens disease severity but is attenuated by *Bifidobacterium*. *PLoS One* 14:e0210798. doi: 10.1371/journal.pone.0210798

Panpetch, W., Spinler, J. K., Versalovic, J., and Tumwasorn, S. (2016). Characterization of *Lactobacillus salivarius* strains B37 and B60 capable of inhibiting IL-8 production in *Helicobacter pylori*-stimulated gastric epithelial cells. *BMC Microbiol.* 16:242. doi: 10.1186/s12866-016-0861-x

Paone, P., and Cani, P. D. (2020). Mucus barrier, mucins and gut microbiota: the expected slimy partners? *Gut* 69, 2232–2243. doi: 10.1136/gutjnl-2020-322260

Pfaffl, M. W. (2001). A new mathematical model for relative quantification in real-time RT-PCR. *Nucleic Acids Res.* 29:e45.

Pothoulakis, C. (2000). Effects of *Clostridium difficile* toxins on epithelial cell barrier. *Ann. N. Y. Acad. Sci.* 915, 347–356.

Reeves, A. E., Koenigsknecht, M. J., Bergin, I. L., and Young, V. B. (2012). Suppression of *Clostridium difficile* in the gastrointestinal tracts of germfree mice inoculated with a murine isolate from the family Lachnospiraceae. *Infect. Immun.* 80, 3786–3794. doi: 10.1128/IAI.00647-12

Reeves, A. E., Theriot, C. M., Bergin, I. L., Huffnagle, G. B., Schloss, P. D., and Young, V. B. (2011). The interplay between microbiome dynamics and pathogen dynamics in a murine model of *Clostridium difficile* infection. *Gut Microbes* 2, 145–158. doi: 10.4161/gmic.2.3.16333

Reid, G., Younes, J. A., Van Der Mei, H. C., Gloor, G. B., Knight, R., and Busscher, H. J. (2011). Microbiota restoration: natural and supplemented recovery of human microbial communities. *Nat. Rev. Microbiol.* 9, 27–38. doi: 10.1038/nrmicro2473

Ritchie, M. L., and Romanuk, T. N. (2012). A meta-analysis of probiotic efficacy for gastrointestinal diseases. *PLoS One* 7:e34938.

Roychowdhury, S., Cadnum, J., Glueck, B., Obrenovich, M., Donskey, C., and Cresci, G. A. M. (2018). *Faecalibacterium prausnitzii* and a prebiotic protect intestinal health in a mouse model of antibiotic and *Clostridium difficile* exposure. *JPEN J. Parenter. Enteral Nutr.* 42, 1156–1167. doi: 10.1002/jpen.1053

Savidge, T. C., Pan, W. H., Newman, P., O'brien, M., Anton, P. M., and Pothoulakis, C. (2003). *Clostridium difficile* toxin B is an inflammatory enterotoxin in human intestine. *Gastroenterology* 125, 413–420. doi: 10.1016/s0016-5085(03)00902-8

Schloss, P. D., Westcott, S. L., Ryabin, T., Hall, J. R., Hartmann, M., Hollister, E. B., et al. (2009). Introducing mothur: open-source, platform-independent, community-supported software for describing and comparing microbial communities. *Appl. Environ. Microbiol.* 75, 7537–7541. doi: 10.1128/AEM.01541-09

Shekels, L. L., Lyftogt, C. T., and Ho, S. B. (1996). Bile acid-induced alterations of mucin production in differentiated human colon cancer cell lines. *Int. J. Biochem. Cell Biol.* 28, 193–201. doi: 10.1016/1357-2725(95)00125-5

Shen, N. T., Maw, A., Tmanova, L. L., Pino, A., Ancy, K., Crawford, C. V., et al. (2017). Timely use of probiotics in hospitalized adults prevents *Clostridium difficile* infection: a systematic review with meta-regression analysis. *Gastroenterology* 152, 1889–1900.e1889. doi: 10.1053/j.gastro.2017.02.003

Spinler, J. K., Auchtung, J., Brown, A., Boonma, P., Oezguen, N., Ross, C. L., et al. (2017). Next-generation probiotics targeting *Clostridium difficile* through precursor-directed antimicrobial biosynthesis. *Infect. Immun.* 85, e303–e317. doi: 10.1128/IAI.00303-17

Sun, X., Savidge, T., and Feng, H. (2010). The enterotoxicity of *Clostridium difficile* toxins. *Toxins (Basel)* 2, 1848–1880. doi: 10.3390/toxins2071848

Thomas, C. M., Hong, T., Van Pijkeren, J. P., Hemarajata, P., Trinh, D. V., Hu, W., et al. (2012). Histamine derived from probiotic *Lactobacillus reuteri* suppresses TNF via modulation of PKA and ERK signaling. *PLoS One* 7:e31951. doi: 10.1371/journal.pone.0031951

Thomas, C. M., Saulnier, D. M., Spinler, J. K., Hemarajata, P., Gao, C., Jones, S. E., et al. (2016). FolC2-mediated folate metabolism contributes to suppression of inflammation by probiotic *Lactobacillus reuteri*. *Microbiologyopen* 5, 802–818. doi: 10.1002/mbo3.371

Trejo, F. M., Perez, P. F., and De Antoni, G. L. (2010). Co-culture with potentially probiotic microorganisms antagonises virulence factors of *Clostridium difficile in vitro*. *Antonie Van Leeuwenhoek* 98, 19–29. doi: 10.1007/s10482-010-9424-6

Velcich, A., and Augenlicht, L. H. (1993). Regulated expression of an intestinal mucin gene in HT29 colonic carcinoma cells. *J. Biol. Chem.* 268, 13956–13961.

Viswanathan, V. K., Hodges, K., and Hecht, G. (2009). Enteric infection meets intestinal function: how bacterial pathogens cause diarrhoea. *Nat. Rev. Microbiol.* 7, 110–119.

Voth, D. E., and Ballard, J. D. (2005). *Clostridium difficile* toxins: mechanism of action and role in disease. *Clin. Microbiol. Rev.* 18, 247–263. doi: 10.1128/CMR.18.2.247-263.2005

Wei, Y., Yang, F., Wu, Q., Gao, J., Liu, W., Liu, C., et al. (2018). Protective effects of bifidobacterial strains against toxigenic *Clostridium difficile*. *Front. Microbiol.* 9:888. doi: 10.3389/fmicb.2018.00888

Xu, Q., Gu, S., Chen, Y., Quan, J., Lv, L., Chen, D., et al. (2018). Protective effect of *Pediococcus pentosaceus* LI05 against *Clostridium difficile* infection in a mouse model. *Front. Microbiol.* 9:2396.

Xue, Y., Zhang, H., Wang, H., Hu, J., Du, M., and Zhu, M. J. (2014). Host inflammatory response inhibits *Escherichia coli* O157:H7 adhesion to gut epithelium through augmentation of mucin expression. *Infect. Immun.* 82, 1921–1930. doi: 10.1128/IAI.01589-13

Yong, C. C., Lim, J., Kim, B. K., Park, D. J., and Oh, S. (2019). Suppressive effect of *Lactobacillus fermentum* Lim2 on *Clostridioides difficile* 027 toxin production. *Lett. Appl. Microbiol.* 68, 386–393. doi: 10.1111/lam.13124

Zemljic, M., Rupnik, M., Scarpa, M., Anderluh, G., Palu, G., and Castagliuolo, I. (2010). Repetitive domain of *Clostridium difficile* toxin B exhibits cytotoxic effects on human intestinal epithelial cells and decreases epithelial barrier function. *Anaerobe* 16, 527–532. doi: 10.1016/j.anaerobe.2010.06.010

Conflict of Interest: The authors declare that the research was conducted in the absence of any commercial or financial relationships that could be construed as a potential conflict of interest.

Publisher's Note: All claims expressed in this article are solely those of the authors and do not necessarily represent those of their affiliated organizations, or those of the publisher, the editors and the reviewers. Any product that may be evaluated in this article, or claim that may be made by its manufacturer, is not guaranteed or endorsed by the publisher.

Copyright © 2021 Panpetch, Phuengmaung, Cheibchalard, Somboonna, Leelahavanichkul and Tumwasorn. This is an open-access article distributed under the terms of the Creative Commons Attribution License (CC BY). The use, distribution or reproduction in other forums is permitted, provided the original author(s) and the copyright owner(s) are credited and that the original publication in this journal is cited, in accordance with accepted academic practice. No use, distribution or reproduction is permitted which does not comply with these terms.

frontiers in Immunology

REVIEW
published: 10 December 2021
doi: 10.3389/fimmu.2021.775526

The Gut-Liver Axis in Health and Disease: The Role of Gut Microbiota-Derived Signals in Liver Injury and Regeneration

*Zhipeng Zheng and Baohong Wang**

State Key Laboratory for Diagnosis and Treatment of Infectious Diseases, National Clinical Research Center for Infectious Diseases, Collaborative Innovation Center for Diagnosis and Treatment of Infectious Diseases, The First Affiliated Hospital, Zhejiang University School of Medicine, Hangzhou, China

Diverse liver diseases undergo a similar pathophysiological process in which liver regeneration follows a liver injury. Given the important role of the gut-liver axis in health and diseases, the role of gut microbiota-derived signals in liver injury and regeneration has attracted much attention. It has been observed that the composition of gut microbiota dynamically changes in the process of liver regeneration after partial hepatectomy, and gut microbiota modulation by antibiotics or probiotics affects both liver injury and regeneration. Mechanically, through the portal vein, the liver is constantly exposed to gut microbial components and metabolites, which have immense effects on the immunity and metabolism of the host. Emerging data demonstrate that gut-derived lipopolysaccharide, gut microbiota-associated bile acids, and other bacterial metabolites, such as short-chain fatty acids and tryptophan metabolites, may play multifaceted roles in liver injury and regeneration. In this perspective, we provide an overview of the possible molecular mechanisms by which gut microbiota-derived signals modulate liver injury and regeneration, highlighting the potential roles of gut microbiota in the development of gut microbiota-based therapies to alleviate liver injury and promote liver regeneration.

Keywords: gut microbiota (GM), liver injury and regeneration, lipopolisaccharide (LPS), bile acid (BA), SCFA (short chain fatty acids), tryptophan metabolites, gut microbial metabolites

OPEN ACCESS

Edited by:
Alina Maria Holban, University of Bucharest, Romania

Reviewed by:
Daisuke Tokuhara, Osaka City University, Japan
Naschla Gasaly, University of Chile, Chile
Marcela A. Hermoso Ramello, University of Chile, Chile, in collaboration with reviewer NG

***Correspondence:**
Baohong Wang
wangbaohongzju@zju.edu.cn

Specialty section:
This article was submitted to Microbial Immunology, a section of the journal Frontiers in Immunology

Received: *14 September 2021*
Accepted: *19 November 2021*
Published: *10 December 2021*

Citation:
Zheng Z and Wang B (2021) The Gut-Liver Axis in Health and Disease: The Role of Gut Microbiota-Derived Signals in Liver Injury and Regeneration. Front. Immunol. 12:775526. doi: 10.3389/fimmu.2021.775526

INTRODUCTION

The liver has an outstanding regenerative capacity (1). Liver regeneration is a well-orchestrated biological process that depends on a large series of signals. Following different types of damage, the remnant liver initiates different types of reprogramming events, which activate different progenitor cells to replace injured cells (2). The regenerating liver undergoes numerous adaptive responses in gene expression, growth factor production, and morphological structure, which have been extensively described (1, 3). The essential gene expressions required for liver regeneration cover cytokine, growth factor, and metabolic, which interact with each other and fine-tune regenerative

responses to maintain hepatic homeostasis according to body demands (4). The classical mechanisms of liver regeneration focus on signaling pathways within the liver. However, recent studies have evidenced that commensal gut microbiota plays local and systematic roles in tissue repair and regeneration (5). Therefore, it is extremely important to describe the interaction between gut microbiota and liver in the regulation of liver injury and regeneration.

Through the portal vein, the liver is constantly exposed to bacterial components and gut microbial metabolites. Lipopolysaccharide (LPS) is a cell wall component of gram-negative bacteria, and a mild release of LPS from the gut can stimulate liver regeneration and tissue repair (6–8). Besides, gut microbial metabolites, such as bile acids, short-chain fatty acids (SCFAs), and tryptophan metabolites, affect host metabolism and immune system (9, 10), which may indirectly influence liver injury and regeneration. Herein, the review aims to elucidate the potential molecular mechanisms that gut microbiota interacts with the liver from the perspective of injury and regeneration, which may provide valuable clues to develop gut microbiota-based therapies for liver diseases.

GUT MICROBIOTA AND LIVER DISEASES

Gut microbiota dysbiosis has been found in liver diseases with distinct etiologies, including acute liver injury, viral hepatitis, non-alcoholic fatty liver disease (NAFLD), alcohol-related liver disease, autoimmune hepatitis (AIH), primary biliary cholangitis (PBC), and primary sclerosing cholangitis (PSC) (11, 12). (**Table 1**) Diverse liver diseases undergo a similar pathophysiological process, in which the damaged liver needs repair and gut microbiota may play an important role.

In pre-cirrhotic liver disease, the gut microbiota has changed. The ratio of *Bifidobacteria*/Enterobacteriaceae is gradually reduced in healthy individuals, hepatitis B virus carriers, patients with chronic hepatitis B, and patients with decompensated cirrhosis (13), suggesting that the alteration of gut microbiota is associated with disease progression in hepatitis B patients. In NASH patients, the relative abundance of *Bacteroides* significantly increases and *Prevotella* decreases, whereas the relative abundance of *Ruminococcus* is higher in F ≥ 2 fibrosis patients (14). A recent study finds that high-alcohol-producing *Klebsiella pneumoniae* is associated with almost 60% of NAFLD, and high-alcohol-producing *Klebsiella pneumoniae* supplement by oral gavage induces NAFLD in mice (15), suggesting that endogenous alcohol production by gut microbiota drives NAFLD in some cases. In addition, a gut microbiota-based metagenomic signature can be used to distinguish mild and moderate NAFLD from advanced fibrosis (23). For AIH, increased abundance of *Veillonella dispar* is linked to disease severity, and the combination of *Veillonella*, *Lactobacillus*, *Oscillospira*, and *Clostridiales* discriminates AIH from controls (16). The relative abundance of *Veillonella* is also enriched in PSC compared with healthy controls and ulcerative colitis patients without liver diseases (17). Microbial diversity is significantly reduced in PBC patients, and *Faecalibacterium* is further decreased in gp210-positive than gp210-negative PBC patients (18). These correlations between pre-cirrhotic liver diseases and gut microbiota indicate that the primary injury of liver diseases shape, and are shaped by, changes in gut microbiota composition.

Gut dysbiosis is more obvious in liver cirrhosis, the pathological end-stage of chronic liver disease, and can cause complications. The enrichment of potentially pathogenic bacteria Enterobacteriaceae and Streptococcaceae and the reduction of beneficial bacteria Lachnospiraceae in patients with liver cirrhosis have a positive and negative correlation with the Child-Turcotte-Pugh score, which is used to assess the severity of cirrhosis based on five clinical parameters, respectively (19). Quantitative metagenomics reveals that a combination of 15 optimal microbiota-targeted gene markers (NLF009_gene_80134, H16_gene_75905, et al.) discriminates liver cirrhosis patients from healthy individuals with a training AUC value of 0.918 and a validating AUC value of 0.836 (24). Decompensated liver cirrhosis could be accompanied by a severe central nervous system, namely hepatic encephalopathy (HE). There is no difference in stool microbiota between HE and no-HE patients, but mucosal microbiota obtained by sigmoidoscopy is different with increased abundance of *Enterococcus*, *Veillonella*, *Megasphaera*, and *Burkholderia* and decreased abundance of *Roseburia* in HE patients (20). The further development of decompensated liver cirrhosis towards acute-on-chronic liver failure (ACLF). The cirrhosis dysbiosis ratio (Lachnospiraceae +

TABLE 1 | Gut dysbiosis in liver diseases.

Liver disease	Organism	Reference
Hepatitis B	*Bifidobacteria*/Enterobacteriaceae ↓	(13)
NASH	*Bacteroides* ↑, *Prevotella* ↓, *Ruminococcus* ↑	(14)
NAFLD	High-alcohol-producing *Klebsiella pneumoniae* ↑	(15)
AIH	*Veillonella dispar* ↑	(16)
PSC	*Veillonella*↑	(17)
PBC	Microbial diversity ↓, *Faecalibacterium* ↓	(18)
Liver cirrhosis	Enterobacteriaceae ↑, Streptococcaceae ↑, Lachnospiraceae ↓	(19)
Liver cirrhosis with HE	*Enterococcus*↑, *Veillonella* ↑, *Megasphaera* ↑ *Burkholderia* ↑, *Roseburia* ↑	(20)
ACLF	Lachnospiraceae + Ruminococcaceae + Veillonellaceae + Clostridiales Cluster XIV/Enterobacteriaceae + Bacteroidaceae ↓	(21)
HCC	Actinobacteria ↑, Verrucomicrobia ↓	(22)

Ruminococcaceae + Veillonellaceae + Clostridiales Cluster XIV/ Enterobacteriaceae + Bacteroidaceae) is lower in patients who progress to ACLF and associated with an elevated risk of extra-hepatic failure and death (21). Besides, most hepatocellular carcinoma (HCC) develops in the setting of advanced liver cirrhosis. Dysbiosis of gut microbiota is associated with increased inflammation, impaired intestinal barrier, and immune system disorders, which are involved in HCC development (22). The complexity and role of gut microbiota in end-stage chronic liver disease suggest that gut microbiota modulation may be a way to deal with difficulties in liver injury and regeneration.

Consequently, these studies suggest that gut microbiota may have a significant impact on the pathophysiology of liver diseases, in which abnormal ductular responses, excessive fibrosis, and impaired innate immunity can inhibit normal regeneration and lead to liver failure or tumors. How to restore the regenerative ability of the failed liver is an essential problem to be solved in clinical scenarios. A comprehensive understanding of the underlying mechanisms may enable appropriate targets of gut microbiota-based therapies to reduce the factors that inhibit liver regeneration or directly stimulate liver regeneration.

GUT MICROBIOTA DYNAMICALLY CHANGES DURING LIVER REGENERATION

The relationship between gut microbiota and liver regeneration has been studied in the animal partial hepatectomy models (**Figure 1**). Dynamic changes of gut microbiota are observed in mice from 0 hours to 9 days after partial hepatectomy (25). Partial hepatectomy leads to a distinct change in the composition of gut microbiota, early at 1 hour after partial hepatectomy, with steadily increased Bacteroidetes and decreased Firmicutes, which account for the most abundant phyla. At the family level, increased S24-7 and Rikenellaceae make up the most abundant taxa within Bacteroidetes phylum, while decreased Clostridiaceae, Lachnospiraceae and Ruminococcaceae are the most abundant representatives in Firmicutes phylum. Moreover, alteration of S24-7, Lachnospiraceae, and Ruminococcaceae is closely associated with hepatic metabolism and proliferation. The shifts of bacterial populations persist for 9 days in mice after partial hepatectomy, which almost covers all of the priming phase, proliferative phase, and termination phase of regenerating liver (25).

In the other study, fluctuating alterations of gut microbiota are observed in rats after partial hepatectomy (26). In this study, the abundance of Bacteroidetes rapidly decreases at 12 hours after partial hepatectomy, but steadily increases to the initial level at 48 hours, and then decreases to a low level again at 72 hours and lasts to the endpoint. Compared with Bacteroidetes, the alteration of Firmicutes shows a different trend. The ratio of Firmicutes to Bacteroidetes (F/B) is fluctuant throughout the process of liver regeneration. Notably, the abundance of Proteobacteria has a remarkable elevation at 48 hours after partial hepatectomy, but it almost decreases to the initial level before the endpoint. At the family level, Lachnospiraceae and Ruminococcaceae increase in 12-24 hours and 3-14 days after partial hepatectomy, but they are decreased in 30-48 hours.

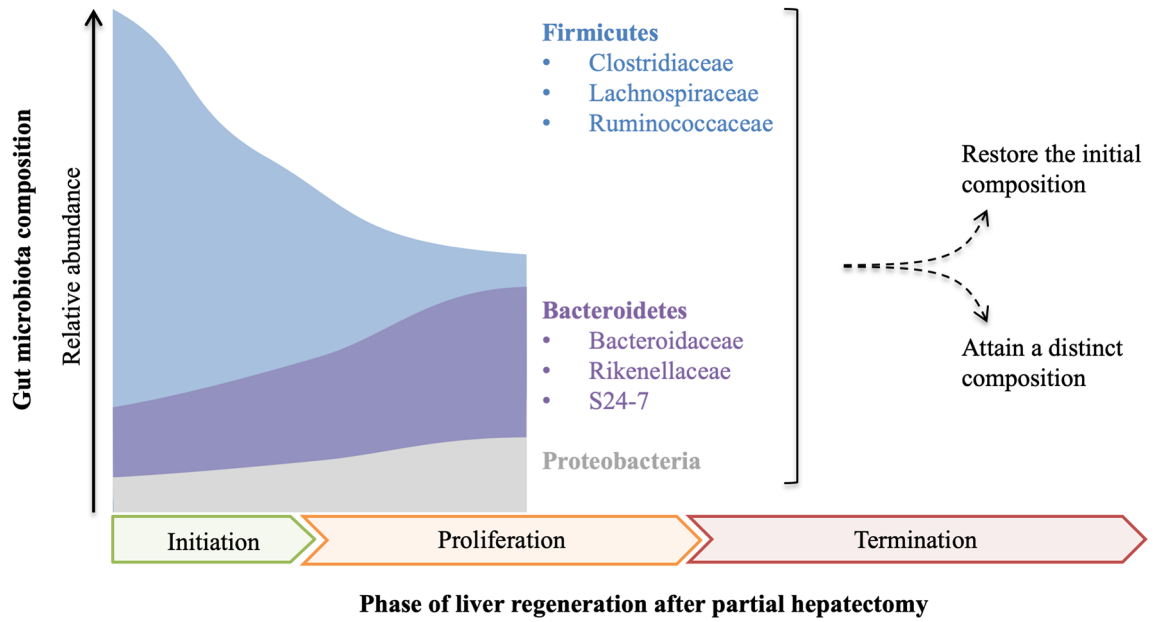


FIGURE 1 | The composition of gut microbiota is fluctuant in the course of liver regeneration. After partial hepatectomy, the relative abundance of Firmicutes decreases while Bacteroidetes and Proteobacteria increase, which probably continues until the middle of the proliferation phase of liver regeneration. As proliferation and termination of liver regeneration progress, the final composition of gut microbiota remains controversial and needs further study.

Furthermore, cluster analysis indicates that the composition of gut microbiota is different along with the process of liver regeneration (26).

Although the changing trends of gut microbiota are not identical in the only two published studies, which may be the consequence of different experimental designs, increased Bacteroidetes and decreased Firmicutes are recognized in the priming phase and the partial proliferative phase of liver regeneration. As the proliferation and termination of liver regeneration progress, whether the composition of gut microbiota is finally restored or attains a new state remains unclear and needs further study. These data indicate that gut microbiota has a potential influence on the regenerating liver or vice versa.

GUT MICROBIOTA MANIPULATIONS AFFECT LIVER INJURY AND REGENERATION

Gut microbiota is depleted in germ-free model and can be modulated by antibiotics, probiotics, prebiotics, such as dietary fibers (27), fecal microbiota transplant (FMT), and colon resection. All of these gut microbiota manipulations influence liver injury and regeneration (**Figure 2**).

Gut bacterial depletion using oral non-absorbable antibiotics depresses liver regeneration in rats after partial hepatectomy, and liver regeneration is also impaired in germ-free mice with partial hepatectomy (7, 8). Likewise, liver regeneration is suppressed in rats with simultaneous liver and colon partial resection (28). These studies indicate that gut microbiota is required for normal liver regeneration. Interestingly, gut microbiota participates in liver injury as well as liver regeneration. Oral antibiotics prevent liver injury induced by hepatotoxic agents, such as CCl_4, acetaminophen, D-Gal, and alcohol (29), whereas a complete absence of gut microbiota as in germ-free rodents can exacerbate the acute liver injury (30), suggesting that gut microbiota also contributes to the pathophysiology of drug-induced liver injury.

Moreover, FMT normalizes impaired liver regeneration in rats with gut decontamination by antibiotics (26), which further manifests that normal gut microbiota plays a driving role in liver regeneration. Probiotics improve the outcome of partial hepatectomy, not only in animal experiments but also in some clinical trials (31–33). Probiotic supplement improves mitosis in the liver of rats with simultaneous 70% partial hepatectomy and colon anastomosis probably by preventing bacteria translocation (31). In hepatocellular carcinoma (HCC) patients receiving

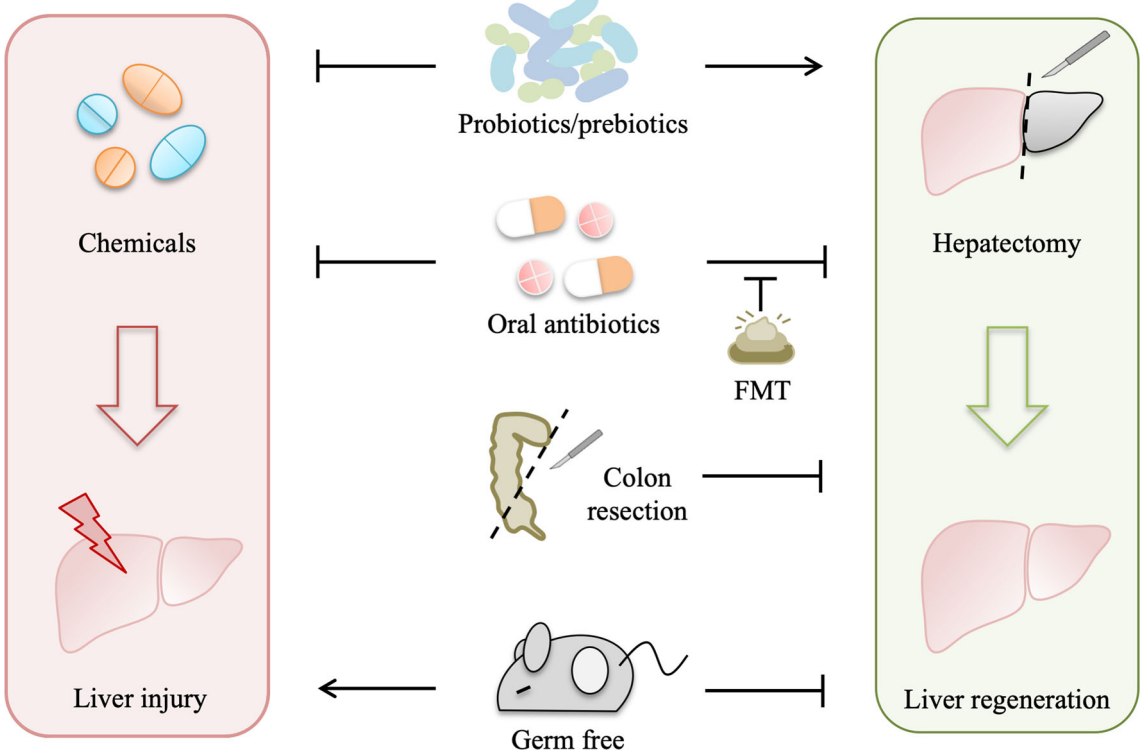


FIGURE 2 | Gut microbiota manipulations affect liver injury and regeneration. Gut microbiota depletion by several approaches, including germ-free, antibiotics, and colon resection, suppresses liver regeneration to varying degrees, while fecal microbiota transplant (FMT) can normalize liver regeneration in the antibiotic-treated model, and probiotics/prebiotics can promote liver regeneration. In addition, both probiotics and oral antibiotics alleviate drug-induced acute liver injury, which is aggravated in germ-free rodents.

hepatic resection, preoperative and postoperative probiotics improve liver function and reduce complications (32). In another pilot study with 19 patients subjected to right hepatectomy, symbiotics can improve liver function after liver resection in the uncomplicated subgroup (33). Likewise, emerging evidence demonstrates that probiotics alleviate drug-induced liver injury in animal experiments. *Lactobacillus rhamnosus* improves liver function and ameliorates alcohol-induced liver injury in mice (34, 35). *Bifidobacterium adolescentis*, *Bacillus cereus*, and *Lactobacillus helveticus* pretreatments can modify the gut microbiota and alleviate liver injury in D-Gal-treated rats (36–38). *Akkermansia muciniphila* protects mice from immune-mediated liver injury (39).

Dynamic changes of gut microbiota during liver regeneration and the benefits of FMT and probiotics on liver injury and regeneration indicate that the crosstalk between the liver and gut microbiota is important for liver regeneration, which is probably mediated by gut microbiota-derived components and metabolites.

GUT-DERIVED LPS HAVE MULTIPLE EFFECTS ON LIVER INJURY AND REGENERATION

Gut-derived LPS, produced by enteric gram-negative bacteria, are continually presented to the liver (6), and low-grade portal venous LPS can be cleared by the liver (40). Under normal conditions, gut-derived LPS can be phagocytized and detoxified by Kupffer cells in the liver reticuloendothelial system (RES) (41). When the liver suffers from an extended injury, homeostasis between the formation and removal of gut-derived LPS is broken, which may be due to the following reasons. First, sensitivity to gut-derived LPS is increased after the initial liver damage. Second, RES injury leads to hampered detoxification and clearance of gut-derived LPS. Third, gut barrier dysfunction allows more translocation of LPS. Last, bacteria overgrowth and delay of gastrointestinal motility increase production and spillover of gut-derived LPS.

Gut-Derived LPS Aggravate the Liver Injury

Gut-derived LPS as a cofactor plays a universal role in acute liver injury, which has been demonstrated in acute liver injury models induced by different hepatotoxic agents, including CCl_4, acetaminophen, alcohol, and D-Gal (29). Under primary liver damage, gut-derived LPS can activate Kupffer cells to release pro-inflammatory mediators, such as TNF-α, interleukins (IL-1 and IL-10), lysosomal enzymes (protease and phosphatase), and superoxide, which aggravate inflammatory responses and necrosis (29). Induction of LPS tolerance protects rats from CCl_4-induced liver necrosis, and LPS-binding protein also has a protective effect on acute liver injury (29).

In addition to acute liver injury, gut-derived LPS plays a critical role in chronic liver injury. Elevated plasma endotoxin is observed in patients with alcoholic liver disease (ALD) and experimental models of alcoholic liver injury, which can be attenuated by oral antibiotics (42, 43). However, LPS alone fails to mimic ethanol-induced steatosis, but together with ethanol, which is metabolized to acetaldehyde by gut bacteria and intestinal mucosa, leads to hepatocyte steatosis (42). Besides, fibrogenesis usually occurs in the advanced ALD and other chronic liver diseases, such as nonalcoholic fatty liver disease (NAFLD) and chronic hepatitis B (CHB), which can develop into cirrhosis (44). Chronic liver diseases are accompanied by dysbiosis of gut microbiota, which contributes to intestinal dysmotility, inflammation, and mucosal leakage, leading to continuous and excessive liver exposure to gut-derived LPS (45). Toll-like receptor-4 (TLR4) mutation and gut sterilization prevent hepatic fibrosis in mice, revealing that gut-derived LPS contribute to hepatic fibrosis (46). On one hand, when the liver is exposed to increased gut-derived LPS, TLR4 activation of hepatic stellate cells upregulates the production of chemokine (CCL2) and induces chemotaxis of Kupffer cells (47). On the other hand, LPS binding to TLR4 on hepatic stellate cells downregulates transforming growth factor β (TGF-β) pseudoreceptor BAMBI through Myd88- NF-κB-dependent signals, which sensitizes hepatic stellate cells to TGF-β released by Kupffer cells, promoting transdifferentiation of quiescent hepatic stellate cells to activated scar-forming myofibroblasts (46), and myofibroblasts generate extracellular matrix (ECM) materials, including collagen, laminin, and fibronectin. Excessive deposition of ECM will cause aberrant scar formation and fibrosis, which diminishes liver regeneration (48).

In addition, chronic liver diseases are driven by vicious cycles of liver injury, inflammation, repair, and regeneration, which make an opportunity for hepatocellular carcinoma (HCC) development (49). Previous TLR4-deficient, gut-sterilized, germ-free, and LPS-treated animal experiments have evidenced that gut-derived LPS contribute to hepatocarcinogenesis (50, 51). Mechanistically, the LPS-TLR4 pathway contributes to liver tumor promotion by increasing proliferation and preventing apoptosis of non-bone marrow-derived resident liver cells, and in the early phases of HCC, TLR4-dependent secretion of hepatomitogen epiregulin by hepatic stellate cells mediates HCC promotion (51).

The broad roles of gut-derived LPS in liver injury are well established and accepted, but applicating this knowledge to develop an effective treatment remains challenging, which needs further study.

Gut-Derived LPS Promote Liver Regeneration

Gut-derived LPS also plays an important role in liver regeneration. Restriction of gut-derived LPS by gut bacterial depletion, endotoxin neutralization, and induction of endotoxin tolerance significantly impairs liver regeneration in rats, which is reversed by exogenous LPS supplements (7). In addition, impaired liver regeneration is also observed in germ-free mice receiving partial hepatectomy and in rats simultaneously receiving partial hepatectomy and colon bowel resection (8, 28).

When the liver is subjected to an experimental physical or a chemical injury, gut-derived LPS will pass through the compromised liver and spill into the general circulation, leading to low-grade systemic endotoxemia, which elicits hepatotrophic factors production, such as insulin, glucagon, epidermal growth factor (EGF), vasopressin and triiodothyronine (T3) (6, 52). In addition, gut-derived LPS activates Kupffer cells by binding to TLR-4 for activation of NF-κB and subsequently stimulates the production of TNF-α, which in return activates Kupffer cells to secrete interleukin-6 (IL-6) (53). IL-6 trans-signaling through the soluble IL-6/IL-6R complex induces hepatic stellate cells to produce hepatocyte growth factor (HGF) (54). HGF cooperates with other extrahepatic factors, such as T3, insulin, and EGF, allowing the remnant hepatocytes to overcome cell-cycle checkpoint control to proliferate, which is essential for the priming phase of liver regeneration after partial hepatectomy (53, 54). Finally, when the liver regenerates sufficiently and the phagocytosis function of the Kupffer cell is restored, gut-derived LPS in the portal blood can be detoxified again (6).

Therefore, gut-derived LPS are important for liver regeneration as well as liver injury, liver fibrosis, and liver tumors, which may depend on the degree and duration of exposure (**Figure 3**). However, it is difficult to determine the beneficial level of gut-derived LPS for the liver in different scenarios to avoid the deleterious effects of excessive TLR-4 activation. One promising strategy is modulating gut microbiota by probiotics, prebiotics, and perhaps appropriate antibiotics, such as rifaximin, to control gut-derived LPS.

GUT MICROBIOTA-ASSOCIATED BILE ACID METABOLISM IS INVOLVED IN LIVER INJURY AND REGENERATION

Bile acids (BAs), produced from cholesterol, are assembled as primary conjugated BAs in the liver and actively transported into the biliary system. A small fraction of BAs circulates from cholangiocytes to the liver through the cholangio-hepatic shunt, while most of them are stored in the gallbladder and released into the duodenum after food intake. Approximately 95% of BAs are reabsorbed *via* the apical sodium-dependent bile acid transporter (ASBT) in the terminal small intestine and return to the liver through the portal vein. Conjugated primary BAs can also be deconjugated by the gut microbiota and escape reabsorption, further dehydroxylated by microbial bioconversion to secondary BAs. A part of secondary BAs is passively absorbed by colonic cells. Spillover of BAs into systemic circulation can be cleared *via* urinary excretion. Bile acids that are lost in urinary and fecal excretion are replenished by hepatic synthesis (55, 56).

In normal conditions, BAs almost recycle within the enterohepatic circulation, which has important physiological roles in nutrient absorption and biliary secretion of lipids and toxic metabolites, and only traces of BAs escape to the systemic circulation. After partial hepatectomy, BAs that are reabsorbed from the intestine suddenly become too high for the remnant liver, which leads to an abrupt and massive spillover of BAs to the systemic circulation (57, 58). Bile acids overload beyond a certain threshold is deleterious (59). However, BAs are also necessary for normal liver regeneration. Depletion of BAs by cholestyramine (a BA-sequestering resin) leads to suppression of liver regeneration (60). In rats after partial hepatectomy and mice with CCl_4-induced injury, elevated BAs accelerate liver regeneration, while low levels of BAs impair liver regeneration (60, 61). The similar phenomenon is observed in clinical scenarios, following a major hepatectomy, patients without external biliary drainage have better liver regeneration than those with external biliary drainage (62). Gut microbiota-dependent BA metabolism is likely to participate in liver injury and regeneration by modifying the quality (conjugated vs deconjugated and primary vs secondary BAs) and quantity of the BA pool (**Figure 4**).

Gut Microbiota-Mediated Deconjugation of BAs Participates in Liver Injury and Regeneration

After partial hepatectomy, to protect the remnant liver and biliary tree from excess BAs, the basolateral uptake and BAs production are decreased and the basolateral efflux and biliary excretion are increased. Deconjugation (removal of the glycine or taurine) by gut microbiota with bile salt hydrolase (BSH) prevents reabsorption of BAs in the small intestine (63). BSH is enriched in the human gut microbiota and mediates bile tolerance (64). Conjugated BAs are transported by sodium taurocholate cotransporting polypeptide (NTCP) and organic anion-transporting polypeptide (OATP) isoform, which are the major uptake transports of BAs in the liver. The mRNA levels of *NTCP*, *OATP1*, and *OATP2* are decreased with the most prominent decrease of *NTCP*, while the protein level of NTCP is markedly decreased during the initial phase of liver regeneration (65). Downregulated NTCP relieves basolateral over uptake of BAs in the liver, but OATP expressing hepatocytes could ensure ongoing basolateral uptake of BAs after partial hepatectomy. However, one study demonstrates that the mRNA and protein levels of NTCP are unchanged after partial hepatectomy (66).

Despite the conflicting effects of partial hepatectomy on NTCP expression, high levels of BAs in the remnant liver are generally accepted. BAs overload inhibits the synthesis of BAs by negative feedback regulation through the nuclear receptor farnesoid X receptor (FXR), which is highly expressed in the liver and ileum (63). Chenodeoxycholic acid (CDCA) is the most potent efficacious ligand of FXR, followed by lithocholic acid (LCA), deoxycholic acid (DCA), and cholic acid (CA) (67). LCA and DCA are secondary BAs transformed from primary BAs by microbial 7α-dehydroxylation, which is a characteristic of *Clostridium* and *Eubacaterium* (68, 69). In the liver, FXR activation induces expression of small heterodimer partner 1 (SHP-1), which can inhibit expression of CYP7A1, the rate-limiting enzyme of BAs synthesis, by reducing the activity of liver receptor homolog 1 (LRH-1) (70). Therefore, BAs overload leads to decreased BAs production by repressing the transcription of

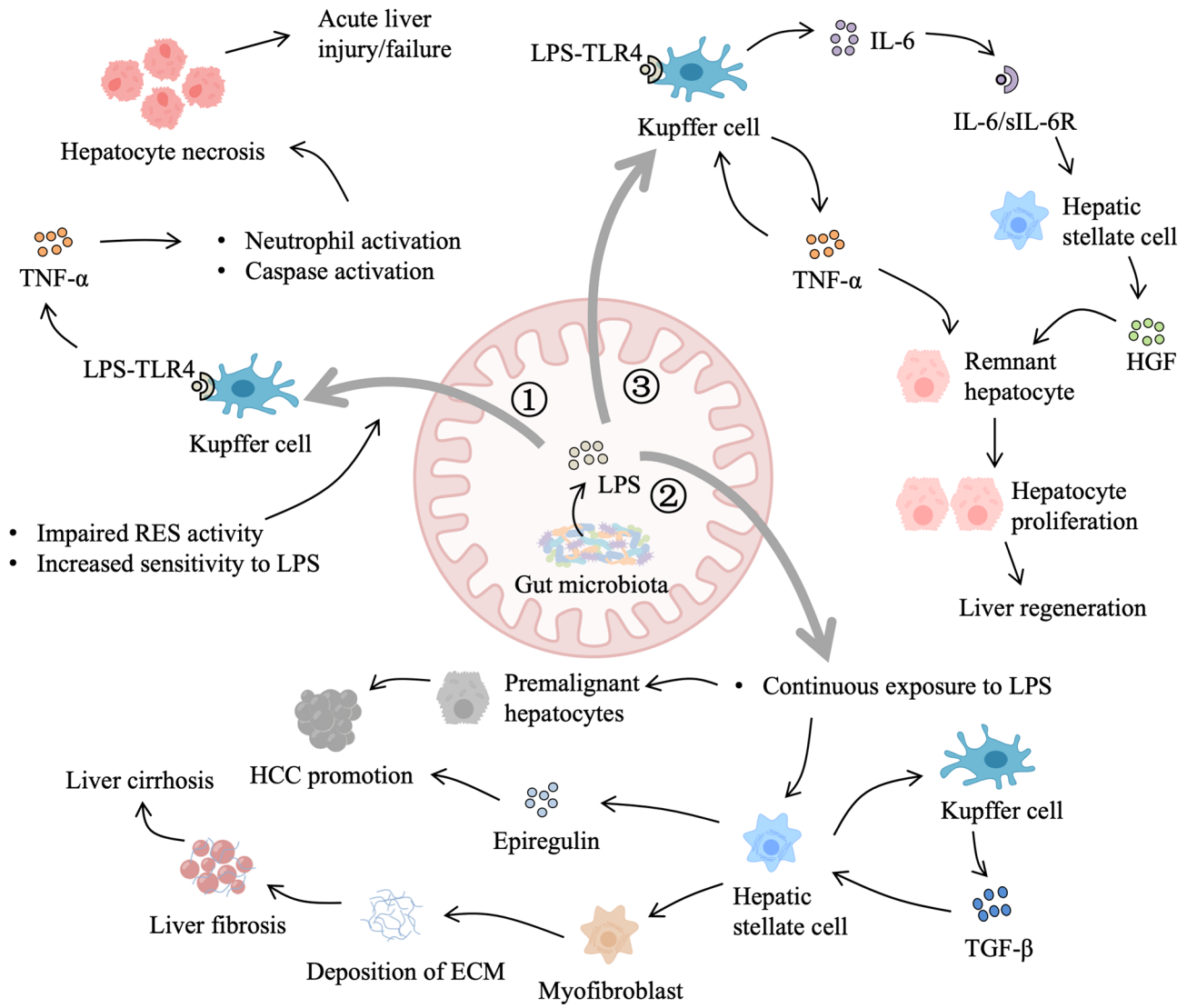


FIGURE 3 | Role of gut-derived LPS in liver injury and regeneration. 1) When the liver suffers from an acute injury, primary damage reduces the activity of the reticuloendothelial system (RES) and increases liver sensitivity to LPS. LPS binding to Toll-like receptor 4 (TLR4) on Kupffer cells triggers the production of tumor necrosis factor-α (TNF-α), which leads to hepatocyte necrosis and aggravates the primary damage. 2) In addition, gut-derived LPS also contributes to chronic liver injury. Dysbiosis of gut microbiota leads to elevated LPS and impaired gut barrier function. Continuous LPS exposure sensitizes hepatic stellate cells to transforming growth factor-β (TGF-β) and promotes the transdifferentiation of hepatic stellate cells into myofibroblasts, resulting in the generation of extracellular matrix (ECM) materials. Excessive deposition of ECM interferes with normal regeneration, leading to liver cirrhosis and hepatocellular carcinoma (HCC) promotion. Besides, LPS accelerates the development of premalignant hepatocytes and stimulates hepatic stellate cells to secret epiregulin, which facilitates HCC promotion. 3) Moreover, after partial hepatectomy, gut-derived LPS activate Kupffer cells to secrete TNF-α, which in return stimulates Kupffer cells to produce interleukin-6 (IL-6). IL-6/IL-6 receptor complex induces the production of hepatocyte growth factor (HGF) by hepatic stellate cells. In addition, gut-derived LPS that escape Kupffer cells spilling into the general circulation elicit systemic hepatotrophic factors production. HGF, TNF-α, and other hepatotrophic factors allow remnant hepatocytes to overcome cell-cycle checkpoint and support liver regeneration.

the rate-limiting enzyme in BAs synthesis. In addition, increased basolateral efflux and biliary excretion of BAs reduce BAs concentrations in hepatocytes, which protects the liver from BA-induced liver injury. Conjugated BAs are primarily secreted into bile *via* the canalicular bile salt export pump (BSEP) (55). The expression of BSEP is increased from days 1 to 3 after partial hepatectomy, which depends on the activation of FXR (60). Thus, the remnant liver copes with the BAs overload *via* FXR to maintain normal BAs levels, including both repressions of synthesis and induction of export.

Besides, hepatic FXR plays a critical role in the expression of Foxm1b, a key regulator of the hepatic cell cycle, promoting liver regeneration after either partial hepatectomy or CCl_4-induced liver injury (71). Moreover, compared with liver-specific FXR

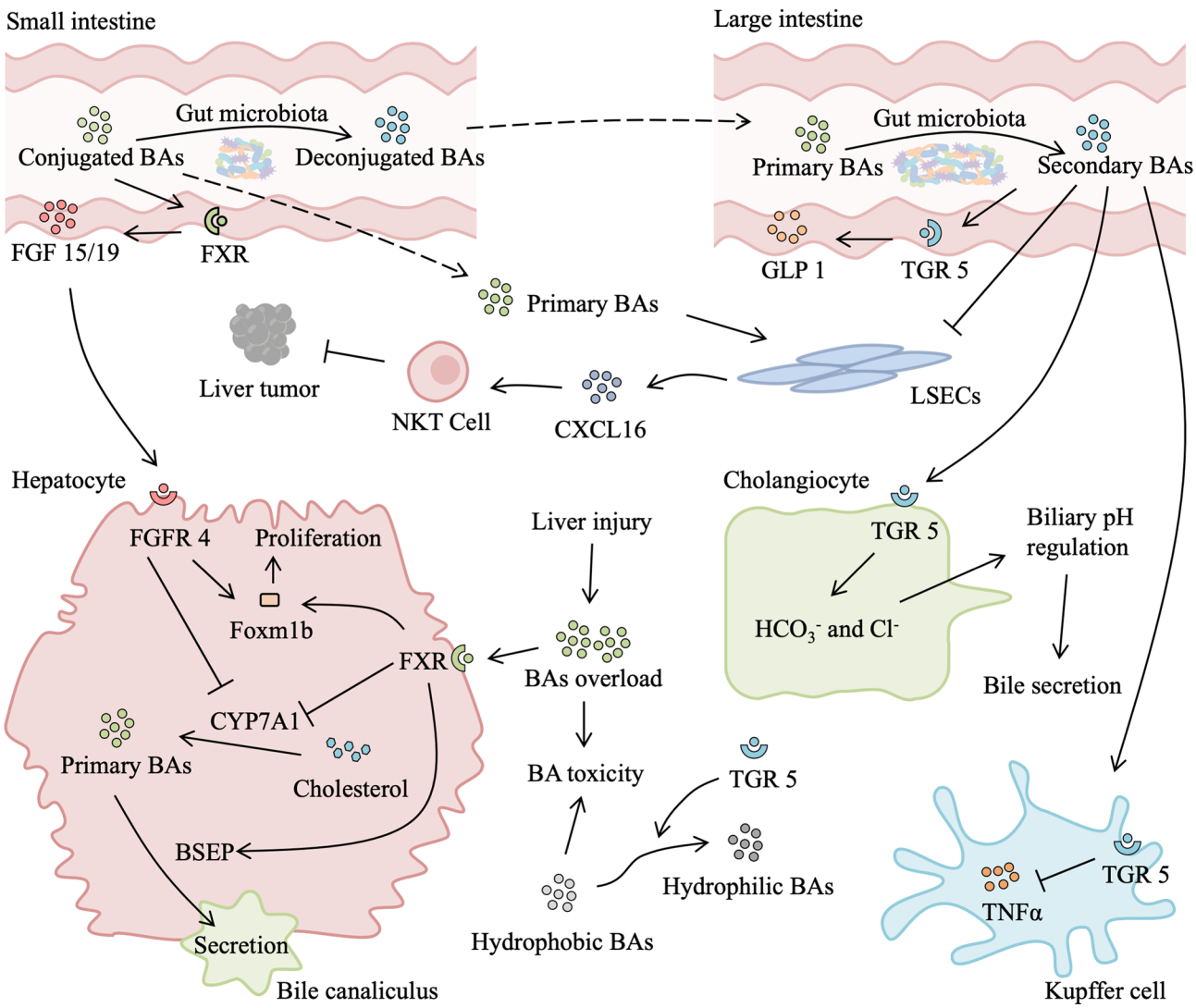


FIGURE 4 | Role of gut microbiota-associated bile acids metabolism in liver injury and regeneration. After a liver injury or partial hepatectomy, bile acids (BAs) absorbed from the intestine suddenly become too high for the remnant liver, leading to secondary liver injury. Excessive BAs binding to hepatic farnesoid X receptor (FXR) inhibits transcription of cytochrome P450 family 7 subfamily A member 1 (CYP7A1), which reduces the production of primary BAs. In addition, activated FXR can promote the secretion of primary BAs into bile canaliculus and upregulate expression of Foxm1b, thus relieving BAs overload and facilitating liver regeneration. Meanwhile, in the small intestine, BAs activate intestinal FXR to secret fibroblast growth factor (FGF) 15/19, which binds to fibroblast growth factor receptor 4 (FGFR4). FGFR4/agonist also induces expression of Foxm1b and improves proliferation. Gut microbiota is responsible for secondary BAs production in the large intestine. Secondary BAs binding to intestinal transforming growth factor 5 (TGR5) elicits secretion of glucagon-like peptide 1 (GLP1), which activates the insulin signaling pathway. Absorbed secondary BAs binding to hepatic TGR5 has an anti-inflammatory effect by suppressing the release of TNF-α from the Kupffer cell. TGR5 activation also promotes BAs secretion by secreting HCO_3^- and Cl^- from cholangiocyte and increasing transformation of hydrophilic BAs from hydrophobic BAs, which reduce BAs load and BAs toxicity-induced liver injury, promoting liver regeneration. Moreover, primary BAs stimulate and secondary BAs suppress the expression of chemokine (C-X-C motif) ligand 16 (CXCL16) by liver sinusoidal endothelial cells (LSECs). CXCL16 is a chemokine that recruits natural killer T (NKT) cells, which suppress liver tumors.

knock-out (KO) mice, conventional FXR KO mice show significantly decreased liver regeneration response at 36 h and 72 h after partial hepatectomy, suggesting that FXR activation in other tissues also contribute to liver regeneration (71).

Intestinal FXR may participate in the promotion of liver regeneration through secreting fibroblast growth factor (FGF) 15 in mice or FGF19 in humans. Trans-enterocytic BAs flux from the intestinal lumen to the basolateral side drives FXR-dependent FGF15 synthesis in the ileum (72). FGF15 reaches the liver and regulates BA homeostasis by an FGFR4-dependent activation of c-Jun N-terminal kinase (JNK) and extracellular signal-regulated kinase (ERK) pathways, leading to transcriptional inhibition of CYP7A1 in hepatocytes (72). Therefore, BAs-mediated intestinal FXR-dependent FGF15

production appears as a necessary gut-derived signal for liver protection after partial hepatectomy by maintaining BAs homeostasis. Besides, FGF15 may directly contribute to liver regeneration by stimulating the proliferation of hepatocytes and cholangiocytes (73). Mechanistically, the FGF15-FGFR4-STAT3 signaling pathway, which is required for Foxm1 transcription and cell cycle progression, controls hepatocyte proliferation in the regenerating liver (74). Furthermore, it should be noted that FXR is expressed in the kidney at high levels and in the thymus, spleen, ovary, testes, heart, and eyes at lower levels (63). Increased systemic BAs after partial hepatectomy may also act on these tissues and organs in an FXR-dependent manner and indirectly affect liver regeneration, which needs further exploration.

Taken together, gut microbiota-mediated deconjugation improves the reabsorption of BAs and the abundance of colonic primary conjugated BAs, which may induce protective as well as proliferative cascades in the damaged liver by initiating FXR-dependent responses.

Gut Microbiota-Dependent Production of Secondary BAs Facilitates Liver Regeneration

Gut microbiota dehydrogenates primary BAs to secondary BAs mainly in the colon. Secondary BAs are the most efficient agonists of Taketa G-protein-coupled receptor 5 (TGR5) (75). TGR5 is ubiquitously expressed in many tissues, including the liver, gallbladder, intestine, brown and white adipose tissue, skeletal muscle, and so on (63). In the liver, TGR5 is highly expressed in cholangiocytes, Kupffer cells, and endothelial cells but weakly or not expressed in hepatocytes (76). Therefore, TGR5-dependent protective effects against BAs overload are likely due to other mechanisms rather than regulation of BAs synthesis. TGR5 regulates BA size and composition by reducing hydrophobicity and increasing secretion. A shift towards a more hydrophobic BAs pool is associated with inhibition of liver regeneration (77). TGR5-KO mice have a more hydrophobic BAs composition and hydrophobic BAs accumulation in the liver leads to toxic injury, which is alleviated by a BA resin enriched diet (58). In addition, TGR5 promotes cystic fibrosis transmembrane conductance regulator (CFTR)-dependent Cl^- secretion and BAs uptake into biliary epithelia and reduces biliary bile acid concentrations (78). TGR5-dependent increased output of biliary HCO_3^- and Cl^- after partial hepatectomy also enhances bile secretion, which prevents the remnant liver from BAs-induced toxicity (58). Furthermore, the production and release of the cytokine after partial hepatectomy are crucial for normal liver regeneration. It has been demonstrated that the immunosuppressive effect of secondary BAs on macrophage is mediated by TGR5 (79), which inhibits LPS-induced expression of cytokines and reduces liver injury (80), by suppressing NF-κB transcription activity and its target gene expression (81). Therefore, gut microbiota-controlled activation of TGR5 may contribute to liver regeneration by regulating hepatic inflammatory response and limiting hepatocyte necrosis after partial hepatectomy. Moreover, TGR5 in skeletal muscle and brown adipose tissue promotes energy expenditure through iodothyronine deiodinase 2 enzyme (DIO2), which converts inactive thyroxine into active thyroid hormone (63). TGR5 in colonic L cells mediates synthesis and secretion of intestinal glucagon-like peptide-1 (GLP-1), which could stimulate insulin secretion (82). Thyroid hormone and insulin cooperated with other growth factors allow the hepatocyte to overcome cell-cycle checkpoint control, initiating and regulating liver regeneration (53).

Gut microbiota-dependent conversion of primary BAs to secondary BAs is also involved in the development of liver cancer (83). Primary BAs stimulate, whereas secondary BAs

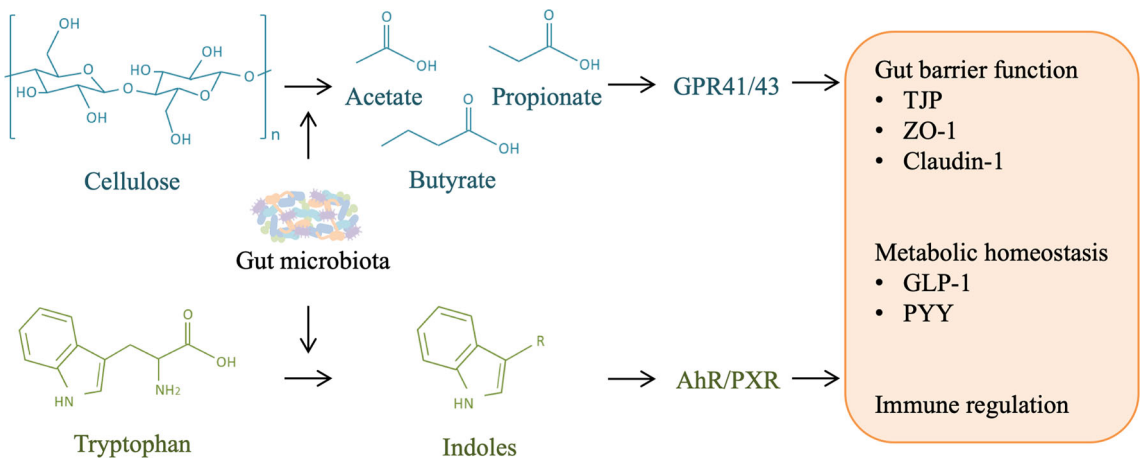


FIGURE 5 | Role of other microbial metabolites in liver injury and regeneration. Gut microbiota is responsible for the production of short-chain fatty acids (SCFAs) and indoles from cellulose and tryptophan in food-intake, respectively. SCFAs can activate host G-protein-coupled receptor (GPR) 41/43, and indoles can activate aryl hydrocarbon receptor (AHR)/pregnane X receptor (PXR), contributing to gut barrier protection, metabolism homeostasis, and immune regulation, which may facilitate liver regeneration by alleviating liver injury.

suppress, the expression of chemokine (C-X-C motif) ligand 16 (CXCL16) by liver sinusoidal endothelial cells, which induces accumulation of hepatic CXCR6+ natural killer T (NKT) cells and production of interferon-γ, inhibiting both primary and metastatic liver tumors.

In general, gut microbiota-dependent production of secondary BAs may reduce the inflammatory response and promote liver regeneration by TGR5-dependent regulation of the BA pool and production of T3 and GLP-1. Elucidating ways to fine-tune gut microbiota-BAs-host interaction is a promising strategy to assist normal liver regeneration.

GUT MICROBIAL METABOLITES SHORT-CHAIN FATTY ACIDS AND INDOLES MAY ASSIST LIVER REGENERATION IN A SIMILAR WAY

Short Chain Fatty Acids May Assist Liver Regeneration

Short-chain fatty acids (SCFAs) produced by gut microbial fermentation have multiple physiological functions (84). The most abundant SCFAs in the gut are acetate, propionate, and butyrate (85, 86). Bacteroidetes produce acetate and propionate, and Firmicutes are the primary butyrate producers (87–90).

The intestinal tract is the major site of SCFAs production and the biological concentration gradient falls from the gut to the peripheral tissues. Butyrate is largely metabolized in the intestinal epithelium, and the rest is degraded in the liver (91, 92). Most propionate is degraded in the liver, and a substantial portion of acetate passes into the systemic circulation (92, 93). SCFAs function as extracellular agonists for G-protein-coupled receptor (GPR) 41 and GPR43 (94). Butyrate, but not acetate or propionate, also activates the GPR109A (95). GPR41, GPR43, and GPR109A are expressed by intestinal epithelial cells and immune cells (84). Stimulation of GPRs by SCFAs activates ERK1/2, c-JNK, and p38/mitogen-activated protein kinases (MAPKs) (96). In addition, butyrate broadly affects transcription by activating histone acetyltransferases (HATs) and suppressing nuclear class I histone (HDACs) (84). Butyrate can also act as an extracellular agonist activating peroxisome proliferator-activated receptor γ (PPAR-γ), which plays anti-inflammatory effects (97, 98).

SCFAs are important substrates for the integrity of the epithelial barrier, which limits pro-inflammatory load to the liver. Butyrate enhances gut barrier function by increasing the expression of claudin-1 and zonula occludens-1 (ZO-1), decreasing LPS translocation and inhibiting downstream inflammatory responses (99, 100). Therefore, SCFAs may indirectly affect liver injury and regeneration through maintaining gut barrier function.

In addition, SCFAs play potential roles in metabolism homeostasis during liver regeneration. Acetate, propionate, and butyrate regulate hepatic glucose and lipid homeostasis in a PPAR-γ dependent manner (101). Acetate and propionate inhibit adipocyte lipolysis *via* GPR43, which reduces free fatty acid (FFA) flux to the liver and ameliorates the deterioration of glucose homeostasis caused by fatty liver (102, 103). Propionate and butyrate have metabolic benefits through activating gluconeogenesis gene expression (104). Moreover, SCFAs stimulate gut hormone production of GLP-1 and peptide YY (PYY), improving the metabolic phenotype (105). Butyrate inhibits NF-κB activation in lamina propria macrophages and reduces the responsiveness of lamina propria macrophages to commensal bacteria (106, 107). Butyrate alleviates ischemia-reperfusion liver injury by preventing NF-κB activation and reducing inflammatory factors production (108). Propionate and butyrate have potential roles in the production and function of regulatory T cells *via* inhibiting histone deacetylase (HDAc) (109, 110).

These studies highlight the interaction between gut microbiota-derived SCFAs and the immune and metabolic homeostasis of the host, which may play an important role in liver injury and regeneration (**Figure 5**).

Indoles May Assist Liver Regeneration

Tryptophan is one of the essential amino acids and must be supplied by dietary uptake. The majority of tryptophan is absorbed in the small intestine, and a significant fraction may also reach the colon. Intestinal tryptophan metabolism follows three major pathways: (1) the kynurenine pathway in epithelial and immune cells through indoleamine 2,3-dioxygenase 1 (IDO1); (2) the serotonin pathway in enterochromaffin cells through tryptophan hydroxylase 1 (TpH1); and (3) direct transformation by commensal bacteria into indole and indole derivatives (111). Numerous bacterial species can metabolize tryptophan, which has been described in a previous review (112). Indole is the most abundant metabolite of gut microbial tryptophan, which is followed by indol-3-acetic acid (IAA) and indole-3-propionic acid (IPA), in adults (112). Indole and many indole derivatives, such as IAA, IPA, indole-3-aldehyde (IAld), tryptamine (TA), 3-methylindole (skatole), and indoxyl-3-sulfate (I3S), are endogenous ligands of aryl hydrocarbon receptor (AhR) (113). AhR is initially well-known for its major role in the metabolism and elimination of environmental toxicants, but it also serves as a key transcription factor controlling many critical cellular functions and organ homeostasis (114).

Given the production site, the role of gut microbial tryptophan metabolism is preponderant in intestinal AhR activity. Activation of AhR in the gut improves intestinal barrier function by decreasing gut permeability and mucosal inflammation (83). Indole upregulates the expression of genes involved in the maintenance of epithelial-cell tight-junction resistance (115, 116). Indoleacrylic acid (IA) improves intestinal epithelial barrier function by promoting goblet cell differentiation and mucus production, which is possibly mediated by AhR activation (117). Moreover, in the context of indole, IPA also regulates intestinal barrier function by acting as a ligand for the pregnane X receptor (PXR) (118). These studies suggest that tryptophan metabolites enhance the intestinal epithelial barrier function by AhR and PXR signaling pathways, which decreases translocation of gut-derived LPS and then could participate in liver injury and regeneration.

Similar to SCFAs, indole is also able to modulate the secretion of GLP-1 from colonic L cells and influence host metabolism in an AhR-dependent manner (119, 120). GLP-1 has an important role in glucose homeostasis and liver function, which is probably involved in liver regeneration.

In addition, AhR is expressed by many immune cells and plays an important role in the regulation of immune response in health and disease (113). Gut microbiota-derived IAA and TA reduce inflammatory responses in macrophages and hepatocytes (121), suggesting that gut microbial tryptophan metabolites could regulate immune responses in the liver as well, which indicates their potential roles in liver injury and regeneration. However, the exact effects of gut microbial tryptophan metabolites on liver regeneration still need further research (**Figure 5**).

CONCLUSION

Mechanisms of liver regeneration are complex. The crosstalk between gut microbiota and liver allows that gut-derived signals are orchestrated in liver injury and regeneration. Gut-derived LPS and gut microbiota-associated bile acid metabolism appear to have multiple effects on liver injury and regeneration, while SCFAs and tryptophan metabolites produced by gut microbiota have potential benefits in liver regeneration. A comprehensive understanding of these roles of gut-derived signals in liver injury and regeneration will enable the further development of rational specific therapies to either directly improve liver regeneration or prevent complications that appear in the process of liver regeneration. The role of gut-derived signals in animal models of liver regeneration has been briefly described in this review, but lessons learned from animal models still need to be confirmed in more clinical settings, such as chronic liver injury with abnormal liver architecture and advanced liver fibrosis, in which normal regeneration of compromised liver is expected. However, gut-derived signals have the promise to motivate translational and interventional studies of liver injury and regeneration.

AUTHOR CONTRIBUTIONS

ZZ managed the literature research and wrote the first draft of the manuscript. BW critically reviewed the manuscript and provided valuable discussions and criticisms. All authors contributed to the article and approved the submitted version.

FUNDING

This study was supported by National Natural Science Foundation of China [grant numbers 82170668 and 81790633], Sino-German Center for Research Promotion [grant numbers GZ1546], and CAMS Innovation Fund for Medical Sciences [grant numbers 2019-I2M-5-045].

REFERENCES

1. Michalopoulos GK. Hepatostat: Liver Regeneration and Normal Liver Tissue Maintenance. *Hepatology* (2017) 65(4):1384–92. doi: 10.1002/hep.28988
2. Michalopoulos GK, Khan Z. Liver Stem Cells: Experimental Findings and Implications for Human Liver Disease. *Gastroenterology* (2015) 149(4):876–82. doi: 10.1053/j.gastro.2015.08.004
3. Forbes SJ, Newsome PN. Liver Regeneration - Mechanisms and Models to Clinical Application. *Nat Rev Gastroenterol Hepatol* (2016) 13(8):473–85. doi: 10.1038/nrgastro.2016.97
4. Fausto N, Campbell JS, Riehle KJ. Liver Regeneration. *Hepatology* (2006) 43 (2 Suppl 1):S45–53. doi: 10.1002/hep.20969
5. Shavandi A, Saeedi P, Gerard P, Jalalvandi E, Cannella D, Bekhit AE, et al. The Role of Microbiota in Tissue Repair and Regeneration. *J Tissue Eng Regener Med* (2020) 14(3):539–55. doi: 10.1002/term.3009
6. Cornell RP. Gut-Derived Endotoxin Elicits Hepatotrophic Factor Secretion for Liver Regeneration. *Am J Physiol* (1985) 249(5 Pt 2):R551–62. doi: 10.1152/ajpregu.1985.249.5.R551
7. Cornell RP. Restriction of Gut-Derived Endotoxin Impairs DNA Synthesis for Liver Regeneration. *Am J Physiol* (1985) 249(5 Pt 2):R563–9. doi: 10.1152/ajpregu.1985.249.5.R563
8. Cornell RP, Liljequist BL, Bartizal KF. Depressed Liver Regeneration After Partial Hepatectomy of Germ-Free, Athymic and Lipopolysaccharide-Resistant Mice. *Hepatology* (1990) 11(6):916–22. doi: 10.1002/hep.1840110603
9. Van Treuren W, Dodd D. Microbial Contribution to the Human Metabolome: Implications for Health and Disease. *Annu Rev Pathol* (2019) 24(15):345–69. doi: 10.1146/annurev-pathol-020117-043559
10. Garrett WS. Immune Recognition of Microbial Metabolites. *Nat Rev Immunol* (2019) 20(2):91–2. doi: 10.1038/s41577-019-0252-2
11. Bajaj JS, Khoruts A. Microbiota Changes and Intestinal Microbiota Transplantation in Liver Diseases and Cirrhosis. *J Hepatol* (2020) 72 (5):1003–27. doi: 10.1016/j.jhep.2020.01.017
12. Tokuhara D. Role of the Gut Microbiota in Regulating Non-Alcoholic Fatty Liver Disease in Children and Adolescents. *Front Nutr* (2021) 8:700058. doi: 10.3389/fnut.2021.700058
13. Lu H, Wu Z, Xu W, Yang J, Chen Y, Li L, et al. Intestinal Microbiota was Assessed in Cirrhotic Patients With Hepatitis B Virus Infection. Intestinal Microbiota of HBV Cirrhotic Patients. *Microb Ecol* (2011) 61(3):693–703. doi: 10.1007/s00248-010-9801-8
14. Boursier J, Mueller O, Barret M, Machado M, Fizanne L, Araujo-Perez F, et al. The Severity of Nonalcoholic Fatty Liver Disease Is Associated With Gut Dysbiosis and Shift in the Metabolic Function of the Gut Microbiota. *Hepatology* (2016) 63(3):764–75. doi: 10.1002/hep.28356
15. Yuan J, Chen C, Cui J, Lu J, Yan C, Wei X, et al. Fatty Liver Disease Caused by High-Alcohol-Producing Klebsiella Pneumoniae. *Cell Metab* (2019) 30 (4):675–88.e7. doi: 10.1016/j.cmet.2019.08.018
16. Wei Y, Li Y, Yan L, Sun C, Miao Q, Wang Q, et al. Alterations of Gut Microbiome in Autoimmune Hepatitis. *Gut* (2020) 69(3):569–77. doi: 10.1136/gutjnl-2018-317836
17. Kummen M, Holm K, Anmarkrud JA, Nygard S, Vesterhus M, Hoivik ML, et al. The Gut Microbial Profile in Patients With Primary Sclerosing Cholangitis Is Distinct From Patients With Ulcerative Colitis Without Biliary Disease and Healthy Controls. *Gut* (2017) 66(4):611–9. doi: 10.1136/gutjnl-2015-310500
18. Tang R, Wei Y, Li Y, Chen W, Chen H, Wang Q, et al. Gut Microbial Profile Is Altered in Primary Biliary Cholangitis and Partially Restored After UDCA Therapy. *Gut* (2018) 67(3):534–41. doi: 10.1136/gutjnl-2016-313332
19. Chen Y, Yang F, Lu H, Chen W, Chen H, Wang Q, et al. Characterization of Fecal Microbial Communities in Patients With Liver Cirrhosis. *Hepatology* (2011) 54(2):562–72. doi: 10.1002/hep.24423
20. Bajaj JS, Hylemon PB, Ridlon JM, Heuman DM, Daita K, White MB, et al. Colonic Mucosal Microbiome Differs From Stool Microbiome in Cirrhosis and Hepatic Encephalopathy and Is Linked to Cognition and Inflammation. *Am J Physiol Gastrointest Liver Physiol* (2012) 303(6):G675–85. doi: 10.1152/ajpgi.00152.2012

21. Bajaj JS, Vargas HE, Reddy KR, Lai JC, O'Leary JG, Tandon P, et al. Association Between Intestinal Microbiota Collected at Hospital Admission and Outcomes of Patients With Cirrhosis. *Clin Gastroenterol Hepatol* (2019) 17(4):756–65.e3. doi: 10.1016/j.cgh.2018.07.022
22. Rattan P, Minacapelli CD, Rustgi V. The Microbiome and Hepatocellular Carcinoma. *Liver Transpl* (2020) 26(10):1316–27. doi: 10.1002/lt.25828
23. Loomba R, Seguritan V, Li W, Long T, Klitgord N, Bhatt A, et al. Gut Microbiome-Based Metagenomic Signature for Non-Invasive Detection of Advanced Fibrosis in Human Nonalcoholic Fatty Liver Disease. *Cell Metab* (2017) 25(5):1054–62.e5. doi: 10.1016/j.cmet.2017.04.001
24. Qin N, Yang F, Li A, Prifti E, Chen Y, Shao L, et al. Alterations of the Human Gut Microbiome in Liver Cirrhosis. *Nature* (2014) 513(7516):59–64. doi: 10.1038/nature13568
25. Liu HX, Rocha CS, Dandekar S, Wan YJ. Functional Analysis of the Relationship Between Intestinal Microbiota and the Expression of Hepatic Genes and Pathways During the Course of Liver Regeneration. *J Hepatol* (2016) 64(3):641–50. doi: 10.1016/j.jhep.2015.09.022
26. Bao Q, Yu L, Chen D, Li L. Variation in the Gut Microbial Community Is Associated With the Progression of Liver Regeneration. *Hepatol Res* (2019) 50(1):121–36. doi: 10.1111/hepr.13424.
27. Gasaly N, de Vos P, Hermoso MA. Impact of Bacterial Metabolites on Gut Barrier Function and Host Immunity: A Focus on Bacterial Metabolism and Its Relevance for Intestinal Inflammation. *Front Immunol* (2021) 12:658354. doi: 10.3389/fimmu.2021.658354
28. Miyazaki M, Kohda S, Itoh H, Kaiho T, Kimura F, Ambiru S, et al. Inhibition of Hepatic Regeneration After 70% Partial Hepatectomy by Simultaneous Resection of the Bowel in Rats. *Eur Surg Res* (1995) 27(6):396–405. doi: 10.1159/000129426
29. Nolan JP. The Role of Intestinal Endotoxin in Liver Injury: A Long and Evolving History. *Hepatology* (2010) 52(5):1829–35. doi: 10.1002/hep.23917
30. Hartmann P, Chu H, Duan Y, Schnabl B. Gut Microbiota in Liver Disease: Too Much Is Harmful, Nothing at All Is Not Helpful Either. *Am J Physiol Gastrointest Liver Physiol* (2019) 316(5):G563–73. doi: 10.1152/ajpgi.00370.201
31. Seehofer D, Rayes N, Schiller R, Stockmann M, Muller AR, Schirmeier A, et al. Probiotics Partly Reverse Increased Bacterial Translocation After Simultaneous Liver Resection and Colonic Anastomosis in Rats. *J Surg Res* (2004) 117(2):262–71. doi: 10.1016/j.jss.2003.11.021
32. Rifatbegovic Z, Mesic D, Ljuca F, Zildzic M, Avdagic M, Grbic K, et al. Effect of Probiotics on Liver Function After Surgery Resection for Malignancy in the Liver Cirrhotic. *Med Arh* (2010) 64(4):208–11.
33. Rayes N, Pilarski T, Stockmann M, Bengmark S, Neuhaus P, Seehofer D. Effect of Pre- and Probiotics on Liver Regeneration After Resection: A Randomised, Double-Blind Pilot Study. *Benef Microbes* (2012) 3(3):237–44. doi: 10.3920/BM2012.0006
34. Wang Y, Kirpich I, Liu Y, Ma Z, Barve S, McClain CJ, et al. Lactobacillus Rhamnosus GG Treatment Potentiates Intestinal Hypoxia-Inducible Factor, Promotes Intestinal Integrity and Ameliorates Alcohol-Induced Liver Injury. *Am J Pathol* (2011) 179(6):2866–75. doi: 10.1016/j.ajpath.2011.08.039
35. Wang Y, Liu Y, Kirpich I, Ma Z, Wang C, Zhang M, et al. Lactobacillus Rhamnosus GG Reduces Hepatic TNFalpha Production and Inflammation in Chronic Alcohol-Induced Liver Injury. *J Nutr Biochem* (2013) 24 (9):1609–15. doi: 10.1016/j.jnutbio.2013.02.001
36. Li Y, Lv L, Ye J, Fang D, Shi D, Wu W, et al. Bifidobacterium Adolescentis CGMCC 15058 Alleviates Liver Injury, Enhances the Intestinal Barrier and Modifies the Gut Microbiota in D-Galactosamine-Treated Rats. *Appl Microbiol Biotechnol* (2019) 103(1):375–93. doi: 10.1007/s00253-018-9454-y
37. Li YT, Ye JZ, Lv LX, Xu H, Yang LY, Jiang XW, et al. Pretreatment With Bacillus Cereus Preserves Against D-Galactosamine-Induced Liver Injury in a Rat Model. *Front Microbiol* (2019) 10:1751. doi: 10.3389/fmicb.2019.01751
38. Wang Q, Lv L, Jiang H, Wang K, Yan R, Li Y, et al. Lactobacillus Helveticus R0052 Alleviates Liver Injury by Modulating Gut Microbiome and Metabolome in D-Galactosamine-Treated Rats. *Appl Microbiol Biotechnol* (2019) 103(23-24):9673–86. doi: 10.1007/s00253-019-10211-8
39. Wu W, Lv L, Shi D, Ye J, Fang D, Guo F, et al. Protective Effect of Akkermansia Muciniphila Against Immune-Mediated Liver Injury in a Mouse Model. *Front Microbiol* (2017) 8:1804. doi: 10.3389/fmicb.2017.01804
40. Prytz H, Holst-Christensen J, Korner B, Liehr H. Portal Venous and Systemic Endotoxaemia in Patients Without Liver Disease and Systemic Endotoxaemia in Patients With Cirrhosis. *Scand J Gastroenterol* (1976) 11 (8):857–63. doi: 10.1080/00365521.1976.12097199
41. Nolan JP. Endotoxin, Reticuloendothelial Function, and Liver Injury. *Hepatology* (1981) 1(5):458–65. doi: 10.1002/hep.1840010516
42. Rao R. Endotoxemia and Gut Barrier Dysfunction in Alcoholic Liver Disease. *Hepatology* (2009) 50(2):638–44. doi: 10.1002/hep.23009
43. Adachi Y, Moore LE, Bradford BU, Gao W, Thurman RG. Antibiotics Prevent Liver Injury in Rats Following Long-Term Exposure to Ethanol. *Gastroenterology* (1995) 108(1):218–24. doi: 10.1016/0016-5085(95)90027-6
44. Bataller R, Brenner DA. Liver Fibrosis. *J Clin Invest* (2005) 115(2):209–18. doi: 10.1172/JCI24282
45. Carotti S, Guarino MP, Vespasiani-Gentilucci U, Morini S. Starring Role of Toll-Like Receptor-4 Activation in the Gut-Liver Axis. *World J Gastrointest Pathophysiol* (2015) 6(4):99–109. doi: 10.4291/wjgp.v6.i4.99
46. Seki E, De Minicis S, Osterreicher CH, Kluwe J, Osawa Y, Brenner DA, et al. TLR4 Enhances TGF-Beta Signaling and Hepatic Fibrosis. *Nat Med* (2007) 13(11):1324–32. doi: 10.1038/nm1663
47. Krenkel O, Tacke F. Liver Macrophages in Tissue Homeostasis and Disease. *Nat Rev Immunol* (2017) 17(5):306–21. doi: 10.1038/nri.2017.11
48. Issa R, Zhou X, Trim N, Millward-Sadler H, Krane S, Benyon C, et al. Mutation in Collagen-1 That Confers Resistance to the Action of Collagenase Results in Failure of Recovery From CCl4-Induced Liver Fibrosis, Persistence of Activated Hepatic Stellate Cells, and Diminished Hepatocyte Regeneration. *FASEB J* (2003) 17(1):47–9. doi: 10.1096/fj.02-0494fje
49. Yu LX, Schwabe RF. The Gut Microbiome and Liver Cancer: Mechanisms and Clinical Translation. *Nat Rev Gastroenterol Hepatol* (2017) 14(9):527–39. doi: 10.1038/nrgastro.2017.72
50. Yu LX, Yan HX, Liu Q, Yang W, Wu HP, Dong W, et al. Endotoxin Accumulation Prevents Carcinogen-Induced Apoptosis and Promotes Liver Tumorigenesis in Rodents. *Hepatology* (2010) 52(4):1322–33. doi: 10.1002/hep.23845
51. Dapito DH, Mencin A, Gwak GY, Pradere JP, Jang MK, Mederacke I, et al. Promotion of Hepatocellular Carcinoma by the Intestinal Microbiota and TLR4. *Cancer Cell* (2012) 21(4):504–16. doi: 10.1016/j.ccr.2012.02.007
52. Cornell RP. Endotoxin-Induced Hyperinsulinemia and Hyperglucagonemia After Experimental Liver Injury. *Am J Physiol* (1981) 241(6):E428–35. doi: 10.1152/ajpendo.1981.241.6.E428
53. Taub R. Liver Regeneration: From Myth to Mechanism. *Nat Rev Mol Cell Biol* (2004) 5(10):836–47. doi: 10.1038/nrm1489
54. Fazel Modares N, Polz R, Haghighi F, Lamertz L, Behnke K, Zhuang Y, et al. IL-6 Trans-Signaling Controls Liver Regeneration After Partial Hepatectomy. *Hepatology* (2019). doi: 10.1016/S0618-8278(19)30621-8
55. Chiang JYL, Ferrell JM. Bile Acid Metabolism in Liver Pathobiology. *Gene Expr* (2018) 18(2):71–87. doi: 10.3727/105221618X15156018385515
56. Schneider KM, Albers S, Trautwein C. Role of Bile Acids in the Gut-Liver Axis. *J Hepatol* (2018) 68(5):1083–5. doi: 10.1016/j.jhep.2017.11.025
57. Doignon I, Julien B, Serriere-Lanneau V, Garcin I, Alonso G, Nicou A, et al. Immediate Neuroendocrine Signaling After Partial Hepatectomy Through Acute Portal Hyperpressure and Cholestasis. *J Hepatol* (2011) 54(3):481–8. doi: 10.1016/j.jhep.2010.07.012
58. Pean N, Doignon I, Garcin I, Besnard A, Julien B, Liu B, et al. The Receptor TGR5 Protects the Liver From Bile Acid Overload During Liver Regeneration in Mice. *Hepatology* (2013) 58(4):1451–60. doi: 10.1002/hep.26463
59. Merlen G, Ursic-Bedoya J, Jourdainne V, et al. Bile Acids and Their Receptors During Liver Regeneration: "Dangerous Protectors". *Mol Aspects Med* (2017) 56:25–33. doi: 10.1016/j.mam.2017.03.002
60. Huang W, Ma K, Zhang J, Qatanani M, Cuvillier J, Liu J, et al. Nuclear Receptor-Dependent Bile Acid Signaling Is Required for Normal Liver Regeneration. *Science* (2006) 312(5771):233–6. doi: 10.1126/science.1121435
61. Ueda J, Chijiiwa K, Nakano K, Zhao G, Tanaka M. Lack of Intestinal Bile Results in Delayed Liver Regeneration of Normal Rat Liver After Hepatectomy Accompanied by Impaired Cyclin E-Associated Kinase Activity. *Surgery* (2002) 131(5):564–73. doi: 10.1067/msy.2002.123008
62. Otao R, Beppu T, Isiko T, Mima K, Okabe H, Hayashi H, et al. External Biliary Drainage and Liver Regeneration After Major Hepatectomy. *Br J Surg* (2012) 99(11):1569–74. doi: 10.1002/bjs.8906

63. Wahlstrom A, Sayin SI, Marschall HU, Backhed F. Intestinal Crosstalk Between Bile Acids and Microbiota and Its Impact on Host Metabolism. *Cell Metab* (2016) 24(1):41–50. doi: 10.1016/j.cmet.2016.05.005
64. Jones BV, Begley M, Hill C, Gahan CG, Marchesi JR. Functional and Comparative Metagenomic Analysis of Bile Salt Hydrolase Activity in the Human Gut Microbiome. *Proc Natl Acad Sci USA* (2008) 105(36):13580–5. doi: 10.1073/pnas.0804437105
65. Vos TA, Ros JE, Havinga R, Moshage H, Kuipers F, Jansen PL, et al. Regulation of Hepatic Transport Systems Involved in Bile Secretion During Liver Regeneration in Rats. *Hepatology* (1999) 29(6):1833–9. doi: 10.1002/hep.510290638
66. Csanaky IL, Aleksunes LM, Tanaka Y, Klaassen CD. Role of Hepatic Transporters in Prevention of Bile Acid Toxicity After Partial Hepatectomy in Mice. *Am J Physiol Gastrointest Liver Physiol* (2009) 297 (3):G419–33. doi: 10.1152/ajpgi.90728.2008
67. Chiang JY. Bile Acid Metabolism and Signaling. *Compr Physiol* (2013) 3 (3):1191–212. doi: 10.1002/cphy.c120023
68. Ridlon JM, Kang DJ, Hylemon PB. Isolation and Characterization of a Bile Acid Inducible 7alpha-Dehydroxylating Operon in Clostridium Hylemonae TN271. *Anaerobe* (2010) 16(2):137–46. doi: 10.1016/j.anaerobe.2009.05.004
69. Ridlon JM, Harris SC, Bhowmik S, Kang DJ, Hylemon PB. Consequences of Bile Salt Biotransformations by Intestinal Bacteria. *Gut Microbes* (2016) 7 (1):22–39. doi: 10.1080/19490976.2015.1127483
70. Goodwin B, Jones SA, Price RR, Watson MA, McKee DD, Moore LB, et al. A Regulatory Cascade of the Nuclear Receptors FXR, SHP-1, and LRH-1 Represses Bile Acid Biosynthesis. *Mol Cell* (2000) 6(3):517–26. doi: 10.1016/S1097-2765(00)00051-4
71. Zhang L, Wang YD, Chen WD, Wang X, Lou G, Liu N, et al. Promotion of Liver Regeneration/Repair by Farnesoid X Receptor in Both Liver and Intestine in Mice. *Hepatology* (2012) 56(6):2336–43. doi: 10.1002/hep.25905
72. Inagaki T, Choi M, Moschetta A, Peng L, Cummins CL, McDonald JG, et al. Fibroblast Growth Factor 15 Functions as an Enterohepatic Signal to Regulate Bile Acid Homeostasis. *Cell Metab* (2005) 2(4):217–25. doi: 10.1016/j.cmet.2005.09.001
73. Uriarte I, Fernandez-Barrena MG, Monte MJ, Latasa MU, Chang HC, Carotti S, et al. Identification of Fibroblast Growth Factor 15 as a Novel Mediator of Liver Regeneration and its Application in the Prevention of Post-Resection Liver Failure in Mice. *Gut* (2013) 62(6):899–910. doi: 10.1136/gutjnl-2012-302945
74. Padrissa-Altes S, Bachofner M, Bogorad RL, Pohlmeier L, Rossolini T, Bohm F, et al. Control of Hepatocyte Proliferation and Survival by Fgf Receptors Is Essential for Liver Regeneration in Mice. *Gut* (2015) 64(9):1444–53. doi: 10.1136/gutjnl-2014-307874
75. Martinot E, Sedes L, Baptissart M, Lobaccaro JM, Caira F, Beaudoin C, et al. Bile Acids and Their Receptors. *Mol Aspects Med* (2017) 56:2–9. doi: 10.1016/j.mam.2017.01.006
76. Chiang JYL. Bile Acid Metabolism and Signaling in Liver Disease and Therapy. *Liver Res* (2017) 1(1):3–9. doi: 10.1016/j.livres.2017.05.001
77. Garcia-Rodriguez JL, Barbier-Torres L, Fernandez-Alvarez S, Gutierrez-de Juan V, Monte MJ, Halilbasic E, et al. SIRT1 Controls Liver Regeneration by Regulating Bile Acid Metabolism Through Farnesoid X Receptor and Mammalian Target of Rapamycin Signaling. *Hepatology* (2014) 59 (5):1972–83. doi: 10.1002/hep.26971
78. Keitel V, Cupisti K, Ullmer C, Knoefel WT, Kubitz R, Haussinger D. The Membrane-Bound Bile Acid Receptor TGR5 Is Localized in the Epithelium of Human Gallbladders. *Hepatology* (2009) 50(3):861–70. doi: 10.1002/hep.23032
79. Kawamata Y, Fujii R, Hosoya M, Harada M, Yoshida H, Miwa M, et al. A G Protein-Coupled Receptor Responsive to Bile Acids. *J Biol Chem* (2003) 278 (11):9435–40. doi: 10.1074/jbc.M209706200
80. Keitel V, Donner M, Winandy S, Kubitz R, Haussinger D. Expression and Function of the Bile Acid Receptor TGR5 in Kupffer Cells. *Biochem Biophys Res Commun* (2008) 372(1):78–84. doi: 10.1016/j.bbrc.2008.04.171
81. Wang YD, Chen WD, Yu D, Forman BM, Huang W. The G-Protein-Coupled Bile Acid Receptor, Gpbar1 (TGR5), Negatively Regulates Hepatic Inflammatory Response Through Antagonizing Nuclear Factor Kappa Light-Chain Enhancer of Activated B Cells (NF-KappaB) in Mice. *Hepatology* (2011) 54(4):1421–32. doi: 10.1002/hep.24525
82. Thomas C, Gioiello A, Noriega L, Strehle A, Oury J, Rizzo G, et al. TGR5-Mediated Bile Acid Sensing Controls Glucose Homeostasis. *Cell Metab* (2009) 10(3):167–77. doi: 10.1016/j.cmet.2009.08.001
83. Ma C, Han M, Heinrich B, Fu Q, Zhang Q, Sandhu M, et al. Gut Microbiome-Mediated Bile Acid Metabolism Regulates Liver Cancer *via* NKT Cells. *Science* (2018) 360(6391). doi: 10.1126/science.aan5931
84. Koh A, De Vadder F, Kovatcheva-Datchary P, Backhed F. From Dietary Fiber to Host Physiology: Short-Chain Fatty Acids as Key Bacterial Metabolites. *Cell* (2016) 165(6):1332–45. doi: 10.1016/j.cell.2016.05.041
85. Macfarlane GT, Macfarlane S. Bacteria, Colonic Fermentation, and Gastrointestinal Health. *J AOAC Int* (2012) 95(1):50–60. doi: 10.5740/jaoacint.SGE_Macfarlane
86. Cummings JH, Pomare EW, Branch WJ, Naylor CP, Macfarlane GT. Short Chain Fatty Acids in Human Large Intestine, Portal, Hepatic and Venous Blood. *Gut* (1987) 28(10):1221–7. doi: 10.1136/gut.28.10.1221
87. El Kaoutari A, Armougom F, Gordon JI, Raoult D, Henrissat B. The Abundance and Variety of Carbohydrate-Active Enzymes in the Human Gut Microbiota. *Nat Rev Microbiol* (2013) 11(7):497–504. doi: 10.1038/nrmicro3050
88. Flint HJ, Duncan SH, Scott KP, Louis P. Links Between Diet, Gut Microbiota Composition and Gut Metabolism. *Proc Nutr Soc* (2015) 74(1):13–22. doi: 10.1017/S0029665114001463
89. Levy M, Thaiss CA, Elinav E. Metabolites: Messengers Between the Microbiota and the Immune System. *Genes Dev* (2016) 30(14):1589–97. doi: 10.1101/gad.284091.116
90. Rios-Covian D, Ruas-Madiedo P, Margolles A, Gueimonde M, de Los Reyes-Gavilan CG, Salazar N, et al. Intestinal Short Chain Fatty Acids and Their Link With Diet and Human Health. *Front Microbiol* (2016) 7:185. doi: 10.3389/fmicb.2016.00185
91. Donohoe DR, Collins LB, Wali A, Bigler R, Sun W, Bultman SJ. The Warburg Effect Dictates the Mechanism of Butyrate-Mediated Histone Acetylation and Cell Proliferation. *Mol Cell* (2012) 48(4):612–26. doi: 10.1016/j.molcel.2012.08.033
92. Bloemen JG, Venema K, van de Poll MC, Olde Damink SW, Buurman WA, Dejong CH. Short Chain Fatty Acids Exchange Across the Gut and Liver in Humans Measured at Surgery. *Clin Nutr* (2009) 28(6):657–61. doi: 10.1016/j.clnu.2009.05.011
93. Morrison DJ, Preston T. Formation of Short Chain Fatty Acids by the Gut Microbiota and Their Impact on Human Metabolism. *Gut Microbes* (2016) 7 (3):189–200. doi: 10.1080/19490976.2015.1134082
94. Brown AJ, Goldsworthy SM, Barnes AA, Eilert MM, Tcheang L, Daniels D, et al. The Orphan G Protein-Coupled Receptors GPR41 and GPR43 Are Activated by Propionate and Other Short Chain Carboxylic Acids. *J Biol Chem* (2003) 278(13):11312–9. doi: 10.1074/jbc.M211609200
95. Thangaraju M, Cresci GA, Liu K, Ananth S, Gnanaprakasam JP, Browning DD, et al. GPR109A Is a G-Protein-Coupled Receptor for the Bacterial Fermentation Product Butyrate and Functions as a Tumor Suppressor in Colon. *Cancer Res* (2009) 69(7):2826–32. doi: 10.1158/0008-5472.CAN-08-4466
96. Seljeset S, Siehler S. Receptor-Specific Regulation of ERK1/2 Activation by Members of the "Free Fatty Acid Receptor" Family. *J Recept Signal Transduct Res* (2012) 32(4):196–201. doi: 10.3109/10799893.2012.692118
97. Alex S, Lange K, Amolo T, Grinstead JS, Haakonsson AK, Szalowska E, et al. Short-Chain Fatty Acids Stimulate Angiopoietin-Like 4 Synthesis in Human Colon Adenocarcinoma Cells by Activating Peroxisome Proliferator-Activated Receptor Gamma. *Mol Cell Biol* (2013) 33(7):1303–16. doi: 10.1128/MCB.00858-12
98. Croasdell A, Duffney PF, Kim N, Lacy SH, Sime PJ, Phipps RP. PPARgamma and the Innate Immune System Mediate the Resolution of Inflammation. *PPAR Res* (2015) 2015:549691. doi: 10.1155/2015/549691
99. Wang HB, Wang PY, Wang X, Wan YL, Liu YC. Butyrate Enhances Intestinal Epithelial Barrier Function *via* Up-Regulation of Tight Junction Protein Claudin-1 Transcription. *Dig Dis Sci* (2012) 57(12):3126–35. doi: 10.1007/s10620-012-2259-4
100. Liu B, Qian J, Wang Q, Ma Z, Qiao Y. Butyrate Protects Rat Liver Against Total Hepatic Ischemia Reperfusion Injury With Bowel Congestion. *PloS One* (2014) 9(8):e106184. doi: 10.1371/journal.pone.0106184
101. den Besten G, Bleeker A, Gerding A, van Eunen K, Havinga R, van Dijk TH, et al. Short-Chain Fatty Acids Protect Against High-Fat Diet-Induced

Obesity *via* a PPARgamma-Dependent Switch From Lipogenesis to Fat Oxidation. *Diabetes* (2015) 64(7):2398–408. doi: 10.2337/db14-1213
102. Crouse JR, Gerson CD, DeCarli LM, Lieber CS. Role of Acetate in the Reduction of Plasma Free Fatty Acids Produced by Ethanol in Man. *J Lipid Res* (1968) 9(4):509–12. doi: 10.1016/S0022-2275(20)42731-2
103. Ge H, Li X, Weiszmann J, Wang P, Baribault H, Chen JL, et al. Activation of G Protein-Coupled Receptor 43 in Adipocytes Leads to Inhibition of Lipolysis and Suppression of Plasma Free Fatty Acids. *Endocrinology* (2008) 149(9):4519–26. doi: 10.1210/en.2008-0059
104. De Vadder F, Kovatcheva-Datchary P, Goncalves D, Vinera J, Zitoun C, Duchampt A, et al. Microbiota-Generated Metabolites Promote Metabolic Benefits *via* Gut-Brain Neural Circuits. *Cell* (2014) 156(1-2):84–96. doi: 10.1016/j.cell.2013.12.016
105. Kaji I, Karaki S, Kuwahara A. Short-Chain Fatty Acid Receptor and Its Contribution to Glucagon-Like Peptide-1 Release. *Digestion* (2014) 89 (1):31–6. doi: 10.1159/000356211
106. Luhrs H, Gerke T, Muller JG, Melcher R, Schauber J, Boxberge F, et al. Butyrate Inhibits NF-kappaB Activation in Lamina Propria Macrophages of Patients With Ulcerative Colitis. *Scand J Gastroenterol* (2002) 37(4):458–66. doi: 10.1080/003655202317316105
107. Chang PV, Hao L, Offermanns S, Medzhitov R. The Microbial Metabolite Butyrate Regulates Intestinal Macrophage Function via Histone Deacetylase Inhibition. *Proc Natl Acad Sci USA* (2014) 111(6):2247–52. doi: 10.1073/pnas.1322269111
108. Qiao YL, Qian JM, Wang FR, Ma ZY, Wang QW. Butyrate Protects Liver Against Ischemia Reperfusion Injury by Inhibiting Nuclear Factor Kappa B Activation in Kupffer Cells. *J Surg Res* (2014) 187(2):653–9. doi: 10.1016/j.jss.2013.08.028
109. Arpaia N, Campbell C, Fan X, Dikiy S, van der Veeken J, deRoos P, et al. Metabolites Produced by Commensal Bacteria Promote Peripheral Regulatory T-Cell Generation. *Nature* (2013) 504(7480):451–5. doi: 10.1038/nature12726
110. Furusawa Y, Obata Y, Fukuda S, Endo TA, Nakato G, Takahashi D, et al. Commensal Microbe-Derived Butyrate Induces the Differentiation of Colonic Regulatory T Cells. *Nature* (2013) 504(7480):446–50. doi: 10.1038/nature12721
111. Agus A, Planchais J, Sokol H. Gut Microbiota Regulation of Tryptophan Metabolism in Health and Disease. *Cell Host Microbe* (2018) 23(6):716–24. doi: 10.1016/j.chom.2018.05.003
112. Roager HM, Licht TR. Microbial Tryptophan Catabolites in Health and Disease. *Nat Commun* (2018) 9(1):3294. doi: 10.1038/s41467-018-05470-4
113. Gutierrez-Vazquez C, Quintana FJ. Regulation of the Immune Response by the Aryl Hydrocarbon Receptor. *Immunity* (2018) 48(1):19–33. doi: 10.1016/j.immuni.2017.12.012
114. Roman AC, Carvajal-Gonzalez JM, Merino JM, Mulero-Navarro S, Fernandez-Salguero PM. The Aryl Hydrocarbon Receptor in the Crossroad of Signalling Networks With Therapeutic Value. *Pharmacol Ther* (2018) 185:50–63. doi: 10.1016/j.pharmthera.2017.12.003
115. Bansal T, Alaniz RC, Wood TK, Jayaraman A. The Bacterial Signal Indole Increases Epithelial-Cell Tight-Junction Resistance and Attenuates Indicators of Inflammation. *Proc Natl Acad Sci USA* (2010) 107(1):228–33. doi: 10.1073/pnas.0906112107
116. Shimada Y, Kinoshita M, Harada K, Mizutani M, Masahata K, Kayama H, et al. Commensal Bacteria-Dependent Indole Production Enhances Epithelial Barrier Function in the Colon. *PloS One* (2013) 8(11):e80604. doi: 10.1371/journal.pone.0080604
117. Wlodarska M, Luo C, Kolde R, d'Hennezel E, Annand JW, Heim CE, et al. Indoleacrylic Acid Produced by Commensal Peptostreptococcus Species Suppresses Inflammation. *Cell Host Microbe* (2017) 22(1):25–37.e6. doi: 10.1016/j.chom.2017.06.007
118. Venkatesh M, Mukherjee S, Wang H, Li H, Sun K, Benechet AP, et al. Symbiotic Bacterial Metabolites Regulate Gastrointestinal Barrier Function *via* the Xenobiotic Sensor PXR and Toll-Like Receptor 4. *Immunity* (2014) 41(2):296–310. doi: 10.1016/j.immuni.2014.06.014
119. Chimerel C, Emery E, Summers DK, Keyser U, Gribble FM, Reimann F. Bacterial Metabolite Indole Modulates Incretin Secretion From Intestinal Enteroendocrine L Cells. *Cell Rep* (2014) 9(4):1202–8. doi: 10.1016/j.celrep.2014.10.032
120. Natividad JM, Agus A, Planchais J, Lamas B, Jarry AC, Martin R, et al. Impaired Aryl Hydrocarbon Receptor Ligand Production by the Gut Microbiota Is a Key Factor in Metabolic Syndrome. *Cell Metab* (2018) 28 (5):737–49.e4. doi: 10.1016/j.cmet.2018.07.001
121. Krishnan S, Ding Y, Saedi N, Choi M, Sridharan GV, Sherr DH, et al. Gut Microbiota-Derived Tryptophan Metabolites Modulate Inflammatory Response in Hepatocytes and Macrophages. *Cell Rep* (2018) 23(4):1099–111. doi: 10.1016/j.celrep.2018.03.109

Conflict of Interest: The authors declare that the research was conducted in the absence of any commercial or financial relationships that could be construed as a potential conflict of interest.

Publisher's Note: All claims expressed in this article are solely those of the authors and do not necessarily represent those of their affiliated organizations, or those of the publisher, the editors and the reviewers. Any product that may be evaluated in this article, or claim that may be made by its manufacturer, is not guaranteed or endorsed by the publisher.

Copyright © 2021 Zheng and Wang. This is an open-access article distributed under the terms of the Creative Commons Attribution License (CC BY). The use, distribution or reproduction in other forums is permitted, provided the original author(s) and the copyright owner(s) are credited and that the original publication in this journal is cited, in accordance with accepted academic practice. No use, distribution or reproduction is permitted which does not comply with these terms.

frontiers in Immunology

ORIGINAL RESEARCH
published: 16 December 2021
doi: 10.3389/fimmu.2021.760475

Critical Roles of Spätzle5 in Antimicrobial Peptide Production Against *Escherichia coli* in *Tenebrio molitor* Malpighian Tubules

Maryam Ali Mohammadie Kojour[1], *Tariku Tesfaye Edosa*[1,2], *Ho Am Jang*[1], *Maryam Keshavarz*[1,3], *Yong Hun Jo*[1]* *and Yeon Soo Han*[1]*

[1] Department of Applied Biology, Institute of Environmentally-Friendly Agriculture (IEFA), College of Agriculture and Life Sciences, Chonnam National University, Gwangju, South Korea, [2] Ethiopian Institute of Agricultural Research, Ambo Agricultural Research Center, Ambo, Ethiopia, [3] Department of Evolutionary Biology, Institute of Biology, Free University of Berlin, Berlin, Germany

OPEN ACCESS

Edited by:
Carmen Mariana Chifiriuc, University of Bucharest, Romania

Reviewed by:
Fengliang Jin, South China Agricultural University, China
Susanna Valanne, Tampere University, Finland

***Correspondence:**
Yeon Soo Han
hanys@jnu.ac.kr
Yong Hun Jo
yhun1228@jnu.ac.kr

Specialty section:
This article was submitted to Microbial Immunology, a section of the journal Frontiers in Immunology

Received: 18 August 2021
Accepted: 22 November 2021
Published: 16 December 2021

Citation:
Ali Mohammadie Kojour M, Edosa TT, Jang HA, Keshavarz M, Jo YH and Han YS (2021) Critical Roles of Spätzle5 in Antimicrobial Peptide Production Against Escherichia coli in Tenebrio molitor Malpighian Tubules. Front. Immunol. 12:760475. doi: 10.3389/fimmu.2021.760475

The dimeric cytokine ligand Spätzle (Spz) is responsible for Toll pathway activation and antimicrobial peptide (AMP) production upon pathogen challenge in *Tenebrio molitor*. Here, we indicated that *Tm*Spz5 has a functional role in response to bacterial infections. We showed that the highest expression of *TmSpz5* is induced by *Candida albicans*. However, *TmSpz5* knockdown reduced larval survival against *Escherichia coli* and *Staphylococcus aureus*. To evaluate the molecular mechanism underlying the observed survival differences, the role of *TmSpz5* in AMP production was examined by RNA interference and microbial injection. *T. molitor* AMPs that are active against Gram-negative and -positive bacteria, including *Tm*tenecins, *Tm*attacins, *Tm*coleoptericins, *Tm*taumatin-like-proteins, and *Tm*cecropin-2, were significantly downregulated by *TmSpz-5* RNAi in the Malpighian tubules (MTs) following a challenge with *E. coli* and *S. aureus*. However, upon infection with *C. albicans* the mRNA levels of most AMPs in the ds*TmSpz5*-injected group were similar to those in the control groups. Likewise, the expression of the transcription factors NF-κB, *TmDorX2*, and *TmRelish* were noticeably suppressed in the MTs of *TmSpz5*-silenced larvae. Moreover, *E. coli*-infected *TmSpz5* knockdown larvae showed decreased antimicrobial activity in the MTs and hindgut compared with the control group. These results demonstrate that *Tm*Spz5 has a defined role in *T. molitor* innate immunity by regulating AMP expression in MTs in response to *E. coli*.

Keywords: *Tenebrio molitor*, innate immune response, spätzle 5, antimicrobial peptides, NF-κB, Toll signaling pathway, Malpighian tubules

INTRODUCTION

Insects have been the largest and most diverse class over millions of years of evolution and have adapted to survive in a vast range of ecological territories (1–3). Owing to their exposure to various pathogen sources including bacteria, fungi, parasites, and viruses, they have evolved several multifunctional defense mechanisms, making them an exceptional model for immunity studies

(4, 5). Unlike mammals, insects do not have an adaptive immunity (2). However, they do possess a functional innate immune system, involving both humoral and cellular immune responses (6). Cellular immunity, mediated by hemocytes (insect blood cells), involves nodulation (7), encapsulation (8), and phagocytosis (9). Humoral immune response, on the other hand, is mainly mediated by fat bodies (the equivalent of the mammalian liver) and soluble plasma proteins. The production of antimicrobial peptides (AMPs) is the main determinant of humoral immunity (6). Following invader recognition, AMP production is stimulated by the activation of two major signaling pathways, the immune deficiency (Imd) and Toll pathways (6, 10).

The Toll signaling pathway was initially identified as a dorso-ventral axis establishment regulator during embryonic development in *Drosophila melanogaster* (11). Since then, extensive molecular and mapping studies have provided insight into the roles of the Toll pathway and its components in the *Drosophila* immune system. The key activator of the Toll transmembrane-associated receptor is the endogenous cytokine-like polypeptide Spätzle (Spz) (12). Invader detection by peptidoglycan recognition proteins (PGRPs) or β-1,3-glucan recognition protein (βGRP)/Gram-negative-binding proteins (GNBPs) in *Drosophila* leads to a proteolytic cascade that eventually results in Spätzle cleavage and activation. Spätzle can then bind to the Toll receptor and activate downstream signaling pathways, leading to AMP production (10, 13, 14). In addition to its role in *D. melanogaster*, Spätzle has been shown to have significant roles in different species and taxa, including mosquitoes (15–17), *Manduca sexta* (18), *Bombyx mori* (19), shrimp (20), and *Tenebrio molitor* (21).

Comprehensive biochemical studies of innate immunity claim for a relatively large insect model to enable the collection of sufficient hemolymph samples. Thus, in the last two decades, *T. molitor* has become a common model for biochemical and molecular studies on innate immunity pathways and their components (22).

Toll signaling in *T. molitor* is activated when PGRP-SA and GNBP1 recognize *meso*-diaminopimelic acid (DAP)-type peptidoglycan (PGN) of Gram-negative bacteria and some *Bacillus* species, and the lysine-type peptidoglycan of Gram-positive bacteria (21, 23–26). However, in *Drosophila*, the PGRP-SA/GNBP1 complex solely recognizes Gram-positive bacterial and fungal infections, whereas Gram-negative bacteria can be sensed by the alternative receptors PGRP-LC and PGRP-LE and triggers the Imd signaling pathway (6, 27–31). Following recognition, a proteolytic cascade activation, including modular serine protease (MSP), Spz-processing enzyme (SPE)-activating enzyme (SAE), and SPE, leads to the cleavage of Spätzle zymogen, and eventually, mature Spätzle recruitments to the Toll receptor (32, 33). Upon Spz–Toll association in *T. molitor*, an intracellular cascade is activated, resulting in the engagement of myeloid differentiation factor 88 (MyD88), tube, pelle, pellino, and tumor necrosis factor receptor associated factor (TRAF). This ultimately leads to the binding of cactin to cactus, a dorsal-related immunity factor (Dif) and dorsal inhibitor (34, 35). These transcription factors translocate to the nucleus (36, 37), where they bind to NF-κB-response elements and induce AMP genes transcription (38–43). We have identified nine *Spätzle* genes (*TmSpz-like*, *-1b*, *-3*, *-4*, *-5*, *-6*, *-7*, *-7a*, and *-7b*) in *T. molitor*. However, the functional importance of these isoforms is poorly understood. To date, only two *T. molitor Spätzle* genes (*TmSpz4* and *TmSpz6*) have been functionally characterized (44, 45). In this study, we focused on the immunological significance of *Tm*Spz5 against microbial infection (**Supplementary Table 1**).

MATERIALS AND METHODS

Insect Rearing

T. molitor larvae were reared under dark conditions at 26 ± 1°C and 60 ± 5% relative humidity in an environmental chamber established in the laboratory. Larvae were fed an artificial diet consisting of 1.1 g sorbic acid, 1.1 ml propionic acid, 20 g bean powder, 10 g brewer's yeast powder, and 200 g wheat bran in 4,400 ml distilled water. The feed was autoclaved at 121°C for 15 min and fed to healthy 10th–12th instar larvae for all experiments.

Microorganism Preparation

The Gram-negative bacterium *Escherichia coli* (strain K12), Gram-positive bacterium *Staphylococcus aureus* (strain RN4220), and fungus *Candida albicans* (strain AUMC 13529) were used as pathogenic invaders. *E. coli* and *S. aureus* were cultured in Luria–Bertani (LB) broth, and *C. albicans* was cultured in Sabouraud's dextrose broth overnight at 37°C. The microorganisms were harvested and washed twice in phosphate-buffered saline (PBS; pH 7.0) and then centrifuged at 3,500 × g for 15 min. Subsequently, the samples were suspended in PBS, and concentrations were measured at 600 nm (OD_{600}) by spectrophotometry (Eppendorf, Hamburg, Germany). *E. coli* and *S. aureus* were diluted to 1×10^6 cells/μl, and *C. albicans* was diluted to 5×10^4 cells/μl for immune challenge studies.

Computational Sequence Analysis of *TmSpz5*

The *TmSpz5* gene sequence (accession number: MW916536) was obtained from the *T. molitor* RNAseq analysis (unpublished) and NCBI Expressed Sequence Tag (EST) database. The *Tribolium castaneum* Spz5 amino acid sequence (accession number: XP_008193940.1) was used as the query for identification by local-tblastn searches. The full-length open reading frame (ORF) and deduced amino acid sequences of *TmSpz5* were analyzed using BLASTp (NCBI; https://blast.ncbi.nlm.nih.gov/Blast.cgi). The domain architectures of the protein sequences were retrieved using InterProScan (https://www.ebi.ac.uk/interpro/search/sequence-search). Signal peptides were predicted using the SignalP 5.0 server (http://www.cbs.dtu.dk/services/SignalP/).

A multiple-sequence alignment of the *Tm*Spz5 amino acid sequence with representative Spätzle amino acid sequences from other insects (retrieved from GenBank) was generated using ClustalX 2.1 (46). Estimation of the percent identity and

phylogenetic analyses were performed using ClustalX 2.1 (pim as the output file) and MEGA version 7.0 (47), respectively. Evolutionary relationships were inferred using the neighbor-joining method (48), and the bootstrap consensus tree was inferred from 1,000 replicates. Several protein sequences were used to generate the phylogenetic tree, including those of *Tc*Spz5, *Tribolium castaneum* spätzle 5 isoform X1 (XP_008193940.1); *Tc*Spz5, *Tribolium castaneum* spätzle 5 isoform X2 (XP_015836109.1); *At*Spz5like, *Aethina tumida* spätzle 5-like (XP_019879590.1); *So*Spz5like, *Sitophilus oryzae* spätzle 5-like (XP_030767938.1); *Ms*Spz5, *M. sexta* spätzli 5 (XP_037299529.1); *Bm*Spz5, *B. mori* spätzli 5 (XP_004924790.1); *Aa*Spz5like, *Anopheles albimanus* spätzle 5-like (XP_035790066.1); *Dme*Spz5, *D. melanogaster* spätzle5 (NP_647753.1); *Dma*Spz5, *Drosophila mauritiana* spätzle 5 (XP_033160799.1); *Ar*Spz5, *Athalia rosae* spätzli 5 (XP_012261687.1); *Pg*Spz5, *Pseudomyrmex gracilis* spätzle 5 isoform X3 (XP_020284715.1); and *Pv*Spz4, *Penaeus vannamei* spätzle 4 (ANJ04742.1).

Analysis of *TmSpz5* Expression and Induction

The protocols for the developmental stage- and tissue-specific analyses have been reported previously (44, 45, 49). Briefly, total RNA was isolated from different developmental stages (eggs, young larvae (instars 10–12), late larvae (instars 14-15), pre-pupae, 1- to 7-day-old pupae, and 1- to 5-day-old adults) and tissues [integument, gut, fat bodies, Malpighian tubule (MT), hemocytes of last instar larvae and 5-day-old adults, and ovary and testis of 5-day-old adults] of *T. molitor*.

To analyze the induction of *TmSpz5*, suspensions containing 1×10^6 cells/μl of *E. coli* and *S. aureus* and 5×10^4 cells/μl of *C. albicans* were injected into *T. molitor* larvae at instars 10–12 (n = 20). PBS-injected *T. molitor* larvae were used as the control group. Samples were collected at 3, 6, 9, 12, and 24 h post-microbial challenge.

Total RNA was isolated using the Clear-S Total RNA Extraction Kit (Invirustech Co., Gwangju, South Korea) according to the manufacturer's instructions. Then, 2 μg of total RNA was used as the template to synthesize cDNA using the Oligo (dT)12–18 primers under the following reaction conditions: 72°C for 5 min, 42°C for 1 h, and 94°C for 5 min. The MyGenie96 Thermal Block (Bioneer, Daejeon, Korea) and AccuPower® RT PreMix (Bioneer) were used according to the manufacturer's instructions. cDNA was stored at -20°C until further use.

Relative quantitative PCR (qRT-PCR) was performed using AccuPower® 2X GreenStar qPCR Master Mix (Bioneer) with synthesized cDNAs and specific primers (*TmSpz5*_qPCR_Fw and *TmSpz5*_qPCR_Rv), as depicted in **Table 1**, with an initial denaturation of 95°C for 20 s, followed by 40 cycles at 95°C for 5 s and 60°C for 20 s. *T. molitor* ribosomal protein *L27a* (*TmL27a*) was used as an internal control, and the results were analyzed using the $2^{-\Delta\Delta Ct}$ method (50). The results are presented as means ± standard error (SE) of three biological replicates.

RNA Interference

To synthesize the double-stranded RNA (dsRNA) of the *TmSpz5* gene, primers containing the T7 promoter sequence at their 5′ ends were designed using SnapDragon-Long dsRNA Design (**Table 1**). PCR was performed using AccuPower® Pfu PCR PreMix with the *TmSpz5*_Fw and *TmSpz5*_Rv primers (**Table 1**) and according to the developmental expression pattern of *TmSpz5*, cDNA synthesized from pre-pupae (whole bodies) as a template under the following cycling conditions: an initial denaturation step at 94°C for 2 min followed by 35 cycles of denaturation at 94°C for 30 s, annealing at 53°C for 30 s, and extension at 72°C for 30 s, with a final extension step at 72°C for 5 min. PCR products were purified using the AccuPrep PCR Purification Kit (Bioneer), and dsRNA was synthesized using the AmpliScribe T7-Flash Transcription Kit (Epicentre Biotechnologies, Madison, WI, USA) according to the manufacturer's instructions. After synthesis, the dsRNA was purified by precipitation with 5 M ammonium acetate and 80% ethanol, followed by quantification using an Epoch spectrophotometer (BioTek Instruments, Inc., Winooski, VT, USA). The dsRNA for enhanced green fluorescent protein (ds*EGFP*) was synthesized for use as a control and was stored at -20°C until use.

Effect of *TmSpz5* Gene Silencing on Larval Mortality Against Microbial Challenge

To study the importance of *Tm*Spz5 in the *T. molitor* immune response, ds*TmSpz5* (1 μg/μl) was first injected into early-instar larvae (instars 10–12; n = 30) using disposable needles mounted onto a micro-applicator (Picospritzer III Micro Dispense System; Parker Hannifin, Hollis, NH, USA). An equal amount of ds*EGFP* was injected in the larvae at the same stage as the negative control. The efficiency of *TmSpz5* knockdown was evaluated by qRT-PCR, and over 86% knockdown was achieved at 4 days postinjection. The *TmSpz5*-silenced and ds*EGFP*-injected larval groups were challenged with *E. coli* (10^6 cells/μl), *S. aureus* (10^6 cells/μl), or *C. albicans* (5×10^4 cells/μl) in triplicate experiments. The challenged larvae were maintained for 10 days, and the number of surviving larvae was recorded. The survival rates of *TmSpz5*-silenced larvae were compared with those of the control larvae. Relevant analysis was performed using Kaplan–Meier plots (51).

Effect of ds*TmSpz5* on AMP Expression in Response to Microbial Challenge

To evaluate the functional properties of *TmSpz5* in the regulation of AMP gene expression in response to pathogens, RNAi was used for *TmSpz5* gene silencing, followed by the injection of larvae with *E. coli*, *S. aureus*, or *C. albicans*. ds*EGFP* and PBS were used as the negative and injection controls, respectively. At 24 h postinjection, the hemocytes, fat body, gut, and MTs were dissected, total RNA was extracted from each tissue, and cDNA was synthesized as described above. Next, qRT-PCR was performed with specific primers (**Table 1**) to analyze the temporal expression patterns of 14 AMP genes: *TmTenecin-1*, *-2*, *-3*, and *-4* (*TmTene1*, *2*, *3*, and *4*), *TmAttacin-1a*, *-1b*, and *-2* (*TmAtt1a*, *1b* and *2*), *TmDefensin* (*TmDef*), *TmDefensin-like* (*TmDef-like*), *TmColeoptericin-A* and *-B* (*TmColeA* and *B*), *TmCecropin-2* (*TmCec-2*), and *TmThaumatin like protein-1* and *-2* (*TmTLP1* and *2*).

TABLE 1 | Sequences of the primers used in this study.

Primer name	Sequence (5′–3′)
TmSpz5-qPCR-Fw	CAGTACGATGCACGAGAGGA
TmSpz5-qPCR-Rv	AACTGGGAAACCAGAACACG
TmSpz5-T7-Fw	TAATACGACTCACTATAGGGTCAGTACGATGCACGAGAGGA
TmSpz5-T7-Rv	TAATACGACTCACTATAGGGTAACTGGGAAACCAGAACACG
TmSpz5-cloning-Full ORF-Fw	CGCACATGTTGATGCATATTGAC
TmSpz5-cloning-Full ORF-Rv	TCTTTGTCTAACCGTTCGAGATG
TmL27a-qPCR-Fw	TCATCCTGAAGGCAAAGCTCCAGT
TmL27a-qPCR-Rv	AGGTTGGTTAGGCAGGCACCTTTA
dsEGFP-Fw	TAATACGACTCACTATAGGGTCGTAAACGGCCACAAGTTC
dsEGFP-Rv	TAATACGACTCACTATAGGGTTGCTCAGGTAGTGTTGTCG
TmTenecin-1_Fw	CAGCTGAAGAAATCGAACAAGG
TmTenecin-1_Rv	CAGACCCTCTTTCCGTTACAGT
TmTenecin-2_Fw	CAGCAAAACGGAGGATGGTC
TmTenecin-2_Rv	CGTTGAAATCGTGATCTTGTCC
TmTenecin-3_Fw	GATTTGCTTGATTCTGGTGGTC
TmTenecin-3_Rv	CTGATGGCCTCCTAAATGTCC
TmTenecin-4_Fw	GGACATTGAAGATCCAGGAAAG
TmTenecin-4_Rv	CGGTGTTCCTTATGTAGAGCTG
TmDefensin_Fw	AAATCGAACAAGGCCAACAC
TmDefencin_Rv	GCAAATGCAGACCCTCTTTC
TmDefencin-like_Fw	GCGATGCCTCATGAAGATGTAG
TmDefencin-like_Rv	CCAATGCAAACACATTCGTC
TmColeoptericinA_Fw	GGACAGAATGGTGGATGGTC
TmColeoptericinA_Rv	CTCCAACATTCCAGGTAGGC
TmColeoptericinB_Fw	CAGCTGTTGCCCACAAGTG
TmColeoptericinB_Rv	CTCAACGTTGGTCCTGGTGT
TmAttacin-1a_Fw	GAAACGAAATGGAAGGTGGA
TmAttacin-1a_Rv	TGCTTCGGCAGACAATACAG
TmAttacin-1b_Fw	GAGCTGTGAATGCAGGACAA
TmAttacin-1b_Rv	CCCTCTGATGAAACCTCCAA
TmAttacin-2_Fw	AACTGGGATATTCGCACGTC
TmAttacin-2_Rv	CCCTCCGAAATGTCTGTTGT
TmCecropin-2_Fw	TACTAGCAGCGCCAAAACCT
TmCecropin-2_Rv	CTGGAACATTAGGCGGAGAA
TmThaumatin-like protein-1_Fw	CTCAAAGGACACGCAGGACT
TmThaumatin-like protein-1_Rv	ACTTTGAGCTTCTCGGGACA
TmThaumatin-like protein-2_Fw	CCGTCTGGCTAGGAGTTCTG
TmThaumatin-like protein-2_Rv	ACTCCTCCAGCTCCGTTACA

Underline indicates T7 promotor sequence.

Effects of ds*TmSpz5* on NF-κB Gene Expression

To study the effects of ds*TmSpz5* on the expression of NF-κB genes, including *TmDorsal isoform X2* (*TmDorX2*) and *TmRelish* (*TmRel*), *TmSpz5* was silenced in early-instar larvae and *E. coli*, *S. aureus*, and *C. albicans* were injected at 4 days post-double-strand treatment. At 24 h after pathogen injection, the MTs, hemocytes, gut, and fat bodies were dissected. Total RNA extraction and cDNA synthesis were performed as described above.

Effects of *TmSpz5* RNAi on Antimicrobial Activity Against *E. coli*

The AMPs and NF-κB gene expression patterns led us to perform colony-forming unit (CFU) assay to assess the *in vitro* AMP activity against Gram-negative bacteria. Therefore, *TmSpz5* dsRNA-treated young instar larvae of *T. molitor* were injected with *E. coli* (10^6 cells). At 48 h post–pathogen injection, the hemolymph, midgut, hindgut, and Malpighian tubules were isolated in 100 µl 1× PBS. PBS and ds*EGFP* were injected as uninfected and dsRNA control groups, respectively. Tissue samples were homogenized and centrifuged at 15,000 rpm at 4°C for 10 min, and then the supernatants were boiled at 100°C for 10 min and centrifuged again at 15,000 rpm at 4°C for 10 min. Consequently, the protein content of extracted peptides has been measured by an Epoch machine and 50 ng of tissue samples was assayed with 10^6 cells of *E. coli* in 1× PBS at 37°C for 2 h (52). Eventually, 2,000-fold serial dilutions were performed, and 100 µl of the resulting mixture was plated onto LB agar, followed by incubation at 37°C for 16 h. The colony numbers of assayed plates were then counted.

Data Analysis

Statistical analyses were performed using SAS 9.4 (SAS Institute, Inc., Cary, NC, USA), and cumulative survival was analyzed by Tukey's multiple-comparison test, with a significance level of $p < 0.05$. Fold change in expression of the AMP genes compared to

the levels of the internal control (*TmL27a*) and external control (PBS) was calculated using the $2^{-\Delta\Delta Ct}$ method.

RESULTS

In Silico Analysis of *TmSpz5*

To acquire the full-length cDNA sequence of *TmSpz5*, a local blast search of the *T. molitor* RNAseq database was performed using the *T. castaneum* Spätzle5 protein sequence as the query. The *TmSpz5* full-length ORF consisted of 1,062 bp, encoding a polypeptide of 353 amino acid residues (**Figure 1**). As determined using InterProScan, the *Tm*Spz5 amino acid sequence contained a cystine-knot domain at the C-terminus (which binds to the Toll receptor), one cleavage site predicted to be processed by SPE, and a predicted signal peptide at the N-terminus (**Figure 1**). Additionally, the conserved domains in *Tm*Spz5 were compared at the amino acid level using ClustalX 2.1 and multiple-sequence alignment. *Tm*Spz5 sequences were conserved at the protein level among insect species (**Figure 2A**). A phylogenetic analysis illustrated that *Tm*Spätzle5 in the order Coleoptera formed a group with other isoforms of Spätzle5 from *T. castaneum* (**Figure 2B**).

Temporal and Spatial Expression of *TmSpz5*

TmSpz5 mRNA expression patterns were evaluated by qRT-PCR at different developmental stages and in various tissues in larvae and adults. *TmSpz5* was observed at essentially all developmental

```
      G CCC GGG GTA GCG CAC ATG TTG ATG CAT ATT GAC TCT TCA CTT AAG CTA ATG TTT
GCG AAC TTA CGA TCA GTG CTG GTT CTC GTG CTT GCC ATT TTC TGA CTC GAC TCG CCT GTG

ATG AGC GGC ACA AAG ACC CAA ACC ATC TGC CTA GTC CTC ATC GCG CTG GTG CTA CCC GCA    60
 M   S   G   T   K   T   Q   T   I   C   L   V   L   I   A   L   V   L   P   A    20

AAG AGT CAC TCC TAC TGT ACC AAC ACC TAT GGG ACA GAA ATC TGC AGT TTC CTG CCG GCA   120
 K   S   H   S   Y   C   T   N   T   Y   G   T   E   I   C   S   F   L   P   A    40

GCT CCT GGA AAA ACT CCT CCG TGT GCC CTT CCA GGA CTC ACC TAC TGC GAG CAC CTA GAG   180
 A   P   G   K   T   P   P   C   A   L   P   G   L   T   Y   C   E   H   L   E    60

CAC TAC CCC GGG CAA AGA ATC GAG TAC TTG ATT CAA AAA TGG CGT TTC GAC CAC TCT ACG   240
 H   Y   P   G   Q   R   I   E   Y   L   I   Q   K   W   R   F   D   H   S   T    80

ACT CTC GTG GAC GAG TCC AAG GAA GAC TTC ACC TCT TAC TAC TAC CCT CCC CCG TCT TAC   300
 T   L   V   D   E   S   K   E   D   F   T   S   Y   Y   Y   P   P   P   S   Y   100

AAA TAC GGA CCG AGC AAC AAC ATC AAA CAA GAG GGT TAC TAC CCC GAA CCC ATT TAC ATC   360
 K   Y   G   P   S   N   N   I   K   Q   E   G   Y   Y   P   E   P   I   Y   I   120

CCC AAG CCT AAC TAC GCG TTC GAT CCT AGC ACG AGG GTG GGA AAC GCG TAC ATT CCC CCG   420
 P   K   P   N   Y   A   F   D   P   S   T   R   V   G   N   A   Y   I   P   P   140

CAT CCT TAC AAC GCC ACC CAG AGC TTC GCG GGT TAT CCT GAC AGG GCA CAA TAC TAC AAT   480
 H   P   Y   N   A   T   Q   S   F   A   G   Y   P   D   R   A   Q   Y   Y   N   160

TAC AAA TAT TCG AAT AAC ATT CCG CCG AGT GGT GCG CCT AGA GAC GTG TAC GGT CCT TCA   540
 Y   K   Y   S   N   N   I   P   P   S   G   A   P   R   D   V   Y   G   P   S   180

GCT GCC TAC TCG GCG TTG ATC CTC CCC CAG GTC AAC CCT TAC GTG AAC AAG GTG TGG AAC   600
 A   A   Y   S   A   L   I   L   P   Q   V   N   P   Y   V   N   K   V   W   N   200

AGG AAG GAC GAG AAG TAC GGT AAA GCG ATC TTG ATA AGG AAG AAG CGA TCG GAG ATG GTG   660
 R   K   D   E   K   Y   G   K   A   I   L   I   R   K   K   R   S   E   M   V   220

TCG CGG AAG ATG AGG AAG TTG AAG TCG ATT GGT CAG CAC AAC AAC AGT ACG ATG CAC GAG   720
 S   R   K   M   R   K   L   K   S   I   G   Q   H   N   N   S   T   M   H   E   240

AGG ACG AAG AGA CAA AGT GCT TTG ACT GGA CAG AGT CTC TGC ACG GCG AGG TCT CAG TTT   780
 R   T   K   R   Q   S   A   L   T   G   Q   S   L   C   T   A   R   S   Q   F   260

ATC ATG CCC AGG GCT GCG TTG AAT AAT AAA GGC AAC TGG ATG TAT GTT GTC AAC ATG CCA   840
 I   M   P   R   A   A   L   N   N   K   G   N   W   M   Y   V   V   N   M   P   280

GAA CTG GAC AAC AGA TTT ACT CAG CTC GTC AAG AGT GAA ACT TGT GCG TCG CAG ACT TGC   900
 E   L   D   N   R   F   T   Q   L   V   K   S   E   T   C   A   S   Q   T   C   300

AGC GGC CTC TGC GGT CTT CCG CTA GGG TAT ACG TCC AGA TGC GAG CAG AAG TAC GTC CAG   960
 S   G   L   C   G   L   P   L   G   Y   T   S   R   C   E   Q   K   Y   V   Q   320

AAA AGA CTA GTA GCG CTG GAG GGC GGC GGG AAC GAC CTC TAC ACC GAC GTG TTC TGG TTC  1020
 K   R   L   V   A   L   E   G   G   G   N   D   L   Y   T   D   V   F   W   F   340

CCC AGT TGT TGT GTA TGT ACC ATC TCG AAC GGT TAG                                  1056
 P   S   C   C   V   C   T   I   S   N   G   *                                    351

ACA AAG ATT TTT GAA TAA TAT GTA GGC GCT AAT TTT ATA TTT TTT CAA TTA TAG TTA CCA
AAA GGC GAA A
```

FIGURE 1 | Nucleotide and deduced amino acid sequences of *T. molitor Spätzle5* (*TmSpz5*). The *Tm*Spz5 full-length open reading frame (ORF) consisted of 1,062 bp, encoding a polypeptide of 353 amino acid residues. The cystine-knot domain is shown in a yellow box, and the signal peptide region and cleavage site are indicated by red and blue arrows, respectively. The stop codon is shown with an asterisk.

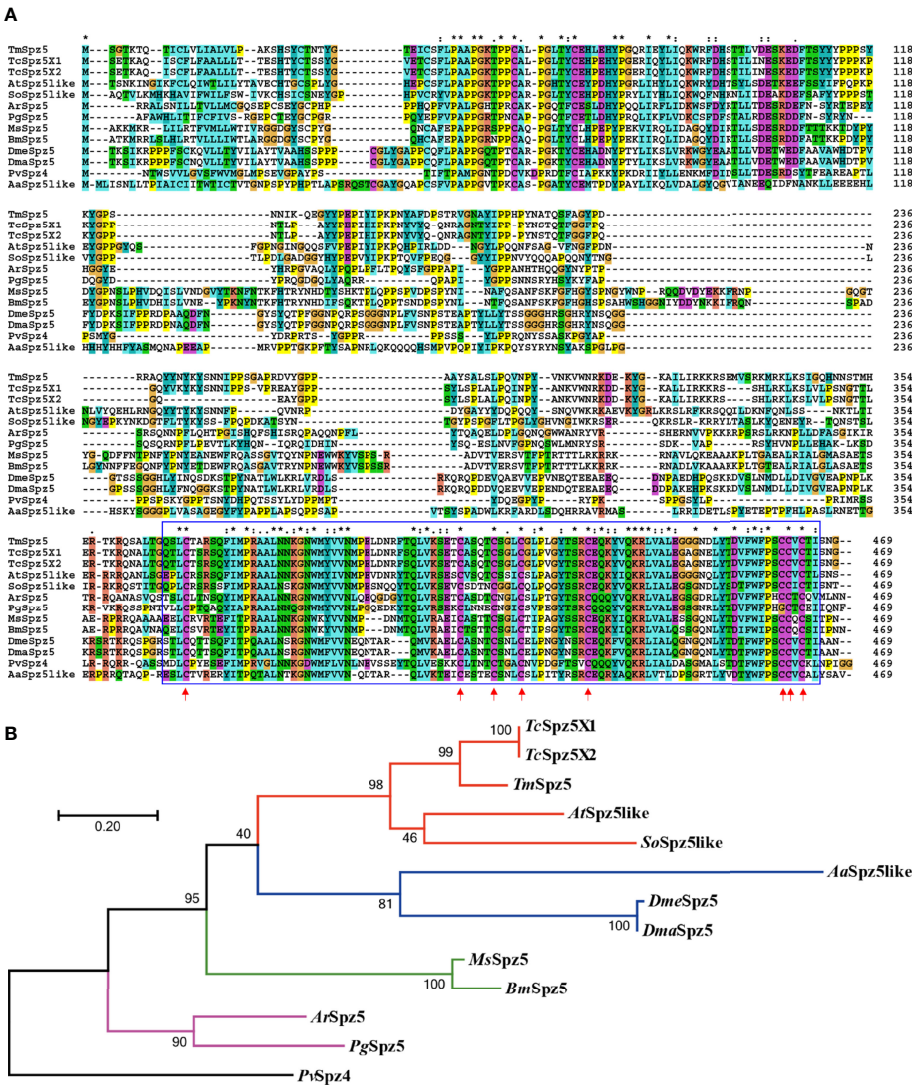


FIGURE 2 | Multiple-sequence alignment **(A)** and phylogenetic analysis **(B)** of *T. molitor* Spätzle5 (*Tm*Spz5). A domain analysis was performed using ClustalX2, and the phylogenetic tree was constructed using MEGA7 with the maximum likelihood method and 1,000 bootstrap replicates (where numbers at nodes indicate bootstrap support). The representative Spätzle 5 protein sequences showed high homology at the conserved domains marked in blue boxes, and the red arrows indicate conserved cystine-knot domain scores between groups. A neighbor-joining (NJ) tree was constructed based on the protein sequences of *Tc*Spz5, *Tribolium castaneum* spätzle 5 isoform X1 (XP_008193940.1); *Tc*Spz5, *Tribolium castaneum* spätzle 5 isoform X2 (XP_015836109.1); *At*Spz5like, *A. tumida* spätzle 5-like (XP_019879590.1); *So*Spz5like, *S. oryzae* spätzle 5-like (XP_030767938.1); *Ms*Spz5, *M. sexta* spätzle 5 (XP_037299529.1); *Bm*Spz5, *B. mori* spätzle 5 (XP_004924790.1); *Aa*Spz5like, *A. albimanus* spätzle 5-like (XP_035790066.1); *Dme*Spz5, *D. melanogaster* spaetzle5 (NP_647753.1); *Dma*Spz5, *D. mauritiana* spätzle 5 (XP_033160799.1); *Ar*Spz5, *A. rosae* spätzle 5 (XP_012261687.1); *Pg*Spz5, *P. gracilis* spätzle 5 isoform X3 (XP_020284715.1); and *Pv*Spz4, *P. vannamei* spätzle 4 (ANJ04742.1) which was used as the outgroup. Colored lines indicate different insect orders; red: Coleopteran, green: Lepidopteran, blue: Dipteran, purple: Hymenopteran. *Pv*Spz4, illustrated black, belongs to the Crustacean class.

stages (**Figure 3A**). However, the highest expression levels were seen in embryos and pupae. The mRNA levels decreased at the larval stage, and in late larvae, it shows the lowest expression. We observed fluctuations in the expression pattern during pupal stages with a plateau phase in late pupae. Overall, increased *TmSpz5* mRNA levels were observed during molting and each ecdysis, with a gradual fall across each individual stage.

With respect to tissue expression patterns (**Figures 3B, C**), *TmSpz5* expression levels were highest in MTs, followed by (in decreasing order) the hemocytes, fat bodies, integument, and gut in larvae. Contrarily, in adults, the mRNA expression of *TmSpz5* was low in MTs and highest in the gut.

Patterns of *TmSpz5* Induction

TmSpz5 expression in immune-challenged *T. molitor* larvae was examined after *E. coli*, *S. aureus*, and *C. albicans* injections (**Figure 4**), using PBS injection as the control. Four tissues, including the fat bodies (**Figure 4A**), hemocytes (**Figure 4B**), gut

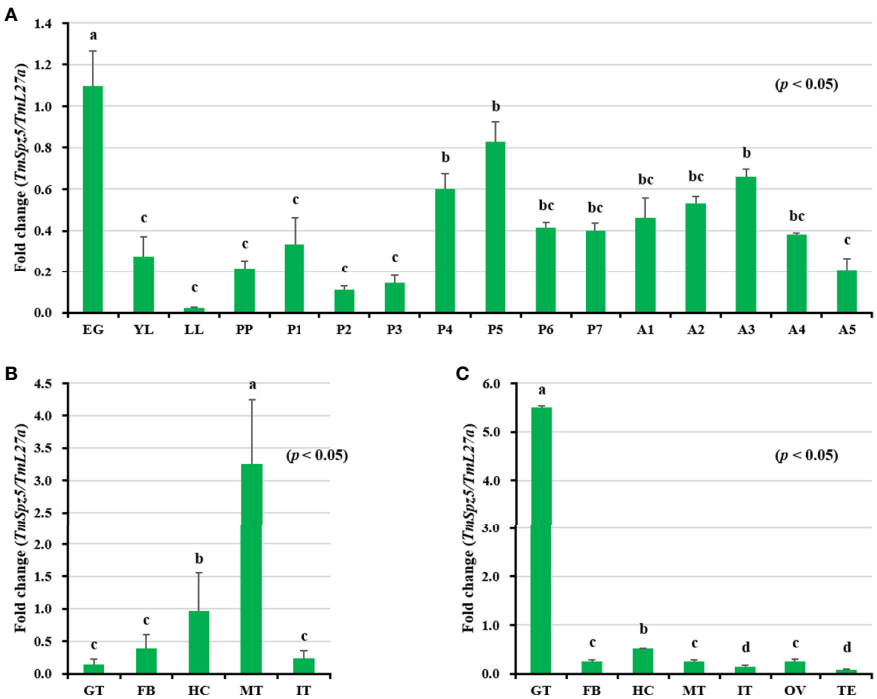


FIGURE 3 | Developmental stage- and tissue-specific expression patterns of *TmSpz5* measured by qRT-PCR. **(A)** Relative *TmSpz5* mRNA levels in eggs (EG), young larvae (YL), late-instar larvae (LL), pre-pupae (PP), 1- to 7-day-old pupae (P1–P7), and 1- to 5-day-old adults (A1–A5) are illustrated. Expression levels were the highest in the eggs and the pupae. The mRNA levels decreased in the larval stage and were lowest in the late larval stage. Increases in *TmSpz5* transcript levels were detected during molting and in each ecdysis with a gradual decrease across each individual stage. *TmSpz5* tissue expression patterns in late instar larvae **(B)** and adults **(C)** were also examined. Total RNA was extracted from different tissues, including the integument (IT), Malpighian tubule (MT), gut (GT), hemocytes (HC), and fat bodies (FB) of late instar larvae and the integument (IT), Malpighian tubule (MT), gut (GT), hemocytes (HC), fat bodies (FB), ovary (OV), and testis (TE) of 5-day-old adults. Total RNA was isolated from 20 mealworms and *T. molitor* 60S ribosomal protein 27a (*TmL27a*) primers were used as internal control (N = 3). One-way ANOVA and Tukey's multiple-range test at a 95% confidence level were used for comparisons. Bars with the same letter are not significantly different by Tukey's multiple-range test ($p < 0.05$).

(**Figure 4C**), and MTs (**Figure 4D**), were collected at 3, 6, 9, 12, and 24 h post-pathogen injection for total RNA extraction. *TmSpz5* expression was considerably upregulated in response to bacterial and fungal infections. *TmSpz5* expression varied in tissue- and time-dependent manners. The highest expression levels were seen in the gut at 12 and 24 h and in the fat bodies at 9 and 24 h after infection (in that order), in response to all three pathogens. Of note, in the fat bodies, the expression of *TmSpz5* was lowest at 12 h, possibly due to fluctuations in mRNA expression after infection as also reported earlier (35, 44, 49, 53). In MTs, there was also a noticeable upregulation in response to *C. albicans* and *E. coli* at 3 h post injection and in response to *S. aureus* at 9 h postinjection. *C. albicans* also induced *TmSpz5* expression in the hemocytes at 12 h postinjection.

Effect of *TmSpz5* RNAi on *T. molitor* Survival

Considering our observation that *TmSpz5* expression is induced by different pathogens, we further examined the survival rate of *TmSpz5*-silenced larvae using the RNAi technique. *TmSpz5* mRNA levels were decreased by 86% 4 days after ds*TmSpz5* injection (**Figure 5A**), confirming the efficiency of the RNAi.

Subsequent to confirmation of RNAi efficiency, pathogens of interest were injected. Survival rates of *TmSpz5*-silenced larvae were then evaluated over 10 days following microbial infection. ds*EGFP* was used as the control group for ds*TmSpz5*. PBS-injected larvae showed no statistically significant differences in survival between the ds*TmSpz5* and ds*EGFP* groups (data not shown). ds*TmSpz5* larvae showed considerable reductions in survival in response to *E. coli* and *S. aureus* (survival rates of approximately 33% and 58%, respectively) (**Figures 5B, C**). Interestingly, *C. albicans*-injected larvae showed similar survival rates to those of the PBS group (**Figure 5D**).

Effect of *TmSpz5* Gene Silencing on Antimicrobial Peptide Production

The survival analysis indicated that *TmSpz5* gene silencing accelerated the vulnerability of larvae challenged with *E. coli* and *S. aureus*, but not *C. albicans*. We further evaluated the induction of AMPs following challenge with *E. coli*, *S. aureus*, and *C. albicans* in *TmSpz5*-silenced *T. molitor* larvae. In particular, we knocked down *TmSpz5* and evaluated the levels of 14 AMP genes 24 h after the microbial challenge.

According to the results of the survival analysis, we expected *TmSpz5* silencing to lead to AMP downregulation in response to

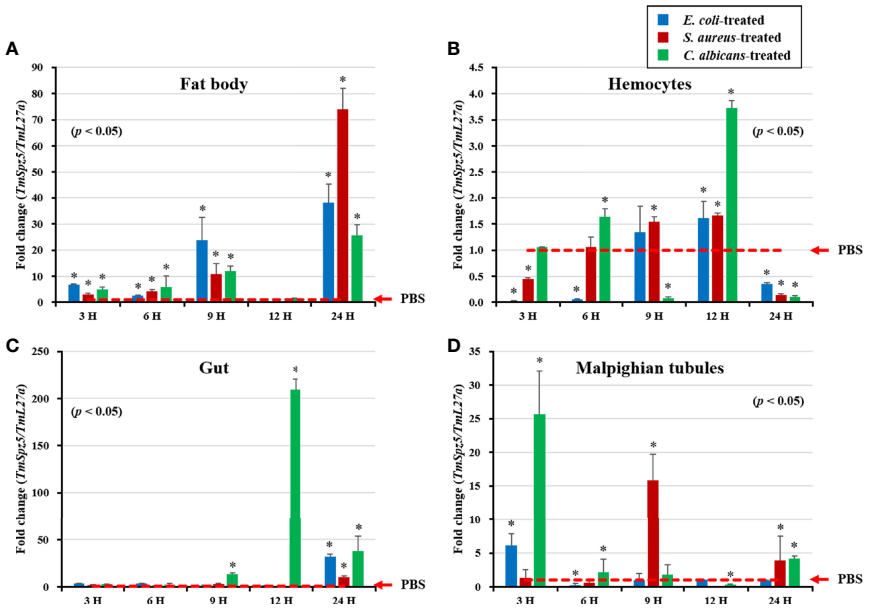


FIGURE 4 | Temporal expression patterns of *TmSpz5* in immune-challenged *T. molitor* larvae. Levels of *TmSpz5* mRNA in the fat bodies **(A)**, hemocytes **(B)**, gut **(C)**, and Malpighian tubules **(D)** were examined by qRT-PCR 3, 6, 9, 12, and 24 h after infection with *E. coli* (10^6 cells/μl), *S. aureus* (10^6 cells/μl), and *C. albicans* (5×10^4 cells/μl). *TmSpz5* expression was highly induced in the presence of *C. albicans* and *S. aureus* in various tissues. PBS was used as an injection control, and *T. molitor* 60S ribosomal protein 27a (*TmL27a*) primers were used as internal control (n = 3). Asterisks indicate significant differences between infected and PBS-injected larval groups by Student's *t*-test ($p < 0.05$). Vertical bars indicate means ± SD (n = 20).

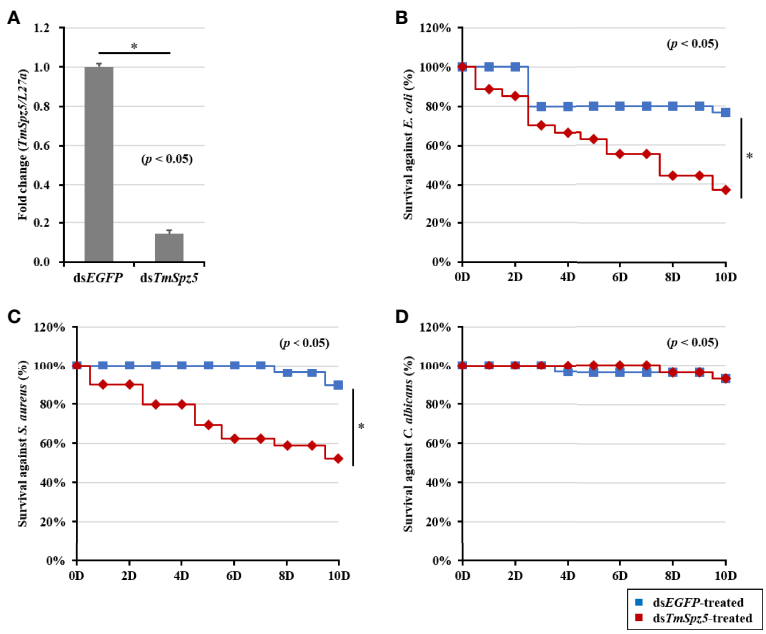


FIGURE 5 | Effect of *TmSpz5* gene silencing on the survival of *T. molitor* larvae. The silencing efficiency of ds*TmSpz5* was measured by qRT-PCR at 4 days postinjection **(A)**. *TmSpz5*-silenced larvae were injected with *E. coli* **(B)**, *S. aureus* **(C)**, and *C. albicans* **(D)**, and survival rates were studied over 10 days post-pathogen injection (n = 10 per group). Larval survival rates at 10 days post-microbial injection were 33% after *E. coli* injection, 58% after *S. aureus* injection, and 90% after *C. albicans* injection compared with the levels in the ds*EGFP*-injected control group. The data are reported as averages of three biologically independent replicates. Asterisks indicate significant differences between ds*TmSpz5*- and ds*EGFP*-injected groups. The survival analysis was performed using Kaplan–Meier plots (log-rank chi-squared test; $^*p < 0.05$).

E. coli and *S. aureus*. Our data illustrated that following confirmation of the *TmSpz5* knockdown efficiency (**Supplementary Figure 1**), 10 out of 14 AMP genes were significantly downregulated in the MTs of *TmSpz5*-silenced larvae after *E. coli* and *S. aureus* injections but not after fungal infection. In particular, the *E. coli* challenge resulted in reductions in the levels of *TmTene1*, *TmTene2*, *TmTene3*, *TmTene4*, *TmColeA*, *TmColeB*, *TmAtt1a*, *TmAtt1b*, *TmAtt2*, *TmTLP1*, and *TmTLP2* and the *S. aureus* challenge resulted in substantial reductions in the levels of *TmTene2*, *TmTene4*, *TmColeA*, *TmColeB*, *TmAtt1a*, *TmAtt1b*, *TmAtt2*, *TmTLP1*, and *TmTLP2* (**Figure 6**). In the gut, silencing of *TmSpz5* suppressed the *E. coli*-induced upregulation of *TmColeA*, *TmAtt1a*, and *TmAtt1b* as well as the S. *aureus*-induced regulation of *TmTene2*, *TmTene4*, *TmColeB*, *TmAtt1a*, and *TmAtt1b* (**Figures 7B, D, H–K**). In the hemocytes, *TmTene1*, *TmDef*, and *TmAtt2* were downregulated in response to *E. coli* and *TmDef* and *TmAtt2* were downregulated in response to *S. aureus* (**Figures 8A, E, L**). Moreover, in response to *C.albicans*, mRNA levels of TmTen3 and TmCec2 were downregulated

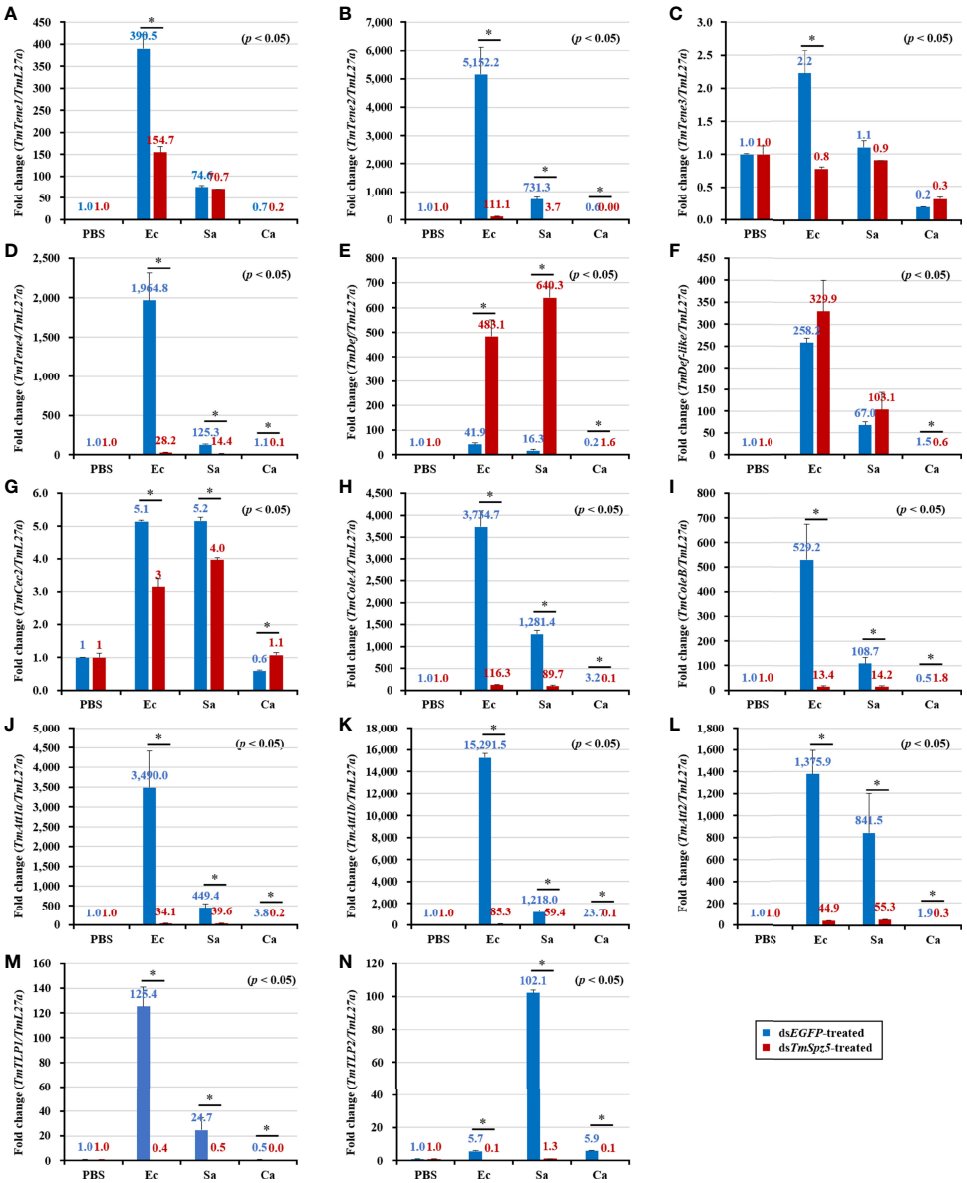


FIGURE 6 | Induction of 14 AMP genes in the Malpighian tubules of *TmSpz5*-silenced *T. molitor* larvae infected with *E. coli* (Ec), *S. aureus* (Sa), and *C. albicans* (Ca) using PBS as control. At 24 h after microbial injection, AMP genes, including *TmTene1* **(A)**, *TmTene2* **(B)**, *TmTene3* **(C)**, *TmTene4* **(D)**, *TmDef* **(E)**, *TmDef-like* **(F)**, *TmCec2* **(G)**, *TmColeA* **(H)**, *TmColeB* **(I)**, *TmAtt1a* **(J)**, *TmAtt1b* **(K)**, *TmAtt2* **(L)**, *TmTLP1* **(M)**, and *TmTLP2* **(N)** were examined by qPCR using ds*EGFP* as a knockdown control and *T. molitor ribosomal protein* (*TmL27a*) as an internal control. All experiments were performed in triplicate. Asterisks indicate significant differences between ds*TmSpz5*- and ds*EGFP*-treated groups determined by Student's *t*-test ($p < 0.05$).

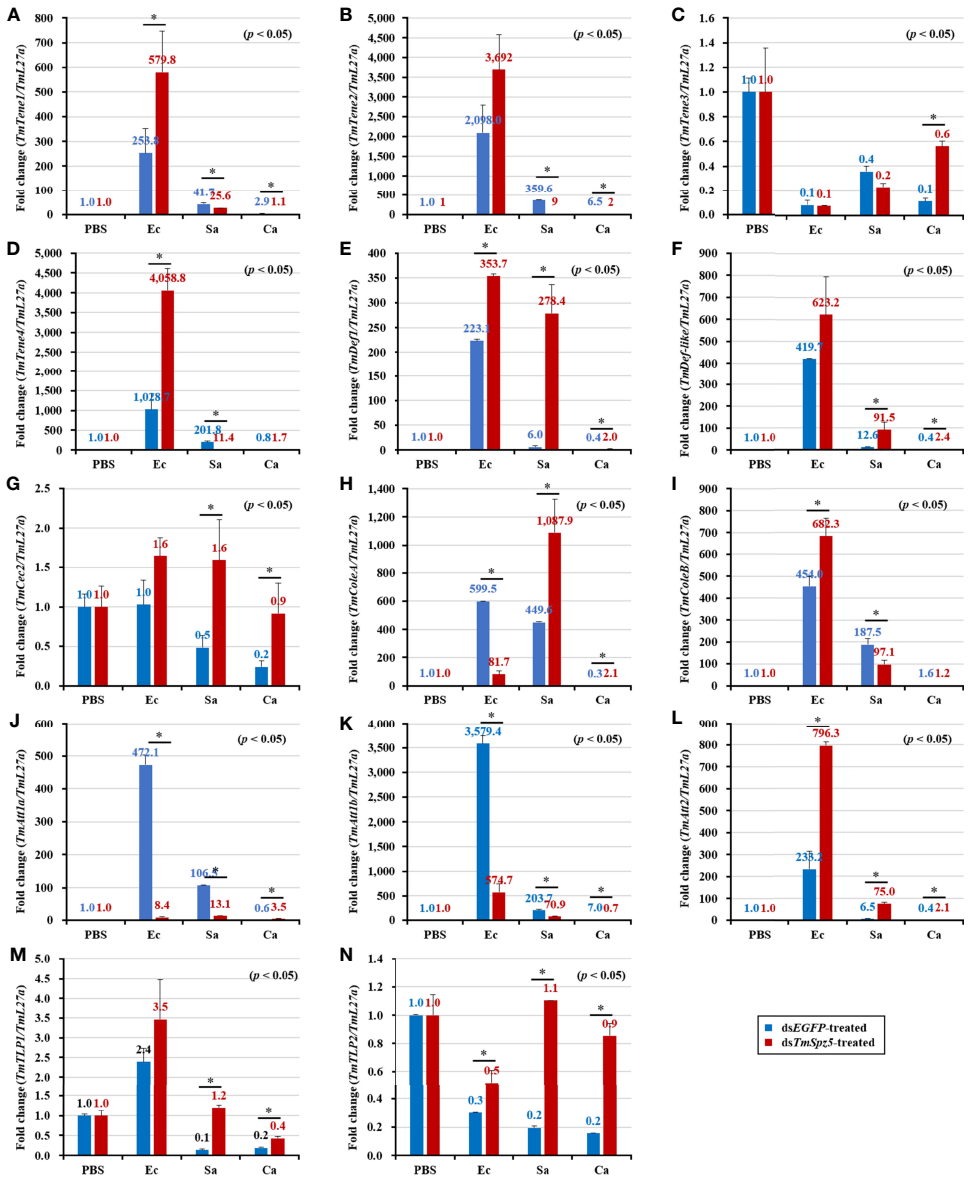


FIGURE 7 | Effect of *TmSpz5* gene silencing on antimicrobial peptide (AMP) gene expression levels in the *T. molitor* gut. Four days after *TmSpz5* RNAi treatment, pathogens including *E. coli* (Ec), *S. aureus* (Sa), and *C. albicans* (Ca) and PBS as control were injected. Levels of the AMP genes, including *TmTene1* **(A)**, *TmTene2* **(B)**, *TmTene3* **(C)**, *TmTene4* **(D)**, *TmDef* **(E)**, *TmDef-like* **(F)**, *TmCec2* **(G)**, *TmColeA* **(H)**, *TmColeB* **(I)**, *TmAtt1a* **(J)**, *TmAtt1b* **(K)**, *TmAtt2* **(L)**, *TmTLP1* **(M)**, and *TmTLP2* **(N)** were evaluated by qRT-PCR at 24 h post-microbial injection. ds*EGFP* was injected as a negative control, and *TmL27a* expression was evaluated as an internal control. All experiments were performed in triplicate. Asterisks indicate significant differences between ds*TmSpz5*- and ds*EGFP*-treated groups when compared using Student's *t*-test ($p < 0.05$).

(**Figures 8C, G**). In the fat bodies, only the levels of *TmTene4*, *TmDef*, and *TmTLP1* were reduced in response to *E. coli* infection (**Figures 9D, E, M**). Surprisingly, ds*TmSpz5* elevated the mRNA levels of some AMPs in response to pathogens in all dissected tissues, particularly the levels of the *Cecropin*, *Attacin*, and *Tencin* families in the gut, fat bodies, and hemocytes (**Figures 7A, C, E–G, 8B, D, F,** and **9A–C, F–L, N**). Finally, mRNA levels of almost all AMPs did not differ between the ds*TmSpz5* group and the control group in response to *C. albicans.*

Following the same protocol used to evaluate the expression of AMP genes following knockdown, the NF-κB pathway genes *TmDorX2* and *TmRelish* were examined (**Figure 10**). ds*TmSpz5* considerably depleted *TmDorX2* expression levels in MTs following *E. coli* and *S. aureus* infection (**Figure 10A**). A less substantial reduction in *TmRelish* expression was observed in MTs (**Figure 10B**). Moreover, following the microbial challenge, *TmDorX2* was upregulated in the fat bodies and gut and *TmRelish* was upregulated in the fat bodies.

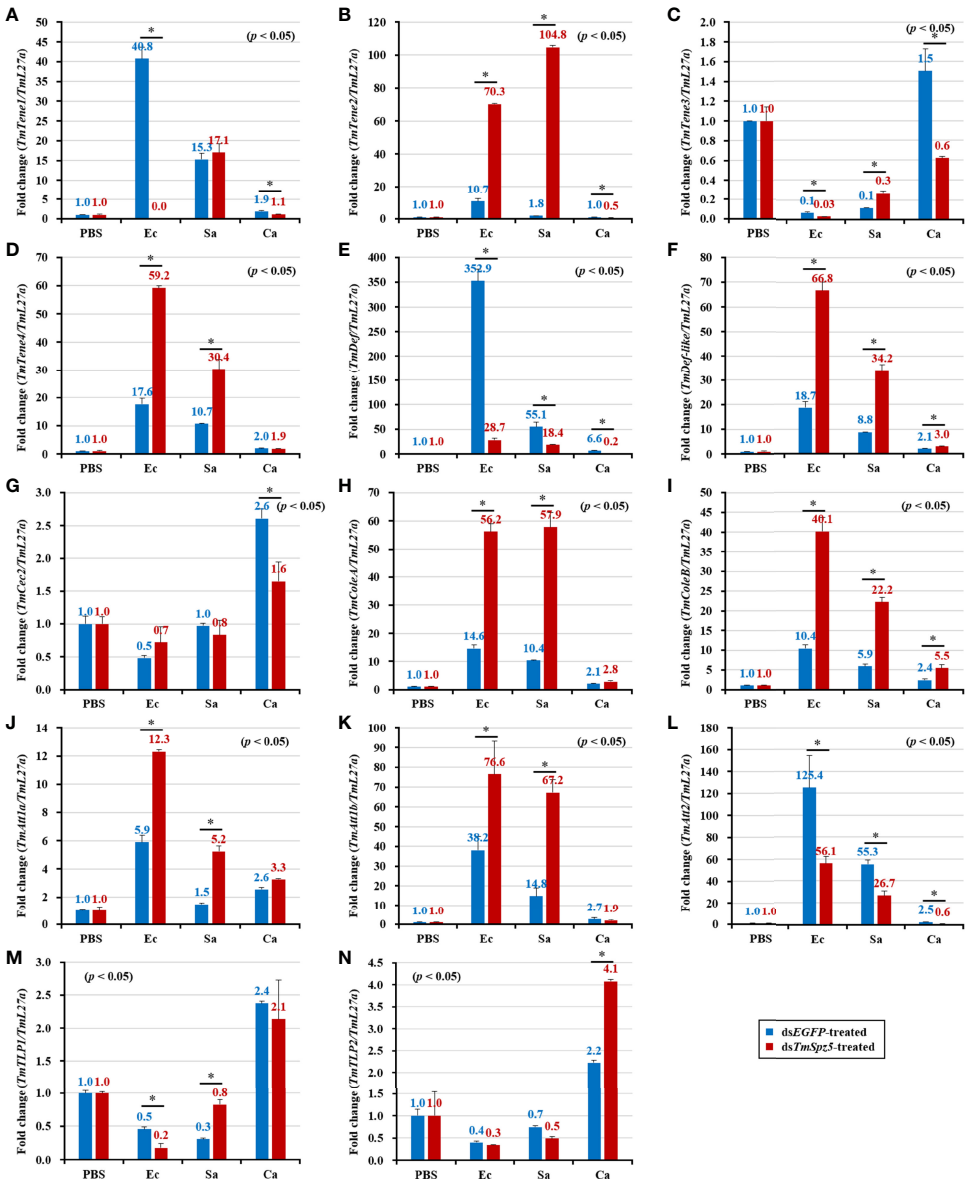


FIGURE 8 | The mRNA expression levels of 14 antimicrobial peptide (AMP) genes after *TmSpz5* gene silencing in the hemocytes of *T. molitor*. Four days after *TmSpz5* dsRNA treatment, *E. coli* (Ec), *S. aureus* (Sa), and *C. albicans* (Ca) and PBS as a control were injected. At 24 h after injecting the microbes, the expression levels of *TmTene1* **(A)**, *TmTene2* **(B)**, *TmTene3* **(C)**, *TmTene4* **(D)**, *TmDef* **(E)**, *TmDef-like* **(F)**, *TmCec2* **(G)**, *TmColeA* **(H)**, *TmColeB* **(I)**, *TmAtt1a* **(J)**, *TmAtt1b* **(K)**, *TmAtt2* **(L)**, *TmTLP1* **(M)**, and *TmTLP2* **(N)** were evaluated by qRT-PCR. ds*EGFP* was injected as a negative control, and *TmL27a* expression was measured as an internal control. All experiments were performed in triplicate. Asterisks indicate significant differences between ds*TmSpz5*- and ds*EGFP*-treated groups when compared using Student's *t*-test ($p < 0.05$).

Loss of Antimicrobial Activity in ds*TmSpz5*-Treated Larvae

The AMP assay result clearly demonstrated that *E. coli* and *S. aureus* infection in ds*TmSpz5*-treated larvae induced AMP expression significantly in Malpighian tubules and partially in the gut. Thus, we examined whether this suppression would affect bacterial growth in the hemolymph, MTs, midgut, and hindgut by CFU assay. Following ds*EGFP* and ds*TmSpz5* injection, larvae were exposed to *E. coli*, and the aforementioned tissues were dissected 48 h postinfection and cultured with *E. coli* on LB agar plates. Elevated antimicrobial activity was observed in all dissected tissues in *E. coli*-injected larvae compared with the PBS-injected group (**Figures 11A, C, E, G**). Moreover, it was found that *E. coli* growth was hindered in the ds*EGFP*-injected gut, compared to the ds*TmSpz5*-injected larvae in the MTs, hindgut, and midgut (in decreasing order) (**Figures 11D, F, H**). In contrast, in the

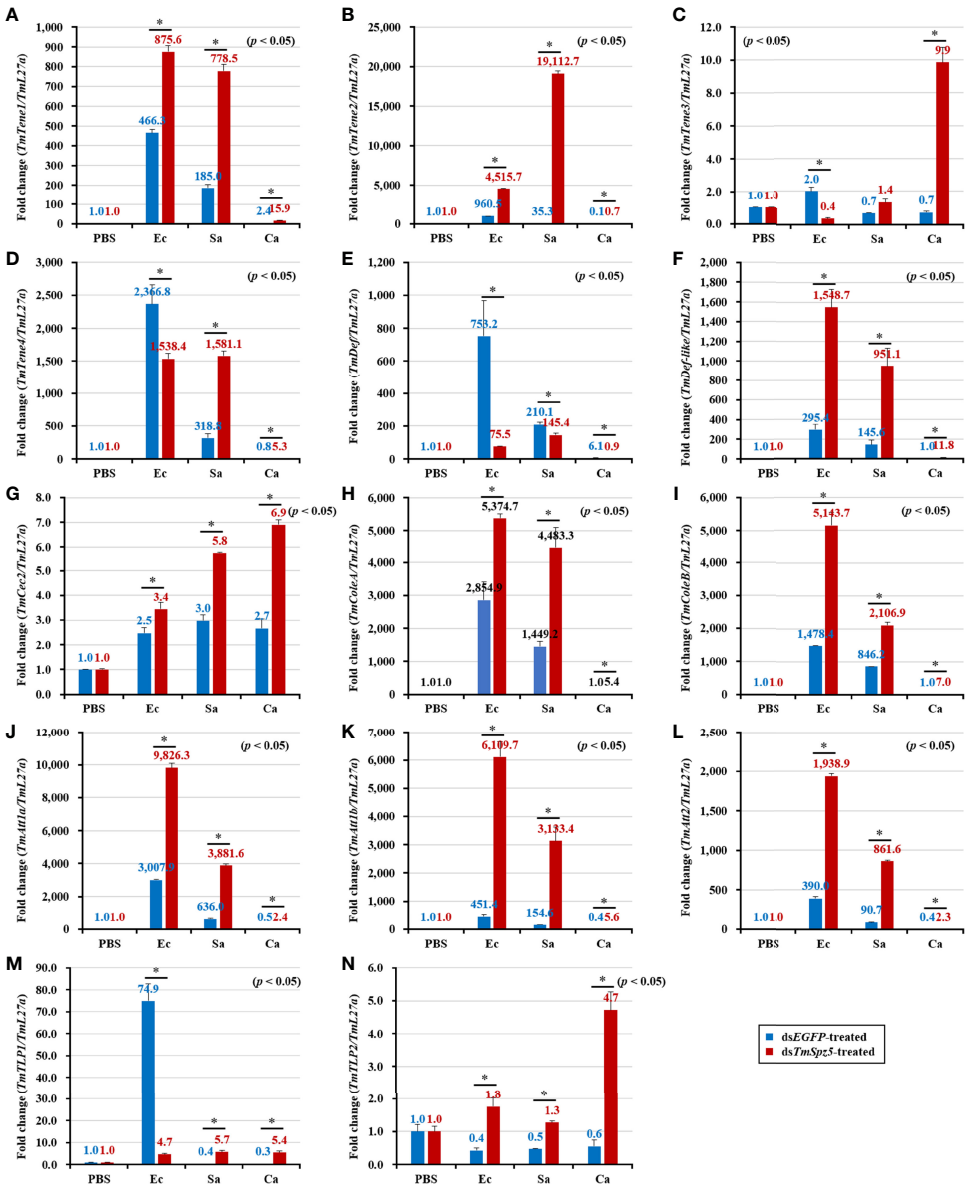


FIGURE 9 | Antimicrobial peptide expression patterns in the fat bodies of ds*TmSpz5*-treated *T. molitor* larvae in response to microbial challenge. At 24 h post-infection by *E. coli* (Ec), *S. aureus* (Sa), and *C. albicans* (Ca), the mRNA levels of *TmTene1* **(A)**, *TmTene2* **(B)**, *TmTene3* **(C)**, *TmTene4* **(D)**, *TmDef* **(E)**, *TmDef-like* **(F)**, *TmCec2* **(G)**, *TmColeA* **(H)**, *TmColeB* **(I)**, *TmAtt1a* **(J)**, *TmAtt1b* **(K)**, *TmAtt2* **(L)**, *TmTLP1* **(M)**, and *TmTLP2* **(N)** were evaluated by qRT-PCR. PBS was administered to the non-infected control group. ds*EGFP* was injected as a negative control, and *TmL27a* expression was measured as an internal control. All experiments were performed in triplicate. Asterisks indicate significant differences between ds*TmSpz5*- and ds*EGFP*-treated groups determined using Student's t-test ($p < 0.05$).

hemolymph, no significant difference in proliferation inhibition was observed between the ds*EGFP*- and ds*TmSpz5*-injected larvae (**Figure 11B**). These results imply that the effect of *TmSpz5* knockdown on AMP gene depletion in MTs causes suppressed antimicrobial activity against Gram-negative bacteria. Additionally, while antimicrobial activity in hemolymph remained indifferent, downregulation of AMP genes in MTs subsequent to *TmSpz5* knockdown exhibits reduced antimicrobial activity in the hindgut.

DISCUSSION

Drosophila is one of the most potent genetic model systems for characterization of the Toll and Imd signaling pathways (24, 54, 55). Nevertheless, the focus on this model limits our understanding of the biochemical mechanisms of the Toll proteolytic cascade. For instance, the activation protocol (i.e., developmental factors or infection) influences pathway activity, making it difficult to comprehensively characterize the underlying mechanisms (12, 31).

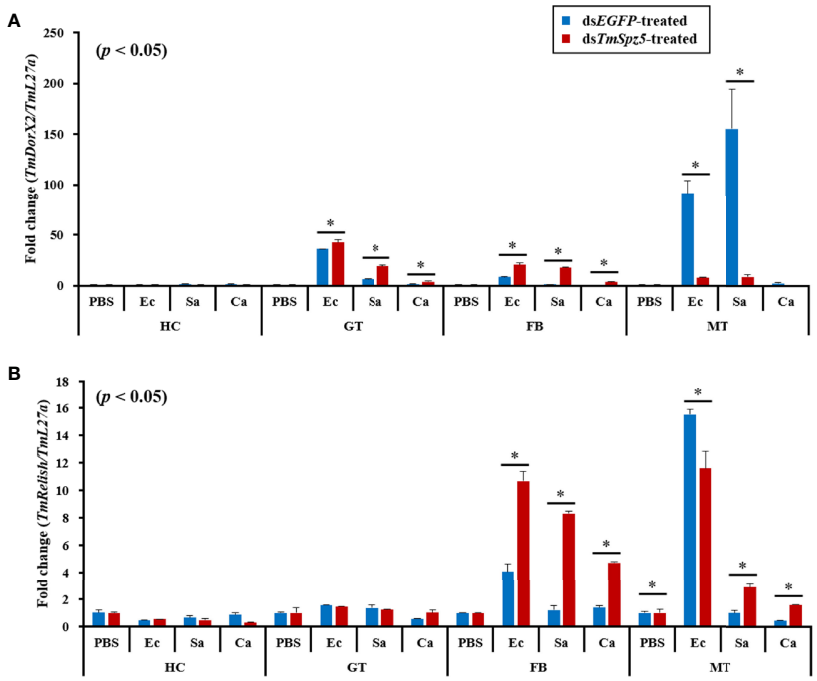


FIGURE 10 | Effect of *Tmspz5* gene silencing on NF-κB gene expression patterns. ds*Tmspz5*-treated *T. molitor* larvae were infected with *E. coli*, *S. aureus* and *C. albicans* and 24 h post-pathogen injection, mRNA levels of NF-κB genes, including *TmDorX2* **(A)** and *TmRel* **(B)**, were measured by RT-qPCR. EGFP dsRNA was assessed as a negative control and *T. molitor ribosomal protein* (*TmL27a*) was used as an internal control. All experiments were performed in triplicate. Asterisks indicate significant differences between ds*TmSpz5*- and ds*EGFP*-treated groups determined using Student's *t*-test ($p < 0.05$).

T. molitor Toll signaling activation by Gram-positive bacteria or fungi, its compartments, and its relevant AMPs have been well elucidated (24). Surprisingly, similar to Lys-type PGN, *Tm*PGRP-SA can recognize polymeric DAP-type PGN of Gram-negative bacteria, subsequently leading to activation of a three-step proteolytic cascade and the production of mature Spätzle (53, 56).

During *Drosophila* developmental stages, expression of the Spätzle gene is regulated by hormonal alteration. Radio-immunoassays have illustrated that ecdysone activity is high during prepupal and pupal stages (57). Likewise, cross talk between the steroid hormone 20-hydroxyecdysone (20E) and immune-regulatory genes in *Drosophila* has been reported (57, 58). Additionally, *Drosophila* MTs do not undergo histological alterations during pupal metamorphosis and therefore play an important role in innate immunity during this process (59, 60). Our developmental stage- and tissue-specific gene expression data revealed that *TmSpz5* levels are high during the embryonic stage as well as at each ecdysis, consequently increasing susceptibility to possible attacks, showing that *TmSpz5* contributes to both insect dorso-ventral axis formation during development and immune responses, respectively (11). The fact that *TmSpz5* expression is the highest in larval MTs and in the adult gut supports its important role in epithelial defense organs.

Toll signaling is activated upon the recognition of Gram-positive bacteria and fungi by the cleavage of the cytokine-like polypeptide Spätzle (2, 6, 27). We detected a high and early expression of *TmSpz5* following *C. albicans* and *S. aureus* challenge in descending order in all dissected tissues. The observed *TmSpz5* expression in response to *E. coli* infection in MTs provides evidence for cross talk between the Toll and Imd signaling pathways. The unexpected results of the survival analysis demonstrated the importance of *TmSpz5* in *T. molitor* immunity against *E. coli* and *S. aureus*, but not *C. albicans*. Consistently, *TmSpz5* silencing leads to *T. molitor* vulnerability toward *E. coli* and *S. aureus* by decreasing AMP production in the presence of pathogens. Our results were predominantly consistent with those of previous studies on AMP production after treatment with ds*TmSpz5*. In *Drosophila*, attacin, diptericin, cecropin, and drosocin are active against Gram-negative bacteria, and metchnikowin and defensin act against Gram-positive bacteria (59, 61–65). In this study, *TmCecropin-2* was also induced by Gram-positive bacteria and fungi. Surprisingly, the elevated mRNA levels of some AMPs in various tissues may suggest that there are alternative mechanisms to regulate gene expression. As it has been demonstrated previously, different *T. molitor Spätzle* RNAi treatments (*TmSpz4*, *TmSpz6*, *TmSpzlike*) resulted in an increased expression of AMPs following microbial challenges (44, 45, 49). Additionally, the monomeric DAP-type peptidoglycan of Gram-negative bacteria activates *Tm*IMD protein which triggers the expression of nine AMP genes (66). Likely, results of this study propose a possibility that the effect of *TmSpz5* RNAi leads to the overexpression of other *Spätzle* genes with a similar function. Overexpression of some AMP genes,

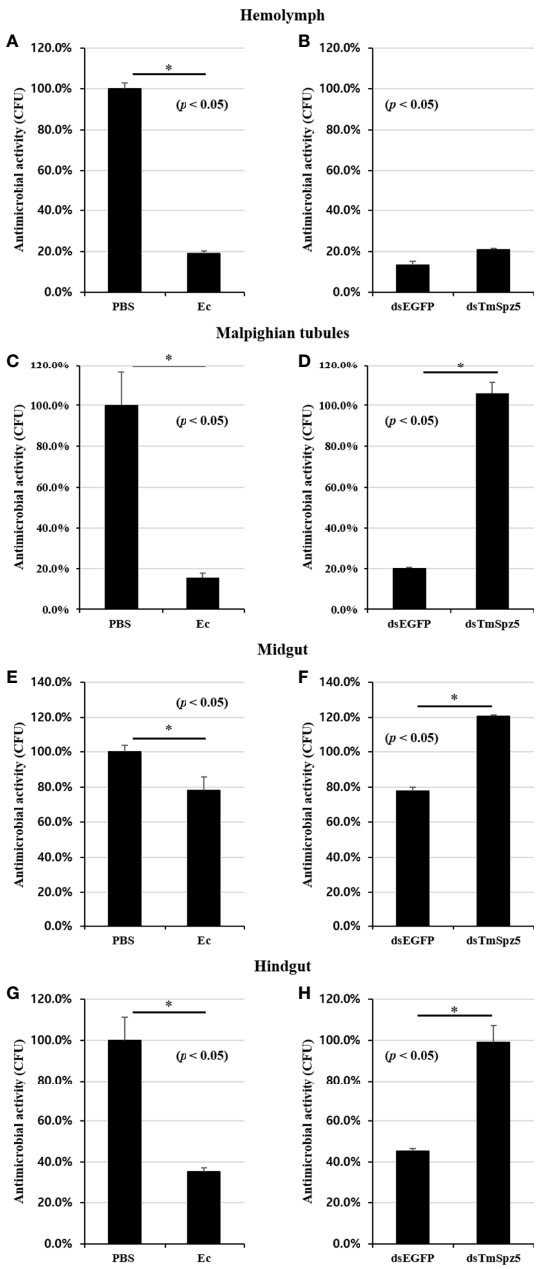


FIGURE 11 | Antimicrobial activity against *E. coli* in *TmSpz5*-silenced larvae hemolymph, Malpighian tubules, midgut, and hindgut by CFU assay. **(A, C, E, G)** Antimicrobial activity evoked by *E. coli* (Ec) (10^6 cells/μl) elicitation. PBS-injected *T. molitor* was used as a negative control (Cont). *E. coli*-injected *T. molitor* hemolymph and Malpighian tubules had higher antimicrobial activity compared with control group **(A, C)**. **(B, D, F, H)** *E. coli* (10^6 cells/μl) was injected into ds*TmSpz5*-treated *T. molitor* larvae. ds*EGFP*-treated larvae were used as a negative control. The result shows that the antimicrobial activity was decreased by treatment of ds*Spz5* compared with the ds*EGFP*-treated group majorly in Malpighian tubules **(D)**, hindgut **(H)**, and midgut **(F)** in a depleting manner. *E. coli* proliferation remained indifferent in the ds*TmSpz5*-treated group compared with ds*EGFP*-treated larvae in hemolymph **(B)**. Asterisks indicate significant differences between ds*TmSpz5*- and dsEGFP-injected groups.

mostly in hemolymph and fat bodies, maintains homeostasis. Moreover, other signaling pathways such as Imd can trigger an elevated expression of AMPs (35). Since the Imd signaling pathway has not been fully clarified, further studies regarding possible synergistic effects on induction of different AMPs are required to have a crystal understanding of Toll and Imd pathway association with regulation of AMP genes. Furthermore, the lack of change in mRNA levels of most AMPs in the ds*TmSpz5* group in response to *C. albicans* appeared to be inconsistent with the induction data.

NF-κB family members in *Drosophila*, activated by the Toll and Imd pathways, regulate the expression of AMP genes (27). The Toll signaling pathway mediates activation of the transcription factors Dorsal and Dif and is predominantly actuated by the detection of Gram-positive bacteria and fungi (6, 40, 67, 68). In contrast, Gram-negative bacteria activate the Imd pathway, which triggers the NF-κB transcription factor Relish (6, 43, 69). In agreement with the AMP expression results, *TmDorX2* was significantly suppressed in the MTs of *TmSpz5*-silenced larvae following challenges with *E. coli* and *S. aureus*, indicating that *TmSpz5* is involved in regulating the expression of *TmDorX2*.

With respect to antimicrobial activity, AMPs extracted from all tissues except the hemolymph effectively inhibited *E. coli* growth. The effective inhibition of bacterial proliferation in the MTs and hindgut were consistent with the AMP mRNA expression and NF-κB results, suggesting that *TmSpz5* acts as an immune component in the MTs and subsequently the hindgut. Further investigations are needed to verify these results.

Drosophila fat bodies are considered as the insect equivalent of the mammalian liver and are the main AMP-producing tissues, allowing an effective response to infection (6). Epithelial cells in the gut, MTs, genital tract, and trachea play important roles in systemic immunity by mediating the local response to invaders (70, 71). These epithelial tissues constitute the first line of defense toward possible invaders, and if pathogens invade these barriers, cellular and humoral immunity is induced (60, 71). Insect MTs form by hindgut–midgut joint invagination, and thus its secretions and hemolymph waste products are constantly transported to the hindgut (72). Thereupon, *Drosophila* MTs have osmoregulatory activity function as detoxification compartments in the hemolymph, acting as major innate immune organs (73). They are able to recognize pathogens and induce the production of high levels of AMPs (59, 60). They do not endure metamorphosis caused by ecdysone induction and are conveyed from larvae to adults. PGRP-LC expression is elevated by MT ecdysone production and has a marked effect on boosting host immunity (60). Additionally, PGRP-LE and PGRP-SC1 are immune elements predominantly functioning in the posterior midgut and anterior hindgut (74).

Our results show that MTs are critical immune organs in *T. molitor*, as has been observed in *Drosophila*. The radical shrinkage of the expression of almost all AMP genes and *TmDorX2* in the MTs of *TmSpz5*-silenced larvae following *E. coli* infection suggests that DAP-type PGN is recognized by PRRs

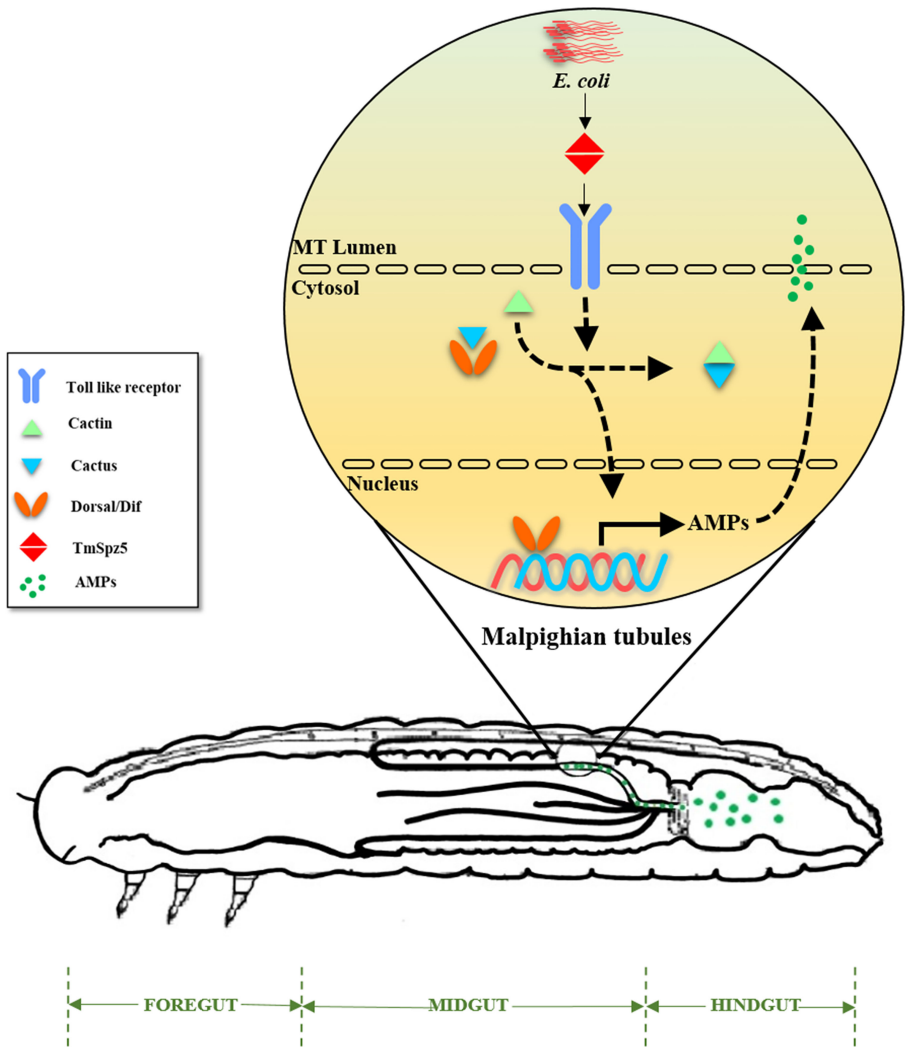


FIGURE 12 | A schematic summary of *TmSpz5* positive regulation in antimicrobial peptide production in Malpighian tubules (MTs) of bacterial infected larvae. 10 AMP-encoding genes including *TmTen-1*, *TmTen-2*, *TmTen-4*, *TmColA*, *TmColB*, *TmAtt-1a*, *TmAtt-1b*, *TmAtt-2*, *TmTLP-1*, and *TmTLP-2* are positively regulated by *TmSpz5* upon bacterial infections in MTs and produced peptides along with rest of tubules content, eventually flow to hindgut.

and the relevant proteolytic cascade leads to the activation of mature *Tm*Spz5. Consequently, activated *Tm*Spz5 binds to the Toll receptor and positively regulates the expression of the NF-κB response elements and AMP genes. In contrast to the lack of change in AMP expression in the gut of *Tm*Spz5 knockdown larvae, the CFU results not only demonstrate the pivotal role of *Tm*Spz5 in antibacterial activity of MT AMPs but also show that these AMPs act as hindgut disinfectants (**Figure 12**).

Our molecular analyses deepen our current knowledge of *T. molitor* immunity. Notably, the role of MTs in the innate immunity of *T. molitor* against the Gram-negative bacteria, *E. coli*, supports the results of previous studies, showing that polymeric DAP-type PG can be sensed by PGRP-SA, and Toll pathway activation leads to *Tm*Spz5 cleavage and AMP production. A comprehensive understanding of these proteolytic cascades could provide a basis for the development of diagnostic kits and novel clinical trials for innate immune system-related diseases.

DATA AVAILABILITY STATEMENT

The datasets presented in this study can be found in online repositories. The names of the repository/repositories and accession number(s) can be found in the article/**Supplementary Material**.

AUTHOR CONTRIBUTIONS

YH, YJ, and MA conceived and designed the experiments. MA performed the experiments. YH contributed reagents/materials/

analysis tools. MA, YJ, and HJ analyzed the data. MA wrote the first draft of the manuscript. YJ, MK, TE, HJ, and YH revised and edited the manuscript. All authors contributed to the article and approved the submitted version.

FUNDING

This research was supported by the Basic Science Research Program through the National Research Foundation of Korea (NRF) funded by the Ministry of Science, ICT and Future Planning (Grant No. 2018R1A2A2A05023367) and by the Korea Institute of Planning and Evaluation for Technology in Food, Agriculture, Forestry and Fisheries (IPET) through the Export Promotion Technology Development Program (Grant no. 617077-5), funded by the Ministry of Agriculture, Food, and Rural Affairs (MAFRA).

SUPPLEMENTARY MATERIAL

The Supplementary Material for this article can be found online at: https://www.frontiersin.org/articles/10.3389/fimmu.2021.760475/full#supplementary-material

REFERENCES

1. Coope G. Several Million Years of Stability Among Insect Species Because of, or in Spite of, Ice Age Climatic Instability? *Philos Trans R Soc Lond Ser B Biol Sci* (2004) 359(1442):209–14. doi: 10.1098/rstb.2003.1393
2. Ferrandon D, Imler J-L, Hoffmann JA. Sensing Infection in Drosophila: Toll and Beyond. *Semin Immunol* (2004) 16(1):43–53. Elsevier. doi: 10.1016/j.smim.2003.10.008
3. Grimaldi D, Engel MS, Engel MS, Engel MS. *Evolution of the Insects*. New York: Cambridge University Press (2005).
4. Janeway CA Jr, Medzhitov R. Innate Immune Recognition. *Annu Rev Immunol* (2002) 20(1):197–216. doi: 10.1146/annurev.immunol.20.083001.084359
5. Medzhitov R, Janeway CA. Decoding the Patterns of Self and Nonself by the Innate Immune System. *Science* (2002) 296(5566):298–300. doi: 10.1126/science.1068883
6. Hoffmann JA. The Immune Response of Drosophila. *Nature* (2003) 426 (6962):33–8. doi: 10.1038/nature02021
7. Miller JS, Nguyen T, Stanley-Samuelson DW. Eicosanoids Mediate Insect Nodulation Responses to Bacterial Infections. *Proc Natl Acad Sci* (1994) 91 (26):12418–22. doi: 10.1073/pnas.91.26.12418
8. Pech LL, Strand MR. Granular Cells Are Required for Encapsulation of Foreign Targets by Insect Haemocytes. *J Cell Sci* (1996) 109(8):2053–60. doi: 10.1242/jcs.109.8.2053
9. Leonard C, Ratcliffe NA, Rowley AF. The Role of Prophenoloxidase Activation in Non-Self Recognition and Phagocytosis by Insect Blood Cells. *J Insect Physiol* (1985) 31(10):789–99. doi: 10.1016/0022-1910(85)90072-1
10. Tauszig S, Jouanguy E, Hoffmann JA, Imler J-L. Toll-Related Receptors and the Control of Antimicrobial Peptide Expression in Drosophila. *Proc Natl Acad Sci* (2000) 97(19):10520–5. doi: 10.1073/pnas.180130797
11. Belvin MP, Anderson KV. A Conserved Signaling Pathway: The Drosophila Toll-Dorsal Pathway. *Annu Rev Cell Dev Biol* (1996) 12(1):393–416. doi: 10.1146/annurev.cellbio.12.1.393
12. Weber AN, Tauszig-Delamasure S, Hoffmann JA, Lelièvre E, Gascan H, Ray KP, et al. Binding of the Drosophila Cytokine Spätzle to Toll Is Direct and Establishes Signaling. *Nat Immunol* (2003) 4(8):794–800. doi: 10.1038/ni955
13. Shia AK, Glittenberg M, Thompson G, Weber AN, Reichhart J-M, Ligoxygakis P. Toll-Dependent Antimicrobial Responses in Drosophila Larval Fat Body Require Spätzle Secreted by Haemocytes. *J Cell Sci* (2009) 122(24):4505–15. doi: 10.1242/jcs.049155
14. Ming M, Obata F, Kuranaga E, Miura M. Persephone/Spätzle Pathogen Sensors Mediate the Activation of Toll Receptor Signaling in Response to Endogenous Danger Signals in Apoptosis-Deficient Drosophila. *J Biol Chem* (2014) 289(11):7558–68. doi: 10.1074/jbc.M113.543884
15. Richman AM, Dimopoulos G, Seeley D, Kafatos FC. Plasmodium Activates the Innate Immune Response of Anopheles Gambiae Mosquitoes. *EMBO J* (1997) 16(20):6114–9. doi: 10.1093/emboj/16.20.6114
16. Christophides GK, Zdobnov E, Barillas-Mury C, Birney E, Blandin S, Blass C, et al. Immunity-Related Genes and Gene Families in Anopheles Gambiae. *Science* (2002) 298(5591):159–65. doi: 10.1126/science.1077136
17. Cui C, Wang Y, Liu J, Zhao J, Sun P, Wang S. A Fungal Pathogen Deploys a Small Silencing RNA That Attenuates Mosquito Immunity and Facilitates Infection. *Nat Commun* (2019) 10(1):1–10. doi: 10.1038/s41467-019-12323-1
18. An C, Jiang H, Kanost MR. Proteolytic Activation and Function of the Cytokine Spätzle in the Innate Immune Response of a Lepidopteran Insect, Manduca Sexta. *FEBS J* (2010) 277(1):148–62. doi: 10.1111/j.1742-4658.2009.07465.x
19. Yu B, Sang Q, Pan G, Li C, Zhou Z. A Toll-Spätzle Pathway in the Immune Response of Bombyx Mori. *Insects* (2020) 11(9):586. doi: 10.3390/insects11090586
20. Huerlimann R, Wade NM, Gordon L, Montenegro JD, Goodall J, McWilliam S, et al. *De Novo* Assembly, Characterization, Functional Annotation and Expression Patterns of the Black Tiger Shrimp (Penaeus Monodon) Transcriptome. *Sci Rep* (2018) 8(1):1–14. doi: 10.1038/s41598-018-31148-4
21. Roh K-B, Kim C-H, Lee H, Kwon H-M, Park J-W, Ryu J-H, et al. Proteolytic Cascade for the Activation of the Insect Toll Pathway Induced by the Fungal Cell Wall Component. *J Biol Chem* (2009) 284(29):19474–81. doi: 10.1074/jbc.M109.007419
22. Park JB, Choi WH, Kim SH, Jin HJ, Han YS, Kim NJ. Developmental Characteristics of Tenebrio Molitor Larvae (Coleoptera: Tenebrionidae) in Different Instars. *Int J Ind Entomol* (2014) 28(1):5–9. doi: 10.7852/ijie.2014.28.1.5
23. Gilbert LI. *Insect Molecular Biology and Biochemistry*. London: Academic Press (2012).
24. Ali Mohammadie Kojour M, Han YS, Jo YH. An Overview of Insect Innate Immunity. *Entomol Res* (2020) 50(6):282–91. doi: 10.1111/1748-5967.12437
25. Keshavarz M, Jo YH, Edosa TT, Bae YM, Han YS. TmPGRP-SA Regulates Antimicrobial Response to Bacteria and Fungi in the Fat Body and Gut of Tenebrio Molitor. *Int J Mol Sci* (2020) 21(6):2113. doi: 10.3390/ijms21062113
26. Keshavarz M, Jo YH, Edosa TT, Han YS. Tenebrio Molitor PGRP-LE Plays a Critical Role in Gut Antimicrobial Peptide Production in Response to Escherichia Coli. *Front Physiol* (2020) 11:320. doi: 10.3389/fphys.2020.00320
27. Hoffmann JA. Innate Immunity of Insects. *Curr Opin Immunol* (1995) 7(1):4–10. doi: 10.1016/0952-7915(95)80022-0
28. Choe KM, Werner T, Stoven S, Hultmark D, Anderson KV. Requirement for a Peptidoglycan Recognition Protein (PGRP) in Relish Activation and Antibacterial Immune Responses in Drosophila. *Science* (2002) 296 (5566):359–62. doi: 10.1126/science.1070216
29. Gottar M, Gobert V, Michel T, Belvin M, Duyk G, Hoffmann JA, et al. The Drosophila Immune Response Against Gram-Negative Bacteria Is Mediated by a Peptidoglycan Recognition Protein. *Nature* (2002) 416(6881):640–4. doi: 10.1038/nature734
30. Rämet M, Manfruelli P, Pearson A, Mathey-Prevot B, Ezekowitz RAB. Functional Genomic Analysis of Phagocytosis and Identification of a Drosophila Receptor for E. Coli. *Nature* (2002) 416(6881):644–8. doi: 10.1038/nature735
31. Gobert V, Gottar M, Matskevich AA, Rutschmann S, Royet J, Belvin M, et al. Dual Activation of the Drosophila Toll Pathway by Two Pattern Recognition Receptors. *Science* (2003) 302(5653):2126–30. doi: 10.1126/science.1085432
32. Yang YT, Lee MR, Lee SJ, Kim S, Nai YS, Kim JS. Tenebrio Molitor Gram-Negative-Binding Protein 3 (TmGNBP3) Is Essential for Inducing Downstream Antifungal Tenecin 1 Gene Expression Against Infection With Beauveria Bassiana JEF-007. *Insect Sci* (2018) 25(6):969–77. doi: 10.1111/1744-7917.12482

33. Vigneron A, Jehan C, Rigaud T, Moret Y. Immune Defenses of a Beneficial Pest: The Mealworm Beetle, Tenebrio Molitor. *Front Physiol* (2019) 10:138. doi: 10.3389/fphys.2019.00138
34. Patnaik BB, Patnaik HH, Seo GW, Jo YH, Lee YS, Lee BL, et al. Gene Structure, cDNA Characterization and RNAi-Based Functional Analysis of a Myeloid Differentiation Factor 88 Homolog in Tenebrio Molitor Larvae Exposed to Staphylococcus Aureus Infection. *Dev Comp Immunol* (2014) 46 (2):208–21. doi: 10.1016/j.dci.2014.04.009
35. Jo YH, Kim YJ, Park KB, Seong JH, Kim SG, Park S, et al. TmCactin Plays an Important Role in Gram-Negative and -Positive Bacterial Infection by Regulating Expression of 7 AMP Genes in Tenebrio Molitor. *Sci Rep* (2017) 7:46459. doi: 10.1038/srep46459
36. Keshavarz M, Jo YH, Park KB, Ko HJ, Edosa TT, Lee YS, et al. TmDorX2 Positively Regulates Antimicrobial Peptides in Tenebrio Molitor Gut, Fat Body, and Hemocytes in Response to Bacterial and Fungal Infection. *Sci Rep* (2019) 9(1):16878. doi: 10.1038/s41598-019-53497-4
37. Keshavarz M, Jo YH, Patnaik BB, Park KB, Ko HJ, Kim CE, et al. TmRelish is Required for Regulating the Antimicrobial Responses to Escherichia Coli and Staphylococcus Aureus in Tenebrio Molitor. *Sci Rep* (2020) 10(1):4258. doi: 10.1038/s41598-020-61157-1
38. Jang HA, Park KB, Kim BB, Ali Mohammadie Kojour M, Bae YM, Baliarsingh S, et al. *In Silico* Identification and Expression Analyses of Defensin Genes in the Mealworm Beetle Tenebrio Molitor. *Entomol Res* (2020) 50(12):575–85 doi: 10.1111/1748-5967.12468
39. Jo YH, Park S, Park KB, Noh MY, Cho JH, Ko HJ, et al. *In Silico* Identification, Characterization and Expression Analysis of Attacin Gene Family in Response to Bacterial and Fungal Pathogens in Tenebrio Molitor. *Entomol Res* (2018) 48 (1):45–54. doi: 10.1111/1748-5967.12287
40. Keshavarz M, Jo YH, Park KB, Ko HJ, Edosa TT, Lee YS, et al. Tm DorX2 Positively Regulates Antimicrobial Peptides in Tenebrio Molitor Gut, Fat Body, and Hemocytes in Response to Bacterial and Fungal Infection. *Sci Rep* (2019) 9(1):1–19. doi: 10.1038/s41598-019-53497-4
41. Ali Mohammadie Kojour M, Jang HA, Edosa TT, Keshavarz M, Kim BB, Bae YM, et al. Identification, *In Silico* Characterization, and Expression Analysis of Tenebrio Molitor Cecropin-2. *Entomol Res* (2020) 51(2):74–82. doi: 10.1111/1748-5967.12476
42. Jang HA, Park KB, Kim BB, Ali Mohammadie Kojour M, Bae YM, Baliarsingh S, et al. Bacterial But Not Fungal Challenge Up-Regulates the Transcription of Coleoptericin Genes in Tenebrio Molitor. *Entomol Res* (2020) 50(9):440–9. doi: 10.1111/1748-5967.12465
43. Keshavarz M, Jo YH, Patnaik BB, Park KB, Ko HJ, Kim CE, et al. Tm Relish Is Required for Regulating the Antimicrobial Responses to Escherichia Coli and Staphylococcus Aureus in Tenebrio Molitor. *Sci Rep* (2020) 10(1):1–18. doi: 10.1038/s41598-020-61157-1
44. Edosa TT, Jo YH, Keshavarz M, Bae YM, Kim DH, Lee YS, et al. TmSpz4 Plays an Important Role in Regulating the Production of Antimicrobial Peptides in Response to Escherichia Coli and Candida Albicans Infections. *Int J Mol Sci* (2020) 21(5):1878. doi: 10.3390/ijms21051878
45. Edosa TT, Jo YH, Keshavarz M, Bae YM, Kim DH, Lee YS, et al. TmSpz6 Is Essential for Regulating the Immune Response to Escherichia Coli and Staphylococcus Aureus Infection in Tenebrio Molitor. *Insects* (2020) 11 (2):105–19. doi: 10.3390/insects11020105
46. Larkin MA, Blackshields G, Brown NP, Chenna R, McGettigan PA, McWilliam H, et al. Clustal W and Clustal X Version 2.0. *Bioinformatics* (2007) 23(21):2947–8. doi: 10.1093/bioinformatics/btm404
47. Kumar S, Stecher G, Li M, Knyaz C, Tamura K. MEGA X: Molecular Evolutionary Genetics Analysis Across Computing Platforms. *Mol Biol Evol* (2018) 35(6):1547–9. doi: 10.1093/molbev/msy096
48. Saitou N, Nei M. The Neighbor-Joining Method: A New Method for Reconstructing Phylogenetic Trees. *Mol Biol Evol* (1987) 4(4):406–25.
49. Jang HA, Patnaik BB, Ali Mohammadie Kojour M, Kim BB, Bae YM, Park KB, et al. TmSpz-Like Plays a Fundamental Role in Response to E. Coli But Not S. Aureus or C. Albican Infection in Tenebrio Molitor *via* Regulation of Antimicrobial Peptide Production. *Int J Mol Sci* (2021) 22(19):10888. doi: 10.3390/ijms221910888
50. Livak KJ, Schmittgen TD. Analysis of Relative Gene Expression Data Using Real-Time Quantitative PCR and the 2(-Delta Delta C(T)) Method. *Methods* (2001) 25(4):402–8. doi: 10.1006/meth.2001.1262
51. Goel MK, Khanna P, Kishore J. Understanding Survival Analysis: Kaplan-Meier Estimate. *Int J Ayurveda Res* (2010) 1(4):274. doi: 10.4103/0974-7788.76794
52. Moon HJ, Lee SY, Kurata S, Natori S, Lee BL. Purification and Molecular Cloning of cDNA for an Inducible Antibacterial Protein From Larvae of the Coleopteran, Tenebrio Molitor. *J Biochem* (1994) 116(1):53–8. doi: 10.1093/oxfordjournals.jbchem.a124502
53. Park S, Jo YH, Park KB, Ko HJ, Kim CE, Bae YM, et al. TmToll-7 Plays a Crucial Role in Innate Immune Responses Against Gram-Negative Bacteria by Regulating 5 AMP Genes in Tenebrio Molitor. *Front Immunol* (2019) 10:310. doi: 10.3389/fimmu.2019.00310
54. Anthoney N, Foldi I, Hidalgo A. Toll and Toll-Like Receptor Signalling in Development. *Development* (2018) 145(9):dev156018. doi: 10.1242/dev.156018
55. Harnish JM, Link N, Yamamoto S. Drosophila as a Model for Infectious Diseases. *Int J Mol Sci* (2021) 22(5):2724. doi: 10.3390/ijms22052724
56. Kim CH, Kim SJ, Kan H, Kwon HM, Roh KB, Jiang R, et al. A Three-Step Proteolytic Cascade Mediates the Activation of the Peptidoglycan-Induced Toll Pathway in an Insect. *J Biol Chem* (2008) 283(12):7599–607. doi: 10.1074/jbc.M710216200
57. Borst DW, Bollenbacher WE, O'Connor JD, King DS, Fristrom JW. Ecdysone Levels During Metamorphosis of Drosophila Melanogaster. *Dev Biol* (1974) 39(1):308–16. doi: 10.1016/S0012-1606(74)80032-1
58. Meister M, Richards G. Ecdysone and Insect Immunity: The Maturation of the Inducibility of the Diptericin Gene in Drosophila Larvae. *Insect Biochem Mol Biol* (1996) 26(2):155–60. doi: 10.1016/0965-1748(95)00076-3
59. Verma P, Tapadia MG. Immune Response and Anti-Microbial Peptides Expression in Malpighian Tubules of Drosophila Melanogaster Is Under Developmental Regulation. *PloS One* (2012) 7(7):e40714. doi: 10.1371/journal.pone.0040714
60. Zheng W, Rus F, Hernandez A, Kang P, Goldman W, Silverman N, et al. Dehydration Triggers Ecdysone-Mediated Recognition-Protein Priming and Elevated Anti-Bacterial Immune Responses in Drosophila Malpighian Tubule Renal Cells. *BMC Biol* (2018) 16(1):60. doi: 10.1186/s12915-018-0532-5
61. Bulet P, Hetru C, Dimarcq JL, Hoffmann D. Antimicrobial Peptides in Insects; Structure and Function. *Dev Comp Immunol* (1999) 23(4-5):329–44. doi: 10.1016/s0145-305x(99)00015-4
62. Ekengren S, Hultmark D. Drosophila Cecropin as an Antifungal Agent. *Insect Biochem Mol Biol* (1999) 29(11):965–72. doi: 10.1016/s0965-1748(99)00071-5
63. Tzou P, Ohresser S, Ferrandon D, Capovilla M, Reichhart JM, Lemaitre B, et al. Tissue-Specific Inducible Expression of Antimicrobial Peptide Genes in Drosophila Surface Epithelia. *Immunity* (2000) 13(5):737–48. doi: 10.1016/s1074-7613(00)00072-8
64. Imler JL, Bulet P. Antimicrobial Peptides in Drosophila: Structures, Activities and Gene Regulation. *Chem Immunol Allergy* (2005) 86:1–21. doi: 10.1159/000086648
65. Lemaitre B, Hoffmann J. The Host Defense of Drosophila Melanogaster. *Annu Rev Immunol* (2007) 25:697–743. doi: 10.1146/annurev.immunol.25.022106.141615
66. Jo YH, Patnaik BB, Hwang J, Park KB, Ko HJ, Kim CE, et al. Regulation of the Expression of Nine Antimicrobial Peptide Genes by TmIMD Confers Resistance Against Gram-Negative Bacteria. *Sci Rep* (2019) 9(1):10138. doi: 10.1038/s41598-019-46222-8
67. Meng X, Khanuja BS, Ip YT. Toll Receptor-Mediated Drosophila Immune Response Requires Dif, an NF-kappaB Factor. *Genes Dev* (1999) 13(7):792–7. doi: 10.1101/gad.13.7.792
68. Rutschmann S, Jung AC, Hetru C, Reichhart JM, Hoffmann JA, Ferrandon D. The Rel Protein DIF Mediates the Antifungal But Not the Antibacterial Host Defense in Drosophila. *Immunity* (2000) 12(5):569–80. doi: 10.1016/S1074-7613(00)80208-3
69. Kaneko T, Yano T, Aggarwal K, Lim JH, Ueda K, Oshima Y, et al. PGRP-LC and PGRP-LE Have Essential Yet Distinct Functions in the Drosophila Immune Response to Monomeric DAP-Type Peptidoglycan. *Nat Immunol* (2006) 7(7):715–23. doi: 10.1038/ni1356
70. Brey PT, Lee WJ, Yamakawa M, Koizumi Y, Perrot S, François M, et al. Role of the Integument in Insect Immunity: Epicuticular Abrasion and Induction of Cecropin Synthesis in Cuticular Epithelial Cells. *Proc Natl Acad Sci USA* (1993) 90(13):6275–9. doi: 10.1073/pnas.90.13.6275
71. Huttner KM, Bevins CL. Antimicrobial Peptides as Mediators of Epithelial Host Defense. *Pediatr Res* (1999) 45(6):785–94. doi: 10.1203/00006450-199906000-00001

72. McGavin GC. *Essential Entomology: An Order-by-Order Introduction*. New York: Oxford University Press (2001).
73. McGettigan J, McLennan RKJ, Broderick KE, Kean L, Allan AK, Cabrero P, et al. Insect Renal Tubules Constitute a Cell-Autonomous Immune System That Protects the Organism Against Bacterial Infection. *Insect Biochem Mol Biol* (2005) 35(7):741–54. doi: 10.1016/j.ibmb.2005.02.017
74. Broderick NA. Friend, Foe or Food? Recognition and the Role of Antimicrobial Peptides in Gut Immunity and Drosophila–Microbe Interactions. *Philos Trans R Soc B: Biol Sci* (2016) 371(1695):20150295. doi: 10.1098/rstb.2015.0295

Conflict of Interest: The authors declare that the research was conducted in the absence of any commercial or financial relationships that could be construed as a potential conflict of interest.

Publisher's Note: All claims expressed in this article are solely those of the authors and do not necessarily represent those of their affiliated organizations, or those of the publisher, the editors and the reviewers. Any product that may be evaluated in this article, or claim that may be made by its manufacturer, is not guaranteed or endorsed by the publisher.

Copyright © 2021 Ali Mohammadie Kojour, Edosa, Jang, Keshavarz, Jo and Han. This is an open-access article distributed under the terms of the Creative Commons Attribution License (CC BY). The use, distribution or reproduction in other forums is permitted, provided the original author(s) and the copyright owner(s) are credited and that the original publication in this journal is cited, in accordance with accepted academic practice. No use, distribution or reproduction is permitted which does not comply with these terms.

frontiers in Microbiology

REVIEW
published: 22 December 2021
doi: 10.3389/fmicb.2021.790442

Exploitation of the Host Ubiquitin System: Means by *Legionella pneumophila*

Jingjing Luo[1], Lidong Wang[1], Lei Song[1] and Zhao-Qing Luo[2]**

[1] Department of Respiratory Medicine, Center for Pathogen Biology and Infectious Diseases, Key Laboratory of Organ Regeneration and Transplantation of the Ministry of Education, The First Hospital of Jilin University, Changchun, China, [2] Department of Biological Sciences, Purdue University, West Lafayette, IN, United States

Ubiquitination is a commonly used post-translational modification (PTM) in eukaryotic cells, which regulates a wide variety of cellular processes, such as differentiation, apoptosis, cell cycle, and immunity. Because of its essential role in immunity, the ubiquitin network is a common target of infectious agents, which have evolved various effective strategies to hijack and co-opt ubiquitin signaling for their benefit. The intracellular pathogen *Legionella pneumophila* represents one such example; it utilizes a large cohort of virulence factors called effectors to modulate diverse cellular processes, resulting in the formation a compartment called the Legionella-containing vacuole (LCV) that supports its replication. Many of these effectors function to re-orchestrate ubiquitin signaling with distinct biochemical activities. In this review, we highlight recent progress in the mechanism of action of *L. pneumophila* effectors involved in ubiquitination and discuss their roles in bacterial virulence and host cell biology.

Keywords: ubiquitin, intracellular pathogen, effector, immunity, virulence

OPEN ACCESS

Edited by:
Monica Cartelle Gestal, Louisiana State University Health Shreveport, United States

Reviewed by:
Yury Belyi, N. F. Gamaleya Scientific Research Institute of Epidemiology and Microbiology (RAMS), Russia
Tomoe Kitao, Gifu University, Japan
Stanimir Ivanov, Louisiana State University Health Shreveport, United States
Vincent Joseph Starai, University of Georgia, United States

****Correspondence:***
Lei Song
lsong@jlu.edu.cn
Zhao-Qing Luo
luoz@purdue.edu

Specialty section:
This article was submitted to Infectious Agents and Disease, a section of the journal Frontiers in Microbiology

Received: *06 October 2021*
Accepted: *30 November 2021*
Published: *22 December 2021*

Citation:
Luo J, Wang L, Song L and Luo Z-Q (2021) Exploitation of the Host Ubiquitin System: Means by Legionella pneumophila. Front. Microbiol. 12:790442. doi: 10.3389/fmicb.2021.790442

INTRODUCTION

Ubiquitin (Ub) is a small, 76-amino acid protein that highly conserved in all eukaryotes (Liu et al., 2013; Shaid et al., 2013). The attachment of ubiquitin to client proteins forms a covalent modification known as ubiquitination, resulting in changes in the stability, cellular localization and/or activity of the substrates. Classical ubiquitination is a three-reaction cascade catalyzed by three types of enzymes (**Figure 1**). The first reaction is carried out by the ubiquitin-activating enzyme (E1), which catalyzes acyl adenylation on the carboxyl terminus of Ub by hydrolyzing an ATP molecule. The labile intermediate AMP-Ub then reacts with E1, resulting in linkage of the Ub moiety to its active cysteine residue by a thioester bond and the release of AMP (Hershko and Ciechanover, 1998). The Ub on E1 is then delivered to the active cysteine residue of ubiquitin-conjugating enzyme (E2) (Olsen and Lima, 2013). Charged E2s carrying a Ub moiety work together with ubiquitin ligation enzymes (E3) to transfer the modifier onto a substrate (Buetow and Huang, 2016). Whereas E2s often dictate the chain type of ubiquitination (Stewart et al., 2016), E3s normally determine substrate specificity (Buetow and Huang, 2016). There are three major classes of E3 enzymes that utilize distinct mechanisms to transfer Ub from E2 or E3 itself to the substrate (Buetow and Huang, 2016). In most cases, Ub is attached to substrates by an isopeptide bond formed between its carboxyl terminus and the ε-amino group of Lys residues in target protein or in the preceding Ub moiety (Hershko and Ciechanover, 1998).

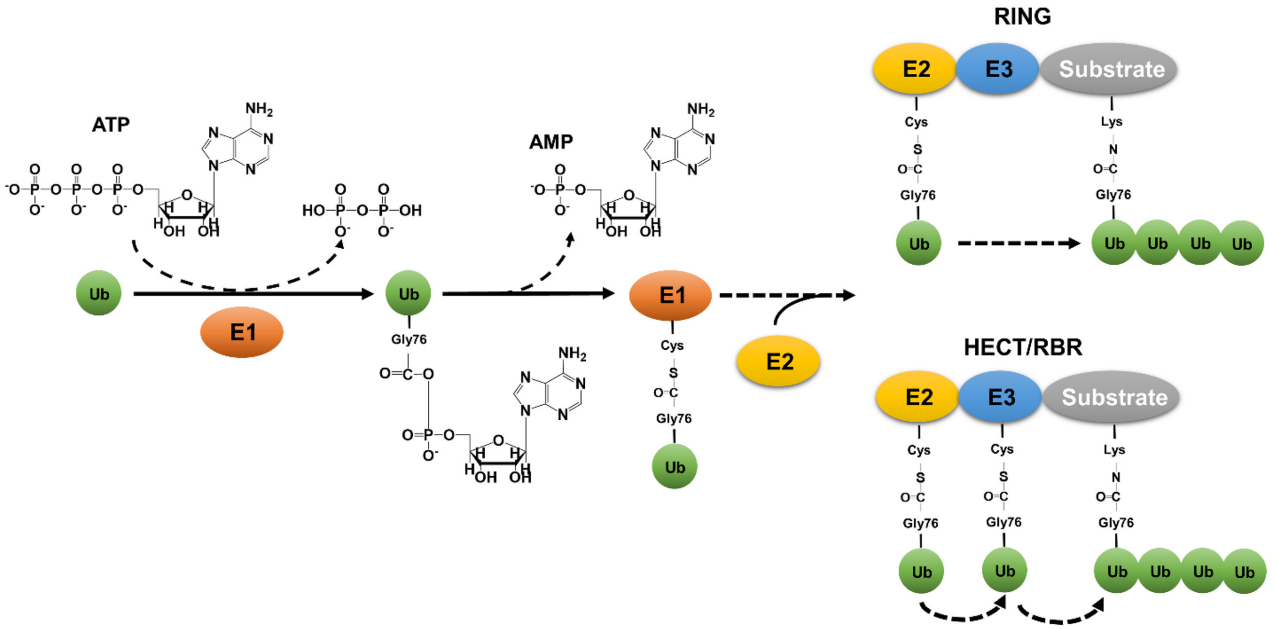


FIGURE 1 | Canonical eukaryotic ubiquitination by the three-enzyme cascade. Canonical ubiquitination is initiated by E1-mediated acyl adenylation on the carboxyl terminus of Ub by hydrolyzing an ATP molecule, followed by a linkage of Ub to the active cysteine residue of E1 and the release of AMP. The Ub on E1 is then delivered to the active cysteine residue of E2, which works together with E3 to transfer Ub to lysine residue of substrates. E3 ligases are categorized into three different classes: RING (Really Interesting New Gene) type, HECT (Homologous to the E6-AP Carboxyl Terminus) type, and the RBR (RING-between-RING) type. While the RING domain-containing E3 ligases transfer ubiquitin from the thioester-conjugated E2 directly to the isopeptide bond of lysine residues in the substrates, HECT- or RBR-containing E3 enzymes receives ubiquitin on a cysteine residue from E2, which is then delivered to substrate proteins.

Ubiquitination can be reversed by deubiquitinases (Dubs), which are a large family of enzymes that cleave the isopeptide bond between Ub and its substrate or between Ub moieties, leading to the release of free Ub and the return of the substrate protein to its original state (Sowa et al., 2009). Together with E3 ligases, Dubs regulate a wide variety of cellular processes, such as apoptosis, cell cycle and division, mutation repair, transcription, differentiation, development, inflammation and immune responses (Hershko and Ciechanover, 1998). Under certain disease and development conditions, ubiquitin signaling is regulated by posttranslational modifications on one or more of the enzymes or Ub itself, which allow the cell to fine-tune specific signal transduction cascades regulated by ubiquitination (Song and Luo, 2019). Furthermore, a recent exciting discovery demonstrates that the lipid A moiety of bacterial lipopolysaccharide (LPS) is ubiquitinated by the E3 ubiquitin ligase RNF213, an event critical for the elimination of invading pathogenic *Salmonella* Typhimurium (Otten et al., 2021). The identification of non-proteinaceous substrates has greatly expanded the scope of the biological processes regulated by this posttranslational modification.

Because of the involvement of ubiquitination in diverse cellular processes, particularly in immunity, it is fulfilling to realize that many pathogens elaborate various pathogenic factors to co-opt ubiquitin signaling to facilitate their survival and replication in their hosts. Virulence factors involved in interference of the host ubiquitin network have been identified in a wide spectrum of pathogens (Zhou and Zhu, 2015; Vozandychova et al., 2021). Among these, the opportunistic pathogen *Legionella pneumophila* is emerging as a unique model in this regard because of the sheer number of bacterial proteins involved and the richness in their mechanisms of action (Qiu and Luo, 2017b).

L. pneumophila is a Gram-negative bacterium ubiquitously found in fresh water environments where it exists as a parasite for protists. Inhalation of bacteria-contaminated aerosol by susceptible individuals can lead to the development of a severe form of pneumonia called Legionnaires' disease (Newton et al., 2010). *L. pneumophila* employs similar strategies to survive and replicate in amoebae and human macrophages, in both cases, it utilizes the Dot/Icm type IV secretion system to transport more than 330 effector proteins into host cells to construct the *Legionella*-containing vacuole (LCV) supportive for bacterial growth (Swanson and Isberg, 1995; Finsel and Hilbi, 2015; Ensminger, 2016). The LCV highly resembles the endoplasmic reticulum (ER) in term of protein composition and other cell biological features (Swanson and Isberg, 1995; Kagan and Roy, 2002). These Dot/Icm effectors interfere with a wide range of host processes with diverse biochemical activities (Qiu and Luo, 2017b). Among them, close to 20 effectors have been found to co-opt the host ubiquitin network by diverse biochemical mechanisms (**Table 1**; Qiu and Luo, 2017a). Here, we will highlight recent progress in the study of *Legionella* proteins that hijack host ubiquitination and their roles in bacterial pathogenesis and in the study of host cell biology.

TABLE 1 | *L. pneumophila* Dot/Icm effectors involved in ubiquitination pathway.

Effectors (Gene ID)	Aliases	Interactor/substrate	Enzymatic activity	Function	References
Canonical E3 ligases					
lpg0171	legU1	SKP1, Cullin 1, BAT3	F-Box protein, E3 ligase	Unknown	Ensminger and Isberg, 2010; Skaar et al., 2013
lpg1111	RavN	Unknown	U-box-like protein, E3 ligase	Unknown	Lin et al., 2018
lpg1408	licA	SKP1	F-Box protein	Unknown	Ensminger and Isberg, 2010
lpg2144/lpp2082	legAU13/ankB	SKP1, Cullin 1, Parvin B	F-Box protein, E3 ligase	Intracellular replication; Recruitment of ubiquitinated proteins to the LCV	Al-Khodor et al., 2008; Price et al., 2009; Ensminger and Isberg, 2010; Lomma et al., 2010; Skaar et al., 2013
lpg2224	PpgA	Unknown	F-Box protein	Unknown	Ensminger and Isberg, 2010
lpg2370	HipA	Unknown	E3 ligase	Unknown	Lin et al., 2018
lpg2455	GobX	Unknown	U-Box protein, E3 ligase	Unknown	Lin et al., 2015
lpg2498	MavJ	Unknown	E3 ligase	Unknown	Lin et al., 2018
lpg2525		Unknown	F-Box protein	Unknown	
lpg2577	MavM	Unknown	E3 ligase	Unknown	Lin et al., 2018
lpg2830	LegU2/LubX	Clk1, SidH	U-Box protein, E3 ligase	SidH degradation	Luo and Isberg, 2004; Kubori et al., 2008, 2010; Quaile et al., 2015
SidC family					
lpg2452	LegA14/SdcB	Unknown	Cys-His-Asp domain protein, E3 ligase	Unknown	Lin et al., 2018
lpg2510 lpg2511	SidC SdcA	Rab10	Cys-His-Asp domain protein, E3 ligase	Recruitment of ER vesicles and ubiquitinated proteins including Rab10 to LCV	Weber et al., 2006; Ragaz et al., 2008; Hsu et al., 2014; Luo et al., 2015; Jeng et al., 2019
Non-canonical E3 ligases					
lpg0234 lpg2153 lpg2156 lpg2157	SidE SdeC SdeB SdeA	Rab1, Rab6a, Rab30, Rab33b, Rtn4, FAM134C	All-in-one ubiquitin conjugation enzyme; Deubiquitinase	Intracellular replication; regulation of ubiquitin dynamics on the LCV; Recruitment of ER markers to the LCV; ER tubule Rearrangement.	Bhogaraju et al., 2016; Qiu et al., 2016; Kotewicz et al., 2017; Wan et al., 2019a; Shin et al., 2020b; Kawabata et al., 2021
lpg2147	MavC	UBE2N	Transglutaminase activity	inhibits NFκB activation	Valleau et al., 2018; Gan et al., 2019a; Guan et al., 2020; Puvar et al., 2020
Dubs					
lpg0160	RavD	Unknown	Cleaves linear Ub chains	Benefits L. pneumophila by suppressing host immune responses	Wan et al., 2019b
lpg0227	Ceg7	Unknown	Targets K6-, K11-, K48-, and K63- Ub chains	Unknown	Hermanns et al., 2020; Schubert et al., 2020
lpg1148	LupA	LegC3	Typical bacterial CE clan Dubs	Removes Ub modification of LegC3	Urbanus et al., 2016
lpg1621	LotB	Sec22b	Targets K63- Ub chains	Abolishes the interaction between Sec22b on the LCV and the syntaxin 3	Kitao et al., 2020b; Shin et al., 2020a

(Continued)

TABLE 1 | (Continued)

Effectors (Gene ID)	Aliases	Interactor/substrate	Enzymatic activity	Function	References
lpg2248	LotA	Unknown	Targets K13-, K48-, and K63- Ub chains	Removes ubiquitinated proteins from the surface of LCV	Kubori et al., 2018
lpg2529	LotC/Lem27	Rab10	Targets K6-, K11-, K48-, and K63- Ub chains	Removes ubiquitinated Rab10 from the surface of LCV	Liu et al., 2020; Schubert et al., 2020; Shin et al., 2020a

CANONICAL E3 LIGASES

The U-box type of E3s usually contain a conserved U-box sequence of 70 amino acids at their carboxyl termini (Miyamoto and Saito, 2018). LubX (Lpg2830) and GobX (Lpg2455) are *L. pneumophila* effectors that belong to this E3 family. Interestingly, LubX contains two U-box motifs with distinctly different functions: only U-box1 confers E3 activity (Quaile et al., 2015) and the proteins targeted by this enzyme appear structurally diverse. First, it attacks SidH (Lpg2829), a large Dot/Icm substrate (Luo and Isberg, 2004) encoded by a gene next to *lubX* by ubiquitination and subsequent degradation by the proteasome (Kubori et al., 2010). Because LubX functions to regulate the activity of another effector, it was designated as a metaeffector (Kubori et al., 2010). Interestingly, metaeffectors seem to be used in the regulation of a large cohort of *Legionella* effectors (Urbanus et al., 2016; Joseph and Shames, 2021; McCloskey et al., 2021). Second, LubX mediates ubiquitination of the Cdc2-like kinase 1 (CLK1) in host cells, leading to its degradation, but the biological significance of this degradation remains unknown (Kubori et al., 2008).

The effector GobX is the second U-box E3 ligase encoded by *L. pneumophila*, this enzyme is *S*-palmitoylated in host cells, thus allowing it to specifically target to the Golgi apparatus (Lin et al., 2015). Although its substrate has not yet been identified, such localization suggests that GobX functions to modulate cellular activity associated with this organelle (Lin et al., 2015). Recently, Lin et al. (2018) reported the amino terminal portion of RavN (Lpg1111) contains a U-box-like motif that has E3 activity. These authors also found that HipA (Lpg2370), MavM (Lpg2577), and MavJ (Lpg2498) have E3 ligase activity despite the fact that they share very limited homology to eukaryotic E3s. Unfortunately, the substrates of these E3s are currently unknown, so is their biological significance in *L. pneumophila* infection.

The SCF complex is a multi-subunit ubiquitin ligase consisting of RING-Box1 (RBXI), cullin 1 (CUL1), S-phase kinase-associated protein 1 (SPK1) and an F-box motif containing protein (FBP) (Nguyen and Busino, 2020). Whereas the first three proteins serve as structural scaffold for the complex to interact with other proteins, particularly an appropriate E2 enzyme, FBP contributes to substrate specificity of the SCF complex by modules involved in protein-protein interaction such as leucine-rich repeats and WD repeats (Nguyen and Busino, 2020). The *L. pneumophila* strain Philadelphia 1 encodes at least 5 FBP-like effectors to engage ubiquitination (Ensminger and Isberg, 2010; Skaar et al., 2013). Among these, LegU1 (Lpg0171) and AnkB (Lpg2144) contain *bona fide* F-box motifs and have been demonstrated to form active SCF complexes by interacting with SKP1. LicA (Lpg1408) harbors an F-box motif and this protein interacts with SKP1 but does not detectably bind CUL1 (Ensminger and Isberg, 2010). The E3 ligase complex formed by LegU1 catalyzes ubiquitination of the HLAB-associated transcript-3 (BAT3) (Ensminger and Isberg, 2010), a protein involved in the regulation of a wide range of cellular processes, including apoptosis in higher eukaryotes (Sasaki et al., 2007; Corduan et al., 2009). By a yeast two-hybrid screen, Lomma et al. (2010) identified ParvB as a substrate for AnkB and found that the bacterial F-box protein functions to reduce ParvB ubiquitination induced by endogenous enzymes. Yet whether ParvB is a specific substrate ubiquitylated by AnkB needs further study. AnkB is required for optimal intracellular growth of *L. pneumophila* strains AA100 and Paris in human monocyte derived macrophages (hMDMs) and for lung colonization in A/J mice (Price et al., 2009; Lomma et al., 2010). However, AnkB is dispensable for intracellular replication of strain Paris in *Acanthamoeba castellanii* (Lomma et al., 2010), while it is required for proficient replication of strain AA100 in *A. polyphaga* (Al-Khodor et al., 2008). These discrepancies may be due to differential effector redundancy in different strains of *L. pneumophila* or/and different protozoa infection models used. Finally, although both PpgA (Lpg2224) and Lpg2525 are predicted to harbor an F-box by bioinformatic analysis, neither has been shown to interact with SKP1 (Ensminger and Isberg, 2010). Whether these proteins have E3 ligase activity remained to be determined.

SidC AND SdcA

One prominent feature of the LCV is that this organelle dynamically recruits and retains an array of proteins of either host or *L. pneumophila* origin. In some cases, the anchoring of bacterial proteins on the LCV is mediated by their binding to phosphatidylinositol-4-phosphate (PI4P), an important signaling lipid whose enrichment on the bacterial phagosome is achieved in part by sequential action of three independent effectors that coordinate to biosynthesize PI4P from phosphatidylinositol (Hsu et al., 2012; Dong et al., 2016; Li et al., 2021). SidC (Lpg2511) and its ortholog SdcA anchor on the LCV by binding to PI4P via a lipid-interacting domain localized in the carboxyl portion of these proteins (Weber et al., 2006; Ragaz et al., 2008; Luo et al., 2015). These two highly similar effectors function to facilitate

the recruitment of ER-derived vesicles and ubiquitylated proteins to the LCV, which is executed by an activity conferred by their amino terminal domain (Ragaz et al., 2008), a region later found to possess E3 ligase activity (Hsu et al., 2014). The biochemical basis of ubiquitination catalyzed by SidC and SdcA is unique, which requires a Cys-His-Asp catalytic triad (Hsu et al., 2014), which often is associated with proteases (Buller and Townsend, 2013). Although these two proteins are of 72% identical in their primary sequences, SidC prefers the E2 UbcH7 for its activity and predominantly catalyzes the formation of K11- and K33-linked polyubiquitin chains. In contrast, SdcA displays the highest activity when working together with the E2 UbcH5 (Hsu et al., 2014). The E3 ligase activity of SidC and SdcA is essential for their role in the recruitment of ER components to the LCV (Hsu et al., 2014; Luo et al., 2015). Intriguingly, structural analysis reveals that the four α-helix bundles of the PI4P-binding motif blocks the catalytic site for the E3 activity embedded in the SNL (SidC N-terminal ubiquitin ligase) domain (Luo et al., 2015). In biochemical reactions, truncation mutants lacking the PI4P-binding domain exhibits more robust E3 ligase activity than the full-length protein. Consistently, inclusion of PI(4)P in reactions with full-length SidC enhances its E3 ligase activity (Luo et al., 2015). Thus, SidC and SdcA become more active in the presence of PI(4)P, which may allow them to selectively ubiquitinate their substrates on the surface of the LCV. Interestingly, Lpg2452 (SdcB) also possess a domain structurally resembling the catalytic center of SidC important for its E3 ligase activity, thus had been included as a member of the SidC family (Lin et al., 2018).

The small GTPase Rab1 is monoubiquitinated in macrophages infected with wild-type *L. pneumophila* but not the Δ*sidCsdcA* mutant, suggesting that Rab1 is a substrate of these E3 enzymes (Horenkamp et al., 2014). However, ubiquitination of Rab1 by SidC or SdcA was not detected in cells co-expressing these proteins by transfection or in biochemical reactions with recombinant proteins (Horenkamp et al., 2014; Hsu et al., 2014). How infection of wild-type *L. pneumophila* induces Rab1 ubiquitination remains to be investigated. Recently, Jeng et al. (2019) identified the GTPase Rab10 as a substrate of SidC and SdcA. Consistent with the non-degradative K11- and K33-types of polyubiquitin chains induced by SidC and SdcA, Rab10 is not degraded by SidC or SdcA. Instead, ubiquitination leads to its recruitment to the LCV (Jeng et al., 2019). How ubiquitination of Rab10 and its recruitment to the bacterial phagosome benefit the bacterium is unknown.

DUBS

Ubiquitination can be reversed by enzymes of the deubiquitinase superfamily. Members of this large family of proteases function to cleave Ub from ubiquitinated substrates by hydrolyzing the isopeptide bond between Ub moieties and between Ub and the substrate (Harrigan et al., 2018). The specificity of Dubs toward their substrates is dictated by multiple factors, including their topography, the polyubiquitin chain types, and the way the enzyme makes contact with Ub moieties (Ronau et al., 2016). *L. pneumophila* codes for multiple Dubs that participate in various aspects of its interactions with host cells (Kitao et al., 2020a). Among these, LupA (Lpg1148) is the first described Dub in this pathogen, it harbors a Cys-His-Asp catalytic triad associated with typical bacterial CE clan Dubs (Urbanus et al., 2016). LupA is able to suppress the yeast toxicity of LegC3 (Lpg1701), another Dot/Icm substrate that appears to modulate membrane fusion in host cells (Urbanus et al., 2016). LegC3 undergoes ubiquitination in host cells probably by a yet unidentified host E3 ligase and LupA can remove such modification in a process that requires an intact Cys-His-Asp catalytic triad (Urbanus et al., 2016). How the Dub activity of LupA suppresses the yeast toxicity of LegC3 is not fully understood. One possibility is that ubiquitination activates the enzymatic activity of LegC3, which causes yeast toxicity and the removal of the Ub by LupA thus will put the toxicity under check.

LotA (Lpg2248) harbors two ovarian tumor (OTU)-like domains each possessing its own catalytic cysteine residue (Cys13 and Cys303, respectively). Whereas the domain using Cys13 mainly cleaves Lys6-linked polyubiquitin chains, the other prefers Lys48/Lys63-linked polyubiquitin (Kubori et al., 2018). Although its target is unknown, LotA contributes to the removal of ubiquitinated proteins from the surface of the LCV and is required for proficient intracellular growth of *L. pneumophila* (Kubori et al., 2018). LotB (Lpg1621) is another OTU-like Dub that specifically removes Lys63-linked ubiquitin chains (Ma et al., 2020; Schubert et al., 2020; Shin et al., 2020a). Structural analysis reveals that except for the ubiquitin binding site S1, LotB harbors an additional site S1', which confers its specificity in cleavage of the Lys63-linked chains (Shin et al., 2020a). The SNARE protein Sec22b involved in membrane fusion is a substrate of LotB; this protein is ubiquitinated in cells infected with *L. pneumophila* and LotB appears to function to counteract such modification (Shin et al., 2020a). The removal of ubiquitin from Sec22b abolishes the interaction between Sec22b on the LCV and the t-SNARE syntaxin 3, resulting in the dissociation of the latter from the bacterial phagosome (Kitao et al., 2020b). Interestingly, ubiquitination and recruitment of Rab10 to the LCV by SidC and SdcA are regulated by a third OUT-like Dub Lem27 (Lpg2529) (also known as LotC) coded for by *L. pneumophila* (Schubert et al., 2020; Shin et al., 2020a). Lem27 appears to modulate Rab10 ubiquitination by counteracting the activity of SidC and SdcA (Liu et al., 2020). Ceg7 (Lpg0227) has also been shown to possess Dub activity and belongs to the OUT-like family (Hermanns et al., 2020; Schubert et al., 2020). This enzyme broadly targets K6-, K11-, K48-, and K63-linked polyubiquitin chains in biochemical assays but the biological significance of this activity is unclear (Schubert et al., 2020). A recent structural study revealed that an extended helical lobe (EHL) domain commonly shared in LotA, LotB and Lem27 is responsible for their Ub binding, defining the Lot-OTUs as a unique class of Dubs (Takekawa et al., 2021).

RavD (Lpg0160) is an effector that is associated with the LCV by binding to phosphatidylinositol-3-phosphate (PI3P) (Pike et al., 2019). Although no impact on bacterial intracellular growth, deletion of *ravD* led to a significant increase of late endosome/lysosome markers such as LAMP-1 on the LCV (Pike et al., 2019). A more recent study revealed that RavD is a Dub that

specifically cleaves linear ubiquitin chains (Wan et al., 2019b), a unique ubiquitin chain important for signaling in innate and adaptive immunity, and inflammatory signaling (Rittinger and Ikeda, 2017). The removal of the linear ubiquitin chains on the LCV by RavD benefits *L. pneumophila* by suppressing host immune responses (Wan et al., 2019b). The activity of RavD suggests *L. pneumophila* may more extensively interact with higher order hosts, including mammals, because the ubiquitin ligase complex LUBAC responsible for the formation of linear ubiquitin chain is not present in protozoan (Spit et al., 2019).

PHOSPHORIBOSYL UBIQUITINATION AND ITS REGULATION

The SidE family contains SdeA, SdeB, SdeC, and SidE, which are four large proteins. Among these, SidE, SdeA, and SdeC are almost identical at the primary sequence level, only with a few conserved substitutions throughout the proteins of about 1,500 residues. SdeB (1926 aa) is considerably larger than the other three members of the family, it contains an extra region of about 400 aa in its carboxyl end (Luo and Isberg, 2004). Members of the SidE family (SidEs) are functionally redundant in *L. pneumophila* virulence (Bardill et al., 2005). Careful biochemical analysis reveals that these effectors represent a novel Ub ligase that catalyzes ubiquitination by a mechanism that is chemically distinct from the canonical three-enzyme cascade. First, Ub activation in reaction catalyzed by SidEs is energized by nicotinamide adenine dinucleotide (NAD), which is hydrolyzed by a mono-ADP-ribosyltransferase activity (mART) to modify Arg42 of Ub to produce ADP-ribosylated Ub (ADPR-Ub) (Qiu et al., 2016; **Figure 2A**). Whereas the biochemical basis of this catalysis is similar to classical mART often found in bacterial toxins (Mikolcevic et al., 2021), ADPR-Ub produced by this reaction is utilized by a phosphodiesterase (PDE) activity also embedded in each of SidE family member, which cleaves the phosphoanhydride bond between the two phosphate atoms, resulting in the transfer of phosphoribosyl Ub (PR-Ub) to serine residues on substrate proteins and the release of AMP (Bhogaraju et al., 2016; Kotewicz et al., 2017; **Figure 2A**).

Members of the SidE family appear to attack a large cohort of structurally diverse host proteins, including a number of Rab small GTPases and numerous ER resident proteins such as Rtn4 and FAM134C (Bhogaraju et al., 2016; Qiu et al., 2016; Kotewicz et al., 2017; Wan et al., 2019a; Shin et al., 2020b). Although many of these substrates are similarly attacked by each of these ligases (Bhogaraju et al., 2016; Qiu et al., 2016; Kotewicz et al., 2017; Wan et al., 2019a; Shin et al., 2020b), it is not clear whether any of these proteins specifically modifies one or more host proteins. Structural analysis suggests that a binding cleft in the PDE domain is responsible for substrate recognition which engages a sequence motif in which the target serine is in the vicinity of hydrophobic residues and is flanked by proline residues (Kalayil et al., 2018).

During *L. pneumophila* infection, ubiquitination of Rtn4 by SidEs drastically promotes structural transformation of ER tubules, probably by inducing Rtn4 oligomerization, thus providing a scaffold for the formation of tubule matrix-like structures (Kotewicz et al., 2017). For small GTPases such as Rab33b, modification induced by SidEs leads to slight inhibition of its GTPase activity (Qiu et al., 2016). The modification and subsequent recruitment of other ER proteins such as FAM134C to the LCV may prevent the delivery of the bacterial phagosome to the autophagic pathway (Wan et al., 2019a; Shin et al., 2020b). Phosphoribosyl ubiquitination of Rab33b by SidEs recruits this GTPases to the LCV, where its associates with another small GTPase Rab6A, which interacts with the ER via direct interaction with SNAREs. Thus, one role of the SidE family is to promote the fusion between the LCV and the ER (Kawabata et al., 2021).

Members of SidEs family also have classical Dub activity, each conferred by a domain formed by the first 200 residues of the proteins (Sheedlo et al., 2015). The cleavage of isopeptide bond by these Dub domains is catalyzed by a Cys-His-Asp triad commonly found in the CE clan proteases (Sheedlo et al., 2015). This Dub module cleaves Lys11, Lys48, and Lys63-linked polyubiquitin chains, with a distinct preference for Lys63 linkages (Sheedlo et al., 2015). The Dub activity of SidEs function to reduce the association of ubiquitinated proteins on the LCV, which may antagonize the recruitment of host autophagy machinery to the phagosome. In addition, the low chain type specificity of these Dub domains probably function to replenish the Ub pool proximal to the LCV to provide the reaction precursor for phosphoribosyl ubiquitination.

Similar to canonical ubiquitination, modification by SidEs is reversible. The phospho-ribose linkage between Ub and the substrate cannot be cleaved by canonical Dubs. By testing a number of *Legionella* proteins predicted to harbor a PDE domain potentially involved in cleaving phosphodiester bond, two independent studies identified DupA (Lpg2154) and DupB (Lpg2509) as enzymes that function to remove PR-Ub from substrates (Akturk et al., 2018; Wan et al., 2019a; **Figure 2A**). Intriguingly, the Dup family can hydrolyze ADPR-Ub to produce PR-Ub and AMP (Akturk et al., 2018; Wan et al., 2019a; **Figure 2A**).

Structural studies reveal that the distance between the mART domain of SidEs and the PDE domain is approximately 70 Å (Akturk et al., 2018; Dong et al., 2018; Kalayil et al., 2018), suggesting the need of a mechanism to channel the reaction intermediate ADPR-Ub produced by the mART domain to the second reaction center. Because ADPR-Ub is highly toxic to eukaryotic cells by interfering with canonical ubiquitination (Bhogaraju et al., 2016), hydrolysis of this reaction intermediate by DupA and DupB may prevent poisoning of the host cell by ADPR-Ub that accidentally escapes from the mART catalytic pocket. Whether and how PR-Ub, which is also toxic to eukaryotic cells (Bhogaraju et al., 2016), is further reduced to phosphoribose and free Ub is unknown.

In addition to DupA and DupB, which mainly function to reverse ubiquitination induced by SidEs, the activity of this family of Ub ligases is further regulated by SidJ, one protein of a two-member family (Liu and Luo, 2007). SidJ had been reported to disperse SidEs from the LCV (Jeong et al., 2015) and can suppress the toxicity of SidEs to eukaryotic cells (Havey and Roy, 2015; Jeong et al., 2015). Of note is that the regulation of cellular

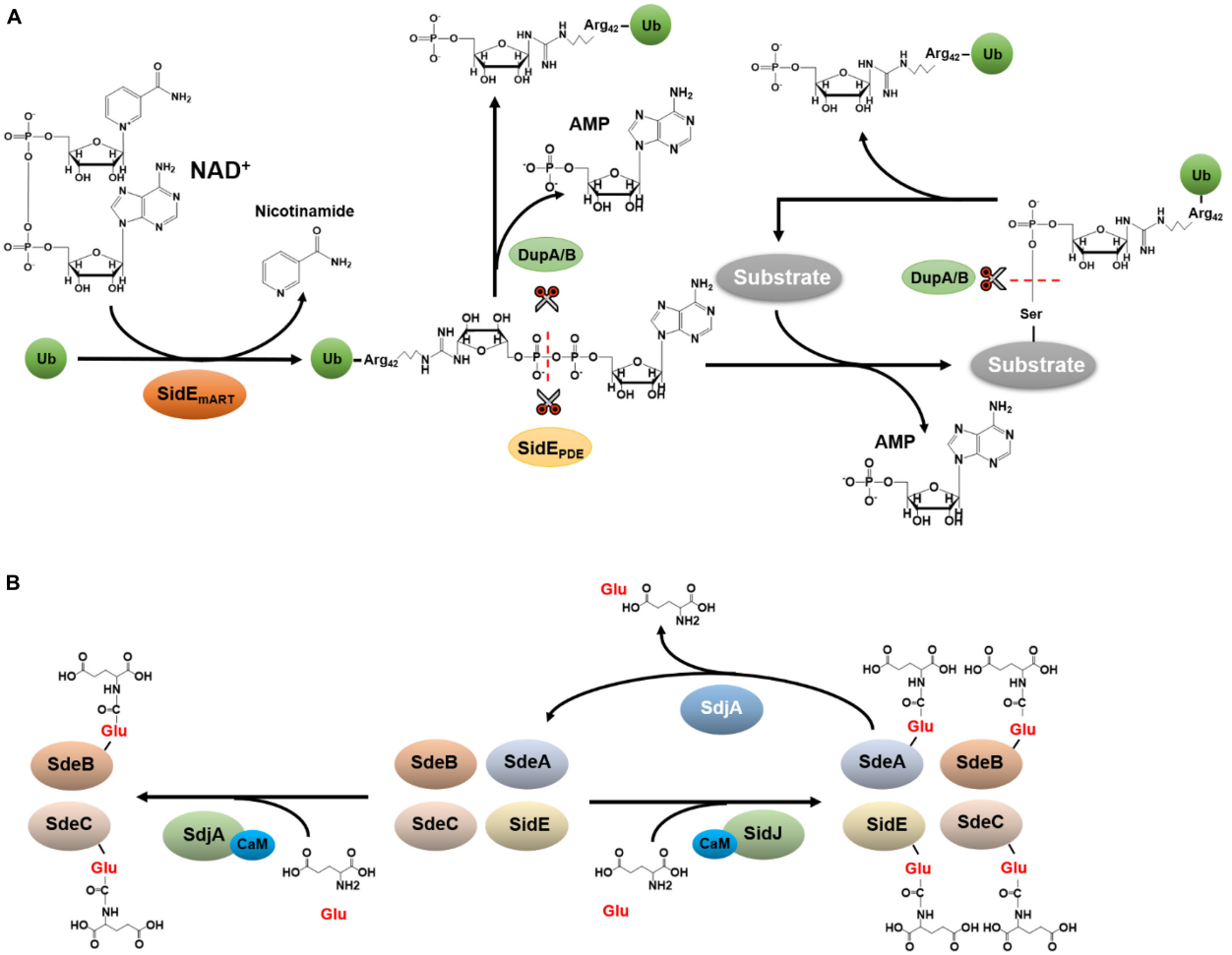


FIGURE 2 | Ubiquitination by the SidE family and its regulation. **(A)** Phosphoribosyl ubiquitination and de-ubiquitination. Phosphoribosyl ubiquitination induced by SidEs is initiated by ADP-ribosylation of Ub at Arg42 by its mART activity, leading to the release of nicotinamide and the production of ADPR-Ub. The phosphodiester bond in ADPR-Ub is subsequently the cleaved by the phosphodiesterase (PDE) domain of SidEs, which is accompanied by the transfer of phosphoribosyl Ub to serine residues of substrate proteins and the release of AMP. **(B)** Glutamylation and de-glutamylation of members of the SidE family. In host cells, SidJ binds to CaM via an IQ motif in its carboxyl end. The complex functions as a glutamylase to attack the first glutamate residue of the ExE motif in the mART domain of SidEs by polyglutamylation, leading to abolishment of the activity of the mART, and thus the inactivation of Ub ligase activity of the SidEs. Despite its high-level similarity to SidJ, SdjA selectively inhibits SdeB and SdeC by glutamylation. In addition to the glutamylase activity, SdjA also exhibits a deglutamylase activity toward glutamylated SdeA.

distribution of SidEs by SidJ was not detected in an independent study (Qiu et al., 2017). Four structural and biochemical studies independently reveal that SidJ is a glutamylase that attacks the first glutamate residue of the ExE motif in the mART domain of SidEs by polyglutamylation (Bhogaraju et al., 2019; Black et al., 2019; Gan et al., 2019b; Sulpizio et al., 2019). This modification abolishes the activity of the mART, thus the Ub ligase activity of the SidEs. Mechanistically, the glutamylation by SidJ is catalyzed by a two-step reaction in which the enzyme first activates the target glutamate residue by acyl-adenylation using a pseudokinase domain (Sreelatha et al., 2018), followed by the replacement of the AMP moiety with glutamate (Bhogaraju et al., 2019; Black et al., 2019; Gan et al., 2019b; Sulpizio et al., 2019), Interestingly, SidJ is activated by the eukaryote-specific calcium-binding protein calmodulin (CaM) which recognizes an IQ motif in its carboxyl end (Bhogaraju et al., 2019; Black et al., 2019; Gan et al., 2019b; Sulpizio et al., 2019). The requirement of CaM restricts the activity of SidJ in the cytosol of the infected cell, thus preventing premature inactivation of SidEs. Despite its high-level similarity to SidJ, SdjA, the other member of the SidJ family, cannot rescue the yeast growth defect caused by SdeA (Qiu et al., 2017; Gan et al., 2019b). Furthermore, SidJ and SdjA are not functionally redundant for the intracellular growth defect of the Δ*sidJ* mutant cannot be complemented by SdjA (Liu and Luo, 2007). A recent study found that SdjA selectively inhibits some members of the SidE family by glutamylation (Osinski et al., 2021; **Figure 2B**). Interestingly, another study shows that in addition to the glutamylase activity against SdeB and SdeC, SdjA exhibits a deglutamylase activity toward SdeA that has been modified by SidJ/CaM (Song et al., 2021; **Figure 2B**). Thus, SdjA functions

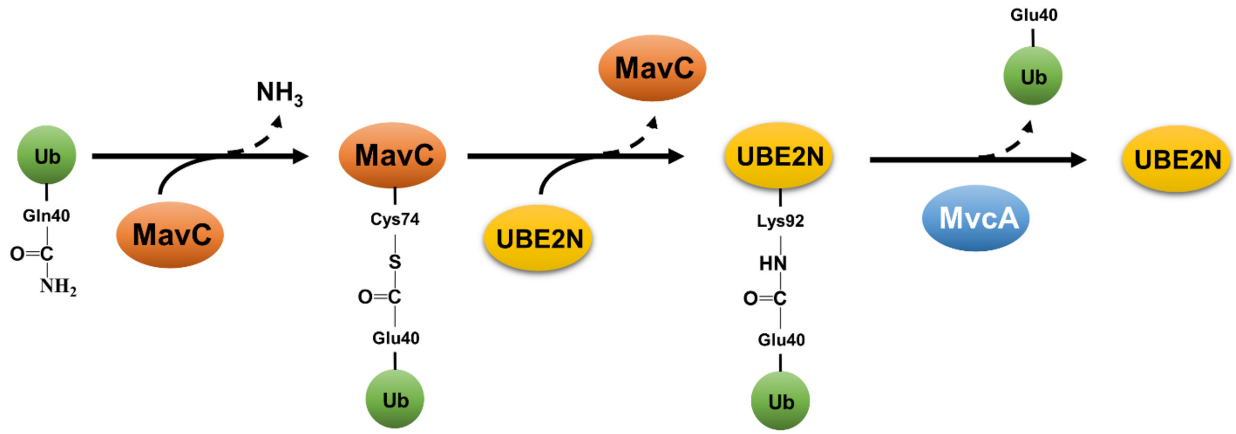


FIGURE 3 | Reversible atypical ubiquitination by MavC and MvcA. Ubiquitination catalyzed by MavC is initiated by the formation of a thioester linkage between the active residue Cys74 and Gln40 of Ub, concomitant with the release of ammonium. The acylated MavC then reacts with the amine donor from a lysine (Lys92) in UBE2N to form an intermolecular isopeptide bond, resulting in ubiquitination of UBE2N. MvcA, a structural ortholog of MavC, functions as a deubiquitinase to cleave the isopeptide bond between Ub and UBE2N catalyzed by MavC, leading to the release of UBE2N and deamidated Ub.

to fine-tune the activity of SidJ and SdeA during *L. pneumophila* infection (Song et al., 2021). Yet, the mechanism by which SdjA catalyzes the cleavage of the isopeptide bond between glutamate residues in glutamylated SdeA needs further investigation.

The SidE effector family has long known to be important for optimal virulence of *L. pneumophila* (Song et al., 2021), and targeting the unique ubiquitin ligase activity with compounds is an anti-virulence strategy to control *L. pneumophila* infection. Several stable NAD^+ analogs capable of inhibiting the activity of SdeC at IC_{50} of 28–39 μM have been developed (Madern et al., 2020). It remains unclear whether these compounds can block intracellular replication of the pathogen.

REVERSIBLE UBIQUITINATION BY TRANSGLUTAMINASES MavC AND MvcA

The second non-canonical ubiquitination mechanism by *L. pneumophila* is exemplified by MavC (Lpg2147) that catalyzes a crosslink reaction between Ub and the E2 enzyme UBE2N (Gan et al., 2019a). MavC is a transglutaminase that induces the formation of a γ-glutamyl-ε-Lys isopeptide between Gln40 of Ub and Lys92 of UBE2N (Gan et al., 2019a). This reaction appears to preferably occur intramolecularly in charged UBE2N that carries a Ub moiety covalently linked to its active site Cys87 (Puvar et al., 2020). The reaction catalyzed by MavC is initiated by the formation of a thioester linkage between its active site Cys74 and the side chain amide of Gln40 of Ub, which is followed by a transglutamination reaction that leads to the installation of an isopeptide bond between Lys92 of UBE2N and Gln40 of Ub (Guan et al., 2020; Puvar et al., 2020; **Figure 3**). Because of its structural homology to bacterial deamidases Cif and CHBP that attack Ub and NEDD8 at Gln40 (Cui et al., 2010), MavC was identified in an earlier study as a Ub deamidase (Valleau et al., 2018). All described transglutaminases exhibit a protein deamidation activity in reactions lacking the crosslink target (Lorand and Graham, 2003). Consistent with this notion, MavC deamidates Ub at Gln_{40} in reactions containing only the enzyme and Ub (Valleau et al., 2018; Gan et al., 2019a). Importantly, the Ub deamidation activity is only detectable in biochemical reactions with large amounts of proteins but not in cells infected with wild-type *L. pneumophila* (Valleau et al., 2018; Gan et al., 2019a). Structurally, the main domain of MavC resembles the structures of Cif effectors (Valleau et al., 2018), the insertion domain is involved in engaging its substrate UBE2N (Guan et al., 2020).

MvcA (Lpg2148) is an ortholog of MavC, these two proteins share 50% identity and 65% similarity in their sequences and the structures of these two proteins are superimposable (Cui et al., 2010). Both MavC and MvcA deamidates Ub at Gln40, and this activity had been suggested to interfere with Ub signaling at different phases of *L. pneumophila* infection (Cui et al., 2010). Despite this high-level similarity, MvcA cannot catalyze protein crosslink between Ub and UBE2N or several other E2 enzymes (Gan et al., 2020). Further biochemical experiments reveal that MvcA functions as deubiquitinase that cleaves the isopeptide bond between Ub and UBE2N in the crosslink product formed by MavC (Gan et al., 2020; Mu et al., 2020; **Figure 3**). MavC and MvcA utilize the same biochemical mechanism to catalyze two reactions that have an opposite effect toward the activity of UBE2N (Gan et al., 2020; Mu et al., 2020). It has been proposed that the outcome of the reaction is determined by the binding affinity of the enzyme to Ub, UBE2N and the product UBE2N-Ub (Guan et al., 2020). The surface charge of the Tail domain of MvcA is repulsive to Ub, which together with the lower binding affinity for UBE2N favor the dissociation of Ub from MvcA, thus resulting in the cleavage of the isopeptide bond (Guan et al., 2020).

A main function of UBE2N is to catalyze the formation of K63-type polyubiquitin chains, which are involved in the regulation of diverse cellular activities, including immunity by

inducing the activation of the NFκB pathway (Hodge et al., 2016). MavC-induced ubiquitination UBE2N inserts the Ub moiety in the catalytic pocket of the E2 enzyme (Gan et al., 2020; Mu et al., 2020), which blocks the entry of activated Ub to its Cys87 active site. Although MavC can effectively induce crosslink between free Ub and UBE2N, charged UBE2N carrying a Ub moiety on its catalytic site Cys87 via a thioester bond appears to be the prefer substrate (Puvar et al., 2020). This modification effectively inhibits NFκB activation by cues that initiate the signaling upstream of UBE2N (Valleau et al., 2018; Gan et al., 2019a). Like many Dot/Icm effectors, MavC expresses at high levels in bacteria grown to the post-exponential phase (Gan et al., 2019a), which facilitates the initial attack of the host defense upon contact. As the infection proceeds to later phases, the activity of UBE2N is restored by MvcA to accommodate the need of NFκB activation for maintaining critical cellular functions such as cell survival (Losick and Isberg, 2006). Consistent with this notion, the expression of MvcA does not become detectable several hours after bacterial uptake (Gan et al., 2020). Interestingly, Lpg2149 which is encoded by a gene in the *mavC* and *mvcA* locus, blocks the activity of both MavC and MvcA by direct binding (Mu et al., 2020). The biological significance of Lpg2149 largely remains mysterious, but its presence further highlights the importance of fine-tuning the activity of UBE2N during *L. pneumophila* infection.

CONCLUSION AND PERSPECTIVES

The study of *L. pneumophila* effectors involved in ubiquitination has greatly expanded our appreciation of the exploitation of Ub signaling by a pathogen. It has also extended our understanding of the chemical basis of ubiquitination. A recent study shows that Ub signaling plays important roles beyond the remodeling of phagosomal membranes (Ong et al., 2021). Several host proteins involved in ubiquitination, particularly the E2 enzyme UBE2E1, and the E3 Ub ligase, CUL7, are important not only for *L. pneumophila* intracellular replication but also for Dot/Icm-mediated protein translocation (Ong et al., 2021). Clearly, the involvement of the Ub system in *L. pneumophila* pathogenesis is deeper and more extensive than we have appreciated. It will be of great interest to determine whether and how these host enzymes impact the functionality of the bacterial protein translocation machinery and its substrates. An equally important question is whether these enzymes are targeted by *L. pneumophila* effectors involved in Ub signaling.

With a few exceptions, the cellular targets of most of the E3 ligases or Dubs remain unknown. Clearly, the identification of their substrates is essential in our understanding of these effectors in the intracellular life cycle of *L. pneumophila.* Because the affinity between E3 ligases and their substrates often is too low to be harnessed for substrate identification (Nagy and Dikic, 2010), new technologies such as orthogonal Ub transfer (OUT) (Zhao et al., 2012), effective proximity labeling by the bacterial biotin ligase BirA (Branon et al., 2018) and substrate trapping by fusion proteins (O'Connor et al., 2015), will surely be useful in this endeavor. It is anticipated that more exciting discoveries will be made in years to come in our investigation of Ub signaling in *L. pneumophila* virulence.

AUTHOR CONTRIBUTIONS

JL and LW drafted the first version of the manuscript. LS and Z-QL revised the manuscript with input from all authors.

FUNDING

Work in our labs was supported by the Jilin Science and Technology Agency grant 20200403117SF (LS) and the National Institutes of Health grant R01AI127465 (Z-QL).

REFERENCES

Akturk, A., Wasilko, D. J., Wu, X., Liu, Y., Zhang, Y., Qiu, J., et al. (2018). Mechanism of phosphoribosyl-ubiquitination mediated by a single *Legionella* effector. *Nature* 557, 729–733. doi: 10.1038/s41586-018-0147-6

Al-Khodor, S., Price, C. T., Habyarimana, F., Kalia, A., and Abu Kwaik, Y. (2008). A Dot/Icm-translocated ankyrin protein of *Legionella pneumophila* is required for intracellular proliferation within human macrophages and protozoa. *Mol. Microbiol.* 70, 908–923. doi: 10.1111/j.1365-2958.2008.06453.x

Bardill, J. P., Miller, J. L., and Vogel, J. P. (2005). IcmS-dependent translocation of SdeA into macrophages by the *Legionella pneumophila* type IV secretion system. *Mol. Microbiol.* 56, 90–103. doi: 10.1111/j.1365-2958.2005.04539.x

Bhogaraju, S., Bonn, F., Mukherjee, R., Adams, M., Pfleiderer, M. M., Galej, W. P., et al. (2019). Inhibition of bacterial ubiquitin ligases by SidJ-calmodulin catalysed glutamylation. *Nature* 572, 382–386. doi: 10.1038/s41586-019-1440-8

Bhogaraju, S., Kalayil, S., Liu, Y., Bonn, F., Colby, T., Matic, I., et al. (2016). Phosphoribosylation of ubiquitin promotes serine ubiquitination and impairs conventional ubiquitination. *Cell* 167, 1636–1649 e13. doi: 10.1016/j.cell.2016.11.019

Black, M. H., Osinski, A., Gradowski, M., Servage, K. A., Pawlowski, K., Tomchick, D. R., et al. (2019). Bacterial pseudokinase catalyzes protein polyglutamylation to inhibit the SidE-family ubiquitin ligases. *Science* 364, 787–792. doi: 10.1126/science.aaw7446

Branon, T. C., Bosch, J. A., Sanchez, A. D., Udeshi, N. D., Svinkina, T., Carr, S. A., et al. (2018). Efficient proximity labeling in living cells and organisms with TurboID. *Nat. Biotechnol.* 36, 880–887. doi: 10.1038/nbt.4201

Buetow, L., and Huang, D. T. (2016). Structural insights into the catalysis and regulation of E3 ubiquitin ligases. *Nat. Rev. Mol. Cell Biol.* 17, 626–642. doi: 10.1038/nrm.2016.91

Buller, A. R., and Townsend, C. A. (2013). Intrinsic evolutionary constraints on protease structure, enzyme acylation, and the identity of the catalytic triad. *Proc. Natl. Acad. Sci. U.S.A.* 110, E653–E661. doi: 10.1073/pnas.1221050110

Corduan, A., Lecomte, S., Martin, C., Michel, D., and Desmots, F. (2009). Sequential interplay between BAG6 and HSP70 upon heat shock. *Cell Mol. Life Sci.* 66, 1998–2004. doi: 10.1007/s00018-009-9198-z

Cui, J., Yao, Q., Li, S., Ding, X., Lu, Q., Mao, H., et al. (2010). Glutamine deamidation and dysfunction of ubiquitin/NEDD8 induced by a bacterial effector family. *Science* 329, 1215–1218. doi: 10.1126/science.1193844

Dong, N., Niu, M., Hu, L., Yao, Q., Zhou, R., and Shao, F. (2016). Modulation of membrane phosphoinositide dynamics by the phosphatidylinositide 4-kinase activity of the Legionella LepB effector. *Nat. Microbiol.* 2:16236. doi: 10.1038/nmicrobiol.2016.236

Dong, Y., Mu, Y., Xie, Y., Zhang, Y., Han, Y., Zhou, Y., et al. (2018). Structural basis of ubiquitin modification by the *Legionella* effector SdeA. *Nature* 557, 674–678. doi: 10.1038/s41586-018-0146-7

Ensminger, A. W. (2016). *Legionella pneumophila*, armed to the hilt: justifying the largest arsenal of effectors in the bacterial world. *Curr. Opin. Microbiol.* 29, 74–80. doi: 10.1016/j.mib.2015.11.002

Ensminger, A. W., and Isberg, R. R. (2010). E3 ubiquitin ligase activity and targeting of BAT3 by multiple *Legionella pneumophila* translocated substrates. *Infect. Immun.* 78, 3905–3919. doi: 10.1128/IAI.00344-10

Finsel, I., and Hilbi, H. (2015). Formation of a pathogen vacuole according to *Legionella pneumophila*: how to kill one bird with many stones. *Cell Microbiol.* 17, 935–950. doi: 10.1111/cmi.12450

Gan, N., Guan, H., Huang, Y., Yu, T., Fu, J., Nakayasu, E. S., et al. (2020). *Legionella pneumophila* regulates the activity of UBE2N by deamidase-mediated deubiquitination. *EMBO J.* 39:e102806. doi: 10.15252/embj.2019102806

Gan, N., Zhen, X., Liu, Y., Xu, X., He, C., Qiu, J., et al. (2019b). Regulation of phosphoribosyl ubiquitination by a calmodulin-dependent glutamylase. *Nature* 572, 387–391. doi: 10.1038/s41586-019-1439-1

Gan, N., Nakayasu, E. S., Hollenbeck, P. J., and Luo, Z. Q. (2019a). *Legionella pneumophila* inhibits immune signalling via MavC-mediated transglutaminase-induced ubiquitination of UBE2N. *Nat. Microbiol.* 4, 134–143. doi: 10.1038/s41564-018-0282-8

Guan, H., Fu, J., Yu, T., Wang, Z. X., Gan, N., Huang, Y., et al. (2020). Molecular basis of ubiquitination catalyzed by the bacterial transglutaminase MavC. *Adv. Sci.* 7:2000871. doi: 10.1002/advs.202000871

Harrigan, J. A., Jacq, X., Martin, N. M., and Jackson, S. P. (2018). Deubiquitylating enzymes and drug discovery: emerging opportunities. *Nat. Rev. Drug Discov.* 17, 57–78. doi: 10.1038/nrd.2017.152

Havey, J. C., and Roy, C. R. (2015). Toxicity and SidJ-mediated suppression of toxicity require distinct regions in the SidE family of *Legionella pneumophila* effectors. *Infect. Immun.* 83, 3506–3514. doi: 10.1128/IAI.00497-15

Hermanns, T., Woiwode, I., Guerreiro, R. F., Vogt, R., Lammers, M., and Hofmann, K. (2020). An evolutionary approach to systematic discovery of novel deubiquitinases, applied to *Legionella*. *Life Sci. Alliance* 3:e202000838. doi: 10.26508/lsa.202000838

Hershko, A., and Ciechanover, A. (1998). The ubiquitin system. *Annu. Rev. Biochem.* 67, 425–479.

Hodge, C. D., Spyracopoulos, L., and Glover, J. N. (2016). Ubc13: the Lys63 ubiquitin chain building machine. *Oncotarget* 7, 64471–64504. doi: 10.18632/oncotarget.10948

Horenkamp, F. A., Mukherjee, S., Alix, E., Schauder, C. M., Hubber, A. M., Roy, C. R., et al. (2014). *Legionella pneumophila* subversion of host vesicular transport by SidC effector proteins. *Traffic* 15, 488–499. doi: 10.1111/tra.12158

Hsu, F., Luo, X., Qiu, J., Teng, Y. B., Jin, J., Smolka, M. B., et al. (2014). The *Legionella* effector SidC defines a unique family of ubiquitin ligases important for bacterial phagosomal remodeling. *Proc. Natl. Acad. Sci. U.S.A.* 111, 10538–10543. doi: 10.1073/pnas.1402605111

Hsu, F., Zhu, W., Brennan, L., Tao, L., Luo, Z. Q., and Mao, Y. (2012). Structural basis for substrate recognition by a unique *Legionella* phosphoinositide phosphatase. *Proc. Natl. Acad. Sci. U.S.A.* 109, 13567–13572. doi: 10.1073/pnas.1207903109

Jeng, E. E., Bhadkamkar, V., Ibe, N. U., Gause, H., Jiang, L., Chan, J., et al. (2019). Systematic identification of host cell regulators of *Legionella pneumophila* pathogenesis using a genome-wide CRISPR screen. *Cell Host Microbe* 26, 551–563.e6. doi: 10.1016/j.chom.2019.08.017

Jeong, K. C., Sexton, J. A., and Vogel, J. P. (2015). Spatiotemporal regulation of a *Legionella pneumophila* T4SS substrate by the metaeffector SidJ. *PLoS Pathog.* 11:e1004695. doi: 10.1371/journal.ppat.1004695

Joseph, A. M., and Shames, S. R. (2021). Affecting the effectors: regulation of *Legionella pneumophila* effector function by metaeffectors. *Pathogens* 10:108. doi: 10.3390/pathogens10020108

Kagan, J. C., and Roy, C. R. (2002). *Legionella* phagosomes intercept vesicular traffic from endoplasmic reticulum exit sites. *Nat. Cell Biol.* 4, 945–954. doi: 10.1038/ncb883

Kalayil, S., Bhogaraju, S., Bonn, F., Shin, D., Liu, Y., Gan, N., et al. (2018). Insights into catalysis and function of phosphoribosyl-linked serine ubiquitination. *Nature* 557, 734–738. doi: 10.1038/s41586-018-0145-8

Kawabata, M., Matsuo, H., Koito, T., Murata, M., Kubori, T., Nagai, H., et al. (2021). Legionella hijacks the host Golgi-to-ER retrograde pathway for the association of *Legionella*-containing vacuole with the ER. *PLoS Pathog.* 17:e1009437. doi: 10.1371/journal.ppat.100943

Kitao, T., Nagai, H., and Kubori, T. (2020a). Divergence of *Legionella* effectors reversing conventional and unconventional ubiquitination. *Front. Cell Infect. Microbiol.* 10:448. doi: 10.3389/fcimb.2020.00448

Kitao, T., Taguchi, K., Seto, S., Arasaki, K., Ando, H., Nagai, H., et al. (2020b). Legionella manipulates non-canonical SNARE pairing using a bacterial deubiquitinase. *Cell Rep.* 32:108107. doi: 10.1016/j.celrep.2020.108107

Kotewicz, K. M., Ramabhadran, V., Sjoblom, N., Vogel, J. P., Haenssler, E., Zhang, M., et al. (2017). A single *Legionella* effector catalyzes a multistep ubiquitination pathway to rearrange tubular endoplasmic reticulum for replication. *Cell Host Microbe* 21, 169–181. doi: 10.1016/j.chom.2016.12.007

Kubori, T., Hyakutake, A., and Nagai, H. (2008). Legionella translocates an E3 ubiquitin ligase that has multiple U-boxes with distinct functions. *Mol. Microbiol.* 67, 1307–1319. doi: 10.1111/j.1365-2958.2008.06124.x

Kubori, T., Kitao, T., Ando, H., and Nagai, H. (2018). LotA, a *Legionella* deubiquitinase, has dual catalytic activity and contributes to intracellular growth. *Cell Microbiol.* 20:e12840. doi: 10.1111/cmi.12840

Kubori, T., Shinzawa, N., Kanuka, H., and Nagai, H. (2010). Legionella metaeffector exploits host proteasome to temporally regulate cognate effector. *PLoS Pathog* 6:e1001216. doi: 10.1371/journal.ppat.1001216

Li, G., Liu, H., Luo, Z. Q., and Qiu, J. (2021). Modulation of phagosome phosphoinositide dynamics by a *Legionella* phosphoinositide 3-kinase. *EMBO Rep.* 22:e51163. doi: 10.15252/embr.202051163

Lin, Y. H., Doms, A. G., Cheng, E., Kim, B., Evans, T. R., and Machner, M. P. (2015). Host cell-catalyzed S-palmitoylation mediates golgi targeting of the legionella ubiquitin ligase GobX. *J. Biol. Chem.* 290, 25766–25781. doi: 10.1074/jbc.M115.637397

Lin, Y. H., Lucas, M., Evans, T. R., Abascal-Palacios, G., Doms, A. G., Beauchene, N. A., et al. (2018). RavN is a member of a previously unrecognized group of *Legionella pneumophila* E3 ubiquitin ligases. *PLoS Pathog.* 14:e1006897. doi: 10.1371/journal.ppat.1006897

Liu, S., Luo, J., Zhen, X., Qiu, J., Ouyang, S., and Luo, Z. Q. (2020). Interplay between bacterial deubiquitinase and ubiquitin E3 ligase regulates ubiquitin dynamics on Legionella phagosomes. *Elife* 9:e58114. doi: 10.7554/eLife.58114

Liu, X., Wang, Q., Chen, W., and Wang, C. (2013). Dynamic regulation of innate immunity by ubiquitin and ubiquitin-like proteins. *Cytokine Growth Factor Rev.* 24, 559–570. doi: 10.1016/j.cytogfr.2013.07.002

Liu, Y., and Luo, Z. Q. (2007). The *Legionella pneumophila* effector SidJ is required for efficient recruitment of endoplasmic reticulum proteins to the bacterial phagosome. *Infect. Immun.* 75, 592–603. doi: 10.1128/IAI.01278-06

Lomma, M., Dervins-Ravault, D., Rolando, M., Nora, T., Newton, H. J., Sansom, F. M., et al. (2010). The *Legionella pneumophila* F-box protein Lpp2082 (AnkB) modulates ubiquitination of the host protein parvin B and promotes intracellular replication. *Cell Microbiol.* 12, 1272–1291. doi: 10.1111/j.1462-5822.2010.01467.x

Lorand, L., and Graham, R. M. (2003). Transglutaminases: crosslinking enzymes with pleiotropic functions. *Nat. Rev. Mol. Cell Biol.* 4, 140–156. doi: 10.1038/nrm1014

Losick, V. P., and Isberg, R. R. (2006). NF-kappaB translocation prevents host cell death after low-dose challenge by *Legionella pneumophila*. *J. Exp. Med.* 203, 2177–2189. doi: 10.1084/jem.20060766

Luo, X., Wasilko, D. J., Liu, Y., Sun, J., Wu, X., Luo, Z. Q., et al. (2015). Structure of the *Legionella* virulence factor, SidC reveals a unique PI(4)P-specific binding domain essential for its targeting to the bacterial phagosome. *PLoS Pathog.* 11:e1004965. doi: 10.1371/journal.ppat.1004965

Luo, Z. Q., and Isberg, R. R. (2004). Multiple substrates of the *Legionella pneumophila* Dot/Icm system identified by interbacterial protein transfer. *Proc. Natl. Acad. Sci. U.S.A.* 101, 841–846. doi: 10.1073/pnas.0304916101

Ma, K., Zhen, X., Zhou, B., Gan, N., Cao, Y., Fan, C., et al. (2020). The bacterial deubiquitinase Ceg23 regulates the association of Lys-63-linked polyubiquitin molecules on the *Legionella* phagosome. *J. Biol. Chem.* 295, 1646–1657. doi: 10.1074/jbc.RA119.011758

Madern, J. M., Kim, R. Q., Misra, M., Dikic, I., Zhang, Y., Ovaa, H., et al. (2020). Synthesis of stable NAD(+) mimics as inhibitors for the *Legionella pneumophila*

Phosphoribosyl ubiquitylating enzyme SdeC. *Chembiochem* 21, 2903–2907. doi: 10.1002/cbic.202000230

McCloskey, A., Perri, K., Chen, T., Han, A., and Luo, Z. Q. (2021). The metaeffector MesI regulates the activity of the *Legionella* effector SidI through direct protein-protein interactions. *Microbes Infect.* 23:104794. doi: 10.1016/j.micinf.2021.104794

Mikolcevic, P., Hlousek-Kasun, A., Ahel, I., and Mikoc, A. (2021). ADP-ribosylation systems in bacteria and viruses. *Comput. Struct. Biotechnol. J.* 19, 2366–2383. doi: 10.1016/j.csbj.2021.04.023

Miyamoto, K., and Saito, K. (2018). Concise machinery for monitoring ubiquitination activities using novel artificial RING fingers. *Protein Sci.* 27, 1354–1363. doi: 10.1002/pro.3427

Mu, Y., Wang, Y., Huang, Y., Li, D., Han, Y., Chang, M., et al. (2020). Structural insights into the mechanism and inhibition of transglutaminase-induced ubiquitination by the *Legionella* effector MavC. *Nat. Commun.* 11:1774. doi: 10.1038/s41467-020-15645-7

Nagy, V., and Dikic, I. (2010). Ubiquitin ligase complexes: from substrate selectivity to conjugational specificity. *Biol. Chem.* 391, 163–169. doi: 10.1515/bc.2010.021

Newton, H. J., Ang, D. K., Van Driel, I. R., and Hartland, E. L. (2010). Molecular pathogenesis of infections caused by *Legionella pneumophila*. *Clin. Microbiol. Rev.* 23, 274–298. doi: 10.1128/cmr.00052-09

Nguyen, K. M., and Busino, L. (2020). The biology of F-box proteins: the SCF Family of E3 ubiquitin Ligases. *Adv. Exp. Med. Biol.* 1217, 111–122. doi: 10.1007/978-981-15-1025-0_8

O'Connor, H. F., Lyon, N., Leung, J. W., Agarwal, P., Swaim, C. D., Miller, K. M., et al. (2015). Ubiquitin-activated interaction traps (UBAITs) identify E3 ligase binding partners. *EMBO Rep.* 16, 1699–1712. doi: 10.15252/embr.201540620

Olsen, S. K., and Lima, C. D. (2013). Structure of a ubiquitin E1-E2 complex: insights to E1-E2 thioester transfer. *Mol. Cell* 49, 884–896. doi: 10.1016/j.molcel.2013.01.013

Ong, S. Y., Schuelein, R., Wibawa, R. R., Thomas, D. W., Handoko, Y., Freytag, S., et al. (2021). Genome-wide genetic screen identifies host ubiquitination as important for *Legionella pneumophila* Dot/Icm effector translocation. *Cell Microbiol.* 23:e13368. doi: 10.1111/cmi.13368

Osinski, A., Black, M. H., Pawłowski, K., Chen, Z., Li, Y., and Tagliabracci, V. S. (2021). Structural and mechanistic basis for protein glutamylation by the kinase fold. *Mol. Cell* 81, 4527–4539.e8. doi: 10.1016/j.molcel.2021.08.007

Otten, E. G., Werner, E., Crespillo-Casado, A., Boyle, K. B., Dharamdasani, V., Pathe, C., et al. (2021). Ubiquitylation of lipopolysaccharide by RNF213 during bacterial infection. *Nature* 594, 111–116. doi: 10.1038/s41586-021-03566-4

Pike, C. M., Boyer-Andersen, R., Kinch, L. N., Caplan, J. L., and Neunuebel, M. R. (2019). The Legionella effector RavD binds phosphatidylinositol-3-phosphate and helps suppress endolysosomal maturation of the *Legionella*-containing vacuole. *J. Biol. Chem.* 294, 6405–6415. doi: 10.1074/jbc.RA118.007086

Price, C. T., Al-Khodor, S., Al-Quadan, T., Santic, M., Habyarimana, F., Kalia, A., et al. (2009). Molecular mimicry by an F-box effector of *Legionella pneumophila* hijacks a conserved polyubiquitination machinery within macrophages and protozoa. *PLoS Pathog.* 5:e1000704. doi: 10.1371/journal.ppat.1000704

Puvar, K., Iyer, S., Fu, J., Kenny, S., Negron Teron, K. I., Luo, Z. Q., et al. (2020). *Legionella* effector MavC targets the Ube2N˜Ub conjugate for noncanonical ubiquitination. *Nat. Commun.* 11:2365. doi: 10.1038/s41467-020-16211-x

Qiu, J., and Luo, Z. Q. (2017b). *Legionella* and Coxiella effectors: strength in diversity and activity. *Nat. Rev. Microbiol.* 15, 591–605. doi: 10.1038/nrmicro.2017.67

Qiu, J., and Luo, Z. Q. (2017a). Hijacking of the host ubiquitin network by *Legionella pneumophila*. *Front. Cell Infect. Microbiol.* 7:487. doi: 10.3389/fcimb.2017.00487

Qiu, J., Sheedlo, M. J., Yu, K., Tan, Y., Nakayasu, E. S., Das, C., et al. (2016). Ubiquitination independent of E1 and E2 enzymes by bacterial effectors. *Nature* 533, 120–124. doi: 10.1038/nature17657

Qiu, J., Yu, K., Fei, X., Liu, Y., Nakayasu, E. S., Piehowski, P. D., et al. (2017). A unique deubiquitinase that deconjugates phosphoribosyl-linked protein ubiquitination. *Cell Res.* 27, 865–881. doi: 10.1038/cr.2017.66

Quaile, A. T., Urbanus, M. L., Stogios, P. J., Nocek, B., Skarina, T., Ensminger, A. W., et al. (2015). Molecular characterization of LubX: functional divergence of the U-box fold by *Legionella pneumophila*. *Structure* 23, 1459–1469. doi: 10.1016/j.str.2015.05.020

Ragaz, C., Pietsch, H., Urwyler, S., Tiaden, A., Weber, S. S., and Hilbi, H. (2008). The *Legionella pneumophila* phosphatidylinositol-4 phosphate-binding type IV substrate SidC recruits endoplasmic reticulum vesicles to a replication-permissive vacuole. *Cell Microbiol.* 10, 2416–2433. doi: 10.1111/j.1462-5822.2008.01219.x

Rittinger, K., and Ikeda, F. (2017). Linear ubiquitin chains: enzymes, mechanisms and biology. *Open Biol.* 7:170026. doi: 10.1098/rsob.170026

Ronau, J. A., Beckmann, J. F., and Hochstrasser, M. (2016). Substrate specificity of the ubiquitin and Ubl proteases. *Cell Res.* 26, 441–456. doi: 10.1038/cr.2016.38

Sasaki, T., Gan, E. C., Wakeham, A., Kornbluth, S., Mak, T. W., and Okada, H. (2007). HLA-B-associated transcript 3 (Bat3)/Scythe is essential for p300-mediated acetylation of p53. *Genes Dev.* 21, 848–861. doi: 10.1101/gad.1534107

Schubert, A. F., Nguyen, J. V., Franklin, T. G., Geurink, P. P., Roberts, C. G., Sanderson, D. J., et al. (2020). Identification and characterization of diverse OTU deubiquitinases in bacteria. *EMBO J.* 39:e105127. doi: 10.15252/embj.2020105127

Shaid, S., Brandts, C. H., Serve, H., and Dikic, I. (2013). Ubiquitination and selective autophagy. *Cell Death Differ.* 20, 21–30. doi: 10.1038/cdd.2012.72

Sheedlo, M. J., Qiu, J., Tan, Y., Paul, L. N., Luo, Z. Q., and Das, C. (2015). Structural basis of substrate recognition by a bacterial deubiquitinase important for dynamics of phagosome ubiquitination. *Proc. Natl. Acad. Sci. U.S.A.* 112, 15090–15095. doi: 10.1073/pnas.1514568112

Shin, D., Bhattacharya, A., Cheng, Y. L., Alonso, M. C., Mehdipour, A. R., Van Der Heden Van Noort, G. J., et al. (2020a). Bacterial OTU deubiquitinases regulate substrate ubiquitination upon *Legionella* infection. *Elife* 9:e58277. doi: 10.7554/eLife.58277

Shin, D., Mukherjee, R., Liu, Y., Gonzalez, A., Bonn, F., Liu, Y., et al. (2020b). Regulation of phosphoribosyl-linked serine ubiquitination by deubiquitinases DupA and DupB. *Mol. Cell* 77, 164–179.e6. doi: 10.1016/j.molcel.2019.10.019

Skaar, J. R., Pagan, J. K., and Pagano, M. (2013). Mechanisms and function of substrate recruitment by F-box proteins. *Nat. Rev. Mol. Cell Biol.* 14, 369–381. doi: 10.1038/nrm3582

Song, L., and Luo, Z. Q. (2019). Post-translational regulation of ubiquitin signaling. *J. Cell Biol.* 218, 1776–1786. doi: 10.1083/jcb.201902074

Song, L., Xie, Y., Li, C., Wang, L., He, C., Zhang, Y., et al. (2021). The *Legionella* effector SdjA Is a bifunctional enzyme that distinctly regulates Phosphoribosyl ubiquitination. *mBio* 12:e0231621. doi: 10.1128/mBio.02316-21

Sowa, M. E., Bennett, E. J., Gygi, S. P., and Harper, J. W. (2009). Defining the human deubiquitinating enzyme interaction landscape. *Cell* 138, 389–403. doi: 10.1016/j.cell.2009.04.042

Spit, M., Rieser, E., and Walczak, H. (2019). Linear ubiquitination at a glance. *J. Cell Sci.* 132:jcs208512. doi: 10.1242/jcs.208512

Sreelatha, A., Yee, S. S., Lopez, V. A., Park, B. C., Kinch, L. N., Pilch, S., et al. (2018). Protein AMPylation by an evolutionarily conserved Pseudokinase. *Cell* 175, 809-821.e19. doi: 10.1016/j.cell.2018.08.046

Stewart, M. D., Ritterhoff, T., Klevit, R. E., and Brzovic, P. S. (2016). E2 enzymes: more than just middle men. *Cell Res.* 26, 423–440. doi: 10.1038/cr.2016.35

Sulpizio, A., Minelli, M. E., Wan, M., Burrowes, P. D., Wu, X., Sanford, E. J., et al. (2019). Protein polyglutamylation catalyzed by the bacterial calmodulin-dependent pseudokinase SidJ. *Elife* 8:e51162. doi: 10.7554/eLife.51162

Swanson, M. S., and Isberg, R. R. (1995). Association of *Legionella pneumophila* with the macrophage endoplasmic reticulum. *Infect. Immun.* 63, 3609–3620. doi: 10.1128/iai.63.9.3609-3620.1995

Takekawa, N., Kubori, T., Iwai, T., Nagai, H., and Imada, K. (2021). Structural basis of ubiquitin recognition by a bacterial OTU deubiquitinase LotA. *J. Bacteriol.* JB0037621.

Urbanus, M. L., Quaile, A. T., Stogios, P. J., Morar, M., Rao, C., Di Leo, R., et al. (2016). Diverse mechanisms of metaeffector activity in an intracellular bacterial pathogen, *Legionella pneumophila*. *Mol. Syst. Biol.* 12:893. doi: 10.15252/msb.20167381

Valleau, D., Quaile, A. T., Cui, H., Xu, X., Evdokimova, E., Chang, C., et al. (2018). Discovery of Ubiquitin deamidases in the pathogenic arsenal of *Legionella pneumophila*. *Cell Rep.* 23, 568–583. doi: 10.1016/j.celrep.2018.03.060

Vozandychova, V., Stojkova, P., Hercik, K., Rehulka, P., and Stulik, J. (2021). The Ubiquitination system within bacterial host-pathogen interactions. *Microorganisms* 9:638. doi: 10.3390/microorganisms9030638

Wan, M., Wang, X., Huang, C., Xu, D., Wang, Z., Zhou, Y., et al. (2019b). A bacterial effector deubiquitinase specifically hydrolyses linear ubiquitin chains

to inhibit host inflammatory signalling. *Nat. Microbiol.* 4, 1282–1293. doi: 10.1038/s41564-019-0454-1

Wan, M., Sulpizio, A. G., Akturk, A., Beck, W. H. J., Lanz, M., Faca, V. M., et al. (2019a). Deubiquitination of phosphoribosyl-ubiquitin conjugates by phosphodiesterase-domain-containing *Legionella* effectors. *Proc. Natl. Acad. Sci. U.S.A.* 116, 23518–23526. doi: 10.1073/pnas.1916287116

Weber, S. S., Ragaz, C., Reus, K., Nyfeler, Y., and Hilbi, H. (2006). *Legionella pneumophila* exploits PI(4)P to anchor secreted effector proteins to the replicative vacuole. *PLoS Pathog.* 2:e46. doi: 10.1371/journal.ppat.0020046

Zhao, B., Bhuripanyo, K., Zhang, K., Kiyokawa, H., Schindelin, H., and Yin, J. (2012). Orthogonal ubiquitin transfer through engineered E1-E2 cascades for protein ubiquitination. *Chem. Biol.* 19, 1265–1277. doi: 10.1016/j.chembiol.2012.07.023

Zhou, Y., and Zhu, Y. (2015). Diversity of bacterial manipulation of the host ubiquitin pathways. *Cell Microbiol.* 17, 26–34. doi: 10.1111/cmi.12384

Conflict of Interest: The authors declare that the research was conducted in the absence of any commercial or financial relationships that could be construed as a potential conflict of interest.

Publisher's Note: All claims expressed in this article are solely those of the authors and do not necessarily represent those of their affiliated organizations, or those of the publisher, the editors and the reviewers. Any product that may be evaluated in this article, or claim that may be made by its manufacturer, is not guaranteed or endorsed by the publisher.

Copyright © 2021 Luo, Wang, Song and Luo. This is an open-access article distributed under the terms of the Creative Commons Attribution License (CC BY). The use, distribution or reproduction in other forums is permitted, provided the original author(s) and the copyright owner(s) are credited and that the original publication in this journal is cited, in accordance with accepted academic practice. No use, distribution or reproduction is permitted which does not comply with these terms.

frontiers in Immunology

REVIEW
published: 24 December 2021
doi: 10.3389/fimmu.2021.800796

Gut Microbiota and Acute Central Nervous System Injury: A New Target for Therapeutic Intervention

Bin Yuan[1], *Xiao-jie Lu*[1,2*] *and Qi Wu*[3*]

[1] Department of Neurosurgery, The Affiliated Wuxi No. 2 Hospital of Nanjing Medical University, Wuxi, China, [2] Department of Neurosurgery, The Affiliated Hospital of Jiangnan University, Wuxi, China, [3] Department of Neurosurgery, Jinling Hospital, Nanjing University, School of Medicine, Nanjing, China

Acute central nervous system (CNS) injuries, including stroke, traumatic brain injury (TBI), and spinal cord injury (SCI), are the common causes of death or lifelong disabilities. Research into the role of the gut microbiota in modulating CNS function has been rapidly increasing in the past few decades, particularly in animal models. Growing preclinical and clinical evidence suggests that gut microbiota is involved in the modulation of multiple cellular and molecular mechanisms fundamental to the progression of acute CNS injury-induced pathophysiological processes. The altered composition of gut microbiota after acute CNS injury damages the equilibrium of the bidirectional gut-brain axis, aggravating secondary brain injury, cognitive impairments, and motor dysfunctions, which leads to poor prognosis by triggering pro-inflammatory responses in both peripheral circulation and CNS. This review summarizes the studies concerning gut microbiota and acute CNS injuries. Experimental models identify a bidirectional communication between the gut and CNS in post-injury gut dysbiosis, intestinal lymphatic tissue-mediated neuroinflammation, and bacterial-metabolite-associated neurotransmission. Additionally, fecal microbiota transplantation, probiotics, and prebiotics manipulating the gut microbiota can be used as effective therapeutic agents to alleviate secondary brain injury and facilitate functional outcomes. The role of gut microbiota in acute CNS injury would be an exciting frontier in clinical and experimental medicine.

Keywords: gut microbiota, stroke, traumatic brain injury, spinal cord injury, gut-brain axis

OPEN ACCESS

Edited by:
Alina Maria Holban,
University of Bucharest, Romania

Reviewed by:
Stuart Friess,
Washington University in St. Louis, United States
Pia M. Vidal,
Catholic University of the Most Holy Conception, Chile

***Correspondence:**
Xiao-jie Lu
xiaojieluwuxi@163.com
Qi Wu
nswuqi@163.com

Specialty section:
This article was submitted to Microbial Immunology, a section of the journal Frontiers in Immunology

Received: *24 October 2021*
Accepted: *09 December 2021*
Published: *24 December 2021*

Citation:
Yuan B, Lu X-j and Wu Q (2021) Gut Microbiota and Acute Central Nervous System Injury: A New Target for Therapeutic Intervention. Front. Immunol. 12:800796. doi: 10.3389/fimmu.2021.800796

INTRODUCTION

Acute injuries to the central nervous system (CNS), such as stroke, traumatic brain injury (TBI), spinal cord injury (SCI), are critical global health problems that result in lifelong disabilities or death, leading to catastrophic changes to the injured individuals, alongside their family and even the entire community (1, 2). The processes secondary to acute CNS injuries involve a sequence of complex pathophysiological mechanisms, including excitotoxicity, electrolyte imbalance, oxidative stress, inflammation, apoptosis, pyroptosis, ferroptosis, autophagy, and cerebral edema (3). These cellular and molecular damages exacerbate neuronal cell death. Although some preclinical researchers have made many efforts to develop efficacious treatment strategies, patients with

severe acute CNS injuries still have a poor prognosis. Given the prevalence of acute CNS injury-induced disabilities or death, exploring a novel and effective therapeutic regimen is imperative. In addition, a growing body of studies has shown that gut microbiota plays a pivotal role in health and disease in the host, particularly in the CNS (4–7).

Gut microbiota refers to the assemblage of bacteria, archaea, viruses, and eukaryotic microbes that colonize in the digestive tract (8). The gut microbiota contains trillions of microorganisms, over 1000 different species of known bacteria, and approximately 100 ~ 150-fold more genes than the human genome (9). At the phylum level, the gut microbiota primarily consists of Firmicutes, Bacteroidetes, Actinobacteria, Proteobacteria, and Verrucomicrobia (10). Thereinto, Firmicutes, and Bacteroidetes comprise about 90% of all the bacteria (11). Additionally, the composition of gut microbiota among individuals was influenced by diet, age, gender, environment, and genes (12). Although the microbiome is spatially restricted to the gut, it has been shown to regulate the functions of distant organs (13). Notably, advances in the sequencing of gut microbiota have revealed the close correlation between the complex ecosystem and CNS (14). Previous studies focused on exploring the bidirectional communication pathways between gut microbiota and CNS, termed the "microbiota-gut-brain" axis (MGBA) (15). The bidirectional communication pathways between the CNS and gut microbiota involve immunological, endocrine, metabolic, and neural pathways (16, 17). Recent findings have implicated that MGBA partakes in the pathogenesis of many neurological disorders such as neurodegenerative diseases(e.g., Alzheimer's disease and Parkinson's disease), neurodevelopmental and neuropsychiatric diseases (e.g., anxiety, depression, autism, and schizophrenia), autoimmune disease (e.g., multiple sclerosis), and acute CNS injuries (e.g., stroke, TBI and SCI) (7, 15, 18–20). In this review, we provide an update on the link between gut microbiota and acute CNS injuries.

MICROBIOTA-GUT-BRAIN AXIS

Top-Down Signaling: Brain-to-Gut

In top-down signaling, the pathways involve the autonomic nervous system, enteric nervous system, the hypothalamic-pituitary-adrenal (HPA) axis, and immunological pathway (**Figure 1**). The autonomic nervous system regulates intestinal homeostasis, and the neurotransmitters, released by the activated sympathetic and parasympathetic nerve fibers, modulate gut motility, gut barrier permeability, fluid maintenance, bile secretion, resident immune cell activation, and gut microbiota makeup (21). The enteric nervous system is also responsible for gut functions, such as gut motility and fluid maintenance, a neuronal connection between the microbiota and the host. Moreover, the HPA axis is one of the vital nonneuronal transmission pathways within the MGBA, releasing cortisol to influence gut homeostasis in response to various stimuli. With the discovery of meningeal lymphatic vessels, the brain is no longer an immune-privileged site. Functional meningeal lymphatic vessels lined mainly in the dorsal part of the skull are responsible for the clearance of cerebrospinal fluid and drainage of immune cells and the periphery, communicating with the host organs (22).

Bottom-Up Signaling: Gut-to-Brain

Two different mechanisms involved in the bottom-up signaling are neuronal and nonneuronal pathways (**Figure 1**). The vagus nerve, composed of both afferent and efferent fibers (80% vs. 20%), plays a pivotal role in bidirectionally transmitting vital information between the gut and brain. The afferent fibers stimulated by microbial metabolites and enteroendocrine neuropeptides convey hypothalamic neurons that promote pituitary secretions. In addition, the interaction between the gut and brain primarily relies on the nonneuronal pathway. Singh et al. reported that the gut microbiota-mediated neuroprotection was absent in lymphocyte-deficient mice after an experimental stroke of permanent distal middle cerebral artery occlusion (MCAO), indicating that the gut communicate with the brain by immunological pathway (23). In a transient MCAO model, intestinal $CD45^+$ and $CD11c^+$ cells significantly migrated from the gut to the brain and meninges at 3 days post-stroke (24). A study of a thoracic level 9 contusion SCI also showed that commercial probiotics (VSL#3) feeding triggered a protective immune response in gut-associated lymphatic tissues (GALTs) and conferred neuroprotection with the improvement of locomotor recovery after SCI (25). TBI-induced leaky gut released lipopolysaccharide (LPS), a toxic bacterial component, into the circulation that exacerbated neuroinflammation by activating microglia (26).

The MGBA is critical to the development of the human central nervous system. A prospective longitudinal study conducted by Carlson et al. investigated the correlation between gut microbial composition and cognitive ability in 89 infants. It revealed that 2-year-old cognitive function assessed with the Early Learning Composite of Mullen Scale was significantly correlated with the gut microbiota composition at one year (27). Infants with a relatively high abundance of Bacteroides showed higher performance, while those with a relatively high quantity of Faecalibacterium had a lower performance. In another clinical study of 39 infants, the α-diversity of gut microbiota was associated with functional connectivity between the amygdala and thalamus, between the anterior cingulate cortex and anterior insula, and between the supplementary motor area and the inferior parietal lobule (28). Additionally, the functional connectivity was also related to 2-year-old cognitive outcomes. These studies have demonstrated that the gut microbiota significantly affects neurodevelopment in the early stage through the MGBA.

Microbial components and metabolites such as lipopolysaccharide (LPS), long-chain fatty acids (LCFAs), short-chain fatty acids (SCFAs), trimethylamine-N-oxide (TAMO), tryptophan, and polysaccharide A (PSA) are considered to induce neuroinflammation and modulate the function of CNS either directly or by activating migration of peripheral immune cells to the brain. Although this regulation of

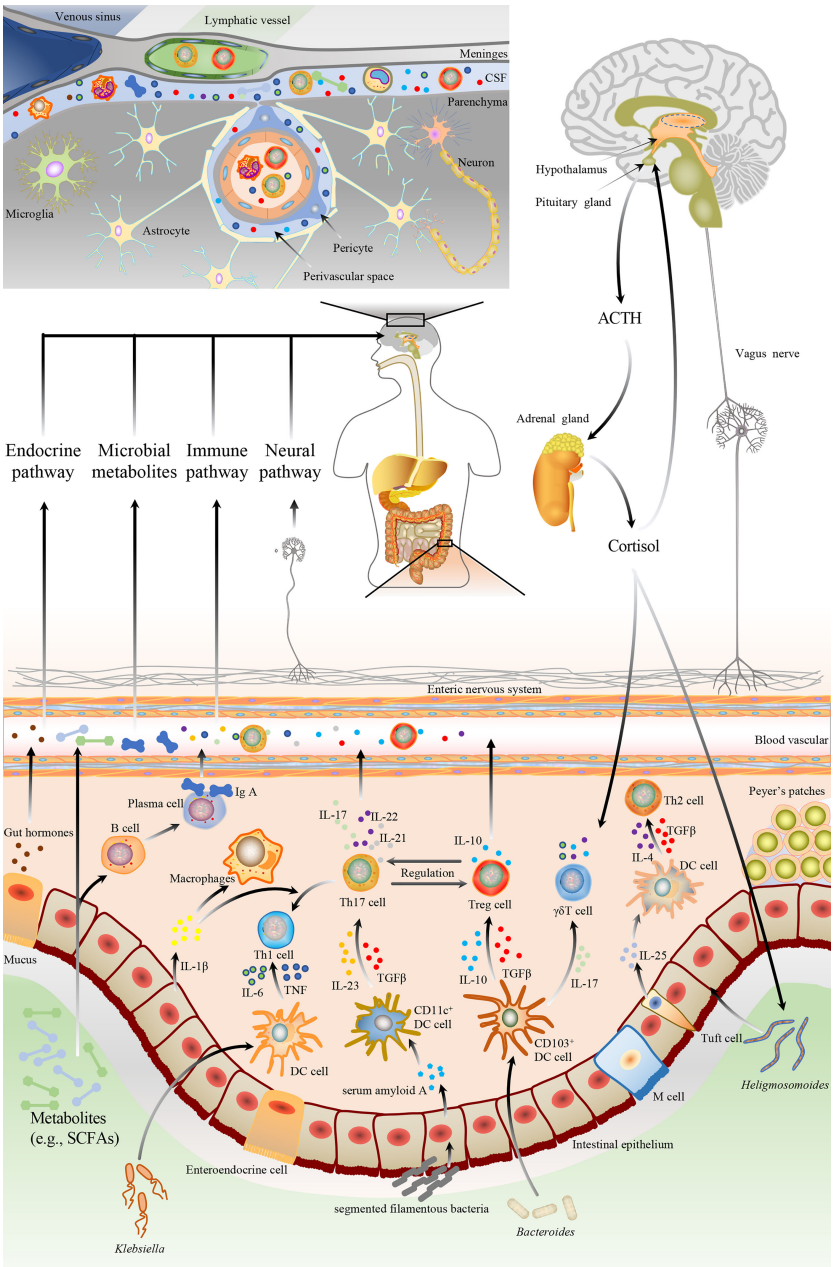


FIGURE 1 | The bidirectional communication pathways between the gut microbiota and brain. The gut microbiota could bi-directionally communicate with the brain through multiple pathways, including neuronal and non-neuronal. The brain regulates the gut microbiota *via* neuronal pathways (e.g., autonomic nervous system and enteric nervous system), hypothalamic-pituitary-adrenal axis, etc. Neuronal pathways release neurotransmitters to modulate gut motility, gut barrier permeability, fluid maintenance, resident immune cell activation, and gut microbiota composition. HPA also releases cortisol to regulate gut homeostasis. Additionally, gut microbiota affects the development and pathophysiology of the brain by immunological, endocrine, metabolic, and neural pathways. Microbiomes and their metabolites could modulate the brain and behavior by affecting intestinal epithelial cells to alter gut barrier function, enteroendocrine cells to secret hormones, as well as dendritic cells and macrophage, to regulate immune and microglia activation. Gut microbiota can modulate the $CD4^+$ T cells differentiation through epithelial cells or DC cells-mediated signals. ① Ectopic colonizing microbes, such as Klebsiella, can invade intestinal epithelium and stimulate DC cells to secrete proinflammatory cytokines, including IL-6 and TNF, which drive the polarization of Th1cells. ② SFB promotes Th17 polarization *via* epithelial cell-mediated $CD11c^+$ DC cells activation. Epithelial cells release serum amyloid A to activate $CD11c^+$ DC cells, leading to the TGF-β, IL-12, and IL-23 secretion. ③ Resident microbes, such as Bacteroides, modulate Treg cells generation by TGF-β and IL-10, which are secreted by $CD103^+$ DC cells. $CD103^+$ DC cells also can release IL-17 to promote γδT cell polarization. ④ Microbiota-associated Th2 cell polarization is correlated with parasite colonization such as Heligmosomoides, mediated by tuft cells secreting IL-25 to DC cells. Then activated DC cells release IL-4 and TGF-β to drive Th2 polarization. DC, dendritic cell; IL, interleukin; TNF, tumor necrosis factor; Th, T helper; TGF-β, transforming growth factor-β; SFB, segmented filamentous bacteria; SCFA, short-chain fatty acid; Treg, regulatory T cell.

immune cells by the microbiota occurs in the gut, peripheral immune cells could also migrate to the brain meninges and modulate the brain function (29).

GUT MICROBIOTA AND IMMUNOMODULATION

Gut Microbiota

Previous studies have shown that the gut microbiota-host interaction contributes to the maturation and modulation of the host immune system. Through constant contact with the gut microbiota, immune cells and epithelial cells located in the gut have achieved a homeostatic state and promote tolerogenic responses to the host commensal microbes. Under physiological conditions, all types of immune cells such as T lymphocytes, B lymphocytes, macrophages, dendritic cells (DCs), etc., counterbalance each other to preserve the host homeostasis. T helper (Th) cells and regulatory T (Treg) cells are a requisite component of the host immune system, especially in the gut-associated immune responses. Compared with germ-free (GF) mice, conventional specific-pathogen-free (SPF) mice had a more significant proportion of $CD4^+$ T cells (30). Th1 cells were polarized by DCs-secreted pro-inflammatory cytokines such as interleukin(IL)-6 and IL-12 stimulated by Klebsiella (31). Parasites, such as Heligmosomoides, could activate Th2 cells through DCs-derived transforming growth factor-β(TGF-β) and IL-4 (32). Besides, segmented filamentous bacteria drive Th17 polarization *via* activation of $CD11c^+$ DCs (33). The activated Th17 cells secrete high-affinity IL-17 and promote IgA transportation, memory $CD4^+$ T cell differentiation, and mucin production (33). Bacteroides fragilis stimulate regulatory $CD4^+$ T cells to make themselves colonize the intestinal epithelium and induce immunosuppression, mediated by $CD103^+$ DCs (34). γδ T cells, another innate immune cell population in the gut epithelium, are vital for gut homeostasis regulation and pathological reaction. $CD103^+$ DCs activated by gut microbiota also communicate with IL-17^+ γδ T cells *via* cell-to-cell contact or different cytokines (35). γδ T cells protect the host from intestinal barrier damage and pathogenic bacterial invasion and exert pro-inflammatory or anti-inflammatory effects depending on the milieu (36). Additionally, the development of intestinal mucosa B cells is regulated by commensal microbes, which promote antibody production and control the expression of a differentiation-related gene through enhancement of fatty acid synthesis, glycolysis, and oxidative phosphorylation (37). Commensal microbiota-induced secretion of IL-1β by mucosal macrophages is closely correlated with the development of steady-state Th17 cells (38)(**Figure 1**).

Microbial Components and Metabolites

Gut microbiota-derived small molecules are inextricably linked with the crosstalk between gut microbiota and host. Moreover, there is now a considerable body of experimental evidence that some metabolites of the intestinal microbiota can participate in the modulation of inflammatory cytokine production and immune cell differentiation. SCFAs produced by gut microbiota such as Faecalibacterium prausnitzii, Roseburia intestinalis, and Anaerostipes butyraticus regulate the activation and differentiation of immune cells (e.g., neutrophils, macrophages, DCs, and T cells), mediated by inhibiting histone deacetylases (HDACs) as well as activating G-protein-coupled receptors (GPCRs) (e.g., GPR41, GPR43, and GPR109A) and olfactory receptor-78 (Olfr-78) (39–41). TMAO is another gut microbiota metabolite oxidized from trimethylamine (TMA) generated by hepatic flavin-containing monooxygenases (FMOs) from dietary nutrients such as choline and L-carnitine. TAMO regulates pro-inflammatory responses *via* activating the NOD-like receptor family, pyrin domain-containing protein 3 (NLRP3) inflammasome, mitogen-activated protein kinase (MAPK), and nuclear factor-κB (NF-κB) signaling pathway (42). Additionally, tryptophan has also been demonstrated to be involved in the functional modulation of intestinal intraepithelial lymphocytes and innate lymphocytes *via* activating the aryl hydrocarbon receptor (AHR) (43). PSA, produced by Bacteroides fragilis, activates toll-like receptor 2 (TLR2) expressed on DCs and Treg cells, triggering anti-inflammatory cytokine IL-10 (43). PSA also regulates the differentiation of naive $CD4^+$ T cells into Th1 cells, skewing Th1/Th2 ratio towards Th1 cells (44). Interestingly, a study found that CD39 expression is required for Treg cells to migrate to the CNS, depending on PSA-driven effects on the Treg cells (45).

GUT MICROBIOTA AND ACUTE CNS INJURIES

Stroke

Stroke is the second leading cause of death worldwide. Morbidity and mortality of stroke grow in many countries, contributing to financial burden and loss of life quality, and thus diminishing national happiness index. Approximately 15 million people around the world are victims of a stroke every year (46). There are two types of strokes: ischemic stroke and hemorrhagic stroke. Recent evidence shows that shifts in the gut microbial composition occur rapidly after stroke in clinical and experimental studies. Therefore, alteration of the gut microbiota directly regulates the reactions secondary to brain injury through central and peripheral immunity and indirectly determines the brain's sequel to these types of catastrophic events.

Ischemic Stroke

Reportedly, ischemic stroke accounts for ~80% of all strokes (47), and the gut microbiota plays an essential role in the pathogenesis and prognosis of ischemic stroke. Multiple studies have shown that ischemic stroke significantly changes the gut microbiota composition (21, 23, 48–66). These studies have been summarized in **Table 1**. Although dysbiosis of the gut microbiota has been proved in previous studies, controversy still exists on the specific microbiota difference. Compelling evidence has been identified that confounding factors such as

TABLE 1 | A summary of preclinical and human studies on the gut microbiota and ischemic stroke.

	Subjects	Methods	Key findings
Yin J, et al. (2015) (48)	322 patients vs. 231 controls	16S rRNA (V4) sequencing & LC-MS	• Patients with stroke and transient ischemic attack presented the gut microbiota dysbiosis, which increased Enterobacter, Megasphaera, Oscillibacter, and Desulfovibrio and decreased Bacteroides, Prevotella, and Faecalibacterium. • Patients with stroke and the transient ischemic attack had lower trimethylamine N-oxide (TMAO) compared with asymptomatic patients.
Stanley D, et al. (2016) (52)	36 patients vs. 9 hospital-based controls vs. 10 healthy controls; middle cerebral artery occlusion (MCAO) mice	16S rRNA sequencing	• Common commensal bacteria resided in the intestinal tracts contributed to the post-stroke infections in patients with ischemic stroke. This was also observed in a mouse model of ischemic stroke. • In the experimental stroke, post-stroke infection was only seen in specific pathogen-free (SPF) mice, not germ-free (GF) mice.
Nie J, et al. (2018) (51)	622 patients vs. 622 controls	LC-MS	• The increment of serum TMAO level increased the risk of the first stroke. • Patients with higher TMAO levels (≥1.79 μmol/L) had a significantly higher risk of the first stroke.
Zeng X, et al. (2019) (50)	141 patients	16S rRNA sequencing & GS-MS	• Compared with the low-risk group, opportunistic pathogens (e.g., Enterobacteriaceae and Veillonellaceae) and lactate-producing bacteria (e.g., Bifidobacterium and Lactobacillus) were increased, as well as butyrate-producing bacteria (e.g., Lachnospiraceae and Ruminococcaceae) were decreased in the high-risk group. • The fecal butyrate concentrations in the high-risk group were lower than those in the low-risk group. Moreover, the concentrations of other short-chain fatty acids (SCFAs) (e.g., acetate, propionate, isobutyrate, isovalerate, and valerate) in the feces were significantly different between the three groups.
Haak BW, et al. (2020) (49)	349 patients vs. 51 controls	16S rRNA (V3-V4) sequencing & LC-MS	• The TMAO level in stroke patients was two-fold lower than that of the healthy controls. • Lower abundance of butyrate-producing bacteria within 24h of hospital admission was an independent predictor of enhanced risk of post-stroke infection, but not of mortality or functional patient outcome.
Xu DJ, et al. (2021) (60)	61 large artery atherosclerotic (LAA) stroke vs. 20 cardioembolic (CE) stroke vs. 51 asymptomatic controls	16S rRNA (V4-V5) sequencing & LC-MS	• The TMAO levels in the plasma of patients with LAA and CE strokes were significantly higher than those in controls. Moreover, the plasma TMAO level in the LAA stroke patients was positively associated with the carotid plaque area. • The composition and the function of gut microbiota in the patients with LAA stroke were significantly different from those in the asymptomatic controls. In contrast, no significant difference between CE stroke patients and the asymptomatic controls was observed in the present study.
Ling Y, et al. (2020) (61)	53 patients with post-stroke cognitive impairment (PSCI) vs. 40 patients with post-stroke non-cognitive impairment (PSNCI)	16S rRNA (V3-V4) sequencing	• Compared with the patient with PSNCI, the abundance of Proteobacteria was highly increased in the patients with PSCI. • The abundances of Clostridia, Clostridiales, Lachnospiraceae, and Lachnospiraceae_other were significantly decreased in the patients with PSCI after adjusting to age. • The Kyoto Encyclopedia of Genes and Genomes analysis showed the progressive enriched module for folding, sorting, and degradation (chaperones and folding catalysts) and the significantly decreased modules related to metabolisms of cofactors and vitamins, amino acid, and lipid in patients with PSCI.
Xiang L, et al. (2020) (62)	20 patients vs. 16 controls	16S rRNA (V3) sequencing	• Stroke patients had fewer Firmicutes than controls. • Two optimal bacterial species, Lachnospiraceae (OTU_45) and Bacteroides served as markers of lacunar infarction. • Two optimal bacterial species, Bilophila and Lachnospiraceae (OTU_338)), served as markers of non-lacunar acute ischemic infarction. • Three optimal bacterial species, Pseudomonas, Sphingomonadaceae, and Akkermansia, served as markers of post-ischemic stroke patients with 15 days of treatment.
Tan C, et al. (2021) (67)	140 patients vs. 92 controls	16S rRNA (V4) sequencing & GS-MS	• Patients with acute ischemic stroke are characterized by a lack of SCFAs-producing bacteria (Roseburia, Bacteroides, Lachnospiraceae, Faecalibacterium, Blautia, and Anaerostipes) and an overload of Lactobacillaceae, Akkermansia, Enterobacteriaceae, and Porphyromonadaceae in their feces. • The SCFAs levels were negatively related to stroke severity and prognosis. • Reduced fecal SCFAs level, especially acetate, was correlated with an increased risk of 3-month unfavorable outcomes.
Zhang J, et al. (2021) (68)	351 patients vs. 150 controls	LC-MS	• Patients with an unfavorable outcome had significantly increased plasma TMAO levels on admission. • Plasma TMAO levels on admission were an independent predictor of functional outcome and mortality after acute ischemic stroke.
Guo Q, et al.	49 patients vs. 30 controls	16S rRNA (V3-V4) sequencing	• The acute ischemic stroke patients treated with Tanhuo Decoction had a better outcome than the controls on both clinical outcome and gut microbiota characteristics.

(Continued)

TABLE 1 | Continued

	Subjects	Methods	Key findings
(2021) (69)			• Tanhuo Decoction treatment significantly decreased the lipopolysaccharide (LPS)-producing bacteria (Bacteroidaceae and Bacteroides) to reduce LPS biosynthesis. • The acute ischemic stroke patients treated with Tanhuo Decoction also exhibited the potential to decrease the biosynthesis of trimethylamine (TMA), the precursor of TMAO, and increase TMA's degradation.
Huang Y, et al. (2021) (63)	76 patients vs. 19 controls	16S rRNA (V3-V4) sequencing	• Stroke patients had a significantly higher abundance of Enterococcus and lower abundances of Bacteroides, Escherichia-Shigella, and Megamonas. • Compared with stroke patients, patients with post-stroke cognitive impairment had a significantly higher proportion of Enterococcus, Bacteroides, and Escherichia-Shigella and a lower content of Faecalibacterium. • Patients with the post-stroke affective disorder had a significantly higher proportion of Bacteroides and Escherichia-Shigella and a lower proportion of Enterococcus and Faecalibacterium.
Sun T, et al. (2021) (70)	953 patients vs. 953 controls	LC-MS/MS	• Plasma TMAO levels in patients with ischemic stroke were significantly increased. • Higher plasma TMAO levels were correlated with increased odds of ischemic stroke. • The adjusted odds ratios for ischemic stroke per 1 μmol/L increase of plasma TMAO was 1.05.
Xu K, et al. (2021) (64)	Cohort 1: 28 patients vs. 28 controls; Cohort 2: 124 patients; MCAO mice	16S rRNA sequencing	• Enriched Enterobacteriaceae was an independent risk factor for acute ischaemic stroke patients in early-stage recovery. • MCAO mice showed rapid gut dysbiosis with Enterobacteriaceae blooming, associated with intestinal ischemia and nitrate production. • Enterobacteriaceae exacerbates brain infarction by accelerating LPS/toll-like receptor 4(TLR4)-mediated systemic inflammation. • Inhibiting Enterobacteriaceae overgrowth by diminishing nitrate generation or inhibiting nitrate respiration alleviates brain infarction.
Houlden A, et al. (2016) (21)	MCAO mice	16S rRNA PCR	• The alteration of the caecal microbiota composition following stroke could be mediated by noradrenaline release from the autonomic nervous system, changing caecal mucoprotein production and goblet cell numbers. • Specific changes in Peptococcaceae and Prevotellaceae after stroke were correlated with the severity of the injury.
Singh V, et al. (2016) (54)	MCAO mice	16S rRNA (V1-V3) sequencing	• Reduced species diversity and bacterial overgrowth of bacteroidetes were associated with intestinal barrier dysfunction and reduced intestinal motility. • GF mice recolonized with poststroke gut microbiota exacerbates infarct volume and functional deficits following stroke, mediated by the migration of intestinal pro-inflammatory T cells to the ischemic brain. • Fecal microbiota transplantation (FMT) could normalize brain lesion-induced dysbiosis and improve stroke outcomes.
Benakis C, et al. (2016) (55)	MCAO mice	16S rRNA (V4-V5) sequencing	• Antibiotic-induced alterations in the gut microbiota reduced brain injury after ischemic stroke. • Dysbiosis following ischemic stroke changed intestinal immune homeostasis, leading to an increase in regulatory T(Treg) cells and a reduction in IL-17+ γδ T cells through altered dendritic cell activity. Moreover, dysbiosis blocked the migration of effector T cells from the gut to the leptomeninges.
Winek K, et al. (2016) (59)	MCAO mice	–	• Microbiota-depleted mice stopped the antibiotic cocktail pretreatment 3 days before surgery significantly decreased survival after MCAO. • Microbiota-depleted animals treated by continuous antibiotic treatment or colonized with SPF microbiota before surgery rescued from severe acute colitis.
Spychala MS, et al. (2018) (53)	MCAO mice	16S rRNA (V4-V5) sequencing	• The Firmicutes to Bacteroidetes ratio in aged mice increased ~9-fold compared to young. • The gut microbiota in the young manipulated by fecal from aged mice increased mortality, decreased behavioral performance, and increased cytokine levels following MCAO, altering the microbiota in the aged by fecal gavage to resemble that of young increased survival and improved recovery following MCAO.
Singh V, et al. (2018) (23)	MCAO mice	16S rRNA (V1-V3) sequencing	• Bacterial colonization reduces stroke volumes by increasing cerebral expression of cytokines and microglia/macrophage cell counts. • The gut microbiota-mediated neuroprotection was absent in lymphocyte-deficient mice.
Benakis C, et al. (2020) (56)	MCAO mice	16S rRNA (V4) sequencing	• Single antibiotic treatment with either ampicillin or vancomycin, but not neomycin, significantly reduced the infarct volume and improved motor sensory function 3 days after stroke. • Bacteroidetes S24.7 and the enzymatic pathway for aromatic metabolism were correlated with infarct size. • The gut microbiota composition in the ampicillin-treated mice was associated with reduced gut inflammation, a long-term favorable outcome, and a reduction of brain tissue loss. • Regulation of SCFAs and tryptophan pathways induced by ampicillin could be predictive of stroke outcomes.

(Continued)

TABLE 1 | Continued

	Subjects	Methods	Key findings
Sadler R, et al. (2020) (57)	MCAO and photothrombotic (PT) mice	GC-MS	• SCFAs supplementation in the drinking water significantly improved recovery of limb motor function by altering contralesional cortex connectivity, which is related to SCFAs-dependent changes in spine and synapse densities. • A substantial impact of SCFAs on microglial activation contributes to the structural and functional remodeling, mediated by the recruitment of T cells to the infarcted brain.
Lee J, et al. (2020) (58)	MCAO mice	16S rRNA (V4) sequencing & LC-MS	• Aged stroke mice transplanted the young fecal improved post-stroke neurological deficits and inflammation, which correlated with higher SCFAs levels and SCFAs-producers such as Bifidobacterium longum, Clostridium symbiosum, Faecalibacterium prausnitzii, and Lactobacillus fermentum.
Jeon J, et al. (2020) (65)	MCAO pig	16S rRNA (V3-V4) sequencing	• Compared with pre-stroke populations, the abundance of the Proteobacteria was significantly increased, while the abundances of Firmicutes and lactic acid bacteria Lactobacillus decreased at 3 days poststroke. • The gut microbial pattern returned to similar values as prestrike at 5 days poststroke.
Benakis C, et al. (2020) (56)	MCAO mice	16S rRNA (V4) sequencing	• Mice treated with a cocktail of antibiotics significantly reduced infarct volume in the acute phase of stroke. • Single antibiotic treatment with either ampicillin or vancomycin, but not neomycin, significantly reduced infarct volume and improved neurological function 3 days after stroke. • Bacteroidetes S24.7 and the enzymatic pathway for aromatic metabolism were associated with infarct size after stroke. • The gut microbiota signature in the ampicillin-treated mice was correlated with reduced intestinal inflammation, long-term favorable outcome and was predictive of SCFAs and tryptophan pathways.
Huang Q, et al. (2021) (71)	MCAO rat	16S rRNA (V3-V4) sequencing & GC-MS	• Compared with non-hemorrhagic transformation (HT) rats, the relative abundances of Proteobacteria and Actinobacteria were enriched in HT rats. • Total SCFAs levels, especially butyrate and valeric acid, were significantly decreased in the cecal contents of HT rats. • The rats colonized with gut microbiota from HT rats showed increased susceptibility to HT.
Zhang P, et al. (2021) (72)	MCAO mice	16S rRNA sequencing & HPLC-MS	• Atorvastatin significantly ameliorated neurological defects and reduced microglia-mediated neuroinflammation after experimental stroke. • Atorvastatin increased the abundance of Firmicutes and Lactobacillus, decreased Bacteroidetes abundance, increased fecal butyrate level, promoted intestinal barrier function by elevating the expression of claudin-1, occludin and mucoprotein 2, as well as regulated intestinal immune function. • Transplantation of atorvastatin-treated mice fecal microbiota alleviated neuroinflammation in MCAO mice.
Huang JT, et al. (2021) (73)	MCAO mice	16S rRNA sequencing	• The transplantation of gut microbiota collected from calorie-restriction-treated mice was eligible to have better long-term rehabilitation. • Bifidobacterium was enriched in calorie-restriction mice. • Bifidobacterium administration improved the long-term rehabilitation of stroke mice
Zhu W, et al. (2021) (74)	MCAO mice	16S rRNA (V4) sequencing & LC-MS	• The human fecal microbial transplantation study showed TMAO production and stroke severity are transmissible traits. • TMAO and choline supplementation exacerbated infarct size and functional impairment. • Gut microbial CutC increased host TMAO levels and aggravated cerebral infarct size and functional deficits after stroke.
Wu W, et al. (2021) (66)	MACO rat	16S rRNA (V3-V4) sequencing & LC-MS	• The abundance of the Firmicutes phylum was decreased, whereas Proteobacteria and Deferribacteres were increased after stroke. • Ruminococcus_sp_15975 might serve as a biomarker for the stroke. • Many metabolites, such as L-leucine, L-valine, and L-phenylalanine, differed between the stroke and sham groups, mainly involved in mineral absorption and cholinergic synapse pathways.
Yuan Q, et al. (2021) (75)	MCAO mice	16S rRNA sequencing & GC-MS	• Lactulose supplementation significantly improved the functional outcome after stroke by downregulating inflammatory reaction and increased anti-inflammatory factors in the brain and gut. • Lactulose supplementation improved intestinal barrier injury and restored gut microbiota dysbiosis after stroke.

16S rRNA, 16S ribosomal RNA.
PCR, polymerase chain reaction.
LC-MS, liquid chromatography-mass spectrometry.
GC-MS, gas chromatography-mass spectrometry.
HPLC-MS, high-performance liquid chromatography-mass spectrometry.

age, diet, behavior, antibiotic use, prolonged stress, environment, and genetics compose the gut microbiota, which may be influenced by the contradictory results of the above studies. Thus, more studies are needed to clarify the role of gut microbiota dysbiosis in the pathogenesis and prognosis of ischemic stroke. Recently, a preclinical study also suggested that the alteration in the gut microbiota was associated with hemorrhagic transformation (HT) (71). The relative abundance of Proteobacteria and Actinobacteria was significantly increased in HT rats after experimental stroke, indicating that the gut microbiota is involved in the progression of ischemic stroke.

Mechanistically, the gut microbiota-mediated neuroprotection greatly depended on the microglia and lymphocyte responses, significantly increasing Th cells, polarized Treg cells, and Th17 cell counts in the intestinal Peyer's patches (23). Pro-inflammatory Th1, Th17, and γδT cells often increase inflammatory damage, while Treg cells suppress post-stroke inflammation by secreting the anti-inflammatory cytokine IL-10. Alteration of gut microbiota following a stroke in the bacterial population triggers pro-inflammatory T cells responses, migrates intestinal immune cells to the meninges involved in secondary brain injury, and worsens stroke outcome. In GF MCAO animal models, mice transplanted with post-stroke fecal content presented increased infarct volume and functional deficits by inducing pro-inflammatory T cell polarization. Moreover, restoration of gut microbiota homeostasis with fecal microbiota transplantation (FMT) reduced infarct volume, improved stroke outcome and promoted the migration of intestinal Treg cells to the ischemic area in the brain (54). Also, intestinal dysbiosis following ischemic stroke was found to regulate immune homeostasis in the small intestine with increased Treg cells and decreased IL-17$^+$ γδT cells, mediated by DCs. The neuroprotective effect of IL-10 was identified as a regulator of Treg cell-mediated IL-17$^+$ γδT cell suppression (55).

Microbial-derived metabolites also correlate with the progression and prognosis of ischemic stroke. Ischemic stroke patients had significant gut microbiota dysbiosis with an increased abundance of SCFAs-producing bacteria such as Odoribacter, Akkermansia, which closely correlated with the stroke outcome (76). However, Zeng et al. reported that people with a high risk of stroke had lower levels of butyrate-producing bacteria (e.g., Lachnospiraceae and Ruminococcaceae) and fecal butyrate (50). Tan et al. also reported a lack of SCFAs-producing bacteria and a low fecal SCFAs level in acute ischemic stroke patients (67). Moreover, the reduced fecal SCFAs were correlated with an increased risk of 3-month unfavorable outcomes (67). The differences in the results of these clinical studies may be due to the small cohorts of the studies. These findings need to be further validated by higher-quality clinical studies with large cohorts. In experimental stroke, reduced plasma SCFAs level correlated with a worse stroke outcome in mice, and SCFAs supplementation improved behavioral recovery with modified poststroke cortical connectivity and synaptic plasticity by recruiting T lymphocytes on modulation of microglial activation, as reflected by the increase in Treg cells (57). Oral gavage of SCFAs-producing bacteria such as Bifidobacterium longum, Clostridium symbiosum, Faecalibacterium prausnitzii, and Lactobacillus fermentum alleviated post-stroke neurological deficits and inflammation by increasing populations of Treg cells and reducing the percentage of IL-17$^+$ γδT cells (58). Pretreatment with Clostridium butyricum improved neurological deficits and decreased hippocampal apoptosis by increasing butyrate and reducing brain oxidative stress in experimental stroke (77). Furthermore, Zhou et al. reported that butyrate alleviated neuronal apoptosis following stroke *via* GPR41/Gβγ/PI3K/Akt pathway (78). SCFAs could also improve outcomes by protecting gut epithelial cells against stroke-induced gut leakiness by enhancing tight junction proteins (79). Furthermore, sodium butyrate reduced infarct volume and improved neurological function Recently, Huang et al. found that the significant decrease of SCFAs in cecal contents, especially butyrate and valeric acid, was closely related hemorrhagic transformation after ischemic stroke (71).

It has been demonstrated that there is a significant association between TMAO level and various diseases, including stroke (80). Although several clinical studies have identified a correlation between TMAO level and stroke, the results remain controversial. Most studies show that the plasma TMAO concentrations in stroke patients are significantly higher than those in control patients, and its high level is positively related to the severity of the stroke (51, 68). A large-scale case-control study with 953 sex- and age-matched pairs performed by Sun et al. suggested that the plasma TMAO concentrations in patients with first acute ischemic stroke were significantly elevated (70). Furthermore, further analysis revealed that the multivariable-adjusted odds ratios for ischemic stroke per 1 μmol/L increase of plasma TMAO level were 1.05. Tan et al. reported that TMAO concentrations decreased with time after stroke, and elevated TMAO levels at an early stage predicted poor stroke outcomes (81). A meta-analysis also showed that compared with non-stroke controls, TMAO increased the stroke risks by 68% and accreted 2.201 umol/L on the average level of TMAO in stroke patients (82). Zhu et al.'s study also suggested gut microbiota can impact stroke severity *via* the gut microbial CutC-mediated TMAO pathway, which exacerbated cerebral infarct size and functional deficits (74).

The activation of the kynurenine pathway for tryptophan degradation correlates with stroke-induced inflammatory responses and unfavorable outcomes[53]. Tryptophan catabolites regulate intestinal immune cell function by activating AHR. Pharmacological and genetic inhibition of neural cell-specific AHR activation improved stroke outcomes in the MCAO mice model (83). Furthermore, tryptophan catabolism positively correlated with the severity of stroke outcome and might be associated with stroke-induced inflammatory response (51). Besides, xenobiotic/aromatic compound metabolism was a predictive marker of the size of the ischemic lesion (56).

Multiple studies have demonstrated that antibiotic-induced dysbiosis promotes the proliferation and differentiation of T cells in the gut to either improve or worsen outcomes in experimental stroke. Mice pretreated with ampicillin or vancomycin

significantly improved the outcome of stroke, whose neuroprotection is related to a shift with increased Proteobacteria and Firmicutes and reduction of Bacteroidetes caused by antibiotics (56). Particularly, Bacteroidetes S24.7 was closely associated with infarct size. However, Winek et al. reported stroke mice pretreated with quintuple broad-spectrum antibiotics presented with the damaged gut epithelium and worsened outcome (59). This controversial result still needs further study to clarify. FMT is a novel and potent treatment strategy in patients with gut microbiota dysbiosis obtained from fecal microbiota in healthy individuals. FMT exerts a neuroprotective effect by altering gut microbial metabolites production and reducing pro-inflammatory gut bacteria, alleviating inflammatory response and oxidative stress in the brain. Restoring gut microbiota homeostasis with FMT from healthy donors reduced lesion size by increasing Treg cells (54). MCAO mice receiving FMT from anti-inflammatory donors reduced the infarct volume by 54% (55). Additionally, FMT from young microbiota was also beneficial to stroke recovery (53). Oral gavage of SCFAs-producing bacteria or SCFAs supplementation also alleviated neurological deficits and improved poststroke recovery by reducing IL-17$^+$ γδT cells in the ischemic brain (57, 58). Recently, Zhang et al. found that atorvastatin significantly alleviated the defects in sensorimotor behaviors and reduced microglia-mediated neuroinflammation by increasing the abundance of Firmicutes and Lactobacillus, decreasing the abundance of Bacteroidetes abundance, increasing fecal butyrate level, promoting intestinal barrier function, as well as regulating intestinal immune function (reduced monocyte chemotactic protein 1(MCP-1), tumor necrosis factor-α(TNF-α) and increased IL-10) in the mice with permanent MCAO (72). Calorie restriction also can promote ischemic stroke rehabilitation *via* enriching the abundance of Bifidobacterium (73). Tanhuo decoction also promoted poststroke recovery by decreasing the biosynthesis of TMA, the precursor of TMAO, and increasing the expression of trimethylamine-corrinoid protein Co-methyltransferase (mttB), which catabolizes TMA to methane (69). Additionally, Lactulose supplementation was shown to significantly improve the functional outcome of stroke, which is possibly mediated by repairing intestinal barrier injury and improving gut microbiota dysbiosis following stroke (75).

Hemorrhagic Stroke

Hemorrhagic stroke includes intracranial and subarachnoid hemorrhage. Intracranial hemorrhage accounts for 80% of hemorrhagic stroke and 10-15% of all strokes, which is primarily caused by hypertension-induced small vessel rupture, while subarachnoid bleeding is mainly due to intracranial aneurysms rupture (84). Hemorrhagic stroke is characterized by high mortality and morbidity, which burdens society and families. However, there are, to date, few studies focused on the exploration of the correlation between hemorrhagic stroke and gut microbiota. A few studies reported that gut microbiota dysbiosis contributes to hypertension and intracranial aneurysms. However, the direct relationship between gut microbiota and hemorrhagic stroke has not been studied. Both clinical and animal studies are warranted in the future.

Gut Microbiota and Intracranial Aneurysms

A case-control metagenome-wide association study showed that the structural heterogeneity of intestinal microbiota in patients with intracranial aneurysm (IA) was significantly decreased compared to healthy controls, which had an increased abundance of Bacteroides, Parabacteroides, Ruminococcus, and Blautia in IA patients and an enrichment of Faecalibacterium, Eubacterium, Collinsella, and Lactobacillus (85). Recently, another multicenter, prospective case-control study reported that the abundance of the genus Campylobacter and Campylobacter ureolyticus was significantly higher in patients with ruptured IA than that in patients with unruptured IA, which may be associated with the rupture of IA (86). Further analysis suggested that gut microbiota promoted the pathogenesis of IA by regulating plasma amino acids (e.g., taurine, hypotaurine, L-histidine, and L-citrulline) and fatty acid levels (85). Compared to mice transplanted with healthy control feces, the incidence of IA in mice transplanted with the feces of IA patients was significantly increased (85). Mechanistically, supplementation with taurine or H.hathewayi reduces the formation and rupture of IA by blunting cerebrovascular inflammatory processes, reducing extracellular matrix remodeling, and maintaining the structural integrity of cerebral blood vessels. Similarly, Fumiaki Shikata et al. also reported that the gut microbiota contributes to the development of IA by modulating inflammation in the experimental IA model (87). Gut microbiota depletion by an oral antibiotic cocktail of ampicillin, metronidazole, neomycin, and vancomycin (AMNV) significantly reduced the incidence of IA *via* decreasing macrophage infiltration and the expression of pro-inflammatory cytokines such as IL-1β and IL-6 in vascular wells (87). These results suggest that gut microbiota is closely correlated with the development of IA. Additionally, human studies are needed to determine the exact contribution of the gut microbiota to the pathophysiology of IA and aneurysmal subarachnoid hemorrhage in humans.

Traumatic Brain Injury (TBI)

Traumatic brain injury (TBI) is one of the most common neurological diseases, with an estimated incidence of approximately 50 million people worldwide annually, leading to thousands of deaths and disabilities (88). TBI induces various secondary progressive brain damage contributing to varied functional outcomes. TBI also influences the gut barrier integrity, gut function, and gut microbiota composition (89). In turn, gut microbiota alterations may regulate a pro-inflammatory response following TBI and aggravate secondary brain injury. However, the information on TBI-induced gut microbiota dysbiosis is scarce for now. The relevant studies are summarized in **Table 2**.

Recently, an observational study investigated the characteristics of gut microbiota in 101 TBI patients and found

TABLE 2 | A summary of preclinical and human studies on the gut microbiota and traumatic brain injury.

	Subjects	Methods	Key findings
Mahajan C, et al. (2021) (90)	101 patients	–	• All organisms belonged to the Proteobacteria phylum, especially Enterobacteriaceae forming the largest group after traumatic brain injury (TBI). • TBI is associated with widespread colonization with Proteobacteria as early as 48 hours after injury.
Hou Y, et al. (2021) (91)	24 patients vs. 10 controls; surgical brain injury (SBI) rat	16S rRNA sequencing & HPLC-MS	• The abundances of Enterococcus, Parabacteroides, Akkermansia, and Lachnoclostridium were significantly increased, whereas the relative abundances of Bifidobacterium and Faecalibacterium were decreased in the patients with TBI. • Oral administration of brain protein combined with probiotics alleviated inflammatory gut damage by affecting tryptophan-related pathways.
Treangen TJ, et al. (2018) (92)	controlled cortical impact (CCI) mice	16S rRNA (V3-V4) sequencing	• At a high-level view, the abundances of Marvinbryantia and Clostridiales were significantly changed after TBI. • Lactobacillus gasseri, Ruminococcus flavefaciens, and Eubacterium ventriosum were decreased at the species level, while Eubacterium sulci and Marvinbryantia formatexigens and were increased after TBI.
Li H, et al. (2018) (93)	weight-drop impact (WDI) mice	–	• Clostridium butyricum treatment improved neurological deficits, brain edema, neurodegeneration, and blood-brain barrier impairment. • Clostridium butyricum treatment increased tight junction proteins, p-Akt, and Bcl-2 and decreased expression of Bax. • Mice treated by Clostridium butyricum showed an increased intestinal Glucagon-like peptide 1(GLP-1) secretion and upregulated the expression of cerebral GLP-1 receptor.
Simon DW, et al. (2020) (89)	CCI mice	16S rRNA (V4) sequencing	• Mice receiving pretreatment of ampicillin, metronidazole, neomycin, and vancomycin(AMNV) before surgery increased CA1's density of hippocampal neuronal and reduced Iba-1 positive cells at 72 h after TBI. • Mice pretreated by AMNV alleviated associative learning deficit and decreased lesion volume after TBI.
Angoa-Pérez M, et al. (2020) (94)	WDI mice	16S rRNA (V4) sequencing	• An early increase in microglial activation persisted from 0-day to 90-day post-injury, compounded by substantial increases in astrocyte reactivity and phosphorylated tau. • Few differences in the microbial community were observed in mice exposed to repetitive, mild TBI (rmTBI). • The progressive emergence of white matter damage and cognitive deficits following rmTBI was not associated with the altered gut microbiota.
Opeyemi OM, et al. (2021) (95)	CCI mice model	16S rRNA (V4) sequencing & HPLC-MS	• Bacteria from Lachnospiraceae, Ruminococcaceae, and Bacteroidaceae families were depleted, while bacteria from the Verrucomicrobiaceae family were enriched. • Fecal SCFAs such as acetate were reduced at 7 days and 28 days following TBI; SCFAs administration improved spatial learning after TBI.
Du D, et al. (2021) (96)	CCI rat	16S rRNA (V3-V4) sequencing & HPLC-MS	• TBI induced significant changes in the gut microbiome, including the alpha- and beta-bacterial diversity and the microbiome composition at 8 days after TBI. Fecal microbiota transplantation (FMT) could rescue these changes and relieve neurological deficits after TBI. • Metabolomics results showed that the level of trimethylamine (TMA) in feces and the level of trimethylamine N-oxide (TMAO) in the ipsilateral brain and serum was increased after TBI. At the same time, FMT decreased TMA levels in the feces and TMAO levels in the ipsilateral brain and serum. • FMT can restore gut microbiota dysbiosis and relieve neurological deficits, possibly through the TMA-TMAO-methionine sulfoxide reductase A (MsrA) signaling pathway after TBI.
You W, et al. (2021) (97)	lateral fluid percussion injury mice model	16S rRNA (V3-V4) sequencing & HPLC-MS	• The diversity of gut microbiota experienced a time-dependent change from 1 h to 7 days post-TBI. • The decreased levels of bile acids, especially secondary bile acids, were related to intestinal inflammation after TBI. • Staphylococcus and Lachnospiraceae may contribute to the bile acid metabolic changes.
Celorrio M, et al. (2021) (98)	CCI mice	PCR	• Antibiotic-induced gut microbial dysbiosis significantly worsened neuronal loss after TBI. • Antibiotic exposure for 1 week after TBI decreased T lymphocyte infiltration, increased microglial pro-inflammatory markers, and reduced cortical infiltration of $Ly6C^{high}$ monocytes. • Gut microbiota dysbiosis was associated with increased hippocampal neuronal loss and fear memory response 3 months after TBI.

16S rRNA, 16S ribosomal RNA.
PCR, polymerase chain reaction.
HPLC-MS, high-performance liquid chromatography-mass spectrometry.

that organisms from rectal swabs obtained on days 0, 3, and 7 after admission belonged to the Proteobacteria phylum, with Enterobacteriaceae forming the largest group (90). Hou et al. also analyzed the gut microbiota composition in a small cohort (10 healthy control volunteers vs. 24 TBI patients) and reported that the abundance of Enterococcus, Parabacteroides, Akkermansia, and Lachnoclostridium were significantly increased, while the abundance of Bifidobacterium and Faecalibacterium were decreased in TBI patients (91).

In the controlled cortical impact (CCI) mouse model, the gut microbiota significantly decreased in Lactobacillus gasseri, Ruminococcus flavefaciens, and Eubacterium ventriosum and increased dramatically in Eubacterium sulci and Marvinbryantia formatexigens at 24h post-CCI (92). In an experimental weight-drop injury model, the severity of TBI is correlated with the alteration in Bacteroidetes, Porphyromonadaceae, Firmicutes, and α-Proteobacteria (21). Nicholson et al. found a reduced Firmicutes/Bacteroidetes ratio in gut microbiota composition occurring at 2h post-injury was significantly related to MRI-determined lesion volume and behavioral function defects (99). In the lateral fluid percussion injury mice model, You et al. also observed the alterations of gut microbiota and bile acid profile

(97). Further analysis found that specific bacterial taxa such as Staphylococcus and Lachnospiraceae could be associated with the bile acid metabolic changes, resulting in intestinal inflammation. Interestingly, Angoa-Pérez et al. found that repetitive, mild TBI did not cause alterations in the gut microbiota composition (94). Although differences in gut microbiota composition have been observed after TBI in animal models, the exact regulatory mechanism remains elusive. A study considered that vagal afferent alterations, TBI-induced increase of cholecystokinin level, might be responsible for gut dysfunction through activation of the vago-vagal NTS-inhibitory pathway (100). Additionally, in another experimental TBI, the gut upregulated the expression of glycoproteins to recruit immune cells and activate inflammatory signals, resulting in altered mucosal integrity (101). The leaky gut allowed toxic bacterial components such as LPS to enter the circulation that mediates neuroinflammation by activating microglia following TBI (26). Furthermore, the permeability of the blood-brain barrier (BBB) can increase up to 4 times more than normal within 6h following TBI. The increased BBB permeability aggravates the gut dysbiosis-induced neuroinflammation by LPS exposure, γδT cell activation, and activated microglia differentiation into the M1 phenotype. A recent preclinical study performed by Celorrio et al. suggested that antibiotic-induced gut microbial dysbiosis established before TBI significantly worsened neuronal loss, reduced cortical infiltration of $Ly6C^{high}$ monocytes and T lymphocyte, increased microglial pro-inflammatory markers, and impaired neurogenesis after TBI (98).

CCI mice pretreated with AMNV 2 weeks before CCI presented increased neuronal density in the hippocampus at 72h post-injury, while mice treated with AMNV right after CCI showed reduced lesion volume and attenuated associative learning deficit at 22 days (89). TBI mice treated by Clostridium butyricum also improved neurological deficits, attenuates brain edema, ameliorated neurodegeneration, and alleviated BBB impairment *via* elevating intestinal Glucagon-like peptide 1(GLP-1) secretion (93). SCFAs supplementation also improved spatial learning following CCI-induced TBI, mediated by activating the neurotrophic tyrosine kinase receptor type 1 (TrkA) pathway (95, 102). Probiotic supplementation also significantly remedied the gut microbiota dysbiosis and decreased the intestinal permeability following experimental TBI by reducing the intestinal mucosa damage, alleviating brain injury (103). In human studies, probiotic treatment could relieve systemic inflammatory response, decrease nosocomial infection rate, and improve the recovery of patients with TBI (104, 105). Interestingly, vagal stimulation reduced gut barrier permeability after TBI, mediated by the suppression of TNF-α release (106). Recently, it has been demonstrated that FMT can restore gut microbiota dysbiosis following TBI and ameliorate neurological deficits, mediated by the TMA-TMAO-MsrA signaling pathway (96).

Spinal Cord Injury (SCI)

Traumatic spinal cord injury (SCI) is another acute CNS injury that affects millions worldwide every year (107). The studies involving SCI and the bidirectional effect on the gut microbiota have been carried out in recent years, which are summarized in **Table 3**. This section reviews the study published on the changes in the gut microbiota that occur following SCI.

In a Chinese cohort study, Zhang et al. observed an increase in Proteobacteria and Verrucomicrobia and reduced Bacteroidaceae and Bacteroides in patients with chronic traumatic complete SCI (109). Lin et al. also analyzed 46 Chinese subjects (23 SCI patients vs. 23 healthy controls) and reported that the abundances of Parabacteroides, Alistipes, Phascolarctobacterium, Christensenella, Barnesiella, Holdemania, Eggerthella, Intestinimonas, Gordonibacter, Bilophila, Flavonifractor, and Coprobacillus were higher in the patients with SCI than those in the health individuals (110). Another clinical study with 54 Turkish participants (41 SCI patients vs. 13 healthy controls) identified that butyrate-producing microbes of the Firmicutes phylum are significantly reduced in SCI patients than healthy controls (108). Recently, Bazzocchi et al. investigated a large Italian SCI population acute phase after injury and age- and gender-matched healthy Italians (112). Their study revealed that the abundance of SCI patients' gut microbiota increased in potentially pathogenic, pro-inflammatory, and mucus-degrading bacteria and decreased in SCFAs producers. Moreover, gut microbiome dysbiosis is closely associated with the severity of the lesion after SCI. A case-control study carried by Yu et al. (45 SCI patients vs. 24 healthy individuals) showed that the abundance of Actinobacteria and Synergistetes in patients with complete thoracic SCI (CTSCI) was significantly higher than that in healthy individuals. At the same time, the Bacteroidetes, Cyanobacteria, and Proteobacteria were significantly decreased in patients with incomplete thoracic SCI (ITSCI) as compared to the healthy (113). Furthermore, they compared the gut microbiota composition between patients with CTSCI and ITSCI and found a significantly increased abundance of Coriobacteriaceae, Synergistetes, Eubacterium, and Cloacibacillus was observed in patients with CTSCI, while patients with ITSCI were abundant with Lactobacillaceae, Lachnospiraceae, Eubacterium, Clostridium, and Sutterella.

Similarly, a thoracic level 9 (T9) contusion SCI-induced gut microbiota dysbiosis in the experimental SCI mice was also characterized by an expansion of Bacteroidetes and a reduction of Firmicutes (115). However, a preclinical work in a T9 contusion SCI mouse model by Kigerl et al. reported that SCI mice presented a decrease in Bacteroidales and an increase in Clostridiales (25). In an SCI rat model, gut microbiota composition was significantly changed with an increased abundance of Lactobacillus intestinalis, Clostridium disporicum, and Bifidobacterium choerinum and a reduced level of Clostridium saccharogumia (114). The difference in the results may be caused by experimental deviation. Additionally, the above analyses of SCI-induced gut microbiota dysbiosis were assessed by 16S rRNA amplicon sequencing, which cannot profile microbiota function or identify viruses (123). Du et al. studied gut microbiota dysbiosis after experimental SCI at T4 or T10 using genome- and gene-resolved metagenomic analysis (122). The results suggested that the abundance of beneficial commensals (Lactobacillus johnsonii and CAG-1031 spp.)

TABLE 3 | A summary of preclinical and human studies on the gut microbiota and spinal cord injury.

	Subjects	Methods	Key findings
Gungor B, et al. (2016) (108)	30 patients vs. 10 controls	16S rRNA (V4) sequencing	• Marvinbryantia was significantly lower in the upper motor neuron (UMN) bowel dysfunction group than in the lower motor neuron (LMN) group after spinal cord injury(SCI). • Compared with healthy groups, Roseburia, Pseudobutyrivibrio, and Megamonas were significantly lower in the LMN bowel dysfunction group; the abundances of Pseudobutyrivibrio, Dialister, and Megamonas genera were significantly lower in the UMN bowel dysfunction group.
Zhang C, et al. (2018) (109)	43 patients vs. 23 controls	16S rRNA (V3-V4) sequencing	• SCI contributed to the increased abundance of Veillonellaceae and Prevotellaceae and the decreased abundance of Bacteroidaceae and Bacteroides. • The abundance of Bacteroidaceae and Bacteroides in the quadriplegia group and Acidaminococcaceae, Blautia, Porphyromonadaceae, and Lachnoclostridium in the paraplegia group were significantly higher compared to the healthy male group. • Following SCI, the gut microbiota composition was significantly associated with serum biomarkers (glucose, high-density lipoprotein, creatinine, and C-reactive protein), neurogenic bowel dysfunction defecation time, and course.
Lin R, et al. (2020) (110)	23 patients vs. 23 controls	16S rRNA (V3-V4) sequencing	• There were no significant differences in the α-diversity indices of the fecal microbiota between the SCI and control groups. • The abundances of Parabacteroides, Alistipes, Phascolarctobacterium, Christensenella, Barnesiella, Holdemania, Eggerthella, Intestinimonas, Gordonibacter, Bilophila, Flavonifractor, and Coprobacillus were higher in the patients with SCI than those in the healthy control.
Li J, et al. (2020) (111)	32 patients (7 acute SCI and 25 long-standing SCI) vs. 25controls	16S rRNA (V4) sequencing	• Compared with the controls, SCI patients had higher abundances of the Erysipelotrichaceae, Acidaminococcaceae, Rikenellaceae, Lachnospiraceae, Rikenellaceae, the Ruminococcaceae families. • The long-standing SCI patients had higher abundances of Lachnospiraceae and Eggerthellaceae, and lower abundances of Campylobacteraceae than the controls. • The acute SCI has a higher abundance of the Desulfovibrionaceae family than the controls.
Bazzocchi G, et al. (2021) (112)	100 patients	16S rRNA (V3-V4) sequencing	• The SCI-induced gut microbiota composition showed distinct dysbiotic signatures with an enriched in potentially pathogenic, pro-inflammatory, and mucus-degrading bacteria and a decreased abundance of short-chain fatty acids (SCFAs) producers. • The gut microbiota dysbiosis is very likely secondary to injury and closely related to the lesion's degree of completeness and severity after SCI.
Yu B, et al. (2021) (113)	45 patients (21 complete thoracic SCI and 24 incomplete thoracic SCI) vs. 24 controls	16S rRNA sequencing	• Compared with healthy individuals, Actinobacteria and Synergistetes were significantly enriched in patients with complete thoracic SCI. Similarly, Bacteroidetes, Cyanobacteria, and Proteobacteria were significantly lower in patients with incomplete thoracic SCI than healthy controls. • Coriobacteriaceae, Synergistetes, Eubacterium, and Cloacibacillus, were significantly increased in patients with complete thoracic SCI, while Lactobacillaceae, Lachnospiraceae, Eubacterium, Clostridium, and Sutterella, were significantly increased in patients with incomplete thoracic SCI.
Kigerl KA, et al. (2016) (25)	T9 contusion mice model	16S rRNA (V4-V5) sequencing	• SCI increased intestinal permeability and bacterial translocation from the gut, associated with immune cell activation in gut-associated lymphoid tissues (GALTs) and the altered gut microbiota composition. • In naive mice, gut dysbiosis induced by oral delivery of broad-spectrum antibiotics before SCI exacerbated neurological impairment and spinal cord pathology after SCI. • SCI mice treated by commercial probiotics (VSL#3) enriched lactic acid-producing bacteria, triggering a protective immune response in GALTs and conferring neuroprotection with improved neurological recovery.
O'Connor G, et al. (2018) (114)	T9 contusion rat model	16S rRNA (V4) sequencing	• Lactobacillus intestinalis, Clostridium disporicum, and Bifidobacterium choerinum were enriched, while Clostridium saccharogumia was depleted following SCI. • Levels of interleukin-1β(IL-1β), IL-12, and macrophage inflammatory protein-2 significantly correlated with changes in β diversity 8-weeks post-SCI.
Myers SA, et al. (2019) (115)	T9 contusion mice model	16S rRNA (V4) sequencing	• SCI led to an increased abundance of Proteobacteria. • The absence of Pde4b improved white matter sparing and recovery of hindlimb locomotion following SCI. Moreover, SCI-induced gut dysbiosis, bacterial overgrowth, and endotoxemia were also reduced in Pde4b$^{-/-}$ mice.
Jing Y, et al. (2019) (116)	T10 contusion mice model	16S rRNA (V3-V4) sequencing	• Daily intraperitoneal injection with melatonin improved enhanced barrier integrity and gastrointestinal motility, reduced proinflammatory cytokines, and promoted locomotor recovery. • Melatonin-treated SCI animals decreased the abundance of Clostridiales and increased the quantity of Lactobacillales and Lactobacillus. • Before surgery, gut dysbiosis induced by broad-spectrum antibiotics exacerbated neurological impairment following SCI, and melatonin treatment improved locomotor recovery and intestinal integrity in antibiotic-treated SCI mice.
Schmidt EKA, et al. (2020) (117)	C5 contusion rat model	16S rRNA (V4) sequencing	• SCI-induced dysbiosis increased symptoms of anxiety-like behavior. • Fecal microbiota transplantation (FMT) prevented SCI-induced dysbiosis and the development of anxiety-like behavior.

(Continued)

TABLE 3 | Continued

	Subjects	Methods	Key findings
Jing Y, et al. (2021) (118)	T10 contusion mice model	16S rRNA (V4) sequencing & HPLC-MS	• FMT-treated SCI mice facilitated functional recovery, promoted neuronal axonal regeneration, and enhanced intestinal barrier integrity and gastrointestinal motility, which short-chain fatty acids (SCFAs) and Nuclear Factor-κB (NF-κB) signaling may mediate. • Butyricimonas were reduced in SCI mice, and FMT significantly reshaped gut microbiota.
Schmidt EKA, et al. (2021) (119)	C5 contusion rat model	16S rRNA (V4) sequencing	• Minocycline had a profound acute effect on the gut microbiota diversity and composition after SCI. • Gut dysbiosis following SCI has been linked to the development of anxiety-like behavior, which was also alleviated by minocycline. • Although minocycline attenuated SCI-induced microglial activation, it did not change the lesion size or promote neurological recovery.
Doelman A, et al. (2021) (120)	T2 or T10 contusion pig model	16S rRNA (V3-V4) sequencing	• In the acute phase (<14d post-SCI), Proteobacteria, Tenericutes, Epsilonbacteraeota, and Cyanobacteria decreased compared to the controls while Bacteroidetes, Firmicutes, and Spirochaetes were enriched. • In the sub-acute phase (>14 days post-SCI), the abundance of Spirochaetes, Cyanobacteria, and Proteobacteria remained statistically significantly different from the controls.
Rong Z, et al. (2021) (121)	T10 contusion mice model	–	• The levels of pro-inflammatory cytokines tumor necrosis factor-α, IL-1β, and IL-6 in SCI mice were increased, while the levels of anti-inflammatory factors IL-4, transforming growth factor-β, and IL-10 were decreased. • Gut microbiota dysbiosis aggravated SCI by activating the toll-like receptor 4(TLR4)/myeloid differentiation factor 88 (MyD88) signaling pathway.
Du J, et al. (2021) (122)	T4 or T10 contusion mice model	genome- and gene-resolved metagenomic analysis	• The abundance of Lactobacillus johnsonii and CAG-1031 spp. decreased, while Weissella cibaria, Lactococcus lactis_A, Bacteroides thetaiotaomicron were enriched after SCI. • Microbial-mediated biosynthesis of tryptophan, vitamin B6, and folate was reduced after SCI. • 1028 mostly novel viral populations were recovered, which expanded known murine gut viral species sequence space. • Phages of beneficial commensal hosts, including CAG-1031, Lactobacillus, and Turicibacter, decreased, while phages of pathogenic hosts, including Weissella, Lactococcus, and class Clostridia, increased after SCI.

16S rRNA, 16S ribosomal RNA.
HPLC-MS, high-performance liquid chromatography-mass spectrometry.

significantly decreased, while potentially pathogenic bacteria (Weissella cibaria, Lactococcus lactis_A, Bacteroides thetaiotaomicron) increased after SCI. Functionally, tryptophan, vitamin B6, and folate biosynthesis, encoded by microbial genes, were reduced in the feces after SCI. Interestingly, the study performed by Du et al. reported that phages of beneficial commensal hosts (CAG-1031, Lactobacillus, and Turicibacter) decreased. In contrast, phages of pathogenic hosts (Weissella, Lactococcus, and class Clostridia) increased after SCI (122). In a Yucatan minipig model with a contusion-compression SCI at T2 or T10, Doelman et al. presented a dynamic view of the microbiome changes following SCI and identified acute stage, 0-14 post-SCI, as a special time-frame that many of the bacterial fluctuations occur before returning to "baseline" levels (120).

SCI promotes intestinal leakiness and bacterial translocation associated with activation of immune cells in GALTs, by increasing the population of B cells, $CD8^+$ T cells, DCs, and macrophages and decreasing $CD4^+$ T cell counts (25). γδT cell-deficient mice improved functional recovery after SCI (124). Moreover, changes in gut microbiota composition following SCI could predict locomotor impairment (125). Additionally, gut microbiota dysbiosis can aggravate SCI by activating the TLR4/Myeloid differentiation factor 88 signaling pathway (121).

SCI mice fed with commercial probiotics (VSL#3) reduced neuropathology, improved locomotor recovery, and promoted an anti-inflammatory response by increasing the number of Treg cells in GALTs (25). Additionally, SCI mice daily treated with melatonin improved gut barrier integrity and functional recovery by reducing the abundance of Clostridiales and enhancing the quantity of Lactobacillales and Lactobacillus, which were related to a more favorable cytokine profile (116). Lactic acid supplementation was also proved to improve functional recovery following SCI (25). FMT prevented both SCI-induced dysbiosis, locomotor function, and the development of anxiety-like behavior (117). FMT could increase the amount of fecal SCFAs and downregulate IL-1β/NF-κB signaling in the spinal cord and NF-κB signaling in the gut following SCI (118). A recent study also reported that minocycline treatment attenuated SCI-induced anxiety-like behavior and systemic inflammatory response *via* altering the Firmicutes/Bacteroidetes ratio (119). Engineered liposomes targeting the MGBA may also be a potential treatment (126).

CONCLUSION AND PERSPECTIVE

Gut microbiota is closely involved in the development and progression of acute CNS disease through multiple mechanisms, including immunological, endocrine, metabolic, and neural pathways. FMT and probiotics significantly improve brain injury by restoring the acute CNS injury-induced gut microbiota dysbiosis. Gut microbiota may be a potential target to assist in the treatment of acute CNS injury.

However, several aspects are still needed to ponder despite a growing number of studies concerning the gut microbiota. Firstly, human gut microbiota composition is different from rodents. Although Firmicutes and Bacteroidetes are the most abundant microbiota both in mice and humans, more than 80% of the bacteria found in the mice intestine are not colonized in the human intestines based on genus level (127). Secondly, immunological features are also different between rodents and humans. A previous study suggests that the intestinal properties of humans are similar to those of mice. However, differences in intestinal immunity between mice and humans have already been found that γδT cells are found significantly less frequently in the intraepithelial compartment of humans than in mice (128). Thirdly, the effects of enteroviruses, fungi, and bacteriophages cannot be ignored. Bacteriophages have high host specificity that shapes the gut microbiota composition and regulates the host immune response by altering bacterial pathogen-associated molecular patterns and maintaining the host mucosal barrier (129). Although the effects of enteroviruses on health and disease are still unclear, phage-virus-fungi-bacterial-host interaction in the gut should also be considered. Moreover, their role in human acute brain injury or animal models has not been studied so far. Fourthly, developmental disturbances in GF mice should be considered. GF mice have hypoplastic immune structures and differ from SPF mice in the intestinal immune cell populations, such as IgA-producing plasma cells and lamina propria $CD4^+$ T cells (130). Additionally, GF mice contain fewer serum immunoglobulins, particularly IgG (131). In the absence of gut microbiota, CNS is also altered with a "leaky" BBB and an abnormal microglia morphology and function (132, 133). Finally, criteria for identifying qualified, healthy donors in the FMT treatment have not yet been fully established. The safety and efficiency of FMT need to be extensively investigated.

AUTHOR CONTRIBUTIONS

BY wrote the manuscript. X-jL and QW revised the manuscript. All authors contributed to the article and approved the submitted version.

FUNDING

This work was supported by the Scientific Research Project of Jiangsu Provincial Health commission under Grant No. H2018066.

REFERENCES

1. Sun P, Liu DZ, Jickling GC, Sharp FR, Yin KJ. Microrna-Based Therapeutics in Central Nervous System Injuries. *J Cereb Blood Flow Metab* (2018) 38 (7):1125–48. doi: 10.1177/0271678x18773871
2. Wang Y, Tan H, Hui X. Biomaterial Scaffolds in Regenerative Therapy of the Central Nervous System. *BioMed Res Int* (2018) 2018(2):7848901–19. doi: 10.1155/2018/7848901
3. Sorby-Adams AJ, Marcoionni AM, Dempsey ER, Woenig JA, Turner RJ. The Role of Neurogenic Inflammation in Blood-Brain Barrier Disruption and Development of Cerebral Oedema Following Acute Central Nervous System (CNS) Injury. *IJMS* (2017) 18(8):1788. doi: 10.3390/ijms18081788
4. Zmora N, Suez J, Elinav E. You are What You Eat: Diet, Health and the Gut Microbiota. *Nat Rev Gastroenterol Hepatol* (2019) 16(1):35–56. doi: 10.1038/s41575-018-0061-2
5. O'Toole PW, Jeffery IB. Gut Microbiota and Aging. *Sci (New York NY)* (2015) 350(6265):1214–5. doi: 10.1126/science.aac8469
6. Sánchez B, Delgado S, Blanco-Míguez A, Lourenço A, Gueimonde M, Margolles A. Probiotics, Gut Microbiota, and Their Influence on Host Health and Disease. *Mol Nutr Food Res* (2017) 61(1):1600240. doi: 10.1002/mnfr.201600240
7. Järbrink-Sehgal E, Andreasson A. The Gut Microbiota and Mental Health in Adults. *Curr Opin Neurobiol* (2020) 62:102–14. doi: 10.1016/j.conb.2020.01.016
8. Sender R, Fuchs S, Milo R. Revised Estimates for the Number of Human and Bacteria Cells in the Body. *PloS Biol* (2016) 14(8):e1002533. doi: 10.1371/journal.pbio.1002533
9. Flowers SA, Ellingrod VL. The Microbiome in Mental Health: Potential Contribution of Gut Microbiota in Disease and Pharmacotherapy Management. *Pharmacotherapy* (2015) 35(10):910–6. doi: 10.1002/phar.1640
10. Arumugam M, Raes J, Pelletier E, Le Paslier D, Yamada T, Mende DR, et al. Enterotypes of the Human Gut Microbiome. *Nature* (2011) 473(7346):174–80. doi: 10.1038/nature09944
11. Tyler Patterson T, Grandhi R. Gut Microbiota and Neurologic Diseases and Injuries. *Adv Exp Med Biol* (2020) 1238:73–91. doi: 10.1007/978-981-15-2385-4_6
12. Takagi T, Naito Y, Inoue R, Kashiwagi S, Uchiyama K, Mizushima K, et al. Differences in Gut Microbiota Associated With Age, Sex, and Stool Consistency in Healthy Japanese Subjects. *J Gastroenterol* (2019) 54(1):53–63. doi: 10.1007/s00535-018-1488-5
13. Delgado Jiménez R, Benakis C. The Gut Ecosystem: A Critical Player in Stroke. *Neuromolecular Med.* (2021) 23(2):236–241. doi: 10.1007/s12017-020-08633-z
14. Knight R, Vrbanac A, Taylor BC, Aksenov A, Callewaert C, Debelius J, et al. Best Practices for Analysing Microbiomes. *Nat Rev Microbiol* (2018) 16 (7):410–22. doi: 10.1038/s41579-018-0029-9
15. Arya AK, Hu B. Brain-Gut Axis After Stroke. *Brain Circ* (2018) 4(4):165–73. doi: 10.4103/bc.bc_32_18
16. Russo R, Cristiano C, Avagliano C, De Caro C, La Rana G, Raso GM, et al. Gut-Brain Axis: Role of Lipids in the Regulation of Inflammation, Pain and CNS Diseases. *Curr Med Chem* (2018) 25(32):3930–52. doi: 10.2174/0929867324666170216113756
17. Fung TC, Olson CA, Hsiao EY. Interactions Between the Microbiota, Immune and Nervous Systems in Health and Disease. *Nat Neurosci* (2017) 20(2):145–55. doi: 10.1038/nn.4476
18. Cryan JF, O'Riordan KJ, Cowan CSM, Sandhu KV, Bastiaanssen TFS, Boehme M, et al. The Microbiota-Gut-Brain Axis. *Physiol Rev* (2019) 99 (4):1877–2013. doi: 10.1152/physrev.00018.2018
19. Benakis C, Martin-Gallausiaux C, Trezzi JP, Melton P, Liesz A, Wilmes P. The Microbiome-Gut-Brain Axis in Acute and Chronic Brain Diseases. *Curr Opin Neurobiol* (2020) 61:1–9. doi: 10.1016/j.conb.2019.11.009
20. Cryan JF, O'Riordan KJ, Sandhu K, Peterson V, Dinan TG. The Gut Microbiome in Neurological Disorders. *Lancet Neurol* (2020) 19(2):179–94. doi: 10.1016/S1474-4422(19)30356-4
21. Houlden A, Goldrick M, Brough D, Vizi ES, Lénárt N, Martinecz B, et al. Brain Injury Induces Specific Changes in the Caecal Microbiota of Mice *via* Altered Autonomic Activity and Mucoprotein Production. *Brain Behav Immun* (2016) 57:10–20. doi: 10.1016/j.bbi.2016.04.003
22. Antila S, Karaman S, Nurmi H, Airavaara M, Voutilainen MH, Mathivet T, et al. Development and Plasticity of Meningeal Lymphatic Vessels. *J Exp Med* (2017) 214(12):3645–67. doi: 10.1084/jem.20170391

23. Singh V, Sadler R, Heindl S, Llovera G, Roth S, Benakis C, et al. The Gut Microbiome Primes a Cerebroprotective Immune Response After Stroke. *J Cereb Blood Flow Metab* (2018) 38(8):1293–8. doi: 10.1177/0271678X18780130
24. Brea D, Poon C, Benakis C, Lubitz G, Murphy M, Iadecola C, et al. Stroke Affects Intestinal Immune Cell Trafficking to the Central Nervous System. *Brain Behav Immun* (2021) 96:295–302. doi: 10.1016/j.bbi.2021.05.008
25. Kigerl KA, Hall JCE, Wang L, Mo X, Yu Z, Popovich PG. Gut Dysbiosis Impairs Recovery After Spinal Cord Injury. *J Exp Med* (2016) 213(12):2603–20. doi: 10.1084/jem.20151345
26. Wen L, You W, Wang H, Meng Y, Feng J, Yang X. Polarization of Microglia to the M2 Phenotype in a Peroxisome Proliferator-Activated Receptor Gamma-Dependent Manner Attenuates Axonal Injury Induced by Traumatic Brain Injury in Mice. *J neurotrauma* (2018) 35(19):2330–40. doi: 10.1089/neu.2017.5540
27. Carlson AL, Xia K, Azcarate-Peril MA, Goldman BD, Ahn M, Styner MA, et al. Infant Gut Microbiome Associated With Cognitive Development. *Biol Psychiatry* (2018) 83(2):148–59. doi: 10.1016/j.biopsych.2017.06.021
28. Gao W, Salzwedel AP, Carlson AL, Xia K, Azcarate-Peril MA, Styner MA, et al. Gut Microbiome and Brain Functional Connectivity in Infants-A Preliminary Study Focusing on the Amygdala. *Psychopharmacology* (2019) 236(5):1641–51. doi: 10.1007/s00213-018-5161-8
29. Harms AS, Thome AD, Yan Z, Schonhoff AM, Williams GP, Li X, et al. Peripheral Monocyte Entry Is Required for Alpha-Synuclein Induced Inflammation and Neurodegeneration in a Model of Parkinson Disease. *Exp Neurol* (2018) 300:179–87. doi: 10.1016/j.expneurol.2017.11.010
30. Mazmanian SK, Liu CH, Tzianabos AO, Kasper DL. An Immunomodulatory Molecule of Symbiotic Bacteria Directs Maturation of the Host Immune System. *Cell* (2005) 122(1):107–18. doi: 10.1016/j.cell.2005.05.007
31. Atarashi K, Suda W, Luo C, Kawaguchi T, Motoo I, Narushima S, et al. Ectopic Colonization of Oral Bacteria in the Intestine Drives TH1 Cell Induction and Inflammation. *Science* (2017) 358(6361):359–65. doi: 10.1126/science.aan4526
32. Fort MM, Cheung J, Yen D, Li J, Zurawski SM, Lo S, et al. IL-25 Induces IL-4, IL-5, and IL-13 and Th2-Associated Pathologies *In Vivo*. *Immunity* (2001) 15(6):985–95. doi: 10.1016/s1074-7613(01)00243-6
33. Wang Y, Yin Y, Chen X, Zhao Y, Wu Y, Li Y, et al. Induction of Intestinal Th17 Cells by Flagellins From Segmented Filamentous Bacteria. *Front Immunol* (2019) 10:2750. doi: 10.3389/fimmu.2019.02750
34. Round JL, Lee SM, Li J, Tran G, Jabri B, Chatila TA, et al. The Toll-Like Receptor 2 Pathway Establishes Colonization by a Commensal of the Human Microbiota. *Sci (New York NY)* (2011) 332(6032):974–7. doi: 10.1126/science.1206095
35. Fleming C, Cai Y, Sun X, Jala VR, Xue F, Morrissey S, et al. Microbiota-Activated CD103(+) Dcs Stemming From Microbiota Adaptation Specifically Drive Gammadeltat17 Proliferation and Activation. *Microbiome* (2017) 5(1):46. doi: 10.1186/s40168-017-0263-9
36. Yang Y, Xu C, Wu D, Wang Z, Wu P, Li L, et al. Γδ T Cells: Crosstalk Between Microbiota, Chronic Inflammation, and Colorectal Cancer. *Front Immunol* (2018) 9:1483. doi: 10.3389/fimmu.2018.01483
37. Wesemann DR, Portuguese AJ, Meyers RM, Gallagher MP, Cluff-Jones K, Magee JM, et al. Microbial Colonization Influences Early B-Lineage Development in the Gut Lamina Propria. *Nature* (2013) 501(7465):112–5. doi: 10.1038/nature12496
38. Shaw MH, Kamada N, Kim Y-G, Núñez G. Microbiota-Induced IL-1β, But Not IL-6, Is Critical for the Development of Steady-State TH17 Cells in the Intestine. *J Exp Med* (2012) 209(2):251–8. doi: 10.1084/jem.20111703
39. Chang PV, Hao L, Offermanns S, Medzhitov R. The Microbial Metabolite Butyrate Regulates Intestinal Macrophage Function *via* Histone Deacetylase Inhibition. *Proc Natl Acad Sci United States America* (2014) 111(6):2247–52. doi: 10.1073/pnas.1322269111
40. Singh N, Gurav A, Sivaprakasam S, Brady E, Padia R, Shi H, et al. Activation of Gpr109a, Receptor for Niacin and the Commensal Metabolite Butyrate, Suppresses Colonic Inflammation and Carcinogenesis. *Immunity* (2014) 40(1):128–39. doi: 10.1016/j.immuni.2013.12.007
41. Parada Venegas D, de la Fuente MK, Landskron G, Gonzalez MJ, Quera R, Dijkstra G, et al. Short Chain Fatty Acids (Scfas)-Mediated Gut Epithelial and Immune Regulation and Its Relevance for Inflammatory Bowel Diseases. *Front Immunol* (2019) 10:277. doi: 10.3389/fimmu.2019.00277
42. Sun X, Jiao X, Ma Y, Liu Y, Zhang L, He Y, et al. Trimethylamine N-Oxide Induces Inflammation and Endothelial Dysfunction in Human Umbilical Vein Endothelial Cells *via* Activating ROS-TXNIP-NLRP3 Inflammasome. *Biochem Biophys Res Commun* (2016) 481(1-2):63–70. doi: 10.1016/j.bbrc.2016.11.017
43. Dasgupta S, Erturk-Hasdemir D, Ochoa-Reparaz J, Reinecker H-C, Kasper DL. Plasmacytoid Dendritic Cells Mediate Anti-Inflammatory Responses to a Gut Commensal Molecule *via* Both Innate and Adaptive Mechanisms. *Cell Host Microbe* (2014) 15(4):413–23. doi: 10.1016/j.chom.2014.03.006
44. Johnson JL, Jones MB, Cobb BA. Polysaccharide a From the Capsule of Bacteroides Fragilis Induces Clonal CD4+ T Cell Expansion. *J Biol Chem* (2015) 290(8):5007–14. doi: 10.1074/jbc.M114.621771
45. Wang Y, Begum-Haque S, Telesford KM, Ochoa-Reparaz J, Christy M, Kasper EJ, et al. A Commensal Bacterial Product Elicits and Modulates Migratory Capacity of CD39(+) CD4 T Regulatory Subsets in the Suppression of Neuroinflammation. *Gut Microbes* (2014) 5(4):552–61. doi: 10.4161/gmic.29797
46. Feigin VL, Norrving B, Mensah GA. Global Burden of Stroke. *Circ Res* (2017) 120(3):439–48. doi: 10.1161/CIRCRESAHA.116.308413
47. Ojaghihaghighi S, Vahdati SS, Mikaeilpour A, Ramouz A. Comparison of Neurological Clinical Manifestation in Patients With Hemorrhagic and Ischemic Stroke. *World J Emerg Med* (2017) 8(1):34–8. doi: 10.5847/wjem.j.1920-8642.2017.01.006
48. Yin J, Liao S-X, He Y, Wang S, Xia G-H, Liu F-T, et al. Dysbiosis of Gut Microbiota With Reduced Trimethylamine-N-Oxide Level in Patients With Large-Artery Atherosclerotic Stroke or Transient Ischemic Attack. *J Am Heart Assoc* (2015) 4(11):e002699. doi: 10.1161/JAHA.115.002699
49. Haak BW, Westendorp WF, van Engelen TSR, Brands X, Brouwer MC, Vermeij J-D, et al. Disruptions of Anaerobic Gut Bacteria Are Associated With Stroke and Post-Stroke Infection: A Prospective Case-Control Study. *Trans Stroke Res* (2020) 11:110–12. doi: 10.1007/s12975-020-00863-4
50. Zeng X, Gao X, Peng Y, Wu Q, Zhu J, Tan C, et al. Higher Risk of Stroke is Correlated With Increased Opportunistic Pathogen Load and Reduced Levels of Butyrate-Producing Bacteria in the Gut. *Front Cell Infect Microbiol* (2019) 9:4. doi: 10.3389/fcimb.2019.00004
51. Nie J, Xie L, Zhao B-X, Li Y, Qiu B, Zhu F, et al. Serum Trimethylamine N-Oxide Concentration Is Positively Associated With First Stroke in Hypertensive Patients. *Stroke* (2018) 49(9):2021–8. doi: 10.1161/STROKEAHA.118.021997
52. Stanley D, Mason LJ, Mackin KE, Srikhanta YN, Lyras D, Prakash MD, et al. Translocation and Dissemination of Commensal Bacteria in Post-Stroke Infection. *Nat Med* (2016) 22(11):1277–84. doi: 10.1038/nm.4194
53. Spychala MS, Venna VR, Jandzinski M, Doran SJ, Durgan DJ, Ganesh BP, et al. Age-Related Changes in the Gut Microbiota Influence Systemic Inflammation and Stroke Outcome. *Ann Neurol* (2018) 84(1):23–36. doi: 10.1002/ana.25250
54. Singh V, Roth S, Llovera G, Sadler R, Garzetti D, Stecher B, et al. Microbiota Dysbiosis Controls the Neuroinflammatory Response After Stroke. *J Neurosci* (2016) 36(28):7428–40. doi: 10.1523/JNEUROSCI.1114-16.2016
55. Benakis C, Brea D, Caballero S, Faraco G, Moore J, Murphy M, et al. Commensal Microbiota Affects Ischemic Stroke Outcome by Regulating Intestinal Γδ T Cells. *Nat Med* (2016) 22(5):516–23. doi: 10.1038/nm.4068
56. Benakis C, Poon C, Lane D, Brea D, Sita G, Moore J, et al. Distinct Commensal Bacterial Signature in the Gut Is Associated With Acute and Long-Term Protection From Ischemic Stroke. *Stroke* (2020) 51(6):1844–54. doi: 10.1161/STROKEAHA.120.029262
57. Sadler R, Cramer JV, Heindl S, Kostidis S, Betz D, Zuurbier KR, et al. Short-Chain Fatty Acids Improve Poststroke Recovery *via* Immunological Mechanisms. *J Neurosci* (2020) 40(5):1162–73. doi: 10.1523/JNEUROSCI.1359-19.2019
58. Lee J, d'Aigle J, Atadja L, Quaicoe V, Honarpisheh P, Ganesh BP, et al. Gut Microbiota-Derived Short-Chain Fatty Acids Promote Poststroke Recovery in Aged Mice. *Circ Res* (2020) 127(4):453–65. doi: 10.1161/CIRCRESAHA.119.316448
59. Winek K, Engel O, Koduah P, Heimesaat MM, Fischer A, Bereswill S, et al. Depletion of Cultivatable Gut Microbiota by Broad-Spectrum Antibiotic

Pretreatment Worsens Outcome After Murine Stroke. *Stroke* (2016) 47 (5):1354–63. doi: 10.1161/STROKEAHA.115.011800
60. Xu DJ, Wang KC, Yuan LB, Li HF, Xu YY, Wei LY, et al. Compositional and Functional Alterations of Gut Microbiota in Patients With Stroke. *Nutr Metab Cardiovasc Dis* (2021) 31(12):3434–48. doi: 10.1016/j.numecd.2021.08.045
61. Ling Y, Gong T, Zhang J, Gu Q, Gao X, Weng X, et al. Gut Microbiome Signatures Are Biomarkers for Cognitive Impairment in Patients With Ischemic Stroke. *Front Aging Neurosci* 12:511562. doi: 10.3389/fnagi.2020.511562
62. Xiang L, Lou Y, Liu L, Liu Y, Zhang W, Deng J, et al. Gut Microbiotic Features Aiding the Diagnosis of Acute Ischemic Stroke. *Front Cell Infect Microbiol* (2020) 10:587284. doi: 10.3389/fcimb.2020.587284
63. Huang Y, Shen Z, He W. Identification of Gut Microbiome Signatures in Patients With Post-Stroke Cognitive Impairment and Affective Disorder. *Front Aging Neurosci* (2021) 13:706765. doi: 10.3389/fnagi.2021.706765
64. Xu K, Gao X, Xia G, Chen M, Zeng N, Wang S, et al. Rapid Gut Dysbiosis Induced by Stroke Exacerbates Brain Infarction in Turn. *Gut* (2021) 70:1486–94. doi: 10.1136/gutjnl-2020-323263
65. Jeon J, Lourenco J, Kaiser EE, Waters ES, Scheulin KM, Fang X, et al. Dynamic Changes in the Gut Microbiome at the Acute Stage of Ischemic Stroke in a Pig Model. *Front Neurosci* (2020) 14:587986. doi: 10.3389/fnins.2020.587986
66. Wu W, Sun Y, Luo N, Cheng C, Jiang C, Yu Q, et al. Integrated 16S Rrna Gene Sequencing and LC-MS Analysis Revealed the Interplay Between Gut Microbiota and Plasma Metabolites in Rats With Ischemic Stroke. *J Mol Neurosci* (2021) 71(10):2095–106. doi: 10.1007/s12031-021-01828-4
67. Tan C, Wu Q, Wang H, Gao X, Xu R, Cui Z, et al. Dysbiosis of Gut Microbiota and Short-Chain Fatty Acids in Acute Ischemic Stroke and the Subsequent Risk for Poor Functional Outcomes. *JPEN J Parenter Enteral Nutr* (2021) 45(3):518–29. doi: 10.1002/jpen.1861
68. Zhang J, Wang L, Cai J, Lei A, Liu C, Lin R, et al. Gut Microbial Metabolite TMAO Portends Prognosis in Acute Ischemic Stroke. *J Neuroimmunol* (2021) 354:577526. doi: 10.1016/j.jneuroim.2021.577526
69. Guo Q, Jiang X, Ni C, Li L, Chen L, Wang Y, et al. Gut Microbiota-Related Effects of Tanhuo Decoction in Acute Ischemic Stroke. *Oxid Med Cell Longev* (2021) 2021:5596924. doi: 10.1155/2021/5596924
70. Sun T, Zhang Y, Yin J, Peng X, Zhou L, Huang S, et al. Association of Gut Microbiota-Dependent Metabolite Trimethylamine N-Oxide With First Ischemic Stroke. *J Atheroscler Thromb* (2021) 28(4):320–8. doi: 10.5551/jat.55962
71. Huang Q, Di L, Yu F, Feng X, Liu Z, Wei M, et al. Alterations in the Gut Microbiome With Hemorrhagic Transformation in Experimental Stroke. *CNS Neurosci Ther* (2022) 28(1):77–91. doi: 10.1111/cns.13736
72. Zhang P, Zhang X, Huang Y, Chen J, Shang W, Shi G, et al. Atorvastatin Alleviates Microglia-Mediated Neuroinflammation *via* Modulating the Microbial Composition and the Intestinal Barrier Function in Ischemic Stroke Mice. *Free Radic Biol Med* (2021) 162:104–17. doi: 10.1016/j.freeradbiomed.2020.11.032
73. Huang JT, Mao YQ, Han B, Zhang ZY, Chen HL, Li ZM, et al. Calorie Restriction Conferred Improvement Effect on Long-Term Rehabilitation of Ischemic Stroke *via* Gut Microbiota. *Pharmacol Res* (2021) 170:105726. doi: 10.1016/j.phrs.2021.105726
74. Zhu W, Romano KA, Li L, Buffa JA, Sangwan N, Prakash P, et al. Gut Microbes Impact Stroke Severity *via* the Trimethylamine N-Oxide Pathway. *Cell Host Microbe* (2021) 29(7):1199–208. doi: 10.1016/j.chom.2021.05.002
75. Yuan Q, Xin L, Han S, Su Y, Wu R, Liu X, et al. Lactulose Improves Neurological Outcomes by Repressing Harmful Bacteria and Regulating Inflammatory Reactions in Mice After Stroke. *Front Cell Infect Microbiol* (2021) 11:644448. doi: 10.3389/fcimb.2021.644448
76. Li N, Wang X, Sun C, Wu X, Lu M, Si Y, et al. Change of Intestinal Microbiota in Cerebral Ischemic Stroke Patients. *BMC Microbiol* (2019) 19 (1):191–8. doi: 10.1186/s12866-019-1552-1
77. Sun J, Ling Z, Wang F, Chen W, Li H, Jin J, et al. Clostridium Butyricum Pretreatment Attenuates Cerebral Ischemia/Reperfusion Injury in Mice *via* Anti-Oxidation and Anti-Apoptosis. *Neurosci Lett* (2016) 613:30–5. doi: 10.1016/j.neulet.2015.12.047
78. Zhou Z, Xu N, Matei N, McBride DW, Ding Y, Liang H, et al. Sodium Butyrate Attenuated Neuronal Apoptosis *via* GPR41/Gbetagamma/PI3K/Akt Pathway After MCAO in Rats. *J Cereb Blood Flow Metab* (2021) 41 (2):267–81. doi: 10.1177/0271678X20910533
79. Yan H, Ajuwon KM. Butyrate Modifies Intestinal Barrier Function in IPEC-J2 Cells Through a Selective Upregulation of Tight Junction Proteins and Activation of the Akt Signaling Pathway. *PloS One* (2017) 12(6):e0179586. doi: 10.1371/journal.pone.0179586
80. Wu C, Li C, Zhao W, Xie N, Yan F, Lian Y, et al. Elevated Trimethylamine N-Oxide Related to Ischemic Brain Lesions After Carotid Artery Stenting. *Neurology* (2018) 90(15):e1283–90. doi: 10.1212/WNL.0000000000005298
81. Tan C, Wang H, Gao X, Xu R, Zeng X, Cui Z, et al. Dynamic Changes and Prognostic Value of Gut Microbiota-Dependent Trimethylamine-N-Oxide in Acute Ischemic Stroke. *Front Neurol* (2020) 11:2020.00029. doi: 10.3389/fneur.2020.00029
82. Farhangi MA, Vajdi M, Asghari-Jafarabadi M. Gut Microbiota-Associated Metabolite Trimethylamine N-Oxide and the Risk of Stroke: A Systematic Review and Dose-Response Meta-Analysis. *Nutr J* (2020) 19(1):76. doi: 10.1186/s12937-020-00592-2
83. Chen W-C, Chang L-H, Huang S-S, Huang Y-J, Chih C-L, Kuo H-C, et al. Aryl Hydrocarbon Receptor Modulates Stroke-Induced Astrogliosis and Neurogenesis in the Adult Mouse Brain. *J Neuroinflamm* (2019) 16 (1):187–13. doi: 10.1186/s12974-019-1572-7
84. Macdonald RL, Schweizer TA. Spontaneous Subarachnoid Haemorrhage. *Lancet* (2017) 389(10069):655–66. doi: 10.1016/S0140-6736(16)30668-7
85. Li H, Xu H, Li Y, Jiang Y, Hu Y, Liu T, et al. Alterations of Gut Microbiota Contribute to the Progression of Unruptured Intracranial Aneurysms. *Nat Commun* (2020) 11(1):3218. doi: 10.1038/s41467-020-16990-3
86. Kawabata S, Takagaki M, Nakamura H, Oki H, Motooka D, Nakamura S, et al. Dysbiosis of Gut Microbiome is Associated With Rupture of Cerebral Aneurysms. *Stroke* (2021), STROKEAHA121034792. doi: 10.1161/STROKEAHA.121.034792
87. Shikata F, Shimada K, Sato H, Ikedo T, Kuwabara A, Furukawa H, et al. Potential Influences of Gut Microbiota on the Formation of Intracranial Aneurysm. *Hypertension* (2019) 73(2):491–6. doi: 10.1161/HYPERTENSIONAHA.118.11804
88. Maas AIR, Menon DK, Adelson PD, Andelic N, Bell MJ, Belli A, et al. Traumatic Brain Injury: Integrated Approaches to Improve Prevention, Clinical Care, and Research. *Lancet Neurol* (2017) 16(12):987–1048. doi: 10.1016/S1474-4422(17)30371-X
89. Simon DW, Rogers MB, Gao Y, Vincent G, Firek BA, Janesko-Feldman K, et al. Depletion of Gut Microbiota Is Associated With Improved Neurologic Outcome Following Traumatic Brain Injury. *Brain Res* (2020) 1747:147056. doi: 10.1016/j.brainres.2020.147056
90. Mahajan C, Khurana S, Kapoor I, Sokhal S, Kumar S, Prabhakar H, et al. Characteristics of Gut Microbiome After Traumatic Brain Injury. *J Neurosurg Anesthesiol* (2021). doi: 10.1097/ANA.0000000000000789
91. Hou Y, Xu L, Song S, Fan W, Wu Q, Tong X, et al. Oral Administration of Brain Protein Combined With Probiotics Induces Immune Tolerance Through the Tryptophan Pathway. *Front Mol Neurosci* (2021) 14:634631. doi: 10.3389/fnmol.2021.634631
92. Treangen TJ, Wagner J, Burns MP, Villapol S. Traumatic Brain Injury in Mice Induces Acute Bacterial Dysbiosis Within the Fecal Microbiome. *Front Immunol* (2018) 9:2757. doi: 10.3389/fimmu.2018.02757
93. Li H, Sun J, Du J, Wang F, Fang R, Yu C, et al. Clostridium Butyricum Exerts a Neuroprotective Effect in a Mouse Model of Traumatic Brain Injury *via* the Gut-Brain Axis. *Neurogastroenterol Motil* (2018) 30(5):e13260. doi: 10.1111/nmo.13260
94. Angoa-Pérez M, Zagorac B, Anneken JH, Briggs DI, Winters AD, Greenberg JM, et al. Repetitive, Mild Traumatic Brain Injury Results in a Progressive White Matter Pathology, Cognitive Deterioration, and a Transient Gut Microbiota Dysbiosis. *Sci Rep* (2020) 10(1):8949. doi: 10.1038/s41598-020-65972-4
95. Opeyemi OM, Rogers MB, Firek BA, Janesko-Feldman K, Vagni V, Mullett SJ, et al. Sustained Dysbiosis and Decreased Fecal Short-Chain Fatty Acids After Traumatic Brain Injury and Impact on Neurologic Outcome. *J Neurotrauma* (2021) 38(18):2610–21. doi: 10.1089/neu.2020.7506

96. Du D, Tang W, Zhou C, Sun X, Wei Z, Zhong J, et al. Fecal Microbiota Transplantation Is a Promising Method to Restore Gut Microbiota Dysbiosis and Relieve Neurological Deficits After Traumatic Brain Injury. *Oxid Med Cell Longevity* (2021) 2021:5816837. doi: 10.1155/2021/5816837
97. You W, Zhu Y, Wei A, Du J, Wang Y, Zheng P, et al. Traumatic Brain Injury Induces Gastrointestinal Dysfunction and Dysbiosis of Gut Microbiota Accompanied by Alterations of Bile Acid Profile. *J Neurotrauma* (2021). doi: 10.1089/neu.2020.7526
98. Celorrio M, Abellanas MA, Rhodes J, Goodwin V, Moritz J, Vadivelu S, et al. Gut Microbial Dysbiosis After Traumatic Brain Injury Modulates the Immune Response and Impairs Neurogenesis. *Acta Neuropathol Commun* (2021) 9(1):40. doi: 10.1186/s40478-021-01137-2
99. Nicholson SE, Watts LT, Burmeister DM, Merrill D, Scroggins S, Zou Y, et al. Moderate Traumatic Brain Injury Alters the Gastrointestinal Microbiome in a Time-Dependent Manner. *Shock* (2019) 52(2):240–8. doi: 10.1097/SHK.0000000000001211
100. Blanke EN, Holmes GM, Besecker EM. Altered Physiology of Gastrointestinal Vagal Afferents Following Neurotrauma. *Neural Regener Res* (2021) 16(2):254–63. doi: 10.4103/1673-5374.290883
101. Hang C-H, Shi J-X, Li J-S, Li W-Q, Yin H-X. Up-Regulation of Intestinal Nuclear Factor Kappa B and Intercellular Adhesion Molecule-1 Following Traumatic Brain Injury in Rats. *World J Gastroenterol* (2005) 11(8):1149–54. doi: 10.3748/wjg.v11.i8.1149
102. Lu J, Frerich JM, Turtzo LC, Li S, Chiang J, Yang C, et al. Histone Deacetylase Inhibitors Are Neuroprotective and Preserve NGF-Mediated Cell Survival Following Traumatic Brain Injury. *Proc Natl Acad Sci United States America* (2013) 110(26):10747–52. doi: 10.1073/pnas.1308950110
103. Zhang X, Jiang X. Effects of Enteral Nutrition on the Barrier Function of the Intestinal Mucosa and Dopamine Receptor Expression in Rats With Traumatic Brain Injury. *JPEN J Parenter Enteral Nutr* (2015) 39(1):114–23. doi: 10.1177/0148607113501881
104. Wan G, Wang L, Zhang G, Zhang J, Lu Y, Li J, et al. Effects of Probiotics Combined With Early Enteral Nutrition on Endothelin-1 and C-Reactive Protein Levels and Prognosis in Patients With Severe Traumatic Brain Injury. *J Int Med Res* (2020) 48(3):300060519888112. doi: 10.1177/0300060519888112
105. Tan M, Zhu J-C, Du J, Zhang L-M, Yin H-H. Effects of Probiotics on Serum Levels of Th1/Th2 Cytokine and Clinical Outcomes in Severe Traumatic Brain-Injured Patients: A Prospective Randomized Pilot Study. *Crit Care (London England)* (2011) 15(6):R290–10. doi: 10.1186/cc10579
106. Bansal V, Costantini T, Ryu SY, Peterson C, Loomis W, Putnam J, et al. Stimulating the Central Nervous System to Prevent Intestinal Dysfunction After Traumatic Brain Injury. *J Trauma* (2010) 68(5):1059–64. doi: 10.1097/TA.0b013e3181d87373
107. Stothers L, Macnab AJ, Mukisa R, Mutabazi S, Bajunirwe F. Traumatic Spinal Cord Injury in Uganda: A Prevention Strategy and Mechanism to Improve Home Care. *Int J Epidemiol* (2017) 46(4):1086–90. doi: 10.1093/ije/dyx058
108. Gungor B, Adiguzel E, Gursel I, Yilmaz B, Gursel M. Intestinal Microbiota in Patients With Spinal Cord Injury. *PloS One* (2016) 11(1):e0145878. doi: 10.1371/journal.pone.0145878
109. Zhang C, Zhang W, Zhang J, Jing Y, Yang M, Du L, et al. Gut Microbiota Dysbiosis in Male Patients With Chronic Traumatic Complete Spinal Cord Injury. *J Trans Med* (2018) 16(1):353–16. doi: 10.1186/s12967-018-1735-9
110. Lin R, Xu J, Ma Q, Chen M, Wang L, Wen S, et al. Alterations in the Fecal Microbiota of Patients With Spinal Cord Injury. *PloS One* (2020) 15(8):e0236470. doi: 10.1371/journal.pone.0236470
111. Li J, van der Pol W, Eraslan M, McLain A, Cetin H, Cetin B, et al. Comparison of the Gut Microbiome Composition Among Individuals With Acute or Long-Standing Spinal Cord Injury vs. Able-Bodied Controls. *J Spinal Cord Med* (2020) 4:1–9. doi: 10.1080/10790268.2020.1769949
112. Bazzocchi G, Turroni S, Bulzamini MC, D'Amico F, Bava A, Castiglioni M, et al. Changes in Gut Microbiota in the Acute Phase After Spinal Cord Injury Correlate With Severity of the Lesion. *Sci Rep* (2021) 11(1):12743. doi: 10.1038/s41598-021-92027-z
113. Yu B, Qiu H, Cheng S, Ye F, Li J, Chen S, et al. Profile of Gut Microbiota in Patients With Traumatic Thoracic Spinal Cord Injury and Its Clinical Implications: A Case-Control Study in a Rehabilitation Setting. *Bioengineered* (2021) 12(1):4489–99. doi: 10.1080/21655979.2021.1955543
114. O'Connor G, Jeffrey E, Madorma D, Marcillo A, Abreu MT, Deo SK, et al. Investigation of Microbiota Alterations and Intestinal Inflammation Post-Spinal Cord Injury in Rat Model. *J Neurotrauma* (2018) 35(18):2159–66. doi: 10.1089/neu.2017.5349
115. Myers SA, Gobejishvili L, Saraswat Ohri S, Garrett Wilson C, Andres KR, Riegler AS, et al. Following Spinal Cord Injury, PDE4B Drives an Acute, Local Inflammatory Response and a Chronic, Systemic Response Exacerbated by Gut Dysbiosis and Endotoxemia. *Neurobiol Dis* (2019) 124:353–63. doi: 10.1016/j.nbd.2018.12.008
116. Jing Y, Yang D, Bai F, Zhang C, Qin C, Li D, et al. Melatonin Treatment Alleviates Spinal Cord Injury-Induced Gut Dysbiosis in Mice. *J Neurotrauma* (2019) 36(18):2646–64. doi: 10.1089/neu.2018.6012
117. Schmidt EKA, Torres-Espin A, Raposo PJF, Madsen KL, Kigerl KA, Popovich PG, et al. Fecal Transplant Prevents Gut Dysbiosis and Anxiety-Like Behaviour After Spinal Cord Injury in. *PloS One* (2020) 15(1):e0226128. doi: 10.1371/journal.pone.0226128
118. Jing Y, Yu Y, Bai F, Wang L, Yang D, Zhang C, et al. Effect of Fecal Microbiota Transplantation on Neurological Restoration in a Spinal Cord Injury Mouse Model: Involvement of Brain-Gut Axis. *Microbiome* (2021) 9(1):59–21. doi: 10.1186/s40168-021-01007-y
119. Schmidt EKA, Raposo PJF, Torres-Espin A, Fenrich KK, Fouad K. Beyond the Lesion Site: Minocycline Augments Inflammation and Anxiety-Like Behavior Following SCI in Rats Through Action on the Gut Microbiota. *J Neuroinflammation* (2021) 18(1):144. doi: 10.1186/s12974-021-02123-0
120. Doelman A, Tigchelaar S, McConeghy B, Sinha S, Keung MS, Manouchehri N, et al. Characterization of the Gut Microbiome in a Porcine Model of Thoracic Spinal Cord Injury. *BMC Genomics* (2021) 22(1):775. doi: 10.1186/s12864-021-07979-3
121. Rong Z, Huang Y, Cai H, Chen M, Wang H, Liu G, et al. Gut Microbiota Disorders Promote Inflammation and Aggravate Spinal Cord Injury Through the TLR4/Myd88 Signaling Pathway. *Front Nutr* (2021) 8:702659. doi: 10.3389/fnut.2021.702659
122. Du J, Zayed AA, Kigerl KA, Zane K, Sullivan MB, Popovich PG. Spinal Cord Injury Changes the Structure and Functional Potential of Gut Bacterial and Viral Communities. *mSystems* (2021) 6(3):e01356–20. doi: 10.1128/mSystems.01356-20
123. Kigerl KA, Zane K, Adams K, Sullivan MB, Popovich PG. The Spinal Cord-Gut-Immune Axis as a Master Regulator of Health and Neurological Function After Spinal Cord Injury. *Exp Neurol* (2020) 323:113085. doi: 10.1016/j.expneurol.2019.113085
124. Sun G, Yang S, Cao G, Wang Q, Hao J, Wen Q, et al. Γδ T Cells Provide the Early Source of IFN-Γ to Aggravate Lesions in Spinal Cord Injury. *J Exp Med* (2018) 215(2):521–35. doi: 10.1084/jem.20170686
125. Kigerl KA, Mostacada K, Popovich PG. Gut Microbiota are Disease-Modifying Factors After Traumatic Spinal Cord Injury. *Neurotherapeutics* (2018) 15(1):60–7. doi: 10.1007/s13311-017-0583-2
126. Wang X, Wu J, Liu X, Tang K, Cheng L, Li J, et al. Engineered Liposomes Targeting the Gut-CNS Axis for Comprehensive Therapy of Spinal Cord Injury. *J Control Release* (2021) 331:390–403. doi: 10.1016/j.jconrel.2021.01.032
127. Ley RE, Bäckhed F, Turnbaugh P, Lozupone CA, Knight RD, Gordon JI. Obesity Alters Gut Microbial Ecology. *Proc Natl Acad Sci USA* (2005) 102(31):11070–5. doi: 10.1073/pnas.0504978102
128. Mann ER, Landy JD, Bernardo D, Peake STC, Hart AL, Al-Hassi HO, et al. Intestinal Dendritic Cells: Their Role in Intestinal Inflammation, Manipulation by the Gut Microbiota and Differences Between Mice and Men. *Immunol Lett* (2013) 150(1-2):30–40. doi: 10.1016/j.imlet.2013.01.007
129. De Paepe M, Leclerc M, Tinsley CR, Petit M-A. Bacteriophages: An Underestimated Role in Human and Animal Health? *Front Cell Infect Microbiol* (2014) 4:39. doi: 10.3389/fcimb.2014.00039
130. Sommer F, Bäckhed F. The Gut Microbiota–Masters of Host Development and Physiology. *Nat Rev Microbiol* (2013) 11(4):227–38. doi: 10.1038/nrmicro2974
131. Macpherson AJ, Harris NL. Interactions Between Commensal Intestinal Bacteria and the Immune System. *Nat Rev Immunol* (2004) 4(6):478–85. doi: 10.1038/nri1373

132. Erny D, Hrabě de Angelis AL, Jaitin D, Wieghofer P, Staszewski O, David E, et al. Host Microbiota Constantly Control Maturation and Function of Microglia in the CNS. *Nat Neurosci* (2015) 18(7):965–77. doi: 10.1038/nn.4030
133. Braniste V, Al-Asmakh M, Kowal C, Anuar F, Abbaspour A, Tóth M, et al. The Gut Microbiota Influences Blood-Brain Barrier Permeability in Mice. *Sci Transl Med* (2014) 6(263):263ra158–263ra158. doi: 10.1126/scitranslmed.3009759

Conflict of Interest: The authors declare that the research was conducted in the absence of any commercial or financial relationships that could be construed as a potential conflict of interest.

Publisher's Note: All claims expressed in this article are solely those of the authors and do not necessarily represent those of their affiliated organizations, or those of the publisher, the editors and the reviewers. Any product that may be evaluated in this article, or claim that may be made by its manufacturer, is not guaranteed or endorsed by the publisher.

Copyright © 2021 Yuan, Lu and Wu. This is an open-access article distributed under the terms of the Creative Commons Attribution License (CC BY). The use, distribution or reproduction in other forums is permitted, provided the original author(s) and the copyright owner(s) are credited and that the original publication in this journal is cited, in accordance with accepted academic practice. No use, distribution or reproduction is permitted which does not comply with these terms.

frontiers in Immunology

ORIGINAL RESEARCH
published: 03 January 2022
doi: 10.3389/fimmu.2021.791780

Disturbance of Gut Bacteria and Metabolites Are Associated with Disease Severity and Predict Outcome of NMDAR Encephalitis: A Prospective Case–Control Study

Xue Gong[1,2,3], *Yue Liu*[1,2,3], *Xu Liu*[1,2,3], *Aiqing Li*[1,2,3], *Kundian Guo*[1,2,3], *Dong Zhou*[1,2] *and Zhen Hong*[1,2,3*]

[1] Department of Neurology, West China Hospital, Sichuan University, Chengdu, China, [2] Institute of Brain Science and Brain-Inspired Technology of West China Hospital, Sichuan University, Chengdu, China, [3] Department of Neurology, Chengdu Shangjin Nanfu Hospital, Chengdu, China

OPEN ACCESS

Edited by:
Alina Maria Holban, University of Bucharest, Romania

Reviewed by:
Choong-Kyun Noh, Ajou University, South Korea
Xu Zhang, Health Canada, Canada

***Correspondence:**
Zhen Hong
hongzhengoog@aliyun.com

Specialty section:
This article was submitted to Microbial Immunology, a section of the journal Frontiers in Immunology

Received: *09 October 2021*
Accepted: *02 December 2021*
Published: *03 January 2022*

Citation:
Gong X, Liu Y, Liu X, Li A, Guo K, Zhou D and Hong Z (2022) Disturbance of Gut Bacteria and Metabolites Are Associated with Disease Severity and Predict Outcome of NMDAR Encephalitis: A Prospective Case–Control Study. Front. Immunol. 12:791780. doi: 10.3389/fimmu.2021.791780

Objective: We aimed to investigate the associations between the intestinal microbiota, metabolites, cytokines, and clinical severity in anti-*N*-methyl-D-aspartate receptor (NMDAR) encephalitis and to further determine the predictive value of the intestinal microbiota or metabolites in clinical prognosis.

Methods: In this prospective observational cohort study of 58 NMDAR encephalitis patients and 49 healthy controls, fecal microbiota, metabolites, and cytokines were quantified and characterized by16S rRNA gene sequencing, liquid chromatography–mass spectrometry, and the Luminex assay, respectively.

Results: There were marked variations in the gut microbiota composition and metabolites in critically ill patients. We identified 8 metabolite modules (mainly characterized by fatty acid, glycerophosphoethanolamines, and glycerophosphocholines) that were distinctly classified as negatively or positively associated with bacterial co-abundance groups (CAGs). These CAGs were mainly composed of *Bacteroides*, *Eubacterium_hallii_group*, *Anaerostipes*, *Ruminococcus*, *Butyricicoccus*, and *Faecalibacterium*, which were substantially altered in patients. In addition, these fecal and serum metabolic modules were further correlated with the serum cytokines. Additionally, the combination of clinical features, microbial marker (*Granulicatella*), and a panel of metabolic markers could further enhance the performance of prognosis discrimination significantly, which yielded an area under the receiver operating characteristic curve of (AUC) of 0.94 (95%CI = 0.7–0.9). Patients with low bacterial diversity are more likely to develop relapse than those with higher bacterial diversity (log-rank $p = 0.04$, HR = 2.7, 95%CI = 1.0–7.0).

Interpretation: The associations between the multi-omics data suggested that certain bacteria might affect the pathogenesis of NMDAR encephalitis by modulating the metabolic pathways of the host and affecting the production of pro-inflammatory

cytokines. Furthermore, the disturbance of fecal bacteria may predict the long-term outcome and relapse in NMDAR encephalitis.

Keywords: NMDAR encephalitis, microbiome, metabolomics, prognosis marker, multi-omic analysis

1 INTRODUCTION

Anti-*N*-methyl-D-aspartate receptor (NMDAR) encephalitis is the most prevalent and severe autoimmune encephalitis type, with significant economic burden (1, 2). Nearly 75% of patients may require care in the intensive care unit, and 20%–25% of cases may have poor prognosis or further relapse (3, 4). However, there are no biomarkers to inform therapy or predict outcomes. Despite some clinical signs (including orofacial dyskinesia and central hypoventilation) (3), higher antibody titers in the cerebrospinal fluid (5), increased cytokines (CXCL13, TNF-α, IL-6, or IL-10) (6, 7), or abnormal MRI (8, 9) suggesting potential associations with poor clinical outcomes, these associations were weak and need longitudinal assessments. Thus, biomarkers are still urgently needed for the prediction of disease prognosis and evaluation of disease severity in NMDAR encephalitis.

The microbiota could modulate the host immune response and affect the secretion of cytokines and antibodies (10–13). It has been reported that dysbiotic microbiota is involved in the pathogenesis of various antibody-mediated diseases such as multiple sclerosis, neuromyelitis optica, Guillain–Barré syndrome, and systemic lupus erythematosus (14–17). One leading hypothesis is that molecular mimicry leads to cross-reactivity (18, 19) and, in turn, to autoimmune attack. In our prior study, an increase of pro-inflammatory fecal bacteria was also observed in NMDAR encephalitis patients with several relapses (20). In addition, *via* fecal transplantation, one study reported that transplantation of the "NMDAR encephalitis microbiota" into specific pathogen-free (SPF) mice can induce abnormal behaviors and T helper 17 (Th17) response (21). Taken together, these studies have provided initial proof that microbial dysbiosis or imbalance may potentially contribute to the onset of this disorder.

Metabolomics is a new method for elucidating the pathomechanisms and biomarkers and for assessing the environmental impact of a disease. Metabolome (serum and fecal) also represent end products from microbial metabolism, and they are functionally more important when compared to specific bacterial species (22, 23). Therefore, exploring links between the microbiota and metabolic and immune function may reveal new insights into disease etiology and pathophysiology. However, as far as we know, no data are currently available for investigating the molecular mediators of the effects of the microbiota on NMDAR encephalitis. Furthermore, research on whether altered microbiota and metabolites are associated with or could predict the risk of susceptibility to severe status and worse outcomes in NMDAR encephalitis has not been determined yet.

Herein, for the first time, we present a comprehensive comparison of the intestinal microbiota and systemic metabolomes from a large and prospective cohort of 107 individuals. We first established the features of the gut microbiota and the host metabolite profiles that are correlated with disease severity. We then integrated extensive multilevel omics findings to elucidate the gut microbial ecosystem, and its significance, in NMDAR encephalitis. In addition, the predictive value of the intestinal microbiota or metabolites in the clinical prognosis of NMDAR encephalitis was revealed.

2 METHODS

2.1 Study Design and Human Participants

Figure 1 depicts the overall design of the study. Briefly, fecal specimens from a prospective cohort of 58 treatment-naive NMDAR encephalitis patients and 49 household healthy controls (HCs) were evaluated using high-throughput 16S ribosomal DNA (rDNA) gene sequencing and untargeted metabolomics. Serum samples were collected from a subset of these same NMDAR encephalitis patients (n = 39) and HC individuals (n = 31) for untargeted metabolic and cytokine study. All patients were followed for at least 6 months, after which the fecal and serum samples of 30 patients were collected at the remission phase.

All participants in this study were enrolled between December 2019 and March 2021 from West China Hospital of Sichuan University, in which treatment-naive patients with unknown triggers at initial onset (n = 58) had been diagnosed based on the definitions of NMDAR encephalitis from a recent consensus statement (1). The detailed diagnostic criteria of NMDAR encephalitis patients are summarized in *eMethods* in the *Electronic Supplementary Material* (ESM). We included spouse (n = 30), sibling (n = 14), or parents (n = 5) as controls free from neurological disorders living within the same community and sharing a similar diet for at least 5 years (to minimize the potential effects of confounding by factors, including diet, housing conditions, and lifestyle) (24, 25).

The exclusion criteria for HCs and patients were: 1) patients with identified trigger for disease (tumor or herpes simplex virus encephalitis); 2) participants who received treatment with any immunotherapies (steroids, immunoglobulin, cyclophosphamide, rituximab, or plasma exchange); 3) participants who received antibiotics or probiotics, or prebiotics within 1 month before sampling; 4) participants who experienced marked bloating, abdominal pain, diarrhea, or infections of the respiratory tract in the previous month; 5) alcohol or any other substance (apart from tobacco) dependence or abuse within 3 months before enrollment; 6) participants with chronic diseases such as hypertension and diabetes; 7) history of other autoimmune diseases (systemic lupus erythematosus,

rheumatoid arthritis, type 1 diabetes, etc.); 8) history of bowel surgery; 9) lactation or pregnancy; and 10) any history of neuropsychiatric disorders, such as depression, schizophrenia, anxiety, or multiple sclerosis.

This study was conducted in accordance with the Declaration of Helsinki and was granted permission by the Institutional Review Boards of the Ethics Committee of West China Hospital of Sichuan University. Prior to their enrolment, all participants provided informed consent (registration no. ChiCTR2100042215; Chinese Clinical Trial Registry, http://www.chictr.org). The patient cohort included in this study was independent from our previous cohorts (20).

2.2 Clinical Evaluations and Follow-Up Assessment

Participants were subjected to various clinical evaluations, such as medical history, physical and neurological examinations, laboratory assessments, and neuropsychological tests. All clinical information [demographic, medical, follow-up, and body mass index (BMI) data] was collected according to standard procedures (see details in *eMethods* in ESM). Assessment of dietary intake was done using a locally validated Food Frequency Questionnaire (FFQ) including 136 food items and analyzed by a competent nutritionist, as previously reported (20, 26).

The modified Rankin scale (mRS) score was employed to assess disease severity and outcome grading of NMDAR encephalitis. The initial severity status was classified according to mRS scores of moderate (0–3) and severe (4–5). The respective definitions of long-term favorable or poor functional outcomes were as follows: mRS score of ≤2 and mRS score of >2 at 6 months after admission (27–29). Patients were routinely followed up every 2 months for up to at least 6 months. The primary outcome was the long-term outcome. The secondary end point was clinical relapse, which was defined as a new symptomatic onset or worsening after an initial stabilization or improvement for ≥2 months (1).

2.3 Specimen Collection and Quality Control

Determination of the sample sizes was based on previous studies (20). The participants were given a written protocol for stool collection (to avoid contamination of the sample) and transportation. Briefly, disposable sterile potty and tubes were distributed to participants in advance. Firstly, participants discharged their feces into the sterile potty, washed their hands, wore disposable gloves, took the middle part of the feces, instantly put them on ice, and transported the sample to the laboratory, where it was stored it at −80°C within 1–2 h after sample collection.

Serum samples were collected from patients who consented to participate in the study. For each participant, one 6-ml overnight fasting peripheral blood sample was obtained in the morning of the day after admission. Blood was centrifuged at room temperature for 10 min at 3,000 × *g*, then the serum was collected, and 1–2 ml aliquots were transferred into pre-labeled cryovials. Within 1 h of collection, the samples were kept at −20°C for 24 h for freezing and then stored at −80°C for further analyses.

2.4 DNA Extraction, Amplification, and Sequencing

Fecal samples stored at −80°C were used in this assay, which was performed at Majorbio BioPharm Technology Co., Ltd. (Shanghai, China). Extraction of microbial DNA from fecal samples was conducted using the E.Z.N.A.® Soil DNA Kit (Omega Bio-Tek, Norcross, GA, USA) as described by the manufacturer. The final DNA concentrations were determined with a NanoDrop 2000 UV–vis spectrophotometer (Thermo Scientific, Wilmington, DE, USA), while DNA quality was evaluated with 1% agarose gel electrophoresis. Specific primers (806 R: 5′-GGACTACHVGGGTWTCTAAT-3′; 338 F: 5′-ACTCCTACGGGAGGCAGCAG-3′) were used to amplify the V3–V4 hypervariable regions of the bacterial 16S rRNA gene *via* a thermocycler PCR system (GeneAmp 9700; ABI, Foster City, CA, USA). The PCR conditions were as follows: 3 min of denaturation at 95°C, 27 cycles at 95°C for 30 s, annealing at 55°C for 30 s, elongation for 45 s at 72°C, and a final extension for 10 min at 72°C. The PCR assays were conducted in triplicate in a 20-μl mixture of 4 μl 5× FastPfu Buffer, 2.5 mmol/L dNTPs (2 μl), 0.8 μl of each primer (5 μmol/L), FastPfu polymerase (0.4 μl), and template DNA (10 ng). Extraction of the PCR products was done on 2% agarose gel, purified using a AxyPrep DNA Gel Extraction Kit (Axygen Biosciences, Union City, CA, USA) and quantified using QuantiFluor™-ST (Promega, Madison, WI, USA) as described by the respective manufacturers. Amplicons (purified) were pooled in equimolar, followed by paired-end sequencing (2 × 300) on an Illumina MiSeq system (Illumina, San Diego, CA, USA).

2.5 Processing of Sequencing Data

This procedure was conducted at Majorbio Bio-Pharm Technology Co., Ltd. (Shanghai, China). Raw fastq files were demultiplexed, filtered by Trimmomatic for quality, followed by merging by FLASH as described previously (30, 31). Details related to the processing of sequencing data can be found in *eMethods* in ESM.

2.6 Untargeted Metabolomics Analyses

Fecal samples (50 mg) and serum samples (100 μl) were spiked with 40 μl of a methanol/water (4:1, *v*/*v*) solution (Merck, Darmstadt, Germany) and extracted as described by the manufacturer (Majorbio Bio-Pharm Technology Co., Ltd., Shanghai, China). The extracted samples were evaluated by liquid chromatography–mass spectrometry (LC-MS) (Shimadzu, Tokyo, Japan). Aliquots from all extracted samples were pooled to form a quality control (QC) sample, which was analyzed as done for the analytical samples (*eMethods* in ESM).

2.7 Inflammatory Biomarker Assays

The concentrations of serum cytokines (CCL4, IFN-α, IFN-γ, IL-1β, IL-7, IFN-β, IL-1ra, IL-10, IL-4, IL-6, IL-8, IL-12 p40, IL-18, IL-17, and TNF-α) were analyzed employing xMAPtechnology

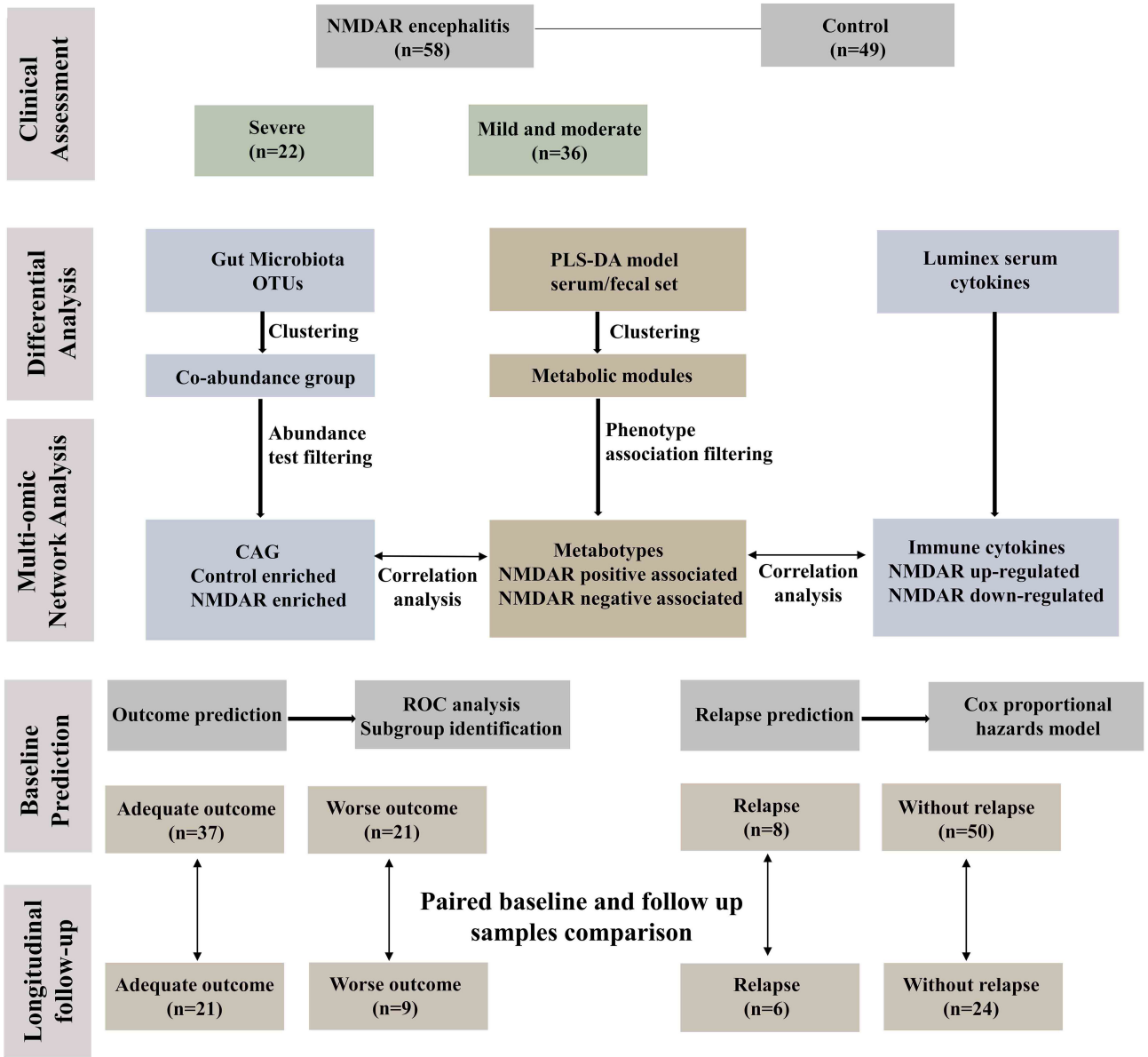


FIGURE 1 | Workflow integrating anti-*N*-methyl-D-aspartate receptor (NMDAR) encephalitis gut microbiome, fecal and serum metabolomes, and cytokines. Fifty-eight patients with a definite diagnosis of NMDAR encephalitis were divided into different severity groups: severe (n = 22) and moderate (n = 36); there were 49 healthy controls. We next constructed a co-abundance network with 294 operational taxonomic units (OTUs) and clustered them into 19 co-abundance groups (CAGs). Subsequently, we identified the important CAGs that were strikingly prevalent in patients with more severe status. We then identified the serum and fecal metabolome and cytokine features between NMDAR encephalitis patients and healthy controls. Serum and fecal metabolites were summarized as co-abundance metabolic modules. Next, we identified the relationships between the markedly altered gut microbiome composition, host metabolic profiles, and the major dysregulated cytokines. Finally, fecal and serum samples from 30 patients after 6 months of follow-up were collected to investigate longitudinal deviations in dysbiosis and establish associations between disease outcome markers and dysbiosis.

(LXSAHM-20, R&D Systems Inc., Minneapolis, MN, USA; HGAMMAG-301K-03, Merck Millipore, Burlington, MA, USA). Detailed method can be found in *eMethods* in ESM.

2.8 Statistical Analysis

Data are shown as the mean ± SEM. Differences in the clinical features between groups were evaluated using *t*-tests, chi-square, and Mann–Whitney *U* test in SPSS version 20.0. Differences among groups were analyzed by one-way ANOVA with Tukey's test or false discovery rate (FDR) correction. The cutoff for significance was $p \leq 0.05$. Differential abundance of the microbial taxa and LC-MS-based metabolites were determined by negative binomial distribution and the Wald test (1.0 was the threshold for log fold change). Microbial taxa whose sequences

were <1,000 and present in <20% of the whole cohort were filtered. Microbial and metabolite characteristics with FDR-adjusted $p < 0.01$ were considered significant. Effect sizes were assessed by comparisons of the fold changes. Identification of co-abundant metabolite clusters was done using "WGCNA21" in R, along with official tutorials (https://horvath.genetics.ucla.edu). Associations between specific metabolites, microbial, predicted pathways, and clinical variables in the NMDAR encephalitis patient subgroup were determined by correlation network analysis with a >1 threshold for the correlation coefficient (based on Spearman's rank correlation) and FDR-adjusted $p < 0.05$ (using the Benjamini–Hochberg procedure). Finally, potential microbiota-dependent predictors of outcomes were assessed by age, gender, and the NEOS score, which is known to be a predictor of the 1-year functional status of NMDAR encephalitis patients (28, 32). We analyzed time to relapse with the Cox proportional hazards model, including the alpha diversity index as a factor, and provided the results as hazard ratios (HRs) with 95% confidence intervals (CIs).

3 RESULTS

3.1 Demographic and Clinical Features of the Recruited Subjects

Fifty-eight patients with NMDAR encephalitis (mean age = 34.4 years, SEM = 1.8), among whom 36 patients had mRS scores of 2–3 (mean age = 35.3 years, SEM = 2.2), 22 patients had mRS scores of 4–5 (mean age = 33.1 years, SEM = 3.0), and 49 were HCs (mean age = 32.0 years, SEM = 1.5), were enrolled. The detailed demographics of the participants are shown in **Table 1**. The differences in age, female-to-male ratios, BMI, and nutritional factors among all of the groups were not significant. In addition, no obvious effect of sex and age on the gut microbiome structures was observed in this cohort (analysis of similarities: $p > 0.05$; **Supplementary Figure S1**).

3.2 Fecal Microbiota Are Significantly Different in the Severe Disease Group

We sequenced fecal 16S rRNA genes in V3–V4 regions to evaluate variations in the gut microbiome in NMDAR encephalitis subgroups. Differences in the diversity of the gut microbiota between patients in the moderate status and HC groups were not significant. However, the severe group exhibited significantly lower values of the Chao1 (310 ± 78 vs. 345 ± 89, $p = 0.04$; **Figure 2A**) and Shannon (2.6 ± 0.8 vs. 3.1 ± 0.6, $p = 0.006$; **Figure 2B**) indices than those of HCs. Then, a score plot of the principal coordinate analysis (PCoA) based on unweighted UniFrac distances was built to evaluate the gut microbiota structure. The microbial structure and composition markedly varied between patients with different severity grades and HCs ($R = 0.12$, $p = 0.002$; **Figure 2C**).

Since bacteria form functional groups in the gut, we constructed a co-abundance network, whereby 294 operational taxonomic units (OTUs) were shared by ≥20% of samples based on SparCC correlation coefficients, and clustered the OTUs into 19 CAGs. Among them, CAG6 and CAG12 decreased and CAG11 increased markedly in patients in the group with more severe disease relative to patients with moderate status and to HCs (Wilcoxon rank-sum test: $p < 0.05$; **Figure 2D**). Among the OTUs in these CAGs depleted in the severe group, 80% belonged to *Bacteroides*, *Eubacterium_hallii_group*, *Anaerostipes*, *Megamonas*, *Ruminococcus*, *Butyricicoccus*, and *Faecalibacterium*, the members of which may alleviate inflammation. On the other hand, CAG11 comprised *Enterococcus*, *Oscillospirales*, *Fusicatenibacter*, and *Sellimonas*, which are opportunistic pathogens or pathogens (33) (**Figure 2E**).

We then determined the log of [abundance in microbes increased in NMDAR encephalitis] over [abundance of microbes decreased in NMDAR encephalitis] for all samples, defined as the microbial dysbiosis index (MD-index) (34). The MD-index, which was disease phenotype-based, revealed strong positive correlations with disease severity (mRS score, $p < 0.0001$; **Figure 3A**) and negative associations with species richness ($p < 0.0001$; **Figure 3B**), implying that a severe disease status exhibits a markedly reduced species diversity, with a preference for extreme dysbiosis. Moreover, this index captured the overall beta diversity, resulting in a clear gradient by which samples grouped across all sample types (**Figure 3C**).

3.3 Metabonomics of the Fecal and Serum Specimens From NMDAR Encephalitis Patients Are Distinct From Those of Controls

All 107 participants were enrolled in the fecal metabonomic study, and a subset of 70 participants (39 patients with NMDAR encephalitis and 31 HCs) from this study was included in the serum metabonomic study. Identification of the differentially enriched metabolites that were significant was based on a variable importance in projection (VIP) threshold >1 and $p < 0.05$. Overall, 298 known fecal metabolites, 158 elevated and 140 suppressed, were identified in patients relative to HCs, which were visualized in a volcano plot (see **Supplementary Figure S2A**). The top priority metabolites identified were L-carnitine, samin, lysophosphatidic acid (lysoPA, a-25:0/0:0), and phenylalanyl-lysine, among others (see **Supplementary Figure S2B**). For the serum samples, 378 known metabolites, 58 elevated and 320 suppressed, separated patients with NMDAR encephalitis from normal controls (**Supplementary Figure S2C**). The top serum metabolites included 2-deoxy-D-gluconate, theophylline, and guanosine (**Supplementary Figure S2D**).

The partial least squares discriminant analysis (PLS-DA) plot showed the global fecal metabolic changes in NMDAR encephalitis patients and HCs (**Figure 4A**). A separation between patients with different disease severity status and HCs was also obtained with the PLS-DA method (**Figure 4B**). The serum data recapitulated the distinction, classifying the patients into different severity grading and HC groups (**Figures 4C, D**). However, the Q2 values (**Figure 4B**) for all the comparisons were low or negative, which means that the statistical model may not be reliable. Thus, in this study, NMDAR encephalitis patients did not show significantly different metabolite profiles relative to

TABLE 1 | Extrinsic host factor profile including diet, stool consistency, and lifestyle in anti-*N*-methyl-D-aspartate receptor (NMDAR) encephalitis patients and control individuals.

	NMDAR Encephalitis	Control	*p*-value
No. of patients	58	49	
Sex (F/M)	36/22	31/18	0.9[b]
Age (years), mean (SEM)	34.4 (1.8)	32.0 (1.5)	0.4[c]
Initial presentation			
Psychogenic, *n* (%)	28 (48.3)	0	
Seizure, *n* (%)	15 (25.8)	0	
Other, *n* (%)	15 (25.8)	0	
MRI, abnormality, *n* (%)	30 (51.7)	0	
EEG, abnormality, *n* (%)	40 (68.9)	0	
CSF, abnormality, *n* (%)	29 (50)	0	
ICU admission, *n* (%)	14 (24.1)	0	
NEOS score, median (IQR)	2 (1–3)	0	
Gastrointestinal distress			0.4[b]
Frequently, *n* (%)	4 (6.8)	1 (2.0)	
Occasionally, *n* (%)	16 (27.5)	13 (26.5)	
None, *n* (%)	38 (65.5)	35 (71.4)	
Diarrhea (nearly 3 months)	7 (12.0)	5 (10.2)	0.7[b]
Defecation frequency			0.001[b]
3 times/day, *n* (%)	6 (10.3)	1 (2.0)	
1–2 times/day, *n* (%)	21 (36.2)	31 (42.8)	
Once/2 days, *n* (%)	15 (25.8)	17 (34.7)	
Once/3 days, *n* (%)	16 (27.6)	0 (0)	
Defecation consistency[a]			0.1[b]
Separate, hard lumps	2 (3.5)	0 (0)	
Lumpy, sausage-shaped	5 (8.6)	2 (4.1)	
Sausage-shaped with cracks	8 (13.8)	4 (8.1)	
Smooth and soft	32 (55.2)	28 (57.1)	
Soft with edges	9 (15.5)	15 (30.6)	
Mushy with ragged edges	2 (3.4)	0 (0)	
Liquid	0 (0)	0 (0)	
Dietary intake, median (IQR)			
Energy	1,827.2 (784.1–1988.2)	2,492.6 (802.4–2,691.1)	<0.001[d]
Protein	73.1 (57.7–99.3)	93.7 (69.4–125.7)	0.01[d]
Fat	71.2 (32.8–108.4)	82.2 (67.4–132.0)	0.05[d]
Fiber	18.5 (9.9–32.6)	23.9 (14.2–31.3)	0.2[d]
Carbohydrate	232.9 (158.1–294.6)	304.7 (219.4–479.5)	<0.001[d]
Cholesterol	128.3 (76.7–243.0)	164.6 (109.7–270.8)	0.5[d]
Retinol equivalent	818.3 (336.1–1,333.3)	1,053.0 (694.8–1,368.0)	0.5[d]
Vitamin B1 (mg)	1.3 (0.9–1.9)	1.5 (1.0–2.3)	0.3[d]
Vitamin B2 (mg)	1.4 (0.7–2.5)	1.3 (1.1–1.9)	0.6[d]
Vitamin B12 (μg)	0.44 (0.3–0.0)	0.34 (0.30–0.91)	0.2[d]
Folvite (μg)	450.8 (290.3–478.2)	473.9 (106.1–500.1)	0.7[d]
Vitamin E (mg)	36.0 (16.9–61.3)	49.6 (40.1–78.4)	0.1[d]
Vitamin C (mg)	166.1 (62.9–274.9)	211.9 (136.7–275.1)	0.5[d]
Na (mg)	3,284.8 (928.3–7250.7)	5,024.4 (3,585.5–7,265.2)	0.1[d]
Ca (mg)	672.9 (217.9–1290.2)	876.1 (620.5–1,135.0)	0.2[d]
Fe (mg)	28.0 (17.3–44.3)	35.1 (25.3–49.3)	0.08[d]
I (mg)	3.0 (1.9–3.4)	2.9 (0.7–3.2)	0.7[d]

Measurement data are expressed as the median (IQR). NEOS score, delayed treatment, improvement delay, abnormal CSF and MRI were strongly associated with the probability of poor functional status.

IQR, interquartile range; MRI, magnetic resonance imaging; EEG, electroencephalogram; CSF, cerebrospinal fluid; ICU, intensive care unit; NEOS score, anti-NMDAR encephalitis one-year functional status score

[a]*Defecation consistency was assessed by type 4 Bristol stool scale.*

[b]χ^2 *test.*

[c]*Student's t-test.*

[d]*Mann–Whitney U test.*

HCs. In addition, the metabolite levels did not shift with disease severity.

Sub-pathways shared by metabolites provide meaningful groups and are vital for elucidation of disease mechanisms. In multivariate models controlling for three potential confounders, namely, age, sex, and BMI, we identified 277 differential fecal metabolites across 51 sub-pathways and 12 super-pathways. Similarly, for serum, we identified 221 differential metabolites across 47 sub-pathways and 9 super-pathways. **Figures 5A, B** illustrate the fecal and serum metabolites with the highest variations in abundance between the disease cases and HCs, respectively.

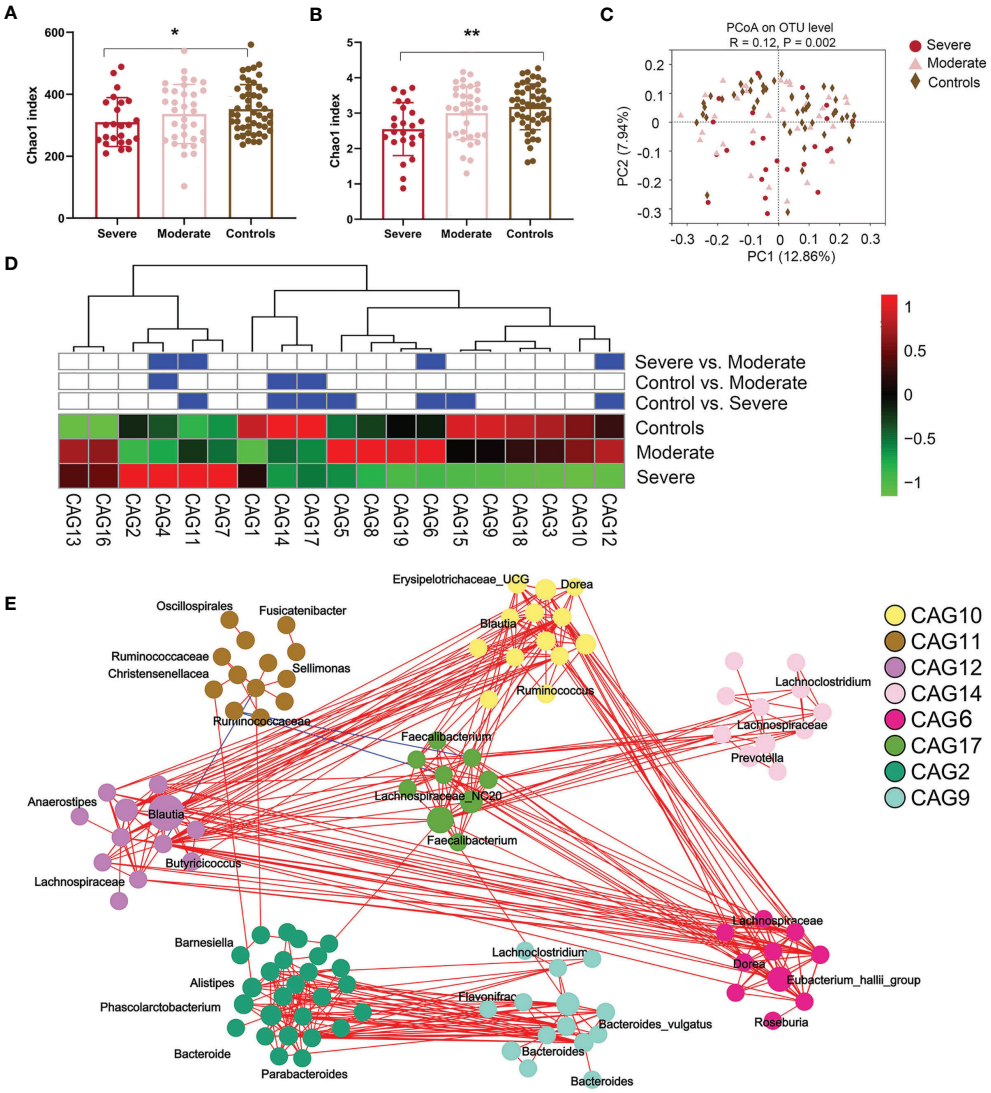


FIGURE 2 | The fecal microbiota from anti-*N*-methyl-D-aspartate receptor (NMDAR) encephalitis patients with more severe status are distinct from those of healthy controls. **(A, B)** Comparison of the Chao 1 **(A)** and Shannon **(B)** indices between the different disease severity groups and healthy controls. A significantly decreased intestinal microbiota diversity in NMDAR encephalitis patients with more severe disease status was found. The mean values and standard deviations are presented as *bars*. $^{*}p < 0.05$, $^{**}p < 0.01$. *P*-values are from the Kruskal–Wallis test. **(C)** The overall bacterial signatures between the three groups were markedly different (unweighted Unifrac, PERMANOVA: $p = 0.003$). **(D)** Abundances of the 19 co-abundance groups (CAGs) in various NMDAR encephalitis severity subgroups. Abundances were transmuted into *Z* scores by subtracting the average abundances and dividing the standard deviations for all samples. *Z* scores were negative (shown in *green*) when row abundance was below the mean. CAGs at $p < 0.05$ (by Wilcoxon rank-sum test) are shown in *blue*. **(E)** Operational taxonomic unit (OTU)-level diagram for the enrichment of OTUs in various groups based on the markedly altered CAGs. *Node size* denotes the mean abundance of each OTU. Bacteria denoted on *nodes* were of the lowest classification status that could be identified by the RDP classifier. *Lines between nodes* denote associations, with *line width* showing association magnitudes, *red* denotes positive association, and *blue* denotes negative associations. *Lines* corresponding to associations with magnitudes >0.4 were drawn.

Fecal metabolomics pathway enrichment assessments revealed significantly overrepresented sub-pathways among the differentially abundant metabolites. PLS-DA revealed 17 sub-pathways, including, among the most significant, beta-alanine metabolism, phenylpropanoid biosynthesis, choline metabolism in cancer, aminobenzoate degradation, bile secretion, pentose and glucuronate interconversions, and tryptophan metabolism, as represented by the dot plot (**Figure 5C**). For serum pathway enrichment analysis, PLS-DA identified 13 sub-pathways that were significantly different between disease cases and HCs, including choline metabolism in cancer, D-glutamine and D-glutamate metabolism, purine metabolism, glycerophospholipid metabolism, ABC transporters, and arginine and proline metabolism (**Figure 5D**).

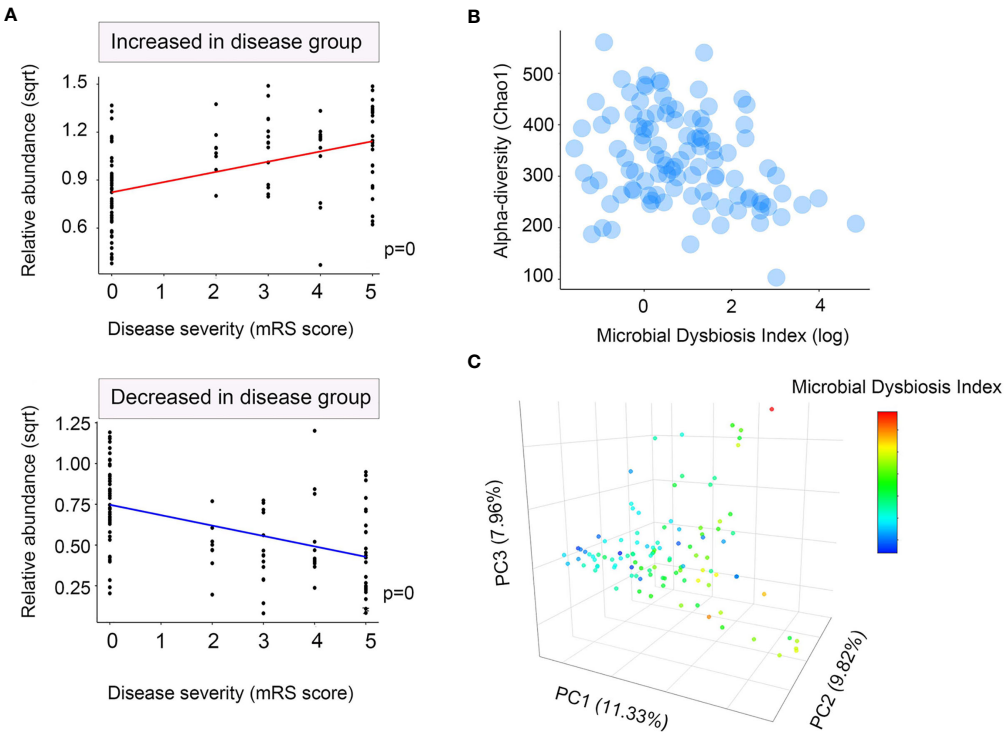


FIGURE 3 | Microbial dysbiosis index (MD-index) characterizing anti-*N*-methyl-D-aspartate receptor (NMDAR) encephalitis severity. **(A)** Scatter plot of arcsine square root transmuted abundance for all summed abundances for the taxa decreased (*bottom*) or increased (*top*) in patients with NMDAR encephalitis versus the modified Rankin scale (mRS) score as a disease severity measure. **(B)** Scatter density plot for species richness vs. the MD-index for each sample. In samples with a high MD-index, a strong reduction in the species richness was observed. **(C)** Principal coordinate plot for unweighted UniFrac distance, colored using the MD-index. It can be noticed that the three principal coordinates stratified the samples by MD-index, which exhibited negative correlations with species richness. *Sqrt*, square root.

The enrichment analysis suggested that the choline metabolism in cancer pathway and the bile secretion pathway were altered significantly in both serum and fecal samples in patients with NMDAR encephalitis, indicating that these two metabolic pathways are important in NMDAR encephalitis.

3.4 The Differential Genera Showed a Correlation with Dysregulated Cytokines in NMDAR Encephalitis

In various immune-associated disorders, cytokines are key drivers of inflammation and tissue damage (35). Commensal microbiome modulates cytokine-mediated immune reactions (36, 37). To establish the relationship between cytokines and the gut microbiota in NMDAR encephalitis patients, we evaluated the serum levels of inflammatory cytokines in NMDAR encephalitis patients relative to HCs (**Figures 6A–I**). Nine cytokines exhibited significantly higher levels in the patient group than in HCs, including IFN-β, IFN-γ, IL-3, IL-6, IL-1, IL-7, IL-18, IL-33, and TNF-α. These cytokines were elevated in patients with severe status and were suppressed in HCs, while a small increase in patients with moderate status further verified that cytokines are associated with disease severity grading (data not shown).

To identify the immune disorder-associated bacteria in NMDAR encephalitis patients, correlation analyses of the various genera and different cytokines between any two groups were performed. **Figure 6J** shows that *Bifidobacterium*, *Enterococcus*, *Clostridium_innocuum_group*, and *Roseburia*, which were the significantly increased genera in the severe disease status group relative to HCs, were positively correlated with the levels of cytokines, which revealed these bacterial genera to be the core bacteria involved in the stimulation of these immune factors. In contrast, *Butyricicoccus*, *Eubacterium_hallii_group*, *Lachnospiraceae_NC2004_group*, *Faecalibacterium*, *Lachnospiraceae_NK4A136_group*, and *Prevotella*, which were significantly reduced in severe NMDAR encephalitis patients, showed a strong negative association with immune factors, implying that these genera could reduce the inflammatory cytokine levels in NMDAR encephalitis patients. However, there was a relatively small marked positive association between the different genera and immune factors in HCs and moderate groups.

3.5 Association Between Metabolites, Cytokines, and Gut Microbiota in NMDAR Encephalitis

At an FDR of 5%, five gut microbiota CAGs were markedly associated with 8 serum metabolic modules, while 7 gut microbiota CAGs were markedly associated with 8 fecal metabolic modules. These metabolic modules were also respectively associated with serum cytokines.

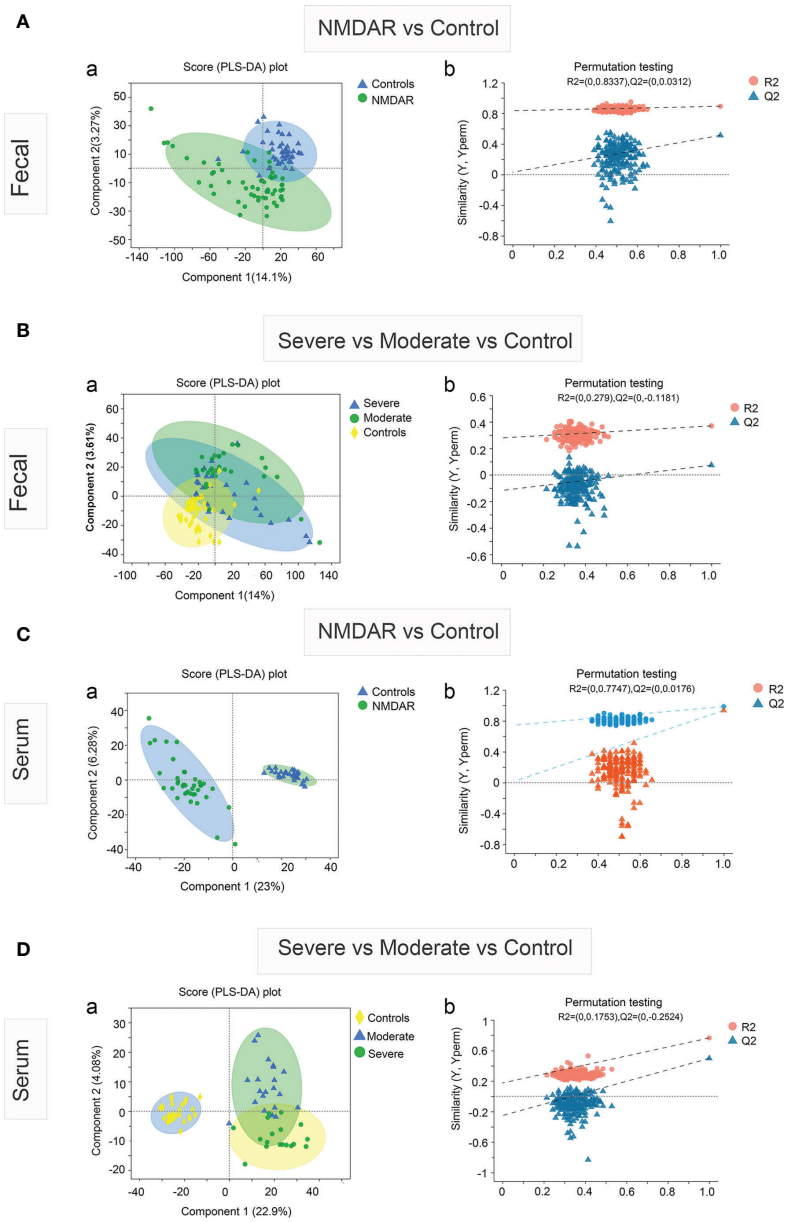


FIGURE 4 | Partial least squares discriminant analysis (PLS-DA) of the fecal and serum metabolomes in anti-*N*-methyl-D-aspartate receptor (NMDAR) encephalitis cases versus healthy controls. Fecal **(A)** and serum **(C)** metabolomics PLS-DA score plot of NMDAR encephalitis cases (*blue*) vs. controls (*green*). Each *dot* denotes an individual subject. Permutation test for the PLS-DA model: 999 permutations led to intercepts of R^2 = 0.833, Q2 = 0.03 (fecal) and R^2 = 0.774, Q2 = 0.017 (serum), implying an acceptable model minus overfitting. Fecal **(B)** and serum **(D)** metabolomics PLS-DA score plot of NMDAR encephalitis cases with severe status (*blue*) and moderate status (*green*) versus controls (*yellow*). Each *dot* represents an individual subject. PLS-DA model permutation test: 999 permutations led to intercepts of R^2 = 0.279, Q2 = –0.118 and R^2 = 0.175, Q2 = –0.252, implying an acceptable model minus overfitting.

The correlation between CAGs, fecal metabolic module, and cytokines can be seen in **Figure 7A**. The light cyan metabolic module (characterized by prenol lipids, steroids, and steroid derivatives) enriched in NMDAR encephalitis, was positively correlated with CAG11 (more abundant in the severe disease group) and negatively correlated with CAG12 (enriched in HCs). CAG11 also showed a negative association with the cyan module enriched in HCs (characterized by glycerophospholipids and fatty acyls; *p*-value for interaction, <0.05).

The correlation between CAGs, serum metabolic module, and cytokines can be seen in **Figure 7B**. CAG6, enriched in the NMDAR encephalitis patients, was positively correlated with the serum metabolic modules that were "NMDAR encephalitis-positive associated", such as the gray module (enriched in

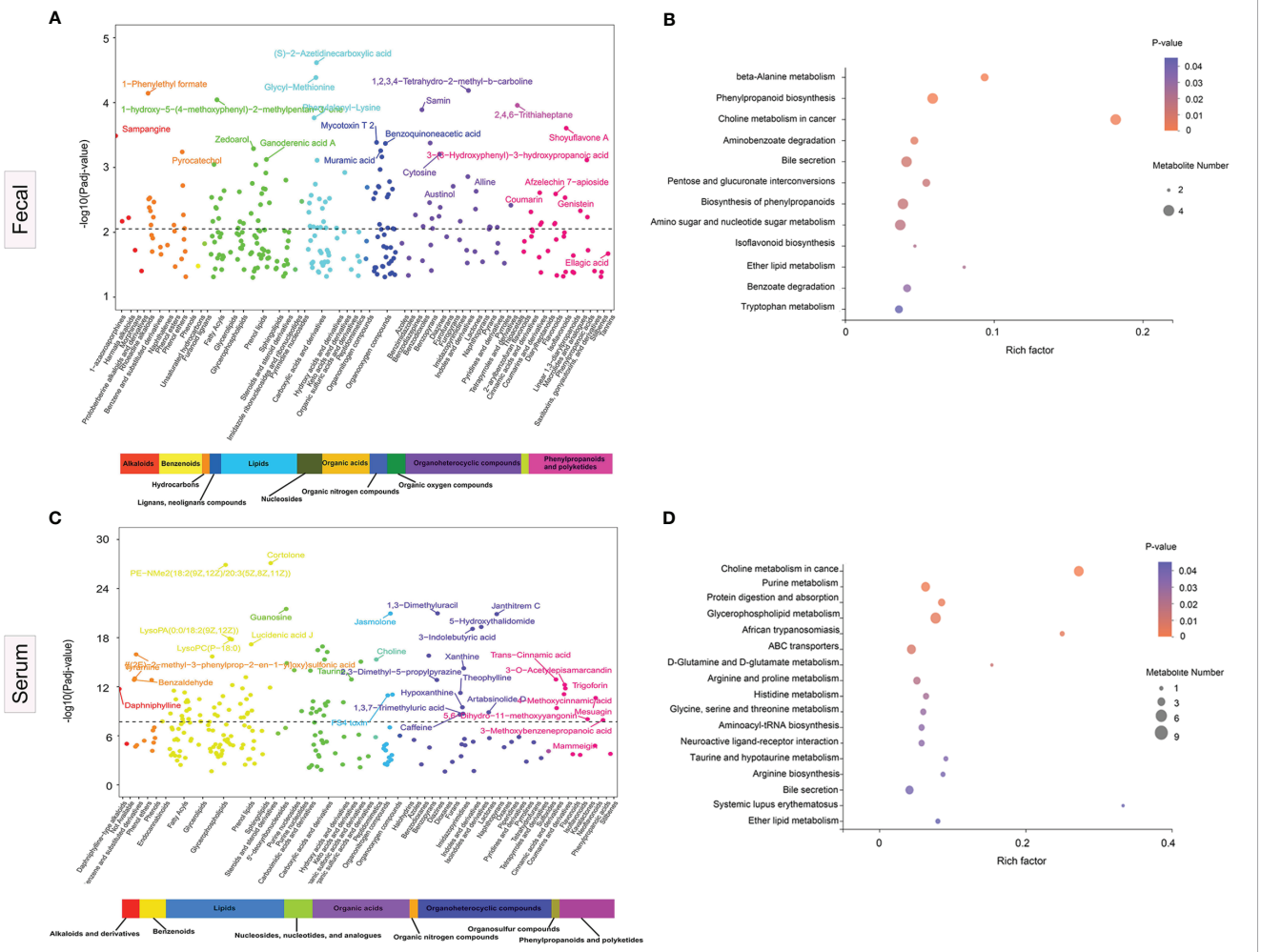


FIGURE 5 | Significance plot for the adjusted selected differential metabolites in anti-*N*-methyl-D-aspartate receptor (NMDAR) encephalitis cases vs. healthy controls by sub- and super-pathway level. **(A, C)** Each significantly selected fecal **(A)** and serum **(C)** metabolites sub-pathway is represented. The –log10(P_{adj}) for each metabolite is displayed by respective sub- and super-pathway (P_{adj}, adjusted *p*-value). Unadjusted Wilcoxon rank-sum test *p*-values were adjusted for multiple comparisons using Benjamini–Hochberg (BH) correction to yield adjusted *p*-values. The *dashed line* represents the adjusted *p*-value. *Asterisks* represent compounds that were not verified against a standard, but whose identity the analytical platform was confident in. **(B, D)** Significantly enriched sub-pathways from metabolites selected using partial least squares discriminant analysis (PLS-DA) models are illustrated in dot plots. Each significantly selected fecal **(B)** and serum **(D)** sub-pathway is denoted by a *circle* described by three parameters. *Circle size* shows how many of the metabolites were selected in the sub-pathway (see legend in *gray* to the *right of the plot* for relative sizes). *Circle shades* from *light pink* to *red* denote selected sub-pathway significance levels based on –log10(*p*-value) (see *legend to the right of the plot* for relative color gradient). Sub-pathways were markedly enriched if $p < 0.05$, which was comparable to –log10(*p*-value) > 1.3. *Circle position along the rich factor axis* shows the abundance of the selected metabolites from the sub-pathway against all sub-pathway metabolites.

organic acids and derivatives and fatty acids; *p*-value for interaction, <0.05). On the other hand, CAG14, CAG17, and CAG15, enriched in the HC group, were negatively associated with metabolic modules that were enriched in the disease group, including the brown, dark orange module (characterized by glycerophosphocholines and glycerophosphoethanolamine-related metabolites; *p*-value for interaction, <0.05), sky blue module (characterized by lipid-like molecules, organic acids and derivatives, and amino acids; *p*-value for interaction, <0.05), and the gray module (characterized by organic acids and derivatives; *p*-value for interaction, <0.05). Particularly, CAG14, mainly consisting of Lachnospiraceae and *Prevotella*, was closely associated with 7 serum modules, implying that it might have vital functions in the maintenance of normal physiology by interacting with various serum metabolites.

Based on the marked associations between distinctive metabolic characteristics in fecal and serum samples and the disorderly gut microbiota in NMDAR encephalitis, it is possible that gut microbiota dysbiosis initiated the disordered microbial functions, leading to the deficiency of anti-inflammation protective metabolites and dysregulation of cytokines, thereby increasing vulnerability to NMDAR encephalitis.

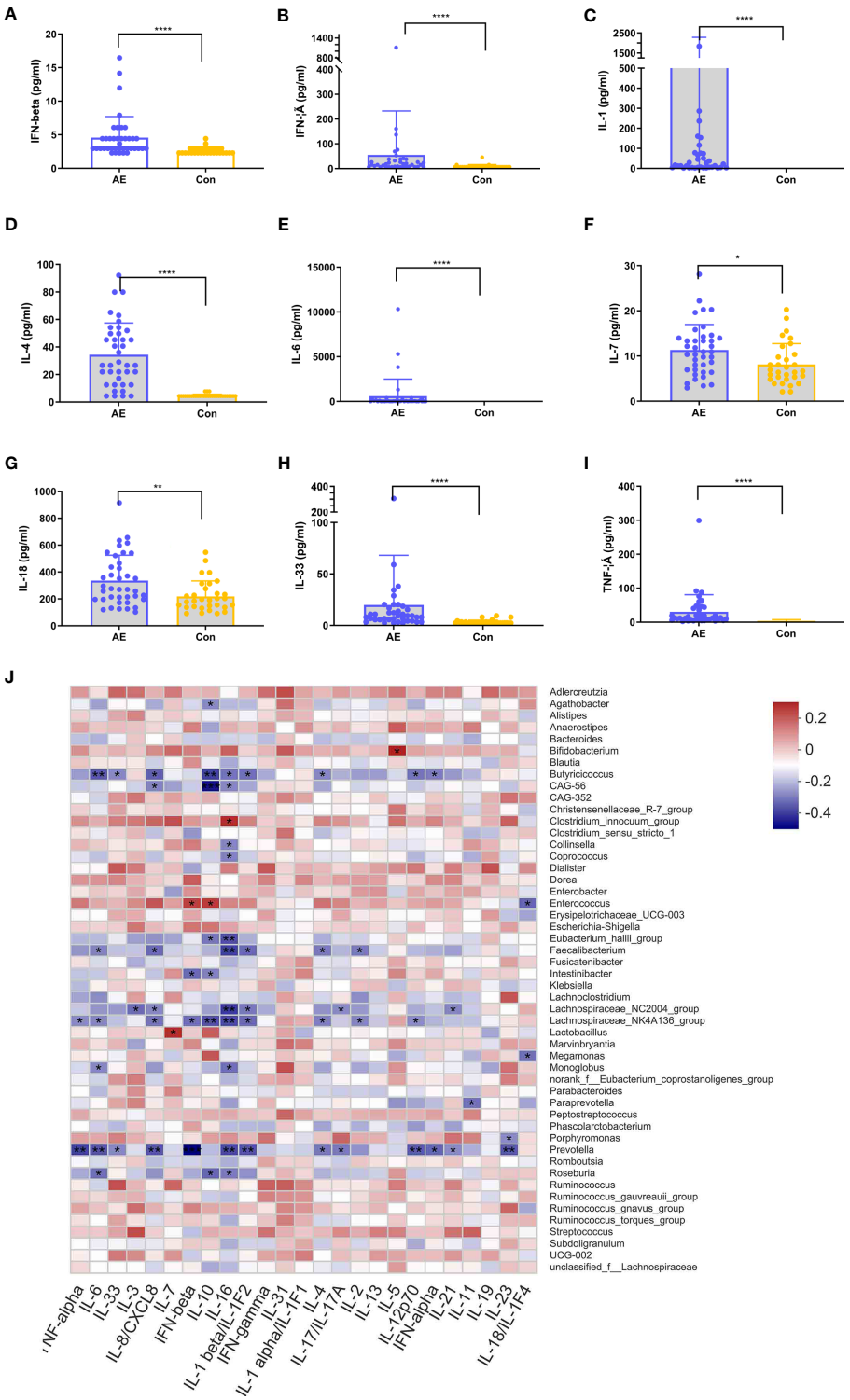


FIGURE 6 | Correlation between dysregulated cytokines and differential genera in anti-*N*-methyl-D-aspartate receptor (NMDAR) encephalitis. **(A–I)** Analysis of 12 immune cytokines in patients with NMDAR encephalitis and in healthy controls (HCs). Participants' sera were run on Luminex. Differences are determined by a *t*-test. **(J)** Correlation analyses of cytokines and differentially enriched genera between any two groups. Abundance rates of differentially enriched species (top 30) in HCs and NMDAR encephalitis were evaluated for association with differential immune factors using Spearman's correlation analysis. Correlations are shown by color gradients from *green* (negatively correlated) to *purple* (positively correlated). Correlation coefficients and *p*-values (*$p < 0.05$, **$p < 0.01$, ***$p < 0.001$, **** $p < 0.0001$) are shown.

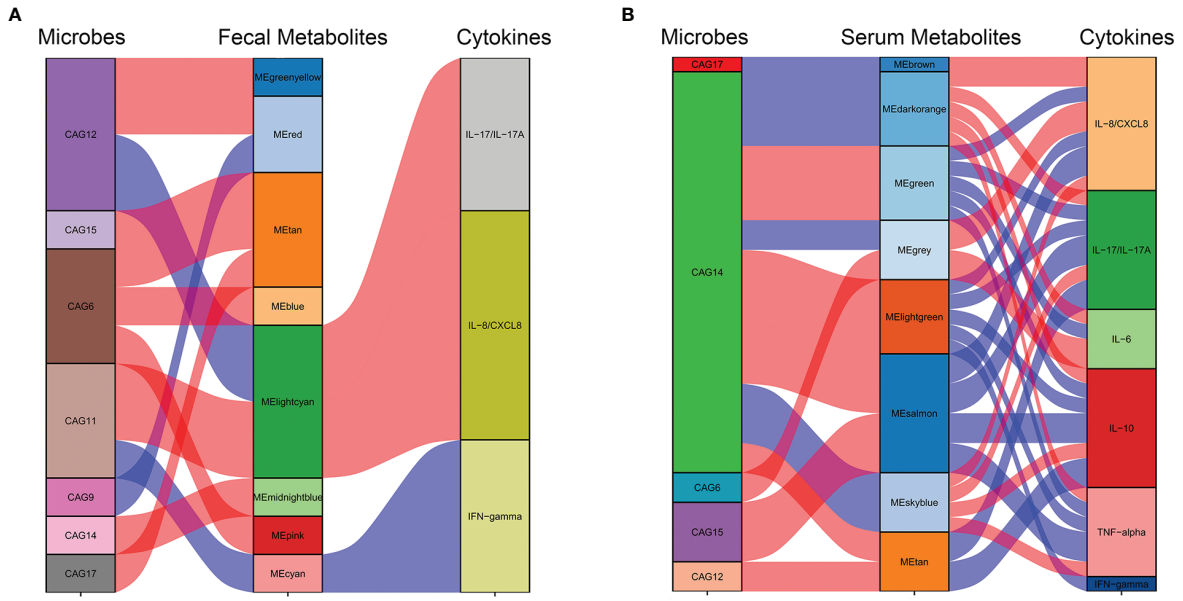


FIGURE 7 | Interrelationships between the gut microbiota composition, host metabolic profiles, and cytokine phenotypes. Correlation network between the gut microbiota of significant co-abundance groups (CAGs), fecal **(A)** and serum **(B)** metabolites, and cytokines. *Red lines* denote positive correlations (FDR < 0.05), while *blue lines* denote negative correlations (FDR < 0.05). In the gut microbiota column, *green* stratum denotes CAGs highly enriched in the control group. Stratum in *brown* denotes microbiota increased in the more severe group. In the metabolomics column, *orange* and red *strata* denote anti-*N*-methyl-D-aspartate receptor (NMDAR) encephalitis-negative metabotypes, while *blue* and *green* strata denote NMDAR encephalitis-positive metabotypes.

3.6 Fecal Microbiota and Metabolites Are Predictive of Clinical Outcomes in NMDAR Encephalitis Patients

Outcomes were evaluated in all 58 patients: 21 (36.2%) patients had an unfavorable outcome at 6 months, including 1 (1.7%) who died within 3 months after admission. Then, we determined whether the key characteristics of the fecal microbiome (bacterial diversity and community composition) or metabolites (fecal and serum) are predictive of the clinical outcomes of NMDAR encephalitis patients. The mRS score, which was the main outcome, was measured at 6 months post-admission. The secondary outcome was clinical relapse.

Firstly, we evaluated whether the community composition of fecal bacteria can predict NMDAR encephalitis outcomes. By using a random forest to assess poor outcome-associated taxa, we identified 10 OUTs most strongly predictive of higher mRS scores at 6 months after admission. The value of the area under the receiver operating characteristic curve (AUC) was 0.84 (the sensitivity and specificity were 72% and 86%, respectively) (**Figure 8A**). Then, we evaluated whether these taxa can predict long-term functional outcomes. **Figure 8B** shows that OTU512 (*Granulicatella*) was highly predictive of favorable disease outcomes. The association between the other OTUs detected and disease outcomes was not significant ($p > 0.05$). Logistic multivariate regression analysis indicated that a high abundance of OTU512 was correlated with a reduced risk of developing worse outcomes, independent of age, sex, disturbance of consciousness, and the NEOS score [odds ratio (OR) = 0.11, 95%CI = 0.02–0.5, multivariate $p = 0.007$]. The combination of clinical features (NEOS score), microbial marker (OUT-512), and a panel of metabolic markers in serum (kynurenine and choline) and feces (lysoPA and L-carnitine) could further enhance the performance of this discrimination significantly, which yielded an AUC of 0.94 (95%CI = 0.7–0.9) (**Figure 8A**).

We next investigated whether the diversity of fecal bacteria predicts NMDAR encephalitis outcomes. Bacterial diversity (as evaluated by the Shannon diversity index) was not a significant predictor of worse outcomes in NMDAR encephalitis ($p = 0.9$). Then, survival analysis showed the relationship between further relapse and microbial diversity (**Figure 8C**). In the low-bacterial-diversity (α-diversity < median, $n = 29$) group, the risk of patients developing relapse was significantly higher than that in the high-diversity (α-diversity > median, $n = 29$) group (log-rank $p = 0.04$, HR = 2.7, 95%CI = 1.0–7.0).

Subsequently, after at least 6 months of follow-up, we collected fecal sample from 30 NMDAR encephalitis patients of the same cohort (21 patients with favorable outcomes and 9 patients with poor outcomes in the recovery phase). We explored the longitudinal changes in dysbiosis and further validated the relationship between disease outcome markers and dysbiosis. The results showed that patients with worse outcomes had a significantly lower OTU512 than patients with favorable outcomes (**Figure 8D**). Moreover, patients with higher microbial diversity did not have relapse during the follow-up (**Figures 8E, F**).

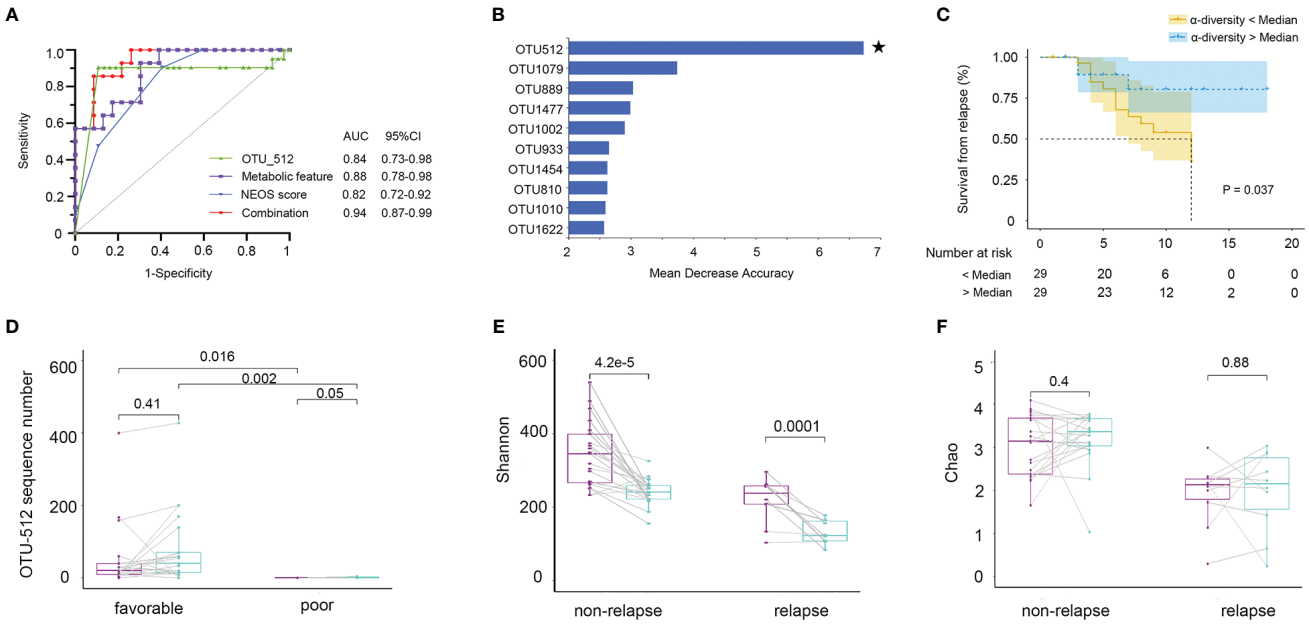


FIGURE 8 | Fecal microbiota and outcomes in anti-*N*-methyl-D-aspartate receptor (NMDAR) encephalitis patients. The community composition of fecal bacteria was significantly predictive of functional outcomes at 6 months. **(A)** Diagnostic outcomes are presented *via* receiver operating characteristic (ROC) curves for the outcomes at 6 months of NMDAR encephalitis patients. **(B)** Detailed explanatory variables that are based on random forest models for comparison of favorable and worse outcomes. *Bar lengths* in the histogram denote the mean decrease accuracy, showing the significance of operational taxonomic units (OTUs) for classification. Random forest identified the fecal-associated OTU512 (*Granulicatella*) as the strongest predictor of favorable outcome. **(C)** Cox proportional hazards model of the association of relapse. Patients were grouped into two: α-diversity < median and α-diversity > median, for which at least 6-month Kaplan–Meier survival plot is shown. Fifty-eight NMDAR encephalitis patients were grouped based on Shannon index median (log-rank $p = 0.037$, HR = 2.74, 95%CI = 1.06–7.05). Numbers below the curve represent the at-risk patients per group. *Yellow line*, below the median; *blue line*, above the median. Analyses were done using quantitative values, and grouping by quantiles was used for graphical presentation only. Patients with unfavorable outcomes did not improve microbiota abnormalities compared to patients with favorable outcomes. **(D)** Patients with paired baseline and long-term (6 ± 1 months) fecal samples are represented ($n = 30$). The measured parameters were genera OTU512. **(E, F)** Patients without relapse had an overall improvement of the Shannon and Chao indices over time compared to patients with one or several relapses. Wilcoxon signed-rank test for comparisons of paired baseline and long-term change.

We thus concluded that, in NMDAR encephalitis patients, poor clinical outcomes and relapse are both predicted by metabolites, community composition, and microbial diversity.

4 DISCUSSION

This is the first multi-omics-based study to comprehensively evaluate the associations of the gut microbiome with fecal and serum metabolites and inflammatory cytokines from a large and prospective cohort including 107 individuals. This is also the first study to simultaneously show that differences in the fecal microbiota are a predictor of clinical outcomes in NMDAR encephalitis patients. The core findings of this study were as follows: i) both the gut microbiota and circulation metabolites markedly changed in patients with more severe disease than in patients with moderate status and HCs, which indicates that dysbiosis could increase the risk of susceptibility to severe disease; ii) two key features of the fecal microbiome at admission—enrichment of OTU512 and higher bacterial diversity—predicted favorable long-term outcomes and reduced further relapse in patients with NMDAR encephalitis; iii) the strong correlations between the distinguishing metabolic features, disordered gut microbiota, and cytokines in NMDAR encephalitis suggested that the fecal microbiome might play vital roles in the maintenance of normal physiological conditions by interacting with several metabolites and pro-inflammatory factors.

The results of the microbial features obtained in this investigation were largely consistent with those previously reported by Herken et al. (38), Xu et al. (39), and Chen et al. (21), namely, an increase in *Oscillospirales* and *Enterococcus* and a decrease in various organic acid-producing bacteria such as Lachnospiraceae, *Ruminococcus*, *Faecalibacterium*, *Anaerostipes*, and *Prevotella*. We further confirmed that these taxa were altered significantly in patients with more severe disease compared with those of moderate status and the HCs. Notably, we also found some taxa depleted in NMDAR encephalitis that were not observed in previous studies, including *Eubacterium_hallii_group*, *Megamonas*, and *Butyricicoccus*. In contrast, Herken et al. described that both patients and controls

had a normal gut microbiome (38). In the study of Chen et al. (21), *Bacteroides* were shown to be higher in NMDAR patients, yielding opposite results in comparison with our study. Previous reviews suggested that *Bacteroides* plays an important role in polysaccharide metabolism and host immune regulation (40, 41). This lack of reproducibility among studies probably resulted from several factors including population heterogeneity, sequencing methods and depths (raw reads per sample ranging ~40K in the previous V4 region of bacterial 16S rRNA gene sequencing studies compared to ~110K in this study), small sample size, different disease stages, a less rigorous inclusion criteria (included 3 ovarian teratoma patients with an identified trigger), and inadequate control of important confounding factors, particularly immunotherapy, antibiotic treatment, and diet.

Furthermore, ecologically, gut bacteria exist as functional groups referred to as "guilds" (42). In response to changes in physiological and environmental resources, key members of co-abundance groups could thrive or decline together (43). Thus, relative to the conventional taxon-based analysis, CAG-based analysis provides a more ecologically relevant method for facilitating the identification of functionally vital gut microbiota in NMDAR encephalitis. In our study, the abundance of CAG11 significantly increased in patients with severe status. This CAG contained several pathogens or opportunistic pathogenic bacteria, such as *Enterococcus*, Oscillospirales, *Fusicatenibacter*, and *Sellimonas*. Thus, these bacteria may initiate innate immune responses through lipopolysaccharide production and elicit successive inflammatory responses that are a result of local cytokine generation.

Our study also provided the important information that a reduced fecal bacterial diversity, including the Shannon and Chao1 indices, predicts further relapse and correlates positively with disease status (mRS score). The mRS score is an important informative parameter for disease severity in numerous neurological diseases (44). A low alpha diversity is a dysbiosis marker and denotes "worse" health (45–47). By using random forest analysis, the combination of microbial taxa, metabolic makers, and the NEOS score at admission can even distinguish patients with adequate outcomes from those with worse outcomes, with an AUC of 0.94. This result was validated by the longitudinal microbiota analysis. Thus, combination with fecal microbiome could also be useful in the early identification of patients with poor prognostic outcomes and inform whether early second-line immunotherapy or other novel salvage treatments can be administered to NMDAR encephalitis patients.

Metabolomes reflect the cumulative effects of endogenous physiological processes and exogenous factors (48). The human gut microbiome comprehensively interacts with the host *via* substrate co-metabolism and metabolic exchange. PLS-DA, highly used for the identification of metabolites that markedly separate controls from cases, identified L-carnitine and lysoPA as differential fecal metabolites in NMDAR encephalitis patients versus controls. L-Carnitine is an amino acid derivative that participates in the transport of long-chain fatty acids into the mitochondria. It improves mitochondrial functions and exerts beneficial effects in neurological disorders (49). An upregulated lysoPA correlated with the occurrence of several inflammatory conditions, such as asthma (50), cancer (51), and autoimmune hepatitis (52). We identified phosphatidylserine (PS), phosphatidylethanolamine (PE), and lysoPA as differential serum metabolites in NMDAR encephalitis patients versus controls. According to most previous studies, these glycerolipids (glycerophosphocholines and glycerophosphoethanolamines) are the major pro-inflammatory glycerolipid derivatives that are absorbed into the bloodstream (53, 54). Phosphocholines, which are low-density lipoprotein (LDL, "bad") cholesterol components, interact with C-reactive proteins in a pro-inflammatory and pro-atherosclerotic manner (55–57).

The pathway enrichment analysis in our study suggested that the choline metabolism pathway and the bile secretion pathway were significantly altered in both serum and fecal samples in patients with NMDAR encephalitis. Several studies have shown that choline metabolism plays pathophysiological roles in central nervous system (CNS) diseases. For instance, choline metabolism has a potentially prognostic role in cognitive impairment after stoke (58). Choline is the precursor of neurotransmitter acetylcholine and also acts as an agonist for the receptors that could regulate CNS immune responses, and their dysregulation is associated with the pathogenesis of several neurological diseases (59).

The main strengths of this study were as follows: i) the gut microbiota in cohabiting spouses exhibit high similarities relative to non-cohabiting age-matched male–female pairs; thus, recruiting paired spousal and sibling controls could largely minimize potential confounding. ii) Although some studies have highlighted the inconsistent sex and age influences on the gut microbiome, no obvious effects of sex and age on the gut microbiome structures were observed in this cohort based on beta diversity (**Supplementary Figure S2**). iii) The paired fecal and serum samples of the same cohort may provide more insights that deviations in gut microbial communities are associated with disease severity *via* mediation of fecal and serum metabolites. iv) The relatively large sample size and prospective follow-up data, along with longitudinal microbiome analysis, enabled us to better understand the specific bacteria that may contribute to susceptibility, worse prognosis, and relapse.

We also acknowledge various limitations of this study. Firstly, participants were recruited from Western China; thus, the reported results might not be applicable to Western populations or other populations with specific genetic backgrounds and diets. Secondly, in our study, drugs including immunotherapies and antibiotic were not used on all patients, but other drug use was inevitable since most NMDAR encephalitis require anti-seizure (diazepams, phenobarbital, or midazolam) or anti-antipsychotic drugs at initial onset during emergency care. Hence, although we have obtained the samples from patients as soon as possible, so that the impacts of the above drugs have been reduced to a very low level, the potential impacts of the above drugs on the gut microbiota and metabolites cannot be completely excluded. In addition, similar to other human studies, even though our results were significant when controlled for crucial confounders, we did not control for

all potential clinical exposures. For example, dietary data were obtained using food questionnaires, and inaccuracies of self-reported data can weaken the power in dietary analyses. Furthermore, NMDAR encephalitis patients at disease onset had higher constipation or diarrhea rate in comparison with healthy controls (38% vs. 2%) since autonomic dysfunction is a common symptom in patients with NMDAR encephalitis. A previous study also reported that the incidences of constipation account for nearly one-third of NMDAR encephalitis patients. However, differences between stool frequencies would make it difficult to explain the causal relationship between stool characteristics and microbiota alterations. Finally, the LC-MS platform has certain limitations, e.g., metabolites need to be ionized in order to be detected, and it tends to be highly susceptible to variability. Thus, the combination of MS and NMR methods could be used for complementary sets of metabolites, thereby allowing for a comprehensive assessment of the metabolome. In conclusion, despite our findings highlighting the clinical relevance of the gut microbiome and metabolite changes in NMDAR encephalitis, various knowledge gaps remain. Fecal microbiota may not provide or reflect the whole bowel microbial environment; thus, mechanistic experimental models, and independent validation cohort, and human interventional studies targeting precise metabolic/microbial features should be performed to unravel how they contribute to various physiological roles and pathological outcomes.

DATA AVAILABILITY STATEMENT

The datasets presented in this study can be found in online repositories. The names of the repository/repositories and accession number(s) can be found below: https://www.ncbi.nlm.nih.gov/, BioProject: PRJNA764676.

ETHICS STATEMENT

The studies involving human participants were reviewed and approved by the Institutional Review Boards of the Ethics Committee of West China Hospital of Sichuan University. The patients/participants provided written informed consent to participate in this study.

AUTHOR CONTRIBUTIONS

XG drafted and revised the manuscript, carried out the statistical analysis, and interpreted the data. YL, XL, AL, and KG collected the samples. DZ and ZH conceptualized and designed the study and revised the manuscript. All authors contributed to the article and approved the submitted version.

FUNDING

This study is supported by the National Science Foundation of China (grants 81671291, 81420108014, and 81971213) and the National Key R&D Program of China (2018YFC1312300).

ACKNOWLEDGMENTS

We thank our colleagues and the agencies or institutions that contributed to this study.

SUPPLEMENTARY MATERIAL

The Supplementary Material for this article can be found online at: https://www.frontiersin.org/articles/10.3389/fimmu.2021.791780/full#supplementary-material

REFERENCES

1. Graus F, Titulaer MJ, Balu R, Benseler S, Bien CG, Cellucci T, et al. A Clinical Approach to Diagnosis of Autoimmune Encephalitis. *Lancet Neurol* (2016) 15 (4):391–404. doi: 10.1016/S474-4422(15)00401-9
2. Li A, Gong X, Guo K, Lin J, Zhou D, Hong Z. Direct Economic Burden of Patients With Autoimmune Encephalitis in Western China. *Neurol Neuroimmunol Neuroinflamm* (2020) 7(6):e891. doi: 10.1212/NXI.0000000000000891
3. Gable MS, Sheriff H, Dalmau J, Tilley DH, Glaser CA. The Frequency of Autoimmune N-Methyl-D-Aspartate Receptor Encephalitis Surpasses That of Individual Viral Etiologies in Young Individuals Enrolled in the California Encephalitis Project. *Clin Infect Dis* (2012) 54(7):899–904. doi: 10.1093/cid/cir38
4. Prüss H, Dalmau J, Harms L, Höltje M, Ahnert-Hilger G, Borowski K, et al. Retrospective Analysis of NMDA Receptor Antibodies in Encephalitis of Unknown Origin. *Neurology* (2010) 75(19):1735–9. doi: 10.212/WNL.0b013e3181fc2a06
5. Gresa-Arribas N, Titulaer MJ, Torrents A, Aguilar E, McCracken L, Leypoldt F, et al. Antibody Titres at Diagnosis and During Follow-Up of Anti-NMDA Receptor Encephalitis: A Retrospective Study. *Lancet Neurol* (2014) 13 (2):167–77. doi: 10.1016/S474-4422(13)70282-5
6. Leypoldt F, Höftberger R, Titulaer MJ, Armangue T, Gresa-Arribas N, Jahn H, et al. Investigations on CXCL13 in Anti-N-Methyl-D-Aspartate Receptor Encephalitis: A Potential Biomarker of Treatment Response. *JAMA Neurol* (2015) 72(2):180–6. doi: 10.1001/jamaneurol.2014.956
7. Chen J, Ding Y, Zheng D, Wang Z, Pan S, Ji T, et al. Elevation of YKL-40 in the CSF of Anti-NMDAR Encephalitis Patients Is Associated With Poor Prognosis. *Front Neurol* (2018) 9:727. eCollection 2018. doi: 10.3389/fneur.2018.00727. eCollection 2018
8. Dalmau J, Gleichman AJ, Hughes EG, Rossi JE, Peng X, Lai M, et al. Anti-NMDA-Receptor Encephalitis: Case Series and Analysis of the Effects of Antibodies. *Lancet Neurol* (2008) 7(12):1091–8. doi: 10.16/S474-4422(08)70224-2
9. Iizuka T, Kaneko J, Tominaga N, Someko H, Nakamura M, Ishima D, et al. Association of Progressive Cerebellar Atrophy With Long-Term Outcome in Patients With Anti-N-Methyl-D-Aspartate Receptor Encephalitis. *JAMA Neurol* (2016) 73(6):706–13. doi: 10.1001/jamaneurol.2016.0232
10. Schirmer M, Smeekens SP, Vlamakis H, Jaeger M, Oosting M, Franzosa EA, et al. Linking the Human Gut Microbiome to Inflammatory Cytokine Production Capacity. *Cell* (2016) 167(4):1125–36.e8. doi: 10.016/j.cell.2016.10.020
11. Buffie CG, Pamer EG. Microbiota-Mediated Colonization Resistance Against Intestinal Pathogens. *Nat Rev Immunol* (2013) 13(11):790–801. doi: 10.1038/nri3535

12. Kamada N, Chen GY, Inohara N, Núñez G. Control of Pathogens and Pathobionts by the Gut Microbiota. *Nat Immunol* (2013) 14(7):685–90. doi: 10.1038/ni.2608
13. Rosenblum MD, Remedios KA, Abbas AK. Mechanisms of Human Autoimmunity. *J Clin Invest* (2015) 125(6):2228–33. doi: 10.1172/JCI78088
14. Kadowaki A, Saga R, Lin Y, Sato W, Yamamura T. Gut Microbiota-Dependent CCR9+CD4+ T Cells are Altered in Secondary Progressive Multiple Sclerosis. *Brain* (2019) 142(4):916–31. doi: 10.1093/brain/awz012
15. Cree BA, Spencer CM, Varrin-Doyer M, Baranzini SE, Zamvil SS. Gut Microbiome Analysis in Neuromyelitis Optica Reveals Overabundance of Clostridium Perfringens. *Ann Neurol* (2016) 80(3):443–7. doi: 10.1002/ana.24718
16. Brooks PT, Brakel KA, Bell JA, Bejcek CE, Gilpin T, Brudvig JM, et al. Transplanted Human Fecal Microbiota Enhanced Guillain Barré Syndrome Autoantibody Responses After Campylobacter Jejuni Infection in C57BL/6 Mice. *Microbiome* (2017) 5(1):92. doi: 10.1186/s40168-017-0284-4
17. Choi SC, Brown J, Gong M, Ge Y, Zadeh M, Li W, et al. Gut Microbiota Dysbiosis and Altered Tryptophan Catabolism Contribute to Autoimmunity in Lupus-Susceptible Mice. *Sci Transl Med* (2020) 12(551):eaax2220. doi: 10.1126/scitranslmed.aax2220
18. Blank M, Barzilai O, Shoenfeld Y. Molecular Mimicry and Auto-Immunity. *Clin Rev Allergy Immunol* (2007) 32(1):111–8. doi: 10.1007/BF02686087
19. Cusick MF, Libbey JE, Fujinami RS. Molecular Mimicry as a Mechanism of Autoimmune Disease. *Clin Rev Allergy Immunol* (2012) 42(1):102–11. doi: 10.1007/s12016-011-8294-7
20. Gong X, Liu X, Li C, Chen C, Lin J, Li A, et al. Alterations in the Human Gut Microbiome in Anti-N-Methyl-D-Aspartate Receptor Encephalitis. *Ann Clin Transl Neurol* (2019) 6(9):1771–81. doi: 10.002/acn3.50874
21. Chen H, Chen Z, Shen L, Wu X, Ma X, Lin D, et al. Fecal Microbiota Transplantation From Patients With Autoimmune Encephalitis Modulates Th17 Response and Relevant Behaviors in Mice. *Cell Death Discovery* (2020) 6:75. doi: 10.1038/s41420-020-00309-8. eCollection 2020
22. Holmes E, Li JV, Marchesi JR, Nicholson JK. Gut Microbiota Composition and Activity in Relation to Host Metabolic Phenotype and Disease Risk. *Cell Metab* (2012) 16(5):559–64. doi: 10.1016/j.cmet.2012.10.007
23. Cho I, Blaser MJ. The Human Microbiome: At the Interface of Health and Disease. *Nat Rev Genet* (2012) 13(4):260–70. doi: 10.1038/nrg3182
24. Tremlett H, Bauer KC, Appel-Cresswell S, Finlay BB, Waubant E. The Gut Microbiome in Human Neurological Disease: A Review. *Ann Neurol* (2017) 81(3):369–82. doi: 10.1002/ana.24901
25. Song SJ, Lauber C, Costello EK, Lozupone CA, Humphrey G, Berg-Lyons D, et al. Cohabiting Family Members Share Microbiota With One Another and With Their Dogs. *Elife* (2013) 2:e00458. doi: 10.7554/eLife.00458
26. Gong X, Liu X, Chen C, Lin J, Li A, Guo K, et al. Alteration of Gut Microbiota in Patients With Epilepsy and the Potential Index as a Biomarker. *Front Microbiol* (2020) 11:517797. eCollection 2020. doi: 10.3389/fmicb.2020.517797. eCollection 2020
27. Titulaer MJ, McCracken L, Gabilondo I, Armangué T, Glaser C, Iizuka T, et al. Treatment and Prognostic Factors for Long-Term Outcome in Patients With Anti-NMDA Receptor Encephalitis: An Observational Cohort Study. *Lancet Neurol* (2013) 12(2):157–65. doi: 10.1016/S474-4422(12)70310-1
28. Balu R, McCracken L, Lancaster E, Graus F, Dalmau J, Titulaer MJ. A Score That Predicts 1-Year Functional Status in Patients With Anti-NMDA Receptor Encephalitis. *Neurology* (2019) 92(3):e244–e52. doi: 10.1212/WNL.0000000000006783
29. Lee WJ, Lee ST, Shin YW, Lee HS, Shin HR, Kim DY, et al. Teratoma Removal, Steroid, IVIG, Rituximab and Tocilizumab (T-SIRT) in Anti-NMDAR Encephalitis. *Neurotherapeutics* (2020) 3(10):020–00921. doi: 10.1007/s13311-020-00921-7
30. Magoč T, Salzberg SL. FLASH: Fast Length Adjustment of Short Reads to Improve Genome Assemblies. *Bioinformatics* (2011) 27(21):2957–63. doi: 10.1093/bioinformatics/btr507
31. Kuczynski J, Stombaugh J, Walters WA, González A, Caporaso JG, Knight R. Using QIIME to Analyze 16S rRNA Gene Sequences From Microbial Communities. *Curr Protoc Bioinf* (2011) Unit 10.7. doi: 10.1002/0471250953.bi1007s36
32. Peng Y, Dai F, Liu L, Chen W, Yan H, Liu A, et al. Validation of the NEOS Score in Chinese Patients With Anti-NMDAR Encephalitis. *Neurol Neuroimmunol Neuroinflamm* (2020) 7(5):e860. doi: 10.1212/NXI.0000000000000860
33. Shah ASV, McAllister DA, Gallacher P, Astengo F, Rodríguez Pérez JA, Hall J, et al. Incidence, Microbiology, and Outcomes in Patients Hospitalized With Infective Endocarditis. *Circulation* (2020) 141(25):2067–77. doi: 10.1161/CIRCULATIONAHA.119.044913
34. Gevers D, Kugathasan S, Denson LA, Vázquez-Baeza Y, Van Treuren W, Ren B, et al. The Treatment-Naive Microbiome in New-Onset Crohn's Disease. *Cell Host Microbe* (2014) 15(3):382–92. doi: 10.1016/j.chom.2014.02.005
35. Moudgil KD. Interplay Among Cytokines and T Cell Subsets in the Progression and Control of Immune-Mediated Diseases. *Cytokine* (2015) 74(1):1–4. doi: 10.1016/j.cyto.2015.05.006
36. Fatkhullina AR, Peshkova IO, Dzutsev A, Aghayev T, McCulloch JA, Thovarai V, et al. An Interleukin-23-Interleukin-22 Axis Regulates Intestinal Microbial Homeostasis to Protect From Diet-Induced Atherosclerosis. *Immunity* (2018) 49(5):943–57.e9. doi: 10.1016/j.immuni.2018.09.011
37. Guo M, Wang H, Xu S, Zhuang Y, An J, Su C, et al. Alteration in Gut Microbiota is Associated With Dysregulation of Cytokines and Glucocorticoid Therapy in Systemic Lupus Erythematosus. *Gut Microbes* (2020) 11(6):1758–73. doi: 10.080/19490976.2020.1768644
38. Herken J, Bang C, Rühlemann MC, Finke C, Klag J, Franke A, et al. Normal Gut Microbiome in NMDA Receptor Encephalitis. *Neurol Neuroimmunol Neuroinflamm* (2019) 6(6):e632. doi: 10.1212/NXI.0000000000000632
39. Xu R, Tan C, He Y, Wu Q, Wang H, Yin J. Dysbiosis of Gut Microbiota and Short-Chain Fatty Acids in Encephalitis: A Chinese Pilot Study. *Front Immunol* (2020) 11:1994. eCollection 2020. doi: 10.3389/fimmu.2020.01994. eCollection 2020
40. Stefan KL, Kim MV, Iwasaki A, Kasper DL. Commensal Microbiota Modulation of Natural Resistance to Virus Infection. *Cell* (2020) 183(5):1312–24.e10. doi: 10.016/j.cell.2020.10.047
41. Chen BD, Jia XM, Xu JY, Zhao LD, Ji JY, Wu BX, et al. An Autoimmunogenic and Proinflammatory Profile Defined by the Gut Microbiota of Patients With Untreated Systemic Lupus Erythematosus. *Arthritis Rheumatol* (2021) 73(2):232–43. doi: 10.1002/art.41511
42. Liu H, Chen X, Hu X, Niu H, Tian R, Wang H, et al. Alterations in the Gut Microbiome and Metabolism With Coronary Artery Disease Severity. *Microbiome* (2019) 7(1):68. doi: 10.1186/s40168-019-0683-9
43. Faust K, Raes J. Microbial Interactions: From Networks to Models. *Nat Rev Microbiol* (2012) 10(8):538–50. doi: 10.1038/nrmicro2832
44. van Swieten JC, Koudstaal PJ, Visser MC, Schouten HJ, van Gijn J. Interobserver Agreement for the Assessment of Handicap in Stroke Patients. *Stroke* (1988) 19(5):604–7. doi: 10.1161/01.str.19.5.604
45. Frost F, Kacprowski T, Rühlemann M, Pietzner M, Bang C, Franke A, et al. Long-Term Instability of the Intestinal Microbiome is Associated With Metabolic Liver Disease, Low Microbiota Diversity, Diabetes Mellitus and Impaired Exocrine Pancreatic Function. *Gut* (2021) 70(3):522–30. doi: 10.1136/gutjnl-2020-322753
46. Heinzel S, Aho VTE, Suenkel U, von Thaler AK, Schulte C, Deuschle C, et al. Gut Microbiome Signatures of Risk and Prodromal Markers of Parkinson Disease. *Ann Neurol* (2020) 88(2):320–31. doi: 10.1002/ana.25788
47. Yeoh YK, Zuo T, Lui GC, Zhang F, Liu Q, Li AY, et al. Gut Microbiota Composition Reflects Disease Severity and Dysfunctional Immune Responses in Patients With COVID-19. *Gut* (2021) 70(4):698–706. doi: 10.1136/gutjnl-2020-323020
48. Goutman SA, Boss J, Guo K, Alakwaa FM, Patterson A, Kim S, et al. Untargeted Metabolomics Yields Insight Into ALS Disease Mechanisms. *J Neurol Neurosurg Psychiatry* (2020) 91(12):1329–38. doi: 10.136/jnnp-2020-323611
49. Mota SI, Pita I, Águas R, Tagorti S, Virmani A, Pereira FC, et al. Mechanistic Perspectives on Differential Mitochondrial-Based Neuroprotective Effects of Several Carnitine Forms in Alzheimer's Disease *In Vitro* Model. *Arch Toxicol* (2021) 24(10):021–03104. doi: 10.1007/s00204-021-03104-1
50. Naz S, Kolmert J, Yang M, Reinke SN, Kamleh MA, Snowden S, et al. Metabolomics Analysis Identifies Sex-Associated Metabotypes of Oxidative Stress and the autotaxin-lysoPA Axis in COPD. *Eur Respir J* (2017) 49(6):1602322. doi: 10.1183/13993003.02322-2016
51. Emoto S, Kurano M, Kano K, Matsusaki K, Yamashita H, Nishikawa M, et al. Analysis of Glycero-Lysophospholipids in Gastric Cancerous Ascites. *J Lipid Res* (2017) 58(4):763–71. doi: 10.1194/jlr.P072090

52. Li SS, Niu M, Jing J, Huang Y, Zhang ZT, Chen SS, et al. Metabolomic Signatures of Autoimmune Hepatitis in the Development of Cirrhosis. *Front Med (Lausanne)* (2021) 8:644376. eCollection 2021. doi: 10.3389/fmed.2021.644376. eCollection 2021
53. Quehenberger O, Armando AM, Brown AH, Milne SB, Myers DS, Merrill AH, et al. Lipidomics Reveals a Remarkable Diversity of Lipids in Human Plasma. *J Lipid Res* (2010) 51(11):3299–305. doi: 10.1194/jlr.M009449
54. Ou J, Xiao M, Huang Y, Tu L, Chen Z, Cao S, et al. Serum Metabolomics Signatures Associated With Ankylosing Spondylitis and TNF Inhibitor Therapy. *Front Immunol* (2021) 12:630791. eCollection 2021. doi: 10.3389/fimmu.2021.630791. eCollection 2021
55. Berliner JA, Subbanagounder G, Leitinger N, Watson AD, Vora D. Evidence for a Role of Phospholipid Oxidation Products in Atherogenesis. *Trends Cardiovasc Med* (2001) 11(3-4):142–7. doi: 10.1016/s50-738(01)00098-6
56. Chang MK, Binder CJ, Torzewski M, Witztum JL. C-Reactive Protein Binds to Both Oxidized LDL and Apoptotic Cells Through Recognition of a Common Ligand: Phosphorylcholine of Oxidized Phospholipids. *Proc Natl Acad Sci USA* (2002) 99(20):13043–8. doi: 10.1073/pnas.192399699
57. Allaband C, Lingaraju A, Martino C, Russell B, Tripathi A, Poulsen O, et al. Intermittent Hypoxia and Hypercapnia Alter Diurnal Rhythms of Luminal Gut Microbiome and Metabolome. *mSystems* (2021) 29(10):00116–21. doi: 10.1128/mSystems.00116-21
58. Zhong C, Lu Z, Che B, Qian S, Zheng X, Wang A, et al. Choline Pathway Nutrients and Metabolites and Cognitive Impairment After Acute Ischemic Stroke. *Stroke* (2021) 52(3):887–95. doi: 10.1161/STROKEAHA.120.031903
59. Velazquez R, Ferreira E, Knowles S, Fux C, Rodin A, Winslow W, et al. Lifelong Choline Supplementation Ameliorates Alzheimer's Disease Pathology and Associated Cognitive Deficits by Attenuating Microglia Activation. *Aging Cell* (2019) 18(6):e13037. doi: 10.1111/acel

Conflict of Interest: The authors declare that the research was conducted in the absence of any commercial or financial relationships that could be construed as a potential conflict of interest.

Publisher's Note: All claims expressed in this article are solely those of the authors and do not necessarily represent those of their affiliated organizations, or those of the publisher, the editors and the reviewers. Any product that may be evaluated in this article, or claim that may be made by its manufacturer, is not guaranteed or endorsed by the publisher.

Copyright © 2022 Gong, Liu, Liu, Li, Guo, Zhou and Hong. This is an open-access article distributed under the terms of the Creative Commons Attribution License (CC BY). The use, distribution or reproduction in other forums is permitted, provided the original author(s) and the copyright owner(s) are credited and that the original publication in this journal is cited, in accordance with accepted academic practice. No use, distribution or reproduction is permitted which does not comply with these terms.

frontiers in Immunology

ORIGINAL RESEARCH
published: 13 January 2022
doi: 10.3389/fimmu.2021.811803

IL-17 Aggravates *Pseudomonas aeruginosa* Airway Infection in Acute Exacerbations of Chronic Obstructive Pulmonary Disease

Fengming Ding[1†], *Lei Han*[1†], *Qiang Fu*[1], *Xinxin Fan*[2], *Rong Tang*[3], *Chengjian Lv*[1], *Yishu Xue*[1], *Xue Tian*[1] *and Min Zhang*[1*]

[1] *Department of Respiratory and Critical Care Medicine, Shanghai General Hospital, Shanghai Jiao Tong University School of Medicine, Shanghai, China,* [2] *Department of Tuberculosis, Fuzhou Pulmonary Hospital of Fujian Province, Fuzhou, China,* [3] *Department of Clinical Laboratory, Shanghai General Hospital, Shanghai Jiao Tong University School of Medicine, Shanghai, China*

OPEN ACCESS

Edited by:
Alina Maria Holban, University of Bucharest, Romania

Reviewed by:
Muriel Pichavant, U1019 Centre d'Infection et Immunité de Lille (CIIL) (INSERM), France
Amol Suryawanshi, Auburn University, United States

***Correspondence:**
Min Zhang
maggie_zhangmin@163.com

†These authors have contributed equally to this work and share first authorship

Specialty section:
This article was submitted to Microbial Immunology, a section of the journal Frontiers in Immunology

Received: *09 November 2021*
Accepted: *22 December 2021*
Published: *13 January 2022*

Citation:
Ding F, Han L, Fu Q, Fan X, Tang R, Lv C, Xue Y, Tian X and Zhang M (2022) IL-17 Aggravates Pseudomonas aeruginosa Airway Infection in Acute Exacerbations of Chronic Obstructive Pulmonary Disease. Front. Immunol. 12:811803. doi: 10.3389/fimmu.2021.811803

Pseudomonas aeruginosa airway infection increases risks of exacerbations and mortality in chronic obstructive pulmonary disease (COPD). We aimed to elucidate the role of IL-17 in the pathogenesis. We examined the expression and influences of IL-23/IL-17A in patients with stable COPD (n = 33) or acute COPD exacerbations with *P. aeruginosa* infection (n = 34). A mouse model of COPD (C57BL/6) was used to investigate the role of IL-17A in host inflammatory responses against *P. aeruginosa* infection through the application of IL-17A–neutralizing antibody or recombinant IL-17A. We found that *P. aeruginosa* infection increased IL-23/17A signaling in lungs of both COPD patients and COPD mouse models. When COPD mouse models were treated with neutralizing antibody targeting IL-17A, *P. aeruginosa* induced a significantly less polymorphonuclear leukocyte infiltration and less bacterial burden in their lungs compared to those of untreated counterparts. The lung function was also improved by neutralizing antibody. Furthermore, IL-17A-signaling blockade significantly reduced the expression of pro-inflammatory cytokine IL-1β, IL-18, TNF-α, CXCL1, CXCL15 and MMP-9, and increased the expression of anti-inflammatory cytokine IL-10 and IL-1Ra. The application of mouse recombinant IL-17A exacerbated *P. aeruginosa*-mediated inflammatory responses and pulmonary dysfunction in COPD mouse models. A cytokine protein array revealed that the expression of retinol binding protein 4 (RBP4) was down-regulated by IL-17A, and exogenous RBP4-recombinant protein resulted in a decrease in the severity of *P. aeruginosa*-induced airway dysfunction. Concurrent application of IL-17A-neutralizing antibody and ciprofloxacin attenuated airway inflammation and ventilation after inoculation of *P. aeruginosa* in COPD mouse models. Our results revealed that IL-17 plays a detrimental role in the pathogenesis of *P. aeruginosa* airway infection during acute exacerbations of COPD. Targeting IL-17A is a potential therapeutic strategy in controlling the outcomes of *P. aeruginosa* infection in COPD patients.

Keywords: COPD, IL-17, *Pseudomonas aeruginosa*, cytokine profile, lung function

INTRODUCTION

Pseudomonas aeruginosa is a common cause of bacterial infection in Chronic Obstructive Lung Disease (COPD), which can be isolated from sputum samples of 4%-15% of adult COPD patients (1, 2). COPD patients in whom *P. aeruginosa* can be cultured from the airways had a markedly increased risk of exacerbations and mortality (3), which are more likely to be seen in patients who have received recent antibiotic therapy, and those who require mechanical ventilation (4). In most cases, the carriage of a strain lasts for a short time, however a subset of patients can be persistently colonized with *P. aeruginosa* for several years (5). The main factors contributing to the pathogenicity of *P. aeruginosa* are the type III secretion-linked cytotoxicity and production of quorum-sensing regulated virulence factors, such as pyocyanin, alkaline proteases, and elastase (6). Several conserved microbial structures have been implicated in activating the host immune responses through the cell surface and endosomal Toll-like receptors (TLRs), such as TLR4 and TLR5 (7, 8).

However, the immune responses to *P. aeruginosa* infection are not always protective, and an excessive host inflammatory response can cause lung injury (9). For example, neutrophils are crucial for the clearance of bacterial pathogens, but persistent neutrophil recruitment and excessive release of proteases from neutrophils, such as neutrophil elastase (NE) and matrix metalloproteinase-9 (MMP-9), leads to excessive extracellular matrix (ECM) degradation and tissue damage (10). Neutrophils degranulation also releases excessive oxidants, including hydrogen peroxide and hydroxyl radicals that attack host tissues (11). The ability of *P. aeruginosa* to activate the NLRC4 inflammasome-mediated production of IL-1β and IL-18 is responsible for a substantial amount of the pathology associated with acute pneumonia, and inhibition of IL-1β, caspase-1, IL-1R, and IL-18R limits pathological consequences of infection and improves bacterial clearance (12, 13). Therefore, rapid resolution of *P. aeruginosa* infection-induced inflammation is important for reducing the lung injuries, which involves the balance of pro- and anti-inflammatory immune responses including the expression of cytokines and chemokines. The IL-17 family of cytokines is one of such group that can influence the balance of immune responses.

The IL-17 cytokine family consists of six related proteins, IL-17A-F (14). IL-17A is the prototypical member of this family, and signals through a multimeric receptor consisting of IL-17RA and IL-17RC, along with IL-17F that sharing 50% homology to IL-17A. Other family members signal through receptor complex, sharing the common chain with IL-17RA (15). Although Th17 cells are a major source of IL-17 cytokines which are induced by IL-23, they can also be produced by innate immune cells, including dendritic cells (DCs), macrophages, γδT cells, and type 3 innate lymphoid cells (16). The role of IL-17 family cytokines in COPD has emerged rapidly in the last decade. Both stable COPD and acute exacerbations of COPD (AECOPD) have been associated with elevated levels of IL-17A or IL-17A-producing cells in clinical studies (17). IL-17 receptor signaling was shown to be critical for the development of lung inflammation and emphysema in a study using murine models of cigarette smoke-induced COPD, suggesting a critical role for IL-17 in chronic lung injury associated with chronic airway inflammation (18).

In infectious diseases, IL-17 has been shown to play both protective and pathogenic roles. Proper IL-17 signaling enhances the immunity that protects the host from bacterial, fungal and viral invasion (19–21). It is reported that IL-17 rather than antibody is a key element in host defense against chronic pulmonary infection with *P. aeruginosa* (22). In contrast, aberrant IL-17 signaling can lead to excess pulmonary inflammation which can lead to immunopathology and inflammation-induced tissue destruction, such as acute respiratory distress syndrome (ARDS) (23). IL-17A also plays a detrimental role in the pathogenesis of other bacterial mucosal disorders such as *P. aeruginosa* keratitis (24). Therefore, IL-17 are not only involved in the host defense against infection but also in the tissue damage caused by inflammation.

Given the two sides of IL-17 in mucosal immunity, we are interested in understanding the expression of IL-17 signaling and its role in AECOPD with *P. aeruginosa* infection. In this study, we found blockade of IL-17 signaling significantly attenuated the severity of *P. aeruginosa* airway infection by suppressing infection-induced cytokines, suggesting IL-17A may be used as a target of adjunctive therapy, in combination with antibiotics, to treat AECOPD patients with *P. aeruginosa* infection.

MATERIALS AND METHODS

Paticipants and Clinical Variables

Patients with AECOPD with *P. aerugionosa* infection were recruited between August 2020 to July 2021 from two centers of Shanghai General Hospital (Shanghai, China). One center was at north Hongkou Campus in the urban area, and the other center was at south Songjiang Campus in the suburban area. Chest HRCT scans and spirometries were performed in suspected patients with chronic coughing, expectoration, and trachypnea, and diagnosis of COPD was confirmed according to the Global Initiative for Chronic Obstructive Lung Disease (GOLD) guidelines (25). AECOPD is defined as an acute, sustained (> 48 hours) worsening of respiratory symptoms, such as cough, sputum production, and/or dyspnea, which is beyond normal day-to-day variations, and leads to a change in medication. All these enrolled AECOPD patients presented with purulent sputum at the time of admission into hospital. Culture and subsequent detection of microbial isolates were performed in sputum samples or bronchoalveolar lavage fluid (BALF), and *P. aeruginosa* was positive in the samples of all recruited patients. The density of *P. aeruginosa* in sputum sample was more than 10^7 CFU/mL, and in BALF sample was more than 10^4 CFU/mL. These patients didn't have history of *P. aeruginosa* isolation in previous cultures of lower respiratory tract samples. Patients with malignancy, bronchiectasis, significant immuno-deficiencies, or co-colonized with other detected pathogens (eg.

Staphylococcus aureus, *Haemophilus influenza* and *Tuberculous mycobacteria*) were excluded. Controls were from a collection of stable COPD patients who had no pathogen found in either sputum or BALF samples. Written informed consent was obtained from all subjects, and this study was proved by the Ethics Committee of Shanghai General Hospital, and performed in accordance with relevant guidelines and regulations.

Characteristics of participants were collected as follows: anthropometric data (age, gender, body mass index and smoking history); spirometry results [percentages of predicted values of forced expiratory volume in one second ($FEV_{1.0}$), forced vital capacity (FVC), the ratio of $FEV_{1.0}$/FVC, peak exiratory flow (PEF), maximal mid-expiratory flow (MMEF), and forced oscillation test (FOT)]; blood indicators (neutrophil absolute counts, neutrophils%); neutrophil counts and cytokines concentrations (IL-17A, IL-23) in BALF.

Animals and Establishment of COPD Model

Specific pathogen-free male C57BL/6 mice (8-12 weeks of age, 18-22 g) were obtained from Shanghai SLAC Laboratory Animal Co. Ltd (Shanghai, China), and were housed under specific pathogen-free conditions with standard mouse chow (#7001, Harlan Teklad). Animals were exposed to ozone produced from an ozoniser (Model 500 Sander Ozoniser, Germany), mixed with air, for 3 h at a concentration 2.5 parts per million (ppm) in a sealed perspex container, twice a week for 6 weeks. Ozone concentration was continuously monitored with an ozone probe (ATi Technologies, Ashton-U-Lyne, UK). Lung function were measured 24 hours after the last exposure to confirm the COPD model (26, 27). Mice exposed to air were used as controls. All animal procedures were performed in compliance with guide for the care and use of laboratory animals (28) and were approved by the institutional animal care and use committee of Shanghai Jiao Tong University.

Intratracheal Inoculation With Agar-Entrapped *P. aeruginosa*

After **exposure to ozone or air**, mice were inoculated with agar-entrapped *P. aeruginosa* as previously described (29). Briefly, a virulent laboratory strain PAO1 was embedded in the agarose beads at a final concentration of 2.0×10^6 CFU/mL phosphate buffer solution (PBS). Mice were anesthetized with an i.p. injection of pentobarbital sodium (50 mg/kg) before surgical procedures. The trachea was cannulated, and 50 μL of PAO1-laden agarose beads solution was introduced into the lung. Mice were monitored, and allowed to recover until euthanized by CO_2 asphyxiation. Mortality rate related to the procedure was 1%.

Administration of Neutralizing Antibody, Recombinant Proteins and Ciprofloxacin

To apply neutralizing antibody or recombinant proteins, mice were intraperitoneally injected with IL-17A–neutralizing antibody (2 mg/kg, 0.1 ml; R&D Systems, Minneapolis, MN, USA), recombinant mouse (rm)-IL-17A (1.6 mg/kg, 0.1 ml; R&D Systems, Minneapolis, MN, USA) or recombinant mouse retinol binding protein 4 (RBP4, 5 μg/kg, 0.1 ml; Abcam, Cambridge, MA, USA) 4 h before the inoculation with *P. aeruginosa* intrabronchially. To explore the clinical use of anti–IL-17 treatment, anti–IL-17 antibody (2 mg/kg, 0.1 ml) was administered intraperitoneally starting 16 h after *P. aeruginosa* inoculation and continuing every 4 h after initial treatment. Meanwhile, ciprofloxacin (5 mg/kg, Sangon Biotech, Shanghai, China) was administered orally at the same starting point with anti–IL-17 antibody, and continuing every 12 hours after the initial dose.

Spirometry for COPD Mouse Models Using the Forced Manoeuvres System

Twenty-four hours after the last challenge, mice were anesthetized with an anesthetic solution containing tiletamine hydrochloride and zolazepam hydrochloride (25 mg/kg, Virbac S. A., France) and xylazine hydrochloride (10 mg/kg, Chang Sha Best Biological Technology Institute Co., Ltd, Hunan, China) *via* intraperitoneal injection. Mice were tracheostomized, cannulated endotracheally, and ventilated with a pneumotachograph connected to a transducer (EMMS, Hants, UK) at 250 breaths/min and tidal volume of 250 ml. To mimic clinical spirometry, the lungs of mice were inflated to a set tracheal pressure, and then exposed to a large negative pressure reservoir, forcing the mouse to exhale as quickly as possible. Variables, including the FVC, FEV_{50}, MMEF, FEF_{50} and FEF_{75}, were calculated.

Lung Histology and Immunofluorescence

The right low lobes were embedded in paraffin, cut into slices (5 μm), and stained with hematoxylin and eosin. Infiltrate scores were assigned to the infected tissues for the assessment of peribronchial infiltrate severity in a blinded fashion (30). For immunohistochemistry, 6 μm thick sections were cut, mounted to poly-L-lysine–coated glass slides, and blocked with PBS containing 2% BSA for 1 h at room temperature. Sections were then incubated with primary anti-mouse IL-17RA antibody (1:50; Santa Cruz Biotechnology, Dallas, TX, USA) and anti-mouse Ly-6G antibody (1: 100; Cell Signaling Technology, Beverly, MA, USA), followed by the secondary antibodies, including FITC-conjugated anti-rabbit IgG and Cy3-conjugated anti-mouse IgG (1:500; Jackson ImmunoResearch Laboratories, West Grove, PA, USA). The sections were finally counterstained with 4′,6-diamidino-2-phenylindole to visualize the nuclei. Controls were similarly treated with corresponding IgG from the same animal as the primary antibody.

Quantification of *P. aeruginosa* Burden, and Myeloperoxidase Concentration

The remaining right lobes were excised aseptically and homogenized in 0.5 mL of normal saline. Minced lung tissues were quantitatively cultured by serial dilution on LB agar plates overnight at 37°C. The homogenates were further lysed for myeloperoxidase (MPO) measurement. MPO activities were determined using a MPO Activity Assay kit (Nanjing Jiancheng Bioengineering Institute, Nanjing, China).

Semiquantitative and Quantitative PCR

Lungs were lysed in TRIzol and total RNA was extracted. For semiquantitative PCR, cDNA was amplified with DreamTaq Green DNA polymerase (Takara Bio., Dalian, Liaoning, China). PCR products were subjected to electrophoresis on 2% agarose gels containing ethidium bromide. For quantitative PCR (q-PCR), cDNA was amplified using a StepOnePlus™ Real-Time PCR Systems with SYBR Green PCR Master Mix (Applied Biosystems, University Park, IL, USA). Data were analyzed by using the $2^{-\Delta\Delta Ct}$ method with β-actin as the internal control. The primers used in this study are listed in **Table S1**.

Western Blot, ELISA and Cytokine Array

Proteins from lung tissues were extracted using a Nuclear and Cytoplasmic Protein Extraction kit (Beyotime Institute of Biotechnology, Haimen, Jiangsu, China) and protein concentrations were evaluated using a BCA protein assay. For Western blot analysis, A total of 24 μg aliquots of protein samples mixed with a loading buffer were separated by 10% SDS–PAGE and transferred onto polyvinylidene fluoride membranes. The membranes were blocked with 5% milk and subsequently incubated with primary and secondary Abs. The protein bands were illuminated using the enhanced chemiluminescence method (GE Healthcare Life Sciences, Little Chalfont, Buckinghamshire, UK), and quantified by densitometry analyses using ImageJ software version 1.8.0. The primary Abs used included anti-IL-23 (Boster Biological Technology, Wuhan, Hubei, China), anti-IL-23R (Proteintech Group, IL, USA), anti-IL-17A (Proteintech Group, IL, USA), anti-IL-17RA (Servicebio Biological Technology, Wuhan, Hubei, China), anti-RBP4 (R&D Systems, Minneapolis, MN, USA), and anti-β-actin (BioTNT, Shanghai, China). ELISA and Cytokine array (Proteome Profiler Array Mouse XL Cytokine Array Kit; R&D Systems, Minneapolis, MN, USA) were performed following manufacturer's protocols.

Statistical Analysis

SAS version 8.1 statistical software (SAS Institute, Inc., Cary, NC, USA) was used for data analysis. Normally distributed quantitative variables were analyzed using *t*-tests, and non-normally distributed variables were analyzed using Mann–Whitney U test. Qualitative variables were analyzed using the chi-squared test. *P* values < 0.05 were considered statistically significant.

RESULTS

BALF IL-23/IL-17A Levels Were Elevated in *P. aeruginosa*-Infected COPD Patients

A total of 67 COPD patients were enrolled in the study, including 33 patients with stable COPD (con-COPD group) and 34 patients with *P. aeruginosa*-infected AECOPD (PA-COPD group). The demographic and clinical characteristics of the participants are presented in **Table 1**. There was no significant difference of age, gender, body mass index, pack-years of smoking and baseline lung function between the two groups.

TABLE 1 | Baseline characteristics of COPD patients with or without *P. aeruginosa* infection.

Characteristic	Con-COPD (n = 33)	PA-COPD (n = 34)	Statistic value*	*P*-value
Age, years	70.7 (10.4)	76.3 (16.3)	1.95	0.0548
Male, *n* (%)	29 (87.9)	24 (70.6)	3.03	0.0818
BMI, kg/m^2	22.3 (3.4)	21.2 (3.4)	1.32	0.1925
Smoking history, pack-years	26.8 (11.8)	32.1 (16.6)	1.51	0.1347
Previous exacerbations, *n***	2.7 (0.7)	3.0 (0.9)	1.8	0.07
mMRC dyspnea scores, *n****	2.6 (0.6)	2.8 (0.7)	1.2	0.24
GOLD group	D	D	/	/
spirometric GOLD grade	2	2	/	/
Baseline lung function				
$FEV_{1.0}$% predicted	69.5 (10.5)	65.1 (8.8)	1.85	0.0685
FVC% predicted	81.7 (11.5)	77.2 (7.7)	1.89	0.0636
FEV_1/FVC (%)	69.2 (7.7)	67.7 (4.3)	0.99	0.3240
PEF, L/s	6.5 (1.3)	5.9 (2.0)	1.61	0.1117
MMEF, L/s	1.19 (0.53)	1.22 (0.70)	0.60	0.5529
R at 5 Hz (R_5), kPa/(L/s)	0.51 (0.05)	0.49 (0.06)	1.76	0.0825
R at 20 Hz (R_{20}), kPa/(L/s)	0.42 (0.04)	0.40 (0.04)	1.74	0.0852
R_5-R_{20}, kPa/(L/s)	0.091 (0.02)	0.086 (0.02)	0.97	0.3368
Antibiotic treatment****				
Fluoroquinolone, *n* (%)	7 (21.2)	14 (41.2)	3.10	0.0782
β-lactam, *n* (%)*****	4 (12.1)	10 (29.4)	3.03	0.0818
Aminoglycoside, *n* (%)	1 (3.0)	4 (11.8)	1.85	0.1738

Data are presented as median (SD) unless otherwise indicated.

Con-COPD, control COPD group (patients with stable COPD); PA-COPD, P. aeruginosa-infected COPD group (patients with acute exacerbations of COPD with P. aeruginosa infection); BMI, body mass index; FEV1.0, forced expiratory volume in one second; FVC, forced vital capacity; PEF, peak exiratory flow; MMEF, maximal mid-expiratory flow.

**Quantitative variables were analyzed using t-tests, and qualitative variables were analyzed using the chi-squared test.*

***COPD exacerbations in the past year.*

****mMRC (Modified Medical Research Council) dyspnea scores.*

*****Antibiotic treatment in 7 days prior the study.*

******β-lactams included β-lactamase inhibitors.*

Many AECOPD patients received antibiotics before collecting the samples. To avoid the impact of antibiotics on our results, we included some control stable COPD patients who also received antibiotics for infection of other tissues, such as urinary tract and mucous membrane. No significant difference in antibiotic treatment was observed between con-COPD group and PA-COPD group in this study. Compared with con-COPD patients, PA-COPD patients had higher absolute and percent numbers of neutrophils in BALF, but not in blood (**Figures 1A, B**). Spirometry results showed that PA-COPD patients had significantly more severe airflow obstruction and small airway dysfunction during exacerbations than con-COPD patients (**Figures 1C-E**). Significantly higher IL-23 and IL-17A levels were observed in the BALF of PA-COPD patients (**Figure 1F**), and there was a notable positive correlation between levels of the two cytokines (r = 0.8347, P < 0.0001; **Figure 1G**). Further regression analysis revealed that IL-23 might be an important factor contributing to elevation of IL-17A (R^2 = 0.6967, regression coefficient =1.5330; **Figure 1H**). IL-17A levels also showed a significantly positive correlation with the levels of absolute neutrophil numbers in BALF (r = 0.7889, P < 0.0001; **Figure 1I**), and a negative correlation with the spirometry results ($FEV_{1.0}$% predicted, r = -0.5477, P < 0.0001, **Figure 1J**; $FEV_{1.0}$/FVC%, r = -0.3800, P = 0.0015, **Figure 1K**; MMEF, r = -0.1977, P = 0.0390, **Figure 1L**).

IL-23/IL-17 Axis Signaling Was Increased by *P. aeruginosa* Infection in COPD Mouse Models

Having identified the increased expression of IL-23/IL-17 in BALF of *P. aeruginosa*-infected AECOPD patients, we investigated the expression of IL-23/IL-17 signaling axis in airways of COPD mouse models in response to *P. aeruginosa* infection. The COPD models were established using ozone exposure, which presented with chronic airway inflammation, mucus hypersecretion, airway remodeling and emphysema. IL-17A and IL-23 levels were higher in BALF of COPD models compared to air-control mice (**Figure S1).** Then COPD mouse models were transbronchially inoculated with sterile agar beads (con-COPD group) or agar-entrapped *P. aeruginosa* (PA-COPD group). We found more mucus production was observed in PA-COPD group one day post inoculation (**Figure 2A**). At both mRNA and protein levels, IL-23 and its receptor IL-23R, IL-17A and its receptor IL-17RA were significantly increased in PA-COPD lungs compared to con-COPD lungs (**Figures 2B, C**). Immunofluorescence showed that in PA-COPD lungs, more IL-17RA-positive neutrophils were seen around airway (**Figure 2D**). In addition, we found there was negative correlation between lung function and number of IL-17RA-positive neutrophils in the lungs (r = -0.6928, P = 0.0263, **Figure 2E**). The air-control mice presented with similar response when challenged with *P. aeruginosa*. However, the magnitude was less than that in COPD mice (**Figure S1**). These data suggested that genes of IL-23/IL-17-signaling pathway were over-activated by *P. aeruginosa* infection in COPD, which might play a detrimental role in the pathogenesis of airway inflammation.

IL-17A-Signaling Aggravates Airway Dysfunction in *P. aeruginosa*-Infected COPD Mouse Models

To determine the role of IL-17A in the airway dysfunction induced by *P. aeruginosa* infection in COPD mouse models, we investigated the effects of IL-17A activity in PA-COPD mice by application of IL-17A–neutralizing antibody and exogenous mouse rm-IL-17A, respectively. Both IL-17A–neutralizing antibody and rm-IL-17A protein were administered 4 h prior to *P. aeruginosa* inoculation. Blockade of IL-17A resulted in reduced severity of *P. aeruginosa* airway inflammation, compared with those injected with control IgG (**Figure 3A**). The MPO activity and bacterial load assigned to anti-IL-17A mice were significantly lower than those of control IgG group (**Figures 3B, C**). We next administrated rm-IL-17A prior to *P. aeruginosa* inoculation. In contrast to blockade of IL-17A, the presence of exogenous IL-17A markedly increased the susceptibility of COPD mouse lungs to *P. aeruginosa* infection, with higher infiltrate scores (**Figure 3D**), MPO activity (**Figure 3E**) and bacterial burden (**Figure 3F**) compared with the BSA control group. Immunofluorescence analysis revealed that in contrast to IL-17A blockade, which decreased the number of infiltrated Ly-$6G^+$IL-$17RA^+$ cells, exogenous rm-IL-17A greatly increased the number of infiltrated Ly-$6G^+$IL-$17RA^+$ cells around the airways (**Figure 3G**). Both FVC and FEV_{50} were exacerbated by exogenous rm-IL-17A, however only FEV_{50} was improved by the blockade of IL-17A. On the contrary, the small airway parameters MMEF and FEF_{75} were improved by the IL-17A blockade, however only MMEF were exacerbated by rm-IL-17A (**Figure 3H**). Taken together, the results of the two complementary approaches indicated that IL-17A aggravated airway dysfunction induced by *P. aeruginosa* infection in COPD mouse models. As for air-control mice, their Ly-$6G^+$IL-$17RA^+$ cells were also significantly induced by IL-17A in response to *P. aeruginosa* infection, but their MPO level, bacterial burden, infiltrate scores, and lung function could not be improved by IL-17A blockade (**Figure S2**).

IL-17A Altered Immune Responses to *P. aeruginosa* Infection in COPD Mouse Models

We next assessed the effects of IL-17A on the expression of several innate immune responsive genes in COPD mouse models using IL-17A–neutralizing antibody and rm–IL-17A 4 h pior to *P. aeruginosa* inoculation. We performed real-time PCR for those genes which were shown to be associated with the pathogenesis of *P. aeruginosa* infection. At one day post inoculation, IL-17A–neutralizing antibody dampened, whereas rm–IL-17A protein augmented the expression of proinflammatory genes of IL-1β, IL-18, TNF-α, CXCL1, CXCL15 and MMP-9 in response to *P. aeruginosa* infection in COPD mouse lungs. Furthermore, the expression of the anti-inflammatory gene IL-10 and IL-1Ra was augmented by IL-17A–neutralizing antibody, and dampened by rm–IL-17A protein (**Figure 4**). The protein levels of these genes

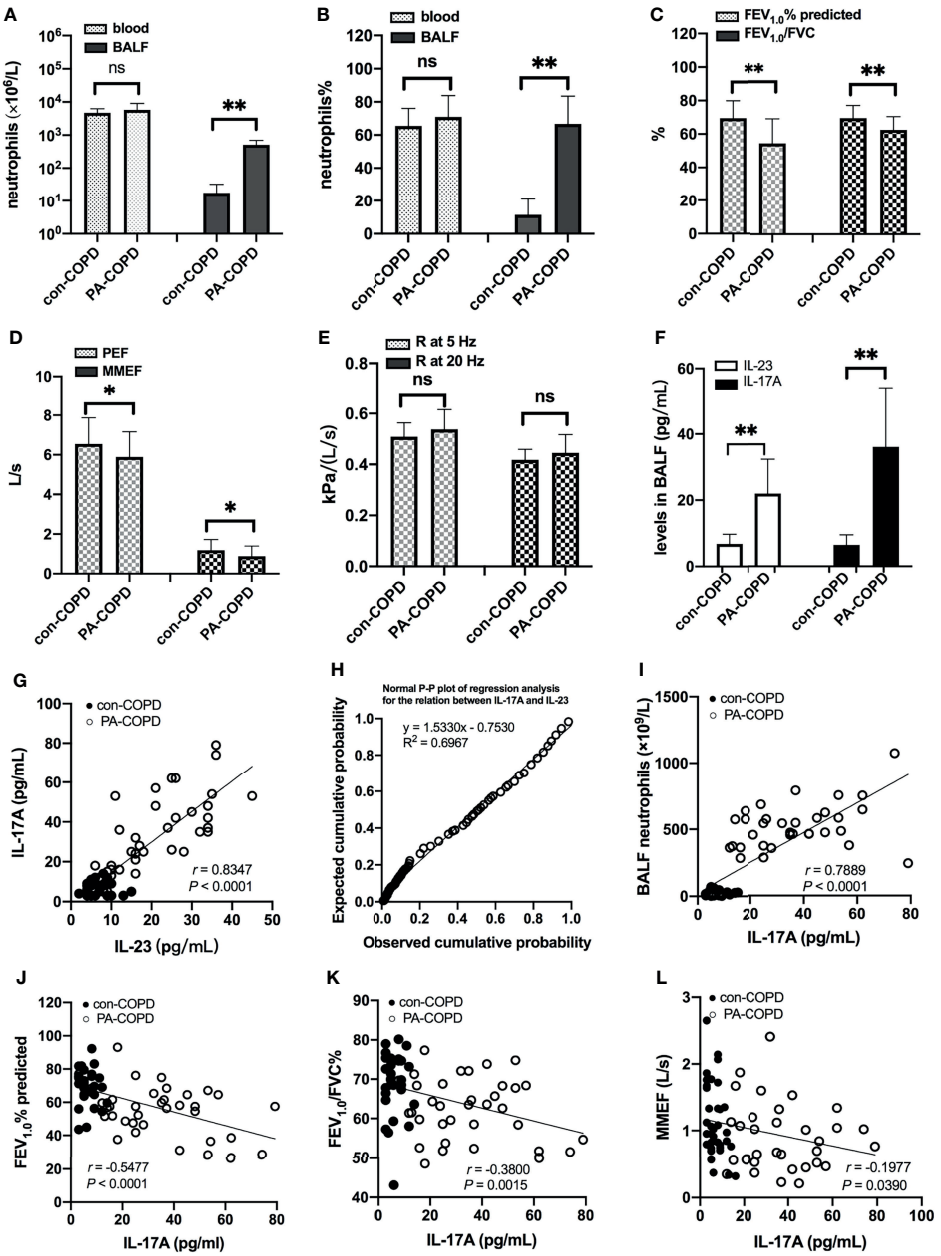


FIGURE 1 | Neutrophils, lung function and BALF IL-23/IL-17A levels between patients with stable COPD (con-COPD, *n* = 33) and patients with *P. aeruginosa*-infected COPD (PA-COPD, *n* = 34). PA-COPD patients had higher absolute and percent numbers of neutrophils in BALF, but not in blood **(A, B)**. Forced expiratory volums **(C)**, expiratory flows **(D)** and forced oscillation tests **(E)** were compared between con-COPD and PA-COPD patients. IL-23 and IL-17A levels were significantly elevated in patients with PA-COPD **(F)**. Data were presented as mean ± SD. $^{*}P < 0.05$, $^{**}P < 0.01$, ns, non-significant. Correlation analysis showed that there was a notably positive correlation between the two cytokines **(G)**, and further regression analysis revealed that IL-23 might be an important factor contributing to elevation of IL-17A **(H)**. There was also a significantly positive correlation between IL-17A levels and absolute neutrophil numbers in BALF **(I)**. The spirometry results, including $FEV_{1.0}$% predicted **(J)**, $FEV_{1.0}$/FVC% **(K)** and MMEF **(L)** were negatively correlated with the levels of IL-17A. BALF, bronchoalveolar lavage fluid; COPD, chronic obstructive pulmonary disease; IL, interleukin; $FEV_{1.0}$, forced expiratory volume in one second; FVC, forced vital capacity; MMEF, maximal mid-expiratory flow.

were consistent with their mRNA levels (**Figure 5**). For air-control mice, only the mRNA and protein expression of IL-1β, IL-18, TNF-α, and MMP-9 were significantly affected by both IL-17A–neutralizing antibody and rm–IL-17A (**Figures S3**, **S4**).

We used the XL mouse cytokine array to assess the effects of IL-17A on the expression of cytokines, chemokines, and growth factors. Among 111 proteins in the array, RBP4 protein levels were abundant in con-COPD lungs and became low in PA-

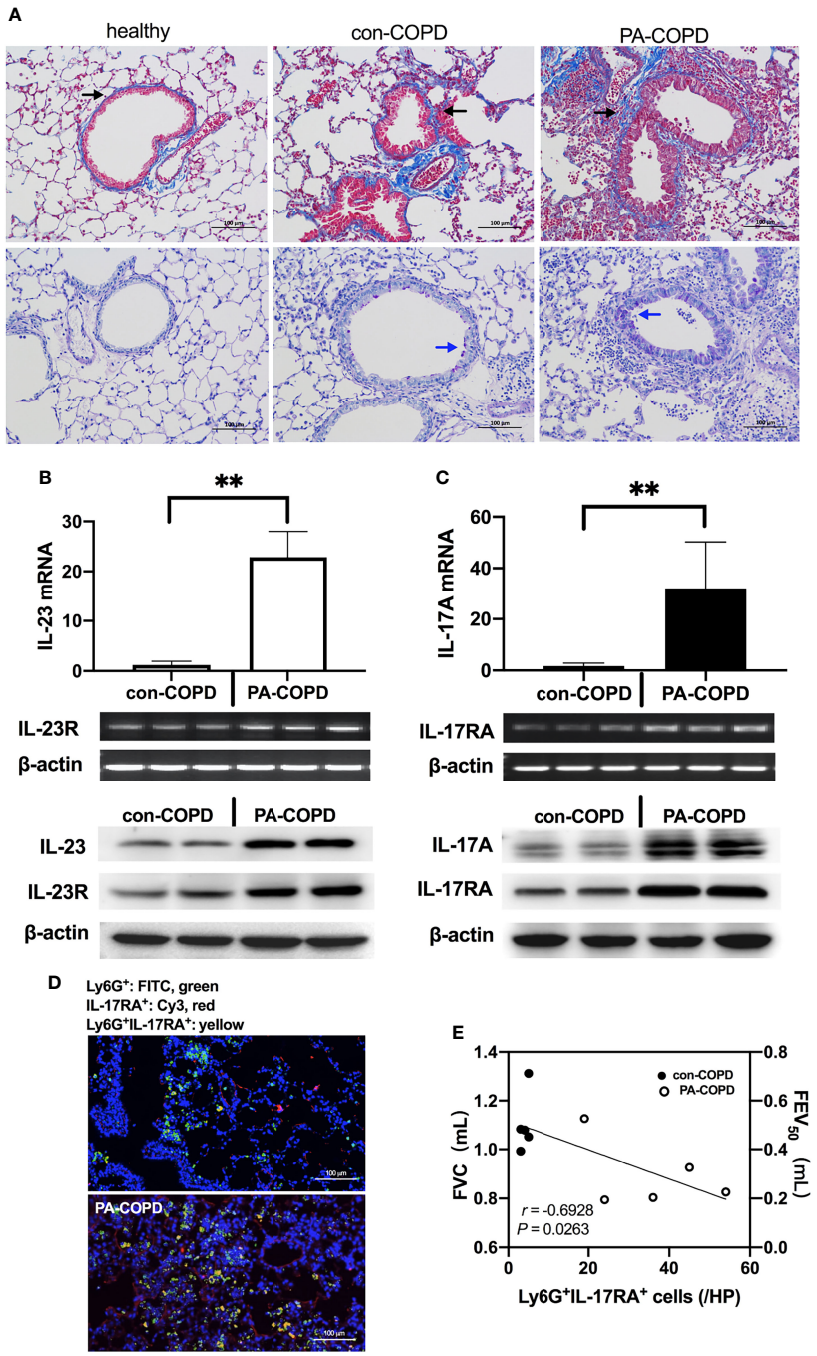


FIGURE 2 | *P. aeruginosa* infection increased IL-23/IL-17 axis signaling in the lungs of COPD mouse models. C57BL/6 mice were exposed to ozone twice a week for 6 weeks to establish COPD models, and then were intrabronchially inoculated with sterile agar beads (con-COPD) or 1.0×10^5 CFU agar-entrapped P. aeruginosa (PA-COPD). Lungs were excised at one day post inoculation, and were sectioned and stained with masson trichrome to measure tissue fibrosis (**A**, upper row), and PAS to quantify glycogen [**(A)**, bottom row]. Blue areas around airways were identified as collagen deposition (indicated by black arrows), and purple areas within tracheal cavity were identified as mucus production and goblet cell hyperpasia (indicated by blue arrows). Internal scale bar = 100 μm. Quantitative real-time PCR, semiquantitative RT-PCR, and western-blot analysis of IL-23 and its receptor **(B)**, and IL-17A and its receptor **(C)** were performed using lung tissues. β-actin serves as the loading control. Data were presented as mean ± SD (n = 5 per group). $^{**}P < 0.01$. The lungs were processed for immunofluorescent analysis **(D)**, and the sections were stained with anti-IL-17RA (red) and anti-Ly6G (green), and DAPI (blue) for nuclei. Internal scale bar = 100 μm. Two independent experiments were performed. Correlation analysis showed that there was a significantly negative correlation between the numbers of $Ly6G^+IL\text{-}17RA^+$ cells and the spirometry results **(E)**. COPD, chronic obstructive pulmonary disease; CFU, colony-forming units; IL, interleukin; FVC, forced vital capacity; FEV_{50}, volume expired in the first 50 ms of fast expiration.

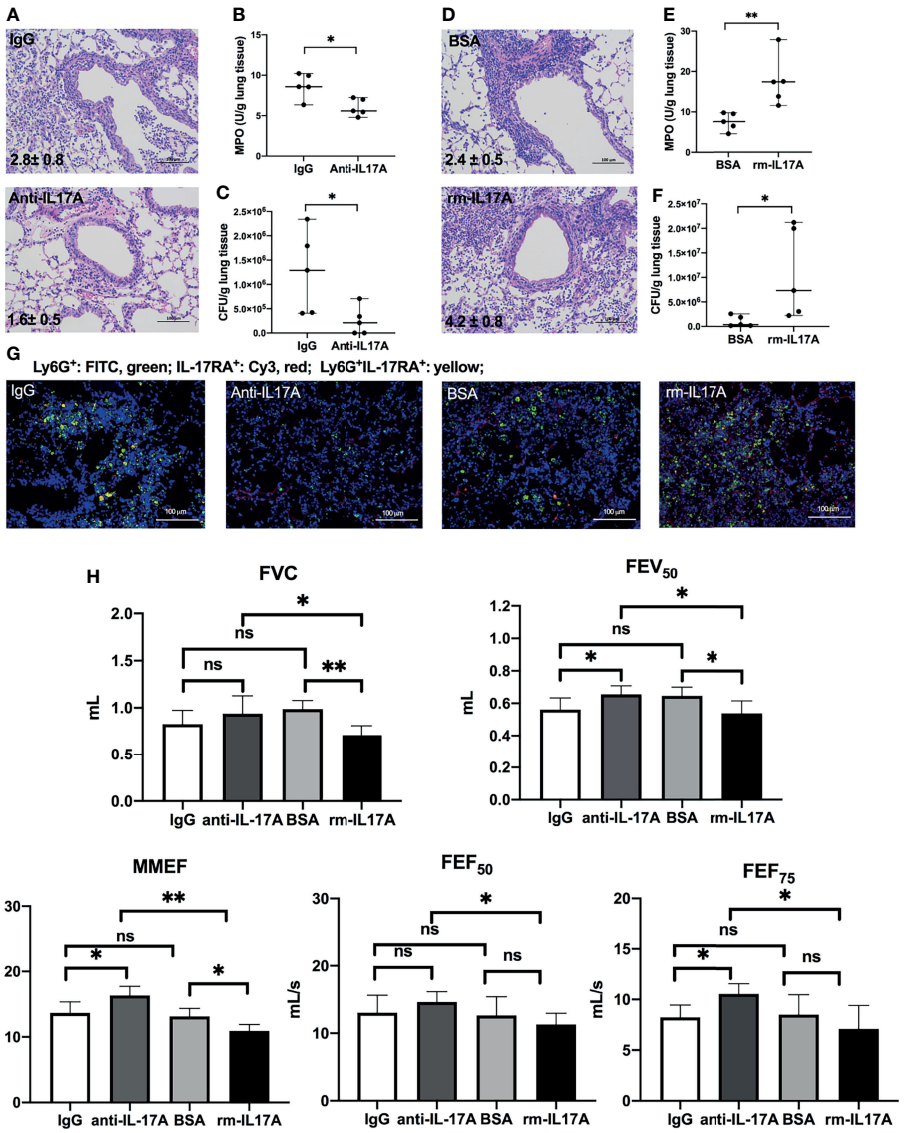


FIGURE 3 | IL-17A-signaling promoted lung injury in *P. aeruginosa*-infected COPD mouse models. COPD mouse models were intraperitoneally injected with IL-17A–neutralizing antibody (2 mg/kg) or recombinant-IL-17A (1.6 mg/kg) 4 h before the inoculation with 1.0×10^5 CFU *P. aeruginosa*. Mouse IgG and BSA serve as controls, respectively. Lungs were excised, sectioned and stained with hematoxylin and eosin (internal scale bar = 100 μm) at one day post inoculation **(A, D)**. The numbers within each lung microphotograph are the infiltrate scores assigned. MPO unit determination **(B, E)**, bacterial plate counting **(C, F)** were performed. The lung sections were immunofluorescently stained with anti-IL-17RA (red) and anti-Ly6G (green), and DAPI (blue) for nuclei **(G)**. Internal scale bar = 100 μm. The results of spirometry tests, including FVC, FEV_{50}, MMEF, FEF_{50}, and FEF_{75} were compared among different groups **(H)**. Data are presented as mean ± SD (n = 5). $^*P < 0.05$, $^{**}P < 0.01$, ns, non-significant. COPD, chronic obstructive pulmonary disease; MPO, myeloperoxidase; CFU, colony-forming units; BSA, bovine serum albumin; IL, interleukin; FVC, forced vital capacity; FEV_{50}, volume expired in the first 50 ms of fast expiration; MMEF, maximal mid-expiratory flow; FEF_{50}, forced expiratory flow at 50% FVC; FEF_{75}, forced expiratory flow at 75% FVC.

COPD lungs. IL-17A–neutralizing antibody increased, whereas rm–IL-17A protein further decreased, the expression of RBP4 at one day post inoculation (**Figure 6A**). Quantitative RT-PCR (qRT-PCR) was performed to confirm the results of cytokine array. We found that RBP4 transcripts were significantly down-regulated in the PA-COPD lungs in comparison to con-COPD lungs; in anti–IL-17A–treated lungs, there was a significant induction of RBP4 transcription, whereas in rm–IL-17A–treated lungs, there was a significant reduction of RBP4 transcription (**Figure 6B**).

RBP4 Regulates IL-17A Expression, and Protect COPD Mouse Models From PA-Induced Airway Dysfunction

Having identified the regulation of RBP4 by IL-17A in PA-COPD lungs, we next investigated the role of RBP4 in the *P.*

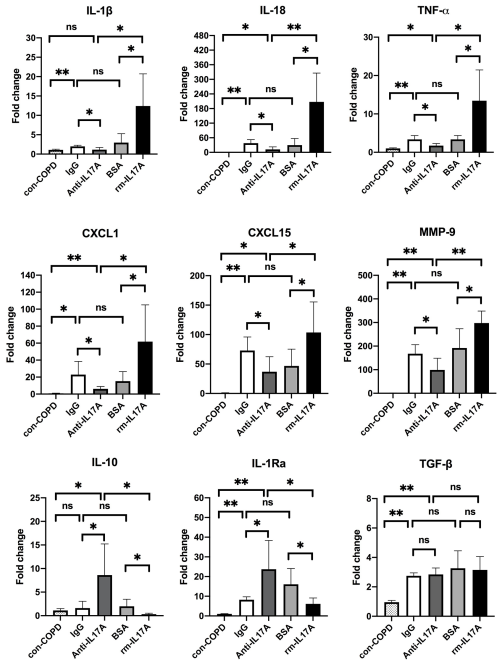


FIGURE 4 | IL-17A affected transcription of inflammatory genes in responses to *P. aeruginosa* infection in COPD mouse models. Mice were intraperitoneally injected with IL-17A–neutralizing antibody (2 mg/kg) or recombinant-IL-17A (1.6 mg/kg) 4 h before the inoculation with 1.0×10^5 CFU *P. aeruginosa*. Mouse IgG and BSA served as controls, respectively. COPD mouse models inoculated with sterile agar beads served as blank control (con-COPD). Lungs were excised at 24 h post inoculation and analyzed by real-time PCR. Data are presented as mean ± SD (n = 5 per group). $^*P < 0.05$, $^{**}P < 0.01$, ns, non-significant. COPD, chronic obstructive pulmonary disease; BSA, bovine serum albumin; IL, interleukin; CXCL, C-X-C motif chemokine ligand; MMP, matrix metalloproteinase.

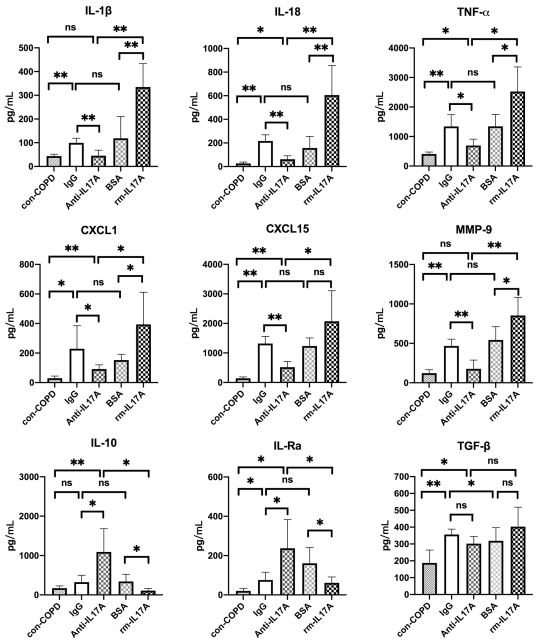


FIGURE 5 | IL-17A affected protein expression of inflammatory genes in response to *P. aeruginosa* infection in COPD mouse models. Mice were intraperitoneally injected with IL-17A–neutralizing antibody (2 mg/kg) or recombinant-IL-17A (1.6 mg/kg) 4 h before the inoculation with 1.0×10^5 CFU *P. aeruginosa*. Mouse IgG and BSA served as treatment controls, respectively. COPD mouse models inoculated with sterile agar beads served as blank control (con-COPD). Lungs were excised at 24 h post inoculation and analyzed by real-time PCR. Data are presented as mean ± SD (n = 5 per group). $^*P < 0.05$, $^{**}P < 0.01$, ns, non-significant. COPD, chronic obstructive pulmonary disease; BSA, bovine serum albumin; IL, interleukin; CXCL, C-X-C motif chemokine ligand; MMP, matrix metalloproteinase.

aeruginosa-induced airway dysfunction in COPD mouse models. We found RBP4 recombinant protein, which was administered 4 h prior to *P. aeruginosa* inoculation, decreased the severity of airway inflammation in PA-COPD mice, including lower infiltrate scores, and reduced MPO activity, when compared with those PA-COPD mice injected with control BSA (**Figures 6C, D**). Importantly, the RBP4 protein significantly decreased the levels of IL-17A transcripts in the lung tissues of PA-COPD mice (**Figure 6E**). When we subconjunctivally injected IL-17A– and RBP4-recombinant protein simultaneously in COPD mouse models 4 h prior to inoculation, the RBP4 protein dampened the severity of rm–IL-17A–induced airway inflammation at one day post inoculation, including a decreased infiltrate score and MPO activity compared with rm–IL-17A–only-treated PA-COPD mice as the control (**Figures 6C, D**). Although the exogenous RBP4 treatment didn't significantly improve the lung function of PA-COPD mice, it alleviated the further decline of FVC and FEV_{50} caused by rm–IL-17A (**Figures 6F, G**). Among the small airway parameters, the decline of FEF_{50} was also alleviated by RBP4 (**Figures 6H–J**). Therefore, the downregulation of RBP4 by IL-17A is partially responsible for the airway dysfunction in *P. aeruginosa*-infected COPD mouse models. RBP4 treatment in PA-infected air-control mice had the similar situation (**Figure S5**).

Adjunctive Therapy of IL-17A–Neutralizing Antibody to Antibiotics Improved the Outcome of *P. aeruginosa*-Infected COPD Mouse Models

To explore the potential clinical application of anti–IL-17A treatment as an adjunctive therapy in AECOPD patients **with** *P. aeruginosa* infection, we orally applied ciprofloxacin concurrently with intraperitoneally administered IL-17A–neutralizing antibody in COPD mouse models starting at 16 h post *P. aeruginosa* inoculation. The addition of anti–IL-17A antibody significantly reduced the severity of lung injury compared with control IgG on day 3 post treatment initiation (**Figure 7A**). Both the infiltrate scores and MPO levels in anti–IL-17A group was significantly decreased compared with ciprofloxacin control group (**Figures 7B, C**). There was no significant difference in the bacterial clearance between two groups (**Figure 7D**). The levels of IL-23 and IL-17 were significantly decreased by combination therapy (**Figures 7E, F**),

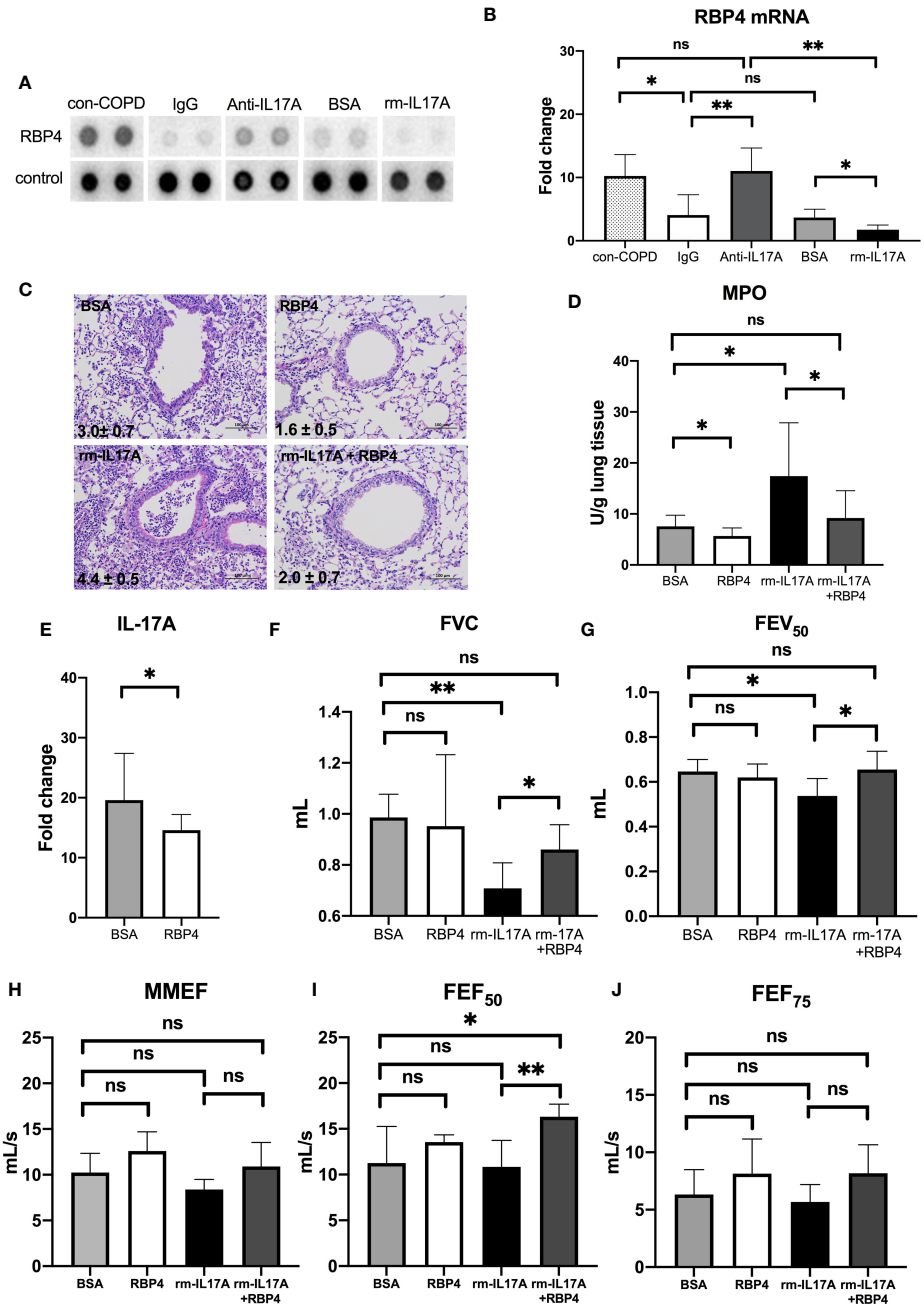


FIGURE 6 | The interaction between IL-17A and RBP4 in the lungs of COPD mouse models in response to *P. aeruginosa* infection. COPD mouse models were intraperitoneally injected with IL-17A–neutralizing antibody (2mg/kg) or recombinant–IL-17A protein (1.6 mg/kg) 4 h before the inoculation with 1.0×10^5 CFU *P. aeruginosa* (PA-COPD). Mouse IgG and BSA served as controls, respectively. COPD mouse models inoculated with sterile agar beads served as blank control (con-COPD). Lungs were excised at one day post inoculation. The effect of IL-17A on cytokine expression were determined using protein array analysis. Selected images for RBP4 was shown **(A)**. Realtime-PCR analysis of RBP4 were performed in lung homogenates. β-actin served as the loading control **(B)**. Data are presented as mean ± SD ($n = 5$ per group). $^*P < 0.05$, $^{**}P < 0.01$, ns = non-significant. Then COPD mouse models were intraperitoneally injected with recombinant RBP4 (5 μg/kg), recombinant–IL-17A protein (1.6 mg/kg) or IL-17A– and RBP4-recombinant protein simultaneously 4 h before the inoculation with 1.0×10^5 CFU *P. aeruginosa*. Mouse BSA served as control. Mouse lungs were excised, sectioned and stained with hematoxylin and eosin (internal scale bar = 100 μm) at one day post inoculation **(C)**. The numbers within each lung microphotograph are the infiltrate scores assigned. Lungs were subjected to MPO unit determination **(D)** and real-time PCR analysis on the transcription of IL-17A **(E)**. The spirometry results, including FVC **(F)**, FEV_{50} **(G)**, MMEF **(H)**, FEF_{50} **(I)**, and FEF_{75} **(J)** were performed and compared between groups. Data were presented as mean ± SD ($n = 5$ per group). $^*P < 0.05$, $^{**}P < 0.01$. COPD, chronic obstructive pulmonary disease; BSA, bovine serum albumin; IL, interleukin; RBP4, retinol binding protein 4; MPO, myeloperoxidase; FVC, forced vital capacity; FEV_{50}, volume expired in the first 50 ms of fast expiration; MMEF, maximal mid-expiratory flow; FEF_{50}, forced expiratory flow at 50% FVC; FEF_{75}, forced expiratory flow at 75% FVC.

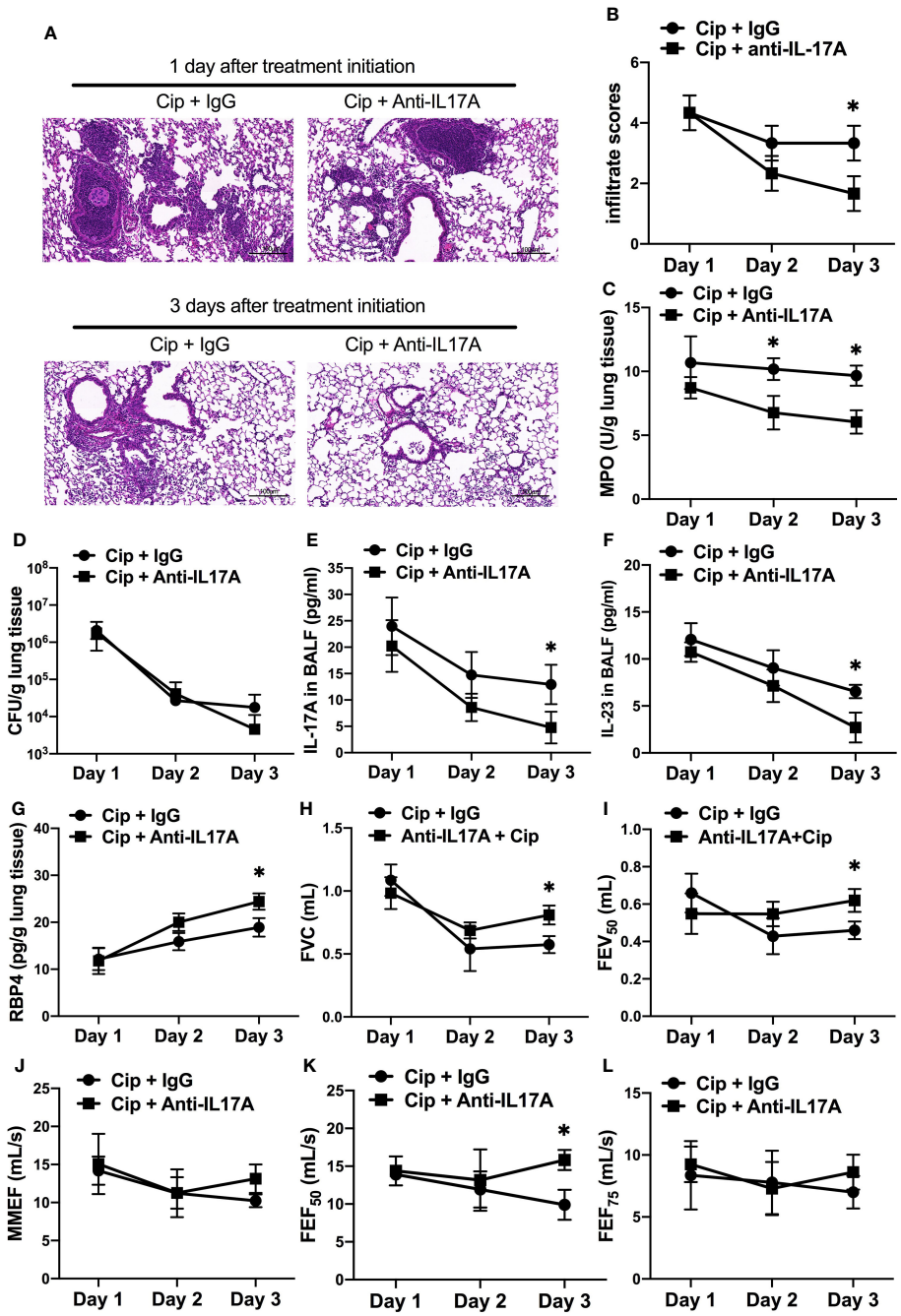


FIGURE 7 | Adjunctive therapy of IL-17A–neutralizing antibody to antibiotic improved the outcome of *P. aeruginosa* infection in COPD mouse models. COPD mouse models were intrabronchially inoculated with 1.0×10^5 CFU agar-entrapped *P. aeruginosa*. Oral ciprofloxacin (5 mg/kg, every 12 h) was applied concurrently with intraperitoneally administered IL-17A–neutralizing antibody (2 mg/kg, every 4 h) or IgG starting at 16 h post inoculation. Mouse lungs were excised, sectioned and stained with hematoxylin and eosin (internal scale bar = 100 μm) after treatment **(A)**, and the infiltrate scores **(B)** and MPO activity **(C)** were determined on each day. Bacterial plate counting **(D)**, protein levels of IL-17A **(E)**, IL-23 **(F)**, and RBP4 **(G)**, and spirometry tests, including FVC **(H)**, FEV_{50} **(I)**, MMEF **(J)**, FEF_{50} **(K)**, and FEF_{75} **(L)**, were performed and compared between groups treated with and without IL-17A block. Data are representative of three independent experiments, and are presented as mean ± SD (n = 3 per group). *$P < 0.05$. COPD, chronic obstructive pulmonary disease; Cip, ciprofloxacin; CFU, colony-forming units; MPO, myeloperoxidase; FVC, forced vital capacity; FEV50, volume expired in the first 50 ms of fast expiration; MMEF, maximal mid-expiratory flow; FEF_{50}, forced expiratory flow at 50% FVC; FEF_{75}, forced expiratory flow at 75% FVC.

while the RBP4 level (**Figure 7G**) and lung function parameters (FVC, FEV_{50}, FEF_{50}) were significantly increased (**Figures 7H–L**). Hence, anti–IL-17 treatment is a potential adjunct therapy to antibiotics for treating *P. aeruginosa* infection in COPD. The combination treatment didn't show advantage over ciprofloxacin alone in PA-infected air-control mice (**Figure S6**).

DISCUSSION

In this study, we found IL-17 signal pathway was upregulated in COPD patients and COPD mouse models in response to *P. aeruginosa* infection, which was associated with deterioration of lung function. The blockade of IL-17A decreased, whereas rm–IL-17A exacerbated the infection-induced airway inflammation and lung dysfunction in COPD mouse models. We also found that IL-17A suppressed RBP4 expression in *P. aeruginosa*–infected mouse models, and exogenous administration of RBP4 downregulated IL-17A expression, and partially attenuated *P. aeruginosa*-induced airway dysfunction. Finally, concurrent application of IL-17A–neutralizing antibody and ciprofloxacin improved *P. aeruginosa* infection–associated inflammation and lung function in mouse models. Taken together, these results suggest that IL-17 signaling plays a pathological role in AECOPD caused by *P. aeruginosa* infection, which includes the induction of proinflammatory cytokine/chemokine and decrease in lung function. These pathological changes are partly related to the suppression of RBP4 expression.

Although IL-17A is a key factor controlling extracellular bacterial and fungal infection under normal condition, its role in AECOPD seems to be complicated (17). Previous studies reported that IL-17A was not involved in the clearance of nontypeable *Haemophilus influenzae* (NTHi) (31), and its response to *Streptococcus Pneumoniae* (32) was defective during COPD exacerbations. Those studies suggested the protective role of IL-17A against bacteria infection was limited in AECOPD. In this study, we found in the mouse models of COPD, despite decreased neutrophil recruitment after treatment with IL-17A–neutralizing antibody, no increased bacterial burden was observed in the lungs, suggesting IL-17A was not critical in the clearance of *P. aeruginosa* during AECOPD. Instead, we found IL-17A induced severe inflammation in the airways and caused lung function decline in mouse models. Our data supported the impaired balance between the role of antibacterial and hyperinflammatory activities for IL-17A in AECOPD, which could result in the bacterial colonisation and persistent neutrophilic inflammation in the airways.

IL-23 is an important mediator of tissue inflammation, which induces the differentiation of naive $CD4^+$ T cells into highly pathogenic helper T cells (Th17) that produce IL-17A, IL-17F, IL-6, and TNF-α, but not IFN-γ and IL-4 (33). In addition, IL-23 produced by residential dendritic cells is likely to be an initial step in the inflammatory cascade that drives the infiltration of innate defense cells such as neutrophils, NK cells, and innate lymphoid cells, most of which are capable of secreting IL-17A (34). Our results showed that IL-17A and IL-23 concentrations were significantly increased in BALF of AECOPD patients with *P. aeruginosa* infection, and there was a notable positive correlation between the two cytokines. The mouse models also showed increased expressions of IL-23/17 axis–signaling molecules by *P. aeruginosa* infection, including IL-23, IL-23R, IL-17A, and IL-17RA. Notably, the infiltrated neutrophils, which were IL-17RA positive, were increased around airways. These data indicated the involvement of IL-23/IL-17 axis in the neutrophilic airway inflammation by *P. aeruginosa* infection in AECOPD.

To investigate the mechanism by which IL-17A drives airway inflammatory response to *P. aeruginosa* infection in COPD, we assessed the effects of IL-17A on the expression of genes known to be involved in the airway immune defense against microbial infection. We found that IL-17A–neutralizing antibody dampened, whereas rm–IL-17A protein augmented the expression of proinflammatory genes of IL-1β, IL-18, TNF-α, CXCL1, CXCL15 and MMP-9 in the lung tissues one day after *P. aeruginosa* inoculation. In contrast, the expression of the anti-inflammatory gene IL-10 and IL-1Ra was augmented by IL-17A–neutralizing antibody, and dampened by rm–IL-17A. IL-1β and IL-18 are members of the IL-1 family, and both induces T cells to produce IL-17 and promote autoimmune responses to specific antigens (35). CXCL1 and CXCL15 are potent neutrophil chemoattractants, which can be released by airway epithelial cells in the response of IL-17 signaling against *P. aeruginosa* (36, 37), whereas IL-10 and IL-1Ra are anti-inflammatory cytokines that counteracts LPS in recruiting neutrophils (38, 39). TNF-α is known to trigger cell activation, migration, or proliferation against pathogens, and is involved in the pathogenesis of inflammatory and autoimmune diseases. TNF-α can induce the release of cytokines IL-6, IL-1β, and IL-8, which can be enhanced by IL-17 (40). MMP-9 is produced by a variety of cells including epithelial cells, fibroblasts, dendritic cells, macrophages, and granulocyteshas in response to *P. aeruginosa* infection, and has the capacity to degrade both elastin and partially hydrolyzed collagen resulting in lung structure injury (41). Our data supported that IL-17 signaling can increase the expression of proinflammatory cytokines and decrease the expression of anti-inflammatory cytokines in *P. aeruginosa*-infected COPD mouse models, which suggested that IL-17 signaling blockade is a potential approach to resolute infection-associated inflammation in AECOPD.

As we are interested in exploring the mechanisms underlying IL-17A's influence on *P. aeruginosa* infection in AECOPD, a cytokine protein array was used, which showed that the protein levels of RBP4 were most dramatically down-regulated in the lungs of COPD mouse models in response to *P. aeruginosa* infection. Furthermore, IL-17A neutralizing promoted, and exogenous IL-17A suppressed, the transcription and expression of RBP4 in the lung tissues. In the functional study, exogenous RBP4 attenuated the severity of IL-17A-induced neutrophilic airway inflammation. RBP4 is synthesized in the liver and adipose tissue, and is the circulating transporter for vitamin A. Previous reports indicated that RBP4 levels in patients with

AECOPD were significantly lower than those in stable COPD and healthy subjects (42, 43). Serum RBP4 levels were associated with nutritional status, which is related to respiratory impairment and systemic inflammation in patients with AECOPD (44). Malnutrition increases the incidence of complications and mortality, and can be identified as a risk factor associated with short-term mortality of elderly AECOPD patients. Our data showed that IL-17A signaling could influence the production of RBP4, which to our knowledge is the first report to link RBP4 expression to IL-17 signaling in AECOPD that caused by *P. aeruginosa* infection. It's notable that the exogenous RBP4 could downregulate IL-17A transcription, suggesting a negative feedback response of RBP4 expression to IL-17A signaling. Our data supported that AECOPD patients with *P. aeruginosa* infection might benefit from vitamin A supplementation during IL-17-induced inflammatory injury. The link between IL-17 and RBP4 in *P. aeruginosa*-infected AECOPD still needs further investigation.

At last, we tested therapeutic potential of IL-17 neutralization on controlling infection-induced airway inflammation in combination with the treatment of oral antibiotics in *P. aeruginosa*-infected AECOPD. Although ciprofloxacin is one of the most active drugs against *P. aeruginosa* among the quinolones (45), inflammation may remain due to the virulence factors, such as LPS, released by the dissolved pathogen (46). Our data showed that the combination treatment of ciprofloxacin and IL-17A–neutralizing antibody reduced airway inflammation associated with *P. aeruginosa* infection as assessed by infiltrate scores and MPO examination. Notably, IL-17A neutralizing could benefit the improvement of lung function in COPD mice after *P. aeruginisa* infection. These data suggested the value of applying concurrent therapy of IL-17A–neutralizing antibody and antibiotics in the treatment of *P. aeruginisa*-infected AECOPD.

Our study focused on IL-17-medated cytokine alternation and its impact on lung function and histopathology in AECOPD with *P. aeruginosa* infection. Limitation of this study included lack of molecular mechanisms on celluar immunity and cross-regulation between IL-17A and RBP4 during AECOPD. Further investigations are needed to support these results of our study.

In conclusion, our study indicated that IL-17 signaling pathway aggravated *P. aeruginosa*-induced airway dysfunction in AECOPD, which is partly related to the downregulation of RBP4 expression. These data supported the therapeutic value of targeting IL-17A in the treatment of *P. aeruginosa* infection in AECOPD.

DATA AVAILABILITY STATEMENT

The original contributions presented in the study are included in the article/**Supplementary Material**. Further inquiries can be directed to the corresponding author.

ETHICS STATEMENT

The studies involving human participants were reviewed and approved by the Ethics Committee of Shanghai General Hospital. The patients/participants provided their written informed consent to participate in this study. The animal study was reviewed and approved by the institutional animal care and use committee of Shanghai Jiao Tong University.

AUTHORS CONTRIBUTIONS

FD, LH, and MZ conceived of and designed the entire study. XT, RT, and CL contributed to data collection and statistical analyses. YX, LH, and QF performed the experiments. FD and LH wrote the manuscript, supervised by MZ. All authors critically reviewed and approved the final version. All authors agreed to be accountable for all aspects of the work in ensuring that questions related to the accuracy or integrity of any part of the work are appropriately investigated and resolved.

FUNDING

This work was supported by the National Natural Science Foundation of China (Grant No. 81970006 and Grant No. 81873402); Project of Science and Technology Commission of Shanghai Municipality (Grant No. 20ZR1444300, Grant No. 20Y11902400 and Grant No. 20Z11900903); Appropriate Technique Application Program of Shanghai Municipal Health System (Grant No. 2019SY042); Three-year Action Plan of Shanghai Shenkang Hospital Development Center (Grant No. SHDC2020CR5010).

ACKNOWLEDGMENTS

The authors would like to thank all the persons who participated in the research.

SUPPLEMENTARY MATERIAL

The Supplementary Material for this article can be found online at: https://www.frontiersin.org/articles/10.3389/fimmu.2021.811803/full#supplementary-material

Supplementary Figure 1 | IL-23/IL-17 axis signaling between the lungs of COPD mouse models and air-control mice in response to *P. aeruginosa* infection. C57BL/6 mice were exposed to ozone twice a week for 6 weeks to establish COPD models, and then were intrabronchially inoculated with sterile agar beads (con-COPD) or 1.0×10^5 CFU agar-entrapped *P. aeruginosa* (PA-COPD). Mice exposed to air were used as controls and also inoculated with sterile agar beads (con-air) or 1.0×10^5 CFU agar-entrapped *P. aeruginosa* (PA-air). Mice were euthanized at one day post inoculation. Quantitative real-time PCR and ELISA analysis of IL-23 **(A, B)**, and IL-17A **(C, D)** were performed using lung tissues or BALF. Data were presented as mean ± SD ($n = 5$ per group). $^*P < 0.01$, $^{**}P < 0.01$. The lungs were processed for immunofluorescent analysis **(E)**, and correlation analysis showed that there was a significantly negative correlation between the numbers of $Ly6G^+IL\text{-}17RA^+$ cells and spirometry results in the study population**(F)**. COPD, chronic obstructive pulmonary disease; CFU, colony-forming units; IL, interleukin; FVC, forced vital capacity; FEV_{50}, volume expired in the first 50 ms of fast expiration.

Supplementary Figure 2 | The effect of IL-17A-signaling on lung injury in *P. aeruginosa*-infected air-control mice. C57BL/6 control mice that exposed to air were intrabronchially inoculated with sterile agar beads (con-air) or 1.0×10^5 CFU agar-entrapped *P. aeruginosa* (PA-air). Mice were intraperitoneally injected with IL-17A–neutralizing antibody (2 mg/kg) or recombinant-IL-17A (1.6 mg/kg) 4 h before the inoculation with 1.0×10^5 CFU *P. aeruginosa*. Mouse IgG and BSA serve as treatment controls, respectively. Lungs were excised, sectioned and stained with hematoxylin and eosin at one day post inoculation. MPO unit determination **(A)**, bacterial plate counting **(B)** and infiltrate scoring **(C)** were performed. The lung sections were analysed immunofluorescently for the expression of $Ly6G^+IL\text{-}17RA^+$ cells **(D)**. The results of spirometry tests, including FVC **(E)**, FEV_{50} **(F)**, MMEF **(G)**, FEF_{50} **(H)**, and FEF_{75} **(I)** were compared among different groups. Data are presented as mean ± SD ($n = 5$). $^*P < 0.05$, $^{**}P < 0.01$. COPD, chronic obstructive pulmonary disease; MPO, myeloperoxidase; CFU, colony-forming units; BSA, bovine serum albumin; FVC, forced vital capacity; FEV_{50}, volume expired in the first 50 ms of fast expiration; MMEF, maximal mid-expiratory flow; FEF_{50}, forced expiratory flow at 50% FVC; FEF_{75}, forced expiratory flow at 75% FVC.

Supplementary Figure 3 | The effect of IL-17A on inflammatory gene transcription in response to *P. aeruginosa* infection by air-control mice. C57BL/6 control mice that exposed to air were intraperitoneally injected with IL-17A–neutralizing antibody (2 mg/kg) or recombinant-IL-17A (1.6 mg/kg) 4 h before the inoculation with 1.0×10^5 CFU *P. aeruginosa* (PA-air). Mouse IgG and BSA served as treatment controls, respectively. Mice inoculated with sterile agar beads served as blank control (con-air). Lungs were excised at 24 h post inoculation and analyzed by real-time PCR. Data are presented as mean ± SD (n = 5 per group). $^*P < 0.05$, $^{**}P < 0.01$. COPD, chronic obstructive pulmonary disease; BSA, bovine serum albumin; IL, interleukin; CXCL, C-X-C motif chemokine ligand; MMP, matrix metalloproteinase.

Supplementary Figure 4 | The effect of IL-17A on inflammatory factor expression in response to *P. aeruginosa* infection by air-control mice. C57BL/6 control mice that exposed to air were intraperitoneally injected with IL-17A–neutralizing antibody (2 mg/kg) or recombinant-IL-17A (1.6 mg/kg) 4 h before the inoculation with 1.0×10^5 CFU *P. aeruginosa* (PA-air). Mouse IgG and BSA served as treatment controls, respectively. Mice inoculated with sterile agar beads served as blank control (con-air). Lungs were excised at 24 h post inoculation and analyzed by real-time PCR. Data are presented as mean ± SD (n = 5 per group). $^*P < 0.05$, $^{**}P < 0.01$. COPD, chronic obstructive pulmonary disease; BSA, bovine serum albumin; IL, interleukin; CXCL, C-X-C motif chemokine ligand; MMP, matrix metalloproteinase.

Supplementary Figure 5 | The interaction between IL-17A and RBP4 in the lungs of air-control mice in response to *P. aeruginosa* infection. C57BL/6 control mice that exposed to air were intraperitoneally injected with IL-17A–neutralizing antibody (2mg/kg) or recombinant–IL-17A protein (1.6 mg/kg) 4 h before the inoculation with 1.0×10^5 CFU *P. aeruginosa* (PA-air). Mouse IgG and BSA served as treatment controls, respectively. Mice inoculated with sterile agar beads served as blank control (con-air). Realtime-PCR and ELISA analysis of RBP4 were performed in lung homogenates **(A, B)**. Data are presented as mean ± SD ($n = 5$ per group). $^*P < 0.05$, $^{**}P < 0.01$. Then air-control mice were intraperitoneally injected with recombinant RBP4 (5 μg/kg), recombinant–IL-17A protein (1.6 mg/kg) or IL-17A– and RBP4-recombinant protein simultaneously 4 h before the inoculation with 1.0×10^5 CFU *P. aeruginosa*. Mouse BSA served as control. Lungs were excised and subjected to MPO unit determination **(C)**. The spirometry results, including FVC (D), FEV_{50} **(E)**, MMEF **(F)**, FEF_{50} **(G)**, and FEF_{75} **(H)** were performed and compared between groups. Data were presented as mean ± SD ($n = 5$ per group). $^*P < 0.05$, $^{**}P < 0.01$. COPD, chronic obstructive pulmonary disease; BSA, bovine serum albumin; IL, interleukin; RBP4, retinol binding protein 4; MPO, myeloperoxidase; FVC, forced vital capacity; FEV_{50}, volume expired in the first 50 ms of fast expiration; MMEF, maximal mid-expiratory flow; FEF_{50}, forced expiratory flow at 50% FVC; FEF_{75}, forced expiratory flow at 75% FVC.

Supplementary Figure 6 | Combination therapy of IL-17A–neutralizing antibody and antibiotic in *P. aeruginosa*-infected air-control mice. C57BL/6 control mice that exposed to air were intrabronchially inoculated with 1.0×10^5 CFU agar-entrapped *P. aeruginosa*. Oral ciprofloxacin (5 mg/kg, every 12 h) was applied concurrently with intraperitoneally administered IL-17A–neutralizing antibody (2 mg/kg, every 4 h) or IgG starting at 16 h post inoculation. Mouse lungs were excised, sectioned and stained with hematoxylin and eosin after treatment. The infiltrate scores **(A)**, MPO activity **(B)**, bacterial plate counting **(C)**, $Ly6G^+IL\text{-}17RA^+$ cell numbers **(D)**, protein expression of IL-17 **(E)** and IL-23 **(F)**, and RBP4 **(G)**, and spirometry tests, including FVC **(H)**, FEV_{50} **(I)**, MMEF **(J)**, FEF_{50} **(K)**, and FEF_{75} **(L)**, were performed and compared between groups treated with and without IL-17A block. Data are representative of three independent experiments, and are presented as mean ± SD ($n = 3$ per group). $^*P < 0.05$, $^{**}P < 0.01$. COPD, chronic obstructive pulmonary disease; Cip, ciprofloxacin; CFU, colony-forming units; MPO, myeloperoxidase; FVC, forced vital capacity; FEV50, volume expired in the first 50 ms of fast expiration; MMEF, maximal mid-expiratory flow; FEF_{50}, forced expiratory flow at 50% FVC; FEF_{75}, forced expiratory flow at 75% FVC.

REFERENCES

1. Patel IS, Seemungal TA, Wilks M, Lloyd-Owen SJ, Donaldson GC, Wedzicha JA. Relationship Between Bacterial Colonisation and the Frequency, Character, and Severity of COPD Exacerbations. *Thorax* (2002) 57:759–64. doi: 10.1136/thorax.57.9.759
2. Groenewegen KH, Wouters EF. Bacterial Infections in Patients Requiring Admission for an Acute Exacerbation of COPD; A 1-Year Prospective Study. *Respir Med* (2003) 97:770–7. doi: 10.1016/s0954-6111(03)00026-x
3. Murphy TF, Brauer AL, Eschberger K, Lobbins P, Grove L, Cai X, et al. Pseudomonas Aeruginosa in Chronic Obstructive Pulmonary Disease. *Am J Respir Crit Care Med* (2008) 177:853–60. doi: 10.1164/rccm.200709-1413OC
4. Lode H, Allewelt M, Balk S, De Roux A, Mauch H, Niederman M, et al. A Prediction Model for Bacterial Etiology in Acute Exacerbations of COPD. *Infection* (2007) 35:143–9. doi: 10.1007/s15010-007-6078-z
5. Martínez-Solano L, Macia MD, Fajardo A, Oliver A, Martinez JL. Chronic Pseudomonas Aeruginosa Infection in Chronic Obstructive Pulmonary Disease. *Clin Infect Dis* (2008) 47:1526–33. doi: 10.1086/593186
6. Kipnis E, Sawa T, Wiener-Kronish J. Targeting Mechanisms of Pseudomonas Aeruginosa Pathogenesis. *Med Mal Infect* (2006) 36:78–91. doi: 10.1016/j.medmal.2005.10.007
7. Feuillet V, Medjane S, Mondor I, Demaria O, Pagni PP, Galán JE, et al. Involvement of Toll-Like Receptor 5 in the Recognition of Flagellated Bacteria. *Proc Natl Acad Sci USA* (2006) 103:12487–92. doi: 10.1073/pnas.0605200103
8. Faure K, Sawa T, Ajayi T, Fujimoto J, Moriyama K, Shime N, et al. TLR4 Signaling Is Essential for Survival in Acute Lung Injury Induced by Virulent Pseudomonas Aeruginosa Secreting Type III Secretory Toxins. *Respir Res* (2004) 5:1. doi: 10.1186/1465-9921-5-1
9. Courtney JM, Ennis M, Elborn JS. Cytokines and Inflammatory Mediators in Cystic Fibrosis. *J Cyst Fibros* (2004) 3:223–31. doi: 10.1016/j.jcf.2004.06.006
10. Smith JA. Neutrophils, Host Defense, and Inflammation: A Double-Edged Sword. *J Leukoc Biol* (1994) 56:672–86. doi: 10.1002/jlb.56.6.672
11. Weiss SJ. Tissue Destruction by Neutrophils. *N Engl J Med* (1989) 320:365–76. doi: 10.1056/nejm198902093200606
12. Cohen TS, Prince AS. Activation of Inflammasome Signaling Mediates Pathology of Acute P. Aeruginosa Pneumonia. *J Clin Invest* (2013) 123:1630–7. doi: 10.1172/jci66142
13. Wonnenberg B, Bischoff M, Beisswenger C, Dinh T, Bals R, Singh B, et al. The Role of IL-1β in Pseudomonas Aeruginosa in Lung Infection. *Cell Tissue Res* (2016) 364:225–9. doi: 10.1007/s00441-016-2387-9
14. Jin W, Dong C. IL-17 Cytokines in Immunity and Inflammation. *Emerg Microbes Infect* (2013) 2:e60. doi: 10.1038/emi.2013.58
15. Iwakura Y, Ishigame H, Saijo S, Nakae S. Functional Specialization of Interleukin-17 Family Members. *Immunity* (2011) 34:149–62. doi: 10.1016/j.immuni.2011.02.012
16. Cua DJ, Tato CM. Innate IL-17-Producing Cells: The Sentinels of the Immune System. *Nat Rev Immunol* (2010) 10:479–89. doi: 10.1038/nri2800
17. Le Rouzic O, Pichavant M, Frealle E, Guillon A, Si-Tahar M, Gosset P. Th17 Cytokines: Novel Potential Therapeutic Targets for COPD Pathogenesis and Exacerbations. *Eur Respir J* (2017) 50:1602434. doi: 10.1183/13993003.02434-2016
18. Chen K, Pociask DA, McAleer JP, Chan YR, Alcorn JF, Kreindler JL, et al. IL-17RA Is Required for CCL2 Expression, Macrophage Recruitment, and

Emphysema in Response to Cigarette Smoke. *PloS One* (2011) 6:e20333. doi: 10.1371/journal.pone.0020333
19. Conti HR, Gaffen SL. IL-17-Mediated Immunity to the Opportunistic Fungal Pathogen Candida Albicans. *J Immunol* (2015) 195:780–8. doi: 10.4049/jimmunol.1500909
20. Happel KI, Zheng M, Young E, Quinton LJ, Lockhart E, Ramsay AJ, et al. Cutting Edge: Roles of Toll-Like Receptor 4 and IL-23 in IL-17 Expression in Response to Klebsiella Pneumoniae Infection. *J Immunol* (2003) 170:4432–6. doi: 10.4049/jimmunol.170.9.4432
21. Ma WT, Yao XT, Peng Q, Chen DK. The Protective and Pathogenic Roles of IL-17 in Viral Infections: Friend or Foe? *Open Biol* (2019) 9:190109. doi: 10.1098/rsob.190109
22. Bayes HK, Ritchie ND, Evans TJ. Interleukin-17 Is Required for Control of Chronic Lung Infection Caused by Pseudomonas Aeruginosa. *Infect Immun* (2016) 84:3507–16. doi: 10.1128/iai.00717-16
23. Confalonieri M, Salton F, Fabiano F. Acute Respiratory Distress Syndrome. *Eur Respir Rev* (2017) 26:160116. doi: 10.1183/16000617.0116-2016
24. Me R, Gao N, Dai C, Yu FX. IL-17 Promotes Pseudomonas Aeruginosa Keratitis in C57BL/6 Mouse Corneas. *J Immunol* (2020) 204:169–79. doi: 10.4049/jimmunol.1900736
25. Vogelmeier CF, Criner GJ, Martinez FJ, Anzueto A, Barnes PJ, Bourbeau J, et al. Global Strategy for the Diagnosis, Management, and Prevention of Chronic Obstructive Lung Disease 2017 Report. GOLD Executive Summary. *Am J Respir Crit Care Med* (2017) 195:557–82. doi: 10.1164/rccm.201701-0218PP
26. Wiegman CH, Li F, Clarke CJ, Jazrawi E, Kirkham P, Barnes PJ, et al. A Comprehensive Analysis of Oxidative Stress in the Ozone-Induced Lung Inflammation Mouse Model. *Clin Sci (Lond)* (2014) 126:425–40. doi: 10.1042/cs20130039
27. Wiegman CH, Li F, Ryffel B, Togbe D, Chunget KF. Oxidative Stress in Ozone-Induced Chronic Lung Inflammation and Emphysema: A Facet of Chronic Obstructive Pulmonary Disease. *Front Immunol* (2020) 11:1957. doi: 10.3389/fimmu.2020.01957
28. Carbone L. Pain Management Standards in the Eighth Edition of the Guide for the Care and Use of Laboratory Animals. *J Am Assoc Lab Anim Sci* (2012) 51(3):322–8.
29. van Heeckeren AM, Schluchter MD. Murine Models of Chronic Pseudomonas Aeruginosa Lung Infection. *Lab Anim* (2002) 36:291–312. doi: 10.1258/002367702320162405
30. Dubin PJ, Kolls JK. IL-23 Mediates Inflammatory Responses to Mucoid Pseudomonas Aeruginosa Lung Infection in Mice. *Am J Physiol Lung Cell Mol Physiol* (2007) 292:L519–28. doi: 10.1152/ajplung.00312.2006
31. Roos AB, Sethi S, Nikota J, Wrona CT, Dorrington MG, Sandén C, et al. IL-17A and the Promotion of Neutrophilia in Acute Exacerbation of Chronic Obstructive Pulmonary Disease. *Am J Respir Crit Care Med* (2015) 192:428–37. doi: 10.1164/rccm.201409-1689OC
32. Pichavant M, Sharan R, Le Rouzic O, Olivier C, Hennegrave F, Rémy G, et al. IL-22 Defect During Streptococcus Pneumoniae Infection Triggers Exacerbation of Chronic Obstructive Pulmonary Disease. *EBioMedicine* (2015) 2:1686–96. doi: 10.1016/j.ebiom.2015.09.040
33. Iwakura Y, Ishigame H. The IL-23/IL-17 Axis in Inflammation. *J Clin Invest* (2006) 116:1218–22. doi: 10.1172/jci28508
34. Li Y, Zhu L, Chu Z, Yang T, Sun HX, Yang F, et al. Characterization and Biological Significance of IL-23-Induced Neutrophil Polarization. *Cell Mol Immunol* (2018) 15:518–30. doi: 10.1038/cmi.2017.39
35. Dinarello CA. Overview of the IL-1 Family in Innate Inflammation and Acquired Immunity. *Immunol Rev* (2018) 281:8–27. doi: 10.1111/imr.12621
36. Eyerich K, Dimartino V, Cavani A. IL-17 and IL-22 in Immunity: Driving Protection and Pathology. *Eur J Immunol* (2017) 47:607–14. doi: 10.1002/eji.201646723
37. Tobin JM, Nickolich KL, Ramanan K, Pilewski MJ, Lamens KD, Alcorn JF, et al. Influenza Suppresses Neutrophil Recruitment to the Lung and Exacerbates Secondary Invasive Pulmonary Aspergillosis. *J Immunol* (2020) 205:480–8. doi: 10.4049/jimmunol.2000067
38. Conaway EA, de Oliveira DC, McInnis CM, Snapper SB, Horwitz BH. Inhibition of Inflammatory Gene Transcription by IL-10 Is Associated With Rapid Suppression of Lipopolysaccharide-Induced Enhancer Activation. *J Immunol* (2017) 198:2906–15. doi: 10.4049/jimmunol.1601781
39. Arend WP, Malyak M, Guthridge CJ, Gabay C. Interleukin-1 Receptor Antagonist: Role in Biology. *Annu Rev Immunol* (1998) 16:27–55. doi: 10.1146/annurev.immunol.16.1.27
40. Beringer A, Miossec P. IL-17 and TNF-α Co-Operation Contributes to the Proinflammatory Response of Hepatic Stellate Cells. *Clin Exp Immunol* (2019) 198:111–20. doi: 10.1111/cei.13316
41. Zheng L, Lam WK, Tipoe GL, Shum IH, Yan C, Leung R, et al. Overexpression of Matrix Metalloproteinase-8 and -9 in Bronchiectatic Airways. *vivo Eur Respir J* (2002) 20(1):170–6. doi: 10.1183/09031936.02.00282402
42. Jin Q, Chen Y, Lou Y, He X. Low Serum Retinol-Binding Protein-4 Levels in Acute Exacerbations of Chronic Obstructive Pulmonary Disease at Intensive Care Unit Admission is a Predictor of Mortality in Elderly Patients. *J Inflammation (Lond)* (2013) 10:31. doi: 10.1186/1476-9255-10-31
43. Landi F, Onder G, Gambassi G, Pedone C, Carbonin P, Bernabei R. Body Mass Index and Mortality Among Hospitalized Patients. *Arch Intern Med* (2000) 160(17):2641–4. doi: 10.1001/archinte.160.17.2641
44. Bone RC, Balk RA, Cerra FB, Dellinger RP, Fein AM, Knaus WA, et al. Definitions for Sepsis and Organ Failure and Guidelines for the Use of Innovative Therapies in Sepsis. The ACCP/SCCM Consensus Conference Committee. American College of Chest Physicians/Society of Critical Care Medicine. *Chest* (1992) 101:1644–55. doi: 10.1378/chest.101.6.1644
45. Follath F, Bindschedler M, Wenk M, Frei R, Stalder H, Reber H. Use of Ciprofloxacin in the Treatment of Pseudomonas Aeruginosa Infections. *Eur J Clin Microbiol* (1986) 5:236–40. doi: 10.1007/bf02013997
46. Kirikae T, Kirikae F, Saito S, Tominaga K, Tamura H, Uemura Y, et al. Biological Characterization of Endotoxins Released From Antibiotic-Treated Pseudomonas Aeruginosa and Escherichia Coli. *Antimicrob Agents Chemother* (1998) 42:1015–21. doi: 10.1128/aac.42.5.1015

Conflict of Interest: The authors declare that the research was conducted in the absence of any commercial or financial relationships that could be construed as a potential conflict of interest.

Publisher's Note: All claims expressed in this article are solely those of the authors and do not necessarily represent those of their affiliated organizations, or those of the publisher, the editors and the reviewers. Any product that may be evaluated in this article, or claim that may be made by its manufacturer, is not guaranteed or endorsed by the publisher.

Copyright © 2022 Ding, Han, Fu, Fan, Tang, Lv, Xue, Tian and Zhang. This is an open-access article distributed under the terms of the Creative Commons Attribution License (CC BY). The use, distribution or reproduction in other forums is permitted, provided the original author(s) and the copyright owner(s) are credited and that the original publication in this journal is cited, in accordance with accepted academic practice. No use, distribution or reproduction is permitted which does not comply with these terms.

frontiers in Immunology

REVIEW
published: 13 January 2022
doi: 10.3389/fimmu.2021.814709

The cGAS-STING Pathway in Bacterial Infection and Bacterial Immunity

Nanxin Liu[1†], *Xiaoxiao Pang*[1†], *Hua Zhang*[2*] *and Ping Ji*[1*]

[1] *Chongqing Key Laboratory of Oral Diseases and Biomedical Sciences, Chongqing Municipal Key Laboratory of Oral Biomedical Engineering of Higher Education, Stomatological Hospital of Chongqing Medical University, Chongqing, China,*
[2] *Department of Obstetrics and Gynaecology, The First Affiliated Hospital of Chongqing Medical University, Chongqing, China*

Cyclic guanosine monophosphate (GMP)-adenosine monophosphate (AMP) (cGAMP) synthase (cGAS), along with the adaptor stimulator of interferon genes (STING), are crucial components of the innate immune system, and their study has become a research hotspot in recent years. Many biochemical and structural studies that have collectively elucidated the mechanism of activation of the cGAS-STING pathway with atomic resolution have provided insights into the roles of the cGAS-STING pathway in innate immunity and clues to the origin and evolution of the modern cGAS-STING signaling pathway. The cGAS-STING pathway has been identified to protect the host against viral infection. After detecting viral dsDNA, cGAS synthesizes a second messenger to activate STING, eliciting antiviral immune responses by promoting the expression of interferons (IFNs) and hundreds of IFN-stimulated genes (ISGs). Recently, the cGAS-STING pathway has also been found to be involved in response to bacterial infections, including bacterial pneumonia, melioidosis, tuberculosis, and sepsis. However, compared with its functions in viral infection, the cGAS-STING signaling pathway in bacterial infection is more complex and diverse since the protective and detrimental effects of type I IFN (IFN-I) on the host depend on the bacterial species and infection mode. Besides, STING activation can also affect infection prognosis through other mechanisms in different bacterial infections, independent of the IFN-I response. Interestingly, the core protein components of the mammalian cGAS-STING signaling pathway have been found in the bacterial defense system, suggesting that this widespread signaling pathway may have originated in bacteria. Here, we review recent findings related to the structures of major molecules involved in the cGAS-STING pathway and the effects of the cGAS-STING pathway in various bacterial infections and bacterial immunity, which may pave the way for the development of new antibacterial drugs that specifically kill bacteria without harmful effects on the host.

Keywords: cGAS, STING, bacteria, infection, innate immunity, CGAMP

OPEN ACCESS

Edited by:
Alina Maria Holban,
University of Bucharest, Romania

Reviewed by:
Chunfu Zheng,
University of Calgary, Canada
Sarang Tartey,
IGM Biosciences, United States

***Correspondence:**
Ping Ji
jiping@hospital.cqmu.edu.cn
Hua Zhang
zh2844@gmail.com

[†]These authors have contributed equally to this work

Specialty section:
This article was submitted to Microbial Immunology, a section of the journal Frontiers in Immunology

Received: *14 November 2021*
Accepted: *21 December 2021*
Published: *13 January 2022*

Citation:
Liu N, Pang X, Zhang H and Ji P (2022) The cGAS-STING Pathway in Bacterial Infection and Bacterial Immunity. Front. Immunol. 12:814709. doi: 10.3389/fimmu.2021.814709

INTRODUCTION

Bacterial infections caused by opportunistic pathogens or invading pathogenic bacteria are the major infectious diseases worldwide, causing many diseases, including pneumonia, periodontitis, tuberculosis, conjunctivitis, gastroenteritis, and sepsis (1–5). Although antibiotics have enabled great success in preventing and treating bacterial infections, overconsumption and misuse have unfortunately increased the prevalence of muti-drug-resistant (MDR) microbes (6, 7). A study that collected the total medical expenditure of inpatients in China from 2013 to 2015 reported an additional medical expenditure of US $15,557.25 per inpatient with a healthcare-associated infection (HAI) caused by antimicrobial resistance (AMR) infection compared with that without an HAI (8). The mortality rate of AMR infections increases every year, and it is estimated to kill 10 million people per annum by 2050 (9). Thus, the resurgence of bacterial infections has made them a pressing public health concern once again. In this context, researchers are striving to develop new strategies to treat bacterial infections and avoid drug resistance, among which immunotherapy is an important research direction due to its breakthroughs and advantages in the treatment of cancer and autoimmune diseases (7, 10).

Through a complex network of biological processes, the immune system protects the body from diseases by recognizing and eliminating invading pathogens to sustain the organism's homeostasis. The mammalian innate immune system has evolved various pattern recognition receptors (PRRs) to detect pathogens and damage-associated molecular patterns (PAMPs and DAMPs) to trigger the host's defense rapidly (11). DNA sensors recognize pathogen DNA or misplaced host DNA to initiate innate immune responses and shape adaptive immunity (12–14). cGAS has been identified as the main DNA sensor that can generate the second messenger 2'3'-cGAMP upon detection of cytosolic DNA. Then, STING binds with 2'3'-cGAMP, and the complex is transferred from the endoplasmic reticulum (ER) to the Golgi complex, leading to the activation of TANK-binding kinase 1 (TBK1) and interferon regulatory factor 3 (IRF3) for IFN-I and inflammatory cytokine production (15) (**Figure 1**).

Over evolutionary time, cGAS has adopted multiple detection strategies to recognize various pathogens sensitively. First, cGAS is located in the cytoplasm, plasma membrane, and nucleus, allowing it to rapidly recognize DNA in different infectious contexts and initiate a downstream immune transcription cascade (16–19). Second, the sensitivity of cGAS to DNA can be increased by various factors during infection. For example, DNA that is prearranged by mitochondrial transcription factor A (TFAM) or modified by reactive oxygen species (ROS) can facilitate the detection of DNA by cGAS (20, 21). Third, inflammatory cytokines or cGAMP released from infected cells

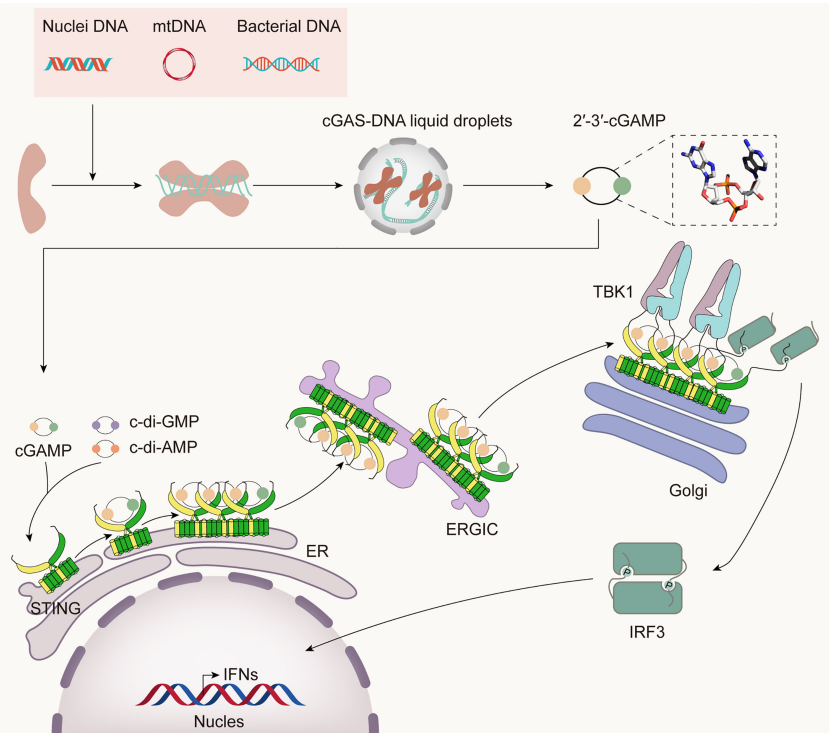


FIGURE 1 | The cGAS-STING pathway. Cytosolic DNA from bacteria, damaged mitochondria, or nuclei is sensed by cGAS, leading to the formation of cGAS-DNA liquid droplets, in which ATP and GTP are catalyzed to 2'3'-cGAMP. It binds STING and initiates the traffic of STING from ER to Golgi and post-Golgi compartments. During the translocation process, STING recruits TBK1 and IRF3. TBK1 phosphorylates STING in its CTT, then phosphorylates IRF3, which then translocates into the nucleus, inducing the expression of IFN-I and many other inflammatory cytokines.

act as alarm signals, giving rise to the activation of the cGAS-STING pathway in bystander cells (22).

This strong surveillance pathway has attracted intense attention in the field of innate immunity and is widely believed to be effective in preventing viruses from entry, replication, or budding during infection (23–26). Additionally, the cGAS-STING pathway has also been involved in bacterial infections, but it does not always defend against bacteria, sometimes promoting their replication and survival (27–29). Moreover, unlike the case in viruses, bacterial lipopolysaccharide (LPS) and cyclic di-nucleotides (CDNs, including c-di-AMP, c-di-GMP, 2'2'-cGAMP, and 3'3'-cGAMP) can activate the cGAS-STING pathway, in addition to bacterial DNA (30–35). Both extracellular CDNs (eCDNs) and intracellular CDNs (iCDNs) can activate STING independently of cGAS to initiate the host immune response (**Figure 1**), while recent studies have found that cGAS facilitates sensing of eCDNs to activate innate immunity (36). After eCDNs pass through the lipid bilayer of cells *via* a folate-organic phosphate antiporter or clathrin-dependent endocytosis (37), they directly bind cGAS, induce dimerization, and promote the interaction between cGAS and STING. In this process, cGAS acts as a scaffold protein to nucleate perinuclear signalosomes containing eCDNs/cGAS/STING, thus activating STING in a 2'-3'-cGAMP-independent manner (36). LPS, another important PAMP, has recently been reported to induce the cytosolic release of mitochondrial DNA (mtDNA), which subsequently activates the cGAS-STING pathway (35). Interestingly, the cGAS-STING pathway, which mediates the development and prognosis of bacterial infection in mammalian cells in various ways, has been found to originate as a bacterial immune system that confers immunological protection against viral infection (38). Therefore, a better understanding of the role of the cGAS-STING pathway in bacterial infection and bacterial immunity will be of great value in many areas of research, such as the development of small molecule drugs targeting the bacterial cGAS-STING pathway without adverse effects on the host.

In this review, we summarize current knowledge on structural insights into the cGAS-STING signaling pathway and further review the activation mechanism and specific functions of the cGAS-STING pathway during the infection of intracellular gram-positive bacteria, including *Listeria monocytogenes* and *Staphylococcus aureus*; extracellular gram-positive bacteria including *Streptococcus pyogenes* and *Streptococcus pneumoniae*; intracellular gram-negative bacteria including *Brucella abortus*, *Burkholderia pseudomallei*, and *Francisella tularensis*; and extracellular gram-negative bacteria, such as *Pseudomonas aeruginosa*; and *Mycobacterium tuberculosis*, with a special focus on LPS due to its controversial role in the activation of the cGAS-STING pathway. Next, we present recent advances in understanding how the bacterial cGAS-STING pathway protects bacteria against phage infection and discuss the similarities and differences of the cGAS-STING pathway in bacteria and humans. The cGAS-STING pathway, which protects both bacteria and humans, has become a shining star in innate immunity. New ideas for treating bacterial infections may be discovered by reviewing the structure, signal transduction process, and role of the cGAS-STING pathway in bacterial infection and bacterial immunity.

STRUCTURAL MECHANISM OF THE ACTIVATION OF THE cGAS-STING PATHWAY

In 2013, Chen's team discovered the existence of cGAS in mammalian cells and its ability to synthesize cGAMP as the second messenger to activate STING directly (39, 40). The cGAS-STING pathway has since been identified to be extensively involved in various physiological and pathological processes (41). Due to its important role in immunity, many studies have analyzed the structure of key proteins and molecules in this pathway. Early structural studies of inactive human cGAS (hcGAS), mouse cGAS, and other mammalian homologs did not provide structural information of DNA recognition by activated hcGAS (42–46). Recently, researchers have identified the structural mechanism of dsDNA sensing by hcGAS in an active conformation (47) and cGAS inhibition by nucleosomes (48, 49), deepening our understanding of cGAS activation and providing guidance for the design of drugs that target cGAS. Since STING was discovered in 2008, a large number of studies have carefully analyzed the structure of STING, generating an elegant model of STING activation in which upon cGAMP binding, STING rotates inwardly toward the ligand-binding pocket, closes its ligand-binding pocket, and releases its CTT to recruit TBK1 and IRF3 (50–52). Here, we review recent high-impact structural work on cGAS and STING to increase our understanding of this signaling pathway at atomic resolution and promote the development of novel therapeutics for cGAS-STING-related diseases.

cGAS

cGAS belongs to the structurally conserved cGAS/DncV-like nucleotidyltransferase (CD-NTase) superfamily, consisting of an N-terminal domain and a C-terminal catalytic domain. The catalytic domain comprises the NTase core and Mab21 domains and adopts a bilobed structure that comprises a central catalytic domain and two different positively charged surfaces (41, 53). A long helix 'spine' at the N-terminus of the catalytic domain bridges the N-terminal lobe, which possesses the NTase fold with a two-leaved, highly twisted β-sheet, and the C-terminal lobe, which contains a tight helix bundle (**Figure 2A**) (54, 55). The catalytic site is located at the edge of the deep groove between the two lobes of cGAS. Once the positively charged surface of cGAS interacts with dsDNA in a sequence-independent manner, a significant structural switch occurs such that the catalytic pocket of cGAS is rearranged to initiate the cyclization of guanosine triphosphate (GTP) and adenosine triphosphate (ATP).

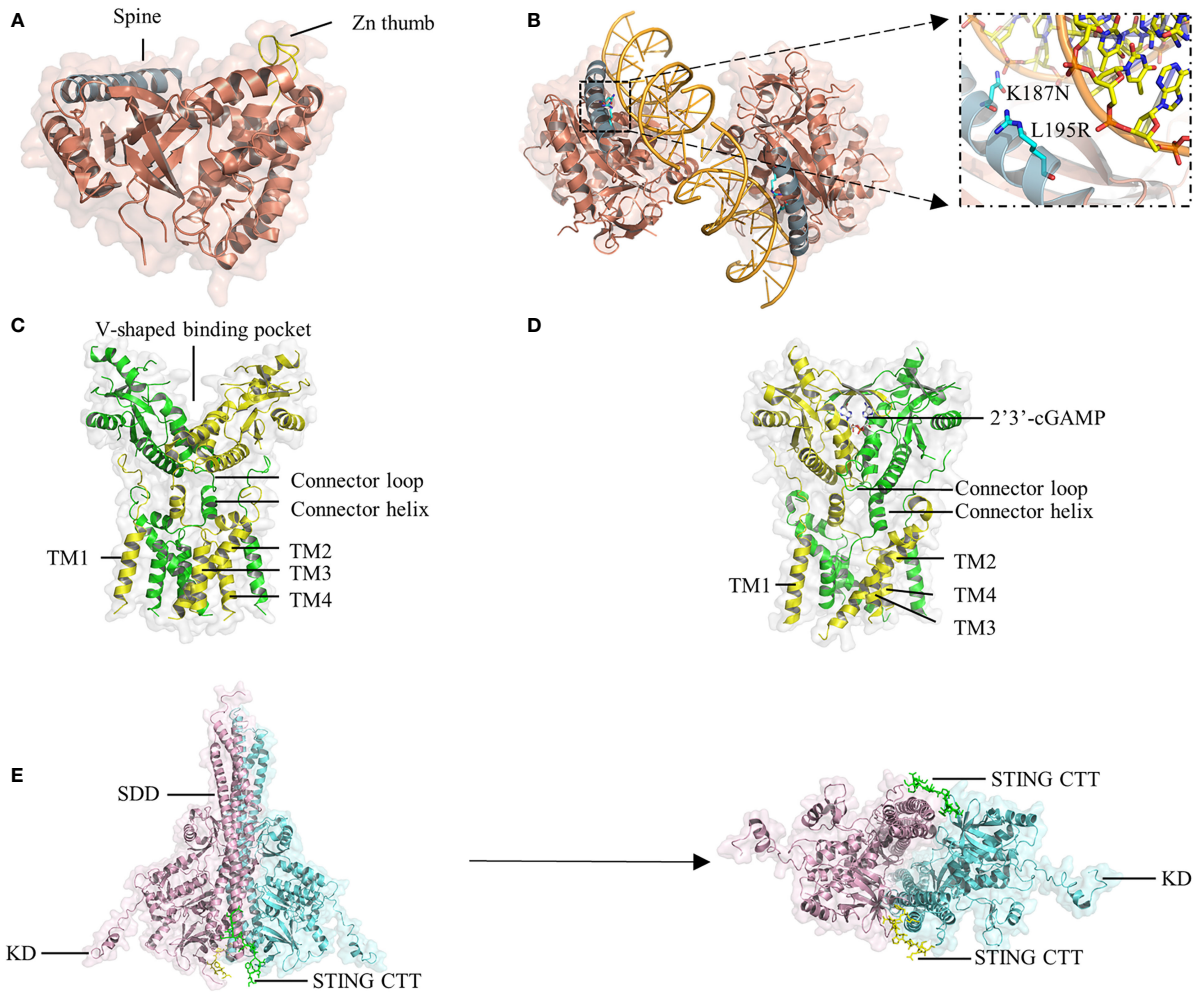


FIGURE 2 | Crystal structure of cGAS, STING, and TBK1. **(A)** The hcGAS model is shown as ribbon representation with annotated structures including 'spine' in blue and 'Zn thumb' in yellow. **(B)** Schematic and overview of the 2:2 hcGAS:dsDNA complex structure. Zoom-in cutaways of the locations of K187 and L195 substitutions in hcGAS that are responsible for its long dsDNA preference. **(C)** Representation of the structure of full-length human STING in the apo state. **(D)** Structure of STING bound to cGAMP. **(E)**, Ribbon representations of the structure of mouse TBK1 in complex with the human STING CTT in a side view (left) and a bottom view (right).

A unique protrusion called the 'Zn thumb' connects the two lobes and promotes the interaction of cGAS and the sugar-phosphate backbone of the DNA] duplex (**Figure 2A**) (45). Binding to dsDNA brings the two lobes of cGAS close to each other and activates cGAS (44, 46, 56). Four cGAS molecules assemble into a 2:2 mouse cGAS-dsDNA complex after binding dsDNA through extensive electrostatic interactions and hydrogen bonds. In these complexes, two dsDNA molecules are cross-linked with a cGAS dimer, and the two cGAS dimers bind to the dsDNA asymmetrically to avoid steric clashes of the two dsDNA duplexes (45). Similar to the mouse model of the cGAS-dsDNA complex, cGAS can oligomerize to a functionally active 2:2 cGAS-dsDNA state (41). Although oligomerization is beneficial for regulating enzymatic function, it is unclear whether it is necessary for cGAS activation.

HcGAS can discriminate the length of DNA and prefers long dsDNA, causing its cGAMP production level to be significantly lower than that of other mammals. Both the human-specific substitutions K187N and L195R (47) (**Figure 2B**) and the ladder-like networks formed between cGAS dimers and dsDNA (20) may explain the preference of human cGAS for long dsDNA, leading to a reduced immune response by reshaping the balance between the sensitivity and tolerance of dsDNA. In cGAS-DNA liquid droplets, a linear dinucleotide 5'-pppG(2'-5')pA is first formed and then flips over to promote the generation of the second 3'-5' phosphodiester bond, resulting in the formation of 2'3'-cGAMP (39, 57). Moreover, in addition to a positively charged surface, another cGAS-dsDNA interface (labeled site-C) was found to enhance the enzymatic activity of cGAS. These studies will provide insights facilitating the design of drugs targeting the active site of cGAS.

STING

As an adaptor protein, STING is the core component in the signaling cascade of the innate immune response (58, 59). The small protein (~40 kDa) is anchored to the ER membrane by an N-terminal portion containing four transmembrane helices (TM1-4). The C-terminal domain (CTD) of STING consists of a ligand-binding domain (LBD) that is responsible for binding 2'3'-cGAMP and CDNs, and a C-terminal tail (CTT) that is capable of binding TBK1, both of which face the cytosol (60, 61). Recently, cryo-electron microscopy analyses have revealed that STING in apo states exists as a dimer in which a domain-swapped architecture is adopted through organizing the eight transmembrane helices and two CTDs (52). In the dimeric TM domain, one layer is the central layer formed by TM2 and TM4, and the other layer is the outer layer composed of TM1 and TM3. The LBD domain contains five β strands and four α helices, of which α-helix 1 is linked to TM4 by the connector helix (residues 141-149) and connector loop (residues 150-156) (52). Two STING CTDs dimerize mainly *via* hydrophobic interactions, generating a V-shaped binding pocket (**Figure 2C**).

Upon cGAMP binding, a four-stranded β-sheet lid-like structure forms over the ligand-binding pocket of STING to hold cGAMP tightly; this is described as the 'closed' conformation (**Figure 2D**). Interestingly, the crystal structure of STING bound to c-di-GMP is in an 'open' conformation, similar to the structure of apo STING (59, 62, 63). Moreover, a linked amidobenzimidazole compound can bind to and activate STING in an 'open' structure (64). However, the binding affinity of human STING to c-di-GMP is weaker than that of STING to cGAMP (65). Therefore, it is likely that closure of the ligand-binding domain is not required for STING activation but is beneficial for increasing binding affinity (50). Another conformational change induced by cGAMP is that the LBD of STING rotates 180° relative to the TM domain, causing the two connector LBDα1 elements, which form a right-handed crossover in the apo state, to become parallel to each other (52).

Moreover, cGAMP initiates intracellular transport of STING by interrupting the interaction between STING and ER-resident protein stromal interaction molecule 1. Then, STING travels anterogradely from the ER to the Golgi apparatus depending on SEC24C, a component of the canonical coat protein complex II (COPII), *via* the ER-Golgi intermediate compartments (ERGICs) upon STING oligomer formation (66). STING dimers are not the only functionally active units in STING; tetramers and higher-order oligomers are also observed to form through the rotation of the LBD and the conformational change of the connector loop (41). The polymerization of STING also contributes to its activation (67–69), but the size and minimum activation length of functional STING polymers are unclear.

THE STING CTT AND TBK1

The STING CTT plays a vital role in activating STING-TBK1-IRF3 by mediating the recruitment and activation of TBK1 and IRF3. TBK1 exits as an elongated dimer containing the scaffold and dimerization domain (SDD), a ubiquitin-like domain (ULD), and the kinase domain (KD) (**Figure 2E**) (51, 70). The N-terminal lobe of the KD interacts with the SDD of the dimer partner. The TBK1-binding motif (TBM) within the STING CTT interacts with TBK1 at many sites, including a groove between the KD of one monomer and the SDD of another monomer in the same TBK1 dimer; a deep hydrophobic pocket in the middle of the groove; Phe585, Tyr55, and Arg405 in the SDD; and Lys 30 in the KD (51). Although the TBK1 dimer binds flexibly to C-terminal TBMs from the STING dimer, it has little or no contact with the LBD of STING. Recently, some residues in the TBM were identified to constitute a highly conserved PLPLRT/SD motif, which is responsible for TBK1 recruitment (70). However, even if a large amount of TBK1 already binds to these preformed STING dimers on the ER, phosphorylation in *trans* will be blocked by steric hindrance. TBK1 can only be activated if parallel-stacking of STING homodimers is disrupted by the conformational change induced by cGAMP to interfere with CTT sequestration, which is essential for controlling basal STING activation (71). The TBK1 dimer binds two peptides from STING, and each peptide simultaneously binds two TBK1 monomers to form a 2:2 complex. In the STING-TBK1 complex, the autophosphorylation of TBK1 is mediated by the proximity in trans induced by adjacent STING molecules. High-order oligomerization of STING and TBK1 promotes the TNK1-induced phosphorylation of the serine residue in the pLxlS motif of STING, which not only enhances the binding of STING with TBK1 (51) but also provides a docking site for STING to bind IRF3. The recruited IRF3 is phosphorylated by adjacent TBK1 binding to the CTT of STING and then dimerizes and enters the nucleus to initiate the production of inflammatory cytokines, including IFN-I (**Figure 1**), proving that STING may scaffold the interaction between TBK1 and IRF3. Nuclear factor (NF)-κB signaling is also downstream of STING activation (72). However, it is unclear which of the two signaling pathways is activated or comes first. Moreover, although the important role of CTT in STING signal propagation has been confirmed, the detailed structure of CTT is still unknown.

cGAS-STING SIGNALING PATHWAY IN BACTERIAL INFECTION

The immune system is required for protecting the body by controlling bacterial infections but can also lead to pathology. On the one hand, IFN-I induced by the cGAS-STING pathway can fight against bacterial infections and inhibit the overactivation of the immune response (73, 74). On the other hand, it had been identified to increase susceptibility to several bacteria, such as *Listeria monocytogenes* (75, 76). Furthermore, in the face of bacterial infection, the activation of STING not only initiates the IFN-I response but also interacts with bacteria by regulating metabolism or other downstream pathways (27, 77). Recently, c-di-AMP produced by live gram-positive bacteria, whether intracellular bacteria such as *Staphylococcus aureus* and

Listeria monocytogenes or extracellular bacteria such as *Streptococcus pyogenes*, has been reported to induce a previously unappreciated cell-autonomous response by STING to elicit an augmented IFN-I response in host defense against infection caused by live bacteria (78). The mRNA of live gram-negative bacteria, rather than c-di-AMP, induces innate responses *via* STING-independent signaling pathways (79). Therefore, the activation mechanisms and effects of the cGAS-STING pathway differ between invading bacteria and infected tissues or cells. The interaction between the cGAS-STING pathway and gram-positive or gram-negative bacteria will be discussed in detail below (**Table 1** and **Figure 3**).

INTRACELLULAR GRAM-POSITIVE BACTERIA

Staphylococcus aureus

Staphylococcus aureus is the etiological pathogen of many diseases, ranging from superficial skin infections to life-threatening infections such as pneumonia (80, 81). The c-di-AMP released from *S. aureus* biofilms activates STING to upregulate the expression of IFN-I in macrophages. The STING-dependent IFN-I response promotes macrophage polarization to an anti-inflammatory phenotype, resulting in impaired *S. aureus* clearance and exacerbated infectious outcomes (82). Moreover, the cGAS-STING pathway can be activated in response to live but not dead *S. aureus* by sensing *S. aureus* DNA. During the early stage of *S. aureus* infection, the Toll-like receptor (TLR) and cGAS-STING pathways are both activated by live *S. aureus* but exhibit opposite roles in the host immune response to *S. aureus*. TLR signaling restricts infection, while the cGAS-STING pathway enhances bacterial growth (83, 84). The transcription and expression of IFN-I are well-known to be induced by phosphorylation of IRF3. However, IRF3 phosphorylation in dendritic cells acts independently of activating the cGAS-STING pathway to drive IFN-I expression in response to inactivated *S. aureus* treated by ultraviolet irradiation (85).

Meanwhile, the production of many cytokines induced by live or inactivated *S. aureus* is different (85, 86), suggesting that the viability of *S. aureus* may influence the host immune response to its infection. Previous studies reported that the cGAS-STING pathway was involved in initiating necroptosis in macrophages in an IFN-I-dependent manner (87, 88). However, in the context of *S. aureus* pneumonia, STING was reported to facilitate the restriction of *S. aureus* infection and protect the architecture and function of the lung by suppressing macrophage necroptosis (89). According to these studies, IFN-I induced by the cGAS-STING pathway seems to be related to immune evasion of *S. aureus*, while the activation of STING may also contribute to controlling pulmonary *S. aureus* infection. Therefore, the protective effect of STING against *S. aureus* pneumonia needs to be confirmed first. Next, how STING suppresses necroptosis in the presence of increased IFN-I needs to be further studied.

Listeria monocytogenes

Listeria monocytogenes can cause listeriosis, which usually manifests as self-limited gastroenteritis, although a few cases may develop into sepsis, meningitis, and monocytosis, mainly in newborns, the elderly, and immunocompromised individuals (90, 91). The IFN-I response has been reported to stimulate excessive immune activation as an important component of listeriosis pathology (76, 92, 93). During *L. monocytogenes* infection, STING is activated by bacterial DNA-activated cGAS

TABLE 1 | The activation of the cGAS-STING pathway in various bacterial infections.

Pathogens	DNA	CDNs	IFN-I response induced by the cGAS-STING pathway	Additional functions of STING activation	Refs
Staphylococcus aureus	live *S. aureus* DNA	c-di-AMP	i. Promote macrophage polarization to an anti-inflammatory phenotype ii. Promote bacterial growth	Control pulmonary *S. aureus* infection	(80–89)
Listeria monocytogenes	*Listeria* DNA	c-di-AMP	Detrimental effect	i. Reduce the influx of inflammatory monocytes ii. Promote Evs formation, and dampen the immunological activity of T cells	(73, 76, 90–96)
Streptococcus pneumoniae	Pneumococcal DNA, mtDNA	c-di-AMP	Suppress inflammation-related damage and lethality	Regulate blood coagulation	(74, 77, 97–100)
Streptococcus pyogenes	Unclear	Unclear	Suppress the inflammatory response	Unclear	(101–103)
Brucella abortus	*B.abortus* DNA	c-di-GMP	i. Anti-bacterial response ii. Induce UPR expression to promote *B.abortus* replication	Mediate cellular metabolism to control *B.abortus* replication	(27, 28, 104–106)
Burkholderia	Micronuclei (dsDNA)	Unclear	Irrelevant to the antibacterial response	Autophagic cell death	(107–114)
Francisella novicida	*Francisella* DNA	Unclear	i. Induce cell apoptosis ii. Promote bacteriolysis and additional DNA release	Promote Evs formation, and dampen the immunological activity of T cells	(115–118)
Pseudomonas aeruginosa	*Pseudomonas* DNA	Unclear	Fight against bacterial infection	i. Enhance NO synthase expression ii. Inhibit proinflammatory cytokines	(119–122)
Mycobacterium tuberculosis	Mycobacterial DNA	c-di-AMP	Antibacterial defense	unclear	(1, 123–134)

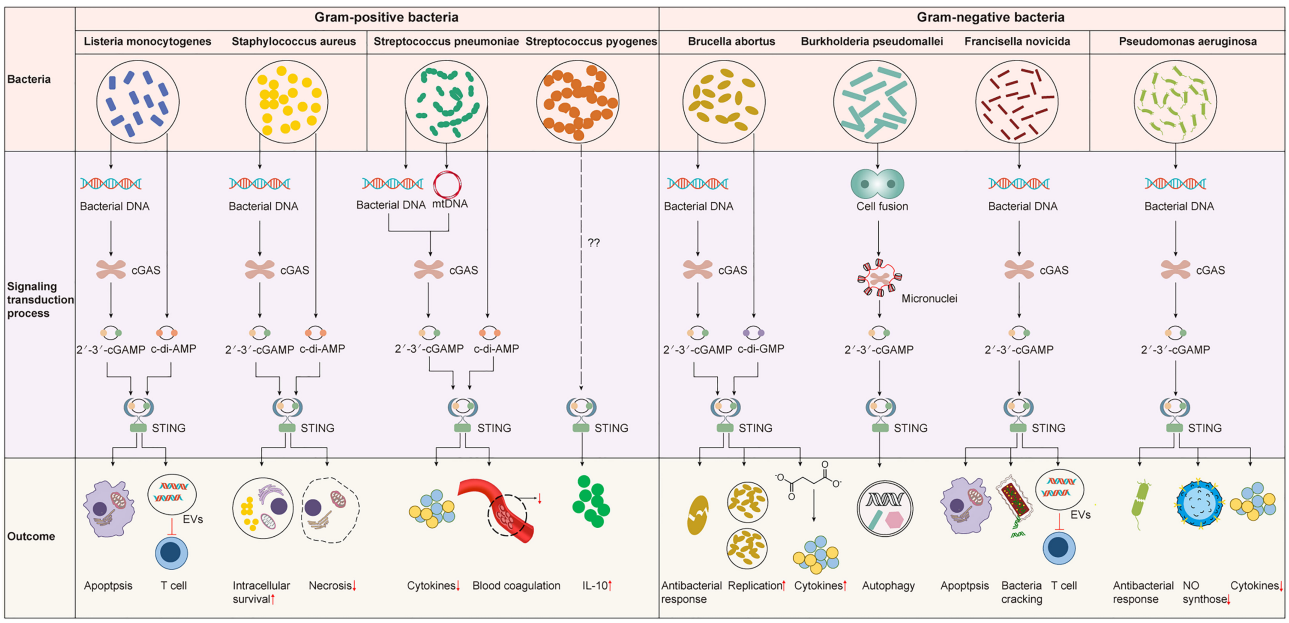


FIGURE 3 | The cGAS-STING pathway in bacterial infection. The cGAS-STING pathway is widely involved in various bacterial infections. However, the signaling transduction process and outcome upon the activation of the cGAS-STING pathway are different. STING is activated by 2′3′-cGAMP produced by cGAS or bacterial CDNs to induce an IFN-I response that may be protective or detrimental for the host. STING can also influence the infection outcome by mediating other important biological or physiological processes like blood coagulation or metabolism independent of IFN-I response.

or another DNA sensor, IFI16, or by binding c-di-AMP secreted by *L. monocytogenes via* multidrug efflux pumps (MDRs), in both cases leading to the production of IFN-I (73, 94). Therefore, *L. monocytogenes* trigger IFN responses *via* the cGAS-STING pathway, making it a novel therapeutic target for listeriosis. Recently, the endogenous anaphylatoxins C5a and C3a have been found to suppress the expression of STING and phosphorylated TBK1 and IFN-β during *L. monocytogenes* infection, consequently attenuating the detrimental effect of IFN-β production, for example, inhibiting *L. monocytogenes*-mediated-apoptosis of immune cells (73). However, the STING-dependent immune response was suggested to defend against *L. monocytogenes* by reducing the influx of inflammatory monocytes and systemic bacterial loads during enterocolitis (95). This result indicated that in addition to the IFN-I response, STING activation in enterocolitis could also exert immunomodulatory effects through other mechanisms that need further investigation. *L. monocytogenes* has evolved to manipulate STING strategically for its benefit instead of evading it. For example, its DNA is sorted into extracellular vesicles (EVs) in a process that depends on STING, TBK1, and multivesicular body protein (MVB12b) and is then delivered to bystander cells to further activate the cGAS-STING pathway. Both EVs that dampened the immunological activity of T cells and increased IFN-I production in bystander cells promote the establishment of infection in a STING-dependent manner (96). Other intracellular bacteria, including *Francisella tularensis* and *Legionella pneumophila*, also adopt this strategy to impair antibacterial defense. According to these studies, the cGAS-STING pathway dominantly enhances host susceptibility to *L. monocytogenes* by upregulating IFN-I production but may play an antibacterial role in some diseases in an IFN-independent manner. However, the underlying mechanism of STING resistance to *L. monocytogenes* infection remains unclear.

EXTRACELLULAR GRAM-POSITIVE BACTERIA

Streptococcus pneumoniae

Streptococcus pneumoniae can colonize the upper respiratory tract asymptomatically or cause diseases such as bacterial pneumonia and meningitis (97, 98). It enters mature phagolysosomes and releases nucleic acids and c-di-AMP into the host cytosol *via* a secretion system or following partial lysis. *S. pneumoniae* c-di-AMP initiates host innate immune responses by activating STING directly and increasing the expression of IFN-β (99). IFN-β production is also induced by pneumolysin (Ply), a pore-forming protein and a major virulence factor of *S. pneumoniae*. It can initiate oxidative damage to mitochondria in macrophages, leading to the cytosolic translocation of mtDNA and triggering IFN-β expression in a cGAS-STING dependent manner (97). Although cGAS has been reported to sense pneumococcal DNA and then stimulate STING, resulting in the activation of IFN-I response in mouse macrophages, how pneumococcal DNA enters the cytoplasm of host cells has not been clarified. Notably, IFN-I induced by *S. pneumoniae* has

been identified to be protective to the host by suppressing inflammation-related damage and lethality (74). Moreover, STING can regulate coagulation by increasing cytosolic calcium and then triggering the release of a key initiator of blood coagulation independent of TBK1 or IRF3 activation, thus limiting the severity of sepsis caused by *S. pneumoniae* (77). These results reveal that the cGAS-STING signaling pathway plays an immunoprotective role in *S. pneumoniae* infection by generating IFN-I and regulating coagulation. Conversely, *Ruiz-Moreno* et al. reported that although the cGAS-STING pathway sensed *S. pneumoniae* invasion and induced an IFN-I response, it was dispensable for defense against *S. pneumoniae* infection (100). Hence, the exact role of the cGAS-STING pathway in anti-pneumococcal defense needs to be further studied.

Streptococcus pyogenes

Streptococcus pyogenes can cause a range of symptoms, from mild illness to life-threatening infections such as necrotizing fasciitis (101). A previous study suggested that the activation of the STING pathway and the subsequent increase in IFN-I production were probably initiated by cGAS upon sensing cytosolic nuclear acids in *S. pyogenes*-infected macrophages and dendritic cells (102). However, *Movert* et al. reported that *S. pyogenes* activated the STING pathway independent of cytosolic dsDNA because neither bacterial nor host DNA could be detected in the cytosol of *S. pyogenes* infected macrophages (103). In addition, *S. pyogenes* promoted the production of anti-inflammatory IL-10 to curb the inflammatory response through the activation of the STING signaling pathway mediated by the streptococcal M protein, a surface-anchored virulence factor (103). Thus, IFN-I signaling was exploited by *S. pyogenes* to avoid life-threatening inflammation. Although the activation of STING has been suggested to be independent of cGAMP generated by cGAS during *S. pyogenes* infection (103), whether it is activated by c-di-AMP synthesized by *S. pyogenes* remains unknown.

INTRACELLULAR GRAM-NEGATIVE BACTERIA

Brucella abortus

Brucella abortus replicates and survives in macrophages and dendritic cells by forming *Brucella*-containing vacuoles (BCVs) (104). *B. abortus* c-di-GMP binds to STING, triggers the TBK1-IRF3 signaling cascade, and initiates the IFN-I response independently of cGAS. Subsequently, IFN-I signaling upregulates the expression of guanylate-binding proteins (GBPs), which can promote *B. abortus* DNA translocation from the BCV to the cytosol to activate AIM2 and increase IL-1β secretion (105). However, whether cGAS senses *B. abortus* genomic DNA and further amplifies the IFN-I signaling pathway and whether cGAS and AIM2 can cooperate to protect the host from *B. abortus* infection remain unclear. Moreover, STING controls *B. abortus* replication by regulating the metabolic reprogramming of macrophages. STING increases the levels of succinate to stabilize hypoxia-inducible factor-1 alpha (HIF-1α), resulting in the production of proinflammatory cytokines to limit *B. abortus* infection (27). However, the STING and IFN-I signaling pathway was reported to be required for an increase in unfolded protein response (UPR) expression, which facilitates *B. abortus* replication (28). According to these studies, STING is critical in host protective immunity by triggering the IFN-I pathway and mediating cellular metabolism. Thus, we speculate that when STING responds to *B. abortus* infection, the response that defends against *B. abortus* may be stronger than that promoting bacterial replication. The specific mechanism of these antagonistic effects needs to be further elucidated. In addition, *B. abortus* can decrease the expression of STING in the early stage of infection by upregulating miR-24-2 *via* a type IV secretion system, providing an environment in which *Brucella* can replicate in host cells free from the threat of the cytosolic surveillance pathway (106). In the future, appropriate utilization of miRNAs targeting STING may prevent excessive inflammation induced by *B. abortus* infection.

Burkholderia

Burkholderia pseudomallei affects immune function *via* manipulating the caspase system, causing melioidosis with high morbidity and mortality (107, 108). Unlike many other intracellular bacteria, *B. pseudomallei* induces host cell fusion, an important aspect of melioidosis pathogenesis (109, 110). Cell fusion leads to the formation of multinucleated giant cells (MNGCs), which facilitate intracellular dissemination of *B. pseudomallei* without exposure to extracellular host defenses or antimicrobials (111, 112). cGAS responds to *B. pseudomallei* infection by colocalizing with micronuclei formed during aberrant and abortive mitotic events (110). Upon activation of the cGAS-STING pathway, autophagic cell death is induced to limit aberrant cell division and cellular transformation. Intriguingly, transcriptional changes rather than IFN-I production are induced by the cGAS-STING pathway (110). *Burkholderia thailandensis*, a close relative of *B. pseudomallei* (113), also invades the cytosol, induces cell-cell fusion allowing intracellular diffusion, and forms MNGCs to promote bacterial replication. Downstream signaling molecules rather than upstream molecules, such as cGAS/STING for IFN-I, are critical to restrict MNGC formation and bacterial actin motility during *B. thailandensis* infection (114). These results indicate that the IFN-I production induced by the cGAS-STING pathway may be irrelevant to the antibacterial response.

Francisella novicida

During *Francisella novicida* infection, cGAS and interferon-γ inducible protein 16 (IFI16) synergistically sense cytosolic *Francisella* DNA to fully activate the STING-dependent IFN-I response, which plays a detrimental role by inducing apoptotic cell death (115, 116). In addition, IFN-I signaling is required to activate the AIM2 inflammasome by promoting bacteriolysis and bacterial DNA release (117). In turn, the AIM2 inflammasome negatively regulates the IFN-I response by mediating the interferon regulatory module, thus restraining the cGAS-driven IFN-I response (118). However, IFN-I signaling overrides the

protective AIM2 inflammasome responses and plays a dominant role in exacerbating *F. novicida* infection (117). Since the relative expression levels of cGAS, IFI16, and AIM2-like receptors vary in different cell types, the specific reaction and interaction mechanisms in specific cells need to be further studied. Furthermore, *F. novicida* can suppress antibacterial defense by forming EVs in a STING-dependent manner to promote infection, similar to *L. monocytogenes*.

EXTRACELLULAR GRAM-NEGATIVE BACTERIA

Pseudomonas aeruginosa

Pseudomonas aeruginosa is an opportunistic bacterium that can easily cause infection in immunocompromised people (119). The cGAS-STING pathway has been reported to have a protective effect in *P. aeruginosa* infection by promoting host resistance against *P. aeruginosa* infection and negatively modulating host inflammatory responses (120, 121). After penetrating *P. aeruginosa* into host cells, its genomic DNA can be sensed by cGAS, which mediates the IFN-I response by activating STING. Although the secretion of IFN-I increased, the level of proinflammatory cytokines decreased due to the inhibition of p38, JNK, ERK, and NF-κB activity by STING. In addition, STING can enhance NO synthase expression to eliminate invaded *P. aeruginosa* (121). Overall, cGAS-STING restrains P. aeruginosa infection by inducing the expression of IFN or NO synthase and protects host cells by suppressing excessive production of inflammatory cytokines. Recently, an X-ray-inactivated whole-cell vaccine was found to resist *P. aeruginosa* infection by stimulating the cGAS-STING pathway in dendritic cells (DCs) to foster its maturation which boosts T cells (122). Notably, the vaccine also protected against an MDR strain (122). Although the specific mechanism by which bacterial DNA enters the cytoplasm and whether host DNA is involved in the activation of cGAS during *P. aeruginosa* infection remains unclear, the critical role of the cGAS-STING pathway in the recognition and restriction of *P. aeruginosa* has been proven. In summary, immunotherapy targeting the cGAS-STING signaling pathway to treat AMR infections is a reliable line of research.

OTHERS

Mycobacterium tuberculosis

Mycobacterium tuberculosis, neither gram-positive nor gram-negative bacteria, is the etiological agent of tuberculosis, which has been a major threat to human health since its discovery more than a century ago (1). *M. tuberculosis* survives primarily within macrophages, with the ESX-1 secretion system as the virulence factor. Numerous previous studies have suggested that the passive leakage of mycobacterial DNA into the cytosol with the help of ESX-1 can activate the cGAS-STING pathway to induce antibacterial defenses (123–127). What's more, a recently revised model indicated that ESX-1 was involved in the mobilization of the cytosolic release of mitochondrial and nuclear host DNA by permeabilizing host membranes *via* genetically separable mechanisms (128). But the underlying mechanism in which ESX-1 affects the membrane integrity of the phagosome, nucleus, and mitochondria remains unclear. In addition, Mycobacterial c-di-AMP activates STING directly independent of ESX-1 (30, 129).

During the parallel evolution between host cells and *M. tuberculosis*, *M. tuberculosis* has developed many strategies to evade the surveillance of the cGAS-STING pathway to establish infection (130–133). For example, *M. tuberculosis* coding protein Rv0753c (MmsA) can not only decrease STING levels and subsequent IRF3 activation by binding and colocalizing with STING, but also facilitate STING autophagic degradation by binding with p62, resulting in the inhibition of STING-TBK1-IRF3 pathway (130); *M. tuberculosis* phosphodiesterase (PDE) can inhibit STING activation by cleaving both c-di-AMP and cGAMP to blunt the antibacterial response (133); *M. tuberculosis* isolates associated with severe tuberculosis can evade cGAS-STING surveillance system by accumulating mutations in the ESX components or generating sigA recognition boxes, and at the same time, IL-1β secretion caused by these isolates is significantly decreased (131). Furthermore, both CDNs-adjuvanted protein subunit vaccine and inhibitors of *M. tuberculosis* PDE can protect the host from infection by *M. tuberculosis* through eliciting a stronger anti-inflammatory response (132, 134). Thus, vaccine design and therapeutic development should consider genetic diversity and the continuous evolution of *M. tuberculosis* isolates in the future.

LPS

LPS, localized in the outer layer of the membrane of gram-negative bacteria, has been widely recognized to cause various infections by activating TLR4. Extracellular LPS-induced activation of the TLR4-dependent cGAS-STING-NLRP3 axis is responsible for acute lung injury (ALI). LPS was reported to promote the cytosolic release of mtDNA, which activated cGAS to induce inflammation and oxidative stress in BMDMs. cGAS inhibition could mitigate inflammation by blocking the activation of STING and the NLRP3 inflammasome in LPS-treated BMDMs (135). In contrast, *Cao* reported that cGAS was dispensable for the LPS-induced inflammatory response in BMDMs because LPS and IFN-γ elicited a robust increase in inflammatory cytokines in both cGAS-null and wild-type cells (136). Both studies found that inflammatory cytokine secretion was significantly decreased in cGAS-silenced or cGAS-knockout BMDMs, while higher mRNA levels of these inflammatory cytokines were observed in cGAS-null cells than in cells not treated with LPS, which indicated that other critical factors participate in promoting the inflammatory response in LPS-stimulated BMDMs. The difference in roles of cGAS in the inflammatory response of BMDMs might also be explained by the different treatment modalities used, one stimulated by LPS only and the other stimulated by LPS in combination with IFN-γ. As for STING, it is activated by cGAMP produced by cGAS to aggravate inflammation and oxidative stress in LPS-induced ALI (135).

Meanwhile, its expression in BMDMs is upregulated by the transcription factor c-Myc, the expression of which is enhanced by LPS (135). However, LPS was reported to induce the perinuclear translocation of STING mediated by TLR4 to activate the phosphorylation and nuclear translocation of IRF3 in mice or neonatal rat cardiomyocytes (NRCMs) without affecting the protein expression of STING (137). Therefore, STING activation may not necessarily be accompanied by increased protein expression in some cell types. STING plays a vital role in LPS-induced cardiac dysfunction, inflammation, apoptosis, and pyroptosis by triggering the activation of the NLRP3 inflammasome in an IRF3-dependent manner (137). Above all, targeting the cGAS-STING pathway is an efficient strategy to inhibit LPS-induced acute lung injury and cardiac dysfunction.

Intriguingly, STING expression was repressed by LPS in human cells through a metabolism-dependent pathway (138). During the metabolic reprogramming of human cells after LPS stimulation, a cell-permeable derivative of itaconate (4-octyl-itaconate, 4-OI) accumulated and then activated the transcription factor Nrf2 (nuclear factor (erythroid-derived 2)-like 2), which decreased STING expression and negatively regulated the STING-dependent IFN-I response. However, inhibition of STING by Nrf2 following LPS treatment was observed in neither BMDMs nor RAW264.7 cells. Additionally, the phosphorylation and expression of STING were enhanced in LPS-treated mouse cells within 12 h, and the peak was reached at 6 h, whereas LPS inhibited the expression of STING in human cells from 24 to 72 h (138), and this inhibition strengthened with time. These results suggest that the effect of LPS on STING may be cell-dependent and time-dependent. Additionally, it is necessary to study further whether LPS can inhibit the expression of STING in mouse cells after prolonged treatment, whether the effect of LPS on STING is consistent in human and mouse macrophages, and what role STING plays in the crosstalk between metabolism and innate immunity; these findings will benefit the identification of a potential treatment target in STING-dependent inflammatory diseases.

LPS from extracellular bacteria can also gain access to the cytosol of host cells through endocytosis mediated by outer membrane vesicles (OMVs) in a TLR4-independent manner (139). Internalized LPS activates the noncanonical caspase-11 inflammasome, which cleaves Gasdermin D (GSDMD), leading to the generation of GSDMD N-terminal fragments (GSDMD-NT) and subsequent pyroptosis in bacterial sepsis (140, 141). Recently, activation of caspase-11 and formation of GSDMD-NT by cytosolic LPS were reported to initiate a decrease in mitochondrial membrane potential (MMP) and the release of mtDNA into the cytosol in lung microvascular endothelial cells (LMVECs). The DNA-sensing cGAS-STING pathway is activated by cytosolic mtDNA, leading to the impairment of endothelial regeneration after inflammatory lung injury (35). It is worth noting that internalized LPS induces a decrease in MMP, while extracellular LPS causes an increase in MMP (35, 142). Although this difference may be due to differences in cell type, the finding that intracellular LPS transfection activated cGAS-STING through the caspase-11-GSDMD pathway independent of TLR4 activation reveals that LPS can induce mitochondrial injury through different intracellular and extracellular pathways, which requires further investigation (**Table 2**).

cGAS-STING SIGNALING PATHWAY IN BACTERIAL IMMUNITY AGAINST VIRAL INFECTION

With a deeper understanding of the diversity and complexity of bacterial immune systems, researchers have speculated that these defense systems mirror those of animals. The bacterial CRISPR-Cas system, for example, is similar to the human adaptive immune system, which can form immune memories to fight specific pathogens upon re-infection (38). The cGAS-STING pathway is a crucial signaling cascade in innate immunity that regulates inflammatory diseases, autoimmune diseases, senescence, and cancer (15). Currently, most of the work regarding the relationship between the cGAS-STING signaling pathway and bacteria focuses on the controversial role of the cGAS-STING pathway during bacterial infection. Strikingly, several recent studies have reported that cGAS-like and STING-like proteins that protect bacteria against viral infection are found in bacteria, raising the possibility that the cGAS-

TABLE 2 | The cGAS-STING pathway response to LPS.

LPS administration	cGAS expression	Cytosolic mtDNA level	cGAMP production	STING expression	STING localization	STING phosphorylation	The role of the cGAS-STING pathway	Refs
LPS transfection	NA	upregulate	upregulate	NA	NA	NA	LPS activates the cGAS-STING pathway to promote inflammatory injury	(35)
LPS added to the culture medium	Upregulate	upregulate	upregulate	upregulate	NA	upregulate	LPS activates the cGAS-STING pathway to promote lung injury	(135)
LPS added to the culture medium	NA	NA	NA	NA	NA	NA	cGAS is dispensable for the inflammatory response induced by LPS	(136)
LPS added to the culture medium	NA	NA	NA	No change	Promote its perinuclear translocation	NA	LPS induces cardiac inflammation *via* the STING-IRF3-NLRP3 axis	(137)
LPS added to culture medium	NA	NA	NA	downregulate	NA	NA	LPS negatively regulate STING *via* an Nrf2-dependent way	(138)

NA, not available.

STING pathway originates from the bacterial immune system (110, 143, 144). Next, we will review the structure and function of the cGAS-STING pathway in bacterial immunity (**Figure 4**).

cGAS-LIKE ENZYMES AND CDNs

A bacterial four-gene operon system that contains cGAS-like and downstream effector-encoding genes and two additional genes, known as the CDN-based anti-phage signaling system (CBASS), initiates a second messenger-dependent antiviral response that is similar to that in mammalian cells (145, 146). Bacterial CD-NTases can use all four ribonucleotides to synthesize many types of CDNs and cyclic trinucleotide products. The *Vibrio cholerae* CD-NTase dinucleotide cyclase in *Vibrio* (DncV) synthesizes the second messenger 3'3'-cGAMP, *Escherichia coli* CdnE (CD-NTase in clade E) produces 3'3' cyclic UMP-AMP, Flavobacteriaceae sp. CdnE synthesizes 3'3' c-di-GMP, and *Enterobacter cloacae* CdnD synthesizes 3'3'3' cyclic AMP-AMP-GMP and 3'3'-cGAMP. These bacterial CDNs or cyclic trinucleotide molecules can be distinguished from 2'3'-cGAMP, which is critical for STING activation in mammalian cells by their phosphodiester linkage specificity. The asymmetric pattern of the phosphodiester bonds in 2'3'-cGAMP has been reported in multicellular animals rather than bacteria, indicating structural changes in STING's dominant ligand and CDN-binding pocket during evolution, which will be discussed later. However, why the phosphodiester bonds between GMP and AMP change during evolution remains unknown.

Acinetobacter. baumannii CdnD (*Ab*CdnD) has been unexpectedly identified to produce the noncanonical 2'-5'-linked second messenger for antiviral immunity, demonstrating that incorporation of 2'-5' and 3'-5' phosphodiester linkages is not a unique adaptation that evolved in eukaryotes but is also present in bacteria to subvert viral resistance (143, 147–149). CD-NTase-associated protein 4 (Cap4), a founding member of a major family of downstream bacterial receptors, can recognize various CD-NTase signals, including 2'-5'- and 3'-5'-linked bacterial nucleotide second messengers, in CBASS immunity (143). Cap4 contains a ligand-binding SAVED domain, a fusion of two CRISPR-associated Rossman fold (CARF) domains, and a promiscuous DNA endonuclease domain. After nucleotide second messenger recognition in the SAVED domain, the

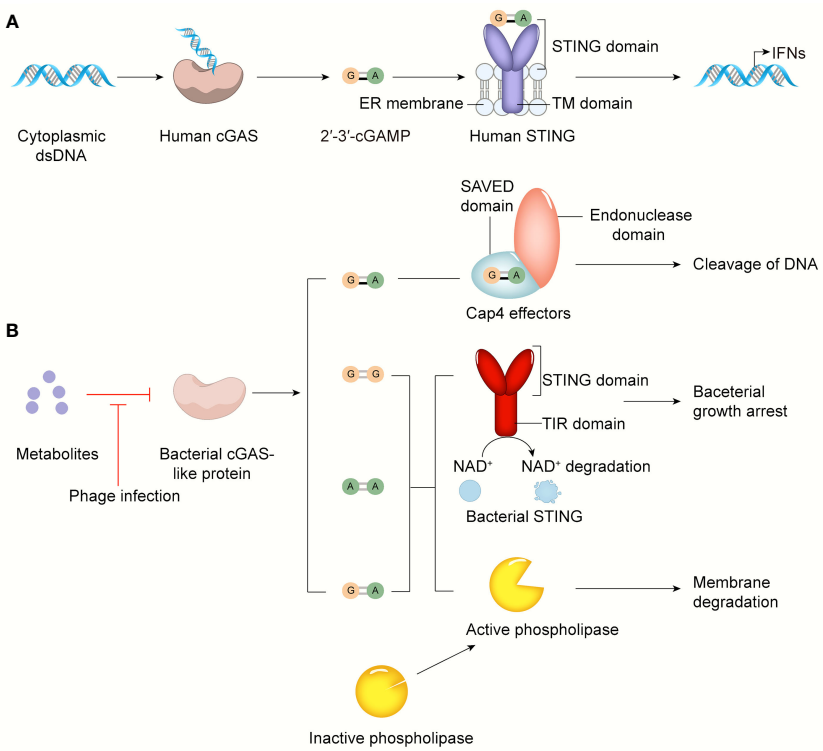


FIGURE 4 | The cGAS-STING pathway in bacterial infection and bacterial immunity. **(A)** cGAS senses cytosolic dsDNA, catalyzes 2'3'-cGAMP that binds and activates STING anchored on ER, leading to IFN-I production. **(B)** The activity of the bacterial cGAS-like enzyme is inhibited by some metabolites or other unknown molecules in normal conditions. In response to phage infection, the inhibition of bacterial cGAS-like enzyme is relieved. Surprisingly, in addition to 3'3'-cGAMP, c-di-AMP, c-di-GMP, 2'3'-cGAMP can be generated by *Ab*CdnD. The SAVED domain of Cap4 recognizes 2'3'-cGAMP, then its endonuclease domain cleaves viral DNA to defend against phage infection. Bacterial STING-TIR fusion protein activated by its ligands like c-di-GMP induces bacterial growth arrest by degrading NAD^+. Upon activated by 3'3'-cGAMP, phospholipase degrades bacterial membrane to control phage infection.

endonuclease domain of Cap4 is subsequently activated through ligand-induced oligomerization and induces promiscuous DNA cleavage to restrict phage replication (**Figure 4**). These SAVED CARF family proteins provide a precondition for cGAMP signaling to be a part of an antiphage defense system and suggest that the importance of linkage specificity reaches far beyond the mammalian cGAS-STING pathway.

Another unresolved question is how bacterial CD-NTase enzymes are activated to catalyze nucleotide second messenger synthesis during phage infection. To date, researchers have found that bacterial cGAS-like proteins are constitutively active *in vitro*. Moreover, DncV seems to be liberated from the inhibition of folate-like molecules only when phage infection has occurred (150). Based on the present studies, we speculate that the activity of bacterial cGAS-like proteins is normally inhibited by certain molecules, such as some metabolites, but when phages invade, these molecules are degraded or depleted under the regulation of some mechanism, thus activating the antiviral immune response. These specific molecular mechanisms need to be further explored. The bacterial antiviral response initiated by the CBASS system is independent of IFN-I, which is crucial for the mammalian antipathogen response. For example, the bacterial cGAS-like enzyme dinucleotide cyclase in *Vibrio* (DncV) synthesizes the second messenger 3'3'-cGAMP, which subsequently activates a downstream effector like phospholipase and results in the degradation of the inner bacterial membrane and cell death, thereby limiting phage replication and protecting the remaining bacterial population during phage infection (151–153) (**Figure 4**).

Intriguingly, 3'3' c-di-GMP is considered to coordinate many different aspects of bacterial growth, behavior, and intracellular signaling, including polymer cellulose synthesis, biofilm formation, motility, virulence, and cell cycle progression (33). However, its role in the CBASS immune system, which kills bacteria or induces bacterial growth arrest, contradicts its original biological function described above. Thus, whether 3'3' c-di-GMP, which is secreted continuously to maintain normal bacterial homeostasis, can activate CBASS downstream effector proteins is very important for bacterial survival. Researchers have conducted a series of experiments to answer this question, including analyzing the genomes of bacteria containing cGAS-STING pathways. The results showed that bacterial STING and other signaling pathways involving 3'3' c-di-GMP rarely coexist in bacteria. In this way, bacteria can effectively avoid potentially catastrophic conflicts caused by the dual effects of 3'3' c-di-GMP.

STING-LIKE PROTEIN

Many structurally divergent effector domains can be activated by CD-NTase products to fight against phage infection, including proteases, phosphodiesterases, and potentially pore-forming transmembrane proteins (145, 154). Among them, some proteins are found to contain a C-terminal STING domain, further suggesting that the intact cGAS-STING pathway may be preserved from bacteria to humans. X-ray crystallography analysis showed that the crystal structures of proteins in *Flavobacteriaceae* sp. and *Capnocytophaga granulosa* exhibited obvious homology to human STING. Bacterial STING is encoded within bacterial defense islands and has been newly identified as a prokaryotic member of the STING family of functional cyclic dinucleotide receptors (144).

The overall architecture of bacterial STING is similar to that of mammalian STING, and both adopt a canonical V-shaped, homodimeric architecture with a hydrophobic α-helix stem. However, the bacterial STING protein is 20% smaller and more compact than mammalian STING, mainly due to a lack of extension in the β-strand lid domain, a terminal α-helix, and an unstructured C-terminal tail (51, 66, 70, 72). These mammalian-specific insertions allowed STING to evolve to induce autophagy and regulate innate immune responses dependent on IFN-I. This structural difference partly explains why the bacterial CBASS immune system takes a suicidal approach rather than relying on the IFN-I response to fight against phage infection.

In addition, there are differences in the amino acid residues of the CDN-binding pockets of bacterial STING and human STING (144), indicating that they may have different ligand preferences. Unlike human STING, which binds CDNs with no sequence-specific contact, a conserved residue in the CDN-binding pocket of bacterial STING makes sequence-specific contacts to the guanosine nucleobase of c-di-GMP, which is consistent with its high-affinity recognition of c-di-GMP. Furthermore, bacterial STING exhibits a weaker affinity for 3'3'-cGAMP, and it cannot recognize mammalian 2'3'-cGAMP since there is not enough space in its CDN-binding pocket to accommodate the free 3'-OH of 2'3'-cGAMP due to the presence of another conserved residue in bacterial STING; in contrast, human STING recognizes 2'3'-cGAMP with high affinity by making an additional contact between the human STING residue and the phosphodiester backbone (155).

Bacterial STING exists as a fusion protein appended to the Toll/interleukin-1 receptor (TIR) adaptor domain or predicted transmembrane (TM) effector modules, and the STING-TIR fusion protein is the most dominant form of STING. The TLR domain has been widely recognized to play an important role in protein-protein interactions to defend against various pathogens in mammals. Some TIR domains can degrade β-nicotinamide adenine dinucleotide (NAD^+), required for cellular metabolism (156, 157).

After recognizing c-di-GMP, bacterial STING assembles into long-ordered filaments with fourfold symmetry. Filaments contain parallel-stacked STING homodimers arranged in an orderly manner, consistent with the activation mechanism of human STING discussed above (51, 71). In contrast to c-di-GMP, the weak agonist 3'3'-cGAMP induced only partial formation of filaments, suggesting that c-di-GMP plays a crucial role in the process by which bacterial STING oligomerizes into filaments. Mutations in the CDN-binding

domain of bacterial STING blocks the formation of filaments without affecting the binding of c-di-GMP and leads to the loss of STING NADase activity, confirming that filament formation controls the activation of STING, as well as the rapid cleavage of NAD^+ mediated by the TIR domain (144). NAD^+ destruction that occurs after the activation of STING-TIR fusion proteins results in cell death to halt phage propagation, which is different from the immune response activated by human STING, which relies on the expression of antipathogen-related genes and proteins (158) (**Figure 4**).

STING-TIR fusion proteins also exist in some invertebrates, such as *Crassostrea gigas*. However, STING-TIR fusion proteins in *C.gigas* can bind tightly to 2'3'-cGAMP (144). In addition, the residues of STING CTT differ across species, resulting in different activation preferences for downstream pathways, including IFN-I response and NF-κB response. These findings indicate that the structure, composition, and function of STING are all changing under selective pressure, but the reasons for these changes are still unknown.

In summary, bacterial CBASS immunity uses the CD-NTase enzyme, a hcGAS homolog, to catalyze the production of diverse nucleotide second messengers, recognized by the bacterial STING-TIR fusion protein to initiate an antiviral response by driving the destruction of NAD^+. Although there are many differences in the cGAS-STING pathways of mammals and bacteria, each of the fundamental components that define the human cGAS-STING pathway is functionally and structurally shared within ancient bacterial CBASS immunity. The preserved antipathogen defense from bacteria to humans provides a deeper understanding of how the modern cGAS-STING pathway has been shaped during evolution, providing directions for developing therapeutics for cGAS-STING-related diseases.

DISCUSSION

In the last decade, a series of studies in cytosolic surveillance systems have made fruitful progress and demonstrated a critical role of the cGAS-STING signaling pathway in bacterial infection. Both extracellular and intracellular bacteria activate cGAS-STING signaling in host cells through PAMPs, including bacterial DNA, CDNs, and LPS, or DAMPs, such as cytosolic DNA released from host mitochondria and the nucleus. Structural information about the main molecules of cGAS-STING signaling has uncovered their regulatory mechanisms, ligand-binding sites, conformational changes, intracellular localization, and function in signal propagation. Moreover, unlike its protective effect against viruses, the activity of the cGAS-STING signaling pathway in bacterial infection may not always be protective. In addition to the induction of cell apoptosis by the IFN-I response during *F. novicida* and *L.monocytogenes* infection, activation of the cGAS-STING pathway can promote bacterial replication during *B. abortus* infection and intracellular bacterial survival during *S. aureus* infection. The cGAS-STING pathway can also affect the outcomes of bacterial infections by participating in the mediation of some important physiological or pathological processes such as blood coagulation and autophagy. The cGAS-STING pathway has also been found in bacteria to defend against phage infection, which provides evolutionary insights into the development of mammalian cGAS-STING signaling and the ongoing host-bacterial arms race.

In addition to the cytoplasm and membrane, hcGAS is also found in the nucleus, easily contact genomic DNA. Structural analysis showed that cGAS is anchored to the nucleosome acidic patch of histone H2A-H2B. Binding to the nucleosome blocks the interaction of cGAS with dsDNA by occupying the strong dsDNA binding surface on cGAS and preventing cGAS dimerization, contributing to the inhibition of cGAS activity. The self-nonself discrimination of host nuclear dsDNA by cGAS can protect the host from autoimmune attack (49, 56, 159). Bacterial cGAS-like enzymes also have easy access to dsDNA, exposed in the cytoplasm without a nuclear membrane. Similarly, the activity of bacterial cGAS-like enzymes is suppressed under normal conditions to avoid the induction of bacterial death by aberrant cGAS activation. The differences and similarities in the mechanism of cGAS inhibition between bacteria and humans remain to be studied.

Despite the current progress, many questions remain to be answered in the future. For instance, can STING mediate physiological or pathological processes other than innate immune responses, such as cell metabolism, independent of cGAS or TBK1, and how are these functions finely orchestrated to maintain cellular homeostasis?

Are there any rules determining whether the cGAS-STING signaling pathway has protective or detrimental effects in various bacterial infections? Does cGAS-STING play different roles in different diseases caused by the same bacteria? Precisely how is STING transported from the ER to the Golgi complex? What is the significance of certain small changes that occurred in the cGAS-STING pathway during evolution? With the resolution of these questions in the future, we expect to effectively control bacterial infection and protect the host from injury by fine-tuning the cGAS-STING signaling pathway.

AUTHOR CONTRIBUTIONS

NL and XP have contributed equally to this work. PJ and HZ are corresponding authors. All authors contributed to the article and approved the submitted version.

ACKNOWLEDGMENTS

We would like to acknowledge the National Natural Science Foundation of China (82001058 and 82071115).

REFERENCES

1. Chai Q, Zhang Y, Liu CH. Mycobacterium Tuberculosis: An Adaptable Pathogen Associated With Multiple Human Diseases. *Front Cell Infect Microbiol* (2018) 8:158. doi: 10.3389/fcimb.2018.00158
2. Marchesan JT, Girnary MS, Moss K, Monaghan ET, Egnatz GJ, Jiao Y, et al. Role of Inflammasomes in the Pathogenesis of Periodontal Disease and Therapeutics. *Periodontol 2000* (2020) 82:93–114. doi: 10.1111/prd.12269
3. Wilson DJ, Gabriel E, Leatherbarrow AJ, Cheesbrough J, Gee S, Bolton E, et al. Tracing the Source of Campylobacteriosis. *PloS Genet* (2008) 4: e1000203. doi: 10.1371/journal.pgen.1000203
4. Pen DL, Yan GF, He LY, Yan WL, Chen WM, Liu J, et al. The Role of Bacterial Colonization of Ventilator Circuit in Development of Ventilator-Associated Pneumonia: A Prospective Observational Cohort Study. *Clin Microbiol Infect* (2021) 27:467.e1– e7. doi: 10.1016/j.cmi.2020.04.008
5. Orsini J, Frawley BJ, Gawlak H, Gooch R, Escovar J. Severe Sepsis With Septic Shock as a Consequence of a Severe Community-Acquired Pneumonia Resulting From a Combined Legionella Pneumophila and Streptococcus Pneumoniae Infection. *Cureus* (2020) 12:e10966. doi: 10.7759/cureus.10966
6. The Lancet Gastroenterology H. The Challenge of Antimicrobial Resistance. *Lancet Gastroenterol Hepatol* (2016) 1:173. doi: 10.1016/S2468-1253(16)30121-2
7. McCulloch TR, Wells TJ, Souza-Fonseca-Guimaraes F. Towards Efficient Immunotherapy for Bacterial Infection. *Trends Microbiol* (2021). doi: 10.1016/j.tim.2021.05.005
8. Liu X, Cui D, Li H, Wang Q, Mao Z, Fang L, et al. Direct Medical Burden of Antimicrobial-Resistant Healthcare-Associated Infections: Empirical Evidence From China. *J Hosp Infect* (2020) 105:295–305. doi: 10.1016/j.jhin.2020.01.003
9. Bassetti M, Poulakou G, Ruppe E, Bouza E, Van Hal SJ, Brink A. Antimicrobial Resistance in the Next 30 Years, Humankind, Bugs and Drugs: A Visionary Approach. *Intensive Care Med* (2017) 43:1464–75. doi: 10.1007/s00134-017-4878-x
10. Naran K, Nundalall T, Chetty S, Barth S. Principles of Immunotherapy: Implications for Treatment Strategies in Cancer and Infectious Diseases. *Front Microbiol* (2018) 9:3158. doi: 10.3389/fmicb.2018.03158
11. Broz P, Monack DM. Newly Described Pattern Recognition Receptors Team Up Against Intracellular Pathogens. *Nat Rev Immunol* (2013) 13:551–65. doi: 10.1038/nri3479
12. Akira S, Uematsu S, Takeuchi O. Pathogen Recognition and Innate Immunity. *Cell* (2006) 124:783–801. doi: 10.1016/j.cell.2006.02.015
13. Roers A, Hiller B, Hornung V. Recognition of Endogenous Nucleic Acids by the Innate Immune System. *Immunity* (2016) 44:739–54. doi: 10.1016/j.immuni.2016.04.002
14. West AP, Shadel GS. Mitochondrial DNA in Innate Immune Responses and Inflammatory Pathology. *Nat Rev Immunol* (2017) 17:363–75. doi: 10.1038/nri.2017.21
15. Hopfner KP, Hornung V. Molecular Mechanisms and Cellular Functions of cGAS-STING Signalling. *Nat Rev Mol Cell Biol* (2020) 21:501–21. doi: 10.1038/s41580-020-0244-x
16. Sun L, Wu J, Du F, Chen X, Chen ZJ. Cyclic GMP-AMP Synthase is a Cytosolic DNA Sensor That Activates the Type I Interferon Pathway. *Science* (2013) 339:786–91. doi: 10.1126/science.1232458
17. Barnett KC, Coronas-Serna JM, Zhou W, Ernandes MJ, Cao A, Kranzusch PJ, et al. Phosphoinositide Interactions Position cGAS at the Plasma Membrane to Ensure Efficient Distinction Between Self- and Viral DNA. *Cell* (2019) 176:1432–46 e11. doi: 10.1016/j.cell.2019.01.049
18. Gentili M, Lahaye X, Nadalin F, Nader GPF, Lombardi EP, Herve S, et al. The N-Terminal Domain of cGAS Determines Preferential Association With Centromeric DNA and Innate Immune Activation in the Nucleus. *Cell Rep* (2019) 26:3798. doi: 10.1016/j.celrep.2019.03.049
19. Mackenzie KJ, Carroll P, Martin CA, Murina O, Fluteau A, Simpson DJ, et al. cGAS Surveillance of Micronuclei Links Genome Instability to Innate Immunity. *Nature* (2017) 548:461–5. doi: 10.1038/nature23449
20. Andreeva L, Hiller B, Kostrewa D, Lassig C, de Oliveira Mann CC, Jan Drexler D, et al. cGAS Senses Long and HMGB/TFAM-Bound U-Turn DNA by Forming Protein-DNA Ladders. *Nature* (2017) 549:394–8. doi: 10.1038/nature23890
21. Gehrke N, Mertens C, Zillinger T, Wenzel J, Bald T, Zahn S, et al. Oxidative Damage of DNA Confers Resistance to Cytosolic Nuclease TREX1 Degradation and Potentiates STING-Dependent Immune Sensing. *Immunity* (2013) 39:482–95. doi: 10.1016/j.immuni.2013.08.004
22. Zhou C, Chen X, Planells-Cases R, Chu J, Wang L, Cao L, et al. Transfer of cGAMP Into Bystander Cells *via* LRRC8 Volume-Regulated Anion Channels Augments STING-Mediated Interferon Responses and Anti-Viral Immunity. *Immunity* (2020) 52:767–81.e6. doi: 10.1016/j.immuni.2020.03.016
23. Ma Z, Damania B. The cGAS-STING Defense Pathway and Its Counteraction by Viruses. *Cell Host Microbe* (2016) 19:150–8. doi: 10.1016/j.chom.2016.01.010
24. Franz KM, Neidermyer WJ, Tan YJ, Whelan SPJ, Kagan JC. STING-Dependent Translation Inhibition Restricts RNA Virus Replication. *Proc Natl Acad Sci USA* (2018) 115:E2058–E67. doi: 10.1073/pnas.1716937115
25. Carty M, Guy C, Bowie AG. Detection of Viral Infections by Innate Immunity. *Biochem Pharmacol* (2021) 183:114316. doi: 10.1016/j.bcp.2020.114316
26. Zahid A, Ismail H, Li B, Jin T. Molecular and Structural Basis of DNA Sensors in Antiviral Innate Immunity. *Front Immunol* (2020) 11:613039. doi: 10.3389/fimmu.2020.613039
27. Gomes MTR, Guimaraes ES, Marinho FV, Macedo I, Aguiar E, Barber GN, et al. STING Regulates Metabolic Reprogramming in Macrophages *via* HIF-1alpha During Brucella Infection. *PloS Pathog* (2021) 17:e1009597. doi: 10.1371/journal.ppat.1009597
28. Guimaraes ES, Gomes MTR, Campos PC, Mansur DS, Dos Santos AA, Harms J, et al. Brucella Abortus Cyclic Dinucleotides Trigger STING-Dependent Unfolded Protein Response That Favors Bacterial Replication. *J Immunol* (2019) 202:2671–81. doi: 10.4049/jimmunol.1801233
29. Marinho FV, Benmerzoug S, Oliveira SC, Ryffel B, Quesniaux VFJ. The Emerging Roles of STING in Bacterial Infections. *Trends Microbiol* (2017) 25:906–18. doi: 10.1016/j.tim.2017.05.008
30. Dey B, Dey RJ, Cheung LS, Pokkali S, Guo H, Lee JH, et al. A Bacterial Cyclic Dinucleotide Activates the Cytosolic Surveillance Pathway and Mediates Innate Resistance to Tuberculosis. *Nat Med* (2015) 21:401–6. doi: 10.1038/nm.3813
31. Woodward JJ, Iavarone AT, Portnoy DA. C-Di-AMP Secreted by Intracellular Listeria Monocytogenes Activates a Host Type I Interferon Response. *Science* (2010) 328:1703–5. doi: 10.1126/science.1189801
32. Elmanfi S, Yilmaz M, Ong WWS, Yeboah KS, Sintim HO, Gursoy M, et al. Bacterial Cyclic Dinucleotides and the cGAS-cGAMP-STING Pathway: A Role in Periodontitis? *Pathogens* (2021) 10:675. doi: 10.3390/pathogens10060675
33. Jenal U, Reinders A, Lori C. Cyclic Di-GMP: Second Messenger Extraordinaire. *Nat Rev Microbiol* (2017) 15:271–84. doi: 10.1038/nrmicro.2016.190
34. Zaver SA, Woodward JJ. Cyclic Dinucleotides at the Forefront of Innate Immunity. *Curr Opin Cell Biol* (2020) 63:49–56. doi: 10.1016/j.ceb.2019.12.004
35. Huang LS, Hong Z, Wu W, Xiong S, Zhong M, Gao X, et al. mtDNA Activates cGAS Signaling and Suppresses the YAP-Mediated Endothelial Cell Proliferation Program to Promote Inflammatory Injury. *Immunity* (2020) 52:475–86.e5. doi: 10.1016/j.immuni.2020.02.002
36. Liu H, Moura-Alves P, Pei G, Mollenkopf HJ, Hurwitz R, Wu X, et al. cGAS Facilitates Sensing of Extracellular Cyclic Dinucleotides to Activate Innate Immunity. *EMBO Rep* (2019) 20:e46293. doi: 10.15252/embr.201846293
37. Luteijn RD, Zaver SA, Gowen BG, Wyman SK, Garelis NE, Onia L, et al. SLC19A1 Transports Immunoreactive Cyclic Dinucleotides. *Nature* (2019) 573:434–8. doi: 10.1038/s41586-019-1553-0
38. Jenson J, Chen ZJ. Bacteria Sting Viral Invaders. *Nature* (2020) 586:363–4. doi: 10.1038/d41586-020-02712-8
39. Wu J, Sun L, Chen X, Du F, Shi H, Chen C, et al. Cyclic GMP-AMP is an Endogenous Second Messenger in Innate Immune Signaling by Cytosolic DNA. *Science* (2013) 339:826–30. doi: 10.1126/science.1229963
40. Gao D, Wu J, Wu YT, Du F, Aroh C, Yan N, et al. Cyclic GMP-AMP Synthase Is an Innate Immune Sensor of HIV and Other Retroviruses. *Science* (2013) 341:903–6. doi: 10.1126/science.1240933
41. Zhang X, Bai XC, Chen ZJ. Structures and Mechanisms in the cGAS-STING Innate Immunity Pathway. *Immunity* (2020) 53:43–53. doi: 10.1016/j.immuni.2020.05.013

42. Kranzusch PJ, Lee AS, Berger JM, Doudna JA. Structure of Human cGAS Reveals a Conserved Family of Second-Messenger Enzymes in Innate Immunity. *Cell Rep* (2013) 3:1362–8. doi: 10.1016/j.celrep.2013.05.008
43. Civril F, Deimling T, de Oliveira Mann CC, Ablasser A, Moldt M, Witte G, et al. Structural Mechanism of Cytosolic DNA Sensing by cGAS. *Nature* (2013) 498:332–7. doi: 10.1038/nature12305
44. Kato K, Ishii R, Goto E, Ishitani R, Tokunaga F, Nureki O. Structural and Functional Analyses of DNA-Sensing and Immune Activation by Human cGAS. *PloS One* (2013) 8:e76983. doi: 10.1371/journal.pone.0076983
45. Li X, Shu C, Yi G, Chaton CT, Shelton CL, Diao J, et al. Cyclic GMP-AMP Synthase Is Activated by Double-Stranded DNA-Induced Oligomerization. *Immunity* (2013) 39:1019–31. doi: 10.1016/j.immuni.2013.10.019
46. Zhang X, Wu J, Du F, Xu H, Sun L, Chen Z, et al. The Cytosolic DNA Sensor cGAS Forms an Oligomeric Complex With DNA and Undergoes Switch-Like Conformational Changes in the Activation Loop. *Cell Rep* (2014) 6:421–30. doi: 10.1016/j.celrep.2014.01.003
47. Zhou W, Whiteley AT, de Oliveira Mann CC, Morehouse BR, Nowak RP, Fischer ES, et al. Structure of the Human cGAS-DNA Complex Reveals Enhanced Control of Immune Surveillance. *Cell* (2018) 174:300–11 e11. doi: 10.1016/j.cell.2018.06.026
48. Kujirai T, Zierhut C, Takizawa Y, Kim R, Negishi L, Uruma N, et al. Structural Basis for the Inhibition of cGAS by Nucleosomes. *Science* (2020) 370:455–8. doi: 10.1126/science.abd0237
49. Pathare GR, Decout A, Gluck S, Cavadini S, Makasheva K, Hovius R, et al. Structural Mechanism of cGAS Inhibition by the Nucleosome. *Nature* (2020) 587:668–72. doi: 10.1038/s41586-020-2750-6
50. Ergun SL, Li L. Structural Insights Into STING Signaling. *Trends Cell Biol* (2020) 30:399–407. doi: 10.1016/j.tcb.2020.01.010
51. Zhang C, Shang G, Gui X, Zhang X, Bai XC, Chen ZJ. Structural Basis of STING Binding With and Phosphorylation by TBK1. *Nature* (2019) 567:394–8. doi: 10.1038/s41586-019-1000-2
52. Shang G, Zhang C, Chen ZJ, Bai XC, Zhang X. Cryo-EM Structures of STING Reveal Its Mechanism of Activation by Cyclic GMP-AMP. *Nature* (2019) 567:389–93. doi: 10.1038/s41586-019-0998-5
53. Gao P, Ascano M, Wu Y, Barchet W, Gaffney BL, Zillinger T, et al. Cyclic [G (2',5')pA(3',5')p] Is the Metazoan Second Messenger Produced by DNA-Activated Cyclic GMP-AMP Synthase. *Cell* (2013) 153:1094–107. doi: 10.1016/j.cell.2013.04.046
54. Ding C, Song Z, Shen A, Chen T, Zhang A. Small Molecules Targeting the Innate Immune Cgasstingtbk1 Signaling Pathway. *Acta Pharm Sin B* (2020) 10:2272–98. doi: 10.1016/j.apsb.2020.03.001
55. Kranzusch PJ. cGAS and CD-NTase Enzymes: Structure, Mechanism, and Evolution. *Curr Opin Struct Biol* (2019) 59:178–87. doi: 10.1016/j.sbi.2019.08.003
56. Cao D, Han X, Fan X, Xu RM, Zhang X. Structural Basis for Nucleosome-Mediated Inhibition of cGAS Activity. *Cell Res* (2020) 30:1088–97. doi: 10.1038/s41422-020-00422-4
57. Ablasser A, Goldeck M, Cavlar T, Deimling T, Witte G, Rohl I, et al. cGAS Produces a 2'-5'-Linked Cyclic Dinucleotide Second Messenger That Activates STING. *Nature* (2013) 498:380–4. doi: 10.1038/nature12306
58. Ishikawa H, Barber GN. STING Is an Endoplasmic Reticulum Adaptor That Facilitates Innate Immune Signalling. *Nature* (2008) 455:674–8. doi: 10.1038/nature07317
59. Zhang X, Shi H, Wu J, Zhang X, Sun L, Chen C, et al. Cyclic GMP-AMP Containing Mixed Phosphodiester Linkages Is an Endogenous High-Affinity Ligand for STING. *Mol Cell* (2013) 51:226–35. doi: 10.1016/j.molcel.2013.05.022
60. Cavlar T, Deimling T, Ablasser A, Hopfner KP, Hornung V. Species-Specific Detection of the Antiviral Small-Molecule Compound CMA by STING. *EMBO J* (2013) 32:1440–50. doi: 10.1038/emboj.2013.86
61. Chin KH, Tu ZL, Su YC, Yu YJ, Chen HC, Lo YC, et al. Novel C-Di-GMP Recognition Modes of the Mouse Innate Immune Adaptor Protein STING. *Acta Crystallogr D Biol Crystallogr* (2013) 69:352–66. doi: 10.1107/S0907444912047269
62. Shang G, Zhu D, Li N, Zhang J, Zhu C, Lu D, et al. Crystal Structures of STING Protein Reveal Basis for Recognition of Cyclic Di-GMP. *Nat Struct Mol Biol* (2012) 19:725–7. doi: 10.1038/nsmb.2332
63. Shu C, Yi G, Watts T, Kao CC, Li P. Structure of STING Bound to Cyclic Di-GMP Reveals the Mechanism of Cyclic Dinucleotide Recognition by the Immune System. *Nat Struct Mol Biol* (2012) 19:722–4. doi: 10.1038/nsmb.2331
64. Ramanjulu JM, Pesiridis GS, Yang J, Concha N, Singhaus R, Zhang SY, et al. Design of Amidobenzimidazole STING Receptor Agonists With Systemic Activity. *Nature* (2018) 564:439–43. doi: 10.1038/s41586-018-0705-y
65. Ouyang S, Song X, Wang Y, Ru H, Shaw N, Jiang Y, et al. Structural Analysis of the STING Adaptor Protein Reveals a Hydrophobic Dimer Interface and Mode of Cyclic Di-GMP Binding. *Immunity* (2012) 36:1073–86. doi: 10.1016/j.immuni.2012.03.019
66. Gui X, Yang H, Li T, Tan X, Shi P, Li M, et al. Autophagy Induction *via* STING Trafficking Is a Primordial Function of the cGAS Pathway. *Nature* (2019) 567:262–6. doi: 10.1038/s41586-019-1006-9
67. Tanaka Y, Chen ZJ. STING Specifies IRF3 Phosphorylation by TBK1 in the Cytosolic DNA Signaling Pathway. *Sci Signal* (2012) 5:ra20. doi: 10.1126/scisignal.2002521
68. Hansen AL, Buchan GJ, Ruhl M, Mukai K, Salvatore SR, Ogawa E, et al. Nitro-Fatty Acids Are Formed in Response to Virus Infection and are Potent Inhibitors of STING Palmitoylation and Signaling. *Proc Natl Acad Sci USA* (2018) 115:E7768–E75. doi: 10.1073/pnas.1806239115
69. Mukai K, Konno H, Akiba T, Uemura T, Waguri S, Kobayashi T, et al. Activation of STING Requires Palmitoylation at the Golgi. *Nat Commun* (2016) 7:11932. doi: 10.1038/ncomms11932
70. Zhao B, Du F, Xu P, Shu C, Sankaran B, Bell SL, et al. A Conserved PLPLRT/SD Motif of STING Mediates the Recruitment and Activation of TBK1. *Nature* (2019) 569:718–22. doi: 10.1038/s41586-019-1228-x
71. Ergun SL, Fernandez D, Weiss TM, Li L. STING Polymer Structure Reveals Mechanisms for Activation, Hyperactivation, and Inhibition. *Cell* (2019) 178:290–301 e10. doi: 10.1016/j.cell.2019.05.036
72. de Oliveira Mann CC, Orzalli MH, King DS, Kagan JC, Lee ASY, Kranzusch PJ. Modular Architecture of the STING C-Terminal Tail Allows Interferon and NF-kappaB Signaling Adaptation. *Cell Rep* (2019) 27:1165–75 e5. doi: 10.1016/j.celrep.2019.03.098
73. Mueller-Ortiz SL, Calame DG, Shenoi N, Li YD, Wetsel RA. The Complement Anaphylatoxins C5a and C3a Suppress IFN-Beta Production in Response to Listeria Monocytogenes by Inhibition of the Cyclic Dinucleotide-Activated Cytosolic Surveillance Pathway. *J Immunol* (2017) 198:3237–44. doi: 10.4049/jimmunol.1601420
74. Castiglia V, Piersigilli A, Ebner F, Janos M, Goldmann O, Dambock U, et al. Type I Interferon Signaling Prevents IL-1beta-Driven Lethal Systemic Hyperinflammation During Invasive Bacterial Infection of Soft Tissue. *Cell Host Microbe* (2016) 19:375–87. doi: 10.1016/j.chom.2016.02.003
75. O'Connell RM, Saha SK, Vaidya SA, Bruhn KW, Miranda GA, Zarnegar B, et al. Type I Interferon Production Enhances Susceptibility to Listeria Monocytogenes Infection. *J Exp Med* (2004) 200:437–45. doi: 10.1084/jem.20040712
76. Stockinger S, Materna T, Stoiber D, Bayr L, Steinborn R, Kolbe T, et al. Production of Type I IFN Sensitizes Macrophages to Cell Death Induced by Listeria Monocytogenes. *J Immunol* (2002) 169:6522–9. doi: 10.4049/jimmunol.169.11.6522
77. Zhang H, Zeng L, Xie M, Liu J, Zhou B, Wu R, et al. TMEM173 Drives Lethal Coagulation in Sepsis. *Cell Host Microbe* (2020) 27:556–70 e6. doi: 10.1016/j.chom.2020.02.004
78. Moretti J, Roy S, Bozec D, Martinez J, Chapman JR, Ueberheide B, et al. STING Senses Microbial Viability to Orchestrate Stress-Mediated Autophagy of the Endoplasmic Reticulum. *Cell* (2017) 171:809–23 e13. doi: 10.1016/j.cell.2017.09.034
79. Sander LE, Davis MJ, Boekschoten MV, Amsen D, Dascher CC, Ryffel B, et al. Detection of Prokaryotic mRNA Signifies Microbial Viability and Promotes Immunity. *Nature* (2011) 474:385–9. doi: 10.1038/nature10072
80. Miller LS, Cho JS. Immunity Against Staphylococcus Aureus Cutaneous Infections. *Nat Rev Immunol* (2011) 11:505–18. doi: 10.1038/nri3010
81. Olaniyi R, Pozzi C, Grimaldi L, Bagnoli F. Staphylococcus Aureus-Associated Skin and Soft Tissue Infections: Anatomical Localization, Epidemiology, Therapy and Potential Prophylaxis. *Curr Top Microbiol Immunol* (2017) 409:199–227. doi: 10.1007/82_2016_32

82. Gries CM, Bruger EL, Moormeier DE, Scherr TD, Waters CM, Kielian T. Cyclic Di-AMP Released From Staphylococcus Aureus Biofilm Induces a Macrophage Type I Interferon Response. *Infect Immun* (2016) 84:3564–74. doi: 10.1128/IAI.00447-16
83. Scumpia PO, Botten GA, Norman JS, Kelly-Scumpia KM, Spreafico R, Ruccia AR, et al. Opposing Roles of Toll-Like Receptor and Cytosolic DNA-STING Signaling Pathways for Staphylococcus Aureus Cutaneous Host Defense. *PloS Pathog* (2017) 13:e1006496. doi: 10.1371/journal.ppat.1006496
84. Zhou Y, Zhao S, Gao X, Jiang S, Ma J, Wang R, et al. Staphylococcus Aureus Induces IFN-Beta Production *via* a CARMA3-Independent Mechanism. *Pathogens* (2021) 10:300. doi: 10.3390/pathogens10030300
85. Cruciani M, Sandini S, Etna MP, Giacomini E, Camilli R, Severa M, et al. Differential Responses of Human Dendritic Cells to Live or Inactivated Staphylococcus Aureus: Impact on Cytokine Production and T Helper Expansion. *Front Immunol* (2019) 10:2622. doi: 10.3389/fimmu.2019.02622
86. Yokota M, Haffner N, Kassier M, Brunner M, Shambat SM, Brennecke F, et al. Staphylococcus Aureus Impairs Dermal Fibroblast Functions With Deleterious Effects on Wound Healing. *FASEB J* (2021) 35:e21695. doi: 10.1096/fj.201902836R
87. Sarhan J, Liu BC, Muendlein HI, Weindel CG, Smirnova I, Tang AY, et al. Constitutive Interferon Signaling Maintains Critical Threshold of MLKL Expression to License Necroptosis. *Cell Death Differ* (2019) 26:332–47. doi: 10.1038/s41418-018-0122-7
88. Brault M, Olsen TM, Martinez J, Stetson DB, Oberst A. Intracellular Nucleic Acid Sensing Triggers Necroptosis Through Synergistic Type I IFN and TNF Signaling. *J Immunol* (2018) 200:2748–56. doi: 10.4049/jimmunol.1701492
89. Liu ZZ, Yang YJ, Zhou CK, Yan SQ, Ma K, Gao Y, et al. STING Contributes to Host Defense Against Staphylococcus Aureus Pneumonia Through Suppressing Necroptosis. *Front Immunol* (2021) 12:636861. doi: 10.3389/fimmu.2021.636861
90. Barbuddhe SB, Chakraborty T. Listeria as an Enteroinvasive Gastrointestinal Pathogen. *Curr Top Microbiol Immunol* (2009) 337:173–95. doi: 10.1007/978-3-642-01846-6_6
91. Charlier C, Perrodeau E, Leclercq A, Cazenave B, Pilmis B, Henry B, et al. Clinical Features and Prognostic Factors of Listeriosis: The MONALISA National Prospective Cohort Study. *Lancet Infect Dis* (2017) 17:510–9. doi: 10.1016/S1473-3099(16)30521-7
92. Auerbuch V, Brockstedt DG, Meyer-Morse N, O'Riordan M, Portnoy DA. Mice Lacking the Type I Interferon Receptor Are Resistant to Listeria Monocytogenes. *J Exp Med* (2004) 200:527–33. doi: 10.1084/jem.20040976
93. Carrero JA, Calderon B, Unanue ER. Type I Interferon Sensitizes Lymphocytes to Apoptosis and Reduces Resistance to Listeria Infection. *J Exp Med* (2004) 200:535–40. doi: 10.1084/jem.20040769
94. Hansen K, Prabakaran T, Laustsen A, Jorgensen SE, Rahbaek SH, Jensen SB, et al. Listeria Monocytogenes Induces IFNbeta Expression Through an IFI16-, cGAS- and STING-Dependent Pathway. *EMBO J* (2014) 33:1654–66. doi: 10.15252/embj.201488029
95. Louie A, Bhandula V, Portnoy DA. Secretion of C-Di-AMP by Listeria Monocytogenes Leads to a STING-Dependent Antibacterial Response During Enterocolitis. *Infect Immun* (2020) 88:e00407–20. doi: 10.1128/IAI.00407-20
96. Nandakumar R, Tschismarov R, Meissner F, Prabakaran T, Krissanaprasit A, Farahani E, et al. Intracellular Bacteria Engage a STING-TBK1-MVB12b Pathway to Enable Paracrine cGAS-STING Signalling. *Nat Microbiol* (2019) 4:701–13. doi: 10.1038/s41564-019-0367-z
97. Hu X, Peng X, Lu C, Zhang X, Gan L, Gao Y, et al. Type I IFN Expression is Stimulated by Cytosolic MtDNA Released From Pneumolysin-Damaged Mitochondria *via* the STING Signaling Pathway in Macrophages. *FEBS J* (2019) 286:4754–68. doi: 10.1111/febs.15001
98. Drijkoningen JJ, Rohde GG. Pneumococcal Infection in Adults: Burden of Disease. *Clin Microbiol Infect* (2014) 20 Suppl 5:45–51. doi: 10.1111/1469-0691.12461
99. Wooten AK, Shenoy AT, Arafa EI, Akiyama H, Martin IMC, Jones MR, et al. Unique Roles for Streptococcus Pneumoniae Phosphodiesterase 2 in Cyclic Di-AMP Catabolism and Macrophage Responses. *Front Immunol* (2020) 11:554. doi: 10.3389/fimmu.2020.00554
100. Ruiz-Moreno JS, Hamann L, Jin L, Sander LE, Puzianowska-Kuznicka M, Cambier J, et al. The cGAS/STING Pathway Detects Streptococcus Pneumoniae But Appears Dispensable for Antipneumococcal Defense in Mice and Humans. *Infect Immun* (2018) 86:e00849–17. doi: 10.1128/IAI.00849-17
101. Ralph AP, Carapetis JR. Group a Streptococcal Diseases and Their Global Burden. *Curr Top Microbiol Immunol* (2013) 368:1–27. doi: 10.1007/82_2012_280
102. Gratz N, Hartweger H, Matt U, Kratochvill F, Janos M, Sigel S, et al. Type I Interferon Production Induced by Streptococcus Pyogenes-Derived Nucleic Acids Is Required for Host Protection. *PloS Pathog* (2011) 7:e1001345. doi: 10.1371/journal.ppat.1001345
103. Movert E, Lienard J, Valfridsson C, Nordstrom T, Johansson-Lindbom B, Carlsson F. Streptococcal M Protein Promotes IL-10 Production by cGAS-Independent Activation of the STING Signaling Pathway. *PloS Pathog* (2018) 14:e1006969. doi: 10.1371/journal.ppat.1006969
104. de Figueiredo P, Ficht TA, Rice-Ficht A, Rossetti CA, Adams LG. Pathogenesis and Immunobiology of Brucellosis: Review of Brucella-Host Interactions. *Am J Pathol* (2015) 185:1505–17. doi: 10.1016/j.ajpath.2015.03.003
105. Costa Franco MM, Marim F, Guimaraes ES, Assis NRG, Cerqueira DM, Alves-Silva J, et al. Brucella Abortus Triggers a cGAS-Independent STING Pathway To Induce Host Protection That Involves Guanylate-Binding Proteins and Inflammasome Activation. *J Immunol* (2018) 200:607–22. doi: 10.4049/jimmunol.1700725
106. Khan M, Harms JS, Liu Y, Eickhoff J, Tan JW, Hu T, et al. Brucella Suppress STING Expression *via* miR-24 to Enhance Infection. *PloS Pathog* (2020) 16:e1009020. doi: 10.1371/journal.ppat.1009020
107. Limmathurotsakul D, Golding N, Dance DA, Messina JP, Pigott DM, Moyes CL, et al. Predicted Global Distribution of Burkholderia Pseudomallei and Burden of Melioidosis. *Nat Microbiol* (2016) 1:15008. doi: 10.1038/nmicrobiol.2015.8
108. Wiersinga WJ, Virk HS, Torres AG, Currie BJ, Peacock SJ, Dance DAB, et al. Melioidosis. *Nat Rev Dis Primers* (2018) 4:17107. doi: 10.1038/nrdp.2017.107
109. Conejero L, Patel N, de Reynal M, Oberdorf S, Prior J, Felgner PL, et al. Low-Dose Exposure of C57BL/6 Mice to Burkholderia Pseudomallei Mimics Chronic Human Melioidosis. *Am J Pathol* (2011) 179:270–80. doi: 10.1016/j.ajpath.2011.03.031
110. Ku JWK, Chen Y, Lim BJW, Gasser S, Crasta KC, Gan YH. Bacterial-Induced Cell Fusion Is a Danger Signal Triggering cGAS-STING Pathway via Micronuclei Formation. *Proc Natl Acad Sci USA* (2020) 117:15923–34. doi: 10.1073/pnas.2006908117
111. Whiteley L, Meffert T, Haug M, Weidenmaier C, Hopf V, Bitschar K, et al. Entry, Intracellular Survival, and Multinucleated-Giant-Cell-Forming Activity of Burkholderia Pseudomallei in Human Primary Phagocytic and Nonphagocytic Cells. *Infect Immun* (2017) 85:e00468–17. doi: 10.1128/IAI.00468-17
112. Kespichayawattana W, Rattanachetkul S, Wanun T, Utaisincharoen P, Sirisinha S. Burkholderia Pseudomallei Induces Cell Fusion and Actin-Associated Membrane Protrusion: A Possible Mechanism for Cell-to-Cell Spreading. *Infect Immun* (2000) 68:5377–84. doi: 10.1128/IAI.68.9.5377-5384.2000
113. Sangsri T, Saiprom N, Tubsuwan A, Monk P, Partridge LJ, Chantratita N. Tetraspanins are Involved in Burkholderia Pseudomallei-Induced Cell-to-Cell Fusion of Phagocytic and non-Phagocytic Cells. *Sci Rep* (2020) 10:17972. doi: 10.1038/s41598-020-74737-y
114. Place DE, Briard B, Samir P, Karki R, Bhattacharya A, Guy CS, et al. Interferon Inducible GBPs Restrict Burkholderia Thailandensis Motility Induced Cell-Cell Fusion. *PloS Pathog* (2020) 16:e1008364. doi: 10.1371/journal.ppat.1008364
115. Storek KM, Gertsvolf NA, Ohlson MB, Monack DM. cGAS and Ifi204 Cooperate to Produce Type I IFNs in Response to Francisella Infection. *J Immunol* (2015) 194:3236–45. doi: 10.4049/jimmunol.1402764
116. Almine JF, O'Hare CA, Dunphy G, Haga IR, Naik RJ, Atrih A, et al. IFI16 and cGAS Cooperate in the Activation of STING During DNA Sensing in Human Keratinocytes. *Nat Commun* (2017) 8:14392. doi: 10.1038/ncomms14392

117. Zhu Q, Man SM, Karki R, Malireddi RKS, Kanneganti TD. Detrimental Type I Interferon Signaling Dominates Protective AIM2 Inflammasome Responses During Francisella Novicida Infection. *Cell Rep* (2018) 22:3168–74. doi: 10.1016/j.celrep.2018.02.096
118. Banerjee I, Behl B, Mendonca M, Shrivastava G, Russo AJ, Menoret A, et al. Gasdermin D Restrains Type I Interferon Response to Cytosolic DNA by Disrupting Ionic Homeostasis. *Immunity* (2018) 49:413–26 e5. doi: 10.1016/j.immuni.2018.07.006
119. Wilhelmus KR. Review of Clinical Experience With Microbial Keratitis Associated With Contact Lenses. *CLAO J* (1987) 13:211–4.
120. Zhou CM, Wang B, Wu Q, Lin P, Qin SG, Pu QQ, et al. Identification of cGAS as an Innate Immune Sensor of Extracellular Bacterium Pseudomonas Aeruginosa. *iScience* (2021) 24:101928. doi: 10.1016/j.isci.2020.101928
121. Chen K, Fu Q, Liang S, Liu Y, Qu W, Wu Y, et al. Stimulator of Interferon Genes Promotes Host Resistance Against Pseudomonas Aeruginosa Keratitis. *Front Immunol* (2018) 9:1225. doi: 10.3389/fimmu.2018.01225
122. Ma C, Ma X, Jiang B, Pan H, Liao X, Zhang L, et al. A Novel Inactivated Whole-Cell Pseudomonas Aeruginosa Vaccine That Acts Through the cGAS-STING Pathway. *Signal Transduct Target Ther* (2021) 6:353. doi: 10.1038/s41392-021-00752-8
123. Conrad WH, Osman MM, Shanahan JK, Chu F, Takaki KK, Cameron J, et al. Mycobacterial ESX-1 Secretion System Mediates Host Cell Lysis Through Bacterium Contact-Dependent Gross Membrane Disruptions. *Proc Natl Acad Sci USA* (2017) 114:1371–6. doi: 10.1073/pnas.1620133114
124. Majlessi L, Brosch R. Mycobacterium Tuberculosis Meets the Cytosol: The Role of cGAS in Anti-Mycobacterial Immunity. *Cell Host Microbe* (2015) 17:733–5. doi: 10.1016/j.chom.2015.05.017
125. Peng X, Jiang G, Liu W, Zhang Q, Qian W, Sun J. Characterization of Differential Pore-Forming Activities of ESAT-6 Proteins From Mycobacterium Tuberculosis and Mycobacterium Smegmatis. *FEBS Lett* (2016) 590:509–19. doi: 10.1002/1873-3468.12072
126. Collins AC, Cai H, Li T, Franco LH, Li XD, Nair VR, et al. Cyclic GMP-AMP Synthase Is an Innate Immune DNA Sensor for Mycobacterium Tuberculosis. *Cell Host Microbe* (2015) 17:820–8. doi: 10.1016/j.chom.2015.05.005
127. Watson RO, Bell SL, MacDuff DA, Kimmey JM, Diner EJ, Olivas J, et al. The Cytosolic Sensor cGAS Detects Mycobacterium Tuberculosis DNA to Induce Type I Interferons and Activate Autophagy. *Cell Host Microbe* (2015) 17:811–9. doi: 10.1016/j.chom.2015.05.004
128. Lienard J, Nobs E, Lovins V, Movert E, Valfridsson C, Carlsson F. The Mycobacterium Marinum ESX-1 System Mediates Phagosomal Permeabilization and Type I Interferon Production via Separable Mechanisms. *Proc Natl Acad Sci USA* (2020) 117:1160–6. doi: 10.1073/pnas.1911646117
129. Zhang Y, Yang J, Bai G. Cyclic Di-AMP-Mediated Interaction Between Mycobacterium Tuberculosis DeltacnpB and Macrophages Implicates a Novel Strategy for Improving BCG Vaccination. *Pathog Dis* (2018) 76. doi: 10.1093/femspd/fty008
130. Sun Y, Zhang W, Dong C, Xiong S. Mycobacterium Tuberculosis MmsA (Rv0753c) Interacts With STING and Blunts the Type I Interferon Response. *mBio* (2020) 11:e03254–19. doi: 10.1128/mBio.03254-19
131. Sousa J, Ca B, Maceiras AR, Simoes-Costa L, Fonseca KL, Fernandes AI, et al. Mycobacterium Tuberculosis Associated With Severe Tuberculosis Evades Cytosolic Surveillance Systems and Modulates IL-1beta Production. *Nat Commun* (2020) 11:1949. doi: 10.1038/s41467-020-15832-6
132. Karanja CW, Yeboah KS, Sintim HO. Identification of a Mycobacterium Tuberculosis Cyclic Dinucleotide Phosphodiesterase Inhibitor. *ACS Infect Dis* (2021) 7:309–17. doi: 10.1021/acsinfecdis.0c00444
133. Dey RJ, Dey B, Zheng Y, Cheung LS, Zhou J, Sayre D, et al. Inhibition of Innate Immune Cytosolic Surveillance by an M. Tuberculosis Phosphodiesterase. *Nat Chem Biol* (2017) 13:210–7. doi: 10.1038/nchembio.2254
134. Van Dis E, Sogi KM, Rae CS, Sivick KE, Surh NH, Leong ML, et al. STING-Activating Adjuvants Elicit a Th17 Immune Response and Protect Against Mycobacterium Tuberculosis Infection. *Cell Rep* (2018) 23:1435–47. doi: 10.1016/j.celrep.2018.04.003
135. Ning L, Wei W, Wenyang J, Rui X, Qing G. Cytosolic DNA-STING-NLRP3 Axis Is Involved in Murine Acute Lung Injury Induced by Lipopolysaccharide. *Clin Transl Med* (2020) 10:e228. doi: 10.1002/ctm2.228
136. Cao DJ, Schiattarella GG, Villalobos E, Jiang N, May HI, Li T, et al. Cytosolic DNA Sensing Promotes Macrophage Transformation and Governs Myocardial Ischemic Injury. *Circulation* (2018) 137:2613–34. doi: 10.1161/CIRCULATIONAHA.117.031046
137. Li N, Zhou H, Wu H, Wu Q, Duan M, Deng W, et al. STING-IRF3 Contributes to Lipopolysaccharide-Induced Cardiac Dysfunction, Inflammation, Apoptosis and Pyroptosis by Activating NLRP3. *Redox Biol* (2019) 24:101215. doi: 10.1016/j.redox.2019.101215
138. Olagnier D, Brandtoft AM, Gunderstofte C, Villadsen NL, Krapp C, Thielke AL, et al. Nrf2 Negatively Regulates STING Indicating a Link Between Antiviral Sensing and Metabolic Reprogramming. *Nat Commun* (2018) 9:3506. doi: 10.1038/s41467-018-05861-7
139. Vanaja SK, Russo AJ, Behl B, Banerjee I, Yankova M, Deshmukh SD, et al. Bacterial Outer Membrane Vesicles Mediate Cytosolic Localization of LPS and Caspase-11 Activation. *Cell* (2016) 165:1106–19. doi: 10.1016/j.cell.2016.04.015
140. Cheng KT, Xiong S, Ye Z, Hong Z, Di A, Tsang KM, et al. Caspase-11-Mediated Endothelial Pyroptosis Underlies Endotoxemia-Induced Lung Injury. *J Clin Invest* (2017) 127:4124–35. doi: 10.1172/JCI94495
141. Hagar JA, Powell DA, Aachoui Y, Ernst RK, Miao EA. Cytoplasmic LPS Activates Caspase-11: Implications in TLR4-Independent Endotoxic Shock. *Science* (2013) 341:1250–3. doi: 10.1126/science.1240988
142. Mills EL, Kelly B, Logan A, Costa ASH, Varma M, Bryant CE, et al. Succinate Dehydrogenase Supports Metabolic Repurposing of Mitochondria to Drive Inflammatory Macrophages. *Cell* (2016) 167:457–70 e13. doi: 10.1016/j.cell.2016.08.064
143. Lowey B, Whiteley AT, Keszei AFA, Morehouse BR, Mathews IT, Antine SP, et al. CBASS Immunity Uses CARF-Related Effectors to Sense 3'-5'- and 2'-5'-Linked Cyclic Oligonucleotide Signals and Protect Bacteria From Phage Infection. *Cell* (2020) 182:38–49 e17. doi: 10.1016/j.cell.2020.05.019
144. Morehouse BR, Govande AA, Millman A, Keszei AFA, Lowey B, Ofir G, et al. STING Cyclic Dinucleotide Sensing Originated in Bacteria. *Nature* (2020) 586:429–33. doi: 10.1038/s41586-020-2719-5
145. Cohen D, Melamed S, Millman A, Shulman G, Oppenheimer-Shaanan Y, Kacen A, et al. Cyclic GMP-AMP Signalling Protects Bacteria Against Viral Infection. *Nature* (2019) 574:691–5. doi: 10.1038/s41586-019-1605-5
146. Ye Q, Lau RK, Mathews IT, Birkholz EA, Watrous JD, Azimi CS, et al. HORMA Domain Proteins and a Trip13-Like ATPase Regulate Bacterial cGAS-Like Enzymes to Mediate Bacteriophage Immunity. *Mol Cell* (2020) 77:709–22 e7. doi: 10.1016/j.molcel.2019.12.009
147. Danilchanka O, Mekalanos JJ. Cyclic Dinucleotides and the Innate Immune Response. *Cell* (2013) 154:962–70. doi: 10.1016/j.cell.2013.08.014
148. Kranzusch PJ, Wilson SC, Lee AS, Berger JM, Doudna JA, Vance RE. Ancient Origin of cGAS-STING Reveals Mechanism of Universal 2',3' cGAMP Signaling. *Mol Cell* (2015) 59:891–903. doi: 10.1016/j.molcel.2015.07.022
149. Margolis SR, Wilson SC, Vance RE. Evolutionary Origins of cGAS-STING Signaling. *Trends Immunol* (2017) 38:733–43. doi: 10.1016/j.it.2017.03.004
150. Zhu D, Wang L, Shang G, Liu X, Zhu J, Lu D, et al. Structural Biochemistry of a Vibrio Cholerae Dinucleotide Cyclase Reveals Cyclase Activity Regulation by Folates. *Mol Cell* (2014) 55:931–7. doi: 10.1016/j.molcel.2014.08.001
151. Davies BW, Bogard RW, Young TS, Mekalanos JJ. Coordinated Regulation of Accessory Genetic Elements Produces Cyclic Di-Nucleotides for V. Cholerae Virulence. *Cell* (2012) 149:358–70. doi: 10.1016/j.cell.2012.01.053
152. Severin GB, Ramliden MS, Hawver LA, Wang K, Pell ME, Kieninger AK, et al. Direct Activation of a Phospholipase by Cyclic GMP-AMP in El Tor Vibrio Cholerae. *Proc Natl Acad Sci USA* (2018) 115:E6048–E55. doi: 10.1073/pnas.1801233115
153. Kranzusch PJ, Lee ASY, Wilson SC, Solovykh MS, Vance RE, Berger JM, et al. Structure-Guided Reprogramming of Human cGAS Dinucleotide Linkage Specificity. *Cell* (2014) 158:1011–21. doi: 10.1016/j.cell.2014.07.028
154. Burroughs AM, Zhang D, Schaffer DE, Iyer LM, Aravind L. Comparative Genomic Analyses Reveal a Vast, Novel Network of Nucleotide-Centric Systems in Biological Conflicts, Immunity and Signaling. *Nucleic Acids Res* (2015) 43:10633–54. doi: 10.1093/nar/gkv1267
155. Gao P, Ascano M, Zillinger T, Wang W, Dai P, Serganov AA, et al. Structure-Function Analysis of STING Activation by C[G(2',5')pA(3',5')p] and Targeting by Antiviral DMXAA. *Cell* (2013) 154:748–62. doi: 10.1016/j.cell.2013.07.023
156. Wan L, Essuman K, Anderson RG, Sasaki Y, Monteiro F, Chung EH, et al. TIR Domains of Plant Immune Receptors Are NAD(+)-Cleaving Enzymes That Promote Cell Death. *Science* (2019) 365:799–803. doi: 10.1126/science.aax1771

157. Horsefield S, Burdett H, Zhang X, Manik MK, Shi Y, Chen J, et al. NAD(+) Cleavage Activity by Animal and Plant TIR Domains in Cell Death Pathways. *Science* (2019) 365:793–9. doi: 10.1126/science.aax1911
158. Millman A, Melamed S, Amitai G, Sorek R. Diversity and Classification of Cyclic-Oligonucleotide-Based Anti-Phage Signalling Systems. *Nat Microbiol* (2020) 5:1608–15. doi: 10.1038/s41564-020-0777-y
159. Boyer JA, Spangler CJ, Strauss JD, Cesmat AP, Liu P, McGinty RK, et al. Structural Basis of Nucleosome-Dependent cGAS Inhibition. *Science* (2020) 370:450–4. doi: 10.1126/science.abd0609

Conflict of Interest: The authors declare that the research was conducted in the absence of any commercial or financial relationships that could be construed as a potential conflict of interest.

Publisher's Note: All claims expressed in this article are solely those of the authors and do not necessarily represent those of their affiliated organizations, or those of the publisher, the editors and the reviewers. Any product that may be evaluated in this article, or claim that may be made by its manufacturer, is not guaranteed or endorsed by the publisher.

Copyright © 2022 Liu, Pang, Zhang and Ji. This is an open-access article distributed under the terms of the Creative Commons Attribution License (CC BY). The use, distribution or reproduction in other forums is permitted, provided the original author(s) and the copyright owner(s) are credited and that the original publication in this journal is cited, in accordance with accepted academic practice. No use, distribution or reproduction is permitted which does not comply with these terms.

frontiers in Microbiology

ORIGINAL RESEARCH
published: 25 February 2022
doi: 10.3389/fmicb.2022.700894

Accessory Gene Regulator (*agr*) Allelic Variants in Cognate *Staphylococcus aureus* Strain Display Similar Phenotypes

Li Tan[1†], Yuyang Huang[2†], Weilong Shang[1], Yi Yang[1], Huagang Peng[1], Zhen Hu[1], Yuting Wang[1], Yifan Rao[1], Qiwen Hu[1], Xiancai Rao[1], Xiaomei Hu[1], Ming Li[1], Kaisen Chen[3] and Shu Li[1]**

[1] College of Basic Medical Sciences, Army Medical University, Chongqing, China, [2] Queen Mary College, Nanchang University, Nanchang, China, [3] The First Affiliated Hospital of Nanchang University, Nanchang, China

The accessory gene regulator (*agr*) quorum-sensing system is an important global regulatory system of *Staphylococcus aureus* and contributes to its pathogenicity. The *S. aureus agr* system is divided into four *agr* groups based on the amino acid polymorphisms of AgrB, AgrD, and AgrC. The *agr* activation is group-specific, resulting in variations in *agr* activity and pathogenicity among the four *agr* groups. Strains with divergent *agr* system always have different phenotypes. In the present report, we, respectively, exchanged the *agr* system of a certain *S. aureus* with other three *agr* alleles and assessed the corresponding phenotypes of these congenic strains. Replacement of the *agr* system led to significant variations in hemolytic activity, protein expression, and virulence gene expression comparing with that of the parental strain. Interestingly, we found that the biological characteristics of these *agr* congenic strains in the same strain background were highly similar to each other, and the allele-dependent differences of the *agr* systems were weakened. These findings indicate that the allele-dependent *agr* predilections of *S. aureus* are determined by some factors in addition to the polymorphisms of AgrB, AgrD, and AgrC. Future studies may reveal the novel mechanism to improve our understanding of the *agr* network.

Keywords: *Staphylococcus aureus*, quorum sensing system, accessory gene regulator (*agr*) alleles, *agr* polymorphisms, virulence factors

OPEN ACCESS

Edited by:
Alina Maria Holban, University of Bucharest, Romania

Reviewed by:
James Q. Boedicker, University of Southern California, United States
Tao Xu, Fudan University, China

***Correspondence:**
Kaisen Chen
chenks100@126.com
Shu Li
1416234121@qq.com

[†]These authors have contributed equally to this work

Specialty section:
This article was submitted to Infectious Agents and Disease, a section of the journal Frontiers in Microbiology

Received: *27 April 2021*
Accepted: *14 January 2022*
Published: *25 February 2022*

Citation:
Tan L, Huang Y, Shang W, Yang Y, Peng H, Hu Z, Wang Y, Rao Y, Hu Q, Rao X, Hu X, Li M, Chen K and Li S (2022) Accessory Gene Regulator (agr) Allelic Variants in Cognate Staphylococcus aureus Strain Display Similar Phenotypes. Front. Microbiol. 13:700894. doi: 10.3389/fmicb.2022.700894

INTRODUCTION

The accessory gene regulator (*agr*) quorum-sensing system, a globe transcriptional regulator of *Staphylococcus aureus*, plays a key role in its pathogenesis and resistance (Bernabè et al., 2021) and has been intensively studied to aid drug and vaccine development (Tan et al., 2018). The *agr* locus comprises two adjacent transcripts, RNAII and RNAIII, which are controlled by P2 and P3 promoters, respectively (Ji et al., 1995). RNAII is composed of four genes, *agrB*, *agrD*, *agrC*, and *agrA* (Novick et al., 1995). *agrD* encodes the propeptide for an autoinducing peptide (AIP). *agrB* encodes an endopeptidase that is the processor of AIP. AgrC and AgrA, encoded by *agrC* and *agrA*, function as a two-component regulatory system. When *agr* system is activated, AIP propeptide is processed to an octapeptide by AgrB and secreted to extracellular space (Queck et al., 2008). As AIP reaches a threshold, the membrane-bound histidine kinase AgrC autophosphorylates and becomes activated, which leads to the phosphorylation of its cognate response regulator, AgrA

(Queck et al., 2008). Phosphorylated AgrA activates the transcription of its own RNAII transcript to produce more AIP and also activates promoter P3 to increase the expression of RNAIII (Queck et al., 2008; Wang and Muir, 2016). The two main intracellular effectors, AgrA and RNAIII, regulate expression of virulence factors and contribute to the pathogenicity of *S. aureus* (Bronesky et al., 2016). AgrA can activate the synthesis of phenol soluble modulin (PSM) peptides, which are the only known toxins regulated by AgrA (Queck et al., 2008). RNAIII was shown to regulate primarily the expression of many important virulence factors and several transcriptional regulators (Wang and Muir, 2016).

The amino acid sequences of AgrB, AgrD, and AgrC are variable (**Supplementary Figure 1**), whereas AgrA, RNAIII, and their promoter regions are highly conserved (**Supplementary Figure 2**). According to the polymorphisms of AgrB, AgrD, and AgrC, the *agr* system in *S. aureus* is divided into four types named *agr*I, *agr*II, *agr*III, and *agr*IV. Each *agr* variant produces its own specific AIP, which triggers autoinduction. The heterologous pairing of AIP inhibits the response of other *agr* types and leads to heterologous mutual inhibition (Ji et al., 1997). The variations of *agr* specificity may form specific functional units that drive evolutionary diversification in *Staphylococcus* and also have significant implications for host disease (Wright et al., 2005). Cues between special *agr* groups and some disease predilections have been reported by previous studies. For example, most of *agr*II clinical *S. aureus* strains are isolated from acute infection, and half of clinical methicillin-resistant *S. aureus* (MRSA) bloodstream isolates are in the *agr*II group. Menstrual toxic shock syndrome is usually caused by *agr*III and *agr*IV *S. aureus* (Jarraud et al., 2002), and *agr*IV strains are associated with exfoliative syndromes and bullous impetigo (Gomes et al., 2005). The *agr*II and *agr*IV strains exhibit higher biofilm formation capacity (Khoramrooz et al., 2016). The distributions of certain toxin genes and mobile genetic elements also show *agr* group specificity (Wright et al., 2005). It has been reported that the specific lineage and geographical distribution of *S. aureus* may correlate with *agr* types (Holtfreter et al., 2007). In summary, clinical symptoms caused by some staphylococcal strains are closely associated with their *agr* subgroups (Traber et al., 2008). However, it is not known whether there are any other factors involved in the *agr* predilection and *agr*-specific virulence genotypes of *S. aureus* in addition to the specific *agr* type, or the polymorphous AgrB, AgrD, and AgrC.

In this study, we replaced the *agr* system of *S. aureus* Newman strain (*agr*I type) or N315 (*agr*II type) with different *agr* alleles. The resulting four congenic strains were assessed for their *agrA* activity, hemolytic activity, pigmentation, exoprotein expression, and virulence factor expressions.

MATERIALS AND METHODS

Bacterial Strains, Plasmids, Primers, and Growth Conditions

S. aureus strain Newman, an *agr* group I prototype used as the backbone strain in this study, was originally isolated from a secondarily infected tubercular osteomyelitis lesion (Duthie and Lorenz, 1952). N315, an *agr*II prototype MRSA with defective *agr* system, was also used as control background strain (Tsompanidou et al., 2011). MW2 is a prototypical *agr* group III strain originally isolated from a child with fatal septicemia and septic arthritis (Mei et al., 2011). XQ is a clinical community-associated MRSA belongs to group IV prototype strain isolated from an adolescent patient with staphylococcal scalded skin syndrome (Rao et al., 2015). *Escherichia coli* strain DH5α was used for plasmid construction and genetic manipulation. All strains were stored in 10% glycerol at −80°C (**Supplementary Table 1**). *E. coli* strains were grown in Luria–Bertani broth, whereas *S. aureus* strains were cultivated in trypticase soy broth (TSB; Sigma) or brain–heart infusion medium (Sigma). When necessary, ampicillin (100 μg/mL) and chloramphenicol (20 μg/mL) were added to the medium. The temperature-sensitive *S. aureus* plasmid pBT2 and *E. coli–S. aureus* shuttle plasmid pLI50 kindly provided by Prof. Baolin Sun (University of Science and Technology of China, China) were used for gene mutation and complementation assay, respectively. Transformations of *S. aureus* strains were performed by electroporation (Bio-Rad Gene Pulser). The primers used in this study were presented in **Supplementary Table 2**.

Construction of Accessory Gene Regulator Gene Markerless Deletion Mutant

The Newman Δ*agrBDC* and N315 Δ*agrBDCA* markerless deletion mutants were constructed with pBT2 plasmid using homologous recombinant strategy as described previously (Yuan et al., 2013). Take Newman Δ*agrBDC* construction as an example, a 803-bp DNA fragment upstream of *agrBDC* locus was amplified from Newman genome DNA using primer pairs, Δ*agrBDC* up-for and Δ*agrBDC* up-rev (**Supplementary Table 2**). The polymerase chain reaction (PCR) product was digested with *Hin*dIII and *Sal*I and subcloned into the same site of pBT2 to obtain plasmid p*agrBDC*F. Then, a 957-bp DNA fragment downstream of *agrBDC* locus was amplified and subcloned into the *Bam*HI and *Eco*RI site of p*agrBDC*F, yielding the Δ*agrBDC* knockout plasmid (p*agrBDC*). The p*agrBDC* plasmid was identified by restriction enzyme digestion and DNA sequencing and then electrotransformed into *S. aureus* RN4220 and Newman to construct Newman Δ*agrBDC* markerless deletion mutant by homologous recombination. The mutants were screened and confirmed by PCR amplification and DNA sequencing. The N315 Δ*agrBDCA* markerless deletion mutant was constructed with similar strategy.

Construction of Accessory Gene Regulator Gene Allele Replacement Strains

The *agrBDC* fragments of *agr*II, *agr*III, and *agr*IV were separately obtained from N315, MW2, and XQ by PCR amplification and were, respectively, inserted into the *Sal*I and *Bam*HI sites of pBT2

plasmid to yield p*agrBDC*-II, p*agrBDC*-III, and p*agrBDC*-IV knock-in vectors. Then, these p*agrBDC* vectors were sequentially introduced into *S. aureus* RN4220 and NewmanΔ*agrBDC* deletion mutant strain to construct allelic replacement strains *via* homologous recombination. The substitution of *agrBDC* fragments of allelic congenic strains was also verified by PCR amplification and DNA sequencing.

Construction of *agrBDCA* Plasmid Complemented Strains

Full gene DNA of types I through IV *agr* clusters and their promoters were separately amplified from Newman, N315, MW2, and XQ using the primers described in **Supplementary Table 2** and subcloned into the pLI50 plasmid. All positive recombinant plasmids were confirmed by DNA sequencing. Then, these plasmids were, respectively, transformed into *E. coli* DH5α, *S. aureus* RN4220, and finally into NewmanΔ*agrBDC* or N315Δ*agrBDCA* mutant to construct types I–IV *agrBDCA* genes complemented strains.

Biological Characteristic Analysis

The hemolytic activity, pigment formation, exoprotein production, and gene transcription of *agr* allelic congenic strains were analyzed to assess the influence of *agr* system replacement on *S. aureus* biological characteristics.

For hemolytic activity assessment, overnight culture of each single *S. aureus* colony was diluted into the same colony-forming units (CFUs) and plated on rabbit's blood agar plates, followed by overnight growth at 37°C for hemolysis analysis. Furthermore, the hemolytic activity was also evaluated according to the hemolysis of rabbit erythrocytes. As the method described previously (Pader et al., 2014), 100 μL overnight culture supernatant was mixed with 6% rabbit blood in phosphate-buffered saline and then incubated at 37°C for 20 min. The unlysed blood cells were removed by centrifugation, and the erythrocyte lysis was determined with the OD543 values of supernatant.

To evaluate staphyloxanthin production, the diluted overnight inoculation of *S. aureus* strains was also cultured on TSB plate to assess the effect of *agr* replacement on pigment formation. Moreover, staphyloxanthin productions were also quantitatively analyzed and adapted from a previously published method (Liu et al., 2018). Cells in 1-mL overnight culture were collected and washed thrice with sterilized water and then resuspended with 200 μL methanol and heated at 55°C for 3 min. After the cells were centrifuged at 10,000 × *g* for 1 min, the OD462 value of supernatant was detected.

The overnight culture supernatants of *S. aureus* were collected by centrifugation. Proteins in supernatants were precipitated with trichloroacetic acid and analyzed by sodium dodecyl sulfate–polyacrylamide gel electrophoresis (SDS-PAGE) in a 12% polyacrylamide gel.

The change in gene transcription was appraised with quantitative real-time PCR (qRT-PCR). Cells were harvested at 6 h after inoculation, which represent the mid-log phase of the *S. aureus* growth. The total bacterial RNA was isolated using SV Total RNA Isolation System kit (Z3100; Promega, United States). The contaminated genomic DNA in RNA was degraded with DNaseI. The cDNA was prepared using PrimeScript RT Reagent Kit (RR047A; Takara, Japan) and used for qRT-PCR using GoTaq® qPCR Master Mix (A6001; Promega, United States) on an ABI SimpliAmp PCR detection system (United States). Specific primers for qRT-PCR (**Supplementary Table 3**) were designed according to the target gene sequences. All PCR reactions were performed in triplicate, with 16S rDNA as internal control. The relative expression of gene products was normalized to the housekeeping gene 16S and calculated using the $2^{-\Delta\Delta CT}$ method.

RESULTS

Construction of Congenic Strains Containing Accessory Gene Regulator Alleles

The *agr* systems were divided into four *agr* groups named *agr*I, *agr*II, *agr*III, and *agr*IV in *S. aureus* (Wang and Muir, 2016). AgrA is highly conserved, whereas AgrB, AgrD, and AgrC are variable among the four *agr* groups (**Supplementary Figure 1**). In this study, *S. aureus* Newman and N315 were selected for *agr* congenic strains construction to assess the effects of divergent *agr* alleles. The whole RNAII transcripts (involved *agrB*, *agrD*, *agrC*, and *agrA* genes) were allelic substituted to construct congenic strains in N315, whereas only *agrB*, *agrD*, and *agrC* genes were replaced in Newman congenic strains. The congenic strains were constructed *via* homologous recombination and confirmed by PCR amplification (**Figure 1** and **Supplementary Table 2**) and DNA sequencing.

Effects of Accessory Gene Regulator Alleles on Hemolytic Activity

S. aureus is able to secrete a variety of toxins, such as α-hemolysin, bicomponent leukocidins, γ-hemolysin, Panton–Valentine leukocidin (PVL), β-hemolysin, δ-hemolysin, PSMs, and so on (Cheung and Otto, 2012). These exotoxins have leukotoxic and hemolytic activities and are widely associated with the pathogenicity of *S. aureus* (Powers et al., 2015; Seilie and Bubeck Wardenburg, 2017). α-Hemolysin, γ-hemolysin, PVL, δ-hemolysin, and PSM belong to pore-forming toxins capable of forming transmembrane aqueous channel and leading to host cell lysis (Reyes-Robles and Torres, 2017). β-Hemolysin is a neutral sphingomyelinase capable of digesting sphingomyelin into ceramide and phosphorylcholine (Vandenesch et al., 2012). The production of hemolysins in *S. aureus* is tightly regulated, and the *agr* system plays an important role in this process (Johansson et al., 2019). It was reported that the *agr* system controls the expression of α-, β-, and γ-hemolysin and PVL by RNAIII and regulates the transcription of δ-hemolysin and PSMs through AgrA (Arya and Princy, 2013; Singh and Ray, 2014). The hemolytic capabilities of *S. aureus* vary with their *agr* types. As shown in **Figure 2A**, the Newman (*agr*I) and XQ (*agr*IV) strains have strong hemolytic

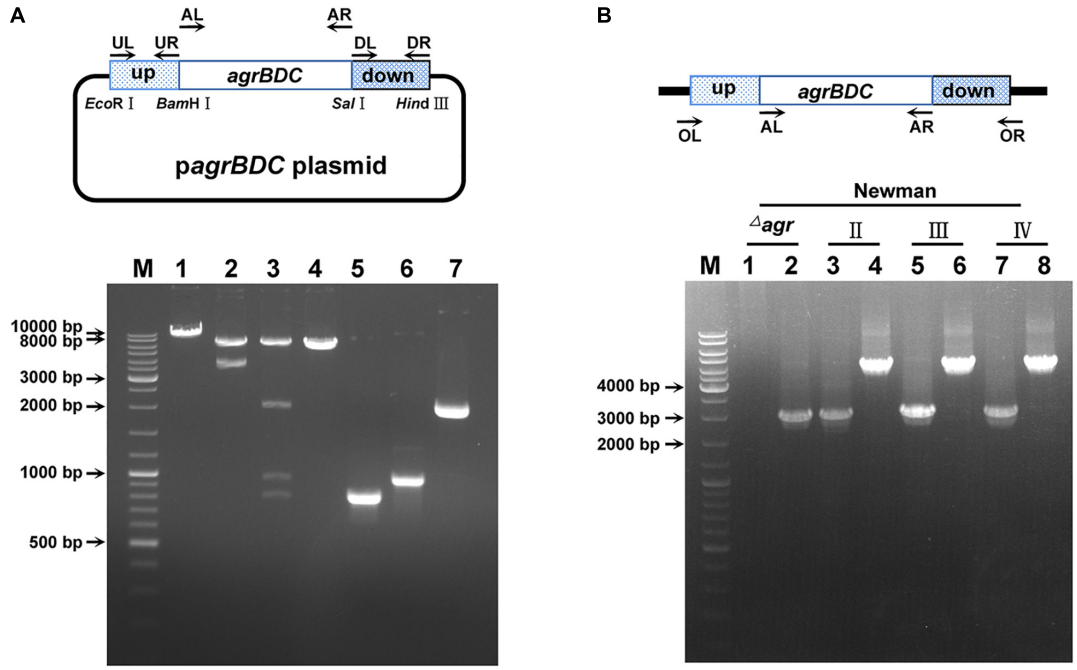


FIGURE 1 | The identification of *agr* allelic mutant in *S. aureus* Newman. **(A)** The confirmation of *agr* allele replacement plasmid by restriction enzyme digestion (take type II *agrBDC* replacement as an example). Bands 1, 2, and 3 are the single (*Bam*HI), double (*Eco*RI + *Hin*dIII), and four (*Bam*HI, *Eco*RI, *Hin*dIII, and *Sal*I) enzymes digestion patterns of *agrBDC*-II allelic replacement plasmid, respectively. Band 4 is the pattern of empty pBT2 plasmid linearized by *Bam*HI. Bands 5, 6, and 7 are patterns of the PCR amplification products of *agrBDC*-up (Band5, primers UL + UR), *agrBDC*-down (Band6, primers DL + DR), and *agrBDC*-II from N315 (Band7, primers AL + AR) fragments, respectively. **(B)** The confirmation of *agr* allelic replacement strains in Newman background by PCR amplification with primers AL + AR (Bands 1, 3, 5, 7) and primers OL + OR (Bands 2, 4, 6, 8). Bands 1–2 refer to the PCR products of Newman Δ*agrBDC* mutants, Bands 3–4 are the PCR products of the congenic strain harbor *agrBDC*-II sequence, bands 5–6 refer to PCR products of the congenic strain with *agrBDC*-III replacement, and bands 7–8 for *agrBDC*-IV replacement. All primers are shown in **Supplementary Table 2**.

activities, the MW2 (*agr*III) strain showed weak hemolysis, and the N315 (*agr*II) strain presented the lowest hemolytic toxicity (**Figure 2A**).

To assess the effects of different *agr* alleles on *S. aureus* hemolytic activity, the *agrBDC* genes in Newman strain (*agrBDC*-I) were deleted and *in situ* substituted with other three *agrBDC* alleles (*agrBDC*-II, *agrBDC*-III, and *agrBDC*-IV). As expected, the hemolytic activity of the NewmanΔ*agrBDC* strain was significantly lower than that of the wild strain (**Figure 2B**). The knock-in of type I *agrBDC* genes back to the genome of NewmanΔ*agrBDC* mutant recovered the hemolytic activity of revertant strain (**Figure 2B**). Contrary to our expectations, no visible hemolysis and very low hemolytic activity were discovered on three congenic replacement strains harboring heterologous *agr* systems (**Figure 2B**). The hemolytic activity controlled by *agr* system seemed to be severely suppressed when the three heterologous *agr* alleles were *in situ* recombined into the genome of NewmanΔ*agrBDC* mutant.

To investigate this further, four recombinant pLI50 plasmids containing types I to IV *agrBDCA* genes and their promoter sequences were, respectively, transformed into the Δ*agrBDC* mutant strains of Newman or N315. As shown in **Figures 2C,D**, the four *agr* complemented strains showed similar hemolytic activities to each other. The differences in hemolysis across *agr* groups were significantly weakened in the same Newman or N315 background when compared with the standard *agr* allelic strains.

Effects of Accessory Gene Regulator Alleles on Pigment Formation

Staphyloxanthin, a carotenoid pigment produced by *S. aureus*, protects bacteria from neutrophil oxidants (Xue et al., 2019). When the *agrBDC* sequence was deleted, NewmanΔ*agrBDC* mutant strain lost staphyloxanthin production and formed white colonies (**Figures 3B,C**). All congenic strains of Newman constructed by genomic replacement or plasmid complemented did not bring back the yellow color of wild Newman strain and showed white colonies (**Figures 3B,C**). The deletion of genes *agrBDCA* of N315 did not lead to visible color change (**Figure 3D**). However, four *agr* alleles complemented mutants in N315 presented white colonies in contrast to the golden colonies from the wild N315 and N315Δ*agrBDCA* mutant strains (**Figure 3D**).

Five genes, *crtOPQMN*, organized in an operon are responsible for the biosynthesis of staphyloxanthin (Xue et al., 2019). Two colorless farnesyl diphosphate successively catalyzed by five enzymes (CrtM, CrtN, CrtP, CrtQ, CrtO) to yield orange staphyloxanthin. Dehydrosqualene desaturase, CrtN, catalyzes the formation of the first deep yellow-colored carotenoid

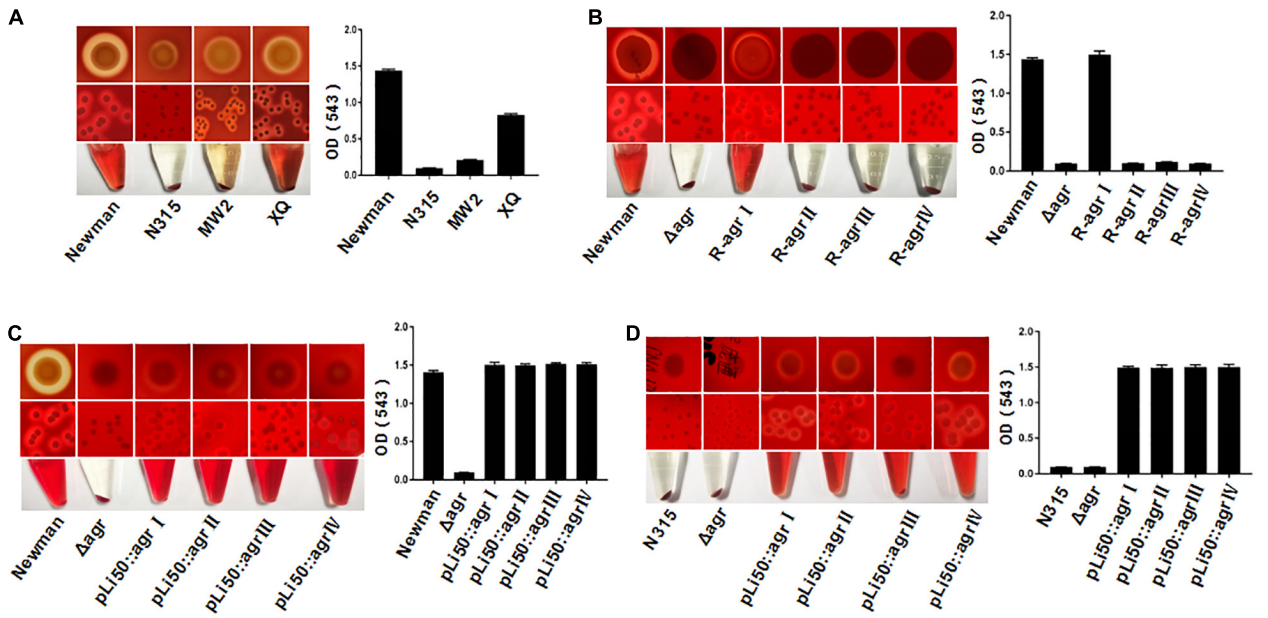


FIGURE 2 | Effects of *agr* alleles on the hemolytic activities of *S. aureus*. The overnight cultures of *S. aureus* strains with the same CFUs were plated on Columbia blood agar plates and grown for 24 h at 37°C. **(A)** Hemolytic activities of the four wild *agr* allelic strains: *agr*I (Newman), *agr*II (N315), *agr*III (MW2), and *agr*IV (XQ). **(B)** Hemolytic activities of the wild Newman strain, NewmanΔ *agrBDC*, and *agr* genomic *in situ* replacement mutants of Newman (*agr*I to *agr* IV). Hemolytic activities of the wild type, Δ*agrBDC* mutants and pLI50-*agr* plasmid complement mutants of Newman **(C)** and N315 **(D)**. The hemolytic activities of the relative strains were determined by measuring the optical density (OD543).

intermediate product, 4,4′-diaponeurosporene (Wieland et al., 1994). The sigma factor B (SigB) plays an essential role in regulating staphyloxanthin biosynthesis by binding to the promoter that laid in upstream of *crtO* (Kullik et al., 1998; Pelz et al., 2005). In the present study, the transcription levels of genes *crtN* and *sigB* were analyzed and found to be down-regulated in congenic strains when compared with the wild strains, Newman or N315 (**Figure 4**). It can be inferred that the down-regulated transcriptions of *crt* operon, especially that of *crtN*, are responsible for the weaken pigmentations of congenic strains, and the decreased SigB expression may play an important role in these processes.

Effects of Accessory Gene Regulator Alleles on Exoprotein Productions

To explore the influences of *agr* alleles on *S. aureus* exoprotein expressions, overnight culture supernatants were collected and analyzed by SDS-PAGE. As shown in **Figure 5A**, each *agr* type strain has its distinctive exoprotein profiles. Deletion of *agrBDC* genes led to significant changes in exoprotein expressions of Newman (**Figure 5A**). The knock-in of *agr*II, *agr*III, or *agr*IV *agrBDC* genes did not change the exoprotein expressions of NewmanΔ*agrBDC*; the three allelic strains exhibited similar exoprotein profiles as that of NewmanΔ*agrBDC* mutant (**Figure 5A**). However, when the four allelic *agrBDCA* genes were introduced by the pLI50 plasmid, the exoprotein patterns of four *agr* allelic complemented strains changed, which were highly similar to each other (**Figure 5B**) but different from those of wild *agr* allelic strains and the genomic replacement strains (**Figures 5A,B**). The *agr* allele–dependent difference in exoprotein expression was diminished when in the same Newman background. The similar results were also observed in N315 (**Figure 5C**). These complement strains exhibited significantly higher exoprotein expression than wild strains (**Figures 5B,C**). The two most abundant bands at approximately 25 and 35 kDa were identified as bicomponent hemolysin, α-hemolysin, or serine protease with mass spectrometry (**Supplementary Tables 4, 5**), which have been demonstrated to be regulated by *agr* system.

Effects of Accessory Gene Regulator Alleles on Virulence Gene Regulations

The ability of *S. aureus* to invade host tissues and cause infections depends on the production of a number of virulence factors. Many of them are regulated by the *agr* system such as α-toxin, β-toxin, δ-toxin, serine protease, fibrinolysin, PSM, and enterotoxin B (Seilie and Bubeck Wardenburg, 2017). In this study, we sought to examine the effects of different *agr* alleles on the transcription of virulence factors as *hla*, *hlb*, *hld*, *hlg*, *psmα*, *psmβ*, *pvl*, and *aur* (**Figure 6** and **Supplementary Figure 4**).

We found that the transcription of most toxins that are known to be activated by *agr* system (Bronesky et al., 2016) was now down-regulated in the NewmanΔ*agrBDC* mutant strain; the transcriptional factors and some surface proteins (Foster et al., 2014) that are usually inhibited by *agr* were now up-regulated. When the *agrBDC* genes of Newman strain (*agr*I) were genomically replaced by *agrBDC* genes from the other three *agr* alleles, the resulting mutants showed very

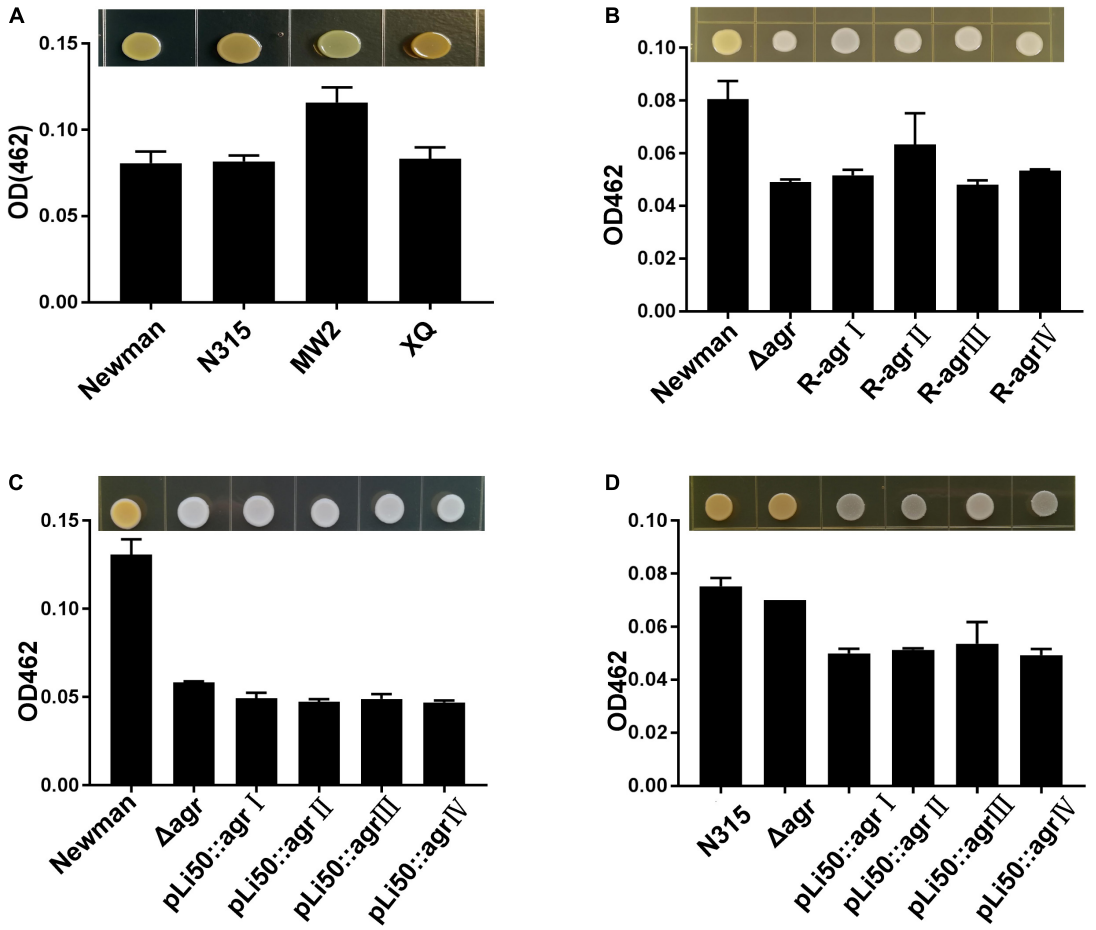


FIGURE 3 | Effects of *agr* alleles on the pigment formations of *S. aureus*. The overnight cultures of *S. aureus* strains with the same CFUs were plated on TSB agar plates and grown for 24 h at 37°C. **(A)** Pigment productions of the four wild *agr* allelic strains: *agr*I (Newman), *agr*II (N315), *agr*III (MW2), and *agr*IV (XQ). **(B)** Pigment productions of the wild Newman strain, NewmanΔ*agrBDC*, and *agr* genomic *in situ* replacement mutants (R-*agr*Ito *agr*IV) of Newman. Pigment productions of the wild type, Δ*agrBDC* mutants, and pLI50-*agr* plasmid complement mutants of Newman **(C)** and N315 **(D)**. Pigment productions of the relative strains were determined by measuring the optical density (OD462).

low *agr* expression (data not shown). This is consistent with the finding of hemolytic assay, staphyloxanthin formation test, and exoprotein profile analysis. As the *agrBDC* deletion was complemented by plasmid pLI50, the transcription of *agrA* and RNAIII of NewmanΔ*agrBDC* returned to the original level of wild Newman (**Supplementary Figures 3B,E**). While the relative mRNA level of *agrA* increased 30–50 times and the RNAIII increased about thousand folds compared with that of wild N315 (**Supplementary Figures 3C,F**), the virulence factor transcription of these allelic complemented strains constructed in the same background varied in the same trend, showing an elimination of *agr*-dependent difference in identical background (**Figure 6** and **Supplementary Figure 4**). For example, the transcription levels of *hla* gene of four *agr* congenic Newman strains increased 15–30 times compared with the wild Newman (**Figure 6B**), whereas they significantly increased 150–300 times when the four *agr* alleles were, respectively, complemented in *agr* defective N315 by plasmid pLI50 (**Figure 6C**). The *hlb* mRNA level showed 260- to 990-fold increase in N315 background, whereas only 30- to 72-fold in Newman background (**Figures 6E,F**). Similar changes were also observed in transcriptions of proteases such as aureolysin-encoding gene (*aur*, **Figures 6H,I**) and PVL-encoding gene (*pvl*, **Figures 6K,L**). Interestingly, the levels of *psm*α and *psm*β in all the four complemented strains were significantly decreased in the Newman background (**Supplementary Figures 4H,K**) compared with the wild Newman strain, but increased hundreds or thousands of folds in the N315 background (**Supplementary Figures 4I,L**).

DISCUSSION

The *agr* quorum-sensing system is a global regulator in *S. aureus* and controls the expression of numerous surface molecules, secreted enzymes, and cytotoxins (Ford et al., 2020). The amino acid polymorphisms in AgrB, AgrD, and AgrC separate the *agr* system into four groups. Strains with divergent *agr* groups

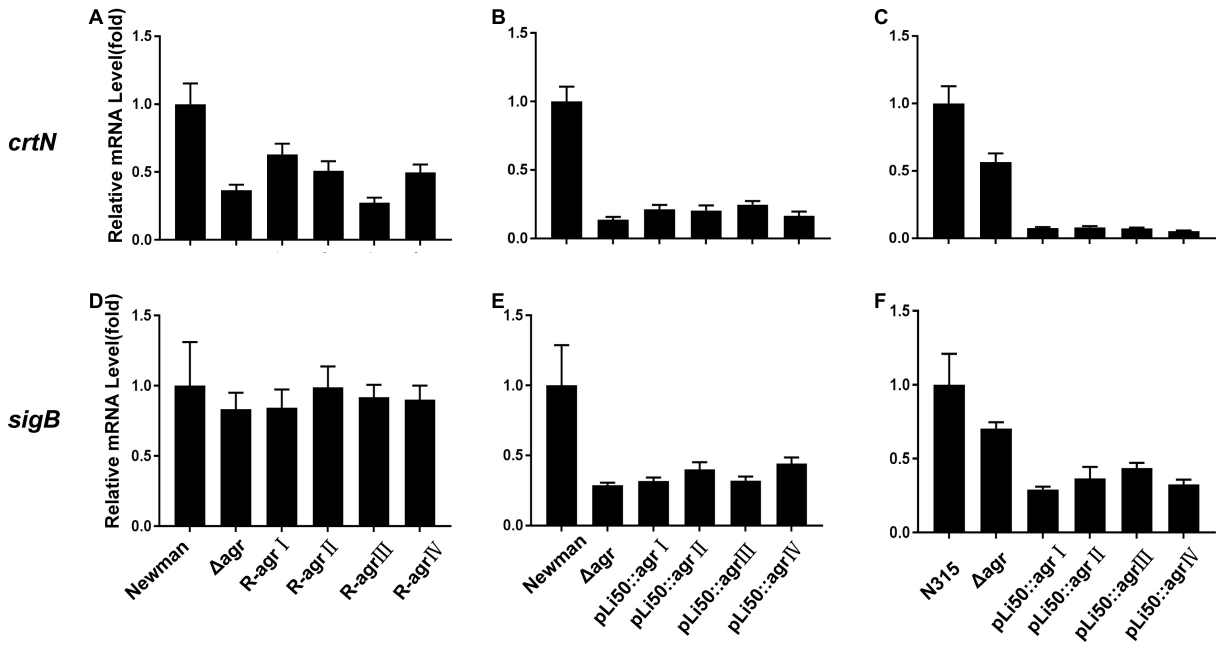


FIGURE 4 | Effects of *agr* alleles on the transcriptions of staphyloxanthin biosynthesis–related genes. The relative transcription levels of *crtN* **(A–C)** and *sigB* **(D–F)** were determined. **(A,D)** The relative transcription levels of wild Newman strain, Newman Δ*agrBDC* mutant, and *agr* genomic *in situ* replacement mutants (R-*agr*Ito *agr*IV) of Newman. **(B,E)** The relative transcription levels of wild Newman strain, Newman Δ*agrBDC* mutant, and four *agr* plasmid complemented strains in Newman background. **(C,F)** The relative transcription levels of wild N315 strain, N315 Δ*agrBDCA* mutant, and four *agr* plasmid complemented strains in N315 background.

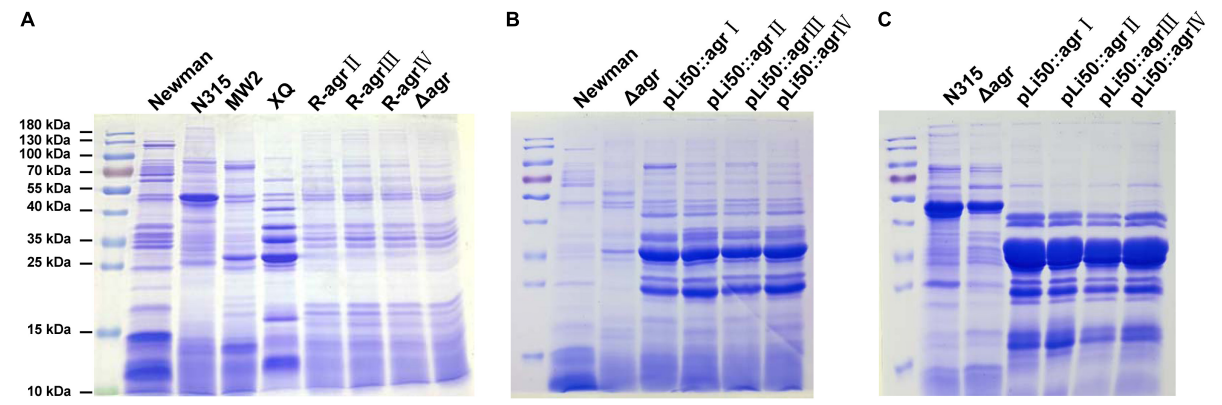


FIGURE 5 | Effects of *agr* alleles on the exoprotein productions of *S. aureus*. Overnight culture supernatants of *S. aureus* strains were collected and analyzed with SDS-PAGE. **(A)** Exoprotein profiles of the four wild *agr* allelic strains (*agr*I/Newman, *agr*II/N315, *agr*III/MW2, and *agr*IV/XQ), Newman Δ*agrBDC* mutant and three *agr* genomic *in situ* replacement strains in Newman background. **(B)** Exoprotein profiles of wild Newman strain, Newman Δ*agrBDC* mutant, and four *agr* plasmid complemented strains in Newman background. **(C)** Exoprotein profiles of wild N315 strain, Δ*agrBDCA*-N315 mutant, and four *agr* plasmid complemented strains in N315 background.

also show different biological phenotypes and virulence factor production. However, the influence factors of the *S. aureus agr*-specific genotypes and virulence remain poorly understood. To dissect the contributions of four divergent *agr* alleles on *S. aureus* biological properties, Geisinger et al. (2012) constructed *agr* congenic strains by individually inserting different *agr* allele at the staphylococcal pathogenicity island (SaPI)-1 *attC* locus site of the same background strain. They found that divergent *agr* alleles showed different *agr* activation dynamic and virulence factor production, and the allele-dependent differences are mediated by the polymorphisms in *agrBDCA* genes (Geisinger et al., 2012). In our study, the *agrBDC* genes of Newman (*agr*I) and the *agrBDCA* genes of N315 (*agr*II) were, respectively, replaced with those of other three *agr* groups by *in situ* genomic substitution or plasmid complementation. As expected, the knockout of *agrBDC* genes led to significant variations in hemolysis activity, pigment formation, exoprotein expression, and virulence factor expressions of Newman Δ*agrBDC* mutant.

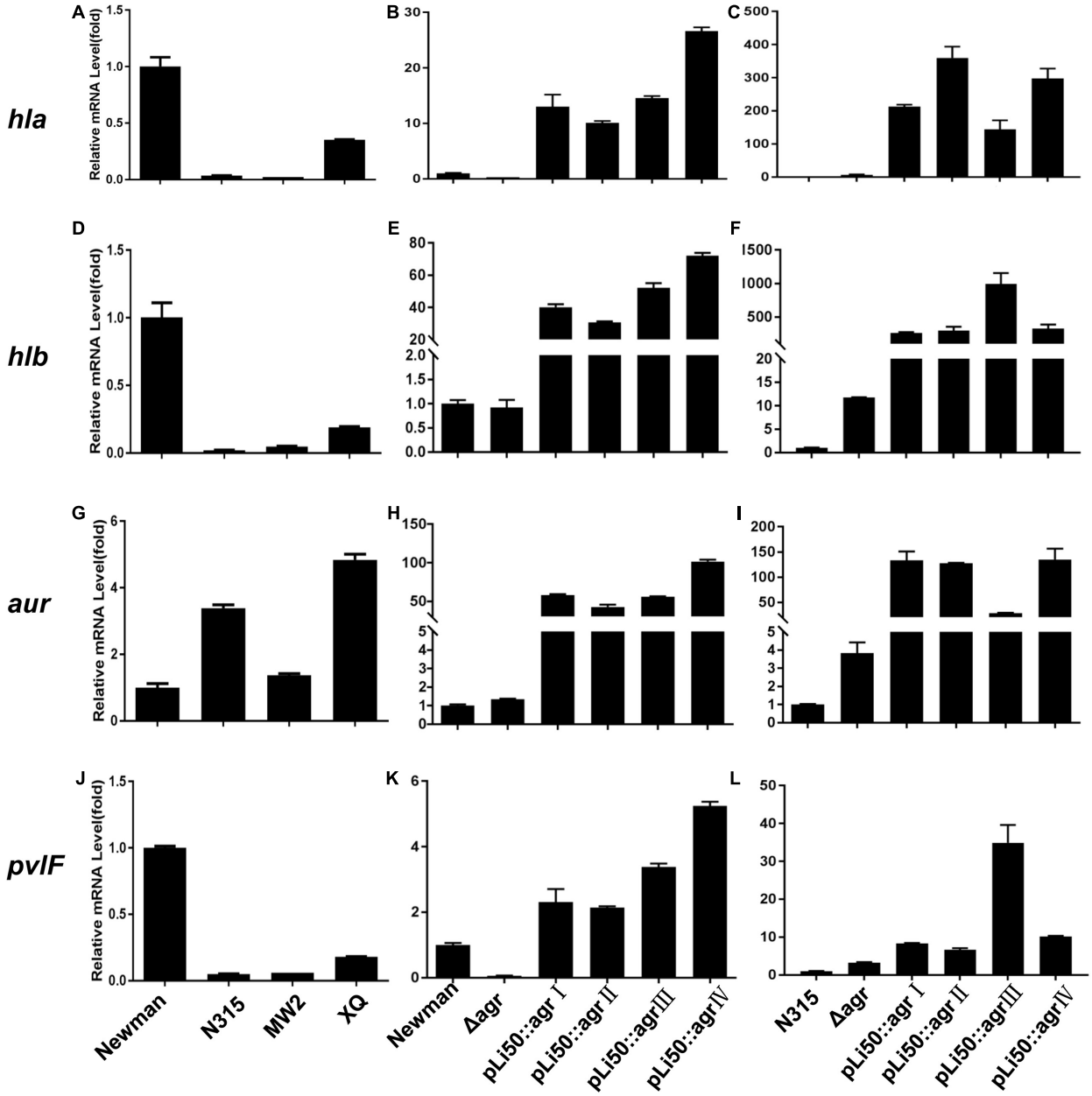


FIGURE 6 | Effects of *agr* alleles on virulence gene transcriptions of *S. aureus*. The relative transcription levels of *hla* **(A–C)**, *hlb* **(D–F)**, *aur* **(G–I)**, and *pvlF* **(J–L)** among the four wild *agr* allelic strains (*agr*I/Newman, *agr*II/N315, *agr*III/MW2, and *agr*IV/XQ) (left); *agr* plasmid complemented congenic strains in Newman (middle); or N315 (right) background were analyzed. Error bars represent the average standard deviation (SD) of three separate experiments.

No discernible difference was observed between wild N315 and N315Δ*agrBDCA* mutant because of the low activity of the N315 *agr* system under normal condition (**Figures 2–6**). However, when the three heterologous *agr* alleles (*agr*II, *agr*III, and *agr*IV) were individually introduced into the native *agr* site of NewmanΔ*agrBDC* genome, the hemolytic activity, pigment formation, and exoprotein expression of three congenic strains were almost identical to those of NewmanΔ*agrBDC* mutant. In addition, the *agrBDCA* and promoter regions of four *agr* alleles were also introduced into *S. aureus* Δ*agrBDC* strain (Newman or N315) by plasmid complementation. The hemolysis, exoprotein expression, pigment formation and virulence gene transcription of these plasmid complemented congenic strains were different from the wild strains harboring divergent *agr* allele (Newman for *agr*I, N315 for *agr*II, MW2 for *agr*III, and XQ for *agr*IV) and background strains (Newman or N315), but exactly similar to each other. According to the findings of our study, the congenic strains present similar biological properties when different *agr* alleles are individually introduced in the same background strain whether by *in situ* genomic replacement or

plasmid complement. It appears that the *agr* allele–dependent differences were weakened when in an identical background, which is distinct to the study by Geisinger et al. (2012) Perhaps, there are some other factors involved in the presentation of *agr*-controlled biological phenotype in addition to the polymorphous in *agrBDCA* genes.

The *agr* system is a critical regulatory system in *S. aureus*. Four allelic variants were reported, and each *agr* variant mediates the autoinduction of its own AIP (Jarraud et al., 2000). The *agr* cross-inhibition may drive evolutionary diversification in *S. aureus*. Our results indicate that cross-inhibition driven by *agr* polymorphisms may be affected by additional unknown factors in addition to the polymorphous of AgrBDCA proteins. It is well known that the *S. aureus agr* system can regulate the transcriptions of many genes and also be directly and indirectly controlled by other regulators (Queck et al., 2008). For example, SarA (Arya and Princy, 2013), SarU (Manna and Cheung, 2003), and MgrA (Manna and Cheung, 2006) are reported to up-regulate the expression of the *agr* system, whereas SigB (Bischoff et al., 2001), SarX (Manna and Cheung, 2006), and CodY (Majerczyk et al., 2010) may lead to the down-regulation of the *agr* system. The transcription levels of *sarA* and *sigB* were analyzed in this study (data not shown). Unfortunately, no direct correlation was observed between the expressions of these regulators and the similar phenotypes of *agr* allelic congenic strains. More in-depth studies are needed to reveal the putative factors and regulation mechanism, which may improve our understanding of the *S. aureus agr* system.

Taken together, our results further indicate that diversities of AgrB, AgrD, and AgrC contribute to the allele-dependent differences in *agr*-regulated activities in *S. aureus*. Additional unknown factors may also interfere with the *agr*-regulated phenotypes in *S. aureus*.

DATA AVAILABILITY STATEMENT

The raw data supporting the conclusions of this article will be made available by the authors, without undue reservation.

AUTHOR CONTRIBUTIONS

SL, XH, and XR conceived and designed this study. LT, SL, and YH carried out the experiments and analyzed the results. YW, ZH, and YR gave important suggestions to the data interpretation. WS, YY, and HP provided guidance in performing the experiments. XR, QH, ML, and KC provided guidance on the ideas for the study. All authors discussed the results and commented on the manuscript.

FUNDING

This work was supported by the National Natural Science Foundation of China (grant nos. 31470241, 31570127, and 31900118).

SUPPLEMENTARY MATERIAL

The Supplementary Material for this article can be found online at: https://www.frontiersin.org/articles/10.3389/fmicb.2022.700894/full#supplementary-material

Supplementary Figure 1 | The amino acids comparisons of AgrB **(A)**, AgrD **(B)**, and AgrC **(C)** among the four *S. aureus agr* allelic strains: *agr*I (Newman), *agr*II (N315), *agr*III (MW2), and *agr*IV (XQ). The sequences were obtained from NCBI (National Center for Biotechnology Information) database and aligned with the Clustal X and DNAMAN software. The blast results show that the amino acid sequences of AgrB, AgrD, and AgrC are variable.

Supplementary Figure 2 | The comparisons of AgrA **(A)**, RNAIII **(B)**, and promoter sequences **(C)** among the four *S. aureus agr* allelic strains: *agr*I (Newman), *agr*II (N315), *agr*III (MW2), and *agr*IV (XQ). The sequences were obtained from NCBI (National Center for Biotechnology Information) database (http://www.ncbi.nlm.nih.gov) and aligned with the Clustal X and DNAMAN software. The blast results show that the AgrA, RNAIII, and promoter region are highly conserved among the four *S. aureus agr* allelic strains.

Supplementary Figure 3 | Effects of *agr* alleles on *agr* transcriptions. The total bacterial RNA was isolated in mid-log phase, and gene transcription was appraised with quantitative RT-PCR. The transcription of *agrA* **(A–C)** and RNAIII **(D–F)** among the four wild *agr* allele strains (*agr*I/Newman, *agr*II/N315, *agr*III/MW2, and *agr*IV/XQ) (left) and *agr* plasmid complemented congenic strains in Newman (middle) or N315 (right) background were analyzed. Error bars represent the average standard deviation (SD) of three separate experiments.

Supplementary Figure 4 | Effects of *agr* alleles on virulence gene transcriptions of *S. aureus*. The total bacterial RNA was isolated in mid-log phase, and gene transcription was appraised with quantitative RT-PCR. The transcription of *hlgB* **(A–C)**, *hld* **(D–F)**, *psm*α **(G–I)**, and *psm*β **(J–L)** among the four wild *agr* allelic strains (*agr*I/Newman, *agr*II/N315, *agr*III/MW2, and *agr*IV/XQ) (left); *agr* plasmid complemented congenic strains in Newman (middle); or N315 (right) background were analyzed. Error bars represent the average standard deviation (SD) of three separate experiments.

REFERENCES

Arya, R., and Princy, S. (2013). An insight into pleiotropic regulators Agr and Sar: molecular probes paving the new way for antivirulent therapy. *Future Microbiol.* 8, 1339–1353. doi: 10.2217/fmb.13.92

Bernabè, G., Dal Pra, M., Ronca, V., Pauletto, A., Marzaro, G., Saluzzo, F., et al. (2021). A novel Aza-derivative inhibits quorum sensing signaling and synergizes Methicillin-Resistant *Staphylococcus aureus* to clindamycin. *Front. Microbiol.* 12:610859. doi: 10.3389/fmicb.2021.610859

Bischoff, M., Entenza, J. M., and Giachino, P. (2001). Influence of a functional sigB operon on the global regulators sar and agr in *Staphylococcus aureus*. *J. Bacteriol.* 183, 5171–5179. doi: 10.1128/JB.183.17.5171-5179.2001

Bronesky, D., Wu, Z., Marzi, S., Walter, P., Geissmann, T., Moreau, K., et al. (2016). *Staphylococcus aureus* RNAIII and its regulon link quorum sensing, stress responses, metabolic adaptation, and regulation of virulence gene expression. *Ann. Rev. Microbiol.* 70, 299–316. doi: 10.1146/annurev-micro-102215-095708

Cheung, G., and Otto, M. (2012). The potential use of toxin antibodies as a strategy for controlling acute *Staphylococcus aureus* infections. *Expert Opin. Ther. Targets* 16, 601–612. doi: 10.1517/14728222.2012.682573

Duthie, E., and Lorenz, L. (1952). Staphylococcal coagulase; mode of action and antigenicity. *J. Gen. Microbiol.* 6, 95–107. doi: 10.1099/00221287-6-1-2-95

Ford, C., Hurford, I., and Cassat, J. (2020). *Staphylococcus aureus* antivirulence strategies for the treatment of infections: a mini review. *Front. Microbiol.* 11:632706. doi: 10.3389/fmicb.2020.632706

Foster, T., Geoghegan, J., Ganesh, V., and Höök, M. (2014). Adhesion, invasion and evasion: the many functions of the surface proteins of *Staphylococcus aureus*. *Nat. Rev. Microbiol.* 12, 49–62. doi: 10.1038/nrmicro3161

Geisinger, E., Chen, J., and Novick, R. (2012). Allele-dependent differences in quorum-sensing dynamics result in variant expression of virulence genes in *Staphylococcus aureus*. *J. Bacteriol.* 194, 2854–2864. doi: 10.1128/jb.06685-11

Gomes, A., Vinga, S., Zavolan, M., and de Lencastre, H. (2005). Analysis of the genetic variability of virulence-related loci in epidemic clones of methicillin-resistant *Staphylococcus aureus*. *Antimicrob. Agents Chemother.* 49, 366–379. doi: 10.1128/aac.49.1.366-379.2005

Holtfreter, S., Grumann, D., Schmudde, M., Nguyen, H., Eichler, P., Strommenger, B., et al. (2007). Clonal distribution of superantigen genes in clinical *Staphylococcus aureus* isolates. *J. Clin. Microbiol.* 45, 2669–2680. doi: 10.1128/jcm.00204-07

Jarraud, S., Lyon, G., Figueiredo, A., Lina, G., Gérard, L., Vandenesch, F., et al. (2000). Exfoliatin-producing strains define a fourth agr specificity group in *Staphylococcus aureus*. *J. Bacteriol.* 182, 6517–6522. doi: 10.1128/jb.182.22.6517-6522.2000

Jarraud, S., Mougel, C., Thioulouse, J., Lina, G., Meugnier, H., Forey, F., et al. (2002). Relationships between *Staphylococcus aureus* genetic background, virulence factors, agr groups (alleles), and human disease. *Infect. Immun.* 70, 631–641. doi: 10.1128/iai.70.2.631-641.2002

Ji, G., Beavis, R., and Novick, R. (1995). Cell density control of staphylococcal virulence mediated by an octapeptide pheromone. *Proc. Natl. Acad. Sci. U.S.A.* 92, 12055–12059. doi: 10.1073/pnas.92.26.12055

Ji, G., Beavis, R., and Novick, R. (1997). Bacterial interference caused by autoinducing peptide variants. *Science* 276, 2027–2030. doi: 10.1126/science.276.5321.2027

Johansson, C., Rautelin, H., and Kaden, R. (2019). *Staphylococcus argenteus* and are cytotoxic to human cells due to high expression of alpha-hemolysin Hla. *Virulence* 10, 502–510. doi: 10.1080/21505594.2019.1620062

Khoramrooz, S., Mansouri, F., Marashifard, M., Malek Hosseini, S., Akbarian Chenarestane-Olia, F., Ganavehei, B., et al. (2016). Detection of biofilm related genes, classical enterotoxin genes and agr typing among *Staphylococcus aureus* isolated from bovine with subclinical mastitis in southwest of Iran. *Microbial. Pathog.* 97, 45–51. doi: 10.1016/j.micpath.2016.05.022

Kullik, I., Giachino, P., and Fuchs, T. (1998). Deletion of the alternative sigma factor sigma B in *Staphylococcus aureus* reveals its function as a global regulator of virulence genes. *J. Bacteriol.* 180, 4814–4820. doi: 10.1128/JB.00536-07

Liu, H., Shang, W., Hu, Z., Zheng, Y., Yuan, J., Hu, Q., et al. (2018). A novel SigB(Q225P) mutation in *Staphylococcus aureus* retains virulence but promotes biofilm formation. *Emerg. Microbes Infect.* 7:72. doi: 10.1038/s41426-018-0078-1

Majerczyk, C., Dunman, P., Luong, T., Lee, C., Sadykov, M., Somerville, G., et al. (2010). Direct targets of CodY in *Staphylococcus aureus*. *J. Bacteriol.* 192, 2861–2877. doi: 10.1128/jb.00220-10

Manna, A. C., and Cheung, A. L. (2003). sarU, a sarA homolog, is repressed by SarT and regulates virulence genes in *Staphylococcus aureus*. *Infect. Immun.* 71, 343–353. doi: 10.1128/IAI.71.1.343-353.2003

Manna, A. C., and Cheung, A. L. (2006). Expression of SarX, a Negative regulator of agr and exoprotein synthesis, Is activated by MgrA in *Staphylococcus aureus*. *J. Bacteriol.* 188, 4288–4299. doi: 10.1128/JB.00297-06

Mei, G. L., Cue, D., Roux, C. M., Dunman, P. M., and Lee, C. Y. (2011). Rsp inhibits attachment and biofilm formation by repressing fnbA in *Staphylococcus aureus* MW2. *J. Bacteriol.* 193, 5231–5241. doi: 10.1128/JB.05454-11

Novick, R., Projan, S., Kornblum, J., Ross, H., Ji, G., Kreiswirth, B., et al. (1995). The agr P2 operon: an autocatalytic sensory transduction system in *Staphylococcus aureus*. *Mol. Gen. Genet.* 248, 446–458. doi: 10.1007/bf02191645

Pader, V., James, E., Painter, K., Wigneshweraraj, S., and Edwards, A. (2014). The Agr quorum-sensing system regulates fibronectin binding but not hemolysis in the absence of a functional electron transport chain. *Infect. Immun.* 82, 4337–4347. doi: 10.1128/IAI.02254-14

Pelz, A., Wieland, K., Putzbach, K., Hentschel, P., Albert, K., and Götz, F. (2005). Structure and biosynthesis of staphyloxanthin from *Staphylococcus aureus*. *J. Biol. Chem.* 280, 32493–32498. doi: 10.1074/jbc.M505070200

Powers, M., Becker, R., Sailer, A., Turner, J., and Bubeck Wardenburg, J. (2015). Synergistic action of *Staphylococcus aureus* α-Toxin on platelets and myeloid lineage cells contributes to lethal sepsis. *Cell Host Microbe* 17, 775–787. doi: 10.1016/j.chom.2015.05.011

Queck, S., Jameson-Lee, M., Villaruz, A., Bach, T., Khan, B., Sturdevant, D., et al. (2008). RNAIII-independent target gene control by the agr quorum-sensing system: insight into the evolution of virulence regulation in *Staphylococcus aureus*. *Mol. Cell* 32, 150–158. doi: 10.1016/j.molcel.2008.08.005

Rao, Q., Zhou, K., Zhang, X., Hu, Q., Zhu, J., Chen, Z., et al. (2015). Fatal multiple organ failure in an adolescent due to community-acquired methicillin-susceptible *Staphylococcus aureus* ST121/agrIV lineage: a case report. *Rev. Med. Microbiol.* 26:1. doi: 10.1097/MRM.0000000000000050

Reyes-Robles, T., and Torres, V. (2017). Staphylococcus aureus pore-forming toxins. *Curr. Topics Microbiol. Immunol.* 409, 121–144. doi: 10.1007/82_2016_16

Seilie, E., and Bubeck Wardenburg, J. (2017). Staphylococcus aureus pore-forming toxins: the interface of pathogen and host complexity. *Semin. Cell Dev. Biol.* 72, 101–116. doi: 10.1016/j.semcdb.2017.04.003

Singh, R., and Ray, P. (2014). Quorum sensing-mediated regulation of staphylococcal virulence and antibiotic resistance. *Future Microbiol.* 9, 669–681. doi: 10.2217/fmb.14.31

Tan, L., Li, S., Jiang, B., Hu, X., and Li, S. (2018). Staphylococcus aureusTherapeutic Targeting of the Accessory Gene Regulator (agr) System. *Front. Microbiol.* 9:55. doi: 10.3389/fmicb.2018.00055

Traber, K., Lee, E., Benson, S., Corrigan, R., and Novick, R. (2008). Agr function in clinical *Staphylococcus aureus* isolates. *Microbiology* 154, 2265–2274. doi: 10.1099/mic.0.2007/011874-0

Tsompanidou, E., Sibbald, M., Chlebowicz, M., Dreisbach, A., Back, J., van Dijl, J., et al. (2011). Requirement of the agr locus for colony spreading of *Staphylococcus aureus*. *J. Bacteriol.* 193, 1267–1272. doi: 10.1128/JB.01276-10

Vandenesch, F., Lina, G., and Henry, T. (2012). *Staphylococcus aureus* hemolysins, bi-component leukocidins, and cytolytic peptides: a redundant arsenal of membrane-damaging virulence factors? *Front. Cell. Infect. Microbiol.* 2:12. doi: 10.3389/fcimb.2012.00012

Wang, B., and Muir, T. (2016). Regulation of virulence in *Staphylococcus aureus*: molecular mechanisms and remaining puzzles. *Cell Chem. Biol.* 23, 214–224. doi: 10.1016/j.chembiol.2016.01.004

Wieland, B., Feil, C., Gloria-Maercker, E., Thumm, G., Lechner, M., Bravo, J., et al. (1994). Genetic and biochemical analyses of the biosynthesis of the yellow carotenoid 4,4'-diaponeurosporene of *Staphylococcus aureus*. *J. Bacteriol.* 176, 7719–7726. doi: 10.1128/jb.176.24.7719-7726.1994

Wright, J., Traber, K., Corrigan, R., Benson, S., Musser, J., and Novick, R. (2005). The agr radiation: an early event in the evolution of staphylococci. *J. Bacteriol.* 187, 5585–5594. doi: 10.1128/jb.187.16.5585-5594.2005

Xue, L., Chen, Y., Yan, Z., Lu, W., and Zhu, H. (2019). Staphyloxanthin: a potential target for antivirulence therapy. *Infect. Drug Resist.* 12, 2151–2160. doi: 10.2147/IDR.S193649

Yuan, W., Hu, Q., Cheng, H., Shang, W., Liu, N., Hua, Z., et al. (2013). Cell wall thickening is associated with adaptive resistance to amikacin in methicillin-resistant *Staphylococcus aureus* clinical isolates. *J. Antimicrob. Chemother.* 68, 1089–1096. doi: 10.1093/jac/dks522

Conflict of Interest: The authors declare that the research was conducted in the absence of any commercial or financial relationships that could be construed as a potential conflict of interest.

Publisher's Note: All claims expressed in this article are solely those of the authors and do not necessarily represent those of their affiliated organizations, or those of the publisher, the editors and the reviewers. Any product that may be evaluated in this article, or claim that may be made by its manufacturer, is not guaranteed or endorsed by the publisher.

Copyright © 2022 Tan, Huang, Shang, Yang, Peng, Hu, Wang, Rao, Hu, Rao, Hu, Li, Chen and Li. This is an open-access article distributed under the terms of the Creative Commons Attribution License (CC BY). The use, distribution or reproduction in other forums is permitted, provided the original author(s) and the copyright owner(s) are credited and that the original publication in this journal is cited, in accordance with accepted academic practice. No use, distribution or reproduction is permitted which does not comply with these terms.

Advantages of publishing in Frontiers

OPEN ACCESS
Articles are free to read for greatest visibility and readership

FAST PUBLICATION
Around 90 days from submission to decision

HIGH QUALITY PEER-REVIEW
Rigorous, collaborative, and constructive peer-review

TRANSPARENT PEER-REVIEW
Editors and reviewers acknowledged by name on published articles

Frontiers
Avenue du Tribunal-Fédéral 34
1005 Lausanne | Switzerland

Visit us: www.frontiersin.org
Contact us: frontiersin.org/about/contact

REPRODUCIBILITY OF RESEARCH
Support open data and methods to enhance research reproducibility

DIGITAL PUBLISHING
Articles designed for optimal readership across devices

FOLLOW US
@frontiersin

IMPACT METRICS
Advanced article metrics track visibility across digital media

EXTENSIVE PROMOTION
Marketing and promotion of impactful research

LOOP RESEARCH NETWORK
Our network increases your article's readership